

Handbook of Optical Constants of Solids

edited by

Edward D. Palik

This book is printed on acid-free paper.

Copyright © 1998 by Academic Press

All rights reserved.
No part of this publication may be reproduced or transmitted in any form or by any means, electronic or mechanical, including photocopy, recording, or any information storage and retrieval system, without permission in writing from the publisher.

ACADEMIC PRESS
525 B Street, Suite 1900, San Diego, CA 92101-4495, USA
1300 Boylston Street, Chestnut Hill, MA 02167, USA
http://www.apnet.com

Academic Press Limited
24–28 Oval Road, London NW1 7DX, UK
http://www.hbuk.co.uk/ap/

Library of Congress Cataloging-in-Publication Data

Library of Congress CIP data pending.

ISBN 0-12-544423-0

Printed in the United States of America
97 98 99 00 01 IC 9 8 7 6 5 4 3 2 1

Contents

List of Contributors xiii
Preface xvii

Part I DETERMINATION OF OPTICAL CONSTANTS

Chapter 1 **Introductory Remarks** 3
EDWARD D. PALIK

I. Introduction 3
II. The Chapters 4
III. The Critiques 5
IV. The Tables 5
V. The Figures of the Tables 5
VI. Corrections, Additions, and Comments 6
References 12

Chapter 2 **Determination of the Far-Infrared Optical Constants of Solids by Dispersive Fourier Transform Spectroscopy** 13
T. J. PARKER, K. A. MASLIN, and G. MIRJALILI

I. Introduction 13
II. The Materials 20
Acknowledgment 55
References 55

Chapter 3 **Photothermal/Photoacoustic Spectroscopic Measurements of Optical Absorption Coefficients in Semiconductors** 59
ANDREAS MANDELIS

I. Introduction 59
II. Photoacoustic Spectroscopy (PAS) 60
III. Photopyroelectric Spectroscopy (PPES) 67
IV. Measurements of $\alpha(\lambda)$ in Semiconductors using Photoacoustic/Photothermal Techniques 69
Acknowledgments 94
References 94

Chapter 4 **Photothermal Deflection Measurements of the Extinction Coefficient *k*** 99
MATTHEW E. BRIGGS

I. Introduction 99
II. Photothermal Deflection 103
III. Conclusions 116
Acknowledgments 117
References 117

Chapter 5 **Determination of Optical Constants by Brillouin Scattering** 121
HACÈNE BOUKARI and NICHOLAS LAGAKOS

I. Definition of Notation 121
II. Introduction 122
III. Background on Brillouin Scattering Technique 123
IV. Equations for Measurement of the Index of Refraction 125
V. Fabry-Perot Interferometers 128
VI. Discussion 128
VII. Brillouin Scattering in Thin Slabs and Optical Fibers 134
VIII. Special Case of Transparent Thin Slabs 135
IX. Brillouin Scattering in Optical Fibers 146
References 153

Chapter 6 **Doped n-Type Silicon (n-Si)** 155
MARK AUSLENDER and SHLOMO HAVA

I. Introduction 155
II. Contributions to Dielectric Function: Optical Properties versus Optical Constants 156
III. Semiclassical Theory of Free-Carrier Contribution to the Dielectric Function: The Drude Approximation 158
IV. Free-Carrier Contribution to the Dielectric Function in Quantum Absorption Regime: Generalized Drude Approach 159
V. Experimental Data Overview 162
VI. Generalized Drude Approximation for n-Si 166
VII. Tabulation of Optical Constants of Doped n-Si 171
References 185

Chapter 7 **Optical Parameters for the Materials in *HOC I, HOC II,* and *HOC III*** 187
EDWARD D. PALIK

I. Introduction 187
II. The Parameters 187
References 225

Part II CRITIQUES

Subpart 1 Metals

Introduction to the Data for Several Metals 233
DAVID W. LYNCH and W. R. HUNTER

I. Introduction 233
References 235
II. Magnesium (Mg) 235
References 235
III. Titanium (Ti) 240
References 241
IV. Manganese (Mn) 249
References 250
V. Ruthenium (Ru) 253
References 254
VI. Indium (In) 261
References 262
VII. Tin (Sn) 268
References 269
VIII. Antimony (Sb) 274
References 275
IX. Rhenium (Re) 278
References 279

Optical Constants of Eight Rare-Earth Elements 287
L. WARD

I. Introduction 287
II. Cerium (Ce) 292
III. Samarium (Sm) 293
IV. Gadolinium (Gd) 294
V. Terbium (Tm) 297
VI. Dysprosium (Dy) 298
VII. Erbium (Er) 300
VIII. Thulium (Tm) 301
IX. Ytterbium (Yb) 302
References 303

Cesium (Cs) 341
T. INAGAKI and E. T. ARAKAWA

References 344

Zirconium Nitride (ZrN), Hafnium Nitride (HfN) 351
CARL G. RIBBING and ARNE ROOS

References 358

Subpart 2 Semiconductors

Aluminum Nitride (AlN) 373
S. LOUGHIN and R. H. FRENCH

References 377

Bismuth Silicon Oxide ($Bi_{12}SiO_{20}$) and Bismuth Germanium Oxide ($Bi_{12}GeO_{20}$) 403
E. D. PALIK

References 408

Boron Nitride (BN) 425
GARY L. DOLL

References 429

Cadmium Germanium Arsenide ($CdGeAs_2$) 445
J. C. RIFE

References 448

Copper Gallium Sulfide ($CuGaS_2$) 459
J. C. RIFE

References 462

Gallium Selenide (GaSe) 473
DAVID F. EDWARDS

References 477

Gallium Telluride (GaTe) 489
DAVID F. EDWARDS

References 491

Iron Pyrite (FeS_2) 507
E. D. PALIK

References 511

Silicon (Si) Revisited (1.1–1.3 eV) 519
JON GEIST

References 524

Silicon (Si) Revisited (1.4–6.0 eV) 531
DAVID F. EDWARDS

References 533

Silicon–Germanium Alloys (Si_xGe_{1-x}) Revisited 537
J. HUMLÍČEK

References 538

Silver Chloride (AgCl), Silver Bromide (AgBr), Silver Iodide (AgI) 553
MASATO TAZAWA and ARMAND HADNI

References 556

Silver Gallium Selenide ($AgGaSe_2$) and Silver Gallium Sulfide ($AgGaS_2$) 573
LUIS ARTÚS

References 577

Zinc Arsenide (Zn_3As_2) 595
J. MISIEWICZ and K. JEZIERSKI

References 596

Zinc Phosphide (Zn_3P_2) 609
J. MISIEWICZ and K. JEZIERSKI

References 612

Zinc Germanium Phosphide ($ZnGeP_2$) 637
J. C. RIFE

References 640

Subpart 3 **Insulators**

Aluminum Oxide (Al_2O_3) Revisited 653
MICHAEL E. THOMAS and WILLIAM J. TROPF

References 657

Barium Fluoride (BaF_2) 683
MICHAEL E. THOMAS and WILLIAM J. TROPF

References 686

Calcium Carbonate, Calcite ($CaCo_3$) 701
WILLIAM J. TROPF

References 703

Cesium Bromide (CsBr) 717
W. J. MOORE

References 719

Cesium Chloride (CsCl) 731
JOHN E. ELDRIDGE

References 733

Cesium Fluoride (CsF) 743
JOHN E. ELDRIDGE

References 745

Beta-Gallium Oxide (β-Ga_2O_3) 753
DAVID F. EDWARDS

References 755

Lead Fluoride (PbF_2) 761
MÁRCIA A. F. DESTRO and ALVARO J. DAMIÃO

References 766

Lithium Tantalate ($LiTaO_3$) 777
FRANÇOIS GERVAIS and VICENTE FONSECA

References 780

Potassium Iodide (KI) 807
MICHAEL E. THOMAS

References 810

Potassium Niobate ($KNbO_3$) 821
IVAN BIAGGIO

References 825

Rubidium Bromide (RbBr) 845
IVAN OHLÍDAL and MILOSLAV OHLÍDAL

References 848

Rubidium Iodide (RbI) 857
IVAN OHLÍDAL and DANIEL FRANTA

References 861

Sodium Nitrate ($NaNO_3$) 871
EDWARD D. PALIK and R. KHANNA

References 873

Strontium Fluoride (SrF_2) 883
MICHAEL E. THOMAS

References 886

Orthorhombic Sulfur (α-S) 899
KIRK A. FULLER, HARRY D. DOWNING, and MARVIN R. QUERRY

References 905

Cubic Thallium(I) Halides 923
WILLIAM J. TROPF

References 931

Yttrium Aluminum Garnet ($Y_3Al_5O_{12}$) 963
WILLIAM J. TROPF

References 966

Zircon ($ZrSiO_4$) 987
EDWARD D. PALIK and R. KHANNA

References 989

List of Contributors

Numbers in parentheses indicate the pages on which the authors' contributions begin.

E. T. ARAKAWA (341), Life Sciences Division, Oak Ridge National Laboratory, Oak Ridge, Tennessee 37831

LUIS ARTÚS (573), Consejo Superior de Investigaciones Cientificas, Instituto Jaime Almera, Sole Sabaris s/n, 08028 Barcelona, Spain

MARK AUSLENDER (155), Department of Electrical and Computer Engineering, Ben-Gurion University of the Negev, Beer-Sheva 84105, Israel

IVAN BIAGGIO (821), Institute of Quantum Electronics, Swiss Federal Institute of Technology, ETH-Hönggerberg, CH-8093 Zürich, Switzerland

HACÈNE BOUKARI (121), Institute for Physical Science and Technology, University of Maryland, College Park, Maryland 20742

MATTHEW E. BRIGGS (99), Department of Physics, 201 James Fletcher Building, University of Utah, Salt Lake City, Utah 84112

ALVARO J. DAMIÃO (761), Centro Técnico Aeroespacial, Instituto de Estudos Avançados, São José dos Campos, São Paulo, Brasil

MÁRCIA A. F. DESTRO (761), Centro Técnico Aeroespacial, Instituto de Estudos Avancados, São José dos Campos, Sao Paulo, Brasil

GARY L. DOLL (425), Mail Code RES-04, The Timken Company, 1835 Dueber Avenue, S.W., Canton, Ohio 44706

HARRY D. DOWNING (899), Department of Physics and Astronomy, Stephen F. Austin State University, Nacogdoches, Texas 75962

DAVID F. EDWARDS (473, 489, 531, 753), 8820 W. Valpico Road, Tracy, California 95376

JOHN E. ELDRIDGE (731, 743), Department of Physics, 6224 Agriculture Road, The University of British Columbia, Vancouver, B. C. V6T 1Z1, Canada

VICENTE FONSECA (777), Centre de Recherches sur la Physique de Hautes Températures, 1D, Avenue de la Recherche Scientifique, 45071 Orléans Cedex, France

DANIEL FRANTA (857), Department of Solid State Physics, Faculty of Science, Masaryk University Brno, Kotlárská 2, 611 37 Brno, Czech Republic

ROGER H. FRENCH (373), DuPont Central Research and Development, Experimental Station Building E265-384, Wilmington, Delaware 19880-0356

KIRK A. FULLER (899), Department of Atmospheric Science, Colorado State University, Fort Collins, Colorado 80521
JON GEIST (519), 4008 Fulford Street, Olney, Maryland 20832
FRANÇOIS GERVAIS (777), Centre de Recherches sur la Physique de Hautes Temperatures, 1D, Avenue de la Recherche Scientifique, 45071 Orléans Cedex, France
ARMAND HADNI (553), Université Henri Poincaré, Nancy I, 54506 Vandoeuvre-les-Nancy Cedex, France
SHLOMO HAVA (155), Department of Electrical and Computer Engineering, Ben-Gurion University of the Negev, Beer-Sheva 84105, Israel
JOSEF HUMLÍČEK (537), Department of Solid State Physics, Faculty of Science, Masaryk University Brno, Kotlárská 2, 611 37 Brno, Czech Republic
W. R. HUNTER (233), SFA Inc., 1401 McCormack Drive, Largo, Maryland 20774
T. INAGAKI (341), Division of Natural Sciences, Osaka Kyoiku University, Osaka, Japan
K. JEZIERSKI (595, 609), Institute of Physics, Technical University of Wroclaw, Wybrzeze Wyspianskiego 27, 50-370 Wroclaw, Poland
R. KHANNA (871, 987), Department of Chemistry and Biochemistry, University of Maryland, College Park, Maryland 20742
NICHOLAS LAGAKOS (121), Code 7134, Naval Research Laboratory, Washington, D.C. 20375
STEPHEN LOUGHIN (373), Lockheed Martin Astro Space, Building B-29B12, P.O. Box 8555, Philadelphia, Pennsylvania 19101-8555
DAVID W. LYNCH (233), Department of Physics and Astronomy and Ames Laboratory, USDOE, Iowa State University, Ames, Iowa 50011
ANDREAS MANDELIS (59), Photothermal and Optoelectronic Diagnostics Laboratories, Department of Mechanical and Industrial Engineering, University of Toronto, 5 King's College Road, Toronto M5S3G8 Canada
K. A. MASLIN (13), Royal Holloway, University of London, Egham, Surrey TW20 OEX, United Kingdom
G. MIRJALILI* (13), Department of Physics, University of Essex, Colchester CO4 3SQ, United Kingdom
J. MISIEWICZ (595, 609), Institute of Physics, Technical University of Wroclaw, Wybrzeze Wyspianskiego 27, 50-370 Wroclaw, Poland
W. J. MOORE (717), Code 6870, Naval Research Laboratory, Washington, D.C. 20375
IVAN OHLÍDAL (845, 857), Department of Solid State Physics, Faculty of Science, Masaryk University Brno, Kotlárská 2, 611 37 Brno, Czech Republic
MILOSLAV OHLÍDAL (845), Institute of Physical Engineering, Technical University, Brno, Czech Republic

* Present address: Department of Physics, University of Yazd, Yazd, Iran

EDWARD D. PALIK (3, 187, 403, 507, 871, 987), Institute for Physical Science and Technology, University of Maryland, College Park, Maryland 20742

T. J. PARKER (13), Department of Physics, University of Essex, Colchester CO4 3SQ, United Kingdom

MARVIN R. QUERRY (899), Department of Physics, University of Missouri-Kansas City, Kansas City, Missouri 64110

CARL G. RIBBING (351), School of Engineering, Department of Technology, Uppsala University, Box 534, S-751 Uppsala, Sweden

J. C. RIFE (445, 459, 637), Code 6680, Naval Research Laboratory, 4555 Overlook Avenue, S.W., Washington, D. C. 20375

ARNE ROOS (351), School of Engineering, Department of Technology, Uppsala University, Box 534, S-751 Uppsala, Sweden

MASATO TAZAWA (553), National Industrial Research Institute of Nagoya, Nagoya 462, Japan

MICHAEL E. THOMAS (653, 683, 807, 883), The Johns Hopkins University, Applied Physics Laboratory, Johns Hopkins Road, Laurel, Maryland 20723-6099

WILLIAM J. TROPF (653, 683, 701, 923, 963), The Johns Hopkins University, Applied Physics Laboratory, Johns Hopkins Road, Laurel, Maryland 20723-6099

L. WARD (287), School of Natural and Environmental Sciences, Coventry University, Priory Street, Coventry CV1 5FB, United Kingdom

Preface

The *Handbook of Optical Constants of Solids* has now grown to three volumes. The publication of *HOC I* in 1985 and *HOC II* in 1991 has reduced but not exhausted the available materials of scientific and technological interest. One can ask what materials are left to critique. There are several candidates.

There is a trickle of recently published papers remeasuring "old" materials already critiqued in *HOC I* and *HOC II.* This is the case for Si, Al_2O_3, Si_xGe_{1-x}, which are revisited in *HOC III.* This will be worthwhile to do for several other materials from time to time.

We have not developed the courage to attack the III–V ternary and quaternary materials in detail except for $Al_xGa_{1-x}As$ *(HOC II),* so important in laser and electronic applications. We looked at the II–VI ternary compound $Hg_{1-x}Cd_xTe$ *(HOC II),* important in infrared-detector applications, as well as the IV-VI compound $Pb_{1-x}Sn_xTe$ *(HOC II).*

Our dream of critiquing all the alkali halides from LiF to CsBr is not yet fulfilled.

We have noticed a lack of data for the index of refraction n but not for the extinction coefficient k for gemstones. The gemologist only seems interested in n at the Na D line. We noticed from a scan of several gem books that n is not given throughout the visible. For most purposes, n is considered a constant. But to the physicist, n is not a constant. Since gemstones must be "full of impurities" to give them their wide variety of colors, the gemologist does measure the visible absorption spectrum to determine the impurity absorption bands. The physicist usually prefers pure crystals (at least insulators). We have previously critiqued diamond, sapphire, quartz, and spinel in pure form, the latter three being the starting point for several gemstones including ruby, amethyst, agate, opal, and chrysoberyl. In *HOC III* we add yttrium aluminum garnet and zircon. There are no n measurements in the visible except at 589.0 nm for zircon. We need to find more technology uses for gemstones which, in turn, will spur measurements of n and k! We could not find a critiquer for cubic zirconia, which to us is quite different from diamond in optical properties, but serves as "fake" diamond for many people.

As with *HOC I* and *HOC II,* I am indebted to the many scientists for their work in *HOC III,* writing chapters on still more ways to measure optical constants and writing critiques tabulating the optical constants of more than 60 additional materials.

June, 1997 EDWARD D. PALIK

Chapter 1

Introductory Remarks

EDWARD D. PALIK
Institute for Physical Science and Technology
University of Maryland
College Park, Maryland

I. Introduction 3
II. The Chapters 4
III. The Critiques 5
IV. The Tables 5
V. The Figures of the Tables 5
VI. Corrections, Additions, and Comments 6
A. Optical Constants of CdS 6
B. Optical Constants of Metal Films 6
C. Henke Model for the Elements 8
D. More-Recent Papers about Optical Constants 9
E. Optical Constants on Disk 12
References 12

INTRODUCTION I

The two previous volumes of *Handbook of Optical Constants of Solids (HOC I* and *HOC II)* contained about 85 materials. The present volume adds about 58 more materials, roughly divided into equal numbers of metals, semiconductors, and insulators. A long list of potential materials was circulated among possible critiquers. They chose and/or recommended the ones presented here. There are still some materials omitted because of a lack of critiquers. These include Bi, B, Ba, Ca, Cd, Pb, Zn, Zr, ZnO, HgS, HgSe, $Pb_xSn_{1-x}Se$, PbO, MoS_2, Cd_3As_2, GaS, LiOH, NaBr, NaI, KF, LiCl, LiBr, ZrO_2, BaO, and NiO. Note that 43 of the 92 chemical elements are done and 143 of the 100,000 (or more) chemical compounds. We have omitted glasses generally, which are covered to some extent by Efimov [1] and Tropf *et al.* [2].

There is some loose use of the words *semiconductor* and *insulator* in *HOC I* and *HOC II* based primarily on the band gap being less or greater than

Copyright © 1998 by Academic Press.
All rights of reproduction in any form reserved
ISBN 0-12-544423-0/$25.00.

3 eV. AgCl, AgBr, AgI, BSO, and BGO are considered as semiconductors because their electrical properties can be controlled by doping during growth of the crystals, but they may end up in either category. Diamond is invariably thought of as an insulator, although natural diamonds can be found with semiconducting properties.

II THE CHAPTERS

The chapters are meant to describe experimental techniques for measuring n and k.

In Chapter 2, Parker *et al.* discuss the determination of n and k by differential Fourier transform spectroscopy in the far infrared. This is an elegant way to obtain n and k from the reflection amplitude and phase and has been applied to many semiconductors and insulators. It is of interest to compare these newer optical constants with those in *HOC I* or *HOC II,* which have generally been obtained by Kramers-Kronig (K-K) analysis or classical oscillator fit.

In Chapter 3, Mandelis describes the use of photoacoustic spectroscopy to determine k. While this chapter stresses semiconductors, several variations of the technique have also found widespread use for other materials.

In Chapter 4, Briggs discusses photothermal deflection as a method of determining k. It is done with two intense beams, one to heat up a small spot on a sample and a second to detect bending of the sample as it expands locally.

In Chapter 5, Boukari and Lagakos describe the determination of n and k by Brillouin scattering. While not usually thought of as a technique for determining optical constants, there are novel ways to determine n an k in highly absorbing materials and n in transparent slabs and thin films.

In Chapter 6, Auslender and Hava develop models for calculating n and k in n-Si for the infrared region for free-electron concentrations from 10^{16} to 10^{20} cm^{-3}.

In Chapter 7, Palik collects a number of optical parameters for all the materials in *HOC I, HOC II,* and *HOC III* including crystal structure, space group symmetry, unit cell dimensions, number of molecules/unit cell, optic and acoustic irreducible representation, transverse and longitudinal lattice vibration frequencies, plasma frequency, band gap, and d.c. dielectric constant.

There were suggestions for chapters on the loss-tangent method at low frequencies and on the prism minimum-deviation technique (still the best way to determine n), but these could not be done at this time.

THE CRITIQUES III

The critiques are meant to be the critiquer's own judgment of the best room-temperature values of n and k over the widest spectral range. As the volumes have progressed, we have expanded the range a little with a few critiques including above and below room-temperature data. Sometimes there are two overlapping sets of data from two different laboratories which can be compared. This sometimes happens in the far infrared where reflectivity is K-K analyzed and/or a classical oscillator model is applied. Generally, it is not a good idea to give the reader a choice of data—it is the job of the critiquer to make the choice. Sometimes, however, a comparison sheds light on the problems arising in the measurement of optical constants such as wavelength calibration and determination of absolute reflectivity. Recently, spectroscopic ellipsometry has grown into a wide-spread technique for the 1.5–6 eV region, probably supplanting K-K analysis of reflectivity.

We have returned to a few materials done in previous volumes because more data have become available. Therefore, we revisit Al_2O_3, Si_xGe_{1-x} and Si.

THE TABLES IV

The tables of n and k have become more individual to meet the needs of the individual critiquers. We maintain the columns labeled eV, cm^{-1}, μm, n, k and proceed down the column in decreasing eV. Reference brackets [1] start at the top of a given data column and are understood down the column until a new data set occurs, which is then labeled [2], for example. We promoted exponential notation especially of k, ideally for every column, but have not yet reached that stage of uniformity.

To facilitate editing the tables for the Optical Society of America, we have requested that the exponential notation be used at every row, rather than omitting the exponent until it changes value somewhere down the column.

THE FIGURES OF THE TABLES V

The critiquers have taken more leeway with the figures, since they had to produce them with whatever graphics software they had available. In previous editions, all the figures were prepared by the same artist who kept the style uniform. Now critiquers can use data points (usually ○○○ for n and △△△ for k). Data points can be connected with lines, or just lines can be used (usually —— for n and --- for k). In the past, both n and k were plotted on the same

figure with the same log-log scale. Since the extent of k determined the number of decades of the log scale for the ordinate, ($10^{-7} < k < 10^{1}$), n was squeezed. Also, for solids with a lot of vibration bands, this region got very busy. Now some critiquers have separated n and k plots to show the structure more clearly.

The drawbacks in having each critiquer make his own figure are the many problems of font size, tick-mark position, and border thickness, remembering that the figure will be reduced in published form.

VI CORRECTIONS, ADDITIONS, AND COMMENTS

A Optical Constants of CdS

A correction and addition to the data for CdS from *HOC II* needs to be made according to the critiquer, L. Ward. Data of Dutton[1] near the band edge has been added. The extinction coefficient for both $\mathbf{E}_{\|c}$ and $\mathbf{E}_{\perp c}$ has been determined by transmission measurements of thin slabs of different thicknesses. These can be compared to data of Cardona and Harbeke[2] for bulk-oriented samples obtained from K-K analysis of reflectivity with polarized light. Data of Khawaja and Tomlin[3] for films deposited on quartz substrates (assumed to be polycrystalline) were obtained from transmittance and reflectance measurements; these data have been reassessed to correct an error in reading the wavelength scale. The results are presented in Table I. While above the band gap the results for k are comparable, below the band gap where absorption decreases orders of magnitude, the results differ drastically among the three data sets. We suspect that K-K analysis of reflectivity in Cardona and Harbeke gives poor results for $k \ll 1$ compared to transmittance of slabs in Dutton. For the polycrystalline films in Khawaja and Tomlin, it is not obvious why k is so much larger compared to the data of Dutton below the band gap. Perhaps there was significant light scattering from defected material, which was mistaken for absorption.

B Optical Constants of Metal Films

The optical constants of metals in *HOC I, II,* and *III* can be compared with those given in Optimatr, a computer program to calculate optical prop-

[1] D. Dutton, Fundamental absorption edge in cadmium sulfide. *Phys. Rev.* **112,** 785 (1958).

[2] M. Cardona and G. Harbeke, Optical properties and band structure in wurtzite-type crystals and rutile. *Phys. Rev.* **A137,** 1467 (1965).

[3] E. E. Khawaja and S. G. Tomlin, The optical constants of thin evaporated films of cadmium and zinc sulphide. *J. Phys. D: Appl. Phys.* **8,** 581 (1975).

TABLE I

Values of n and k for Cadmium Sulfide from Various References

eV	cm^{-1}	μm	n	k	$n\perp$	$k\perp$	$n\parallel$	$k\parallel$	$k\perp$	$k\parallel$
			[3]		[2]		[2]		[1]	
4.133	33333	0.30	2.68	0.70						
4.0	32260	0.3100			2.64	0.64	2.40	0.81		
3.75	30245	0.3306			2.64	0.62	2.38	0.74		
3.542	28571	0.35	2.58	0.47						
3.5	28230	0.3542			2.62	0.56	2.38	0.65		
3.25	26213	0.3815			2.62	0.49	2.36	0.61		
3.100	25000	0.40	2.55	0.37						
3.0	24196	0.4133			2.63	0.44	2.37	0.56		
2.755	22222	0.45	2.62	0.32						
2.75	22180	0.4509			2.70	0.41				
2.7	21777	0.4592					2.47	0.54		
2.6	20970	0.4769							0.32	0.32
2.575	20769	0.4815							0.32	0.32
2.55	20567	0.4862							0.32	0.32
2.525	20365	0.4910							0.29	0.22
2.5	20164	0.4959			2.81	0.36	2.62		0.28	0.16
2.475	19962	0.5009	2.72	0.15					0.25	0.15
2.45	19760	0.5061							0.081	0.022
2.425	19559	0.5113							0.014	0.0028
2.4	19357	0.5166							0.0016	0.00033
2.375	19155	0.5220							0.00019	
2.254	18182	0.55	2.45	0.01						
2.25	18147	0.5510			2.57	0.04	2.53	0.26		
2.066	16667	0.60	2.40							
2.0	16130	0.6199			2.48	0.02	2.44	0.18		

erties of materials. This software is available from ARSoftware, 8201 Corporate Dr., Suite 1110, Landover, MD 20785. It is copyrighted by the Johns Hopkins University/Applied Physics Laboratory and ARSoftware, Inc. The calculational procedures, based on several literature models for determining optical properties of solids, are based on the works of M. E. Thomas and W. J. Tropf. The data for metals in Optimatr were essentially that of Ordal *et al.*, who fitted a Drude model to many sets of existing data. In comparing the optical constants of metals from Optimatr and *HOC* in the visible and near-infrared regions, one finds for Au and Ag especially, significant variations in n and k (up to a factor of two). This is due to the fact that data from different laboratories were used. Where the data from the same laboratories were used, the agreement is much better, of course.

This general problem of the variation of optical constants of metal films deposited at different laboratories and with different deposition techniques, has been discussed by Aspnes *et al.* with regard to gold. They find that voids

and grain size in the films can account for significant variations in n and k, as demonstrated by their spectroscopic-ellipsometry measurements in the 1.5–6 eV spectral region. Therefore, it would appear that metal films (and especially Au and Ag) should be measured directly if the optical constants are needed for an application. Also, it would be good to measure the optical constants of single crystals of the metal, if polishing the surface can be accomplished with minimal damage. Since k is so large (generally > 1), the optical skin depth is typically less than a few hundred Angstroms. Native oxides can also pose a problem.

We list a number of papers about Au which trace this problem and may be of interest to the reader.

H. E. Bennett and J. M. Bennett, Validity of the Drude theory for silver, gold and aluminum in the infrared. *In* "Optical Properties and Electronic Structure of Metals and Alloys," (F. Abeles, ed.), p. 175. North-Holland, Amsterdam, 1966.

M.-L. Theye, Investigation of the optical properties of Au by means of thin semitransparent films. *Phys. Rev. B* **2,** 3060. (1970).

D. E. Aspnes, E. Kinsbron and D. D. Bacon, Optical properties of Au: Sample effects. *Phys. Rev. B* **21,** 3290 (1980), and references therein.

M. A. Ordal, L. L. Long, R. J. Bell, S. E. Bell, R. R. Bell, R. W. Alexander, Jr., and C. A. Ward, Optical properties of the metals Al, Co, Cu, Au, Fe, Pb, Ni, Pd, Pt, Ag, Ti, and W in the infrared and far infrared. *Appl. Opt.* **22,** 1099 (1983).

M. A. Ordal, R. J. Bell, R. W. Alexander, Jr., L. L. Long, and M. R. Querry, Optical properties of fourteen metals in the infrared and far infrared: Al, Co, Cu, Au, Fe, Pb, Mo, Ni, Pd, Pt, Ag, Ti, V, and W. *Appl. Opt.* **24,** 4493 (1985).

M. Yamamoto and T. Namioka, In situ ellipsometric study of optical properties of ultrathin films. *Appl. Opt.* **31,** 1612 (1992).

F. Xingwei, S. Yi, M. Hongzhou, C. Liangyao, and Q. Youhua, Precision of determination of optical constant of Au film by spectroscopic ellipsometry. *Chin. J. Infrared Millimeter Waves* **12,** 107 (1993).

C Henke Model for the Elements

The most recent update for the scattering factors of the chemical elements has appeared in B. L. Henke, E. M. Gullikson and J. C. Davis, X-Ray interactions: Photoabsorption, scattering, transmission, and reflection at E = 50–30000 eV, Z = 1–92. *At. Data Nucl. Data Tables* **54,** 181 (1993).

These data are also available by computer. In fact, the calculation of n and k can be carried out at

http://www-cxro.lbl.gov/optical_constants

Extension to compounds is also possible, although the values will not be correct at energies near bonding energies. Deep-lying K and L absorption edges are well approximated, however.

More-Recent Papers about Optical Constants D

Since 1985 for the materials in *HOC I,* and since 1991 for the materials in *HOC II,* more papers have appeared discussing optical constants. We list those papers below which we have noticed.

Occasionally, an older paper of interest, missed or omitted by the critiquer, has been included (without comment).

Metals 1

B. Henke, E. M. Gullikson and J. C. Davis, X-ray interactions; photoabsorption, scattering, transmission, and reflection at E = 50-30000 eV, Z = 1-92. *At. Data Nucl. Data Tables* **54,** 181 (1993).

M. Yamamoto and T. Namioka, In situ ellipsometric study of optical properties of ultrathin films. *Appl. Opt.* **31,** 1612 (1992). (C, Si, Ni, Nb, Mo, Ru, Rh, Pd, Ag, W, Re, Au.)

D. L. Windt, XUV optical constants of single-crystal GaAs and sputtered C, Si, Cr_3C_2, Mo, and W. *Appl. Opt.* **30,** 15 (1991).

D. L. Windt, W. C. Cash, Jr., M. Scott, P. Arendt, B. Newnam, R. F. Fisher, and A. B. Swartzlander, Optical constants for thin films of Ti, Zr, Nb, Mo, Ru, Rh, Pd, Ag, Hf, Ta, W, Re, Ir, Os, Pt, and Au from 24 Å to 1216 Å. *Appl. Opt.* **27,** 246 (1988).

D. L. Windt, W. C. Cash, Jr., M. Scott, P. Arendt, B. Newnam, R. F. Fisher, A. B. Swartzlander, P. Z. Takacs, and J.M. Pinneo, Optical constants for thin films of C, diamond, Al, Si and CVD SiC from 24 Å to 1216 Å. *Appl. Opt.* **27,** 279 (1988).

F. Xingwei, S. Yi, M. Hongzhou, C. Liangyao and Q. Youhua, Precision of determination of optical constants of Au film by spectroscopic ellipsometry. *Chin. J. Infrared Millimeter Waves* **12,** 107 (1993).

M. Yanagihara, J. Cao, M. Yamamoto, A. Arai, S. Nakayama, T. Mizuide, and T. Namioka, Optical constants of very thin gold films in the soft x-ray region. *Appl. Opt.* **30,** 2807 (1991).

J. Cao, M. Yanagihara, M. Yamamoto, Y. Goto, and T. Namioka, Simultaneous determination of the optical constants and thickness of very thin films by using soft-x-ray reflectance measurements. *Appl. Opt.* **33,** 2013 (1994). (Au, C.)

R. Wolf, H.-G. Birken, C. Blessing, and C. Kunz, Optical constants of gold in the soft-x-ray region from reflection and transmission measurements. *Appl. Opt.* **33,** 2683 (1994).

T. Maehara, M. Yanagihara, M. Yamamoto, and T. Namioka, Optical constants of very thin Pt and Rh films determined from soft-x-ray reflectance and photoelectric yield measurements. *Nucl. Instrum. Methods Phys. Res.* **B47,** 362 (1993).

B. T. Sullivan, Optical properties of palladium in the visible and near UV spectral regions. *Appl. Opt.* **29,** 1964 (1990).

J. I. Larruquert, J. A. Méndez, and J. A. Aznárez, Far-ultraviolet reflectance measurements and optical constants of unoxidized aluminum films. *Appl. Opt.* **34,** 4892 (1995).

J. I. Larruquert, J. A. Méndez, and J. A. Aznárez, Optical constants of aluminum films in the extreme ultraviolet interval of 82-77 nm. *Appl. Opt.* **35,** 5692 (1996).

Semiconductors 2

J. Geist, A. Migdall, and H. Baltes, Shape of the silicon absorption coefficient spectrum near 1.63 eV. *Appl. Opt.* **29,** 3548 (1990).

J. Geist, A. Migdall, and H. P. Baltes, Analytic representation of the silicon absorption coefficient in the indirect transition region. *Appl. Opt.* **27,** 3777 (1988).

H. A. Weakliem and D. Redfield, Temperature dependence of the optical properties of silicon *J. Appl. Phys.* **50,** 1491 (1979).

J. Geist, A. R. Schaefer, J.-F. Song, Y. H. Wang, and E. F. Zalewski, An accurate value for the absorption coefficient of silicon at 633 nm. *J. Res. Natl. Inst. Stand. Technol.* **95,** 549 (1990).

G. E. Jellison, Jr., and F. A. Modine, Optical functions of silicon at elevated temperatures. *J. Appl. Phys.* **76,** 3758 (1994).

G. E. Jellison, Jr., Optical functions of silicon determined by two-channel polarization modulation ellipsometry. *Opt. Mater.* **1,** 41, (1992).

G. E. Jellison, Jr., and F. A. Modine, Optical functions of silicon between 1.7 and 4.7 eV at elevated temperatures. *Phys. Rev.* **B27,** 7466 (1983); G. E. Jellison, Jr., and F. A. Modine, Optical absorption of silicon between 1.6 and 4.7 eV at elevated temperatures. *Appl. Phys. Lett.* **41,** 180 (1992).

J. F. Seely, W. R. Hunter, J. C. Rife, and M. P. Kowalski, Optical constants of thin silicon films near the silicon $L_{2,3}$ absorption edge. *Appl. Opt.* **31,** 7367 (1992).

G. E. Jellison, Jr., T. E. Haynes, and H. H. Burke, Optical functions of silicon-germanium alloys determined using spectroscopic ellipsometry. *Opt. Mater.* **2,** 105 (1993).

J. Humlíček and M. Garriga, Temperature dependence of the refractive index of crystalline germanium-silicon alloys. *Appl. Phys.* **A56,** 259 (1993).

J. Humlíček, A. Röseler, T. Zettler, M. G. Kekoua, and E. V. Khoutsishvili, Infrared refractive index of germanium-silicon alloy crystals. *Appl. Opt.* **31,** 90 (1992).

S. Chen, R. Jiang, and D. Mo, Ultraviolet-visible ellipsometric spectra and optical constants of sputtered amorphous silicon. *Acta Opt. Sin. (Guangxue Xuebao)* **4,** 49 (1984).

G. E. Jellison, Jr., Optical functions of GaAs, GaP, and Ge determined by two-channel polarization modulation ellipsometry. *Opt. Mater.* **1,** 151 (1992).

T. A. Kudykina, "Index of refraction of $A^{III}B^{V}$ compounds in the region of fundamental absorption. *Phys. Status Solidi B* **188,** K39 (1995).

C. M. Herzinger, H. Tao, P. G. Snyder, F. G. Celii, Y.-C. Kao, B. Johs, and J. A. Woollam, Determination of AlAs optical constants by variable angle spectroscopic ellipsometry and a multisample analysis. *J. Appl. Phys.* **77,** 4677 (1995).

C. M. Herzinger, P. G. Snyder, B. Johs and J. A. Woollam, InP optical constants between 0.7 and 5 eV determined by variable-angle spectroscopic ellipsometry. *J. Appl. Phys.* **77,** 1715 (1995).

C. M. Herzinger, P. G. Snyder, F. G. Celii, Y.-C Kao, D. Chow, B. Johs, and J. A. Woollam, Studies of thin stressed GaAs, AlAs and AlSb layers by spectroscopic ellipsometry. *J. Appl. Phys.* **79,** 2667 (1996).

W. J. Moore and R. T. Holm, Infrared dielectric constant of gallium arsenide. *J. Appl. Phys.* **80,** 6939 (1996).

L. Pajasová, P. Pajas, A. Šimunek, and O. A. Makarov, A study of the optical properties of semiconductors with synchrotron radiation from the VEPP-2M storage ring. *Nucl. Instrum. Methods Phys. Res.* **A261,** 131 (1987). (GaAs.)

V. Vaicikauskas, Far infrared surface electromagnetic waves propagation on A^3B^5 semiconductors. *Int. J. Infrared Millimeter Waves* **15,** 303 (1994). (InSb, InP, GaAs.)

J. A. McCaulley, T. W. M. Dommelly, M. Vernon, and I. Taha, Temperature dependence of the near-infrared refractive index of silicon, gallium arsenide, and indium phosphide. *Phys. Rev. B* **49,** 7408 (1994).

P. Martin, E. M. Skouri, L. Chusseau, and C. Milert, Accurate refractive index measurements of doped and undoped InP by a grating coupling technique. *Appl. Phys. Lett.* **67,** 881 (1995).

R. G. Kaufman, C. R. Hulse, D. J. Vezzetti, A. L. Moretti, K. A. Stair, G. P. Devane, and T. E. Bird, Measurement of the refractive index of $Al_xGa_{1-x}As$ and the mode indices of guided modes by a grating coupling technique. *J. Appl. Phys.* **75,** 8053 (1994).

R. J. Deri and M. A. Emanuel, Consistent formula for the refractive index of $Al_xGa_{1-x}As$ below the band edge. *J. Appl. Phys.* **77,** 4667 (1995).

C.-H. Lin and J. M. Meese, Optical properties of bulk $Al_xGa_{1-x}As$. *J. Appl. Phys.* **74,** 6341 (1993).
D. B. Chenault and R. A. Chipman, Infrared birefringence spectra for cadmium sulfide and cadmium selenide. *Appl. Opt.* **32,** 4223 (1993).
D. Dutton, Fundamental absorption edge in cadmium sulfide. *Phys. Rev.* **112,** 785 (1958).
P. Hofmann, K. Horn, A. M. Bradshaw, R. L. Johnson, D. Fuchs, and M. Cardona, Dielectric function of cubic and hexagonal CdS in the vacuum ultraviolet region. *Phys. Rev. B* **47,** 1639 (1993).
M. Schäffner, X. Bao, and A. Penzkofer, Principal optical constants measurement of uniaxial crystal CdSe in the wavelength region between 380 and 950 nm. *Appl. Opt.* **31,** 4546 (1992).
J. M. Hoffman and W. L. Wolfe, Cryogenic refractive indices of ZnSe, Ge, and Si at 10.6 μm. *Appl. Opt.* **30,** 4014 (1991).
C. A. Klein, R. P. Miller, and D. L. Stierwalt, Surface and bulk absorption characteristics of chemically vapor-deposited zinc selenide in the infrared. *Appl. Opt.* **33,** 4304 (1994).
E. N. Kotlikov, Analysis of absorption in zinc selenide and fluoride mirrors and films. *Opt. Spectrosc.* **70,** 490 (1991); *Opt. Spektrosk.* **70,** 838 (1991).
W. J. Moore, Errors in film refractive-index determinations from interference fringes. *Appl. Opt.* **33,** 4164 (1994). (3C-SiC films.)
W. J. Moore, R. T. Holm, M. J. Yang, and J. A. Freitas, Jr., Infrared dielectric constant of cubic SiC. *J. Appl. Phys.* **78,** 7255 (1995).
S. Ninomoya and S. Adachi, Optical constants of 6N-SiC single crystal. *Jpn. J. Appl. Phys.* **33,** 2479 (1994).
J. B. Kortright and D. L. Windt, Amorphous silicon carbide coatings for extreme ultraviolet optics. *Appl. Opt.* **27,** 2841 (1988).
M. Yanagihara, M. Niwano, T. Koide, S. Sata, T. Miyahara, Y. Iguchi, S. Yamaguchi, and T. Sasaki, Soft x-ray reflection from SiC, TiC, and WC mirrors. *Appl. Opt.* **25,** 4586 (1986).
C. Junhao and M. Zhengyu, Absorption and reflection spectra of HgCdTe *Chin. J. Infrared Millimeter Waves* **8,** 91 (1989).
A. I. Belogorokhov, A. G. Belov, and E. P. Rashevskaya, Effect of free charge carriers on $Cd_xHg_{1-x}Te$ solid-solution reflection spectra in the far infrared. *Opt. Spectrosc.* **69,** 86 (1990); *Opt. Spektrosk.* **69,** 139 (1990).
S. Farjami Shayesteh, T. Dumflow, T. J. Parker, T. I. Benushis, S. N. Ershov, and M. I. Vasilevskiy, Determination of the far infrared optical constants of n-doped bulk $Cd_xHg_{1-x}Te$ (CMT) by dispersive Fourier transform spectroscopy. *Int. J. Infrared Millimeter Waves* **16,** 763 (1995).
M. Nianxin, Y. Hongjuan, S. Xuechu, H. Zhihong, and L. Anxiang, Far-infrared reflectance spectra of naturally occuring PbS (galena). *Chin. J. Infrared Millimeter Waves* **13,** 91 (1994).

Insulators 3

J. M. Siqueiros, R. Machorro, and L. E. Regalado, Determination of the optical constants of MgF_2 and ZnS from spectrophotometric measurements and the classical oscillator method. *Appl. Opt.* **27,** 2549 (1988).
S. Cunsolo, P. Dore, and C. P. Varsamis, Refractive index of crystals from transmission and reflection measurements: MgO in the far-infrared region. *Appl. Opt.* **31,** 4554 (1992).
S. Cunsolo, P. Dore, S. Lupi, and P. Maselli, Complex refractive index of MgO in the far infrared from transmission and reflection measurements. *Infrared Phys.* **33,** 539 (1992).
X. Gerbaux, A. Hadni, M. Tazawa, and J. C. Villegier, Far-infrared spectra of magnesium oxide. *Appl. Opt.* **33,** 57 (1994).
J. Nithianandam and J. C. Rife, Synchrotron x-ray optical properties of natural diamond. *Phys. Rev. B* **47,** 3517 (1993).
G. Davies, A. T. Collins, and P. Spear, Sharp infrared absorption lines in diamond. *Solid State Commun.* **49,** 433 (1984).

Y. Pastol, G. Arjavalingam, G. V. Kopcsay, and J.-M. Halbout, Dielectric properties of uniaxial crystals measured with optoelectronically generated microwave transient radiation. *Appl. Phys. Lett.* **55,** 2277 (1989). (Al_2O_3, x-SiO_2.)

R. T. Swimm, Y. Xiao, and M. Bass, Calorimetric study of optical absorption of Suprasil W-1 fused quartz at visible, near-IR and near-UV wavelengths. *Appl. Opt.* **24,** 322 (1985).

M. L. Lang and W. L. Wolfe, Optical constants of fused silica and sapphire from 0.3 to 25 μm. *Appl. Opt.* **22,** 1267 (1983).

E. E. Khawaja and F. Bouamrane, Determination of the optical constants *(n, k)* of thin dielectric films. *Appl. Opt.* **32,** 1168 (1993). (deposited TiO_2.)

U. Schlarb and K. Betzler, Refractive indices of lithium niobate as a function of wavelength and composition. *J. Appl. Phys.* **73,** 3472 (1993).

A. V. Soldatov, I. E. Shtekhin, and A. Biankoni, Fine structure analysis of the L_2 edge of x-ray absorption by Ca in CaF_2 using multiple-scattering method. *Opt. Spectrosc.* **74,** 514 (1993); *Opt. Spektrosk.* **74,** 862 (1992).

A. B. Sushkov and E. A. Tishchenko, Ellipsometry of a convergent beam in the far infrared. *Opt. Spectrosc.* **72,** 265 (1992): *Opt. Spektrosk.* **72,** 491 (1992). ($SrTiO_3$.)

M. E. Thomas, W. J. Tropf, and S. L. Gilbert, Vacuum-ultraviolet characterization of sapphire, ALON, and spinel near the band gap. *Opt. Eng.* **32,** 1340 (1993).

M. E. Thomas, Optical properties of IR materials. *Thin Solid Films* **206,** 241 (1991). (MgO, SiO_2, Al_2O_3, Y_2O_3, $MgAl_2O_4$.)

G. Compagnini, Optical constants of hydrogenated and unhydrogenated amorphous carbon in the 0.5–12-eV range. *Appl. Opt.* **33,** 7377 (1994).

L. Kou, D. Labrie, and P. Chylek, Refractive indices of water and ice in the 0.65– to 2.5-μm spectral range. *Appl. Opt.* **32,** 3531 (1993).

V. M. Zoloratev and A. V. Demin, Optical constants of water over a broad range of wavelengths, 0.1Å–1m. *Opt. Spectrosc.* **43,** 157 (1977); *Opt. Spektrosk.* **43,** 271 (1977).

H. R. Zelsmann, Temperature dependence of the optical constants for liquid H_2O and D_2O in the far infrared region. *J. Mol. Struct.* **350,** 95 (1995).

M. E. Innocenzi, R. T. Swimm, M. Bass, R. H. French, A. B. Villaverde, and M. R. Kokta, Room-temperature optical absorption in undoped α-Al_2O_3. *J. Appl. Phys.* **67,** 7542 (1990).

M. Zukic, D. G. Torr, J. F. Spann, and M. R. Torr, Vacuum ultraviolet thin films. 1: Optical constants of BaF_2, CaF_2, LaF_3, MgF_2, Al_2O_3, HfO_2, and SiO_2 thin films. *Appl. Opt.* **29,** 4284 (1990).

E Optical Constants on Disk

The tables of *n* and *k* from *HOC I* and *HOC II* have been edited and put on disk by the Optical Society of America. One 3.5″ disk in MS DOS version in compressed format is available from Electronic Products, Optical Society of America, 2010 Massachusetts Ave., N.W., Washington, D.C. 20036. Hopefully, this can be expanded to include the materials in *HOC III* shortly.

REFERENCES

1. A. M. Efimov, "Optical Constants of Inorganic Glasses." CRC Press, Boca Raton, Florida, 1995.
2. W. J. Tropf, M. E. Thomas and T. J. Harris, Properties of crystals and glasses. *In* "Handbook of Optics, Volume II, Devices, Measurements and Properties," (M. Bass, E. W. Van Stryland, D. R. Williams and W. L. Wolfe, eds.), 2nd Ed. McGraw-Hill, New York, 1995.

Chapter 2

Determination of the Far-Infrared Optical Constants of Solids by Dispersive Fourier Transform Spectroscopy

T. J. PARKER[1], K. A. MASLIN[2], and G. MIRJALILI[1*]
[1]Department of Physics, University of Essex
Colchester, United Kingdom
[2]Royal Holloway, University of London
Egham, Surrey, United Kingdom

I. Introduction 13
II. The Materials 20
A. Alkali Halides 20
B. Semiconductors 32
C. II–VI Semiconductors 33
D. III–V Semiconductors 38
Acknowledgment 55
References 55

I INTRODUCTION

We present values of the far-infrared optical constants of a selection of alkali halide crystals (NaCl, KCl, KBr, KI, and RbCl), II–VI semiconductors (CdTe, ZnSe) and III–V semiconductors (GaP, GaAs, GaSb, InP, InAs, and InSb) determined by dispersive Fourier transform spectroscopy (DFTS). DFTS is a technique for determining the optical constants of materials in the solid, liquid, or gas phase from direct measurements of the amplitude and phase reflection or transmission coefficients of suitable samples as a function of frequency, $f = c/\lambda$, or wavenumber, $\nu = 1/\lambda$, where c is the speed of light in vacuo and λ is the wavelength. The technique was pio-

* Present address: Department of Physics, University of Yazd, Yazd, Iran

Copyright © 1998 by Academic Press.
All rights of reproduction in any form reserved
ISBN 0-12-544423-0/$25.00.

neered in the early 1960s by Chamberlain and colleagues [1–3] at the National Physical Laboratory in the United Kingdom, and by Bell and colleagues [4–6] at the Ohio State University in the United States. A number of extensive reviews of the applications of DFTS in solid, liquid, and gas state spectroscopy have been written over the past twenty years [7–10]; we shall not repeat that material here, but shall very briefly summarize the principles of the technique and then concentrate on aspects of the method which have a direct bearing on the accuracy of the determination of the optical constants.

In DFTS, a suitable sample, usually prepared with plane-parallel surfaces, is placed in one arm, usually the fixed arm, of a two-beam Michelson interferometer for measurements either in reflection or transmission; three geometrical arrangements have been described in the literature [8], and these are illustrated schematically in Fig. 1. Two interferograms are usually recorded, a sample interferogram $I_S(x)$, measured as a function of optical path difference, x, with the sample in place in the interferometer, and a reference, or background interferogram, $I_B(x)$, recorded after replacing the sample with a suitable reference material: in reflection DFTS, the reference material would be a reference mirror placed in the plane previously occupied by the sample; in transmission DFTS, the reference material would be the slab of vacuum left in the instrument after removing the sample. In either case, the information containing the frequency dependence of the amplitude and phase reflection or transmission coefficients is obtained by computing the ratio

$$L(\nu) = L_0(\nu)\exp i\phi_L(\nu) = \frac{FT[I_S(x)]}{FT[I_B(x)]} \tag{1}$$

of the complex Fourier transforms, $FT[I_S(x)]$ and $FT[I_B(x)]$, of the two recorded interferograms. The exact form of the relationship between $L(\nu)$, commonly known as the complex insertion loss, and the optical constants, (n, k), is determined by the details of the experimental arrangement.

In this article we shall review the optical constants of a selection of simple binary solids calculated from amplitude and phase reflection coefficients determined by reflection DFTS. In this geometry (Fig 1(c)), as already pointed out, the background interferogram is recorded after replacing the sample by a reference mirror. This is the simplest geometry encountered in DFTS, and the complex insertion loss is equal to the ratio of the complex amplitude reflection coefficients of the sample and the reference mirror. Thus, for reflection DFTS, or amplitude reflection spectroscopy as it is frequently known, the complex insertion loss is given by

$$L_0(\nu)\exp i\phi_L(\nu) = \frac{r_s(\nu)\exp i\phi_s(\nu)}{r_m(\nu)\exp i\phi_m(\nu)} \tag{2}$$

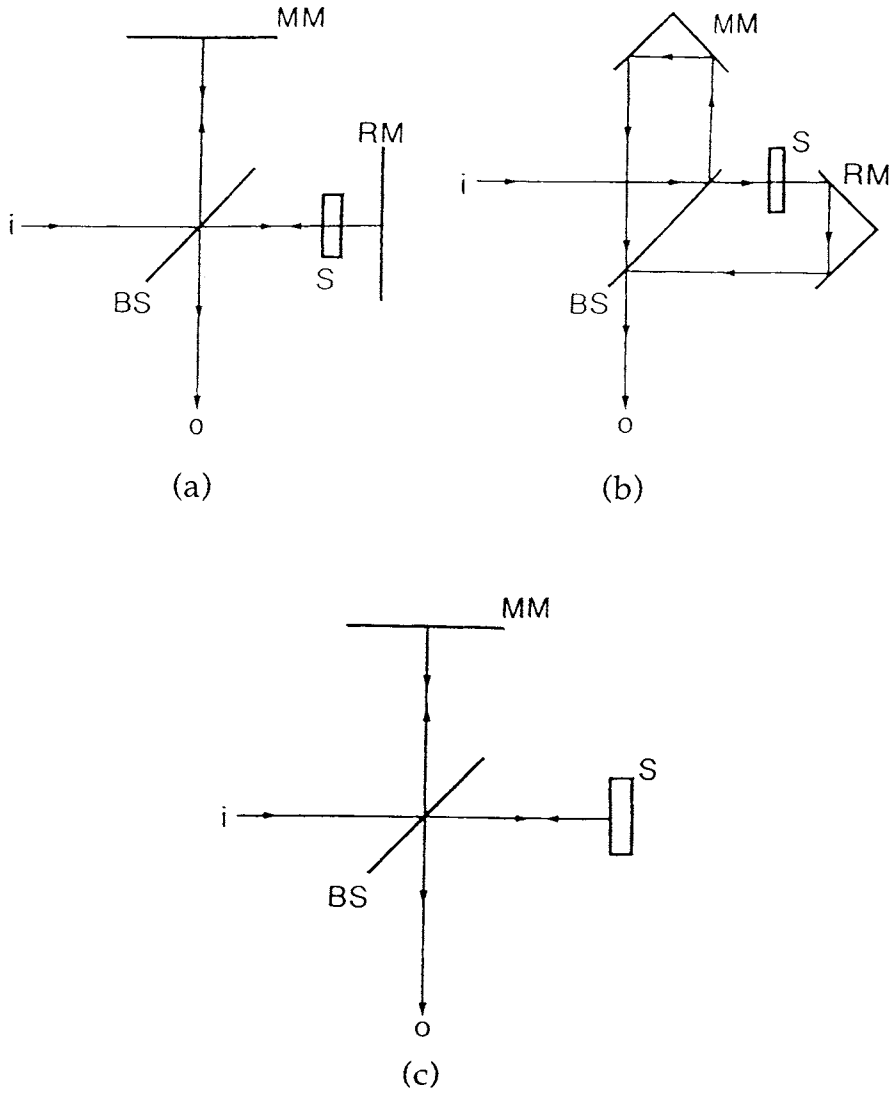

Fig. 1. Schematic drawing of the three experimental arrangements used in DFTS. (a) Double-pass transmission DFTS, (b) Single-pass transmission DFTS, and (c) Reflection DFTS, or amplitude-reflection spectroscopy. Key: *i,* input beam; *o,* output beam; *MM,* moving mirror; *RM,* reference mirror; *BS,* beam splitter; *S,* sample.

In DFTS in the far infrared, it is common practice to regard the reference mirror as a perfect mirror with a complex-amplitude reflection coefficient

$$r_m(\nu) \exp i\phi_m(\nu) = \exp i\pi. \tag{3}$$

Consequently, the amplitude and phase reflection coefficients of the sample are determined in a straightforward way from the measured interferograms, as

$$r_s(\nu) = L_0(\nu), \qquad \text{and} \qquad \phi_s(\nu) = \phi_L(\nu) + \pi. \tag{4}$$

In reflection DFTS, measurements are usually made at or at very nearly normal incidence, and samples are chosen with sufficient thickness to suppress all but the primary reflected partial wave from the front surface of the sample. Under these conditions, the simplest form of Fresnel's equations can be used, and the optical constants and amplitude and phase reflection coefficients are related by

$$n(\nu) + ik(\nu) = \frac{1 + r_s(\nu)\exp i\phi_s(\nu)}{1 - r_s(\nu)\exp i\phi_s(\nu)} \tag{5}$$

The intensity reflection coefficient, or reflectivity, $R_s(\nu)$, is related to the amplitude reflection coefficient by

$$R_s(\nu) = \boldsymbol{r}_s(\nu)\, \boldsymbol{r}_s{}^*(\nu), \qquad \text{where} \qquad \boldsymbol{r}_s(\nu) = r_s(\nu) \exp i\phi_s(\nu) \tag{6}$$

is the complex amplitude reflection coefficent, and $\boldsymbol{r}_s{}^*(\nu)$ is its complex conjugate.

DFTS has the advantage that both the amplitude and the phase are measured directly at all frequencies in the measured range; this eliminates uncertainties in $\phi_s(\nu)$ which arise due to truncation of the measured spectrum when the phase is calculated from the measured reflectivity using the Kramers-Kronig dispersion relations. As already mentioned, DFTS is invariably used at normal, or near-normal incidence, so that the simplest forms of the Fresnel equations can be used. Frequently a combination of reflection and transmission DFTS can be used very effectively to determine n and k at most frequencies. When R_s is small, as can be seen from Eq. (6), measuring r is an advantage; Johnson and Bell [11] have shown that values of R_s as small as 4×10^{-4} can be measured reliably by reflection DFTS. However, when R_s is large, this is a disadvantage because r_s for the sample then differs from the value for the reference mirror by even less than R_s. Finally, reflection DFTS cannot be used to determine reliable values of $k(\nu)$ in spectral regions where the sample is transparent, because the phase is then very small, as discussed further below.

In reflection DFTS, applicable here, it is convenient to consider uncertainties in the measured amplitude and phase reflection coefficients separately. Uncertainties in the amplitude arise in the same way as they do in

other forms of spectroscopy in which, usually, in reflection spectroscopy, it is the intensity, R_s, of the reflection coefficient which is measured. Provided that adequate precautions have been taken to eliminate systematic errors, uncertainties in r_s or R_s arise primarily from random uncertainties in the detector response. However, when using metal reference mirrors which are usually fabricated by metallizing optically flat glass blanks, systematic errors also arise due to lack of perfect reflection of the metal surface. This latter point has been discussed by Eldridge and Staal [12] and Staal and Eldridge [13] and corrections to both the amplitude and the phase reflection coefficient associated with such mirrors were taken into account in their determinations of the optical constants of NaCl by reflection DFTS. Comparisons of published data for NaCl, KCl, and KBr presented in this article indicate that such corrections are necessary if the technique is to be used to full advantage. Birch [14] has shown how, by using a thick transparent slab of a material such as silicon as a reference reflector, a combination of reflection and transmission DFTS can be used to determine absolute values of the amplitude and phase reflection coefficients of thin metal mirrors in the far infrared.

In the case of the phase reflection coefficient, a number of additional systematic errors can arise which are associated mainly with the way in which the comparatively small wavelengths encountered in the far infrared ($\lambda \sim 20$–500 μm) translate into a need for very precise technology for sampling the interferograms and handling optical components (such as the sample and reference mirror surfaces). In most reflection DFTS experiments, the sample and reference mirror surfaces must be precisely interchanged during the experiment. Let us first consider the possible sources of systematic phase error which are encountered in a far-infrared interferometer equipped with a mechanical step-drive mechanism for scanning the moving mirror. It will be convenient to begin by taking as the goal for our phase measurements a systematic error which is equal to the random phase error equivalent to the random error in the amplitude reflection coefficient. A convenient yardstick is a signal-to-noise ratio of 100, leading directly to an uncertainty in the amplitude reflection coefficient of $\delta r_s = 0.01$, or 1%. The equivalent uncertainty in the phase is $\delta\phi_s = 0.01 \times \pi$ radian, or $\delta\phi_s \sim 0.5°$. The most serious systematic phase errors are as follows.

1. Potentially most serious of all is the phase error resulting from failure to place the reference-mirror surface precisely in the same plane as the sample reflecting surface. If we consider measurements at 100 cm^{-1}, for instance, then a phase uncertainty of 0.5° would occur if the error in the positioning of the two optical components were $\delta x = (\lambda/2 \times 360)\,\delta\phi_s \sim 0.1$ μm. This is a very severe constraint indeed, bearing in mind that the limiting precision of most mechanical engineering work lies in the range between 2.5 and 25 μm.

2. Mechanical step drives for interferometers and, in particular, backlash errors which occur when such drives are operated over a sequence of scans, as required when recording background and sample interferograms in turn, can often introduce uncertainties in the position of the moving mirror of a magnitude $\delta x \sim 0.1$ μm.
3. Differential thermal expansion in the two arms of the interferometer can be the cause of significant systematic phase errors. If the optical components are at a distance L from the beam divider, then a relative change in the temperature of the two arms of the interferometer of δT will result in a differential change in the lengths of the two arms of the interferometer of $\delta L = \alpha L \delta T$, where α is the coefficient of thermal expansion of the material from which the interferometer is constructed. If we take $L = 30$ cm, and $\alpha = 2 \times 10^{-5}$ K^{-1}, corresponding to Al, then we must have $\delta T < 0.015$ K, if $\delta L < 0.1$ μm. Temperature control with this level of precision is fairly easily achievable, but the figure for δT does indicate that this aspect of instrument design cannot be ignored.
4. The flatness of the sample and reference mirror surfaces should also satisfy the criterion calculated in (1) above, i.e., the surface flatness should be within ~ 0.1 μm at all points across the surface. Apart from placing severe requirements on the quality of the flatness and the optical polish of these optical components, the two components must also be cut from material which is sufficiently thick to maintain the quality of the surface for the duration of the measurements. Usually, this means that for optical components of ~ 10 mm in diameter, the thickness should not be less than ~ 6 mm.

Fortunately, there are ways of avoiding most of these phase errors. Parker *et al.* [15] have described how the need for the accurate replacement of reflecting surfaces can be avoided by metallizing part of the sample surface for use as a reference mirror, and this technique has been used by a number of authors, including Pai *et al.* [16], Eldridge and Staal [12], Staal and Eldridge [13], and Plumb and Birch [17]. Maslin and Parker [18] have shown that by designing an interferometer with a subsidiary He-Ne laser beam running along the optical axis of the far-infrared beam and using laser fringe-counting techniques, the second and third of the systematic phase errors listed above can also be avoided. It has been shown by Wan Abdullah and Parker [19] that this method also significantly reduces noise in the measured spectrum arising from random errors in sampling the interferogram; such errors are often present when a mechanical step drive is used for the moving mirror. Burton and Parker [20, 21] have demonstrated that systematic phase errors arising from non-flatness of the sample surface can be reduced to the order of one degree when $\lambda > 0.4$ μm (i.e., for DFTS at all wavelengths exceeding those in the UV) by suitably coating the sample surface and reusing it as the reference surface; the method requires the use of four interferograms and has been demon-

strated with reflection DFTS measurements in the visible region of the spectrum, but it has not yet been used in the far-infrared. Birch [22, 23] has investigated these so-called pseudocoherence effects associated with nonflatness of optical components theoretically.

By far the greatest single difficulty in reflection DFTS is the need for the accurate mechanical replacement of the reference mirror and sample reflecting surfaces. However, careful consideration of the form of the Fresnel equations for reflection readily demonstrates that this difficult operation can often be avoided. In many materials of interest, and that applies to those considered in this article, there are frequency ranges in the measured range in which the extinction coefficient is very small compared with the real refractive index, i.e., $k(\nu) \ll n(\nu)$. In the limit of small k, it follows from Eq. (5) that n and k are given by

$$n(\nu) \sim \frac{1 + r_s(\nu)}{1 - r_s(\nu)} \text{ and } k(\nu) \sim \frac{2r_s(\nu)\phi_s(\nu)}{[1 - r_s(\nu)]^2}. \tag{7}$$

The smallest measurable value of $\phi_s(\nu)$, corresponding to the noise limit if the signal-to-noise ratio is 100, is 0.01 radian. For the semiconductors studied by Maslin *et al.* [24], $r_s(\nu) \sim 0.5$ well above the reststrahl region where $\phi_s(\nu)$ is small. From Eq. (7), the corresponding lower limit for the value of k which can be measured by reflection DFTS is then $k \sim 0.04$, and the associated experimental uncertainty would be $\sim$100%. In regions where k is much smaller and the sample is transparent, it follows from Eq. (7) that for practical purposes, $\phi_s(\nu)$ approaches zero. In the alkali-halide crystals where ϵ_∞ is smaller, smaller values of k are accessible to reflection DFTS, but the accuracy of the determination of k is still severely limited by the difficulty of measuring $\phi_s(\nu)$. At a suitable reference frequency, ν_H, sufficiently far above the reststrahl band of a binary solid, we can set $\phi_s(\nu_H) = 0$ on physical grounds. $\phi_s(\nu) = 0$ also at $\nu = 0$. It follows that we can dispense with the experimental requirement to mechanically locate the reference mirror and sample surfaces in precisely the same plane. Instead, a much simpler experimental requirement of placing them in precisely parallel planes will suffice; planes separated by $\delta x \sim$ a few microns are easily achievable experimentally and this will not introduce systematic errors in $r_s(\nu)$, even if the radiation is poorly collimated. Then, after recording the two interferograms and computing the sample phase reflection coefficient, $\phi_s(\nu)$, using Eq. (4), the value of $\delta x = \phi_s(\nu_H)/4\pi\nu$ required to correct the measured phase $\phi_s(\nu_H)$ at ν_H can be calculated and a linear phase correction

$$\delta\phi_s(\nu) = 4\pi\nu\ \delta x \tag{8}$$

applied throughout the phase spectrum. This procedure was followed by Maslin *et al.* [24] when they used reflection DFTS to determine the optical constants of the II–VI and III–V semiconductors presented here. The origi-

nal numerical data were lost when the group moved their laboratory from London to Colchester in 1991; computer-generated graphs of the numerical data for all samples were presented on paper 25 × 20 cm^2 in area in the Ph.D. thesis by Maslin [25], and the data for semiconductors presented here has been obtained by carrying out digital scans of those graphs. We consider that the errors introduced by this process have not significantly added to the spectroscopic errors of the original data.

A detailed statistical analysis of experimental uncertainties in reflection DFTS was carried out by Pai *et al.* [16]. They used a method in which part of the sample surface was metallized [15] and used to provide the reference phase measurement, thus obviating the need for the precise mechanical replacement of reflecting surfaces. They listed values of n and k, and of the associated experimental uncertainties Δn and Δk, throughout the reststrahl bands of eight alkali halide crystals: NaF, NaCl, KCl, KBr, KI, RbCl, RbBr, and RbI at 100 and 300 K. We reproduce their estimates of Δn and Δk in Tables I–V for five alkali-crystals here: NaCl, KCl, KBr, KI, and RbCl. Because of the similarity between the far-infrared optical properties of the alkali halides and the II–VI and III–V semiconductors, these experimental uncertainties provide a useful guide to the frequency dependence of the experimental uncertainties for the II–VI and III–V semiconductors listed here.

II THE MATERIALS

A Alkali Halides

1 *NaCl*

The far-infrared optical constants of NaCl determined by Pai *et al.* [16] at 300 K at a resolution of 2 cm^{-1} using DFTS are shown in Fig. 2 and listed in Table I, where they are compared with values measured by reflection DFTS by Eldridge and Staal [12], and listed numerically by Eldridge and Palik [26]. Pai *et al.* [16] also published numerical values for n and k for NaCl at 100 K. The two sets of values listed in Table I are generally in reasonable agreement, within the limits of the experimental errors listed by Pai *et al.*, differing at most by a few percent except in the region of high reflectivity where n and k have their highest values. Eldridge and Staal used aluminium as a reference surface and corrected for the fact that aluminium is not a perfect reflector and does not have a phase reflectivity of exactly π: this could account for the difference between the two sets of data in Table I where n and k are large. This is supported by the data presented below for

TABLE I

Values of *n* and *k* for Sodium Chloride from Various Sources

cm^{-1}	n	k	Δn, Δk	n	k
50	2.47	0.05	0.03 [16]	2.45	0.047 [12, 26]
60	2.51	0.06			
70	2.50	0.05			
80	2.52	0.06			
90	2.57	0.07			
100	2.62	0.09		2.74	0.087
110	2.76	0.06			
120	2.98	0.09			
130	3.21	0.15	0.04	3.31	0.135
135	3.37	0.17			
140	3.54	0.20			
144	3.85	0.24			
148	4.08	0.44			
152	4.46	0.47			
156	5.16	0.84	0.01		
160	6.16	1.31	0.13	6.92	2.14
162	6.73	2.45	0.16		
164	6.12	4.81	0.18		
166	3.84	5.79	0.14		
170	1.59	5.42	0.09	1.35	6.03
174	0.76	4.19	0.05		
178	0.59	3.46			
182	0.56	3.08	0.03		
186	0.45	2.79			
190	0.33	2.50		0.19	2.63
194	0.27	2.20	0.02		
198	0.28	1.99			
202	0.25	1.88			
206	0.23	1.69			
210	0.23	1.50		0.18	1.56
214	0.22	1.38			
218	0.24	1.16			
222	0.28	1.03			
226	0.32	0.90	0.01		
230	0.42	0.86		0.43	0.87
234	0.49	0.82			
238	0.43	0.78			
242	0.49	0.68			
246	0.53	0.64			
250	0.603	0.645		0.58	0.66
254	0.593	0.648			
258	0.487	0.616			
262	0.409	0.482	0.006		
266	0.433	0.359			

(continued)

TABLE I *(Continued)*

Sodium Chloride

cm^{-1}	n	k	Δn, Δk	n	k
270	0.482	0.208			
274	0.570	0.200			
278	0.652	0.199			
282	0.74	0.18			
286	0.78	0.15			
290	0.80	0.13			
294	0.83	0.12			
300	0.86	0.11	0.01	0.85	1.1 E-3
320	1.01	0.05			
340	1.10	0.02			
360	1.17	0.01			
380	1.22	0.01			
400	1.27		0.01	1.27	3.5 E-3

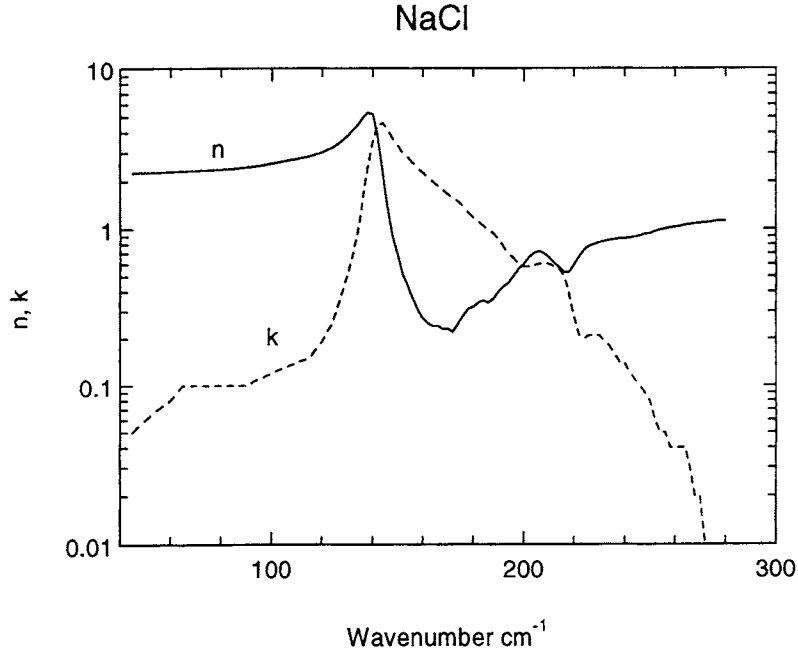

Fig. 2. Log-linear plot of the far-infrared optical constants, *n* and *k*, versus wavenumber for NaCl at 300 K. (From Pai *et al.* [16] with permission from the publisher.)

KCl and KBr; we can conclude that the corrections to the reference-mirror reflectivity carried out by Eldridge and Staal are worthwhile and to be recommended. Below 110 cm^{-1} and above 340 cm^{-1} where the phase reflection coefficient is very small, Eldridge and Staal [12] obtained the phase indirectly from transmission measurements on cleaved crystals, which yielded directly the absorption coefficient.

KCl 2

The far-infrared optical constants of KCl determined by Pai *et al.* [16] at 300 K at a resolution of 2 cm^{-1} using DFTS are shown in Fig. 3 and listed in Table II. They also published numerical values for n and k for KCl at 100 K. Johnson and Bell [11] also determined the optical constants of KCl at 300 K by reflection DFTS at 2 cm^{-1} resolution, and Palik [27] obtained numerical values by reading their graphs: a selection of these values is given in Table II, and it can be seen that there is very good agreement between the two sets of data, somewhat better than the agreement reported above between the data of Pai *et al.* [16] and Eldridge and Staal [12] for NaCl. Nei-

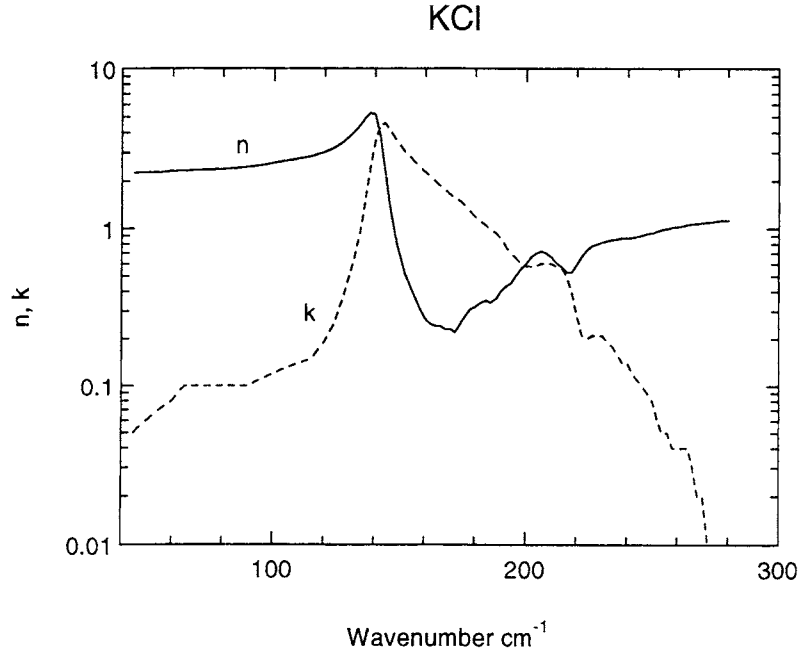

Fig. 3. Log-linear plot of the far-infrared optical constants, n and k, versus wavenumber for KCl at 300 K. (From Pai *et al.* [16] with permission from the publisher.)

TABLE II

Values of *n* and *k* for Potassium Chloride from Various Sources

cm^{-1}	n	k	Δn, Δk	n	k
50	2.27	0.06	0.03 [16]	2.2	[11, 27]
60	2.30	0.08		2.3	5.3 E-2
70	2.33	0.10		2.4	9.2 E-2
75	2.34	0.10			
80	2.37	0.10		2.5	0.11
85	2.40	0.10			
90	2.44	0.10		2.6	6.6 E-2
95	2.50	0.11			
100	2.57	0.12	0.03	2.7	0.11
110	2.75	0.14		2.9	0.15
120	3.02	0.19	0.04	3.3	0.20
124	3.22	0.25			
128	3.57	0.39			
132	4.09	0.66	0.07		
136	4.89	1.46	0.09		
140	5.20	3.47	0.13	5.3	4.0
144	2.36	4.58	0.08		
148	0.90	3.68	0.04		
152	0.52	3.01			
156	0.37	2.61			
160	0.27	2.27	0.02	0.17	2.2
164	0.24	1.99			
168	0.23	1.76			
172	0.22	1.56	0.01		
176	0.28	1.38			
180	0.32	1.18		0.31	1.05
190	0.40	0.86			
200	0.60	0.58			
204	0.70	0.59			
208	0.70	0.61			
212	0.61	0.58			
216	0.53	0.50			
220	0.59	0.28	0.01	0.53	0.35
224	0.74	0.20			
228	0.80	0.21			
232	0.84	0.19			
236	0.86	0.16			
240	0.87	0.14			
250	0.94	0.08			
260	1.03	0.04		0.99	4.2 E-2
264	1.06	0.04			
268	1.08	0.02			
272	1.10	0.01			
276	1.12	0.01			
280	1.13	0.01	0.01	1.10	2.3 E-2

ther set of data for KCl was corrected for the reference-mirror reflectivity; this supports the view that differences in the data of Pai *et al.* [16] and Eldridge and Staal [12] for NaCl can be attributed to the corrections which Eldridge and Staal made for the reflectivity of their Al reference mirror. Thus, for measurements with this accuracy, corrections for the imperfect reflectivity of metallized reference mirrors are to be recommended.

KBr 3

The far-infrared optical constants of KBr determined by Pai *et al.* [16] at 300 K at a resolution of 2 cm^{-1} using DFTS are shown in Fig. 4 and listed in Table III. They also published numerical values for n and k for KBr at 100 K. Johnson and Bell [11] also determined the optical constants of KBr at 300 K by reflection DFTS at 2 cm^{-1} resolution, and Palik [28] obtained numerical values by reading their graphs: a selection of these values is also given in Table III, and it can be seen that, as in the case of KCl, there is very good agreement between the two sets of data. Again, the agreement is significantly better than the agreement reported above between the data of Pai *et al.* [16] and Eldridge and Staal [12] for NaCl. Neither set of data for

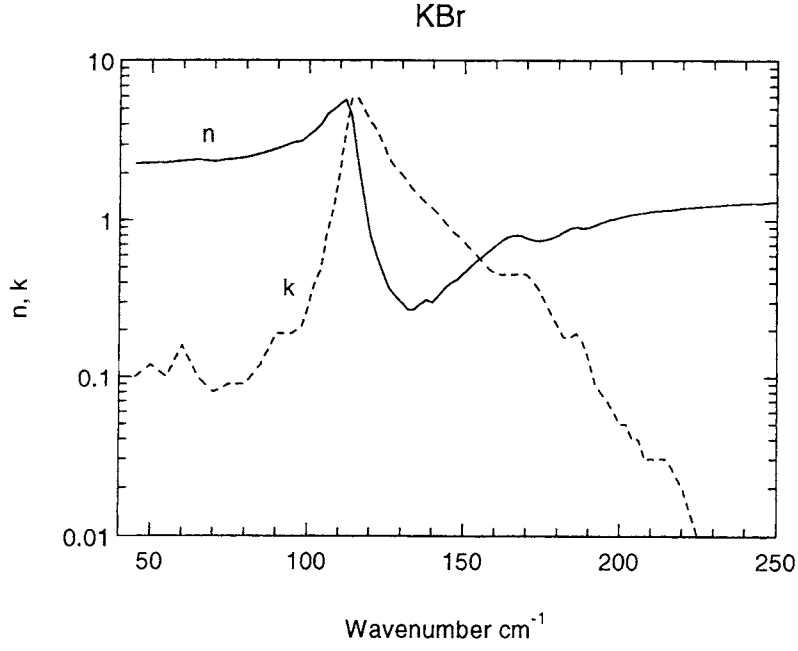

Fig. 4. Log-linear plot of the far-infrared optical constants, n and k, versus wavenumber for KBr at 300 K. (From Pai *et al.* [16] with permission from the publisher.)

TABLE III

Values of *n* and *k* for Potassium Bromide from Various Sources

cm^{-1}	n	k	Δn, Δk	n	k
50	2.30	0.12	0.03 [16]	2.30	9.3 E-2 [11, 28]
60	2.38	0.16		2.35	0.11
70	2.36	0.08		2.40	0.12
80	2.49	0.09	2.52	0.125	
85	2.65	0.12			
90	2.83	0.19		2.80	0.15
95	3.07	0.19	0.04		
98	3.17	0.21			
100	3.42	0.28		3.40	0.33
104	4.02	0.48			
110	5.35	1.98	0.11	5.50	1.0
114	4.55	5.84	0.16		
118	1.39	4.89	0.07		
122	0.60	3.64	0.04		
126	0.37	2.43	0.02		
130	0.30	1.97		0.30	2.0
134	0.27	1.54			
138	0.31	1.28	0.01		
142	0.33	1.08			
146	0.40	0.86			
150	0.46	0.73	0.01	0.48	0.72
154	0.55	0.60			
158	0.64	0.49			
162	0.74	0.45			
166	0.80	0.45			
170	0.77	0.45		0.76	0.44
174	0.74	0.36			
178	0.77	0.25			
182	0.85	0.18			
186	0.90	0.19			
190	0.90	0.13		0.90	0.18
194	0.97	0.08			
200	1.05	0.05	0.01		
210	1.14	0.03			
220	1.20	0.02			
230	1.25	0.01		1.30	
235	1.27	0.01			
240	1.29	0.01			
245	1.30	0.01			
250	1.32	0.01	0.01		
255	1.33				
260	1.35				
265	1.35				
270	1.36		0.01		

KBr was corrected for the reference-mirror reflectivity; this again supports the view that differences in the data of Pai *et al.* [16] and Eldridge and Staal [12] for NaCl can be attributed to the corrections which Eldridge and Staal made for the reflectivity of their Al reference mirror. Thus, for measurements with this accuracy, corrections for the imperfect reflectivity of metallized reference mirrors are to be recommended.

KI 4

The far-infrared optical constants of KI determined by Pai *et al.* [16] at 300 K at a resolution of 2 cm^{-1} using DFTS are shown in Fig. 5 and listed in Table IV. They also published numerical values for n and k for KI at 100 K. These values are generally in agreement, within the limits of the experimental uncertainties listed by Pai *et al.* [16], with other determinations of n and k for KI by DFTS reported by Berg and Bell [29] and Memon and Parker [30]. Thomas [31] has presented a critique of KI in this volume using the data in Refs. 16 and 29.

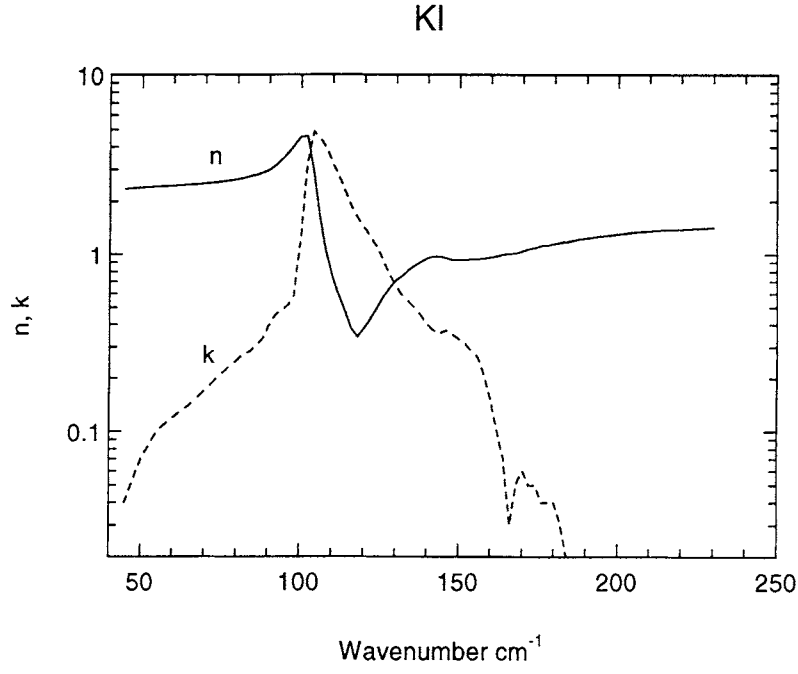

Fig. 5. Log-linear plot of the far-infrared optical constants, n and k, versus wavenumber for KI at 300 K. (From Pai *et al.* [16] with permission from the publisher.)

TABLE IV

Values of *n* and *k* for Potassium Iodide from Ref. [16]

cm^{-1}	n	k	Δn, Δk
45	2.33	0.04	0.03 [16]
50	2.38	0.07	
55	2.41	0.10	
60	2.44	0.12	
65	2.46	0.14	
70	2.51	0.17	
75	2.57	0.21	
80	2.65	0.25	
84	2.75	0.28	
88	2.88	0.33	0.04
92	3.16	0.45	
96	3.72	0.51	0.06
98	4.09	0.58	0.07
100	4.54	1.24	0.08
102	4.62	3.21	0.10
104	2.92	4.88	0.10
106	1.66	4.51	0.07
108	1.03	3.96	0.05
110	0.75	3.28	0.03
112	0.59	2.75	0.03
114	0.48	2.27	0.02
116	0.38	1.87	0.01
118	0.34	1.60	
120	0.38	1.42	
122	0.43	1.26	
124	0.49	1.11	
126	0.57	0.92	
128	0.64	0.77	
130	0.71	0.67	0.01
132	0.75	0.59	
134	0.81	0.54	
136	0.86	0.50	
138	0.91	0.45	
140	0.95	0.40	
142	0.97	0.37	
144	0.97	0.36	
146	0.95	0.37	
148	0.93	0.35	
150	0.93	0.33	0.01
160	0.96	0.15	
170	1.05	0.06	
180	1.16	0.04	
190	1.24	0.02	
200	1.31	0.02	0.01
210	1.37	0.01	
220	1.40	0.01	
230	1.43	0.01	
240	1.45		
250	1.47		0.01

RbCl 5

The far-infrared optical constants of RbCl determined by Pai *et al.* [16] at 300 K at a resolution of 2 cm^{-1} using DFTS are shown in Fig. 6 and listed in Table V. They also published numerical values for n and k for RbCl at 100 K. These are the only values of n and k determined by DFTS for RBCl reported in the literature. As in the case of all the alkali halide crystals studied by Pai *et al.*, the value of ν_{TO} determined from the peak in the conductivity, $\sigma(\nu) = \nu\epsilon''(\nu)/2$, calculated from these results is in good agreement with values reported by Jones *et al.* [32], Wilkinson [33], and Lowndes and Martin [34].

NaF, RbBr, and RbI 6

Pai *et al.* [16] also determined the optical constants of NaF, RbBr, and RbI in the optical phonon region at both 300 K and 100 K by DFTS at a resolution of 2 cm^{-1}. A critique of NaF was published by Ohlídal and Navrátil [35] in *HOC II* using the far-infrared data of Pai *et al.* [16]. The optical constants of RbBr and RbI are reviewed by Ohlídal and Ohlídal [36] and Ohlídal and Franta [37], respectively, elsewhere in this volume.

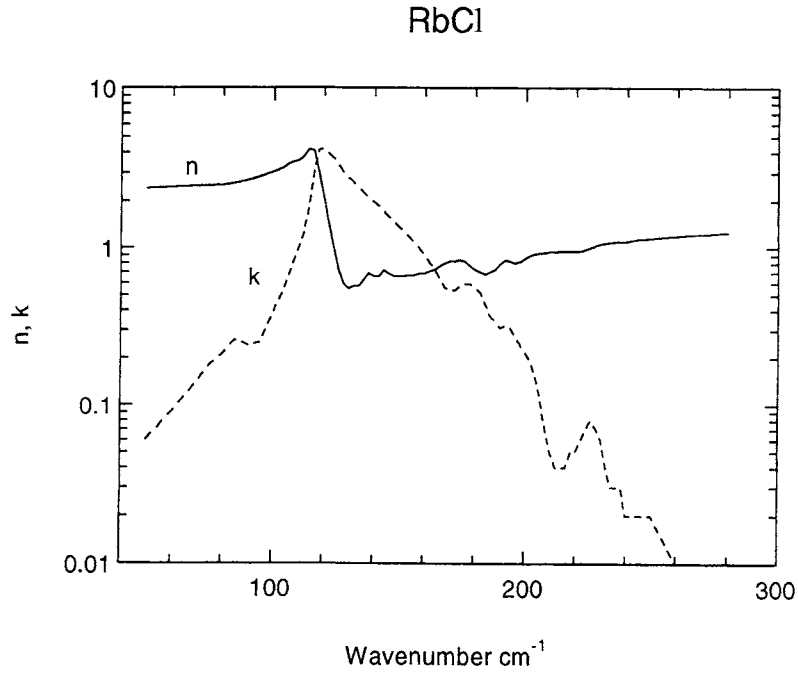

Fig. 6. Log-linear plot of the far-infrared optical constants, n and k, versus wavenumber for RbCl at 300 K. (From Pai *et al.* [16] with permission from the publisher.)

TABLE V

Values of *n* and *k* for Rubidium Chloride from Ref. [16]

cm^{-1}	n	k	Δn, Δk
50	2.40	0.06	0.03 [16]
60	2.44	0.09	
70	2.47	0.14	
75	2.50	0.18	
80	2.51	0.21	
85	2.58	0.26	
90	2.69	0.24	
95	2.85	0.25	
100	3.03	0.38	
102	3.12	0.45	
104	3.23	0.53	0.05
106	3.40	0.65	
108	3.52	0.81	
110	3.56	0.99	
112	3.76	1.22	
114	4.16	1.81	0.07
116	4.13	3.05	
118	3.04	4.15	
120	2.11	4.21	
122	1.48	3.93	
124	1.00	3.66	0.04
126	0.72	3.34	
128	0.59	2.99	
130	0.55	2.77	
132	0.57	2.59	
134	0.57	2.41	0.02
136	0.63	2.23	
138	0.69	2.07	
140	0.66	1.96	
142	0.66	1.86	
144	0.72	1.73	0.01
146	0.69	1.59	
148	0.66	1.48	
150	0.66	1.36	0.01
152	0.66	1.26	
154	0.67	1.18	
156	0.67	1.07	
158	0.69	0.99	
160	0.69	0.89	
162	0.71	0.81	
164	0.73	0.73	
166	0.77	0.64	
168	0.80	0.56	
170	0.83	0.54	
172	0.83	0.54	

(continued)

TABLE V *(Continued)*

Rubidium Chloride

cm^{-1}	n	k	Δn, Δk
174	0.84	0.57	
176	0.82	0.59	
178	0.77	0.59	
180	0.73	0.56	
182	0.70	0.52	
184	0.68	0.44	
186	0.70	0.37	
188	0.73	0.34	
190	0.79	0.31	
192	0.84	0.32	
194	0.82	0.31	
196	0.80	0.27	
198	0.82	0.24	
200	0.86	0.22	0.01
202	0.90	0.19	
204	0.92	0.15	
206	0.93	0.11	
208	0.94	0.07	
210	0.95	0.05	
212	0.95	0.04	
214	0.96	0.04	
216	0.96	0.04	
218	0.96	0.05	
220	0.96	0.05	
222	0.96	0.06	
224	0.98	0.07	
226	1.01	0.08	
228	1.04	0.07	
230	1.06	0.06	
232	1.08	0.04	
234	1.09	0.03	
236	1.10	0.03	
238	1.11	0.03	
240	1.11	0.02	
245	1.14	0.02	
250	1.16	0.02	0.01
260	1.20	0.01	
270	1.23	0.01	
280	1.26	0.01	
290	1.28		
300	1.30		0.01

B Semiconductors

Values of n and k measured by reflection DFTS in the far-infrared for the eight semiconductors CdTe, ZnSe, GaP, GaAs, GaSb, InP, InAs, and InSb are listed in Tables VII–XIV and log-linear graphs of the DFTS data are presented in Figs. 7–14. For each of these materials the phonon response has been modelled using a Lorentz model for a damped, simple harmonic oscillator:

$$\epsilon' + i\epsilon'' = (n + ik)^2 = \epsilon_\infty + \frac{\rho \nu_{TO}{}^2}{\nu_{TO}{}^2 - \nu^2 - i\nu\gamma}, \tag{9}$$

where ϵ' and ϵ'' are the real and imaginary parts of the complex dielectric response function, ϵ_∞ is the limiting high frequency value of the real part of the dielectric constant, ν_{TO} is the frequency of the transverse optic phonon mode at the center of the Brillouin zone, γ is the phonon damping parameter, ρ is the dipole strength defined by

$$\rho = \epsilon_0 - \epsilon_\infty, \tag{10}$$

and ϵ_0 is the static dielectric constant.

In the case of the four materials exhibiting free-carrier behavior at frequencies below their reststrahl bands, i.e., GaAs, GaSb, InAs, and InSb, a term has been added to Eq. (9) to account for the plasma response, i.e.,

$$\epsilon' + i\epsilon'' = (n + ik)^2 = \epsilon_\infty + \frac{\rho \nu_{TO}{}^2}{\nu_{TO}{}^2 - \nu^2 - i\nu\gamma} - \frac{\epsilon_\infty \nu_p{}^2}{\nu^2 + i\nu\gamma_p}, \tag{11}$$

where ν_p is the plasma frequency and γ_p is the plasmon damping parameter. The plasma frequency is given by

$$\nu_p{}^2 = \frac{ne^2}{\epsilon_\infty \epsilon_0 m^*}, \tag{12}$$

where n is the free-carrier concentration, e is the charge on the electron, and m^* is the effective mass of the free carriers. For fitting the experimental data, ν_p has been taken as the minimum in the measured amplitude reflectivity. In some cases the plasma frequency lies outside the range of data presented here [25].

The values of the parameters ϵ_0, ϵ_∞, ν_{TO}, γ, ν_p, and γ_p, which are needed to fit the spectra of each of the eight semiconductors, are listed in Table VI. The values of ϵ_0 and ϵ_∞, are taken from Kunc *et al.* [38]. Also listed are the values of the ratio m^*/m_0, where m_0 is the mass of the free-electron, taken from Gray [39] for the four samples which showed free-carrier effects at frequencies below the reststrahl bands.

TABLE VI

Parameters Used in Modelling the Contributions of the Lattice Resonance and the Free Carriers to the Far-Infrared Dielectric Response of Eight Semiconductor Crystals

	ϵ_0	ϵ_∞	ρ	ν_{TO} (cm^{-1})	γ (cm^{-1})	ν_P (cm^{-1})	γ_p (cm^{-1})	m^*/m_0
CdTe	10.2	7.10	3.10	141	6.63	—	—	—
ZnSe	8.80	5.9	2.9	207	6.50	—	—	—
GaP	11.01	9.07	1.945	367	9.0	—	—	—
GaAs	12.80	10.90	1.9	269	6.5	60	35	0.070
GaSb	15.80	14.44	1.36	227.5	3.0	30	25	0.047
InP	12.46	9.61	2.85	304	8.0	—	—	—
InAs	15.15	12.25	2.90	218.5	6.0	71	40	0.026
InSb	17.77	15.68	2.09	181.0	6.50	75	15	0.015

Numerical values for n and k calculated from Eq. (11) after fitting the model to the experimental data are quoted for comparison throughout each table. Doping has a very large effect on the far-infrared optical constants of semiconductors, not only in the region of the plasma resonance, but also throughout the reststrahl region because of the strong effect of plasmon-LO phonon coupling. This is likely to be the dominant reason for differences between the optical constants of (different) samples measured in different laboratories. The overall agreement between the calculated and measured values of n is generally quite fair throughout the spectrum for most materials. The most notable exceptions to this occur for GaP, InP, and to a lesser extent, GaAs, in the region between ν_{TO} and ν_{LO}, where n is small. In the case of k, reasonable agreement between calculated and measured values is generally found only in the reststrahl and free-carrier regions where k is large. In regions where k is small, a more sophisticated model is required to take account of the effects of additional absorption arising from anharmonicity and the non-linear dipole moment [40, 41]; apart from this, there is a large uncertainty in values of k determined by DFTS in regions where the phase reflection coefficient is small, as mentioned above.

II–VI Semiconductors C

CdTe 1

The far-infrared optical constants of CdTe determined by Maslin *et al.* [24] at 300 K using DFTS at a resolution of 2 cm^{-1} are shown in Fig. 7 and listed in Table VII, where they are compared with values calculated from the oscillator model, Eq. (11) [OM]. The optical constants of CdTe

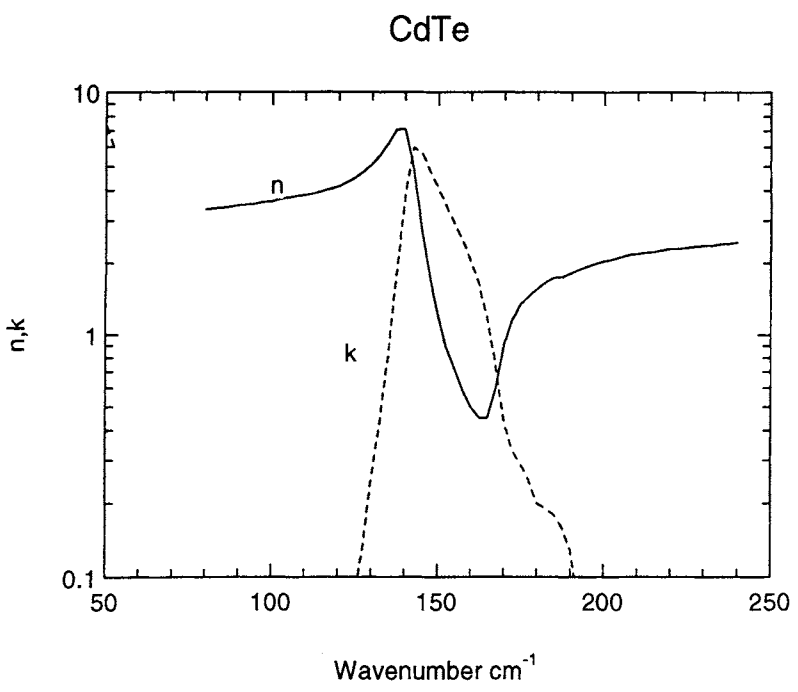

Fig. 7. Log-linear plot of the far-infrared optical constants, n and k, versus wavenumber for CdTe at 300 K.

have also been determined at 300 K using reflection DFTS by Birch and Murray [42] at a resolution of 1 cm^{-1}; their data contained much fine structure a little above the noise level and many features were later assigned by Mok *et al.* [43] as multi-phonon combination bands excited via lattice anharmonicity [40]. Numerical values of n and k read from Birch and Murray's graph by Palik [44] are also listed in Table VII. Differences in the values of n and k in the reststrahl region may be due to the differences in resolution. Apart from this, and poor agreement between the values of k outside the reststrahl region where DFTS is known to be unreliable for measuring k, the overall agreement is reasonable. The transverse optic phonon frequency determined from these data, $\nu_{TO} = 141$ cm^{-1}, is in excellent agreement with previous experimental values; 140.5 cm^{-1} determined by far-infrared reflection-DFTS [42], and 140 cm^{-1} determined by Raman spectroscopy [45] and near-infrared absorption spectroscopy [46]. The longitudinal optic phonon frequency, $\nu_{LO} = 167.5$ cm^{-1}, is in good agreement with previous experimental values for undoped CdTe: 167.5 cm^{-1}, determined by reflection-DFTS [42], and 171 cm^{-1}, determined by Raman spectroscopy [45]; Slack *et al.* [46] carried out an infrared investigation of substitutionally Fe^{2+}-doped CdTe and reported a value of $\nu_{LO} = 180$ cm^{-1}.

TABLE VII

Values of n and k for Cadmium Telluride from Various Sources

cm^{-1}	n	k		n	k	n	k	
80.0	3.34		[24]	3.42	2.6 E-2 [OM]	3.32	0.2	[42]
85.0	3.39							
90.0	3.47					3.45	0.2	
95.0	3.53							
100.0	3.61					3.62	0.2	
105.0	3.72							
110.0						3.9	0.25	
115.0	3.96	0.05						
120.0	4.16	0.03		4.26	0.19	4.4	0.3	
125.0	4.51	0.08				4.7	0.55	
130.0	5.10	0.25				5.1	0.8	
132.5	5.60	0.43						
135.0	6.23	0.83				6.75	2.2	
137.5	7.03	1.78						
140.0	7.07	3.86		6.76	4.50	5.5	5.5	
142.5	4.93	5.96						
145.0	2.81	5.70		2.41	5.50	1.8	5.2	
147.5	1.77	4.82						
150.0	1.20	4.06		1.02	3.81	0.8	3.7	
155.0	0.72	2.92						
160.0	0.50	2.03		0.51	1.89	0.2	1.81	
65.0	0.45	1.17						
170.0	0.91	0.43		0.80	0.52	0.8	0.5	
175.0	1.34	0.29						
180.0	1.56	0.20		1.50	0.16	1.5	0.1	
185.0	1.73	0.18						
190.0	1.81	0.13		1.82	8.0 E-2	1.9		
192.5	1.87	0.08						
195.0	1.93	0.06						
197.5	1.98	0.04						
200.0	2.03	0.03		2.01	5.0 E-2	2.05		
202.5	2.07	0.01						
205.0	2.11	0.01						
207.5	2.16	0.03						
210.0	2.18	0.01						
212.5	2.21	0.00						
215.0	2.23	0.00						
217.5	2.27	0.01						
220.0	2.30	0.01		2.22	2.5 E-2			
222.5	2.30	0.01						
225.0	2.32	0.02						
227.5	2.35	0.01						
230.0								
232.5	2.37	0.03						
235.0	2.40	0.05						
237.5	2.41	0.05						
240.0	2.44	0.04		2.34	1.5 E-2			

2 ZnSe

The far-infrared optical constants of ZnSe determined by Maslin *et al.* [24] at 300 K at a resolution of 4 cm^{-1} using DFTS are shown in Fig. 8 and listed in Table VIII, where they are compared with values calculated from the oscillator model, Eq. (11) [OM], and with values taken from the work of Feldman *et al.* [47], Cardona [48], and Thomas and Hopfield [49], and by Ward [50]. Values of the optical constants of ZnSe determined by transmission DFTS in the millimeter region have been reported by Afsar [51]. Previous data for n and k for ZnSe in the optical phonon region were listed by Ward [50] in *HOC II,* who tabulated the data of Manabe *et al.* [52] and Hattori *et al.* [53]. At frequencies up to about 200 cm^{-1}, i.e., up to the ZnSe transverse optic phonon frequency, the present data for n are in good agreement with the values listed by Ward. Between about 200 and 250 cm^{-1}, where the phase reflection coefficient has its largest values and $r_s(\nu)$ and $\phi_s(\nu)$ change most rapidly, the disagreement with the earlier data is largest, rising to about 60% in n. This is the region in which reflection DFTS is expected to have its greatest advantage. At higher frequencies, the DFTS and reflectivity data for n are again in relatively good agreement (i.e., within

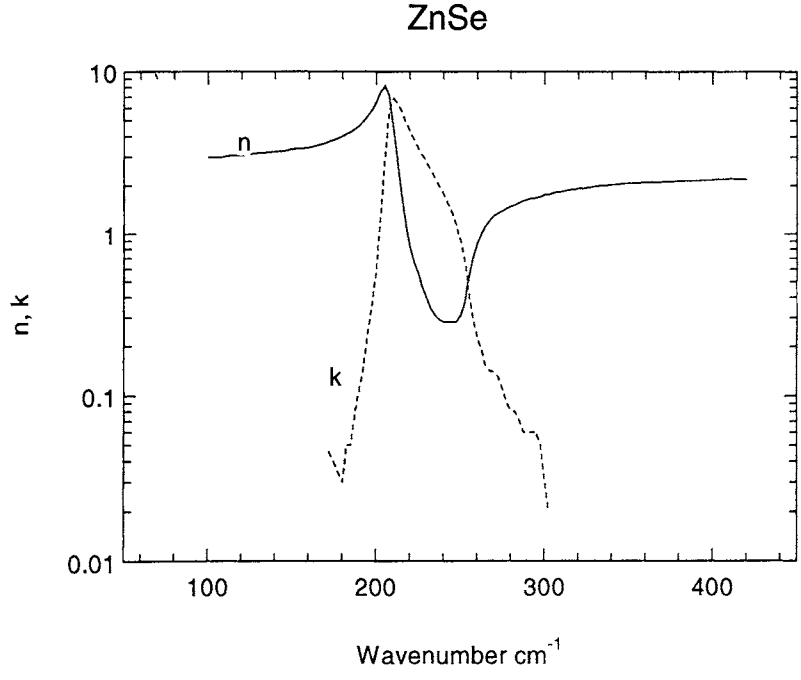

Fig. 8. Log-linear plot of the far-infrared optical constants, n and k, versus wavenumber for ZnSe at 300 K.

TABLE VIII

Values of n and k for Zinc Selenide from Various Sources

cm^{-1}	n	k	n	k	n	k
100.0	2.97	[24]	3.11	1.2 E-2 [OM]		
110.0	3.01					
120.0	3.06		3.20	1.9 E-2		
125.0	3.12				2.90 [47]	
130.0	3.17					
140.0	3.23		3.35	3.1 E-2		
150.0	3.34					
155.0	3.38					
160.0	3.43		3.62	6.0 E-2		
165.0	3.54					
166.7					3.54	0.08 [48]
170.0	3.66		3.84	9.1 E-2		
173.9					3.71	0.11
175.0	3.83					
180.0	4.04	0.03	4.2	0.16		
181.8					3.83	0.14
182.5	4.16	0.05				
185.0	4.30	0.05				
185.2					4.00	0.18
187.5	4.48	0.08				
188.7					4.29	0.23 [47]
190.0	4.69	0.11	4.88	0.33		
192.5	4.98	0.15				
192.3					4.64	0.43
195.0	5.36	0.24				
196.1					5.07	0.58
197.5	5.86	0.36				
200.0	6.56	0.59	6.60	1.25	6.09	0.87
202.0					6.75	1.83
202.5	7.55	1.26				
203.7					7.68	2.52
204.1					7.54	3.62
205.0	8.16	3.00	8.07	4.18		
206.2					3.20	6.20
207.5	7.22	5.74				
208.3					3.19	6.20
210.0	4.43	6.86	3.45	7.17		
210.5					2.10	6.10
212.5	2.81	6.44				
212.8					1.16	4.93
215.0	1.75	5.69	1.24	5.20		
217.4					0.58	3.62
217.5	1.14	4.90				
220.0	0.83	4.27	0.69	3.94		
222.2					0.43	2.90

(continued)

TABLE VIII *(Continued)*

Zinc Selenide

cm^{-1}	n	k	n	k	n	k
222.5	0.66	3.77				
225.0	0.56	3.37				
235.0	0.31	2.21				
240.0	0.28	1.75	0.28	1.58		
250.0	0.31	0.91			1.01	0.32 [49]
260.0	0.87	0.22				
270.0	1.30	0.14				
280.0	1.49	0.08				
285.7					1.60	2.1 E-2
287.5	1.62	0.06				
290.0	1.65	0.06				
300.0	1.75	0.03	1.81	3.0 E-2		
310.0	1.84	0.00				
320.0	1.92					
333.3					2.15	7.0 E-3
340.0	2.02					
360.0	2.09					
380.0	2.15	0.02				
400.0	2.18				2.25	6.0 E-3
420.0	2.19	0.03	2.23	4.3 E-3		

a few percent). The transverse and longitudinal optic phonon frequencies determined from these data, $\nu_{TO} = 207$ cm^{-1} and $\nu_{LO} = 253$ cm^{-1}, are in reasonable agreement with previous experimental values of 206 cm^{-1} and 250 cm^{-1}, respectively, determined by Raman spectroscopy [54]. Patel *et al.* [55] have analyzed fine structure and assigned features to phonon combination bands excited via lattice anharmonicity [40].

D III–V Semiconductors

1 GaP

The far-infrared optical constants of GaP determined by Maslin *et al.* [24] at 300 K at a resolution of 4 cm^{-1} using DFTS are shown in Fig. 9 and listed in Table IX, where they are compared with values calculated from the oscillator model, Eq. (11) [OM], and values listed by Borghesi and Guizzetti [56] taken from the work of Barker [57]. The transverse and longitudinal optic phonon frequencies determined from the data of Maslin *et al.*, $\nu_{TO} = 367$ cm^{-1} and $\nu_{LO} = 403$ cm^{-1}, are in good agreement with previ-

TABLE IX

Values of n and k for Gallium Phosphide from Various Sources

cm^{-1}	n	k	n	k	n	k
100.0	3.30	[24]	3.34	2.3 E-3 [OM]	3.3639	3.0 E-4 [56]
110.0	3.27					
120.0	3.32					
130.0	3.32					
140.0	3.37	0.02	3.37	3.7 E-3		
142.9					3.3947	5.2 E-4
150.0	3.38	0.00				
160.0	3.38	0.03				
170.0	3.43	0.02				
180.0	3.45	0.03	3.41	5.9 E-3		
190.0	3.46	0.03				
200.0	3.51	0.03			3.470	1.06 E-3
210.0	3.53	0.03				
220.0	3.57	0.03	3.48	1.0 E-2		
230.0	3.61	0.05				
240.0	3.65	0.05				
250.0	3.69	0.06			3.606	2.31 E-3
260.0	3.73	0.10	3.60	1.9 E-2		
270.0	3.80	0.10				
280.0	3.89	0.11				
285.7					3.809	5.18 E-3
290.0	3.99	0.13				
300.0	4.12	0.18	3.86	4.6 E-2		
310.0	4.28	0.21				
315.0	4.39	0.24				
320.0	4.50	0.30	4.14	8.7 E-2		
325.0	4.65	0.35				
330.0	4.86	0.42				
333.3					4.765	6.5 E-2
335.0	5.03	0.53				
340.0	5.29	0.69	4.74	0.23		
340.1					5.182	0.16
342.5	5.46	0.76				
344.8					5.578	0.31
345.0	5.62	0.86				
347.5	5.83	1.00				
350.0	6.12	1.19	5.43	0.48		
352.1					6.431	0.78
352.5	6.44	1.49				
355.0	6.77	1.93				
357.1					7.348	1.54
357.5	7.07	2.54				
360.0	7.35	3.50	6.96	1.67		
362.5	7.58	4.66				
365.0	7.14	6.79			10.314	8.62

(continued)

TABLE IX *(Continued)*

Gallium Phosphide

cm^{-1}	n	k	n	k	n	k
367.5	4.15	8.65				
370.0	1.84	8.08	4.11	6.64		
372.5	0.81	6.62				
373.1					0.515	5.86
375.0	0.43	5.49				
377.5	0.28	4.66				
378.8					0.208	4.05
380.0	0.21	3.98	1.06	4.01		
382.5	0.13	3.45				
385.0	0.11	3.02				
387.5	0.11	2.64				
387.6					0.103	2.52
390.0	0.11	2.30				
392.5	0.11	1.98				
395.0	0.13	1.70				
397.5	0.14	1.39				
400.0	0.17	1.05	0.60	1.20	0.108	0.89
402.5	0.29	0.65				
405.0	0.64	0.26				
407.5	0.96	0.16				
409.8					1.208	4.6 E-2
410.0	1.20	0.14				
412.5	1.38	0.11				
415.0	1.52	0.11				
416.7					1.585	2.6 E-2
420.0	1.76	0.11	1.69	0.17		
430.0	2.04	0.11				
440.0	2.27	0.16				
450.0	2.39	0.14				
460.0	2.55	0.16				
480.0	2.66	0.13				
500.0	2.74	0.22	2.61	1.7 E-2	2.606	

ous experimental values: $\nu_{TO} = 366\ cm^{-1}$ and $\nu_{LO} = 402\ cm^{-1}$ determined by far-infrared spectroscopy [58], and $\nu_{TO} = 367\ cm^{-1}$ and $\nu_{LO} = 403\ cm^{-1}$, determined by Raman spectroscopy [59]. No free-carrier response was observable in this sample at frequencies down to $20\ cm^{-1}$ [25].

2 GaAs

The far-infrared optical constants of GaAs determined by Maslin *et al.* [24] at 300 K at a resolution of $4\ cm^{-1}$ using DFTS are shown in Fig. 10

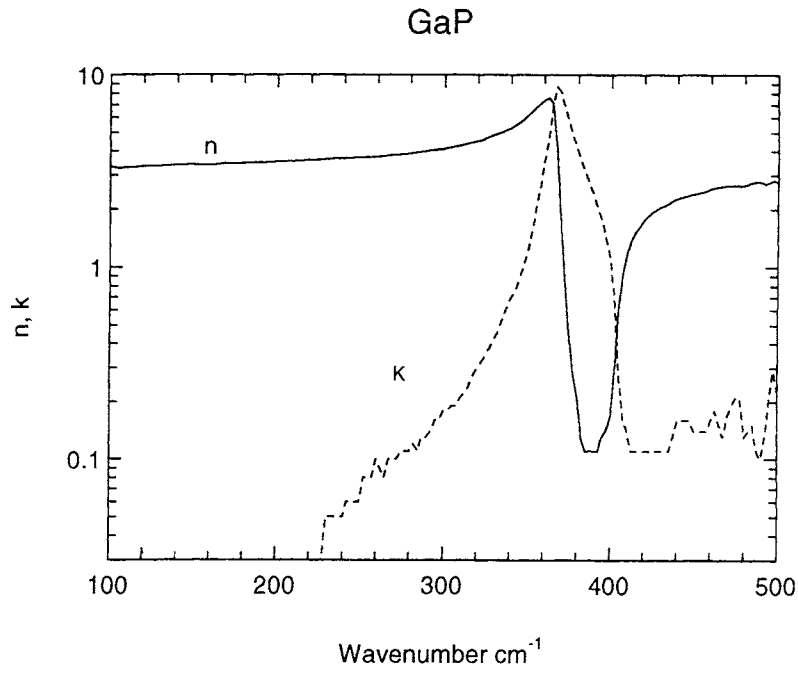

Fig. 9. Log-linear plot of the far-infrared optical constants, n and k, versus wavenumber for GaP at 300 K.

and listed in Table X, where they are compared with values calculated from Eq. (11) [OM] and values of n and k derived from the far-infrared reststrahl work of Kachare *et al.* [60] and Holm *et al.* [61], and values of k determined by Stolen [62], as listed by Palik [63]. Values of the millimeter-wave optical constants of GaAs determined by transmission DFTS have been reported by Afsar and Button [64] and Afsar [65]. The transverse and longitudinal optic phonon frequencies determined from the data of Maslin *et al.*, $\nu_{TO} = 269$ cm^{-1}, and $\nu_{LO} = 293$ cm^{-1}, are in reasonable agreement with previous experimental values, $\nu_{TO} = 269$ cm^{-1} and $\nu_{LO} = 291$ cm^{-1}, determined by Raman spectroscopy [66], and $\nu_{TO} = 271$ cm^{-1} and $\nu_{LO} = 295$ cm^{-1}, determined by far-infrared spectroscopy [67]. The sample was n-type and the onset of the free-carrier response can be seen at frequencies below 150 cm^{-1}. The plasma minimum in the reflectivity occurred at 60 cm^{-1} [25]; using $m^* = 0.07\ m_0$, Table VI [39], the free-carrier concentration is found to be 3.0×10^{16} cm^{-3}. Small differences in the LO frequencies may arise from differences in plasmon-LO phonon coupling for samples with different carrier concentrations.

TABLE X

Values of *n* and *k* for Gallium Arsenide from Various Sources

cm^{-1}	n	k	n	k	n	k
50.0	2.67	0.85 [24]	2.78	1.41 [OM]	3.615 [60, 61]	1.8 E-3 [62]
60.0	2.67	0.54				
70.0	2.85	0.34	2.90	0.67		
80.0	2.88	0.21				
90.0	3.09	0.07	3.10	0.35		
100.0	3.15	0.02			3.650	3.6 E-3
110.0	3.23		3.26	0.20		
120.0	3.33					
130.0	3.40		3.38	0.13		
140.0	3.45					
150.0	3.52					
160.0	3.57					
170.0	3.60		3.58	6.7 E-2		
180.0	3.66					
190.0	3.74		3.70	5.7 E-2		
200.0	3.81				3.93	8.49 E-3 [60, 61]
210.0	3.90		3.86	5.9 E-2	4.02	1.15 E-2
220.0	4.03				4.13	1.63 E-2
230.0	4.18		4.15	8.5 E-2	4.30	2.49 E-2
240.0	4.43	0.02			4.57	4.26 E-2
250.0	4.90	0.11	4.89	0.24	5.08	9.02 E-2
255.0	5.30	0.21			5.57	1.53 E-1
257.5	5.62	0.29				
260.0	6.01	0.41	6.05	0.76	6.47	0.323
262.5	6.56	0.60	6.62	1.20		
265.0	7.38	1.05			8.87	1.20
267.5	8.21	2.05				
270.0	7.84	4.92	5.52	6.49	4.66	11.0
272.5	4.42	7.09				
275.0	2.59	6.41			0.713	5.49
277.5	1.59	5.33				
280.0	1.03	4.40	0.95	3.37	0.358	3.48
282.5	0.71	3.64				
285.0	0.54	2.99			0.270	2.23
287.5	0.46	2.42				
290.0	0.43	1.88	0.77	1.25	0.323	1.09
292.5	0.48	1.37				
295.0	0.62	0.85			1.151	0.201
297.5	1.04	0.37				
300.0	1.40	0.22			1.707	9.59 E-2
305.0	1.82	0.11			2.020	6.02 E-2
310.0	2.06	0.10	2.18	0.13	2.229	4.21 E-2
315.0	2.24	0.06			2.380	3.14 E-2
320.0	2.38	0.03			2.495	2.43 E-2
330.0	2.58		2.61	5.3 E-2	2.659	1.59 E-2
340.0	2.70				2.7701	1.13 E-2

TABLE X *(Continued)*

Gallium Arsenide

cm^{-1}	n	k	n	k	n	k
342.5	2.72					
345.0	2.75					
347.5	2.78					
350.0	2.80		2.80	3.1 E-2	2.851	8.40 E-3
352.5	2.83					
355.0	2.85					
357.5	2.85					
360.0	2.86				2.913	6.50 E-3
362.5	2.88					
365.0	2.90					
367.5	2.91					
370.0	2.93		2.91	2.1 E-2		
372.5	2.94					
375.0	2.96					
377.5	2.98					
379.1					2.997	
380.0	2.98					
382.5	2.99					
385.0	2.99					
387.5	3.01					
390.0	3.01		2.99	1.5 E-2		
392.5	3.01					
395.0	3.01					
397.5	3.02					
399.2					3.058	
400.0	3.04					
402.5	3.04					
405.0	3.04	0.02				
407.5	3.04	0.02				
410.0	3.06	0.02	3.03	1.2 E-2		
412.5	3.07	0.02				
415.0	3.07	0.02				
417.5	3.09	0.02				
419.4					3.100	
420.0	3.09					
422.5	3.09					
425.0	3.09	0.01				
427.5	3.09	0.02				
430.0	3.09	0.03	3.077	9.3 E-2		
432.5	3.09	0.03				
435.0	3.09	0.03				
435.5					3.126	
437.5	3.09	0.03				
440.0	3.10	0.06				
442.5	3.10	0.10				
445.0	3.09	0.08				
447.5	3.09	0.05				
450.0	3.09	0.05	3.11	7.6 E-3		

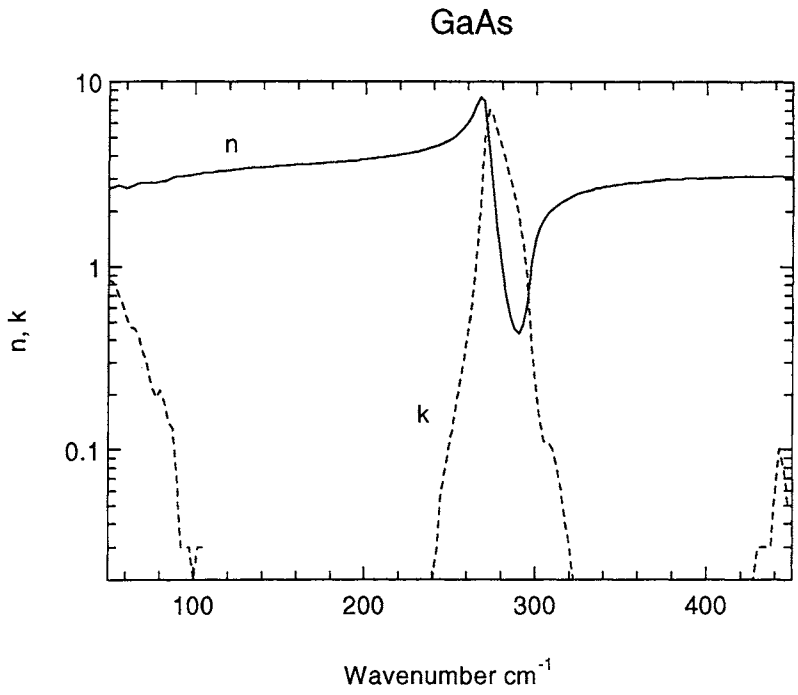

Fig. 10. Log-linear plot of the far-infrared optical constants, n and k, versus wavenumber for GaAs at 300 K.

3 GaSb

The far-infrared optical constants of GaSb determined by Maslin *et al.* [24] at 300 K at a resolution of 4 cm^{-1} using DFTS are shown in Fig. 11 and listed in Table XI, where they are compared with values calculated from the oscillator model, Eq. (11) [OM]. Hass and Henvis [68] measured the fundamental lattice reflection bands of several III-V semiconductors, including GaSb, at liquid-helium temperature and fitted a classical, damped harmonic oscillator model to their data. Edwards and White [69] have listed values of n and k for GaSb at liquid-helium temperature calculated from this model, but no previous numerical values for n and k for GaSb at 300 K have been found in the literature. The sample measured by Maslin *et al.* was n-type, and the onset of the free-carrier plasma response can be seen in Fig. 11 at frequencies below about 150 cm^{-1}. The presence of free carriers will modify the optical constants of the sample throughout the optical-phonon region, making it difficult to compare data for different samples. The transverse and longitudinal optic phonon frequencies determined from the data of Maslin *et al.*, $\nu_{TO} = 227.5$ cm^{-1}, and $\nu_{LO} = 237.5$ cm^{-1}, are in reason-

TABLE XI

Values of n and k for Gallium Antimonide from Various Sources

cm^{-1}	n	k	n	k
50.0	3.29	1.07 [24]	2.92	1.21 [OM]
60.0	3.33	0.81		
70.0	3.31	0.68	3.26	0.49
80.0	3.40	0.50		
90.0	3.56	0.34	3.52	0.24
100.0	3.61	0.24		
110.0	3.74	0.14	3.69	0.13
120.0	3.84	0.14		
130.0	3.90	0.08	3.81	8.2 E-2
140.0	3.99	0.08		
150.0	4.09	0.05	3.92	5.6 E-2
160.0	4.09	0.03		
170.0	4.17	0.03	4.04	4.3 E-2
180.0	4.30	0.02		
190.0	4.45	0.02	4.25	4.3 E-2
195.0	4.54	0.00		
200.0	4.63	0.04		
205.0	4.83	0.03		
210.0	5.03	0.06	4.80	9.8 E-2
212.5	5.19	0.09		
215.0	5.44	0.16		
217.5	5.78	0.22		
220.0	6.28	0.34		
222.5	7.11	0.59		
225.0	8.87	1.36		
227.5	5.34	8.32		
230.0	2.08	7.14	1.87	5.52
232.5	0.82	4.48		
235.0	0.66	2.60		
237.5	0.92	1.49		
240.0	1.62	0.47		
242.5	2.24	0.23		
245.0	2.54	0.17		
247.5	2.79	0.11		
250.0	2.92	0.11	2.74	0.10
252.5	3.03	0.10		
255.0	3.11	0.08		
257.5	3.19	0.06		
260.0	3.25	0.05		
262.5	3.32	0.05		
265.0	3.35	0.04		
267.5	3.42	0.03		
270.0	3.43	0.03	3.27	3.0 E-2
280.0	3.51	0.02		
290.0	3.59	0.01		
300.0	3.66			
310.0	3.69			

(continued)

TABLE XI *(Continued)*

Gallium Antimonide

cm^{-1}	n	k	n	k
320.0	3.72			
330.0	3.75		3.59	8.4 E-3
340.0	3.77			
350.0	3.79			
360.0	3.77			
370.0	3.79			
380.0	3.8			
390.0	3.80		3.68	4.4 E-3
400.0	3.79			
410.0	3.80			
420.0	3.80			
430.0	3.79			
440.0	3.71			
450.0	3.75		3.71	2.7 E-3

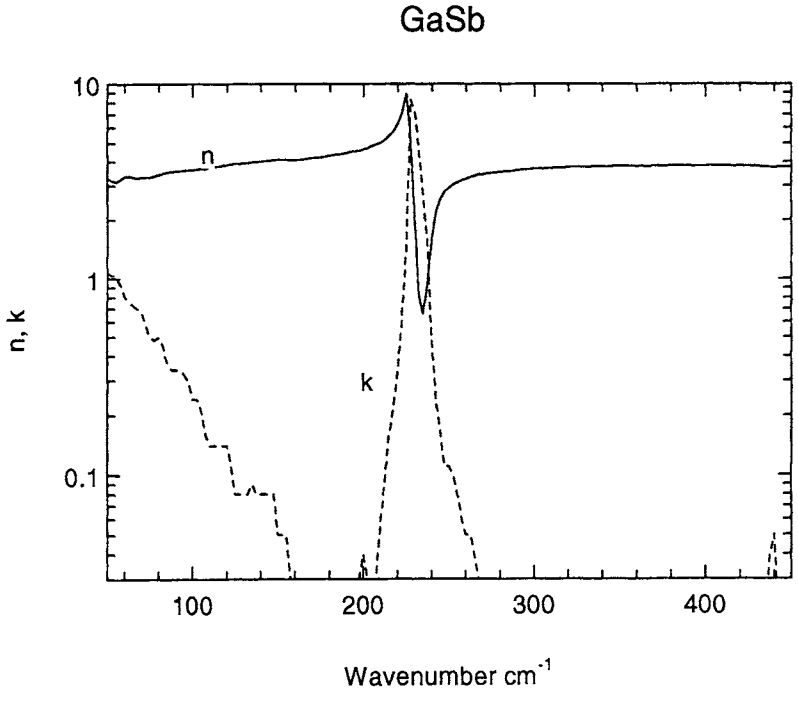

Fig. 11. Log-linear plot of the far-infrared optical constants, n and k, versus wavenumber for GaSb at 300 K.

able agreement with previous experimental values, $\nu_{TO} = 227$ cm^{-1} and $\nu_{LO} = 237$ cm^{-1}, determined by Raman spectroscopy [70], and $\nu_{TO} = 231$ cm^{-1} and $\nu_{LO} = 240$ cm^{-1}, determined by far-infrared spectroscopy [71]. The plasma minimum in the reflectivity occurred at 30 cm^{-1} [25]; using $m^* = 0.047\ m_0$ [39], the free-carrier concentration is found to be 6.7×10^{15} cm^{-3}. Small differences in the LO frequencies may arise from differences in plasmon-LO phonon coupling for samples with different carrier concentrations.

InP 4

The far-infrared optical constants of InP determined by Maslin *et al.* [24] at 300 K at a resolution of 2 cm^{-1} using DFTS are shown in Fig. 12 and listed in Table XII, where they are compared with values calculated from the oscillator model, Eq. (11) [OM], and values listed by Glembocki and Piller [72]. The values of n are the work of Pikhtin and Yas'kov [73], who fitted a lattice-vibration oscillator model to the refractive-index data of

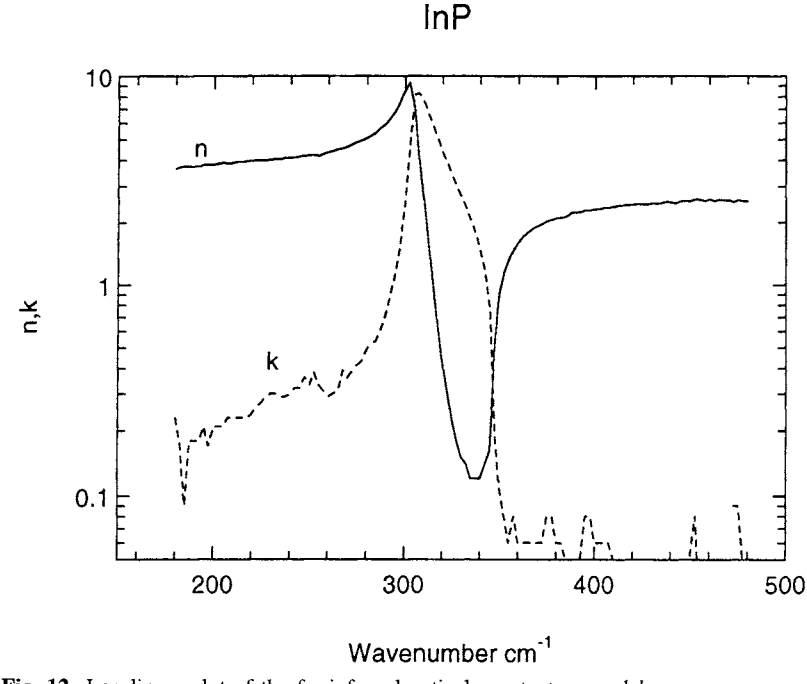

Fig. 12. Log-linear plot of the far-infrared optical constants, n and k, versus wavenumber for InP at 300 K.

TABLE XII

Values of *n* and *k* for Indium Phosphide from Various Sources

cm^{-1}	n	k	n	k	n	k
180.0	3.63	0.23 [24]	3.74	1.4 E-2 [OM]		
190.0	3.73	0.18				
200.0	3.82	0.21			3.81 [73]	8.7 E-3 [72]
210.0	3.88	0.23				
220.0	3.96	0.24	3.95	3.0 E-2		
225.0	3.99	0.27				
227.5	3.99	0.29				
230.0	4.02	0.30				
232.5	4.04	0.30				
235.0	4.05	0.29				
237.5	4.11	0.29				
240.0	4.10	0.30	4.14	5.0 E-2		
242.5	4.13	0.32				
245.0	4.17	0.32				
247.5	4.19	0.36				
250.0	4.20	0.33			4.27	3.0 E-2
252.5	4.23	0.38				
255.0	4.19	0.33				
257.5	4.28	0.31				
260.0	4.36	0.29	4.49	9.8 E-2		
262.5	4.42	0.30				
265.0	4.50	0.31				
267.5	4.56	0.39				
270.0	4.66	0.36			4.79	6.8 E-2
272.5	4.76	0.39				
275.0	4.87	0.41				
277.5	4.95	0.43				
280.0	5.08	0.49	5.29	0.28	5.31	0.124
282.5	5.24	0.52				
285.0	5.41	0.54				
287.5	5.66	0.61				
290.0	5.93	0.71	6.28	0.65		
292.5	6.31	0.88				
295.0	6.83	1.12				
297.5	7.60	1.49				
300.0	8.56	2.44	8.83	3.16	10.4	2.13
302.5	9.27	4.45				
305.0	7.02	8.14				
307.5	4.10	8.29				
310.0	2.52	7.50	2.45	6.75	1.81	7.32
312.5	1.62	6.60				
315.0	0.99	5.74				
317.5	0.61	5.00				
320.0	0.42	4.36	0.80	3.97	0.350	3.94
322.5	0.30	3.84				
325.0	0.22	3.36				

TABLE XII *(Continued)*

Indium Phosphide

cm^{-1}	n	k	n	k	n	k
327.5	0.18	3.00				
330.0	0.15	2.66			0.221	2.41
332.5	0.14	2.34				
335.0	0.12	2.05				
337.5	0.12	1.76				
340.0	0.12	1.46	0.49	1.35 [OM]	0.234	1.20
342.5	0.14	1.15				
345.0	0.16	0.78				
347.5	0.51	0.20				
350.0	0.90	0.11			1.069	0.16
352.5	1.15	0.08				
355.0	1.33	0.06				
357.5	1.48	0.08				
360.0	1.59	0.06	1.61	0.17	1.653	7.0 E-2
362.5	1.71	0.06				
365.0	1.79	0.06				
367.5	1.87	0.06				
370.0	1.92	0.06				
372.5	1.97	0.06				
375.0	2.03	0.08				
377.5	2.06	0.08				
380.0	2.11	0.06	2.14	6.9 E-2	2.163	2.9 E-3
382.5	2.12	0.06				
385.0	2.15	0.05				
387.5	2.23	0.05				
390.0	2.25	0.05				
392.5	2.26	0.05				
395.0	2.30	0.08				
397.5	2.31	0.08				
400.0	2.32	0.06	2.39	3.8 E-2	2.411	
402.5	2.34	0.06				
405.0	2.37	0.06				
407.5	2.37	0.06				
410.0	2.40	0.05				
415.0	2.43	0.03				
420.0	2.46	0.03	2.55	2.5 E-2		
430.0	2.49	0.02				
440.0	2.52					
450.0	2.55	0.05				
460.0	2.61	0.03	2.72	1.3 E-2		
470.0	2.58					
480.0	2.56		2.78	9.5 E-3		

Pettit and Turner [74], measured for an *n*-type sample with a carrier density of 5×10^{16} cm^{-3}. The values of k were calculated by Glembocki and Piller [72] using an oscillator model, with optical-phonon frequencies taken from Mooradian and Wright [75] and ϵ_∞ taken from Hass [76]. The transverse and longitudinal optic phonon frequencies determined from the data of Maslin *et al.*, $\nu_{TO} = 304$ cm^{-1}, and $\nu_{LO} = 346.5$ cm^{-1}, are in excellent agreement with previous experimental values, $\nu_{TO} = 304.5$ cm^{-1} and $\nu_{LO} = 346.4$ cm^{-1}, determined by Raman spectroscopy [77]. No free-carrier response was observable in this sample at frequencies down to 25 cm^{-1}, which puts an upper limit on the (*n*-type) free-carrier concentration of 7×10^{15} cm^{-3}.

5 InAs

The far-infrared optical constants of InAs determined by Maslin *et al.* [24] at 300 K at a resolution of 4 cm^{-1} using DFTS are shown in Fig. 13 and listed in Table XIII, where they are compared with values calculated from

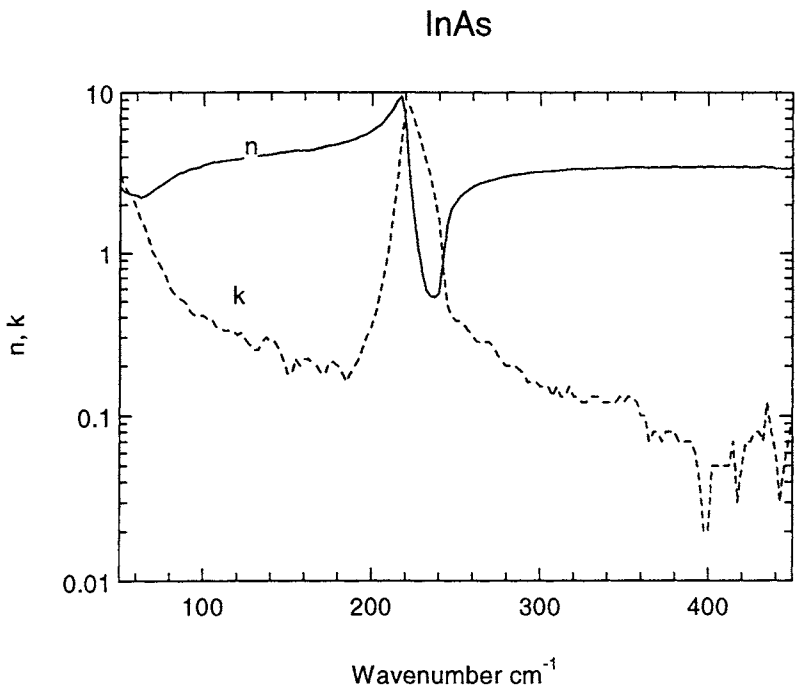

Fig. 13. Log-linear plot of the far-infrared optical constants, n and k, versus wavenumber for InAs at 300 K.

TABLE XIII

Values of n and k for Indium Arsenide from Various Sources

cm^{-1}	n	k	n	k	n	k
60.0	2.29	1.92 [24]	2.47	1.61 [OM]		
80.0	2.91	0.61				
100.0	3.54	0.41	3.27	0.33		
120.0	3.85	0.31				
140.0	4.14	0.28	3.78	0.13		
145.0	4.23	0.25				
150.0	4.31	0.18	3.90	0.11		
155.0	4.38	0.22			5.30	0.51 [80]
160.0	4.38	0.22	4.02	0.10		
165.0	4.42	0.21				
170.0	4.57	0.18	4.19	0.10		
175.0	4.70	0.21			5.58	0.20
180.0	4.80	0.20	4.41	0.12		
185.0	4.95	0.16				
190.0	5.19	0.20	4.73	0.16		
195.0	5.44	0.26			6.42	8 E-2
200.0	5.84	0.35	5.32	0.28		
205.0	6.35	0.57			7.48	0.48
210.0	7.33	1.04	6.76	0.89		
212					9.13	1.53
212.5	7.97	1.62				
216					9.24	3.50
215.0	8.83	2.75				
217.5	9.44	4.98				
220.0	6.82	8.13	5.43	7.76	7.50	6.40
222.5	3.09	8.15				
224					4.90	6.12
225.0	1.74	6.99				
227.5	1.08	5.63				
228					3.85	5.60
230.0	0.75	4.55	0.90	3.84		
232					2.79	5.17
232.5	0.59	3.71				
235.0	0.54	2.93				
236					1.27	4.20
237.5	0.53	2.21				
240.0	0.56	1.61	0.64	1.72	0.92	2.77
242.5	0.90	0.81				
244					1.24	1.44
245.0	1.53	0.48				
247.5	1.87	0.41				
248					1.88	0.97
250.0	2.07	0.38	1.46	0.38	2.03	0.83
252.5	2.26	0.38				
255.0	2.36	0.36			2.37	0.50
257.5	2.48	0.33				

(continued)

TABLE XIII *(Continued)*

Indium Arsenide

cm^{-1}	n	k	n	k	n	k
260.0	2.58	0.31	2.11	0.16	2.73	0.40
265.0	2.75	0.28			2.92	0.40
270.0	2.85	0.28			2.92	0.39
275.0	2.94	0.23				
280.0	3.01	0.20			3.00	0.17
285.0	3.09	0.20				
290.0	3.13	0.18	2.78	5.1 E-2	3.18	4 E-2
295.0	3.19	0.16				
300.0	3.22	0.15				
310.0	3.28	0.15	2.96	3.2		
320.0	3.36	0.13				
330.0	3.39	0.13				
340.0	3.40	0.12	3.11	2.0 E-2		
350.0	3.42	0.12				
360.0	3.46	0.10				
370.0	3.45	0.08				
380.0	3.47	0.08				
390.0	3.45	0.07	3.24	1.1 E-2		
400.0	3.47	0.02				
410.0	3.47	0.05				
420.0	3.44	0.05				
430.0	3.45	0.08				
440.0	3.40	0.06				
450.0	3.44	0.10	3.32	6.4 E-3		

the oscillator model, Eq. (11) [OM]. The far-infrared optical constants of InAs determined by reflection DFTS were previously reported by Gast and Genzel [78]. The transverse optic phonon frequency determined from these data, $\nu_{TO} = 218.5\ cm^{-1}$, is in good agreement with a previous experimental value, 217.3 cm^{-1}, determined by Raman spectroscopy [79]. The longitudinal optic phonon frequency, $\nu_{LO} = 242.5\ cm^{-1}$, is somewhat higher than a previous experimental value, 238.6 cm^{-1}, determined by Raman spectroscopy [79]. The plasma minimum in the reflectivity occurred at 71 cm^{-1} [25]; using $m^* = 0.026\ m_0$, Table VI [39], the free-carrier concentration is found from Eq. (12) to be $1.8 \times 10^{16}\ cm^{-3}$. Small differences in the LO frequencies may arise from differences in plasmon-LO phonon coupling for samples with different carrier concentrations. Also shown in the table are values of n and k determined by Memon *et al.* [80] for a different sample by DFTS. There are significant differences in the reststrahl region, particularly in the region of ν_{LO} which may also be due to different plasmon-phonon coupling in the two samples.

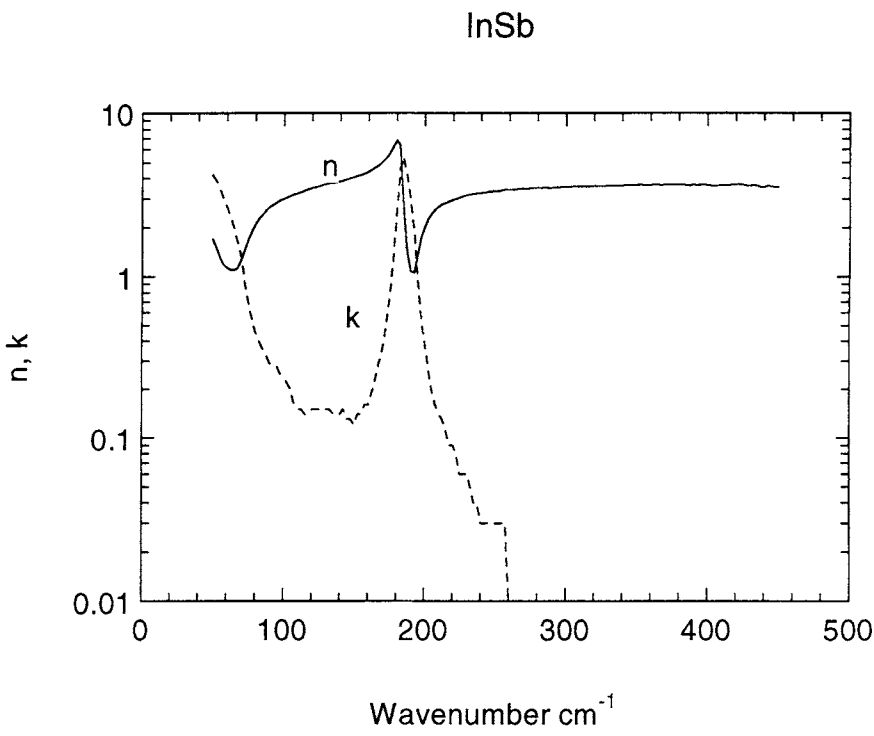

Fig. 14. Log-linear plot of the far-infrared optical constants, n and k, versus wavenumber for InSb at 300 K.

InSb 6

The far-infrared optical constants of InSb determined by Maslin *et al.* [24] at 300 K at a resolution of 4 cm^{-1} using DFTS are shown in Fig. 14 and listed in Table XIV where they are compared with values calculated from the oscillator model, Eq. (11) [OM], and the data of Sanderson [81] as listed by Holm [82]. Measurements of the far-infrared optical constants of InSb determined by reflection DFTS have also been reported by Gast and Genzel [78] and Afsar *et al.* [83]. The transverse optic and longitudinal optic phonon frequencies determined from the data of Maslin *et al.*, $\nu_{TO} = 181$ cm^{-1}, and $\nu_{LO} = 193$ cm^{-1}, are in excellent agreement with previous experimental values, $\nu_{TO} = 182.4$ cm^{-1}, and $\nu_{LO} = 193.0$ cm^{-1}, determined by Raman spectroscopy [84]. The plasma minimum in the reflectivity occurred at 75 cm^{-1} [25]; using $m^* = 0.015\ m_0$, Table VI [39], the free-carrier concentration is found from Eq. (12) to be 1.5×10^{16} cm^{-3}. Small differences in the LO frequencies may arise from differences in plasmon-LO phonon coupling for samples with different carrier concentrations.

TABLE XIV

Values of *n* and *k* for Indium Antimonide from Various Sources

cm^{-1}	n	k	n	k	n	k
50.0	1.70	4.20 [24]	1.22	3.99 [OM]	0.894	4.72 [81]
55.0	1.31	3.44				
60.0	1.13	2.67			0.771	3.21
65.0	1.10	1.98				
70.0	1.27	1.32	1.54	1.21	0.881	1.79
75.0	1.68	0.69				
80.0	2.10	0.45			1.68	0.633
85.0	2.40	0.36				
90.0	2.67	0.29	2.82	0.32	2.45	0.310
95.0	2.85	0.28				
100.0	3.01	0.24			2.92	0.193
105.0	3.13	0.20				
110.0	3.25	0.15	3.44	0.16	3.25	0.134
115.0	3.37	0.14				
120.0	3.50	0.15			3.51	0.100
125.0	3.57	0.15				
130.0	3.68	0.15	3.85	0.11	3.74	8.08 E-2
135.0	3.75	0.14				
140.0	3.83	0.14			3.96	7.15 E-2
145.0	3.93	0.13				
150.0	4.06	0.12	4.29	0.12	4.24	7.43 E-2
155.0	4.20	0.14				
160.0	4.37	0.16			4.66	0.105
162.5	4.49	0.19				
165.0	4.63	0.23				
167.5	4.80	0.29				
170.0	5.01	0.36	5.41	0.46	5.69	0.291
172.5	5.29	0.50				
175.0	5.67	0.76			7.32	0.963
177.5	6.22	1.26				
180.0	6.78	2.52			5.34	8.56
182.5	6.36	4.59				
185.0	2.74	5.40			0.884	4.10
187.5	1.44	4.22				
190.0	1.07	2.88	1.34	2.56	0.618	1.88
192.5	1.06	1.86				
195.0	1.35	0.94				
197.5	1.74	0.56				
200.0	2.02	0.39			2.22	0.165
205.0	2.43	0.20				
210.0	2.69	0.14	2.79	0.15	2.82	6.92 E-2
215.0	2.84	0.11				
220.0	2.96	0.09				
222.5	3.01	0.08				
225.0	3.06	0.06				
230.0	3.15	0.06	3.26	5.5 E-2		

TABLE XIV *(Continued)*

Indium Antimonide

cm^{-1}	n	k	n	k	n	k
235.0	3.21	0.04				
240.0	3.26	0.03				
250.0	3.35	0.03	3.46	3.0 E-2	3.45	1.75 E-2
260.0	3.41	0.01				
270.0	3.46	0.01	3.57	2.0 E-2		
280.0	3.49	0.01				
285.0	3.52	0.01				
290.0	3.51	0.01				
295.0	3.53	0.01				
300.0	3.55				3.662	7.84 E-3
302.5	3.55					
305.0	3.56					
310.0	3.57		3.70	1.1 E-2	320.0	3.59
330.0	3.61				3.708	
340.0	3.63				3.743	
350.0	3.64					
360.0	3.64					
370.0	3.65					
380.0	3.65					
400.0	3.64					
425.0	3.65					
450.0	3.54		3.85	2.8 E-3		

ACKNOWLEDGMENT

G. Mirjalili wishes to acknowledge the award of a scholarship by the Islamic Republic of Iran and the University of Yazd.

REFERENCES

1. J. E. Chamberlain, J. E. Gibbs, and H. A. Gebbie, *Nature (London)* **198**, 874 (1963).
2. J. E. Chamberlain and H. A. Gebbie, *Nature (London)* **208**, 480 (1965).
3. J. E. Chamberlain, F. D. Findlay, and H. A. Gebbie, *Appl. Opt.* **4**, 1382 (1965).
4. E. E. Bell, *Jpn. J. Appl. Phys.* **4**(Suppl. 1), 412 (1965).
5. E. E. Bell, *Infrared Phys.* **6**, 1382 (1965).
6. E. E. Russell and E. E. Bell, *Infrared Phys.* **6**, 75 (1966).
7. E. E. Bell, *Handb. Phys.* **25**, 1 (1967).
8. J. R. Birch and T. J. Parker, *in* "Infrared and Millimeter Waves" (K. J. Button, ed.), Vol. 2, Chap. 3. Academic Press, New York, 1979.
9. J. R. Birch, *Proc. SPIE* **289**, 362 (1981).
10. T. J. Parker, *Contemp. Phys.* **31**, 335 (1990).
11. K. W. Johnson and E. E. Bell, *Phys. Rev.* **187**, 1044 (1969).
12. J. E. Eldridge and P. R. Staal, *Phys. Rev. B* **16**, 4608 (1977).
13. P. R. Staal and J. E. Eldridge, *Can. J. Phys.* **57**, 1784 (1979).
14. J. R. Birch, *Infrared Phys.* **18**, 613 (1978).
15. T. J. Parker, W. G. Chambers, and J. F. Angress, *Infrared Phys.* **14**, 207 (1974).

16. K. F. Pai, T. J. Parker, N. E. Tornberg, R. P. Lowndes, and W. G. Chambers, *Infrared Phys.* **18**, 199 (1978).
17. G. O. Plumb and J. R. Birch, *Infrared Phys.* **24**, 315 (1984).
18. K. A. Maslin and T. J. Parker, *Proc. 14th Int. Conf. Infrared Millimeter. Waves, Wurzburg, October 2–6, 1989; Proc. SPIE* **1240**, 476 (1989).
19. A. K. Wan Abdullah and T. J. Parker, *Infrared Phys.* **29**, 799 (1989).
20. N. J. Burton and T. J. Parker, *Opt. Commun.* **45**, 367 (1983).
21. N. J. Burton and T. J. Parker, *Infrared Phys.* **24**, 291 (1984).
22. J. R. Birch, *Infrared Phys.* **28**, 345 (1988).
23. J. R. Birch, *Infrared Phys.* **28**, 425 (1988).
24. K. A. Maslin, C. Patel, and T. J. Parker, *Infrared Phys.* **18**, 199 (1978).
25. K. A. Maslin, Ph.D. Thesis, University of London, London (1986).
26. J. E. Eldridge and E. D. Palik, *in* "Handbook of Optical Constants of Solids" (E. D. Palik, ed.), p. 775. Academic Press, Orlando, Florida, 1985.
27. E. D. Palik, *in* "Handbook of Optical Constants of Solids," (E. D. Palik, ed.), p. 703. Academic Press, Orlando, Florida, 1985.
28. E. D. Palik, *in* "Handbook of Optical Constants of Solids II" (E. D. Palik, ed.), p. 989. Academic Press, Orlando, Florida, 1991.
29. J. I. Berg and E. E. Bell, *Phys. Rev. B* **10**, 3572 (1971).
30. A. Memon and T. J. Parker, *Int. J. Infrared Millim. Waves* **2**, 839 (1981).
31. M. E. Thomas, in this volume.
32. G. O. Jones, D. H. Martin, P. A. Mawer, and C. H. Perry, *Proc. R. Soc. London Ser. A* **261**, 10 (1961).
33. G. R. Wilkinson, *in* "Infrared Spectroscopy and Molecular Structure" (M. Davies, ed.), p. 85. Elsevier, Amsterdam, 1963.
34. R. P. Lowndes and D. H. Martin, *Proc. R. Soc. London Ser. A* **308**, 473 (1969).
35. I. Ohlídal and K. Navrátil, *in* "Handbook of Optical Constants of Solids II" (E. D. Palik, ed.), p. 1021. Academic Press, Orlando, Florida, 1991.
36. I. Ohlídal and M. Ohlídal, in this volume.
37. I. Ohlídal and D. Franta, in this volume.
38. K. Kunc, M. Balkanski, and M. A. Numisovici, *Phys. Status Solidi B* **72**, 229 (1975).
39. D. E. Gray, ed., "American Institute of Physics Handbook," 3rd Ed., pp. 9–59. McGraw-Hill, New York, 1972.
40. R. A. Cowley, *Adv. Phys.* **12**, 421 (1963).
41. R. Geick, *Phys. Rev.* **138**, 1495 (1965).
42. J. R. Birch and D. K. Murray, *Infrared Phys.* **18**, 283 (1978).
43. C. L. Mok, T. J. Parker, and J. R. Birch, *Solid State Commun.* **34**, 567 (1980).
44. E. D. Palik, *in* "Handbook of Optical Constants" (E. D. Palik, ed.), p. 409. Academic Press, Orlando, Florida 1985.
45. A. Mooradian and G. B. Wright, "Proceedings of The Ninth International Conference on The Physics of Semiconductors, Moscow," Vol. 2, p. 1020. Nauka, Leningrad, 1968.
46. G. A. Slack, F. S. Ham, and R. M. Chrenko, *Phys. Rev.* **152**, 376 (1971).
47. A. Feldman, I. Malitson, D. Horwitz, R. M. Waxler, and M. J. Dodge, *Natl. Bur. Stand. (U.S.), Tech. Note* **993**, 63 (1979).
48. M. Cardona, "Proceedings of the Seventh International Conference on The Physics of Semiconductors, Paris," p. 181. Dunod, Paris, and Academic Press, New York, 1964.
49. D. G. Thomas and J. J. Hopfield, *Phys. Rev.* **128**, 2135 (1969).
50. L. Ward, *in* "Handbook of Optical Constants of Solids II" (E. D. Palik, ed.), p. 737. Academic Press, Orlando, Florida, 1991.
51. M. N. Afsar, "Proceedings of the Third International Conference on Infrared Physics, Zurich" (W. Ruegsegger and F. K. Kneubuhl, eds.), p. 714. ETH, Zurich, 1984.
52. A. Manabe, A. Mitsuishi, and H. Yoshinaga, *Jpn. J. Appl. Phys.* **6**, 593 (1967).

53. T. Hattori, Y. Homma, and A. Mitsuishi, *Opt. Commun.* **7**, 229 (1973).
54. J. C. Irwin and J. La Combe, *Can. J. Phys.* **50**, 2596 (1972).
55. C. Patel, K. A. Maslin, and T. J. Parker, "Proceedings of the Second International Conference on Phonon Physics," p. 927. Phonon '85, Budapest, 1985.
56. A. Borghesi and G. Guizzetti, *in* "Handbook of Optical Constants of Solids" (E. D. Palik, ed.), p. 445. Academic Press, Orlando, Florida, 1985.
57. A. S. Barker, Jr., *Phys. Rev.* **165**, 917 (1968).
58. D. A. Kleinman and W. G. Spitzer, *Phys. Rev.* **118**, 110 (1960).
59. M. V. Hobden and J. P. Russell, *Phys. Lett.* **13**, 39 (1964).
60. A. H. Kachare, W. G. Spitzer, F. K. Euler, and A. Kahan, *J. Appl. Phys.* **45**, 2938 (1974).
61. R. T. Holm, J. W. Gibson, and E. D. Palik, *J. Appl. Phys.* **48**, 212 (1977).
62. R. H. Stolen, *Phys. Rev. B* **11**, 767 (1975); R. H. Stolen, *Appl. Phys. Lett.* **15**, 74 (1969).
63. E. D. Palik, *in* "Handbook of Optical Constants of Solids" (E. D. Palik, ed.), p. 429. Academic Press, Orlando, Florida, 1985.
64. M. N. Afsar and K. J. Button, *IEEE Trans. Microwave Theory Tech.* **MTT-31**, 217 (1983).
65. M. N. Afsar, *IEEE Trans. Microwave Theory Tech.* **MTT-32**, 1598 (1984).
66. T. Sekine, K. Uchinokura, and E. Matsuura, *J. Phys. Chem. Solids* **38**, 1091 (1977).
67. E. S. Koteles and W. R. Datars, *Can. J. Phys.* **54**, 1676 (1976).
68. M. Hass and B. W. Henvis, *J. Phys. Chem. Solids.* **23**, 1099 (1962).
69. D. F. Edwards and R. H. White, *in* "Handbook of Optical Constants of Solids II" (E. D. Palik, ed.), p. 597. Academic Press, Orlando, Florida, 1991.
70. T. Sekine, K. Uchinokura, and E. Matsuura, *Solid State Commun.* **18**, 1337 (1976).
71. S. S. Mitra, *Phys. Rev.* **132**, 986 (1963).
72. O. J. Glembocki and H. Piller, *in* "Handbook of Optical Constants of Solids" (E. D. Palik, ed.), p. 503. Academic Press, Orlando, Florida, 1985.
73. A. N. Pikhtin and A. D. Yas'kov, *Sov. Phys. Semicond. (Engl. Transl.)* **12**, 622 (1978); A. N. Pikhtin and A. D. Yas'kov, *Fiz. Tekh. Poluprovodu.* **12**, 1047 (1978).
74. G. D. Pettit and W. J. Turner, *J. Appl. Phys.* **36**, 2081 (1965).
75. A. Mooradian and G. B. Wright, *Solid State Commun.* **4**, 431 (1966).
76. M. Hass, *in* "Semiconductors and Semimetals" (R. K. Willardson and A. C. Beer, eds.), Vol. 3, p. 3. Academic Press, New York, 1967.
77. G. F. Alfrey and P. H. Borcherds, *J. Phys. C* **5**, 275 (1972).
78. J. Gast and L. Genzel, *Opt. Commun.* **8**, 26 (1973).
79. R. Carles, N. Saint-Cricq, J. B. Renucci, M. A. Renucci, and A. Zwick, *Phys. Rev. B* **22**, 4804 (1980).
80. A. Memon, T. J. Parker, and J. R. Birch, *Proc. 1981 Int. Conf. Fourier Transform Spectroscopy, Proc. SPIE* **289**, 20 (1981).
81. R. B. Sanderson, *J. Phys. Chem. Solids* **26**, 803 (1965).
82. R. T. Holm, *in* "Handbook of Optical Constants of Solids" (E. D. Palik, ed.), p. 491. Academic Press, Orlando, Florida 1985.
83. M. N. Afsar, J. R. Birch, and J. Chamberlain, *Proc. Conf. Dielectric Mater. Measurements Appl., IEE Conf. Publ.* **129**, 131 (1975).
84. W. Kiefer, W. Richter, and M. Cardona, *Phys. Rev. B* **12**, 2346 (1975).

Chapter 3

Photothermal/Photoacoustic Spectroscopic Measurements of Optical Absorption Coefficients in Semiconductors

ANDREAS MANDELIS
Photothermal and Optoelectronic Diagnostics Laboratories
Department of Mechanical and Industrial Engineering
University of Toronto
Toronto, ON, Canada

I. Introduction 59
II. Photoacoustic Spectroscopy (PAS) 60
III. Photopyroelectric Spectroscopy (PPES) 67
IV. Measurements of $\alpha(\lambda)$ in Semiconductors
Using Photoacoustic/Photothermal Techniques 69
Acknowledgments 94
References 94

INTRODUCTION I

Photothermal- and photoacoustic-based spectroscopic techniques have proliferated in recent years as primary methodologies for measuring the optical absorption coefficient, α, in broad ranges of solids, which may, or may not, be easily measurable by other, more conventional spectroscopic techniques. An increasing body of literature concerning these measurements can be consulted by the interested reader, including a number of monographs, review books and treatises on the state-of-the-art in these fields [1–7]. It should be noted that the foregoing techniques are now widely used to measure *directly* the optical absorption coefficient $\alpha(\lambda)$ from a dynamic measurement of the heat released *via* the spatial rate of optical-to-thermal energy conversion in a material, rather than the extinction coefficient, $k(\lambda)$.

HANDBOOK OF OPTICAL CONSTANTS OF SOLIDS III

Copyright © 1998 by Academic Press.
All rights of reproduction in any form reserved
ISBN 0-12-544423-0/$25.00.

The two measurements are, of course, equivalent and are related through the defining equation of the former

$$\alpha(\lambda) = 4\pi k(\lambda)/\lambda \qquad [\text{cm}^{-1}]. \tag{1}$$

As a result of this peculiarity of the photoacoustic/photothermal techniques, all the spectroscopic plots and data to be discussed in this chapter will be given in terms of $\alpha(\lambda)$. The major α-measuring methodologies in this field include in order of historical sequence a) gas-cell and piezoelectric photoacoustic spectroscopy (PAS); various photothermal spectroscopies (PTS), such as b) photothermal beam-deflection spectroscopy (PDS), otherwise known as Mirage-Effect spectroscopy; c) Fourier-transform infrared photoacoustic (FTIR-PAS) spectroscopies; and d) photopyroelectric spectroscopy (PPES). The PDS family of techniques has been well described by Briggs in Chapter 4 and, therefore, will not be discussed further in this chapter, except where necessary for complementary measurements of α, especially with regard to semiconducting amorphous thin-films. Again, for historical reasons the presentation of the material in this chapter will be done as follows: i) technique description and instrumental implementation; and ii) applications to optical-property measurements of semiconductors, specifically of α at a single wavelength or within a spectral range.

II PHOTOACOUSTIC SPECTROSCOPY (PAS)

A Gas-Cell—Microphone Photoacoustics

The photoacoustic effect in solids was first described quantitatively by Parker [8] in 1973 and was later generalized by what has come to be known as the "Rosencwaig–Gersho (RG) Theory" [9]. Figure 1 shows a cross-section of a typical photoacoustic cell used for the measurement of α in sol-

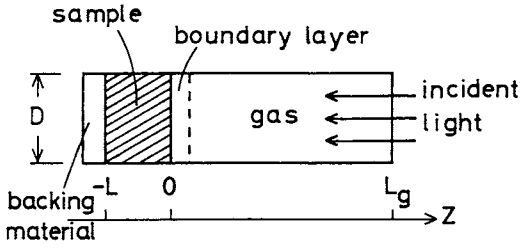

Fig. 1. Cross-sectional view of a simple cylindrical photoacoustic cell. (From Rosencwaig and Gersho [9] with permission from the publisher.)

ids. The gas-cell—microphone PA signal is generated as an acoustic disturbance in a hermetically sealed chamber equipped with a sensitive microphone, following the incidence and absorption of optical power by a solid sample inside the acoustic chamber. The incident radiation penetrates the cell through a transparent window, and the intensity is mechanically chopped or otherwise modulated at a constant frequency $f = \omega/2\pi$. The absorbed radiation is subsequently converted into heat through non-radiative relaxation mechanisms in the bulk and/or at the surface of the solid. Conduction heat transfer to the surrounding gaseous medium (air) at the frequency f is almost always the predominant energy-transport process and the one that generates the harmonic acoustic disturbance detected by the sensitive microphone. The absorption of photons by a solid followed by energy conversion and de-excitation pathways is described schematically in Fig. 2. Non-radiative conversion is but one such pathway, which, nevertheless, is usually the dominant de-excitation mechanism in solids, leading to production of heat. Other possible energy transformations and conversions are also shown in Fig. 2. The PA signal from the microphone is demodulated by a lock-in amplifier, and the amplitude and phase are stored and displayed on a computer screen for quantitative analysis. A typical experimental set-up is shown in Fig. 3.

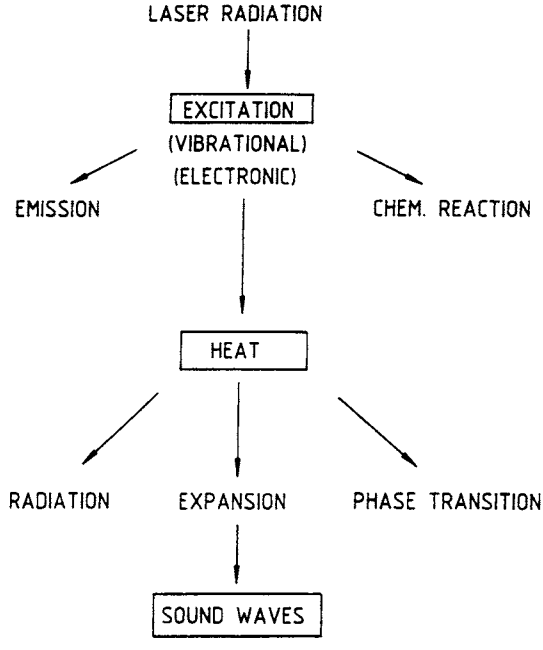

Fig. 2. Optical energy conversion pathways in a photoacoustic experiment.

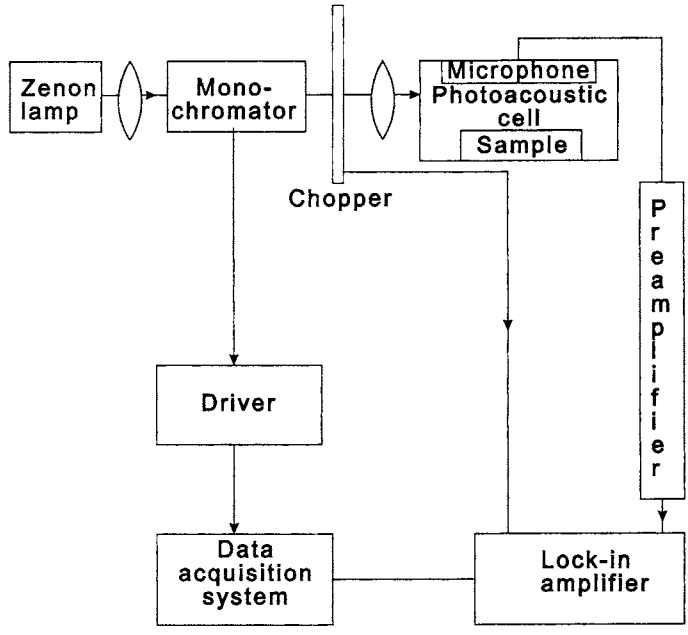

Fig. 3. Typical experimental set-up for gas-cell—microphone PAS of solids.

Assuming a spatially broad, homogeneous and isotropic, sinusoidally chopped/modulated monochromatic light source with wavelength, λ, impinging on an absorbing solid of optical absorption coefficient, $\alpha(\lambda)$, with intensity

$$I(t) = \frac{1}{2} I_0(1 + \cos\omega t) \qquad [\mathrm{W/cm^2}], \tag{2}$$

the heat density produced at depth x from the surface of the solid is given by

$$Q(x,t) = \frac{1}{2}\alpha I_0 e^{-\alpha x} Re(1 + e^{i\omega t}) \qquad [\mathrm{W/cm^3}]. \tag{3}$$

Coupled heat-diffusion equations in the gas, solid, and backing regions of Fig. 1 can be solved to give the a.c. temperature oscillation in the PA chamber [9]. This is the thermal-wave responsible for the acoustic oscillation (the pressure wave) detected by the microphone. From the real and imaginary parts of the complex thermal-wave signal *at the surface of the solid,* the PA signal expressions are worked out in the RG theory assuming the validity of the ideal gas law and the adiabatic gas law in the hermetically sealed

chamber/cell. The PA amplitude and phase can thus be calculated in the general case from the real and imaginary parts of the signal. These are complicated expressions, and they are generally non-linear in the parameter α. Nevertheless, substantial simplifications occur in a number of limiting cases of the RG theory:

Optically Transparent Solids ($\alpha^{-1} > L$)

Case 1a: Thermally Thin Solids ($\mu > L$; $\mu >$ or $< \alpha^{-1}$): The symbol μ, a function of the chopping frequency, stands for the thermal-wave penetration depth in the solid material of thickness L,

$$\mu(\omega) = \sqrt{2\beta/\omega}, \tag{4}$$

where β is the thermal diffusivity of the sample [cm^2/s]. In this limiting case, the optical radiation is assumed to obey the Beer-Lambert Law and is absorbed throughout the length of the solid. A fraction of it exits the back surface of the sample and impinges on the backing material, which is assumed to be transparent and of infinite thickness. In this limit, whether $\alpha >$ or $< \sqrt{2}/\mu(\omega)$, the complex magnitude of the PA signal is approximately given by

$$Q \approx Y\mu_g(\mu_b/\kappa_b)Y\frac{(1-i)\alpha L}{2}, \tag{5}$$

where the subscript *"b"* indicates the backing material, *"g"* indicates the surrounding gas (almost always air), κ stands for thermal conductivity [W/cm K], μ_j has the definition of Eq. (4) for $j = g$ or b. Y is a constant (real) pre-factor independent of the optical absorption coefficient of the sample, but generally dependent on wavelength through its linear dependence on the reflectivity in the form $[1 - R(\lambda)]$. Equation (5) shows that the PA signal in this limit is proportional to αL and inversely proportional to ω. Furthermore, the thermal properties of the backing play a role in this thermally thin situation.

Case 1b: Thermally Thick Solids ($\mu < L$; $\mu \ll \alpha^{-1}$): The complex magnitude of the PA signal is now approximated by

$$Q \approx -iY\mu_g(\mu/\kappa)\frac{\alpha\mu}{2}. \tag{6}$$

Here the signal is proportional to $\alpha\mu$, rather than αL, that is only the radiation that is absorbed within the optical absorption length α^{-1} contributes to the signal, even though optical absorption takes place throughout the thickness of the sample. Since the sample is now thermally "thick", the thermal properties of the backing material have been replaced by those of the solid, and the frequency dependence is $\omega^{-3/2}$.

Optically Opaque Solids ($\alpha^{-1} \ll L$)

Case 2a: Thermally Thin Solids ($\mu \gg L$, $\mu \gg \alpha^{-1}$): In this case the Beer-Lambert Law yields $e^{-\alpha L} \approx 0$, and the complex magnitude of the PA signal becomes

$$Q \approx Y(\mu/\kappa)\frac{(1-i)\mu_g}{2}. \tag{7}$$

In this case, the signal is independent of the optical absorption coefficient (*photoacoustic saturation*) and decreases with increasing frequency as ω^{-1}. No spectroscopic information can be derived in this limit.

Case 2b: Thermally Thick Solids ($\mu < L$, $\mu > \alpha^{-1}$): When the modulation/chopping frequency rises well above the limits represented in Case 2a, the PA signal becomes

$$Q \approx Y\mu_g(\mu/\kappa)\frac{(1-i)}{2}. \tag{8}$$

Again, this case lies within the range of photoacoustic saturation, and no spectroscopic information may be derived from experiments in this (intermediate) frequency range.

Case 2c: Thermally Thick Solids ($\mu \ll L$, $\mu < \alpha^{-1}$): This situation obtains at very high frequencies, so that the sample is entirely thermally thick, and the PA signal comes out of photoacoustic saturation with frequency dependence $\omega^{-3/2}$:

$$Q \approx -Y\mu_g(\mu/\kappa)\frac{\alpha\mu}{2}. \tag{9}$$

Even though theoretically this is a legitimate special case where PAS operates as an absorption spectroscopy, in practice the modulation frequencies required to satisfy the conditions of the case may be too high to yield an acceptable signal-to-noise ratio.

B Piezoelectric Photoacoustics

In the case of gas-microphone PA detection, the optically generated heat is coupled to the non-absorbing gas of the sample chamber, and the ensuing time-dependent pressure fluctuation is detected by a sensitive microphone. An alternative signal-transduction methodology is through coupling of the thermal energy released following optical absorption to the vibrational modes of the sample, i.e., through coupling to its acoustic phonon spectrum. In this

thermoelastic mode, the speed of energy transfer is governed by the speed of sound and is limited by the sample/transducer geometry and the boundary conditions at the sample-gas and sample-transducer interfaces. The thermoelastic theory of this PAS mode has been presented adequately by White [10]. The generated harmonic pressure pulse in the sample is communicated to an intimately attached piezoelectric transducer. This pressure pulse results in a harmonic electrical signal across the piezoelectric transducer, which may be demodulated by a lock-in amplifier (LIA) as in the case of gas-cell—microphone PAS. A more complete theory directly applicable to piezoelectric PAS of condensed matter was developed by Jackson and Amer [11], commonly known as the "Jackson–Amer (JA) model." A simple outline of this detection principle is shown in Fig. 4. The expansion of the central region causes displacement of the sample surface by two separate mechanisms. First, the enlargement of the central region causes the general expansion of both surfaces of the sample at $z = 0$ and $z = L$, Fig. 4(a). Second, in the case of strongly absorbing solids, the heat in the illuminated region decays spatially throughout the thickness of the sample; consequently, the front part of the sample expands more than the rear part, resulting in bending, Fig. 4(b). Such bending compresses the rear surface at $z = L$ and causes further expansion to the front surface, which adds to the general expansion. These displacements of the sample surfaces are sensed by a sufficiently thin piezoelectric transducer, the generated voltage being detected by appropriate electrodes.

The general expression of the piezoelectric PA signal is quite complicated

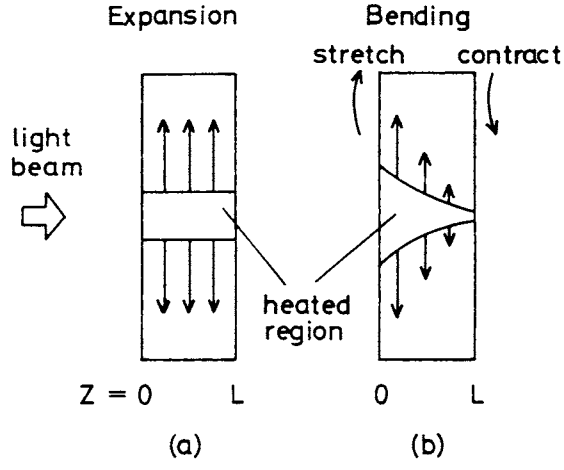

Fig. 4. Sources of surface strain for the average expansion (a) or bending (b) of an irradiated absorbing solid. The PA piezoelectric transducer may be attached to either side of the sample. (From Jackson and Amer [11] with permission from the publisher.)

and hard to interpret physically. For lucidity, Jackson and Amer [11] worked out a few special cases of the JA model, neglecting the surface thermal conduction of the solid to the surrounding gas and considering sample-parameter-limiting situations similar to those presented in the RG model. For front-surface illumination of a solid sample ($z = 0$) and the piezoelectric transducer at $z = L$, a convenient form of these special cases was given by Ikari *et al.* [12]

Optically opaque solids:

Case 1a: Thermally Thick Solid:

The complex magnitude of the PA signal is given by

$$Q \approx -\frac{2MPa_t}{i\omega L\rho_s C_s}, \tag{10}$$

where a_t is the linear expansion coefficient of the solid, P is the incident power corrected for the sample reflectivity $R(\lambda)$; M is a constant calculated by means of piezoelectric and dielectric constants; and ρ_s, C_s are the density and specific heat capacity of the solid, respectively.

Case 1b: Thermally Thin Solid: In this situation the complex signal is

$$Q \approx \frac{MPa_t}{i\omega L\rho_s C_s}. \tag{11}$$

Optically transparent solids:

In the thermally thick limit the expression for the PA signal is an explicit function of the optical absorption coefficient

$$Q \approx \frac{MPa_t}{i\omega L\rho_s C_s}\left[1 - e^{-\alpha L} \pm (6/L\alpha)[1 - (L\alpha/2) - e^{-\alpha L}(1 + L\alpha/2)]\right]. \tag{12}$$

The negative sign applies in the case where the transducer is away from the optical beam ($z = L$), and the positive sign is applicable when the transducer is toward the beam ($z = 0$).

In terms of the utility of piezoelectric PAS as a spectroscopic tool for the measurement of α, Eq. (12) shows that for small values of α the signal is directly proportional to this parameter. For high values of α, however, the position of the piezoelectric with respect to the incident beam yields significantly different results: In the position $z = L$, as α increases the signal decreases, eventually passing through zero and changing sign at higher values of α. In this limit, the bending compression exceeds the expansion due to heating. On the other hand, in the position $z = 0$, the signal shows little photoacoustic saturation up to some very high values of α. In this case the bending and the expansion terms add, thus increasing the observed signal.

From the foregoing discussion it is apparent that the mechanism generat-

ing the PA signal is greatly dependent on the position of the transducer, and the resulting spectra are frequently too complicated to understand quantitatively. The peaks and valleys in the spectra are sometimes inverted as well [13]. An alternative spectroscopic technique using a pyroelectric element [14] has been developed to detect photothermal waves in solids [15]. Photopyroelectric spectroscopy has distinct advantages over piezoelectric PAS, such as the simplicity of calibration, insensitivity to acoustic noise and mechanical resonances, a high potential for signal-to-noise-ratio improvement, and a flat response in the range 0.1 to 10^{-7} K/s. This technique has been useful for solids exhibiting complicated PA spectra.

PHOTOPYROELECTRIC SPECTROSCOPY (PPES) III

A one-dimensional geometry of a PPE system is shown in Fig. 5 [15]. The sample is in intimate contact with a pyroelectric transducer, most likely a thin polyvinylidene fluoride film (PVDF) of thickness ℓ. The pyroelectric

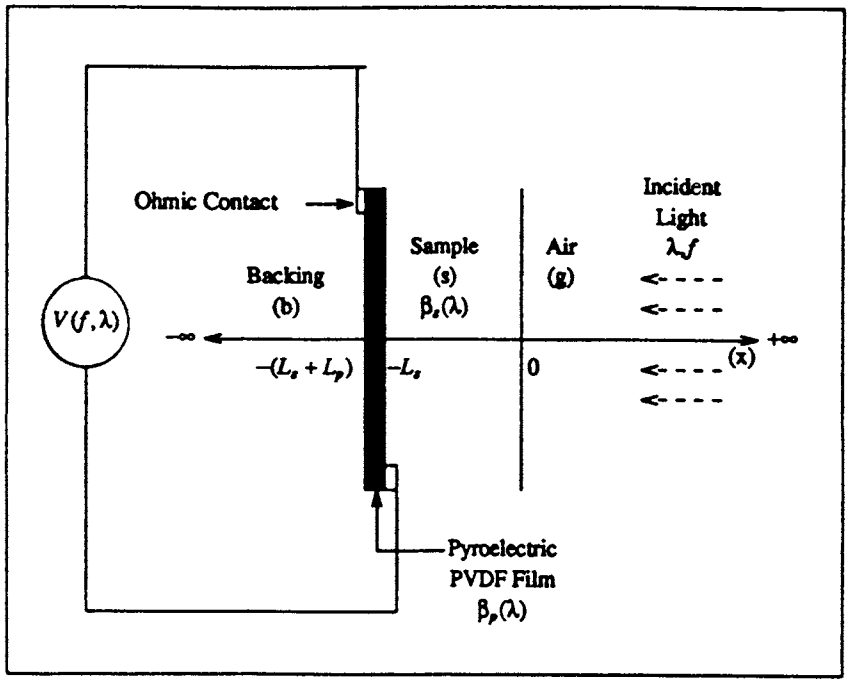

Fig. 5. One-dimensional geometry of a frequency-domain photopyroelectric system. (From Mandelis and Zver [15] with permission from the publisher.)

coefficient of the detector is p. The sample/transducer system is supported by a transparent (semi-infinite) backing material. The PPE cell, unlike the PA cell, does not require hermetic closure (open geometry). Light absorption by the sample and nonradiative energy conversion to heat increases the temperature of the pyroelectric thin-film transducer. This temperature increase results in a potential difference between the upper and lower surfaces of the transducer due to the pyroelectric effect [14]. This voltage $V[\omega, \alpha(\lambda)]$ amounts to an electrical signal, which is measured in the external circuit through the connection of Ohmic leads to the pyroelectric as shown in Fig. 5. The demodulation of the PPE voltage is done in a manner similar to that used for PAS, and the rest of the experimental system is also similar. The charge accumulated in the pyroelectric due to a change $T_p(t)$ in temperature is given by

$$q(t) = pT_p(t). \tag{13}$$

The PPE voltage across the transducer electrodes is

$$V(\omega,\alpha) = \frac{i\omega A < T_p(\omega,\alpha) > R}{(1 + i\omega\tau_E)}, \tag{14}$$

where A is the area of the pyroelectric exposed to temperature variation, R is the total resistance of the equivalent circuit, and τ_E is the RC time constant of the equivalent circuit [16]. The average value of the pyroelectric temperature oscillation is taken over the thickness of the pyroelectric element:

$$< T_p(\omega,\alpha) > = \frac{1}{\ell} \int_{\ell} T_p(x;\omega,\alpha)\, dx. \tag{15}$$

The expression for the average thermal-wave field across the pyroelectric is given by a treatment of coupled heat-diffusion equations similar to that derived for PAS [9]. For practical spectroscopic applications, Mandelis and Zver have developed a one-dimensional PPE model, valid for broad optical-excitation beams compared to both sample thickness and pyroelectric-element thickness, and known as the "Mandelis–Zver (MZ) model" [15]. In terms of the ability of the technique to measure optical absorption coefficients, a more extensive analysis of the signals has also been conducted by Chirtoc and Mihailescu [17]. According to the MZ model, the PPE signal depends linearly on the sample optical absorption coefficient

$$V(\omega,\alpha) \propto \alpha, \tag{16}$$

when *the sample is optically opaque,* $\alpha^{-1} \ll L$, *and thermally thick,* a case likely to occur at high modulation/chopping frequencies, such that $\mu << L$

and $\mu < \alpha^{-1}$. The signal magnitude, however, decreases exponentially with the square root of modulation frequency, $\exp(-L/\mu)$; therefore, the signal-to-noise ratio (SNR) is expected to be poor.

When the sample is *optically transparent,* $\alpha^{-1} > L$, *and thermally thick,* this case is of strong experimental interest, because the complex magnitude of the PPE signal is

$$V(\omega,\alpha) \propto 1 - \alpha L, \tag{17}$$

and the signal decreases only as ω^{-1}, so the SNR is expected to be satisfactory. This limit is achieved when $\mu < L$ and $\mu \ll \alpha^{-1}$. The two foregoing cases are the only ones which can yield direct spectroscopic information about the optical absorption coefficient of the sample material, as the result of thermal and optical transmission, respectively [18, 19].

IV MEASUREMENTS OF $\alpha(\lambda)$ IN SEMICONDUCTORS USING PHOTOACOUSTIC/PHOTOTHERMAL TECHNIQUES

In this section, several examples will be given of optical absorption spectra of simple semiconducting solids, which have been measured by means of photoacoustic or photothermal techniques. The selection of this particular family of solids is in order to keep the volume of material in this chapter within reason as a first photothermal/photoacoustic presentation in the *Handbook of Optical Constants of Solids* series, and reflects the extraordinary importance of these materials in science and technology in the 1990s. The major advantage of the methodologies discussed in Sects. I–III over their purely optical spectroscopic counterparts, is the superior dynamic range of the former, especially at low α ranges. This stems from the linear dependence of the photothermal signals on α (or αL in the case of thin layers), which renders the signal proportional to the thermal energy released following absorption, as opposed to optical reflectance or transmittance detection: in the former situation the transducer only registers the amount of converted thermal energy which is proportional to α; in the latter situation, two large optical signals must be subtracted (incident − transmitted energy) to calculate the amount absorbed and thus to estimate α. This subtraction procedure becomes increasingly less accurate as α decreases toward zero, and it is in this range where PAS, PPES, and PDS excel as zero-baseline spectroscopies. An excellent discussion of this crucial aspect of the photoacoustic/photothermal spectroscopies has been given by Boccara and Fournier [20]. Absolute measurements of α can be obtained using photoacoustic and photothermal methods, by normalizing sample spectra by the spectrum of a totally optically

opaque (reference) material. Such a spectrum is photothermally saturated [9, 19]; therefore, it is independent of the absorption coefficient of the reference and its spectral signature depends solely on the optical fluence of the source and on the thermal/acoustic and signal transduction characteristics of the sample chamber and the instrumentation. Quantitative $\alpha(\lambda)$ spectra of a material may be obtained from the ratio of the signal amplitude with that of the reference, and from the difference of the signal phase from the phase of the reference (normalization). Xerox toner is the usual reference material in the photoacoustic literature.

The PA or PT spectra in this section will be presented or discussed according to the following rules: 1) Quantitative spectra of α (cm^{-1}) will be presented from the original reference(s), whereas qualitative-only spectra will be briefly discussed and references will be given; 2) Spectra of semiconductors whose optical spectra (α, k, or n) have already appeared in the *HOC I, II,* or *III* will be given priority over other spectra. Historically, the complementary nature of PAS or PTS to optical spectroscopies has manifested itself through the measurement of spectra of materials in states complementary to those conventionally measured (e.g., powders instead of single crystals). Furthermore, the high dynamic range of the PAS or PTS signals has been taken advantage of in extending the low spectral (or α) ranges beyond those conventionally measured by optical techniques.

1 Si

Qualitative measurements of gas-cell microphonic PA spectra of Si in the 200–1200 nm region were performed by Tokumoto *et al.* [21]. The measurements were performed at low chopping frequencies so as to be in the thermally thin regime. An abrupt change was observed at 1100 nm (1.12 eV) which corresponds to the fundamental absorption edge, E_G. In the above-band-gap regime (photoacoustic saturation region) the only wavelength-dependent term of the PA signal is the $[1\text{-}R(\lambda)]$ factor embedded in Y, Eq. (7) or Eq. (8). Good correlation of the observed "dips" with optical reflectance spectra was found, thus verifying the origin of these features in the electronic band structure of Si. Ram *et al.* [22] recorded qualitative gas-cell—microphone PA spectra of powdered Si in the range 800–1300 nm and estimated the value of E_G to be 1.18 eV $\pm$ 0.01 eV. Quantitative $\alpha(\lambda)$ spectra of a 400 μm-thick crystalline Si wafer were obtained by Christofides *et al.* [23] using PPES. These authors used both PPE amplitude and phase data and the MZ theory to determine α from a single-modulation-frequency experiment in the range 1100–1400 nm: this procedure allowed the unambiguous determination of α at several frequencies in regimes intermediate between thermally thin and thick. The resulting spectra are shown in Fig. 6 [23–25].

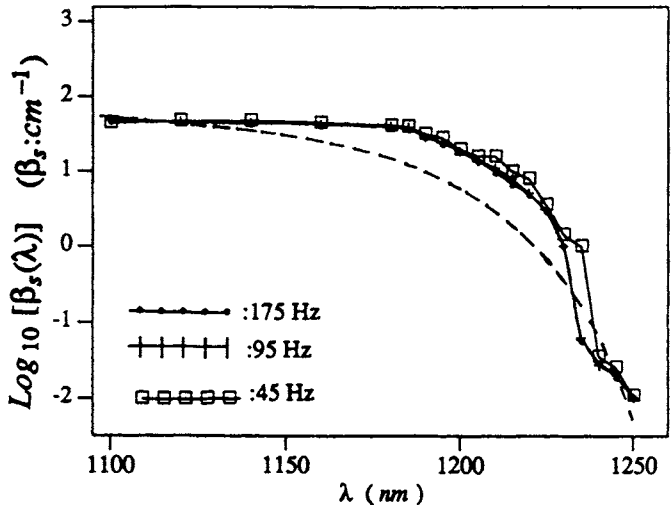

Fig. 6. Logarithm of the optical-absorption-spectrum calculation for Si. Data were taken from several PPE amplitude and phase data sets at 45, 95, and 175 Hz. Flatness in the short wavelength region is due to PPE saturation. The dashed curve is from Sze [24] and Kirev [25]. (From Christofides *et al.* [23] with permission from the publisher.)

Ge 2

Tokumoto *et al.* [21] presented a qualitative gas-cell PA spectrum of Ge in the 200–1000 nm region. Above-bandgap features due to the spectral variation of the reflectance were observed in the PA amplitude and were well correlated to optical reflectance spectra. Welsch *et al.* [26] used a thermoelastic variant of photothermal deflection spectroscopy (see Chapter 4), developed by Olmstead *et al.* [27] to obtain the absorption coefficient of a thin-film Ge sample at 10.6 μm, as characteristic of IR optical-component absorption. They found α_{Ge} (10.6 μm) = 0.0019 cm^{-1}. Fig. 7 shows quantitative $\alpha = \beta_s(\lambda)$ spectra of a wafer of crystalline Ge obtained using PPES at various chopping frequencies in the thermally thin limit of Eq. (17) [28]. Real-time spectrum normalization by the Xe-lamp throughput was employed. The high-energy flat regions are due to PPE saturation: this phenomenon sets in at ~ 1850 nm for the 14 Hz spectrum and at 1800 nm for the higher-chopping-frequency spectra. The very reproducible absorption feature centered at 1933 nm does not appear in the conventional optical transmission spectra of Ge [24,25]. It is believed to be a surface damage or contamination feature as a result of the fabrication and polishing process. This feature does not appear in the PPE phases corresponding to Fig. 7 (not shown), and such a correlation between amplitude and phase spectra would be expected from absorption features homogeneously distributed throughout the wafer

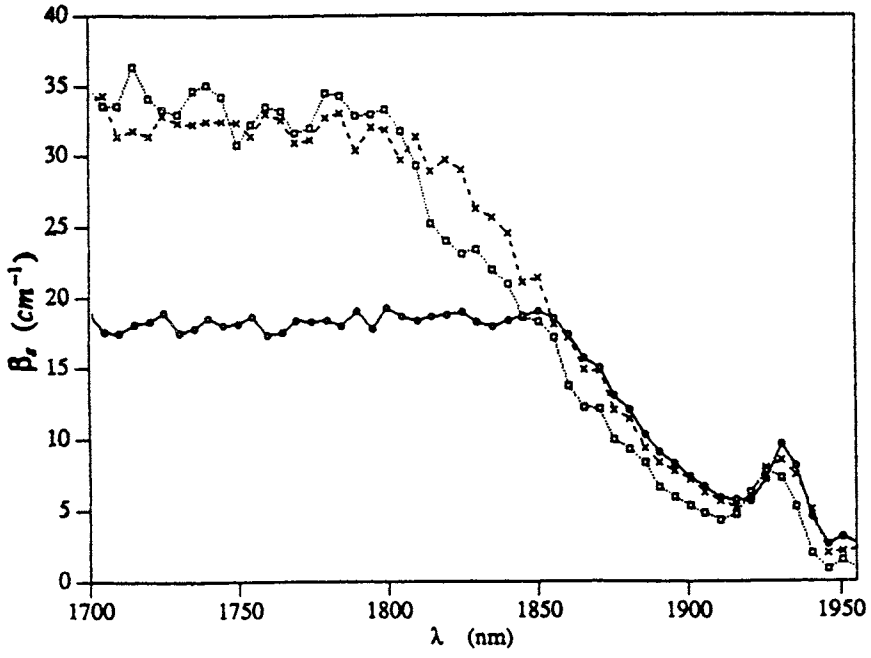

Fig. 7. Optical-absorption-coefficient $\alpha = \beta_s(\lambda)$ calculation for Ge as a function of wavelength. Data taken at various frequencies: - • - : 14 Hz; - x - : 41 Hz; - □ - : 75 Hz. (From Christofides *et al.* [28] with permission from the publisher.)

bulk according to the MZ theory [15]. Assuming a parabolic density-of-states approximation of the conduction-band structure of Ge, a plot of $\sqrt{\alpha h\nu}$ vs. photon energy E and a least-squares fit to the straight line obtained from the $f = 75$ Hz spectrum of Fig. 7, yielded an intercept which gave the energy-gap value for germanium [28] $E_G = 0.652$ eV. This value is in agreement with the one previously reported [24, 25].

3 AgCl

Low and Parodi [29] have used a home-made, single-beam, dispersive infrared PA spectrometer constructed from a Perkin-Elmer Model 421 bed and Model 421 or 621 interchange to obtain spectra of several inorganic solids, including AgCl in the 4000–800 cm^{-1} region. The spectra were normalized by that of carbon black and were presented in qualitative units as ratios of PA signals. Other IR spectra studied by these authors include aspirin, polyethylene, sucrose, siloxane, $BaI_2 \cdot 2H_2O$, KNO_4, $CaSO_4$, KBr, MgO, S, Cu_2O, and Ag_2S.

ZnS 4

Welsch *et al.* [26], using the thermoelastic variant of PDS developed by Olmstead *et al.* [27], measured the absorption coefficient of a thin-film of ZnS at 10.6 μm:

$$\alpha_{ZnS} = 0.18 \text{ cm}^{-1}$$

Rosencwaig [30] measured the qualitative gas-cell—microphonic PA spectrum of ZnS and obtained the band-gap value of 3.7 eV, compared with 3.6 eV from specular-reflectance measurements. Ram *et al.* [22] repeated those measurements with the same technique and estimated a value of 3.81 eV at room temperature. The *Handbook of Chemistry and Physics* value of E_G for ZnS is 3.67 eV [31].

ZnSe 5

The optical absorption coefficient of ZnSe has been measured at 10.6 μm by Welsch *et al.* [26] as discussed above, and by Fernelius [32] who fitted gas-cell—microphone PA frequency responses from a ZnSe window with an AR coating to a two-layer extension [33, 34] to the RG theory [9]. The results are

$$\alpha_{ZnSe} = 0.0055 \text{ cm}^{-1} \quad \text{(Thin-film; Welsch et al. [26])}$$

$$\alpha_{ZnSe} = 0.0064 \text{ cm}^{-1} \quad \text{(Bulk laser window; Fernelius [32]).}$$

Fernelius also measured an uncoated CVD ZnSe window [35] using the same technique. He found

$$\alpha_{CVD\text{-}ZnSe} = 4.06 \times 10^{-3} \text{ cm}^{-1}.$$

CdTe 6

The bandgap energy of this semiconductor at room temperature has been measured from the gas-cell microphonic PA spectrum by several investigators:

$$E_G = 1.58 \text{ eV} \quad \text{(Ram } et\ al. \text{ [22])}$$

$$E_G = 1.50 \text{ eV} \quad \text{(Nicolic and Todorovic [36]).}$$

These values compare well with the conventional value [31] of 1.50 eV.

7 GaAs

Microphonic PA measurements in the saturation region of III–V semiconducting GaAs samples lapped by alumina powder and etched by appropriate etchants, were measured by Tokumoto *et al.* [21]. This qualitative spectrum was shown to correlate well with the calculated $1 - R(\lambda)$ spectrum as expected in the optically opaque regime, and yielded the value $E_G = 1.43$ eV. Ikari *et al.* [37] performed piezoelectric PA measurements on 530–139 μm-thick samples of liquid-encapsulated-Czochralski-grown n-GaAs at room temperature. A continuous broad band below 1.35 eV and a peak at 1.383 eV were observed in the amplitude spectrum. The comparison with optical absorption spectra concluded that the broad band was due to the electronic transition involving the EL2 deep-level defect. The same group used the same technique [38] and investigated PA spectra of semi-insulating (SI) and n-type GaAs at 90 K. A distinctive peak at 0.92 eV and a hump near 1.2 eV were observed for these materials. Comparison with optical and electron photoionization spectra concluded that these features were due to electron transitions involving the EL2-level defect. Quantitative spectroscopic results at the 514.5 nm line of the Ar-ion laser photoexciting Si-implanted GaAs were obtained by Zammit *et al.* [39] by fitting their gas-cell—microphonic PA frequency data in the theory by Mandelis *et al.* [33]:

Si^+ implantation dose (cm^{-2})	$\alpha_{514.5}$ (cm^{-1})
5×10^{13}	$(1.17 \pm 0.04) \times 10^5$
1×10^{14}	$(1.23 \pm 0.04) \times 10^5$
1×10^{15}	$(1.42 \pm 0.04) \times 10^5$.

Figure 8 shows the near-bandgap (1.30–1.44 eV) $\alpha(\lambda)$ spectrum of GaAs immersed in cedar oil in order to produce a high signal-to-noise ratio by use of the PDS technique [40].

The optical absorption properties of Cr-doped GaAs crystals were measured at 1200 nm using gas-cell microphonic PAS at 40 Hz [41]. The fundamental absorption edge was found to be at 870 nm. The spectral peak at 1200 nm is well-known to be due to the Cr^{2+} center. The RG model was used for the quantitative results given in terms of α(1200 nm) vs. concentration. An increasing non-linearity with increased Cr content was thus found due to the presence of several Cr states, such as neutral Cr^{3+} and doubly-ionized Cr^+ states besides the Cr^{2+} state. Wasa *et al.* [42] used a piezoelectric ZnO transducer and obtained GaAs spectra in the 0.8–1.3 eV range. The bandgap was determined to be approximately at 0.88 eV and several peaks appeared which were ascribed to light absorption by non-radiative centers within the bandgap, formed by dislocations and Cr impurities. Qualitative piezoelectric PA spectra of molecular-beam-epitaxy (MBE)-grown GaAs lay-

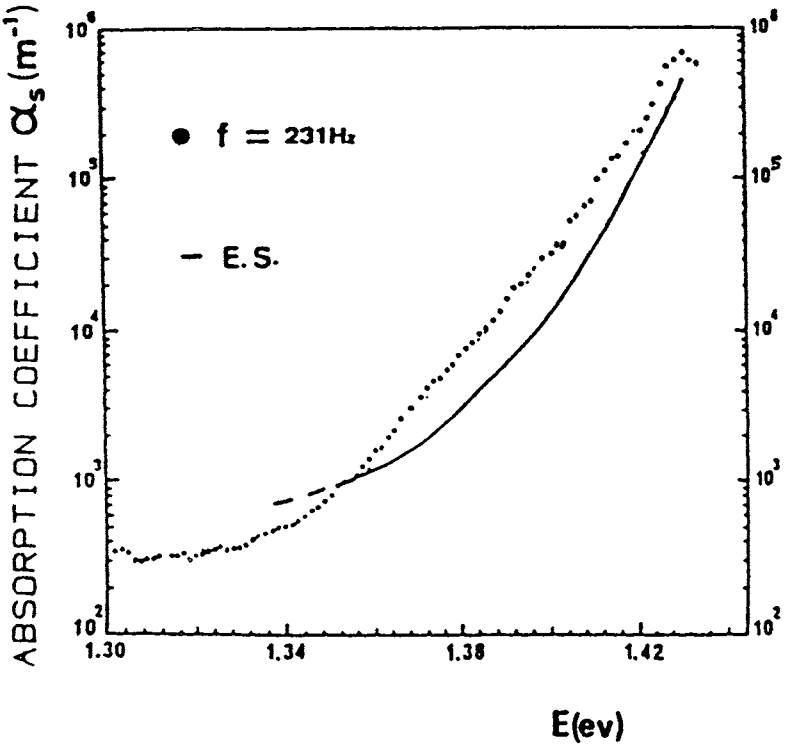

Fig. 8. Optical absorption spectrum of GaAs deduced from PDS data and compared with ellipsometry (E. S.). (From Fournier *et al.* [40] with permission from the publisher.)

ers on GaAs substrates in the photon energy range 1.1–1.5 eV and in the temperature range of 90 to 290 K were produced by Ikari *et al.* [43]. A broad (*D*) band ranging from 0.8 to 1.44 eV with a maximum near 1.3 eV, and a sharp (*Q*) peak at 1.485 eV were observed in the 90 K spectra. These features vanished under secondary illumination. The *D*-band was found to originate in electronic transitions involving EL2-level defects in the GaAs substrate. The *Q*-peak was attributed to electronic transitions from shallow acceptors such as carbon in GaAs.

GaP 8

Qualitative microphonic PA spectra in the saturation regime were obtained by Tokumoto *et al.* [21], showing abrupt changes at 540 nm, which corresponds to the fundamental absorption edge of GaP. This has led to a calculation of the indirect bandgap of GaP at 2.30 eV. For a coarse-powder sample, the indirect bandgap of GaP was measured by Rosencwaig [30] to be

approx. 2.80 eV. Pankove [44] reports 2.30 eV for the GaP bandgap. Fesquet *et al.* [45] used a method of measurement of $\alpha(\lambda)$ of thick GaP based on a simplified version of the RG model, which allowed them to deduce this parameter directly from the PA amplitude signal measurement, irrespective of the light-modulation frequency. The equation for the normalized gas-cell—microphonic PA signal (Cases 1b, 2b, and 2c of the RG model) valid for all optical-absorption-coefficient ranges becomes

$$Q = \frac{\alpha\mu}{[1 + (1 + \alpha\mu)^2]^{1/2}}. \tag{18}$$

Here, normalization is meant with respect to the maximum value Q_s of the PAS signal obtained for high values of α (PA saturation region). Application of Eq. (18) to the PA data yielded the absorption spectrum of Fig. 9. Along with the PAS-deduced spectrum Fig. 9 also shows data (solid line) obtained using ellipsometry in the range between 450 and 550 nm [46]. There is good agreement between the two sets of results in the overlap region 459 nm $\leq \lambda \leq$ 539 nm and for modulation frequencies 90 Hz $\leq f \leq$ 620 Hz. Complementary gas-cell—microphonic PA spectroscopic data were obtained from 0.2–1 mm-thick GaP crystals by Fathallah and Zouaghi [47], in the range 2.1–2.3 eV, and are shown in Fig. 10. These spectra correspond to optical absorption coefficients in the 15–200 cm^{-1} range and could not be obtained with the front-surface-illumination method. The authors used back-surface illumination with the microphone positioned to receive PA signals in the transmission mode, and used the modified RG theory relevant to this type of detection [48].

9 InSb

Tokumoto *et al.* [21] have reported a qualitative PA InSb spectrum obtained by the gas-cell—microphonic method in the PA saturation region, which correlates well with the complement of the conventional reflectance spectrum, 1-$R(\lambda)$, and exhibits three minima corresponding to E_2, $E_1 + \Delta_1$ and E_1 transitions. Baltassare and Cingolani [49] obtained a reflectivity spectrum of InSb from the microphonic PA spectrum. The reflectivity was calculated from the PA signal $Q(\lambda)$ as

$$Q(\lambda)/I_0(\lambda) = 1 - R(\lambda), \tag{19}$$

where I_0 (λ) is the intensity of the incident radiation. These authors quantified the various electronic transitions in InSb at 2.42 eV (E_1'), 2.75 eV (E_1), 3.30 eV (E_2), 4.32 eV (E_3) and 4.80 eV (E_4), all corresponding with optical peaks identified by Piacentini *et al.* [50].

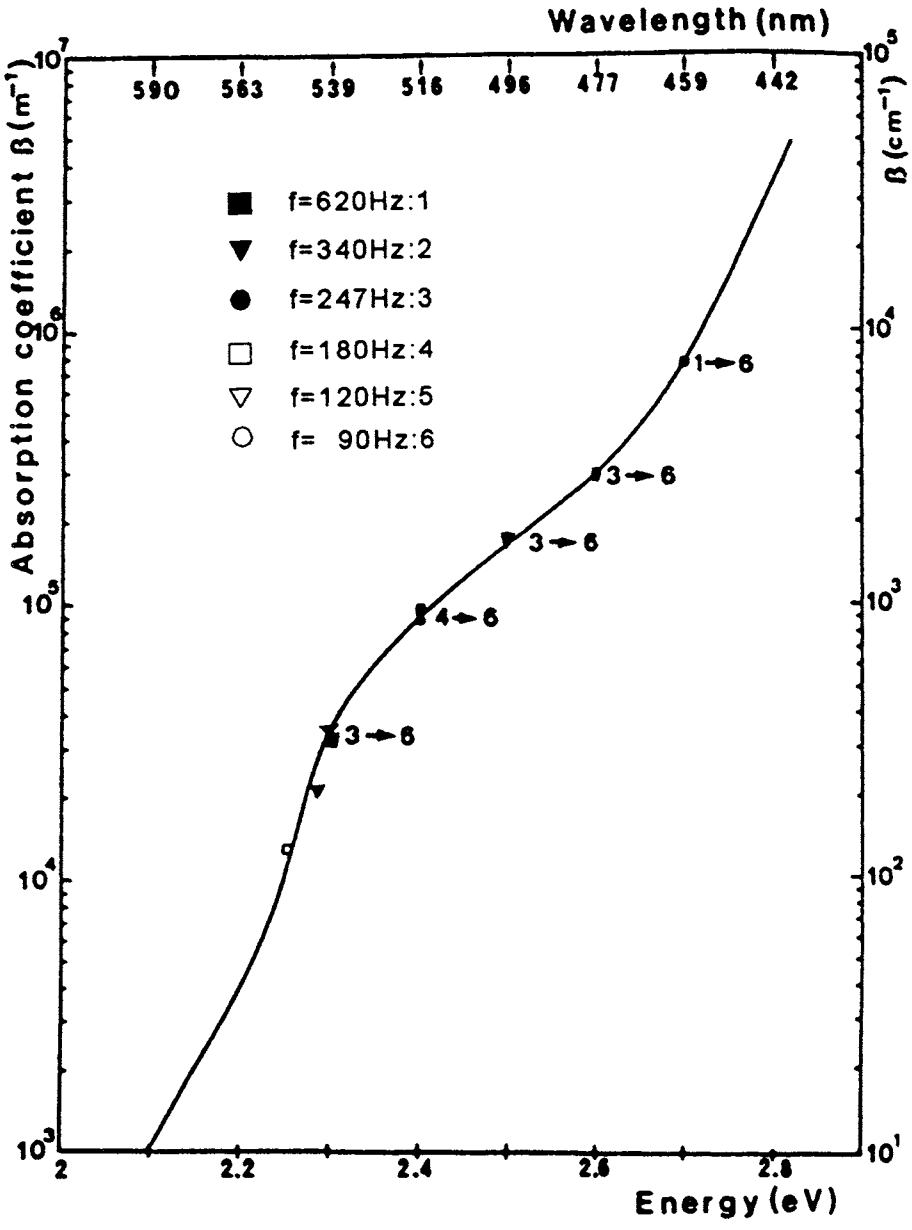

Fig. 9. Experimental results of $\alpha = \beta(\lambda)$ corresponding to various modulation frequencies (1–6) for GaP in the 2.1–2.9 eV range. The $\beta(\lambda)$ curve (solid line) was obtained from optical measurements using ellipsometry. The points on the curve correspond to two light-intensity-modulation frequencies, numbered as shown in the caption. The two unmarked, lowest-absorption-coefficient points correspond to 340 Hz (inverted triange) and 100 Hz (square). Both $\beta(\lambda)$ ordinates are PAS results: the left scale is graded in m^{-1}; the right scale is graded in cm^{-1}. (From Fesquet *et al.* [45] with permission from the publisher.)

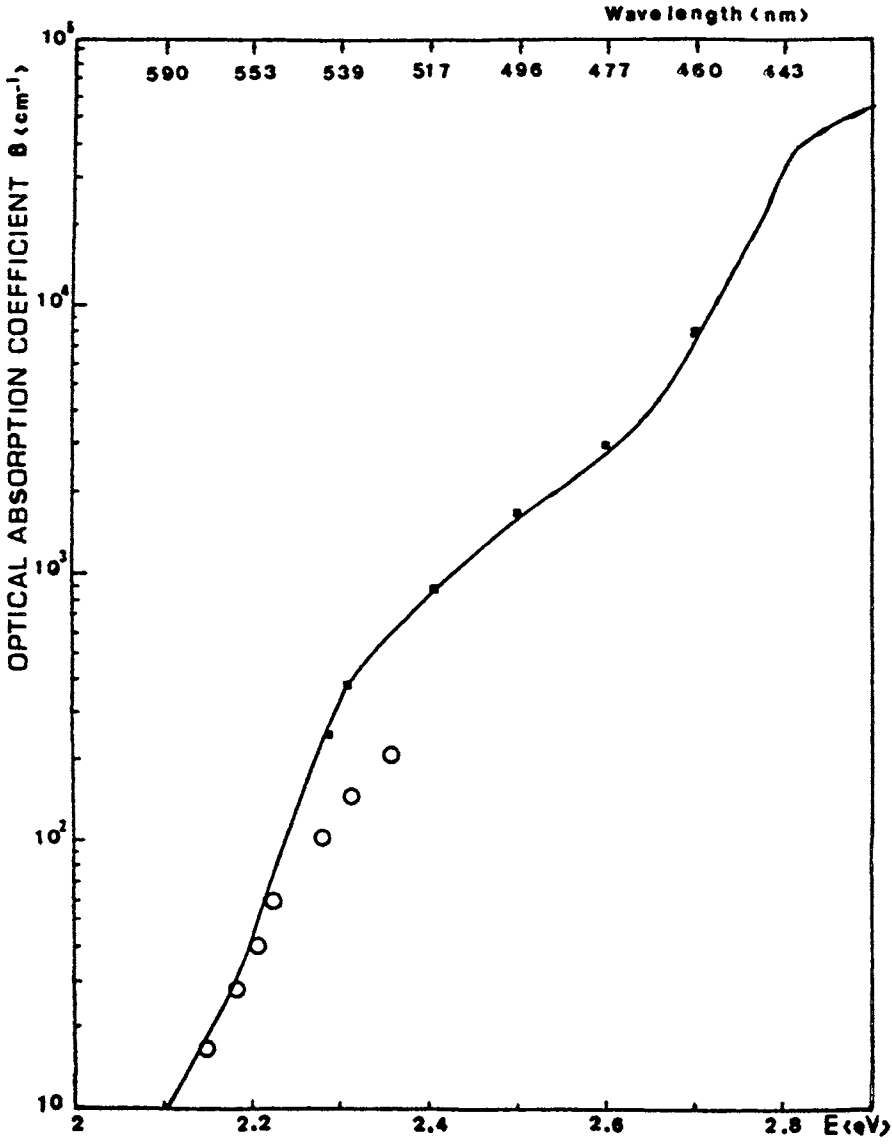

Fig. 10. Optical absorption spectrum $\alpha = \beta(\lambda)$ of GaP obtained by ellipsometry [46] (solid curve); front-side PA detection (■); and reverse-side PA detection (○). (From Fathallah and Zouaghi [47] with permission from the publisher.)

10 InP

Piezoelectric PAS with a PZT transducer was used by Yoshinaga *et al.* [51] to obtain spectra of InP in the range 400–1200 nm and various implantation fluences, including an unimplanted sample. The spectra were qualita-

tive and their shape depended on the optical reflectance as 1-$R(\lambda)$ above the bandgap, where $\alpha \sim 10^4$ cm^{-1}. The band edge yielded the PA value for the bandgap $E_G = 1.34$ eV.

GaSe 11

This material is characteristic of layered semiconductors. The gas-cell microphonic PA spectra of crystalline GaSe have been studied extensively in the neighborhood of the intrinsic absorption edge by Todorovic and Nicolic [36, 52]. The measurements were carried out at room temperature with 100 μm-thick samples. A peak appears in the PA spectrum at 2.02 eV, and the PA signal remains photon-energy independent above that peak. Comparing the results with optical absorption data, the authors concluded that the peak at 2.02 eV is due to formation of excitons. The RG theory was applied to experimental PA data with the absorption coefficient of GaAs given approximately by [52]

$$\alpha(E) = \alpha_0 \frac{\exp[\pi\sqrt{(E - E_G)/E_e}]}{2\sinh[\pi\sqrt{(E - E_G)/E_e}]}, \tag{20}$$

where E_e is the exciton binding energy, and α_0 is the absorption coefficient calculated neglecting Coulomb effects. This equation was fitted to the PA data with E_e being treated as a fitting parameter and E_G being defined by the position of the exciton peak, which is at $E_G - E_e$. The absorption profile of Fig. 11(a) was thus obtained with the following parameters:

$\alpha_0 = 1430$ cm^{-1}; $\quad E_e = 17.5 \pm 0.5$ meV; $\quad E_G = 2.017 \pm 0.003$ eV.

Rochon and Racey [53] measured the optical transmission of two single-crystal GaSe specimens, and also used gas-cell microphonic PAS to measure the near-gap region photoacoustically and compare it to the optical spectrum. They observed that whereas the optical $\alpha(\lambda)$ spectra of the two samples were essentially identical around the band-gap edge, large differences appeared in the (thermally thin) PA spectra. They concluded that the PAS technique is not very appropriate for determining E_G for GaSe, but its usefulness centers around the study of near-gap phenomena, such as impurity states and the Urbach tail.

Ikari *et al.* [54] have studied the piezoelectric PA spectra of p-GaSe at 99, 113 and 295 K. The thickness of the sample was 350 μm, and a sputtered ZnO film transducer was used as the PA detector. A maximum was observed at 2.0 eV at 295 K, in good agreement with the direct-exciton formation [52]. The exciton ground-state ionization energy (Rydberg energy) was estimated to be 19.5 meV. A detailed discussion of low-temperature GaSe spectral features appears in Mandelis [2], Chapter 17, pp. 426–440.

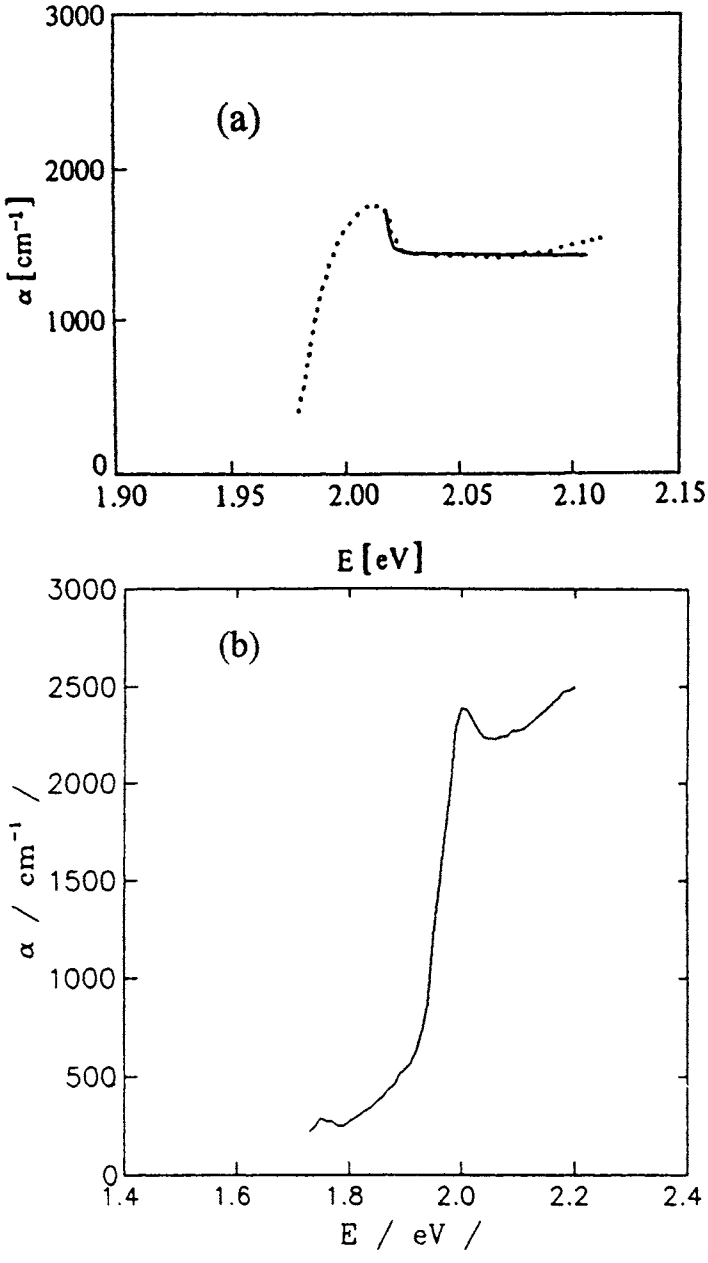

Fig. 11. a) Absorption edge of GaSe: experimental (.....) and theoretical (_____) absorption coefficients; b) Extended $\alpha(\lambda)$ spectrum of GaSe obtained from an analysis of PA amplitude and phase data. (From Todorovic and Nicolic [52] with permission from the publisher.)

Much PAS work has been done in measuring the band-gap energy of the direct semiconductor CdS:

E_G (eV)	T (°C)	Reference	Comments
2.4	Room	[30]	Powder
2.45	Room	[22]	Powder
2.40 ± 0.01	80	[55]	Polycrystalline films
2.35 ± 0.01	240	[55]	"
2.28 ± 0.01	300	[55]	"
2.34 ± 0.01	360	[55]	"
2.37 ± 0.01	470	[55]	"
2.38 ± 0.01	505	[55]	"

These values are to be compared to optically obtained data at room temperature: 2.42 eV [31]; and 2.48 eV [56]. Table I shows the spectral positions of seven states in CdS measured by gas-cell—microphone PAS compared to measurements made with photoconductivity and photoluminescence techniques. Table II shows the locations of the A-, B-, and C-exciton absorption in CdS measured by piezoelectric PAS in the transmission mode ("TPAS") with the transparent $LiNbO_3$ transducer contacting the back of the sample. Comparisons with optical absorption, electroreflectance, and photoconductivity measurements are also given. These tables and detailed discussions on CdS PAS can be found in Mandelis [57].

TABLE I[a]

The Values of Wavelength Corresponding to the Light Absorption Due to Seven States in CdS Measured by Various Methods (units:nm)

	Photoconductivity[b]	Photoluminescence[c]	PAS	Nature
P_1	507.5	—	509	nonradiative
P_2	513.5	514	513	radiative
P_3	517	—	518	nonradiative
P_4	522.5	524	523	radiative
P_5	532	531	534	radiative
P_6	542	—	544	nonradiative
P_7	555	—	554	radiative

[a] K. Wasa, K. Tsubouchi and N. Mikoshiba, *Jpn. J. Appl. Phys.* **19,** L475 (1980).
[b] I. Uchida, *J. Phys. Soc. Jpn.* **22,** 770 (1967).
[c] Obtained by the same sample as that used in PAS measurement.

TABLE II[a]

The Values of Wavelength Corresponding to A, B, C-exciton Absorption in CdS Measured by Various Methods (units:nm)

	Light absorption[b]	Electroreflectance[c]	Photoconductivity[d]	TPAS
A-exciton	501.5	505.7	501.5	506
B-exciton	498.5	502.8	498	503
C-exciton	486.1	491.0	485.5	490

[a] K. Wasa, K. Tsubouchi and N. Mikoshiba, *Jpn. J. Appl. Phys.* **19,** L475 (1980).
[b] E. Gutsche and I. Voigt, "II-VI Semiconducting Compounds," (D. G. Thomas, ed.), p. 337, Benjamin, New York, (1967).
[c] M. Cardona, K. L. Shaklee and F. H. Pollak, *Phys. Rev.* **154,** 696 (1967).
[d] I. Uchida, *J. Phys. Soc. Jpn.* **22,** 770 (1967).

13 CdSe

Powders of CdSe were examined using gas-cell—microphonic PAS [22]. The band gap was calculated to be $E_G = 1.88$ eV compared with 1.74 eV (optical) [31]; 1.75 eV (powder; PAS) [30]) and 1.8 eV (optical) [44].

14 CuO

Toyoda and co-workers have made extensive gas-cell—microphone PA spectroscopic measurements of Cu and its various oxides (including the semiconducting CuO) in the X-ray absorption, near-edge structure (XANES) regions using synchrotron radiation. These spectra are not directly comparable with existing data in *HOC I* or *II,* but they represent novel PAS applications in spectral regions hereto uncharted. These spectra were compared to optical-density X-ray spectroscopy in the 8.95–9.10 keV range [58]. The two sets of spectra were similar; however, the results showed that the increase and changes of the PAS-signal detailed structure at the XANES region were different from those of the X-ray absorption coefficient. Other Cu compounds studied by these authors included Cu_2O and pure Cu metal.

15 As_2S_3

Tanaka *et al.* [59] have utilized PPES in the thermally thin limit of the MZ model, with experimental data obtained using a PVDF thin-film transducer, thin-transparent CuI electrodes and an amorphous As_2S_3 film sample. The $\alpha(\lambda)$ spectrum thus obtained is shown in Fig. 12. A comparison with

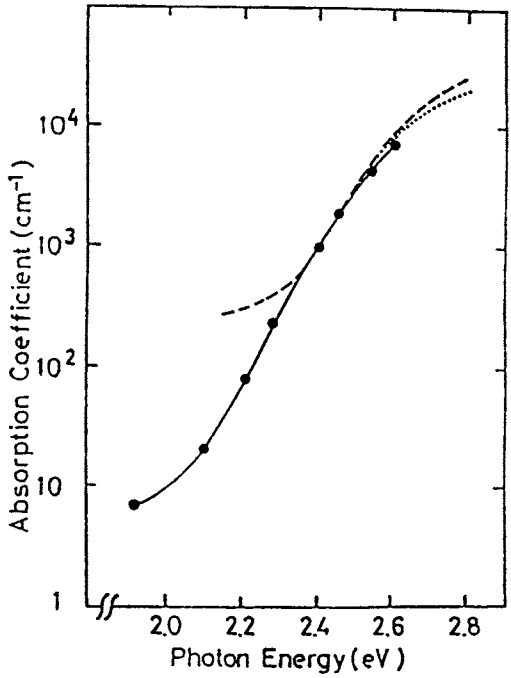

Fig. 12. Spectral dependence of the absorption coefficient of evaporated As_2S_3 films, measured with PPES (solid line). For comparison, results obtained by thermocouple photothermal spectroscopy (dashed line) and by conventional transmission spectroscopy (dotted line) are also shown. (From Mandelis [2] with permission from the publisher.)

conventional transmission spectroscopy and with thermocouple photothermal spectroscopy (PTS) is also shown in Fig. 12. It is seen that the dynamic range of PPES ($\sim$10 cm^{-1}) is superior to the conventional spectroscopies, giving reliable results down to 1.9 eV photon energy. The transmission technique yielded reproducible results for $\alpha \geq 5 \times 10^3$ cm^{-1}, and PTS had a higher dynamic range of $\alpha \geq 5 \times 10^2$ cm^{-1}. A qualitative gas-cell—microphone PA spectrum of a layered single-crystal As_2S_3 sample was also presented by Nicolic and Todorovic [36]. From the "knee" of the spectrum these authors calculated the bandgap energy $E_G = 2.65$ eV.

Tanaka *et al.* [60] employed a $LiTaO_3$ pyroelectric crystal transducer and CuI electrodes to produce the PPE absorption spectrum of the annealed amorphous semiconductor As_2S_3 shown in Fig. 13. This configuration was used instead of a PVDF transducer so as to withstand annealing temperatures of the samples at approximately 180°C. The difference in the absorption edge between the annealed and the illuminated state at 300 K corresponds to the so-called reversible photodarkening effect [60].

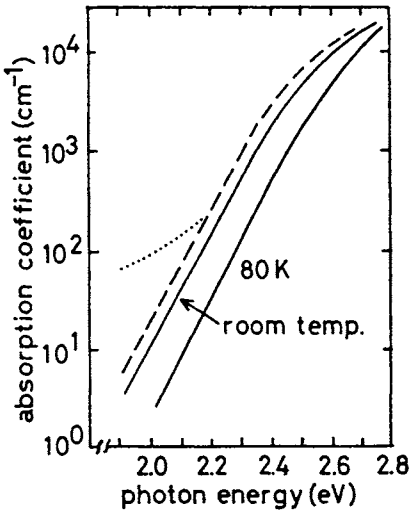

Fig. 13. The optical absorption edges of an annealed As_2S_3 film at room temperature and 80 K (solid lines). The characteristics at room temperature after illumination (dashed line) and under illumination (dotted line) are also shown. (From Tanaka *et al.* [60] with permission from the publisher.)

16 Se

Tanaka *et al.* [60] employed a 9-μm-thick PVDF film transducer to produce PPE spectra of amorphous Se. Figure 14 shows the resulting $\alpha(\hbar\omega)$ spectrum in the optical gap region, overlapping the Urbach tail represented by

$$\alpha \propto \exp(\Gamma\hbar\omega), \tag{21}$$

where Γ is the steepness parameter [61]. Figure 14 also shows the results obtained by Ceasar *et al.* [62] using the gas-cell—microphonic PAS technique. The high-energy end of the Urbach tails agree between these two sets of data, with the PPES technique exhibiting sensitivity of $\alpha L \geq 10^{-2}$. The PPE spectra in the $\leq$ 1.8 eV region deviate from the Urbach tail, because they are due to stray absorptions in the pyroelectric sensor.

Ram *et al.* [22] have measured qualitative PA spectra of powdered Se at room temperature. They found the bandgap energy to be E_G = 1.85 eV to be compared to the optical value of 1.80 eV [63].

17 $Ga_{1-x}Al_xAs$

In this case, and others involving multilayered structures, photothermal investigations have led to the determination of both the substrate *and* the film. The major rival methodology is ellipsometry, which is very convenient

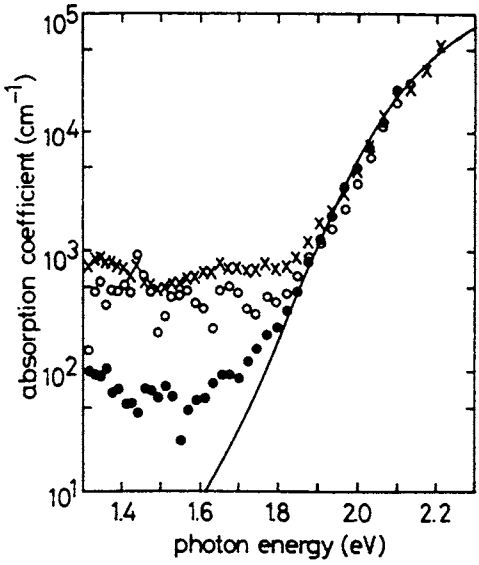

Fig. 14. The optical absorption edge of amorphous Se evaluated with PPES and from a PAS measurement (solid line). The PPES data are given for film thicknesses of 1.43 μm (•); 0.96 μm (○); and 0.74 μm (×). (From Tanaka *et al.* [60] with permission from the publisher.)

for monitoring the growth process of films, as polarized light is mainly sensitive to both the film thickness and the real part of the refractive index. Nevertheless, for low absorptions photothermal methods exhibit higher sensitivity [40]. Fournier and Boccara [40] and Yacoubi [64] utilized the two-layer theory of the PA/PT effect [33, 34] along with PDS-derived spectroscopic data from substrate GaAs to obtain the quantitative $\alpha(\lambda)$ spectrum of $Ga_{1-x}Al_xAs$ films deposited on GaAs. x is the mole-fraction of Al in the ternary GaAlAs alloy-semiconductor crystal matrix. The results are shown in Fig. 15.

Kubota *et al.* [65] measured the qualitative piezoelectric PA spectra of epitaxial layers (1.5 μm) of $Ga_{1-x}Al_xAs$ on GaAs wafers (300 μm). The incident light impinged on the epitaxial layer, and the PZT transducer was attached to the GaAs substrate. A steep rise of the PA signal at 1.42 eV due to the direct band-to-band transition of GaAs, as well as a less sharp decrease around 1.90 eV was observed. This energy is nearly equal to the indirect transition edge of $Ga_{1-x}Al_xAs$. Therefore, it was found by means of PZT PAS that $E_{G,GaAlAs}^{indirect} \approx 1.90$ eV for both $x = 0.25$ and 0.3.

a-Si 18

Quantitative $\alpha(\lambda)$ spectra of amorphous Si abound in the photothermal literature. Amer and Jackson [66] presented a detailed discussion on the appli-

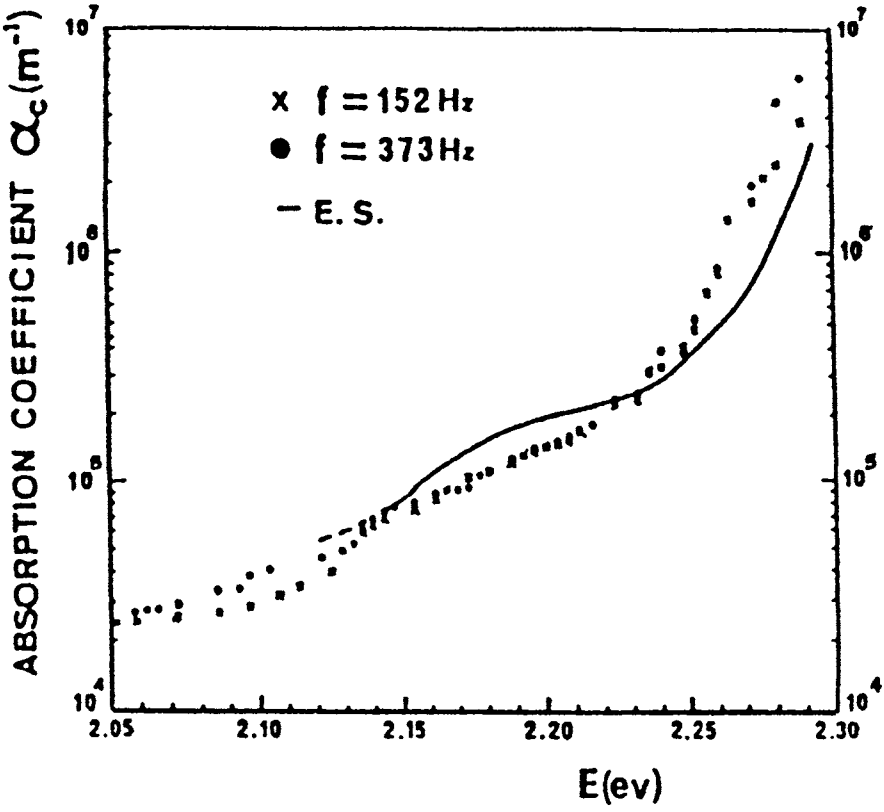

Fig. 15. Optical absorption spectrum of $Ga_{1-x}Al_xAs$ obtained using PDS data; x is the mole-fraction of Al in the ternary alloy semiconductor. The solid line is the spectrum obtained for comparison with the ellipsometric technique (E. S.). (From Fournier and Boccara [40] with permission from the publisher.)

cability of PDS to the measurement of the optical absorption coefficient of a-Si thin films under a variety of growth conditions. The advantage of photothermal techniques, such as PDS, is in the low-α region of the thin-film spectrum, where the film is entirely thermally thin and optically transparent: In this limit, the PDS signal is simply given by

$$< S(\lambda)/S_{\text{sat}} > = 1 - \exp[-\alpha_f(\lambda)\ell], \tag{22}$$

which gives the thin-film absorptance for an incoherent pump source. In Eq. (22) $< >$ denotes averaging of the interference fringes on a logarithmic scale, and S_{sat} is the saturated PDS signal obtained in the high-α region. Figures 16–20 are quantitative PDS spectra of a-Si in the 0.5 eV–2.0 eV range, measured by Amer and Jackson and their co-workers [67–70]. Figure 16 shows the effect of substrate temperature on the optical absorption spectrum: The sub-gap absorption is lowest for material deposited at 230°C and

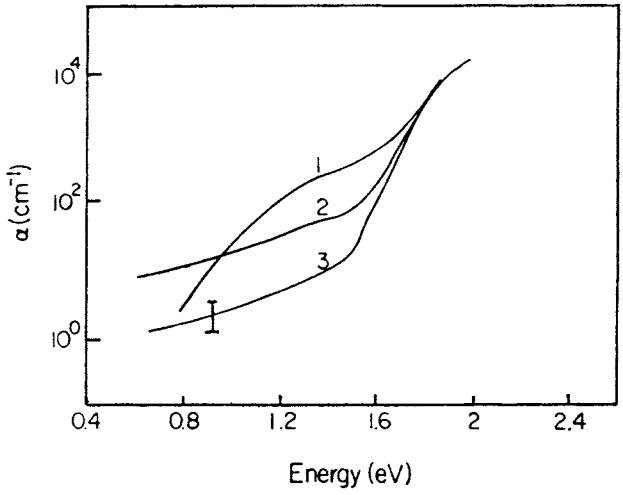

Fig. 16. The substrate temperature dependence of gap-state absorption (undoped a-Si): (1): 100°C; (2): 330°C; (3): 230°C. (From Jackson and Amer [67] with permission from the publisher.)

increases for both lower and higher deposition temperatures. The effect on $\alpha(\lambda)$ of increasing film-deposition power density on the sub-gap absorption for a constant substrate temperature is shown in Fig. 17. The shoulder which appears in the 1.25 eV range is due to large defect densities in the high-deposition power a-Si films. The effects of single doping are shown in Fig. 18. The $\alpha(\lambda)$ spectra for various phosphorus doping levels are shown in

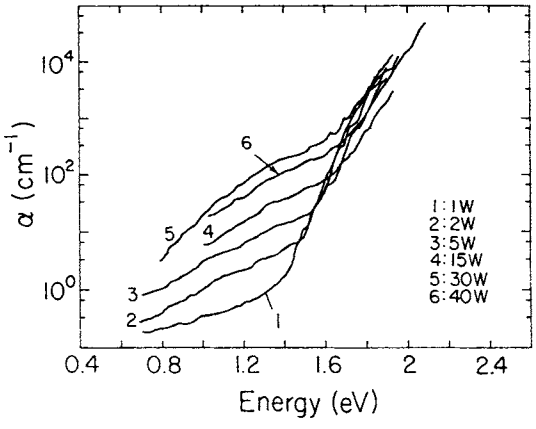

Fig. 17. The dependence of gap-state absorption on deposition power (undoped material). (1): 1 W; (2): 2 W; (3): 5 W; (4): 15 W; (5): 30 W; and (6): 40 W. (From Jackson and Amer [68] with permission from the publisher.)

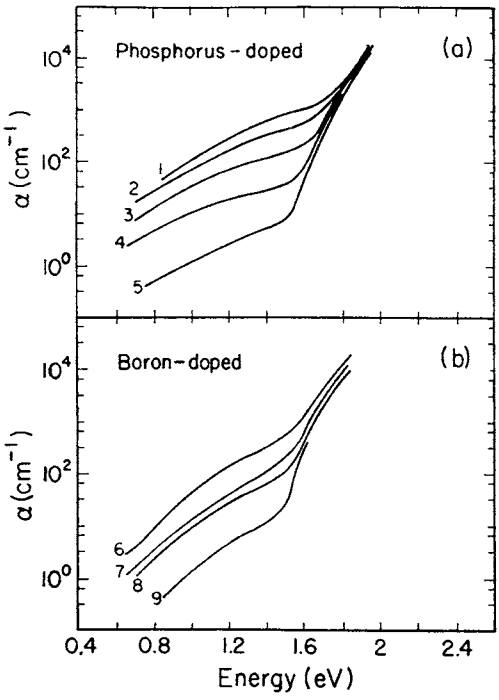

Fig. 18. The dependence of gap-state absorption on the type and level of doping. (a) PH_3 doping concentration: (1): 10^{-2}; (2): 10^{-3}; (3): 3×10^{-4}; (4): 10^{-5}; and (5): 10^{-6}. (b) B_2H_6 doping concentration: (6): 10^{-3}; (7): 3×10^{-4}; (8): 10^{-4}; and (9): 10^{-5}. All doping concentrations refer to gas-phase concentration. Substrate temperature is 230°C, and the rf deposition power is 2 W. (From Jackson and Amer [68] with permission from the publisher.)

Fig. 18a. The gap-state absorption increases and the Urbach edge broadens as the *P*-concentration is increased. Figure 18(b) shows that boron-doping has a similar qualitative effect on the absorption spectrum. The results of Figs. 16–18 demonstrate that the optical absorption coefficient of a-Si thin films is highly sensitive to doping and deposition conditions. The number of defects can be estimated by separating the sub-gap defect absorption from the exponential band-tail absorption [68]. The excess optical absorption α_{ex} due to gap-state defect absorption is given by:

$$\alpha_{ex}(E) = \alpha - \alpha_0 \exp\left(\frac{\hbar\omega}{E_0}\right), \tag{23}$$

where a_0 and E_0 are obtained from a fit to the exponential absorption. The defect number density is related to the sub-gap optical absorption by [66]:

$$N_s = 7.9 \times 10^{15} \int \alpha_{ex}(E)\, dE. \tag{24}$$

By combining Eq. (24) with the PDS results of a thickness-dependence study [69], it was found that for low-defect a-Si the film surface (or its interface with the substrate) has a defect density of $\sim 10^{22}$ cm^{-2} dangling bonds, (see Fig. 19). The absorption spectra are consistent with a defective surface layer of $\sim$ 5 nm thickness and is similar to that obtained from the highly defective bulk a-Si:H. Figure 20 shows the effect of illumination with broad-band light on the gap-state absorption of an undoped a-Si sample. The spectra show a clear and reproducible enhancement in the gap-state absorption coefficient after illumination. Annealing at 150°C in the dark restores the magnitude of $\alpha(\lambda)$ to its original value [70]. By using Eq. (24), the density and energy position of the optically induced defects can be determined.

Amato *et al.* [71] have introduced a new method for determining the surface-state absorption in a-Si thin films, based on the enhancement of the interference fringe amplitude in PDS spectra due to the presence of surface states in the region below 1.5 eV.

Ceasar *et al.* [72] have used gas-cell—microphone PAS to estimate the density of defect states responsible for the sub-gap tail of $\alpha(\lambda)$ of a-Si:H thin films prepared by ion-beam deposition. The values of α measured by PAS were found to be complimentary to those estimated by optical transmission and lay further toward the low-absorption, infrared region, down to

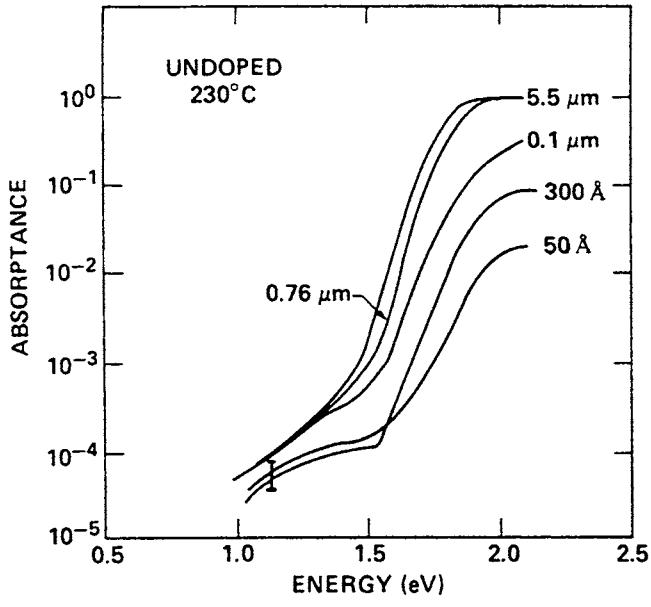

Fig. 19. Thickness dependence of the absorption coefficient in undoped a-Si at 230°C. (From Jackson *et al.* [69] with permission from the publisher.)

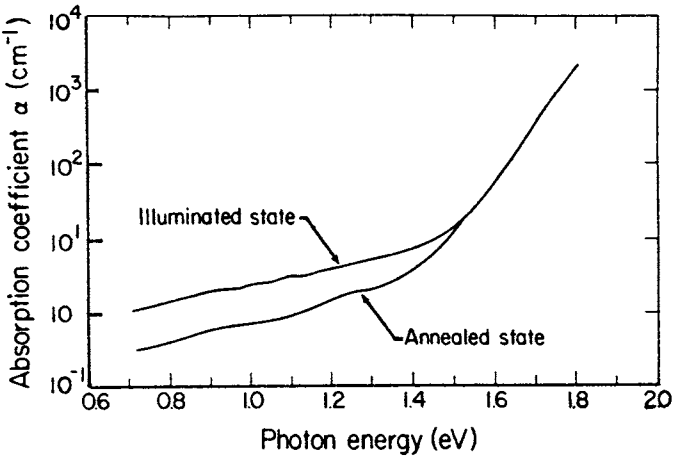

Fig. 20. The effect of illumination on the absorption spectrum of undoped a-Si:H. (From Amer *et al.* [70] with permission from the publisher.)

0.4 eV (see Fig. 21). The extension of the $\alpha(\hbar\omega)$ dynamic range to this sub-gap regime is a clear advantage of photothermal-based spectroscopies over purely optical techniques. Yamasaki [73] has also performed gas-cell—microphonic PAS studies of undoped hydrogenated a-Si as a function of the ambient temperature, the deposition temperature and the post-annealing temperature. The resulting absorption-coefficient spectra were determined between 2.0 and 0.6 eV and were of similar quality to those derived by Amer and Jackson [66]. Amato *et al.* [74] investigated the optical absorption coefficient of low-pressure, chemical-vapor-deposition (LPCVD) a-Si:H by using a combination of analytical techniques: Optical spectroscopy for the above-bandgap transitions, PAS in the sub-gap range, and the constant photocurrent method (CPM) in both regions. Differences in sensitivity to surface states and to inhomogeneities in the material along the growth axis were found. Figure 22 shows those differences between PAS and CPM spectroscopic measurements of $\alpha(\hbar\omega)$. Based on these spectra, a simple growth-kinetic model suggested that the growth kinetics could change during the film-deposition process. Ishiguro and Tokumoto [75] also reported on the improved resolution and accuracy of gas-cell—microphonic PA spectra from undoped and doped a-Si thin films over optical transmission data (see Fig. 23). The spectral photon-energy ranges were > 0.5 eV, similar to those studied by Ceasar *et al.* [72]. Tanaka [76] gives a detailed discussion on the physics behind the variations of the optical absorption coefficients of amorphous semiconductor thin-films as measured by photothermal spectroscopies.

More recently, PPES has been applied to the quantitative simultaneous measurement of two important spectroscopic parameters of amorphous Si thin-films: the optical absorption coefficient and the nonradiative quantum

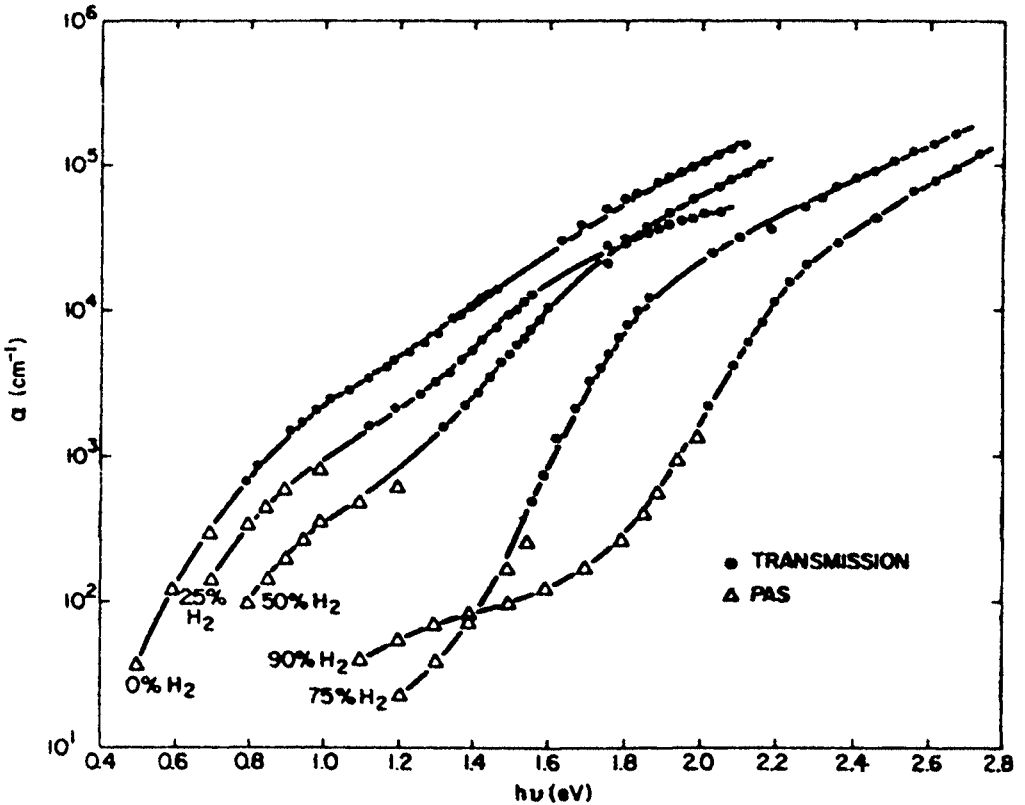

Fig. 21. Optical absorption-coefficient spectra for a-Si:H films made with ion beams of various H_2 compositions. (From Ceasar *et al.* [72] with permission from the publisher.)

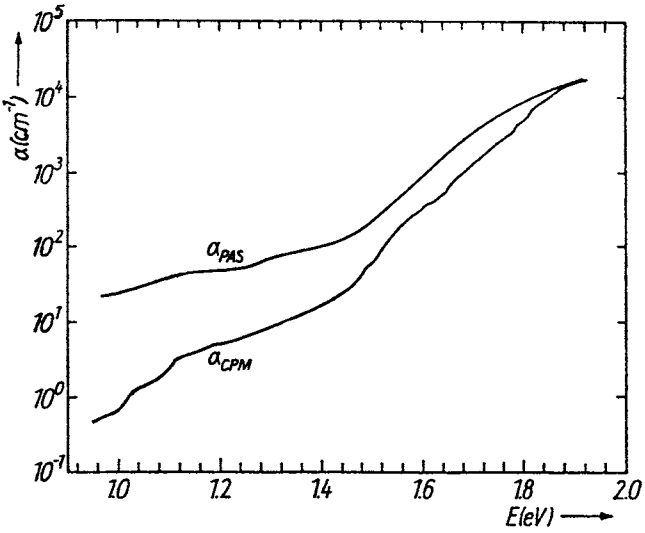

Fig. 22. Optical absorption-coefficient spectra obtained by means of PAS and CPM on a typical LPCVD a-Si:H sample. (From Amato *et al.* [74] with permission from the publisher.)

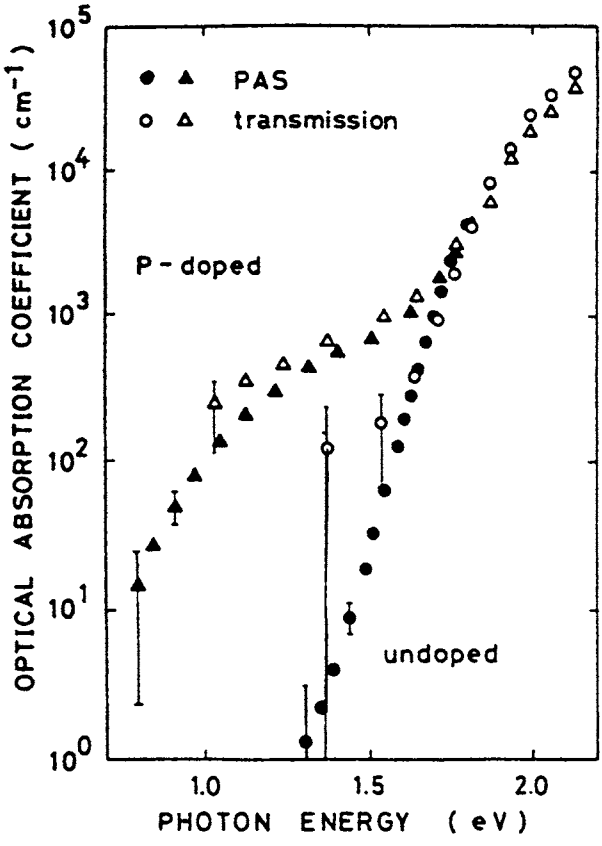

Fig. 23. Comparison of optical absorption-coefficient spectra obtained by the optical transmission method and PAS, for undoped and doped a-Si thin films. (From Ishiguro and Tokumoto [75] with permission from the publisher.)

efficiency [77]. As a back-surface (thermal-wave transmission) detection technique, PPES can be used to measure the absorption-coefficient spectrum in the thermally thick configuration of Eq. (17), whereas it can measure the optical-to-thermal energy conversion efficiency spectrum in the thermally thin configuration of Eq. (16). Based on this feature of PPES, Mandelis *et al.* [77] and Fan and Kakalios [78] obtained both spectra for a-Si:H samples for photon energies from 0.8 eV to 2.5 eV. This technique yielded a sensitivity of $\alpha\ell > 10^{-3}$, where ℓ is the thin-film thickness. This is of the same order as PDS with similar quality $\alpha(\hbar\omega)$ spectra. Unlike PDS, no coupling fluid is necessary (see Chapter 4 by Briggs in this volume), and the experimental geometry is simpler, enabling easy measurement of α as a function of temperature.

ZnO 19

Qualitative PA spectra of ZnO powders were measured by Ram *et al.* [22]. These authors reported the room-temperature bandgap energy of the powders as $E_G = 3.46$ eV, to be compared to 3.20 eV for the solid crystalline ZnO reported earlier [31] by means of optical spectroscopy. Toyoda *et al.* [79] measured the hard-X-ray spectrum of ZnO thin films in the EXAFS (extended X-ray absorption fine structure) region using synchrotron radiation (9.35–10.35 keV) and gas-cell—microphone PAS detection in the thermally thin limit (23–45 Hz). These spectra reflect the heat-production processes in radio-frequency-sputtered ZnO thin layers (~7 μm-thick), which exhibit oscillatory behavior with a peak at 9.95 keV. More work needs to be done to quantify these deep-energy-level features. The same group [80] performed photothermal studies of the optical spectral range, around the band-gap energy of ZnO thin films (2.6–3.4 eV). These spectra were obtained using a thermistor in contact with the sample (PTS). By ratioing the PTS signal to the absorptance 1-*T*-*R* (*T*: transmittance; *R*: reflectance) spectrum, Toyoda and Okonagi [80] showed that the mechanism for heat generation is different from the total rate of optical energy absorption below the fundamental absorption edge. It is this author's opinion that the interpretation of these phenomena may rest with the behavior of the nonradiative quantum-efficiency spectrum.

SnS 20

Nicolic and Todorovic [81] produced the microphonic PA spectrum of a prismatically shaped single crystal of SnS of 0.3 mm-thickness. The value of the bandgap energy was calculated from the spectrum to be $E_G \approx 1.24$ eV. A PA minimum at 0.85 μm (1.46 eV) was also observed, an ill-understood effect of the specific band structure of SnS. The fundamental direct energy gap of 1.5 eV was also measured from an abrupt drop of the PAS signal.

This feature was found to be in good agreement with a photovoltaic-effect spectrum [82].

21 InSe

This layered semiconductor belongs to the same family as GaSe; it is photosensitive, and is used for photovoltaic energy-converter device fabrication. Ikari *et al.* [83] have studied the piezoelectric PA spectra of 470-μm- and 115-μm- thick crystal of InSe extensively, both at room temperature and at 116 K, using a ZnO transducer. They discovered two peaks at 1.250 and at 1.212 eV at room temperature. The energy and the temperature variation of the 1.250 peak were well explained in terms of a free-exciton ($n = 1$) annihilation. The other peak was interpreted as a surface-state-related transition. These authors found that the optical absorption spectrum of InSe correlates well with the intensity of the PA spectrum in the near-band-gap region ($\sim$1.2 eV at room temperature), but no quantitative photoacoustic/photothermal measurement of $\alpha(\lambda)$ has been presented in the literature for InSe.

22 $GeSe_2$

This layered semiconductor can be grown in the form of a single crystal similar to GaSe and InSe. Nicolic and Todorovic [36] have estimated the bandgap energy from the gas-cell microphonic PA spectrum to be at $E_G \approx$ 2.53 eV.

ACKNOWLEDGMENTS

The author wishes to acknowledge the continuing support of the Natural Sciences and Engineering Research Council of Canada (NSERC) through multiple sustained Research Grants and an ongoing Collaborative Research Grant with Professor H. Ruda, which made partially possible his laboratories' contributions described in this chapter.

REFERENCES

1. A. Rosencwaig, "Photoacoustics and Photoacoustic Spectroscopy." Wiley, New York, 1980.
2. A. Mandelis, ed., "Photoacoustic and Thermal Wave Phenomena in Semiconductors." North-Holland Publ., New York, 1987.
3. J. A. Sell, ed., "Photothermal Investigations of Solids and Fluids." Academic Press, San Diego, 1989.
4. P. Hess, ed., "Photoacoustic, Photothermal and Photochemical Processes at Surfaces and Thin Films." Springer-Verlag, Heidelberg, 1989.
5. A. Mandelis, ed., "Progress in Photothermal and Photoacoustic Science and Technology, Volume I, Principles and Perspectives of Photothermal and Photoacoustic Phenomena." Elsevier, New York, 1992; A. Mandelis, ed., "Progress in Photothermal and Photoacoustic

Science and Technology, Volume II, Non-Destructive Evaluation." PTR Prentice-Hall, Englewood Cliffs, New Jersey, 1994; A. Mandelis and P. Hess, eds., "Progress in Photothermal and Photoacoustic Science and Technology, Volume III, Life and Earth Sciences." SPIE Publ., Bellingham, Washington, 1997.
6. D. P. Almond and P. M. Patel, "Photothermal Science and Techniques." Chapman & Hall, London, 1996.
7. S. E. Bialkowski, "Photothermal Spectroscopy Methods for Chemical Analysis." Wiley, New York, 1996.
8. J. G. Parker, *Appl. Opt.* **12**, 2974 (1973).
9. A. Rosencwaig and A. Gersho, *J. Appl. Phys.* **47**, 64 (1976).
10. R. M. White, *J. Appl. Phys.* **34**, 3559 (1963).
11. W. Jackson and N. M. Amer, *J. Appl. Phys.* **51**, 3343 (1980).
12. T. Ikari, S. Shigetomi, and Y. Koga, *in* "Photoacoustic and Thermal Wave Phenomena in Semiconductors," A. Mandelis, ed., Chap. 16, pp. 404–406. North-Holland Publ., New York, 1987.
13. T. Hata, Y. Sato, Y. Nagai, and T. Hada, *Jpn. J. Appl. Phys. Suppl.* **23-1**, 75 (1984).
14. J. Cooper, *Rev. Sci. Instrum.* **33**, 92 (1962).
15. A. Mandelis and M. M. Zver, *J. Appl. Phys.* **57**, 4421 (1985).
16. E. H. Putley, *in* "Semiconductors and Semimetals." (R. K. Willardson and A. C. Beer, eds.), Vol. 5, p. 259. Academic Press, New York, 1970.
17. M. Chirtoc and G. Mihailescu, *Phys. Rev. B* **40**, 9606 (1989).
18. H. Coufal, *Appl. Phys. Lett.* **45**, 516 (1984).
19. A. Mandelis, *Chem. Phys. Lett.* **108**, 388 (1984).
20. A. C. Boccara and D. Fournier, *in* "Progress in Photothermal and Photoacoustic Science and Technology, Volume I, Principles and Perspectives of Photothermal and Photoacoustic Phenomena," A. Mandelis, ed., Chap. 1. Elsevier, New York, 1992.
21. H. Tokumoto, M. Tokumoto, and T. Ishiguro, *J. Phys. Soc. Jpn.* **50**, 602 (1981).
22. R. S. Ram, O. M. Prakash, and A. N. Pandey, *Pramana* **28**, 293 (1987).
23. C. Christofides, A. Engel, and A. Mandelis, *Ferroelectrics* **118**, 411 (1991).
24. S. M. Sze, "Physics of Semiconductor Devices," Chap. 2. Wiley(Interscience), New York, 1969.
25. P. Kirev, "The Physics of Semiconductors," Chap. 8. Mir, Moscow, 1975.
26. E. Welsch, H.-G. Walther, K. Friedrich, and P. Eckardt, *J. Appl. Phys.* **67**, 6575 (1990).
27. M. A. Olmstead, N. M. Amer, S. Kohn, D. Fournier, and A. C. Boccara, *Appl. Phys. A* **32**, 141 1983.
28. C. Christofides, A. Mandelis, K. Ghandi, and R. Wagner, *Rev. Sci. Instrum.* **61**, 2360 (1990).
29. M. J. D. Low and G. A. Parodi, *J. Photoacoust.* **1**, 131 (1982).
30. A. Rosencwaig, *Anal. Chem.* **47**, 592A (1975).
31. R. C. Weast, ed., "CRC Handbook of Chemistry and Physics." CRC Press, Cleveland, Ohio, 1977.
32. N. C. Fernelius, "Proceedings on Laser Induced Damage in Optical Materials: 1979," p. 301. NIST, Gaithersburg, Maryland, 1980.
33. A. Mandelis, Y. C. Teng, and B. S. H. Royce, *J. Appl. Phys.* **50**, 7138 (1979).
34. N. C. Fernelius, *J. Appl. Phys.* **51**, 650 (1980).
35. N. C. Fernelius, "Proceedings on Laser Induced Damage in Optical Materials: 1981," p. 129. NIST, Gaithersburg, Maryland, 1983.
36. P. M. Nicolic and D. M. Todorovic, *Prog. Quantum Electron.* **13**, 107 (1989).
37. T. Ikari, K. Miyazaki, A. Fukuyama, H. Yokoyama, K. Maeda, and K. Futagami, *J. Appl. Phys.* **71**, 2408 (1992).
38. A. Fukuyama, T. Ikari, K. Miyazaki, K. Maeda, and K. Futagami, *Jpn. J. Appl. Phys. Suppl.* **31-1**, 20 (1992).
39. U. Zammit, M. Marinelli, F. Scudieri, and S. Martelucci, *Appl. Phys. Lett.* **50**, 830 (1987).

40. D. Fournier and A.C. Boccara, *in* "Photoacoustic and Thermal Wave Phenomena in Semiconductors," (A. Mandelis, ed.), Chap. 10, p. 247. North-Holland Publ., New York, 1987; D. Fournier and A. C. Boccara, *Mater. Sci. Eng.* **B5,** 83 (1990).
41. H. Tokumoto and T. Ishiguro, *Jpn. J. Appl. Phys. Suppl.* **22-3**, 202 (1983).
42. K. Wasa, K. Tsubouchi, and N. Mikoshiba, *Jpn. J. Appl. Phys.* **19**, L636 (1980).
43. T. Ikari, A. Fukuyama, K. Maeda, K. Futagami, S. Shigetomi, and Y. Akashi, *Phys. Rev. B* **46**, 10 173 (1992-II).
44. J. I. Pankove, "Optical Processes in Semiconductors." Prentice-Hall, New York, 1971.
45. J. Fesquet, B. Girault, and M. D. M. Razafindrandriatsimaniry, *Appl. Opt.* **23**, 2784 (1984).
46. D. E. Aspnes and A. A. Studna, *Phys. Rev. B* **27**, 123 (1983).
47. M. Fathallah and M. Zouaghi, *Solid State Commun.* **54**, 317 (1985).
48. R. Takaue, M. Matsunaga, and K. Hosokawa, *J. Appl. Phys.* **56**, 1543 (1984).
49. L. Baltassare and A. Cingolani, *Solid State Commun.* **44**, 705 (1982).
50. M. Piacentini, E. Doni, R. Girlanda, V. Grasso, and A. Balzarotti, *Nuovo Cimento B* **54**, 269 (1979).
51. H. Yoshinaga, J. Kawai, T. Agui, F. Uehara, and T. Matsumori, *Nucl. Instrum. Methods Phys. Res. B* **80/81**, 591 (1993).
52. D. M. Todorovic and P. M. Nicolic, *Appl. Opt.* **24**, 2252 (1985).
53. P. Rochon and T J. Racey, *J. Photoacoust.* **1**, 475 (1983–1984).
54. T. Ikari, S. Shigetomi, Y. Koga, and S. Shigetomi, *Rev. Sci. Instrum.* **57**, 17 (1986).
55. O. Zelaya-Angel, J. J. Alvarado-Gil, R. Lozada-Morales, H. Vargas, and A. Ferreira da Silva, *Appl. Phys. Lett.* **64**, 291 (1994).
56. A. F. Gibson, "Progress in Semiconductors," Vol. 3. Haywood, London, 1958.
57. A. Mandelis, *in* "Photoacoustic and Thermal Wave Phenomena in Semiconductors," A. Mandelis, ed., Chap. 15, pp. 353–395. North-Holland Publ., New York, 1987.
58. T. Toyoda, T. Masujima, H. Shiwaku, and M. Ando, *Jpn. J. Appl. Phys. Suppl.* **30-1**, 274 (1991); T. Toyoda, T. Masujima, H. Shiwaku, and M. Ando, *Appl. Phys. Lett.* **59**, 3657 (1991).
59. K. Tanaka, K. Sindoh, and A. Odajima, *Rep. Progr. Polymer Phys. Jpn.* **29**, 367 (1986).
60. K. Tanaka, Y. Ichimura, and K. Sindoh, *J. Appl. Phys.* **63**, 1815 (1988).
61. N. F. Mott and E. A. Davis, "Electronic Processes in Non-Crystalline Materials," Sections 6,9, and 10. Oxford Univ. Press (Clarendon), Oxford, 1979.
62. G. P. Ceasar, M. Abkowitz, and J. W.-P. Lin, *Phys. Rev. B* **29**, 2353 (1984).
63. R. A. Smith, "Semiconductors." Cambridge Univ. Press, London, 1968.
64. N. Yacoubi, Ph.D. Thesis, University of Montpellier, France (1986).
65. K. Kubota, H. Murai, and H. Nakatsu, *J. Appl. Phys.* **55**, 1520 (1984).
66. N. M. Amer and W. B. Jackson, *in* "Semiconductors and Semimetals: Hydrogenated Amorphous Silicon; Optical Properties," (J. I. Pankove, ed.), Vol. 21, Chap. 3. Academic Press, Orlando, Florida, 1984.
67. W. B. Jackson and N. M. Amer, *J. Phys. Colloq.* **42**, C4-293 (1981).
68. W. B. Jackson and N. M. Amer, *Phys. Rev. B* **25**, 5559 (1982).
69. W. B. Jackson, D. K. Biegelsen, R. J. Nemanich, and J. C. Knights, *Appl. Phys. Lett.* **42**, 105 (1983).
70. N. M. Amer, A. Skumanich, and W. B. Jackson, *Physica Utrecht* **117B & 118B**, 897 (1983).
71. G. Amato, G. Benedetto, L. Boarino, and R. Spagnolo, *Appl. Phys. A* **50**, 503 (1990).
72. G. P. Ceasar, K. Okumura, J. Lin, M. A. Machonkin, and L. Dudek, *J. Non-Cryst. Solids* **59 & 60**, 289 (1983).
73. S. Yamasaki, *Philos. Mag. B* **56**, 79 (1987).
74. G. Amato, G. Benedetto, F. Fizzotti, C. Manfredotti, and R. Spagnolo, *Phys. Status Solidi A* **119**, 169 (1990).
75. T. Ishiguro and H. Tokumoto, *Jpn. J. Appl. Phys. Suppl.* **21-3**, 11 (1982).
76. K. Tanaka, *in* "Photoacoustic and Thermal Wave Phenomena in Semiconductors," A. Mandelis, ed., Chap. 18, pp. 441–468. North-Holland Publ., New York, 1987.

77. A. Mandelis, R. E. Wagner, K. Ghandi, R. Baltman, and P. Dao, *Phys. Rev. B* **39**, 5254 (1989-I).
78. J. Fan and J. Kakalios, *Proc. MRS Meet.* **258** (1991).
79. T. Toyoda, T. Masujima, and M. Ando, *Jpn. J. Appl. Phys.* **32**, 2550 (1993).
80. T. Toyoda and K. Okonagi, *Proc. 2nd Int. Symp. Sputtering Plasma Processes (ISSP'93)*, 237 (1993).
81. P. M. Nicolic and D. M. Todorovic, *J. Phys. C: Solid State Phys.* **19**, L717 (1986).
82. D. Trbojevic, P. M. Nicolic, B. Perovic, and V. Cvekic, *Appl. Phys. Lett.* **38**, 362 (1981).
83. T. Ikari, S. Shigetomi, Y. Koga, and S. Shigetomi, *J. Phys. C: Solid State Phys.* **17**, L969 (1984).

Chapter 4

Photothermal Deflection Measurements of the Extinction Coefficient *k*

MATTHEW E. BRIGGS
Physics Department
University of Utah
Salt Lake City, Utah

I. Introduction 99
II. Photothermal Deflection 103
A. Advantages and Disadvantages 103
B. Examples of Deflection Techniques 104
C. Summary of Strengths and Weaknesses 105
D. Measurements of *k* Using Photothermal Deflection 106
E. Working Equations 114
III. Conclusions 116
Acknowledgments 117
References 117

INTRODUCTION I

The optical properties of a material can be studied using photothermal techniques when the energy absorbed from incident light dissipates mainly as heat. This is the case for most materials, so that photothermal techniques are used on a variety of materials to characterize thermal, optical, and surface properties. We will focus on one such technique, *photothermal deflection* [1], as shown in Fig. 1. A transparent material absorbs some light from a tightly focused heating-beam, and dissipates this energy as heat. This creates a hot spot in the material, and a laser probe-beam is deflected by gradients in the refractive index $\partial n/\partial r$ that arise from thermal expansion around the hot spot. The experimenter measures the deflection of the probe-beam, first calibrating the deflection with a standard sample in which the absorption is known, and then moving on to unkown samples. Such a measure-

HANDBOOK OF OPTICAL CONSTANTS OF SOLIDS III

Copyright © 1998 by Academic Press.
All rights of reproduction in any form reserved
ISBN 0-12-544423-0/$25.00.

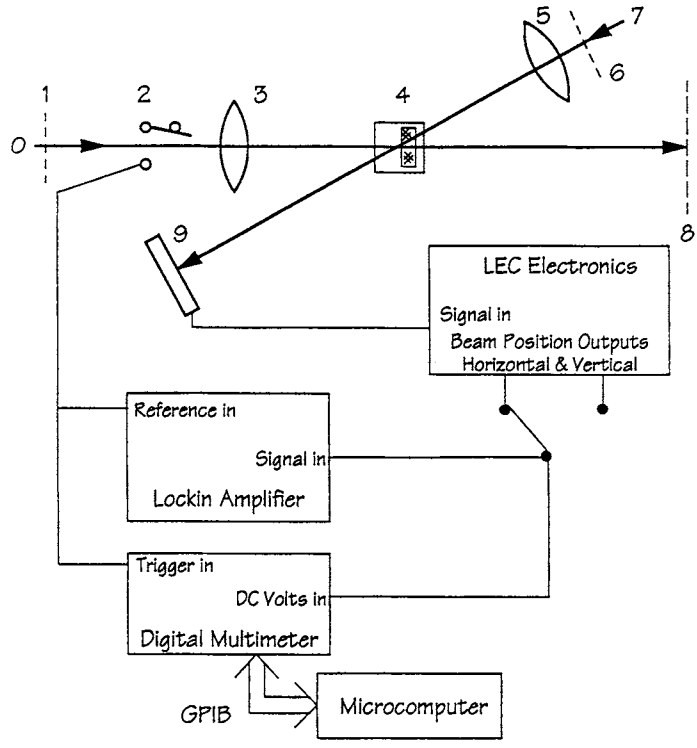

0 - pump laser 1 - attenuator (neutral density filter) 2 - shutter or chopper
3 - focusing lens for pump 4 - beams crossing in the fluid in front of a surface absorption
5 - focusing lens for the probe, on an x-z translation stage
6 - attenuator (neutral density filter) 7 - probe laser
8 - view -screen for pump (flows or lensing distortions) 9 - position sensor (lateral effects cell)

Fig. 1. A schematic of a collinear photothermal deflection apparatus used for measuring a surface absorption.

ment reveals the absorptance A of the material, which is the fraction of the power P that is travelling through the material which is absorbed,[1] and which is thus directly connected to the extinction coefficient k in the medium (see Section IID.)

We want to emphasize two features of photothermal deflection. First, it is a *localized* measurement—the effect relies on temperature *gradients* (Sec-

[1] P must take into account power lost to reflection (and scatter, if the material or its surface is highly scattering [2]), i.e., P must be given by the incident power P_i minus the reflected and scattered powers. Photothermal techniques have at best 10% accuracy and are usually (but not always) applied to transparent materials with polished surfaces. Under these conditions, the scatter and the $\approx 4\%$ reflection can be neglected, so that $P \approx P_i$, and the usual expression $A = P_a/P_i$ holds.

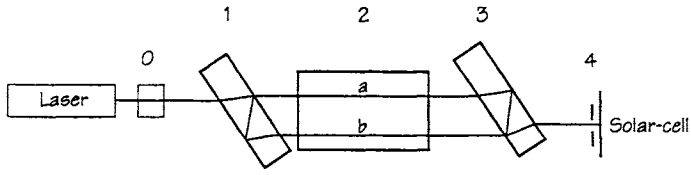

Fig. 2. An interferometer of the type used by Stone [8] to measure optical absorption in liquids.

tion IIE), and so is strongest at point sources such as the focused heating beam shown in Fig. 1. This first feature leads to two important capabilities: because the location of the region which the probe-beam senses is selected by where it crosses the heating-beam, surface and bulk absorptions can easily be separated in bulk samples (Sections IID1, IID13 give examples for bulk and film samples). For similar reasons, photothermal deflection finds widespread use as a form of microscopy, in which surface and sub-surface features of a material are found by scanning the sample and looking for changes in the deflection signal. The second feature we would like to emphasize is that photothermal deflection is *highly sensitive:* The high flux of a focused, laser heating-beam, the high sensitivity of photodiode-based beam-position sensors, and the use of a chopper to modulate the heating beam for lock-in detection combine to allow background levels equivalent to $A = 10^{-6}$ routinely [3], and $A = 10^{-9}$ more recently [4–6]. We should also mention a practical feature: the technique is simple to implement and inexpensive, if a laser source is already available with a power >100 mW.

We will finish the introduction with a few general comments about photothermal techniques, and then narrow the discussion to deflection techniques in Section II. We refer the reader to the reviews of Welsch [7] for a more detailed comparison and extensive bibliography. We divide photothermal techniques into two classes: *localized* measurements such as the deflection example just given, and *extended* measurements, typified by the interferometric measurement shown in Fig. 2 [8]. In photothermal interferometry, the experimenter places the sample in one leg of an interferometer, and detects the change in the fringe pattern that occurs when the heating beam is introduced into the sample. The difference between the classes is that the localized techniques detect the effect at a point in the sample, while the extended techniques *integrate* the thermal effect along the entire length in the material. Other examples of extended techniques include photothermal lensing (the first photothermal technique discovered) [9–11], and Fabry-Perot *etalon* work [12], as well as photoacoustic techniques, which can be adapted to both extended and localized measurements (see Chapter 3 by Mandelis, this

volume). The applications reflect the extendedness of the measurement, and include bulk optical-absorption measurements [8, 13], and trace detection of parts-per-billion impurities in bulk gases and liquids [14]. The two classes have much in common: it is the density change from heating which causes the signal, the source of the heating is usually the optical absorption from a focused heating beam, the heating beam is modulated to allow lock-in detection, and sensitivities are at least as good as $A = 10^{-6}$. In fact, photothermal techniques are the only means for detecting optical absorptions below 10^{-4} (Fig. 3); the traditional spectrophotometric approach is more appropriate for stronger absorbers because the absorption is found from the difference between large signals, the incident power minus the sum of the reflected and transmitted powers. Photothermal techniques now employ all the tools of modern optics—pulsed lasers, Fourier-transform techniques, microwave stimulation, to name a few, and have been applied to a wide range

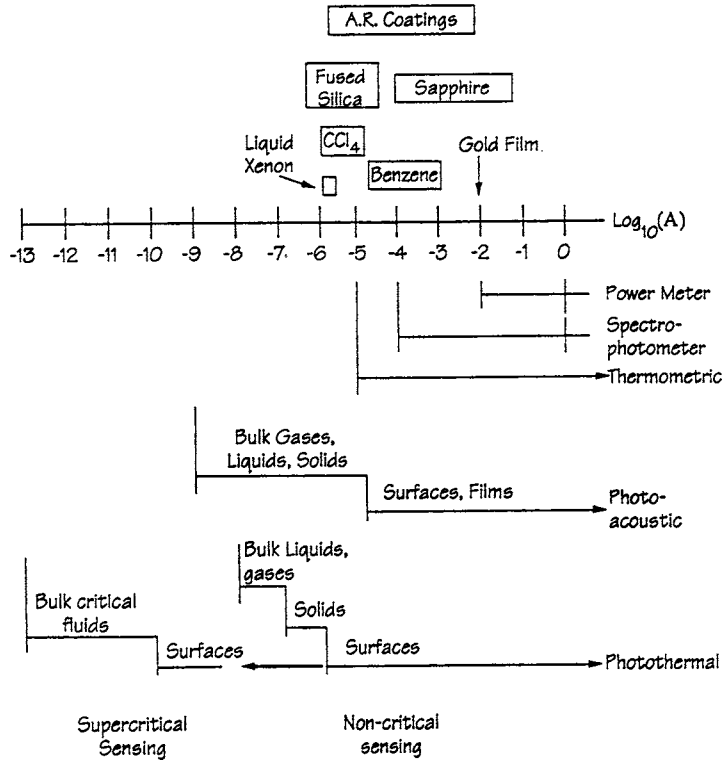

Fig. 3. A logarithmic guide to absorption measurements, giving the minimum detectable fractional absorption, $A \equiv P_{\text{absorbed}}/P_{\text{incident}}$, for various techniques, under a 1 W cw illumination. For bulk absorptions, the length l is taken to be 1 cm, where $A = \alpha l$. The arrows pointing to the right are intended to emphasize that these techniques can be used for opaque materials.

of samples for a variety of thermal, spectroscopic, and diagnostic studies. The review articles by Welsch [7], texts by Mandelis [15] and Sell [16], and others [17, 18] will quickly inform the interested reader.

PHOTOTHERMAL DEFLECTION II

Advantages and Disadvantages A

Figures 1 and 4–6 show several configurations for photothermal deflection measurements. The collinear arrangement (Figs. 1 and 6) senses the absorption at the location where the beams cross—either bulk or surface absorptions can be measured by choosing the location appropriately. In bulk measurements, the volume that contributes to the signal is set by the overlap of the heating and probe beams and the diameter of the heating beam, i.e., a cylinder $\sim$ 0.5 (mm long) $\times$ 0.05 (mm diameter). Surface measurements sense an area determined by the diameter of the heating beam, because the absorption at the surface is usually much stronger than the bulk absorption, so that the bulk can be neglected [19]. Treatments of the separation of bulk and surface contributions can be found elsewhere in [20–22], and examples in optical-constants measurements are discussed in Sections IID1 and IID13. The sensitivity for surface absorptions of solids can be increased strongly by immersing the sample in a fluid and placing the intersection of the probe and heating beams just above the surface, in the fluid. This is because the higher thermal-expansion coefficient of the fluid leads to a stronger optical effect (Section IIE.)

Though highly sensitive, the *accuracy* of this technique has been limited to the 10% level since the start of this research field. The difficulty in improving the accuracy arises because k is found from the amplitude of the deflection, which depends on quantities that are difficult to reproduce or know accurately at the site where the beams cross, principally the diameter of the heating and probe beams and the alignment between the two beams. The surface polish and sample handling must be specified for measurements of surface absorption, because the surface roughness and cleanliness strongly effect the absorption. Further, convection is an issue when working in liquids or at surfaces in air, and it is important in these types of measurements to reduce the heating power until good linearity of the signal with power is observed [6, 23]. Attempts to model these issues will be mentioned in Section II E. As a rule of thumb, only a careful calibration using known absorbers with thermophysical, geometrical, and optical properties chosen to match the unknowns will allow an accurate measurement of k. Photothermal deflection is, therefore, applied to the measurement of k in systems that de-

mand either a high sensitivity, a non-contact measurement, or a localized measurement. Photothermal deflection can also be applied to determine how much of the relaxation is thermal; transmission measurements reveal the total absorption, while photothermal techniques reveal only that portion of the absorption which relaxes thermally. For example, results from these two techniques are used by Montecchi and Masetti [24] to find the vibrational relaxation efficiency for films of gold, chromium, zinc selenide, and amorphous-carbon thin-films.

B Examples of Deflection Techniques

An example of the 10% accuracy available from deflection techniques is provided by the first exhaustive photothermal deflection study, which still serves as an instruction manual for getting started in this technique [1,3]. These authors demonstrate the accuracy of their collinear-deflection apparatus by achieving 10% agreement and repeatability between calculated and calibrated bulk-absorption measurements. They use a dye-laser heating beam to measure the spectrum of the sixth harmonic of theC—H stretching excitation of benzene at various concentrations of benzene in carbon tetrachloride from $\lambda = 580$ to 620 nm. The carbon tetrachloride serves as a non-absorbing medium in which the known amount of benzene present allows the authors to test the accuracy of the deflection measurements at various absorption levels against separate spectrophotometric measurements. In the same paper, the authors report a similar level of success for measurements of the surface-absorption spectra of In and CdS *films* on glass substrates, again calibrating the absorption in separate spectrophotometric measurements.

The "mirage" configuration shown in Fig. 4 allows the experimenter to work on opaque samples, and simplifies the process of scanning the sample [3]. Here the deflection arises from thermal expansion in the gas above the hot spot created by the absorption of the heating beam at the surface of the material. Changing the frequency and noting the phase shift in the response allows an analysis of the depth of the absorption. Alternatively, the probe beam can travel through the substrate, sensing the mirage effect from the (weaker) thermal expansion of the substrate material under the surface absorption [25]. This would be useful for detecting the absorption in processes for which the region above the surface is not optically good, such as laser ablation.

Although Murphy and Aamodt [23] find 10% accuracy and agreement with theory for mirage measurements on an electrically heated surface, in the more common case of heating from optical absorption, the agreement between the mirage measurements and theory is not as good [25, 26]. This presumably is because of the more complex geometry and alignment requirements. The convenience of the technique for imaging problems makes this an important

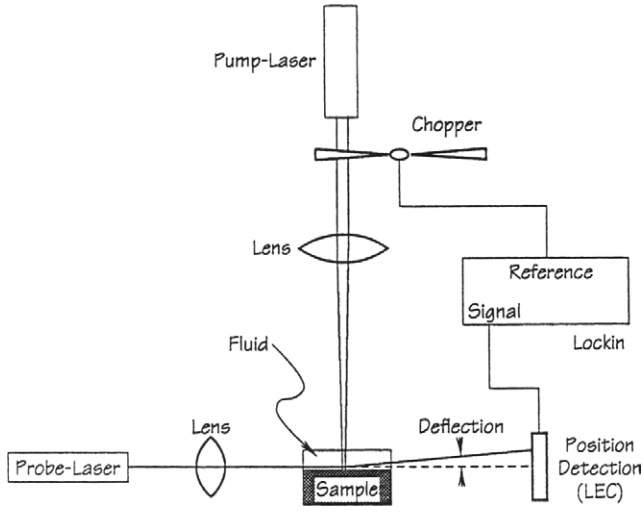

Fig. 4. A mirage photothermal-deflection apparatus using the refractive-index distortions created in the fluid or gas above the region of the absorption as a measure of the absorption.

technique, but until the mechanisms of the measurement are understood well enough to allow the measured amplitude to agree with theory, the transfer of absolute absorption levels from calibration samples to unknowns will have a larger margin of doubt than other photothermal techniques.

The remaining deflection techniques fall under the title *photothermal surface-deformation,* an example of which is shown in Fig. 5. These techniques offer advantages in imaging applications similar to the mirage technique, and in addition contain information about the thermal-expansion properties of the material itself (rather than the gas above the material.) Examples of these configurations of photothermal apparatus are available elsewhere [23, 27, 28]. A further advantage is that the surface-deformation approach gives agreement with theory closer to 10% [28, 29], presumably because the optical alignment is less demanding than for the mirage technique. Because the signal depends on the coefficient of thermal expansion of the material, surface-deflection techniques are typically used on metal films; it would be less appropriate on the low-thermal-expansion optical glasses, where one would turn to the collinear or mirage approach.

Summary of Strengths and Weaknesses C

Strengths of the deflection techniques thus generally include: 1) a combination of simplicity and very high sensitivity, 2) non-contact *in-situ* measurements, 3) adaptable to transparent, turbid or opaque samples, 4) either

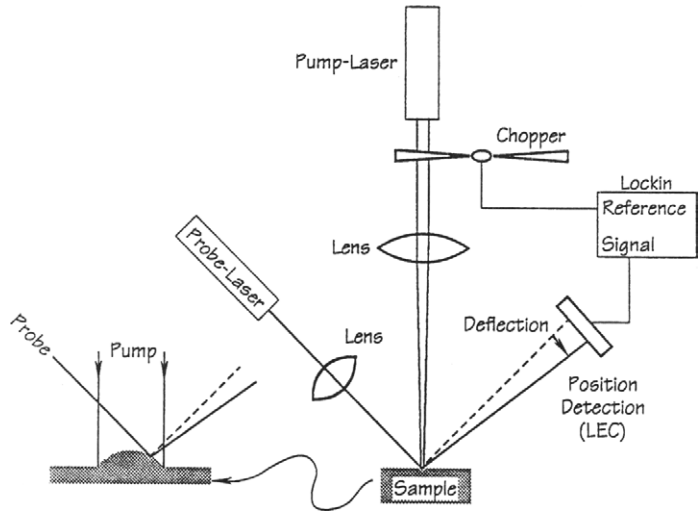

Fig. 5. A reflective photothermal deflection apparatus using the thermal expansion of the sample surface at the site of the absorption as a convex mirror, to change the angle of reflection in proportion to the absorption.

strongly absorbing or weakly absorbing and any phase (gas, liquid, solid), 5) either surface or bulk, spatial resolution to a few μm's, and 6) ability to measure dynamic processes. We should also mention that the technique has been used at cryogenic temperatures (see Section IID13). Weaknesses of the technique generally include: 1) necessity for careful optical alignment, 2) accuracy is not high, 3) modeling of 3-D heat flow is needed to understand full dynamic range, 4) provides only local measurements, and 5) requires laser with power $\gtrsim$ 100 mW. Because *deflection* measurements are localized, the measurement of k in bulk materials is probably better done using one of the *extended* techniques mentioned in the introduction—unless the surface absorption needs to be removed from the measurement. The dominant applications for *deflection* techniques today are the microscopy and characterization of surfaces, which will be evident from the following discussion. However, anyone using a single number for the absorption in a material must consider the possible effects of local variations if their application pushes the performance or depends critically on the performance of the material. The absorptance can vary locally by a factor of 100 around a surface, and 10 in bulk materials.

D Measurements of *k* Using Photothermal Deflection

The photothermal techniques yield the absorptance $A \equiv P_a/P$, where P_a is the power absorbed from a heating beam of power P in the material (see the

footnote in the introduction). In order to find the imaginary part of the refractive index, k, we first find from the absorptance A the absorption coefficient $\alpha(\text{cm}^{-1})$, which describes the spatial rate at which optical energy is converted into thermal energy, and then use $\alpha = 4\pi k/\lambda$. For example, in the simplest case of normal incidence on a semi-infinite material we have

$$A \equiv P_a/P_i = 1 - e^{-\alpha z}, \tag{1}$$

where z is the path length travelled in the absorbing material, and P_i is the power transmitted into the sample through the interface. Finding α from A can be a challenging problem: for the case of intereference coatings, Eq. (1) must take into account the multiple reflections of the heating beam within the coating, which requires careful calculation of the path length and interference effects [19, 30].

A detailed schematic of a collinear apparatus we used for precise measurement of optical absorptions is shown in Fig. 6. We include this to provide as detailed an example of an experimental set-up as we can. This is an implementation of the apparatus described by Jackson *et al.* [3], which still serves as an excellent cookbook for setting up such an apparatus, as well as for an introduction to the theory. Along with this, we recommend papers by Commandré et al. [19], Bennet *et al.* [26], Commandré and Pelletier [30] as examples of how to make a thorough study of the optical properties of a material using photothermal deflection (See Section IID14).

We now discuss materials for which k has been measured using photothermal deflection techniques. In all cases, the process involves an initial calibration using a known absorber with similar optical properties, such as the substrate thermophysical properties and film multilayer structure, in the case of thin films. We will attempt to present the strength and weakness of the individual measurements, bearing in mind that often the primary goal of the authors was to diagnose the presence of impurities or defects, rather than to produce absolute measurements of optical constants.

Aluminum Oxide and Fused Silica Glasses (Al_2O_3, SiO_2 Glasses) 1

Fused silica provides an excellent example of the role photothermal deflection can play in the measurement of optical properties: the absorption of this material is sufficiently low that it had not been measured yet [31]. The collinear-deflection technique has since been used to measure $\alpha \approx 10^{-6}$ cm^{-1} at 514.5 and 632.8 nm for synthetic fused silica, and $16\text{–}600 \times 10^{-6}$ cm^{-1} for natural fused silica [19, 32]. This gives an extinction coefficient for synthetic fused-silica of $k = 3 \times 10^{-12}$. The reason for using the deflection technique rather than an extended technique is that by crossing the beams in the bulk of the sample, the workers were able to avoid surface absorption effects which might dominate the bulk absorption. The loss in intensity due to reflections and scatter in these materials is small enough that workers take

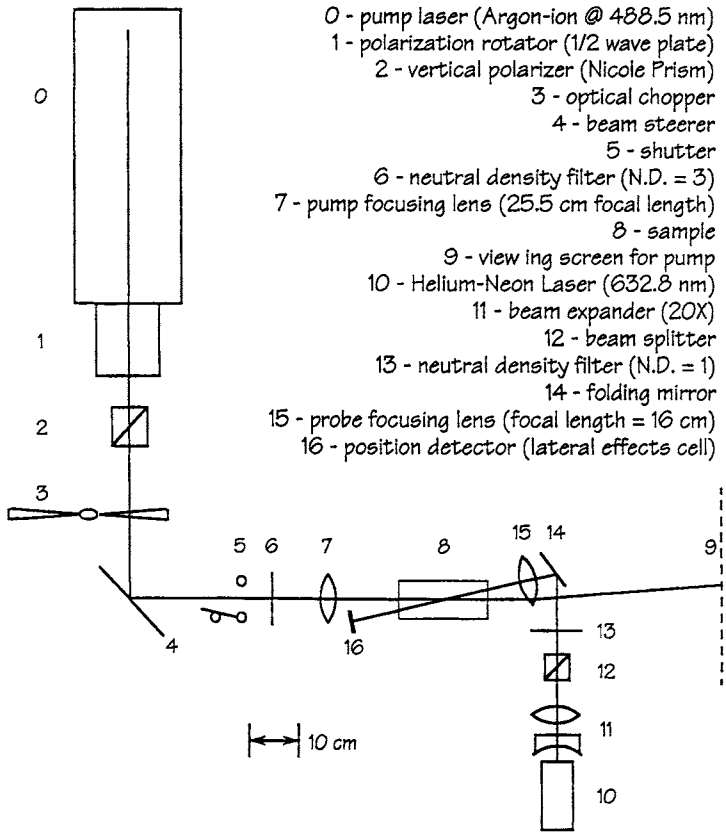

Fig. 6. A scale drawing of a typical photothermal deflection apparatus that allows a convenient variation of the power through rotation of the polarization of the Ar^+ output beam, and is characterized by a 20 μm radius probe beam and 50 μm radius heating beam at the sample location.

the intensity in the bulk to be equal to the intensity incident on the surface. Other techniques are generally forced to include the surface absorption with the bulk, and the surface absorption will usually be much stronger. We have not found bulk measurements using deflection techniques for sapphire. Our own work on surface absorptions in these materials reveals a wide range of absorptances, $10^{-5}-10^{-3}$ at 632.8 nm, depending on surface polish and cleaning [6] (recall that surface measurements can only report the fraction of light absorbed, not α). A good collection of different treatments of the problem of surface absorption in optical materials can be found elsewhere [18]. Several papers in the section on absorption losses in this reference show that surface absorptances in fused silica can be as low as $A = 10^{-6}$. Our own best fused-silica surfaces, which were superpolished by the same com-

pany that supplied some of the 10^{-6} surfaces reported in this collection, showed levels of 10^{-5}. This suggests the presence of a low-level contaminant on the surface, despite our use of modern UHV procedures to prepare the perfect sample. Workers in supercritical fluids should take note of this observation.

Amorphous Carbon Films (a-C:H) 2

Photothermal deflection was chosen for its sensitivity in recent work mapping the effects of hydrogenation on the optical absorption in amorphous-carbon films [33]. Results are given for α, which we convert to an approximate value of k using $k = \lambda\alpha/4\pi$. For example, at $\lambda = 0.6328$ μm, this gives $k = 2 \times 10^{-3}$ at an atomic fraction of hydrogen in the film of $X_H = 0.44$. This should be compared to the values $k = 0.217, 0.0348$ from transmission measurements, as tabulated by Piller [34], for which X_H was not quoted. A careful study of the absorption in a-C:H must include careful treatment of X_H, as in Compagnini *et al.* [33].

Copper (Cu) 3

The absorption spectrum of copper for $500\text{nm} < \lambda < 700\text{nm}$ is given by Spear and Russo [25] for a 0.2 μm-thick layer sputtered onto acrylic. This is a demonstration of the mirage technique performed in the substrate, and not an optical-properties paper, so the level is equivilant to the calibration from reflectance measurements, and no value for α is given. The experimental deflection is an order of magnitude lower than expected from theory, which seems to be a typical problem for the mirage approach, making it less desirable for the measurement of optical constants.

Gallium Arsenide and Amorphous Gallium Arsenide (GaAs, a-GaAs:H) 4

The absorption of 1 μm thick MBE layers of GaAs has been reported between 0.8 and 2 μm as a function of temperature of the substrate during growth [35]. The photothermal deflection technique was chosen for its sensitivity; these results fall into an area of low extinction coefficient in the subgap region not previously measured [31]. Subgap absorption-levels vary strongly with substrate growth temperature, $\alpha \approx 10^1$–10^3cm^{-1} as λ goes from 2 to 0.8μm. These results are used by the authors to determine defect-density behavior. Unhydrogenated amorphous GaAs layers show 100× higher absorption than the crystalline films and a shift to lower energies [36], similar to behavior observed for GaP (next section) and Se (Section IID7).

The hydrogenated amorphous film showed similar behavior to the crystalline film, however.

5 Gallium Phosphide (GaP)

The effect of substrate temperature during sputtering of amorphous GaP films appears to have only a slight effect on the optical absorption in the subgap region [37], in contrast to the behavior reported for GaAs (Section IID4). A smoothing of the exponential absorption edge is observed by these authors, similar to that found for amorphous Se (Section IID7), as well as a shift by a factor of 3 to lower energy compared to the absorption edge in crystalline GaP. The observed α ranges from 0.1 to 10^5 cm^{-1} as the wavelength decreases from 0.5 to 2.5 μm. Much of this region had not been explored before [38].

6 Amorphous Hydrogenated Germanium (a-Ge:H)

The amorphous thin-films of germanium and silicon (Section IID13) have been extensively studied with photothermal deflection, because the sensitivity allows the measurement of the absorption in the sub-gap region up into the more highly absorptive region where classical approaches work. For example, the region from 0.5 to 1.5 eV has been measured in a-Ge:H using photothermal deflection [39], showing the change from $\alpha = 10$ cm^{-1} at the flat absorption below the gap rising up to 10^5 cm^{-1} at the gap. Generally, these studies map the absorption as a function of the degree of hydrogenation and the defect density.

7 Amorphous GeSe and Selenium Films (a-GeSe, a-Se)

Annealing effects on 1–1.5 μm-thick GeSe films have been reported by Theye *et al.* [40], in which the authors use photothermal deflection in the subgap region. The resulting absorption ranges from $\alpha = 10^1$ to 10^3 cm^{-1} as λ goes from 1.2 to 0.5 μm. The authors find strongly reduced absorption with annealing over most of the range, but find an indication of *increased* absorption for the annealed sample at the lowest energy. Theye and co-workers later study absorption versus concentration of Se from 0 to 100% [41], over a broader range of wavelengths than their first study. The material shows a gradually increasing absorption with energy, $\alpha = 3$ to 10^5 cm^{-1} as the wavelength changes from $\lambda = 2.5$ to 0.5 μm. They note that the amorphous selenium films lack the sharp exponential absorption edge found in bulk Se.

Gold Films (Au) 8

Gold has been measured using photothermal deflection in demonstration measurements for a new surface-deformation technique [28]. The authors show the equivalence between the absorption measured on gold films using photothermal deflection with that measured using the reflectance, and demonstrate agreement between the expected and measured signal levels. The absorption coefficient they measure is $\alpha = 7.6 \times 10^5\ \text{cm}^{-1}$ at $\lambda = 0.488\ \mu\text{m}$, which gives $k = \lambda\alpha/4\pi = 2.4$, compared to $k \approx 1.8$ in Lynch and Hunter [42]. The difference is presumably due to differences in the deposition and surface finish of the film, and reinforces our point that reports of surface absorptions must include a careful specification of the surface condition at the time of measurement.

Indium Phosphide (InP) 9

Polished wafers of InP were tested by Horita *et al.* [43] for demonstrating a double-pass method to enhance the sensitivity of mirage detection. In addition, these workers used the high sensitivity to extend the measurements of k reported by Glembocki and Piller [44] to wavelengths between 1 and 1.2 μm, where the absorption had been too low to measure previously. The new results map smoothly onto the old ones, and dip down to $\alpha = 2 \times 10^{-2}\ \text{cm}^{-1}$ at 1.2 μm. As usual for the mirage technique, the calibration cannot be calculated correctly from theory. However, there is good overlap with the data of Glembocki and Piller [44], which is taken as the calibration. This is appropriate for their demonstration work, but leaves open the possibility of an offset (due, for example, to surface roughness) between the actual and reported absorption of the sample. We just want to emphasize the importance of an independent calibration and agreement with theoretical signal-levels in measurements of optical constants. The absorption of this material was also measured using photothermal deflection [45], as part of a study of the utility of photothermal deflection in the characterization of quantum wells. The authors report that they are successful in determining the absolute absorption of the quantum wells, and in addition report the absorption spectrum for the InP substrate from $\lambda = 1$ down to 2 μm, extending the work of Horita *et al.* [43] further into the relatively flat absorption region ($k \approx 10^{-2}$) below the gap at 1.3 eV.

Iron Disilicide ($FeSi_2$) 10

k and α are reported in Dimitriadis *et al.* [46] using photothermal deflection in conjunction with spectroscopic ellipsometry and X-ray diffraction in

a thorough study of this material between $\lambda = 0.5$ and 2.5 μm. Photothermal deflection was chosen for its sensitivity. The resulting k is found to grow from 1 to 3 with energy in this range, for both bulk and thin-film samples. The results establish a band gap at 0.8 μm.

11 *Lead Lanthanum Zirconate Titanate Ceramics (PLZT)*

The subgap absorption in this material has been measured in a study of the absorption centers and the effects of illumination [47]. The authors find a smooth increase in the absorption coefficient from 10^{-2} to 10^{2} cm^{-1}, for incident light between 1 and 3.5 eV. In the method of calibration, the authors show an appreciation for the need to duplicate the thermal properties of the unkown materials: they paint the surface of an identical sample with black paint to increase the absorption sufficiently to allow a cross-calibration with transmission. This still leaves serious doubt, however, in that the thermal impedance at the boundary between the paint and the sample will be very different from that of the surface absorption to the bulk in the unpainted material.

12 *Silicon (Si)*

The same work we discussed in the Section IID9 also reported measurements of α for a polished silicon wafer. Again, the results dip down smoothly from the literature values used for calibration [48], and end with $\alpha = 10^{-2}$, cm^{-1} at 1.2 μm, similar to InP. This small region is interesting because previous measurements had stopped at 1.1 μm [48], and Horita *et al.* [43] show that the absorption continues to plummet, dropping two more decades between 1.1 and 1.2 μm. Because work by Edwards [48] is used for calibration, the results of Horita *et al.* [43] are locked into consistency with the earlier work. A calibration offset may exist for this mirage work, as discussed in Section IID9.

13 *Amorphous Silicon and Hydrogenated Silicon (a-Si, a-Si:H)*

The absorptions of a-Si and a-Si:H thin films have now been measured using all of the techniques that we have mentioned. This work provides another example of the interplay between these techniques: The transmission work cited by Piller [34] lacks the sensitivity to measure the absorption in the sub-gap region of the thin film. Since then, photothermal (and other) techniques have measured the absorption in this region, revealing a wide variety of levels associated with different levels of hydrogenation (X_H) and

sample purity [49]. The surface absorption is distinguished from the film interior absorption by Umezu *et al.* [50] by studying the absorption versus the thickness of the film from 0.02 to 5 μm. The work is carried out at wavelengths starting in the supgap region and extending up over the band-edge, from 0.6 to 1.2 μm, for the purpose of exploring the nature of the surface states; α is not given. The difficulty in reaching conclusions about the absolute absorption α arises from the interpretation of interference effects, as we discussed in our general review of the technique. A treatment of this effect for amorphous silicon films can be found elsewhere [51]. These authors apply a thin-film optical analysis to extract α for 0.3 μm-thick films of a-Si:H between $\lambda = 0.6$ and 1.2 μm. They find α increasing from 10^1 to 10^4 cm^{-1} with energy in this region, with the gap edge at 0.8 μm. They attempt to resolve surface and bulk levels by fitting, to obtain the surface density of states and how these depend on light soaking and thermal annealing. A more thorough discussion of the application of thin-film optical analyis can be found in the work on TiO_2 discussed in the next section. A review of earlier work using photothermal deflection on a-Si can be found elsewhere [52]. Finally, we note that this material was studied at liquid-nitrogen temperatures, with α decreasing smoothly from 10^5 to 10^2 cm^{-1} between $\lambda = 0.5$ and 1.2 μm [53].

Titanium Dioxide Films (TiO_2) 14

Photothermal techniques are critical for measuring k in TiO_2 (and other transparent films) where the extinction coefficient is so small in the entire visible region that it was previously inaccessible [31]. The optical properties of this material have been thoroughly measured in the literature using photothermal deflection [19, 26, 30]. This work gives $k = 1 \times 10^{-5}$–5×10^{-4}, depending principally on the sample roughness and preparation method, and independent of wavelength in the visible range where these studies were done. Note that the crossover from this flat region to the strong wavelength dependence evident in Ribarsky [54] for $\lambda < 0.4$ μm and $\lambda > 10$ μm has not been explored to our knowledge. The value of k reported at these wavelengths is $k \approx .05$, rising quickly to $k \approx 2$ [54]. This is one of the most studied materials, and one can go to the above references to find work on the effects of multilayer interference, and comparison with the more traditional techniques.

Zinc Sulfide (ZnS) 15

A single layer of ZnS was used as a calibration signal by Commandré *et al.* [19]. In order to extract an extinction coefficient from their data, we cal-

culate k from the formula and parameters given by Commandré *et al.* [19] that take into account interference effects, with $n_1 = 2.4$ at $\lambda = 610$ nm [55]. This gives $k = 7 \times 10^{-4}$, somewhat higher than the value for cubic ZnS given by Palik and Addamiano [55], but not inconsistent with variations noted for surface absorptions in general. See references in Palik and Addamiano [55].

E Working Equations

Here we give the working equations for the simplest deflection measurement, a collinear deflection apparatus making bulk measurements. Our intention is to show, in general, how the different materials' properties affect the signal. The absolute calculation for a particular experiment must take into account any peculiarities of the new experiment and be verified against calibration standards. If such a comparison is unsuccessful, then the confidence in using the calibration standards to judge the absolute absorption of an unknown is diminished. Several workers have reported good success with models, treating the heat flow in the proper number of dimensions and taking into account the presence of surfaces [3, 6, 56–58].

When a material is heated, thermal expansion causes the density of the material to decrease, and this lowers the refractive index of the material—the speed of light increases as the density goes down. The optical effect of the change in density dominates the change in polarizability. This phenomenon is well described by a dipole approximation described by the Clausius-Mossotti equation [59], and if one takes the derivative of this equation with respect to density ρ, one finds a simple expression for the temperature derivative of the refractive index, dn/dT,

$$\frac{dn}{dT} = \frac{\partial n}{\partial \rho}\frac{\partial p}{\partial T} = -\frac{(n^2 - 1)(n^2 + 2)}{6n}\beta_p, \tag{2}$$

where we have substituted the thermal expansion coefficient at constant pressure β_p,

$$\beta_p \equiv -(1/\rho)(\partial \rho/\partial T)_p. \tag{3}$$

The signal turns out to be proportional to this term, so that the coefficient of thermal expansion plays a crucial role in the signal level: the sensitivity of the mirage approach is due to the thermal expansion in the gas above the heated surface, the use of sensing fluids in collinear measurements on solids is due to the 100× larger thermal expansion in liquids compared to solids, and the enhancement to the signal provided by supercritical fluids arises because the thermal-expansion coefficient diverges with proximity to the criti-

cal point [4, 6]. The coefficient of thermal expansion of liquids is β_p (liquid) $\approx 10^{-3}$ (K^{-1}), while for fused silica, β_p has the very low value 1.6×10^{-6} (K^{-1}). The strength of the thermal effect on n, therefore, varies from $dn/dT \approx 5 \times 10^{-4}$ or 0.03%, down to 7×10^{-7} or 5×10^{-5}% (K^{-1}). These are small effects, but they are entirely due to the process of interest, unlike the transmission approach, which deduces the absorption from the small amount of light lost from the incident beam.

The deflections are small enough that we can assume that a beam travelling in some direction z will always be deflected by gradients perpendicular to z, $\partial n/\partial r$, according to the simple expression

$$d\theta = \frac{1}{n}\frac{\partial n}{\partial r}dz, \tag{4}$$

where $d\theta$ is the angular deviation from the z-axis. This can be seen directly by considering the change in the velocity along the wavefront of a plane-wave travelling in a medium with a gradient in the refractive index along the wavefront [59]. We express this gradient in terms of the temperature gradient from which it arises, $\partial n/\partial r = (dn/dT)\partial T/\partial r$, and integrate this along the path of the probe-beam through the heated region of the sample. Assume this heated region arises from the absorption coefficient α (cm^{-1}) of a heating beam of power P, focused to a Gaussian waist-radius w_0 and chopped at a frequency ω. We take the heating and probe-beams to overlap at an angle ϕ, which gives an effective overlap length l of $l = 2w_0/\sin\phi$. If the frequency is low enough that a steady state is reached during each shutter opening, the effect will be limited by the thermal conductivity Λ of the sample, so that the final expression for the root-mean-square angular variation of the probe beam is:

$$\theta_{rms} = \frac{\beta_p}{\Lambda}\rho\frac{\partial n}{\partial \rho}\frac{\alpha l P}{\sqrt{2}\pi^2 w_0}\left[\frac{1 - e^{-2r^2/\omega_0^2}}{r/w_0}\right], \tag{5}$$

where we have assumed that the materials are transparent, i.e., that the power in the heating beam is not significantly diminished by the absorption before and while overlapping with the probe beam. If on the other hand, the frequency is high enough that the temperature is increasing at its maximum rate throughout the time the shutter is open, the signal is limited by the heat capacity of the sample c_p, and obeys

$$\theta_{rms} = \frac{\beta_p}{\omega\rho c_p}\rho\frac{\partial n}{\partial \rho}\frac{16\alpha l P}{\sqrt{2}\pi^2 w_0^3}\left[\frac{r}{w_0}e^{-2r^2/w_0^2}\right]. \tag{6}$$

The intermediate frequencies are described by integral equations that must be solved numerically [3, 6, 15, 16, 60].

The qualitative behavior common to both the low- and high-frequency forms is then a signal which is proportional to the illuminating power P and the absorption αl or A. The low-frequency signal level rolls-off to frequency-limited behavior at a frequency $f_r \equiv 4D/(\pi w_0^2)$, where D is the thermal diffusivity of the fluid, and w_0 is the waist radius of the heating beam. Low-frequency signals will be independent of frequency, and proportional to the ratio of the thermal-expansion coefficient β_p to the thermal conductivity Λ. The maximum signal will be found with the probe at $r = 0.8w_0$ from the axis of the heating beam. High-frequency signals fall off with frequency like $1/f$, and are proportional to the ratio of β_p to the constant-pressure heat capacity c_p. The probe position at maximum signal will move in, to a separation $r = w_0/2$ from the heating beam.

We repeat that the above calculations describe the signal in a collinear photothermal deflection experiment measuring the bulk absorption of a transparent material. We wanted to illustrate how the modulation frequency, heat capacity, thermal conductivity, and coefficient of thermal expansion affect the signal. These equations, and generalizations of these equations, have been applied successfully to predict signal levels in a variety of experimental situations, as mentioned in the first paragraph of this section.

III CONCLUSIONS

The photothermal deflection techniques are highly sensitive techniques of 10% accuracy which find their greatest applicability in characterizing the effects on materials of production processes and handling. These non-contact, *in-situ* inspection techniques are in demand in both research and industrial applications in semiconductors and optics [17, 18], and photothermal techniques have been applied to a broad range of sample geometries and materials [7]. The localized nature of these techniques has revealed the fact that impurities, defects, and surface conditions alter dramatically the local absorption level of a material [61]. This has shown us that we must think of a material as having a distribution of absorption levels in order to anticipate the behavior of the material in modern research and technology. The extended techniques we mentioned in the introduction are used more commonly than the deflection techniques for measuring "the" optical constants of materials, because they average over the local variations. However, if one wishes to separate bulk from surface absorption in a transparent material, the ability to choose the measurement location with the beam crossing in the collinear-deflection technique is very useful. One must also realize that the local variations are hidden by the extended techniques—and turn to a local technique to get a complete picture of k in demanding applications.

ACKNOWLEDGEMENTS

This work was supported by the Department of Physics at the University of Utah, 201 James Fletcher Building, University of Utah, Salt Lake City, UT 84112.

REFERENCES

1. A. C. Boccara, D. Fournier, W. B. Jackson, and N. M. Amer, Sensitive photothermal deflection technique for measuring absorption in optically thin media. *Opt. Lett.* **5**, 377 (1980).
2. J. D. Spear, R. E. Russo, and R. J. Silva, Collinear photothermal deflection spectroscopy with light-scattering samples. *Appl. Opt.* **29**, 4225 (1990).
3. W. B. Jackson, N. M. Amer, A. C. Boccara, and D. Fournier, Photothermal deflection spectroscopy and detection. *Appl. Opt.* **20**, 1333 (1981).
4. R. A. Leach and J. M. Harris, Supercritical fluids as spectroscopic solvents for thermooptical absorption measurements. *Anal. Chem.* **56**, 1481 (1984).
5. V. Loriette, L. Pinard, A. C. Boccara, and J. M. Mackowski, Multilayers coatings characterisation for interferometric gravitational waves detection, Optical Interference Coatings. (F. Abelès, ed.), *SPIE Proc.* **2253**, 1031 (1994).
6. M. E. Briggs and R. W. Gammon, Photothermal deflection in a supercritical fluid. *Int. J. Thermophys.* **16**, 1439 (1995).
7. E. Welsch, Photothermal measurements on optical thin films. *Appl. Opt.* **34**, 7239 (1995); E. Welsch, Absorption measurements, *in* "Handbook of Optical Properties, Volume 1, Thin Films for Optical Coatings." (R. E. Hummel and K. H. Guenther, eds.), CRC Press, Boca Raton, Florida, 1995.
8. J. Stone, Measurements of the absorption of light in low-loss liquids. *J. Opt. Soc. Am.* **62**, 327 (1972).
9. J. P. Gordon, R. C. C. Leite, R. S. Moore, S. P. S. Porto, and J. R. Whinnery, Long-transient effects in lasers with inserted liquid samples. *J. Appl. Phys.* **36**, 3 (1965).
10. D. Solimini, Loss measurement of organic materials at 6328 Å. *J. Appl. Phys.* **37**, 3314 (1966).
11. J. R. Whinnery, Laser measurement of optical absorption in liquids. *Acc. Chem. Res.* **7**, 225 (1974).
12. H. A. Schuessler, S. H. Chen, Z. Rong, Z. C. Tang, and E. C. Benck, Cavity-enhanced photothermal spectroscopy: Dynamics, sensitivity, and spatial resolution. *Appl. Opt.* **31**, 2669 (1992).
13. J. Stone, Thermooptical technique for the measurement of absorption loss spectrum in liquids. *Appl. Opt.* **12**, 1828 (1973).
14. D. L. Mazzoni and C. C. Davis, Trace detection of hydrazines by optical homodyne interferometry. *Appl. Opt.* **30**, 756 (1991).
15. A. Mandelis, ed., "Principles and Perspectives of Photothermal and Photoacoustic Phenomena." Elsevier, New York, 1992.
16. J. A. Sell, ed., "Photothermal Investigations of Solids and Fluids." (J. A. Sell, ed.), Academic Press, San Diego, 1989.
17. J. C. Murphy, J. W. M. Spicer, L. C. Aamodt, and B. S. H. Royce, eds., "Photoacoustic and Photothermal Phenomena II." Springer-Verlag, New York, 1990.
18. F. Abelès, ed., Optical Interference Coatings. *SPIE Proc.* **2253**, 1021 (1994).
19. M. Commandré, L. Bertrand, G. Albrand, and E. Pelletier, Measurement of absorption losses of optical thin film components by photothermal deflection spectroscopy. Optical Components and Systems. *SPIE* **805**, 128 (1987).
20. Y. X. Nie and L. Bertrand, Separation of surface and volume absorption by photothermal deflection. *J. Appl. Phys.* **65**, 438 (1994).
21. B. C. Li, Y. Deng, and J. Cheng, Separation of optical thin film and substrate absorption by obliquely-crossed photothermal deflection: Theory. *J. Mod. Opt.* **42**, 1093 (1995).

22. H. E. Bennett and D. K. Burge, Simple expressions for predicting the effect of volume and interface absorption and of scattering in high-reflectance or antireflectance multilayer coatings. *J. Opt. Soc. Am.* **70**, 268 (1980).
23. J. C. Murphy and L. C. Aamodt, Photothermal spectroscopy using optical beam probing: Mirage effect. *J. Appl. Phys.* **51**, 4580 (1980).
24. M. Montecchi and E. Masetti, Measurement of vibrational deexcitation efficiencies of gold, chormium, zinc selenide and amorphous carbon thin films. *Phys. Rev. B* **44**, 11649 (1991).
25. J. D. Spear and R. E. Russo, Transverse photothermal beam deflection within a solid. *J. Appl. Phys* **70**, 580 (1991).
26. J. M. Bennet, E. Pelletier, G. Albrand, J. P. Borgogno, B. Lazarides, C. K. Carniglia, R. A. Schmell, T. H. Allen, T. Tuttle-Hart, K. H. Guenther, and A. Saxer, Comparison of the properties of titanium dioxide films prepared by various techniques. *Appl. Opt.* **28**, 3303 (1989).
27. A. Rosencwaig, J. Opsal, and D. L. Willenborg, Thin-film thickness measurements with thermal waves. *J. Phys.* **6**, 483 (1983).
28. H. Saito, M. Haraguchi, and M. Fukui, New type of photothermal spectroscopic technique. *Appl. Opt.* **31**, 2047 (1992).
29. E. Welsch, H. G. Walther, K. Friedrich, and P. Eckardt, Separation of optical thin film and substrate absorption by means of photothermal surface deformation technique. *J. Appl. Phys.* **67**, 6575 (1990).
30. M. Commandré and E. Pelletier, Measurements of absorption losses in TiO_2 films by a collinear photothermal deflection technique. *Appl. Opt.* **29**, 4276 (1990).
31. E. D. Palik, ed., "Handbook of Optical Constants of Solids." Academic Press, Orlando, Florida, (1985).
32. K. A. Strain, J. Hough, N. A. Robertson, and K. Skeldon, Measurement of the absorptance of fused silica at $\lambda = 514.5$ nm. *Opt. Commun.* **117**, 385 (1995).
33. G. Compagnini, U. Zammit, K. N. Madhusoodanan, and G. Foti, Disorder and absorption edges in ion-irradiated hydrogenated amorphous carbon films. *Phys. Rev. B* **51**, 11168 (1995).
34. H. Piller, Silicon (amorphous), *in* "Handbook of Optical Constants of Solids" (E. D. Palik, ed.), Academic Press Orlando, Florida, p. 571, 1985.
35. M. H. Chan, S. K. So, K. T. Chan, and F. G. Kellert, Defect density measurements of low temperature grown molecular beam epitaxial GaAs by photothermal deflection spectroscopy. *Appl. Phys. Lett.* **67**, 834 (1995).
36. R. Murri and N. Pinto, Optical properties of amorphous gallium arsenide films. *J. Non-Cryst. Solids* **164–166**, 889 (1993).
37. N. Elgun and E. A. Davis, Transport and optical properties of a-GaP prepared at different substrate temperatures. *J. Phys.: Condens. Matter* **6**, 779 (1994).
38. A. Borghesi and G. Guizzetti, Gallium phosphide (GaP), *in* "Handbook of Optical Constants of Solids" (E. D. Palik, ed.), Academic Press, Orlando, Florida, p. 445, 1985.
39. L. Zanzig, W. Beyer, and H. Wagner, High quality hydrogenated amorphous germanium prepared by the hot wire technique. *Appl. Phys. Lett.* **67**, 1567 (1995).
40. M. L. Theye, M. F. Kotkata, K. M. Kandil, A. Gheorghiu, C. Senemaud, and J. Dixmier, Studies of evaporated amorphous $GeSe_2$ films as a function of annealing. *J. Non-Cryst. Solids* **137–138**, 963 (1991).
41. M. F. Kotkata, K. M. Kandil, and M. L. Theye, Optical studies of disorder and defects in amorphous Ge_xSe_{1-x} films as a function of composition. *J. Non-Cryst. Solids* **164–166, 1259 (1993).**
42. D. W. Lynch and W. R. Hunter, Optical constants of metals, *in* "Handbook of Optical Constants of Solids" (E. D. Palik, ed.), Academic Press, Orlando, Florida, p. 275, 1985.
43. S. Horita, E. Miyagoshi, M. Ishimaru, and T. Hata, Improvement of sensitivity of photothermal deflection spectroscopy by a double pass method. *Rev. Sci. Instrum.* **63**, 1909 (1992).

44. O. J. Glembocki and H. Piller, Indium phosphide, *in* "Handbook of Optical Constants of Solids" (E. D. Palik, ed.), Academic Press, Orlando, Florida, p. 503, 1985.
45. C. Wetzel, V. Petrova-Koch, F. Koch, and D. Grutzmacher, Photothermal deflection spectroscopy of InGaAs/InP quantum wells. *Semicond. Sci. Technol.* **5**, 702 (1990).
46. C. A. Dimitriadis, J. H. Werner, S. Logothetidis, M. Stutzmann, J. Weber, and R. Nesper, Electronic properties of semiconducting $FeSi_2$ films. *Appl. Phys.* **68**, 1726 (1990).
47. W. L. Warren, C. H. Seager, D. Dimos, and E. J. Friebele, Optically induced absorption and paramagnetism in lead lanthanum zirconate titanate ceramics. *Appl. Phys. Lett.* **61**, 2530 (1992).
48. D. F. Edwards, Silicon, *in* "Handbook of Optical Constants of Solids" (E. D. Palik, ed.), Academic Press, Orlando, Florida, p. 547, 1985.
49. See Chapter 3 by A. Mandelis, this volume.
50. I. Umezu, M. Daigo and K. Maeda, Investigation of surface passivation effect of a-SiN_x:H and a-Si:H by photothermal deflection spectroscopy. *Jpn. J. Appl. Phys.* **33**, L873 (1994).
51. F. Leblanc, Y. Maeda, K. Onisawa and T. Minemura, Bulk and surface densities of states of 0.3 μm thick hydrogenated amorphous-silicon films using photothermal deflection spectroscopy. *Phys. Rev. B* **50**, 14613 (1994).
52. G. Amato, G. Benedetto, L. Boarino, M. Maringelli, and R. Spagnolo, Photoacoustic and photothermal deflection spectroscopy of semiconductors. *IEE Proc. A 139*, 161 (1992).
53. S. Nonomura, H. Hayashi, and S. Nitta, Photothermal deflection spectroscopy at 77 K. *Rev. Sci. Instrum.* **60**, 657 (1989).
54. M. W. Ribarsky, Titanium dioxide (TiO_2) (rutile), *in* "Handbook of Optical Constants of Solids" (E. D. Palik, ed.), Academic Press, Orlando, Florida, p. 795, 1985.
55. E. D. Palik and A. Addamiano, Zinc Sulfide, *in* "Handbook of Optical Constants of Solids" (E. D. Palik, ed.), Academic Press, Orlando, Florida, p. 597, 1985.
56. A. Rose, R. Vyas, and R. Gupta, Pulsed photothermal deflection spectroscopy in a flowing medium: A quantitative investigation. *Appl. Opt.* **25**, 4626 (1986).
57. E. L. Lasalle, F. Lepoutre, and J. P. Roger, Probe beam size effects in photothermal deflection experiments. *J. Appl. Phys.* **64**, 1 (1988).
58. J. A. Sell, Optical ray tracing for crossed beam photothermal deflection spectroscopy. *Appl. Opt.* **26**, 336 (1987).
59. M. V. Klein, "Optics." Wiley, New York, 1970.
60. J. F. Power, Frequency modulation time delay thermal lens effect spectrometry: A new technique of transient photothermal calorimetry. *Appl. Opt.* **29**, 841 (1990).
61. N. Kaiser, H. Uhlig, U.B. Schallenberg, B. Anton, U. Kaiser, K. Mann, and E. Eva, High damage threshold Al_2O_3/SiO_2 dielectric coatings for excimer lasers. *Thin Solid Films* **260**, 86 (1995).

Chapter 5

Determination of the Optical Constants by Brillouin Scattering

HACÈNE BOUKARI
Institute for Physical Science and Technology
University of Maryland
College Park, Maryland

and

NICHOLAS LAGAKOS
Naval Research Laboratory
Washington, D.C.

I. Definition of Notation 121
II. Introduction 122
III. Background of Brillouin Scattering Technique 123
IV. Equations for Measurement of the Index of Refraction 125
A. Scattering in Transparent Materials 126
B. Scattering from Absorbing Materials 127
V. Fabry-Perot Interferometers 128
VI. Discussion 129
VII. Brillouin Scattering in Thin Slabs and Optical Fibers 134
VIII. Special Case of Transparent Thin Slabs 135
A. Side Illumination (90° External Scattering) 135
B. Edge Illumination (90° External Scattering) 138
C. Special Geometries 140
D. Examples 141
E. Side Illumination at Normal Incidence 144
IX. Brillouin Scattering in Optical Fibers 146
A. Examples 147
References 153

I DEFINITION OF NOTATION

k_i wavevector incident inside sample
k_s wavevector scattered inside

HANDBOOK OF OPTICAL CONSTANTS OF SOLIDS III

Copyright © 1998 by Academic Press.
All rights of reproduction in any form reserved
ISBN 0-12-544423-0/$25.00.

q	acoustic phonon wavevector
ω	angular frequency in rad/s
ν	frequency in Hertz
n	complex index of refraction
η	index of refraction
κ	extinction coefficient
α_0	absorption coefficient
β_0	phase coefficient
λ_0	wavelength in vacuum
$\lambda_i = \lambda_0/\eta$	wavelength in sample
θ	scattering angle
Ω	Brillouin line frequency
v_s	velocity of sound
F_R	reflective finesse
Δ	free spectral range
t	spacing between Fabry-Perot plates
R	reflectivity of Fabry-Perot plates
c	speed of light in vacuum
Γ_q	damping constant of acoustic phonon
γ_q	sound attenuation constant
η_f	index of refraction of medium between the Fabry-Perot plates
δ	optical skin depth
α, β, γ	angles describing side and edge illumination for thin films
d	film thickness
Y	Young's modulus
σ	Poisson's ratio
ρ	density
P	Pockels coefficient

II INTRODUCTION

Brillouin scattering is known to be a very valuable tool to investigate the elastic properties of various materials. Typically, one can derive considerable information about the acoustic phonons from the measured Brillouin peaks. The shift and the width of the peaks can be directly related to the phonon velocity and the phonon attenuation constant, respectively.

In a pioneering work, Sandercock [1] showed, however, that the Brillouin-scattering technique can be applied also to measure the optical constants of absorbing materials and determined accurately the refractive index and the absorption coefficient of germanium and silicon. For this purpose he used a high-resolution, multipass Fabry-Perot interferometer to examine the broadening effect due to absorption on the Brillouin peaks of these materials. In this chapter we describe this broadening effect and its usefulness in measuring the optical constants of absorbing materials.

BACKGROUND ON BRILLOUIN SCATTERING TECHNIQUE

In a typical Brillouin-scattering experiment, a laser beam is directed onto a scattering medium. The scattered light passes through a Fabry-Perot interferometer and is then collected by a detector positioned at a scattering angle, θ, with respect to the incident beam. One obtains, in principle, the spectrum of scattered light (see Fig. 1) from the scattering sample—a plot of the distribution of scattered intensities as a function of frequency. The shape of the measured spectrum depends on the underlying physical processes responsible for the scattering phenomenon. The theoretical task is to identify these processes and calculate the corresponding spectral lineshape.

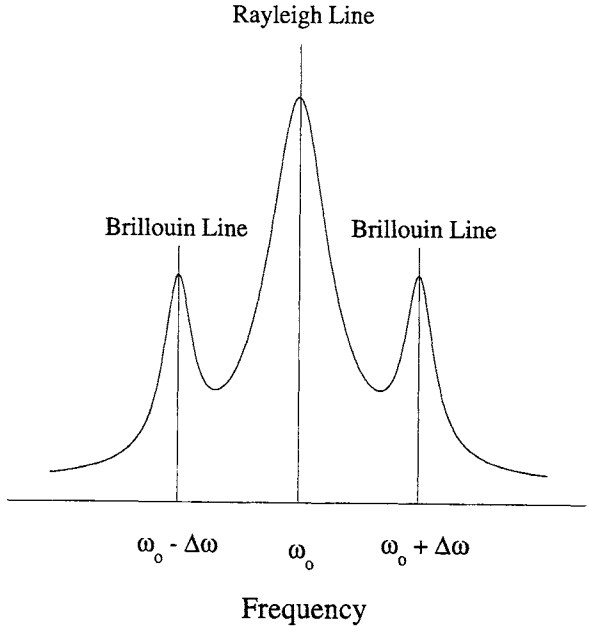

Fig. 1. Typical Brillouin spectrum of a fluid.

As an example, if we consider scattering from a single-component fluid sample, the spectrum of light scattered in a given direction contains three components for a fixed scattering geometry [2, 3]. First, a central Rayleigh line at a non-shifted frequency of the source. This elastic component is caused by density fluctuations in the fluid in thermodynamic equilibrium. These fluctuations cause, in turn, fluctuations in the dielectric constant responsible for the scattering of light. Second, two symmetric, shifted lines. These lines, commonly named Brillouin lines, are caused by inelastic scattering from longitudinal acoustic waves (phonons) propagating in the fluid at a frequency determined by the speed of sound.

In the case of crystals, the spectrum of most light-scattering experiments is composed of a central, non-shifted component and up to three pairs of the phonon components (Brillouin lines): one pair corresponds to longitudinal phonons, and two other pairs correspond to transverse phonons [4–6]. In contrast to the central component in fluids, the non-shifted line is caused by elastic scattering from imperfections either from the surface or bulk of the sample. The Brillouin lines are caused by a collective mode of vibrations of the molecules or atoms forming the sample crystal. We should mention that in crystals, additional components caused by other acoustic quasiparticles such as acoustic magnons, can appear in the spectrum [7].

In the following we will focus only on the Brillouin line as it pertains closely to the application of the Brillouin-scattering technique on the measurement of optical constants. First, there has been extensive progress in understanding and describing the details of the interaction of the incident beam with the scattering system, allowing the calculation of the complete spectral lineshape [4–6, 8]. Second, development of high-contrast, multipass Fabry-Perot interferometers has motivated several experimentalists into applying the Brillouin-scattering technique as a valuable tool in their investigation of elementary excitations in various materials. By increasing the contrast of the instrument, it is possible to detect the weak Brillouin lines and suppress the dominant Rayleigh line [1, 9–13].

The scattering processes can be examined within either a wave (classical) or a quasi-particle (quantum) picture. In the first picture the incident electromagnetic wave, $E \sim e^{i(\omega_i t - \mathbf{k}_i \mathbf{r})}$, is scattered, for example, by the sound waves acting as diffraction gratings. Here we define ω_i and $\mathbf{k}_i$ as the angular frequency and wavevector of the electric field. If the grating were fixed in space, the scattered light would have the frequency of the incident field, ω_i. However, since sound waves propagate with phase velocity, v_s, the gratings move with the same velocity as well. As a result, the back-reflected beam is reduced by a Doppler shift of $2v_s\omega_i/c_m$, c_m being the speed of light in the scattering medium [2]. One can further this analysis and apply the general Maxwell's equations coupled with the elastic properties of the materials to derive the scattering spectrum representing this Doppler-shift line, a challenging theoretical work for complicated structures of the system.

In the quasi-particle picture one can regard the same scattering process as inelastic collisions between photons and phonons [11]. The incident photon has an energy $\hbar\omega_i$ and momentum $\hbar\mathbf{k_i}$, whereas the scattered photon has an energy $\hbar\omega_s$ and momentum $\hbar\mathbf{k_s}$. Conservation of energy and momentum is then applied to extract the form of the normal-mode dispersion relations by requiring that

$$\hbar\mathbf{q} = \hbar\mathbf{k_i} \pm \hbar\mathbf{k_s} \quad (\textit{momentum conservation}), \tag{1}$$

$$\hbar\omega = \hbar\omega_i \pm \hbar\omega_s \quad (\textit{energy conservation}). \tag{2}$$

Two solutions are derived from the above relations: 1) $\mathbf{k_s} = \mathbf{q} - \mathbf{k_i}$ with $\omega_s = \omega - \omega_i$, and 2) $\mathbf{k_s} = \mathbf{k_i} - \mathbf{q}$ with $\omega_s = \omega_i - \omega$. The solutions $\mathbf{q}$ and ω correspond to the annihilation ("anti-Stokes") and creation ("Stokes") of a phonon, respectively. Note that in phonon creation, the scattered photon has a lower frequency than the incident photon, a consistent picture with red-shift tendency.

IV EQUATIONS FOR MEASUREMENT OF THE INDEX OF REFRACTION

We define the complex index of refraction as $n = \eta + i\kappa$, with κ as the extinction coefficient and η as the real-part of the index of refraction of the system (for simplicity we call η the index of refraction). Since our interest is in the measurement of η and κ of a material, our use of a measured Brillouin spectrum is directed to this purpose. So, unlike the common application of the Brillouin-scattering technique as a tool to investigate acoustic phonons in crystals or hydrodynamic modes in fluids, we intend to use the scattering property of the acoustic phonons to determine these optical constants. On the theoretical side, we need to determine the relation between η and κ of the scattering medium and the quantities that can be derived from the measured Brillouin spectrum. On the practical side, we need to design the appropriate spectrometer to measure accurately the Brillouin spectrum. More importantly, we need to discuss the limitations of the Brillouin-scattering technique.

We first note that the energy of acoustic phonons is, at most, of order $E = 10^{-2}$ eV, whereas energy of a visible photon is typically a few eV [11]. Second, for crystals the photon wavevectors are small (of order 10^5 cm^{-1}) compared with typical Brillouin-zone dimensions (of order 10^8 cm^{-1}) [11]. The length scale probed by visible light is long compared with distances between the atoms or molecules constituting the crystal, justifying the application of a continuum picture in the calculations. By applying the above observations, one can find that the magnitude of the wavevector of the incident photon in the medium is conserved in the scattering process. As a re-

sult the momentum-transfer vector q of the phonon probed by the experiment is given by:

$$q = |\mathbf{k_i} - \mathbf{k_s}| = 2k_i \sin(\theta/2), \tag{3}$$

with $|\mathbf{k_i}| = |\mathbf{k_s}|$ being the magnitude of the incident and scattering wavevectors inside the scattering medium. For a laser beam of wavelength λ_0 in vacuum, k_i is given by

$$k_i = \frac{2\pi\eta}{\lambda_0}, \tag{4}$$

where η is the index of refraction of the scattering medium.

The expression in Eq. (3) is commonly known as Bragg's condition. It is an exact relation for elastic scattering and an excellent approximation for most light-scattering situations. The q-value in Eq. (3) can be varied over a wide range by either varying θ or λ (see Eq. (4)) or both. For practical reasons, it is much easier to vary θ. In most experiments, however, θ is fixed and usually set at 90°, although backscattering configuration with $\theta = 180°$ has become a familiar configuration, especially for scattering from opaque materials and thin films.

A Scattering in Transparent Materials

In transparent materials ($\kappa = 0$) the wavevector of the probed phonon is determined uniquely by the wavelength of the incident laser beam and the scattering geometry, specifically the angle θ. The q-wavevector represents one specific Fourier-component of the phonon spectrum. For the observed Brillouin lines, the line shift, Ω, is directly related to the velocity of sound, v_s. This shift is

$$\Omega = v_s q = \frac{4\pi v_s \eta \sin(\theta/2)}{\lambda_0}, \tag{5}$$

where we use the expressions of Eqs. (3) and (4).

Immediately, one can see from Eq. (5) that the shift of the Brillouin line is directly proportional to the index of refraction. If v_s is known, η can be determined, since λ_0 and θ are known. If we neglect the width due to the inherent and natural lifetime of the scattering phonons as well as the width from the instrument (see Section B below), the lineshape of the Brillouin line is very sharp without a width, a theoretical $\delta(q)$-function centered at wavevector q, whose frequency is $\Omega = v_s q$. This can be explained by the uniqueness of the q-vector. The measured intensity is constructed from the

scattered electric fields that add up to form one single peak at the frequency, $\omega_i + \Omega$. Determination of η of transparent materials with such an approach is not commonly pursued, as η can be determined with higher precision using other optical techniques such as prism-minimum deviation and transmission-reflection techniques. The measured Brillouin spectrum is more appropriately used to determine v_s.

Scattering from Absorbing Materials B

Unlike transparent materials, absorbing materials are characterized by a complex refractive index, $n = \eta + i\kappa$, inducing a scale length over which the intensity of the optical field falls off exponentially in the medium. As the varying optical field traverses the material, a range of phonon wavevectors q is covered, adding up to the formed spectrum of the scattered beam [1, 12, 13]. This effect can be readily observed as a broadening of the Brillouin peaks. Here we note that this broadening is an additional effect to that due to the lifetime of the phonon.

For the backscattering configuration, two expressions have been applied to fit the observed Brillouin line, i.e., is, the distribution of the scattered intensity as a function of q wavevector. Initially, Sandercock [1] derived a Lorentzian distribution,

$$L(q) = \frac{1}{\pi} \frac{\alpha_0}{(\beta_0 - q)^2 + {\alpha_0}^2}, \tag{6}$$

where $\beta_0 = 2\omega_i\eta/c$ and $\alpha_0 = 2\omega_i\kappa/c$, ω_i being the angular frequency of the incident beam and c being the speed of light.

However, Dresselhaus and Pine [13] noted later that in the derivation of Eq. (6) the contribution from the reflected optical fields to the total spectrum was neglected. The lineshape of the Brillouin spectrum is not actually symmetric as the Lorentzian function of Eq. (6) suggests. For the same backscattering configuration, the lineshape is rather asymmetric around its maximum and is more accurately described by the following expression:

$$G(q) = \frac{Bq}{({\beta_0}^2 + {\alpha_0}^2 - q^2)^2 + (2q\alpha_0)^2}. \tag{7}$$

In contrast to Eq. (6), the expression in Eq. (7) vanishes at $q = 0$ and falls off as q^{-3} for large q. We further note that $G(q)$ in Eq. (7) and the Lorentzian in Eq. (6) are nearly identical in the limit of a weak absorbent ($\alpha_0 \ll \beta_0$). For a strong absorbent we have ($\alpha_0 \sim \beta_0$), and Eq. (7) appears to be appropriate to the real case.

The calculation for backscattering has been extended to an arbitrary direction of the incident beam [8, 12]. The situation becomes more complicated by the contribution of surface waves of the Rayleigh type to the scattered intensity. Further, the acoustic phonons (bulk) in solids are modified because longitudinal and transverse polarizations are coupled near the surface and cannot be considered independent.

V FABRY-PEROT INTERFEROMETERS

The frequency range of acoustic phonons falls in the Gigahertz, a range suitable to Fabry-Perot interferometers. Nowadays, high-resolution Fabry-Perot interferometers are commercially available and operated routinely to measure Brillouin spectra of various systems. A simple description of the interferometer and its principle of operation can be found in several textbooks [9, 10, 14]. In a simple design, a Fabry-Perot interferometer consists of two plane mirrors held parallel to each other. The inner surfaces are highly reflecting with a reflectivity exceeding 90%. If we examine the case of an ideal Fabry-Perot interferometer, where the plates are considered parallel and free of surface-defects, the instrumental function describing the interferometer is described by an Airy function:

$$I(\omega) = \frac{I_0}{[1 + F \sin^2(\pi\omega/\Delta)]}. \tag{8}$$

Equation (8) represents the lineshape that is obtained if an extremely narrow beam (described by a δ-like function) traverses the interferometer. In Eq. (8) we have $F = 4R/(1 - R)^2$ and $\Delta = c/2\eta_f t$ is the free spectral range, η_f being the index of the medium (usually air) between the mirror plates of reflectivity R, t the spacing between the plates, and c the speed of light in vacuum.

If one varies the spacing, t, or the index of refraction, η_f, one can change the condition of the transmission of light of a given frequency through the interferometer. If a scattered light contains two frequencies set at ω_0 and $\omega_0 + \delta\omega_0$ with ω_0 being at resonance frequency, the peak of the shifted line can be detected by varying t to cover at least one order of interference. Here the conditions for the observation of the shifted peak are determined by two important characteristics of the interferometer: finesse and contrast. First, the finesse, F_R, is the ratio of the free spectral range over the full width at half maximum of the Airy line and describes the capability of the instrument in separating various peaks. For an ideal interferometer it is defined as

$$F_R = \pi\sqrt{R}/(1 - R), \tag{9}$$

and depends only on the reflectivity.

Second, the contrast, C, is the ratio of the maximum over the minimum of the instrumental line, providing an idea on the power of the instrument to detect weak signals. For an ideal interferometer, it is given by

$$C = 1 + (4/\pi^2)F_R^2. \tag{10}$$

Both expressions of Eqs. (9) and (10) show that as R is increased, both finesse and contrast increase. In principle, one can then improve the performance of the interferometer by just changing R. However, imperfections such as surface defects and misalignment introduce a limit to the finesse and contrast [9, 10]. In the interferometers now available, F_R does not usually exceed ~ 50 and $C < 10^3$. This contrast number is particularly too small if one intends to measure very weak peaks, such as those of phonons in highly absorbing materials. For this purpose, a multipassing technique has been devised to increase the contrast [9, 10]. Here, the beam of light passes through the interferometer several times. It can be shown that the resultant contrast, C_n, is

$$C_n = C^n, \tag{11}$$

where n is the number of passes of the beam through the interferometer, and C is the contrast for one pass. In practice, two corner cubes are usually used to achieve multipassing by reflecting and appropriately directing the beam from the various facets of the two cubes. It is now possible to achieve a contrast as high as 10^{12}.

The schematic diagram of a typical set-up for the measurements of acoustic phonons by a multi-pass Fabry-Perot interferometer is shown in Fig. 2. The setup may operate either on 90°-geometry or in backscattering. The light of a laser beam (~200 mW) is focused and directed to a sample by the lens L_1 (90°) or L_2 (backscattering). The scattered light is collected by the lens L_2 and directed onto the input aperture of the Fabry-Perot interferometer. Here, the spacing between the plates t is scanned by piezoelectric rods to cover a number of orders of interference. The output beam passes through the collimator formed by the lenses L_2 and L_3, and is directed to a sensitive photomultiplier (PMT-1) usually with a low dark count (~1 ct/s). The output signal from the photomultiplier is amplified and further processed by a photon-counting circuit. The processed signal is fed to a multichannel analyzer. A second photomultiplier (PMT-2) in combination with a stabilization system is used in a feedback mode to control the plate separation by adjusting the piezoelectric spacers.

VI DISCUSSION

The main information obtained from a measured Brillouin spectrum are the line shift, the linewidth, and the distribution of intensity as a function of frequency, including the maximum peak.

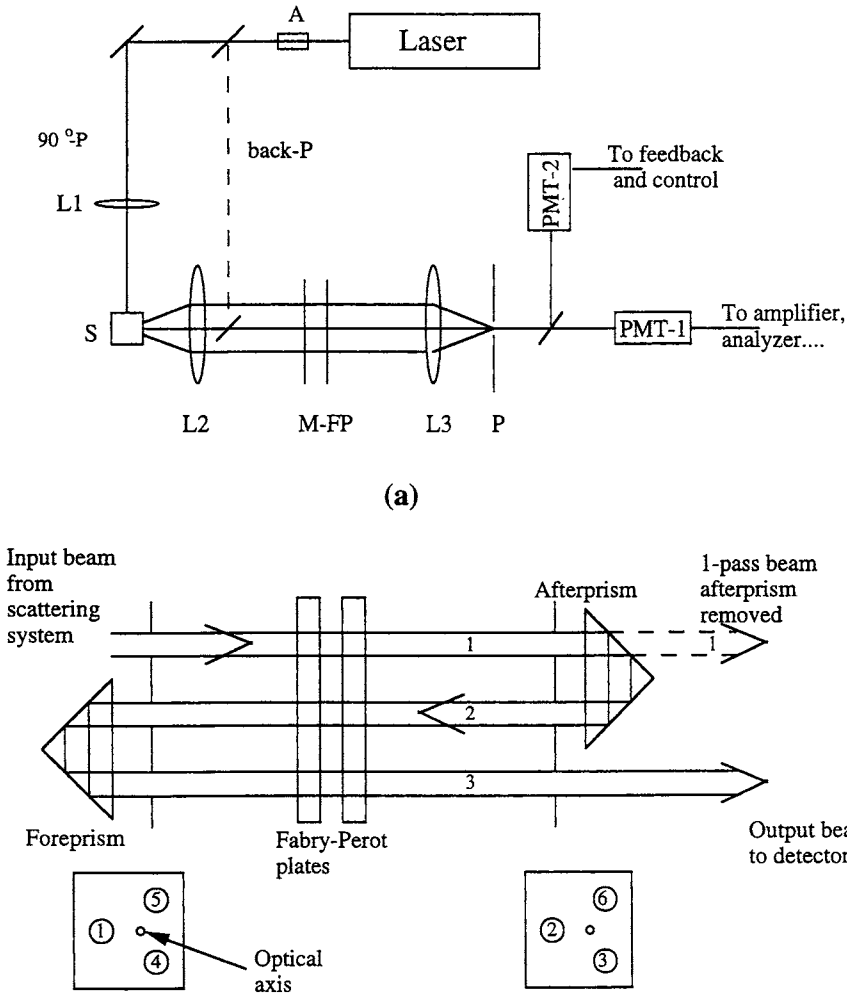

Fig. 2(a). Schematic diagram of an experimental setup to measure the Brillouin spectrum of a sample *S*. Two configurations are shown 90° (90°-*P*) and backscattering (back-*P*). L1, L2, and L3 are optical lenses, *M-FP* the Fabry-Perot interferometer, *P* the collecting pinhole, *PMT*-1 and *PMT*-2 the photomultiplier tubes. **(b)** Details of the 3-pass aperture and retroreflection prism of a 3-pass Fabry-Perot interferometer.

The line shift is directly related to the phonon velocity and is given by Eq. (5). Equation (5) shows that the shift depends on the velocity as well as the index of refraction. As discussed earlier for transparent materials, it is much more appropriate to use the Brillouin spectrum to determine the phonon velocity instead of η, since other optical techniques such as transmission-

reflection and prism-minimum deviation techniques are much more precise in measuring η. However, for practical reasons and experimental difficulties, the Brillouin-scattering technique is sometimes used to determine η. For example Zha *et al.* [15] applied the technique to investigate the effect of high pressure on transparent SiO_2 glass. For this purpose, they measured the Brillouin line shift at two different angles, 90° and 135°, (two q-vectors) and determined simultaneously both η and v_s from the ratio of the shifts. As the pressure was varied, they observed changes in η and v_s indicating changes in the structural properties of the glass. We should note, however, that this two-angle method is appropriate when the material is isotropic with one phonon velocity, therefore simplifying the problem. For anisotropic crystals, complications arise as the phonon velocity changes as a function of optical axis or q-vector. It is not possible then to separate η and v_s, since both vary as a function θ (q-vector).

Information on linewidth is much more useful in the case of absorbing materials as κ is related to the width. The experiments are performed in a backscattering configuration with a high-resolution, multi-pass Fabry-Perot interferometer, allowing the detection of weak Brillouin peaks [1, 16]. To get an accurate value of the width due to just broadening from absorption, corrections are needed to remove contributions from the phonon lifetime and the instrumental function that may include effects due to the finite size of the collection pinhole (see Refs. 9, 10, and 17–19 for more discussion).

Several methods have been developed to correct for contributions from the instrumental linewidth. One can fit the instrumental function with some familiar functions such as a Gaussian or Voigt function and deconvolute numerically the observed spectrum from the fitted instrumental function (see Refs. 17 and 18 and references therein). A more elaborate deconvolution scheme can be performed by first deriving an analytical form of the instrumental function (see Refs. 17–19 for more discussion). Here, the Airy function of the ideal Fabry-Perot interferometer is modified to include various defects in the instrument. Then, this analytical function is convoluted with the predicted scattering function (expression of Eq. (6) or Eq. (7) in our case). The resulting function is fit with the observed spectrum to determine the appropriate parameters (optical constants).

It is sometimes important to correct also for the broadening effect due to the finite size of the collecting pinhole on the spectrum. Indeed, the pinhole introduces a finite solid angle, collecting a range of q-wavevectors instead of the unique q defined in the above theoretical treatment. Experimentally, one has to compromise between reducing the pinhole size to avoid significant broadening and opening it to collect more signal [18].

In Table I we list η and κ for numerous materials which have been studied by Brillouin-scattering technique [20–36]. We should point out that only a few of these materials could yield linewidth information (Si, Ge, CdS, GaAs). Of particular interest is the ratio of the width of the lineshape to the

TABLE I

Index of Refraction and Extinction Coefficient of Numerous Materials

Material	η (5145 Å)	κ (5145 Å)	$\Delta\omega/\Omega = 2\kappa/\eta$	δ (cm)	Reference
CaF_2	1.43	$< 1 \times 10^{-7}$	$< 1.4 \times 10^{-7}$	> 41	[34, 35]
AlN	2.4	$< 1 \times 10^{-6}$	$< 1 \times 10^{-6}$	> 4.1	[36]
ZnO	2.05	$< 1 \times 10^{-6}$	$< 1 \times 10^{-6}$	> 4.1	[28]
GaP	3.55	1.2×10^{-3}	5.6×10^{-4}	3.41×10^{-3}	[23]
CdS†	2.7	4.1×10^{-3}	3.0×10^{-3}	1×10^{-3}	[20–22]
Si	4.21	0.06	0.028	6.82×10^{-5}	[1, 33]
GaAs	4.2	0.37	0.17	1.1×10^{-5}	[33]
TiN	1.2	1.6	2.66	2.56×10^{-6}	[32]
Ta	2.68	1.92	1.43	2.13×10^{-6}	[33]
Au	0.61	2.1	6.9	1.93×10^{-6}	[26, 29]
Ge	4.6	2.45	1.06	1.67×10^{-6}	[1, 33]
Cu	1.12	2.60	4.4	1.57×10^{-6}	[33]
Ni	1.7	3.1	3.77	1.33×10^{-6}	[25, 33]
Co	1.90	3.6	3.77	1.14×10^{-6}	[30]
Fe	2.8	3.7	2.64	1.11×10^{-6}	[33]
Mo	3.6	3.8	2.11	1.08×10^{-6}	[27]
Cr	2.75	4.46	3.24	9.2×10^{-7}	[33]
Al	0.84	6.2	14.7	6.6×10^{-7}	[24, 31, 33]

† Values for electric field polarization perpendicular to c-axis.

frequency shift. Assuming the lineshape to be Lorentzian, one can derive from Eq. (6)

$$\frac{\Delta\omega}{\Omega} = \frac{2\kappa}{\eta}, \tag{12}$$

where $\Delta\omega$ is the full width at half maximum of the line. Equation (12) can be expressed in terms of the absorption coefficient $\alpha_0 = 4\pi\kappa/\lambda_0$ or the skin depth $\delta = 1/\alpha_0$, yielding the following practical relation:

$$\frac{\Delta\omega}{\Omega} = \frac{2\kappa}{\eta} = \frac{\lambda_0}{2\pi\eta\delta}. \tag{13}$$

First, we emphasize that the relation in Eq. (12) is exact only when the lineshape is Lorentzian, a case applicable for low-absorbing materials such as Si. For highly absorbing systems such as Ge, the expression in Eq. (7) describes more accurately the measured lineshape, and Eq. (12) is just an approximation. We show in Fig. 3 the lineshape of the Brillouin lines of Si and Ge as measured by Sandercock [1]. Here we contrast the symmetric line observed for Si with the asymmetric line of Ge, a point already made by Dresselhaus and Pine [13].

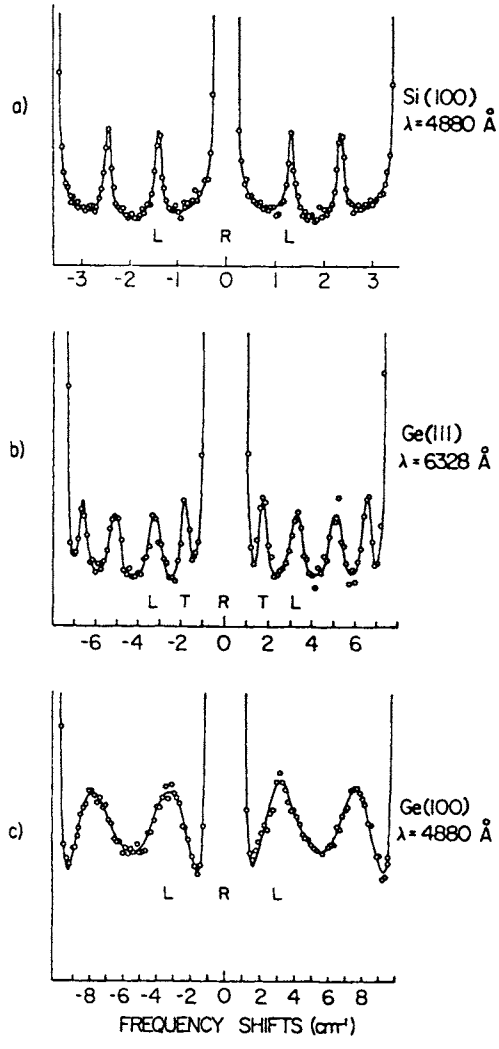

Fig. 3. Brillouin peaks of Si and Ge obtained by Sandercock [1].

Second, we note that the ratio, $\Delta\omega/\Omega$, can be obtained directly from the measured line. Sood and Cardona [16] measured the change in ratio $\Delta\omega/\Omega$ in Si as a function of concentration of a n-type dopant, which changes its absorption coefficient. We show in Fig. 4 their results. The determination of κ or η from the measured line requires previous knowledge of η or κ from another technique. If both η and κ are unknown, one needs the phonon velocity, v_s, which can be determined from ultrasonic measurements, for example. This approach was followed by Sandercock [1] in his analysis of his

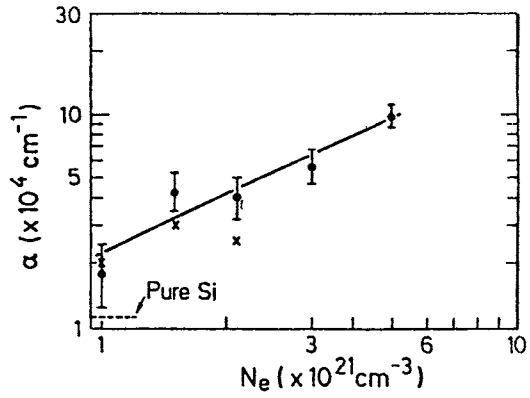

Fig. 4. Optical absorption coefficient of Si is shown as a function of concentration of dopant. The data were determined from the broadening of the measured Brillouin peaks. (From Sood and Cardona [16] with permission from the publisher.)

Si and Ge measurements. In this way, the Brillouin technique works as a complementary technique.

Third, Table I indicates further that the ratio in Eq. (12) becomes larger in highly absorbing materials such as metals. It may then be difficult to observe the peak, as its width can be larger than its frequency shift. Indeed, as κ is increased, the linewidth increases, extending the wings of the Brillouin peak to interfere with the next order of the Fabry-Perot lines. Another way, if the skin depth is of the order of the wavelength of the beam in the scattering medium ($\delta = \lambda_0/\eta$), Eq. 13 yields $\Delta\omega/\Omega \simeq 1/6$, showing a big broadening effect already. Since for metals, $\Delta\omega/\Omega \geq 2$, this is probably why bulk acoustic phonons have not been reported for metals. Practically speaking, materials with $0.01 < \Delta\omega/\Omega < 1$ show probably a measurable linewidth dependence on absorption.

VII BRILLOUIN SCATTERING IN THIN SLABS AND OPTICAL FIBERS

In the second part of this chapter, Brillouin scattering is considered in thin samples, such as thin slabs and single-mode optical fibers, where the dimension of the sample becomes of the same order as the light wavelength. Contrary to the bulk-sample case where both light and phonon energy and momentum are well defined, in thin samples, the light scattered over the thickness of the film develops an envelope of frequencies (and wavevectors), which, therefore, encompass more phonon energies and wavevectors. First, the formulas for calculating the refractive index in slabs are given for several convenient scattering geometries. Then, some examples of Brillouin spectra from the literature are considered, and the refractive index of the

samples is calculated using the given formulas. Finally, phonon propagation in thin slabs and single-mode fibers is discussed.

SPECIAL CASE OF TRANSPARENT THIN SLABS VIII

The refractive index η of a sample can be determined from the Brillouin shift Ω of an acoustic excitation or phonon from one of the two following relationships:

$$\Omega = \frac{4\pi v_s \eta}{\lambda_0} \sin\frac{\theta_s}{2}, \quad q = \frac{4\pi\eta}{\lambda_0} \sin\frac{\theta_s}{2}, \tag{14}$$

where v_s is the velocity of sound of the phonon generated by the light scattering, λ_0 is the wavelength of the incident light in vacuum, and θ_s is the scattering angle in the sample. The dispersion curve for acoustic phonons is given by $\Omega = \omega = qv_s$, where ω is often used, and q is the phonon wavevector. The Brillouin scattering in thin samples can be done by using side illumination [37–40] or edge illumination [40].

Side Illumination (90° External Scattering) A

Most Brillouin spectra in thin samples have been measured by using the side illumination, which is shown schematically in Fig. 5. In this figure, light is incident from the side of the sample (which has 1.458 refractive index, as that of silica), and the scattered light is observed at 90°. The internal scattered angle is not 90°. As can be seen from Fig. 5 (where the notation of Wang *et al.* [37] has been used), two different phonons are generated (created or destroyed depending on whether it is Stokes or anti-Stokes) with the refracted and reflected beams to produce the scattered light inside the sample. Note that for a typical material with $\eta = 1.5$, at a reflection most of the light is refracted out of the slab; only ~4% is reflected for modest angles of incidence. As shown in Fig. 5, in the first case, the phonon has q_1 wavevector, and the scattering angle is θ_1; while in the second case, the phonon has q_2 wavevector, and the scattering angle is θ_2. The two scattering angles can be determined from the following equations:

$$\theta_1 = \beta + \gamma, \quad \theta_2 = \pi - \beta + \gamma, \tag{15}$$

where β and γ are related to the refractive index η:

$$\eta\sin\beta = \sin\alpha, \quad \eta\sin\gamma = \cos\alpha, \tag{16}$$

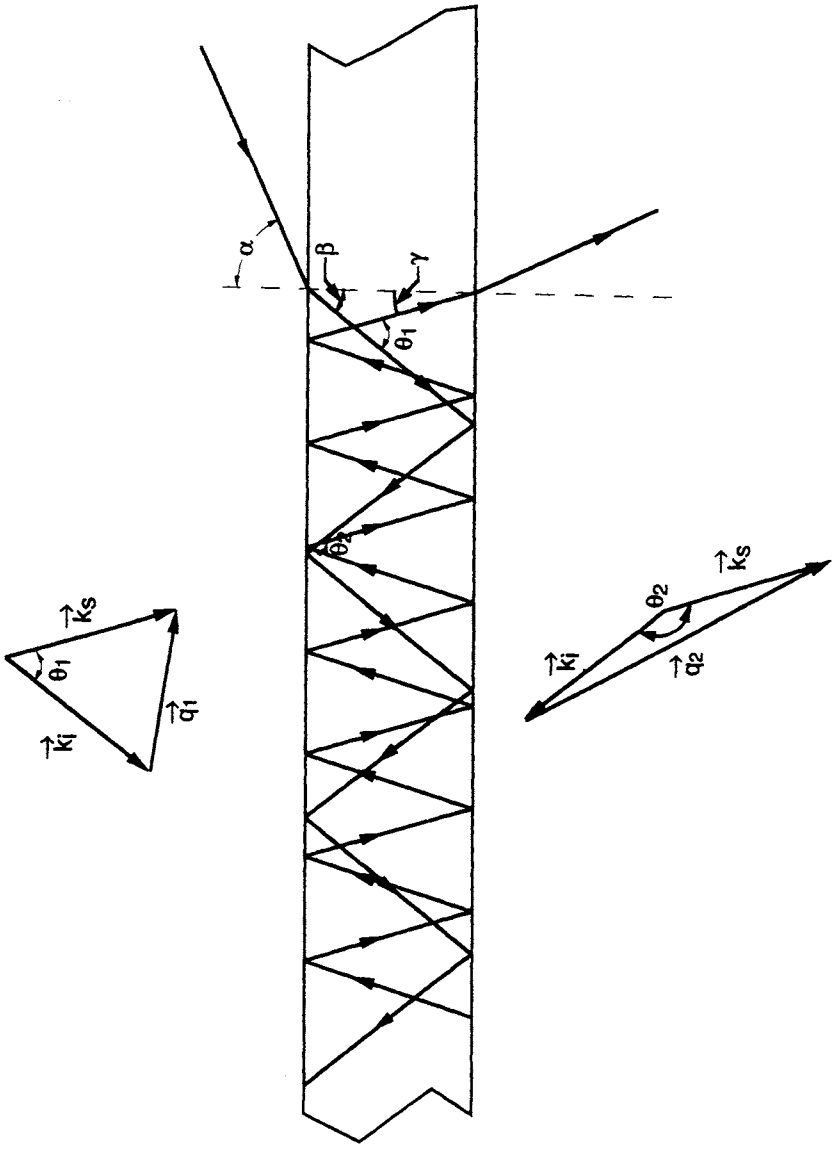

Fig. 5. Side illumination with 90° external scattering.

where α is the incident angle (not to be confused with the absorption coefficient, α_0) and β is the refraction angle (not to be confused with the phase coefficient, β_0). In the second Eq. (16), $\cos\alpha = \sin\alpha'$, since a 90° scattering is considered. Here, α' is the angle formed by the external scattered light and the normal to the sample surface. Note that in Fig. 5 the q_2 phonon is involved with near-backscattering internally.

Using the above equations, it can be shown that the phonon velocity v_s [Eq. (14)] can be expressed in terms of η and the incident angle α as follows [37]:

$$v_{s,1} = \frac{\Omega_1 \lambda_i}{[2\eta^2 + \sin 2\alpha - 2(\eta^4 - \eta^2 + \frac{1}{4}\sin^2 2\alpha)^{1/2}]^{1/2}}, \tag{17}$$

$$v_{s,2} = \frac{\Omega_2 \lambda_i}{[2\eta^2 + \sin 2\alpha + 2(\eta^4 - \eta^2 + \frac{1}{4}\sin^2 2\alpha)^{1/2}]^{1/2}}, \tag{18}$$

where Ω_1 and Ω_2 are the Brillouin shifts corresponding to the phonons with q_1 and q_2 wavevectors, respectively. For many transparent materials, one usually knows η in advance, so the phonon velocity is determined. For a cubic crystal oriented so that the principal axes are along the slab edges, these phonons will, in general, have different velocities. For an isotropic sample ($v_{s,1} = v_{s,2}$), from the above Eqs. (17) and (18), the following equation is obtained

$$\frac{\Omega_1^2}{\Omega_2^2} = \frac{2\eta^2 + \sin 2\alpha - 2(\eta^4 - \eta^2 + \frac{1}{4}\sin^2 2\alpha)^{1/2}}{2\eta^2 + \sin 2\alpha + 2(\eta^4 - \eta^2 + \frac{1}{4}\sin^2 2\alpha)^{1/2}}. \tag{19}$$

Fused silica can serve as an example of an isotropic sample. From this equation the refractive index η can be found from the Brillouin shifts Ω_1 and Ω_2 for any incident angle α.

45°–45° Scattering When the incident angle α is 45°, Eq. (19) has a very simple form. This geometry, in which the sample bisects the incident and the scattered light (45°–45°), has been used extensively in the literature to obtain the refractive index of thin samples and films [37–40]. In this case, $\beta = \gamma$ and $\alpha = 45°$ (see Fig. 5). The q_2 phonon is involved in internal backscattering. Then, from Eqs. (14), (15), and (16) one obtains:

$$v_{s,1} = \frac{\Omega_1 \lambda_i}{\sqrt{2}}, \tag{20}$$

$$v_{s,2} = \frac{\Omega_2 \lambda_i}{2\eta}. \tag{21}$$

Therefore, for an isotropic sample the refractive index η can be obtained from the following equation:

$$\eta = \frac{1}{\sqrt{2}} \frac{\Omega_2}{\Omega_1}. \tag{22}$$

B Edge Illumination (90° External Scattering)

This geometry, in which light is incident at the edge of the sample, has been discussed extensively by Takagi and Gammon [40], and it is shown schematically in Fig. 6. Our notation continues to be that found by Wang *et al.* [37]. One of the positive characteristics of this geometry is that the intensity of the phonon peaks is much stronger than that with the side illumination [40]. This is probably due to the larger volume per reflection implied by Fig. 6 compared to Fig. 5. Similarly to the side-illumination case, as can be seen from Fig. 6, two different phonons are involved in the scattering of the refracted and the reflected beams inside the sample. In the first case, the phonon has q_1 wavevector, and the scattering angle (inside the sample) is θ^*_1, while in the second case the phonon has q_2 wavevector, and the scattering angle is θ^*_2. The two scattering angles can be determined by the following equations:

$$\theta^*_1 = \pi - \beta - \gamma, \quad \theta^*_2 = \pi - \beta + \gamma, \tag{23}$$

where β and γ are related to the refractive index η through Eq. (16). Note that in Fig. 6, the q_2 phonon is involved with internal near-backscattering. Using Eqs. (14), (16), and (23) one obtains:

$$\nu^*_{s,1} = \frac{\Omega^*_1 \lambda_i}{[2\eta^2 - \sin 2\alpha + 2(\eta^4 - \eta^2 + \frac{1}{4}\sin^2 2\alpha)^{1/2}]^{1/2}}, \tag{24}$$

$$\nu^*_{s,2} = \frac{\Omega^*_2 \lambda_i}{[2\eta^2 + \sin 2\alpha + 2(\eta^4 - \eta^2 + \frac{1}{4}\sin^2 2\alpha)^{1/2}]^{1/2}}. \tag{25}$$

Note that Eqs. (18) and (25) are the same. From Eqs. (24) and (25) for an isotropic sample, we obtain the following equation:

$$\frac{\Omega^{*2}_1}{\Omega^{*2}_2} = \frac{2\eta^2 - \sin 2\alpha + 2(\eta^4 - \eta^2 + \frac{1}{4}\sin^2 2\alpha)^{1/2}}{2\eta^2 + \sin 2\alpha + 2(\eta^4 - \eta^2 + \frac{1}{4}\sin^2 2\alpha)^{1/2}}. \tag{26}$$

From this equation, the refractive index η can be found from the Brillouin shifts Ω^*_1 and Ω^*_2 for any incident angle α.

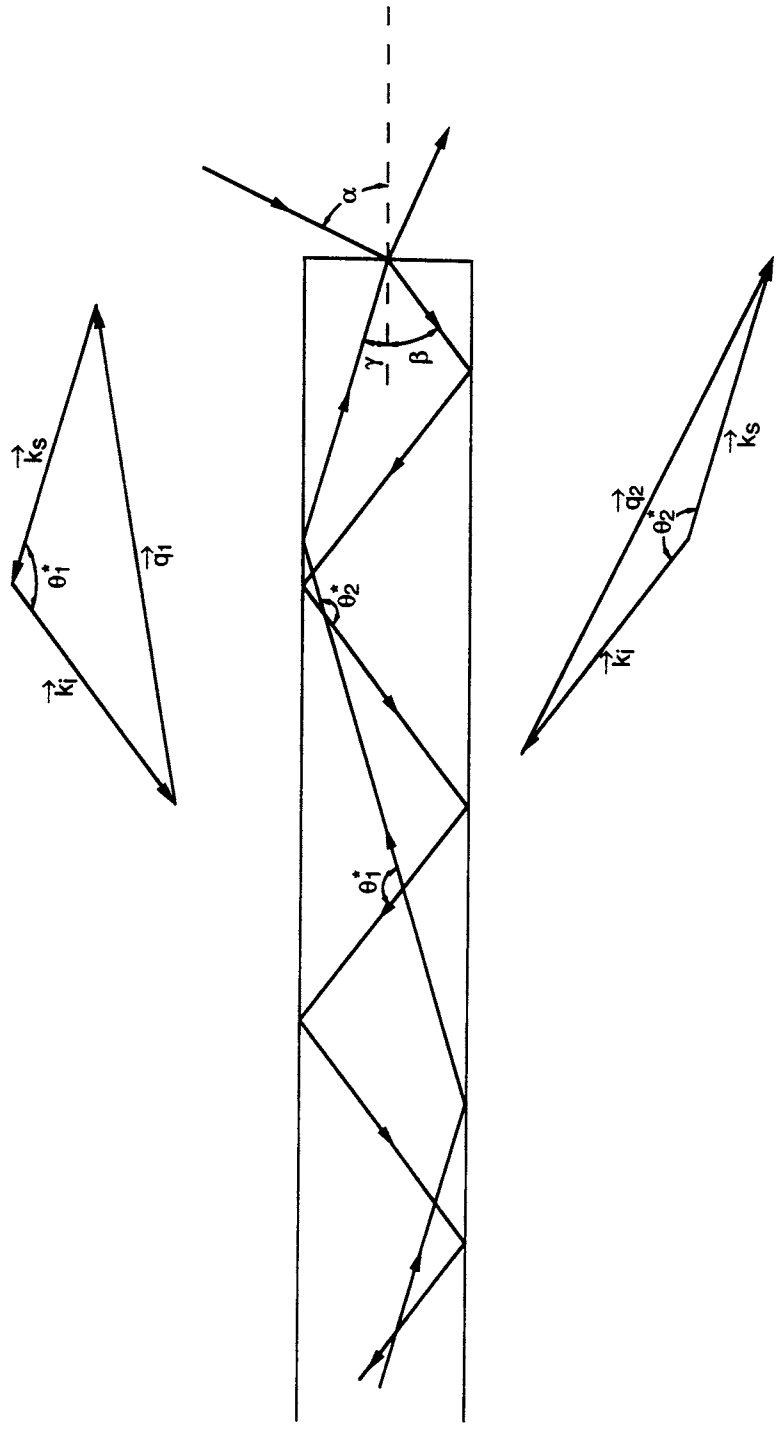

Fig. 6. Edge illumination with 90° external scattering.

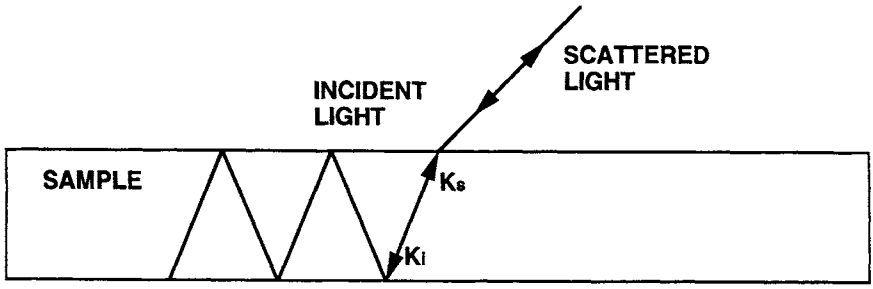

Fig. 7. Side illumination with 180° external backscattering.

45°–45° Scattering In this geometry we have $\beta = \gamma$ and $\alpha = 45°$. The q_2 phonon is involved exactly in backscattering internally. Then, from Eqs. (14), (16), and (23) one obtains:

$$v_{s,1} = \frac{\Omega^*{}_1 \lambda_i}{\sqrt{2}(2\eta^2 - 1)^{1/2}}, \tag{27}$$

$$v_{s,2} = \frac{\Omega^*{}_2 \lambda_i}{2\eta}. \tag{28}$$

Note that Eqs. (21) and (28) are the same. Therefore, the refractive index of an isotropic sample can be found from the following equation:

$$\eta = \frac{1}{\sqrt{2}[1 - \Omega^{*2}{}_1/\Omega^{*2}{}_2]^{1/2}}. \tag{29}$$

C Special Geometries

1 External Backscattering

Two examples of external backscattering (rather than 90° external scattering) are shown in Figs. 7 and 8, where backscattering is done from the side and the edge of the thin slab. For external backscattering for both side and edge illumination, the same phonon with wavevector q_2 is observed as described by Eqs. (18) and (25) or for the 45°–45° position, by Eqs. (21) and (28). Note that since only one q_2 phonon is observed (and q_2 is along k_s), Eqs. (17) and (24) are not pertinent. These results hold for an isotropic material or for a cubic material with the principal crystal axes along the edges of the thin slab. For an isotropic sample it can be shown from selection-rule analysis that for the backscattering geometry (180°), only the longitudinal phonon will be present, while no transverse phonon can be seen [41].

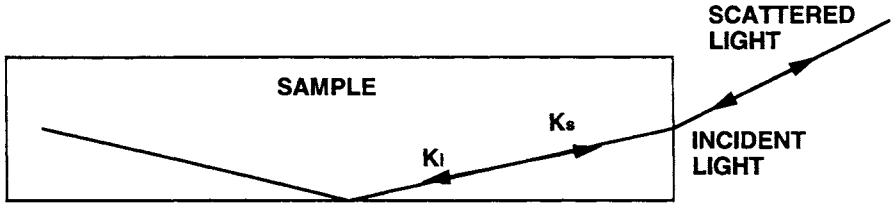

Fig. 8. Edge illumination with 180° external backscattering.

Classical 90° Scattering 2

For the traditional 90° scattering from a bulk sample shown in Fig. 9, $\theta_s = 90°$ in Eq. (14) and, thus:

$$v_s = \frac{\Omega\lambda_i}{\sqrt{2}\eta}. \tag{30}$$

Note that the phonon propagates at 45° to the plate edge. Contrary to the backscattering case, in the 90° scattering both the longitudinal phonon and the transverse phonons (only one transverse phonon for an isotropic sample) will be present.

Examples D

Here, some Brillouin spectra from thin plates and films are used from the literature to calculate their refractive index.

Isotropic Samples 1

Glass Plate The Brillouin spectra of a thin glass plate (150 μm thick) for the 45°–45° geometry for the side and edge illumination, is shown in

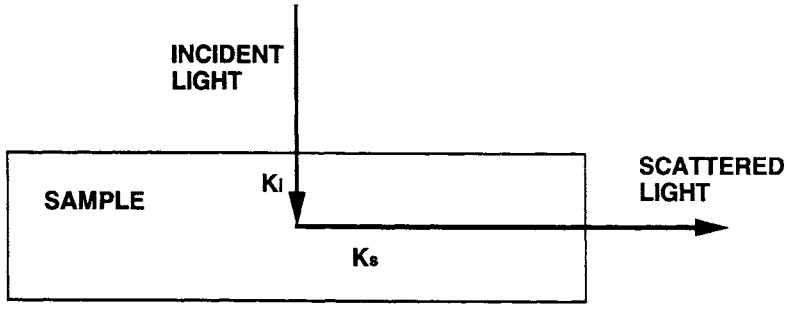

Fig. 9. Classical 90° scattering.

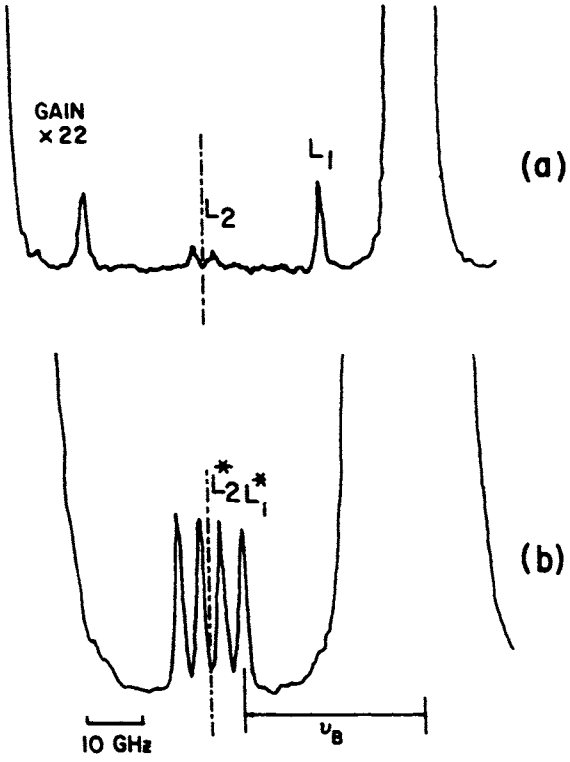

Fig. 10. Typical Brillouin spectra of thin glass plate (150 μm thick). $FSR = 77$; $\alpha = 45°$. (a) Side illumination; (b) Edge illumination. (After Takagi and Gammon [40].)

Fig. 10 [40]. The spectra were obtained using the VV scattering geometry, where only the longitudinal phonons can be seen for an isotropic sample.

In Fig. 10(a) the side illumination was used to obtain the ratio of the Brillouin shifts of the two longitudinal phonons L_1 and L_2 (with q_1 and q_2 wavevectors in Figs. 5 and 6). Then, using this ratio from Eq. (22), the refractive index of the isotropic thin glass plate is calculated to be 1.52.

In Fig. 10(b) the edge illumination was used to obtain the ratio of the Brillouin shifts of the two longitudinal phonons L^*_1 and L^*_2. Using this ratio, from Eq. (29) the refractive index of the thin glass plate is calculated to be 1.51, which is close to the 1.52 obtained from the side illumination. While this type of glass was not described, the fused-silica refractive index is 1.458, which is close to that obtained above.

Polymer Film: Mylar-PET The Brillouin spectra obtained from a polymer film, Mylar-PET, which is a commercial film used as a transparency sheet for overhead projectors can be seen elsewhere [40]. In this case, the side illumination and the 45°–45° scattering geometry were used to obtain

the Brillouin spectra shown in Fig. 11. From the ratio of the Brillouin shifts of the two longitudinal phonons L_1 and L_2, the refractive index of the isotropic Mylar-PET film is found from Eq. (22) to be 1.28. Most plastics have refractive indexes in the range 1.42–1.65, so this value appears too low [42, 43].

DNA Films The refractive index and the sound speed of DNA films has been studied using backscattering and 45°–45° geometry [39]. It was found that the refractive index decreases as the relative humidity of the DNA films increases (for dry DNA, $\eta = 1.50$).

Uniaxially Stretched Films 2

For nonisotropic films, the formulas given above for determining the refractive index are not expected to hold.

PET Film Brillouin scattering has been used in polyethylene terephalate (PET) films to study the sound velocity and the elastic constants as a function of the film stretching ratio [38]. The refractive index of the unoriented PET film is 1.588 at 4880 Å, which is within the range of plastics [42, 43]. It was found that, even though the refractive index of the film is not sensitive to stretching, the elastic constants strongly depend on the stretching ratio of the uniaxially stretched film [38]. The refractive index of the uniaxially stretched PET was found from the Brillouin spectra (side excitation; 45°–45° geometry) [38] using Eq. (22) to be 1.06, a value too low for plastics [42, 43]. This discrepancy is due probably to the fact that Eq. (22) holds only for isotropic samples.

Polyvinylidene Fluoride (PVF_2) Films Brillouin scattering was also used to study the sound velocity and the elastic constants of uniaxially stretched PVF_2 films [37]. Similar to the PET case, while the refractive index is not

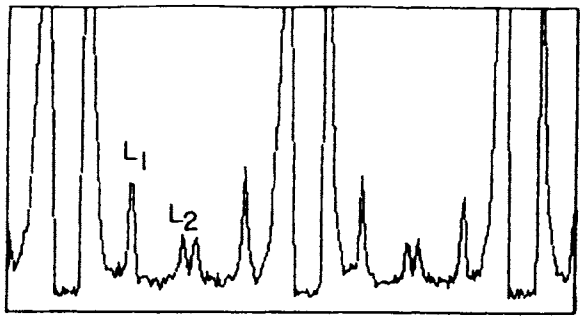

Fig. 11. Brillouin spectra of polymer film Mylar-PET with side illumination. *FSR* = 40 GHz. (After Takagi and Gammon [40].)

sensitive to stretching ($\eta = 1.43$), the sound velocity and the elastic constants are sensitive to the stretching ratio. From the Brillouin spectra (side illumination; 45°–45° geometry) seen elsewhere [37], it was found (using Eq. (22)) that the refractive index of the PVF_2 in the form I is 1.05, while in the form II it is 1.02, values too low for plastics. As in the previous case, this discrepancy is due probably to the fact that the film is not isotropic.

E Side Illumination at Normal Incidence

Brillouin scattering has been used to study phonon propagation in thin films. Following Sandercock [44], for the case of backscattering (180°) perpendicular to the film surface, we have the following distinct regimes.

a. With a real refractive index η, for a semi-infinite thick film, the Brillouin spectrum is typical with the normal Brillouin shift $\Omega = 2\eta k_0 v_s$, as illustrated in Fig. 12(a), where some instrumental and phonon-lifetime broadening of the peaks has been assumed.

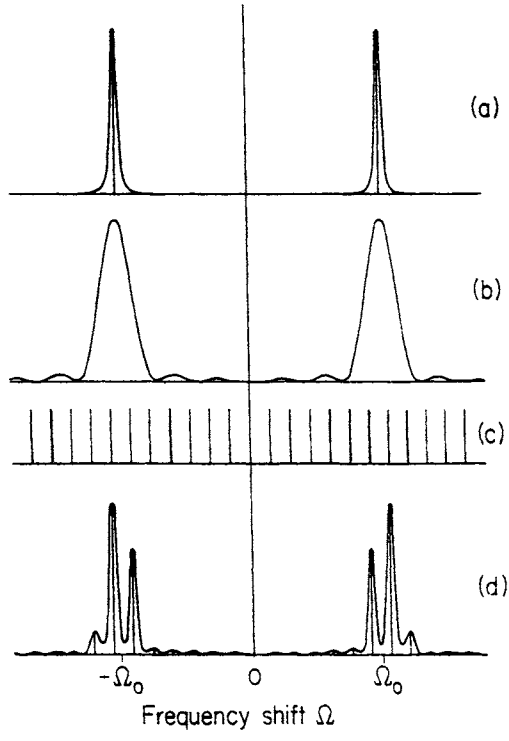

Fig. 12. (a) A normal Brillouin spectrum, (b) the expected spectrum from a thin supported film, (c) the possible frequency shifts in the spectrum from a thin unsupported film, and (d) the observable spectrum from a thin unsupported film. (After Sandercock [44].)

b. With a real η, there is a special case of a film supported on a substrate with the special properties that the substrate has the same acoustic impedance (so phonons can propagate across the boundary freely), but the substrate has very different elasto-optic properties, so that scattering occurring in the film is distinguishable from scattering in the substrate. Such a film/substrate sample probably does not exist, so the spectrum in Fig. 12(b) is not observable. Since film and substrate have the same acoustic properties, all values of q perpendicular to the surface are allowed. However, the Brillouin peaks are broadened due to the finite summation of the scattered electric fields as the incident beam traverses the film. The line shape is given by a $\sin^2 x/x^2$, as shown schematically in Fig. 12(b). Here, $x = (\Omega_0 - \Omega)d/2v_s$, where d is the film thickness, Ω_0 is the Brillouin shift corresponding to the phonon frequency, and Ω is the variable frequency.

c. If further, the film is unsupported, the boundary conditions require that the component of the phonon wavevector perpendicular to the surface be an integral multiple of π/d. In this case, the Brillouin spectrum would have peaks at the frequency shifts $\Omega = qv_s = p\pi v_s/d$ (p is an integer), as shown in Fig. 8(c).

d. Moreover, these phonon lines have a relative amplitude determined by the $\sin^2 x/x^2$ envelope (Fig. 8(b)). Thus, the resulting Brillouin spectrum will be similar to that shown in Fig. 12(d), where again, some instrumental and lifetime broadening has been assumed. The exact form of the peaks of Fig. 12(d) depends on the thickness d, but in general they show triplet or quadruplet structure within the main peak of the $\sin^2 x/x^2$ envelope. With reference to the dispersion curve shown schematically in Fig. 13, the quantized acoustic-phonon modes would be along the q-axis, while the measured phonon frequencies would occur along the ω-axis. Furthermore, the observed modes would be attenuated severely.

e. With a complex index of refraction n, a near-Lorentzian broadening of the Brillouin peaks occurs, as has been discussed in Section IVB. Therefore, the Brillouin components in Fig. 12(d) should be broadened.

From the above discussion the main conclusion is that while normal Brillouin scattering (from a large volume) determines precisely both the energy (from the spectrum) and the momentum (from the scattering geometry) of the phonon involved, the backscattering from a thin film normal to the surface measures phonons within a range of momenta and correspondingly, having a range of energies.

The predicted triplet in the Brillouin spectrum of a thin unsupported film (Fig. 12(d)) has been observed experimentally in Mn_2PS_4 films [44]. Figure 14 shows the observed Brillouin spectrum from two specimens of Mn_2PS_4 of thickness 1.1 and 2.0 μm. In both these spectra the triplets are clear; as the thickness of the film increases, however, the secondary peaks of the triplet get much weaker (Fig. 14(b)).

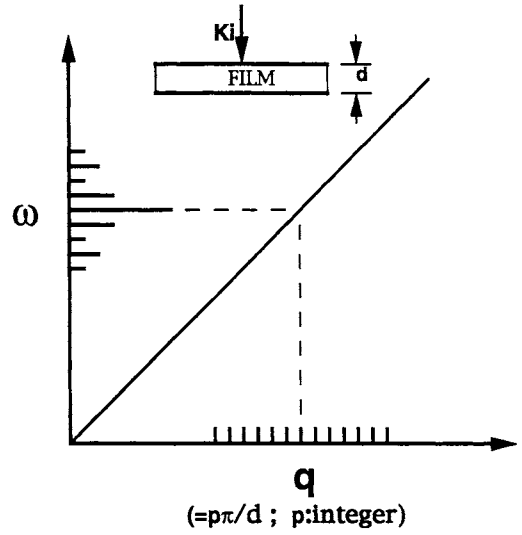

Fig. 13. Frequency vs. wavevector for acoustic phonons propagating perpendicular to the surface of a thin unsupported film. While the incident light energy and wavevector are well defined, the light backscattered over the thickness of the film contains an envelope of frequencies which contain several of the phonons, thus giving the multiple structure.

IX BRILLOUIN SCATTERING IN OPTICAL FIBERS

Brillouin scattering has also been used to study phonon propagation in optical fibers. Most of the work has been done with single-mode fibers in the core of which only one optical mode (photon) propagates. The core is surrounded by the cladding (clad) which has a slightly lower refractive index than that of the core, so that light can propagate in the core in a total-internal-reflection mode. In the simplest case of the backscattering geometry, which we consider here and in which only the longitudinal phonon is present, both the phonon and the photon are propagating almost along the fiber axis. Similar to the thin-film case, phonon propagation in single-mode fibers is expected to be strongly affected by the boundary conditions at the core-clad interface, since light is confined to propagate in the fiber core, which has a diameter (few microns) of the same order as the propagating light wavelength. Indeed, it has been found that [45]: the normal acoustic modes are linear combinations of transverse and longitudinal phonons in both the core and the clad, and the relative field amplitudes are dependent on the boundary conditions at both surfaces. Second, the density of phonon states is not uniform in q and ω space. Finally, the wavevector is not conserved in this acousto-optic interaction for a direction normal to the surface, i.e., the radial direction, and scattering is allowed over a continuum of phonons.

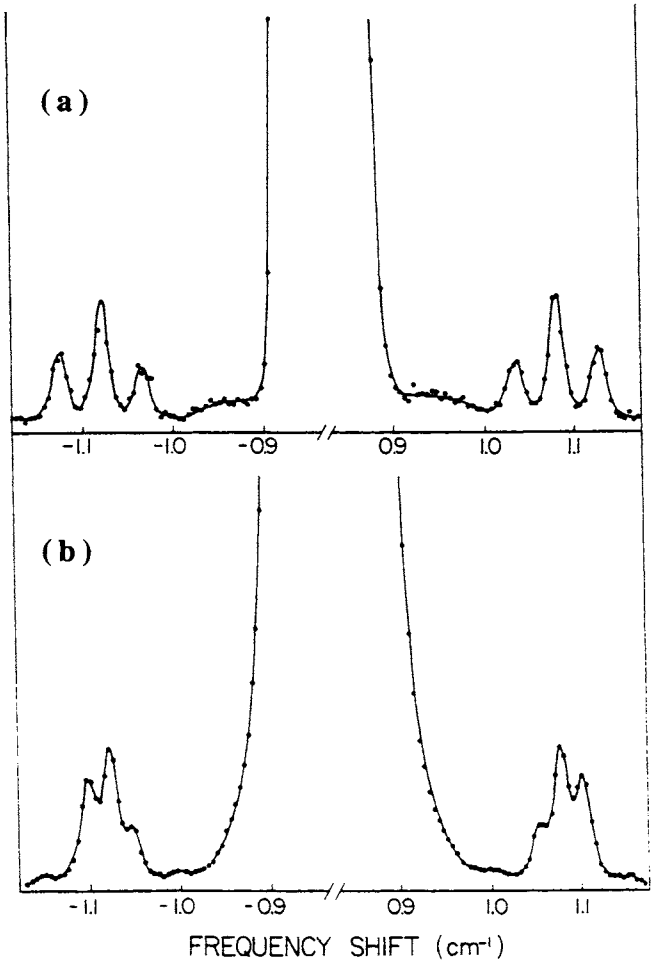

Fig. 14. Observed spectra from (a) and (b) two specimens of Mn_2PS_4 of thickness 1.1 and 2.0 μm, respectively. After Sandercock [44].

Even with the added complexities of a cylinder compared with a flat plate, some comparison can be made with the results for plates given in Eqs. (14–28).

Examples A

Brillouin scattering in optical fibers has been done using 180° and 90° geometry, which are shown schematically in Fig. 15.

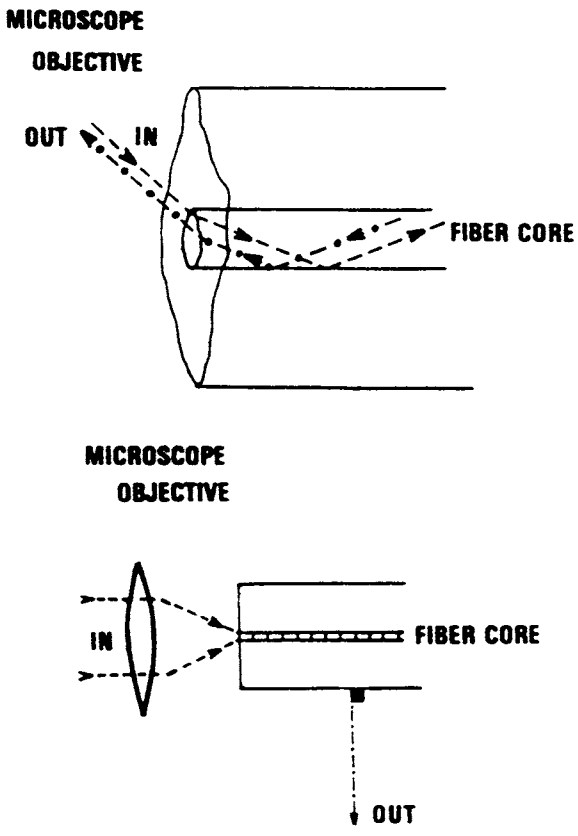

Fig. 15. Schematic of Brillouin scattering in an optical fiber (a) 180° scattering; (b) 90° scattering. After Thomas *et al.* [45].

1 *180° Scattering*

Using the Brillouin backscattering shown in Fig. 15, in which only the longitudinal phonon can be seen, phonon propagation has been studied in single-mode fibers (3 μm core diameter), which is shown in Fig. 16 [45]. In this figure we can see the longitudinal phonons propagating in the core only and in the core-clad space. In Thomas *et al.* [45] the refractive indexes of the core and the clad are given to be 1.462 and 1.457, respectively. From the spectrum of Fig. 16 and the refractive indexes, the sound velocities were calculated using Eq. (28) (backscattering phonon):

$$v_c = 6.026 \times 10^5 \quad \text{cm/sec}, \quad v_{cl} = 5.160 \times 10^5 \quad \text{cm/sec}. \tag{31}$$

Using Eq. (28), which has been derived for thin slabs, is an approximation for the cylindrical fibers, and it probably holds only for the optical rays passing through the fiber axis. These rays propagate in planes containing the

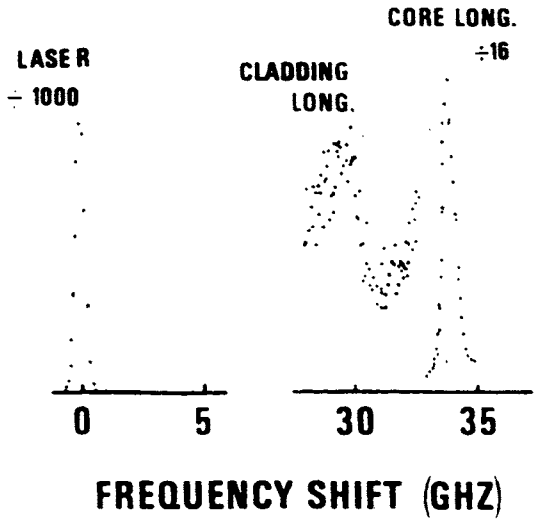

Fig. 16. Experimental Brillouin spectrum from a single optical fiber (180° scattering geometry). (After Thomas *et al.* [45].)

fiber axis. For the skew rays which do not pass through the fiber axis, the above equations would not hold; however, the skew modes attenuate fast in a fiber, and in the steady state of propagation only the rays passing through the center are present.

Even though the exact composition of the fiber was not given, as it can be seen below, the velocities listed in Eq. (31) correspond to standard fibers. In this example, the refractive indexes were given, and the sound velocities were found. However, the opposite is also true: Given the sound velocity, the refractive index can be found using the formula of Eq. (25) or (28).

90° Scattering 2

Single-Mode Fiber Using the 90° scattering shown in Fig. 15, the Brillouin spectrum was obtained in the fiber which was also used in Fig. 16, which is shown schematically in Fig. 17. This spectrum contains both the longitudinal phonons of the core and the clad and the transverse phonon of the core. For the Brillouin shift of the longitudinal core phonon (23.9 GHz), using Eq. (30), it is found that $\eta = 1.463$, a value very close to 1.462 found from the backscattering experiment of Fig. 16.

Single-Mode Fiber Preforms The elastic and elasto-optic (Pockels) coefficients of single-mode fibers have been studied doing Brillouin scattering

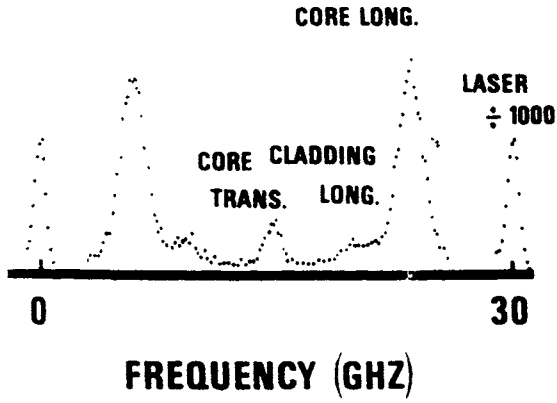

Fig. 17. Experimental Brillouin scattering from an optical fiber (classical 90° scattering geometry). (After Thomas *et al.* [45].)

(90°) on the glass preforms from which the fibers were drawn [46]. The preforms were cylinders 5 cm long and 7 mm in diameter with optically polished end faces. Two different fiber preforms were studied, one with numerical aperture $NA = 0.1$ composed of a fused-silica core with traces of GeO_2, and a clad of 5% B_2O_3 + 95% SiO_2 and another with $NA = 0.15$ composed of a 3% GeO_2 + 97% SiO_2 core, and a 15% B_2O_3 + 85% SiO_2 clad. The longitudinal (L) and the transverse (T) phonons were studied from the (V,V) and the (V,H) Brillouin spectra, respectively. The sound velocities of the phonons were calculated from Eq. (30), where the refractive index had been obtained using the prism method. From the two sound speeds, for an isotropic sample the elastic moduli, i.e., Young's modulus Y and Poisson's ratio σ, can be calculated using the following formulas:

$$Y = \rho v_T^2 \frac{(3v_L^2 - 4v_T^2)}{v_L^2 - v_T^2}, \quad \sigma = \frac{v_L^2 - 2v_T^2}{2(v_L^2 - v_T^2)}, \tag{32}$$

where ρ is the glass density.

The Pockels coefficients were also found by comparing the Brillouin spectra of the preforms to that of a fused-silica preform, whose Pockels coefficients are known, using the following formula for the L phonon [6]:

$$I = \frac{K\eta^8 P_{12}^2}{\rho v_s^2}, \tag{33}$$

where K is a geometrical and temperature factor, and P_{12} is the Pockels coefficient. Keeping the scattering geometry of the fused silica and the preforms identical, the K factor was eliminated by dividing the intensities of the spectra of the fused silica by those of the preforms [46]. This demonstrates the power of the Brillouin-scattering spectra from which, not only all the elastic moduli can be determined at once, but also the (very difficult to

measure) Pockels coefficients can by obtained. It should be also noticed from Eq. (33) that the intensity of the Brillouin spectra has the very strong dependence on the 8th power of the refractive index η.

The results of these experiments on the two fiber preforms for the coefficients of the longitudinal phonon for the core and the clad are listed below: Fiber $NA = 0.1$:

$$\eta_c = 1.4580, \quad \eta_{cl} = 1.4546, \quad v_{c,L} = 5.944 \times 10^5 \text{ cm/sec}, \quad v_{cl,L} = 5.605 \times 10^5 \text{ cm/sec}. \tag{34}$$

Fiber $NA = 0.15$:

$$\eta_c = 1.4624, \quad \eta_{cl} = 1.4547, \quad v_{c,L} = 5.806 \times 10^5 \text{ cm/sec}, \quad v_{cl,L} = 5.164 \times 10^5 \text{ cm/sec}. \tag{35}$$

A close comparison of the sound velocities in Eq. (31) to those in Eqs. (34) and (35) identifies the composition of the fiber used in the 180° scattering to be close to that of the 0.15 *NA*. Also the refractive indexes of these two glasses are very close ($\eta_c = 1.462$ vs. 1.4624, $\eta_{cl} = 1.457$ vs. 1.4547).

Edge Illumination (90° External Scattering) 3

Pyrex Glass The edge illumination (90° external scattering) has been used [40] to obtain the Brillouin spectrum of the longitudinal phonon of a 600 μm diameter glass rod (Pyrex), which is shown in Fig. 18(a). The incidence angle was ~45° for the 45°–45° geometry [47]. If the slab model holds for the cylinder, which seems to be the case in the examples above, two phonons should be observed in the cylinder. If $\Omega_1{}^{*2}/\Omega_2{}^{*2} = 0.844$ is obtained from Fig. 18(a), $\eta = 1.8$ is calculated from Eq. (29), while for Pyrex $\eta = 1.471$ [48]. The correct value for the refractive index of Pyrex can be found from Eq. (26) with $\alpha = 20°$ or 69° for the angle of incidence. Only with these incidence angles for a 90° external scattering, can the peaks shown in Fig. 18(a) correspond to $L_1{}^*$ and $L_2{}^*$ phonons discussed in Section VIII.B, as has been assumed by Takagi and Gammon [40].

Optical Fibers The Brillouin spectra of a multimode and a single-mode fiber are also given and are shown in Figs. 18(b) and 18(c), respectively [40]. For the multimode fiber, $\Omega_1{}^{*2}/\Omega_2{}^{*2} = 0.855$ (Fig. 18(b)), which gives $\eta = 1.8$ for the 45°–45° geometry; this is too large for an optical fiber, which is probably a high-silica glass. Conversely, Eq. (26) gives $\alpha = 17°$ or 72° (with $\eta = 1.458$ for silica), which is not in agreement with experiment.

For the single-mode fiber, $\Omega_1{}^{*2}/\Omega_2{}^{*2} = 0.849$ (Fig. 18(c)), which gives $\eta = 1.8$ for the 45°–45° geometry; again, this is too large for an optical fi-

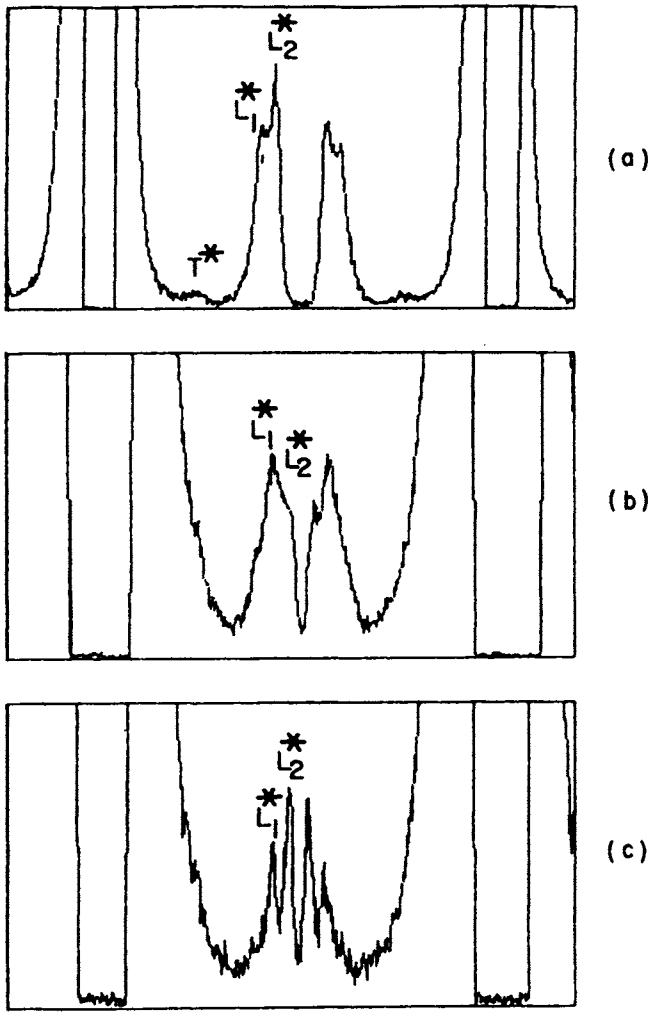

Fig. 18. Brillouin spectra with edge illumination at $FSR = 77$ GHz; (a) glass rod (600 μm), (b) multimode optical fiber, and (c) single-mode optical fiber. After Takagi and Gammon [40].

ber. Conversely, Eq. (26) gives $\alpha = 19°$ or $71°$, which is not in agreement with experiment.

However, for the case of the fibers another possibility is that the two longitudinal phonons correspond to the core and the clad phonons, similar to the ones observed in Figs. 16 and 17, and not to the L_1* and L_2* phonons, as were assigned by Tagaki and Gammon [40].

REFERENCES

1. J. R. Sandercock, *Phys. Rev. Lett.* **28**, 237 (1972).
2. B. Chu, "Laser Light Scattering." Academic Press, New York, 1974.
3. B. Berne and R. Pecora, "Dynamic Light Scattering." Wiley, New York, 1976.
4. G. B. Benedek and K. Fritsch, *Phys. Rev.* **149**, 647 (1966).
5. A. Griffin, *Rev. Mod. Phys.* **40**, 167 (1968).
6. M. Born and K. Huang, "Dynamic Theory of Crystal Lattices." Oxford Univ. Press (Clarendon) Oxford, 1954.
7. A. S. Borovik-Romanov and N. W. Kreines, *Phys. Rep.* **81**, 351 (1982).
8. N. L. Rowell and G. I. Stegeman, *Phys. Rev. B* **18**, 2598 (1978).
9. J. M. Vaughan, "The Fabry-Perot Interferometer." Hilger, London, 1989.
10. G. Hernandez, "Fabry-Perot Interferometers." Cambridge Univ. Press, Cambridge, 1986.
11. N. W. Ashcroft and N. D. Mermin, "Solid State Physics." Sanders College, Philadelphia, 1976.
12. R. Loudon, *J. Phys. C: Solid State Phys.* **11**, 403 1978.
13. G. Dresselhaus and A. S. Pine, *Solid State Commun.* **16**, 1001 (1975).
14. M. Born and E. Wolf, "Principles of Optics," Chap. 7, p. 328. Pergamon, London, 1959.
15. C. S. Zha, R. J. Hemsley, H. K. Mao, T. S. Duffy, and C. Meade, *Phys. Rev. B* **50**, 13105 (1994).
16. A. K. Sood and M. Cardona, *Solid State Commun.* **49**, 299 (1984).
17. E. D. Palik, H. Boukari, and R. W. Gammon, *Appl. Opt.* **34**, 58 (1995).
18. H. Boukari, E. D. Palik, and R. W. Gammon, *Appl. Opt.* **34**, 69 (1995).
19. E. D. Palik, H. Boukari, and R. W. Gammon, *Appl. Opt.* **35**, 48 (1996).
20. A. S. Pine, "Light Scattering in Solids: Topics in Applied Physics," (M. Cardona, ed.), Vol. 28, Chap. 6. Springer-Verlag, Berlin, 1975.
21. A. S. Pine, *Phys. Rev. B* **5**, 2997 (1972).
22. A. S. Pine, *Phys. Rev. B* **5**, 3003 (1972).
23. J. Zuk, H. Kiefte, and M. J. Clouter, *J. Appl. Phys.* **72**, 3504 (1992).
24. R. Bhadra, M. Grimsditch, I. K. Schuller, and F. Nizzoli, *Phys. Rev. B* **39**, 12456 (1989).
25. R. Jorna, D. Visser, V. Bortolani, and F. Nizzoli, *J. Appl. Phys.* **65**, 718 (1989).
26. B. Hillebrands, P. Baumgart, R. Mock, G. Güntherodt, and P. S. Bechthold, *J. Appl. Phys.* **58**, 3167 (1985).
27. J. A. Bell, W. R. Bennett, R. Zanoni, G. I. Stegeman, C. M. Falco, and F. Nizzoli, *Phys. Rev. B* **35**, 4127 (1987).
28. G. Carlotti, D. Fioretto, L. Palmieri, G. Socino, L. Verdini, and E. Verona, IEEE ultrasonic symposium, p. 1201, (1989).
29. M. Grimsditch, R. Bhadra, and I. K. Schuller, *Phys. Rev. Lett.* **58**, 1216 (1987).
30. S. Subramanian, R. Sooryankumar, G. A. Prinz, B. T. Jonker, and Y. U. Idzerda, *Phys. Rev. B* **49**, 17319 (1994).
31. F. Nizzoli, R. Bhadra, O. F. de Lima, M. B. Brodsky, and M. Grimsditch, *Phys. Rev. B* **37**, 1007 (1988).
32. M. Elena, M. Bonelli, C. E. Bottani, G. Ghislotti, A. Miotello, P. Mutti, and P. M. Ossi, *Thin Solid Films* **236**, 209 (1993).
33. J. R. Sandercock, *Solid State Commun.* **26**, 547 (1978).
34. J. M. Karanikas, R. Sooryakumar, and J. M. Phillips, *J. Appl. Phys.* **65**, 3407 (1989).
35. J. M. Karanikas, R. Sooryakumar, and J. M. Phillips, *Phys. Rev. B* **39**, 1388 (1989).
36. L. E. McNeil, M. Grimsditch, and R. H. French, *J. Am. Ceram. Soc.* **76**, 1132 (1993).
37. C. H. Wang, D. B. Cavanaugh, and Y. Hagashigaki, *J. Polym. Sci., (Polym. Phys. Ed.)* **19**, 941–950 (1981).
38. D. B. Cavanaugh and C. H. Wang, *J. Appl. Phys.* **52**, 5998 (1981).
39. M. B. Hakin, S. M. Lindsay, and J. Powell, *Biopolymers* **23**, 1185 (1984).
40. Y. Takagi and R. W. Gammon, *J. Appl. Phys.* **61**, 2030 (1987).

41. J. Pelous and R. Vacher, *Solid State Commun.* **16**, 279 (1975); R. Vacher and J. Pelous, Phys. Rev. *B* **14**, 823 (1976).
42. J. D. Lytle, Polymeric optics, *in* "Handbook of Optics, Devices, Measurements and Properties," (M. Bass, ed.), 2nd Ed., Vol. 2, Chap. 34. McGraw-Hill, New York, 1995.
43. B. H. Billings, Optics, *in* "American Institute of Physics Handbook," (D. E. Gray, ed.), 3rd Ed., Section 6, pp. 6–108. McGraw-Hill, New York, 1982.
44. J. R. Sandercock, *Phys. Rev. Lett.* **29**, 1735 (1972).
45. P. J. Thomas, N. l. Rowell, H. M. van Driel, and G. I. Stegeman, *Phys. Rev. B* **19**, 4986 (1979).
46. N. Lagakos, J. A. Bucaro, and R. Hughes, *Appl. Opt.* **19**, 3668 (1980).
47. Y. Takagi, private communication (1996).
48. J. Schroeder, *J. Non-Cryst. Solids* **40**, 549 (1980).

Chapter 6

Doped n-Type Silicon (n-Si)

MARK AUSLENDER and SHLOMO HAVA
Ben-Gurion University of the Negev
Department of Electrical and Computer Engineering
Beer-Sheva, Israel

I. Introduction 155
II. Contributions to Dielectric Function: Optical Properties versus Optical Constants 156
III. Semiclassical Theory of Free-Carrier Contribution to the Dielectric Function: The Drude Approximation 158
IV. Free-Carrier Contribution to the Dielectric Function in Quantum Absorption Regime: Generalized Drude Approach 159
V. Experimental Data Overview 162
VI. Generalized Drude Approximation for n-Si 166
A. Electron-Phonom Scattering 167
B. Electron-Impurity Scattering 168
VII. Tabulation of Optical Constants of Doped n-Si 171
References 185

INTRODUCTION I

The importance of knowing optical constants was excellently outlined in the introduction to *HOC I* [1]. In the case of silicon, one can also point out technologically important applications of this knowledge. A partial list includes the determination of epilayer thickness [2] and the losses in all-silicon integrated optical devices [3], silicon-wafer thermometry [4], IR emissivity, and absorbance enhancement in silicon gratings [5, 6]

To be self-contained, this critique includes an overview of dielectric-function partition and the relation of optical constants to measured optical properties (Section II), semiclassical, and quantum absorption theory (Sections III and IV). In order to avoid multiple repetition when citing textbook materials, we refer in advance to well-known books on optics [7], semiconductor optics [8], and physics [9], and quantum mechanics [10]; in Section IV we also introduce the generalized Drude approximation. Section V is an

HANDBOOK OF OPTICAL CONSTANTS OF SOLIDS III

Copyright © 1998 by Academic Press.
All rights of reproduction in any form reserved
ISBN 0-12-544423-0/$25.00.

overview of experimental data and the Drude formula with empirically adjusted parameters. In Section VI we present a first-principle theory of free-carrier contribution to optical constants in doped n-Si based on the generalized Drude approximation. We outline the calculations and emphasize the difficulties that the theory is faced with when being used to describe available experimental data.

II CONTRIBUTIONS TO DIELECTRIC FUNCTION: OPTICAL PROPERTIES VERSUS OPTICAL CONSTANTS

Electromagnetics of homogeneous material is completely defined by the dielectric function (DF): $\epsilon = \epsilon_1 + i\epsilon_2$, a function of radiation frequency ω or vacuum wavelength $\lambda = 2\pi c/\omega$. The basic quantity of optics, however, is *complex refractive index* $\sqrt{\epsilon} = n + ik$, where the *refractive index, n,* and *extinction coefficient, k,* are related to ϵ_1 and ϵ_2 via equations

$$n^2 - k^2 = \epsilon_1, \tag{1}$$

$$2nk = \epsilon_2. \tag{2}$$

The lattice and free-carriers, which arise from doping, give additive contributions to the DF:

$$\epsilon = \epsilon_l + \epsilon_c. \tag{3}$$

Here, $\epsilon_l = (n_l + ik_l)^2$ is the lattice contribution, and ϵ_c is that due to the carriers

$$\epsilon_c = i\frac{4\pi\sigma(\omega)}{\omega}, \tag{4}$$

where $\sigma(\omega)$ is conductivity at optical frequencies. Though doping also affects $\epsilon_l$via band-gap reduction [11], in the IR this effect is negligible as compared to ϵ_c. The tables of n_l and k_l for intrinsic silicon were presented by Edwards [12]; such tables for Si: O_2 were also reported [13]. In the near and mid IR, n_l decreases from 3.4490 at 5000 cm^{-1} to 3.4201 at 400 cm^{-1}, the largest values of $k_l \sim 10^{-3}$ are achieved in a narrow band near 606 cm^{-1}. It seems that this variation is negligible on the scale of ϵ_c for doping in excess of 10^{16} cm^{-3}; in most papers, n_l is taken to be constant, and k_l is neglected.

Experimentally, n and k are determined using measurements of various optical properties of quality samples with simple geometry. For smooth

opaque samples, the only quantity of interest is the complex amplitude reflectance

$$r = -\frac{\sqrt{\epsilon} - 1}{\sqrt{\epsilon} + 1} = \sqrt{R}\exp(i\Phi), \tag{5}$$

where R is the Fresnel reflectance of the sample's surface

$$R = |r|^2 = \frac{(n-1)^2 + k^2}{(n+1)^2 + k^2}, \tag{6}$$

and Φ is the argument of the complex reflectance

$$\tan(\Phi) = \frac{2k}{n^2 + k^2 - 1}. \tag{7}$$

The spectrum of R is measured using reflectometry techniques; with R measured, Φ is determined using Kramers-Kronig analysis (KKA) [14]. With both spectra available, Eqs. (6, 7) are solved simultaneously to yield n and k. For a transparent slab, the apparent reflectance R_a and transmittance T_a are measured. In many practical cases, interference oscillations (fringes) in the spectra of R_a and T_a are averaged out. This leads to simple equations:

$$R_a = R\left[1 + \left|1 - r^2\right|^2 \frac{\exp(-2\alpha d)}{1 - R^2\exp(-2\alpha d)}\right], \tag{8}$$

$$T_a = \left|1 - r^2\right|^2 \frac{\exp(-\alpha d)}{1 - R^2\exp(-2\alpha d)}, \tag{9}$$

in which d is the thickness of the slab, and

$$\alpha = \frac{4\pi k}{\lambda} \tag{10}$$

is the EM *power attenuation coefficient.* It is referred to as the *absorption coefficient* in the case $n > k$ ($\epsilon_1 > \epsilon_2$). At $n \gg k$, $r^2 = R$ in Eqs. (8, 9), and *spectral absorbance* $A = 1 - R_a - T_a$ takes the following form when used in silicon-wafer thermometry [4]:

$$A = \frac{(1-R)[1 - \exp(-\alpha d)]}{1 - R\exp(-\alpha d)}. \tag{11}$$

III SEMICLASSICAL THEORY OF FREE-CARRIER CONTRIBUTION TO THE DIELECTRIC FUNCTION: THE DRUDE APPROXIMATION

An approach to calculating ϵ_c, which combines an account of band structure and scattering with the merit of being simple, is based on quasi-classical Boltzmann transport equation. This is restricted by the requirement that the radiation quantum is much smaller than the mean electron energy: $\hbar\omega \ll \langle E \rangle$. In the relaxation-time approximation, the Boltzmann equation can be solved in a closed form for an arbitrary band spectrum $E(\mathbf{k})$. This gives in Eq. (4)

$$\epsilon_c = -\frac{4\pi e^2 N}{\omega}\langle(\omega + i\tau^{-1})^{-1}\mathbf{m}^{-1}\rangle. \tag{12}$$

Here, N is the carrier concentration, τ and $\mathbf{m}$ are the energy-dependent relaxation time and effective-mass tensors, respectively, $\langle ... \rangle$ denotes average over energies E with normalized-to-unity weight $-\frac{\partial f(E)}{\partial E}\cdot\frac{N(E)}{N}$, where $N(E)$ is the number of band states with energies less than E, and f is the Fermi-Dirac distribution. The conduction band in silicon has six equivalent minima (valleys) in the Γ-X directions. Constant-energy surfaces are those of revolution, so $\mathbf{m}$ has two principal values $m_\parallel$ and $m_\perp$. Near the minima ($E < 0.15$ eV), they are constant: $m_\parallel \approx 0.98m_0$, $m_\perp \approx 0.19m_0$, and the constant-energy surfaces are ellipsoids. At larger E's, the masses (mostly $m_\perp$) increase with increasing E, and the ellipsoids become warped [15]. The tensor τ has the same principal axes as $\mathbf{m}$, with principal values $\tau_\parallel$ and $\tau_\perp$. Deformation acoustic (DA)-phonon scattering is nearly isotropic ($\tau_\parallel \approx \tau_\perp$), and deformation optical (DO)-phonon and point-defect scattering are isotropic. For ionized-impurity scattering, tensor τ, introduced as an approximation, is essentially anisotropic.

At $\omega\tau \ll 1$, Eq. (12) gives

$$\epsilon_1 = n_1^2, \quad \epsilon_2 = 2n_1k_1 + n_1^2\frac{\omega_p^2\tau_{dc}}{\omega}, \tag{13}$$

and at $\omega\tau \gg 1$

$$\epsilon_1 = n_1^2(1 - \omega_p^2/\omega^2), \quad \epsilon_2 = 2n_1k_1 + n_1^2\frac{\omega_p^2}{\omega^3\tau_{ac}}. \tag{14}$$

In Eqs. (13, 14) ω_p is the electron plasma frequency defined by

$$\omega_p = \frac{1}{n_1}\sqrt{\frac{4\pi e^2 N}{m_c}}, \quad \frac{1}{m_c} = \langle\frac{1}{3m_\parallel} + \frac{2}{3m_\perp}\rangle, \tag{15}$$

τ_{dc} and $1/\tau_{ac}$ are the combined energy-valley averages of the tensor τ, and the tensor inverse to τ, respectively:

$$\tau_{dc} = m_c \left\langle \frac{\tau_\parallel}{3m_\parallel} + \frac{2\tau_\perp}{3m_\perp} \right\rangle, \tag{16}$$

$$\frac{1}{\tau_{ac}} = m_c \left\langle \frac{1}{3m_\parallel \tau_\parallel} + \frac{2}{3m_\perp \tau_\perp} \right\rangle. \tag{17}$$

The quantity m_c is called *optical* or *conductivity effective mass.* With the use of cyclotron-resonance data, the average in Eq. (15) is calculated trivially to give $m_c = 0.26m_0$.

If, for some reasons, τ_{dc} and τ_{ac} are close to each other, the two limits Eq. (13) and Eq. (14) may be interpolated by the simple formula

$$\epsilon = \epsilon_l - \frac{n_l^2 \omega_p^2}{\omega(\omega + i\gamma)}, \quad \gamma = \frac{1}{\tau}, \tag{18}$$

which is the celebrated Drude (also Drude-Lorentz or Drude-Zener) equation, and τ is the relaxation time [8, 9, 16]. For isotropic τ, the closeness of τ_{dc} and τ_{ac} is certainly realized when carriers are degenerate. In n-Si with the valley density-of-state effective mass $m_d = m_\parallel^{1/3} m_\perp^{2/3} \approx 0.33m_0$, no degeneracy occurs unless $N \geq 10^{20}$ cm^{-3}.

In order to validate the Drude equation at all concentrations, the relation $\tau_{dc}/\tau_{ac} = 1.13$, valid for combined DA-phonon and point-defect scattering in non-degenerate statistics, is used. For ionized-impurity scattering another reason must be sought, because $\tau_{dc}/\tau_{ac} \gg 1$ even in the isotropic band. At heavy doping, the allowance of Eq. (18) implies the existence of a mechanism which 'binds' one-particle currents into collective variable, total current, which relaxes as a whole. This mechanism could be electron-electron (*e-e*) interaction, which smears an individual electron momentum but conserves the total one. Then the response of the electron plasma on an external EM field will be described in terms of total momentum, provided that the electron momentum exchange in *e-e* collisions becomes faster than the electron momentum relaxation due other mechanisms, as N increases over some value. However, this picture is only partially adequate because the *e-e* momentum-relaxation rate is of the same order of magnitude as that due to ionized impurities, though detailed estimates are not widely known especially for the anisotropic band.

IV FREE-CARRIER CONTRIBUTION TO THE DIELECTRIC FUNCTION IN QUANTUM ABSORPTION REGIME: GENERALIZED DRUDE APPROACH

The Boltzmann equation becomes invalid at $\hbar\omega > \langle E \rangle$, since in this case radiation influences the scattering process. In the quantum regime, the act of

scattering is a transition between initial state with momentum $\mathbf{k}$ and energy $E(\mathbf{k})$ and final state with momentum $\mathbf{k}'$ and energy $E(\mathbf{k}')$ with radiation quanta absorbed or emitted: $E(\mathbf{k}') = E(\mathbf{k}) \pm \hbar\omega$. In the quantum regime, ϵ_c was calculated in the terms of transition probabilities using time-dependent perturbation theory. The first calculations of this type were reported 40 years ago by Fan *et al.* in connection with the first IR-absorption measurements on Ge [17] and Si [18]. For DA-phonon scattering, the absorption coefficient (Eq.(10)) obeys a power law: $n\alpha \propto \omega^{-1.5} \propto \lambda^{1.5}$ at $\hbar\omega > \langle E \rangle$. At $\langle E \rangle/\hbar > \omega > 1/\tau$, quantum theory gives the same result as semiclassical theory or the Drude approximation at $\omega\tau > 1$ (Eqs. (14, 18) with Eqs. (2, 10))

$$n\alpha \approx \frac{n_1^2}{c\tau}\left(\frac{\omega_p}{\omega}\right)^2 \propto \lambda^2. \tag{19}$$

DO-phonon scattering in n-Ge was also considered by Fan *et al.* [17]; phonon-assisted absorption in a many-valley conduction band was studied by Meyer [19] and Rosenberg and Lax [20]. The method was recapitulated by Dumke [21] in 1960. Ionized impurity-assisted absorption in the Born approximation was studied by Meyer [19] and Rosenberg and Lax [20], and with Coulomb wave functions by Visvanathan [22] and Donovan [23]. It was found that in the quantum regime, $n\alpha \propto \omega^{-3.5} \propto \lambda^{3.5}$. The transition to Eq. (19) may not occur even after $\langle E \rangle$ exceeds $\hbar\omega$. The reason is, though the electron wave packet as a whole starts to move at thermal equilibrium, its breadth δr is still determined by the oscillations in radiation field: $\delta r = \sqrt{\hbar/2m^*\omega}$, m^* being an effective mass. So at $\delta r < r_s$ (screening length) the electrons 'feel' an unscreened impurity for which $n\alpha \propto \omega^{-3} \propto \lambda^3$ in the classical frequency region [22, 23], and the limit of Eq. (19) is reached only at $\delta r > r_s$. The calculations using transition probabilities require throwbacks to first principles, and are recast each time a new mechanism is considered. From the late 1960s to 1970s, studies devoted to the derivation of generalized Boltzmann equations, which could recover both quantum and classical regimes, were carried out. Having no room to review this subject here, we refer to the contribution of Jensen [24]. Note that at $\omega\tau \gg 1$, the quantum Boltzmann equation and the transition-probability methods give close results.

Kubo quantum-admittance formalism [25] with second quantization allowed researchers to automate the calculations at high frequencies in a reasonably correct, unified form. The Kubo formula for dynamical conductivity [25] reads

$$\sigma(\omega) = \int_0^\infty \exp(i\omega t) \int_0^{1/kT} \langle J_x(t - i\hbar s) J_x(0) \rangle_T \, dt ds. \tag{20}$$

Here, J_x is x −(or any) component of electric-current operator,

$$A(t) = \exp(it\mathcal{H}/\hbar) A \exp(-it\mathcal{H}/\hbar), \tag{21}$$

where $\mathscr{H}$ is a Hamiltonian, and $\langle ... \rangle_T$ stands for thermodynamic average with the temperature T. Using integration by parts with respect to time t, in Eq. (20) the free-carrier contribution (Eq. (4)) can be identically transformed to

$$\epsilon_c = -\frac{\Omega_p^2}{\omega^2}\left[1 + \frac{\Pi(\omega)}{i\omega}\right], \quad \Omega_p^2 = 4\pi \int_0^{1/kT} \langle J_x(i\hbar s) J_x(0)\rangle_T \, ds \tag{22}$$

with

$$\Pi(\omega) = 4\pi\Omega_p^{-2} \int_0^\infty \exp(i\omega t) \int_0^{1/kT} \langle \dot{J}_x (t + i\hbar s) \dot{J}_x(0)\rangle_T \, dtds, \tag{23}$$

where the upper dot denotes the time derivative:

$$\dot{A}(t) = \frac{i}{\hbar}[\mathscr{H}, A(t)].$$

Eq. (23) is convenient for the calculation at high frequencies. Indeed, $\Pi(\omega)$ is at least of *second order* with respect to the interactions, since the electric-current operator commutes with the kinetic energy part of $\mathscr{H}$. Thus, at $\omega\tau \gg 1$ the interactions can be neglected when considering the correlation function in Eq. (23). Then the lowest-order estimate of Eq. (23) $\Pi^{(2)}(\omega) = \Gamma(\omega)$ is obtained in a closed form as a sum of the contributions of different scattering mechanisms. It is expedient to note that in this approximation, the *e-e* interaction does not contribute to $\Gamma(\omega)$ for the isotropic band, where J_x is proportional to the total momentum.

With $\Pi(\omega)$ replaced by $\Gamma(\omega)$, Eq. (22) becomes a fragment of the high-frequency expansion of

$$\epsilon_c = -\frac{\Omega_p^2}{\omega[\omega + i\Gamma(\omega)]}. \tag{24}$$

The extention of Eq. (24) to all ω's is called the *generalized Drude approximation* (GDA). The structure of this type may formally be obtained from exact Eq.(22) using the Mori projection ansatz [26]. Of course, the prescription of the structure by no means validates GDA. The validity of GDA in the whole frequency range was extensively discussed by Sernelius [27]. It was applied to simple metals [28], and to an isotropic model of doped n-Si [29, 30]. GDA appears to be a good approximation if the *e-e* collisions dominate, as outlined in Section III.

Since $\Omega_p = n_1\omega_p$ in the leading approximation, the total DF (Eq. (10)) in GDA differs from the Drude formula (Eq. (19)) only in the presence of the relaxation-memory function $\Gamma(\omega)$ *instead of constant relaxation rate* γ. If the valleys are uncoupled, GDA must be applied separately to each valley. The calculations for the valleys of $\langle 100\rangle$, and $\langle 010\rangle$, $\langle 001\rangle$ types give, in

general, two different contributions $\Gamma_{\parallel}(\omega)$, and $\Gamma_{\perp}(\omega)$, respectively. The total DF in this case is

$$\epsilon = \epsilon_1 - \frac{4\pi Ne^2}{3m_{\parallel}\omega[\omega + i\Gamma_{\parallel}(\omega)]} - \frac{8\pi Ne^2}{3m_{\perp}\omega[\omega + i\Gamma_{\perp}(\omega)]}. \tag{25}$$

At the high-frequency limit only the average relaxation function

$$\Gamma(\omega) = \frac{m_c}{3}\left[\frac{\Gamma_{\parallel}(\omega)}{m_{\parallel}} + 2\frac{\Gamma_{\perp}(\omega)}{m_{\perp}}\right] \tag{26}$$

enters Eq. (25), thus comprising the first term of exact perturbation expansion as required. In the presence of a scattering, that couples the valleys, Eq. (25) must be changed (Eq. (3.8) [27]).

V EXPERIMENTAL DATA OVERVIEW

There exists a body of literature on the optical properties of variously doped n-Si crystals in the IR. The equilibrium solubility of atoms of As, P, and Sb in Si does not exceed $5 \times 10^{20}\text{cm}^{-3}$ [31]. The use of advanced ion-implantation technology increased the active dopant density far above this (up to 5×10^{21} cm^{-3}) and allowed plasma effects to be observed in the near IR [32–34].

Basically, these studies used reflection and/or transmission measurements. For bulk-doped samples at $N < 10^{19}\text{cm}^{-3}$, it is technologically possible to prepare slabs suitable for transmission measurements. With the use of Eqs. (6–10), optical constants are retrieved from measured values of R_a and T_a. As is seen from Eq. (14), extrapolating measured ϵ_1 to zero from the region $n \gg k$ gives the plasma frequency, and hence the optical effective mass m_c. Using this method, Spitzer and Fan [18] found $m_c = 0.27m_0$ for $N = 3.6 \times 10^{18}$ cm^{-3}, in excellent agreement with the value cited in Section II. It was pointed out by Fistul [31] that for heavier doping, the method has low reliability, as was seen from the result $m_c = 0.44m_0$ of Cardona *et al.* for $N = 6.5 \times 10^{19}$ and 1.1×10^{20} cm^{-3} [35]. At doping in excess of 10^{19} cm^{-3}, reflectometry was mostly used [33, 36–39]. A comprehensive study of reflection was made by Howarth and Gilbert [36], who measured 16 n-Si samples doped in the range $7.4 \times 10^{18}\text{cm}^{-3}$ $-1.67 \times 10^{20}\text{cm}^{-3}$. For ion-implanted n-Si layers, combined measurements of reflection and transmission were carried out by Streltsov and Titov [40], Miyao *et al.* [32], and Aspnes *et al.* [34].

Two approaches to processing reflectivity data of bulk-doped samples were used. The first one, which relied on the Drude model, was proposed by

Kukharski and Subashiev [38], and advocated by Lambert [41]. In this approach, ω_p and γ are found from the reflectivity minimum frequency, ω_{min} (wavelength λ_{min}), and the value of reflectivity minimum, R_{min}. With known ω_p, one can calculate m_c if N is measured and vice versa; this method is an improvement of widely used approximations: $(n-1)^2 \gg k^2$ or $n \sim 1$, $k \sim 0$ [17, 18, 35–37]. The method of Kukharski and Subashiev [38] was used also for doped n-Si layers in a homogeneous approximation [40] and modified by Slaoui and Siffert [33] for concentration profiles. The second approach is KKA giving n and k independently of the physical model (see Section II). However, as a rule, the retrieved n and k were not displayed, and again, the Drude model was used. Spitzer *et al.* [37] assumed $m_c = 0.28m_0$ and studied the influence of heat treatment on γ in a sample with $N = 7.5 \times 10^{19}$ cm^{-3}. Barta [39] expressed m_c and τ via ϵ_1 and ϵ_2, which were known after KKA (see Eqs. (1, 2)). The parameters were calculated at the zero of ϵ_1, which gave: $m_c = 0.31m_0$ and $m_c = 0.35m_0$ for two samples with $N = 9 \times 10^{19}$ cm^{-3} and 1.6×10^{20} cm^{-3}, respectively, and about the same value of the relaxation parameter $\gamma \sim 1.09 \times 10^{14}$ s^{-1} for both samples.

A variety of spectra of the absorption coefficient α was observed in n-Si. Dubrovsky in his thesis cited by Fistul [31] in the range of $N \sim (0.1 - 1) \times 10^{20} cm^{-3}$ and reported the dependence $\alpha \propto \lambda^{3.5}$, which is characteristic for ionized-impurity scattering (see Section IV). Balkanski *et al.* [42] measured $\alpha \propto \lambda^2$ at $4\mu m < \lambda < 6\mu m$ in bulk-doped samples with $N = 6 \times 10^{18}$, 10^{19} cm^{-3}. On the contrary, in ion-implanted layers with $N \sim (0.5 - 2) \times 10^{20} cm^{-3}$, the dependence $\alpha \propto \lambda^{1.5}$ was observed at $2\mu m < \lambda < 10\mu m$ [40]. Later this was also observed in laser-annealed poly-Si layers with a much larger concentration [34]. Based on the fact that this dependence is obtained for DA-phonon scattering (see Section VI), Streltsov and Titov [40] asserted that the phonon mechanism dominates the scattering processes in n-Si doped in excess of 10^{19} cm^{-3}.

On the one hand, the researchers were disposed to retrieve some physical information rather than tabulate optical constants. On the other hand, such restricted information can hardly be used in practice. For a fast and accurate approximation of optical constants in a wide range of N and ω, Humlíček and Wojtechovsky [43] proposed a KKA-adjusted Drude model for a best fit of reflectivity data. Using the data for the samples of Howarth and Gilbert [36] and three of their own [43], they found fitting values of ω_p and γ for each, and derived linear relations:

$$\begin{aligned} \gamma &= 113 + 0.208\,\omega_p \quad \text{(Si: Sb)}, \\ \gamma &= 153 + 0.265\,\omega_p \quad \text{(Si: As)}, \\ \gamma &= 194 + 0.174\,\omega_p \quad \text{(Si: P)}, \end{aligned} \tag{27}$$

where ω_p and γ are in units cm^{-1}, and $N \geq 5 \times 10^{18}$ cm^{-3}. The authors sought a dependence between m_c, as calculated using the definition of ω_p,

and N. Due to a large scatter, the result (Eq. (15) [43]) seemed so unphysical that they recommended substituting the value $m_c = 0.26m_0$ for interpolation of optical constants using Eq. (27). Thus, at $N \leq 10^{20}$ cm^{-3} it can be put in the Drude equation (Eq. (18)):

$$n_1^2\omega_p^2 = 3.452 \times 10^{-13} N \text{ cm}^{-2}, \tag{28}$$

where N is in units cm^{-3}.

Eq. (28) can be validated by fittting ω_p of Humlíček and Wojtechovsky [43] linearly to N. The result is shown in Fig. 1. We display only the fit for Si: As, which yields $m_c = 0.27m_0$. It fits the data reasonably well up to $\sim 8 \times 10^{19}$ cm^{-3}. The data for Si: Sb also have a small scatter and are fitted with $m_c = 0.28m_0$. The data for Si: P have larger scatter especially at the end concentrations. The linear fit using the data for $N \leq 10^{20}$ cm^{-3} gives $m_c = 0.29m_0$. The point $N = 1.67 \times 10^{20}$ cm^{-3} (not shown in Fig. 1) drops drastically below this fit. Including this point in the fit increases the value of m_c to $0.31m_0$; the calculation using only this point gives $m_c = 0.34m_0$, which are about the same as obtained by Barta [39]. Since m_c must be independent of impurity type, we conclude that its apparent increase at $N \leq 10^{20}$ cm^{-3} is a result of experimental uncertainty. This agrees with band-structure calculations of van Driel [15], which predicted different behavior of m_c: near-to-constant $m_c = (0.26 - 0.27)\, m_0$ at $N \leq 10^{20}$ cm^{-3}, and monotonic in-

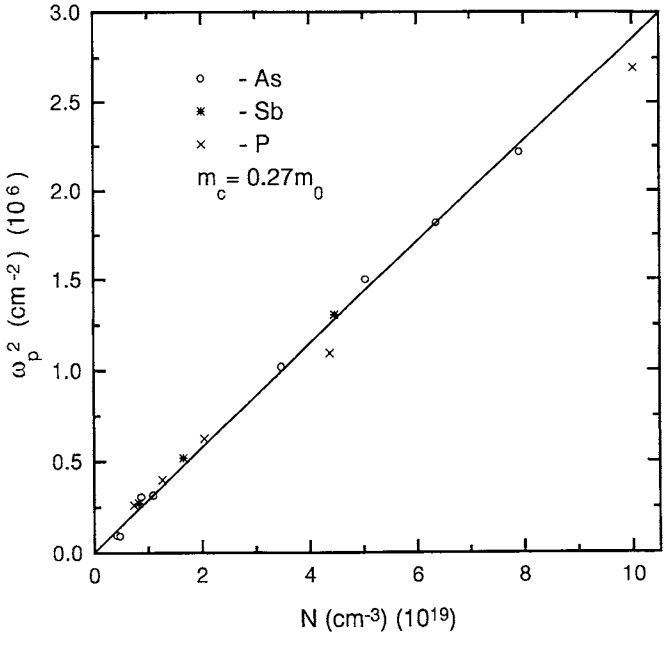

Fig. 1. Plasma frequency squared versus electron concentration for various doped n-Si. Si: As (o), Si: Sb (*), Si: P (×). Straight line is the best linear fit for Si: As giving $m_c = 0.27m_0$.

crease at $N > 10^{20}$ cm^{-3} to about $0.57m_0$ at 5×10^{21} cm^{-3}. This huge increase of m_c was observed in ion-implanted samples [32–34], whereas its onset is seen in the last two Si: P samples of Howarth and Gilbert [36]. As seen from Fig. 2, the agreement of theory [15] and experiment [32–34] is fair.

To derive a fit for γ at $N < 5 \times 10^{18}$ cm^{-3}, the transmission through four samples with $N = 1.4 \times 10^{16}$, 7.5×10^{16}, 10^{17}, and 1.15×10^{17} cm^{-3} was measured by Humlíček and Wojtechovsky [43]. It was found that there is a good agreement between the retrieved γ's and the inverse relaxation times extracted from the mobility data. Using a simplified empirical fit for the mobility, the authors obtained

$$\gamma = 35910 \frac{1 + (10^{-16} N/9.68)^{0.68}}{1427 + 52.2\,(10^{-16} N/9.68)^{0.68}} \text{ cm}^{-1}, \tag{29}$$

where, as usual, N is in units cm^{-3}. Even though optical data between 1.2×10^{17} cm^{-3} and 3.6×10^{18} cm^{-3} are missing, and the mobility data are uncertain, the γ values obtained from Eq. (29) and Eq. (27) match reasonably at $N = 5 \times 10^{18}$ cm^{-3}. To summarize, Eq. (18) (ω in units of cm^{-1}) with Eq. (28) and empirically adjusted relaxation parameter given by Eq. (29)

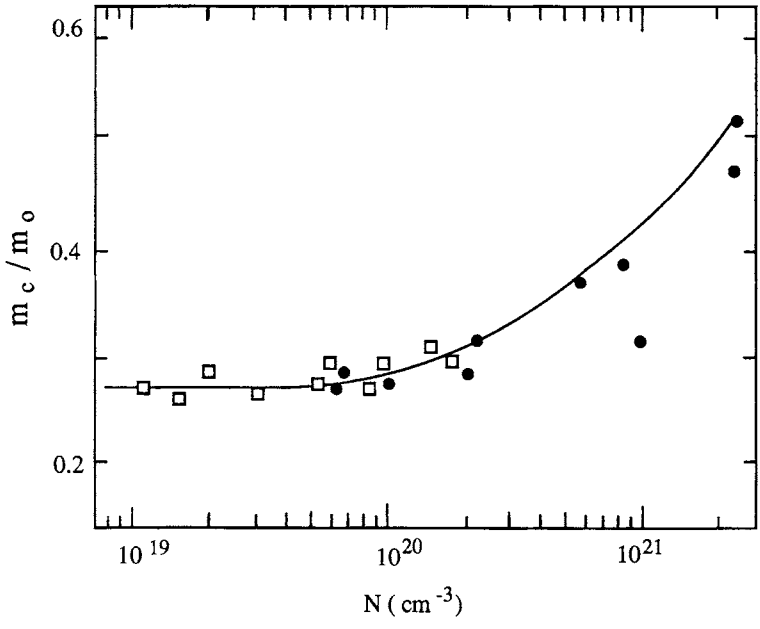

Fig. 2. Dependence of optical effective mass in n-Si on free-carrier concentration. The solid line represents theoretical curve after van Driel [15]. Open squares and solid circles are experimental data after Howarth and Gilbert [36] (□) and Miyao *et al.* [32] (●). Reprinted with permission.

or Eq. (27), can be used for modelling the optical constants in n-Si versus both wavenumber and electron concentration. At light doping, spectral variation of ϵ_l in Eq. (18) is to be taken into account. For this purpose, the real part of ϵ_l can be modeled using the known Sellmeier-type formula [12], and the imaginary part can be taken from the tables [12, 13]. At doping levels well above 10^{19} cm^{-3} the relaxation time τ retrieved from experimental data of Miyao *et al.* [32] and Slaoui and Siffert [33] is smoothly decreasing with the increase of N and then saturated to 3×10^{-15} s near $N = 5 \times 10^{21}$ cm^{-3} as shown in Fig. 3.

It is worthwhile to mention that the reflectivity data are affected by the state of the sample's surface. For example, Spitzer *et al.* [37] noted that for surfaces specially polished or etched, $R_{min} \sim 0.11$, whereas with standard polishing technique, values lower than 0.139 did not occur [36, 37]. Moreover, heat treatment, without affecting λ_{min}, lowered R_{min} to 0.067 [37]. An analysis of this reflectivity curve indicated that relaxation time must depend on λ [37].

VI GENERALIZED DRUDE APPROXIMATION FOR n-Si

In this section we consider all the necessary ingredients for the application of GDA to n-Si. This is done to point out that the results of this treat-

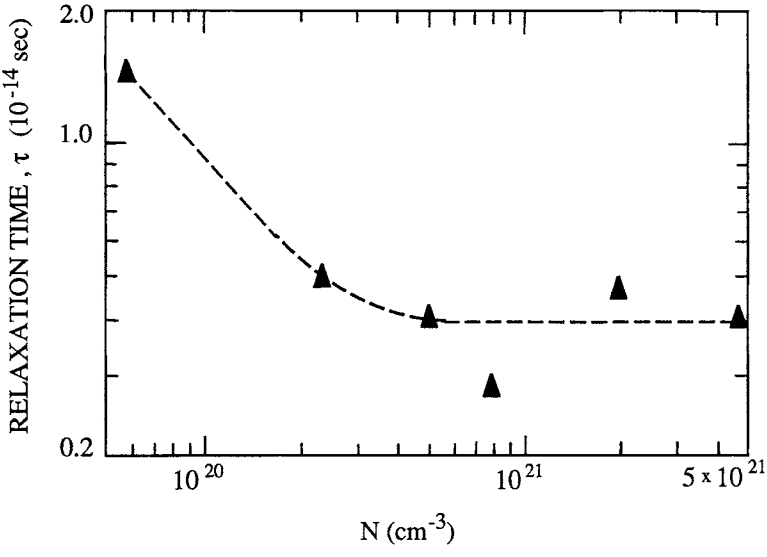

Fig. 3. Dependence of relaxation time τ, which enters the Drude Eq. (18), on free-carrier concentration in ion-implanted n-Si. Solid triangles are experimental data after Miyao *et al.* [32]; dashed line is a guide for the eye. Reprinted with permission.

ment conflict with the Drude approximation, since screened-impurity-potential models lead to a strong spectral dependence of the relaxation functions. In turn, the allowance of a constant τ contradicts some experimental data at short wavelengths [31, 34, 41], and, though less certainly, near λ_{min} [37]. Ideally, one might hope that for a much-studied material like n-Si, the theory and experiment would agree. In reality, poor knowledge of impurity potentials in heavily doped n-Si (see below), as well as the uncertainties of experimental data, make disagreement quite possible. Let us first consider the contributions to the relaxation functions existing in n-Si.

Electron-Phonon Scattering A

Electron-phonon scattering dominates in lightly doped n-Si. The actual mechanisms are DA-phonon and intervalley-phonon scattering. Unlike n-Ge, in n-Si, DO-phonon scattering is not allowed [44]. There are two types of intervalley scattering. In the first, *g*-type, an electron is transferred from a given valley to a valley with the same orientation, and in the second, *f*-type, to one of the four valleys with a different orientation. The *g*-transition uses an LO-phonon with wavevector at the point Δ and energy $\hbar\omega_{LO} \approx 735$K. Two *f*-transitions are assisted by the two phonons with wavevector at the point S: TO ($\hbar\omega_{TO} \approx 690$K) and LA ($\hbar\omega_{LA} \approx 510$K). Matrix elements of these transitions are unknown, but fortunately DA-phonon scattering more or less accounts for room-temperature mobility in lightly doped n-Si ($\mu_{300} \approx 1350$ cm^2 V^{-1}s^{-1}, the mobility relaxation time $\tau_0 \approx 2.00 \times 10^{-13}$ s). The intervalley processes contribute negligibly at room temperature because the corresponding phonon occupation numbers are rather small.

For DA-phonon scattering Eq. (23), neglecting weak anisotropy factors, gives:

$$\Gamma_{\upsilon}^{(ep)}(\omega) = \frac{\Gamma_{DA}}{F_{1/2}(\eta)} \int_0^{\infty} \frac{x}{\bar{\omega}} \ln\left[\frac{1 + \exp(\eta - x - \bar{\omega}^2/16x + \bar{\omega}/2)}{1 + \exp(\eta - x - \bar{\omega}^2/16x - \bar{\omega}/2)}\right] dx, \qquad \upsilon = \parallel, \perp, \quad (30)$$

where $\bar{\omega} = \hbar\omega/kT$, $\eta = \zeta/kT$ is the reduced chemical potential, $F_r(\eta)$ are the Fermi integrals,

$$\Gamma_{DA} = \frac{4\Xi_u^2}{3\hbar\rho u_l^2}\left(\frac{2m_d kT}{\pi\hbar^2}\right)^{3/2}, \quad (31)$$

where Ξ_u is shear-deformation potential, ρ is the crystal density, and u_l is the longitudinal sound velocity. With known values of $\Xi_u \approx 9.6$ eV, the band

and lattice parameters, one obtains $\Gamma_{DA} \approx 0.566 \times 10^{13}\ s^{-1}$ at $T = 300K$. In the non-degenerate case, one obtains

$$\Gamma^{(ep)}(\omega) = \Gamma_{DA}\left(\frac{\overline{\omega}}{4}\right)\sinh\left(\frac{\overline{\omega}}{2}\right)K_2\left(\frac{\overline{\omega}}{2}\right), \tag{32}$$

where $K_2(x)$ is the McDonald function. At $\overline{\omega}/\max(\eta,1) \gg 1$, Eq.(30) gives the asymptotic form of the absorption coefficient (see Section IV):

$$n\alpha^{(ep)} \approx \frac{16Ne^2}{9c\tau m_c\omega^2}\left(\frac{\pi\hbar\omega}{kT}\right)^{1/2}, \quad \tau = \tau_0 \exp(-\eta)F_{1/2}(\eta), \tag{33}$$

where τ_0 is DA-phonon mobility relaxation time for light doping. In Streltsov and Titov [40] the absorption spectra retrieved from the transmission data for ion-implanted Si: P layers with $N = (0.5 - 2) \times 10^{20}\ cm^{-3}$ were shown to fit Eq. (33). Using qualitative arguments, the authors stated that ionized-impurity scattering should 'switch-off' in the spectral interval under study, so observed absorption is due to acoustic phonons; the same conclusion was also drawn by Aspnes *et al.* [34]. At $N = 10^{20}\ cm^{-3}$ the fit by Streltsov and Titov [40] needed τ about 15 times smaller than τ_0, and the formula in Eq. (33) gives a factor ~ 3. The rest, however, is *not necessary* due to the increase of electron-phonon interaction as was claimed by Streltsov and Titov [40]. Actually, any short-range interaction leads to the same spectral dependence as given by Eq. (33), but with another τ_0. It might be the short-range part of electron-donor interaction (see next subsection). In this case, the asymptotic form in Eq. (33) is almost *independent* of T, whereas in the case of phonons, it is *linear* with respect to the temperature. Thus, the origin of $\lambda^{1.5}$-absorption spectrum can not be identified until its temperature dependence is studied experimentally. More seriously, the concept of Aspnes *et al.* [34] and Streltsov and Titov [40] implies impurity scattering *to play no role* also at DC. Indeed, the fit values of τ attributed by Streltsov and Titov [40] *solely* to electron-phonon interaction correspond to the mobilities in the range (61–88) $cm^2\ V^{-1}s^{-1}$, typical for the *measured* mobility at the studied concentrations.

B Electron-Impurity Scattering

A key problem in the theoretical description of electron-donor scattering is to determine the electron-donor interaction potential. Usually it is taken in the form of screened Coulomb potential

$$V_i(\mathbf{r}) = -\frac{e\exp(-|\mathbf{r} - \mathbf{R}_D|/r_s)}{\epsilon_l|\mathbf{r} - \mathbf{R}_D|}, \tag{34}$$

where e is the electron charge, $\mathbf{R}_D$ is a donor position, and r_s is a screening length. The lowest-order calculation of Eq. (23) with respect to this potential can be performed easily no matter what model for r_s is chosen. In the Debye-Thomas-Fermi model and isotropic valleys, the calculation was carried out in our paper [29]. In a theory that seems more consistent, the screening is not introduced but is *derived* in perturbative electron-gas calculations, electron-impurity, and *e-e* interactions being treated simultaneously. For many-valley bands such a calculation of Eq. (23) was performed by Sernelius [27] using a diagrammatic method. His result for the impurity contribution can be transformed to:

$$\Gamma_v^{(ei)}(\omega) = \frac{6e^2}{m_d\omega}\mathrm{Im}\int\frac{d^3q}{(2\pi)^3}q^2 a_\nu(\mathbf{q})V_i(\mathbf{q};\omega)V_i(\mathbf{q},0)[\chi_0(q,\omega) - \chi_0(q,0)], \quad (35)$$

where $a_\parallel(\mathbf{q}) = \cos^2\theta$, $a_\perp(\mathbf{q}) = 1/2\ \sin^2\theta$, $\chi_0(q,\omega)$ is the wavevector-frequency-dependent electron polarizability in one parabolic valley (Lindhard function) with effective mass m_d;

$$V_i(\mathbf{q},\omega) = \frac{-4\pi e}{\epsilon_l q^2\left(\dfrac{m_\parallel a_\parallel}{m_d} + \dfrac{m_\perp a_\perp}{m_d}\right) + 8\pi e^2\sum\limits_{k=1}^{3}\chi_0(q_k,\omega)} \quad (36)$$

is the space-time Fourier transform of the effective interaction potential, where: $q_1 = q$, $q_2 = qK^{1/2}\,[\cos^2\theta + K^{-1}(\cos^2\varphi + K^{-1}\sin^2\varphi)]^{1/2}$, $q_3 = qK^{1/2}\,[\cos^2\theta + K^{-1}(\sin^2\varphi + K^{-1}\cos^2\varphi)]^{1/2}$, $K = m_\parallel/m_\perp$, θ and φ being the polar and azimuthal angles, respectively. In the isotropic valleys Eq. (35) reduces to our result [29] by putting $\omega = 0$, $q = 0$ in the polarizability term of Eq. (36), that is also obtained using transition-probability method. Sernelius [27] obtained an expression for an *e-e* contribution that describes 'friction' damping of relative momentum of differently oriented valleys. It changes the structure of Eq. (25) at general ω, but at high frequencies contributes only an additive term to Eq. (26).

Both screening models take into consideration only the long-range part of electron-donor interaction potential. For uncompensated n-Si at $T = 300$K, because of full donor ionization, they predict independence of the scattering rate from impurity type. At the same time, there exists experimental evidence of such dependence for the mobility [31] and for IR reflectance [34] (see Section III). The dependence is probably due to a short-range potential, for which at least two sources can be pointed out. The first is the difference between the atomic potentials of Si and the donor atom, which is responsible for the deviation of dopant ionization energy from the Bohr energy, and for the difference in those for different dopants. These substitution potentials for the three dopants in Si were estimated by Viña and Cardona [11]. The second is a local deformation in the vicinity of the impurity that affects the valleys through the deformation potential the same way as the lattice

vibrations do. We have not found a reliable estimation of this effect in the literature. The near-IR absorption spectra [34, 40] offer an additional evidence that a short-range potential emerges with doping (see Subsection VIA).

The calculation of DC mobility is a crucial test for the model, because without agreeement between theory and experiment at DC, the disagreement will appear also in the IR. As is well known, the mobility calculated in the Born approximation with respect to the Debye-Thomas-Fermi potential, and isotropic-valley approximation (Brooks-Herring mobility) disagrees strongly with experimental data [45]. The calculations in GDA with (q, ω)-screening model (Eqs. (25, 35, 36)) include triple integration of complicated function with respect to q, θ, φ. This is a formidable task for desktop-computer simulations (a Cray-type supercomputer was used by Serrelius [27]). In our case $K^{1/2} \approx 2.27$, the mean values of $q_{2,3}$ appear to be close to q, so we could put $q_{2,3} = q$ in Eq. (35), but retain angular dependence through the functions $a_\nu(\mathbf{q})$. After this, the angle integration is carried out analytically. The relaxation functions are expressed via the integrals with respect to the reduced-energy variable x as in Eq. (30), but with much more complicated integrands. Despite this complexity, they still allow a fast desktop-computer calculation. The calculations become much faster in the Debye-Thomas-Fermi limit.

Neglecting *e-e* scattering, the DC relaxation time is found using GDA extrapolated to $\omega = 0$:

$$\tau = \frac{m_c}{3m_\parallel \Gamma_\parallel(0)} + \frac{2m_c}{3m_\perp \Gamma_\perp(0)}. \tag{37}$$

At maximum *e-e* scattering, τ changes from this value to $\Gamma^{-1}(0)$, where $\Gamma(\omega)$ is given by Eq. (26) [27]. We calculated τ for $N = 10^{17}$, 10^{18}, 10^{19}, and 10^{20} cm^{-3} and obtained: $\tau = 1.31 \times 10^{-13}$, $(7.22\text{–}7.07) \times 10^{-14}$, $(3.90\text{–}3.77) \times 10^{-14}$, and $(2.58\text{–}2.51) \times 10^{-14}$ s, respectively. The second value in the brackets shows the effect of *e-e* scattering, which thus proves to be small. Corresponding 'experimental' values of τ calculated using Eqs. (27–29) are: 1.08×10^{-13}, 4.22×10^{-14}, $(1.83\text{–}1.69) \times 10^{-14}$, and $(1.09\text{–}1.02) \times 10^{-14}$ s, respectively. In the last two data, the first value corresponds to Si: P and the second to Si: As; close values are extracted from the Irvin resistivity curves [46]. We see systematic discrepancy between the theoretical and experimental values of τ by a factor which increases with the increase of N from ~ 1.2 to ~ 2.3 -2.5. The Debye-Thomas-Fermi model gives a larger factor (3.5–3.7 at $N = 10^{20}$ cm^{-3}). To the best of our knowledge this discrepancy has not yet been resolved, and is still discussed in the literature [47]. Thus, the disagreement between optical constants calculated by GDA using the screening models and those calculated using the empirically adjusted Drude approach [43], arises even if the static values of the relaxation functions are substituted into Eq. (25). Including full frequency de-

pendence does not make the situation better. Moreover, as seen from Fig. 4, the relaxation functions appear to strongly decrease with decreasing λ, so their values at short wavelengths are too small to account for observed absorption. In addition, at heavy doping ($N > 3 \times 10^{18}$ cm^{-3}) the relaxation functions acquire peaks near the plasma wavelength, which are more pronounced for $\Gamma_\perp$ (see Figs. 4, 5). Mathematically, these peaks arise from the poles of $V_i(\mathbf{q},\omega)$ in the complex (q,ω)-plane. Physically, they display the response of plasma waves excited by scattered electrons in the screening electron cloud, a feature that cannot appear in the Debye-Thomas-Fermi model. These peaks produce weak humps on the reflectivity curves near λ_{min}, which have never been observed experimentally. In our opinion, this is one more reason to recast the donor potential issue in n-Si.

TABULATION OF OPTICAL CONSTANTS OF DOPED n-Si VII

We tabulated n and k for practical use at nine concentrations in the range from 10^{16} cm^{-3} to 10^{20} cm^{-3}, with roughly a factor-of-three increase for each step, using the fit of Humlíček and Wojtechovsky [43] given by

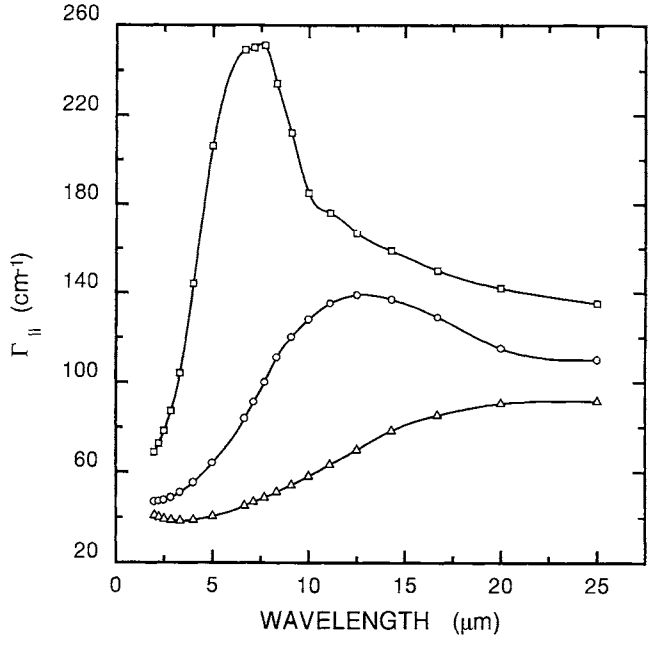

Fig. 4. Theoretical spectra of ⟨100⟩ relaxation function $\Gamma_\parallel$ calculated using Eqs. (35, 36) for three electron concentrations: (Δ) $N = 10^{19}$ cm^{-3}; (○) $N = 3 \times 10^{19}$ cm^{-3}; (□) $N = 10^{20}$ cm^{-3}.

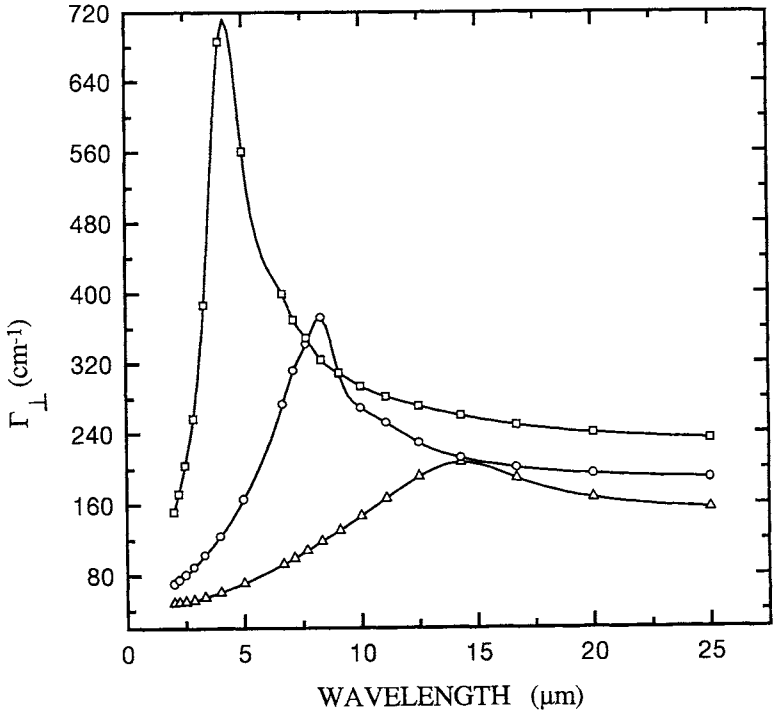

Fig. 5. Theoretical spectra of ⟨010⟩ relaxation function $\Gamma_\perp$ calculated using Eqs. (35, 36) for three electron concentrations: (Δ) $N = 10^{19}$ cm^{-3}; (○) $N = 3 \times 10^{19}$ cm^{-3}; (□) $N = 10^{20}$ cm^{-3}.

Eqs. (27, 28) and Drude Eq. (18). The results are placed in Tables I to IX in the columns headed by abbreviation 'HW'. For heavy doping we display different values for Si: P and Si: As. The fit for Si: Sb (first line of Eq. (27)) was not used because we found that three data points available for this dopant fit a linear function of N better than that of $\sqrt{N}$. Each table covers a spectral interval from 2μm either to 100μm at light and moderate dopings, or to 25μm at heavy doping. The tables can be easily extended to wider intervals using Eqs. (27, 28, 18).

For sake of comparison, in each table we added the columns with theoretical values calculated by us using Eqs. (35, 36) with Eq. (25) as outlined above; they are abbreviated by 'GDA'. It is seen that at light and moderate doping the disagreement between theory and the empirical fit is not so strong. It is more or less concordant with the disagreement at DC discussed above. In some cases, where the fit overestimates γ, theory may be in a better agreement with direct experimental data (see Fig. 6). At heavy doping (Tables VII–IX), the disagreement becomes more drastic especially near the peaks of the relaxation functions. Fig. 7 shows some plots of n and k.

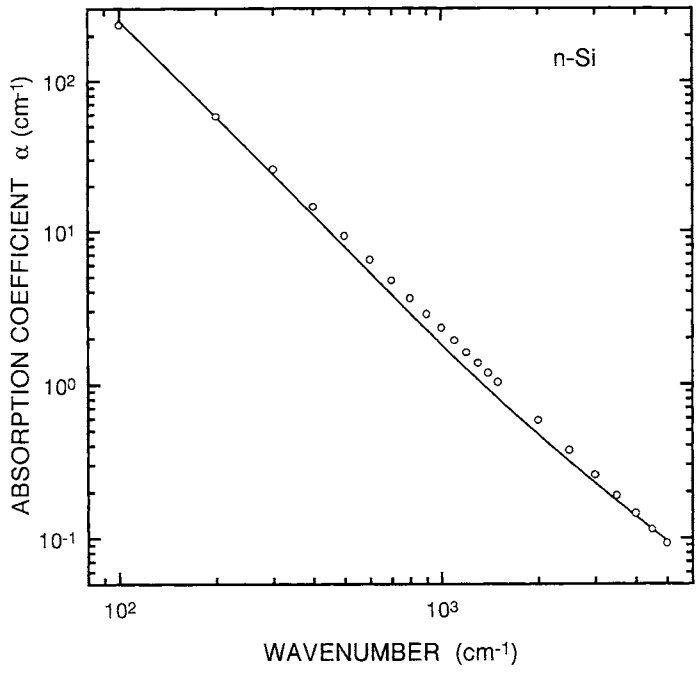

Fig. 6. Absorption spectrum for $N = 10^{17}$ cm^{-3} with lattice absorption extracted. The solid line represents theoretical curve. Open circles are the experimental data for Si: As [43].

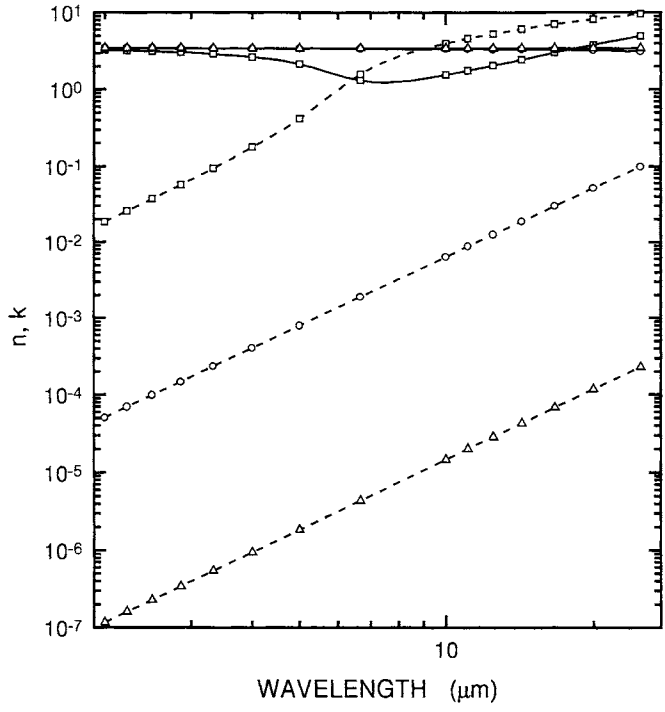

Fig. 7. Log-plot of n and k calculated using Eqs. (18, 27, 29) for three electron concentrations: (Δ) $N = 10^{16}$ cm^{-3}; ($\circ$) $N = 10^{18}$ cm^{-3}; ($\square$) $N = 10^{20}$ cm^{-3}. Lines: solid-n, dashed-k. The difference in values of n as well as its spectral variation for (Δ) and ($\circ$) are small.

TABLE I

n-Si, $N = 10^{16}$ cm^{-3}

			n		k	
eV	cm^{-1}	μm	HW[a]	GDA[b]	HW[a]	GDA[b]
0.6199	5000	2.000	3.453	3.453	1.160 E–7	1.514 E–7
0.5579	4500	2.222	3.447	3.447	1.594 E–7	2.006 E–7
0.4959	4000	2.500	3.441	3.441	2.273 E–7	2.751 E–7
0.4339	3500	2.857	3.435	3.435	3.398 E–7	3.945 E–7
0.3720	3000	3.333	3.431	3.431	5.403 E–7	6.001 E–7
0.3100	2500	4.000	3.427	3.427	9.347 E–7	9.912 E–7
0.2480	2000	5.000	3.424	3.424	1.827 E–6	1.850 E–6
0.1860	1500	6.667	3.421	3.421	4.334 E–6	4.210 E–6
0.1240	1000	10.00	3.419	3.419	1.463 E–5	1.392 E–5
0.1116	900	11.11	3.419	3.419	2.006 E–5	1.910 E–5
0.09919	800	12.50	3.419	3.419	2.856 E–5	2.727 E–5
0.08679	700	14.29	3.418	3.418	4.262 E–5	4.092 E–5
0.07439	600	16.67	3.418	3.418	6.765 E–5	6.549 E–5
0.06199	500	20.00	3.417	3.417	1.168 E–4	1.143 E–4
0.04959	400	25.00	3.416	3.416	2.278 E–4	2.259 E–4
0.03720	300	33.33	3.413	3.413	5.382 E–4	5.413 E–4
0.03472	280	35.71	3.412	3.412	6.612 E–4	6.669 E–4
0.03224	260	38.46	3.411	3.411	8.247 E–4	8.341 E–4
0.02976	240	41.67	3.410	3.410	1.047 E–3	1.061 E–3
0.02728	220	45.45	3.408	3.408	1.356 E–3	1.379 E–3
0.02480	200	50.00	3.406	3.406	1.799 E–3	1.834 E–3
0.02232	180	55.56	3.399	3.399	3.481 E–3	3.563 E–3
0.01984	160	62.50	3.403	3.403	2.458 E–3	2.511 E–3
0.01736	140	71.43	3.394	3.394	5.154 E–3	5.284 E–3
0.01488	120	83.33	3.385	3.385	8.085 E–3	8.297 E–3
0.01240	100	100.0	3.372	3.372	1.370 E–2	1.405 E–2

[a] Values calculated using the fit of Ref. [43].
[b] Values calculated using GDA (unpublished)

TABLE II

n-Si, $N = 3 \times 10^{16}$ cm^{-3}

			n		*k*	
eV	cm^{-1}	μm	HW[a]	GDA[b]	HW[a]	GDA[b]
0.6199	5000	2.000	3.453	3.453	6.273 E–7	4.547 E–7
0.5579	4500	2.222	3.447	3.447	8.622 E–7	6.025 E–7
0.4959	4000	2.500	3.441	3.441	1.230 E–6	8.264 E–7
0.4339	3500	2.857	3.435	3.435	1.838 E–6	1.185 E–6
0.3720	3000	3.333	3.431	3.431	2.923 E–6	1.804 E–6
0.3100	2500	4.000	3.427	3.427	5.056 E–6	2.982 E–6
0.2480	2000	5.000	3.424	3.424	9.884 E–6	5.571 E–6
0.1860	1500	6.667	3.421	3.421	2.344 E–5	1.271 E–5
0.1240	1000	10.00	3.418	3.418	7.913 E–5	4.223 E–5
0.1116	900	11.11	3.417	3.418	1.085 E–4	5.808 E–5
0.09919	800	12.50	3.416	3.417	1.545 E–4	8.312 E–5
0.08679	700	14.29	3.415	3.416	2.306 E–4	1.251 E–4
0.07439	600	16.67	3.413	3.415	3.660 E–4	2.010 E–4
0.06199	500	20.00	3.410	3.413	6.320 E–4	3.528 E–4
0.04959	400	25.00	3.405	3.410	1.233 E–3	7.025 E–4
0.03720	300	33.33	3.394	3.402	2.913 E–3	1.704 E–3
0.03472	280	35.71	3.391		3.579 E–3	
0.03224	260	38.46	3.386		4.464 E–3	
0.02976	240	41.67	3.381		5.667 E–3	
0.02728	220	45.45	3.374		7.342 E–3	
0.02480	200	50.00	3.365	3.381	9.745 E–3	5.888 E–3
0.02232	180	55.56	3.352		1.887 E–3	
0.01984	160	62.50	3.336		1.332 E–2	
0.01736	140	71.43	3.311		2.796 E–2	
0.01488	120	83.33	3.275		4.391 E–2	
0.01240	100	100.0	3.218	3.279	7.453 E–2	4.695 E–2

TABLE III

n-Si, $N = 10^{17}$ cm^{-3}

			n		k	
eV	cm^{-1}	μm	HW[a]	GDA[b]	HW[a]	GDA[b]
0.6199	5000	2.000	3.453	3.453	2.856 E–6	1.519 E–6
0.5579	4500	2.222	3.446	3.446	3.925 E–6	2.013 E–6
0.4959	4000	2.500	3.440	3.440	5.598 E–6	2.763 E–6
0.4339	3500	2.857	3.435	3.435	8.369 E–6	3.965 E–6
0.3720	3000	3.333	3.430	3.430	1.331 E–5	6.042 E–6
0.3100	2500	4.000	3.426	3.426	2.302 E–5	1.000 E–5
0.2480	2000	5.000	3.422	3.423	4.500 E–5	1.875 E–5
0.2356	1900	5.263	3.421		5.250 E–5	
0.2232	1800	5.556	3.421		6.175 E–5	
0.2108	1700	5.882	3.420		7.331 E–5	
0.1984	1600	6.250	3.419		8.794 E–5	
0.1860	1500	6.667	3.418	3.419	1.067 E–4	4.300 E–5
0.1736	1400	7.143	3.417	3.419	1.313 E–4	5.268 E–5
0.1612	1300	7.692	3.4165	3.418	1.640 E–4	6.561 E–5
0.1488	1200	8.333	3.415	3.417	2.085 E–4	8.333 E–5
0.1364	1100	9.091	3.414	3.416	2.708 E–4	1.083 E–4
0.1240	1000	10.00	3.413	3.415	3.604 E–4	1.446 E–4
0.1116	900	11.11	3.410	3.413	4.944 E–4	1.997 E–4
0.09919	800	12.50	3.408	3.411	7.039 E–4	2.874 E–4
0.08679	700	14.29	3.404	3.409	1.051 E–3	4.355 E–4
0.07439	600	16.67	3.399	3.405	1.668 E–3	7.061 E–4
0.06199	500	20.00	3.390	3.400	2.882 E–3	1.255 E–3
0.05951	480	20.83	3.387		3.257 E–3	
0.05703	460	21.74	3.384		3.700 E–3	
0.05455	440	22.73	3.381		4.228 E–3	
0.05207	420	23.81	3.377		4.861 E–3	
0.04959	400	25.00	3.373	3.387	5.626 E–3	2.542 E–3
0.04771	380	26.32	3.368		6.561 E–3	
0.04463	360	27.78	3.365		7.715 E–3	
0.04215	340	29.41	3.356		9.156 E–3	
0.03968	320	31.25	3.348		1.098 E–2	
0.03720	300	33.33	3.338	3.362	1.332 E–2	6.326 E–3
0.03472	280	35.71	3.326		1.638 E–2	
0.03224	260	38.46	3.312		2.045 E–2	
0.02976	240	41.67	3.294		2.599 E–2	
0.02728	220	45.45	3.271		3.372 E–2	
0.02480	200	50.00	3.241	3.294	4.485 E–2	2.283 E–2
0.02232	180	55.56	3.201		6.147 E–2	
0.01984	160	62.50	3.146		8.744 E–2	
0.01736	140	71.43	3.069		1.304 E–1	
0.01488	120	83.33	2.956		2.068 E–1	
0.01240	100	100.0	2.786	2.957	3.567 E–1	1.995 E–1

TABLE IV

n-Si, $N = 3 \times 10^{17}$ cm^{-3}

			n		*k*	
eV	cm^{-1}	μm	HW[a]	GDA[b]	HW[a]	GDA[b]
0.6199	5000	2.000	3.452	3.453	1.286 E–5	4.580 E–6
0.5579	4500	2.222	3.446	3.446	1.768 E–5	6.078 E–6
0.4959	4000	2.500	3.439	3.440	2.522 E–5	8.355 E–6
0.4339	3500	2.857	3.434	3.434	3.770 E–5	1.202 E–5
0.3720	3000	3.333	3.429	3.429	5.995 E–5	1.837 E–5
0.3100	2500	4.000	3.424	3.425	1.037 E–4	3.056 E–5
0.2480	2000	5.000	3.419	3.420	2.028 E–4	5.774 E–5
0.2356	1900	5.263	3.417		2.365 E–4	
0.2232	1800	5.556	3.416		2.782 E–4	
0.2108	1700	5.882	3.415		3.304 E–4	
0.1984	1600	6.250	3.413		3.963 E–4	
0.1860	1500	6.667	3.412	3.415	4.811 E–4	1.344 E–4
0.1736	1400	7.143	3.410	3.413	5.918 E–4	1.654 E–4
0.1612	1300	7.692	3.408	3.412	7.393 E–4	2.071 E–4
0.1488	1200	8.333	3.405	3.410	9.401 E–4	2.647 E–4
0.1364	1100	9.091	3.402	3.408	1.221 E–3	3.466 E–4
0.1240	1000	10.00	3.398	3.405	1.625 E–3	4.671 E–4
0.1116	900	11.11	3.392	3.401	2.230 E–3	6.522 E–4
0.09919	800	12.50	3.385	3.396	3.177 E–3	9.513 E–4
0.08679	700	14.29	3.374	3.388	4.745 E–3	1.467 E–3
0.07439	600	16.67	3.358	3.377	7.542 E–3	2.431 E–3
0.06199	500	20.00	3.331	3.358	1.305 E–2	4.446 E–3
0.05951	480	20.83	3.324		1.476 E–2	
0.05703	460	21.74	3.316		1.678 E–2	
0.05455	440	22.73	3.306		1.918 E–2	
0.05207	420	23.81	3.295		2.207 E–2	
0.04959	400	25.00	3.283	3.324	2.556 E–2	9.367 E–3
0.04771	380	26.32	3.268		2.984 E–2	
0.04463	360	27.78	3.251		3.513 E–2	
0.04215	340	29.41	3.232		4.176 E–2	
0.03968	320	31.25	3.208		5.017 E–2	
0.03720	300	33.33	3.180	3.250	6.100 E–2	2.464 E–2
0.03472	280	35.71	3.145		7.522 E–2	
0.03224	260	38.46	3.103		9.424 E–2	
0.02976	240	41.67	3.051		1.203 E–1	
0.02728	220	45.45	2.985		1.571 E–1	
0.02480	200	50.00	2.900	3.041	2.107 E–1	9.695 E–2
0.02232	180	55.56	2.790		2.923 E–1	
0.01984	160	62.50	2.647		4.227 E–1	
0.01736	140	71.43	2.465		6.431 E–1	
0.01612	130	76.92	2.364		8.094 E–1	
0.01488	120	83.33	2.267		1.030 E 0	
0.01364	110	90.91	2.193		1.314 E 0	
0.01240	100	100.0	2.163	2.137	1.664 E 0	9.947 E–1

TABLE V

n-Si, $N = 10^{18}$ cm^{-3}

			n		k	
eV	cm^{-1}	μm	HW[a]	GDA[b]	HW[a]	GDA[b]
0.6199	5000	2.000	3.451	3.451	5.030 E–5	1.556 E–5
0.5579	4500	2.222	3.444	3.444	6.913 E–5	2.072 E–5
0.4959	4000	2.500	3.438	3.438	9.860 E–5	2.863 E–5
0.4339	3500	2.857	3.431	3.431	1.474 E–4	4.149 E–5
0.3720	3000	3.333	3.425	3.425	2.344 E–4	6.408 E–5
0.3100	2500	4.000	3.419	3.419	4.054 E–4	1.083 E–4
0.2480	2000	5.000	3.411	3.411	7.925 E–4	2.100 E–4
0.2356	1900	5.263	3.410		9.244 E–4	
0.2232	1800	5.556	3.407		1.087 E–3	
0.2108	1700	5.882	3.405		1.291 E–3	
0.1984	1600	6.250	3.402		1.548 E–3	
0.1860	1500	6.667	3.399	3.399	1.879 E–3	5.121 E–4
0.1736	1400	7.143	3.396	3.395	2.312 E–3	6.385 E–4
0.1612	1300	7.692	3.391	3.391	2.887 E–3	8.120 E–4
0.1488	1200	8.333	3.386	3.385	3.671 E–3	1.056 E–3
0.1364	1100	9.091	3.379	3.378	4.766 E–3	1.412 E–3
0.1240	1000	10.00	3.370	3.369	6.343 E–3	1.951 E–3
0.1116	900	11.11	3.358	3.357	8.700 E–3	2.804 E–3
0.09919	800	12.50	3.342	3.340	1.239 E–2	4.234 E–3
0.08679	700	14.29	3.318	3.315	1.848 E–2	6.806 E–3
0.07439	600	16.67	3.282	3.277	2.934 E–2	1.187 E–2
0.06199	500	20.00	3.224	3.213	5.068 E–2	2.309 E–2
0.05951	480	20.83	3.208		5.727 E–2	
0.05703	460	21.74	3.190		6.507 E–2	
0.05455	440	22.73	3.169		7.435 E–2	
0.05207	420	23.81	3.146		8.548 E–2	
0.04959	400	25.00	3.120	3.100	9.896 E–2	5.252 E–2
0.04771	380	26.32	3.090		1.154 E–1	
0.04463	360	27.78	3.055		1.358 E–1	
0.04215	340	29.42	3.014		1.612 E–1	
0.03968	320	31.25	2.967		1.934 E–1	
0.03720	300	33.33	2.912	2.844	2.349 E–1	1.525 E–1
0.03472	280	35.71	2.847		2.891 E–1	
0.03224	260	38.46	2.771		3.613 E–1	
0.02976	240	41.67	2.682		4.594 E–1	
0.02728	220	45.45	2.582		5.953 E–1	
0.02480	200	50.00	2.474	2.149	7.862 E–1	6.685 E–1
0.02232	180	55.56	2.374		1.054 E 0	
0.02108	170	58.82	2.337		1.222 E 0	
0.01984	160	62.50	2.314		1.416 E 0	
0.01860	150	66.67	2.312		1.634 E 0	
0.01736	140	71.43	2.336		1.875 E 0	
0.01612	130	76.92	2.388		2.137 E 0	
0.01488	120	83.33	2.474		2.420 E 0	
0.01364	110	90.91	2.596		2.723 E 0	
0.01240	100	100.0	2.758	2.122	3.048 E 0	3.868 E 0

TABLE VI

n-Si, $N = 3 \times 10^{18}$ cm^{-3}

			n		*k*	
eV	cm^{-1}	μm	HW[a]	GDA[b]	HW[a]	GDA[b]
0.6199	5000	2.000	3.447	3.447	2.482 E–4	4.914 E–5
0.5579	4500	2.222	3.439	3.439	3.412 E–4	6.614 E–5
0.4959	4000	2.500	3.431	3.431	4.866 E–4	9.264 E–5
0.4339	3500	2.857	3.423	3.423	7.275 E–4	1.367 E–4
0.3720	3000	3.333	3.414	3.414	1.157 E–3	2.168 E–4
0.3100	2500	4.000	3.403	3.403	2.001 E–3	3.807 E–4
0.2480	2000	5.000	3.386	3.386	3.913 E–3	7.826 E–4
0.2356	1900	5.263	3.382		4.565 E–3	
0.2232	1800	5.556	3.377		5.370 E–3	
0.2108	1700	5.882	3.371		6.376 E–3	
0.1984	1600	6.250	3.363		7.650 E–3	
0.1860	1500	6.667	3.355	3.354	9.286 E–3	2.097 E–3
0.1736	1400	7.143	3.345	3.343	1.142 E–2	2.683 E–3
0.1612	1300	7.692	3.332	3.330	1.427 E–2	3.510 E–3
0.1488	1200	8.333	3.317	3.314	1.815 E–2	4.714 E–3
0.1364	1100	9.091	3.297	3.293	2.358 E–2	6.531 E–3
0.1240	1000	10.00	3.272	3.266	3.141 E–2	9.391 E–3
0.1116	900	11.11	3.237	3.228	4.312 E–2	1.412 E–2
0.09919	800	12.50	3.190	3.176	6.148 E–2	2.244 E–2
0.08679	700	14.29	3.123	3.099	9.198 E–2	3.820 E–2
0.07439	600	16.67	3.023	2.980	1.466 E–1	7.099 E–2
0.06199	500	20.00	2.866	2.782	2.553 E–1	1.477 E–1
0.05951	480	20.83	2.825		2.892 E–1	
0.05703	460	21.74	2.780		3.294 E–1	
0.05455	440	22.73	2.729		3.774 E–1	
0.05207	420	23.81	2.674		4.352 E–1	
0.04959	400	25.00	2.615	2.435	5.052 E–1	3.728 E–1
0.04771	380	26.32	2.550		5.906 E–1	
0.04463	360	27.78	2.483		6.953 E–1	
0.04215	340	29.41	2.414		8.241 E–1	
0.03968	320	31.25	2.349		9.816 E–1	
0.03720	300	33.33	2.294	1.677	1.172 E 0	1.110 E 0
0.03472	280	35.71	2.258		1.398 E 0	
0.03224	260	38.46	2.249		1.659 E 0	
0.02976	240	41.67	2.277		1.953 E 0	
0.02728	220	45.45	2.347		2.275 E 0	
0.02480	200	50.00	2.464	1.600	2.625 E 0	3.324 E 0
0.02232	180	55.56	2.635		3.004 E 0	
0.01984	160	62.50	2.866		3.416 E 0	
0.01736	140	71.43	3.170		3.868 E 0	
0.01488	120	83.33	3.567		4.375 E 0	
0.01240	100	100.0	4.088	3.571	4.963 E 0	7.154 E 0

TABLE VII

n-Si, $N = 10^{19}$ cm^{-3}

			n		k	
eV	cm^{-1}	μm	HW[a]	GDA[b]	HW[a]	GDA[b]
0.6199	5000	2.000	3.432[P]		1.239 E–3	
			3.434[As]	3.433	1.233 E–3	1.929 E–4
0.5579	4500	2.222	3.420		1.703 E–3	
			3.422	3.422	1.695 E–3	2.672 E–4
0.4959	4000	2.500	3.408		2.432 E–3	
			3.410	3.409	2.419 E–3	3.883 E–4
0.4339	3500	2.857	3.392		3.641 E–3	
			3.395	3.394	3.620 E–3	6.013 E–4
0.3720	3000	3.333	3.372		5.802 E–3	
			3.376	3.375	5.765 E–3	1.015 E–3
0.3100	2500	4.000	3.342		1.007 E–2	
			3.349	3.346	1.000 E–2	1.940 E–3
0.2480	2000	5.000	3.290		1.984 E–2	
			3.301	3.296	1.963 E–2	4.478 E–3
0.2356	1900	5.263	3.275		2.319 E–2	
			3.288		2.293 E–2	
0.2232	1800	5.556	3.258		2.735 E–2	
			3.272		2.702 E–2	
0.2108	1700	5.882	3.237		3.257 E–2	
			3.253		3.214 E–2	
0.1984	1600	6.250	3.213		3.922 E–2	
			3.231		3.865 E–2	
0.1860	1500	6.667	3.184		4.782 E–2	
			3.205	3.190	4.706 E–2	1.413 E–2
0.1736	1400	7.143	3.148		5.916 E–2	
			3.173	3.155	5.810 E–2	1.883 E–2
0.1612	1300	7.692	3.105		7.444 E–2	
			3.133	3.110	7.292 E–2	2.577 E–2
0.1488	1200	8.333	3.050		9.557 E–2	
			3.084	3.054	9.330 E–2	3.636 E–2
0.1364	1100	9.091	2.979		1.257 E–1	
			3.021	2.981	1.222 E–1	5.321 E–2
0.1240	1000	10.00	2.888		1.703 E–1	
			2.940	2.884	1.645 E–1	8.135 E–2
0.1116	900	11.11	2.765[P]		2.395 E–1	
			2.833[As]	2.753	2.293 E–1	1.311 E–1
0.09919	800	12.50	2.598		3.541 E–1	
			2.688	2.572	3.345 E–1	2.240 E–1
0.08679	700	14.29	2.369		5.598 E–1	
			2.492	2.307	5.173 E–1	3.933 E–1
0.08431	680	14.71	2.315		6.194 E–1	
			2.447		5.692 E–1	
0.08183	660	15.15	2.259		6.878 E–1	
			2.399		6.281 E–1	

TABLE VII *(Continued)*

n-Si, $N = 10^{19}$ cm^{-3}

			n		*k*	
eV	cm^{-1}	μm	HW[a]	GDA[b]	HW[a]	GDA[b]
0.07935	640	15.63	2.201		7.662 E–1	
			2.349		6.952 E–1	
0.07690	620	16.13	2.142		8.562 E–1	
			2.299		7.717 E–1	
0.07439	600	16.67	2.085		9.591 E–1	
			2.248	1.847	8.588 E–1	7.106 E–1
0.07180	580	17.24	2.030		1.076 E–1	
			2.198		9.578 E–1	
0.06933	560	17.86	1.980		1.208 E 0	
			2.151		1.070 E 0	
0.06685	540	18.52	1.938		1.355 E 0	
			2.110		1.195 E 0	
0.06438	520	19.23	1.907		1.516 E 0	
			2.075		1.334 E 0	
0.06199	500	20.00	1.887		1.690 E 0	
			2.049	1.274	1.487 E 0	1.565 E 0
0.05951	480	20.83	1.882		1.876 E 0	
			2.035		1.653 E 0	
0.05703	460	21.74	1.890		2.072 E 0	
			2.034		1.830 E 0	
0.05455	440	22.73	1.914		2.277 E 0	
			2.047		2.018 E 0	
0.05207	420	23.81	1.954		2.492 E 0	
			2.075		2.217 E 0	
0.04959	400	25.00	2.009		2.716 E 0	
			2.118	1.197	2.424 E 0	2.943 E 0

[P, As] The superscripts denote Si: P, Si: As respectively.

TABLE VIII

n-Si, $N = 3 \times 10^{19}$ cm^{-3}

			n		k	
eV	cm^{-1}	μm	HW[a]	GDA[b]	HW[a]	GDA[b]
0.6199	5000	2.000	3.397[P]		4.082 E–3	
			3.395[As]	3.393	4.811 E–3	8.340 E–4
0.5579	4500	2.222	3.376		5.626 E–3	
			3.374	3.372	6.629 E–3	1.215 E–3
0.4959	4000	2.500	3.352		8.056 E–3	
			3.349	3.345	9.489 E–3	1.875 E–3
0.4339	3500	2.857	3.319		1.211 E–2	
			3.316	3.310	1.426 E–2	3.121 E–3
0.3720	3000	3.333	3.272		1.944 E–2	
			3.267	3.259	2.287 E–2	5.759 E–3
0.3100	2500	4.000	3.196		3.418 E–2	
			3.191	3.177	4.015 E–2	1.232 E–2
0.2480	2000	5.000	3.060		6.895 E–2	
			3.053	3.025	8.078 E–2	3.331 E–2
0.2356	1900	5.263	3.019		8.124 E–2	
			3.011		9.509 E–2	
0.2232	1800	5.556	2.971		9.671 E–2	
			2.963		1.131 E–1	
0.2108	1700	5.882	2.914		1.165 E–1	
			2.906		1.361 E–1	
0.1984	1600	6.250	2.846		1.423 E–1	
			2.838		1.660 E–1	
0.1860	1500	6.667	2.763		1.768 E–1	
			2.755	2.694	2.057 E–1	1.415 E–1
0.1736	1400	7.143	2.661		2.240 E–1	
			2.655	2.587	2.599 E–1	2.036 E–1
0.1612	1300	7.692	2.534		2.910 E–1	
			2.530	2.453	3.363 E–1	2.886 E–1
0.1488	1200	8.333	2.372		3.903 E–1	
			2.377	2.294	4.483 E–1	4.167 E–1
0.1364	1100	9.091	2.168		5.460 E–1	
			2.188	1.999	6.201 E–1	5.280 E–1
0.1240	1000	10.00	1.921		8.042 E–1	
			1.971	1.609	8.933 E–1	7.725 E–1
0.1116	900	11.11	1.675[P]		1.232 E 0	
			1.774[As]	1.221	1.317 E 0	1.308 E 0
0.09919	800	12.50	1.540		1.842 E 0	
			1.681	1.000	1.893 E 0	2.079 E 0
0.08679	700	14.29	1.571		2.565 E 0	
			1.737	0.966	2.572 E 0	2.948 E 0
0.08431	680	14.71	1.597		2.720 E 0	
			1.767		2.718 E 0	
0.08183	660	15.15	1.628		2.878 E 0	
			1.801		2.868 E 0	

TABLE VIII *(Continued)*

n-Si, $N = 3 \times 10^{19}$ cm^{-3}

			n		*k*	
eV	cm^{-1}	μm	HW[a]	GDA[b]	HW[a]	GDA[b]
0.07935	640	15.63	1.666		3.041 E 0	
			1.843		3.021 E 0	
0.07690	620	16.13	1.711		3.208 E 0	
			1.891		3.178 E 0	
0.07439	600	16.67	1.762		3.380 E 0	
			1.945	1.073	3.340 E 0	3.932 E 0
0.07180	580	17.24	1.820		3.557 E 0	
			2.007		3.506 E 0	
0.06933	560	17.86	1.886		3.739 E 0	
			2.076		3.677 E 0	
0.06685	540	18.52	1.959		3.928 E 0	
			2.153		3.853 E 0	
0.06438	520	19.23	2.042		4.123 E 0	
			2.238		4.035 E 0	
0.06199	500	20.00	2.134		4.325 E 0	
			2.332	1.318	4.223 E 0	5.134 E 0
0.05951	480	20.83	2.236		4.535 E 0	
			2.437		4.418 E 0	
0.05703	460	21.74	2.349		4.754 E 0	
			2.552		4.620 E 0	
0.05455	440	22.73	2.475		4.982 E–0	
			2.679		4.831 E–0	
0.05207	420	23.81	2.614		5.220 E 0	
			2.819		5.050 E 0	
0.04959	400	25.00	2.769		5.469 E 0	
			2.974	1.803	5.278 E 0	6.720 E 0

TABLE IX

n-Si, $N = 10^{20}$ cm^{-3}

			n		k	
eV	cm^{-1}	μm	HW[a]	GDA[b]	HW[a]	GDA[b]
0.6199	5000	2.000	3.270[P]		1.834 E–2	
			3.257[As]	3.247	2.403 E–2	6.131 E–3
0.5579	4500	2.222	3.219		2.549 E–2	
			3.203	3.190	3.341 E–2	9.701 E–3
0.4959	4000	2.500	3.151		3.698 E–2	
			3.130	3.112	4.845 E–2	1.664 E–2
0.4339	3500	2.857	3.053	3.000	5.671 E–2	
			3.027		7.432 E–2	3.232 E–2
0.3720	3000	3.333	2.902		9.410 E–2	
			2.867	2.828	1.233 E–1	8.053 E–2
0.3100	2500	4.000	2.644		1.765 E–1	
			2.597	2.577	2.314 E–1	2.549 E–1
0.2480	2000	5.000	2.138		4.176 E–1	
			2.087	1.990	5.461 E–1	5.336 E–1
0.2356	1900	5.263	1.981		5.226 E–1	
			1.939		6.796 E–1	
0.2232	1800	5.556	1.800		6.717 E–1	
			1.780		8.617 E–1	
0.2108	1700	5.882	1.604		8.873 E–1	
			1.626		1.107 E 0	
0.1984	1600	6.250	1.423		1.188 E 0	
			1.503		1.417 E 0	
0.1860	1500	6.667	1.295		1.566 E 0	
			1.429	0.971	1.777 E 0	1.902 E 0
0.1736	1400	7.143	1.237		1.989 E 0	
			1.411	0.893	2.172 E 0	2.369 E 0
0.1612	1300	7.692	1.239		2.437 E 0	
			1.442	0.873	2.591 E 0	2.859 E 0
0.1488	1200	8.333	1.291		2.911 E 0	
			1.518	0.872	3.037 E 0	3.387 E 0
0.1364	1100	9.091	1.390		3.418 E 0	
			1.642	0.913	3.514 E 0	3.960 E 0
0.1240	1000	10.00	1.540		3.971 E 0	
			1.817	0.985	4.034 E 0	4.603 E 0
0.1116	900	11.11	1.751[P]		4.584 E 0	
			2.057[As]	1.105	4.608 E 0	5.341 E 0
0.09919	800	12.50	2.042		5.278 E 0	
			2.378	1.278	5.251 E 0	6.216 E 0
0.08679	700	14.29	2.444		6.079 E 0	
			2.810	1.530	5.982 E 0	7.282 E 0
0.08431	680	14.71	2.542		6.255 E 0	
			2.913		6.141 E 0	
0.08183	660	15.15	2.646		6.437 E 0	
			3.022		6.305 E 0	

TABLE IX *(Continued)*

n-Si, $N = 10^{20}$ cm^{-3}

			n		*k*	
eV	cm^{-1}	μm	HW[a]	GDA[b]	HW[a]	GDA[b]
0.07935	640	15.63	2.758		6.625 E 0	
			3.139		6.474 E 0	
0.07690	620	16.13	2.877		6.820 E 0	
			3.262		6.649 E 0	
0.07439	600	16.67	3.006		7.022 E 0	
			3.395	1.911	6.829 E 0	8.630 E 0
0.07180	580	17.24	3.143		7.231 E 0	
			3.536		7.015 E 0	
0.06933	560	17.86	3.291		7.448 E 0	
			3.686		7.208 E 0	
0.06685	540	18.52	3.451		7.674 E 0	
			3.846		7.407 E 0	
0.06438	520	19.23	3.622		7.909 E 0	
			4.018		7.614 E 0	
0.06199	500	20.00	3.807		8.154 E 0	
			4.201	2.517	7.829 E 0	1.040 E+1
0.05951	480	20.83	4.006		8.409 E 0	
			4.398		8.052 E 0	
0.05703	460	21.74	4.222		8.675 E 0	
			4.608		8.285 E 0	
0.05455	440	22.73	4.455		8.954 E 0	
			4.835		8.528 E 0	
0.05207	420	23.81	4.707		9.245 E 0	
			5.078		8.782 E 0	
0.04959	400	25.00	4.982		9.551 E 0	
			5.340	3.551	9.048 E 0	1.285 E+1

To conclude, there exists a dicrepancy between theory and experiment for the DF of heavily doped n-Si. This inconsistency is due to an improper model of donor potential, to a much larger extent, than to theoretical shortcomings and experimental uncertainties.

REFERENCES

1. E. D. Palik, *in* "Handbook of Optical Constants of Solids" (E. D. Palik, ed.), p. 3. Academic Press, Orlando, Florida, 1985.
2. P. A. Shumann, Jr., R. P. Phillips, and P. J. Olshefski, *J. Electrochem. Soc.* **113**, 368 (1966).
3. B. R. Hemenway, O. Solgaard, and D. M. Bloom, *Appl. Phys. Lett.* **55**, 349 (1989).
4. J. C. Sturm and C. M. Reaves, *IEEE Trans. Electron Devices* **39**, 81 (1992); P. J. Timans, *J. Appl. Phys.* **74**, 6353 (1993).
5. P. J. Hesketh, J. N. Zemel, and B. Gebhart, *Phys. Rev. B* **37**, 10795 and 10813 (1988).
6. M. Auslender and S. Hava, *Infrared Phys. Technol.* **36**, 1077 (1995); M. Auslender, S. Hava, and J. N. Zemel, *Infrared Phys. Technol.* **37**, 367 (1996).

7. M. Born and E. Wolf, "Principles of Optics." Pergamon, Oxford, 1986.
8. T. S. Moss, "Optical Properties of Semiconductors." Academic Press, New York, 1959.
9. K. Seeger, "Semiconductor Physics" (Springer Series on Solid State Science, Vol. 40). Springer-Verlag, New York, 1982.
10. L. I. Shiff, "Quantum Mechanics." McGraw-Hill, Singapore, 1988.
11. L. Viña and M. Cardona, *Phys. Rev. B* **29**, 6739 (1984).
12. D. F. Edwards, *in* "Handbook of Optical Constants of Solids" (E. D. Palik, ed.), p. 547. Academic Press, Orlando, Florida, 1985.
13. D. E. Aspnes, *in* "Properties of Silicon," Vol. 2.6, p. 79 (Emis Data reviews Ser. No. 4). Inspec IEE, London, 1988.
14. D. Y. Smith, *in* "Handbook of Optical Constants of Solids" (E. D. Palik, ed.), p. 35. Academic Press, Orlando, Florida, 1985.
15. H. M. van Driel, *Appl. Phys. Lett.* **44**, 617 (1984).
16. P. Drude, "Theory of Optics." Dover, New York, 1902.
17. H. Y. Fan, W. G. Spitzer, and R. J. Collins, *Phys. Rev.* **101**, 569 (1956); H. Y. Fan, *Rep. Prog. Phys.* **14**, 119 (1956).
18. W. G. Spitzer and H. Y. Fan, *Phys. Rev.* **106**, 882 (1957).
19. H. J. G. Meyer, *Phys. Rev.* **112**, 298 (1958); H. J. G. Meyer, *J. Phys. Chem. Sol.* **8**, 264 (1959).
20. R. Rosenberg and M. Lax, *Phys. Rev.* **112**, 843 (1958).
21. W. Dumke, *Phys. Rev.* **124**, 1813 (1960).
22. S. Visvanathan, *Phys. Rev.* **120**, 379 (1960).
23. B. Donovan, *Proc. Phys. Soc. (London)* **A76**, 574 (1960).
24. B. Jensen, *in* "Handbook of Optical Constants of Solids" (E. D. Palik, ed.), p. 169. Academic Press, Orlando, Florida, 1985.
25. R. Kubo, *J. Phys. Soc. Jpn.* **12**, 570 (1957).
26. H. Mori, *Prog. Theor. Phys.* **34**, 399 (1965).
27. B. E. Sernelius, *Phys. Rev. B* **41**, 30 (1990).
28. W. Gotze and P. Wolfle, *Phys. Rev. B* **6**, 1226 (1972).
29. M. Auslender and S. Hava, *Phys. Status Solidi B* **174**, 565 (1992); M. Auslender and S. Hava, *Proc. SPIE* **1972**, 210 (1992).
30. S. Hava and M. Auslender, *Appl. Opt.* **32**, 1122 (1993).
31. V. I. Fistul, "Heavily Doped Semiconductors." Plenum, New York, 1969.
32. M. Miyao, T. Motooka, N. Natsuaki, and T. Tokuyama, *Solid State Commun.* **37**, 605 (1981).
33. A. Slaoui and P. Siffert, *Phys. Status Solidi A* **89**, 617 (1985).
34. D. E. Aspnes, A. A. Studna, and E. Kinsbron, *Phys. Rev. B* **29**, 768 (1984).
35. M. Cardona, W. Paul, and H. Brooks, *Z. Naturforsch.* **101**, 329 (1960).
36. L. E. Howarth and J. F. Gilbert, *J. Appl. Phys.* **34**, 236 (1963).
37. W. G. Spitzer, G. W. Gobeli, and F. A. Trumbore, *J. Appl. Phys.* **35**, 206 (1964).
38. A. A. Kukharski and V. K. Subashiev, *Sov. Phys. Solid State,* **8**, 603 (1966).
39. E. Barta, *Infrared Phys.* **17**, 111 (1976).
40. L. N. Streltsov and V. V. Titov, *Sov. Phys. Semicond. (Engl. Transl.)* **4**, 605 (1970).
41. L. M. Lambert, *Phys. Status Solidi A* **11**, 461 (1972).
42. M. Balkanski, E. Aziza, and E. Amzallag, *Phys. Status Solidi* **31**, 323 (1969).
43. J. Humlíček and K. Wojtechovsky, *Czech. J. Phys.* **B38**, 1033 (1988).
44. W. Harrison, *Phys. Rev.* **104**, 1281 (1956).
45. D. Chattopadhyay and H. J. Queisser, *Rev. Mod. Phys.* **53**, 745 (1981).
46. J. C. Irvin, *Bell Syst. Technol. J.* **41**, 387 (1962); S. M. Sze and J. C. Irvin, *Solid-State Electron.* **11**, 559 (1968).
47. H. K. Jung, H. Ohtsuka, K. Taniguchi, and C. Hamaguchi, *J. Appl. Phys.* **79**, 2559 (1996).

Chapter 7

Optical Parameters for the Materials in *HOC I, HOC II,* and *HOC III*

EDWARD D. PALIK
Institute for Physical Science and Technology
University of Maryland
College Park, Maryland

I. Introduction 187
II. The Parameters 187
References 225

INTRODUCTION I

In *HOC II,* we made an attempt to catalog certain optical parameters for all the materials in *HOC I* and *HOC II.* We have continued this work and present in Table I a listing of Material, Crystal Structure, Symmetry Class (Space Group), Unit-Cell Dimensions, Number of Molecular Units per Unit Cell and Primitive Cell, Number of Optic Modes, Optic Irreducible Representation, Acoustic Irreducible Representation, Transverse and Longitudinal Optic Frequencies (ω_T and ω_L), Plasma Frequency for a Metal ω_p (Drude), Fundamental Band Gap E_g (Direct or Indirect), and dc Dielectric Constant ϵ_o.

THE PARAMETERS II

Usually a cubic metal cannot support a transverse or longitudinal optic mode, and this is indicated with *None.* For a cubic diatomic metal, the LO mode may be degenerate with the TO mode, at least at the zone center. It is not obvious that the LO mode has any oscillator strength, since the free charges can move to cancel any longitudinal planes of charge the lattice tries to set up and maintain. We indicate our doubt with a (?). A dashed (- - -)

HANDBOOK OF OPTICAL CONSTANTS OF SOLIDS III

Copyright © 1998 by Academic Press.
All rights of reproduction in any form reserved
ISBN 0-12-544423-0/$25.00.

TABLE I

Collected Optical Parameters

Material	Crystal structure	Symmetry class space group	Unit cell dimensions (Å)	Molecular Units: Unit cell	Molecular Units: Primitive cell	No. of optic modes	Optic irreducible representation	Accoustic irr. rep.	ω_T (cm^{-1})	ω_L (cm^{-1})	ω_P Drude (eV)	E_g (eV)	ϵ_O
$Y_3Al_5O_{12}$	cubic	(230) Ia3d O_h^{10}	12.008	8	4	237	$5A_{1u}(0) + 3A_{1g}(R) + 5A_{2u}(0) + 5A_{2g}(0) + 10E_u(0) + 8E_g(R) + 14F_{1g}(0) + 17F_{1u}(IR) + 14F_{2g}(R) + 16F_{2u}(0)$	F_{1u}	Table a		----	6.5	10.6
Mo	bcc	(229) Im3m O_h^9	3.1473	2	1	0	None	F_{1u}	None	None	7.5	None	−21000
W			3.1646								6.4		−11000
Fe			2.8665								4.1		−50000
Cr			2.8839								xx		xx
Nb			3.3004								xx		xx
K			5.2								4.25		xx
Na			4.2906								5.91		xx
Li			3.5902								xx		xx
Ta			3.3058								6.2		xx
V			3.0240								5.2		−7200
Cs			6.091								xx		xx
Al_2MgO_4	cubic	(227) Fd3m O_h^7	8.0800	8	2	39	$A_{1g}(R) + 2A_{2u}(O) + E_g(R) + 2E_u(O) + F_{1g}(0) + 4F_{1u}(IR) + 3F_{2g}(R) + 2F_{2u}(0)$	F_{1u}	Table b		----	~8	8.29
$Al_{23}O_{27}N_5$	cubic	(227) Fd3m O_h^7	7.948	1	1	162	xxxx	F_{1u}	Table c		----	6–7	~9.36
Si	cubic diamond	(227) Fd3m O_h^7	5.4307	8	2	3	$F_{2g}(R)$	F_{1u}	521	521	----	1.1(i)	11.6
Ge			5.6573						301	301		0.66(i)	16.0
C			3.5667						1332	1332		5.2(i)	5.6
Sn-α gray			6.4912						xxx	?	~8.1	None	xx
Cu	fcc	(225) Fm3m O_h^5	3.6149	4	1	0	None	F_{1u}	None	None	7.4	None	−66000
Au			4.0782								9.0		−114000
Ir			3.8394								xx		xx

Ni			3.5238									4.9		−13000
Pt			3.9231									5.1		−5600
Rh			3.8031									3.8		−251000
Ag			4.0862									9.0		xx
Al			4.0495									14.8		−33000
Pd			3.8898									5.5		−126000
Yb			5.4862									10.0		xx
PbS	cubic NaCl	(225) Fm3m O_h^5	5.935	4	1	3	F_{1u}(IR)	F_{1u}	71	212	----	0.41(d)	169
PbSe			6.122						39	111		0.278(d)	210
PbTe			6.443						32	112		0.31(d)	414
SnTe			6.313						26	139		0.19(d)	1770
NaCl			5.64						164	266		8.6	5.90
KCl			6.2929						142	213		8.5	4.4
KI			7.0655						101	139		~6.2	4.94
LiF			4.0263						307	501		14.2(d)	9.06
KBr			6.6000						113	155		7.8	4.8
NaF			4.620						246	420		10.5	~5.7
MgO			4.215						396	729		7.8(d)	9.8
AgCl			5.547						106	196		3.2(i)	11.1
AgBr			5.7745						79	138		2.6(i)	12.4
CsF			6.008						131	248		10.0	~8.1
RbBr			6.854						88	117		7.7	4.9
RbI			7.342						75	103		~6.1	5.0
TiC			4.3186						537	?	xx	None	xx
TiN			4.235						488	?	xx		xx
HfN			4.512						xx	?	~3		xx
ZrN			4.61						450	?	~3		xx
VC			4.182						590	?	xx		xx
VN			4.128						507	?	xx		xx
CaF_2	cubic fluorite	(225) Fm3m O_h^5	5.4629	4	1	6	F_{1u}(IR) + F_{2g}(R)	F_{1u}	258 F_{1u} 322 F_{2g}	473	----	~11	6.7
BaF_2			6.2001						184 241	319		10.1	7.3
PbF_2-β			5.9273						102 256	337		5.7	27.4
SrF_2			5.7996						217 286	366		3.4	7.69

(continued)

TABLE I *(Continued)*

Collected Optical Parameters

Material	Crystal structure	Symmetry class space group	Unit cell dimensions (Å)	Molecular Units: Unit cell	Molecular Units: Primitive cell	No. of optic modes	Optic irreducible representation	Accoustic irr. rep.	ω_T (cm^{-1})	ω_L (cm^{-1})	ω_P Drude (eV)	E_g (eV)	ϵ_O
Cu_2O	cubic	(224) Pn3m O_h^4	4.2696	2	2	15	$A_{2u}(0) + E_u(0) + F_{2u}(0) + 2F_{1u}(IR) + F_{2g}(R)$	F_{1u}	613 F_{1u} 146 F_{1u} 220 F_{2g} 110 E_u 300 A_{2u}	638 149	----	2.17(d)	~7.5
$SrTiO_3$	cubic perovskite	(221) Pm3m O_h^1	3.9051	1	1	12	$3F_{1u}(IR) + F_{2u}(O)$	F_{1u}	88 F_{1u} 178 F_{1u} 594 F_{1u} xx F_{2u}	173 473 808	----	3.4	311
CsCl	cubic CsCl	(221) Pm3m O_h^1	4.121	1	1	3	$F_{1u}(IR)$	F_{1u}	99	160	----	8.1	6.34
CsBr			4.286						75	113		6.9	6.51
CsI			4.5667						62	93		6.4(d)	6.54
TlCl			3.8452						63	158		3.6	32.7
TlBr			3.9846						43	101		3.1	30.6
Mn-α	cubic	(217) I43m T_d^3	8.894	58	29	84	$5A_1(R) + 2A_2(0) + 7E(R) + 9F_1(0) + 12F_2(IR,R)$	F_2	xx	?	xx	None	xx
ZnS	cubic zincblende	(216) F43m T_d^2	5.4093	4	1	3	$F_2(IR,R)$	F_2	279	351	----	3.68(d)	8.35
ZnSe			5.6676						206	252		2.83(d)	9.0
ZnTe			6.089						179	206		2.3(d)	9.8
CdTe			6.480						141	169		1.5(d)	10.2
GaAs			5.6535						269	292		1.42(i)	13.0
GaP			5.4506						367	403		2.27(i)	11.1
InAs			6.0585						218	240		0.35(d)	14.1
InSb			6.4782						179	190		0.18(d)	17.7
InP			5.8688						304	345		1.34(d)	12.4
SiC-β			4.348						796	972		2.86	9.72
GaSb			6.118						227	237		0.75	15.7

AlSb			6.1347						318	340		1.61(i)	11.2
AlAs			5.62						362	404		2.15(i)	10.06
HgTe			6.460						116	139		0	xx
BN			3.6157						1055	1305		8	7.1
Y_2O_3	bcc	(206) Ia3 T_h^7	10.604	16	8	117	$4A_g(R) + 5A_u(0) + 4E_g(R) +$ $5E_u(0) + 14F_g(R) + 16F_u(IR)$	F_u	Table d		----	~6	11.4
FeS_2	cubic pyrite	(205) Pa3 T_h^6	5.4067	4	4	33	$A_g(R) + 2A_u(0) + E_g(R) +$ $2E_u(0) + 3F_g(R) + 5F_u(IR)$	F_u	Table e		----	~0.9(i)	26.1
$Bi_{12}SiO_{20}$	cubic	(197) I23 T^3	10.1043	2	1	96	8A(R) + 8E(R) + 24F(IR,R)	F	Table f		----	3.25	56
$Bi_{12}GeO_{20}$			10.143									3.25	40
Os	hcp	(194) $P6_3/mmc$ D_{6h}^4	a = 2.7352	2	2	3	$B_{1g}(O) + E_{2g}(R)$	$A_{2u} + E_{1u}$	xx E_{2g}		xx	None	xx
			c = 4.3190						xx B_{1g}				
Co-α			a = 2.5071						xx		4.0		−12000
			c = 4.0686						xx				
Be			a = 2.2866						463		xx		xx
			c = 3.5833						673				
Mg			a = 3.2093						120		xx		xx
			c = 5.2103						241				
Re			a = 2.7608						138		xx		xx
			c = 4.4582						271				
Ru			a = 2.7039						192		xx		xx
			c = 4.2817						267				
Ti			a = 2.950						137		2.5		−2800
			c = 4.686						188				
Dy			a = 3.5903						62		11.8		xx
			c = 5.6475						110				
Er			a = 3.5588						58		6.9		xx
			c = 5.5874						116				
Gd			a = 3.6360						59		9.1		xx
			c = 5.7826						102				
Tb			a = 3.6010						61		11.5		xx
			c = 5.6936						108				
Tm			a = 3.5375						68		6.5		xx
			c = 5.5546						118				
Ce-γ			a = 3.65						xx		8.9		xx
			c = 5.96						xx				
C	hexagonal graphite	(194) $P6_3/mmc$ D_{6h}^4	a = 2.456	4	4	9	$A_{2u}(IR\|) + 2B_{2g}(O) +$ $E_{1u}(IR\perp) + 2E_{2g}(R)$	$A_{2u} + E_{1u}$	Table g		----	xx	5.7(e)
			c = 6.696										

(continued)

TABLE I *(Continued)*

Collected Optical Parameters

Material	Crystal structure	Symmetry class space group	Unit cell dimensions (Å)	Molecular Units: Unit cell	Molecular Units: Primitive cell	No. of optic modes	Optic irreducible representation	Accoustic irr. rep.	ω_T (cm^{-1})	ω_L (cm^{-1})	ω_P Drude (eV)	E_g (eV)	ϵ_O
GaSe-β	hexagonal	(194) $P6_3/mmc$ D^4_{6h}	a = 3.755 c = 15.94	4	4	21	$2A_{1g}(R) + A_{2u}(IR\|) + 2B_{1u}(0) + 2B_{2g}(0) + 2E_{1g}(R) + E_{1u}(IR\perp) + 2E_{2g}(R) + 2E_{2u}(0)$	$A_{2u} + E_{1u}$	Table h		----	2.0(d)	10.6(o) 6.18(e)
GaSe-ϵ	hexagonal	(187) $P\bar{6}m2$ D^1_{3h}	a = 3.755 c = 15.954	4	4	21	$4A_1'(R) + 3A_2''(IR\|,R) + 3E'(IR\perp,R) + 4E''(R)$	$A_2'' + E'$	Table i		-----	~2.0	10.6(o) 6.18(e)
ZnS	hexagonal wurzite	(186) $P6_3mc$ C^4_{6v}	a = 3.811 c = 6.234	2	2	9	$A_1(IR\|,R) + 2B_1(0) + E_1(IR\perp,R) + 2E_2(R)$	$A_1 + E_1$	Table j		-----	3.91	~9.6(o)
CdS			a = 4.1348 c = 6.7490									2.55(d)	9.6(o) 10.7(e)
CdSe			a = 4.2999 c = 7.0109									1.75(d)	9.29(o) 10.16(e)
BeO			a = 2.698 c = 4.380									9.4	6.94(o) 7.65(e)
SiC 6H,$\alpha\Pi$			a = 3.076 c = 5.048									3.1	9.7(o) 10.0(e)
AgI-β			a = 4.5924 c = 7.5104									~5.6	6.8 xx
AlN			a = 3.1127 c = 4.9816									6.2(d)	xx xx
BN			a = 2.504 c = 10.01									3.9(i)	6.86(o) 5.06(e)
GaN			a = 3.1892 c = 5.1850									3.5	9.3(o) 10.4(e)
Si_3N_4-β	hexagonal	(176) $P6_3/m$ C^2_{6h}	a = 7.606 c = 2.909	2	2	39	$4A_g(R) + 2A_u(IR\|) + 3B_g(0) + 4B_u(0) + 2E_{1g}(R) + 4E_{1u}(IR\perp) + 5E_{2g}(R) + 2E_{2u}(0)$	$A_u + E_{1u}$	Table k		----	xx	xx
Al_2O_3	trigonal (hex)	(167) $R\bar{3}c$ D^6_{3d}	a = 5.128 α = 55°20′	6	2	27	$2A_{1g}(R) + 3A_{2g}(O) + 2A_{1u}(O) + 2A_{2u}(IR\|) + 5E_g(R) + 4E_u(IR\perp)$	$A_{2u} + E_u$	Table l		----	8.3	9.49(o) 11.4(e)
Ga_2O_3			a = 5.320 α = 55°48′									xx	24.1(o) 20.6(e)

$NaNO_3$	trigonal (hex)	(167) $R\bar{3}c$ D_{3d}^6	a = 6.3247 α = 47°16′	6	2	27	$A_{1g}(R) + 2A_{1u}(0) + 3A_{2g}(0) +$ $3A_{2u}(IR\parallel) + 4E_g(R) + 5E_u(IR\perp)$	$A_{2u} + E_u$	Table m		----	~5.1	6.85
$CaCO_3$			a = 4.9898 c = 17.060								---- ~8(o) ~9.5(o)	 ~8.6(o) ~8.3(e)	
Sb	trigonal (hex)	(166) $R\bar{3}m$ D_{3d}^5	a = 4.5066 α = 57°6.5′	2	2	3	$A_{1g}(R) + E_g(R)$	$A_{2u} + E_u$	115 A_{1g} 150 Eg		xx	None	xx
Sm			a = 8.996 α = 73°13′						xx xx		~11.7		xx
$LiNbO_3$	trigonal (hex)	(161) R3c C_{3v}^6	a = 5.1483 c = 13.8631	2	2	27	$4A_1(IR\parallel,R) + 5A_2(O) + 9E(IR\perp,R)$	$A_1 + E$	Table n		----	~4.2	43.7(o) 25.6(e)
$LiTaO_3$			a = 5.1543 c = 13.7835								----	~4.5(o)	43.8(o) 46.8(e)
GaSe-γ	trigonal (hex)	(160) R3m C_{3v}^5	a = 3.755 c = 23.92	12	6	33	$11A_1(IR\parallel,R) + 11E(IR\perp,R)$	$A_1 + E$	Table o		----	~2.0	~6.18(o) ~10.6(e)
Si_3N_4-α	trigonal (hex)	(159) P31cC$_{3v}^4$	a = 7.753 c = 5.618	4	4	81	$13A_1(IR\parallel,R) + 14A_2(0) + 27E(IR\perp,R)$	$A_1 + E$	Table p		----	xx	~6.9
SiO_2	trigonal (hex)	(154) $P3_221$ D_3^4	a = 4.9130 c = 5.4046	3	3	24	$4A_1(R) + 4A_2(IR\parallel) + 8E(IR\perp,R)$	$A_2 + E$	Table q		----	~9	4.41(o) 4.62(e)
Se	trigonal (hex)	(152) $P3_121$ $_rD_3^4$	a = 4.3551 c = 4.9494	3	3	6	$A_1(R) + A_2(IR\parallel) + 2E(IR\perp,R)$	$A_2 + E$	Table r		----	~1.6(i)	7.40(o) 12.2(e)
Te			a = 4.4469 c = 5.9149									0.33(d)	30(o) 43(e)
Sn-β	tetragonal (white)	(141) $I4_1/amd$ D_{4h}^{19}	a = 5.8197 c = 3.1749	4	2	3	$B_{2g}(R) + E_g(R)$	$A_{2u} + E_u$	43 124		xx	None	xx
$ZrSiO_4$	tetragonal	(141) I4/amd D_{4h}^{19}	a = 6.6164 c = 6.0150	4	2	33	$2A_{1g}(R) + A_{1u}(0) + A_{2g}(0) +$ $3A_{2u}(IR\parallel) + 4B_{1g}(R) + B_{1u}(0) +$ $B_{2g}(R) + 2B_{2u}(0) + 5E_g(R) + 4E_u(IR\perp)$	$A_{2u} + E_u$	Table s		----	~2.5	xx(o) 10.7(e)
In	tetragonal	(139) I4/mmm D_{4h}^{17}	a = 3.253 c = 4.945	2	1	0	None	$A_{2u} + E_u$	None	None	xx	None	xx
Zn_3P_2	tetragonal	(137) $P4_2/nmc$ D_{4h}^{15}	a = 8.097 c = 11.45	8	8	117	$9A_{1g}(R) + 4A_{1u}(0) + 5A_{2g}(0) +$ $9A_{2u}(IR\parallel) + 10B_{1g}(R) + 5B_{1u}(0) +$ $4B_{2g}(R) + 9B_{2u}(0) + 16E_g(R) + 15E_u(IR\perp)$	$A_{2u} + E_u$	Table t		----	1.3	11
TiO_2	tetragonal SnO_2 rutile	(136) $P4_2/mnm$ D_{4h}^4	a = 4.5937 c = 2.9581	2	2	15	$A_{1g}(R) + A_{2g}(O) + A_{2u}(IR\parallel) +$ $B_{1g}(R) + 2B_{1u}(O) + B_{2g}(R) +$ $E_g(R) + 3E_u(IR\perp)$	$A_{2u} + E_u$	Table u		----	3.06(d,o) 4.3(d,e)	83.7(o) 165(e)

(continued)

TABLE I *(Continued)*

Collected Optical Parameters

Material	Crystal structure	Symmetry class space group	Unit cell dimensions (Å)	Molecular Units: Unit cell	Molecular Units: Primitive cell	No. of optic modes	Optic irreducible representation	Accoustic irr. rep.	ω_T (cm^{-1})	ω_L (cm^{-1})	ω_P Drude (eV)	E_g (eV)	ϵ_O
MgF_2			a = 4.623 c = 3.052									11	5.47(o) 4.62(e)
KH_2PO_4	tetragonal	(122) I42d $D_{2d}^{12} = V_d^{12}$	a = 7.448 c = 6.977	4	2	45	$4A_1(R) + 5A_2(0) + 6B_1(R) +$ $6B_2(IR\parallel,R) + 12E(IR\perp,R)$	$B_2 + E$	Table v		-----	4.96	~44(o) ~21(e)
$AgGaS_2$	tetragonal	(122) I42d $D_{2d}^{12} = V_d^{12}$	a = 5.757 c = 10.304	4	2	21	$A_1(R) + 2A_2(0) + 3B_1(R) +$ $3B_2(IR\parallel,R) + 6E(IR\perp,R)$	$B_2 + E$	Table w		-----	xx ~2.7(d,e)	~10.0(o) ~8.6(e)
$AgGaSe_2$			a = 5.973 c = 10.88									xx ~1.8(d,e)	8.9(o) 7.8(e)
$CdGeAs_2$			a = 5.9432 c = 11.216									xx 0.57(d,e)	18.2(o) 17.9(e)
$CuGaS_2$			a = 5.351 c = 10.480									2.55(d,o) 2.43(d,e)	8.9(o) 7.6(e)
$ZnGeP_2$			a = 5.466 c = 10.722									xx 2.4(d,e)	11.4(o) 11.6(e)
$NH_4H_2PO_4$	tetragonal	(122) I42d $D_{2d}^{12} = V_d^{12}$	a = 7.510 c = 7.564	4	2	69	$7A_1(R) + 7A_2(0) + 8B_1(R) +$ $9B_2(IR\parallel,R) + 19E(IR\perp,R)$	$B_2 + E$	Table x		----	9.92	~56(o) ~15(e)
Zn_3As_2	tetragonal	(110) $I4_1cd$ C_{4v}^{12}	a = 8.316 c = 11.76	32	16	237	$26A_1(IR\parallel,R) + 27A_2(0) +$ $27B_1(0) + 27B_2(R) + 65E(IR\perp,R)$	$A_1 + E$	Table y		----	0.93	10-11.8
$BaTiO_3$	tetragonal	(99) P4mm C_{4v}^1	a = 3.9920 c = 4.0361	1	1	12	$3A_1(IR\parallel,R) + B_1(R) + 4E(IR\perp,R)$	$A_1 + E$	Table z		----	3.27(o) 3.38(e)	xx 31.5(e)

S-α	orthorhombic	(70) Fddd $D_{2h}^{24} = V_h^{24}$	a = 10.467 b = 12.870 c = 24.493	128	32	93	$12A_g(R) + 12A_u(0) + 12B_{1g}(R) +$ $11B_{1u}(IR \parallel z) + 12B_{2g}(R) +$ $11B_{2u}(IR \parallel y) + 2B_{3g}(R) +$ $11B_{3u}(IR \parallel x)$	$B_{1u} +$ $B_{2u} +$ B_{3u}	Table aa	----	4.1(b) 4.2(a)	3.85(b) 3.65(a)
TlI	orthorhombic	(63) Cmcm $D_{2h}^{17} = V_h^{17}$	a = 4.582 b = 12.92 c = 5.251	4	2	9	$2A_u(0) + B_{1u}(IR \parallel z) +$ $3B_{2u}(IR \parallel y) + 3B_{3u}(IR \parallel x)$	$B_{1u} +$ $B_{2u} +$ B_{3u}	Table bb	----	2.8	37.3
$(CH_2)_n$	orthorhombic	(62) Pnma $D_{2h}^{16} = V_h^{16}$	a = 7.40 b = 4.93 c = 2.534	4	4	33	$6A_g(R) + 3A_u(0) + 6B_{1g}(R) +$ $2B_{1u}(IR \parallel z) + 3B_{2g}(R) +$ $5B_{2u}(IR \parallel y) + 3B_{3g}(R) + 5B_{3u}(IR \parallel x)$	$B_{1u} +$ $B_{2u} +$ B_{3u}	Table cc	----	xx	2.29(b) 2.32(c)
$KNbO_3$	orthorhombic	(38) Amm2 C_{2v}^{14}	a = 5.6896 b = 3.9692 c = 5.7256	2	1	12	$4A_1(IR \parallel z,R) + A_2(R) +$ $4B_1(IR \parallel x,R) + 3B_2(IR:y,R)$	$A_1 + B_1$ $+ B_2$	Table dd	----	3.46 3.43 3.46	150-x 985-y 44-z
CuO	monoclinic	(15) B2/b C_{2h}^6 C2/c	a = 4.6837 b = 3.4226 c = 5.1288 β = 99°29′	4	2	9	$A_g(R) + 3A_u(IR \parallel z) +$ $2B_g(R) + 3B_u(IR \parallel x,y)$	$A_u + 2B_u$	Table ee	----	~1.3i	18.1
ThF_4	monoclinic	(15) B2/b C_{2h}^6	a = 12.90 b = 10.93 c = 8.58 β = 126.4°	12	6	87	$20A_g(R) + 22A_u(IR \parallel z) +$ $22B_g(R) + 23B_u(IR \parallel x,y)$	$A_u + 2B_u$	Table ff	----	xx	xx
As_2S_3	monoclinic (unit cell)	(14) $P2_1/b,c$ C_{2h}^5	a = 11.475 b = 9.577 c = 4.256 β = 90°41′	4	4	57	$15A_g(R) + 14A_u(IR \parallel z) +$ $15B_g(R) + 13B_u(IR \parallel x,y)$	$A_u + 2B_u$	Table gg	----	2.43(a,d) 2.45(c,d)	15.2(a) 6.25(b) 13.0(c)
	orthorhombic (layer)	(31) $Pmm2_1$ C_{2v}^1		2	2	27	$7A_1(IR \parallel z,R) + 7A_2(R)$ $7B_1(IR \parallel x,R) + 6B_2(IR \parallel y,R)$					
As_2Se_3			a = 12.053 b = 9.890 c = 4.277 β = 90°28′								~2	14.4(a) 13.0(c)

TABLE I *(Continued)*

Collected Optical Parameters

Material	Crystal structure	Symmetry class space group	Unit cell dimensions (Å)	Molecular Units: Unit cell	Molecular Units: Primitive cell	No. of optic modes	Optic irreducible representation	Accoustic irr. rep.	ω_T (cm^{-1})	ω_L (cm^{-1})	ω_P Drude (eV)	E_g (eV)	ϵ_0
GaTe-α	monoclinic	(12) B2/m C_{2h}^3	a = 17.84 b = 4.07 c = 10.56	12	6	33	$12A_g(R) + 6B_g(R) + 5A_u(IR \parallel z) + 10B_u(IR \parallel x,y)$	$A_u + 2B_u$	Table hh		----	1.67(d) ~1.7	10.58(e) 9.66(o)
(TlBrI, KRS-5)									43	103	----	~2.47	32.5
(TlBrCl, KRS-6)									58	149		3.25	31.8
(AlGaAs) alloy													
(HgCdTe)													
(PbSnTe)													
(Ge-Si)													

(a-Si)			1.77	13.7
amorphous				
(a-SiO_2)		469	~9	3.8
		800		
		1094		
(a-SiO)		1020	~6	4.0
(a-Si_3N_4)		880		3.6
		490		
(a-As_2S_3)				7.45
(a-As_2Se_3)				9.0
(a-ThF_4)				
(a-C:H)				
Hg	liquid			
H_2O				78.3

TABLE a

$Y_3Al_5O_{12}$ [2]

17 F_{1u}(T)(IR)	F_{1u}(L)	14 F_{2g}(R)	8 E_g(R)	3 A_{1g}(R)	16 F_2(0)	14 F_{1g}(0)	10 E_u(0)	5 A_{2g}(0)	5 A_{2u}(0)	5 A_{1u}(0)
122	123	144	162	373	xx	xx	xx	xx	xx	xx
163	172	218	310	561	xx	xx	xx	xx	xx	xx
177	180	243	340	783	xx	xx	xx	xx	xx	xx
219	224	259	403		xx	xx	xx	xx	xx	xx
290	296	296	531		xx	xx	xx	xx	xx	xx
330	340	408	537		xx	xx	xx			
372	378	436	714		xx	xx	xx			
387	388	544	758		xx	xx	xx			
394	402	690			xx	xx	xx			
428	438	719			xx	xx	xx			
445	471	857			xx	xx				
472	511	xx			xx	xx				
516	549	xx			xx	xx				
569	585	xx			xx	xx				
692	712				xx					
723	765				xx					
782	840									

TABLE b

Al_2MgO_4 [2]

4 F_{1u}(T)(IR)	F_{1u}(L)(IR)	1 A_{1g}(R)	1 E_g(R)	3 F_{2g}(R)	2 A_{2u}(0)	2 E_u(0)	1 F_{1g}(0)	2 F_{2u}(0)
305	311	722	410	311	xx	xx	xx	xx
428	xx			492	xx	xx		xx
485	497			611				
670	800							

TABLE c

$Al_{23}O_{27}N_5$ [2]

(T)	(L)
346	xx
395	xx
495	551
634	718
768	869
920	969

TABLE d

Y_2O_3 [2]

16 $F_u(T)(IR)$	$F_u(L)(IR)$	4 $E_g(R)$	4 $A_g(R)$	14 $F_g(R)$	5 $A_u(0)$	5 $E_u(0)$
120	121	333	1184	131	xx	xx
172	173	830	xx	431	xx	xx
182	183	984	xx	469	xx	xx
241	242	xx	xx	596	xx	xx
303	315			xx	xx	xx
335	359			xx		
371	412			xx		
415	456			xx		
461	486			xx		
490	535			xx		
555	620			xx		
xx				xx		
xx				xx		
xx				xx		
xx						
xx						

TABLE e

FeS_2 [2, 19, 20]

5 $F_u(T)(IR)$	$F_u(L)(IR)$	1 $A_g(R)$	1 $E_g(R)$	3 $F_g(R)$	2 $A_u(0)$	2 $E_u(0)$
293	294	379	343	350	xx	xx
348	350			377	xx	xx
401	411			435		
412	421					
422	439					

TABLE f

24 F(T)(IR,R)	F(L)(IR,R)	8 A(R)	8 E(R)
$Bi_{12}SiO_{20}$ [21]			
44	xx	92	68
51		149	88
59		171	132
89		282	252
99		331	xx
106		546	464
xx		785	626
115		xx	xx
136			
175			
195			
208			
237			
288			
314			
353			
367			
462			
496			
509			
531			
579			
609			
825			
$Bi_{12}GeO_{20}$ [21]			
46	xx	89	68
52		148	97
57		170	130
99		273	236
106		326	306
124		543	458
xx		715	623
131		xx	xx
177			
xx			
xx			
207			
232			
271			
303			
338			
356			
459			
481			
xx			
526			
571			
600			
682			

This is the first example of a crystal with the same modes both IR and R active. Often, there is not a one-to-one correspondence, presumably because the IR or R intensity is too weak to be measured. Also, some of the high frequency bands may be combination bands.

TABLE g

C graphite [22]

1 $E_{1u}(T)(IR\perp)$	$E_{1u}(L)(IR\perp)$	1 $A_{2u}(T)(IR\parallel)$	$A_{2u}(L)(IR\parallel)$	2 $E_{2g}(R)$	2 $B_{2g}(O)$
1587.0	1587.5	867.8	868.1	42	127
				1575	xx

$IR\perp$ represents electric field E perpendicular to the c axis (ordinary) and $IR\parallel$ represents electric field E parallel to the c axis (extraordinary). This nomenclature will persist until the orthorhombic crystals are reached, whereupon we must revert to $E\parallel a$, $E\parallel b$, $E\parallel c$ notation. For the remaining monoclinic and triclinic unit cells, the situation becomes more complicated because we must choose a Cartesian coordinate system to describe atomic displacement and electric polarization whose x, y, z axes do not line up with all three a, b, c edges of the unit cell.

TABLE h

GaSe-β [23]

1 $E_{1u}(T)(IR\perp)$	$E_{1u}(L)$	1 $A_{2u}(T)(IR\parallel)$	$A_{2u}(L)$	2 $A_{1g}(R)$	2 $E_{1g}(R)$	2 $E_{2g}(R)$	2 $B_{1u}(0)$	2 $B_{2g}(0)$	2 $E_{2u}(0)$
213.9	254.7	xx	xx	134.6	60.1	19.1	xx	xx	xx
				307.8	249	213.1	xx	xx	xx

Sometimes we omit xx in the longitudinal-mode column because we do not know if such a mode exists until a zero in ϵ_R is found experimentally.

TABLE i

GaSe-ϵ [24]

3 $E'(T)(IR\parallel,R)$	$E'(L)$	3 $A_2''(T)(IR\perp,R)$	$A_2''(L)$	4 $A_1'(R)$	4 $E''(R)$
237	245.5	19.5	254.7	134.3	60.1
xx	xx	213.5	xx	308	211.9
xx	xx	xx	xx	xx	xx
				xx	xx

TABLE j

ZnS [2, 6]

1 $E_1(T)(IR\perp)$	$E_1(L)(IR\perp)$	1 $A_1(T)(IR\parallel)$	$A_1(L)(IR\parallel)$	2 $E_2(R)$	2 $B_1(0)$
224	352	274	352	55	xx
				280	xx
CdS [2, 6]					
243	307	234	305	44	xx
				252	xx
CdSe [2, 6]					
172	210	166	211	34	xx
				xx	xx
BeO [2, 6]					
722	1095	678	1085	340	xx
				684	xx
SiC-α-6H [2, 6]					
794	970	785	970	149	xx
				788	xx
AgI-β [2]					
106	124	106	124	17	xx
				112	xx
AlN [2, 6]					
672	895	659	888	655	xx
				xx	xx
BN [25]					
767	778	783	828	xx	xx
				xx	xx
GaN [2, 6]					
560	746	533	744	145	xx
				568	xx

TABLE k

Si_3N_4-β [26–30]

4 $E_{1u}(T)$ (IR⊥)		2 $A_u(T)$ (IR ∥)		4 $A_g(R)$	2 $E_{1g}(R)$	5 $E_{2g}(R)$	3 $B_g(0)$	4 $B_u(0)$	2 $E_{2u}(0)$
[30]	[27]	[28]	[29]	xx	[29]	[28]			
352						144	xx	xx	xx
371					184	186	xx	xx	xx
378	376	380			206	210	xx	xx	
406					227	229		xx	
443	445	447			449				
460					452	451			
495	496		495		456				
509					617	619			
	537				730	732			
578	580	580	582		742				
600					792				
675					802				
684	680				862	864			
854			854		927	928			
871					938	939			
893					1043	1047			
906	906	910	900						
941									
957									
	980	985	980						
1040	1040	1040	1051						

In most cases, too many lines are seen for each species. Splitting of degenerate modes and combination bands are sometimes invoked to ease this dilemma.

TABLE l

Al_2O_3 [6, 12]

4 $E_u(T)(IR\perp)$	$E_u(L)(IR\perp)$	2 $A_{2u}(T)(IR\parallel)$	$A_{2u}(L)(IR\parallel)$	2 $A_{1g}(R)$	5 $E_g(R)$	3 $A_{2g}(0)$	2 $A_{1u}(0)$
385	388	400	512	418	378	xx	xx
442	480	583	871	645	432	xx	xx
569	625				451	xx	
635	900				578		
					751		
Ga_2O_3 [31]*							
154	xx	xx	xx	xx	xx	xx	xx
230		xx		xx	xx	xx	xx
284					xx	xx	
320					xx		
370					xx		
430							
530							
680							
760							

*Polycrystalline sample measured in transmission. Modes not assigned.

TABLE m

$NaNO_3$ [32]

5 $E_u(T)(IR\perp)$	$E_u(L)(IR\perp)$	3 $A_{2u}(T)(IR\parallel)$	$A_{2u}(L)(IR\parallel)$	1 $A_{1g}(R)$	4 $E_g(R)$	2 $A_{1u}(0)$	3 $A_{2g}(0)$
87	98.5	51.5	90	xx	xx	xx	xx
175.5	184.5	214	262.5		xx	xx	xx
209	257.5	xx	xx		xx		xx
xx	xx				xx		
1356	1468						
$CaCO_3$ [2]							
102	123	92	136	1088	156	xx	xx
223	239	303	387		283	xx	xx
297	381	872	890		714		xx
712	715				1432		
1407	1549						

TABLE n

$LiNbO_3$ [33, 34]

9 E(T)(IR⊥,R)	E(L)(IR⊥,R)	4 A_1(T)(IR ∥,R)	A_1(L)(IR ∥,R)	5 A_2(0)
155	198	255	275	xx
238	243	276	333	xx
265	295	334	436	xx
325	371	633	876	xx
371	428			xx
431	454			
582	668			
668	739			
743	880			
$LiTaO_3$ [35]				
74	80	201	245	xx
140	163	253	347	xx
206	248	356	399	xx
251	278	600	864	xx
316	318			xx
383	452			
462	474			
596	648			
662	870			

TABLE o

GaSe-γ [36]

11 E(T)(IR⊥,R)	E(L)(IR⊥,R)	11 A_1(T)(IR ∥,R)	A_1(L)(IR ∥,R)
20.9	xx	133.5	xx
59.5	xx	235.7	246.5
208.7	xx	307.4	xx
213.9	253.2	xx	
xx		xx	
xx		xx	
xx		xx	
xx		xx	
xx		xx	
xx		xx	
xx		xx	

TABLE p

Si_3N_4-α [26-28, 30, 37]

27 E(T) (IR⊥,R)		13 A_1(T) (IR∥,R)		27 E(R)	13 A_1(R)	14 A_2(0)
[30]	[26]	[27]	[28]	[28]	[37]	
	305		300	153		xx
352	352		355	202	200	xx
371	375		375	231	232	xx
378				258	259	xx
406	403		412	282	280	xx
443				298		xx
460	461		463	306	302	xx
	488			321		xx
495	493	495	499	337		xx
	501			356	356	xx
509	510		518	361	365	xx
578		582	580	383		xx
600	605		600	391		xx
	660				404	xx
	668			460	460	
675	676			470		
684	684		688		484	
	750				505	
854	858	54	855	514	515	
	871		874	537		
893	895		895	569	572	
906		900	909	601	602	
941			935	667	668	
957				691	692	
	985	980	995	763		
1040	1045	1051	1040	848	845	
				868	868	
				914	915	
				951	948	
				975	976	
				1032	1034	
				1107		
					1122	
				1142		
					1205	

The analyses are incomplete. Note that the modes both IR and R active are shown separately. There is poor correlation between IR, R frequencies. Each IR frequency should have an equal R frequency. Raman experimental arrangement was not described adequately—polarization selection rules, etc. No IR polarization was used to distinguish ∥ and ⊥. Powders in mulls were often used.

TABLE q

SiO_2 [12]

8 E(T)(IR⊥,R)	E(L)(IR⊥,R)	4 A_2(T)(IR∥)	A_2(L)IR∥)	4 A_1(R)
127	129	364	387	207
265	270	489	547	356
394	403	777	789	464
450	510	1080	1240	1085
697	699			
796	809			
1076	1161			
1161	1236			

TABLE r

Se [38]

2 E(T)(IR⊥,R)	E(L)(IR⊥,R)	1 A_2(T)(IR∥)	A_2(L)(IR∥)	1 A_1(R)
144	150	102	106	237
225	225			
Te [38]				
92	106	90	96	120
144	145			

TABLE s

$ZrSiO_4$ [39]

4 $E_u(T)(IR\perp)$	$E_u(L)$	3 $A_{2u}(T)(IR\parallel)$	$A_{2u}(L)$	2 $A_{1g}(R)$	4 $B_{1g}(R)$	1 $B_{2g}(R)$	5 $E_g(R)$	1 $A_{1u}(0)$	1 $A_{2g}(0)$	1 $B_{1u}(0)$	2 $B_{2u}(0)$
287	351	338	478	439	214	266	201	xx	xx	xx	xx
389.5	417	608	646	974	393		225				xx
430.5	469	989	1106		1008		357				
885	1034						547				
							1008				

TABLE t

Zn_3P_2 [40, 41]

15 $E_u(T)(IR\perp)$	$E_u(L)$	9 $A_{2u}(T)(IR\parallel)$	$A_{2u}(L)$	9 $A_{1g}(R)$	10 $B_{1g}(R)$	4 $B_{2g}(R)$	16 $E_g(R)$	4 $A_{1u}(0)$	5 $A_{2g}(0)$	5 $B_{1u}(0)$	9 $B_{2u}(0)$
[40]	[40]			[40]	[41]	[40]					
T	L			VV		VH					
44	57			27.5		26					
64	66			37		34.5					
70.5	71			45		39					
78	78.5			50		45					
86	89			61.5		51					
103	104.5			70		61.5					
168.5	169			76		64.5					
182.5	184			86.5		70					
246	276			93		79					
285	307			125		84					
309.5	320			144		92					
338	345			159		94					
351	360			171		99.5					
				190.5		109					
				212		120					
				224.5		132					
				248.5		141					
				258		151.5					
				292		168.5					
				310.5		188					
				331		205					
				340		222					
				345		231.5					
				363		241.5					

(continued)

TABLE t (*Continued*)

Zn_3P_2 [40, 41]

15 $E_u(T)(IR\perp)$	$E_u(L)$	9 $A_{2u}(T)(IR\parallel)$	$A_{2u}(L)$	9 $A_{1g}(R)$	10 $B_{1g}(R)$	4 $B_{2g}(R)$	16 $E_g(R)$	4 $A_{1u}(0)$	5 $A_{2g}(0)$	5 $B_{1u}(0)$	9 $B_{2u}(0)$
				384		256					
				396.5		263					
				411		290					
				430		306.5					
				452		328.5					
				463.5		336					
				486		345					
				499		352.5					
				511		363					
						379.5					
						394					
						403.5					
						423					
						430					
						442					
						450					
						456					
						466.5					
						499					

TABLE u

TiO_2 [6, 42]

3 $E_u(T)(IR\perp)$	$E_u(L)$	2 $A_{2u}(T)(IR\parallel)$	$A_{2u}(L)$	1 $A_{1g}(R)$	1 $B_{1g}(R)$	1 $B_{2g}(R)$	1 $E_g(R)$	1 $A_{2g}(0)$	2 $B_{1u}(0)$
183	373	167	811	612	143	44	763	113	826
388	458	xx							xx
508	831								
MgF_2 [6, 42]									
247	303	399	625	410	92	515	295	326	xx
410	415	xx							xx
450	617								

TABLE v

KH_2PO_4 [2, 43]

12 E(T)(IR⊥,R)	E(L)(IR⊥)	6 $B_2(T)(IR\parallel,R)$	$B_2(L)(IR\parallel)$	4 $A_1(R)$	6 $B_1(R)$	5 $A_2(0)$
86 75	xx	80	xx	360	156	xx
102 95		174		514	479	xx
122 113		xx		918	570	xx
152 190		386		2700	1366	xx
206 320		510			1806	xx
526 490		1350			2390	
xx 530						
xx 568						
xx 960						
xx 1145						
xx 1325						
xx						

Infrared and Raman frequencies do not show a good one-to-one correlation for the *E* mode.

TABLE w

$AgGaS_2$ [2]

6 E(T)(IR⊥,R)	E(L)(IR⊥,R)	3 B_2(T)(IR∥,R)	B_2(L)(IR∥,R)	1 A_1(R)	3 B_1(R)	2 A_2(0)
63	64	195	199	295	118	xx
93	96	215	239		179	xx
158	160	366	400		334	
225	230					
323	347					
368	392					
$AgGaSe_2$ [2]						
78	78	195	199	179	125	xx
133	135	215	239		xx	xx
xx	112	366	400		xx	
160	163					
208	213					
247	274					
$CdGeAs_2$ [2]						
95	98	85	85	188	84	xx
159	161	203	210		167	xx
200	206	270	278		245	
255	258					
280	365					
$CuGaS_2$ [2]						
75	76	259	284	312	138	xx
95	98	339	369		203	xx
147	167	371	402		243	
260	278					
335	352					
365	387					
$ZnGeP_2$ [2]						
94	94	140	xx	328	120	xx
141	141	361	341		247	xx
201	206	411	401		389	
328	330					
369	375					
386	406					

TABLE x

$NH_4H_2PO_4$ [44]

19 E(T)(IR⊥,R)	E(L)(IR⊥,R)	9 B_2(T)(IR∥,R)	B_2(L)(IR∥,R)	7 A_1(R)	8 B_1(R)	7 A_2(0)
51	xx	76	xx	337	178	xx
70		198		520	474	xx
150		450		918	541	xx
164		xx		2700	1298	xx
350		xx		xx	1750	xx
540		xx		xx	2370	xx
xx		xx		xx	xx	xx
xx		xx			xx	
xx		xx				
xx						
xx						
xx						
xx						
xx						
xx						
xx						
xx						
xx						
xx						

TABLE y

Zn_3As_2 [45]

65 E(T)(IR⊥,R)	E(L)	26 A_1(T)(IR∥,R)	A_1(L)	27 B_2(R)	27 A_2(0)	27 B_1(0)
				[45, (HH)]		
xx	xx	xx	xx	34 xx	xx	xx
xx		xx		62 xx	xx	xx
xx		xx		68 xx	xx	xx
xx		xx		74 xx	xx	xx
xx		xx		92 xx	xx	xx
xx		xx		xx	xx	xx
xx		xx		xx	xx	xx
xx		xx	

TABLE y (*Continued*)

Zn_3As_2 [45]

65 E(T)(IR⊥,R)	E(L)	26 A_1(T)(IR ∥,R)	A_1(L)	27 B_2(R)	27 A_2(0)	27 B_1(0)
xx						
xx						
xx						
xx						
xx						
xx						
xx						
xx						
xx						
xx						
xx						
xx						
xx						
xx						
xx						
xx						
xx						
xx						
xx						
xx						

Neither the infrared nor Raman spectrum has been studied in detail or analyzed.

TABLE z

$BaTiO_3$ [2, 46]

4 E(T)(IR⊥,R)	E(L)(IR⊥,R)	3 A_1(T)(IR ∥,R)	A_1(L)(IR ∥,R)	1 B_1(R)
38	180	179	189	305
180	308	276	471	
308	466	515	725	
498	722			

TABLE aa

S [47]

11 $B_{1u}(T)(IR \parallel z)$	$B_{1u}(L)$	11 $B_{2u}(T)(IR \parallel y)$	$B_{2u}(L)$	11 $B_{3u}(T)(IR \parallel x)$	$B_{3u}(L)$	12 A_g	12 B_{1g}	12 B_{2g}	12 B_{3g}	12 $A_u(0)$
44	xx	35	xx	34	xx	45	40	30	30	xx
78		45		47		56	61	46	46	xx
151		74		57		92	79	56	61	xx
181		96		89		159	150	67	70	xx
213		158		155		199	188	79	86	xx
253		197		199		221	217	161	154	xx
408		238		239		249	244	188	183	xx
431		254		256		419	420	239	236	xx
464		437		435		441	434	253	253	xx
472		466		465		470	473	441	443	xx
476		476		471		474	473	472	468	xx
						477	478	472	472	xx

TABLE bb

TII [48]*

1 $B_{1u}(T)(IR \parallel z)$	$B_{1u}(L)$	3 $B_{2u}(T)(IR \parallel y)$	$B_{2u}(L)$	3 $B_{3u}(T)(IR \parallel x)$	$B_{3u}(L)$	2 $A_u(0)$
52	xx	90	xx	xx	xx	xx
		xx		xx		xx
		xx		xx		

* polycrystalline sample

TABLE cc

$(CH_2)_n$ [49, 50]

2 $B_{1u}(T)(IR \parallel z)$	5 $B_{2u}(T)(IR \parallel y)$	5 $B_{3u}(T)(IR \parallel x)$	6 $A_g(R)$	6 $B_{1g}(R)$	3 $B_{2g}(R)$	3 $B_{3g}(R)$	3 $A_u(O)$
86	109	1043	141	1066	1070	101	55
736	721	1177	1138	1297	1293	1137	1041
1478	1472	xx	1175	1371	1373	1176	1181
2851	2853	xx	1445	xx		1458	
2921	2922	xx	2855	xx		2850	
			2885	xx		2889	

Most of the other observed modes in the IR are combination bands of these fundamentals.

TABLE dd

$KNbO_3$ [2]

4 A_1(T)(IR ∥ z,R)	A_1(L)	4 B_1(T)(IR ∥ x,R)	B_1(L)	3 B_2(T)(IR ∥ y,R)	B_2(L)	1 A_2(R)
190	193	187	190	56	189	283
290	296	243	294	195	425	
299	417	267	413	511	838	
607	827	534	842			

TABLE ee

CuO [51]

3 A_u(T)(IR ∥ z)	A_u(L)(IR ∥ z)	3 B_u(T)(IR ∥ x,y)	B_u(L)(IR ∥ x,y)	1 A_g(R)	2 B_g(R)
164	165	145	147	296	346
355	xx	480	593		636
421	xx	603	624		

For this crystal symmetry $a \approx b \approx c$ and $\beta = 99°29'$. The Cartesian coordinate system is taken as $y \parallel b$, $x \parallel a$, leaving z not quite $\parallel$ to c. Note that for species A_u, atomic displacement is along z, and for B_u, it is along x, y.

TABLE ff

ThF_4 [52]

22 $A_u(T)(IR \parallel z)$	$A_u(L)$	23 $B_u(T)(IR \parallel x,y)$	$B_u(L)$	20 $A_g(R)$	22 $B_g(R)$
xx	xx	135	xx	xx	xx
xx		185		xx	xx
xx		xx		xx	xx
xx		xx		xx	xx
xx		xx		xx	xx
xx		xx		xx	xx
xx		xx		xx	xx
xx		xx		xx	xx
xx		xx		xx	xx
xx		xx		xx	xx
xx		xx		xx	xx
xx		xx		xx	xx
xx		xx		xx	xx
xx		xx		xx	xx
xx		xx		xx	xx
xx		xx		xx	xx
xx		xx		xx	xx
xx		xx		xx	xx
xx		xx		xx	xx
xx		xx		xx	xx
xx		xx		xx	xx
xx		xx			xx
xx		xx			xx
		xx			

Obtained from reflection peaks of deposited thin films. Symmetry was not determined.

TABLE gg

As_2S_3 [53]

14 A_u(T)(IR ∥ b)	A_u(L)	15 B_u(T)(IR ∥ a)	B_u(L)	13 B_u(T)(IR ∥ c)	B_u(L)	15 A_g(R)	15 B_g(R)
186	xx	182	189	140	148	136	xx
386	392	246	xx	159	165	154	xx
xx		279	xx	185	189	204	xx
xx		293	328	201	203	311	xx
xx		348	354	260	xx	355	xx
xx		354	369	278	xx	382	xx
xx		369	370	307	326	xx	xx
xx		384	390	355	368	xx	xx
xx		xx		385	390	xx	xx
xx		xx		xx		xx	xx
xx		xx		xx		xx	xx
xx		xx		xx		xx	xx
xx		xx		xx		xx	xx
xx		xx				xx	xx
		xx				xx	xx

As_2Se_3 [53]

xx	xx	106	108	94	97	xx	xx
xx		132	134	105	108	xx	xx
xx		201	209	132	136	xx	xx
xx		224	238	217	232	xx	xx
xx		249		248	250	xx	xx
xx		268		xx		xx	xx
xx		xx		xx		xx	xx
xx		xx		xx		xx	xx
xx		xx		xx		xx	xx
xx		xx		xx		xx	xx
xx		xx		xx		xx	xx
xx		xx		xx		xx	xx
xx		xx		xx		xx	xx
xx		xx		xx		xx	xx
		xx				xx	xx

IR measurements were made with $E \| a$, $E \| b$, $E \| c$, which is probably $E \| x$, $E \| z$, but not quite $E \| y$.

TABLE hh

GaTe-α [54]

10 $B_u(T)(IR \parallel x,y)$	$B_u(L)(IR \parallel x,y)$	5 $A_u(T)(IR \parallel z)$	$A_u(L)(IR \parallel z)$	12 $A_g(R)$	6 $B_g(R)$
49	51	94	98	41	58
89	91	118	120	52	164
97	98	131	132	67	170
112	113	143	144	76	xx
124	125	174	199	110	xx
141	148			115	xx
157	160			155	
193	205			178	
212	214			208	
266	271			233	
				271	
				284	

It is important to establish the *xyz* Cartesian coordinate system with respect to the *a,b,c* edges of the unit cell and then make the appropriate polarization measurements, $E \parallel a$, $E \parallel b$, $E \parallel c$ (not given by group theory), or $E \parallel x$, $E \parallel y$, $E \parallel z$ (given by group theory).

line in the ω_p column signifies that a dielectric has no free-carrier plasma frequency, or in a semiconductor the free-carrier plasma is ignored. A dashed (- - -) line in the E_g column signifies there is no fundamental band gap (in a metal or semimetal). An xxx line in the ω_T, ω_L, ω_p, E_g or ϵ_o column signifies that we could not find a value for this parameter in the literature. Hopefully, this will be filled in later.

When the collection of ω_T, ω_L data is large for a given material, the reader is referred to a separate table often containing a reference.

Even though materials like ThF_4 (monoclinic) and Si_3N_4 (hexagonal and trigonal) have very little room-temperature optical data for crystalline forms, they were tabulated in *HOC I* and *HOC II* in polycrystalline or amorphous forms as deposited in thin films for technological applications. The crystalline parameters available are tabulated in Table I. Sometimes there is more than one crystal form of a material at room temperature, but only one form was critiqued. We often include parameters for the other forms in Table I. There are many optical glasses where the primary interest is the visible index of refraction which is controlled by "doping." Fused silica is an example in *HOC I.* We never tabulated *n* for the many optical glasses, but this is done elsewhere [1, 2].

The numbers in Table I have been obtained from several sources including the original reference to the experimental work. It is not practical to cite every reference. Many of the numbers are from several collections and reviews [3–7] and the references therein. In many cases values of ω_T and ω_L from different laboratories vary by ± a few wavenumbers. Values of E_g vary

by ± a very few tenths of an eV. Some modelling and analysis is necessary to determine whether the gap is direct or indirect.

The irreducible representations at the zone center (Γ point) are obtained from the original literature or were calculated for each symmetry using the reviews by Fateley *et al.* [8] and Rousseau *et al.* [9]. This requires that the site symmetry of each atom in the unit cell be known from other references [4, 5]. While there are 230 space groups in nature, the *HOC's* contain only about 39 (roughly 17%), but surely the *HOC's* contain at least 80% of the materials of optical interest in science and technology. Most of the naturally occuring minerals on Earth have orthorhombic, triclinic, or monoclinic symmetry (thus being biaxial) and have the most complicated optical properties.

On the basis of a Lorentz model for lattice vibrations, there are resonances in ϵ_I defining resonant frequencies for the lattice. The Lorentz model was developed to describe the reaction of a solid to the propagation properties of transverse EM waves in the material. We ultimately associate the resonances at ω_T with propagating transverse optical phonons in the material.

If the oscillator strength for each mode in the material is small, the real part of the dielectric constant ϵ_R is not driven negative (through zero); the medium then cannot support a propagating longitudinal electric field, and there is no ω_L. This is true for a material like polyethylene, but is not true for a material like crystalline SiO_2, where all ω_T's have accompanying ω_L's. If the material only has transverse oscillators, the irreducible representation completely describes the transverse modes giving their IR, R, and silent O activity. In fact, group theory only deals with *x, y, z* atomic displacements and seldom invokes the words transverse, longitudinal, or direction of propagation.

However, as a given oscillator strength increases, the real part of the dielectric constant will be driven to zero at a frequency defined as ω_L. This describes a propagating longitudinal mode with atomic displacements along the direction of propagation; it occurs at a frequency somewhat higher than ω_T. The ω_L mode is not necessarily counted by group theory. The ω_L mode is not directly observed as a resonant absorption line in an IR-reflection experiment, but is located at $\epsilon_R = 0$ and is found by locating the zeroes by Kramers-Kronig analysis of reflectivity R or by a Lorentz-model fit of R. Actually, the ω_L mode can be seen in a thin-film, non-normal-incidence transmission experiment [10] with *p*-polarization. It can also be inferred from reflection measurements at normal incidence as a function of crystal orientation and for a given crystal orientation as a function of angle of incidence [11].

As discussed by several authors [6, 12–14], the Raman-scattering experiment can be used to measure specific transverse and longitudinal phonons propagating in various directions in a uniaxial crystal like ZnS, for example. The principal modes are schematically represented in Fig. 1 for propagation along the *x, y,* and *z* axes, which are usually orthogonal and parallel to the

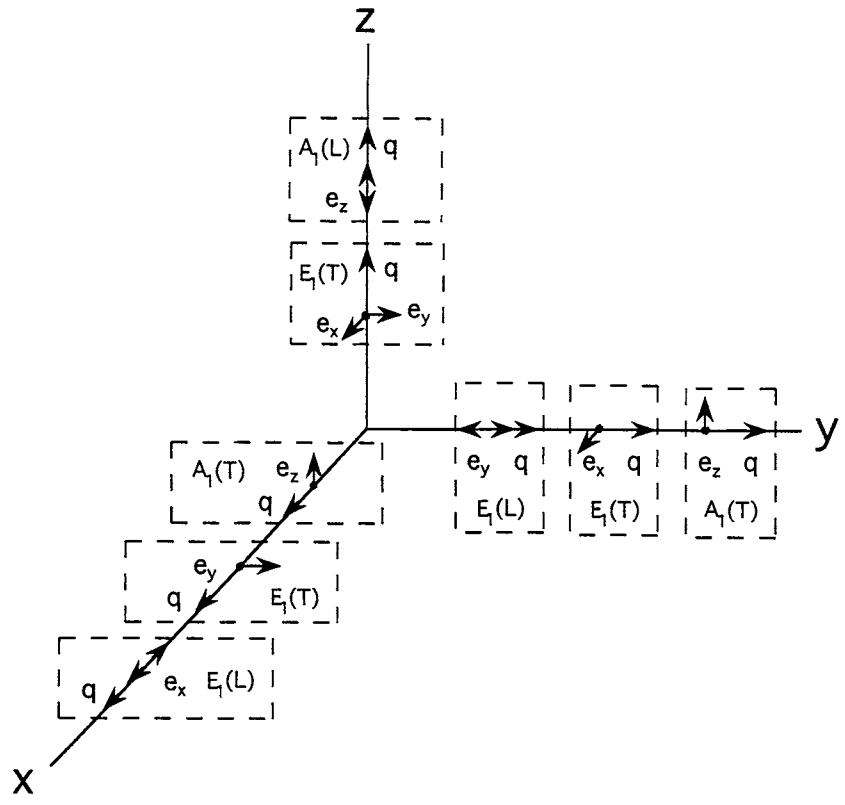

Fig. 1. Schematic representation of various A_1 and E_1 transverse and longitudinal optic modes propagating along principal directions in a CdS-type crystal. The z axis is the c optic axis. Wavevector is indicated by q and atomic displacement by e.

edges of the unit cell (except for monoclinic and triclinic symmetries). For arbitrary direction of propagation, modes are often mixed (transverse and longitudinal). For a C_{6h} crystal with hexagonal symmetry, the optic irreducible representaion is

$$\Gamma = A_1(\mathrm{IR}\|,\mathrm{R}) + 2B_1(\mathrm{O}) + E_1(\mathrm{IR}\perp,\mathrm{R}) + 2E_2(\mathrm{R}).$$

This gives 9 distinct (transverse) optic modes. The A_1 species is to be associated with e_z atomic displacements along the $z(c)$ axis, while the E_1 species is associated with e_x, e_y atomic displacements along the x and y axes. Since group theory is based on symmetry properties of atomic displacements, it tells little about direction of propagation of phonons with respect to atomic displacement of the lattice atoms. Thus, $A_1(\mathrm{IR}\|,\mathrm{R})$ can represent a transverse mode with dipole change (atomic displacement) $\|$ z. This could be a $A_1(T)$ mode propagating along x or y or an $A_1(L)$ mode propagating along z.

These three lattice vibrations have the same atomic displacement along z. Similar considerations for E_1(IR⊥,R) give an $E_1(T)$ species with atomic displacement along $x(y)$ and propagating along $y(x)$ or an $E_1(T)$ mode with atomic displacement along $x(y)$ and propagation along z; and an $E_1(L)$ with atomic displacement along $x(y)$ and propagating along $x(y)$. As mentioned before, the Raman experiment can measure each specific mode by proper orientation of the wave vectors q_i and q_s for the incident and scattered light. In the ω_T, ω_L tables, (for a non-cubic crystal), the total of optic modes will not match the number given by the irreducible representation, as the ω_L modes are "not included" in the irreducible representation.

The x, y, z axes are orthogonal. It is obvious how to define the x, y, z axes system with respect to the a, b, c edges of the unit cell for cubic, tetragonal, orthorhombic and hexagonal and trigonal symmetry (after a bit of thought). But for monoclinic and triclinic symmetries, the a, b, c axes cannot all be selected to coincide with the x, y, z system. The character tables are constructed with x, y, z axes with the resulting selection rules for IR- and Raman-active modes. However, IR experiments are often done with polarization $E \parallel a$, $E \parallel b$, $E \parallel c$. Apparently, the choice of the x, y, z coordinate system is somewhat different in Russian literature as slight systematic differences in irreducible representations seem to occur.

It is pertinent to ask which transverse and longitudinal phonons are observed in an IR reflection experiment. In Fig. 2(a) and (b) for the IR, we show typical reststrahlen reflection spectra of a CdS-type sample with the ω_T, ω_L frequencies marked for light polarizations $\parallel$ and $\perp z$. Note that ω_T (A_1) is somewhat less than ω_T (E_1); ω_L (A_1) is slightly less than ω_L (E_1). In the inset we show the experimental configuration of the sample. At the transverse frequencies light is resonantly absorbed (with a component of dipole moment $\parallel$ and $\perp z$. The longidudinal frequencies occur at the zeroes in ϵ_R. We are tempted to say that for $E \parallel z$ polarization, we measure all $A_1(T)$ modes propagating in the x-y plane; for $E \perp z$, we measure all $E_1(T)$ modes propagating in the x-z plane. Then, where are the corresponding $A_1(L)$ and $E_1(L)$ modes?

For $A_1(T)$ $(E \parallel z)$ with $q \parallel y$ and atomic dispacement $e \parallel z$, there is an $A_1(L)$ mode with $q \parallel z$ and atomic displacement $e \parallel z$. For $E_1(T)$ $(E \perp z)$ with q in the x-z plane and atomic displacement $e \parallel y$, there is an $E_1(L)$ with $q \parallel y$ and atomic displacement $e \parallel y$. A detailed examination of the several ω_T and ω_L frequencies of crystalline SiO_2 indeed suggests such a correlation.

Note that for cubic crystals the IR-active mode is always of F species in some form. Since this is a triply degenerate mode, one can always account for 2 T and 1 L modes. In non-cubic crystals the situation is more complicated. An $A_1(T)$ mode can often change species as the propagation direction is turned from z to x and, indeed, convert to an $E_1(T)$ mode.

Zone-center optic phonons which are silent or Raman active in a metal

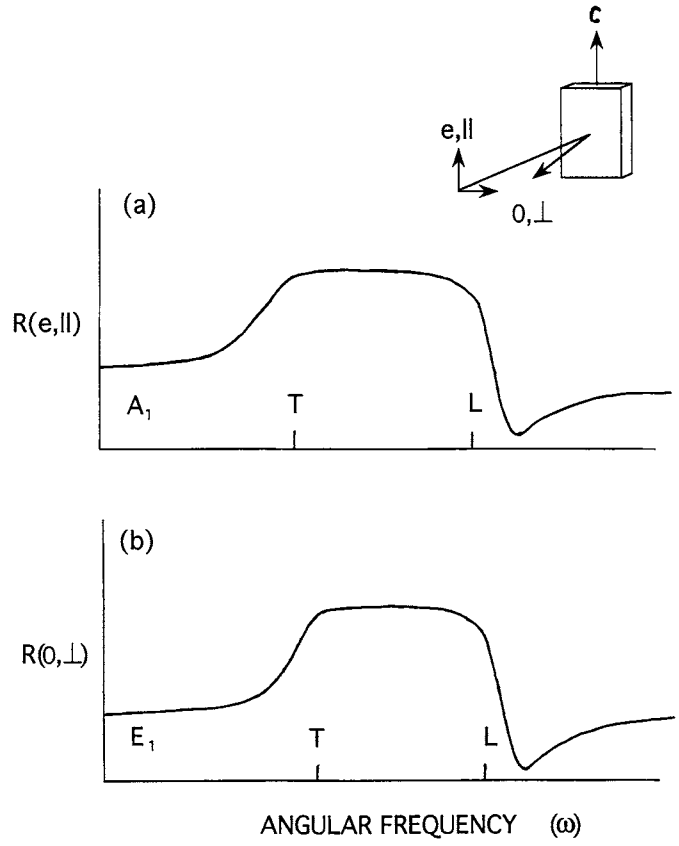

Fig. 2. (a) Reststrahlen spectrum of a CdS-type crystal for incident electric field $E \parallel c$ (extraordinary). Inset shows sample configuration with electric-field polarizations. (b) Reststrahlen spectrum of a CdS-type sample for incident electric field $E \perp c$ (ordinary).

(and therefore not possible or hard to see) can often be seen in neutron-scattering data [15, 16], at least the lower-energy modes. Note that the only metals in Table I which have IR-active modes are cubic Mn-α and the diatomic metals with cubic NaCl symmetry. Since the high free-electron concentration has driven the real dielectric function negative in the IR, these modes would be difficult to measure.

More detailed group theory can be used to calculate the dispersions curves for phonons propagating along various symmetry directions in the crystal, not just for long wavelength phonons at the zone center. This has been done in conjunction with neutron inelastic-scattering experiments. In this case, LA, TA, LO, and TO modes can be assigned to various branches of the dispersion curves in cubic diatomic metals and non-cublic metals such as Sn-β (tetragonal) [17, 18].

REFERENCES

1. A. M. Efimov, "Optical Constants of Inorganic Glasses." CRC Press, Boca Raton, Florida, 1995.
2. W. J. Tropf, M. E. Thomas, and T. J. Harris, Properties of crystals and glasses. *in* "Handbook of Optics, Volume II, Devices, Measurements and Properties" (M. Bass, E. W. Van Stryland, D. R. Wiliams, and W. L. Wolfe, eds.), 2nd Ed., Chap. 33. McGraw-Hill, New York, 1995.
3. K.-H. Hellwege, ed., "Landolt-Börnstein Numerical Data and Functional Relationships in Science and Technology." Springer-Verlag, Berlin, 1983; Several of the volumes treating semiconductors.
4. N. M. F. Henry and K. L. Lonsdak, eds., "International Tables for X-Ray Crystallography." Kynoch Press, Birmingham, U. K., 1952.
5. R. W. G. Wyckoff, "Crystal Structures," Vols. 1–4, Wiley (Interscience), New York, 1965.
6. G. R. Wilkinson, Raman spectra of ionic, covalent, and metallic crystals. *in* "Raman Effect" (A. Anderson, ed.), Vol. 2, Chap. 1. Dekker, New York, 1973.
7. D. E. Gray, ed., "American Institute of Physics Handbook." McGraw-Hill, New York, 1972.
8. W. G. Fateley, F. R. Dollish, M. T. McDevitt, and F. F. Bentley, "Infrared and Raman Selection Rules for Molecular and Lattice Vibrations: The Correlation Method." Wiley (Interscience), New York, 1972.
9. D. L. Rousseau, R. P. Bauman, and S. P. S. Porto, Normal mode determination in crystals. *J. Raman Spectrosc.* **10**, 253 (1981).
10. D. W. Berreman, Infrared absorption at longitudinal optic frequency in cubic crystal films. *Phys. Rev.* **130**, 2193 (1963).
11. C. Decius, R. Frech, and P. Brüesch, Infrared reflection from longitudinal modes in anisotropic crystals." *J. Chem. Phys.* **58**, 4056 (1973).
12. S. P. S. Porto and R. S. Krishnan, Raman effect of corundum. *J. Chem. Phys.* **47**, 1009 (1967).
13. S. M. Shapiro and J. D. Axe, Raman scattering from polar phonons. *Phys. Rev. B* **6**, 2420 (1972).
14. C. A. Arguello, D. L. Rousseau, and S. P. S. Porto, First-order Raman effect in wurtzite-type crystals. *Phys. Rev.* **181**, 1351 (1969).
15. K.-H. Helwege, ed., "Landolt-Börnstein Numerical Data and Functional Relationships in Science and Technology," Section III/Vol. 13a and Section III/Vol. 13b. Springer-Verlag, Berlin, 1983.
16. H. Bilz and W. Kress, "Phonon Dispersion Relations in Insulators." Springer-Verlag, Berlin, 1979.
17. S. H. Chen, Group-theoretical analysis of lattice vibrations in metallic β-Sn. *Phys. Rev.* **163**, 547 (1967).
18. J. M. Rowe, Crystal dynamics of metallic β-Sn at 110 K. *Phys. Rev.* **163**, 547 (1967).
    The preceeding and following references were used to obtain the vibration frequencies for many of the materials in *HOC I, II,* and *III.* The chemical formula for the material precedes the reference or can be inferred from the title of the reference.
    $Y_3Al_5O_{12}$: [2]
    Al_2MgO_4: [2]
    $Al_{23}O_{27}N_5$: [2]
    Y_2O_3: [2]
19. FeS_2: H. D. Lutz, G. Schneider, and G. Kliche, Far-infrared reflection spectra, TO- and LO-phonon frequencies, coupled and decoupled plasmon-phonon modes, dielectric constants, and effective dynamical charges of manganese, iron, and platinum group pyrite type compounds. *J. Phys. Chem. Solids* **46**, 437 (1985).
20. H. Vogt, T. Chattopadhyay, and H. J. Stolz, Complete first-order Raman spectra of the

pyrite structure compounds FeS_2, MnS_2 and SiP_2. *J. Phys. Chem. Solids* **44**, 869 (1983).
Y_2O_3: [2]
21. W. Wojdowski, Vibrational modes in $Bi_{12}GeO_{20}$ and $Bi_{12}SiO_{20}$. *Phys. Status Solidi B* **130**, 121 (1985).
22. C. F. Tuinstra and T. L. Koenig, Raman spectrum of graphite. *J. Chem. Phys.* **53**, 1126 (1970).
23. T. J. Wieting and J. L. Verble, Interlayer bonding and the lattice vibrations of β-GaSe. *Phys. Rev. B* **5**, 1473 (1972).
24. GaSe-ε: J. C. Irwin, R. M. Hoff, B. P. Clayman, and R. A. Bromley, Long wavelength lattice vibrations in GaS and GaSe. *Solid State Commun.* **13**, 1531 (1973).
ZnS: [2, 6]
CdS: [2, 6]
CdSe: [2, 6]
BeO: [2, 6]
SiC-α-6H: [2, 6]
AgI: [2, 6]
AlN: [2, 6]
BN: [25]
GaN: [2, 6]
25. R. Geick, C. H. Perry, and G. Rupprecht, Normal modes in hexagonal boron nitride. *Phys. Rev.* **146**, 543 (1966).
26. Si_3N_4-β: Y. N. Volgin and Y. I. Ukhanov, Vibrational spectra of silicon nitride. *Opt. Spectrosc.* **38**, 412 (1975); *Opt. Spektrosk.* **38**, 727 (1975).
27. Y. N. Volgin, G. P. Dubrovskii, and Y. I. Ukhanov, Lattice vibration spectrum of silicon nitride. *Sov. Phys. Solid State* **17**, 1089 (1975); *Fiz. Tverd. Tela (Leningrad)* **17**, 1671 (1975).
28. N. Wada, S. A. Solin, J. Wong, and S. Prochazka, Raman and IR absorption spectroscopic studies on α, β and amorphous Si_3N_4. *J. Non-Cryst. Solids* **43**, 7 (1981).
29. Y. N. Volgin, V. V. Baptizmanskii, Y. I. Ukhanov, and B. V. Chernovets, Vibrational spectra of β-Si_3N_4. *Sov. Phys. Solid State* **30**, 1105 (1988); *Fiz. Tverd. Tela (Leningrad)* **30**, 1910 (1988).
30. J. P. Luongo, Infrared characterization of α- and β-crystalline silicon nitride. *J. Electrochem. Soc.* **130**, 1560 (1983).
Al_2O_3: [6, 12]
31. Ga_2O_3: E. D. Palik, N. Ginsburg, R. T. Holm, and J. W. Gibson, Optical studies of the anodic oxide on GaAs. *J. Vac. Sci. Technol.* **15**, 1488 (1977).
32. F. Brehat and B. Wyncke, Analysis of the temperature-dependent infrared active modes in the ordered phase of sodium nitrate. *J. Phys. Chem.* **18**, 247 (1985).
$CaCO_3$: [2]
33. I. P. Kaminow and W. D. Johnston, Jr., Quantitative determination of source of the electro-optic effect in $LiNbO_3$ and $LiTaO_3$. *Phys. Rev.* **160**, 519 (1967).
34. R. Claus, Directional dispersion and assignment of optical phonons in $LiNbO_3$. *Z. Naturforsch.* **287A**, 1187 (1972).
35. $LiTaO_3$: J. L. Servoid and F. Gervais, Soft vibrational mode in $LiNbO_3$ and $LiTaO_3$. *Solid State Commun.* **31**, 387 (1979).
36. GaSe-γ: R. M. Hoff, J. C. Irwin and R. M. A. Lieth, Raman scattering in GaSe. *Can. J. Phys.* **53**, 1606 (1975).
37. Si_3N_4-α: T. Kuzuba, K. Kijima, and Y. Bando, Raman-active modes of alpha silicon nitride. *J. Chem. Phys.* **69**, 40 (1978).
SiO_2: [12]
38. Se: G. Lucovsky, A. Mooradian, W. Taylor, G. B. Wright, and R. C. Keezer, Identification of the fundamental vibrational modes of trigonal, α-monoclinic and amorphous films. *Solid State Commun.* **5**, 113 (1967).
Te: [6, 38]

39. P. Dawson, M. M. Hargreave, and G. R. Wilkinson, The vibrational spectrum of zircon ($ZrSiO_4$). *J. Phys. C: Solid State Phys.* **4**, 240 (1971).
40. J. Misiewicz, Optical vibrations in the Zn_3P_2 lattice. *J. Phys. Condens. Matter* **1**, 9283 (1991).
41. G. Pangilinan, R. Sooryakumar, and J. Misiewicz, Raman activity of Zn_3P_2. *Phys. Rev. B* **44**, 2582 (1991).
42. TiO_2: S. P. S. Porto, P. A. Fleury, and T. C. Damen, Raman spectra for TiO_2, MgF_2, ZnF_2, CrF_2, and MnF_2. *Phys. Rev.* **154**, 522 (1967).
43. KH_2PO_4: D. K. Agrawal and C. H. Perry, The temperature dependent Raman spectra of KDP, KD*P, KDA and ADP. *in* "Proceedings of the Second International Conference on Light Scattering Solids," (M. Balkanski, ed.), p. 429. Flammarion, Paris, 1971.
$AgGaS_2$: [2]
$AgGaSe_2$: [2]
$CdGeAs_2$: [2]
$CuGaS_2$: [2]
$ZnGeP_2$: [2]
44. $NH_4H_2PO_4$: T. Kawamura and A. Mitsuishi, *Technol. Rep. Osaka Univ.* **23**, 365 (1973).
45. J. Weszka, A. Zwick, and M. Renucci, Raman scattering in α-Zn_3As_2 crystals. *Acta Phys. Pol. A* **77**, 363 (1990).
46. A. Scalabrin, A. S. Chaves, D. S. Shin, and S. P. S. Porto, Temperature dependence of the A_1 and E optical phonons in $BaTiO_3$. *Phys. Status Solidi B* **79**, 731 (1977).
47. S. G. Gautier and M. Debeau, Spectres de vibration d'un monocristal de soufre orthorhombique. *Spectrochim. Acta* **30A**, 1193 (1974).
48. TlI: J. Claudel, A. Hadni, P. Strimer, and P. Vergnat, Absorption spectra of the thallous halides in the far infrared at low temperatures. *J. Phys. Chem. Solids* **29**, 1539 (1968).
49. $(CH_2)_x$: J. R. Nielsen and A. H. Wollett, Vibrational spectra of polyethylenes and related substances. *J. Chem. Phys.* **26**, 1391 (1957).
50. $(CH_2)_x$: R. Zbinden, "Infrared Spectroscopy of High Polymers." Academic Press, New York, 1964.
$KNbO_3$: [2]
51. S. Guda, D. Peebles, and T. J. Wieting, Zone-center (q = 0) optical phonons in CuO studied by Raman and infrared spectroscopy. *Phys. Rev. B* **43**, 13092 (1991).
52. ThF_4: H. Y. B. Mar, Infrared properties and morphology of ThF_4 films. *J. Vac. Sci. Technol.* **12**, 919 (1975).
53. R. Zallen, M. L. Slade, and A. T. Ward, Lattice vibrations and interlayer interactions in crystalline As_2S_3 and As_2Se_3. *Phys. Rev. B* **3**, 4257 (1971).
54. GaTe-α: M. N. Gasanly, B. M. Dzhavadov, V. I. Tagirov, and E. A. Vinogrdov, Vibrational spectra of a GaTe layer crystal. *Phys. Status. Solidi. (B)* **100**, K53 (1980).

Introduction to the Data for Several Metals

DAVID W. LYNCH
Department of Physics and Astronomy and
Ames Laboratory, USDOE
Iowa State University
Ames, Iowa
and
W. R. HUNTER
SFA Inc.
Largo, Maryland

INTRODUCTION I

Optical data are presented below for eight metals. Mg, In, and Sn are nearly-free-electron polyvalent metals, Ti, Mn, Re, and Ru are transition metals, and Sb is not really a metal, but rather a semimetal. The optical properties of all these metals in the visible and ultraviolet are determined by interband absorption. The threshold for such absorption is, in principle, zero for the transition metals. This means that a fit of the infrared optical properties with a free-electron or Drude model may not be possible. As a practical matter, for b.c.c. and h.c.p. metals there is a threshold for the onset of strong interband absorption, but at energies below this threshold, there is dispersion in the real part of the dielectric function due to the nearby rise in the imaginary part, so a region of "pure" Drude behavior may occur only at very low energies. The polyvalent metals have, in the absence of damping, a threshold for interband absorption, but damping is always present because of electron–electron scattering. For such metals, a Drude model may be fitted at long wavelengths, but the high-energy limit of such a fit is not known reliably at this time. For these reasons we do not report the parameters of Drude fits to the infrared optical properties of any of these metals.

There are four general methods for determining the optical properties (complex refractive index $[n + ik]$ or complex dielectric function $[\epsilon = \epsilon_1 +$

HANDBOOK OF OPTICAL CONSTANTS OF SOLIDS III

Copyright © 1998 by Academic Press.
All rights of reproduction in any form reserved
ISBN 0-12-544423-0/$25.00.

$i\epsilon_2$]) of a material, and in principle, one needs two measurements at each photon energy to determine the real and imaginary parts. Three of the general methods are photometric. When using the first, one measures the reflectance of an opaque sample or thin film, and a second quantity, such as the reflectance at another angle, the transmittance of the film, or the reflectance at nonnormal incidence with a different polarization. The second method is a variant of the first. One measures the reflectance over as wide a range of energies as possible and uses a dispersion integral, or Kramers–Kronig integral, to obtain the unmeasured phase shift upon reflection. These two quantities give the complex refractive index. This method requires, in principle, data over an infinite energy range: data that are usually supplied by the use of measurements of others, and the appeal to simple models for high and low energies. The third method is ellipsometry, which measures the ratio of reflectances for *s*- and *p*-polarized radiation and the relative phase shift between the two, both measured at large angles of incidence. The fourth method is a nonoptical method, electron-energy-loss spectroscopy, which gives a spectrum proportional to $\mathrm{Im}(-1/\epsilon)$. If measured over a wide energy range, this can yield $\mathrm{Re}(-1/\epsilon)$ in a dispersion integral, and ϵ can be obtained, although a scaling factor has to be introduced to obtain absolute units. These measurement methods, and references to them, are described in more detail elsewhere [1]. In the data, we have not made use of any measurements from electron-energy-loss spectroscopy.

By now these methods are able to achieve an accuracy of the order of 1%, but there are discrepancies between the results of different investigators of over 10%. Much of this can be assigned to differences in samples, and how sample deficiencies affect the measured quantities. The first three types of measurement make use of the Fresnel relations derived from Maxwell's equations for the interface between a sample and the ambient medium, air or vacuum in the cases at hand. The interface is assumed to be a mathematical plane and the medium just below it is assumed to be the same as in the bulk of that medium. Real surfaces are not like this. They may be rather rough; the material to be studied may have an oxide film, a cold-worked layer from polishing, or both. Thin films may be highly strained and they may not have the density of the bulk. The effects of these departures from ideality are different for different techniques, and they will depend on the photon energy. For example, an oxide layer may be transparent in the visible but absorbing in the ultraviolet. As a result of these effects, there is not as good agreement between the results of different investigators as may be desired. Moreover, the "correct" optical constants one wants to use may depend on the application. Data resulting from measurements made on strained films may be the best to use if one is calculating anticipated spectra for filters made of strained films.

Several of the materials whose optical constants are given later are anisotropic. These are uniaxial, and two independent spectra of complex optical

constants are required for a complete description of the optical properties of a single crystal. For a polycrystalline sample consisting of randomly oriented crystallites, the dielectric function is given by $\epsilon = (\epsilon_{\parallel} + 2\epsilon_{\perp})/3$, with the c-axis as the reference for polarization. However, films of these materials tend not to have randomly oriented crystallites; the c-axes tend to be oriented normal to the films. They may be closer to a single crystal for optical purposes than to a polycrystal. When available, we have reported a single set of data taken on polycrystalline bulk samples, but for such anisotropic materials, most of those reported here, the reader should consult the references, and should decide how to deal with the anisotropy.

REFERENCES

1. D. W. Lynch, *in* "Handbook on Synchrotron Radiation" (G. V. Marr, ed.), Vol. 2, Chap. 11. Elsevier, Amsterdam, 1987.

MAGNESIUM (Mg) II

Magnesium is a hexagonal close-packed metal. In single-crystal form it is optically anisotropic, uniaxial, with two independent components in the dielectric tensor, one for the electric field parallel to the c-axis and one for the perpendicular orientation. Polycrystalline films may have a texture, growing with the closest-packed plane, the basal plane, in the plane of the film, but with randomly oriented a-axes. If so, the film will be optically anisotropic. If there is truly random orientation of crystallites, the film is isotropic with a complex dielectric function $\epsilon = (\epsilon_{\parallel} + 2\,\epsilon_{\perp})/3$. Mg develops an oxide skin when exposed to air, typically MgO, which is unstable in that it does not protect the metal from further oxidation.

The data presented in Table I and Fig. 1 are those of Hagemann *et al* [1]. These are a result of a Kramers–Kronig analysis of the data of Gesell *et al.* [2], Daudé *et al.* [3], Hacman and Heitmann [4], Kröger and Tomboulian [5], and their own measurements. These represent results on polycrystalline films. Some measurements on single crystals have been published [6–8].

The location of the soft x-ray edges, shown by the short, vertical lines in Fig. 1, are taken from Siegbahn *et al.* [9].

REFERENCES

1. W. Hagemann, W. Gudat, and C. Kunz, *J. Opt. Soc. Am.* **65**, 742 (1975). The data appear in report DESY SR-74/7 from Deutsches Elektronen-Synchrotron, Notkestieg 1, D-2000 Hamburg 52, Germany.
2. T. F. Gesell, E. T. Arakawa, M. W. Williams, and N. R. Hamm, *Phys. Rev. B* **7**, 5141 (1973).
3. A. Daudé, M. Priol, and S. Robin, *Compt. Rend. Ser B* **264**, 1489 (1967).

4. D. Hacman and W. Heitmann, *Appl. Opt.* **12**, 895 (1967).
5. H. Kröger and D. H. Tomboulian, *Phys. Rev.* **130**, 152 (1957).
6. A. P. Lenham and D. M. Treherne, *J. Opt. Soc. Am.* **56**, 752 (1966).
7. D. Jones and A. H. Lettington, *Proc. Phys. Soc. (London)* **92**, 948 (1967).
8. R. H. W. Graves and A. P. Lenham, *J. Opt. Soc. Am.* **58**, 126 (1968).
9. K. Siegbahn, C. Nordling, A. Fahlman, R. Nordberg, K. Hamrin, J. Hedman, G. Johansson, T. Bergmark, S.-E. Karlsson, I. Lindgren, and B. Lindberg, *in* "ESCA Atomic, Molecular, and Solid State Structure Studied by Means of Electron Spectroscopy." Almquist & Wiksell, Uppsala, Sweden, 1967.

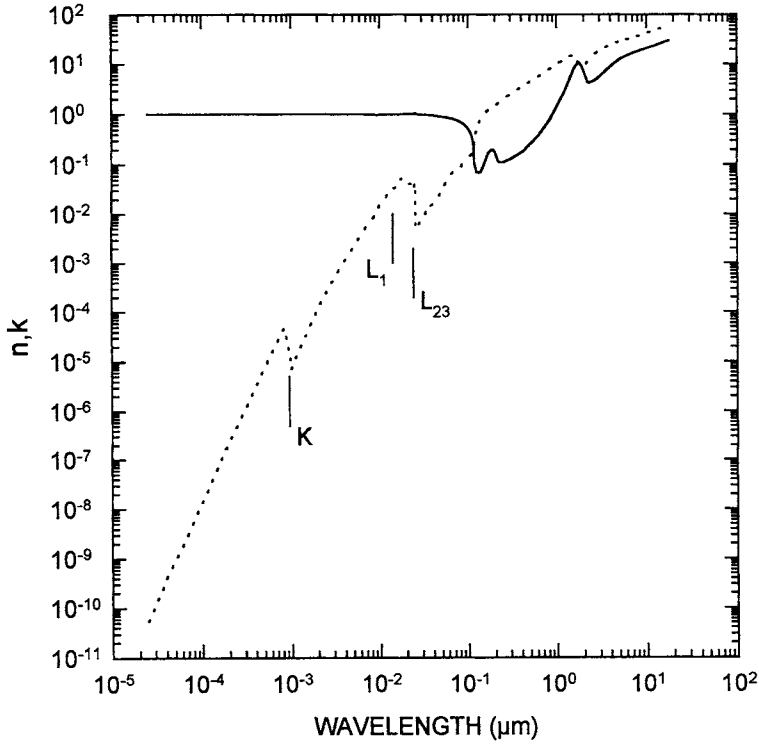

Fig. 1. Log–log plot of n (——) and k (- - - -) versus wavelength in micrometers for magnesium.

TABLE I

Values of n and k Obtained from Various References for Magnesium[a]

eV	cm^{-1}	μm	n	k
50000.	4.033E + 08	2.48E-05	9.999E-01 [1]	5.38E-11 [1]
40000.	3.226E + 08	3.10E-05	9.999E-01	1.35E-10
30000.	2.420E + 08	4.13E-05	9.999E-01	4.80E-10
20000.	1.613E + 08	6.20E-05	9.999E-01	2.04E-09
10000.	8.065E + 07	1.24E-04	9.999E-01	3.33E-08
8000.	6.452E + 07	1.55E-04	9.999E-01	8.27E-08
6000.	4.839E + 07	2.07E-04	9.999E-01	2.75E-07
4000.	3.226E + 07	3.10E-04	9.999E-01	1.19E-06
2000.	1.613E + 07	6.20E-04	9.999E-01	1.75E-05
1500.	1.210E + 07	8.27E-04	9.999E-01	4.76E-05
1300.	1.049E + 07	9.54E-04	9.999E-01	1.50E-05
1260.	1.016E + 07	9.84E-04	9.999E-01	8.15E-06
1250.	1.008E + 07	9.92E-04	9.999E-01	7.09E-06
1200.	9.679E + 06	1.03E-03	9.999E-01	8.94E-06
1000.	8.065E + 06	1.24E-03	9.990E-01	1.86E-05
800.	6.452E + 06	1.55E-03	9.996E-01	4.41E-05
600.	4.839E + 06	2.07E-03	9.990E-01	1.39E-04
500.	4.033E + 06	2.48E-03	9.987E-01	2.66E-04
450.	3.629E + 06	2.76E-03	9.984E-01	3.75E-04
400.	3.226E + 06	3.10E-03	9.977E-01	5.42E-04
350.	2.823E + 06	3.54E-03	9.974E-01	8.11E-04
300.	2.420E + 06	4.13E-03	9.963E-01	1.25E-03
250.	2.016E + 06	4.96E-03	9.948E-01	2.15E-03
200.	1.613E + 06	6.20E-03	9.923E-01	4.07E-03
180.	1.452E + 06	6.89E-03	9.911E-01	5.30E-03
160.	1.290E + 05	7.75E-03	9.891E-01	7.11E-03
150.	1.210E + 06	8.27E-03	9.881E-01	8.16E-03
145.	1.169E + 06	8.55E-03	9.871E-01	8.85E-03
140.	1.129E + 06	8.86E-03	9.860E-01	1.00E-02
135.	1.089E + 06	9.18E-03	9.489E-01	1.16E-02
130.	1.049E + 06	9.54E-03	9.846E-01	1.35E-02
125.	1.008E + 06	9.92E-03	9.847E-01	1.52E-02
120.	9.679E + 05	1.03E-02	9.846E-01	1.66E-02
115.	9.275E + 05	1.08E-02	9.844E-01	1.77E-02
110.	8.872E + 05	1.13E-02	9.829E-01	1.93E-02
105.	8.469E + 05	1.18E-02	9.815E-01	2.25E-02
100.	8.065E + 05	1.24E-02	9.815E-01	2.68E-02
95.	7.662E + 05	1.31E-02	9.838E-01	3.10E-02
90.	7.259E + 05	1.38E-02	9.860E-01	3.30E-02
89.	7.178E + 05	1.39E-02	9.870E-01	3.37E-02
88.	7.098E + 05	1.41E-02	9.870E-01	3.34E-02
87.	7.017E + 05	1.43E-02	9.870E-01	3.34E-02
86.	6.936E + 05	1.44E-02	9.870E-01	3.36E-02
84.	6.775E + 05	1.48E-02	9.880E-01	3.45E-02
82.	6.614E + 05	1.51E-02	9.880E-01	3.52E-02
80.	6.452E + 05	1.55E-02	9.870E-01	3.60E-02
78.	6.291E + 05	1.59E-02	9.860E-01	3.74E-02

(continued)

[a] The references from which the values were extracted are given in brackets.

TABLE I *(Continued)*

Magnesium

eV	cm^{-1}	μm	n	k
76.	6.130E + 05	1.63E-02	9.840E-01	4.14E-02
74.	5.968E + 05	1.68E-02	9.860E-01	4.75E-02
72.	5.807E + 05	1.72E-02	9.920E-01	5.26E-02
70.	5.646E + 05	1.77E-02	1.00	5.33E-02
68.	5.485E + 05	1.82E-02	1.005	5.03E-02
66.	5.323E + 05	1.88E-02	1.008	4.58E-02
64.	5.162E + 05	1.94E-02	1.008	4.32E-02
62.	5.001E + 05	2.00E-02	1.008	4.14E-02
60.	4.839E + 05	2.07E-02	1.008	4.09E-02
59.	4.759E + 05	2.10E-02	1.008	4.10E-02
58.	4.678E + 05	2.14E-02	1.009	4.08E-02
57.	4.597E + 05	2.18E-02	1.01	4.09E-02
56.	4.517E + 05	2.21E-02	1.01	4.18E-02
55.5	4.476E + 05	2.23E-02	1.012	4.12E-02
55.	4.436E + 05	2.25E-02	1.013	4.06E-02
54.5	4.396E + 05	2.27E-02	1.013	3.98E-02
54.	4.355E + 05	2.30E-02	1.014	4.01E-02
53.5	4.315E + 05	2.32E-02	1.015	4.07E-02
53.	4.275E + 05	2.34E-02	1.017	3.93E-02
52.5	4.234E + 05	2.36E-02	1.018	3.39E-02
52.	4.194E + 05	2.38E-02	1.019	3.76E-02
51.5	4.154E + 05	2.41E-02	1.02	3.72E-02
51.	4.113E + 05	2.43E-02	1.021	3.58E-02
50.5	4.073E + 05	2.46E-02	1.023	3.79E-02
50.	4.033E + 05	2.48E-02	1.03	4.17E-02
49.8	4.017E + 05	2.49E-02	1.04	4.18E-02
49.6	4.000E + 05	2.50E-02	1.05	3.38E-02
49.4	3.984E + 05	2.51E-02	1.053	1.06E-02
49.2	3.968E + 05	2.52E-02	1.04	4.92E-03
49.	3.952E + 05	2.53E-02	1.033	4.92E-03
48.5	3.912E + 05	2.56E-02	1.023	4.96E-03
48.	3.871E + 05	2.58E-02	1.018	5.02E-03
46.	3.710E + 05	2.70E-02	1.004	5.97E-03
44.	3.549E + 05	2.82E-02	0.997	6.86E-03
42.	3.388E + 05	2.95E-02	0.989	7.36E-03
40.	3.226E + 05	3.10E-02	0.982	8.84E-03
38.	3.065E + 05	3.26E-02	0.975	1.02E-02
36.	2.904E + 05	3.44E-02	0.967	1.41E-02
34.	2.742E + 05	3.65E-02	0.959	1.41E-02
32.	2.581E + 05	3.87E-02	0.95	1.54E-02
30.	2.420E + 05	4.13E-02	0.939	1.69E-02
28.	2.258E + 05	4.43E-02	0.924	1.96E-02
26.	2.097E + 05	4.77E-02	0.906	2.52E-02
24.	1.936E + 05	5.17E-02	0.885	3.30E-02
22.	1.774E + 05	5.64E-02	0.861	4.54E-02
20.	1.613E + 05	6.20E-02	0.833	5.92E-02
18.	1.452E + 05	6.89E-02	0.798	7.31E-02

TABLE I *(Continued)*

Magnesium

eV	cm^{-1}	μm	n	k
16.	1.290E + 05	7.75E-02	0.741	7.92E-02
15.	1.210E + 05	8.27E-02	0.692	9.16E-02
14.	1.129E + 05	8.86E-02	0.644	1.11E-01
13.	1.049E + 05	9.54E-02	0.577	1.27E-01
12.	9.679E + 04	1.03E-01	0.477	1.45E-01
11.5	9.275E + 04	1.08E-01	0.404	1.58E-01
11.	8.872E + 04	1.13E-01	0.293	1.76E-01
10.5	8.469E + 04	1.18E-01	0.11	2.96E-01
10.	8.065E + 04	1.24E-01	0.0723	4.99E-01
9.5	7.662E + 04	1.31E-01	0.0691	6.47E-01
9.	7.259E + 04	1.38E-01	0.0717	7.87E-01
8.5	6.856E + 04	1.46E-01	0.0858	9.26E-01
8.	6.452E + 04	1.55E-01	0.115	1.06
7.5	6.049E + 04	1.65E-01	0.155	1.19
7.3	5.888E + 04	1.70E-01	0.171	1.23
7.1	5.726E + 04	1.75E-01	0.184	1.27
6.9	5.565E + 04	1.80E-01	0.194	1.31
6.7	5.404E + 04	1.85E-01	0.199	1.35
6.5	5.243E + 04	1.91E-01	0.197	1.39
6.3	5.081E + 04	1.97E-01	0.187	1.44
6.1	4.920E + 04	2.03E-01	0.166	1.49
5.9	4.759E + 04	2.10E-01	0.14	1.56
5.7	4.597E + 04	2.18E-01	0.121	1.64
5.5	4.436E + 04	2.25E-01	0.112	1.74
5.	4.033E + 04	2.48E-01	0.111	2.00
4.	3.226E + 04	3.10E-01	0.132	2.63
3.	2.420E + 04	4.13E-01	0.184	3.66
2.	1.613E + 04	6.20E-01	0.382	5.74
1.5	1.210E + 04	8.27E-01	0.791	7.96
1.	8.065E + 03	1.24	2.977	12.8
0.9	7.259E + 03	1.38	4.776	14.5
0.8	6.452E + 03	1.55	8.269	15.5
0.7	5.646E + 03	1.77	11.2	10.2
0.65	5.243E + 03	1.91	8.809	8.98
0.6	4.839E + 03	2.07	6.056	9.33
0.55	4.436E + 03	2.25	4.194	12.2
0.5	4.033E + 03	2.48	4.509	14.7
0.45	3.629E + 03	2.76	5.056	16.8
0.4	3.226E + 03	3.10	6.069	19.5
0.35	2.823E + 03	3.54	7.519	22.2
0.3	2.420E + 03	4.13	9.516	25.1
0.25	2.016E + 03	4.96	12.3	28.8
0.2	1.613E + 03	6.20	15.2	32.6
0.15	1.210E + 03	8.27	18.9	37.6
0.1	8.065E + 02	12.4	23.8	48.8
0.07	5.646E + 02	17.7	30.3	60.2

III TITANIUM (Ti)

Ti is a hexagonal close-packed metal. In single-crystal form it is optically anisotropic, uniaxial, with two independent components in the dielectric tensor, one for the electric field parallel to the *c*-axis and one for the perpendicular orientation. Polycrystalline films may have a texture, growing with the closest-packed plane, the basal plane, in the plane of the film, but with randomly oriented *a*-axes. If so, the film will be optically anisotropic. If there is truly random orientation, the film is isotropic with a complex dielectric function $\epsilon = (\epsilon_{\parallel} + 2\epsilon_{\perp})/3$. Ti is quite reactive with air. (It is used as a getter pump in vacuum systems.) However, the oxide film is self-limiting, leading to a stable sample. Since there are so many oxides of Ti, it is difficult to model the optical properties of a Ti sample oxidized to equilibrium.

Ti is a transition metal. The incompletely filled 3*d* bands can give rise to interband optical absorption at arbitrarily small energies. This means that reliable fits of optical data to a Drude-model dielectric function cannot be made, except below some unknown low energy. Ordal *et al.* [1] were unable to fit the optical constants of Ti to a Drude model in the 1–12-μm wavelength region because of the presence of interband transitions. According to absorptivity measurements by Lynch *et al.* [2], these transitions give a strong absorption edge at 0.4 eV, although they are present, however weaker, at lower energies. Later, Ordal *et al.* [3] produced a Drude fit to the same data for energies below 0.37 eV.

Ordal *et al.* [4] measured absorptance spectra in the submillimeter-wave region and obtained optical constants by a Kramers–Kronig analysis, using their data and measurements from shorter wavelengths. The data we present in Table II and Fig. 2 are those of Ordal *et al.* [4] and Lynch *et al.* [2], measured on polycrystalline bulk samples and published by Weaver *et al.* [5], Wall *et al.* [6], and Sonntag *et al.* [7]. The last spectra were of the absorption coefficient. They were converted to spectra of the imaginary part of the complex refractive index with the assumption that the real part was unity. The data of Wall *et al.* are the only data on atomically clean surfaces. Comparison with the data of Lynch *et al.*, taken on electropolished surfaces, shows that in the vacuum ultraviolet the effect of the residual oxide is serious.

The data reported for the 1–10 μm region were taken at 4.2 K. At room temperature the peak will broaden considerably. The literature contains a number of additional reports on measurements of the optical constants of Ti [8–20] taken on bulk polycrystalline samples and on evaporated films by several techniques.

Smith [21] has measured the temperature dependence at two wavelengths, 5461 and 6328 Å.

Data in the soft x-ray region, from approximately 10^{-4} to 0.024 μm, are taken from Henke *et al.* [22], and the location of the soft x-ray edges, shown by the short, vertical lines in Fig. 1, are taken from Siegbahn *et al.* [23].

REFERENCES

1. M. A. Ordal, L. L. Long, R. J. Bell, S. E. Bell, R. R. Bell, R. W. Alexander, and C. A. Ward, *Appl. Opt.* **22**, 1099 (1983).
2. D. W. Lynch, C. G. Olson, and J. H. Weaver, *Phys. Rev. B* **11**, 3617 (1975).
3. M. A. Ordal, R. J. Bell, R. W. Alexander, L. L. Long, and M. R. Querry, *Appl. Opt.* **24**, 4493 (1985).
4. M. A. Ordal, R. J. Bell, R. W. Alexander, L. A. Newquist, and M. R. Querry, *Appl. Opt.* **27**, 1203 (1988).
5. J. H. Weaver, C. Krafka, D. W. Lynch, and E.-E. Koch, Physics Data, Optical Properties of Metals, Part I: The Transition Metals, Fachinformationszentrum Karlsruhe, 7514 Eggenstein-Leopoldshafen 2, Germany, 1981.
6. W. Wall, M. W. Ribarsky, and J. R. Stevenson, *J. Appl. Phys.* **51**, 661 (1980).
7. B. Sonntag, R. Haensel, and C. Kunz, *Solid State Commun.* **7**, 597 (1969).
8. G. Hass and A. P. Bradford, *J. Opt. Soc. Am.* **47**, 125 (1957).
9. G. A. Bolotin, A. N. Voloshinskii, M. M. Kirillova, M. M. Noskov, A. V. Sokolov, and B. A. Charikov, *Fiz. Met. Metalloved.* **13**, 823 (1962); *Phys. Met. Metall.* **13**, 24 (1962).
10. M. M. Kirillova and B. A. Charikov, *Opt. Spektrosk.* **17**, 254 (1963); *Opt. Spectrosc.* **17**, 134 (1963).
11. M. M. Kirillova and B. A. Charikov, *Fiz. Met. Metalloved.* **15**, 315 (1963); *Phys. Met. Metall.* **15**, 138 (1963).
12. A. P. Lukirskii, E. P. Savinov, O. A. Ershov, and Yu. F. Shepelev, *Opt. Spektrosk.* **16**, 310 (1964); *Opt. Spectrosc.* **16**, 168 (1964).
13. M. M. Kirillova and B. A. Charikov, *Fiz. Met. Metalloved.* **19**, 495 (1965); *Phys. Met. Metall.* **19**, 13 (1965).
14. A. P. Lenham and D. M. Treherne, *J. Opt. Soc. Am.* **56**, 1137 (1966).
15. M. M. Kirillova, L. V. Nomerovannaya, G. A. Bolotin, V. M. Mayevskiy, M. M. Noskov, and M. L. Bolotina, *Fiz. Met. Metalloved.* **25**, 459 (1968); *Phys. Met. Metall.* **25**, 81 (1968).
16. I. D. Mash and G. P. Motulevich, *Sov. Phys. JETP* **36**, 516 (1973).
17. P. B. Johnson and R. W. Christy, *Phys. Rev. B* **9**, 5056 (1974).
18. J. J. Carroll and A. J. Melmed, *J. Opt. Soc. Am.* **64**, 514 (1974).
19. G. Blondeau, M. Froelicher, M. Froment, and A. Hugot-LeGoff, *Thin Solid Films* **38**, 261 (1976).
20. R. Blickensderfer, D. K. Deardorff, and R. L. Lincoln, *J. Less Common Metals* **51**, 13 (1977).
21. T. Smith, *J. Opt. Soc. Am.* **62**, 774 (1972).
22. B. L. Henke, J. C. Davis, E. M. Gullikson, and R. C. C. Perera, "A Preliminary Report on X-Ray Photoabsorption Coefficients and Atomic Scattering Factors for 92 Elements in the 10–10,000 eV Region," Lawrence Berkeley Lab. Rep. LBL-26259, University of California, Berkeley, California, 1988.
23. K. Siegbahn, C. Nordling, A. Fahlman, R. Nordberg, K. Hamrin, J. Hedman, G. Johansson, T. Bergmark, S.-E. Karlsson, I. Lindgren, and B. Lindberg, "ESCA Atomic, Molecular, and Solid State Structure Studied by Means of Electron Spectroscopy." Almquist & Wiksell, Uppsala, Sweden, 1967.

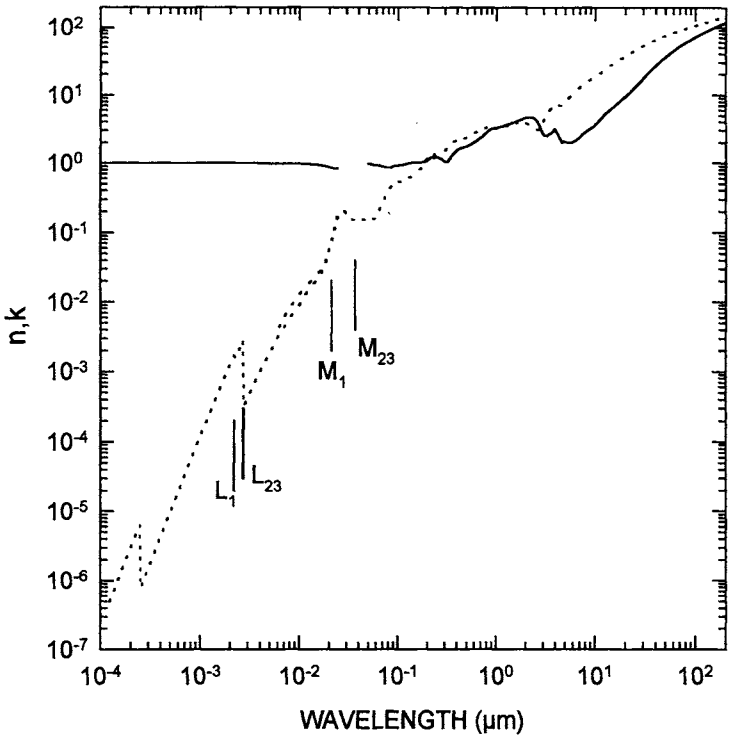

Fig. 2. Log–log plot of n (——) and k (- - - -) versus wavelength in micrometers for titanium.

TABLE II

Values of n and k Obtained from Various References for Titanium[a]

eV	cm^{-1}	μm	n	k
10000	8.101E + 07	1.23E-04	9.9999120E-01 [22]	4.89E-07 [22]
8558	6.902E + 07	1.45E-04	9.999880E-01	9.03E-07
7100	5.726E + 07	1.75E-04	9.999828E-01	1.80E-06
5294	4.269E + 07	2.34E-04	9.999720E-01	5.17E-06
5154	4.157E + 07	2.41E-04	9.999716E-01	5.67E-06
5018	4.048E + 07	2.47E-04	9.999729E-01	6.22E-06
4886	3.941E + 07	2.54E-04	9.999705E-01	7.97E-07
4758	3.837E + 07	2.61E-04	9.999670E-01	8.81E-07
3547	2.861E + 07	3.50E-04	9.999351E-01	2.63E-06
2575	2.077E + 07	4.81E-04	9.99874E-01	8.63E-06
1680	1.355E + 07	7.38E-04	9.99697E-01	4.13E-05
1470	1.186E + 07	8.43E-04	9.99603E-01	6.69E-05
1287	1.038E + 07	9.64E-04	9.99483E-01	1.08E-04
1126	9.081E + 06	1.10E-03	9.99330E-01	1.72E-04
1012	8.161E + 06	1.23E-03	9.99181E-01	2.49E-04
886	7.142E + 06	1.40E-03	9.9896E-01	3.94E-04
735	5.925E + 06	1.69E-03	9.9860E-01	7.40E-04
593	4.786E + 06	2.09E-03	9.9831E-01	1.48E-03
578	4.660E + 06	2.15E-03	9.9834E-01	1.61E-03
563	4.537E + 06	2.20E-03	9.9847E-01	1.52E-03
548	4.417E + 06	2.26E-03	9.9834E-01	1.65E-03
533	4.301E + 06	2.32E-03	9.9832E-01	1.80E-03
492	3.971E + 06	2.52E-03	9.9857E-01	2.31E-03
479	3.866E + 06	2.59E-03	9.9886E-01	2.52E-03
467	3.764E + 06	2.66E-03	9.9945E-01	2.74E-03
454	3.665E + 06	2.73E-03	1.000853	3.24E-04
442	3.568E + 06	2.80E-03	9.9946E-01	3.50E-04
431	3.475E + 06	2.88E-03	9.9887E-01	3.79E-04
321	2.591E + 06	3.86E-03	9.9588E-01	9.19E-04
215	1.736E + 06	5.76E-03	9.9028E-01	2.79E-03
200	1.613E + 06	6.20E-03		4.40E-03 [7]
190	1.532E + 06	6.53E-03		5.10E-03
180	1.452E + 06	6.89E-03		6.00E-03
170	1.371E + 06	7.29E-03		6.90E-03
160	1.290E + 06	7.75E-03		7.90E-03
152	1.227E + 06	8.15E-03	9.817E-01 [22]	6.23E-03 [22]
150	1.210E + 06	8.27E-03		9.10E-03 [7]
140	1.129E + 06	8.86E-03		1.05E-02
130	1.049E + 06	9.54E-03		1.20E-02
120	9.679E + 05	1.03E-02		1.39E-02
110	8.872E + 05	1.13E-02		1.60E-02
102	8.219E + 05	1.22E-02	9.611E-01 [22]	1.45E-02 [22]
100	8.065E + 05	1.24E-02		1.86E-02 [7]
95	7.662E + 05	1.31E-02		2.01E-02

(continued)

[a] The references from which the values were extracted are given in brackets.

TABLE II *(Continued)*

Titanium

eV	cm^{-1}	μm	n	k
90	7.259E + 05	1.38E-02		2.17E-02
85	6.856E + 05	1.46E-02		2.42E-02
80	6.452E + 05	1.55E-02		2.63E-02
75	6.049E + 05	1.65E-02		2.87E-02
74	5.968E + 05	1.68E-02		3.04E-02
72	5.807E + 05	1.72E-02		3.26E-02
70	5.646E + 05	1.77E-02		3.49E-02
68	5.485E + 05	1.82E-02		3.88E-02
66	5.323E + 05	1.88E-02		4.45E-02
64	5.162E + 05	1.94E-02		5.20E-02
62	5.001E + 05	2.00E-02		6.15E-02
60	4.839E + 05	2.07E-02		7.01E-02
55	4.436E + 05	2.25E-02		0.112
52	4.194E + 05	2.38E-02		0.151
50	4.033E + 05	2.48E-02		0.176
48	3.871E + 05	2.58E-02		0.194
46	3.710E + 05	2.70E-02		0.208
44	3.549E + 05	2.82E-02		0.209
42	3.388E + 05	2.95E-02		0.191
40	3.226E + 05	3.10E-02		0.164
38	3.065E + 05	3.26E-02		0.154
25	2.016E + 05	4.96E-02	0.991 [6]	0.151 [6]
24.50	1.976E + 05	5.06E-02	0.987	0.152
24.00	1.936E + 05	5.17E-02	0.982	0.153
23.50	1.895E + 05	5.28E-02	0.977	0.154
23.00	1.855E + 05	5.39E-02	0.972	0.154
22.50	1.815E + 05	5.51E-02	0.961	0.156
22.00	1.774E + 05	5.64E-02	0.951	0.158
21.50	1.734E + 05	5.77E-02	0.941	0.159
21.00	1.694E + 05	5.90E-02	0.936	0.160
20.50	1.653E + 05	6.05E-02	0.932	0.172
20.00	1.613E + 05	6.20E-02	0.930	0.188
19.50	1.573E + 05	6.36E-02	0.922	0.201
19.00	1.532E + 05	6.53E-02	0.920	0.217
18.50	1.492E + 05	6.70E-02	0.902	0.233
18.00	1.452E + 05	6.89E-02	0.891	0.253
17.50	1.411E + 05	7.08E-02	0.883	0.283
17.00	1.371E + 05	7.29E-02	0.882	0.312
16.50	1.331E + 05	7.51E-02	0.871	0.344
16.00	1.290E + 05	7.75E-02	0.852	0.382
15.50	1.250E + 05	8.00E-02	0.853	0.410
15.00	1.210E + 05	8.27E-02	0.860	0.436
14.50	1.169E + 05	8.55E-02	0.872	0.459
14.00	1.129E + 05	8.86E-02	0.892	0.505
13.50	1.089E + 05	9.18E-02	0.903	0.515
13.00	1.049E + 05	9.54E-02	0.912	0.521
12.50	1.008E + 05	9.92E-02	0.923	0.531

TABLE II *(Continued)*

Titanium

eV	cm^{-1}	μm	n	k
12.00	9.679E + 04	1.03E-01	0.932	0.537
11.50	9.275E + 04	1.08E-01	0.940	0.542
11.00	8.872E + 04	1.13E-01	0.951	0.552
10.50	8.469E + 04	1.18E-01	0.966	0.569
10.00	8.065E + 04	1.24E-01	0.993	0.604
9.50	7.662E + 04	1.31E-01	1.00 [2]	0.625 [2]
9.00	7.259E + 04	1.38E-01	1.01	0.645
8.50	6.856E + 04	1.46E-01	1.01	0.691
8.00	6.452E + 04	1.55E-01	1.02	0.763
7.50	6.049E + 04	1.65E-01	1.02	0.810
7.00	5.646E + 04	1.77E-01	1.03	0.873
6.50	5.243E + 04	1.91E-01	1.06	0.947
6.46	5.210E + 04	1.92E-01	1.07	1.11
6.36	5.130E + 04	1.95E-01	1.08	1.14
6.26	5.049E + 04	1.98E-01	1.09	1.16
6.20	5.001E + 04	2.00E-01	1.11	1.18
6.14	4.952E + 04	2.02E-01	1.12	1.19
6.08	4.904E + 04	2.04E-01	1.13	1.20
6.02	4.855E + 04	2.06E-01	1.15	1.21
5.90	4.759E + 04	2.10E-01	1.18	1.22
5.85	4.718E + 04	2.12E-01	1.19	1.22
5.79	4.670E + 04	2.14E-01	1.21	1.22
5.74	4.630E + 04	2.16E-01	1.22	1.22
5.69	4.589E + 04	2.18E-01	1.23	1.21
5.64	4.549E + 04	2.20E-01	1.23	1.21
5.59	4.509E + 04	2.22E-01	1.24	1.21
5.53	4.460E + 04	2.24E-01	1.24	1.20
5.49	4.428E + 04	2.26E-01	1.24	1.19
5.44	4.388E + 04	2.28E-01	1.23	1.19
5.39	4.347E + 04	2.30E-01	1.17	1.16
5.34	4.307E + 04	2.32E-01	1.18	1.41
5.30	4.275E + 04	2.34E-01	1.35	1.21
5.25	4.234E + 04	2.36E-01	1.28	1.20
5.21	4.202E + 04	2.38E-01	1.27	1.20
5.17	4.170E + 04	2.40E-01	1.25	1.20
5.12	4.130E + 04	2.42E-01	1.25	1.20
5.08	4.097E + 04	2.44E-01	1.24	1.21
5.00	4.033E + 04	2.48E-01	1.24	1.21
4.96	4.000E + 04	2.50E-01	1.23	1.21
4.92	3.968E + 04	2.52E-01	1.22	1.22
4.88	3.936E + 04	2.54E-01	1.22	1.22
4.84	3.904E + 04	2.56E-01	1.22	1.23
4.80	3.871E + 04	2.58E-01	1.21	1.23
4.77	3.847E + 04	2.60E-01	1.20	1.23
4.73	3.815E + 04	2.62E-01	1.19	1.24
4.66	3.759E + 04	2.66E-01	1.16	1.27

(continued)

TABLE II *(Continued)*

Titanium

eV	cm^{-1}	μm	n	k
4.66	3.759E + 04	2.66E-01	1.17	1.26
4.59	3.702E + 04	2.70E-01	1.17	1.29
4.56	3.678E + 04	2.72E-01	1.17	1.29
4.53	3.654E + 04	2.74E-01	1.16	1.30
4.49	3.621E + 04	2.76E-01	1.15	1.31
4.46	3.597E + 04	2.78E-01	1.14	1.32
4.43	3.573E + 04	2.80E-01	1.14	1.33
4.40	3.549E + 04	2.82E-01	1.13	1.33
4.36	3.517E + 04	2.84E-01	1.12	1.34
4.34	3.500E + 04	2.86E-01	1.11	1.36
4.30	3.468E + 04	2.88E-01	1.10	1.37
4.28	3.452E + 04	2.90E-01	1.09	1.38
4.25	3.428E + 04	2.92E-01	1.07	1.40
4.22	3.404E + 04	2.94E-01	1.06	1.42
4.19	3.379E + 04	2.96E-01	1.05	1.45
4.16	3.355E + 04	2.98E-01	1.05	1.47
4.13	3.331E + 04	3.00E-01	1.04	1.49
4.11	3.315E + 04	3.02E-01	1.04	1.52
4.08	3.291E + 04	3.04E-01	1.04	1.54
4.05	3.267E + 04	3.06E-01	1.03	1.57
4.03	3.250E + 04	3.08E-01	1.03	1.59
3.99	3.218E + 04	3.11E-01	1.04	1.62
3.97	3.202E + 04	3.12E-01	1.04	1.64
3.95	3.186E + 04	3.14E-01	1.04	1.67
3.92	3.162E + 04	3.16E-01	1.05	1.71
3.90	3.146E + 04	3.18E-01	1.06	1.73
3.87	3.121E + 04	3.20E-01	1.07	1.75
3.85	3.105E + 04	3.22E-01	1.08	1.78
3.80	3.065E + 04	3.26E-01	1.11	1.83
3.70	2.984E + 04	3.35E-01	1.17	1.90
3.60	2.904E + 04	3.44E-01	1.24	1.96
3.50	2.823E + 04	3.54E-01	1.30	2.01
3.40	2.742E + 04	3.65E-01	1.37	2.06
3.30	2.662E + 04	3.76E-01	1.44	2.09
3.20	2.581E + 04	3.87E-01	1.50	2.12
3.10	2.500E + 04	4.00E-01	1.55	2.15
3.00	2.420E + 04	4.13E-01	1.59	2.17
2.90	2.339E + 04	4.28E-01	1.63	2.21
2.80	2.258E + 04	4.43E-01	1.68	2.25
2.70	2.178E + 04	4.59E-01	1.71	2.29
2.60	2.097E + 04	4.77E-01	1.75	2.34
2.50	2.016E + 04	4.96E-01	1.78	2.39
2.40	1.936E + 04	5.17E-01	1.81	2.47
2.30	1.855E + 04	5.39E-01	1.86	2.56
2.20	1.774E + 04	5.64E-01	1.92	2.67
2.10	1.694E + 04	5.90E-01	2.01	2.77
2.00	1.613E + 04	6.20E-01	2.11	2.88

TABLE II *(Continued)*

Titanium

eV	cm^{-1}	μm	n	k
1.95	1.573E + 04	6.36E-01	2.16	2.93
1.90	1.532E + 04	6.53E-01	2.22	2.99
1.85	1.492E + 04	6.70E-01	2.29	3.05
1.80	1.452E + 04	6.89E-01	2.36	3.11
1.75	1.411E + 04	7.08E-01	2.44	3.17
1.70	1.371E + 04	7.29E-01	2.54	3.23
1.65	1.331E + 04	7.51E-01	2.65	3.24
1.60	1.290E + 04	7.75E-01	2.74	3.30
1.55	1.250E + 04	8.00E-01	2.87	3.33
1.50	1.210E + 04	8.27E-01	2.98	3.32
1.45	1.169E + 04	8.55E-01	3.08	3.31
1.40	1.129E + 04	8.86E-01	3.17	3.28
1.35	1.089E + 04	9.18E-01	3.23	3.26
1.30	1.049E + 04	9.54E-01	3.28	3.25
1.25	1.008E + 04	9.92E-01	3.31	3.26
1.20	9.679E + 03	1.03	3.35	3.30
1.15	9.275E + 03	1.08	3.40	3.35
1.10	8.872E + 03	1.13	3.47	3.40
1.05	8.469E + 03	1.18	3.54	3.46
1.00	8.065E + 03	1.24	3.62	3.52
0.98	7.904E + 03	1.27	3.65	3.55
0.96	7.743E + 03	1.29	3.69	3.57
0.94	7.582E + 03	1.32	3.73	3.60
0.92	7.420E + 03	1.35	3.77	3.62
0.90	7.259E + 03	1.38	3.80	3.65
0.88	7.098E + 03	1.41	3.85	3.69
0.86	6.936E + 03	1.44	3.93	3.73
0.84	6.775E + 03	1.48	3.94	3.65
0.82	6.614E + 03	1.51	3.94	3.80
0.80	6.452E + 03	1.55	4.04	3.82
0.78	6.291E + 03	1.59	4.11	3.85
0.76	6.130E + 03	1.63	4.18	3.87
0.74	5.968E + 03	1.68	4.25	3.88
0.72	5.807E + 03	1.72	4.32	3.89
0.70	5.646E + 03	1.77	4.38	3.89
0.68	5.485E + 03	1.82	4.44	3.90
0.66	5.323E + 03	1.88	4.52	3.90
0.64	5.162E + 03	1.94	4.60	3.88
0.62	5.001E + 03	2.00	4.66	3.83
0.60	4.839E + 03	2.07	4.71	3.77
0.58	4.678E + 03	2.14	4.74	3.71
0.56	4.517E + 03	2.21	4.75	3.62
0.54	4.355E + 03	2.30	4.73	3.50
0.52	4.194E + 03	2.38	4.62	3.35
0.50	4.033E + 03	2.48	4.43	3.22
0.49	3.952E + 03	2.53	4.29	3.15

(continued)

TABLE II *(Continued)*

Titanium

eV	cm^{-1}	μm	n	k
0.48	3.871E + 03	2.58	4.11	3.10
0.47	3.791E + 03	2.64	3.89	3.08
0.46	3.710E + 03	2.70	3.62	3.12
0.45	3.629E + 03	2.76	3.35	3.25
0.44	3.549E + 03	2.82	3.10	3.44
0.43	3.468E + 03	2.88	2.88	3.68
0.42	3.388E + 03	2.95	2.69	3.98
0.41	3.307E + 03	3.02	2.56	4.32
0.40	3.226E + 03	3.10	2.49	4.68
0.39	3.146E + 03	3.18	2.48	5.02
0.38	3.065E + 03	3.26	2.52	5.35
0.37	2.984E + 03	3.35	2.59	5.65
0.36	2.904E + 03	3.44	2.67	5.93
0.35	2.823E + 03	3.54	2.74	6.21
0.34	2.742E + 03	3.65	2.82	6.52
0.33	2.662E + 03	3.76	2.95	6.88
0.32	2.581E + 03	3.87	3.17	7.29
0.31	2.500E + 03	4.00	3.60	7.87
0.30	2.420E + 03	4.13	6.39	9.94
0.29	2.339E + 03	4.28	4.15	3.06
0.28	2.258E + 03	4.43	1.43	5.65
0.27	2.178E + 03	4.59	2.00	6.98
0.26	2.097E + 03	4.77	2.08	7.56
0.25	2.016E + 03	4.96	2.05	8.10
0.24	1.936E + 03	5.17	2.01	8.66
0.23	1.855E + 03	5.39	1.98	9.27
0.22	1.774E + 03	5.64	2.00	9.92
0.21	1.694E + 03	5.90	2.04	10.61
0.20	1.613E + 03	6.20	2.12	11.34
0.19	1.532E + 03	6.53	2.23	12.12
0.18	1.452E + 03	6.89	2.41	12.94
0.17	1.371E + 03	7.29	2.60	13.79
0.16	1.290E + 03	7.75	2.81	14.70
0.15	1.210E + 03	8.27	3.00	15.72
0.14	1.129E + 03	8.86	3.22	16.87
0.13	1.049E + 03	9.54	3.49	18.23
0.12	9.679E + 02	10.3	3.90	19.79
0.11	8.872E + 02	11.3	4.48	21.45
0.0992	8.000E + 02	12.5	5.2 [4]	24.40 [4]
0.0868	7.000E + 02	14.3	6.24	27.60
0.0744	6.000E + 02	16.7	7.58	31.80
0.0620	5.000E + 02	20.0	9.67	37.60
0.0558	4.500E + 02	22.2	11.20	41.30
0.0496	4.000E + 02	25.0	13.30	45.80
0.0434	3.500E + 02	28.6	16.30	51.50
0.0372	3.000E + 02	33.3	20.90	58.00
0.0310	2.500E + 02	40.0	27.20	65.90

TABLE II *(Continued)*

Titanium

eV	cm^{-1}	μm	n	k
0.0279	2.250E + 02	44.4	31.30	70.60
0.0248	2.000E + 02	50.0	36.20	75.80
0.0217	1.750E + 02	57.1	42.30	81.80
0.0186	1.500E + 02	66.7	49.90	88.90
0.0155	1.250E + 02	80.0	59.64	97.50
0.0124	1.000E + 02	100	72.50	108.40
0.0099	8.000E + 01	125	86.40	120.00
0.0081	6.500E + 01	154	100.50	131.90
0.0062	5.000E + 01	200	120.00	148.40

MANGANESE (Mn) IV

α-Mn has a complex unit cell, but the lattice is body-centered cubic. α-Mn, therefore, is optically isotropic. There is another cubic phase and a tetragonal phase at high temperature. Mn is quite reactive with oxygen, and this has an effect on all measurements at energies above a few electron volts. Not only does one expect a surface oxide on any film in air, but, as discussed by Atkinson [1], Mn films often contain MnO unless prepared in ultrahigh vacuum. Optical studies have not been carried out on such films.

Mn is a transition metal. The incompletely filled $3d$ bands can give rise to interband optical absorption at arbitrarily small energies. This means that reliable fits of optical data to a Drude-model dielectric function cannot be made, except below some unknown low energy.

With the exception of the work of Lenham and Treherne [2], all optical studies on Mn have been made on thin or thick films. All have possible effects from an oxide. The only infrared data are from Lenham and Treherne [2], obtained by ellipsometry on mechanically polished surfaces of bulk specimens that were not etched after polishing, and from Fouad and Amar [3], obtained on films. The latter match up well with the data of Johnson and Christy [4], taken in the 1–6-eV range on thin films. We present data in Table III and Fig. 3 from both these sources, and the soft x-ray absorption measurements of Sonntag *et al.* [5]. The latter were measurements of the absorption coefficient, converted to a spectrum of the imaginary part of the refractive index with the assumption that the real part was unity. There is a gap between these measurements and the data of Christy *et al.* [4]. In addition, there have been measurements by Steel [6] and Aagard [7].

Data in the soft x-ray region, from approximately 10^{-4} to 0.024 μm, are

taken from Henke *et al.* [8], and the location of the soft x-ray edges, shown by the short, vertical lines in Fig. 3, are taken from Siegbahn *et al.* [9].

REFERENCES

1. R. Atkinson, *Thin Solid Films* **37**, 195 (1976).
2. A. P. Lenham and D. M. Treherne, *J. Opt. Soc. Am.* **56**, 1137 (1966).
3. S. S. Fouad and A. H. Amar, *Physica B* **205**, 285 (1995).
4. P. B. Johnson and R. W. Christy, *Phys. Rev. B* **9**, 5056 (1974).
5. B. Sonntag, R. Haensel, and C. Kunz, *Solid State Commun.* **7**, 597 (1969).
6. M. R. Steel, *J. Phys. F: Metal Phys.* **4**, 873 (1974).
7. R. L. Aagard, *J. Opt. Soc. Am.* **64**, 1456 (1976).
8. B. L. Henke, J. C. Davis, E. M. Gullikson, and R. C. C. Perera, "A Preliminary Report on X-Ray Photoabsorption Coefficients and Atomic Scattering Factors for 92 Elements in the 10–10,000 eV Region," Lawrence Berkeley Lab. Rep. LBL-26259, University of California, Berkeley, California, 1988.
9. K. Siegbahn, C. Nordling, A. Fahlman, R. Nordberg, K. Hamrin, J. Hedman, G. Johansson, T. Bergmark, S.-E. Karlsson, I. Lindgren, and B. Lindberg, "ESCA Atomic, Molecular, and Solid State Structure Studied by Means of Electron Spectroscopy." Almquist & Wiksell, Uppsala, Sweden, 1967.

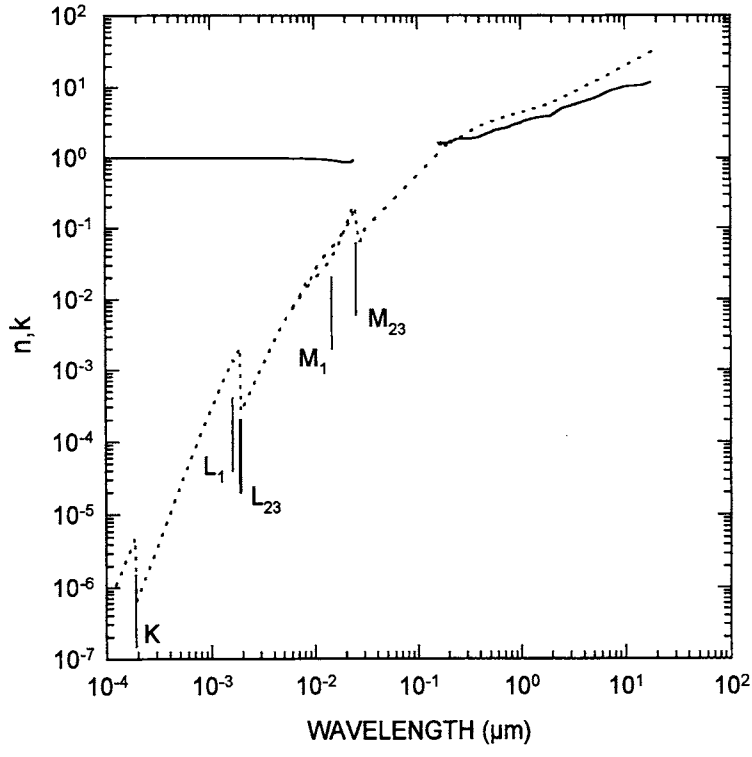

Fig. 3. Log–log plot of n (——) and k (- - - -) versus wavelength in micrometers for manganese.

TABLE III

Values of n and k Obtained from Various References for Manganese[a]

eV	cm^{-1}	μm	n	k
10000.	8.066E + 07	1.24E-04	9.999862E-01 [8]	1.09E-06 [8]
9117.	7.353E + 07	1.36E-04	9.999834E-01	1.54E-06
8123.	6.551E + 07	1.53E-04	9.999795E-01	2.33E-06
7237.	5.837E + 07	1.71E-04	9.999751E-01	3.52E-06
6752.	5.446E + 07	1.84E-04	9.999732E-01	4.48E-06
6598.	5.321E + 07	1.88E-04	9.999737E-01	4.85E-06
6447.	5.200E + 07	1.92E-04	9.999723E-01	6.54E-07
6300.	5.081E + 07	1.97E-04	9.999694E-01	7.11E-07
6156.	4.965E + 07	2.01E-04	9.999673E-01	7.74E-07
5117.	4.127E + 07	2.42E-04	9.999503E-01	1.53E-06
4061.	3.276E + 07	3.05E-04	9.999193E-01	3.63E-06
3299.	2.661E + 07	3.76E-04	9.99876E-01	7.90E-06
2227.	1.797E + 07	5.57E-04	9.99723E-01	3.41E-05
1768.	1.426E + 07	7.01E-04	9.99560E-01	7.92E-05
1539.	1.241E + 07	8.06E-04	9.99423E-01	1.30E-04
1309.	1.056E + 07	9.47E-04	9.99217E-01	2.28E-04
806.	6.501E + 06	1.54E-03	9.9845E-01	1.18E-03
686.	5.530E + 06	1.81E-03	9.9865E-01	1.79E-03
670.	5.404E + 06	1.85E-03	9.9886E-01	1.93E-03
655.	5.281E + 06	1.89E-03	9.9927E-01	2.08E-03
640.	5.160E + 06	1.94E-03	1.00384	2.59E-04
625.	5.042E + 06	1.98E-03	9.9931E-01	2.78E-04
611.	4.927E + 06	2.03E-03	9.9885E-01	2.98E-04
485.	3.911E + 06	2.56E-03	9.9677E-01	6.08E-04
403.	3.251E + 06	3.08E-03	9.9500E-01	1.10E-03
313.	2.521E + 06	3.97E-03	9.9158E-01	2.37E-03
237.	1.911E + 06	5.23E-03	9.863E-01	5.24E-03
232.	1.867E + 06	5.36E-03	9.857E-01	5.52E-03
200.	1.613E + 06	6.20E-03		7.80E-03 [5]
190.	1.532E + 06	6.53E-03		8.80E-03
180.	1.371E + 06	7.29E-03		1.15E-02
175.	1.415E + 06	7.07E-03	9.775E-01 [8]	1.01E-02 [8]
160.	1.290E + 06	7.75E-03		1.38E-02 [5]
150.	1.210E + 06	8.27E-03		1.70E-02
140.	1.129E + 06	8.86E-03		1.63E-02
136.	1.098E + 06	9.11E-03	9.668E-01 [8]	1.67E-02 [8]
130.	1.049E + 06	9.54E-03		2.18E-02 [5]
120.	9.679E + 05	1.03E-02		2.69E-02
111.	8.915E + 05	1.12E-02	9.531E-01 [8]	2.30E-02 [8]
110.	8.872E + 05	1.13E-02		3.20E-02 [5]
100.	8.065E + 05	1.24E-02		3.96E-02
98.5	7.942E + 05	1.26E-02	9.418E-01 [8]	2.75E-02 [8]
95.	7.662E + 05	1.31E-02		4.32E-02 [5]
90.	7.259E + 05	1.38E-02		4.67E-02
85.	6.856E + 05	1.46E-02		5.18E-02

(continued)

[a] The references from which the values were extracted are given in brackets.

TABLE III *(Continued)*

Manganese

eV	cm^{-1}	μm	n	k
83.8	6.756E + 05	1.48E-02	9.195E-01 [8]	3.95E-02 [8]
80.	6.452E + 05	1.55E-02		5.75E-02 [5]
75.	6.049E + 05	1.65E-02		6.39E-02
72.9	5.882E + 05	1.70E-02	0.894 [8]	5.72E-02 [8]
70.	5.646E + 05	1.77E-02		7.40E-02 [5]
65.	5.243E + 05	1.91E-02		9.03E-02
62.	5.004E + 05	2.00E-02	0.864 [8]	0.101 [8]
60.	4.839E + 05	2.07E-02		1.08E-01 [5]
58.	4.678E + 05	2.14E-02		1.16E-01
56.	4.517E + 05	2.21E-02		1.26E-01
55.3	4.458E + 05	2.24E-02	0.864 [8]	0.16 [8]
54.	4.355E + 05	2.30E-02		1.41E-01 [5]
52.	4.194E + 05	2.38E-02		1.67E-01
51.6	4.159E + 05	2.40E-02	0.927 [8]	0.188 [8]
50.	4.033E + 05	2.48E-02		1.96E-01 [5]
48.	3.871E + 05	2.58E-02		1.02E-01
46.	3.710E + 05	2.70E-02		6.38E-02
44.	3.549E + 05	2.82E-02		6.67E-02
42.	3.388E + 05	2.95E-02		8.38E-02
40.	3.226E + 05	3.10E-02		9.78E-02
6.6	5.323E + 04	1.88E-01	1.48 [4]	1.47 [4]
6.47	5.218E + 04	1.92E-01	1.55	1.5
6.35	5.122E + 04	1.95E-01	1.59	1.52
6.22	5.017E + 04	1.62E-01	1.62	1.55
6.1	4.920E + 04	2.03E-01	1.63	1.58
5.98	4.823E + 04	2.07E-01	1.67	1.61
5.85	4.718E + 04	2.12E-01	1.7	1.64
5.73	4.622E + 04	2.16E-01	1.72	1.67
5.6	4.517E + 04	2.21E-01	1.73	1.7
5.48	4.420E + 04	2.26E-01	1.74	1.73
5.36	4.323E + 04	2.31E-01	1.78	1.76
5.23	4.218E + 04	2.37E-01	1.81	1.79
5.11	4.121E + 04	2.43E-01	1.82	1.82
4.98	4.017E + 04	2.49E-01	1.82	1.86
4.86	3.920E + 04	2.55E-01	1.83	1.91
4.74	3.823E + 04	2.62E-01	1.84	1.94
4.61	3.718E + 04	2.69E-01	1.85	1.99
4.49	3.621E + 04	2.76E-01	1.86	2.03
4.36	3.517E + 04	2.84E-01	1.85	2.08
4.24	3.420E + 04	2.92E-01	1.85	2.14
4.12	3.323E + 04	3.01E-01	1.86	2.19
3.99	3.218E + 04	3.11E-01	1.86	2.25
3.87	3.121E + 04	3.20E-01	1.86	2.32
3.74	3.016E + 04	3.32E-01	1.86	2.38
3.62	2.920E + 04	3.43E-01	1.87	2.45
3.5	2.823E + 04	3.54E-01	1.89	2.51
3.37	2.718E + 04	3.68E-01	1.89	2.59

TABLE III *(Continued)*

Manganese

eV	cm^{-1}	μm	n	k
3.25	2.612E + 04	3.81E-01	1.92	2.67
3.12	2.516E + 04	3.97E-01	1.96	2.74
3.	2.420E + 04	4.13E-01	2.0	2.82
2.88	2.323E + 04	4.31E-01	2.06	2.9
2.75	2.218E + 04	4.51E-01	2.11	2.98
2.63	2.121E + 04	4.71E-01	2.19	3.06
2.5	2.016E + 04	4.96E-01	2.25	3.14
2.38	1.920E + 04	5.21E-01	2.32	3.23
2.26	1.823E + 04	5.49E-01	2.39	3.33
2.13	1.718E + 04	5.82E-01	2.47	3.43
2.01	1.621E + 04	6.17E-01	2.51	3.54
1.88	1.516E + 04	6.59E-01	2.56	3.65
1.76	1.420E + 04	7.04E-01	2.62	3.78
1.64	1.323E + 04	7.56E-01	2.7	3.91
1.51	1.218E + 04	8.21E-01	2.83	4.03
1.39	1.121E + 04	8.92E-01	2.97	4.18
1.26	1.016E + 04	9.84E-01	3.1	4.35
1.14	9.195E + 03	1.09	3.3	4.53
1.02	8.227E + 03	1.22	3.48	4.74
0.89	7.178E + 03	1.39	3.65	5.02
0.77	6.210E + 03	1.61	3.78	5.41
0.64	5.162E + 03	1.94	3.89	5.95
0.496	4.000E + 03	2.50	5.0 [3]	7.1 [3]
0.248	2.000E + 03	5.00	7.0	11.8
0.165	1.331E + 03	7.51	9.0	16.0
0.124	1.000E + 03	10.	10.3	20.7
0.099	7.985E + 02	12.5	10.5	24.0
0.083	6.694E + 02	14.9	10.8	28.0
0.071	5.726E + 02	17.5	11.7	31.5
0.062	5.001E + 02	20.		35.7

RUTHENIUM (Ru) V

Ruthenium is a hexagonal close-packed metal. In single-crystal form it is optically anisotropic, uniaxial, with two independent components in the dielectric tensor, one for the electric field parallel to the *c*-axis and one for the perpendicular orientation. Polycrystalline films may have a texture, growing with the closest-packed plane, the basal plane, in the plane of the film, but with randomly oriented *a*-axes. If so, the film will be optically anisotropic. If there is truly random orientation, the film is isotropic with a complex dielectric function $\epsilon = (\epsilon_{\parallel} + 2\epsilon_{\perp})/3$.

Ru is a transition metal. The incompletely filled 4*d* bands can give rise to interband optical absorption at arbitrarily small energies. This means that reliable fits of optical data to a Drude-model dielectric function cannot be made, except below some unknown low energy.

Reliable optical data over a wide spectral range do not exist for polycrystalline bulk samples or thin films of Ru. Therefore, we have chosen to use data taken from the basal plane of a single crystal ($\mathbf{E}\perp\mathbf{c}$) by Weaver *et al.* [1, 2]. These data are from a Kramers–Kronig inversion of absorptance and reflectance data. Where there is overlap of spectral regions, there is good agreement with the data of Kirillova *et al.* [3] obtained by ellipsometry, and with Cox *et al.* [4] from reflectance measurements on films taken at several angles of incidence. Additional measurements have been made by Kress and Lapeyre [5], and by Carroll and Melmed [6].

Data in the soft x-ray region, from approximately 10^{-4} to 0.024 μm, are taken from Henke *et al.* [7], and the location of the soft x-ray edges, shown by the short, vertical lines in Fig. 4, are taken from Siegbahn *et al.* [8]. In order to fill the small gap between the data of Henke *et al.* [7] and Weaver *et al.* [1, 2], we have incorporated some of the data of Cox *et al.* [4].

REFERENCES

1. J. H. Weaver, C. G. Olson, and D. W. Lynch, unpublished, 1981.
2. J. H. Weaver, C. Krafka, D. W. Lynch, and E.-E. Koch, Physics Data, Optical Properties of Metals, Part I: the Transition Metals, Fachinformationszentrum Karlsruhe, 7514 Eggenstein-Leopoldshafen 2, Germany, 1981.
3. M. M. Kirillova, L. V. Nomerovannaya, M. M. Noskov, N. B. Gorina, V. P. Polyakova, and E. M. Savitskii, *Fiz. Tverd. Tela (Leningrad)* **20**, 1718 (1978); *Sov. Phys. Solid State* **20**, 994 (1978).
4. J. T. Cox, G. Hass, J. B. Ramsey, and W. R. Hunter, *J. Opt. Soc. Am.* **64**, 423 (1974).
5. K. A. Kress and G. J. Lapeyre, *Phys. Rev. B* **2**, 2532 (1970).
6. J. J. Carroll and A. J. Melmed, *J. Opt. Soc. Am.* **66**, 1050 (1976).
7. B. L. Henke, J. C. Davis, E. M. Gullikson, and R. C. C. Perera, "A Preliminary Report on X-Ray Photoabsorption Coefficients and Atomic Scattering Factors for 92 Elements in the 10–10,000 eV Region," Lawrence Berkeley Lab. Rep. LBL-26259, University of California, Berkeley, California, 1988.
8. K. Siegbahn, C. Nordling, A. Fahlman, R. Nordberg, K. Hamrin, J. Hedman, G. Johansson, T. Bergmark, S.-E. Karlsson, I. Lindgren, and B. Lindberg, "ESCA Atomic, Molecular, and Solid State Structure Studied by Means of Electron Spectroscopy." Almquist & Wiksell, Uppsala, Sweden, 1967.

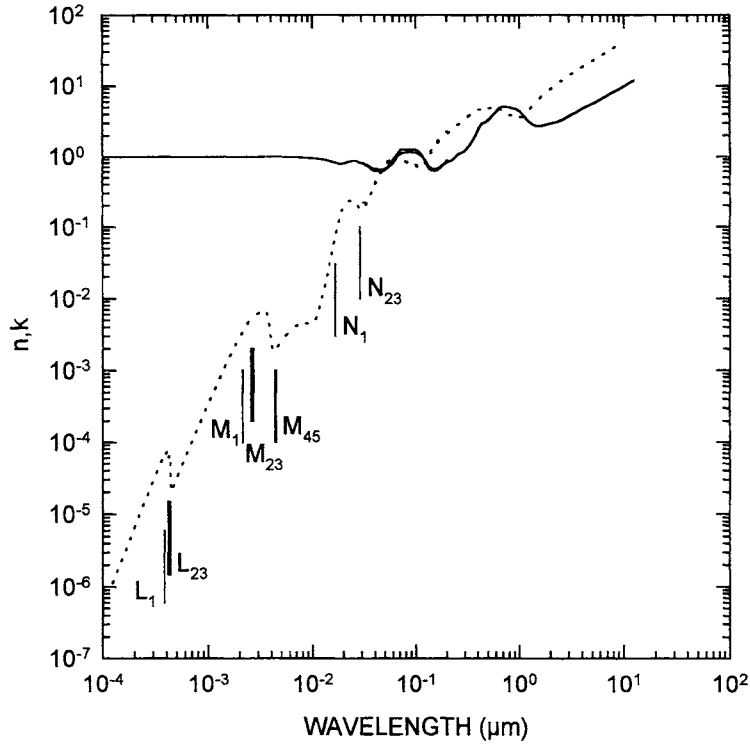

Fig. 4. Log–log plot of n (——) and k (- - - -) versus wavelength in micrometers for ruthenium.

TABLE IV

Values of n and k Obtained from Various References for Ruthenium[a]

eV	cm^{-1}	μm	n	k
10000.	8.066E + 07	1.24E-04	9.999778E-01 [7]	1.14E-06 [7]
9117.	7.353E + 07	1.36E-04	9.999731E-01	1.61E-06
8123.	6.551E + 07	1.53E-04	9.999660E-01	2.48E-06
7072.	5.704E + 07	1.73E-04	9.999550E-01	4.16E-06
6015.	4.852E + 07	2.06E-04	9.999379E-01	7.55E-06
5000.	4.033E + 07	2.48E-04	9.999111E-01	1.48E-05
4062.	3.276E + 07	3.05E-04	9.999870E-01	3.11E-05
3376.	2.723E + 07	3.67E-04	9.99830E-01	5.89E-05
3299.	2.661E + 07	3.76E-04	9.99827E-01	6.37E-05
3224.	2.600E + 07	3.85E-04	9.99828E-01	6.11E-05
3150.	2.541E + 07	3.94E-04	9.99820E-01	6.61E-05
3078.	2.483E + 07	4.03E-04	9.99817E-01	7.16E-05
3008.	2.426E + 07	4.12E-04	9.99821E-01	7.75E-05
2939.	2.371E + 07	4.21E-04	9.99825E-01	6.12E-05
2872.	2.317E + 07	4.32E-04	9.99822E-01	6.63E-05
2806.	2.264E + 07	4.42E-04	9.99825E-01	2.09E-05
2742.	2.212E + 07	4.52E-04	9.99786E-01	2.26E-05
2031.	1.638E + 07	6.10E-04	9.99538E-01	6.42E-05
1809.	1.459E + 07	6.85E-04	9.99410E-01	9.61E-05
1650.	1.330E + 07	7.52E-04	9.99286E-01	1.33E-04
1504.	1.213E + 07	8.24E-04	9.99139E-01	1.83E-04
1371.	1.106E + 07	9.04E-04	9.9897E-01	2.49E-04
1222.	9.854E + 06	1.01E-03	9.9871E-01	3.64E-04
1016.	8.191E + 06	1.22E-03	9.9817E-01	6.70E-04
825.	6.653E + 06	1.50E-03	9.9740E-01	1.29E-03
702.	5.660E + 06	1.77E-03	9.9672E-01	2.12E-03
611.	4.927E + 06	2.03E-03	9.9627E-01	3.11E-03
597.	4.814E + 06	2.08E-03	9.9620E-01	3.28E-03
583.	4.705E + 06	2.12E-03	9.9612E-01	3.46E-03
570.	4.597E + 06	2.18E-03	9.9604E-01	3.66E-03
557.	4.492E + 06	2.23E-03	9.9597E-01	3.90E-03
508.	4.096E + 06	2.44E-03	9.9611E-01	4.79E-03
496.	4.002E + 06	2.50E-03	9.9614E-01	4.94E-03
485.	3.911E + 06	2.56E-03	9.9617E-01	5.09E-03
474.	3.821E + 06	2.62E-03	9.9620E-01	5.23E-03
463.	3.734E + 06	2.68E-03	9.9620E-01	5.37E-03
452.	3.649E + 06	2.74E-03	9.9618E-01	5.53E-03
442.	3.565E + 06	2.80E-03	9.9619E-01	5.74E-03
327.	2.640E + 06	3.79E-03	9.9922E-01	4.60E-03
298.	2.407E + 06	4.15E-03	9.9584E-01	1.82E-03
292.	2.352E + 06	4.25E-03	9.9492E-01	1.90E-03
285.	2.299E + 06	4.35E-03	9.9416E-01	1.97E-03
278.	2.246E + 06	4.45E-03	9.9346E-01	2.04E-03
272.	2.195E + 06	4.56E-03	9.9277E-01	2.13E-03
266.	2.145E + 06	4.66E-03	9.9209E-01	2.24E-03
197.	1.588E + 06	6.30E-03	9.824E-01	3.79E-03

[a] The references from which the values were extracted are given in brackets.

TABLE IV *(Continued)*

Ruthenium

eV	cm^{-1}	μm	n	k
149.	1.204E + 06	8.31E-03	9.672E-01	4.57E-03
101.	8.127E + 05	1.23E-02	9.100E-01	1.02E-02
81.9	6.602E + 05	1.51E-02	0.844	4.02E-02
80.0	6.451E + 05	1.55E-02	0.835	4.78E-02
78.2	6.304E + 05	1.59E-02	0.827	5.68E-02
76.4	6.160E + 05	1.62E-02	0.820	6.59E-02
74.6	6.019E + 05	1.66E-02	0.812	7.53E-02
72.9	5.882E + 05	1.70E-02	0.805	8.60E-02
60.6	4.889E + 05	2.04E-02	0.808	2.05E-01
52.8	4.256E + 05	2.35E-02	0.853	2.35E-01
50.6	4.082E + 05	2.45E-02	0.865 [4]	0.233 [4]
49.6	4.000E + 05	2.50E-02	0.868	0.231
48.6	3.922E + 05	2.55E-02	0.868	0.228
47.7	3.846E + 05	2.60E-02	0.866	0.223
46.8	3.774E + 05	2.65E-02	0.860	0.215
45.9	3.704E + 05	2.70E-02	0.850	0.207
45.1	3.636E + 05	2.75E-02	0.835	0.197
44.3	3.571E + 05	2.80E-02	0.822	0.186
43.5	3.509E + 05	2.85E-02	0.815	0.177
42.8	3.448E + 05	2.90E-02	0.809	0.172
42.0	3.390E + 05	2.95E-02	0.804	0.168
41.3	3.333E + 05	3.00E-02	0.801	0.171
40.0	3.226E + 05	3.10E-02	0.787	0.183
40.0	3.226E + 05	3.10E-02	0.79 [1, 2]	0.22 [1, 2]
39.0	3.146E + 05	3.18E-02	0.77	0.22
38.7	3.125E + 05	3.20E-02	0.774 [4]	0.195 [4]
38.0	3.065E + 05	3.26E-02	0.75 [1, 2]	0.22 [1, 2]
37.6	3.030E + 05	3.30E-02	0.759 [4]	0.208 [4]
37.0	2.984E + 05	3.35E-02	0.73 [1, 2]	0.23 [1, 2]
36.0	2.904E + 05	3.44E-02	0.72	0.25
35.0	2.823E + 05	3.54E-02	0.70	0.26
34.5	2.783E + 05	3.59E-02	0.68	0.27
34.0	2.742E + 05	3.65E-02	0.67	0.28
33.5	2.702E + 05	3.70E-02	0.66	0.30
33.0	2.662E + 05	3.76E-02	0.65	0.31
32.5	2.621E + 05	3.81E-02	0.64	0.32
32.0	2.581E + 05	3.87E-02	0.63	0.34
31.5	2.541E + 05	3.94E-02	0.62	0.37
31.0	2.500E + 05	4.00E-02	0.61	0.40
30.5	2.460E + 05	4.07E-02	0.61	0.43
30.0	2.420E + 05	4.13E-02	0.62	0.45
29.5	2.379E + 05	4.20E-02	0.62	0.46
29.0	2.339E + 05	4.28E-02	0.61	0.48
28.5	2.299E + 05	4.35E-02	0.61	0.50
28.0	2.258E + 05	4.43E-02	0.60	0.53
27.5	2.218E + 05	4.51E-02	0.60	0.56

(continued)

TABLE IV *(Continued)*

Ruthenium

eV	cm^{-1}	μm	n	k
27.0	2.178E + 05	4.59E-02	0.60	0.59
26.5	2.137E + 05	4.68E-02	0.60	0.63
26.0	2.097E + 05	4.77E-02	0.61	0.66
25.5	2.057E + 05	4.86E-02	0.62	0.69
25.0	2.016E + 05	4.96E-02	0.64	0.73
24.5	1.976E + 05	5.06E-02	0.65	0.76
24.0	1.936E + 05	5.17E-02	0.67	0.79
23.5	1.895E + 05	5.28E-02	0.68	0.83
23.0	1.855E + 05	5.39E-02	0.71	0.87
22.5	1.815E + 05	5.51E-02	0.74	0.90
22.0	1.774E + 05	5.64E-02	0.77	0.94
21.8	1.754E + 05	5.70E-02	0.79	0.95
21.5	1.734E + 05	5.77E-02	0.80	0.97
21.3	1.714E + 05	5.83E-02	0.82	0.99
21.0	1.694E + 05	5.90E-02	0.85	1.01
20.8	1.674E + 05	5.98E-02	0.88	1.02
20.5	1.653E + 05	6.05E-02	0.91	1.03
20.3	1.633E + 05	6.12E-02	0.94	1.04
20.0	1.613E + 05	6.20E-02	0.97	1.04
19.8	1.593E + 05	6.28E-02	0.99	1.04
19.5	1.573E + 05	6.36E-02	1.02	1.04
19.3	1.553E + 05	6.44E-02	1.04	1.05
19.0	1.532E + 05	6.53E-02	1.07	1.05
18.8	1.512E + 05	6.61E-02	1.09	1.05
18.5	1.492E + 05	6.70E-02	1.12	1.05
18.3	1.472E + 05	6.79E-02	1.15	1.05
18.0	1.452E + 05	6.89E-02	1.19	1.04
17.8	1.432E + 05	6.99E-02	1.22	1.02
17.5	1.411E + 05	7.08E-02	1.25	1.00
17.3	1.391E + 05	7.19E-02	1.27	0.97
17.0	1.371E + 05	7.29E-02	1.28	0.94
16.8	1.351E + 05	7.40E-02	1.28	0.91
16.5	1.331E + 05	7.51E-02	1.28	0.89
16.3	1.311E + 05	7.63E-02	1.28	0.87
16.0	1.290E + 05	7.75E-02	1.27	0.85
15.8	1.274E + 05	7.85E-02	1.26	0.85
15.6	1.258E + 05	7.95E-02	1.25	0.85
15.4	1.242E + 05	8.05E-02	1.25	0.84
15.2	1.226E + 05	8.16E-02	1.25	0.84
15.0	1.210E + 05	8.27E-02	1.25	0.84
14.8	1.194E + 05	8.38E-02	1.25	0.84
14.6	1.178E + 05	8.49E-02	1.25	0.84
14.4	1.161E + 05	8.61E-02	1.25	0.84
14.2	1.145E + 05	8.73E-02	1.25	0.84
14.0	1.129E + 05	8.86E-02	1.26	0.84
13.8	1.113E + 05	8.98E-02	1.26	0.83
13.6	1.097E + 05	9.12E-02	1.27	0.83

TABLE IV *(Continued)*

Ruthenium

eV	cm^{-1}	μm	n	k
13.4	1.081E + 05	9.25E-02	1.27	0.82
13.2	1.065E + 05	9.39E-02	1.27	0.81
13.0	1.049E + 05	9.54E-02	1.27	0.79
12.8	1.032E + 05	9.69E-02	1.26	0.78
12.6	1.016E + 05	9.84E-02	1.25	0.77
12.4	1.000E + 05	1.00E-01	1.25	0.76
12.2	9.840E + 04	1.02E-01	1.24	0.75
12.0	9.679E + 04	1.03E-01	1.22	0.73
11.8	9.517E + 04	1.05E-01	1.20	0.72
11.6	9.356E + 04	1.07E-01	1.17	0.71
11.4	9.195E + 04	1.09E-01	1.14	0.70
11.2	9.033E + 04	1.11E-01	1.11	0.70
11.0	8.872E + 04	1.13E-01	1.08	0.70
10.8	8.711E + 04	1.15E-01	1.04	0.71
10.6	8.549E + 04	1.17E-01	0.99	0.72
10.4	8.388E + 04	1.19E-01	0.94	0.74
10.2	8.227E + 04	1.22E-01	0.90	0.77
10.0	8.065E + 04	1.24E-01	0.86	0.81
9.8	7.904E + 04	1.27E-01	0.82	0.84
9.6	7.743E + 04	1.29E-01	0.77	0.89
9.4	7.582E + 04	1.32E-01	0.73	0.95
9.2	7.420E + 04	1.35E-01	0.70	1.02
9.0	7.259E + 04	1.38E-01	0.69	1.09
8.8	7.098E + 04	1.41E-01	0.68	1.15
8.6	6.936E + 04	1.44E-01	0.66	1.22
8.4	6.775E + 04	1.48E-01	0.66	1.29
8.2	6.614E + 04	1.51E-01	0.65	1.36
8.0	6.452E + 04	1.55E-01	0.66	1.44
7.8	6.291E + 04	1.59E-01	0.66	1.51
7.6	6.130E + 04	1.63E-01	0.67	1.59
7.4	5.968E + 04	1.68E-01	0.68	1.67
7.2	5.807E + 04	1.72E-01	0.70	1.75
7.0	5.646E + 04	1.77E-01	0.73	1.82
6.8	5.485E + 04	1.82E-01	0.76	1.89
6.6	5.323E + 04	1.88E-01	0.78	1.97
6.4	5.162E + 04	1.94E-01	0.81	2.04
6.2	5.001E + 04	2.00E-01	0.82	2.11
6.0	4.839E + 04	2.07E-01	0.84	2.20
5.9	4.759E + 04	2.10E-01	0.85	2.24
5.8	4.678E + 04	2.14E-01	0.86	2.29
5.7	4.597E + 04	2.18E-01	0.87	2.34
5.6	4.517E + 04	2.21E-01	0.88	2.40
5.5	4.436E + 04	2.25E-01	0.90	2.45
5.4	4.355E + 04	2.30E-01	0.91	2.52
5.3	4.275E + 04	2.34E-01	0.94	2.58
5.2	4.194E + 04	2.38E-01	0.97	2.64

(continued)

TABLE IV *(Continued)*

Ruthenium

eV	cm^{-1}	μm	n	k
5.1	4.113E + 04	2.43E-01	1.00	2.70
5.0	4.033E + 04	2.48E-01	1.03	2.75
4.9	3.952E + 04	2.53E-01	1.06	2.81
4.8	3.871E + 04	2.58E-01	1.09	2.86
4.7	3.791E + 04	2.64E-01	1.11	2.91
4.6	3.710E + 04	2.70E-01	1.13	2.97
4.5	3.629E + 04	2.76E-01	1.14	3.04
4.4	3.549E + 04	2.82E-01	1.16	3.13
4.3	3.468E + 04	2.88E-01	1.18	3.21
4.2	3.388E + 04	2.95E-01	1.21	3.31
4.1	3.307E + 04	3.02E-01	1.25	3.42
4.0	3.226E + 04	3.10E-01	1.29	3.53
3.9	3.146E + 04	3.18E-01	1.35	3.64
3.8	3.065E + 04	3.26E-01	1.41	3.77
3.7	2.984E + 04	3.35E-01	1.50	3.90
3.6	2.904E + 04	3.44E-01	1.60	4.03
3.5	2.823E + 04	3.54E-01	1.71	4.16
3.4	2.742E + 04	3.65E-01	1.84	4.30
3.3	2.662E + 04	3.76E-01	2.00	4.43
3.2	2.581E + 04	3.87E-01	2.18	4.55
3.1	2.500E + 04	4.00E-01	2.40	4.64
3.0	2.420E + 04	4.13E-01	2.64	4.69
2.9	2.339E + 04	4.28E-01	2.87	4.64
2.8	2.258E + 04	4.43E-01	2.99	4.59
2.7	2.178E + 04	4.59E-01	3.06	4.59
2.6	2.097E + 04	4.77E-01	3.14	4.66
2.5	2.016E + 04	4.96E-01	3.27	4.77
2.4	1.936E + 04	5.17E-01	3.44	4.88
2.4	1.895E + 04	5.28E-01	3.56	4.94
2.3	1.855E + 04	5.39E-01	3.69	4.97
2.3	1.815E + 04	5.51E-01	3.82	4.99
2.2	1.774E + 04	5.64E-01	3.94	5.00
2.2	1.734E + 04	5.77E-01	4.05	5.03
2.1	1.694E + 04	5.90E-01	4.21	5.09
2.0	1.613E + 04	6.20E-01	4.61	5.06
1.9	1.532E + 04	6.53E-01	4.96	4.78
1.8	1.452E + 04	6.89E-01	5.10	4.45
1.7	1.371E + 04	7.29E-01	5.12	4.22
1.7	1.331E + 04	7.51E-01	5.11	4.11
1.6	1.290E + 04	7.75E-01	5.08	4.03
1.6	1.250E + 04	8.00E-01	5.04	3.94
1.5	1.210E + 04	8.27E-01	4.99	3.89
1.5	1.169E + 04	8.55E-01	4.93	3.83
1.4	1.129E + 04	8.86E-01	4.86	3.79
1.4	1.089E + 04	9.18E-01	4.77	3.75
1.3	1.049E + 04	9.54E-01	4.66	3.72
1.3	1.008E + 04	9.92E-01	4.51	3.68

TABLE IV *(Continued)*

Ruthenium

eV	cm^{-1}	μm	n	k
1.2	9.679E + 03	1.03E + 00	4.28	3.66
1.2	9.275E + 03	1.08E + 00	4.00	3.73
1.1	8.872E + 03	1.13E + 00	3.69	3.91
1.1	8.469E + 03	1.18E + 00	3.41	4.22
1.0	8.065E + 03	1.24E + 00	3.17	4.59
1.0	7.662E + 03	1.31E + 00	2.97	5.03
0.9	7.259E + 03	1.38E + 00	2.82	5.54
0.9	6.856E + 03	1.46E + 00	2.73	6.12
0.8	6.452E + 03	1.55E + 00	2.73	6.71
0.8	6.049E + 03	1.65E + 00	2.77	7.33
0.7	5.646E + 03	1.77E + 00	2.82	7.99
0.7	5.243E + 03	1.91E + 00	2.90	8.71
0.6	4.839E + 03	2.07E + 00	2.98	9.54
0.6	4.436E + 03	2.25E + 00	3.09	10.50
0.5	4.033E + 03	2.48E + 00	3.27	11.63
0.5	3.629E + 03	2.76E + 00	3.54	12.96
0.4	3.226E + 03	3.10E + 00	3.90	14.51
0.4	2.823E + 03	3.54E + 00	4.30	16.48
0.3	2.420E + 03	4.13E + 00	4.94	18.92
0.3	2.016E + 03	4.96E + 00	5.61	22.27
0.2	1.613E + 03	6.20E + 00	6.68	27.18
0.2	1.210E + 03	8.27E + 00	8.39	35.13
0.1	8.065E + 02	1.24E + 01	11.85	50.81

INDIUM (In) VI

Indium is a tetragonal metal. Its softness and low melting point are well known. In single-crystal form it is optically anisotropic and uniaxial, with two independent components in the dielectric tensor, one for the electric field parallel to the *c*-axis and one for the perpendicular orientation. Polycrystalline films may have a texture, growing with the closest-packed plane, the basal plane, in the plane of the film, but with randomly oriented *a*-axes. If so, the film will be optically anisotropic. If there is truly random orientation, the film is isotropic with a complex dielectric function $\epsilon = (\epsilon_{\parallel} + 2\epsilon_{\perp})/3$. Indium develops an oxide skin when exposed to air.

We present data in Table V and Fig. 5 for polycrystalline In, usually in the form of evaporated films. The film textures usually have not been determined. Studies of the anisotropy in single crystals have been carried out by Lenham and Treherne [1, 2], but on "hand-polished" single crystals. We list the infrared data of Golovashkin *et al.* [3], the visible and ultraviolet data of

Koyama *et al.* [4], and the vacuum ultraviolet and soft x-ray data of Hunter *et al.* [5, 6], Jezequel *et al.* [7], and Leveque *et al.* [8]. All these were taken on evaporated films. The last two references contain spectra of the absorption coefficient that have been converted to spectra of the imaginary part of the refractive index with the assumption that the real part is unity. Other measurements in the visible and near-ultraviolet region are found elsewhere [9–12], and additional measurements in the vacuum ultraviolet are reported by others [13–15]. Measurements at several temperatures were made by Golovashkin *et al.* [3] and Mathewson and Myers [12]. Hodgson [16] and Wilson and Rice [17] have made optical measurements on liquid In.

Data in the soft x-ray region, from approximately 10^{-4} to 0.024 μm, are taken from Henke *et al.* [18], and the location of the soft x-ray edges, shown by the short, vertical lines in Fig. 5, are taken from Siegbahn *et al.* [19].

REFERENCES

1. A. P. Lenham and D. M. Treherne, *Proc. Phys. Soc. (London)* **85**, 167 (1965).
2. A. P. Lenham and D. M. Treherne, *J. Opt. Soc. Am.* **56**, 752 (1966).
3. A. I. Golovashkin, I. S. Levchenko, G. P. Motulevich, and A. A. Shubin, *Sov. Phys. JETP* **24**, 1093 (1967).
4. R. Y. Koyama, N. V. Smith, and W. E. Spicer, *Phys. Rev. B* **8**, 2426, (1973).
5. W. R. Hunter, *J. Opt. Soc. Am.* **54**, 208 (1964).
6. W. R. Hunter, D. W. Angel, and R. Tousey, *Appl. Opt.* **4**, 891 (1965).
7. G. Jezequel, J. Thomas, and J. C. Lemonnier, *Solid State Commun.* **23**, 559 (1977).
8. G. Leveque, C. G. Olson, and D. W. Lynch, *Solid State Commun.* **51**, 377 (1984).
9. J. Bor and C. Bartholomew, *Proc. Phys. Soc. (London)* **90**, 1153 (1967).
10. A. Donnadieu and R. Garrigos, *Compt. Rend. Acad. Sci. Paris* **268**, B698 (1969).
11. M. L. Theye and G. Devant, *Thin Solid Films* **4**, 205 (1969).
12. A. G. Mathewson and H. P. Myers, *J. Phys. C* **5**, 2503 (1972).
13. W. C. Walker, O. P. Rustgi, and G. L. Wiessler, *J. Opt. Soc. Am.* **49**, 471 (1959).
14. J. C. Lemonnier, G. Stephan, Y. Le Calvez, and S. Robin, *J. Phys. Chem. Solids* **30**, 1147 (1969).
15. J. C. Lemonnier, G. Jezequel, and J. Thomas, *J. Phys. C* **8**, 2812 (1975).
16. J. Hodgson, *Philos. Mag.* **7**, 229 (1962).
17. E. G. Wilson and S. A. Rice, *Phys. Rev.* **145**, 55 (1966).
18. B. L. Henke, J. C. Davis, E. M. Gullikson, and R. C. C. Perera, "A Preliminary Report on X-Ray Photoabsorption Coefficients and Atomic Scattering Factors for 92 Elements in the 10–10,000 eV Region," Lawrence Berkeley Lab. Rep. LBL-26259, University of California, Berkeley, California, 1988.
19. K. Siegbahn, C. Nordling, A. Fahlman, R. Nordberg, K. Hamrin, J. Hedman, G. Johansson, T. Bergmark, S.-E. Karlsson, I. Lindgren, and B. Lindberg, "ESCA Atomic, Molecular, and Solid State Structure Studied by Means of Electron Spectroscopy." Almquist & Wiksell, Uppsala, Sweden, 1967.

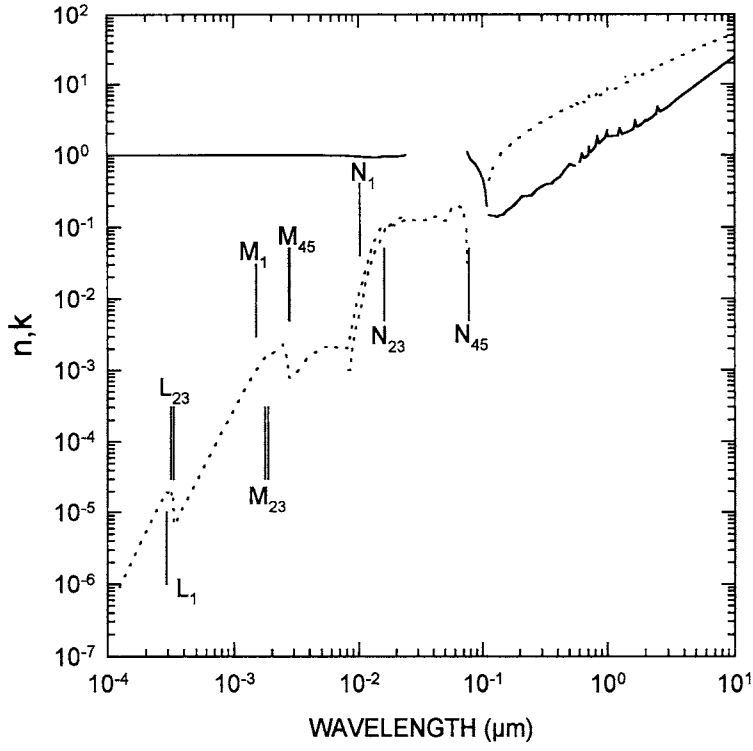

Fig. 5. Log–log plot of n (——) and k (- - - -) versus wavelength in micrometers for indium.

TABLE V

Values of n and k Obtained from Various References for Indium[a]

eV	cm^{-1}	μm	n	k
10000.	8.066E + 07	1.24E-04	9.999872E-01 [18]	9.04E-07 [18]
9117.	7.353E + 07	1.36E-04	9.999844E-01	1.27E-06
8122.	6.551E + 07	1.53E-04	9.999803E-01	1.95E-06
7236.	5.837E + 07	1.71E-04	9.999753E-01	2.99E-06
6156.	4.965E + 07	2.01E-04	9.999662E-01	5.40E-06
5117.	4.127E + 07	2.42E-04	9.999527E-01	1.05E-05
4558.	3.677E + 07	2.72E-04	9.999435E-01	1.58E-05
4454.	3.593E + 07	2.78E-04	9.999418E-01	1.71E-05
4353.	3.511E + 07	2.85E-04	9.999405E-01	1.86E-05
4253.	3.431E + 07	2.91E-04	9.999422E-01	2.01E-05
4156.	3.352E + 07	2.98E-04	9.999381E-01	1.90E-05
4061.	3.276E + 07	3.05E-04	9.999366E-01	2.06E-05
3968.	3.201E + 07	3.12E-04	9.999380E-01	2.24E-05
3878.	3.128E + 07	3.20E-04	9.999357E-01	1.77E-05
3789.	3.057E + 07	3.27E-04	9.999349E-01	1.92E-05
3703.	2.987E + 07	3.35E-04	9.999338E-01	6.59E-06
3618.	2.919E + 07	3.43E-04	9.999247E-01	7.17E-06
2872.	2.317E + 07	4.32E-04	9.99864E-01	1.64E-05
2176.	1.756E + 07	5.70E-04	9.99756E-01	4.29E-05
1727.	1.393E + 07	7.18E-04	9.99613E-01	9.36E-05
1504.	1.213E + 07	8.24E-04	9.99493E-01	1.48E-04
1340.	1.081E + 07	9.25E-04	9.99370E-01	2.17E-04
1166.	9.408E + 06	1.06E-03	9.99192E-01	3.43E-04
1015.	8.191E + 06	1.22E-03	9.9899E-01	5.42E-04
844.	6.809E + 06	1.47E-03	9.9876E-01	9.48E-04
734.	5.927E + 06	1.69E-03	9.9862E-01	1.35E-03
718.	5.792E + 06	1.73E-03	9.9863E-01	1.45E-03
701.	5.660E + 06	1.77E-03	9.9866E-01	1.54E-03
685.	5.530E + 06	1.81E-03	9.9875E-01	1.60E-03
670.	5.404E + 06	1.85E-03	9.9880E-01	1.56E-03
654.	5.281E + 06	1.89E-03	9.9878E-01	1.52E-03
639.	5.160E + 06	1.94E-03	9.9867E-01	1.53E-03
625.	5.042E + 06	1.98E-03	9.9861E-01	1.63E-03
507.	4.096E + 06	2.44E-03	9.9918E-01	2.36E-03
473.	3.821E + 06	2.62E-03	9.9975E-01	1.62E-03
463.	3.734E + 06	2.68E-03	9.9966E-01	1.20E-03
452.	3.649E + 06	2.74E-03	9.9926E-01	8.21E-04
442.	3.565E + 06	2.80E-03	9.9886E-01	7.66E-04
432.	3.484E + 06	2.87E-03	9.9855E-01	7.63E-04
422.	3.404E + 06	2.94E-03	9.9830E-01	7.83E-04
319.	2.580E + 06	3.88E-03	9.9581E-01	1.51E-03
236.	1.911E + 06	5.23E-03	9.9238E-01	2.13E-03
152.	1.232E + 06	8.12E-03	9.761E-01	2.06E-03
150.	1.210E + 06	8.27E-03		1.00E-03 [8]
145.	1.169E + 06	8.55E-03		1.00E-03
140.	1.129E + 06	8.86E-03		2.00E-03

[a] The references from which the values were extracted are given in brackets.

TABLE V *(Continued)*

Indium

eV	cm^{-1}	μm	n	k
135.	1.089E + 06	9.18E-03		3.00E-03
130.	1.049E + 06	9.54E-03		4.00E-03
127.	1.024E + 06	9.77E-03	9.581E-01 [18]	9.81E-03 [18]
125.	1.008E + 06	9.92E-03		5.00E-03 [8]
124.	1.001E + 06	9.99E-03	9.555E-01 [18]	1.14E-02 [18]
121.	9.778E + 05	1.02E-02	9.529E-01	1.32E-02
120.	9.679E + 05	1.03E-02		7.00E-03 [8]
118.	9.555E + 05	1.05E-02	9.500E-01 [18]	1.54E-02 [18]
115.	9.275E + 05	1.08E-02		1.00E-02 [8]
110.	8.872E + 05	1.13E-02		1.60E-02
105.	8.469E + 05	1.18E-02		2.20E-02
100.	8.065E + 05	1.24E-02		3.00E-02
96.2	7.761E + 05	1.29E-02	9.272E-01 [18]	5.68E-02 [18]
95.	7.662E + 05	1.31E-02		4.00E-02 [8]
90.	7.259E + 05	1.38E-02		5.00E-02
85.	6.856E + 05	1.46E-02		6.00E-02
83.8	6.756E + 05	1.48E-02	9.432E-01 [18]	9.34E-02 [18]
81.9	6.602E + 05	1.51E-02	9.479E-01	9.60E-02
80.	6.451E + 05	1.55E-02	9.527E-01	9.85E-02
80.	6.452E + 05	1.55E-02		7.70E-02 [8]
78.2	6.304E + 05	1.59E-02	9.569E-01 [18]	9.83E-02 [18]
76.4	6.160E + 05	1.62E-02	9.589E-01	9.77E-02
75.	6.049E + 05	1.65E-02		9.80E-02 [8]
74.6	6.019E + 05	1.66E-02	9.588E-01 [18]	9.76E-02 [18]
72.9	5.882E + 05	1.70E-02	9.584E-01	9.96E-02
71.3	5.747E + 05	1.74E-02	9.582E-01	1.02E-01
70.	5.646E + 05	1.77E-02		9.60E-02 [8]
69.6	5.616E + 05	1.78E-02	9.576E-01 [18]	1.06E-01 [18]
68.0	5.488E + 05	1.82E-02	9.591E-01	1.11E-01
65.	5.243E + 05	1.91E-02		1.08E-01 [8]
60.	4.839E + 05	2.07E-02		1.03E-01
59.2	4.778E + 05	2.09E-02	9.703E-01 [18]	1.32E-01 [18]
55.	4.436E + 05	2.25E-02		1.21E-01 [8]
54.0	4.356E + 05	2.30E-02	9.830E-01 [18]	1.43E-01 [18]
52.8	4.256E + 05	2.35E-02	9.860E-01	1.45E-01
51.6	4.159E + 05	2.40E-02	9.887E-01	1.48E-01
50.	4.033E + 05	2.48E-02		1.29E-01 [8]
45.	3.629E + 05	2.76E-02		1.26E-01
40.	3.226E + 05	3.10E-02		1.20E-01
28.5	2.299E + 05	4.35E-02		1.44E-01 [7]
28.0	2.258E + 05	4.43E-02		1.40E-01
27.5	2.218E + 05	4.51E-02		1.37E-01
27.0	2.178E + 05	4.59E-02		1.34E-01
26.5	2.137E + 05	4.68E-02		1.28E-01
26.0	2.097E + 05	4.77E-02		1.26E-01
25.5	2.057E + 05	4.86E-02		1.22E-01

(continued)

TABLE V *(Continued)*

Indium

eV	cm^{-1}	μm	n	k
25.0	2.016E + 05	4.96E-02		1.23E-01
24.5	1.976E + 05	5.06E-02		1.25E-01
24.0	1.936E + 05	5.17E-02		1.31E-01
23.5	1.895E + 05	5.28E-02		1.43E-01
23.0	1.855E + 05	5.39E-02		1.53E-01
22.5	1.815E + 05	5.51E-02		1.69E-01
22.0	1.774E + 05	5.64E-02		1.83E-01
21.5	1.734E + 05	5.77E-02		1.92E-01
21.0	1.694E + 05	5.90E-02		2.01E-01
20.5	1.653E + 05	6.05E-02		2.04E-01
20.0	1.613E + 05	6.20E-02		2.01E-01
19.5	1.573E + 05	6.36E-02		1.97E-01
19.0	1.532E + 05	6.53E-02		1.94E-01
18.5	1.492E + 05	6.70E-02		1.90E-01
18.0	1.452E + 05	6.89E-02		1.89E-01
17.9	1.444E + 05	6.93E-02		1.88E-01
17.8	1.436E + 05	6.97E-02		1.86E-01
17.7	1.428E + 05	7.00E-02		1.78E-01
17.6	1.420E + 05	7.04E-02		1.63E-01
17.5	1.411E + 05	7.08E-02		1.47E-01
17.4	1.403E + 05	7.13E-02		1.41E-01
17.3	1.395E + 05	7.17E-02		1.40E-01
17.2	1.387E + 05	7.21E-02		1.41E-01
17.1	1.379E + 05	7.25E-02		1.39E-01
17.0	1.371E + 05	7.29E-02		0.90 [4]
17.0	1.371E + 05	7.29E-02		1.37E-01 [7]
16.9	1.363E + 05	7.34E-02		1.31E-01
16.80	1.355E + 05	7.38E-02		1.22E-01
16.75	1.351E + 05	7.40E-02	1.10 [4]	.
16.70	1.347E + 05	7.42E-02		9.30E-02 [7]
16.60	1.339E + 05	7.47E-02		4.40E-02
16.50	1.331E + 05	7.51E-02		3.20E-02
16.50	1.331E + 05	7.51E-02	1.10 [4]	.
16.25	1.311E + 05	7.63E-02	1.02	
16.00	1.290E + 05	7.75E-02	0.97	
16.00	1.290E + 05	7.75E-02		2.60E-02 [7]
15.75	1.270E + 05	7.87E-02	0.92 [4]	.
15.50	1.250E + 05	8.00E-02	0.88	
15.25	1.230E + 05	8.13E-02	0.85	
15.00	1.210E + 05	8.27E-02	0.83	
14.75	1.190E + 05	8.41E-02	0.80 [4, 5, 6]	.
14.50	1.169E + 05	8.55E-02	0.77	
14.25	1.149E + 05	8.70E-02	0.75	
14.00	1.129E + 05	8.86E-02	0.72	5.00E-02
13.75	1.109E + 05	9.02E-02	0.68	
13.50	1.089E + 05	9.18E-02	0.65	7.00E-02
13.25	1.069E + 05	9.36E-02	0.61	

TABLE V *(Continued)*

Indium

eV	cm^{-1}	μm	n	k
13.00	1.049E + 05	9.54E-02	0.58	8.30E-02
12.75	1.028E + 05	9.72E-02	0.53	
12.50	1.008E + 05	9.92E-02	0.49	1.50E-01
12.25	9.880E + 04	1.01E-01	0.44	
12.00	9.679E + 04	1.03E-01	0.38	1.34E-01
11.75	9.477E + 04	1.06E-01	0.30	
11.50	9.275E + 04	1.08E-01	0.20 [4]	3.00E-01 [4]
11.00	8.872E + 04	1.13E-01	0.15	4.50E-01
10.50	8.469E + 04	1.18E-01	0.15	6.00E-01
10.00	8.065E + 04	1.24E-01	0.15	7.50E-01
9.50	7.662E + 04	1.31E-01	0.14	8.00E-01
9.00	7.259E + 04	1.38E-01	0.15	1.00
8.50	6.856E + 04	1.46E-01	0.15	1.15
8.00	6.452E + 04	1.55E-01	0.17	1.25
7.50	6.049E + 04	1.65E-01	0.18	1.35
7.00	5.646E + 04	1.77E-01	0.20	1.60
6.50	5.243E + 04	1.91E-01	0.23	1.70
6.00	4.839E + 04	2.07E-01	0.27	1.85
5.50	4.436E + 04	2.25E-01	0.27	2.10
5.00	4.033E + 04	2.48E-01	0.28	2.35
4.50	3.629E + 04	2.76E-01	0.34	2.70
4.00	3.226E + 04	3.10E-01	0.38	3.00
3.75	3.025E + 04	3.31E-01	0.40	3.20
3.50	2.823E + 04	3.54E-01	0.40	3.40
3.25	2.621E + 04	3.81E-01	0.45	3.70
3.00	2.420E + 04	4.13E-01	0.50	4.00
2.75	2.218E + 04	4.51E-01	0.60	4.30
2.50	2.016E + 04	4.96E-01	0.75	4.80
2.255	1.819E + 04	5.50E-01	0.70 [3]	4.70 [3]
2.250	1.815E + 04	5.51E-01	0.85	5.50
2.067	1.667E + 04	6.00E-01	0.80	5.02
2.000	1.613E + 04	6.20E-01	1.05	6.00
1.908	1.539E + 04	6.50E-01	0.90	5.42
1.771	1.428E + 04	7.00E-01	1.01	5.83
1.750	1.411E + 04	7.08E-01	1.30	6.90
1.722	1.389E + 04	7.20E-01	1.07	6.00
1.676	1.352E + 04	7.40E-01	1.13	6.18
1.653	1.333E + 04	7.50E-01	1.17	6.26
1.632	1.316E + 04	7.60E-01	1.19	6.31
1.550	1.250E + 04	8.00E-01	1.32	6.60
1.500	1.210E + 04	8.27E-01	1.85	8.00
1.459	1.177E + 04	8.50E-01	1.45	6.78
1.378	1.111E + 04	9.00E-01	1.59	7.18
1.305	1.053E + 04	9.50E-01	1.72	7.44
1.250	1.008E + 04	9.92E-01	2.25	8.80
1.240	1.000E + 04	1.00	1.81	7.77

(continued)

TABLE V *(Continued)*

Indium

eV	cm^{-1}	μm	n	k
1.127	9.090E + 03	1.10	1.84	8.38
1.033	8.332E + 03	1.20	1.87	9.00
1.000	8.065E + 03	1.24	2.40	10.60
0.954	7.694E + 03	1.30	1.95	9.70
0.886	7.146E + 03	1.40	2.06	10.35
0.827	6.670E + 03	1.50	2.19	11.00
0.775	6.251E + 03	1.60	2.33	11.80
0.750	6.049E + 03	1.65	3.10	14.00
0.729	5.880E + 03	1.70	2.49	12.50
0.689	5.557E + 03	1.80	2.64	13.10
0.653	5.267E + 03	1.90	2.80	13.60
0.620	5.001E + 03	2.00	3.13	15.00
0.620	5.001E + 03	2.00	2.97	14.50
0.564	4.549E + 03	2.20	3.30	15.60
0.539	4.347E + 03	2.30	3.48	16.30
0.517	4.170E + 03	2.40	3.81	17.60
0.517	4.170E + 03	2.40	3.65	16.90
0.500	4.033E + 03	2.48	4.80	18.00
0.477	3.847E + 03	2.60	4.00	18.30
0.413	3.331E + 03	3.00	4.70	20.90
0.354	2.855E + 03	3.50	6.00	23.90
0.310	2.500E + 03	4.00	7.27	26.70
0.248	2.000E + 03	5.00	9.77	32.20
0.207	1.670E + 03	5.99	12.40	37.20
0.155	1.250E + 03	8.00	18.40	45.30
0.124	1.000E + 03	10.00	24.80	51.90

VII TIN (Sn)

White tin, β-Sn, is a tetragonal metal. There is also a cubic phase, gray tin, α-Sn, with the diamond structure. Gray tin is the stable form below 18° C, but the transformation from white tin to gray tin is sluggish. We consider here only white tin. In single-crystal form it is optically anisotropic and uniaxial, with two independent components in the dielectric tensor, one for the electric field parallel to the c-axis and one for the perpendicular orientation. Polycrystalline films may have a texture, growing with the closest-packed plane, the basal plane, in the plane of the film, but with randomly oriented a-axes. If so, the film will be optically anisotropic. If there is truly random orientation, the film is isotropic with a complex dielectric function $\epsilon = (\epsilon_{\parallel} + 2\epsilon_{\perp})/3$. Sn develops an oxide skin when exposed to air, typically SnO_2 with a layer of SnO below.

The data reported in Table VI and Fig. 6 were taken on polycrystalline films. However, it is not at all clear that these films had randomly oriented grains. Schwartz [1] made ellipsometric measurements on an oriented single crystal and a polycrystalline film, and it is clear from his data that the spectrum of the film is neither that for **E** in the basal plane nor the polycrystalline average quoted above. Also, the structures in the spectra for the film are broader than those for the single crystal. The data are taken from Golovashkin and Motulevich [2, 3], MacRae *et al.* [4], Girouard and Truong [5], Jezequel *et al.* [6], and Haensel *et al.* [7]. The last have reported only absorption-coefficient spectra. These have been converted to spectra of the imaginary part of the refractive index with the assumption that the real part is unity. Other measurements have been reported by Lenham and Treherne [8] and Mahmoud [9].

Carotenuto *et al.* [10] measured the temperature derivative of the optical constants. Optical studies at different temperatures have been carried out by Schwartz [1] and Golovashkin and Motulevich [2, 3]. Hodgson [11], Comins [12], and Petrakian *et al.* [13] have measured the optical constants of liquid Sn.

Data in the soft x-ray region, from approximately 10^{-4} to 0.024 μm, are taken from Henke *et al.* [14], and the location of the soft x-ray edges, shown by the short, vertical lines in Fig. 6, are taken from Siegbahn *et al.* [15].

REFERENCES

1. H. Schwartz, *Phys. Status. Solidi. B* **44**, 603 (1971).
2. A. I. Golovashkin and G. P. Motulevich, *Sov. Phys. JETP* **19**, 310 (1964).
3. A. I. Golovashkin and G. P. Motulevich, *Sov. Phys. JETP* **20**, 44 (1965).
4. R. A. MacRae, E. T. Arakawa, and M. W. Williams, *Phys. Rev.* **162**, 615 (1967).
5. F. E. Girouard and V. V. Truong, *Appl. Opt.* **15**, 4144 (1981).
6. G. Jezequel, J. Thomas, and J. C. Lemonnier, *Solid State Commun.* **23**, 559 (1977).
7. R. Haensel, C. Kunz, T. Sasaki, and B. Sonntag, *Appl. Opt.* **7**, 301 (1968).
8. A. P. Lenham and D. M. Treherne, J. *Opt. Soc. Am.* **56**, 752 (1966).
9. S. Mahmoud, *J. Mater. Sci.* **22**, 251 (1986).
10. C. Carotenuto, E. Colavita, S. Modesti, and M. Sommacal, *Phys. Rev. B* **14**, 5327 (1976).
11. J. N. Hodgson, *Philos. Mag.* **6**, 509 (1961).
12. N. R. Comins, *Philos. Mag.* **25**, 817 (1972).
13. J. P. Petrakian, A. R. Cathers, J. E. Parks, R. A. MacRae, T. A. Callcott, and E. T. Arakawa, *Phys. Rev. B* **21**, 3043 (1980).
14. B. L. Henke, J. C. Davis, E. M. Gullikson, and R. C. C. Perera, "A Preliminary Report on X-Ray Photoabsorption Coefficients and Atomic Scattering Factors for 92 Elements in the 10–10,000 eV Region," Lawrence Berkeley Lab. Rep. LBL-26259, University of California, Berkeley, California, 1988.
15. K. Siegbahn, C. Nordling, A. Fahlman, R. Nordberg, K. Hamrin, J. Hedman, G. Johansson, T. Bergmark, S.-E. Karlsson, I. Lindgren, and B. Lindberg, "ESCA Atomic, Molecular, and Solid State Structure Studied by Means of Electron Spectroscopy." Almquist & Wiksell, Uppsala, Sweden, 1967.

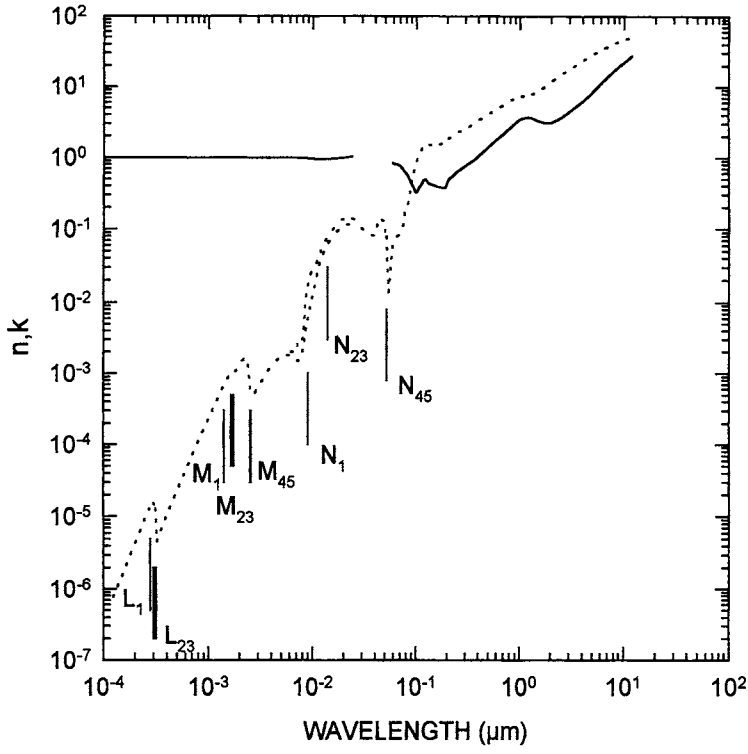

Fig. 6. Log–log plot of n (——) and k (- - - -) versus wavelength in micrometers for tin.

TABLE VI

Values of n and k Obtained from Various References for Tin[a]

eV	cm^{-1}	μm	n	k
10000.	8.066E + 07	1.24E-04	9.999900E-01 [14]	7.65E-07 [14]
9117.	7.353E + 07	1.36E-04	9.999878E-01	1.08E-06
8123.	6.551E + 07	1.53E-04	9.999847E-01	1.66E-06
7072.	5.704E + 07	1.75E-04	9.999800E-01	2.75E-06
6015.	4.852E + 07	2.06E-04	9.999728E-01	4.93E-06
5117.	4.127E + 07	2.42E-04	9.999641E-01	8.70E-06
4665.	3.763E + 07	2.66E-04	9.999591E-01	1.19E-05
4559.	3.677E + 07	2.72E-04	9.999582E-01	1.29E-05
4455.	3.593E + 07	2.78E-04	9.999575E-01	1.24E-05
4353.	3.511E + 07	2.85E-04	9.999561E-01	1.34E-05
4254.	3.431E + 07	2.91E-04	9.999555E-01	1.46E-05
4157.	3.352E + 07	2.98E-04	9.999568E-01	1.58E-05
4062.	3.276E + 07	3.05E-04	9.999540E-01	1.25E-05
3969.	3.201E + 07	3.12E-04	9.999551E-01	1.35E-05
3878.	3.128E + 07	3.20E-04	9.999519E-01	4.55E-06
3790.	3.057E + 07	3.27E-04	9.999456E-01	4.97E-06
2228.	1.797E + 07	5.57E-04	9.99818E-01	3.32E-05
1939.	1.564E + 07	6.39E-04	9.99760E-01	5.29E-05
1728	7.176E + 07	7.18E-04	9.99699E-01	7.77E-05
1688.	1.362E + 07	7.34E-04	9.99686E-01	8.38E-05
1504.	1.213E + 07	8.24E-04	9.99608E-01	1.22E-04
1403.	1.132E + 07	8.84E-04	9.99553E-01	1.54E-04
1309.	1.056E + 07	9.47E-04	9.99493E-01	1.93E-04
1194.	9.628E + 06	1.04E-03	9.99403E-01	2.62E-04
1088.	8.779E + 06	1.14E-03	9.99305E-01	3.55E-04
970.	7.821E + 06	1.28E-03	9.99184E-01	5.36E-04
825.	6.653E + 06	1.50E-03	9.99081E-01	8.24E-04
770.	6.208E + 06	1.61E-03	9.99090E-01	9.78E-04
752.	6.066E + 06	1.65E-03	9.99114E-01	1.02E-03
735.	5.927E + 06	1.69E-03	9.99154E-01	1.03E-03
718.	5.792E + 06	1.73E-03	9.99149E-01	1.00E-03
702.	5.660E + 06	1.77E-03	9.99082E-01	1.00E-03
611.	4.927E + 06	2.03E-03	9.99032E-01	1.42E-03
520.	4.191E + 06	2.39E-03	9.99873E-01	1.27E-03
508.	4.096E + 06	2.44E-03	9.99830E-01	9.19E-04
496.	4.002E + 06	2.50E-03	9.99638E-01	6.63E-04
485.	3.911E + 06	2.56E-03	9.99359E-01	5.34E-04
474.	3.821E + 06	2.62E-03	9.99132E-01	5.14E-04
463.	3.734E + 06	2.68E-03	9.9895E-01	5.12E-04
351.	2.830E + 06	3.53E-03	9.9717E-01	9.62E-04
299.	2.407E + 06	4.15E-03	9.9605E-01	1.36E-03
254.	2.048E + 06	4.88E-03	9.9457E-01	1.66E-03
200.	1.613E + 06	6.20E-03		2.00E-03 [7]
197.	1.588E + 06	6.30E-03	9.9049E-03 [14]	1.72E-03 [14]
190.	1.532E + 06	6.53E-03		2.00E-03 [7]

(continued)

[a] The references from which the values were extracted are given in brackets.

TABLE VI *(Continued)*

Tin

eV	cm^{-1}	μm	n	k
180.	1.452E + 06	6.89E-03		2.00E-03
170.	1.371E + 06	7.29E-03		3.00E-03
160.	1.290E + 06	7.75E-03		3.00E-03
156.	1.261E + 06	7.93E-03	9.808E-01 [14]	1.96E-03 [14]
155.	1.250E + 06	8.00E-03		3.00E-03 [7]
150.	1.210E + 06	8.27E-03		5.00E-03
145.	1.169E + 06	8.55E-03		1.10E-02
140.	1.129E + 06	8.86E-03		1.60E-02
135.	1.089E + 06	9.18E-03		2.00E-02
130.	1.049E + 06	9.54E-03		2.50E-02
125.	1.008E + 06	9.92E-03		2.70E-02
121.	9.778E + 05	1.02E-02	9.608E-01 [14]	1.53E-02 [14]
120.	9.679E + 05	1.03E-02		3.10E-02 [7]
115.	9.275E + 05	1.08E-02		3.40E-02
110.	8.872E + 05	1.13E-02		4.00E-02
105.	8.469E + 05	1.18E-02		4.80E-02
100.	8.065E + 05	1.24E-02		5.90E-02
98.5	7.942E + 05	1.26E-02	9.531E-01 [14]	4.66E-02 [14]
95.	7.662E + 05	1.31E-02		6.70E-02 [7]
90.	7.259E + 05	1.38E-02		7.80E-02
85.7	6.914E + 05	1.45E-02	9.571E-01 [14]	6.81E-02 [14]
85.	6.856E + 05	1.46E-02		8.90E-02 [7]
80.	6.452E + 05	1.55E-02		9.80E-02
75.	6.049E + 05	1.65E-02		0.111
72.9	5.882E + 05	1.70E-02	9.727E-01 [14]	9.21E-02 [14]
70.	5.646E + 05	1.77E-02		0.123 [7]
65.	5.243E + 05	1.91E-02		0.135
60.6	4.889E + 05	2.05E-02	9.984E-01 [14]	1.12E-01 [14]
60.	4.839E + 05	2.07E-02		0.143 [7]
55.	4.436E + 05	2.25E-02		0.146
51.7	4.159E + 05	2.40E-02	1.031 [14]	1.11E-01 [14]
50.	4.033E + 05	2.48E-02		0.137 [7]
45.	3.629E + 05	2.76E-02		0.113
40.	3.226E + 05	3.10E-02		0.098
33.	2.662E + 05	3.76E-02		0.082 [6]
32.5	2.621E + 05	3.81E-02		0.081
32.0	2.581E + 05	3.87E-02		0.081
31.5	2.541E + 05	3.94E-02		0.083
31.0	2.500E + 05	4.00E-02		0.089
30.5	2.460E + 05	4.07E-02		0.095
30.0	2.420E + 05	4.13E-02		0.105
29.5	2.379E + 05	4.20E-02		0.115
29.0	2.339E + 05	4.28E-02		0.124
28.5	2.299E + 05	4.35E-02		0.137
28.0	2.258E + 05	4.43E-02		0.140
27.5	2.218E + 05	4.51E-02		0.134
27.0	2.178E + 05	4.59E-02		0.134

TABLE VI *(Continued)*

Tin

eV	cm^{-1}	μm	n	k
26.5	2.137E + 05	4.68E-02		0.133
26.0	2.097E + 05	4.77E-02		0.131
25.5	2.057E + 05	4.86E-02		0.129
25.0	2.016E + 05	4.96E-02		0.121
24.9	2.008E + 05	4.98E-02		0.107
24.8	2.000E + 05	5.00E-02		0.086
24.7	1.992E + 05	5.02E-02		0.078
24.6	1.984E + 05	5.04E-02		0.077
24.5	1.976E + 05	5.06E-02		0.079
24.4	1.968E + 05	5.08E-02		0.081
24.3	1.960E + 05	5.10E-02		0.083
24.2	1.952E + 05	5.12E-02		0.082
24.1	1.944E + 05	5.14E-02		0.080
24.0	1.936E + 05	5.17E-02		0.079
23.8	1.916E + 05	5.22E-02		0.056
23.4	1.887E + 05	5.30E-02		0.022
23.0	1.855E + 05	5.39E-02		0.014
21.0	1.694E + 05	5.90E-02	0.84 [5]	0.060 [5]
20.0	1.613E + 05	6.20E-02	0.82	0.070
19.0	1.532E + 05	6.53E-02	0.8	0.080
18.0	1.452E + 05	6.89E-02	0.77	0.085
17.5	1.411E + 05	7.08E-02	0.74	0.090
17.0	1.371E + 05	7.29E-02	0.71	0.100
16.5	1.331E + 05	7.51E-02	0.68	0.120
16.0	1.290E + 05	7.75E-02	0.64	0.170
15.5	1.250E + 05	8.00E-02	0.60	0.190
15.0	1.210E + 05	8.27E-02	0.56	0.220
14.5	1.169E + 05	8.55E-02	0.51	0.270
14.0	1.129E + 05	8.86E-02	0.45	0.380
13.5	1.089E + 05	9.18E-02	0.41	0.520
13.0	1.049E + 05	9.54E-02	0.365	0.660
12.5	1.008E + 05	9.92E-02	0.32	0.830
12.0	9.679E + 04	1.03E-01	0.34	1.000
11.5	9.275E + 04	1.08E-01	0.38	1.150
11.0	8.872E + 04	1.13E-01	0.42	1.300
10.5	8.469E + 04	1.18E-01	0.475	1.480
10.0	8.065E + 04	1.24E-01	0.50	1.540
9.5	7.662E + 04	1.31E-01	0.44	1.520
9.0	7.259E + 04	1.38E-01	0.42	1.510
8.5	6.856E + 04	1.46E-01	0.41	1.500
8.0	6.452E + 04	1.55E-01	0.40	1.520
7.5	6.049E + 04	1.65E-01	0.39	1.540
7.0	5.646E + 04	1.77E-01	0.38	1.560
6.5	5.243E + 04	1.91E-01	0.37	1.580
6.0	4.839E + 04	2.07E-01	0.50 [4]	1.900 [4]
5.5	4.436E + 04	2.25E-01	0.55	2.050

(continued)

TABLE VI *(Continued)*

Tin

eV	cm^{-1}	μm	n	k
5.0	4.033E + 04	2.48E-01	0.63	2.300
4.5	3.629E + 04	2.76E-01	0.70	2.400
4.0	3.226E + 04	3.10E-01	0.80	2.600
3.5	2.823E + 04	3.54E-01	0.90	3.000
1.333	1.075E + 04	9.30E-01	3.15 [2]	7.280 [2]
1.253	1.011E + 04	9.90E-01	3.44	7.340
1.033	8.332E + 03	1.20E + 00	3.76	7.630
0.919	7.412E + 03	1.35E + 00	3.57	8.040
0.827	6.670E + 03	1.50E + 00	3.31	8.670
0.729	5.880E + 03	1.70E + 00	3.13	9.880
0.62	5.001E + 03	1.00E + 00	3.10	11.800
0.496	4.000E + 03	2.50E + 00	3.63	14.800
0.413	3.331E + 03	3.00E + 00	4.41	17.800
0.354	2.855E + 03	3.50E + 00	5.27	20.500
0.31	2.500E + 03	3.00E + 00	6.19	23.200
0.248	2.000E + 03	5.00E + 00	8.49	28.500
0.207	1.670E + 03	5.99E + 00	11.0	33.100
0.177	1.428E + 03	7.00E + 00	13.8	37.100
0.155	1.250E + 03	8.00E + 00	16.6	40.600
0.138	1.113E + 03	8.98E + 00	19.3	43.800
0.124	1.000E + 03	1.00E + 01	22.0	46.400
0.113	9.114E + 02	1.10E + 01	24.8	49.000
0.103	8.307E + 02	1.20E + 01	27.8	51.600

VIII ANTIMONY (Sb)

Antimony is a semimetal with a rhombohedral structure. In single-crystal form it is optically anisotropic and uniaxial, with two independent components in the dielectric tensor, one for the electric field parallel to the *c*-axis and one for the perpendicular orientation. Polycrystalline films may have a texture, growing with the closest-packed plane, the basal plane, in the plane of the film, but with randomly oriented *a*-axes. If so, the film will be optically anisotropic. If there is truly random orientation, the film is isotropic with a complex dielectric function $\epsilon = (\epsilon_{\parallel} + 2\epsilon_{\perp})/3$. Sb develops an oxide skin when exposed to air.

Cardona and Greenaway [1] have determined optical constants for a single crystal of Sb with **E** in the basal plane ($\mathbf{E} \perp \mathbf{c}$). We give their data in Table VII and Fig. 7. Data in a more limited, but overlapping, range have been taken by Aspnes [2], Strümpler and Lüth [3], and de Sande *et al.* [4]. Lenham and Treherne [5] and Lenham *et al.* [6] have made measurements in the infrared. Nanney [7] measured the infrared absorptance spectra of a single crystal with $\mathbf{E} \perp \mathbf{c}$ and $\mathbf{E} \parallel \mathbf{c}$ at 300 K and 4.2 K.

Data in the soft x-ray region, from approximately 10^{-4} to 0.024 μm, are taken from Henke *et al.* [8], and the location of the soft x-ray edges, shown by the short, vertical lines in Fig. 7, are taken from Siegbahn *et al.* [9].

REFERENCES

1. M. Cardona and D. L. Greenaway, *Phys. Rev.* **133**, A1685 (1964).
2. D. E. Aspnes, *Phys. Rev. B* **12**, 4008 (1975).
3. R. Strümpler and H. Lüth, *Thin Solid Films* **177**, 287 (1989).
4. J. C. G. de Sande, F. Vega, C. N. Afonso, C. Ortega, and J. Siejka, *Thin Solid Films* **249**, 195 (1994).
5. A. P. Lenham and D. M. Treherne, *J. Opt. Soc. Am.* **56**, 752 (1966).
6. A. P. Lenham, D. M. Treherne, and R. J. Metcalfe, *J. Opt. Soc. Am.* **55**, 1072 (1965).
7. C. Nanney, *Phys. Rev.* **129**, 109 (1963).
8. B. L. Henke, J. C. Davis, E. M. Gullikson, and R. C. C. Perera, "A Preliminary Report on X-Ray Photoabsorption Coefficients and Atomic Scattering Factors for 92 Elements in the 10–10,000 eV Region," Lawrence Berkeley Lab. Rep. LBL-26259, University of California, Berkeley, California, 1988.
9. K. Siegbahn, C. Nordling, A. Fahlman, R. Nordberg, K. Hamrin, J. Hedman, G. Johansson, T. Bergmark, S.-E. Karlsson, I. Lindgren, and B. Lindberg, "ESCA Atomic, Molecular, and Solid State Structure Studied by Means of Electron Spectroscopy." Almquist & Wiksell, Uppsala, Sweden, 1967.

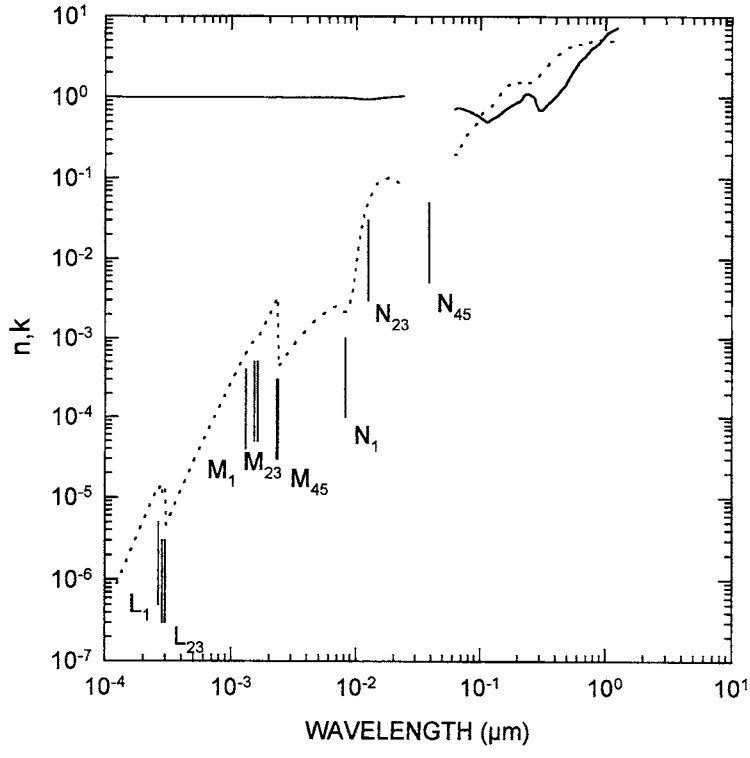

Fig. 7. Log–log plot of n (——) and k (- - - -) versus wavelength in micrometers for antimony.

TABLE VII

Values of n and k Obtained from Various References for Antimony[a]

eV	cm^{-1}	μm	n	k
10000.	8.066E + 07	1.24E-04	9.999885E-01 [8]	8.94E-07 [8]
9117.	7.353E + 07	1.36E-04	9.999860E-01	1.26E-06
8123.	6.551E + 07	1.53E-04	9.999824E-01	1.93E-06
7237.	5.837E + 07	1.71E-04	9.999779E-01	2.95E-06
6156.	4.965E + 07	2.01E-04	9.999701E-01	5.30E-06
5117.	4.127E + 07	2.42E-04	9.999591E-01	1.03E-05
4886.	3.941E + 07	2.54E-04	9.999566E-01	1.21E-05
4775.	3.851E + 07	2.60E-04	9.999558E-01	1.31E-05
4665.	3.763E + 07	2.66E-04	9.999551E-01	1.23E-05
4559.	3.667E + 07	2.72E-04	9.999533E-01	1.34E-05
4455.	3.593E + 07	2.78E-04	9.999529E-01	1.46E-05
4353.	3.511E + 07	2.85E-04	9.999532E-01	1.15E-05
4254.	3.431E + 07	2.91E-04	9.999506E-01	1.25E-05
4157.	3.352E + 07	2.98E-04	9.999512E-01	1.35E-05
4062.	3.276E + 07	3.05E-04	9.999467E-01	4.68E-06
3969.	3.201E + 07	3.12E-04	9.999412E-01	5.10E-06
2806.	2.264E + 07	4.42E-04	9.99868E-01	1.79E-05
2127.	1.716E + 07	5.83E-04	9.99766E-01	4.68E-05
1688.	1.362E + 07	7.34E-04	9.99632E-01	1.02E-04
1504.	1.213E + 07	8.24E-04	9.99542E-01	1.50E-04
1403.	1.132E + 07	8.84E-04	9.99480E-01	1.89E-04
1309.	1.056E + 07	9.47E-04	9.99411E-01	2.37E-04
1166.	9.408E + 06	1.06E-03	9.99284E-01	3.46E-04
1016.	8.191E + 06	1.22E-03	9.99135E-01	5.43E-04
970.	7.821E + 06	1.28E-03	9.99095E-01	6.10E-04
948.	7.642E + 06	1.31E-03	9.99070E-01	6.45E-04
926.	7.468E + 06	1.34E-03	9.99043E-01	6.84E-04
844.	6.809E + 06	1.47E-03	9.9899E-01	8.77E-04
825.	6.653E + 06	1.50E-03	9.9899E-01	8.97E-04
806.	6.501E + 06	1.54E-03	9.9897E-01	9.12E-04
788.	6.353E + 06	1.57E-03	9.9892E-01	9.28E-04
770.	6.208E + 06	1.61E-03	9.9886E-01	9.67E-04
752.	6.066E + 06	1.65E-03	9.9880E-01	1.03E-03
735.	5.927E + 07	1.69E-03	9.9876E-01	1.11E-03
611.	4.927E + 06	2.03E-03	9.9872E-01	2.03E-03
544.	4.389E + 06	2.28E-03	9.9997E-01	2.99E-03.
532.	4.289E + 06	2.33E-03	1.00143	3.23E-03
520.	4.191E + 06	2.39E-03	1.000883	4.40E-04
508.	4.096E + 06	2.44E-03	1.0000560	4.65E-04
496.	4.002E + 06	2.50E-03	9.9966E-01	4.91E-04
394.	3.177E + 06	3.15E-03	9.9788E-01	8.36E-04
298.	2.407E + 06	4.15E-03	9.9576E-01	1.38E-03
197.	1.588E + 06	6.30E-03	9.896E-01	2.37E-03
175.	1.415E + 06	7.07E-03	9.865E-01	2.51E-03
171.	1.383E + 06	7.23E-03	9.857E-01	2.51E-03
168.	1.351E + 06	7.40E-03	9.849E-01	2.44E-03

[a] The references from which the values were taken are given in brackets.

TABLE VII *(Continued)*

Antimony

eV	cm^{-1}	μm	n	k
164.	1.320E + 06	7.57E-03	9.839E-01	2.36E-03
160.	1.290E + 06	7.75E-03	9.828E-01	2.28E-03
156.	1.261E + 06	7.93E-03	9.815E-01	2.20E-03
153.	1.232E + 06	8.12E-03	9.801E-01	2.14E-03
149.	1.204E + 06	8.31E-03	9.785E-01	2.16E-03
121.	9.778E + 05	1.02E-02	9.545E-01	1.13E-02
101.	8.127E + 05	1.23E-02	9.431E-01	4.82E-02
98.5	7.942E + 05	1.26E-02	9.434E-01	5.27E-02
96.2	7.761E + 05	1.29E-02	9.439E-01	5.76E-02
94.	7.584E + 05	1.32E-02	9.452E-01	6.28E-02
80.	6.451E + 05	1.55E-02	9.688E-01	9.17E-02
71.3	5.747E + 05	1.74E-02	9.870E-01	9.89E-02
69.6	5.616E + 05	1.78E-02	9.907E-01	0.100
68.	5.488E + 05	1.82E-02	9.984E-01	0.101
66.5	5.363E + 05	1.86E-02	9.997E-01	0.101
56.6	4.562E + 05	2.19E-02	1.021	8.92E-02
51.5	4.159E + 05	2.40E-02	1.026	7.80E-02
20.	1.613E + 05	6.20E-02	0.72 [1]	0.2 [1]
19.	1.532E + 05	6.53E-02	0.75	0.2
18.	1.452E + 05	6.89E-02	0.74	0.25
17.	1.371E + 05	7.29E-02	0.72	0.3
16.	1.290E + 05	7.75E-02	0.7	0.35
15.	1.210E + 05	8.27E-02	0.67	0.4
14.	1.129E + 05	8.86E-02	0.63	0.45
13.	1.049E + 05	9.54E-02	0.6	0.5
12.	9.679E + 04	1.03E-01	0.55	0.65
11.	8.872E + 04	1.13E-01	0.5	0.7
10.	8.065E + 04	1.24E-01	0.55	0.8
9.	7.259E + 04	1.38E-01	0.6	1.
8.	6.452E + 04	1.55E-01	0.7	1.3
7.	5.646E + 04	1.77E-01	0.8	1.5
6.	4.839E + 04	2.07E-01	0.9	1.5
5.8	4.678E + 04	2.14E-01	0.95	1.6
5.6	4.517E + 04	2.21E-01	1.05	1.6
5.4	4.355E + 04	2.30E-01	1.1	1.6
5.2	4.194E + 04	2.38E-01	1.1	1.55
5.	4.033E + 04	2.48E-01	1.1	1.5
4.8	3.871E + 04	2.58E-01	1.05	1.55
4.6	3.710E + 04	2.70E-01	1.	1.6
4.4	3.549E + 04	2.82E-01	0.8	1.7
4.2	3.388E + 04	2.95E-01	0.7	1.85
4.	3.226E + 04	3.10E-01	0.7	2.1
3.	2.420E + 04	4.13E-01	1.1	3.3
2.8	2.258E + 04	4.43E-01	1.25	3.6
2.6	2.097E + 04	4.77E-01	1.4	3.9
2.4	1.936E + 04	5.17E-01	1.8	4.2

(continued)

TABLE VII *(Continued)*

Antimony

eV	cm^{-1}	μm	n	k
2.2	1.774E + 04	5.64E-01	2.2	4.45
2.	1.613E + 04	6.20E-01	2.8	4.5
1.8	1.452E + 04	6.89E-01	3.2	4.6
1.6	1.290E + 04	7.75E-01	4.	4.9
1.4	1.129E + 04	8.86E-01	4.6	5.1
1.2	9.679E + 03	1.03	6.2	5.1
1.	8.065E + 03	1.24	7.3	4.7

IX RHENIUM (Re)

Rhenium is a hexagonal close-packed metal. In single-crystal form it is optically anisotropic and uniaxial, with two independent components in the dielectric tensor, one for the electric field parallel to the *c*-axis and one for the perpendicular orientation. Polycrystalline films may have a texture, growing with the closest-packed plane, the basal plane, in the plane of the film, but with randomly oriented *a*-axes. If so, the film will be optically anisotropic. If there is truly random orientation, the film is isotropic with a complex dielectric function $\epsilon = (\epsilon_{\parallel} + 2\epsilon_{\perp})/3$.

Re is a transition metal. The incompletely filled 5*d* bands can give rise to interband optical absorption at arbitrarily small energies. This means that reliable fits of optical data to a Drude-model dielectric function cannot be made, except below some unknown low energy.

Reliable optical data over a wide spectral range do not exist for polycrystalline bulk samples or thin films of Re. Therefore, for Table VIII and Fig. 8, we have chosen to use data taken from the basal plane of a single crystal ($\mathbf{E}\perp\mathbf{c}$) by Weaver *et al.* [1, 2]. In the soft x-ray region the absorption-coefficient spectra of Haensel *et al.* [3] have been converted to spectra of the imaginary part of the complex refractive index with the assumption that the real party is unity. Additional optical measurements have been made by Nomerovannaya *et al.* [4] and others [5–8]. Nomerovannaya *et al.* made measurements at 295 and 77 K. Barnes [9] has made measurements of the temperature dependence at higher temperatures.

Data in the soft x-ray region, from approximately 10^{-4} to 0.024 μm, are taken from Henke *et al.* [10], and the location of the soft x-ray edges, shown by the short, vertical lines in Fig. 8 are taken from Siegbahn *et al.* [11].

REFERENCES

1. J. H. Weaver, C. G. Olson, and D. W. Lynch, unpublished.
2. J. H. Weaver, C. Krafka, D. W. Lynch, and E.-E. Koch, Physics Data, Optical Properties of Metals, Part I: the Transition Metals, Fachinformationszentrum Karlsruhe, 7514 Eggenstein-Leopoldshafen 2, Germany, 1981.
3. R. Haensel, K. Radler, B. Sonntag, and C. Kunz, *Solid State Commun.* **7**, 1495 (1969).
4. L. V. Nomerovannaya, M. M. Kirillova, M. M. Noskov, and G. A. Bolotin, *Fiz. Met. Metalloved.* **36**, 1197 (1973); *Phys. Met. Metall.* **36**, 66 (1973).
5. L. J. Leblanc, J. S. Farrell, and D. W. Juenker, *J. Opt. Soc. Am.* **54**, 956, (1964).
6. D. W. Juenker, L. J. Leblanc, and C. R. Martin, *J. Opt. Soc. Am.* **58**, 164 (1968).
7. J. T. Cox, G. Hass, J. B. Ramsey, and W. R. Hunter, *J. Opt. Soc. Am.* **62**, 781 (1972).
8. L. K. Thomas and S. Thurm, *J. Phys. F: Metal Phys.* **6**, 279 (1976).
9. B. T. Barnes, *J. Opt. Soc. Am.* **56**, 1546 (1966).
10. B. L. Henke, J. C. Davis, E. M. Gullikson, and R. C. C. Perera, "A Preliminary Report on X-Ray Photoabsorption Coefficients and Atomic Scattering Factors for 92 Elements in the 10–10,000 eV Region," Lawrence Berkeley Lab. Rep. LBL-26259, University of California, Berkeley, California, 1988.
11. K. Siegbahn, C. Nordling, A. Fahlman, R. Nordberg, K. Hamrin, J. Hedman, G. Johansson, T. Bergmark, S.-E. Karlsson, I. Lindgren, and B. Lindberg, "ESCA Atomic, Molecular, and Solid State Structure Studied by Means of Electron Spectroscopy." Almquist & Wiksell, Uppsala, Sweden, 1967.

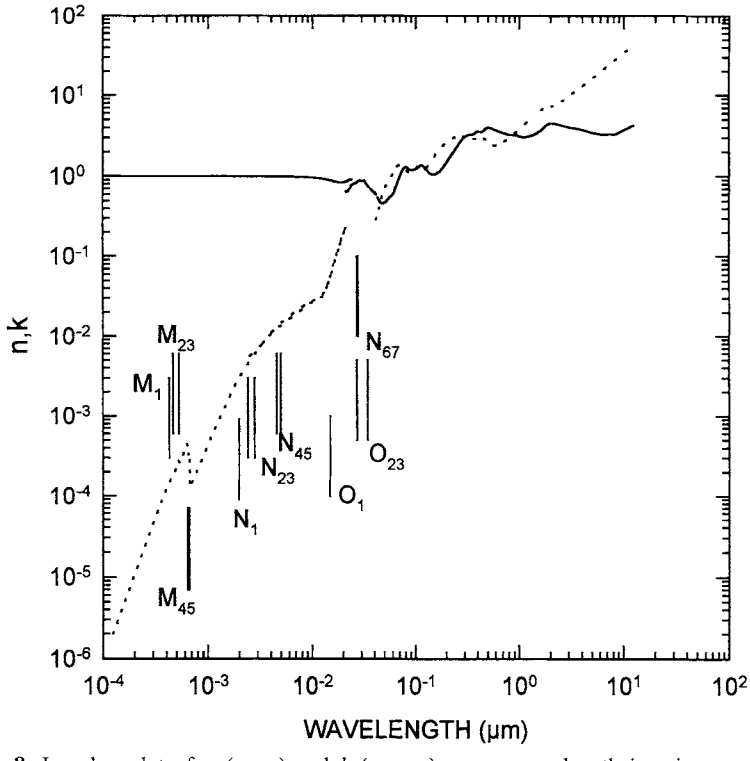

Fig. 8. Log–log plot of n (——) and k (- - - -) versus wavelength in micrometers for rhenium.

TABLE VIII

Values of n and k Obtained from Various References for Rhenium[a]

eV	cm^{-1}	μm	n	k
10000	8.065E + 07	1.24E-04	9.999689E-01 [10]	2.02E-06 [10]
8909.	7.186E + 07	1.39E-04	9.999592E-01	3.06E-06
7937.	6.402E + 07	1.56E-04	9.999479E-01	4.63E-06
7071.	5.703E + 07	1.75E-04	9.999337E-01	6.98E-06
6015.	4.852E + 07	2.06E-04	9.999078E-01	1.24E-05
5000.	4.033E + 07	2.48E-04	9.99866E-01	2.38E-05
4061.	3.276E + 07	3.05E-04	9.99800E-01	4.93E-05
3078.	2.483E + 07	4.03E-04	9.99675E-01	1.28E-04
3007.	2.426E + 07	4.12E-04	9.99664E-01	1.38E-04
2939.	2.371E + 07	4.22E-04	9.99655E-01	1.49E-04
2872.	2.316E + 07	4.32E-04	9.99641E-01	1.55E-04
2806.	2.264E + 07	4.42E-04	9.99628E-01	1.68E-04
2742.	2.212E + 07	4.52E-04	9.99617E-01	1.82E-04
2679.	2.161E + 07	4.63E-04	9.99610E-01	1.85E-04
2618.	2.112E + 07	4.73E-04	9.99593E-01	2.01E-04
2558.	2.064E + 07	4.85E-04	9.99579E-01	2.18E-04
2500.	2.017E + 07	4.96E-04	9.99567E-01	2.36E-04
2443.	1.971E + 07	5.07E-04	9.99561E-01	2.57E-04
2387.	1.926E + 07	5.19E-04	9.99575E-01	2.79E-04
2332.	1.882E + 07	5.31E-04	9.99552E-01	2.59E-04
2279.	1.839E + 07	5.44E-04	9.99530E-01	2.80E-04
2078.	1.676E + 07	5.97E-04	9.99512E-01	3.83E-04
2030.	1.638E + 07	6.10E-04	9.99530E-01	4.14E-04
1984.	1.601E + 07	6.25E-04	9.99580E-01	4.48E-04
1939.	1.564E + 07	6.39E-04	9.99635E-01	3.27E-04
1894.	1.528E + 07	6.54E-04	9.99686E-01	3.56E-04
1851.	1.493E + 07	6.70E-04	9.99600E-01	1.28E-04
1809.	1.459E + 07	6.85E-04	9.99493E-01	1.38E-04
1612.	1.300E + 07	7.69E-04	9.99205E-01	1.99E-04
1403.	1.132E + 07	8.84E-04	9.9888E-01	3.07E-04
1221.	9.854E + 06	1.01E-03	9.9850E-01	4.72E-04
1088.	8.778E + 06	1.14E-03	9.9811E-01	6.67E-04
1015.	8.190E + 06	1.22E-03	9.9785E-01	8.21E-04
904.	7.297E + 06	1.37E-03	9.9736E-01	1.14E-03
806.	6.501E + 06	1.54E-03	9.9679E-01	1.58E-03
685.	5.530E + 06	1.81E-03	9.9590E-01	2.44E-03
670.	5.404E + 06	1.85E-03	9.9576E-01	2.59E-03
654.	5.280E + 06	1.89E-03	9.9564E-01	2.76E-03
639.	5.160E + 06	1.94E-03	9.9553E-01	2.94E-03
625.	5.043E + 06	1.98E-03	9.9543E-01	3.09E-03
610.	4.927E + 06	2.03E-03	9.9531E-01	3.22E-03
596.	4.814E + 06	2.08E-03	9.9517E-01	3.36E-03
544.	4.389E + 06	2.28E-03	9.9450E-01	4.11E-03
531.	4.289E + 06	2.33E-03	9.9439E-01	4.34E-03
519.	4.192E + 06	2.39E-03	9.9427E-01	4.53E-03
507.	4.096E + 06	2.44E-03	9.9412E-01	4.72E-03

[a] The references from which the values were extracted are given in brackets.

TABLE VIII *(Continued)*

Rhenium

eV	cm^{-1}	μm	n	k
500.	4.033E + 06	2.48E-03		5.60E-03 [3]
496.	4.002E + 06	2.50E-03	9.9397E-01 [10]	4.92E-03 [10]
463.	3.734E + 06	2.68E-03	9.9346E-01	5.58E-03
452.	3.649E + 06	2.74E-03	9.9328E-01	5.82E-03
442.	3.566E + 06	2.80E-03	9.9310E-01	6.06E-03
432.	3.484E + 06	2.87E-03	9.9292E-01	6.30E-03
422.	3.404E + 06	2.94E-03	9.9272E-01	6.55E-03
400.	3.226E + 06	3.10E-03		7.30E-03 [3]
312.	2.521E + 06	3.97E-03	9.9002E-01 [10]	1.09E-02 [10]
300.	2.420E + 06	4.13E-03		1.14E-02 [3]
285.	2.299E + 06	4.35E-03	9.891E-01 [10]	1.25E-02 [10]
278.	2.246E + 06	4.45E-03	9.889E-01	1.29E-02
272.	2.195E + 06	4.56E-03	9.887E-01	1.33E-02
265.	2.145E + 06	4.66E-03	9.885E-01	1.37E-02
259.	2.096E + 06	4.77E-03	9.883E-01	1.40E-02
253.	2.048E + 06	4.88E-03	9.880E-01	1.44E-02
248.	2.001E + 06	5.00E-03	9.877E-01	1.48E-02
200.	1.613E + 06	6.20E-03		1.70E-02 [3]
196.	1.588E + 06	6.30E-03	9.836E-01 [10]	1.86E-02 [10]
170.	1.371E + 06	7.29E-03		2.00E-02 [3]
167.	1.351E + 06	7.40E-03	9.789E-01 [10]	2.16E-02 [10]
145.	1.176E + 06	8.50E-03	9.733E-01	2.48E-02
140.	1.129E + 06	8.86E-03		2.43E-02 [3]
124.	1.001E + 06	9.99E-03	9.633E-01 [10]	2.76E-02 [10]
120.	9.679E + 05	1.03E-02		2.76E-02 [3]
100.	8.065E + 05	1.24E-02		3.11E-02
100.	8.130E + 05	1.23E-02	9.364E-01 [10]	3.24E-02 [10]
90.	7.259E + 05	1.38E-02		4.22E-02 [3]
83.8	6.759E + 05	1.48E-02	8.919E-01 [10]	5.52E-02 [10]
80.	6.452E + 05	1.55E-02		6.93E-02 [3]
71.3	5.751E + 05	1.74E-02	8.479E-01 [10]	1.09E-01 [10]
70.	5.646E + 05	1.77E-02		1.25E-01 [3]
65.	5.243E + 05	1.91E-02		1.60E-01
60.6	4.888E + 05	2.05E-02	8.506E-01 [10]	2.11E-01 [10]
60.	4.839E + 05	2.07E-02		2.24E-01 [3]
59.	4.759E + 05	2.10E-02	0.65 [1]	.
58.	4.678E + 05	2.14E-02	0.64	
58.	4.678E + 05	2.14E-02		2.35E-01 [3]
57.	4.597E + 05	2.18E-02	0.65 [1]	.
56.	4.517E + 05	2.21E-02	0.66	
55.	4.436E + 05	2.25E-02	0.68	
55.	4.436E + 05	2.25E-02		2.44E-01 [3]
54.	4.355E + 05	2.30E-02	0.71 [1]	.
53.	4.275E + 05	2.34E-02	0.75	
52.	4.194E + 05	2.38E-02	0.77	
51.6	4.162E + 05	2.40E-02	9.120E-01 [10]	2.34E-01 [10]

(continued)

TABLE VIII *(Continued)*

Rhenium

eV	cm^{-1}	μm	n	k
51.	4.113E + 05	2.43E-02	0.79	
50.	4.033E + 05	2.48E-02	0.8	
50.	4.033E + 05	2.48E-02		2.30E-01 [3]
49.	3.952E + 05	2.53E-02	0.81 [1]	.
48.	3.871E + 05	2.58E-02	0.82	
47.	3.791E + 05	2.64E-02	0.83	
47.	3.791E + 05	2.64E-02		2.69E-01 [3]
46.	3.710E + 05	2.70E-02	0.84 [1]	.
45.	3.629E + 05	2.76E-02	0.87	
45.	3.629E + 05	2.76E-02		2.60E-01 [3]
44.	3.549E + 05	2.82E-02	0.88 [1]	.
43.	3.468E + 05	2.88E-02	0.88	
42.	3.388E + 05	2.95E-02	0.87	
41.	3.307E + 05	3.02E-02	0.87	
40.	3.226E + 05	3.10E-02	0.87	
40.	3.226E + 05	3.10E-02		1.70E-01 [3]
39.	3.146E + 05	3.18E-02	0.88 [1]	.
38.	3.065E + 05	3.26E-02	0.84	
37.	2.984E + 05	3.35E-02	0.8	
36.	2.904E + 05	3.44E-02	0.77	
35.	2.823E + 05	3.54E-02	0.74	
35.	2.823E + 05	3.54E-02		1.95E-01 [3]
34.	2.742E + 05	3.65E-02	0.7 [1]	.
33.	2.662E + 05	3.76E-02	0.67	
32.	2.581E + 05	3.87E-02	0.65	
31.	2.500E + 05	4.00E-02	0.64	
30.	2.420E + 05	4.13E-02	0.59	0.29 [1]
30.	2.420E + 05	4.13E-02		0.2919 [3]
29.	2.339E + 05	4.28E-02	0.55	0.34 [1]
28.	2.258E + 05	4.43E-02	0.51	0.41
27.6	2.226E + 05	4.49E-02	0.49	0.47
27.2	2.194E + 05	4.56E-02	0.48	0.50
26.8	2.162E + 05	4.63E-02	0.47	0.53
26.4	2.129E + 05	4.70E-02	0.46	0.57
26.0	2.097E + 05	4.77E-02	0.46	0.61
25.6	2.065E + 05	4.84E-02	0.46	0.64
25.2	2.033E + 05	4.92E-02	0.47	0.68
24.8	2.000E + 05	5.00E-02	0.47	0.72
24.4	1.968E + 05	5.08E-02	0.48	0.75
24.0	1.936E + 05	5.17E-02	0.49	0.79
23.6	1.903E + 05	5.25E-02	0.50	0.82
23.2	1.871E + 05	5.34E-02	0.52	0.85
22.8	1.839E + 05	5.44E-02	0.53	0.89
22.4	1.807E + 05	5.54E-02	0.55	0.92
22.0	1.774E + 05	5.64E-02	0.56	0.95
21.6	1.742E + 05	5.74E-02	0.57	0.98
21.2	1.710E + 05	5.85E-02	0.58	1.02

TABLE VIII *(Continued)*

Rhenium

eV	cm^{-1}	μm	n	k
20.8	1.678E + 05	5.96E-02	0.60	1.06
20.4	1.645E + 05	6.08E-02	0.61	1.10
20.2	1.629E + 05	6.14E-02	0.64	1.15
20.0	1.613E + 05	6.20E-02	0.65	1.17
19.8	1.597E + 05	6.26E-02	0.67	1.21
19.6	1.581E + 05	6.33E-02	0.72	1.25
19.6	1.581E + 05	6.33E-02	0.70	1.23
19.4	1.565E + 05	6.39E-02	0.74	1.27
19.2	1.549E + 05	6.46E-02	0.76	1.29
19.0	1.532E + 05	6.53E-02	0.79	1.31
18.8	1.516E + 05	6.59E-02	0.82	1.33
18.6	1.500E + 05	6.67E-02	0.85	1.35
18.4	1.484E + 05	6.74E-02	0.88	1.36
18.2	1.468E + 05	6.81E-02	0.92	1.37
18.0	1.452E + 05	6.89E-02	0.95	1.38
17.8	1.436E + 05	6.97E-02	0.99	1.39
17.6	1.420E + 05	7.04E-02	1.03	1.39
17.4	1.403E + 05	7.13E-02	1.06	1.39
17.2	1.387E + 05	7.21E-02	1.10	1.39
17.0	1.371E + 05	7.29E-02	1.14	1.38
16.8	1.355E + 05	7.38E-02	1.17	1.37
16.6	1.339E + 05	7.47E-02	1.21	1.35
16.4	1.323E + 05	7.56E-02	1.24	1.33
16.2	1.307E + 05	7.65E-02	1.26	1.30
16.0	1.290E + 05	7.75E-02	1.28	1.28
15.8	1.274E + 05	7.85E-02	1.29	1.26
15.6	1.258E + 05	7.95E-02	1.31	1.23
15.4	1.242E + 05	8.05E-02	1.31	1.20
15.2	1.226E + 05	8.16E-02	1.31	1.17
15.0	1.210E + 05	8.27E-02	1.29	1.14
14.8	1.194E + 05	8.38E-02	1.27	1.12
14.6	1.178E + 05	8.49E-02	1.24	1.12
14.4	1.161E + 05	8.61E-02	1.22	1.13
14.2	1.145E + 05	8.73E-02	1.21	1.14
14.0	1.129E + 05	8.86E-02	1.20	1.16
13.8	1.113E + 05	8.98E-02	1.19	1.18
13.6	1.097E + 05	9.12E-02	1.19	1.20
13.4	1.081E + 05	9.25E-02	1.20	1.21
13.2	1.065E + 05	9.39E-02	1.20	1.23
13.0	1.049E + 05	9.54E-02	1.21	1.25
12.8	1.032E + 05	9.69E-02	1.22	1.26
12.6	1.016E + 05	9.84E-02	1.23	1.27
12.4	1.000E + 05	1.00E-01	1.23	1.29
12.2	9.840E + 04	1.02E-01	1.25	1.30
12.0	9.679E + 04	1.03E-01	1.26	1.32
11.8	9.517E + 04	1.05E-01	1.28	1.33

(continued)

TABLE VIII *(Continued)*

Rhenium

eV	cm^{-1}	μm	n	k
11.6	9.356E + 04	1.07E-01	1.31	1.34
11.4	9.195E + 04	1.09E-01	1.33	1.34
11.2	9.033E + 04	1.11E-01	1.36	1.33
11.0	8.872E + 04	1.13E-01	1.37	1.31
10.8	8.711E + 04	1.15E-01	1.38	1.28
10.6	8.549E + 04	1.17E-01	1.36	1.25
10.4	8.388E + 04	1.19E-01	1.33	1.23
10.2	8.227E + 04	1.22E-01	1.29	1.22
10.0	8.065E + 04	1.24E-01	1.24	1.24
9.8	7.904E + 04	1.27E-01	1.20	1.27
9.6	7.743E + 04	1.29E-01	1.17	1.31
9.4	7.582E + 04	1.32E-01	1.14	1.36
9.2	7.420E + 04	1.35E-01	1.11	1.41
9.0	7.259E + 04	1.38E-01	1.09	1.46
8.8	7.098E + 04	1.41E-01	1.07	1.52
8.6	6.936E + 04	1.44E-01	1.06	1.58
8.4	6.775E + 04	1.48E-01	1.05	1.66
8.2	6.614E + 04	1.51E-01	1.05	1.74
8.0	6.452E + 04	1.55E-01	1.05	1.83
7.8	6.291E + 04	1.59E-01	1.08	1.93
7.6	6.130E + 04	1.63E-01	1.12	1.98
7.4	5.968E + 04	1.68E-01	1.12	2.08
7.2	5.807E + 04	1.72E-01	1.16	2.19
7.0	5.646E + 04	1.77E-01	1.22	2.28
6.8	5.485E + 04	1.82E-01	1.28	2.37
6.4	5.162E + 04	1.94E-01	1.42	2.56
6.2	5.001E + 04	2.00E-01	1.51	2.64
6.0	4.839E + 04	2.07E-01	1.61	2.74
5.9	4.759E + 04	2.10E-01	1.67	2.78
5.8	4.678E + 04	2.14E-01	1.73	2.81
5.7	4.597E + 04	2.18E-01	1.78	2.85
5.6	4.517E + 04	2.21E-01	1.84	2.88
5.5	4.436E + 04	2.25E-01	1.89	2.92
5.4	4.355E + 04	2.30E-01	1.96	2.96
5.3	4.275E + 04	2.34E-01	2.02	3.00
5.2	4.194E + 04	2.38E-01	2.10	3.04
5.1	4.113E + 04	2.43E-01	2.17	3.08
5.0	4.033E + 04	2.48E-01	2.25	3.12
4.9	3.952E + 04	2.53E-01	2.35	3.14
4.8	3.871E + 04	2.58E-01	2.44	3.17
4.7	3.791E + 04	2.64E-01	2.55	3.19
4.6	3.710E + 04	2.70E-01	2.67	3.18
4.5	3.629E + 04	2.76E-01	2.77	3.17
4.4	3.549E + 04	2.82E-01	2.88	3.15
4.3	3.468E + 04	2.88E-01	2.97	3.11
4.2	3.388E + 04	2.95E-01	3.05	3.06
4.1	3.307E + 04	3.02E-01	3.13	3.01

TABLE VIII *(Continued)*

Rhenium

eV	cm^{-1}	μm	n	k
4.0	3.226E + 04	3.10E-01	3.19	2.94
3.9	3.146E + 04	3.18E-01	3.22	2.88
3.8	3.065E + 04	3.26E-01	3.24	2.84
3.7	2.984E + 04	3.35E-01	3.24	2.81
3.6	2.904E + 04	3.44E-01	3.25	2.83
3.5	2.823E + 04	3.54E-01	3.28	2.84
3.4	2.742E + 04	3.65E-01	3.34	2.88
3.35	2.702E + 04	3.70E-01	3.39	2.90
3.30	2.662E + 04	3.76E-01	3.44	2.89
3.25	2.621E + 04	3.81E-01	3.50	2.88
3.20	2.581E + 04	3.87E-01	3.55	2.84
3.15	2.541E + 04	3.94E-01	3.57	2.79
3.10	2.500E + 04	4.00E-01	3.57	2.74
3.05	2.460E + 04	4.07E-01	3.56	2.71
3.00	2.420E + 04	4.13E-01	3.53	2.71
2.95	2.379E + 04	4.20E-01	3.51	2.72
2.90	2.339E + 04	4.28E-01	3.49	2.75
2.85	2.299E + 04	4.35E-01	3.51	2.83
2.80	2.258E + 04	4.43E-01	3.57	2.88
2.75	2.218E + 04	4.51E-01	3.65	2.91
2.70	2.178E + 04	4.59E-01	3.74	2.92
2.65	2.137E + 04	4.68E-01	3.83	2.88
2.60	2.097E + 04	4.77E-01	3.90	2.84
2.55	2.057E + 04	4.86E-01	3.96	2.78
2.50	2.016E + 04	4.96E-01	4.01	2.70
2.45	1.976E + 04	5.06E-01	4.01	2.60
2.40	1.936E + 04	5.17E-01	4.00	2.55
2.35	1.895E + 04	5.28E-01	3.97	2.47
2.30	1.855E + 04	5.39E-01	3.93	2.44
2.25	1.815E + 04	5.51E-01	3.89	2.40
2.20	1.774E + 04	5.64E-01	3.83	2.38
2.15	1.734E + 04	5.77E-01	3.78	2.39
2.10	1.694E + 04	5.90E-01	3.74	2.40
2.05	1.653E + 04	6.05E-01	3.69	2.41
2.00	1.613E + 04	6.20E-01	3.63	2.43
1.95	1.573E + 04	6.36E-01	3.59	2.46
1.90	1.532E + 04	6.53E-01	3.54	2.50
1.85	1.492E + 04	6.70E-01	3.51	2.57
1.80	1.452E + 04	6.89E-01	3.47	2.59
1.75	1.411E + 04	7.08E-01	3.42	2.65
1.70	1.371E + 04	7.29E-01	3.38	2.72
1.65	1.331E + 04	7.51E-01	3.34	2.80
1.60	1.290E + 04	7.75E-01	3.29	2.88
1.55	1.250E + 04	8.00E-01	3.25	3.01
1.50	1.210E + 04	8.27E-01	3.23	3.12
1.45	1.169E + 04	8.55E-01	3.22	3.25

(continued)

TABLE VIII *(Continued)*

Rhenium

eV	cm^{-1}	μm	n	k
1.40	1.129E + 04	8.86E-01	3.23	3.38
1.35	1.089E + 04	9.18E-01	3.24	3.46
1.30	1.049E + 04	9.54E-01	3.20	3.56
1.25	1.008E + 04	9.92E-01	3.14	3.70
1.20	9.679E + 03	1.03E + 00	3.08	3.89
1.15	9.275E + 03	1.08E + 00	3.04	4.14
1.10	8.872E + 03	1.13E + 00	3.05	4.39
1.05	8.469E + 03	1.18E + 00	3.07	4.65
1.00	8.065E + 03	1.24E + 00	3.09	4.96
0.95	7.662E + 03	1.31E + 00	3.17	5.27
0.90	7.259E + 03	1.38E + 00	3.26	5.61
0.85	6.856E + 03	1.46E + 00	3.39	5.95
0.80	6.452E + 03	1.55E + 00	3.55	6.32
0.77	6.210E + 03	1.61E + 00	3.65	6.53
0.75	6.049E + 03	1.65E + 00	3.77	6.75
0.73	5.888E + 03	1.70E + 00	3.94	6.94
0.70	5.646E + 03	1.77E + 00	4.13	7.09
0.68	5.485E + 03	1.82E + 00	4.30	7.19
0.65	5.243E + 03	1.91E + 00	4.44	7.26
0.63	5.081E + 03	1.97E + 00	4.52	7.31
0.60	4.839E + 03	2.07E + 00	4.53	7.40
0.57	4.597E + 03	2.18E + 00	4.51	7.53
0.55	4.436E + 03	2.25E + 00	4.45	7.73
0.50	4.033E + 03	2.48E + 00	4.34	8.26
0.45	3.629E + 03	2.76E + 00	4.17	9.03
0.40	3.226E + 03	3.10E + 00	3.99	10.15
0.35	2.823E + 03	3.54E + 00	3.93	11.54
0.30	2.420E + 03	4.13E + 00	3.73	13.44
0.25	2.016E + 03	4.96E + 00	3.47	16.27
0.20	1.613E + 03	6.20E + 00	3.28	20.66
0.15	1.210E + 03	8.27E + 00	3.28	28.08
0.10	8.065E + 02	1.24E + 01	4.25	42.83

Optical Constants of Eight Rare Earth Elements: (Ce), (Sm), (Gd), (Tb), (Dy), (Er), (Tm), and (Yb)

L. WARD
Coventry University
Coventry, U.K.

INTRODUCTION I

The 14 rare-earth elements or lanthanides lie in the periodic table between atomic numbers 58 and 71, cerium to lutecium, and are generally characterized by a basic electron configuration of $6s^2\ 5d^1$ and the progressive filling of the $4f$ electron shell. The exceptions to this rule are europium (atomic number 63), which has 7 $4f$ electrons and none in the $5d$ shell, and ytterbium (atomic number 70), which has 14 $4f$ and no $5d$; both of these elements have cubic structures. The rest are hexagonal and so are able to exhibit anisotropic optical properties; some researchers have reported values of optical constants with both $\mathbf{E} \| \mathbf{c}$ and $\mathbf{E} \perp \mathbf{c}$ (the c-axis is at right angles to the hexagonal plane), and these results have been included where suitable. The optical behavior of all the elements in this group between 10 and 10,000 eV is generally governed by the 3, 4, and $5d$ electrons ($M_{4,5}$, $N_{4,5}$, and O_{1-3}) as the $4f$ electrons lie in a narrow localized band and are shielded by the outer $5p$ and $6s$ electrons, which are in overlapping bands giving a high density of states close to the Fermi energy. This situation allows many quantum transitions between these bands and the Fermi energy at low photon energies (1 to 5 eV), giving rise to several absorption peaks in this spectral region. The general shapes of the Fermi surfaces and energy-band structures are complicated but similar in all the heavy rare-earth elements. However, the two elements Eu and Yb are much simpler in this respect, and they behave more like the transition metals.

It is proposed to deal firstly with these elements as a group and then to consider the individual elements later. Eight rare-earth elements will be con-

HANDBOOK OF OPTICAL CONSTANTS OF SOLIDS III

Copyright © 1998 by Academic Press.
All rights of reproduction in any form reserved
ISBN 0-12-544423-0/$25.00.

sidered in this survey: Ce, Sm, Gd, Tb, Dy, Er, Tm, and Yb. The first seven have hexagonal structures, whereas the last, Yb, is cubic. Ce is cubic below 100 K (α-phase) but becomes hexagonal (γ-phase) at higher temperatures.

All the rare-earth metals are highly reactive with oxygen and hydrogen (in water vapor); many of the older measurements that were made in air on solid materials are, therefore, suspect because of possible contamination from these sources, which will cause values of both n and k to be too small. Most modern experimenters have attempted to overcome this problem by carrying out measurements on polycrystalline thick films deposited in a very high vacuum, and so more faith should be given to these more recent results. Where any choice has been available, the later results have been quoted in this article, unless there were compelling reasons otherwise.

Some of the rare-earth metals exhibit paramagnetism at room temperature but become ferromagnetic or antiferromagnetic at lower temperatures. Thus, the light rare-earth metals (Ce to Eu) order antiferromagnetically at low temperatures, whereas the heavy rare-earths (Gd to Tm) may become either ferromagnetic or antiferromagnetic. These effects are connected with the coupling between the uncompensated magnetic moments of the $4f$ electrons and those of the outer electrons by a process known as s–f exchange coupling; depending on the sign of the coupling, either ferro- (positive coupling) or antiferromagnetism (negative coupling) will result. Thus, gadolinium becomes ferromagnetic with a Curie point of 293 K, whereas dysprosium firstly becomes antiferromagnetic with a Néel temperature of 179 K and then ferromagnetic below the Curie temperature of 85 K. Several authors have studied the optical properties of rare-earth metals in low-temperature regions and also at higher temperatures up to about 470 K in order to investigate the effects of these magnetic transformations. Where appropriate, sets of results in all these temperature regions have been included. The values of Curie and Néel temperatures quoted have been obtained from the *Handbook of Physics and Chemistry* [1].

At one time, the rare-earth metals were regarded merely as scientific curiosities that possessed a range of interesting theoretical properties, but now they are finding increasing practical use in a number of commercial applications: for example, as alloys for the storage of computer information, in superconductors, and in optical materials. In recent years, a significant trend in published work in this area has been devoted to the properties of alloys of rare-earth metals with erbium, gadolinium, and ytterbium. The optical properties of these alloys will not be discussed in this chapter, but useful references are Kuron *et al.* [2], Atkinson *et al.* [3], and Memon *et al.* [4]; a triennial conference held by the Rare Earths Research Group is devoted to the properties of such materials [5].

There are comparatively few direct results for n and k for the rare-earth elements. However, some authors have measured the absorption coefficient, α, which is related to k by the equation $\alpha = 4\pi k/\lambda$, so that k may be calcu-

lated, but no value is obtained for n. Similarly, the optical conductivity, σ, may be reported, and this is related to ϵ_2 by $\sigma = \epsilon_2\omega/4\pi$. If both α and ω are measured, n and k can then be determined. There are also scarcities of published values for very low energies (far infrared) and in the range 5–30 eV. Another problem in obtaining accurate data for n and k is that many authors publish their results in graphical form only. In general, it is possible to read off data from these graphs to at best about 1%.

There have been several reviews of the optical and electrical properties of the rare-earth metals. Gasgnier [6] divided his account into three energy ranges, viz.: 0–6 eV, 6–50 eV, and high energies (up to 300 eV). In the low-energy, long-wavelength region, he noted particularly the wide divergences in values by different authors, probably due to surface conditions, crystal structure, and contamination, mainly oxides and hydroxides, and this is borne out in the plots of n and k versus wavelength. The center energy range was dominated by the plasma resonances, whereas the high range featured the N_{4-5} absorption edge.

Knyazev and Noskov [7] have given an in-depth study of the optics of the lanthanides, also looking at different wavelength regions and considering free-electron and interband-absorption mechanisms and also the effect of magnetic transformations. In addition, these authors have published a large number of papers dealing with the optical properties of some of the individual elements, which will be referred to under the appropriate sections. Lynch [8] has given a broad review of the optical properties of these metals in an article in *The Rare Earths in Modern Science and Technology.*

Weaver *et al.* [9] followed their earlier survey of the optical properties of the transition elements by a similar collation of data from various authors that covered the lanthanides and the actinides; they present tables of values of ϵ_1, ϵ_2, n, and k between 0.1 and 5.0 eV.

Another source of the optical constants of the rare-earth metals is Volume 15b of "Landolt–Börnstein New Series" [10], which has tables of n and k versus wavelength for Dy, Sm, Tm, Tb, and Gd, as well as some graphs of σ versus λ for other elements in this group.

For all the rare-earth elements, Henke *et al.* [11, 12] have tables of values of the x-ray interaction coefficients, f_1 and f_2, from which n and k may be calculated, between photon energies of 30 and 10,000 eV, that is, 0.13 and 40 nm.

Thus, $n = 1 - r_0 N f_1 \lambda^2/2\pi$ and $k = r_0 N f_2 \lambda^2/2\pi$, where r_0 = classical electron radius = $2.8179\ 10^{-15}$ m, N = no. of atoms/unit volume = Avogadro's no. $\times$ density/atomic wt., and λ = wavelength in micrometers.

As with other metals, the optical properties of this group of elements are determined by the interactions of the bound and free electrons with the electric field of the incident wave. At wavelengths greater than about 1 μm the free-electron effects are dominant and Drude-like equations may be used to describe their optical properties. Knyazev and Noskov [13] used a two-term Drude equation to describe the properties of samarium, terbium, and dys-

prosium. This makes use of two values each for the electron-relaxation frequency, ω_t, and the plasma frequency, ω_p; the first term in this equation is much larger than the second and agrees well with the values of ω_t and ω_p quoted by other sources. At shorter wavelengths, that is, higher frequencies, interband transitions become significant, and each element shows a series of absorption edges due to the various electron shells; *L, M, N,* and *O* bands are the most significant, and values of the energies for these absorptions will be given for each element considered. Schuler [14] has given a general discussion of these properties, particularly the interband transitions near the symmetry points in the Brillouin zone, where the joint density of states is very high; he gives a table of possible electron transitions in this region.

All the lanthanides show three strong absorption edges in the high-energy region, the N_4 and N_5 transitions between 120 and 180 eV (7 to 10 nm); those between the M_4 and M_5 levels (3*d* electrons) in the range 900 to 1600 eV (0.78 to 1.4 nm); and the *L* band (2*p* electrons) between 6000 and 10,000 eV (0.13 to 0.20 nm). These lines move progressively to larger energies, i.e., shorter wavelengths, as the atomic number increases. The values of the energies of the *L, M, N* and *O* absorption bands quoted have been taken from either Kaye and Laby [15] or the *Physics Handbook* [16].

The energy region between 70 and 500 eV, which includes the N_4 and N_5 electron transitions, has been covered by several groups of workers. Tables by Henke *et al.* [12] cover this region but do not allow the accurate pinpointing of absorption peaks as the values of the photon energies quoted are too far apart. Gribovskii and Zimkina [17, 18] have reported values of the mass absorption coefficients, μ_m, for La, Ce, Pr, Nd, Sm, Gd, Tb, Dy, Ho, Er, Tm, and Yb between 70 and 500 eV, determined by transmission measurements. Their results can be used to calculate values of k ($k = \mu_m \rho \lambda/4\pi$ where ρ = density). In the later paper [18] they used x-ray emission to study the $N_{4,5}$ spectra of Gd, Tb, and Dy in this region.

Formichev *et al.* [19] have published graphs of the absorption coefficient against photon energy for all the rare-earth elements between 95 and 185 eV. Although these are useful in identifying absorption lines, the absorption scale is only arbitrary, and no quantitative information can be extracted. However, their figures give details of the fine-structure maxima for all the lanthanides. Another paper by the same group [20] extended the study to 500 eV for the elements Ce, Pr, Nd, Sm, Eu, Gd, Dy, and Ho. Similarly, Muto *et al.* [21] have studied Eu, Gd, Tb, Dy, and Ho in the 4*d*–4*f* excitation region between 140 and 180 eV using circularly polarized synchrotron radiation as a source to irradiate thin films (~10 nm thick) on polycarbonate cooled to liquid-nitrogen temperature; diagrams show the absorption coefficient (arbitrary units) versus photon energy. The absorption peaks are as follows: Eu 142 eV, Gd 148 eV, Tb 158 eV, Dy 165 eV, and Ho (a flat top) between 167 and 173 eV. These values were also confirmed in the work of Trebbia and Colliex [22].

Kunz [23] observed that all the foregoing results display the systematic absorption behavior due to the progressive lowering in energy of the empty *f* states until these states are finally filled at Lu. The large peak due to transitions into empty 4*f* states migrates towards the ionization limit, while the binding energy of the 4*d* levels increases, producing a shift in the whole absorption feature towards higher photon energies. Finally, when the 4*f* states are filled with 14 electrons, the peak disappears. The fine structures in the absorption coefficient are fairly simple in La but become increasingly complex as the number of filled *f* states increases; in Yb, however, when only one empty *f* state remains, the fine structures become simple again. Gerken *et al.* [24] have noted the energy differences between the emission spectra of the 4*f* electrons from the surface and from the bulk atoms for the lanthanides.

Weaver and Lynch [25] carried out measurements at 4.2 K on the elements Gd, Tb, Dy, Ho, Er, Tm, and Lu in solid form; they measured (a) the optical conductivity, σ, and (b) the optical absorptivity A, defined as $1 - R$ between 0.1 and 5.0 eV in both states of polarization. ϵ_2 may be calculated from σ as described earlier, and n may then be obtained from A using the normal-incidence formula for $1 - R$ [26] to compute ϵ_1. Their results are presented in great detail elsewhere [9]. However, there appear to be errors in all the values of k quoted for these elements. The values of k given in the present article have been recalculated from the values of n and ϵ_2, $(2\ n\ k)$, and now agree with Weaver and Lynch's values for ϵ_1, $(n^2 - k^2)$. In a private communication [27] these authors give optical constants up to 18 eV for dysprosium.

Dzionk *et al.* [28] were able to observe the 5p (*O*) excitations in Gd, Tb, Dy, Er, Tm, and Yb by using the photoionic yields from these elements.

Petrakian [29, 30] adopted a different technique by measuring the reflectance and transmittance of films of thickness d, calculating the absorptivity, A, now defined as $1 - R - T$, and then, using the Wolter formula [31], to obtain $\epsilon_2 = n\ A\ \lambda/2\ \pi\ d\ T$. Petrakian observed that all the lanthanides exhibited an absorption maximum between 5.5 and 6.5 eV, which he ascribed to indirect electron transitions between the 4*f* levels and the Fermi level. In addition, the heavy rare-earths gave an extra peak near 3.1 eV that was not thickness dependent and that he claimed was due to a direct interband transition.

Several authors have reported plasmons in the rare-earth metals. These include Bakulin *et al.* [32], Colliex *et al.* [33], Tsveiman *et al.* [34], and Zashkvara *et al.* [35]. Netzer *et al.* [36] used electron-energy-loss techniques to study plasmons in polycrystalline films of most of the rare-earth metals. Surface plasmons occurred between 4 and 5 eV, whereas bulk plasmons were found between 7 and 14 eV; in both cases, the plasmon energies increased with atomic number. The surface plasmon was found to be very sensitive to oxidation.

Data for each of the rare-earth elements are now presented.

II CERIUM

Crystal structure α = f.c.c., γ = h.c.p.; space group Fm3m O_h^5; atomic number 58; atomic weight 140.1; density α 8.16 $\times$ 10^3 kg/m^3, density γ 6.80 $\times$ 10^3 kg/m^3; electron configuration $4f^1$ $5d^1$ $6s^2$.

Cerium can exist in two phases; at low temperatures the α (f.c.c.) phase is present, and this changes to the γ (hex h.c.p.) phase above about 100 K.

The main absorption edges for cerium are 6516, 6131, and 5690 eV (L) and 1152, 902, and 883 (M_{3-5}) [15]. The $M_{1,2}$ edges occur at 1435 and 1273 eV, whereas N and O edges are at 289 (N_1), 207 ($N_{2,3}$), 112 (N_4), 108 (N_5), 38 (O_1), and 18 eV ($O_{2,3}$) [16]. Henke-model calculations of k [12] show peaks at 885 (M_5) and 131 eV. In the overlap region, the Haensel *et al.* [37] values of k determined from measurements of absorption using synchrotron radiation are in reasonable agreement with the Henke model and indicate a peak between 125 and 130 eV. Suzuki *et al.* [38] have also measured the absorption coefficient for cerium between 100 and 170 eV, recording a broad band peaking at 124 eV, when k = 0.0748, which is very close to the value of Haensel *et al.*

Results for polycrystalline cerium between 0.18 and 6.2 eV have been published by Kirillova *et al.* [39, 40] paying particular attention to the changes due to magnetic and phase transitions. The specimens were electropolished and finally cleaned by bombardment with argon ions; the optical technique used was ellipsometry. It was noted that both n and k increased with the duration of the argon cleaning process until saturation values were obtained after about 200 minutes. The values of both n and k were much larger at 293 K (γ-phase) than at 78 K (α-phase); peaks were observed in n and k in both the α- and γ-phases at about 5.8 eV, as also reported by Petrakian [41]. Two peaks were observed in the curves of conductance versus energy; in the γ-phase there was a narrow peak at 0.35 eV and a wider one at 1.6 eV, whereas in the α-phase the two peaks were of equal width and occurred at 0.75 and 1.8 eV. Kirillova *et al.* claimed that these features supported the theory that, on passing from γ to α, the $4f$ band delocated into a $4f'$ band.

The optical conductivity of thin films of α- and γ-cerium in the range 1.5 to 5.4 eV were studied by Rhee *et al.* [42] using ellipsometry. They found monotonic decreases in σ with energy for both phases and also that σ increased on passing from the γ- to the α-phase because of the increase in the number of electrons per unit volume associated with the change in density that occurs at the phase change.

Plasmons were observed by Zashkvara *et al.* [35]; the bulk plasmon occurred at 8.9 eV and the surface plasmon at 4.1 eV. They also observed the O_{2-3} transition at 20.3 eV and the O_1 transition at 38.6 eV.

Figure 1 shows a log-log plot of n (○) and k (△) versus λ for cerium and incorporating values from Henke [12], Haensel *et al.* [37], and Kirillova *et al.* [39, 40] at 295 K. The n and k curves cross at 0.14 μm, that is, 8.9 eV;

this value of the plasmon energy is in good agreement with that reported by Zashkvara *et al.* [35].

SAMARIUM III

Crystal structure trigonal; space group R3m D_{3d}^5 atomic number 62; atomic weight 150.4; density 7.75×10^3 kg/m^3; electron configuration $4f^6\ 6s^2$.

Absorption edges for samarium occur at 7707 eV (L_1), 7278 (L_2), 6683 (L_3), 1388 (M_3), 1106 (M_4), and 1081 (M_5) [15]; 1728 (M_1), 1546 (M_2), 351 (N_1), 251 ($N_{2,3}$), 137 (N_4), 33 (O_1), and 26 eV ($O_{2,3}$) [16].

Data for the optical constants, n and k, of samarium at high energies have been obtained from Henke's model [12]; these show absorption peaks at about 1120 eV ($M_{4,5}$), and 138 eV (N_4); there is also a slight shoulder at 350 eV (N_1).

The results for k from Gribovskii and Zimkina [17, 18] overlap with Henke's for energies less than 150 eV, and there is reasonably good agreement in this region, the peak at 150 eV being well defined. Haensel *et al.* [37] used synchrotron radiation to determine the absorption coefficients of samarium between 70 and 180 eV, and their values of k agree with Henke's at 170 eV, but are less satisfactory at lower energies.

Knyazev and Noskov [43], working at 293 K, give tables of n and k between 1 and 3 eV. Other, later, sets of results have been published by the same authors [44] between 0.06 and 1.24 eV and at three different temperatures: 85, 293, and 460 K. Where these two groups of results touch at about 1.0 eV, the agreement is excellent. The Néel temperature of samarium is 109 K; results from Knazev and Noskov [44] span this temperature. No dramatic changes in n and k were observed over this magnetic transformation but, in general, k decreases while n increases with temperature up to 460 K over this energy range.

Values of the relaxation and plasma frequencies were calculated by Knyazev and Noskov [44] at all the three temperatures they used and are as follows:

T (K)	ω_t (eV)	ω_p (eV)
80	0.16	11.6
293	0.42	11.7
460	0.59	12.5

Figure 2 shows a log–log plot of n (○) and k (△) versus λ for samarium using values due to Henke [12] Haensel *et al.* [37], Gribovskii and Zimkina [17, 18], and Knyazev and Noskov [43]. It is not easy to get an accurate

value for the crossover point, so the plasma frequency has not been calculated.

IV GADOLINIUM

Crystal structure hex; Space group: $P6_3/mmc$ D_{6h}^4; atomic number 64; atomic weight 157.3; density 7.90×10^3 kg/m^3; electron structure $4f^7$ $5d^1$ $6s^2$.

The L_{1-3} edges are at 8343, 7898, and 7211eV, respectively, whereas the M_{3-5} occur at 1511, 1217, and 1185 eV [15]. The "Physics Handbook" [16] gives 1888 (M_1), 1695 (M_2), 383 (N_1), 311 (N_2), 272 (N_3), 147 (N_4), 142 (N_5), 43 (O_1), and 28 eV (O_2).

Henke *et al.* [12] found M-absorption peaks at 1672 eV (M_2) and 1181 eV (M_5) and also one at about 143 eV (N_5). Results from Gribovskii and Zimkina [17, 18] for k agree well with the Henke-model values at all the overlap energies and also show a clear peak at 146 eV. The O_1 peak near 31 eV is also visible.

Erskine and Flynn [45] have given data for α between 2 and 35 eV using the direct absorption technique. Absorption peaks were found at 7, 8, 24, and 33 eV. These authors claim good agreement with the more accurate ellipsometric measurements of Erskine *et al.* [46] in the overlap region between 4.5 and 5.5 eV (the latter only give ϵ_2, so they are not included in the table of results). Results from Erskine and Flynn fit well with Henke's at 30 eV. Another set of results covering the range 2 to 160 eV has been given by Cukier *et al.* [47]; they found a volume plasmon at 13 eV and the O_2 and O_3 peaks at 25 and 35 eV, respectively. Quemerais *et al.* [48] also covered gadolinium, presenting graphs of ϵ_1, ϵ_2, and σ versus energy up to 15 eV, which overlap with Erskine and Flynn. The agreement is not perfect, but is very good at 12 eV; there were peaks in conductance at 2 and 4–8 eV. Also covering this energy range were Weaver and Lynch [25] at 4.2 K and in both states of polarization; n was smaller for $\mathbf{E} \| \mathbf{c}$, whereas k was larger in this case. At this temperature n showed a peak at 2.0 μm; this was different from the results of Knyazev and Noskov [52], where n continued to increase with wavelength.

Miller *et al.* [49] obtained the optical constants and conductivity of gadolinium from reflectance ratios at oblique incidence on opaque films in the range 1.8 to 3.1 eV. They found optical transitions at 1.95, 2.15, 2.50, 2.75, and 3.1 eV, corresponding to a series of interband transitions. Miller *et al.* [50] used thermally modulated reflectance measurements to study Gd over the energy range 1.45 to 3.2 eV. Another worker with Gd was Myers [51], who employed ellipsometry on thin films; however, he failed to observe the detailed structures described by Miller *et al.* [49]. Instead, the conductivity

only showed some indistinct structure superimposed on a general monotonically decreasing background; a broad peak at 2 eV was identified as due to electron transitions from the Fermi level to the empty *d*-band.

Knyazev and Noskov [52] give values of n and k at 293 K between 1.2 and 3.4 eV. Their experimental technique was to measure the reflectance and phase change on reflection using the method of Bolotin *et al.* [53] on four polycrystalline flat mirrors, mechanically polished. Gadolinium became metallic, i.e., $k > n$ at 1.77 eV. A further series of results by these authors [54] covered the range 1 to 20 μm at temperatures of 80, 293, and 460 K; k was found to decrease with temperature, whereas n increased. There was good agreement where these two sets of values at 293 K touched at 1.0 eV. Knyazev *et al.* [55] have also reported on the infrared absorption of Gd, Tb, and Dy single crystals.

Hodgson and Clayet [56] measured the optical constants of gadolinium at temperatures of 105 and 293 K in the range 0.5 to 2.5 eV using the internal reflectance of evaporated films deposited on silica glass prisms. They found a decrease in n and an increase in k with temperature; they also discovered absorption bands at 0.7 and 1.1 eV. Their results were close to those of Weaver and Lynch [25] and also Krizek and Taylor [57], who employed ellipsometry on evaporated films over the range 0.5 to 2.5 eV and at temperatures of 56 and 300 K. It was only at low energies that ϵ_1 and σ changed rapidly because of the Drude free-electron contribution; there was also a peak at 2.0 eV caused by an interband transition. By assuming that the hexagonal gadolinium could be treated as isotropic, Krizek and Taylor were able to make a theoretical calculation of both the optical conductivity and ϵ_1; this gave the absorption band at 1.6 eV (293 K) and 1.8 eV (105 K).

Petrakian *et al.* [58, 59], who used the technique due to Querry [60] to measure the reflectances in both states of polarization, have reported values of the optical conductivity of gadolinium between 1 and 5 eV at temperatures between 10 K and 300 K. In the ferromagnetic state (below 293 K) an extra peak in conductivity was observed at 0.69 eV and was ascribed to the *s–p* exchange interaction; this peak increased in magnitude as the temperature decreased. Both n and k tended to decrease with temperature, particularly at the lower energies. They compared their results graphically with those of Hodgson and Clayet [56], Erskine *et al.* [46], and Knyazev and Noskov [52]. All the results from investigations over this energy range showed a peak in conductivity at about 1.5 eV and, in addition, two (Petrakian *et al.* [58, 59] and Knyazev and Noskov [52]) indicated a second peak at about 2.5 eV. The most striking feature of this graph, however, was the wide spread of the values of conductivity over this energy range among the various authors, those of Hodgson and Clayet being about three times greater than the values of Knyazev and Noskov, with the other two sets lying between. The results quoted here are taken from both papers by Petrakian *et al.* [58, 59].

Knyazev and Bolotin [61] used polarimetry to measure the optical con-

stants of single crystals of gadolinium both along the hexagonal axis (c) and in the basal plane (a). Transition to the magnetic ordered state was accompanied by the appearance of resonance absorption peaks in the near infrared that may be associated with quantum transitions of electrons between energy bands split by the exchange interaction between the $4f$ and the s and p electrons. This interaction depends on the orientation of the magnetic moment of the unfilled $4f$ shell and consequently may oscillate; if the period of the oscillations is different from that of the lattice, extra gaps form in the energy spectrum. This is the mechanism of exchange-split bands. At 80 K there was a clear extra peak due to this effect at 0.7 eV (1.77 μm) together with smaller peaks at 1.5 and 2.2 eV. The changes in n and k with temperature are comparatively small, but k tends to decrease with increase in temperature, whereas n increases.

Erskine *et al.* [46], using ellipsometry, have measured values of conductivity for gadolinium between 1.25 and 5.5 eV at temperatures of 80 and 295 K; however, σ on its own only allows the calculation of ϵ_2, so their results have not been quoted. But, they, too, present a graph of σ versus eV for gadolinium at room temperature comparing results from Schuler [14], Petrakian *et al.* [58, 59], Hodgson and Clayet [56], Knyazev and Noskov [52], and themselves. A strong peak was observed between 1.5 and 2.5 eV by all the authors, but a second peak at 5–6 eV was found only by Petrakian, Schuler, and themselves. There was again a wide spread in the values of conductivity from the various authors, the lowest being obtained by Knyazev and Noskov and the highest by Petrakian; this is probably due to the reactive nature of this element, which leads to surface contamination.

Daniels [62] claimed to observe plasmons (plasma resonance) at 16.2 eV for gadolinium, but Colliex *et al.* [33] gave a value of 14.2 eV, the difference being probably again due to surface contamination. Other values for plasmons are 9.9 eV (bulk) and 4.7 eV (surface) [35]. The theoretical value is 11.2 eV. Knyazev and Noskov [13] were able to deduce the relaxation and plasma frequencies from their double Drude-like equation and give the following values versus temperature.

T (K)	ω_t (eV)	ω_p (eV)
80	0.43	10.4
293	0.58	9.1
460	0.58	7.2

Ponosov and Bolotin [63], looking at Raman scattering spectra from single crystals of gadolinium, found evidence of a transverse optical phonon at 171.8 μm.

The values of n(○) and k(△) for gadolinium plotted in log–log form in Fig. 3 come from Henke [12], Haensel *et al.* [37], Gribovskii and Zimkina [17],

Knyazev and Noskov [52] (295 K), Krizek and Taylor [57], and Hodgson and Clayet [56]. The n–k plasmon crossover occurs at 10.0 eV, close to that given by Knyazev and Noskov. Figure 3 shows two sets of values for n at wavelengths greater than about 1 μm: those of Knyazev and Noskov [52], in which n increases steadily with wavelength, and those due to Weaver and Lynch at 4.2 K, where there is a peak at 2.0 μm.

TERBIUM V

Crystal structure h.c.p.; space group $P6_3/mmc$ D_{6h}^4; atomic number 65; atomic weight 158.9; density 8.23×10^3 kg/m^3; electron configuration $4f^2\ 6s^2$.

The L_{1-3} absorption edges occur at 8679, 8221, and 7484 eV, respectively, whereas M_{3-5} edges are found at 1583, 1275, and 1241 eV [15]. The "Physics Handbook" [16] gives the following edges in electron volts: 1970 (M_1), 1710 (M_2), 400, 322, 284, 152, 148 (N_{1-5}), 42, and 28 ($O_{1,2}$).

Henke-model results [12] show k peaking at 1240 eV (M_5) and 151 eV (N_4), then falling and rising again at 30 eV. In their overlap region (70 to 170 eV), the results for k from Gribovskii and Zimkina [17,18] show a general agreement with Henke-model values except at 150 eV, where their value is only half that of the Henke model at this peak in k. There is a sharp absorption peak at 151 eV, and the results from Gribovskii and Zimkana may be slightly off peak.

Knyazev and Noskov [64] have published results for terbium at 80, 293, and 450 K in the visible and infrared regions measured by polarimetry, the specimens being mechanically polished and chemically etched before being finally cleaned in an argon discharge. The polarization technique due to Beattie [65] was employed using one reflection in the visible and two for the infrared; an accuracy of between 3 and 5% was claimed.

Values of σ for terbium have also been published by Erskine *et al.* [46] between 1.25 and 5.5 eV and at two temperatures, 80 and 300 K, using an automatic ellipsometer. The Néel temperature of terbium is 230 K, whereas the Curie temperature is close by at 219.5 K. The results of these authors do not show any dramatic change in conductivity over the magnetic transformation points, but generally indicate a simple increase in σ with temperature. Miller *et al.* [49] report values between 1.8 and 3.1 eV using the technique of reflectance ratios; there were optical transitions at 1.90, 2.20, and 2.45 eV due to a number of interband transitions, but only these authors have reported such absorption detail. Krizek and Taylor [57] used ellipsometry to measure both ϵ_1 and σ for terbium films in a similar spectral region (0.35 and 2.5 eV) at temperatures of 20 and 300 K. Weaver and Lynch [25]

have reported values of n and k at 4.2 K for both states of polarization measured by ellipsometry. The agreement between their results and those of Krizek and Taylor is quite good; k increases with temperature over the whole energy range, whereas n decreases below 1.5 eV but increases above 1.5 eV. However, the values of n from Weaver and Lynch peak at 3 μm, whereas those of Knyazev and Noskov show a continuous increase with wavelength. The results of Knyazev *et al.* [55] on single crystals are also included.

Ponosov and Bolotin [63] have also studied terbium by Raman-scattering spectra and found an optical phonon at 166.9 μm.

Colliex *et al.* [33] give a value of the bulk plasmon as 13.3 eV. The following values of ω_t and ω_p were obtained by Knyazev and Noskov [54].

T (K)	ω_t (eV)	ω_p (eV)
80	0.31	11.2
293	0.53	11.5
460	0.86	12.6

$n(\circ)$ and $k(\triangle)$ versus λ for terbium are shown in log–log form in Fig. 4 using data from several references. The crossover of n and k (plasmon) occurs at 13.1 eV. Figure 4 gives two sets of points for n for wavelengths greater than 1.0 μm. The first, due to Knyazev and Noskov, shows n increasing with wavelength, but the second, from Weaver and Lynch [25] at 4.2 K, indicates n reaching a maximum at about 2 μm.

VI DYSPROSIUM

Crystal structure h.c.p.; space group $P6_3/mmc$ D_{6h}^4; atomic number 66; atomic weight 162.5; density 8.54×10^3 kg/m^3; electron configuration $4f^{10}\ 6s^2$.

L-absorption edges occur at 9013 (L_1), 8553 (L_2), and 7762 eV (L_3); M_{3-5} peaks are located at 1642, 1333, and 1295 eV [15]. The following values are for other peaks: 2050 (M_1), 1845 (M_2), 419 (N_1), 339 (N_2), 297 (N_3), 158 (N_4), 155 (N_5), 66 (O_1), and 29 eV (O_2) [16].

Henke's model [12] shows absorption peaks at 1672 eV (M_3), 1295 eV (M_5) and 159 eV (N_4) and a shoulder at 443 eV (N_1). Results from Gribovskii and Zimkina [17, 18] for k below 170 eV are always lower than the Henke-model values by about 30% but show a peak at 160 eV.

A set of results has been published by Quemerais *et al.* [48] using multiangle reflectance measurements, which gives σ and ϵ_1 between 2 and 30 eV in graphical form; this is one of the few studies of the rare-earth elements to cover this spectral range. n and k have been calculated by the

method described earlier and show effects at the $5p^{3/2}$ and $5p^{1/2}$ thresholds. At 30 eV, their values of k are almost 30% lower than the ones from the Henke model, but are in line with those of Gribovskii and Zimkina.

Dysprosium has also been studied by Weaver and Lynch [25] in both the $\mathbf{E} \parallel \mathbf{c}$ and $\mathbf{E} \perp \mathbf{c}$ states of polarization over the energy range 0.1 to 5.0 eV and at 4.2 K as described earlier. As with some other rare-earth metals at this temperature, their values of n showed a peak in the infrared, whereas the results of other workers at higher temperatures show a steady increase in n with increasing wavelength. Krizek and Taylor [57], using ellipsometry, give values of n and k between 0.4 and 2.5 eV at 56 and 300 K; there is a small increase in both n and k as the temperature increases. There was evidence of slight structure in σ at 0.4 eV in the results at 56 and 97 K. Values of σ have also been reported by Erskine *et al.* [46] at 80 K between 1.25 and 5.5 eV, using their automatic-ellipsometer technique. These showed peaks at 22.1 eV ($O_{2,3}$) and 33.5 eV (O_1), but, as it is not possible to deduce n and k, their results have been omitted. Cukier *et al.* [47] found a plasmon at 14 eV and the O-peaks at 25 and 38 eV.

Knyazev *et al.* [40] have given values of n and k between 1 and 4 eV at 293 K and a further set of values occurs in their later paper [54]. Knyazev *et al.* [66] have reported work on single crystals of dysprosium at temperatures between 80 and 293 K both along the hexagonal axis (c) and in the basal plane (a). Dysprosium is paramagnetic at room temperature, becomes antiferromagnetic at 179 K, and finally ferromagnetic below 89 K. A peak developed in the calculated conductivity along the hexagon (c) axis as the temperature decreased for both the anti- and ferromagnetic states. Similar peaks occuring in the conductivity in the basal (a) plane were very much smaller. A further investigation into both states of polarization on single-crystal dysprosium has been carried out by Knyazev *et al.* [55].

Daniels [62] reported a bulk plasma resonance (plasmon) at 15.8 eV for Dy, whereas Colliex *et al.* [33] gave a figure of 14.0 eV, the presence of contamination probably accounting for the difference. Other values of these plasmons are 10.9 eV (bulk) and 5.2 eV (due to the metal–oxide interface) [35]. The following values of ω_t and ω_p were given by Knyazev and Noskov [13] from their double Drude model.

T (K)	ω_t (eV)	ω_p (eV)
80	0.20	10.8
293	0.39	11.8
460	0.64	13.6

Demers *et al.* [67] and also Ponosov and Bolotin [63] using Raman-scattering spectra have reported the presence of an optical phonon in dysprosium at 160.3 μm.

Figure 5 shows log–log plots of $n(\circ)$ and $k(\triangle)$ versus wavelength for dysprosium using data from Henke [12], Gribovskii and Zimkina [17, 18], Quemerais *et al.* [48], Weaver and Lynch [25], Knyazev and Noskov [40, 54], Knyazev *et al.* [55] and Krizek and Taylor [57]. The plasmon crossover between n and k is at 6.9 eV, considerably lower than that observed by Knyazev and Noskov [13].

VII ERBIUM

Crystal structure h.c.p.; space group $P6_3/mmc$ D_{6h}^4; atomic number 68; atomic weight 167.3; density 9.07×10^3 kg/m^3; electron configuration $4f^{12}\ 6s^2$.

L-type edges occur at 9725, 9243, and 8336 eV, corresponding to L_{1-3}, respectively, whereas M_{3-5} edges are at 1783, 1453, and 1409 eV [15]; $M_{1,2}$ are at 2211 and 2010 eV, and N_{1-5} are located at 453, 366, 320, 172, and 169 eV, respectively; $O_{1,2}$ occur at 64 and 33 eV [16].

The absorption peaks revealed by Henke's model [12] are at 1442 eV (M_4), 1401 eV (M_5) and 167 eV (N_5). The values of k derived from the Gribovskii and Zimkina data [17] between 170 and 70 eV are about 10% lower than those of the Henke model in the overlap region but show a sharp peak just above 170 eV.

The imaginary part of the dielectric constant, ϵ_2, can be calculated from values of the optical conductivity σ ($\sigma = \epsilon_2\ \omega/4\ \pi$). Weaver and Lynch [25] and also Krizek and Taylor [57], both using ellipsometry, report values of σ versus ω over the ranges 0.1–5.0 eV and 0.35–2.5 eV, respectively. Weaver and Lynch give values of n and k in two crystallographic directions at 4.2 K; for $\mathbf{E} \parallel \mathbf{c}$, n is larger than for $\mathbf{E} \perp \mathbf{c}$, whereas the opposite is the case for k. (The c-axis is at right angles to the hexagon.) In both orientations, n peaks at about 1.2 μm and then decreases with increasing wavelength. This is the only set of results for temperatures below the Curie point (20 K).

Values of n and k for bulk polycrystalline erbium have been reported by Knyazev and Noskov [68] over the range 0.06 to 4.4 eV and at temperatures between 56 and 293 K; these were determined by polarimetry. n increased with increasing temperature, while k decreased. Both n and k were monotonic between 0.06 and 0.27 eV at all temperatures, indicating that intraband transitions were dominant in this region. The electron relaxation frequency decreased with increasing temperature. Above 0.27 eV interband transitions took over, and there was a broad peak in conductivity centered about 2 eV. Below the Néel temperature (84 K), a new structure appeared in the conductivity at an energy of 0.28 eV, and this was ascribed to the transition to the antiferromagnetic state. In addition, Knyazev and Bolotin [69] measured n and k using ellipsometry on erbium single crystals; values for

both $\mathbf{E} \| \mathbf{c}$ and $\mathbf{E} \perp \mathbf{c}$ were obtained between 0.2 and 5.6 eV and at temperatures of 78 and 293 K, and the errors were estimated at between 2 and 5%. The conductivities in each state were calculated and, when plotted against energy, indicated quantum absorption mainly at about 0.7 eV in a band close to the Fermi surface. Erbium becomes antiferromagnetic at 85 K, and a new peak in the conductivity appeared at about 0.3 eV in both states of polarization for the values at 78 K; the value of this peak predicted from theory was 0.26 eV.

Demers *et al.* [67], using Raman-scattering techniques, discovered an optical phonon in erbium at about 160 μm.

Figure 6 shows log–log plots of $n(\circ)$ and $k(\triangle)$ versus λ for erbium using data from Henke [12], Gribovskii and Zimkina [17], Weaver and Lynch [25], Knyazev and Noskov [68], and Knyazev and Bolotin [69]. The crossover point gives the plasma frequency as 6.9 eV. At wavelengths greater than 1 μm two sets of points for n are plotted. That due to Knyazev and Noskov shows n steadily increasing, whereas that for Weaver and Lynch indicates a peak in n at about 1.5 μm, then a dip to 2.5 μm before n starts to rise again.

THULIUM VIII

Crystal structure h.c.p.; space group $P6_3/mmc$ D_{6h}^4; atomic number 69; atomic weight 168.9; density 9.325×10^3 kg/m^3; electron configuration $4f^{13}\ 6s^2$.

The main absorption edges are as follows: L_1 is at 10,097, L_2 at 9601, and L_3 at 8632 eV, whereas M_{3-5} are at 1861, 1515, and 1468 eV, respectively [15]. Other absorption edges from [16] are 2305 and 2088 ($M_{1,2}$), 470, 382, 333, 180, and 176 eV (N_{1-5}), and 51 and 30 eV ($O_{1,2}$).

The absorption peaks from Henke's model [12] are 1461 eV (M_5) and 183 eV. Gribovskii and Zimkina [17] give values of k between 70 and 170 eV showing a peak developing beyond 180 eV; the agreement with the Henke-model results is within 10%.

Weaver and Lynch [25] have given results for both $\mathbf{E} \| \mathbf{c}$ and $\mathbf{E} \perp \mathbf{c}$ between 0.1 and 5.0 eV at 4.2 K, which is below the Curie temperature of thulium (32 K). n and k are flat between 1 and 2 μm, but although k then resumes its steady increase with increasing wavelength, n decreases at greater wavelengths.

Knyazev and Noskov [70] have published results between 0.062 and 1.24 eV at 80, 293, and 450 K; as the temperature increased, k tended to increase, while n decreased. Knyazev and Bolotin [69] studied single crystals of thulium at 78 and 293 K also with $\mathbf{E} \| \mathbf{c}$ and $\mathbf{E} \perp \mathbf{c}$. Thulium remains paramagnetic down to 58 K, so no magnetic transformations were observed in this work.

Knyazev and Noskov [13] give the following values of ω_t:

T (K)	ω_t (eV)
80	2.93
293	1.00
450	0.69

Figure 7 shows log–log plots of $n(\circ)$ and $k(\triangle)$ versus λ for thulium using data from Henke [12], Gribovskii and Zimkina [17], Knyazev and Noskov [70], and Knyazev and Bolotin [69]; the crossover (plasma resonance) occurs at 6.5 eV, which is smaller than the value given by Knyazev and Noskov. Once again, there are two separate sets of points for n for wavelengths longer than 1 μm, those due to Knyazev and Bolotin and the others from Weaver and Lynch [25]. The latter show that n is flat between 1 and 2 μm and then continues to increase with increasing wavelength.

IX YTTERBIUM

Crystal structure f.c.c.; space group Fm3m O_h^5; atomic number 70; atomic weight 173.0; density 6.996×10^3 kg/m^3; electron configuration $4f^{14}6s^2$.

Ytterbium is the only rare-earth metal in this survey to have a cubic structure. Consequently, it does not exhibit anisotropic optical properties and, in fact, is considered to behave similarly to a transition metal.

The L-absorption edges are at 10479 eV (L_1), 9968 eV (L_2), and 8933 eV (L_3), whereas M_{3-5} occur at 1948, 1576, and 1528 eV [15]; M_1 is at 2397, M_2 at 2172 eV, and N_{1-5} at 487, 399, 346, 189, and 185 eV, whereas $O_{1,2}$ are 53 and 23 eV, respectively [16].

Henke's model [12] indicates absorption peaks at 1550 eV (M_5) and 1943 eV (M_3), as well as at 191 eV (N_4); there is also a shoulder at 393 eV (N_2). The studies of Gribovskii and Zimkina [17] overlap below 170 eV, and their values of k are in very good agreement (5%) with the those derived from Henke's model. No peak is indicated within their range of energies, but a shoulder occurs at 140 eV.

Studies of the optical constants of ytterbium (and europium) have been made by Endriz and Spicer [71] using reflectances over the range 0.5 to 11.5 eV and then employing Kramers–Kronig analysis to obtain ϵ_1, ϵ_2, σ, and α; an overall accuracy of only 20% was claimed for these results. These authors compared their results for these two rare-earth metals with those for the transition elements barium and strontium, which have similar crystal structures and electron configurations; the absorption graphs for these elements were very similar in shape, indicating that the absorption mechanisms were similar in all four elements.

Petrakian [72] measured the conductivity of Yb and also noted that this element behaves similarly to the alkali metal strontium in having broad absorption peaks near 3 and 6 eV. He also published a graph comparing the values of optical conductivity for ytterbium in the energy range 0–6 eV obtained by himself, Muller [73], and Hodgson and Cleyet [56]. These all show a strong peak between 1.5 and 2.0 eV whose height differs markedly between authors. For energies above 2.0 eV, the conductivity values of the three authors differ considerably; this spread is probably because of the differing surface conditions of the specimens.

Muller [73] also studied the same four elements and presented a graph of σ versus E between 0.5 and 5.5 eV. Although his results do not agree well with those of other workers, they have been included in the tables.

Idczak and Zukowska [74] used the ellipsometric technique devised by Idzak *et al.* [75] to measure n and k for thick ytterbium films (350 nm) in the infrared between 1 and 25 μm (0.05 to 0.62 eV); both n and k steadily increase with increasing wavelength in this region where the optical properties are dominated by the free electrons. In addition, Zukowska and Oleszkiewicz [76] have reported single values of n and k for ytterbium using a laser at 632.8 nm. ($n = 1.68$, $k = 3.22$.) They noted that both n and k decreased over a 24-hour period when the specimen was exposed to air, illustrating the effect of oxidation on the optical constants.

A plasmon was detected at 10.0 eV by Bakulin *et al.* [32] using electron energy loss.

Log–log plots of n (○) and k (△) versus λ are shown in Fig. 8, incorporating the results of Henke [12], Gribovskii and Zimkina [17], Endriz and Spicer [71], and Idzak and Zukowska [74]. The plasma frequency given by the crossover point is 11.5 eV, which agrees reasonably well with that just given.

REFERENCES

1. "Handbook of Chemistry and Physics," 1995/6, 76th Ed., pp. 4–115, CRC Press, Roca Raton, Florida, New York, London, and Tokyo.
2. Y.-S. Kuron, T. Suzuki, and T. Kasuya, Physical properties of actinides and rare earth compounds. *Jpn. J. App. Phys., Ser.* **8**, 104–116 (1993).
3. R. Atkinson, R. Gamble, P. F. Gu, and P. H. Lissberger, *Thin Solid Films* **162**, 89 (1988).
4. A. Memon, M. N. Khan, S. Al-Dallal, D. B. Tanner, and C. D. Porter, *Physica C* **185**, 1009 (1991).
5. 20th Rare Earths Research Conference, Monterey, California, Sept. 12–17, 1993.
6. M. Gasgnier, *Phys. Status Solidi A* **57**, 11 (1980).
7. Yu. V. Knyazev and M. M. Noskov, *Phys. Status Solidi B* **80**, 11 (1977).
8. D. W. Lynch, "The Rare Earths in Modern Science and Technology" (G. J. McCarthy and J. J. Rhyne, eds.), p. 461. Plenum, New York and London, 1978.
9. J. H. Weaver, C. Krafta, D. W. Lynch, and E. E. Koch, Physik Daten No. 18–2, Fachinformationszentrum, Karlsruhe, Germany, 1981.
10. "Landolt-Börnstein New Series, Volume III/15(b), Metals: Electronic Transport Phenomena" (K.-H. Kellwege and J. T. Olsen, eds.), Springer-Verlag, Heidelberg, 1985.
11. B. L. Henke, *Am. Inst. Phys., Conf. Proc.* **75**, 146 (1981).

12. B. L. Henke, P. Lee, T. J. Tanaka, R. Shimabukaro, and B. K. Fujikama, *At. Data Nucl. Data Tables* **27**, 1 (1982).
13. Yu. V. Knyazev and M. M. Noskov, *Phys. Met. Metall.* **32**, 1189 (1971).
14. C. C. Schuler, "Optical Properties and Electronic Structure of Metals and Alloys," p. 221. North-Holland, Publ., Amsterdam, 1966.
15. G. W. C. Kaye and T. H. Laby, "Tables of Physical and Chemical Constants," 16th Ed., pp. 384–385. Longmans, Harlow, U.K., 1995.
16. "Physics Handbook," pp. 72–76, Chartwell-Bratt, Bromley, U.K., 1980.
17. S. A. Gribovskii and T. M. Zimkina, *Opt. Spectrosc.* **35**, 104 (1973).
18. S. A. Gribovskii and T. M. Zimkina, *Sov. Phys. Solid State* **15**, 217 (1973).
19. V. A. Fomichev, T. M. Zimkina, S. A. Gribovskii, and I. I. Zhukova, *Sov. Phys. Solid State* **9**, 1163 (1967).
20. T. M. Zimkina, V. A. Fomichev, S. A. Gribovskii, and I. I. Zhukova, *Sov. Phys. Solid State* 9, 1128 (1967).
21. S. Muto, S.-Y. Pak, S. Imada, K. Yamaguchi, Y. Kagoshima, and T. Miyahara, *J. Phys. Soc. Jpn.* **63**, 1179 (1994).
22. P. Trebbia and C. Colliex, *Phys. Status Solidi B* **58**, 523 (1973).
23. C. Kunz, "Optical Properties of Solids—New Developments" (B. O. Seraphin, ed.), p. 473. North-Holland, Amsterdam, 1975.
24. F. Gerken, A. S. Flodstrom, J. Barth, L. I. Johannson, and C. Kunz, *Phys. Scr.* **32**, 43 (1985).
25. J. H. Weaver and D. W. Lynch, *Phys. Rev. Lett.* **34**, 1324 (1975).
26. L. Ward, "Optical Properties of Bulk Materials and Thin Films," 2nd Ed., p. 10. Institute of Physics Publ., Bristol, 1994.
27. J. H. Weaver, private communication, 1996.
28. C. Dzionk, W. Fiedler, M. V. Luche, and P. Zimmermann, *Phys. Rev. A* **41**, 3572 (1990).
29. J. P. Petrakian, *J. Opt. Soc. Am.* **62**, 401 (1972).
30. J. P. Petrakian, *Thin Solid Films* **38**, 83 (1976).
31. H. Wolter, *Z. Phys.* **105**, 269 (1937).
32. E. A. Bakulin, L. A. Balabanova, E. V. Sleppin, and V. V. Shcherbinina, *Sov. Phys. Solid State* **13**, 189 (1969).
33. C. Colliex, M. Gasgnier, and P. Trebbia, *J. Phys. (Paris)* **37**, 397 (1976).
34. E. V. Tsveiman, V. S. Red'kin, V. V. Zashkvara, and M. I. Kovsunskii, *Sov. Phys. Solid State* **58**, 156 (1975).
35. V. V. Zashkvara, E. V. Tsveiman, M. I. Kovsunskii, and V. S. Red'kin, *Sov. Phys. Solid State* **14**, 1564 (1972).
36. F. P. Netzer, G. Strasser, G. Rosina, and J. A. D. Matthew, *Surf. Sci.* **152/153**, 757 (1985).
37. R. Haensel, P. Rabe, and B. Sonntag, *Solid State Commun.* **8**, 1845 (1970).
38. S. Suzuki, T. Ishu, and T. Sagawa, *J. Phys. Soc. Jpn.* **38**, 156 (1975).
39. M. M. Kirillova, Yu. V. Knyazev, and Yu. I. Kuzmin, *Thin Solid Films* **234**, 527 (1993).
40. Yu. V. Knyazev, M. M. Kirillova, Yu. I. Kuzmin, and E. Z. Rivman, *Sov. J. Low Temp. Phys.* **17**, 1143 (1991).
41. J. P. Petrakian, *Thin Solid Films* **13**, 269 (1972).
42. J. T. Rhee, X. Wang, B. N. Harmon, and D. W. Lynch, *Phys. Rev. B* **51**, 17390 (1995).
43. Yu. V. Knyazev and M. M. Noskov, *Phys. Met. Metall.* **30**, 230 (1970).
44. Yu. V. Knyazev and M. M. Noskov, *Phys. Met. Metall.* **33**, 87 (1972).
45. J. L. Erskine and C. F. Flynn, *Phys. Rev. B* **14**, 2197 (1976).
46. J. L. Erskine, G. A. Blake, and C. W. Flaten, *J. Opt. Soc. Am.* **64**, 1322 (1974).
47. M. Cukier, B. Gauthe, and C. Wehenkehl, *J. Phys. (Paris)* **41**, 603 (1980).
48. A. Quemerais, B. Loisel, G. Jezequel, J. Thomas, and J. C. Lemonnier, *J. Phys. F* **11**, 293 (1981).
49. R. F. Miller, L. S. Julian, and A. J. Taylor, *J. Phys. F* **4**, 2338 (1974).
50. R. F. Miller, M. Syms, and L. S. Julien, *J. Phys. D* **12**, 1985 (1979).

51. H. P. Myers, *J. Phys. F* **6**, 141 (1976).
52. Yu. V. Knyazev and M. M. Noskov, *Phys. Met. Metall.* **32**, 71 (1971).
53. G. A. Bolotin, M. M. Noskov, and I. I. Sasovshaya, *Phys. Met. Metall.* **35**, 24 (1973).
54. Yu. V. Knyazev and M. M. Noskov, *Phys. Met. Metall.* **35**, 26 (1973).
55. Yu. V. Knyazev, M. M. Kirillova, and S. A. Nikitin, *Phys. Met. Metall.* **12**, 33 (1990).
56. J. N. Hodgson and B. Clayet, *J. Phys. C* **2**, 97 (1969).
57. J. Krizek and K. W. R. Taylor, *J. Phys. F* **5**, 774 (1975).
58. J. P. Petrakian, N. A. Mokhtar, and R. Fraisse, *Solid State Commun.* **24**, 377 (1977).
59. J. P. Petrakian, N. A. Mokhtar, and R. Fraisse, *J. Phys. F* **7**, 2431 (1977).
60. M. P. Querry, *J. Opt. Soc. Am.* **59**, 876 (1969).
61. Yu. V. Knyazev and G. A. Bolotin, *Phys. Met. Metall.* **58**, 70 (1984).
62. J. Daniels, *Opt. Commun.* **3**, 13 (1977).
63. Yu. S. Ponosov and G. A. Bolotin, *Sov. Phys. Solid State* **35**, 1437 (1993).
64. Yu. V. Knyazev and M. M. Noskov, *Opt. Spectrosc.* **38**, 672 (1975).
65. J. R. Beattie, *Philos. Mag.* **46**, 223 (1955).
66. Yu. V. Knyazev, T. A. Motveyena, and G. A. Bolotin, *Phys. Met. Metall.* **54**, 74 (1982).
67. R. I. Deners, S. Kong, M. V. Klein, R. Du, and C. P. Flynn, *Phys. Rev. B* **38**, 11523 (1988).
68. Yu. V. Knyazev and M. M. Noskov, *Sov. J. Low Temp. Phys.* **4**, 376 (1978).
69. Yu. V. Knyazev and G. A. Bolotin, *Phys. Met. Metall.* **61**, 57 (1986).
70. Yu. V. Knyazev and M. M. Noskov, *Opt. Spectrosc.* **43**, 424 (1977).
71. J. G. Endriz and W. E. Spicer, *Phys. Rev. B* **2**, 1466 (1970).
72. J. P. Petrakian, *Thin Solid Films* **20**, 297 (1974).
73. W. E. Muller, *Phys. Lett.* **17**, 82 (1965).
74. E. Idzak and K. Zukowska, *Thin Solid Films* **75**, 139 (1981).
75. E. Idzak, E. Oleszkiewicz, and K. Zukowska, *J. Phys. E* **22**, 410 (1989).
76. K. Zukowska and E. Oleszkiewicz, *Thin Solid Films* **224**, 217 (1993).

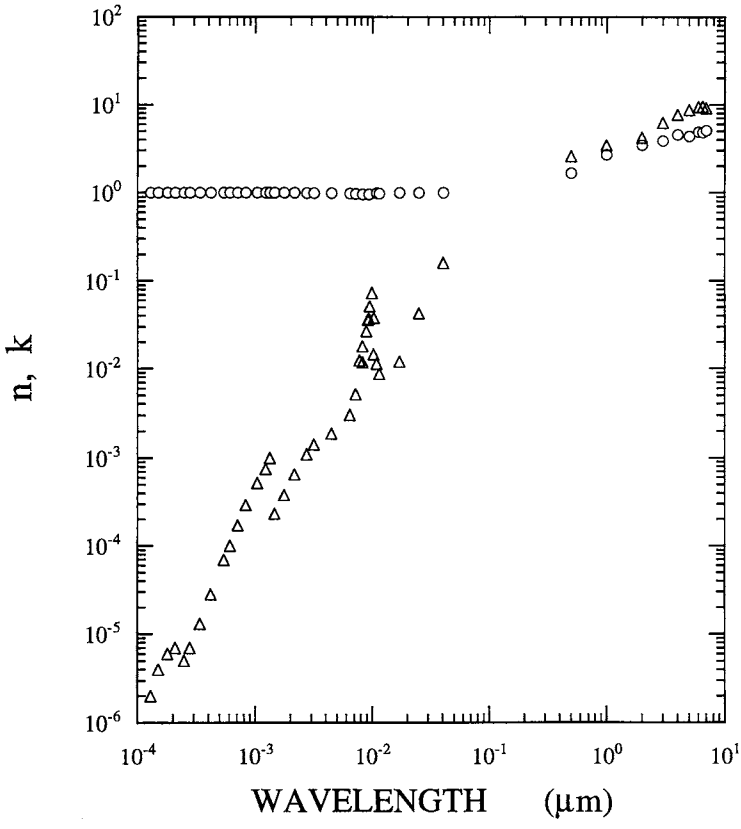

Fig. 1. Log–log plots of n (○) and k (△) versus wavelength in micrometers for cerium (unpolarized radiation).

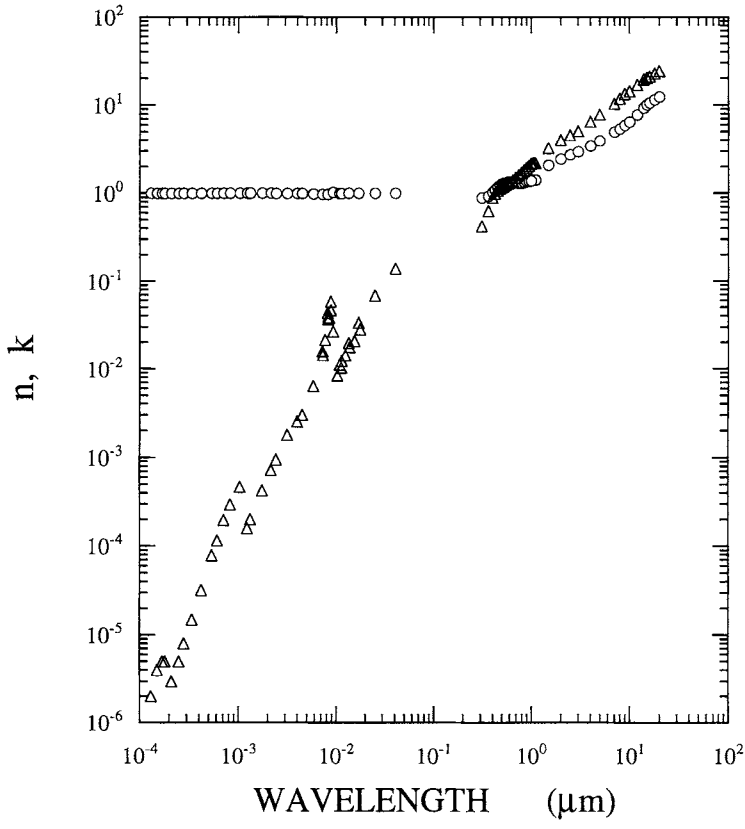

Fig. 2. Log–log plots of n (○) and k (△) versus wavelength in micrometers for samarium (unpolarized radiation).

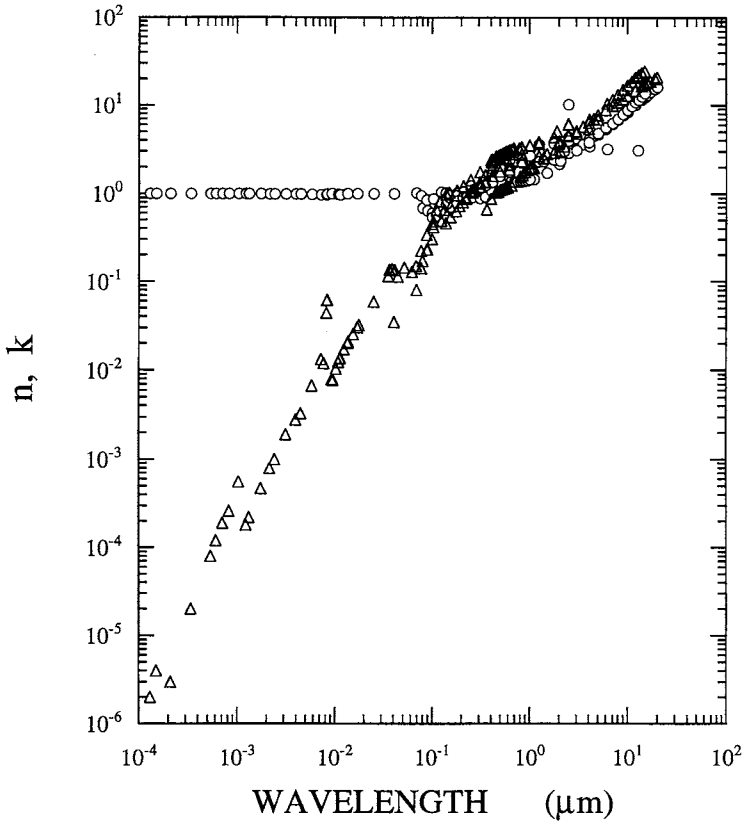

Fig. 3. Log–log plots of n (○) and k (△) versus wavelength in micrometers for gadolinium (unpolarized radiation or polarized $\mathbf{E} \parallel \mathbf{c}$).

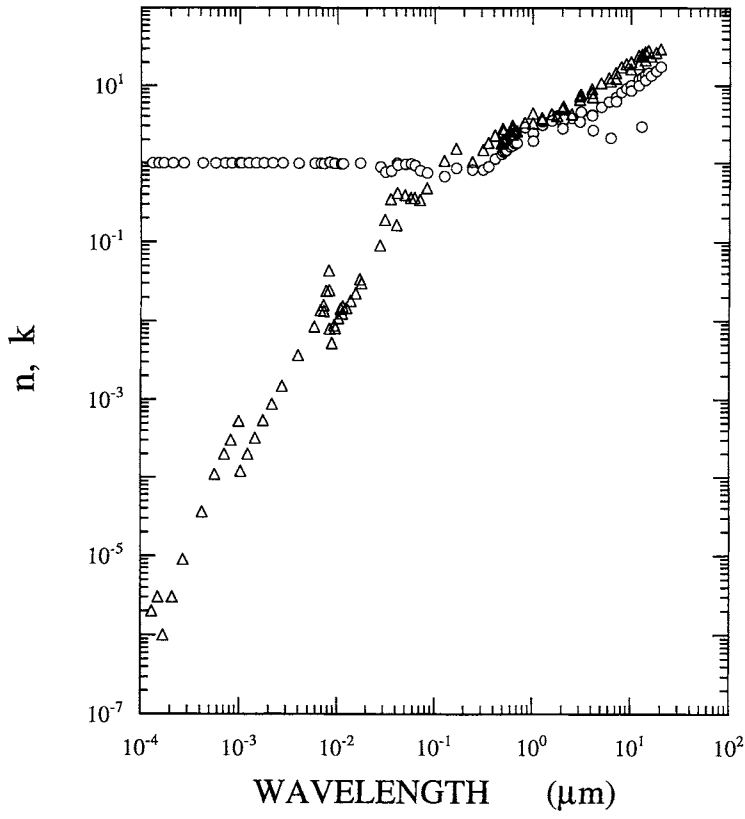

Fig. 4. Log–log plots of n (○) and k (△) versus wavelength in micrometers for terbium (unpolarized radiation or polarized $\mathbf{E} \parallel \mathbf{c}$).

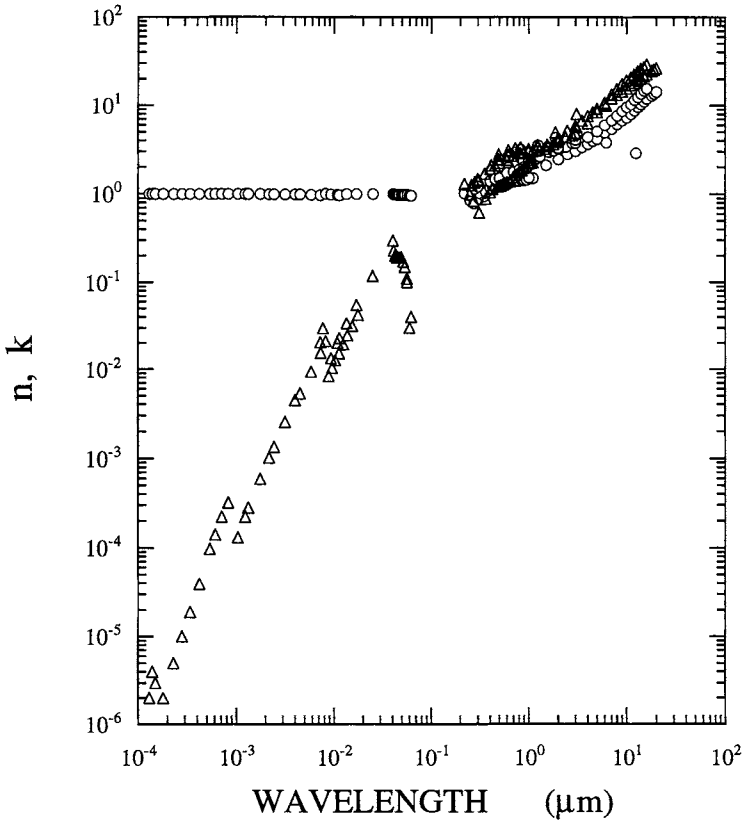

Fig. 5. Log–log plots of n (○) and k (△) versus wavelength in micrometers for dysprosium (unpolarized radiation or polarized $\mathbf{E} \parallel \mathbf{c}$).

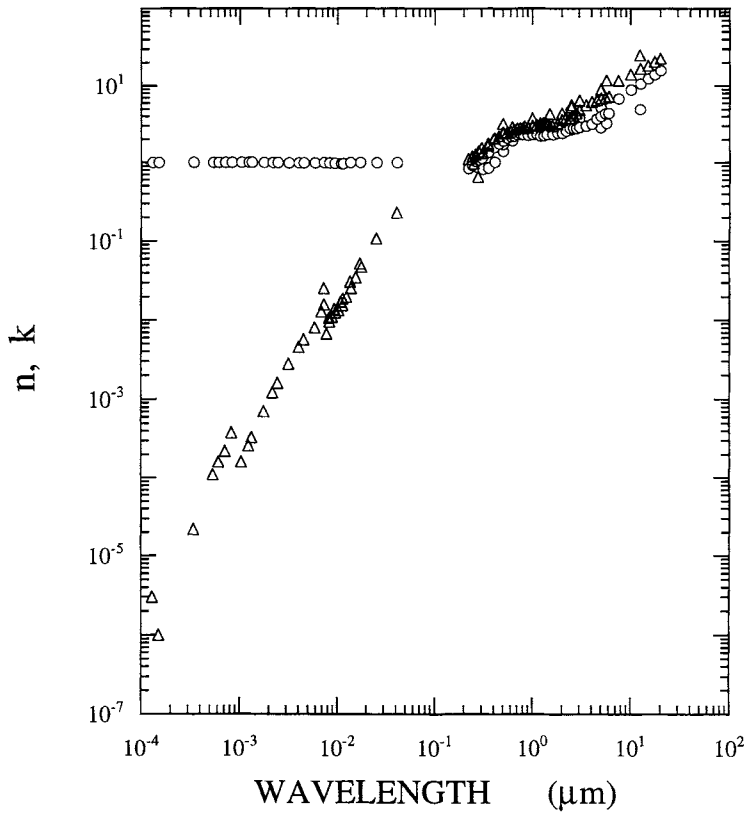

Fig. 6. Log–log plots of n (○) and k (△) versus wavelength in micrometers for erbium (unpolarized radiation or polarized $\mathbf{E} \parallel \mathbf{c}$).

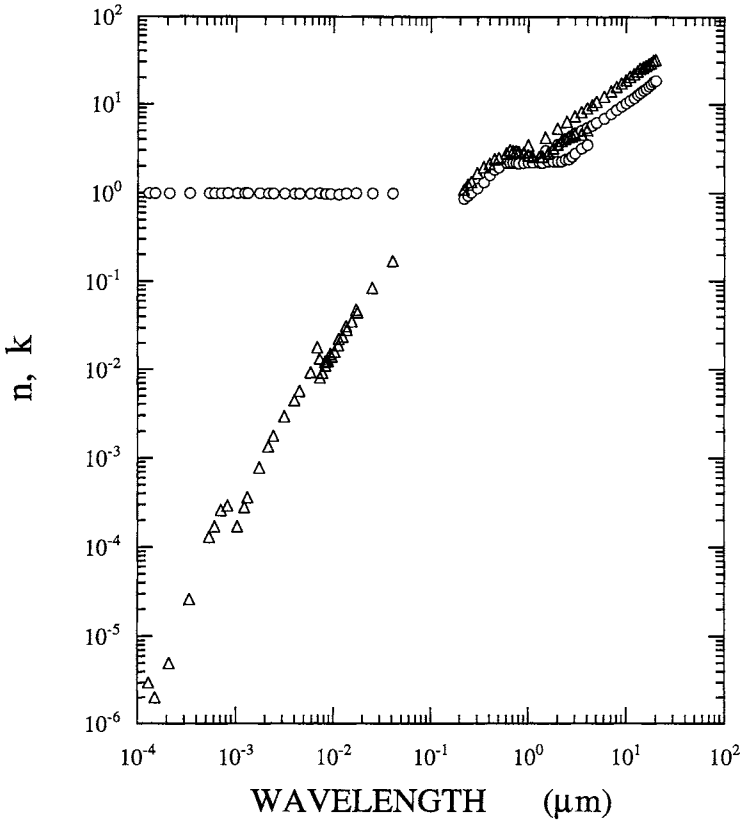

Fig. 7. Log–log plots of n (○) and k (△) versus wavelength in micrometers for thulium (unpolarized radiation or polarized $\mathbf{E} \parallel \mathbf{c}$).

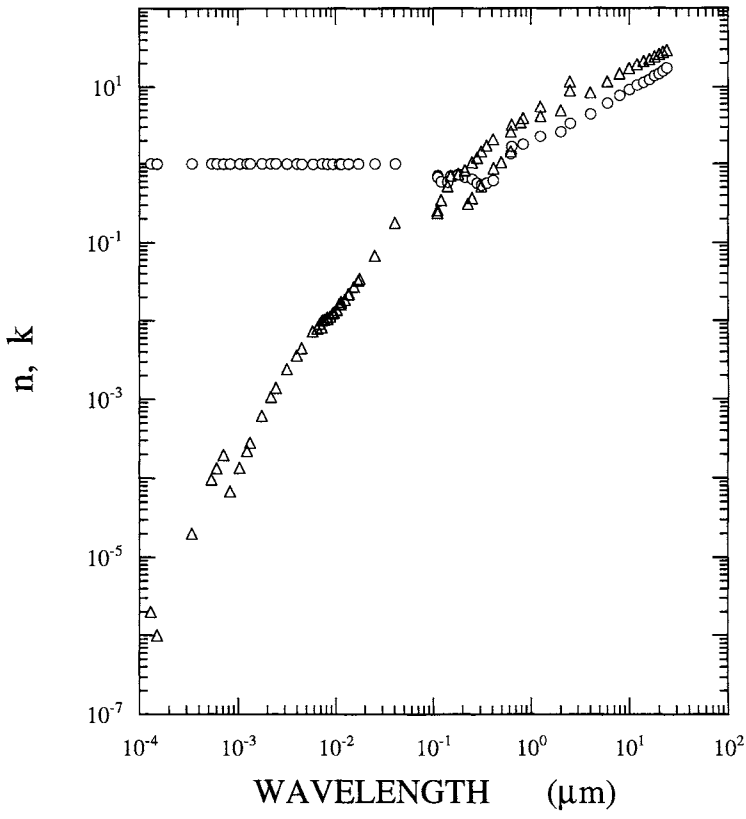

Fig. 8. Log–log plots of n (○) and k (△) versus wavelength in micrometers for ytterbium (unpolarized radiation).

TABLE I

Values of n and k for Cerium from Various References[a]

eV	cm^{-1}	μm	n	k	
9886.40	79738680	0.00013	1.000	0.000002	[12]
8047.80	64909460	0.00015	1.000	0.000004	
6930.30	55896272	0.00018	1.000	0.000006	
5898.80	47576720	0.00021	1.000	0.000007	
4952.20	39941932	0.00025	1.000	0.000005	
4466.30	36022900	0.00028	1.000	0.000007	
3691.70	29775376	0.00034	1.000	0.000013	
2984.30	24069848	0.00042	1.000	0.000028	
2293.20	18495786	0.00054	1.000	0.000069	
2042.40	16472960	0.00061	0.999	0.00010	
1740.00	14033955	0.00071	0.999	0.00017	
1486.70	11990966	0.00083	0.999	0.00029	
1188.00	9581804	0.00104	0.999	0.00052	
1011.70	8159858	0.00123	0.999	0.00075	
929.70	7498488	0.00133	0.999	0.00100	
851.50	6867766	0.00146	0.999	0.00023	
705.00	5686172	0.00176	0.999	0.00038	
572.80	4619914	0.00216	0.998	0.00065	
452.20	3647215	0.00274	0.997	0.00109	
392.40	3164899	0.00316	0.996	0.00141	
277.00	2234141	0.00448	0.993	0.00188	
192.60	1553414	0.00644	0.983	0.00302	
171.70	1384845	0.00722	0.977	0.00513	
151.10	1218696	0.00821	0.967	0.0118	
132.80	1071097	0.00934	0.961	0.0371	
114.00	919466	0.01088	0.991	0.0113	
108.50	875106	0.01143	0.983	0.00875	
72.40	583942	0.01713	1.000	0.0121	
49.30	397629	0.02515	1.000	0.0426	
30.50	245998	0.04065	1.000	0.1603	
160.0	1290478	0.00775		0.0123	[37]
150.0	1209824	0.00827		0.0179	
140.0	1129169	0.00886		0.0268	
135.0	1088847	0.00918		0.0358	
130.0	1048514	0.00954		0.0516	
125.0	1008186	0.00992		0.0734	
120.0	967859	0.01033		0.0378	
115.0	927531	0.01028		0.0146	
2.480	20000	0.50	1.54	2.66	[39]
1.240	10000	1.00	2.64	3.14	78 K
0.620	5000	2.00	3.90	4.50	
0.413	3333	3.00	4.13	5.52	
0.310	2500	4.00	4.09	6.73	
0.248	2000	5.00	3.12	7.99	

[a] The references from which the values were taken are given in brackets.

TABLE I (*Continued*)

Cerium

eV	cm^{-1}	μm	n	k	
0.207	1667	6.00	3.53	8.36	
0.191	1539	6.50	3.29	8.51	
0.177	1429	7.00	3.53	8.36	
2.400	20000	0.50	1.67	2.57	[39]
1.240	10000	1.00	2.68	3.44	295 K
0.620	5000	2.00	3.49	4.20	
0.413	3333	3.00	3.90	6.23	
0.310	2500	4.00	4.59	7.71	
0.248	2000	5.00	4.41	8.74	
0.207	1667	6.00	4.93	9.39	
0.191	1539	6.50	4.85	9.48	
0.177	1429	7.00	5.11	9.20	

TABLE II

Values of *n* and *k* for Samarium for Various References[a]

eV	cm^{-1}	μm	n	k	
9886.40	79738680	0.00013	1.000	0.000002	[12]
8047.80	64909460	0.00015	1.000	0.000004	
7478.20	60315356	0.00017	1.000	0.000005	
6930.30	55896272	0.00018	1.000	0.000005	
5898.80	47576720	0.00021	1.000	0.000003	
4952.20	39941932	0.00025	1.000	0.000005	
4466.30	36022900	0.00028	1.000	0.000008	
3691.70	29775376	0.00034	1.000	0.000015	
2984.30	24069848	0.00042	1.000	0.000032	
2293.20	18495786	0.00054	1.000	0.000078	
2042.40	16472960	0.00061	0.999	0.000115	
1740.00	14033955	0.00071	0.999	0.000196	
1486.70	11990966	0.00083	0.999	0.000295	
1188.00	9581804	0.00104	0.999	0.000465	
1011.70	8159858	0.00123	0.999	0.000158	
929.70	7498488	0.00133	0.999	0.000200	
705.00	5686172	0.00176	0.999	0.000426	
572.80	4619914	0.00216	0.998	0.000721	
511.30	4123886	0.00242	0.997	0.000950	
392.40	3164899	0.00316	0.996	0.00178	
311.70	2514014	0.00398	0.994	0.00251	
277.00	2234141	0.00448	0.993	0.00299	
212.20	1711497	0.00584	0.986	0.00633	
171.70	1384845	0.00722	0.975	0.0159	

(continued)

[a] The references from which the values were taken are given in brackets.

TABLE II *(Continued)*

Samarium

eV	cm^{-1}	μm	n	k	
151.10	1218696	0.00821	0.972	0.0433	
132.80	1071097	0.00934	1.030	0.0268	
114.00	919466	0.01088	0.997	0.0111	
108.50	875106	0.01143	0.992	0.0124	
91.50	737992	0.01355	1.000	0.0197	
72.40	583942	0.01713	1.000	0.0335	
49.30	397629	0.02515	1.000	0.0683	
30.50	245998	0.04065	1.000	0.1395	
170.0	1371133	0.00729		0.0144	[37]
160.0	1290478	0.00775		0.0215	
150.0	1209824	0.00827		0.0362	
148.0	1193693	0.00838		0.0380	
146.0	1177562	0.00849		0.0376	
140.0	1129169	0.00886		0.0465	
150.00	1209833	0.00826		0.0387	[17]
140.00	1129169	0.00886		0.0581	
120.00	967859	0.01033		0.0084	
110.00	887204	0.01127		0.0103	
100.00	806549	0.01240		0.0143	
90.00	725894	0.01377		0.0176	
80.00	645239	0.01550		0.0207	
70.00	564584	0.01771		0.0280	
3.966	31989.8	0.3126	0.89	0.42	[43]
3.397	27397.4	0.365	0.93	0.63	293 K
3.099	25000.0	0.400	1.02	0.89	
2.917	23529.4	0.425	1.09	0.98	
2.755	22222.2	0.450	1.17	1.07	
2.610	21052.6	0.475	1.22	1.12	
2.480	20000.0	0.500	1.27	1.16	
2.362	19047.6	0.525	1.29	1.19	
2.254	18181.8	0.550	1.31	1.24	
2.156	17391.3	0.575	1.33	1.28	
2.066	16666.7	0.600	1.33	1.32	
1.907	15384.7	0.650	1.31	1.39	
1.771	14285.7	0.700	1.31	1.49	
1.653	13333.3	0.750	1.30	1.58	
1.550	12500.0	0.800	1.30	1.70	
1.459	11764.7	0.850	1.32	1.81	
1.378	11111.1	0.900	1.35	1.91	
1.305	10526.3	0.950	1.37	2.02	
1.240	10000.0	1.000	1.38	2.12	
1.181	9523.8	1.050	1.40	2.16	
1.127	9090.9	1.100	1.41	2.16	
1.240	10000.0	1.00	1.39	2.16	[44]
0.827	6666.7	1.50	2.02	3.28	80 K
0.620	5000.0	2.00	2.37	4.13	

TABLE II *(Continued)*

Samarium

eV	cm^{-1}	μm	n	k	
0.496	4000.0	2.50	2.63	4.62	
0.413	3333.3	3.00	2.85	5.12	
0.354	2857.1	3.50	3.14	5.89	
0.310	2500.0	4.00	3.35	6.68	
0.248	2000.0	5.00	3.61	8.15	
0.207	1666.7	6.00	4.03	9.78	
0.177	1428.6	7.00	4.24	11.27	
0.155	1250.0	8.00	4.59	12.75	
0.138	1111.1	9.00	4.81	14.35	
0.124	1000.0	10.00	5.12	15.51	
0.103	833.3	12.00	5.88	18.52	
0.089	714.3	14.00	6.54	21.65	
0.083	666.7	15.00	7.03	22.86	
0.078	625.0	16.00	7.35	24.31	
0.073	588.2	17.00	7.82	25.38	
0.069	555.5	18.00	8.26	26.54	
0.065	526.3	19.00	8.53	27.40	
0.062	500.0	20.00	9.02	28.20	
1.240	10000.0	1.00	1.38	2.12	[44]
0.827	6666.7	1.50	2.07	3.24	293 K
0.620	5000.0	2.00	2.44	4.02	
0.496	4000.0	2.50	2.71	4.53	
0.413	3333.3	3.00	2.96	5.06	
0.310	2500.0	4.00	3.46	6.46	
0.248	2000.0	5.00	3.93	7.81	
0.177	1428.6	7.00	4.97	10.31	
0.155	1250.0	8.00	5.38	11.80	
0.138	1111.1	9.00	5.89	13.26	
0.124	1000.0	10.00	6.51	14.28	
0.103	833.3	12.00	7.76	16.79	
0.089	714.3	14.00	9.32	19.33	
0.083	666.7	15.00	10.08	20.18	
0.078	625.0	16.00	10.61	20.82	
0.069	555.5	18.00	11.55	22.62	
0.062	500.0	20.00	12.43	23.97	
1.240	10000.0	1.00	1.38	2.10	[44]
0.827	6666.7	1.50	2.12	3.18	460 K
0.354	2857.1	3.50	3.34	5.66	
0.248	2000.0	5.00	4.26	7.56	
0.177	1428.6	7.00	5.25	9.92	
0.138	1111.1	9.00	6.37	12.51	
0.103	833.3	12.00	8.38	15.72	
0.083	666.7	15.00	10.79	18.75	
0.073	588.2	17.00	12.26	19.91	
0.065	526.3	19.00	13.51	21.32	
0.062	500.0	20.00	13.98	21.94	

TABLE III

Values of n and k for Gadolinium for Various References[a]

eV	cm^{-1}	μm	n	k	
9886.40	79738680	0.00013	1.000	0.000002	[12]
8047.80	64909460	0.00015	1.000	0.000004	
5898.80	47576720	0.00021	1.000	0.000003	
3691.70	29775376	0.00034	1.000	0.00002	
2293.20	18495786	0.00054	1.000	0.00008	
2042.40	16472960	0.00061	0.999	0.00012	
1740.00	14033955	0.00071	0.999	0.00019	
1486.70	11990966	0.00083	0.999	0.00026	
1188.00	9581804	0.00104	1.000	0.00056	
1011.70	8159858	0.00123	0.999	0.00018	
929.70	7498488	0.00133	0.999	0.00022	
705.00	5686172	0.00176	0.998	0.00047	
572.80	4619914	0.00216	0.997	0.00079	
511.30	4123886	0.00242	0.997	0.0010	
392.40	3164899	0.00316	0.996	0.0019	
311.70	2514014	0.00398	0.994	0.0028	
277.00	2234141	0.00448	0.992	0.0033	
212.20	1711497	0.00584	0.986	0.0067	
171.70	1384845	0.00722	0.976	0.0132	
151.10	1218696	0.00821	0.974	0.0439	
148.70	1199339	0.00834	0.995	0.0622	
132.80	1071097	0.00934	0.999	0.0079	
114.00	919466	0.01088	0.980	0.0123	
108.50	875106	0.01143	0.977	0.0138	
91.50	737993	0.01355	1.000	0.0202	
72.40	583942	0.01713	1.000	0.0304	
49.30	397629	0.02515	1.000	0.0589	
30.50	245997	0.04065	1.000	0.0348	
160.00	1290635	0.00775		0.0120	[17]
150.00	1209970	0.00826		0.0613	
130.00	1048641	0.00954		0.0078	
120.00	967976	0.01033		0.0104	
110.00	887311	0.01127		0.0135	
100.00	806647	0.01240		0.0171	
90.00	725982	0.01377		0.0208	
80.00	645317	0.01550		0.0253	
70.00	564653	0.01771		0.0323	
35.00	282292	0.0354		0.115	[45]
34.00	274227	0.0365		0.135	
32.00	258096	0.0388		0.138	
30.00	241965	0.0413		0.133	
28.00	225834	0.0443		0.114	
24.00	193572	0.0517		0.144	
20.00	161310	0.0620		0.129	

[a] The references from which the values were taken are given in brackets.

TABLE III *(Continued)*

Gadolinium

eV	cm^{-1}	μm	n	k	
18.00	145179	0.0689		0.150	
16.00	129048	0.0775		0.223	
14.00	112917	0.0886		0.337	
12.00	96786	0.1033		0.417	
9.25	74606	0.1340		0.653	
8.00	64524	0.1550		0.719	
6.50	52426	0.1907		0.724	
4.00	32262	0.3100		1.308	
2.00	16131	0.6199		2.128	
15.00	120982	0.08	0.69	0.17	[48]
14.00	112917	0.09	0.64	0.23	
13.00	104851	0.10	0.60	0.30	
12.00	96786	0.10	0.54	0.45	
11.00	88720	0.11	0.56	0.66	
10.00	80655	0.12	0.63	0.81	
9.00	72589	0.14	0.76	0.98	
8.00	64524	0.15	0.92	1.04	
7.00	56458	0.18	1.01	1.09	
6.00	48393	0.21	1.06	1.21	
5.00	40328	0.25	1.12	1.43	
4.00	32262	0.31	1.20	1.75	
3.00	24197	0.41	1.64	2.27	
2.00	16131	0.62	2.35	2.81	
3.10	25003	0.400	1.41	2.39	[49]
3.00	24197	0.413	1.43	2.44	
2.90	23390	0.428	1.45	2.41	
2.80	22583	0.443	1.48	2.46	
2.75	22180	0.451	1.58	2.64	
2.70	21777	0.459	1.59	2.62	
2.60	20970	0.477	1.60	2.66	
2.50	20164	0.496	1.70	2.74	
2.40	19357	0.517	1.73	2.77	
2.30	18551	0.539	1.79	2.82	
2.25	18147	0.551	1.88	2.89	
2.20	17744	0.564	1.91	2.93	
2.15	17308	0.577	1.95	3.00	
2.10	16375	0.590	1.96	2.98	
2.00	16131	0.620	2.10	3.10	
1.90	15324	0.653	2.19	3.14	
1.85	14921	0.670	2.20	3.14	
1.80	14158	0.689	2.34	3.28	
3.397	27397	0.365	1.05	0.66	[52]

(continued)

TABLE III *(Continued)*

Gadolinium

eV	cm^{-1}	μm	n	k	
3.099	25000	0.400	1.12	0.88	293 K
2.755	22222	0.450	1.27	1.04	
2.610	21053	0.475	1.34	1.06	
2.480	20000	0.500	1.37	1.10	
2.362	19048	0.525	1.39	1.12	
2.254	18182	0.550	1.41	1.14	
2.156	17391	0.575	1.42	1.16	
2.066	16667	0.600	1.41	1.19	
1.907	15385	0.650	1.40	1.24	
1.771	14286	0.700	1.36	1.38	
1.550	12500	0.800	1.38	1.55	
1.459	11765	0.850	1.39	1.63	
1.378	11111	0.900	1.41	1.75	
1.305	10526	0.950	1.42	1.86	
1.240	10000	1.000	1.47	1.96	
1.181	9524	1.050	1.49	2.00	
1.127	9091	1.100	1.46	1.96	
1.240	10000	1.00	1.41	2.00	[54]
0.827	6667	1.50	1.70	3.20	80 K
0.620	5000	2.00	2.13	4.01	
0.413	3333	3.00	2.88	5.14	
0.354	2857	3.50	3.36	5.91	
0.310	2500	4.00	3.60	6.92	
0.276	2222	4.50	3.93	7.56	
0.248	2000	5.00	4.18	8.20	
0.207	1667	6.00	4.75	9.38	
0.177	1429	7.00	5.33	10.60	
0.155	1250	8.00	6.03	11.74	
0.124	1000	10.00	7.34	13.96	
0.103	833.3	12.00	8.72	16.25	
0.095	769.2	13.00	9.48	17.19	
0.089	714.3	14.00	10.28	18.07	
0.077	625.0	16.00	11.80	19.97	
0.073	588.2	17.00	12.40	20.71	
0.065	526.3	19.00	13.60	22.12	
0.062	500.0	20.00	14.18	23.24	
1.240	10000	1.00	1.47	1.96	[54]
0.827	6667	1.50	1.73	2.80	293 K
0.620	5000	2.00	2.18	3.89	
0.496	4000	2.50	2.91	4.48	
0.413	3333	3.00	3.26	5.05	
0.354	2857	3.50	3.61	5.71	
0.310	2500	4.00	4.07	6.34	
0.276	2222	4.50	4.52	7.03	
0.248	2000	5.00	4.69	7.72	

TABLE III *(Continued)*

Gadolinium

eV	cm^{-1}	μm	n	k	
0.207	1667	6.00	5.36	8.90	
0.177	1429	7.00	6.14	9.88	
0.155	1250	8.00	6.87	10.75	
0.138	1111	9.00	7.65	11.80	
0.124	1000	10.00	8.40	12.91	
0.103	833.3	12.00	10.12	14.82	
0.089	714.3	14.00	11.71	16.47	
0.083	666.7	15.00	12.45	17.27	
0.077	625.0	16.00	13.20	18.12	
0.073	588.2	17.00	14.09	18.85	
0.065	526.3	19.00	15.38	20.25	
0.062	500.0	20.00	16.20	20.89	
1.240	10000	1.00	1.51	1.95	[54]
0.827	6667	1.50	1.80	2.77	460 K
0.620	5000	2.00	2.30	3.82	
0.413	3333	3.00	3.56	5.02	
0.310	2500	4.00	4.28	6.25	
0.248	2000	5.00	5.06	7.48	
0.207	1667	6.00	5.72	8.46	
0.177	1429	7.00	6.59	9.58	
0.155	1250	8.00	7.47	10.32	
0.138	1111	9.00	8.35	11.40	
0.124	1000	10.00	9.21	12.32	
0.113	909.1	11.00	10.12	13.30	
0.095	769.2	13.00	11.75	15.10	
0.089	714.3	14.00	12.62	15.86	
0.083	666.7	15.00	13.41	16.65	
0.073	588.2	17.00	14.89	18.15	
0.069	555.6	18.00	15.60	18.84	
0.062	500.0	20.00	16.96	20.10	
2.50	20165	0.496	1.96	2.57	[57]
2.00	16132	0.620	2.41	2.93	56 K
1.50	12099	0.827	2.95	3.27	
1.00	8066	1.240	3.52	3.89	
0.50	4033	2.480	4.96	5.44	
2.50	20165	0.496	1.96	2.57	[57]
2.00	16132	0.620	2.44	2.91	300 K
1.50	12099	0.827	3.05	3.25	
1.00	8066	1.240	3.59	3.76	
0.50	4033	2.480	4.27	5.98	
2.50	20165	0.496	2.02	2.62	[56]
2.00	16132	0.620	2.48	2.94	105 K
1.80	14519	0.689	2.71	3.04	

(continued)

TABLE III *(Continued)*

Gadolinium

eV	cm^{-1}	μm	n	k	
1.50	12099	0.827	2.99	3.18	
1.20	9679	1.033	3.23	3.64	
1.00	8066	1.240	3.46	3.93	
0.70	5646	1.771	4.30	4.85	
0.50	4033	2.480	4.86	5.35	
2.50	20165	0.496	1.97	2.56	[56]
2.00	16132	0.620	2.42	2.96	293 K
1.60	12905	0.775	2.89	3.25	
1.50	12099	0.827	3.00	3.33	
1.00	8066	1.240	3.57	3.83	
0.65	5243	1.907	3.87	5.06	
0.50	4033	2.488	4.36	6.10	
5.0	40329	0.248	1.155	1.226	[58, 59]
4.5	36296	0.265	1.167	1.345	50 K
4.0	32263	0.310	1.171	1.543	
3.5	28230	0.354	1.238	1.833	
3.0	24198	0.413	1.381	2.119	
2.5	20165	0.496	1.631	2.357	
2.0	16132	0.620	2.119	2.917	
1.85	14922	0.670	2.310	2.845	
1.4	11292	0.886	2.417	2.719	
1.0	8066	1.240	2.786	3.071	
0.9	7259	1.378	2.81	3.11	
0.8	6452	1.550	3.07	3.39	
0.7	5646	1.771	3.84	3.98	
0.6	4839	2.066	3.22	3.55	
0.55	4439	2.253	4.17	4.28	
0.5	4033	2.480	7.03	5.07	
1.5	12099	0.827	2.21	2.49	[58, 59]
1.0	8066	1.240	2.61	2.80	100 K
0.9	7259	1.378	2.63	2.86	
0.8	6452	1.550	2.68	2.94	
0.7	5646	1.771	2.92	3.20	
0.65	5243	1.907	2.86	3.14	
0.6	4839	2.066	2.88	3.20	
0.55	4439	2.254	3.04	3.44	
0.5	4033	2.480	3.96	4.31	
5.0	40329	0.248	1.226	1.059	[58, 59]
4.5	36296	0.276	1.143	1.095	300 K
4.0	32263	0.310	1.171	1.190	
3.5	28230	0.354	1.250	1.371	
3.0	24198	0.413	1.357	1.583	
2.5	20165	0.496	1.583	1.786	
2.0	16132	0.620	1.774	1.881	

TABLE III *(Continued)*

Gadolinium

eV	cm^{-1}	μm	n	k	n	k	
1.5	12099	0.827	2.238	2.345			
1.0	8066	1.240	2.310	2.667			
0.9	7259	1.378	2.34	2.54			
0.7	5646	1.771	2.44	2.88			
0.6	4839	2.066	2.36	2.99			
0.55	4439	2.253	3.04	3.44			
0.5	4033	2.480	10.18	6.02			
			E ‖ c		**E ⊥ c**		
18.0	145284	0.069	1.02	0.08	[27]		
16.0	129142	0.077	0.95	0.14	4.2 K		
14.0	112999	0.088	0.85	0.23			
12.0	96856	0.103	0.88	0.48			
10.0	80714	0.124	1.05	0.49			
9.0	72642	0.138	1.03	0.46			
8.0	64571	0.155	0.97	0.54			
7.0	56500	0.177	0.95	0.63			
6.0	48428	0.206	0.92	0.79			
5.5	44392	0.225	0.91	0.88			
4.8	38725	0.26	0.91	1.04	0.82	1.03	[25]
4.0	32262	0.31	0.89	1.34	0.75	1.41	
3.5	28229	0.35	0.93	1.62	0.81	1.76	
3.0	24197	0.41	1.07	1.98	1.04	2.17	
2.5	20164	0.50	1.35	2.45	1.41	2.99	
2.0	16131	0.62	1.94	2.81	1.77	2.76	
1.5	12098	0.83	2.43	2.78	2.08	3.46	
1.0	8066	1.24	2.87	3.64	3.16	3.80	
0.7	5646	1.77	3.68	4.32	4.10	4.90	
0.5	4033	2.48	3.96	4.63	4.32	4.43	
0.3	2420	4.10	3.43	6.84	2.58	7.27	
0.2	1613	6.20	3.20	10.48	2.57	12.06	
0.1	806.6	12.80	3.12	21.35	3.32	21.61	
1.240	10000	1.00	2.7	3.5	2.4	3.5	[55]
0.620	5000	2.00	2.8	3.7	2.7	3.6	
0.413	3333	3.00	3.1	4.8	3.4	5.0	
0.310	2500	4.00	3.8	5.4	4.0	5.6	
0.248	2000	5.00	4.8	6.9	4.7	6.7	
0.207	1667	6.00	5.6	8.9	5.1	8.6	
0.177	1429	7.00	6.3	11.5	5.8	10.7	
0.155	1250	8.00	7.0	13.2	6.5	12.4	
0.138	1111	9.00	7.9	15.1	7.4	13.8	
0.124	1000	10.00	8.9	16.8	8.2	15.3	
0.113	909.1	11.00	9.8	18.7	9.2	16.7	
0.103	833.3	12.00	10.9	20.7	10.1	18.0	
0.095	769.2	13.00	11.6	22.1	10.8	19.3	
0.089	714.3	14.00	12.7	23.5	11.6	20.5	
0.083	666.7	15.00	13.8	24.5	12.5	21.8	

TABLE IV

Values of n and k for Terbium for Various References[a]

eV	cm^{-1}	μm	n	k	
9886.4	79748312.	0.00013	1.000	0.000002	[12]
8047.8	64917296	0.00015	1.000	0.000003	
7478.2	60322644	0.00017	1.000	0.000001	
5898.8	47582464	0.00021	1.000	0.000003	
4510.8	36386212	0.00027	1.000	0.000009	
2984.3	24072752	0.00042	1.000	0.000036	
2165.9	17471158	0.00057	1.000	0.00011	
1740.0	14035649	0.00071	1.000	0.00020	
1486.7	11992413	0.00083	1.000	0.00030	
1253.6	10112120	0.00099	1.000	0.00053	
1188.0	9582961	0.00104	1.000	0.00012	
1011.7	8160843	0.00123	1.000	0.00020	
851.5	6868595	0.00146	1.000	0.00032	
705.0	5686859	0.00176	0.998	0.00054	
572.8	4620471	0.00216	0.998	0.00087	
452.2	3647656	0.00274	0.996	0.00148	
311.7	2514317	0.00398	0.994	0.00364	
212.2	1711704	0.00584	0.988	0.00844	
183.3	1478583	0.00676	0.985	0.0137	
171.7	1385012	0.00722	0.983	0.0158	
151.1	1218843	0.00820	1.021	0.0436	
148.7	1199483	0.00834	1.018	0.0080	
132.8	1071227	0.00934	0.987	0.0088	
114.0	919577	0.01087	0.979	0.0142	
108.5	875212	0.01143	0.976	0.0154	
72.4	584012	0.01712	1.000	0.0339	
30.5	246027	0.04065	1.000	0.164	
170.0	1371299	0.00729		0.0134	[17]
160.0	1290635	0.00775		0.0239	
150.0	1209970	0.00826		0.0246	
140.0	1129305	0.00886		0.0052	
130.0	1048641	0.00954		0.0081	
120.0	967976	0.01033		0.0108	
110.0	887311	0.01127		0.0125	
100.0	806647	0.01240		0.0146	
90.0	725982	0.01377		0.0180	
80.0	645317	0.01550		0.0223	
70.0	564653	0.01771		0.0302	
45.0	362947	0.0276	0.89	0.09	[33]
40.0	322620	0.0310	0.77	0.19	
35.0	282292	0.0354	0.80	0.35	
30.0	241965	0.0413	0.94	0.42	
25.0	201637	0.0496	0.97	0.39	
22.0	177441	0.0564	0.98	0.36	
20.0	161310	0.0620	0.93	0.36	

[a] The references from which the values were taken are given in brackets.

TABLE IV *(Continued)*

Terbium

eV	cm^{-1}	μm	n	k	n	k	
17.5	141146	0.0708	0.81	0.34			
15.0	120982	0.0827	0.75	0.48			
10.0	80655	0.1240	0.68	1.07			
7.5	60491	0.1653	0.86	1.54			
				E ∥ c	**E ⊥ c**		
5.0	40328	0.24	0.82	1.04	0.81	1.06	[25]
4.0	32262	0.31	0.82	1.47	0.83	1.46	4.2 K
3.5	28229.	0.35	0.90	1.81	0.90	1.77	
3.0	24197	0.41	1.14	2.24	1.07	2.12	
2.5	20164	0.50	1.59	2.52	1.36	2.57	
2.0	16131	0.62	1.96	2.71	1.94	2.98	
1.0	8066	1.24	3.08	3.63	3.06	3.77	
0.7	5646	1.77	4.05	3.99	3.65	4.29	
0.5	4033	2.48	3.75	4.25	3.76	5.03	
0.3	2420	4.10	2.65	7.07	3.44	7.54	
0.2	1613	6.20	2.10	11.46	3.07	11.44	
0.1	807	12.80	2.94	24.07	3.09	23.76	
1.240	10000	1.00	2.4	4.3	2.2	4.0	[55]
0.620	5000	2.00	3.3	5.1	3.0	4.5	
0.413	3333	3.00	3.5	7.2	3.4	6.5	
0.310	2500	4.00	4.2	9.0	4.1	8.0	
0.248	2000	5.00	5.3	10.8	4.8	9.6	
0.207	1667	6.00	6.2	12.6	5.4	11.0	
0.177	1429	7.00	7.1	14.7	6.2	12.4	
0.155	1250	8.00	8.2	17.5	7.1	13.8	
0.138	1111	9.00	9.2	19.2	7.8	15.3	
0.124	1000	10.00	10.1	20.4	8.6	16.6	
0.103	833.3	12.00	12.2	24.3	10.2	19.6	
0.095	769.2	13.00	12.8	25.6	11.0	20.3	
0.089	714.3	14.00	13.7	27.2	11.8	21.5	
0.083	666.7	15.00	14.8	28.5	12.8	22.7	
2.60	20970	0.476	1.30	1.80	[49]		
2.50	20165	0.496	1.40	1.97			
2.40	19357	0.516	1.42	2.02			
2.30	18551	0.539	1.48	2.11			
2.10	16938	0.590	1.62	2.32			
2.00	16131	0.619	1.67	2.32			
1.90	15325	0.652	1.80	2.54			
1.80	14518	0.688	1.82	2.55			
2.50	20165	0.496	1.83	2.71	[57]		
2.00	16132	0.620	2.35	3.00	77 K		
1.50	12099	0.827	2.80	3.22			

(continued)

TABLE IV *(Continued)*

Terbium

eV	cm^{-1}	μm	n	k	
1.00	8066	1.240	3.40	3.75	
0.80	6453	1.550	3.72	4.22	
0.70	5646	1.771	3.82	4.64	
0.60	4840	2.066	3.98	5.23	
0.40	3226	3.099	4.68	7.07	
2.50	20165	0.496	1.87	2.74	[57]
2.00	16132	0.620	2.36	3.01	300 K
1.50	12099	0.827	2.86	3.27	
1.00	8066	1.240	3.40	3.75	
0.80	6453	1.550	3.47	4.25	
0.60	4840	2.066	3.67	5.34	
0.40	3226	3.099	4.57	7.67	
1.240	10000	1.00	1.79	3.26	[64]
0.620	5000	2.00	2.60	5.23	80 K
0.310	2500	4.00	3.65	8.45	
0.248	2000	5.00	4.26	10.04	
0.177	1429	7.00	5.56	13.46	
0.138	1111	9.00	6.90	16.37	
0.103	833.3	12.00	8.83	20.60	
0.089	714.3	14.00	10.14	23.30	
0.077	625.0	16.00	11.48	26.24	
0.069	555.6	18.00	13.10	29.01	
0.062	500.0	20.00	15.03	31.92	
1.240	10000	1.00	1.92	3.21	[64]
0.620	5000	2.00	2.78	4.94	293 K
0.413	3333	3.00	3.40	6.54	
0.310	2500	4.00	4.12	8.04	
0.177	1429	7.00	6.22	12.42	
0.124	1000	10.00	8.60	16.57	
0.103	833.3	12.00	10.18	19.06	
0.089	714.3	14.00	11.84	21.54	
0.077	625.0	16.00	13.66	24.10	
0.069	555.6	18.00	15.61	26.80	
0.062	500.0	20.00	17.63	29.51	
1.240	10000	1.00	2.20	3.05	[64]
0.620	5000	2.00	3.03	4.72	450 K
0.310	2500	4.00	4.51	7.76	
0.177	1429	7.00	7.10	11.74	
0.138	1111	9.00	8.80	14.15	
0.124	1000	10.00	9.74	15.47	
0.103	833.3	12.00	11.53	17.65	
0.089	714.3	14.00	13.64	20.16	
0.077	625.0	16.00	15.83	22.72	
0.069	555.6	18.00	17.72	24.95	
0.062	500.0	20.00	19.68	27.17	

TABLE V

Values of *n* and *k* for Dysprosium from Various References[a]

eV	cm^{-1}	μm	n	k	
9886.4	79738680	0.00013	1.000	0.000002	[12]
8638.9	69676976	0.00014	1.000	0.000004	
8047.8	64909460	0.00015	1.000	0.000003	
6930.3	55896272	0.00018	1.000	0.000002	
5414.7	43672220	0.00023	1.000	0.000005	
4466.3	36022900	0.00028	1.000	0.000010	
3691.7	29775376	0.00034	1.000	0.000019	
2984.3	24069848	0.00042	1.000	0.000039	
2293.2	18495786	0.00054	1.000	0.000097	
2042.4	16472960	0.00061	1.000	0.00014	
1740.0	14033955	0.00071	1.000	0.00022	
1486.7	11990966	0.00083	0.999	0.00032	
1188.0	9581804	0.00104	0.999	0.00013	
1011.7	8159858	0.00123	0.999	0.00022	
929.7	7498488	0.00133	0.999	0.00028	
705.0	5686172	0.00176	0.998	0.00059	
572.8	4619914	0.00216	0.997	0.00102	
511.3	4123886	0.00242	0.997	0.00135	
392.4	3164899	0.00316	0.995	0.00255	
311.7	2514014	0.00398	0.994	0.00445	
277.0	2234141	0.00448	0.993	0.00528	
212.2	1711497	0.00584	0.988	0.00936	
171.7	1384845	0.00722	0.979	0.0204	
151.1	1218696	0.00821	1.009	0.0210	
132.8	1071097	0.00934	0.989	0.0134	
114.0	919466	0.01088	0.980	0.0201	
108.5	875106	0.01143	0.978	0.0226	
91.5	737992	0.01355	1.000	0.0336	
72.4	583942	0.01713	1.000	0.0552	
49.3	397629	0.02515	1.000	0.1180	
30.5	245998	0.04065	1.000	0.2977	
170.0	1371134	0.00729		0.0154	[17]
160.0	1290479	0.00775		0.0295	
140.0	1129169	0.00886		0.0084	
130.0	1048514	0.00954		0.0104	
120.0	967859	0.01033		0.0127	
110.0	887204	0.01127		0.0153	
100.0	806549	0.01240		0.0194	
90.0	725894	0.01377		0.0244	
80.0	645239	0.01550		0.0316	
70.0	564458	0.01771		0.0422	
30.0	241965	0.0413	0.99	0.23	[48]
29.0	233899	0.0428	0.99	0.20	

(continued)

[a] The references from which the values were taken are given in brackets.

TABLE V *(Continued)*

Dysprosium

eV	cm^{-1}	μm	n	k			
28.0	225834	0.0443	0.98	0.19			
27.0	217768	0.0459	0.98	0.19			
26.0	209703	0.0477	0.98	0.19			
25.5	205670	0.0468	0.98	0.19			
25.0	201637	0.0496	0.98	0.19			
24.0	193572	0.0517	0.98	0.17			
23.0	185506	0.0539	0.98	0.15			
22.0	177441	0.0564	0.98	0.11			
21.7	175424	0.0570	0.98	0.10			
20.8	167359	0.0598	0.97	0.03			
20.0	161310	0.0620	0.97	0.04			
				E ∥ c		**E ⊥ c**	
5.00	40329	0.248	0.86	0.99	0.73	1.21	[25]
4.50	36295	0.276	0.79	0.84	0.73	1.32	4.2 K
4.00	32263	0.310	0.90	1.42	0.75	1.53	
3.50	28229	0.354	0.95	1.69	0.83	1.90	
3.00	24198	0.413	1.12	2.09	1.13	2.36	
2.50	20164	0.496	1.51	2.47	1.64	2.65	
2.00	16132	0.620	2.01	2.75	2.04	2.87	
1.50	12099	0.827	2.53	2.86	2.76	3.21	
1.00	10080	1.240	3.11	3.37	3.20	3.60	
0.80	6452	1.550	3.39	3.58	3.88	3.88	
0.60	4839	2.066	3.50	4.17	3.81	4.15	
0.40	3226	3.100	3.57	5.67	3.30	5.53	
0.20	1613	6.200	3.79	10.03	3.23	10.79	
0.10	806.5	12.400	2.91	20.02	2.23	22.79	
3.966	31990	0.313	1.04	0.62	[43]		
3.397	27397	0.365	1.06	0.89			
3.099	25000	0.400	1.18	1.05			
2.917	23529	0.425	1.24	1.15			
2.610	21053	0.475	1.37	1.20			
2.480	24000	0.500	1.40	1.23			
2.362	19048	0.525	1.41	1.24			
2.254	18182	0.550	1.44	1.28			
2.156	17391	0.575	1.44	1.31			
2.066	16667	0.600	1.40	1.34			
1.907	15385	0.650	1.41	1.40			
1.771	14286	0.700	1.38	1.54			
1.653	13333	0.750	1.40	1.64			
1.550	12500	0.800	1.41	1.76			
1.459	11765	0.850	1.43	1.85			
1.378	11111	0.900	1.43	1.96			
1.305	10526	0.950	1.45	2.09			
1.240	10000	1.000	1.52	2.19			

TABLE V *(Continued)*

Dysprosium

eV	cm^{-1}	μm	n	k	
1.181	9524	1.050	1.51	2.24	
1.127	9091	1.100	1.50	2.26	
1.240	10000	1.00	1.48	2.22	[54]
0.826	6667	1.50	2.06	3.30	80 K
0.620	5000	2.00	2.36	4.25	
0.496	4000	2.50	2.71	5.26	
0.413	3333	3.00	2.90	5.93	
0.354	2857	3.50	3.09	6.81	
0.310	2500	4.00	3.31	7.65	
0.275	2222	4.50	3.51	8.43	
0.248	2000	5.00	3.84	9.40	
0.207	1667	6.00	4.26	10.98	
0.177	1429	7.00	4.88	12.41	
0.155	1250	8.00	5.35	13.94	
0.138	1111	9.00	5.91	15.04	
0.124	1000	10.00	6.61	16.45	
0.103	833.3	12.00	7.75	19.10	
0.089	714.3	14.00	8.74	22.01	
0.077	625.0	16.00	9.92	24.40	
0.069	555.6	18.00	10.82	26.21	
0.065	526.3	19.00	11.22	27.12	
0.062	500.0	20.00	11.70	28.23	
1.240	10000	1.00	1.52	2.19	[54]
0.826	6667	1.50	2.10	3.25	293 K
0.620	5000	2.00	2.46	4.20	
0.496	4000	2.50	2.80	5.13	
0.413	3333	3.00	3.04	5.86	
0.354	2857	3.50	3.36	6.74	
0.310	2500	4.00	3.65	7.58	
0.275	2222	4.50	3.96	8.35	
0.248	2000	5.00	4.16	9.10	
0.207	1667	6.00	4.95	10.76	
0.177	1429	7.00	5.44	12.02	
0.155	1250	8.00	6.13	13.18	
0.138	1111	9.00	6.76	14.40	
0.124	1000	10.00	7.35	15.74	
0.113	909.1	11.00	8.02	16.92	
0.103	833.3	12.00	8.76	17.97	
0.095	769.2	13.00	9.57	19.24	
0.089	714.3	14.00	10.28	20.26	
0.083	666.7	15.00	11.07	21.51	
0.077	625.0	16.00	11.85	22.63	
0.069	555.6	18.00	12.95	24.46	
0.065	526.3	19.00	13.52	25.24	
0.062	500.0	20.00	14.27	26.42	

(continued)

TABLE V *(Continued)*

Dysprosium

eV	cm^{-1}	μm	n	k		
1.240	10000	1.00	1.62	2.16	[54]	
0.826	6667	1.50	2.33	3.17	460 K	
0.620	5000	2.00	2.63	4.09		
0.413	3333	3.00	3.34	5.65		
0.354	2857	3.50	3.63	6.61		
0.310	2500	4.00	3.97	7.39		
0.248	2000	5.00	4.48	8.87		
0.207	1667	6.00	5.38	10.60		
0.177	1429	7.00	5.85	11.71		
0.155	1250	8.00	6.79	12.96		
0.138	1111	9.00	7.42	14.10		
0.124	1000	10.00	8.15	15.40		
0.113	909.1	11.00	9.02	16.62		
0.103	833.3	12.00	9.70	17.65		
0.095	769.2	13.00	10.61	18.70		
0.089	714.3	14.00	11.41	19.61		
0.083	666.7	15.00	12.33	20.52		
0.077	625.0	16.00	13.31	21.60		
0.073	588.2	17.00	14.16	22.11		
0.069	555.6	18.00	14.95	22.91		
0.065	526.3	19.00	15.74	23.73		
0.062	500.0	20.00	16.43	25.09		

eV	cm^{-1}	μm	n	k	n	k	
			E ∥ c		**E ⊥ c**		
5.64	45455	0.22	0.92	1.19	0.96	1.24	[66]
4.77	38462	0.26	0.96	1.21	0.96	1.21	80 K
4.43	35714	0.28	1.06	1.25	1.07	1.29	
4.13	33333	0.30	1.10	1.42	1.14	1.43	
3.54	28571	0.35	1.25	1.64	1.25	1.74	
3.10	25000	0.40	1.35	1.96	1.38	2.05	
2.76	22222	0.45	1.53	2.09	1.57	2.17	
2.25	18182	0.55	1.72	2.31	1.77	2.37	
2.07	16667	0.60	1.80	2.44	1.85	2.49	
1.91	15385	0.65	1.90	2.54	1.93	2.68	
1.65	13333	0.75	2.08	2.66	2.15	2.87	
1.55	12500	0.80	2.13	2.74	2.22	2.95	
1.38	11111	0.90	2.21	2.95	2.30	3.15	
1.24	10000	1.00	2.33	3.08	2.40	3.18	
1.03	8333.3	1.20	2.61	3.25	2.62	3.21	
0.95	7692.3	1.30	2.79	3.26	2.76	3.34	
0.89	7142.9	1.40	2.91	3.37	2.87	3.46	
0.77	6250.0	1.60	3.10	3.56	3.05	3.60	
0.69	5555.6	1.80	3.23	3.79	3.09	3.75	
0.62	5000.0	2.00	3.36	4.05	3.31	3.96	
0.56	4545.5	2.20	3.53	4.19	3.52	4.06	

TABLE V *(Continued)*

Dysprosium

eV	cm^{-1}	μm	n	k	n	k	
0.52	4166.7	2.40	3.68	4.42	3.64	4.32	
0.48	3846.2	2.60	3.84	4.58	3.81	4.53	
0.44	3571.4	2.80	4.02	4.77	4.02	4.59	
0.41	3333.3	3.00	4.15	5.02	4.10	4.91	
5.64	45455	0.22	1.03	1.29	1.04	1.32	[66]
4.77	38462	0.26	1.09	1.26	1.07	1.28	293 K
4.43	35714	0.28	1.16	1.35	1.16	1.35	
4.13	33333	0.30	1.22	1.47	1.22	1.48	
3.10	25000	0.40	1.40	1.92	1.43	1.93	
2.76	22222	0.45	1.48	2.09	1.54	2.05	
2.48	20000	0.50	1.51	2.25	1.56	2.23	
2.07	16667	0.60	1.71	2.40	.75	2.43	
1.77	14286	0.70	1.78	2.67	1.88	2.70	
1.55	12500	0.80	1.88	2.89	2.02	2.92	
1.38	11111	0.90	2.02	2.96	2.14	2.98	
1.24	10000	1.00	2.20	3.04	2.24	3.08	
1.13	9090.9	1.10	2.38	3.05	2.40	3.16	
1.03	8333.3	1.20	2.50	3.12	2.46	3.21	
0.95	7692.3	1.30	2.64	3.18	2.59	3.21	
0.77	6250.0	1.60	2.97	3.42	2.77	3.62	
0.69	5555.6	1.80	3.09	3.66	2.95	3.78	
0.62	5000.0	2.00	3.23	3.85	3.06	3.99	
0.52	4166.7	2.40	3.39	4.36	3.28	4.42	
0.44	3571.4	2.80	3.73	4.59	3.64	4.63	
0.41	3333.3	3.00	3.76	4.86	3.67	4.83	
1.24	10000	1.00	2.4	3.2	2.3	3.1	[55]
0.62	5000	2.00	3.3	4.0	3.4	4.1	
0.413	3333	3.00	4.1	4.9	4.2	5.0	
0.310	2500	4.00	4.4	6.3	4.4	6.2	
0.248	2000	5.00	5.1	8.4	5.2	8.2	
0.207	1667	6.00	6.0	10.5	6.1	10.3	
0.177	1429	7.00	6.8	13.3	6.7	12.5	
0.155	1250	8.00	7.7	15.3	7.3	14.2	
0.138	1111	9.00	8.7	17.5	8.3	15.9	
0.124	1000	10.00	9.6	19.2	9.3	17.2	
0.113	909.1	11.00	10.3	20.7	10.2	19.0	
0.103	833.3	12.00	11.6	22.4	11.0	20.5	
0.095	769.2	13.00	12.4	24.3	11.8	22.4	
0.090	714.3	14.00	13.6	25.8	12.6	23.6	
0.083	666.7	15.00	14.8	26.8	13.4	25.0	
0.078	625.0	16.00	15.6	28.8	14.6	26.1	

(continued)

TABLE V *(Continued)*

Dysprosium

eV	cm^{-1}	μm	n	k	
2.50	20165	0.496	2.04	2.77	[57]
2.00	16132	0.620	2.15	2.76	80 K
1.70	13712	0.729	2.93	3.26	
1.50	12099	0.827	3.17	3.32	
1.00	8065.8	1.240	3.53	3.53	
0.66	5323.4	1.878	3.17	4.84	
0.40	3226.3	3.099	4.47	7.61	
2.50	20165	0.496	2.04	2.77	[57]
2.00	16132	0.620	2.58	3.11	300 K
1.70	13712	0.729	2.95	3.27	
1.50	12099	0.827	3.17	3.32	
1.00	8065.8	1.240	3.56	3.56	
0.66	5323.4	1.878	4.28	4.98	
0.40	3226.3	3.099	4.66	7.98	

TABLE VI

Values of *n* and *k* for Erbium from Various References[a]

eV	cm^{-1}	μm	n	k	
9886.4	79738680	0.00013	1.000	0.000003	[12]
8047.8	64909460	0.00015	1.000	0.000001	
3691.7	29775376	0.00034	1.000	0.000022	
2293.2	18495786	0.00054	1.000	0.00011	
2042.4	16472960	0.00061	1.000	0.00016	
1740.0	14033955	0.00071	1.000	0.00022	
1486.7	11990966	0.00083	1.000	0.00038	
1188.0	9581804	0.00104	0.999	0.00016	
1011.7	8159858	0.00123	0.999	0.00026	
929.7	7498488	0.00133	0.999	0.00033	
705.0	5686172	0.00176	0.998	0.00071	
572.8	4619914	0.00216	0.997	0.00122	
511.3	4123886	0.00242	0.997	0.00161	
392.4	3164899	0.00316	0.995	0.00278	
311.7	2514014	0.00398	0.994	0.00456	
277.0	2234141	0.00448	0.993	0.00564	
212.2	1711497	0.00584	0.990	0.00809	
171.7	1384845	0.00722	0.997	0.0258	
151.1	1218696	0.00821	0.986	0.0107	
132.8	1071097	0.00934	0.982	0.0138	
114.0	919466	0.01088	0.974	0.0171	
108.5	875106	0.01143	0.970	0.0188	
91.5	737992	0.01355	1.000	0.0306	
72.4	583942	0.01713	1.000	0.0518	

[a] The references from which the values were taken are given in brackets.

TABLE VI *(Continued)*

Erbium

eV	cm^{-1}	μm	n	k			
49.3	397629	0.02515	1.000	0.1090			
30.5	245998	0.04065	1.000	0.2315			
180.0	1451964	0.00689		0.0129	[17]		
170.0	1371299	0.00729		0.0158			
160.0	1290635	0.00775		0.0067			
150.0	1209970	0.00826		0.0095			
140.0	1129305	0.00886		0.0109			
130.0	1048641	0.00954		0.0124			
120.0	967976	0.01033		0.0134			
110.0	887311	0.01127		0.0155			
100.0	806647	0.01240		0.0197			
90.0	725982	0.01377		0.0258			
80.0	645317	0.01550		0.0347			
70.0	564653	0.01771		0.0473			
eV	cm^{-1}	μm	n	k	n	k	
				E ∥ c		**E ⊥ c**	
5.0	40328	0.25	0.90	0.97	0.81	0.98	[25]
4.5	36295	0.276	0.86	0.66	0.81	0.64	4.2 K
4.0	32262	0.31	0.82	1.32	0.80	1.43	
3.5	28229	0.35	0.85	1.65	0.89	1.81	
3.0	24197	0.41	1.01	2.07	1.19	2.23	
2.5	20164	0.50	1.40	2.48	1.73	2.54	
2.0	16131	0.62	1.93	2.89	2.25	2.65	
1.5	12098	0.83	2.57	2.96	2.66	2.37	
1.0	8065.5	1.24	2.99	3.14	2.72	2.77	
0.9	7258.9	1.378	3.06	3.22	2.64	2.83	
0.5	4032.8	2.48	2.70	5.24	2.03	5.48	
0.3	2016.4	4.96	2.88	8.75	2.45	9.55	
0.22	1774.4	5.63	3.24	11.75	3.17	12.80	
0.10	806.6	12.40	5.00	24.93	6.98	26.08	
2.48	20000	0.5	1.71	3.21		[68]	
1.24	10000	1.0	2.30	3.75		300 K	
0.83	6666.7	1.5	2.63	4.29			
0.62	5000.0	2.0	2.84	4.39			
0.50	4000.0	2.5	3.32	5.63			
0.41	3333.3	3.0	3.80	6.48			
0.25	2000.0	5.0	5.11	9.00			
0.17	1333.3	7.5	6.89	11.74			
0.12	1000.0	10.0	8.89	14.11			
0.10	800.0	12.5	10.63	16.63			
0.083	666.7	15.0	12.47	18.42			
0.071	571.4	17.5	14.16	20.53			
0.062	500.0	20.0	15.79	22.63			

(continued)

TABLE VI *(Continued)*

Erbium

eV	cm^{-1}	μm	n	k	n	k	
5.64	45455	0.22	0.84	1.10	0.82	1.14	[69]
5.17	41667	0.24	0.92	1.19	0.88	1.24	78 K
4.77	38462	0.26	1.03	1.26	1.01	1.28	
4.43	35714	0.28	1.08	1.40	1.06	1.38	
4.13	33333	0.30	1.14	1.52	1.13	1.44	
3.54	28571	0.35	1.34	1.75	1.32	1.58	
3.10	25000	0.40	1.56	2.03	1.54	1.84	
2.76	22222	0.45	1.75	2.20	1.75	2.02	
2.48	20000	0.50	1.90	2.39	1.94	2.26	
2.25	18182	0.55	2.08	2.45	2.09	2.43	
2.07	16667	0.60	2.17	2.53	2.19	2.66	
1.91	15385	0.65	2.21	2.69	2.24	2.77	
1.77	14286	0.70	2.31	2.78	2.36	2.74	
1.65	13333	0.75	2.36	2.82	2.42	2.76	
1.55	12500	0.80	2.32	2.80	2.41	2.94	
1.38	11111	0.90	2.27	2.84	2.41	3.21	
1.24	10000	1.00	2.30	2.99	2.48	3.39	
1.13	9090.9	1.10	2.30	3.09	2.45	3.52	
1.03	8333.3	1.20	2.21	3.22	2.42	3.45	
0.95	7692.3	1.30	2.23	3.26	2.40	3.34	
0.89	7142.9	1.40	2.30	3.10	2.40	3.20	
0.77	6250.0	1.60	2.30	3.00	2.40	3.40	
0.69	5555.6	1.80	2.40	3.20	2.50	3.50	
0.62	5000.0	2.00	2.40	3.60	2.60	3.80	
0.56	4545.5	2.20	2.60	3.80	2.70	4.00	
0.52	4166.7	2.40	2.80	3.80	2.90	4.20	
0.48	3846.2	2.60	2.80	4.10	2.90	4.60	
0.44	3571.4	2.80	2.80	4.40	3.00	4.90	
0.41	3333.3	3.00	2.90	4.80	3.10	5.10	
0.35	2857.1	3.50	3.00	5.60	3.20	5.90	
0.31	2500.0	4.00	3.20	6.20	3.50	6.20	
0.28	2222.2	4.50	3.70	6.50	3.80	6.50	
0.25	2000.0	5.00	4.00	6.90	4.20	6.70	
0.23	1818.2	5.50	4.30	7.00	4.50	6.60	
0.21	1666.7	6.00	4.40	7.30	4.70	6.70	

TABLE VII

Values of n and k for Thulium from Various References[a]

eV	cm^{-1}	μm	n	k	
9886.4	79738680	0.00013	1.000	0.000003	[12]
8047.8	64909460	0.00015	1.000	0.000002	
5898.8	47576720	0.00021	1.000	0.000005	
3691.7	29775376	0.00034	1.000	0.000026	
2293.2	18495786	0.00054	1.000	0.00013	
2042.4	16472960	0.00061	0.999	0.00017	
1740.0	14033955	0.00071	0.999	0.00026	
1486.7	11990966	0.00083	0.999	0.00029	
1188.0	9581804	0.00104	0.999	0.00017	
1011.7	8159858	0.00123	0.999	0.00028	
929.7	7498488	0.00133	0.999	0.00036	
705.0	5686172	0.00176	0.998	0.00078	
572.8	4619914	0.00216	0.997	0.00135	
511.3	4123886	0.00242	0.997	0.00177	
392.4	3164899	0.00316	0.996	0.00293	
331.7	2514014	0.00398	0.994	0.00444	
277.0	2234141	0.00448	0.993	0.00568	
212.2	1711497	0.00584	0.990	0.00927	
171.7	1384845	0.00722	1.005	0.0133	
151.1	1218696	0.00821	0.987	0.0122	
148.7	1199339	0.00834	0.986	0.0125	
132.8	1071097	0.00934	0.983	0.0152	
108.5	875106	0.01143	0.975	0.0224	
91.5	737992	0.01355	1.000	0.0316	
72.4	583942	0.01713	1.000	0.0475	
49.3	397629	0.02515	1.000	0.0843	
30.5	245998	0.04065	1.000	0.1707	
180.0	1451964	0.00689		0.0179	[17]
170.0	1371299	0.00729		0.0081	
160.0	1290635	0.00775		0.0092	
150.0	1209970	0.00826		0.0110	
140.0	1129305	0.00886		0.0125	
130.0	1048641	0.00954		0.0141	
120.0	967976	0.01033		0.0161	
110.0	887311	0.01127		0.0192	
100.0	806647	0.01240		0.0239	
90.0	725982	0.01377		0.0286	
80.0	645317	0.01550		0.0356	
70.0	564653	0.01771		0.0447	
1.240	10000.0	1.00	2.22	3.75	[70]
0.827	6666.7	1.50	2.67	4.40	80 K
0.620	5000.0	2.00	3.21	5.56	
0.496	4000.0	2.50	3.65	6.51	

(continued)

[a] The references from which the values were taken are given in brackets.

TABLE VII *(Continued)*

Thulium

eV	cm^{-1}	μm	n	k	n	k
0.413	3333.3	3.00	3.86	7.65		
0.354	2857.1	3.50	4.11	8.52		
0.310	2500.0	4.00	4.60	9.37		
0.276	2222.2	4.50	5.03	10.33		
0.248	2000.0	5.00	5.39	11.12		
0.207	1666.6	6.00	6.10	12.94		
0.177	1428.4	7.00	6.92	14.75		
0.155	1250.0	8.00	7.41	16.28		
0.138	1111.1	9.00	7.89	18.15		
0.124	1000.0	10.00	8.40	20.03		
0.113	909.1	11.00	8.68	21.46		
0.103	833.3	12.00	9.53	22.91		
0.095	769.2	13.00	10.02	24.30		
0.089	714.3	14.00	10.68	25.62		
0.083	666.7	15.00	11.35	26.97		
0.078	625.8	16.00	11.77	28.09		
0.073	588.2	17.00	12.21	29.40		
0.069	555.5	18.00	12.64	30.77		
0.065	526.3	19.00	13.10	31.94		
0.062	500.0	20.00	13.60	33.12		
1.240	10000.0	1.00	2.52	3.46	[70]	
0.827	6666.7	1.50	3.02	4.20	293 K	
0.620	5000.0	2.00	3.56	5.30		
0.496	4000.0	2.50	4.15	6.32		
0.413	3333.3	3.00	4.72	7.34		
0.354	2857.1	3.50	5.04	8.15		
0.310	2500.0	4.00	5.46	9.03		
0.276	2222.2	4.50	5.81	9.86		
0.248	2000.0	5.00	6.22	10.72		
0.207	1666.6	6.00	6.94	12.28		
0.177	1422.7	7.00	7.81	14.02		
0.155	1250.0	8.00	8.70	15.81		
0.138	1111.1	9.00	9.54	17.45		
0.124	1000.0	10.00	10.35	18.86		
0.113	909.1	11.00	11.13	20.65		
0.103	833.3	12.00	11.93	22.21		
0.095	769.2	13.00	12.85	23.68		
0.089	714.3	14.00	13.60	25.45		
0.083	666.7	15.00	14.46	26.31		
0.078	625.0	16.00	15.22	27.32		
0.073	588.2	17.00	16.15	28.50		
0.069	555.6	18.00	17.04	29.62		
0.065	526.3	19.00	18.04	31.24		
0.062	500.0	20.00	18.70	31.96		
1.240	10000.0	1.00	2.83	3.31	[70]	
0.827	6666.7	1.50	3.35	3.98	450 K	

TABLE VII *(Continued)*

Thulium

eV	cm^{-1}	μm	n	k			
0.620	5000.0	2.00	3.91	5.07			
0.496	4000.0	2.50	4.48	6.04			
0.413	3333.3	3.00	5.03	6.92			
0.354	2857.1	3.50	5.72	7.70			
0.310	2500.0	4.00	6.24	8.51			
0.276	2222.2	4.50	6.71	9.43			
0.248	2000.0	5.00	7.37	10.40			
0.207	1666.6	6.00	8.36	11.75			
0.177	1428.7	7.00	9.43	13.48			
0.155	1250.0	8.00	10.31	15.36			
0.138	1111.1	9.00	11.25	16.93			
0.124	1000.0	10.00	12.46	18.38			
0.113	909.1	11.00	13.40	20.02			
0.103	833.3	12.00	14.52	21.43			
0.095	769.2	13.00	15.31	22.90			
0.089	714.3	14.00	16.34	24.26			
0.083	666.7	15.00	17.65	25.55			
0.078	625.0	16.00	18.21	26.40			
0.073	588.2	17.00	19.20	27.83			
0.069	555.5	18.00	20.16	29.02			
0.062	500.0	20.00	22.03	31.02			
eV	cm^{-1}	μm	n	k	n	k	
				E ∥ c		**E ⊥ c**	
5.64	45455	0.22	0.87	1.10	0.86	1.09	[69]
5.17	41667	0.24	0.94	1.26	0.92	1.15	78 K
4.77	38462	0.26	1.03	1.34	1.01	1.20	
4.13	33333	0.30	1.15	1.68	1.18	1.40	
3.54	28571	0.35	1.33	1.96	1.29	1.80	
3.10	25000	0.40	1.60	2.13	1.55	1.98	
2.76	22222	0.45	1.85	2.40	1.81	2.16	
2.48	20000	0.50	1.97	2.49	1.92	2.39	
2.07	16667	0.60	2.19	2.80	2.13	2.64	
1.91	15385	0.65	2.23	3.03	2.19	2.81	
1.77	14286	0.70	2.21	2.98	2.23	3.03	
1.65	13333	0.75	2.19	2.98	2.20	3.36	
1.55	12500	0.80	2.18	2.92	2.23	3.48	
1.38	11111	0.90	2.20	2.86	2.24	3.50	
1.24	10000	1.00	2.21	2.66	2.26	3.44	
1.13	9090.9	1.10	2.22	2.56	2.29	3.33	
0.95	7692.3	1.30	2.21	2.55	2.33	3.37	
0.89	7142.9	1.40	2.20	2.60	2.30	3.20	
0.77	6250.0	1.60	2.30	2.80	2.40	3.20	
0.69	5555.6	1.80	2.30	3.20	2.50	2.90	
0.62	5000.0	2.00	2.30	3.50	2.50	2.90	

(continued)

TABLE VII *(Continued)*

Thulium

eV	cm^{-1}	μm	n	k	n	k	
0.56	4545.5	2.20	2.30	3.90	2.60	3.00	
0.52	4166.7	2.40	2.40	4.10	2.80	3.30	
0.48	3846.2	2.60	2.40	4.30	2.80	3.30	
0.44	3571.4	2.80	2.60	4.40	2.90	3.50	
0.41	3333.3	3.00	2.80	4.50	2.90	3.60	
0.35	2857.1	3.50	3.20	4.60	3.20	4.10	
0.31	2500.0	4.00	3.50	5.10	3.40	4.60	
5.0	40327	0.25	0.96	0.94	0.82	1.04	[25]
4.0	32262	0.31	0.90	1.28	0.81	1.51	4.2 K
3.5	28229	0.35	0.94	1.59	0.91	1.91	
3.0	24197	0.41	1.10	2.02	1.35	2.36	
2.5	20164	0.50	1.61	2.50	1.96	2.45	
2.0	16131	0.62	2.30	2.61	2.44	2.52	
1.5	12098	0.83	3.02	2.39	2.84	2.11	
1.0	8065.5	1.24	3.09	2.31	2.34	2.19	
0.5	4032.8	2.48	2.57	5.18	2.80	6.83	
0.3	2419.6	4.13	6.06	5.97	7.96	6.92	
0.2	1613.1	6.20	4.64	5.94	5.32	6.73	
0.1	806.6	12.40	2.21	14.91	2.75	16.60	

TABLE VIII

Values of n and k for Ytterbium from Various References[a]

eV	cm^{-1}	μm	n	k	
9886.4	79738700	0.00013	1.000	0.000002	[12]
8047.8	64909500	0.00015	1.000	0.000001	
3691.7	29775400	0.00034	1.000	0.000020	
2293.2	18495800	0.00054	1.000	0.000096	
2042.4	16473000	0.00061	0.999	0.000134	
1740.0	14034000	0.00071	0.999	0.000197	
1486.7	11991000	0.00083	0.999	0.000068	
1188.0	9581800	0.00104	0.999	0.000135	
1011.7	8159860	0.00123	0.999	0.000220	
929.7	7498490	0.00133	0.999	0.000282	
705.0	5686170	0.00176	0.998	0.000615	
572.8	4619910	0.00216	0.998	0.00106	
511.3	4123880	0.00242	0.998	0.00139	
392.4	3164900	0.00316	0.997	0.00242	
311.7	2514010	0.00398	0.996	0.00360	
277.0	2234140	0.00448	0.995	0.00441	
212.2	1711500	0.00584	0.994	0.00725	
171.7	1384850	0.00722	0.996	0.00812	
151.1	1218700	0.00821	0.991	0.01097	
132.8	1071100	0.00934	0.989	0.0123	
114.0	919466	0.01088	0.986	0.0160	
108.5	875106	0.01143	0.985	0.0171	
91.5	737992	0.01355	1.000	0.0217	
72.4	583942	0.01713	1.000	0.0321	
49.3	397629	0.02515	1.000	0.0680	
30.5	245998	0.04065	1.000	0.1799	
190.0	1532440	0.00652		0.0079	[17]
180.0	1451790	0.00689		0.0091	
170.0	1371130	0.00729		0.0100	
160.0	1290480	0.00775		0.0102	
140.0	1129170	0.00886		0.0112	
150.0	1209830	0.00826		0.0104	
130.0	1048520	0.00954		0.0126	
120.0	967859	0.01033		0.0136	
110.0	887204	0.01127		0.0161	
100.0	806549	0.01240		0.0184	
90.0	725894	0.01377		0.0219	
80.0	645239	0.01550		0.0272	
70.0	564584	0.01771		0.0340	
11.50	92756.9	0.11	0.71	0.24	[71]
11.00	88725.0	0.11	0.68	0.26	
10.00	80658.2	0.12	0.60	0.35	
9.00	72592.4	0.14	0.59	0.52	
8.00	64526.5	0.15	0.70	0.70	

[a] The references from which the values were taken are given in brackets.

TABLE VIII *(Continued)*

Ytterbium

eV	cm^{-1}	μm	n	k	
7.00	56460.7	0.18	0.73	0.73	
6.00	48394.9	0.21	0.68	0.82	
5.00	40329.1	0.25	0.64	1.03	
4.50	36296.2	0.28	0.57	1.19	
4.00	32263.3	0.31	0.54	1.45	
3.50	28230.4	0.35	0.57	1.71	
3.00	24197.5	0.41	0.62	2.09	
2.00	16131.6	0.62	1.34	2.61	
1.50	12098.7	0.83	1.79	3.90	
1.00	8065.8	1.24	2.28	5.49	
0.50	4032.9	2.48	3.37	8.91	
5.50	44361.9	0.225		0.31	[73]
5.00	40329.5	0.248		0.37	
4.00	32263.3	0.310		0.52	
3.00	24197.5	0.413		0.87	
2.50	20164.5	0.496		1.05	
2.00	16131.6	0.620		1.45	
1.60	12905.3	0.775		3.45	
1.00	8065.8	1.240		4.13	
0.50	4032.9	2.480		11.62	
1.959	15802.8	0.633	1.68	3.22	[76]
0.620	5000.0	2.0	2.63	4.92	[74]
0.310	2500.0	4.0	4.43	8.45	
0.207	1666.7	6.0	6.15	11.73	
0.155	1250.0	8.0	7.79	14.68	
0.124	1000.0	10.0	9.23	17.30	
0.104	833.3	12.0	10.58	19.43	
0.089	714.3	14.0	11.48	21.32	
0.078	625.0	16.0	12.38	22.47	
0.069	555.6	18.0	13.86	24.44	
0.062	500.0	20.0	14.84	26.16	
0.056	454.5	22.0	15.99	27.80	
0.052	416.7	24.0	17.47	29.27	

Cesium (Cs)

T. INAGAKI
Division of Natural Science
Osaka Kyoiku University
Osaka, Japan

and

E. T. ARAKAWA
Life Sciences Division
Oak Ridge National Laboratory
Oak Ridge, Tennessee

Cesium is a soft and ductile metal and chemically reactive. The crystalline structure is normally body-centered cubic. The melting point is the lowest (28°C) and the vapor pressure is the highest (ca. 7×10^{-7} torr at room temperature) among the alkali metals. Optical studies have been made usually under ultrahigh vacuum and at low temperatures. However, extensive studies have been made at room temperature [1–6], which is only several degrees below the melting point.

Mirror surfaces of cesium for optical measurements have been produced either by distillation and condensation onto a cooled substrate [1, 2, 6] or by gentle thermal evaporation [3–5, 7, 8, 10–12]. Some measurements have been made on quartz (or calcium fluoride)–Cs interfaces [3–5] to avoid contamination even under ultrahigh vacuum and to avoid the effects of roughening due to the high volatility of Cs. Most measurements have been made, however, on vacuum–cesium interfaces [1, 2, 6–12]. In addition, the optical properties of cesium in the form of semitransparent thin films and the thickness dependencies have been studied by several authors [7, 8, 11, 12] at low temperatures.

The optical properties of cesium in the near infrared to the ultraviolet have been relatively well established [5, 9]. The optical properties are essentially like those of nearly free electrons. The absorption properties given by the optical-conductivity curve show three prominent features: a tail of the Drude absorption below 0.6 eV, a weak absorption with the peak centered at 1.1 eV, and a strong absorption with the peak centered at 5.1 eV.

The weak absorption at 1.1 eV has been assigned conclusively as due to

HANDBOOK OF OPTICAL CONSTANTS OF SOLIDS III

Copyright © 1998 by Academic Press.
All rights of reproduction in any form reserved
ISBN 0-12-544423-0/$25.00.

an interband absorption, whose quantitative features are described by the single-pseudopotential model [5]. The observed onset of this absorption, 0.6 eV, is, however, significantly lower than the theoretical threshold energy, 0.97 eV, of the interband transition. To account for this discrepancy, the contribution from the intrinsic surface state to the total absorption in this region has been studied [13]. The strong absorption at 5.1 eV has been attributed either to an interband transition or to collective excitations [3, 4, 9]. These absorption features are common to the alkali metals except for lithium, but those observed for cesium are considerably stronger than for the other alkali metals [9].

The first modern measurement of the optical constants of cesium at room temperature was made by Mayer and Hietel [2, 6]. They measured a vacuum–cesium interface between 0.5 and 4.18 eV by ellipsometry. Their results show clearly the tail of a Drude absorption below 0.6 eV, the absorption band with peak at around 1.1 eV, and a gradual rise of the absorption above 3.5 eV after leveling off between 2 and 3.5 eV.

Smith [5] remeasured the optical constants of cesium at room temperature between 0.5 and 4.0 eV. He measured multiple (seven) reflections at quartz–cesium interfaces using a split-beam ellipsometer. His measurements reproduced the results of Mayer and Hietel [2, 6] in general. His n values below 1.0 eV are, however, considerably larger than those measured by Mayer and Hietel for vacuum–cesium interfaces. A Kramers–Kronig analysis made by the present authors using a reasonable extrapolation of the k values in the region below 0.5 eV yielded n values that were very close to Smith's values. Smith also found that his n and k values in the region above 2.0 eV agree well with the earlier data by Ives and Briggs [1], which were measured for vacuum–cesium interfaces in 1937.

The optical measurements of cesium have been extended into the vacuum ultraviolet above 6 eV by Whang *et al.* [3, 4] They measured the reflectance from quartz–cesium and calcium fluoride–cesium interfaces as a function of angle of incidence near the critical angle for total internal reflection. Since, in the region of their measurements between 3.6 and 9.6 eV, the k values are small (<0.2), the reflectance curve shows a steep rise at angles given by the n value of cesium relative to that of the substrate. The n values of cesium were obtained from the angle at which the reflectance curve exhibits the steepest rise, and the k values were obtained from the slope by taking account of the effects of the partial polarization of the incident light. Their result of the optical conductivity shows a strong absorption with the peak centered at 5.1 eV. Below 4.2 eV, their results show good agreement with those from Mayer and Hietel [2, 6] and Smith [5].

Whang *et al.* [3, 4] reported that reflectance values measured with calcium fluoride–cesium interfaces were significantly lower than those predicted by theoretical calculations and speculated that it was caused by contamination of the calcium fluoride–cesium interface. They later estimated [9] that

the uncertainty of their optical-conductivity values was less than 30%, and the normalization of the measured reflectance values to the theoretical values rendered the optical conductivity uncertain by an approximately constant factor over the full range of their measurement. A Kramers–Kronig analysis made by the present authors gave n values that are systematically smaller than those reported by Whang *et al.* by 0.080 in the entire range of their measurement. These discrepancies were found too large to attribute to any uncertainties involved in the present Kramers–Kronig analysis, indicating that the major part of the discrepancies came from the uncertainties in the experiments of Whang *et al.*

The optical constants of cesium at low temperatures were studied by Mayer and Hietel [2, 6] by ellipsometry. They measured vacuum–cesium interfaces at 90 and 195 K between 0.5 and 4.18 eV and compared the results with those obtained at room temperature. They found that the ϵ_1 values are rather insensitive to the temperature, but that the ϵ_2 values, and hence the optical conductivity, in the region of the interband transition above 0.6 eV increases, and the 1.1 eV peak shifts slightly to higher energies with decreasing temperature. As pointed out earlier for the room-temperature data, their data below 1.0 eV are possibly subject to a Kramers–Kronig inconsistency.

Monin and Boutry [10] also investigated the vacuum–cesium interface at low temperatures. They prepared the cesium layer at 77 K and measured n and k by ellipsometry between 2 and 5 eV. They found that, below 3 eV, the vacuum–cesium interface exhibited an irreversible change when it was heated to 195 K and cooled down again to 77 K.

The optical properties of cesium in the form of a thin, semitransparent film were studied by Steffen and Mayer [7] between 1.38 and 4.13 eV. They prepared cesium films on a quartz plate kept at 77 K with the thicknesses ranging from 7 to 240 nm. The thickness dependencies of the transmittance and the reflectance were measured by using p- and s-polarized photons incident at 30 and 60°. For the thinner films, they observed an absorption due to plasmon excitation when the photons were p-polarized. They reported the optical constants for the 160-nm-thick film, which did not differ much from those of bulk cesium measured at low temperature [6].

Steffen [11] later reported the optical constants of the rest of the films studied in the previous paper [7]. The ϵ_1 and ϵ_2 values reported for the 14.5-, 80.5-, and 107-nm-thick films show too large a scatter to define dependency of the optical constant values on film thickness.

Hanyu and Yamaguchi [8] also studied the optical properties of cesium films at low temperature between 2.1 and 6.2 eV. They prepared 150- to 170-nm-thick films on a quartz plate kept at 133 K and measured the transmittance and the reflectance of p- and s-polarized photons incident at 45°. The n and k values derived from these data above 3 eV do not differ much from those of bulk cesium measured at room temperature by Smith [5] and Whang *et al.* [4]. Below 3 eV, they found significant deviation of their ϵ_2

values from the bulk values and attributed it to a temperature effect. These authors also reported that the ϵ_2 values found for the 3-μm-thick opaque films were consistently smaller than those found for the 150- to 170-nm-thick films.

The optical constants of cesium in the region of the inner-shell excitation were studied by Sato *et al.* [12] using synchrotron radiation. They prepared semitransparent films of cesium on collodion films supported by metal-mesh screens kept at 77 K. Normal-incidence transmittances of the films were measured between 10 and 37 eV as a function of film thickness. The k values of the films were determined from the slope of the semilog plot of the inverse of the transmittance and the film thickness. Their data show a sharp rise of absorption at 11.8 eV followed by strong absorption extending to 30 eV with a peak at around 16 eV. This absorption was assigned to the transition of electrons in the outermost $5p$ shell to the Fermi and higher levels.

We have made a Kramers–Kronig analysis by combining the k-value data taken at room temperature in the various spectral regions. Below 0.5 eV, we used Drude values of k, which were evaluated from the dc conductivity of cesium to yield a smooth connection with the k values from Smith [5] at 0.5 eV. Between 0.5 and 3.4 eV and between 3.6 and 9.0 eV, we used the data from Smith [5] and Whang *et al.* [4], respectively. Between 10 and 30 eV, we used the data from Sato *et al.* [12] (measured at 77 K), and, above 30 eV, we used the semiempirical data from Henke *et al.* [14] derived from the atomic scattering factors. These data show good agreement with each other in the connecting regions, producing a smoothly connected single curve from $\sim$0 to 30 keV. The result of the sum-rule calculation on these k values was satisfactory.

The n values obtained from the Kramers–Kronig analysis are plotted in Fig. 1 and numerically tabulated in Table I together with the k values. Below 3.4 eV, the n values thus obtained agree well with the data from Smith [5], and between 3.6 and 9.0 eV, they are smaller than the values from Whang *et al.* [4] almost by a constant 0.080, as described earlier. We recommend these n and k values as the most reliable values of the optical constants of cesium at room temperature that are presently available.

ACKNOWLEDGMENT

Sponsored by the Office of Health and Environmental Research, U.S. Department of Energy, under Contract DE-AC05-96OR22464 with Lockheed Martin Energy Research Corporation.

REFERENCES

1. H. E. Ives and H. B. Briggs, *J. Opt. Soc. Am.* **27**, 395 (1937).
2. H. Mayer and B. Hietel, "Optical Properties and Electronic Structures of Metals and Alloys," (F. Abelés, ed.), pp. 47–59. North Holland, Publ., Amsterdam, 1966.
3. U. S. Whang, E. T. Arakawa, and T. A. Callcott, *Phys. Rev. Lett.* **25**, 646 (1970).

4. U. S. Whang, E. T. Arakawa, and T. A. Callcott, *J. Opt. Soc. Am.* **61**, 740 (1971).
5. N. V. Smith, *Phys. Rev. B* **2**, 2840 (1970).
6. H. Mayer and B. Hietel, *Z. Phys.* **254**, 232 (1972).
7. H. Steffen and H. Mayer, *Z. Phys.* **254**, 250 (1972).
8. T. Hanyu and S. Yamaguchi, *J. Phys. Soc. Jpn.* **37**, 994 (1974).
9. U. S. Whang, E. T. Arakawa, and T. A. Callcott, *Phys. Rev. B* **6**, 2109 (1972).
10. J. Monin and G. A. Boutry, *Phys. Rev. B* **9**, 1309 (1974).
11. H. Steffen, *Thin Solid Films* **21**, 59 (1974).
12. S. Sato, T. Miyahara, T. Hanyu, S. Yamaguchi, and T. Ishii, *J. Phys. Soc. Jpn.* **47**, 836 (1979).
13. R. Garron and H. Roubaud, *Surf. Sci.* **146**, 527 (1984).
14. L. Henke, E. M. Gullikson, and J. C. Davis, *At. Data Nucl. Data Tables* **54**, 181 (1993).

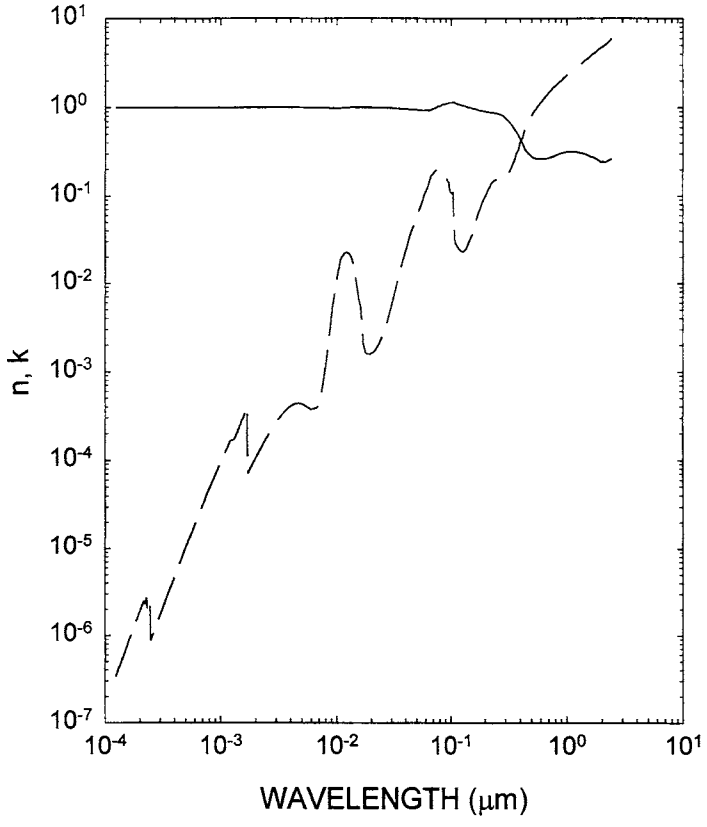

Fig. 1. Log–log plot of n (solid line) and k (dashed line) versus wavelength in micrometers for cesium.

TABLE I

Values of n and k for Cesium Obtained from Various References[a]

eV	cm^{-1}	μm	n	k
10000	8.065E + 07	1.240E-04	0.9999968	3.37E-07[14]
9542	7.696E + 07	1.299E-04	0.9999965	4.00E-07
9106	7.344E + 07	1.362E-04	0.9999961	4.75E-07
8689	7.008E + 07	1.427E-04	0.9999958	5.64E-07
8291	6.687E + 07	1.495E-04	0.9999954	6.68E-07
7912	6.381E + 07	1.567E-04	0.9999949	7.92E-07
7549	6.089E + 07	1.642E-04	0.9999945	9.37E-07
7204	5.810E + 07	1.721E-04	0.999994	1.11E-06
6874	5.544E + 07	1.804E-04	0.9999935	1.31E-06
6560	5.291E + 07	1.890E-04	0.9999929	1.54E-06
6260	5.049E + 07	1.981E-04	0.9999923	1.82E-06
5973	4.818E + 07	2.076E-04	0.9999919	2.14E-06
5700	4.597E + 07	2.175E-04	0.9999919	2.22E-06
5439	4.387E + 07	2.280E-04	0.9999912	2.62E-06
5190	4.186E + 07	2.389E-04	0.9999906	2.27E-06
4952	3.994E + 07	2.504E-04	0.9999902	8.83E-07
4726	3.812E + 07	2.624E-04	0.9999882	1.04E-06
4509	3.637E + 07	2.750E-04	0.9999866	1.23E-06
4303	3.471E + 07	2.881E-04	0.999985	1.46E-06
4106	3.312E + 07	3.020E-04	0.9999833	1.72E-06
3918	3.160E + 07	3.165E-04	0.9999815	2.03E-06
3739	3.016E + 07	3.316E-04	0.9999795	2.40E-06
3568	2.878E + 07	3.475E-04	0.9999774	2.82E-06
3404	2.745E + 07	3.642E-04	0.999975	3.33E-06
3249	2.620E + 07	3.816E-04	0.9999724	3.92E-06
3100	2.500E + 07	4.000E-04	0.9999696	4.61E-06
2958	2.386E + 07	4.192E-04	0.9999666	5.43E-06
2823	2.277E + 07	4.392E-04	0.9999632	6.38E-06
2693	2.172E + 07	4.604E-04	0.9999596	7.50E-06
2570	2.073E + 07	4.824E-04	0.9999556	8.82E-06
2452	1.978E + 07	5.057E-04	0.9999513	1.04E-05
2340	1.887E + 07	5.299E-04	0.9999466	1.22E-05
2233	1.801E + 07	5.552E-04	0.9999414	1.43E-05
2131	1.719E + 07	5.818E-04	0.9999359	1.67E-05
2033	1.640E + 07	6.099E-04	0.9999299	1.96E-05
1940	1.565E + 07	6.391E-04	0.9999235	2.29E-05
1852	1.494E + 07	6.695E-04	0.9999166	2.69E-05
1767	1.425E + 07	7.017E-04	0.9999092	3.14E-05
1686	1.360E + 07	7.354E-04	0.9999015	3.67E-05
1609	1.298E + 07	7.706E-04	0.999893	4.29E-05
1535	1.238E + 07	8.077E-04	0.999885	4.95E-05
1465	1.182E + 07	8.463E-04	0.999877	5.67E-05
1398	1.128E + 07	8.869E-04	0.999867	6.50E-05
1334	1.076E + 07	9.294E-04	0.999857	7.44E-05
1273	1.027E + 07	9.740E-04	0.999847	8.53E-05
1215	9.800E + 06	1.020E-03	0.999837	9.84E-05

[a] The references from which the values were taken are given in brackets.

TABLE I *(Continued)*

Cesium

eV	cm^{-1}	μm	n	k
1159	9.348E + 06	1.070E-03	0.999828	1.13E-04
1106	8.920E + 06	1.121E-03	0.99982	1.29E-04
1055	8.509E + 06	1.175E-03	0.999811	1.48E-04
1007	8.122E + 06	1.231E-03	0.999815	1.68E-04
961.0	7.751E + 06	1.290E-03	0.999812	1.71E-04
917.0	7.396E + 06	1.352E-03	0.999793	1.85E-04
875.0	7.057E + 06	1.417E-03	0.999781	2.15E-04
835.0	6.735E + 06	1.485E-03	0.999782	2.51E-04
796.8	6.427E + 06	1.556E-03	0.999799	2.95E-04
760.3	6.132E + 06	1.631E-03	0.999858	3.47E-04
725.5	5.852E + 06	1.709E-03	1.000264	6.94E-05
692.3	5.584E + 06	1.791E-03	0.999877	7.82E-05
660.6	5.328E + 06	1.877E-03	0.999797	8.82E-05
630.4	5.084E + 06	1.967E-03	0.999739	9.98E-05
601.5	4.851E + 06	2.061E-03	0.999688	1.12E-04
574.0	4.630E + 06	2.160E-03	0.999639	1.26E-04
547.7	4.417E + 06	2.264E-03	0.99959	1.41E-04
522.7	4.216E + 06	2.372E-03	0.99954	1.58E-04
498.7	4.022E + 06	2.486E-03	0.999487	1.75E-04
475.9	3.838E + 06	2.605E-03	0.999432	1.95E-04
454.1	3.663E + 06	2.730E-03	0.999372	2.17E-04
433.3	3.495E + 06	2.861E-03	0.999313	2.40E-04
413.5	3.335E + 06	2.998E-03	0.999248	2.63E-04
394.6	3.183E + 06	3.142E-03	0.999179	2.87E-04
376.5	3.037E + 06	3.293E-03	0.999105	3.11E-04
359.3	2.898E + 06	3.451E-03	0.999025	3.36E-04
342.8	2.765E + 06	3.617E-03	0.99894	3.59E-04
327.2	2.639E + 06	3.789E-03	0.99884	3.81E-04
312.2	2.518E + 06	3.971E-03	0.99874	4.01E-04
297.9	2.403E + 06	4.162E-03	0.99862	4.18E-04
284.3	2.293E + 06	4.361E-03	0.99849	4.30E-04
271.3	2.188E + 06	4.570E-03	0.99835	4.36E-04
258.8	2.087E + 06	4.791E-03	0.99817	4.36E-04
247.0	1.992E + 06	5.020E-03	0.99798	4.30E-04
235.7	1.901E + 06	5.260E-03	0.99774	4.18E-04
224.9	1.814E + 06	5.513E-03	0.99746	4.01E-04
214.6	1.731E + 06	5.778E-03	0.99712	3.85E-04
204.8	1.652E + 06	6.054E-03	0.99672	3.78E-04
195.4	1.576E + 06	6.345E-03	0.99625	3.84E-04
186.5	1.504E + 06	6.648E-03	0.9957	3.88E-04
177.9	1.435E + 06	6.969E-03	0.995	4.30E-04
169.8	1.370E + 06	7.302E-03	0.99414	5.34E-04
162.0	1.307E + 06	7.654E-03	0.9931	7.64E-04
154.6	1.247E + 06	8.020E-03	0.99185	1.15E-03
147.5	1.190E + 06	8.406E-03	0.99028	1.86E-03
140.8	1.136E + 06	8.806E-03	0.9885	3.17E-03

(continued)

TABLE I *(Continued)*

Cesium

eV	cm^{-1}	μm	n	k
134.3	1.083E + 06	9.232E-03	0.9868	5.30E-03
128.2	1.034E + 06	9.671E-03	0.9854	8.35E-03
122.3	9.864E + 05	1.014E-02	0.9852	1.22E-02
116.7	9.412E + 05	1.062E-02	0.9862	1.66E-02
111.4	8.985E + 05	1.113E-02	0.9898	2.02E-02
106.3	8.574E + 05	1.166E-02	0.99366	2.21E-02
101.4	8.178E + 05	1.223E-02	0.99814	2.25E-02
96.77	7.805E + 05	1.281E-02	1.00282	2.20E-02
92.35	7.448E + 05	1.343E-02	1.0074	1.99E-02
88.12	7.107E + 05	1.407E-02	1.0108	1.53E-02
84.09	6.782E + 05	1.474E-02	1.0118	1.06E-02
80.24	6.472E + 05	1.545E-02	1.0104	6.83E-03
76.57	6.176E + 05	1.619E-02	1.00904	5.35E-03
73.06	5.893E + 05	1.697E-02	1.00804	2.06E-03
69.72	5.623E + 05	1.778E-02	1.00458	1.62E-03
66.53	5.366E + 05	1.864E-02	1.00248	1.59E-03
63.48	5.120E + 05	1.953E-02	1.00072	1.58E-03
60.58	4.886E + 05	2.047E-02	0.999	1.64E-03
57.80	4.662E + 05	2.145E-02	0.99738	1.72E-03
55.16	4.449E + 05	2.248E-02	0.996	1.88E-03
52.63	4.245E + 05	2.356E-02	0.99358	2.10E-03
50.23	4.051E + 05	2.468E-02	0.99154	2.38E-03
47.93	3.866E + 05	2.587E-02	0.9896	2.77E-03
45.73	3.688E + 05	2.711E-02	0.9865	3.32E-03
43.64	3.520E + 05	2.841E-02	0.9837	4.12E-03
41.64	3.358E + 05	2.978E-02	0.9808	5.17E-03
39.74	3.205E + 05	3.120E-02	0.9778	6.64E-03
37.92	3.058E + 05	3.270E-02	0.9738	8.62E-03
36.00	2.904E + 05	3.444E-02	0.9700	1.13E-02
34.00	2.742E + 05	3.647E-02	0.9655	1.53E-02
32.00	2.581E + 05	3.875E-02	0.9600	2.02E-02
30.00	2.420E + 05	4.133E-02	0.9540	2.71E-02[12]
29.00	2.339E + 05	4.275E-02	0.9504	3.18E-02
28.00	2.258E + 05	4.428E-02	0.9483	3.69E-02
27.00	2.178E + 05	4.592E-02	0.9459	4.20E-02
26.00	2.097E + 05	4.769E-02	0.9423	4.77E-02
25.00	2.016E + 05	4.959E-02	0.9378	5.46E-02
24.00	1.936E + 05	5.166E-02	0.9340	6.47E-02
23.00	1.855E + 05	5.391E-02	0.9318	7.49E-02
22.00	1.774E + 05	5.636E-02	0.9290	8.90E-02
21.00	1.694E + 05	5.904E-02	0.9296	1.06E-01
20.00	1.613E + 05	6.199E-02	0.9328	1.22E-01
19.50	1.573E + 05	6.358E-02	0.9312	1.33E-01
19.00	1.532E + 05	6.526E-02	0.9352	1.52E-01
18.75	1.512E + 05	6.613E-02	0.9405	1.60E-01
18.50	1.492E + 05	6.702E-02	0.9490	1.69E-01
18.25	1.472E + 05	6.794E-02	0.9574	1.72E-01

TABLE I *(Continued)*

Cesium

eV	cm^{-1}	μm	n	k
18.00	1.452E + 05	6.888E-02	0.9640	1.76E-01
17.75	1.432E + 05	6.985E-02	0.9700	1.79E-01
17.50	1.411E + 05	7.085E-02	0.9761	1.84E-01
17.25	1.391E + 05	7.188E-02	0.9832	1.88E-01
17.00	1.371E + 05	7.293E-02	0.99192	1.93E-01
16.75	1.351E + 05	7.402E-02	1.00000	1.96E-01
16.50	1.331E + 05	7.514E-02	1.00841	1.98E-01
16.25	1.311E + 05	7.630E-02	1.0250	1.97E-01
16.00	1.290E + 05	7.749E-02	1.0326	1.93E-01
15.75	1.270E + 05	7.872E-02	1.0380	1.90E-01
15.50	1.250E + 05	7.999E-02	1.0444	1.91E-01
15.25	1.230E + 05	8.130E-02	1.0536	1.92E-01
15.00	1.210E + 05	8.266E-02	1.0658	1.91E-01
14.75	1.190E + 05	8.406E-02	1.079	1.85E-01
14.50	1.169E + 05	8.551E-02	1.0857	1.72E-01
14.25	1.149E + 05	8.701E-02	1.0878	1.65E-01
14.00	1.129E + 05	8.856E-02	1.0909	1.62E-01
13.75	1.109E + 05	9.017E-02	1.0964	1.61E-01
13.50	1.089E + 05	9.184E-02	1.108	1.57E-01
13.25	1.069E + 05	9.358E-02	1.114	1.47E-01
13.00	1.049E + 05	9.537E-02	1.124	1.44E-01
12.75	1.028E + 05	9.724E-02	1.136	1.22E-01
12.50	1.008E + 05	9.919E-02	1.127	1.10E-01
12.25	9.880E + 04	1.012E-01	1.125	1.06E-01
12.10	9.759E + 04	1.025E-01	1.127	1.05E-01
12.00	9.679E + 04	1.033E-01	1.132	1.07E-01
11.80	9.517E + 04	1.051E-01	1.153	1.10E-01
11.75	9.477E + 04	1.055E-01	1.160	5.79E-02
11.50	9.275E + 04	1.078E-01	1.130	3.17E-02
11.25	9.074E + 04	1.102E-01	1.112	2.86E-02
11.00	8.872E + 04	1.127E-01	1.0963	2.71E-02
10.60	8.549E + 04	1.170E-01	1.0778	2.50E-02
10.20	8.227E + 04	1.216E-01	1.0618	2.33E-02
9.80	7.904E + 04	1.265E-01	1.0467	2.29E-02
9.40	7.582E + 04	1.319E-01	1.0318	2.35E-02
9.04	7.291E + 04	1.372E-01	1.019	2.50E-02[4]
8.74	7.049E + 04	1.419E-01	1.003	2.80E-02
8.39	6.767E + 04	1.478E-01	0.992	3.20E-02
8.07	6.509E + 04	1.536E-01	0.980	3.60E-02
7.76	6.259E + 04	1.598E-01	0.968	4.10E-02
7.63	6.154E + 04	1.625E-01	0.961	4.60E-02
7.35	5.928E + 04	1.687E-01	0.950	5.50E-02
7.08	5.710E + 04	1.751E-01	0.935	6.40E-02
6.82	5.501E + 04	1.818E-01	0.925	7.20E-02
6.66	5.372E + 04	1.862E-01	0.920	7.90E-02
6.53	5.267E + 04	1.899E-01	0.915	8.40E-02

(continued)

TABLE I *(Continued)*

Cesium

eV	cm^{-1}	μm	n	k
6.32	5.097E + 04	1.962E-01	0.905	9.30E-02
6.09	4.912E + 04	2.036E-01	0.896	1.01E-01
5.86	4.726E + 04	2.116E-01	0.888	1.15E-01
5.72	4.613E + 04	2.168E-01	0.883	1.22E-01
5.43	4.380E + 04	2.283E-01	0.873	1.38E-01
5.22	4.210E + 04	2.375E-01	0.865	1.47E-01
5.00	4.033E + 04	2.480E-01	0.858	1.53E-01
4.80	3.871E + 04	2.583E-01	0.845	1.57E-01
4.60	3.710E + 04	2.695E-01	0.830	1.59E-01
4.40	3.549E + 04	2.818E-01	0.808	1.62E-01
4.20	3.388E + 04	2.952E-01	0.775	1.64E-01
4.00	3.226E + 04	3.100E-01	0.730	1.69E-01
3.80	3.065E + 04	3.263E-01	0.678	1.91E-01
3.60	2.904E + 04	3.444E-01	0.618	2.24E-01
3.397	2.740E + 04	3.650E-01	0.548	2.70E-01[5]
3.351	2.703E + 04	3.700E-01	0.535	3.00E-01
3.204	2.584E + 04	3.870E-01	0.480	3.33E-01
3.100	2.500E + 04	4.000E-01	0.441	4.00E-01
2.952	2.381E + 04	4.200E-01	0.388	4.58E-01
2.818	2.273E + 04	4.400E-01	0.340	5.70E-01
2.638	2.128E + 04	4.700E-01	0.303	6.83E-01
2.417	1.949E + 04	5.130E-01	0.273	8.53E-01
2.226	1.795E + 04	5.570E-01	0.263	9.84E-01
2.033	1.640E + 04	6.099E-01	0.261	1.16E + 00
1.842	1.486E + 04	6.731E-01	0.266	1.36E + 00
1.625	1.311E + 04	7.630E-01	0.280	1.65E + 00
1.400	1.129E + 04	8.856E-01	0.303	1.98E + 00
1.219	9.832E + 03	1.017E + 00	0.318	2.36E + 00
1.046	8.436E + 03	1.185E + 00	0.317	2.75E + 00
0.923	7.444E + 03	1.343E + 00	0.306	3.14E + 00
0.864	6.969E + 03	1.435E + 00	0.298	3.41E + 00
0.818	6.598E + 03	1.516E + 00	0.288	3.56E + 00
0.777	6.267E + 03	1.596E + 00	0.280	3.77E + 00
0.734	5.920E + 03	1.689E + 00	0.273	4.02E + 00
0.702	5.662E + 03	1.766E + 00	0.265	4.19E + 00
0.675	5.444E + 03	1.837E + 00	0.257	4.34E + 00
0.651	5.251E + 03	1.905E + 00	0.251	4.54E + 00
0.626	5.049E + 03	1.981E + 00	0.239	4.70E + 00
0.608	4.904E + 03	2.039E + 00	0.246	4.86E + 00
0.587	4.734E + 03	2.112E + 00	0.241	5.04E + 00
0.572	4.613E + 03	2.168E + 00	0.243	5.15E + 00
0.512	4.130E + 03	2.422E + 00	0.263	5.90E + 00

Zirconium Nitride (ZrN)
Hafnium Nitride (HfN)

CARL G. RIBBING and ARNE ROOS
Institute of Technology
Uppsala University
Uppsala, Sweden

The three transition-metal nitrides TiN, ZrN, and HfN belong to a larger group of compounds having NaCl or A15 structure with extreme stability in a generalized sense, i.e., hardness, chemical inertness, and high melting point and Young's modulus. This stability is the basis for their widespread technical use as hard materials on cutting tools, abrasive applications, etc. The larger family of materials includes carbides, nitrides, and oxides of group IVB to VIB transition metals such as vanadium, niobium, tantalum, molybdenum, and tungsten. There are numerous possible stoichiometry variations, since many of these compounds can form stable solid solutions with each other over wide ranges of composition. The basic reason for the high stability is their bonding, which is an intricate mixture of covalent bonds and ionic contributions. Of the three nitrides mentioned, only the two heavier ones constitute the subject of this critique. TiN, which is by far the most investigated of the three, was covered in Vol. II of this handbook [1]. The electronic configurations for the two metals are $[Kr]4d^2 5s^2$ and $[Xe]4f^{14}5d^2 6s^2$, respectively, which form highly directional bonds with N: $1s^2 2s^2 2p^3$ by hybridization. A characteristic and unusual result of this intricate bonding is that these two compounds (as well as TiN) are "ceramic" in terms of hardness, inertness, and directed bonds, but "metallic" with characteristically high electrical and thermal conductivity [2], in fact higher than that of the metal Ti. ZrN becomes superconducting for $T < 10$ K, significantly higher than the critical temperature for the metal T_c (Zr) ≈ 0.55 K. The room-temperature cubic unit-cell sizes of ZrN and HfN are 0.4577 and 0.4526 nm, respectively [2].

The *optical* applications of materials from this group are much less important than their tribological ones, but in particular TiN is used as a cos-

HANDBOOK OF OPTICAL CONSTANTS OF SOLIDS III

Copyright © 1998 by Academic Press.
All rights of reproduction in any form reserved
ISBN 0-12-544423-0/$25.00.

metic coating to replace gold in situations when a noble metal would not be sufficiently wear-resistant. ZrN and HfN have a less yellow but still bright appearance. Their possible use of a color standard has been discussed [3]. This adds to the metallic features just mentioned, and it signals a *free-electron-like* optical behavior that is striking for at least two reasons. Empirical chemical considerations, as well as advanced theoretical calculations, predict that the electrons close to the Fermi-level have a pure *d*-character in spite of the hybridization mentioned earlier. Based on this, one would expect a transition-metal-like behavior and a dull, greyish appearance. This is what is observed for the three carbides of Ti, Zr, and Hf, but the nitrides are radically different. This qualitative shift for only one *p*-electron more or less on the metaloid atom was pointed out by Karlsson [4]. It was suggested to exploit this free-electron-like character of the nitrides in stable optical coatings that are selectively transmitting [5]. Early attempts to prepare a bulk, selective solar absorber from compounds within this group of materials were not sucessful [6–8]. Lately, the use of an inhomogeneously oxidized surface has shown more promise [9].

Free-electron-like optical properties are conventionally described with the Drude-oscillator formalism [10], which models the intraband excitations of an electron gas. In this case of the transition metal nitrides, the *d*-electrons just below the Fermi surface constitute the electron gas. The low dispersion of typical *d*-bands makes it unusual to associate *d*-band compounds with free-electron behavior. Even more striking is that the optical behavior of these nitrides also indicates that interband excitations do not occur at low photon energies, or are at least strongly suppressed. It was suggested that in analogy with atomic spectroscopy, transitions between *d*-bands are forbidden to first order by the selection rule $\Delta l = \pm 1$ [4]. This explanation leaves open the question why the common transition metals, e.g., Fe and Ni, exhibit interband transitions [11] and are not free-electron-like.

In this connection it was of primary interest to compare the experimental optical data with results of band-structure calculations, in particular if integrated to partial densities of state. Already in the period between 1960 and 1970, band-structure calculations correctly predicted general trends within a group such as TiC, TiN, and TiO with regard to the energy band gap [12]. Eibler *et al.* [13] performed LCAO-APW calculations that were well adapted to distinguish between the bands of different character and that gave a more detailed picture than the general chemical arguments above. From the partial density of states a joint density of state function (JDOS) was calculated that, as expected, did not show any suppression at low excitation energies. The matrix elements were approximated in such a way as to show some **k**-dependence, and the product, as an approximation to the imaginary part of the interband dielectric function, $\epsilon_{2,\mathrm{ib}}$, was compared to the corresponding experimental quantity. It was interesting to note that while the JDOS did not show strong supression of *d–d* interband excitations, some of this quench-

ing appeared as a consequence of the matrix-element variation. This point was emphasized further by LMTO calculations [14]. A leap forward in the theoretical understanding has been taken with more recent LMTO calculations of Delin *et al.* [15]. Using the energy-band structure and fully variable matrix elements, an *ab initio* interband dielectric function was calculated. The supression of low-energy interband excitations is confirmed as a consequence of the vanishing dipole excitation probability. A semiempirical Drude-type intraband contribution was added, which resulted in very good agreement between theoretical and experimental reflectance spectra.

Relatively few experimental determinations of the complex index of refraction or dielectric function for bulk samples of *zirconium nitride* have been published. In particular, single crystalline studies are scarce. Schlegel *et al.* [16] prepared ZrN single-crystal samples by CVD growth on a heated graphite substrate from a chloride vapor. The resulting single crystals were polished and the normal-incidence bulk reflectance was measured for photon energies from 0.03 to 12 eV. The spectrum had an interval with high and almost wavelength-independent reflectance in the infrared region and a sharp drop to a minimum in the blue/ultraviolet region, as characteristic for a free-electron-like metal. At shorter wavelengths the reflectance again increases as a consequence of interband excitations. This reflectance spectrum was used as an input to Kramers–Kronig calculations giving primarily the complex dielectric function from which the complex refractive index $N(\lambda) = n(\lambda) + ik(\lambda)$ is easily obtained. The early work of Knosp *et al.* [17] with high-temperature sintered nitrides and carbonitrides had already pointed out that only the nitrides, in contrast to the carbides and even the pure metal, are optically free-electron-like in the visible range. They report reflectance spectra and the dielectric function for the limited wavelength interval 275–750 nm.

For their measurements Karlsson *et al.* [7] also used opaque samples deposited upon molybdenum in a CVD process very similar to that of Schlegel, but at a lower temperature, resulting in a polycrystalline dense film that was subsequently polished to ensure specular reflectance. The room-temperature reflectance spectrum was recorded and Kramers–Kronig inverted as in the two previous cases. The NIR reflectance was about the same, 85–90% in all three cases, but the reflectance minima differed both in magnitude and position [7, 16, 17]. We recall that application of the Drude model requires the introduction of a screening constant in the standard expression:

$$\tilde{\epsilon} = \epsilon_1(\infty) - \frac{\omega_p^2 \tau}{\omega^2 \tau + i\omega}, \tag{1}$$

where $\epsilon_1(\infty) > 1$ is the simplest possible representation, a screening constant, of the dispersion caused by higher-energy excitations not included in the

Drude model. The Drude-model reflectance edge for valence electrons with effective optical mass m^* and volume density n in SI units:

$$\hbar\omega_p = \sqrt{\frac{ne^2}{\epsilon_0 m^*}}. \tag{2}$$

The screening constant corresponds to a rigid shift upward of the real part of the dielectric function $\epsilon_1(\omega)$, which displaces the zero of the corresponding Drude function to a lower photon energy. The plasma edge is therefore shifted by the interband excitations of lower-lying electrons, and if the plasma resonance is sharp, that is, $\omega_p\tau \gg 1$, the screened reflectance-edge position is approximately given by.

$$\hbar\omega_p^* = \sqrt{\frac{ne^2}{\epsilon_1(\infty)\epsilon_0 m^*}}. \tag{3}$$

Equations (1)–(3) apply to the transition-metal nitrides almost as well as to the noble metals, and we find that high IR reflectance, steep plasma edge, and a deep reflectance minimum before the onset of interband transitions all indicate a long relaxation time and therefore a more perfect structure. The reflectance minimum was clearly lower in Refs. [17] and [7], which gives them some preference. The free-electron-like part of the dielectric function was used to calculate the Drude parameters, the plasma and relaxation energies: $\hbar\omega_p$ and $\hbar/\tau$. A comparison revealed some scatter in ω_p-values and lower relaxation energies, that is, longer relaxations times, reported by Knosp and Goretzki [17] and Karlsson *et al.* [7] than by Schlegel *et al.* [16], which somewhat surprisingly indicates fewer defects in the polycrystalline films than in the epitaxial layer.

Using the Drude parameters, the intraband contribution can be subtracted from the experimental dielectric function over the entire experimental region. The remaining, interband-excitation part of the dielectric function is relevant for comparison with band-structure calculations and density-of-state functions, in particular the conspicuous threshold for interband transitions, the position of which explains the color of these nitrides, as well as for the three noble metals. This threshold is close to the reflectance minimum just mentioned, and for ZrN Karlsson *et al.* located it to be at ≈3.5 eV [7]. François *et al.* [18] sputtered 480-nm-thick films on 400° C glass and stainless-steel substrates and measured the bulk-reflectance spectra at elevated temperatures, up to 700° C. The dielectric function was calculated by Kramers–Kronig integration for various temperatures. Already for moderately high temperatures the Drude relaxation time decreased, and at the more elevated temperatures a reduction of the screened plasma energy was also observed. These authors report a lower threshold, 1.5 eV, for interband excitations than previous studies, and also a local maximum in the interband contribution to

ϵ_2 at 2.5 eV, which is not present in papers by Karlsson *et al.* [7] and Schlegel [16]. The resulting optical constants, calculated from their dielectric function, are included in the enlarged-wavelength-scale diagrams in Figs. 2a and b.

Edlou *et al.* [19] deposited the three nitrides on room-temperature optical glass, fused silica, or silicon substrates. Two samples were opaque and two semitransparent with thicknesses 30–40 nm. Reflectance measurements as well as spectroscopic ellipsometry were performed to determine the optical constants. They note that the real part of their refractive index is ≤ 1 in most of the visible range. They also observed that, in particular for the longer wavelengths, the n-values increase, while the k-values are approximately constant when the films are made thinner.

Some reported optical measurements were made on opaque, otherwise unspecified samples and gave results that are difficult to reconcile with present knowledge. Presumably because of oxidation, the material appears dielectric or at least with a dielectric surface layer [20, 21]. The appearance of slowly varying n-values > 1 over the visible range is a typical indicator of such problems [1].

A number of studies on the deposition, mainly by reactive sputtering, of ZrN films and in most cases for tribological applications have been published [22]. The number of detailed reports on the optical constants of opaque or semitransmitting films is limited. In particular, very little has been done outside the visible and near-infrared regions. The report of EELS measurements by Pflüger *et al.* [23] is one of few exceptions, showing plasmon losses at 3.6 and 22.3 eV. We have used data from their diagram in Table II for the photon-energy range 10–50 eV. However, they report a refractive index value $n > 1.1$ at 600 nm and a reduction of the critical temperature for superconductivity T_c to < 5 K, which indicates sample oxidation. We have therefore placed less faith in their results for the visible and infrared regions.

Compared to the much-more-investigated TiN films, ZrN films pose a problem in their poor adhesion to common substrate materials. Bonnot *et al.* [8] sputtered their opaque films reactively upon 500° C silicon or glass substrates. They do not report optical constants, but confirm the transition from ZrN as a strongly colored, free-electron-like metal to the grey, transition-metal-like ZrC by also reporting reflectance spectra for zirconium carbonitrides. Veszelei *et al.* [24] studied optically opaque and semitransmitting ZrN films, reactively sputtered onto heated glass substrates. The optical constants for opaque films were determined by two independent methods: Kramers–Kronig integration of reflectance data was used over the range 0.3–25 μm, beyond which the extrapolation parameter was determined with reflectance measurements using polarized light at 60° incidence [25] at a few short wavelengths. The second method used was spectroscopic ellipsometry for λ from 0.28 to 1 μm. The two methods agreed to within 5% at all wavelengths. The values obtained for opaque films are quoted in Table II. One notices

that the n-values for opaque films are clearly <1, that is, noble-metal-like, over the entire visible region. The variation of the optical constants with film thickness was systematically studied [26], and the same trend as had previously been noted for TiN [27] was established. With decreasing film thickness, the n-values for the visible region increase, and the k-values decrease. For a film thickness < 30 nm, no n-values < 1 are obtained. The usual determination of the intraband part was made without the standard asumption of total dominance for Drude behavior by using the screened version (1) and noting that it corresponds to an exact relation between the real and imaginary parts,

$$\epsilon_1 = \epsilon_1(\infty) - \epsilon_2 \omega\tau, \tag{4}$$

so that the linearity of the plot ϵ_1 versus $\omega\epsilon_2$ will verify that the Drude model is valid, and the slope of the straight line will give an experimental value for the relaxation time τ. In the subsequent step, the second Drude parameter ω_p is determined from the slope of ϵ_1 versus $[(\hbar/\tau)^2 + (\hbar\omega)^2]^{-1}$. It was demonstrated that the screened Drude model very closely predicted the optical constants over the wavelength range 0.3–2 μm, with the constant parameter values $\epsilon_1(\infty) = 6.1$, $\hbar\omega_p = 7.1$ eV, and variations only in τ from 2.3 to 0.49 fs to cover film thicknesses from 300 down to 11 nm.

The number of optical studies of *hafnium nitride* is even more limited than for ZrN. We have not been able to find any report of optical measurements on hafnium-nitride single crystals. The thesis of Fluck on the optical properties of hafnium carbonitrides is a standard reference [28]. Fluck's samples were prepared by sintering at 30 MPa at a temperature of 2800° C in a protective atmosphere of nitrogen. The result was bulk, polycrystalline samples with 10–20 μm grain size. Fluck measured the reflectance spectra over the range 0.1–6.2 eV for the carbonitride series HfC_xN_{1-x} and noted the transition from the noble-metal-like behavior of the nitride, to the transition-metal character of the carbide. He also modeled his spectra with Drude theory, compared with band-structure calculations, and extracted the number of free electrons as a function of composition. However, he only reported values for $\epsilon_2(\omega)$ for samples with $x \geq 0.07$.

Early optical measurements at one wavelength (632.8 nm) on rf-sputtered HfN_x films resulted in optical constants characteristic of a partly oxidized film [29]. Karlsson *et al.* prepared opaque HfN films by CVD deposition in a process similar to that for ZrN [7]. They measured normal-incidence reflectance, made Kramers–Kronig calculations, reported optical constants for λ (0.3–2.1 μm) and separated the intra- and interband contributions to the dielectric function. The n-values were <1 for the visible region and the relaxation energy, $\hbar/\tau$, only 0.45 eV, which indicates a less-defected structure than the sintered samples with $\hbar/\tau = 1.4$ eV.

Thin-film deposition of HfN with reactive dc sputtering and accurate structure determinations was studied in detail by Johansson [30]. It appears as if

the dc sputtering results in less-oxidized films. Two studies of reactively sputtered films give optical constants for the wavelength interval in which measurements can be carried out in air [19, 31]. Edlou *et al.* [19] used spectroscopic ellipsometry to determine $n(\lambda)$ and $k(\lambda)$ for λ from 240 to 1640 nm. Strømme *et al.* [31] combined Kramers–Kronig inversion and ellipsometry to obtain data for the λ-range 230–2000 nm as in Veszelei [24]. Both sets of data are included in Figs. 4a and b. In Table III we quote the data of Karlsson *et al.* [7] considering the lower n-values and higher k-values in the visible region. In one part of the spectrum we have used the data of Strømme *et al.* [31] because of their two independent measurements and wider wavelength range. An increase of the n-values with decreasing film thickness is pointed out elsewhere [19, 31]. A systematic study of the variation of the Drude parameters with film thickness was carried out by Strømme. As for the case with ZrN [26], it is shown that the variation, both in n and in k, can be modeled with a variation of the relaxation time τ alone. An opaque 380-nm-thick film had $\tau = 1.86$ fs, which monotonically decreases to $\tau = 0.60$ fs for a 15-nm-thick film, a variation that is comparable with, but smaller than, that reported for ZrN.

In Fig. 1 we have the standard log–log plot of the optical constants for ZrN from Table II, selected as described below. In Figs. 2a and 2b we have given the more detailed behavior of $n(\lambda)$ and $k(\lambda)$, respectively, in the wavelength range of most optical interest and therein included data from several reports mentioned above. It is striking that there are considerable differences between the various refractive-index curves, $n(\lambda)$ in Fig. 2a, while the extinction coefficients, $k(\lambda)$, in 2b closely agree. In Figs. 3, 4a, and 4b the corresponding representation of HfN-data is given.

In Table I we have collected the Drude parameters for the two materials converted to one set of units, otherwise as reported by the various authors. In Tables II and III, i.e., the major collection of optical constants versus photon energy, we have made the following selection among the available sets of data according to the criteria indicated earlier. For ZrN the high-photon-energy data (10 keV–30 eV) were calculated from atomic data and the density according to Henke [32]. In the range 28–8 eV, the values were extracted from Pflüger *et al.* [23] and at lower energies than 8 eV from Veszelei *et al.* [24]. For HfN in Table III the same source of high-energy data was used [32], which left a gap to the next source for 11–4 eV, an interval where Ref. [31] was used. For 4 eV and below we have chosen the values from Karlsson *et al.* [7]. It should be noted that the Henke values have merely been interpolated across the various atomic absorption edges.

ACKNOWLEDGMENT

We acknowledge many useful and stimulating discussions with Ass. Prof. Björn Karlsson, The Älvkarleby Laboratory, State Power Board, on the subject of this critique.

REFERENCES

1. J. Pflüger and J. Fink, *in* "Handbook of Optical Constants of Solids II" (E. D . Palik, ed.), Chap. 13, Section VIII, p. 307. Academic Press, Orlando, Florida, 1991.
2. L. E. Toth, "Refractory Materials: A Series of Monographs, Volume 7: Transition Metal Carbides and Nitrides." Academic Press, New York, 1971.
3. A. Mumtaz and W. H. Class, Color of titanium nitride prepared by reactive dc magnetron sputtering. *J. Vac. Sci. Technol.* **20**, 345 (1982).
4. B. Karlsson, Optical properties of solids for solar energy conversion. Thesis, Acta Universitatis Upsaliensis No. 620, Uppsala University, Uppsala, Sweden (1981).
5. B. Karlsson and C.-G. Ribbing, Optical properties of transparent heat-mirrors based on thin films of TiN, ZrN and HfN. *Proc SPIE* **324**, 52 (1982); see also B. Zega, M. Kornmann, and J. Amiguet, *Thin Solid Films* **45**, 577 (1977)—Abstract only.
6. L. Roux, J. Hanus, J. C. François, and M. Sigrist, The optical properties of titanium nitrides and carbides: Spectral selectivity and photothermal conversion of solar energy. *Sol. Energy Mater.* **7**, 299 (1982).
7. B. Karlsson, R. P. Shimshock, B. O. Seraphin, and J. C. Haygarth, Optical properties of CVD-coated TiN, ZrN and HfN. *Sol. Energy Mater.* **7**, 401 (1983).
8. A. M. Bonnot, H. Belkhir, D. Pailharey, and P. Mathiez, Reactively sputtered zirconium carbides, carbonitrides and nitride thin films-optical properties. *Sol. Energy Mater.* **14**, 375 (1986).
9. M. Lazarov, A. Brunotte, T. Eisenhammer, R. Sizmann, W. Graf, and W. Wittwer, Effects of roughness in TiN_xO_y-Cu selective absorbers. *Proc. SPIE* **1727**, 34 (1992).
10. F. Wooten, "Optical Properties of Solids," 1st Ed. Academic Press, New York, 1972.
11. P. B. Johnson and R. W. Christy, Optical constants of transition metals: Ti, V, Cr, Mn, Fe, Co, Ni and Pd. *Phys. Rev. B* **9**, 5056 (1974).
12. J.-L. Calais, Band structure of transition metal compounds. *Adv. Phys.* **26**, 847 (1977).
13. R. Eibler, M. Dorrer, and A. Neckel, Calculation of the imaginary part $\epsilon_2(\omega)$ of the dielectric function for TiN and ZrN. *J. Phys. C: Solid State Phys.* **16**, 3137 (1983).
14. A. G. Nargizyan and S. N. Rashkeev, Microscopic analysis of the characteristic energy loss spectra of 3d- and 4d-transition metal carbides and nitrides. *Z. Phys. B Condens. Matter* **82**, 217 (1991).
15. A. Delin, O. Eriksson, R. Ahuja, B. Johansson, M. S. S. Brooks, T. Gasche, S. Auluck, and J. M. Wills, Optical properties of the group IVB refractory metal compounds. *Phys. Rev. B* **54**, 1673 (1996).
16. A. Schlegel, P. Wachter, J. J. Nickl, and H. Lingg, Optical properties of TiN and ZrN. *J. Phys. C: Solid State Phys.* **10**, 4889 (1977).
17. H. Knosp and H. Goretzki, Mikroreflexionsmessungen an druckgesinterten Proben der System Titan-TiN-TiC und Zirkonium-ZrN-ZrC. *Z. Metallkd.* **60**, 587 (1969) and also in H. Knosp and V. Gerold, Die Optische Konstanten in den Systemen Titan-TiN-TiC und Zirconium-ZrN-ZrC. *Z. Metallkd.* **60**, 627 (1969).
18. J. C. François, J. Casset, G. Chassaing, P. Gravier, and M. Sigrist, Optical properties of ZrN as a function of temperature. *J. Appl. Phys.* **58**, 3841 (1985).
19. S. M. Edlou, J. C. Simons, G. A. Al-Jumaily, and N. A. Raouf, Optical and electrical properties of reactively sputtered TiN, ZrN and HfN thin films. *Proc. SPIE* **2262**, 96 (1994).
20. S. A. Kutolin, L. F. Belova, R. N. Samoilova, and O. M. Kotenko, Optical properties and physicochemical spectra of nitrides with the NaCl structure. *Izv. Akad. Nauk SSSR, Met.* **12**, 1299 (1976).
21. B. A. Atamanenko, M. U. Belyi, P. I. Drozd, G. G. Tsebulya, and I. A. Shaikevich, Optical properties of zirconium nitride. *Izv. Akad. Nauk SSSR, Met.* **23**, 1037 (1987).
22. J. E. Sundgren and H. T. G. Hentzell, Critical review: A review of the present state of art in hard coatings grown from the vapor phase. *J. Vac. Sci. Technol. A* **4**, 2259 (1986).

23. J. Pflüger, J. Fink, W. Weber, K. P. Bohnen, and G. Crecelius, Dielectric properties of ZrN, NbC and NbN as determined by electron-energy-loss spectroscopy. *Phys. Rev. B* **31**, 1244 (1985).
24. M. Veszelei, K. Andersson, K. Järrendahl, C.-G. Ribbing, and H. Arwin, Optical constants and Drude analysis of sputtered zirconium nitride films. *Appl. Opt.* **33**, 1993 (1994).
25. J. E. Nestell and R. W. Christy, Derivation of optical constants of metals from thin-film measurements at oblique incidence. *Appl. Opt.* **11**, 643 (1972).
26. M. Veszelei, K. E. Andersson, and A. Roos, Optical characterization of sputtered semi-transparent zirconium nitride films. *Opt. Mater.* **2**, 257 (1993).
27. E. Valkonen, C.-G. Ribbing, and J.-E. Sundgren, Optical constants of thin TiN films: Thickness and preparation effects. *Appl. Opt.* **25**, 3624 (1986).
28. F. W. Fluck, Optische Untersuchungen an Hafniumcarbonitriden HfC_xN_{1-x}. Thesis, Juni 1978, Fakultät für Physik, University of Karlsruhe, Karlsruhe, Germany (1978).
29. P. R Aron and A. Grill, Some properties of RF-sputtered hafnium nitride coatings. *Thin Solid Films* **96**, 87 (1982).
30. B. O. Johansson, Structure and properties of titanium- and hafnium- nitride films prepared by reactive magnetron sputtering. Thesis No. 122, Linköping University, Linköping, Sweden (1984).
31. M. Strømme, R. Karmhag, and C. G. Ribbing, Optical constants of sputtered hafnium nitride films. Intra- and interband contributions. *Opt. Mater.* **4**, 629 (1995).
32. We acknowledge M Sc. Bjoern Gaalnander for demonstrating the E. M. Gullikson website: http://grace.lbl.gov/optical_constants/getdb2.html, which was used for calculating our data.

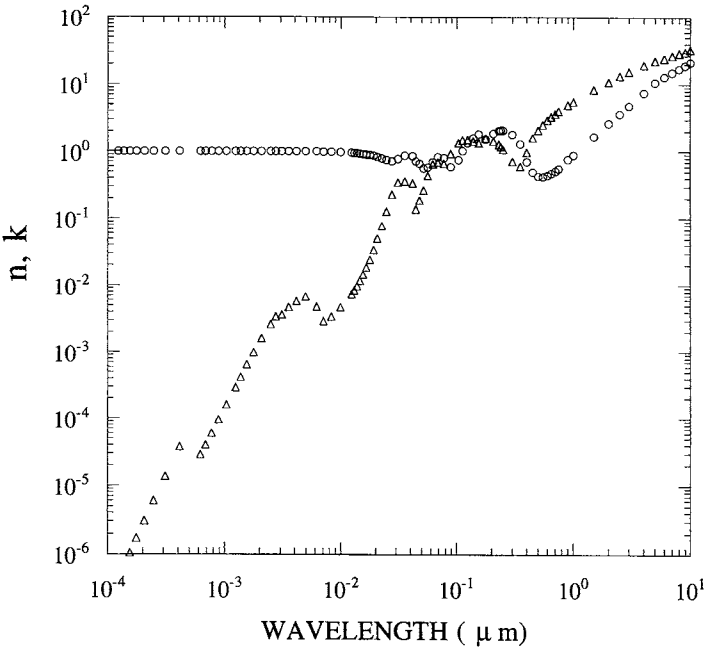

Fig. 1. Complex refractive index, n (○) and k (△), versus photon energy from the x-ray region to the infrared for ZrN according to Table II.

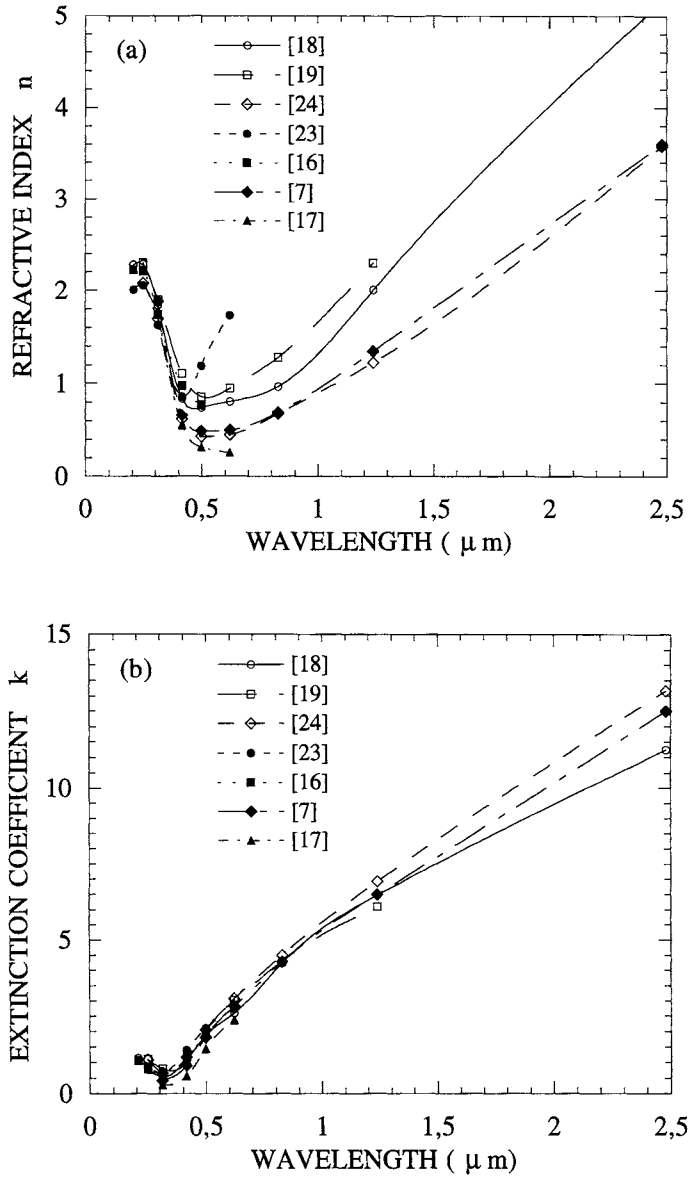

Fig. 2. (a) ZrN n-values versus wavelength in the UV–VIS–NIR range, with values from the different references as indicated in the figure. (b) k-values versus wavelength in the UV–VIS–NIR range, with values from the different references as indicated in the figure.

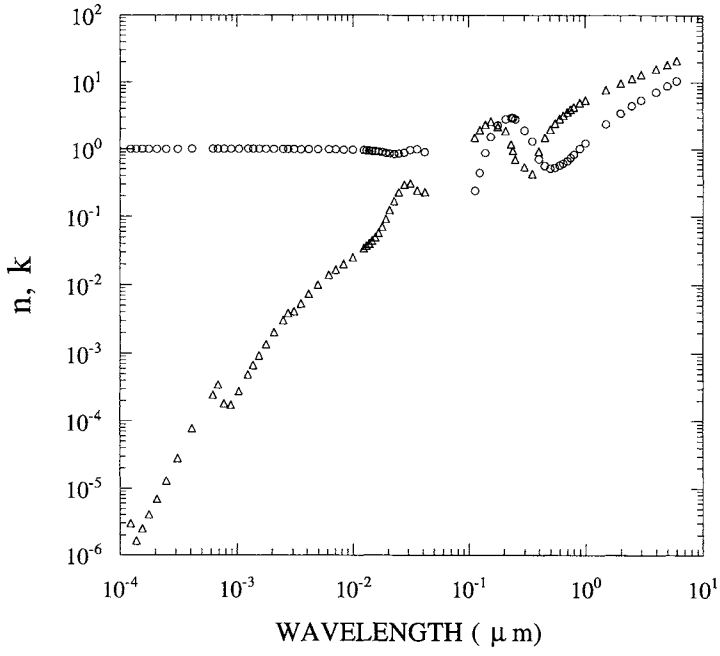

Fig. 3. Complex refractive index, n (○) and k (△), versus photon energy from the x-ray region to the infrared for HfN according to Table III.

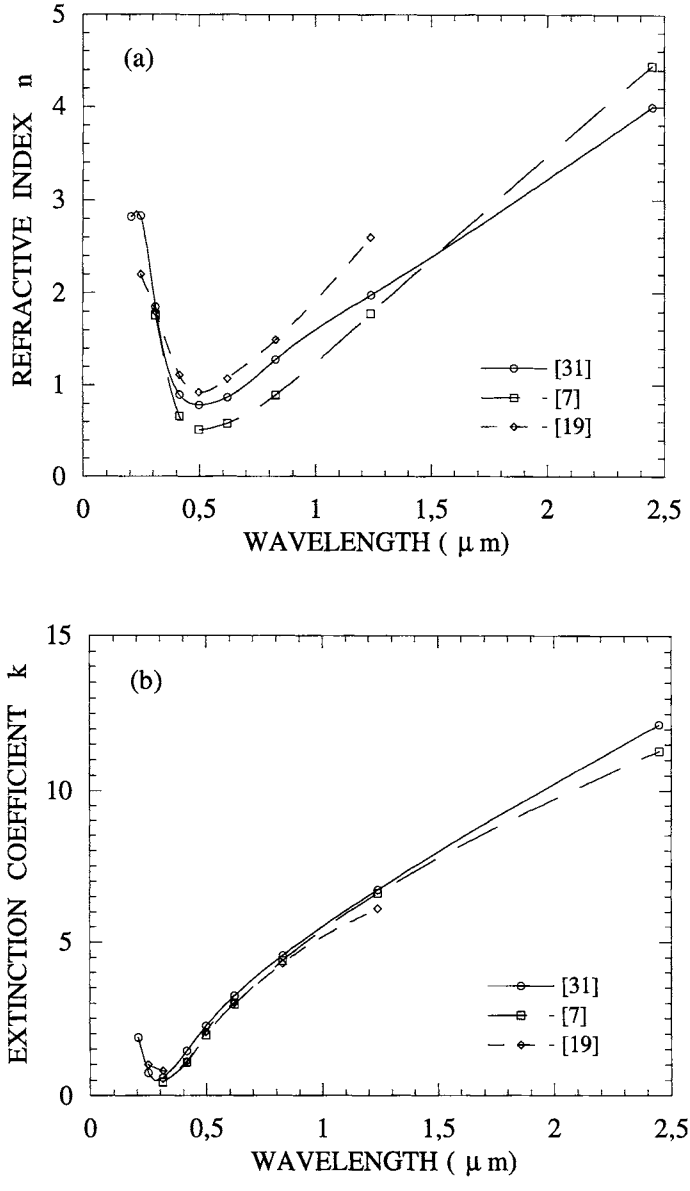

Fig. 4. (a) HfN n-values versus wavelength in the UV–VIS–NIR range with values from the different references as indicated in the figure. (b) k-values versus wavelength in the UV–VIS–NIR range with values from the different references as indicated in the figure.

TABLE I

Drude Parameters: Screened Plasma Energy According to Eq. (3), Drude Plasma Energy According to Eq. (2), Relaxation Energy and Screening Constant as Obtained from the the Indicated Sources

Reference	$\hbar\omega_p^*$ (eV)	$\hbar\omega_p$ (eV)	$\hbar/\tau$ (eV)	$\epsilon_1(\infty)$
ZrN Ref. [7]	3.2	7.17	0.35	
[16]	3.1	7.32	0.62	
[17]	3.20	6.77	0.24	≈7
[18]	3.08	7.35	0.59	
[19]	3.07	6.1	0.73	(2.31)[a]
[24, 26]	3.19	7.35	0.29	6.1
HfN [7]	3.0	7.32	0.45	
[28]	3.11	8.63	1.40	7.7
[19]	3.17	6.1	0.9	(2.74)[a]
[31]	3.88	7.78	0.35	6.4

[a] The two $\epsilon_1(\infty)$-values from Ref. [19] are not comparable with the others because a two-oscillator model was used in the fitting procedure.

TABLE II

Values of *n* and *k* for ZrN Obtained from Various References[a]

e V	cm^{-1}	μm	n	k
1.000E + 4	8.065E + 7	1.240E-1	1.00E + 0 [32]	4.53E-7 [32]
9.000E + 3	7.259E + 7	1.378E-1	1.00E + 0	6.75E-7
8.000E + 3	6.452E + 7	1.550E-1	1.00E + 0	1.05E-6
7.000E + 3	5.646E + 7	1.771E-1	1.00E + 0	1.72E-6
6.000E + 3	4.839E + 7	2.067E-1	1.00E + 0	3.07E-6
5.000E + 3	4.033E + 7	2.480E-1	1.00E + 0	6.01E-6
4.000E + 3	3.226E + 7	3.100E-1	1.00E + 0	1.36E-5
3.000E + 3	2.420E + 7	4.133E-1	1.00E + 0	3.80E-5
2.000E + 3	1.613E + 7	6.200E-1	1.00E + 0	2.86E-5
1.800E + 3	1.452E + 7	6.889E-1	1.00E + 0	4.03E-5
1.600E + 3	1.290E + 7	7.750E-1	1.00E + 0	6.04E-5
1.400E + 3	1.129E + 7	8.857E-1	9.99E-1	9.55E-5
1.200E + 3	9.679E + 6	1.033E + 0	9.99E-1	1.61E-4
1.000E + 3	8.065E + 6	1.240E + 0	9.99E-1	2.91E-4
9.000E + 2	7.259E + 6	1.378E + 0	9.99E-1	4.22E-4
8.000E + 2	6.452E + 6	1.550E + 0	9.98E-1	6.44E-4
7.000E + 2	5.646E + 6	1.771E + 0	9.98E-1	9.90E-4
6.000E + 2	4.839E + 6	2.067E + 0	9.97E-1	1.58E-3
5.000E + 2	4.033E + 6	2.480E + 0	9.97E-1	2.58E-3
4.500E + 2	3.629E + 6	2.756E + 0	9.96E-1	3.37E-3
4.000E + 2	3.226E + 6	3.100E + 0	9.97E-1	3.63E-3
3.500E + 2	2.823E + 6	3.543E + 0	9.96E-1	4.64E-3

(continued)

[a] The references from which the values were taken are given in brackets.

TABLE II *(Continued)*

ZrN

e V	cm^{-1}	μm	n	k
3.000E + 2	2.420E + 6	4.133E + 0	9.95E-1	5.76E-3
2.500E + 2	2.016E + 6	4.960E + 0	9.95E-1	6.73E-3
2.000E + 2	1.613E + 6	6.200E + 0	9.94E-1	4.77E-3
1.750E + 2	1.411E + 6	7.086E + 0	9.89E-1	2.90E-3
1.500E + 2	1.210E + 6	8.267E + 0	9.82E-1	3.36E-3
1.250E + 2	1.008E + 6	9.920E + 0	9.71E-1	4.68E-3
1.000E + 2	8.065E + 5	1.240E + 1	9.51E-1	7.31E-3
9.500E + 1	7.662E + 5	1.305E + 1	9.45E-1	8.30E-3
9.000E + 1	7.259E + 5	1.378E + 1	9.37E-1	9.66E-3
8.500E + 1	6.856E + 5	1.459E + 1	9.28E-1	1.16E-2
8.000E + 1	6.452E + 5	1.550E + 1	9.17E-1	1.43E-2
7.500E + 1	6.049E + 5	1.653E + 1	9.03E-1	1.83E-2
7.000E + 1	5.646E + 5	1.771E + 1	8.85E-1	2.42E-2
6.500E + 1	5.243E + 5	1.908E + 1	8.62E-1	3.40E-2
6.000E + 1	4.839E + 5	2.067E + 1	8.33E-1	5.03E-2
5.500E + 1	4.436E + 5	2.255E + 1	7.96E-1	7.82E-2
5.000E + 1	4.033E + 5	2.480E + 1	7.51E-1	1.29E-1
4.500E + 1	3.629E + 5	2.756E + 1	7.14E-1	2.28E-1
4.000E + 1	3.226E + 5	3.100E + 1	7.81E-1	3.49E-1
3.500E + 1	2.823E + 5	3.543E + 1	8.64E-1	3.58E-1
3.000E + 1	2.420E + 5	4.133E + 1	8.47E-1	3.35E-1
2.800E + 1	2.258E + 5	4.429E + 1	7.21E-1 [23]	1.39E-1 [23]
2.600E + 1	2.097E + 5	4.769E + 1	6.60E-1	1.89E-1
2.400E + 1	1.936E + 5	5.167E + 1	5.66E-1	2.65E-1
2.200E + 1	1.774E + 5	5.636E + 1	5.80E-1	4.31E-1
2.000E + 1	1.613E + 5	6.200E + 1	6.90E-1	6.52E-1
1.800E + 1	1.452E + 5	6.889E + 1	8.27E-1	6.95E-1
1.600E + 1	1.290E + 5	7.750E + 1	7.97E-1	6.59E-1
1.400E + 1	1.129E + 5	8.857E + 1	5.95E-1	9.24E-1
1.200E + 1	9.679E + 4	1.033E + 2	7.52E-1	1.33E + 0
1.100E + 1	8.874E + 4	1.127E + 2	1.02E + 0	1.47E + 0
1.000E + 1	8.065E + 4	1.240E + 2	1.35E + 0	1.49E + 0
8.999E + 0	7.258E + 4	1.378E + 2	1.57E + 0	1.43E + 0
8.000E + 0	6.452E + 4	1.550E + 2	1.82E + 0	1.35E + 0
7.002E + 0	5.647E + 4	1.771E + 2	1.54E + 0 [24]	1.58E + 0 [24]
5.999E + 0	4.838E + 4	2.067E + 2	1.85E + 0	1.43E + 0
5.391E + 0	4.348E + 4	2.300E + 2	2.04E + 0	1.28E + 0
5.167E + 0	4.167E + 4	2.400E + 2	2.08E + 0	1.19E + 0
4.960E + 0	4.000E + 4	2.500E + 2	2.07E + 0	1.07E + 0
4.769E + 0	3.847E + 4	2.600E + 2	2.04E + 0	9.66E-1
4.593E + 0	3.704E + 4	2.700E + 2	1.99E + 0	8.90E-1
4.429E + 0	3.572E + 4	2.800E + 2	1.93E + 0	8.22E-1
4.276E + 0	3.449E + 4	2.900E + 2	1.86E + 0	7.60E-1
4.133E + 0	3.334E + 4	3.000E + 2	1.79E + 0	7.13E-1
4.000E + 0	3.226E + 4	3.100E + 2	1.70E + 0	6.69E-1
3.875E + 0	3.125E + 4	3.200E + 2	1.60E + 0	6.48E-1
3.758E + 0	3.031E + 4	3.300E + 2	1.52E + 0	6.32E-1

TABLE II *(Continued)*

ZrN

e V	cm^{-1}	μm	n	k
3.647E + 0	2.942E + 4	3.400E + 2	1.41E + 0	5.99E-1
3.543E + 0	2.857E + 4	3.500E + 2	1.29E + 0	5.99E-1
3.444E + 0	2.778E + 4	3.600E + 2	1.17E + 0	6.19E-1
3.351E + 0	2.703E + 4	3.700E + 2	1.04E + 0	6.68E-1
3.263E + 0	2.632E + 4	3.800E + 2	9.20E-1	7.60E-1
3.179E + 0	2.564E + 4	3.900E + 2	8.23E-1	8.55E-1
3.100E + 0	2.500E + 4	4.000E + 2	7.06E-1	9.76E-1
3.024E + 0	2.439E + 4	4.100E + 2	6.35E-1	1.12E + 0
2.952E + 0	2.381E + 4	4.200E + 2	5.85E-1	1.24E + 0
2.884E + 0	2.326E + 4	4.300E + 2	5.45E-1	1.36E + 0
2.818E + 0	2.273E + 4	4.400E + 2	5.17E-1	1.48E + 0
2.756E + 0	2.222E + 4	4.500E + 2	4.97E-1	1.59E + 0
2.696E + 0	2.174E + 4	4.600E + 2	4.84E-1	1.69E + 0
2.638E + 0	2.128E + 4	4.700E + 2	4.55E-1	1.80E + 0
2.583E + 0	2.084E + 4	4.800E + 2	4.44E-1	1.90E + 0
2.531E + 0	2.041E + 4	4.900E + 2	4.35E-1	1.99E + 0
2.480E + 0	2.000E + 4	5.000E + 2	4.28E-1	2.09E + 0
2.431E + 0	1.961E + 4	5.100E + 2	4.23E-1	2.18E + 0
2.385E + 0	1.923E + 4	5.200E + 2	4.20E-1	2.27E + 0
2.340E + 0	1.887E + 4	5.300E + 2	4.21E-1	2.35E + 0
2.296E + 0	1.852E + 4	5.400E + 2	4.19E-1	2.44E + 0
2.255E + 0	1.818E + 4	5.500E + 2	4.23E-1	2.52E + 0
2.214E + 0	1.786E + 4	5.600E + 2	4.28E-1	2.60E + 0
2.175E + 0	1.755E + 4	5.700E + 2	4.23E-1	2.68E + 0
2.138E + 0	1.724E + 4	5.800E + 2	4.26E-1	2.76E + 0
2.102E + 0	1.695E + 4	5.900E + 2	4.32E-1	2.84E + 0
2.067E + 0	1.667E + 4	6.000E + 2	4.39E-1	2.92E + 0
2.033E + 0	1.640E + 4	6.100E + 2	4.46E-1	2.99E + 0
2.000E + 0	1.613E + 4	6.200E + 2	4.51E-1	3.07E + 0
1.968E + 0	1.587E + 4	6.300E + 2	4.56E-1	3.14E + 0
1.937E + 0	1.563E + 4	6.400E + 2	4.63E-1	3.22E + 0
1.908E + 0	1.539E + 4	6.500E + 2	4.69E-1	3.29E + 0
1.879E + 0	1.515E + 4	6.600E + 2	4.77E-1	3.36E + 0
1.851E + 0	1.493E + 4	6.700E + 2	4.86E-1	3.44E + 0
1.824E + 0	1.471E + 4	6.800E + 2	4.93E-1	3.51E + 0
1.797E + 0	1.449E + 4	6.900E + 2	5.09E-1	3.58E + 0
1.771E + 0	1.429E + 4	7.000E + 2	5.13E-1	3.64E + 0
1.746E + 0	1.409E + 4	7.100E + 2	5.17E-1	3.71E + 0
1.722E + 0	1.389E + 4	7.200E + 2	5.28E-1	3.78E + 0
1.699E + 0	1.370E + 4	7.300E + 2	5.38E-1	3.85E + 0
1.676E + 0	1.352E + 4	7.400E + 2	5.47E-1	3.92E + 0
1.653E + 0	1.333E + 4	7.500E + 2	5.57E-1	3.99E + 0
1.632E + 0	1.316E + 4	7.600E + 2	5.68E-1	4.06E + 0
1.610E + 0	1.299E + 4	7.700E + 2	5.80E-1	4.13E + 0
1.590E + 0	1.282E + 4	7.800E + 2	5.93E-1	4.20E + 0
1.570E + 0	1.266E + 4	7.900E + 2	6.15E-1	4.27E + 0

(continued)

TABLE II *(Continued)*

ZrN

e V	cm^{-1}	μm	n	k
1.459E + 0	1.177E + 4	8.500E + 2	6.99E-1	4.64E + 0
1.378E + 0	1.111E + 4	9.000E + 2	7.57E-1	4.95E + 0
1.305E + 0	1.053E + 4	9.500E + 2	8.17E-1	5.25E + 0
1.240E + 0	1.000E + 4	1.000E + 3	8.86E-1	5.55E + 0
1.127E + 0	9.092E + 3	1.100E + 3	1.02E + 0	6.13E + 0
1.033E + 0	8.334E + 3	1.200E + 3	1.17E + 0	6.71E + 0
9.538E-1	7.693E + 3	1.300E + 3	1.33E + 0	7.27E + 0
8.857E-1	7.144E + 3	1.400E + 3	1.49E + 0	7.82E + 0
8.267E-1	6.667E + 3	1.500E + 3	1.68E + 0	8.36E + 0
7.750E-1	6.251E + 3	1.600E + 3	1.85E + 0	8.87E + 0
7.294E-1	5.883E + 3	1.700E + 3	2.04E + 0	9.39E + 0
6.889E-1	5.556E + 3	1.800E + 3	2.19E + 0	9.87E + 0
6.526E-1	5.264E + 3	1.900E + 3	2.43E + 0	1.04E + 1
6.200E-1	5.001E + 3	2.000E + 3	2.62E + 0	1.09E + 1
5.905E-1	4.762E + 3	2.100E + 3	2.83E + 0	1.14E + 1
5.636E-1	4.546E + 3	2.200E + 3	3.03E + 0	1.18E + 1
5.391E-1	4.348E + 3	2.300E + 3	3.20E + 0	1.23E + 1
5.167E-1	4.167E + 3	2.400E + 3	3.39E + 0	1.28E + 1
4.960E-1	4.000E + 3	2.500E + 3	3.65E + 0	1.33E + 1
4.769E-1	3.847E + 3	2.600E + 3	4.05E + 0	1.37E + 1
4.593E-1	3.704E + 3	2.700E + 3	4.08E + 0	1.41E + 1
4.429E-1	3.572E + 3	2.800E + 3	4.32E + 0	1.45E + 1
4.276E-1	3.449E + 3	2.900E + 3	4.56E + 0	1.49E + 1
4.133E-1	3.333E + 3	3.000E + 3	4.75E + 0	1.54E + 1
3.100E-1	2.500E + 3	4.000E + 3	7.43E + 0	1.94E + 1
2.480E-1	2.000E + 3	5.000E + 3	1.07E + 1	2.22E + 1
2.066E-1	1.666E + 3	6.002E + 3	1.28E + 1	2.43E + 1
1.771E-1	1.428E + 3	7.003E + 3	1.49E + 1	2.68E + 1
1.550E-1	1.250E + 3	8.000E + 3	1.71E + 1	2.87E + 1
1.378E-1	1.111E + 3	9.001E + 3	1.91E + 1	3.04E + 1
1.240E-1	1.000E + 3	1.000E + 4	2.11E + 1	3.27E + 1
1.127E-1	9.091E + 2	1.100E + 4	2.35E + 1	3.35E + 1
1.033E-1	8.331E + 2	1.200E + 4	2.50E + 1	3.51E + 1
9.536E-2	7.691E + 2	1.300E + 4	2.70E + 1	3.63E + 1
8.853E-2	7.141E + 2	1.401E + 4	2.85E + 1	3.72E + 1
8.258E-2	6.661E + 2	1.501E + 4	3.03E + 1	3.85E + 1
7.750E-2	6.251E + 2	1.600E + 4	3.25E + 1	3.87E + 1
7.291E-2	5.881E + 2	1.701E + 4	3.41E + 1	3.84E + 1
6.882E-2	5.551E + 2	1.802E + 4	3.47E + 1	4.04E + 1
6.523E-2	5.261E + 2	1.901E + 4	3.63E + 1	4.08E + 1
6.200E-2	5.001E + 2	2.000E + 4	3.71E + 1	4.03E + 1
5.903E-2	4.761E + 2	2.101E + 4	3.82E + 1	4.32E + 1
5.630E-2	4.541E + 2	2.203E + 4	3.99E + 1	4.15E + 1
5.382E-2	4.341E + 2	2.304E + 4	4.01E + 1	4.17E + 1
5.159E-2	4.161E + 2	2.404E + 4	4.01E + 1	4.21E + 1

TABLE III

Values of n and k for HfN Obtained from Various References[a]

eV	cm^{-1}	μm	n	k
1.000E + 4	8.065E + 7	1.240E-4	1.00E + 0 [32]	2.97E-6 [32]
9.000E + 3	7.259E + 7	1.378E-4	1.00E + 0	1.63E-6
8.000E + 3	6.452E + 7	1.550E-4	1.00E + 0	2.50E-6
7.000E + 3	5.646E + 7	1.771E-4	1.00E + 0	4.02E-6
6.000E + 3	4.839E + 7	2.067E-4	1.00E + 0	6.94E-6
5.000E + 3	4.033E + 7	2.480E-4	1.00E + 0	1.31E-5
4.000E + 3	3.226E + 7	3.100E-4	1.00E + 0	2.84E-5
3.000E + 3	2.420E + 7	4.133E-4	1.00E + 0	7.70E-5
2.000E + 3	1.613E + 7	6.200E-4	1.00E + 0	2.41E-4
1.800E + 3	1.452E + 7	6.889E-4	1.00E + 0	3.48E-4
1.600E + 3	1.290E + 7	7.750E-4	1.00E + 0	1.80E-4
1.400E + 3	1.129E + 7	8.857E-4	9.99E-1	1.74E-4
1.200E + 3	9.679E + 6	1.033E-3	9.99E-1	2.78E-4
1.000E + 3	8.065E + 6	1.240E-3	9.98E-1	4.88E-4
9.000E + 2	7.259E + 6	1.378E-3	9.98E-1	6.64E-4
8.000E + 2	6.452E + 6	1.550E-3	9.98E-1	9.31E-4
7.000E + 2	5.646E + 6	1.771E-3	9.97E-1	1.36E-3
6.000E + 2	4.839E + 6	2.067E-3	9.96E-1	2.04E-3
5.000E + 2	4.033E + 6	2.480E-3	9.95E-1	3.02E-3
4.500E + 2	3.629E + 6	2.756E-3	9.95E-1	3.88E-3
4.000E + 2	3.226E + 6	3.100E-3	9.95E-1	4.12E-3
3.500E + 2	2.823E + 6	3.543E-3	9.93E-1	5.35E-3
3.000E + 2	2.420E + 6	4.133E-3	9.91E-1	7.31E-3
2.500E + 2	2.016E + 6	4.960E-3	9.89E-1	9.97E-3
2.000E + 2	1.613E + 6	6.200E-3	9.85E-1	1.39E-2
1.750E + 2	1.411E + 6	7.086E-3	9.82E-1	1.65E-2
1.500E + 2	1.210E + 6	8.267E-3	9.77E-1	2.01E-2
1.250E + 2	1.008E + 6	9.920E-3	9.69E-1	2.54E-2
1.000E + 2	8.065E + 5	1.240E-2	9.53E-1	3.43E-2
9.500E + 1	7.662E + 5	1.305E-2	9.47E-1	3.70E-2
9.000E + 1	7.259E + 5	1.378E-2	9.41E-1	4.02E-2
8.500E + 1	6.856E + 5	1.459E-2	9.33E-1	4.42E-2
8.000E + 1	6.452E + 5	1.550E-2	9.23E-1	4.96E-2
7.500E + 1	6.049E + 5	1.653E-2	9.09E-1	5.76E-2
7.000E + 1	5.646E + 5	1.771E-2	8.92E-1	7.09E-2
6.500E + 1	5.243E + 5	1.908E-2	8.73E-1	9.15E-2
6.000E + 1	4.839E + 5	2.067E-2	8.55E-1	1.25E-1
5.500E + 1	4.436E + 5	2.255E-2	8.45E-1	1.69E-1
5.000E + 1	4.033E + 5	2.480E-2	8.48E-1	2.30E-1
4.500E + 1	3.629E + 5	2.756E-2	8.88E-1	2.95E-1
4.000E + 1	3.226E + 5	3.100E-2	9.67E-1	3.13E-1
3.500E + 1	2.823E + 5	3.543E-2	9.98E-1	2.43E-1
3.000E + 1	2.420E + 5	4.133E-2	8.94E-1	2.29E-1
1.100E + 1	8.872E + 4	1.127E-1	2.40E-1 [31]	1.49E + 0 [31]
1.000E + 1	8.065E + 4	1.240E-1	4.43E-1	1.92E + 0

(continued)

[a] References from which the values were taken are given in brackets.

TABLE III *(Continued)*

HfN

eV	cm^{-1}	μm	n	k
8.999E + 0	7.258E + 4	1.378E-1	8.70E-1	2.31E + 0
8.000E + 0	6.452E + 4	1.550E-1	1.52E + 0	2.57E + 0
7.002E + 0	5.647E + 4	1.771E-1	2.26E + 0	2.18E + 0
5.999E + 0	4.838E + 4	2.067E-1	2.82E + 0	1.87E + 0
5.391E + 0	4.348E + 4	2.300E-1	2.95E + 0	1.19E + 0
5.167E + 0	4.167E + 4	2.400E-1	2.96E + 0	9.42E-1
4.960E + 0	4.000E + 4	2.500E-1	2.80E + 0	6.94E-1
4.769E + 0	3.846E + 4	2.600E-1	2.63E + 0	5.38E-1
4.593E + 0	3.704E + 4	2.700E-1	2.30E + 0	4.32E-1
4.429E + 0	3.572E + 4	2.800E-1	2.17E + 0	4.75E-1
4.276E + 0	3.449E + 4	2.900E-1	2.01E + 0	4.87E-1
4.133E + 0	3.333E + 4	3.000E-1	1.91E + 0	5.38E-1
4.000E + 0	3.226E + 4	3.100E-1	1.76E + 0 [7]	4.30E-1 [7]
3.875E + 0	3.125E + 4	3.200E-1	1.66E + 0	4.10E-1
3.758E + 0	3.031E + 4	3.300E-1	1.56E + 0	4.05E-1
3.647E + 0	2.941E + 4	3.400E-1	1.44E + 0	4.05E-1
3.543E + 0	2.858E + 4	3.500E-1	1.31E + 0	4.30E-1
3.444E + 0	2.778E + 4	3.600E-1	1.17E + 0	4.70E-1
3.351E + 0	2.703E + 4	3.700E-1	1.05E + 0	5.40E-1
3.263E + 0	2.632E + 4	3.800E-1	9.00E-1	6.40E-1
3.180E + 0	2.565E + 4	3.900E-1	7.80E-1	7.70E-1
3.100E + 0	2.500E + 4	4.000E-1	7.10E-1	9.20E-1
3.024E + 0	2.439E + 4	4.100E-1	6.60E-1	1.04E + 0
2.952E + 0	2.381E + 4	4.200E-1	6.30E-1	1.16E + 0
2.884E + 0	2.326E + 4	4.300E-1	6.00E-1	1.28E + 0
2.818E + 0	2.273E + 4	4.400E-1	5.70E-1	1.40E + 0
2.756E + 0	2.223E + 4	4.500E-1	5.60E-1	1.50E + 0
2.696E + 0	2.174E + 4	4.600E-1	5.40E-1	1.60E + 0
2.638E + 0	2.128E + 4	4.700E-1	5.30E-1	1.70E + 0
2.583E + 0	2.083E + 4	4.800E-1	5.20E-1	1.80E + 0
2.531E + 0	2.041E + 4	4.900E-1	5.15E-1	1.89E + 0
2.480E + 0	2.000E + 4	5.000E-1	5.10E-1	1.98E + 0
2.431E + 0	1.961E + 4	5.100E-1	5.10E-1	2.07E + 0
2.385E + 0	1.924E + 4	5.200E-1	5.10E-1	2.16E + 0
2.340E + 0	1.887E + 4	5.300E-1	5.15E-1	2.25E + 0
2.296E + 0	1.852E + 4	5.400E-1	5.25E-1	2.34E + 0
2.255E + 0	1.819E + 4	5.500E-1	5.30E-1	2.42E + 0
2.214E + 0	1.786E + 4	5.600E-1	5.35E-1	2.51E + 0
2.175E + 0	1.754E + 4	5.700E-1	5.40E-1	2.59E + 0
2.138E + 0	1.724E + 4	5.800E-1	5.50E-1	2.67E + 0
2.102E + 0	1.695E + 4	5.900E-1	5.60E-1	2.75E + 0
2.067E + 0	1.667E + 4	6.000E-1	5.70E-1	2.83E + 0
2.033E + 0	1.640E + 4	6.100E-1	5.80E-1	2.90E + 0
2.000E + 0	1.613E + 4	6.200E-1	5.85E-1	2.97E + 0
1.968E + 0	1.587E + 4	6.300E-1	5.90E-1	3.05E + 0
1.937E + 0	1.562E + 4	6.400E-1	6.00E-1	3.12E + 0
1.908E + 0	1.539E + 4	6.500E-1	6.10E-1	3.20E + 0

TABLE III *(Continued)*

HfN

eV	cm^{-1}	μm	n	k
1.879E + 0	1.516E + 4	6.600E-1	6.20E-1	3.26E + 0
1.851E + 0	1.493E + 4	6.700E-1	6.30E-1	3.33E + 0
1.823E + 0	1.470E + 4	6.800E-1	6.40E-1	3.40E + 0
1.797E + 0	1.449E + 4	6.900E-1	6.50E-1	3.47E + 0
1.771E + 0	1.428E + 4	7.000E-1	6.60E-1	3.55E + 0
1.746E + 0	1.408E + 4	7.100E-1	6.75E-1	3.62E + 0
1.722E + 0	1.389E + 4	7.200E-1	6.90E-1	3.70E + 0
1.699E + 0	1.370E + 4	7.300E-1	7.10E-1	3.77E + 0
1.676E + 0	1.352E + 4	7.400E-1	7.25E-1	3.85E + 0
1.653E + 0	1.333E + 4	7.500E-1	7.40E-1	3.92E + 0
1.632E + 0	1.316E + 4	7.600E-1	7.60E-1	4.00E + 0
1.610E + 0	1.299E + 4	7.700E-1	7.80E-1	4.05E + 0
1.590E + 0	1.282E + 4	7.800E-1	7.95E-1	4.11E + 0
1.570E + 0	1.266E + 4	7.900E-1	8.15E-1	4.17E + 0
1.550E + 0	1.250E + 4	8.000E-1	8.30E-1	4.24E + 0
1.459E + 0	1.177E + 4	8.500E-1	9.30E-1	4.56E + 0
1.378E + 0	1.111E + 4	9.000E-1	1.03E + 0	4.93E + 0
1.305E + 0	1.053E + 4	9.500E-1	1.15E + 0	5.20E + 0
1.240E + 0	1.000E + 4	1.000E + 0	1.24E + 0	5.45E + 0
1.181E + 0	9.525E + 3	1.050E + 0	1.38E + 0	5.65E + 0
1.127E + 0	9.090E + 3	1.100E + 0	1.45E + 0	5.90E + 0
1.078E + 0	8.695E + 3	1.150E + 0	1.60E + 0	6.15E + 0
1.033E + 0	8.332E + 3	1.200E + 0	1.70E + 0	6.40E + 0
9.920E-1	8.001E + 3	1.250E + 0	1.82E + 0	6.65E + 0
9.539E-1	7.694E + 3	1.300E + 0	1.95E + 0	6.85E + 0
9.185E-1	7.408E + 3	1.350E + 0	2.05E + 0	7.05E + 0
8.857E-1	7.144E + 3	1.400E + 0	2.18E + 0	7.30E + 0
8.552E-1	6.898E + 3	1.450E + 0	2.25E + 0	7.50E + 0
8.267E-1	6.668E + 3	1.500E + 0	2.40E + 0	7.75E + 0
7.750E-1	6.251E + 3	1.600E + 0	2.60E + 0	8.20E + 0
7.294E-1	5.883E + 3	1.700E + 0	2.81E + 0	8.60E + 0
6.889E-1	5.556E + 3	1.800E + 0	3.02E + 0	9.00E + 0
6.526E-1	5.264E + 3	1.900E + 0	3.22E + 0	9.30E + 0
6.200E-1	5.001E + 3	2.000E + 0	3.45E + 0	9.70E + 0
5.905E-1	4.763E + 3	2.100E + 0	3.68E + 0	1.01E + 1
5.636E-1	4.546E + 3	2.200E + 0	3.90E + 0	1.04E + 1
5.391E-1	4.348E + 3	2.300E + 0	4.10E + 0	1.07E + 1
5.167E-1	4.167E + 3	2.400E + 0	4.30E + 0	1.11E + 1
4.960E-1	4.000E + 3	2.500E + 0	4.50E + 0	1.14E + 1
4.769E-1	3.846E + 3	2.600E + 0	4.68E + 0	1.17E + 1
4.593E-1	3.704E + 3	2.700E + 0	4.86E + 0	1.20E + 1
4.429E-1	3.572E + 3	2.800E + 0	5.04E + 0	1.23E + 1
4.276E-1	3.449E + 3	2.900E + 0	5.22E + 0	1.26E + 1
4.133E-1	3.333E + 3	3.000E + 0	5.40E + 0	1.29E + 1
3.100E-1	2.500E + 3	4.000E + 0	7.10E + 0	1.56E + 1
2.480E-1	2.000E + 3	5.000E + 0	8.80E + 0	1.80E + 1
2.067E-1	1.667E + 3	6.000E + 0	1.05E + 1	2.10E + 1

Aluminum Nitride (AlN)

S. LOUGHIN
Lockheed Martin Corporation
Philadelphia, Pennsylvania

and

R. H. FRENCH
DuPont Central Research & Development,
Wilmington, Delaware

INTRODUCTION I

Aluminum nitride (AlN) is a wurtzite structure (space group $P6_3mc$) ceramic material, with lattice parameters [1] of $\vec{a} = \vec{b} = 3.11$ Å and $\vec{c} = 4.98$ Å. The volume of the unit cell is 41.71 Å^3 with two formula units per cell. Interest in this material increased after the pioneering work of Slack [2], who along with McNelly [3, 4], synthesized high-purity single crystals with thermal conductivities of up to 275 W m^{-1} K^{-1}. Since then, this material has found increasing technological application [5] motivating considerable study in theoretical [6–14] and experimental [15] investigations. Here, we critique the literature on the optical properties of AlN, rendering [16] selected data in a table of the real and imaginary components of the index of refraction.

AlN has an affinity for oxygen [17, 18] and all commercially available material contains some oxygen. Previous investigators have correlated oxygen content to changes in thermal conductivity, shifts in luminescence features [19], and changes in the energy dependence of the reflectance spectrum [20] of AlN. A number of authors [21–24] have discussed the thermal stability and oxidation of AlN, noting that AlN is easily oxidized by reaction with water or by heating in the presence of oxygen. Much work [25, 26] has focused on how oxygen is accommodated in AlN and its effect on the electronic structure. Because the electronic structure is altered by the presence of oxygen [27], the optical results most characteristic of the pure phase are obtained on nonaqueously polished samples that have been prepared with

HANDBOOK OF OPTICAL CONSTANTS OF SOLIDS III

Copyright © 1998 by Academic Press.
All rights of reproduction in any form reserved
ISBN 0-12-544423-0/$25.00.

careful attention to minimize oxygen impurities. The difficulty of obtaining and maintaining an oxygen-free AlN surface has complicated many of the experimental investigations of the optical properties of this material. Data from investigations on single crystals or on thin films where oxygen was controlled or mitigated are included in Table I, although a substantially larger body of work is reviewed.

II BAND GAP, BAND-EDGE ABSORPTION, AND BIREFRINGENCE

Estimates of the band gap of AlN from optical measurements have been reported by a number of investigators [28–30] and range from about 5.8 to 6.2 eV. Chu and Kelm [31] report optical absorbance in the region below the fundamental edge and a band gap of 5.9 ± 0.2 eV. Aita *et al.* [32] report a band-gap energy of 6.18 eV.

Zarwasch *et al.* [33] measured the optical absorption of AlN thin films prepared by sputter deposition over the range of 3 to 6.5 eV and discussed their results in comparison to those of Aita *et al.* [32]. Both of these investigations focused on absorption just below the band edge in thin films, which Zarwasch *et al.* attributed to localized states arising from crystalline disorder in the film. The single crystals grown by Slack and McNelly [3, 4] also exhibit absorption below the band edge; however, this has been attributed to nitrogen vacancies [34]. Kaplan and Gerhardt [35] have studied the role of carbon impurities in UV-induced absorption at 0.650 μm. Perry and Rutz [36] measured optical density over the range 5.2–6.4 eV, noting the presence of two absorption features below the fundamental edge attributed to vacancies or oxygen impurities, and report band-gap values of 6.28 eV at 5 K and 6.20 eV at 300 K. Bauer *et al.* [37] prepared films by pyrolytic and plasmachemical vapor deposition and provided the spectral dependence of the real index between 0.1 and 0.4 μm, as well as the absorption coefficient from 4 to 7 eV. They measured band gaps of 5.93 and 6.0 eV with temperature dependancies of -2.8×10^{-4} and -2.5×10^{-4} eV/K, respectively. Barovskii *et al.* [38] reported absorption spectra for oriented, epitaxial AlN films over the range of 2–6 eV and reported the band gap as 5.92 ± 0.05 eV at 300 K.

The temperature dependence of the band gap has been studied in further detail by Guo and Yoshida [39], who provide parameters for the Varshni equation,

$$\Delta E_g(T) = \frac{\alpha T^2}{\beta + T}, \tag{1}$$

and the Bose–Einstein expression,

$$\Delta E_g(T) = \frac{2a_B}{\exp\left(\frac{\Theta}{T}\right) - 1}, \tag{2}$$

over the temperature range 0–300 K as follows: $\alpha = 1.799$ (meV/K) and $\beta = 1462$ K in Eq. (1), and $a_B = 471$ (meV) and $\Theta = 725$ K in Eq. (2).

Yamashita *et al.* [30] prepared epitaxial thin films and obtained spectra for both **(E⊥a)** and **(E∥a).** Ideally, the **(E⊥c)** and **(E∥c)** response would have been compared, however by comparing the ordinary response from **(E⊥a)** with a mixed ordinary–extraordinary response from **(E∥a),** they were able to determine the birefringence of AlN reporting a Δn of order 10^{-2} at about 5 eV, which they attribute to dichroism in the 7- to 8-eV region. They found a direct gap of 6.2 eV but suggested that the Γ_{1v}–Γ_{1c} transition for **(E⊥c)** occurs at lower energy than the Γ_{6v}–Γ_{1c} transition for **(E∥c)** due to crystal-field splitting. Lin *et al.* [40] have studied second-order optical nonlinearity of AlN thin films as a function of incidence angle at a single wavelength (1.06 μm) and have found the effect to be several times larger than that observed in KTP or quartz. Slack [41] reports an index value of 2.2 at 0.589 μm averaged over all directions, and an anisotropy of the index of about 2.3%.

VACUUM ULTRAVIOLET RANGE III

The onset of interband transitions occurs in the UV at approximately 6.1 eV or 0.2 μm. Optical properties in the vacuum UV have been reported by several investigators. Michailin *et al.* [42] employed synchrotron radiation and provide reflectance results between 6 and 40 eV, as well as luminescence. They report features in the reflectance at 7.8 and 8.6 eV.

Jones *et al.* [43] have measured the complex index of refraction below the fundamental absorption edge by ellipsometry, and then used these data in combination with VUV reflectance data of Loughin *et al.* [44] to determine n and k. The ellipsometric data were obtained from a thin-film sample prepared by reactive sputtering, whereas the VUV reflectance data were obtained from a single-crystal specimen prepared by Slack and McNelly [3, 4] and polished non aqueously to avoid oxidation.

The VUV energy range has also been studied by electron-energy-loss spectroscopy [45, 46], although in most cases these results are consistent with those for oxidized material [47].

IV UV/VISIBLE RANGE

Demiryont *et al.* [48] measured thin-film samples of AlN and obtained values for both n and k in this region. Geidur and Yaskov [49] have reported a model for the dispersion of the refractive index of AlN based on experimental data of Roskovcová *et al.* [50]. Optical properties have also been reported by Legrand *et al.* [51], who present the following expression for the index of AlN thin films prepared by sputter deposition over the range of 250 to 800 nm in λ:

$$n = \left[\alpha \exp(-\frac{\lambda}{\beta})\right] + \gamma. \tag{3}$$

α is 2.09, β is 0.1319 μm, and γ varies from 1.8 to 2.5 depending on the nitrogen partial flow rate used in preparing the film. Slack [41] provides the absorption spectrum of single-crystal AlN with less than 340 ppm oxygen over the range 0.25 μm to 10^4 μm.

V INFRARED RANGE

Carlone *et al.* [52] have reported on infrared optical absorption due to phonons, which they used for comparison with Raman-spectroscopy results. Although their IR absorption spectra were not presented quantitatively, they indicate that for **(E⊥c),** strong absorption occurs between 800 and 610 cm^{-1}, and they identify these wave numbers as associated with the E_1(LO) and E_1(TO) modes, respectively. McNeil *et al.* [53] present more recent work on the vibration spectrum of this material obtained with specimens from the single crystals grown by Slack and McNelly [3, 4]. Lewis [54] presents transmission data for AlN thin films between 3 and 15 μm, but these are difficult to interpret because of absorption bands due to ammonium chloride in the films. IR spectra are also given by Li *et al.* [55], but no scale is given for their absorption results. Once again, the work of Slack [41] is considered to be most representative of oxygen-free material.

VI TABLE AND FIGURES

Table I summarizes the available data on the complex index of refraction, $n + ik$, over the wavelength range of λ = 0.0289 μm (42 eV) to 9440 μm (0.00013 eV). These data are presented graphically in Fig. 1, which shows

the real part of the index, n, and Fig. 2, which shows the imaginary part, k, also referred to as the extinction coefficient. The bulk of the data presented in the table are taken from five references: Demiryont *et al.* [48], Geidur and Yaskov [49], Jones *et al.* [43], Slack [41], and Zhilyakov and Kostanovskii [56].

Aside from the general information described earlier, extraordinary ray response data are not available, and the tabular data given here are for the ordinary ray response, with the exception of the polycrystalline films of either Zhilyakov and Kostanovskii [56] or Jones *et al.* [43], averaging both ordinary and extraordinary ray response. The latter data are annotated in the reference column with an "(e)," to distinguish ellipsometric measurements on thin-film samples from their analysis combining both ellipsometric and VUV measurements.

REFERENCES

1. H. Schulz and K. H. Thiemann, Crystal structure refinement of AlN and GaN. *Solid State Commun.* **23**, 815–819 (1977).
2. G. A. Slack, Nonmetallic crystals with high thermal conductivity. *J. Phys. Chem. Solids* **34**, 321–335 (1973).
3. G. A. Slack and T. F. McNelly, Growth of high purity AlN crystals. *J. Cryst. Growth.* **34**, 263–279 (1976).
4. G. A. Slack and T. F. McNelly, AlN single crystals. *J. Cryst. Growth* **42**, 560–563 (1977).
5. L. M. Sheppard, Aluminum nitride: A versatile but challenging material. *Ceram. Bull.* **69**, 1801–1812 (1990).
6. B. Hejda and K. Hauptmanová, Energy band structure of AlN. *Phys. Status Solidi* **36**, K95–K99 (1969).
7. D. Jones and A. H. Lettington, The electronic band structures of the wide band gap semiconductors GaN and AlN. *Solid State Commun.* **11**, 701–705 (1972).
8. A. Kobayashi, O. F. Sankey, S. M. Volz and J. D. Dow, Semiempirical tight-binding band structures of wurtzite semiconductors: AlN, CdS, CdSe, ZnS, and ZnO. *Phys. Rev. B* **28**, 935–945 (1983).
9. M.-Z. Huang and W.-Y. Ching, A minimal basis semi-ab initio approach to the band structures of semiconductors. *J. Phys. Chem. Solids* **46**, 977–995 (1985).
10. W.-Y. Ching and B. N. Harmon, Electronic structure of AlN. *Phys. Rev. B* **34**, 5305–5308 (1986).
11. R. V. Kasowski and F. S. Ohuchi, Electronic structure of Cu overlayers on AlN. *Phys. Rev. B* **35**, 9311–9313 (1987).
12. Y.-N. Xu and W.-Y. Ching, Electronic, optical, and structural properties of some wurtzite crystals. *Phys. Rev. B* **48**, 4335–4351 (1993).
13. E. Ruiz, S. Alvarez, and P. Alemany, Electronic structure and properties of AlN. *Phys. Rev. B* **49**, 7115–7123 (1994).
14. A. K. Solanki, A. Kashyap, T. Nautiyal, and S. Auluck, Optical properties of AlN. *Solid State Commun.* **94** 1009–1012 (1995).
15. F. S. Ohuchi, Cu-AlN interface: electronic structure and adhesion. *J. Phys. (Paris)* **49**, C5-783–789 (1988); *J. Appl. Phys.* **62**, 2286–2289 (1987).
16. F. Wooten, *"Optical Properties of Solids,"* pp. 28 and 49. Academic Press, San Diego, 1972.
17. K. H. Jack, Review: Sialons and related nitrogen ceramics. *J. Mater. Sci.* **11**, 1135–1158 (1976).

18. J. W. McCauley and N. D. Corbin, *Report Submitted to NATO Advanced Study Inst. on Nitrogen Ceramics,* (Aug 1981). see also N. D. Corbin, *The Influences of Carbon, Nitrogen, and Argon on Aluminum Oxynitride Spinel Formation.* Master's Thesis, Massachusetts Institute of Technology, Cambridge (June 1982).
19. J. H. Harris, R. A. Youngman, and R. G. Teller, On the nature of the oxygen related defect in aluminum nitride. *J. Mater. Res.* **5**, 1763–1773 (1990).
20. J. H. Harris and R. A. Youngman, Light induced defects in aluminum nitride ceramics. *J. Mater. Res.* **8**, 154–162 (1993).
21. T. J. Mroz, Jr., Aluminum nitride. *Ceram. Bull.* **70**, 849–850 (1991).
22. M. Sternitzke, Growth of oxide layers on thin aluminum nitride samples measured by electron energy loss spectroscopy. *J. Am. Ceram. Soc.* **76**, 2289–2294 (1993).
23. M. Sternitzke and G. Müller, EELS study of oxygen diffusion in aluminum nitride. *J. Am. Ceram. Soc.* **77**, 737–742 (1994).
24. A. Abid, R. Bensalem, and B. J. Sealy, The thermal stability of AlN." *J. Mater. Sci.* **21**, 1301–1304 (1986).
25. A. D. Westwood, R. A. Youngman, M. R. McCartney, A. N. Cormack, and M. R. Notis, Oxygen incorporation in aluminum nitride via extended defects: Part I. Refinement of the structural model for the planar inversion domain boundary. *J. Mater. Res.* **10**, 1270–1286 (1995); A. D. Westwood, R. A. Youngman, M. R. McCartney, A. N. Cormack, and M. R. Notis, Oxygen incorporation in aluminum nitride via extended defects: Part II. Structure of curved inversion domain boundaries and defect formation. *J. Mater. Res.* **10**, 1287–1300 (1995).
26. F. Ansart, H. Ganda, R. Saporte and J. P. Traverse, Study of the oxidation of aluminum nitride coatings at high temperature. *Thin Solid Films* **260**, 38–46 (1995).
27. S. Pacesová and L. Jastrabík, Radiative recombination at deep impurity centers in AlN : O. *Czech. J. Phys.* **B29**, 913–923 (1979).
28. M. Morita, K. Tsubouchi, and N. Mikoshiba, Optical absorption and cathodoluminescence of epitaxial aluminum nitride films. *Jpn. J. Appl. Phys.* **21**, 1102–1103 (1982).
29. G. Radhakrishnan, Properties of AlN films grown at 350 K by gas-phase excimer laser photolysis. *J. Appl. Phys.* **78**, 6000–6005 (1995).
30. H. Yamashita, K. Fukui, S. Misawa, and S. Yoshida, Optical properties of AlN epitaxial thin films in the vacuum ultraviolet region. *J. Appl. Phys.* **50**, 896–898 (1979).
31. T. L. Chu and R. W. Kelm, Jr., The preparation and properties of aluminum nitride films. *J. Electrochem. Soc.* **122**, 995–1000 (1975).
32. C.R. Aita, C. J. G. Kubiak, and F. Y. H. Shih, Optical behavior near the fundamental absorption edge of sputter-deposited microcrystalline aluminum nitride. *J. Appl. Phys.* **66**, 4360–4364 (1989).
33. R. Zarwasch, E. Rille, and H. K. Pulker, Fundamental optical absorption edge of reactively direct current magnetron sputter-deposited AlN thin films. *J. Appl. Phys.* **71**, 5275–5277 (1992).
34. G. A. Slack, private communication (1996).
35. J. C. Kaplan and R. A. Gerhardt, Effect of trace carbon on the UV-induced behavior of aluminum nitride ceramics. *J. Mater. Res.* **9**, 2209–2212 (1994).
36. P. B. Perry and R. F. Rutz, The optical absorption edge of single crystal AlN prepared by a close spaced vapor process. *Appl. Phys. Lett.* **33**, 319–321 (1978).
37. J. Bauer, L. Biste, and D. Bolze, Optical properties of aluminum nitride prepared by chemical and plasmachemical vapour deposition. *Phys. Status Solidi A* **39**, 173–181 (1977).
38. N. V. Barovskii, U. D. Kudakov, E. B. Sokolov, and V. G. Sredin, Growth and optical properties of AlN epitaxial layers. *Izv. Akad. Nauk SSSR, Neorg. Mat.* **19**, 1589–1591 (1983); *Bull. Acad. Sci USSR. Inorg. Mater.* **19,** 1406 (1983).
39. Q. Guo and A. Yoshida, Temperature dependence of band gap change in InN and AlN. *Jpn. J. Appl. Phys.* **33**, 2453–2456 (1994).

40. W. P. Lin, P. M. Lundquist, G. K. Wong, E. D. Rippert, and J. B. Ketterson, Second order optical nonlinearities of radio frequency sputter-deposited AlN thin films. *Appl. Phys. Lett.* **63**, 2875–2877 (1993).
41. G. A. Slack, "Advanced Materials for Optical Windows," General Electric Technical Information Series No. 79CRD071, under ONR contract N00014-77-C-0649, Schenectady, June 1979.
42. V. V. Michailin, V. E. Oranovskii, S. Pacesová, J. Pastrnák, and A. S. Salamatov, Optical properties of AlN single crystals in the energy region 3 to 40 eV. *Phys. Status Solidi B* **55**, K51–K53 (1973).
43. D. J. Jones, R. H. French, H. Müllejans, S. Loughin, and P. F. Garcia, Optical properties of aluminum nitride determined from vacuum ultraviolet spectroscopy and spectroscopic ellipsometry. To be published.
44. S. Loughin, R. H. French, W.-Y. Ching, Y.-N. Xu, and G. A. Slack, Electronic structure of aluminum nitride: theory and experiment. *Appl. Phys. Lett.* **63**, 1182–1184 (1993).
45. C. G. Olson, J. H. Sexton, D. W. Lynch, A. J. Bevolo, H. R. Shanks, B. N. Harmon, W.-Y. Ching, and D. M. Wieliczka, Photoelectron and electron energy loss spectra of epitaxial aluminum nitride. *Solid State Commun.* **56**, 35–37 (1985).
46. M. Gautier, J. P. Duraud, and C. LeGressus, Electronic structure of an AlN film produced by ion implantation studied by electron spectroscopy. *J. Appl. Phys.* **61**, 574–580 (1987).
47. A. D. Dorneich, R. H. French, H. Müllejans, S. Loughin, and M. Rühle, Quantitative analysis of valence electron energy-loss spectra of aluminum nitride. J. Microsc. to be published.
48. H. Demiryont, L.R. Thompson, and G.J. Collins, Optical properties of aluminum oxinitrides deposited by laser-assisted CVD. *Appl. Opt.* **25**, 1311–1318 (1986).
49. S. A. Geidur and A. D. Yaskov, Dispersion of refractive index and photoelastic effect in semiconductors with a wurtzite structure. *Opt. Spectrosc.* **48**, 618–622 (1980).
50. L. Roskovcová, J. Pastrnák and R. Babusková, The dispersion of the refractive index and the birefringence of AlN. *Phys. Status Solidi* **20**, K29 (1967); J. Pastrnák and L. Roskovcová, Refraction index measurements on AlN single crystal. *Phys. Status Solidi* **14**, K5 (1966).
51. P. B. Legrand, M. Wautelet, B. Dugnoille, J. P. Dauchot and M. Hecq, Optical properties of sputter-deposited aluminum nitride films on silicon. *Thin Solid Films* **248**, 220–223 (1994).
52. C. Carlone, K. M. Lakin, and H. R. Shanks, Optical phonons of aluminum nitride. *J. Appl. Phys.*, **55**, 4010–4014 (1984).
53. L. E. McNeil, M. Grimsditch, and R. H. French, Vibrational spectroscopy of aluminum nitride. *J. Am. Ceram. Soc.* **76**, 1132–1136, (1993).
54. D. W. Lewis, Properties of aluminum nitride derived from $AlCl_3 \cdot NH_3$. *J. Electrochem. Soc.* **117**, 978–982 (1970).
55. Li Xinjiao, Xu Zechuan, He Ziyou, Cao Huazhe, Su Wuda, Chen Zhongcai, Zhou Feng, and Wang Enguang, On the properties of AlN thin films grown by low temperature reactive R. F. sputtering. *Thin Solid Films* **139**, 261–274 (1986).
56. P. A. Zhilyakov and A. V. Kostanovskii, Optical properties of thin films of aluminum nitride. *Teplofiz. Vys. Temp.* **30**, 290–293 (1992).

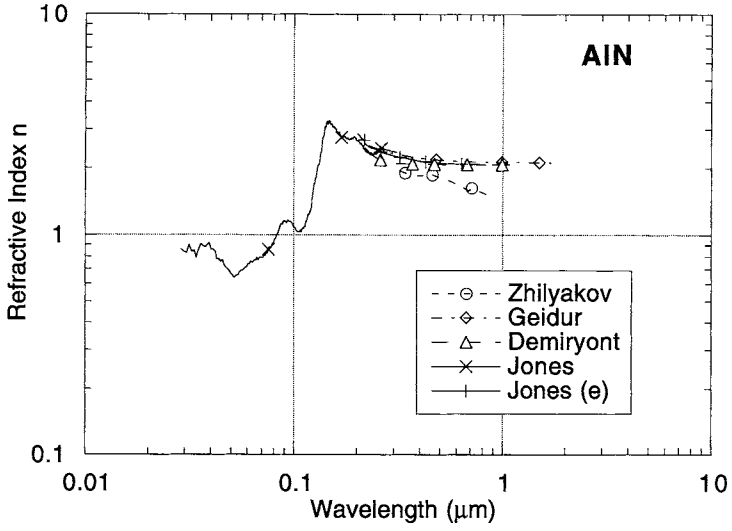

Fig. 1. Log–log plot of n (from Table I) versus wavelength in micrometers for aluminum nitride.

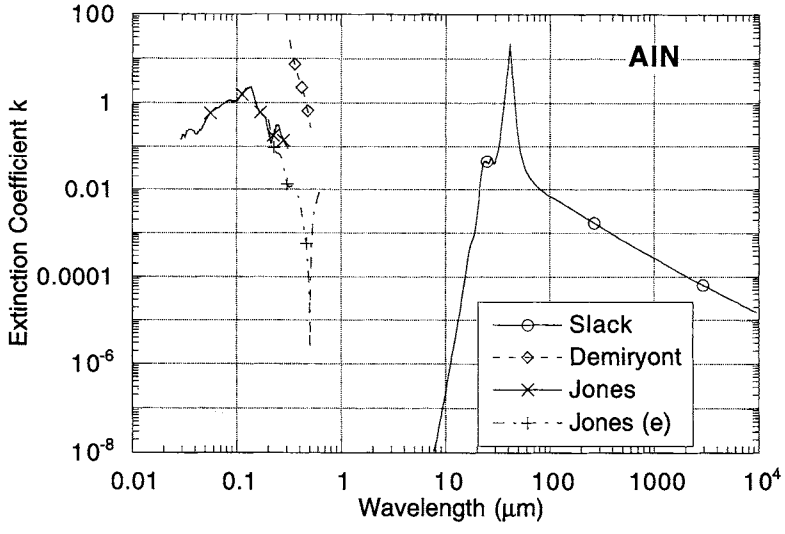

Fig. 2. Log–log plot of k (from Table I) versus wavelength in micrometers for aluminum nitride.

TABLE I

Values of n and k for Aluminum Nitride Obtained from Various References[a]

eV	cm^{-1}	μm	n	k
42.97	346581.	0.0289	0.856 [43]	0.148 [43]
41.70	336312.	0.0297	0.836	0.155
40.50	326634.	0.0306	0.830	0.189
39.36	317498.	0.0315	0.896	0.176
38.29	308858.	0.0324	0.837	0.160
37.28	300677.	0.0333	0.851	0.228
36.32	292917.	0.0341	0.790	0.235
35.40	285548.	0.0350	0.861	0.254
34.53	278541.	0.0359	0.910	0.255
33.71	271870.	0.0368	0.885	0.249
32.92	265510.	0.0377	0.879	0.242
32.17	259441.	0.0385	0.905	0.229
31.45	253644.	0.0394	0.918	0.231
30.76	248100.	0.0403	0.864	0.195
30.10	242793.	0.0412	0.864	0.195
29.47	237708.	0.0421	0.842	0.195
28.87	232832.	0.0429	0.784	0.224
28.29	228152.	0.0438	0.780	0.233
27.73	223656.	0.0447	0.764	0.252
27.19	219335.	0.0456	0.767	0.233
26.68	215177.	0.0465	0.730	0.256
26.18	211169.	0.0474	0.715	0.280
25.70	207312.	0.0482	0.700	0.310
25.24	203594.	0.0491	0.690	0.322
24.80	200006.	0.0500	0.667	0.365
24.37	196543.	0.0509	0.661	0.397
23.95	193198.	0.0518	0.639	0.444
23.55	189964.	0.0526	0.651	0.447
23.17	186837.	0.0535	0.657	0.491
22.79	183812.	0.0544	0.656	0.521
22.43	180882.	0.0553	0.683	0.559
22.07	178045.	0.0562	0.688	0.580
21.73	175295.	0.0570	0.687	0.588
21.40	172629.	0.0579	0.698	0.623
21.08	170043.	0.0588	0.713	0.654
20.77	167533.	0.0597	0.721	0.652
20.47	165097.	0.0606	0.738	0.670
20.18	162730.	0.0615	0.741	0.672
19.89	160430.	0.0623	0.756	0.694
19.61	158194.	0.0632	0.749	0.709
19.34	156019.	0.0641	0.757	0.741
19.08	153904.	0.0650	0.767	0.743
18.83	151845.	0.0659	0.769	0.766
18.58	149840.	0.0667	0.787	0.754
18.34	147888.	0.0676	0.770	0.782

(continued)

[a] The references from which the values were taken are given in brackets.

TABLE I *(Continued)*

Aluminum Nitride

eV	cm^{-1}	μm	n	k
18.10	145986.	0.0685	0.790	0.815
17.87	144132.	0.0694	0.788	0.799
17.65	142325.	0.0703	0.793	0.837
17.43	140563.	0.0711	0.793	0.859
17.21	138843.	0.0720	0.808	0.895
17.01	137165.	0.0729	0.811	0.911
16.80	135528.	0.0738	0.831	0.936
16.61	133928.	0.0747	0.833	0.956
16.41	132367.	0.0755	0.859	0.979
16.22	130841.	0.0764	0.878	0.980
16.04	129350.	0.0773	0.873	0.978
15.86	127892.	0.0782	0.892	1.022
15.68	126467.	0.0791	0.919	1.028
15.51	125074.	0.0800	0.920	1.070
15.34	123711.	0.0808	0.947	1.059
15.17	122377.	0.0817	0.961	1.109
15.01	121072.	0.0826	0.992	1.086
14.85	119792.	0.0835	1.005	1.121
14.70	118541.	0.0844	1.033	1.112
14.55	117316.	0.0852	1.057	1.123
14.40	116116.	0.0861	1.104	1.184
14.25	114940.	0.0870	1.122	1.102
14.11	113788.	0.0879	1.114	1.087
13.97	112658.	0.0888	1.144	1.149
13.83	111551.	0.0896	1.160	1.099
13.70	110466.	0.0905	1.150	1.082
13.56	109401.	0.0914	1.149	1.091
13.43	108357.	0.0923	1.133	1.063
13.31	107332.	0.0932	1.151	1.084
13.18	106327.	0.0940	1.162	1.100
13.06	105340.	0.0949	1.147	1.078
12.94	104371.	0.0958	1.146	1.084
12.82	103420.	0.0967	1.153	1.096
12.71	102486.	0.0976	1.129	1.064
12.59	101569.	0.0985	1.123	1.095
12.48	100668.	0.0993	1.104	1.073
12.37	99789.5	0.1002	1.082	1.103
12.26	98920.8	0.1011	1.081	1.141
12.16	98067.1	0.1020	1.061	1.130
12.05	97228.0	0.1029	1.043	1.177
11.95	96393.9	0.1037	1.039	1.211
11.85	95583.1	0.1046	1.032	1.229
11.75	94785.8	0.1055	1.025	1.276
11.65	94001.7	0.1064	1.031	1.321
11.56	93230.5	0.1073	1.046	1.346
11.47	92471.8	0.1081	1.030	1.365
11.37	91725.4	0.1090	1.060	1.435

TABLE I *(Continued)*

Aluminum Nitride

eV	cm^{-1}	μm	n	k
11.28	90990.9	0.1099	1.071	1.449
11.19	90268.1	0.1108	1.070	1.485
11.10	89556.7	0.1117	1.082	1.511
11.02	88848.6	0.1126	1.090	1.557
10.93	88159.3	0.1134	1.102	1.616
10.85	87480.6	0.1143	1.139	1.660
10.76	86812.3	0.1152	1.155	1.700
10.68	86154.1	0.1161	1.184	1.738
10.60	85505.8	0.1170	1.230	1.774
10.52	84867.2	0.1178	1.232	1.760
10.44	84238.1	0.1187	1.248	1.852
10.37	83618.2	0.1196	1.280	1.883
10.29	83007.4	0.1205	1.294	1.932
10.22	82398.7	0.1214	1.332	2.033
10.14	81805.5	0.1222	1.436	2.137
10.07	81220.8	0.1231	1.532	2.142
10.00	80644.4	0.1240	1.614	2.151
9.928	80076.1	0.1249	1.698	2.159
9.859	79515.8	0.1258	1.704	2.086
9.790	78963.2	0.1266	1.783	2.181
9.723	78418.3	0.1275	1.823	2.148
9.656	77880.9	0.1284	1.881	2.171
9.590	77344.8	0.1293	1.955	2.196
9.525	76821.9	0.1302	2.025	2.191
9.461	76306.0	0.1311	2.061	2.159
9.398	75797.0	0.1319	2.071	2.151
9.335	75294.8	0.1328	2.125	2.209
9.274	74799.2	0.1337	2.240	2.279
9.213	74310.1	0.1346	2.329	2.273
9.153	73827.3	0.1355	2.392	2.264
9.094	73350.7	0.1363	2.551	2.317
9.036	72880.3	0.1372	2.724	2.295
8.978	72410.6	0.1381	2.784	2.174
8.921	71952.1	0.1390	2.800	2.104
8.865	71499.4	0.1399	2.973	2.106
8.809	71052.3	0.1407	3.082	1.999
8.755	70610.8	0.1416	3.059	1.870
8.701	70174.8	0.1425	3.102	1.809
8.647	69744.1	0.1434	3.220	1.739
8.594	69318.6	0.1443	3.247	1.614
8.542	68898.3	0.1451	3.175	1.511
8.491	68483.1	0.1460	3.183	1.473
8.439	68068.2	0.1469	3.282	1.412
8.389	67662.9	0.1478	3.288	1.301
8.340	67262.4	0.1487	3.240	1.213
8.290	66866.6	0.1496	3.171	1.153

(continued)

TABLE I *(Continued)*

Aluminum Nitride

eV	cm^{-1}	μm	n	k
8.242	66475.5	0.1504	3.140	1.118
8.194	66088.9	0.1513	3.179	1.064
8.147	65706.7	0.1522	3.175	0.998
8.100	65329.0	0.1531	3.073	0.967
8.054	64955.5	0.1540	3.069	0.952
8.008	64586.4	0.1548	3.067	0.919
7.962	64217.2	0.1557	3.080	0.884
7.917	63856.4	0.1566	3.057	0.837
7.873	63499.5	0.1575	3.021	0.811
7.829	63146.7	0.1584	3.021	0.772
7.786	62797.7	0.1592	2.997	0.741
7.743	62452.6	0.1601	2.961	0.721
7.701	62111.2	0.1610	2.923	0.708
7.659	61773.6	0.1619	2.922	0.695
7.618	61439.6	0.1628	2.890	0.685
7.576	61105.4	0.1637	2.891	0.667
7.536	60778.6	0.1645	2.920	0.637
7.496	60455.3	0.1654	2.880	0.606
7.456	60135.3	0.1663	2.831	0.600
7.417	59818.8	0.1672	2.796	0.598
7.378	59505.5	0.1681	2.786	0.597
7.339	59195.6	0.1689	2.754	0.610
7.301	58888.8	0.1698	2.755	0.617
7.264	58585.2	0.1707	2.761	0.603
7.226	58284.7	0.1716	2.808	0.592
7.189	57983.9	0.1725	2.756	0.589
7.153	57689.5	0.1733	2.773	0.574
7.117	57398.1	0.1742	2.767	0.563
7.081	57109.7	0.1751	2.770	0.551
7.045	56824.1	0.1760	2.767	0.527
7.010	56541.4	0.1769	2.743	0.531
6.976	56261.4	0.1777	2.717	0.531
6.941	55984.2	0.1786	2.724	0.527
6.907	55709.8	0.1795	2.743	0.511
6.873	55438.0	0.1804	2.736	0.499
6.840	55165.8	0.1813	2.721	0.492
6.807	54899.3	0.1822	2.703	0.492
6.774	54635.3	0.1830	2.697	0.490
6.742	54373.9	0.1839	2.688	0.499
6.709	54115.0	0.1848	2.687	0.497
6.678	53858.5	0.1857	2.725	0.477
6.646	53604.4	0.1866	2.715	0.482
6.615	53352.7	0.1874	2.705	0.471
6.584	53103.4	0.1883	2.723	0.465
6.553	52856.4	0.1892	2.735	0.444
6.523	52608.9	0.1901	2.739	0.439
6.493	52366.5	0.1910	2.724	0.428

TABLE I *(Continued)*

Aluminum Nitride

eV	cm^{-1}	μm	n	k
6.463	52126.3	0.1918	2.745	0.413
6.433	51888.3	0.1927	2.745	0.401
6.404	51652.4	0.1936	2.767	0.367
6.375	51418.7	0.1945	2.775	0.340
6.346	51187.1	0.1954	2.767	0.312
6.318	50957.5	0.1962	2.739	0.307
6.290	50730.0	0.1971	2.728	0.280
6.262	50502.0	0.1980	2.730	0.258
6.234	50278.6	0.1989	2.702	0.258
6.206	50057.1	0.1998	2.670	0.258
6.179	49837.6	0.2007	2.663	0.250
6.152	49619.9	0.2015	2.665	0.244
6.150	49602.7	0.2016	2.858 (e)	0.413 (e)
6.125	49404.2	0.2024	2.653	0.235
6.100	49199.4	0.2033	2.836 (e)	0.383 (e)
6.099	49190.3	0.2033	2.667	0.204
6.073	48978.3	0.2042	2.647	0.213
6.050	48796.2	0.2049	2.823 (e)	0.351 (e)
6.047	48768.1	0.2051	2.634	0.185
6.021	48559.7	0.2059	2.634	0.170
6.000	48392.9	0.2066	2.807 (e)	0.322 (e)
5.995	48350.8	0.2068	2.608	0.177
5.969	48145.9	0.2077	2.570	0.188
5.950	47989.6	0.2084	2.765 (e)	0.298 (e)
5.944	47942.8	0.2086	2.569	0.177
5.919	47741.4	0.2095	2.586	0.151
5.900	47586.3	0.2101	2.736 (e)	0.243 (e)
5.894	47541.6	0.2103	2.580	0.144
5.870	47343.6	0.2112	2.557	0.139
5.850	47183.1	0.2119	2.709 (e)	0.216 (e)
5.846	47147.1	0.2121	2.538	0.130
5.821	46952.3	0.2130	2.532	0.117
5.800	46779.8	0.2138	2.712 (e)	0.195 (e)
5.797	46759.1	0.2139	2.512	0.116
5.774	46567.5	0.2147	2.479	0.134
5.750	46376.5	0.2156	2.688 (e)	0.135 (e)
5.750	46375.3	0.2156	2.460	0.133
5.726	46186.8	0.2165	2.455	0.122
5.703	45999.8	0.2174	2.463	0.117
5.700	45973.2	0.2175	2.680 (e)	0.121 (e)
5.680	45814.4	0.2183	2.420	0.139
5.657	45630.4	0.2192	2.396	0.154
5.650	45570.0	0.2194	2.586 (e)	0.123 (e)
5.636	45454.1	0.22	2.463 [48]	
5.635	45447.9	0.2200	2.386 [43]	0.163 [43]
5.612	45266.9	0.2209	2.381	0.166

(continued)

TABLE I *(Continued)*

Aluminum Nitride

eV	cm^{-1}	μm	n	k
5.600	45166.7	0.2214	2.567 (e)	0.115 (e)
5.590	45087.3	0.2218	2.391	0.161
5.568	44909.1	0.2227	2.379	0.174
5.550	44763.4	0.2234	2.533 (e)	0.108 (e)
5.546	44732.3	0.2236	2.359	0.191
5.524	44554.9	0.2244	2.360	0.177
5.503	44380.9	0.2253	2.368	0.181
5.500	44360.1	0.2254	2.521 (e)	0.101 (e)
5.481	44208.2	0.2262	2.364	0.189
5.460	44036.9	0.2271	2.338	0.198
5.450	43956.9	0.2275	2.498 (e)	0.095 (e)
5.439	43866.9	0.2280	2.342	0.196
5.418	43698.2	0.2288	2.340	0.200
5.400	43553.6	0.2296	2.491 (e)	0.090 (e)
5.397	43530.8	0.2297	2.331	0.210
5.391	43477.8	0.23	2.348 [48]	
5.391	43429.3	0.230	2.523 [49]	
5.377	43364.7	0.2306	2.315 [43]	0.225 [43]
5.356	43199.9	0.2315	2.305	0.240
5.350	43150.3	0.2317	2.481 (e)	0.084 (e)
5.336	43036.3	0.2324	2.299	0.254
5.315	42872.0	0.2333	2.312	0.250
5.300	42747.0	0.2339	2.471 (e)	0.080 (e)
5.296	42710.9	0.2341	2.331	0.243
5.276	42551.0	0.2350	2.352	0.234
5.256	42392.2	0.2359	2.337	0.243
5.250	42343.8	0.2362	2.463 (e)	0.077 (e)
5.236	42234.7	0.2368	2.320	0.253
5.217	42078.3	0.2377	2.304	0.263
5.200	41940.5	0.2384	2.455 (e)	0.073 (e)
5.198	41923.0	0.2385	2.291	0.285
5.179	41769.0	0.2394	2.284	0.303
5.166	41666.3	0.24	2.272 [48]	
5.166	41619.8	0.240	2.485 [49]	
5.160	41616.0	0.2403	2.289 [43]	0.310 [43]
5.150	41537.2	0.2407	2.448 (e)	0.072 (e)
5.141	41462.4	0.2412	2.313	0.308
5.122	41311.7	0.2421	2.344	0.305
5.103	41162.0	0.2429	2.352	0.308
5.100	41133.9	0.2431	2.441 (e)	0.069 (e)
5.085	41013.5	0.2438	2.357	0.308
5.067	40866.0	0.2447	2.358	0.305
5.050	40730.7	0.2455	2.436 (e)	0.070 (e)
5.049	40719.5	0.2456	2.362	0.309
5.031	40574.1	0.2465	2.367	0.313
5.013	40429.8	0.2473	2.367	0.313
5.000	40327.4	0.2480	2.425 (e)	0.070 (e)

TABLE I *(Continued)*

Aluminum Nitride

eV	cm^{-1}	μm	n	k
4.995	40286.5	0.2482	2.374	0.310
4.977	40144.1	0.2491	2.394	0.301
4.960	40001.2	0.2500	2.402	0.299
4.959	39999.6	0.25	2.221 [48]	
4.959	39955.0	0.250	2.447 [49]	
4.950	39924.1	0.2505	2.413 [43]	0.070 [43]
4.942	39860.9	0.2509	2.403	0.300
4.925	39721.6	0.2518	2.400	0.302
4.908	39583.2	0.2526	2.398	0.304
4.900	39520.9	0.2530	2.402 (e)	0.068 (e)
4.891	39445.8	0.2535	2.400	0.306
4.874	39309.3	0.2544	2.410	0.301
4.857	39173.8	0.2553	2.433	0.285
4.850	39117.6	0.2556	2.391 (e)	0.065 (e)
4.840	39039.3	0.2562	2.447	0.278
4.824	38905.6	0.2570	2.451	0.279
4.807	38772.8	0.2579	2.451	0.271
4.800	38714.3	0.2583	2.381 (e)	0.065 (e)
4.791	38639.5	0.2588	2.449	0.258
4.774	38508.6	0.2597	2.458	0.252
4.769	38461.2	0.26	2.180 [48]	
4.769	38418.3	0.260	2.416 [49]	
4.758	38378.5	0.2606	2.468 [43]	0.247 [43]
4.750	38311.0	0.2610	2.372 (e)	0.063 (e)
4.742	38249.3	0.2614	2.465	0.237
4.726	38121.0	0.2623	2.462	0.227
4.711	37993.6	0.2632	2.468	0.219
4.700	37907.8	0.2638	2.362 (e)	0.060 (e)
4.695	37867.0	0.2641	2.472	0.211
4.679	37741.2	0.2650	2.465	0.205
4.664	37616.3	0.2658	2.459	0.199
4.650	37504.5	0.2666	2.352 (e)	0.056 (e)
4.648	37490.7	0.2667	2.460	0.192
4.633	37367.5	0.2676	2.459	0.186
4.618	37245.0	0.2685	2.452	0.185
4.603	37123.3	0.2694	2.445	0.183
4.600	37101.2	0.2695	2.343 (e)	0.052 (e)
4.592	37036.7	0.27	2.146 [48]	
4.592	36995.4	0.270	2.389 [49]	
4.588	37002.4	0.2703	2.443 [43]	0.178 [43]
4.573	36882.3	0.2711	2.441	0.173
4.558	36763.0	0.2720	2.439	0.171
4.550	36697.9	0.2725	2.335 (e)	0.047 (e)
4.543	36644.5	0.2729	2.436	0.169
4.529	36526.7	0.2738	2.434	0.165
4.514	36409.6	0.2747	2.432	0.162

(continued)

TABLE I *(Continued)*

Aluminum Nitride

eV	cm^{-1}	μm	n	k
4.500	36294.7	0.2755	2.327 (e)	0.042 (e)
4.500	36292.0	0.2755	2.430	0.159
4.485	36176.5	0.2764	2.428	0.157
4.471	36061.7	0.2773	2.425	0.154
4.457	35947.6	0.2782	2.423	0.151
4.450	35891.4	0.2786	2.320 (e)	0.037 (e)
4.443	35834.2	0.2791	2.421	0.148
4.429	35721.6	0.2799	2.419	0.146
4.428	35713.9	0.28	2.127 [48]	
4.428	35674.1	0.280	2.366 [49]	
4.415	35609.7	0.2808	2.417 [43]	0.143 [43]
4.401	35498.4	0.2817	2.415	0.141
4.400	35488.1	0.2818	2.312 (e)	0.033 (e)
4.388	35387.9	0.2826	2.413	0.138
4.374	35278.0	0.2835	2.411	0.136
4.360	35167.6	0.2844	2.409	0.134
4.350	35084.8	0.2850	2.305 (e)	0.030 (e)
4.347	35059.1	0.2852	2.407	0.132
4.333	34951.3	0.2861	2.405	0.129
4.320	34844.1	0.2870	2.403	0.127
4.307	34737.6	0.2879	2.401	0.125
4.300	34681.6	0.2883	2.297 (e)	0.025 (e)
4.294	34631.7	0.2888	2.398	0.124
4.281	34526.5	0.2896	2.396	0.122
4.275	34482.4	0.29	2.116 [48]	
4.275	34444.0	0.290	2.346 [49]	
4.268	34421.9	0.2905	2.394 [43]	0.120 [43]
4.255	34317.9	0.2914	2.392	0.119
4.250	34278.3	0.2917	2.288 (e)	0.022 (e)
4.242	34214.6	0.2923	2.389	0.117
4.229	34110.7	0.2932	2.387	0.116
4.217	34008.7	0.2940	2.385	0.115
4.204	33907.2	0.2949	2.383	0.113
4.200	33875.0	0.2952	2.281 (e)	0.019 (e)
4.191	33806.3	0.2958	2.382	0.112
4.179	33706.0	0.2967	2.380	0.111
4.167	33606.3	0.2976	2.378	0.109
4.154	33507.3	0.2984	2.376	0.108
4.150	33471.7	0.2988	2.274 (e)	0.017 (e)
4.142	33408.7	0.2993	2.375	0.107
4.133	33333.0	0.3	2.104 [48]	
4.133	33295.8	0.300	2.329 [49]	
4.130	33310.8	0.3002	2.373 [43]	0.106 [43]
4.118	33213.4	0.3011	2.371	0.105
4.106	33115.6	0.3020	2.370	0.103
4.100	33068.5	0.3024	2.268 (e)	0.015 (e)
4.094	33019.3	0.3029	2.368	0.102

TABLE I *(Continued)*

Aluminum Nitride

eV	cm^{-1}	μm	n	k
4.082	32923.7	0.3037	2.367	0.101
4.070	32828.6	0.3046	2.365	0.100
4.059	32734.0	0.3055	2.364	0.099
4.050	32665.2	0.3061	2.262 (e)	0.013 (e)
4.047	32640.0	0.3064	2.362	0.098
4.035	32546.5	0.3073	2.361	0.097
4.024	32453.5	0.3081	2.359	0.096
4.012	32361.1	0.3090	2.358	0.094
4.000	32261.9	0.3100	2.257 (e)	0.012 (e)
3.999	32257.8	0.31	2.103 [48]	
3.999	32221.8	0.310	2.314 [49]	
3.950	31858.6	0.3139	2.251 [43]	0.012
3.900	31455.4	0.3179	2.245	0.011
3.875	31249.7	0.32	2.100 [48]	26.007 [48]
3.875	31214.8	0.320	2.300 [49]	
3.875	31249.7	0.32	1.950 [56]	[56]
3.850	31052.1	0.3220	2.240 [43]	0.011 [43]
3.800	30648.8	0.3263	2.235 (e)	0.011 (e)
3.757	30302.7	0.33	2.097 [48]	16.997 [48]
3.757	30268.9	0.330	2.287 [49]	
3.750	30245.6	0.3306	2.230 [43]	0.011 [43]
3.700	29842.3	0.3351	2.224 (e)	0.012 (e)
3.650	29439.0	0.3397	2.219 (e)	0.012 (e)
3.647	29411.5	0.34	2.094 [48]	12.270 [48]
3.647	29378.7	0.340	2.275 [49]	
3.647	29411.5	0.34	1.910 [56]	[56]
3.600	29035.7	0.3444	2.214 [43]	0.012 [43]
3.550	28632.5	0.3493	2.208 (e)	0.012 (e)
3.542	28539.3	0.350	2.265 [49]	
3.542	28571.2	0.35	1.880 [56]	[56]
3.500	28229.2	0.3542	2.202 [43]	0.012 [43]
3.450	27825.9	0.3594	2.196 (e)	0.011 (e)
3.444	27777.5	0.36	2.093 [48]	7.405 [48]
3.444	27746.5	0.360	2.255 [49]	
3.400	27422.6	0.3647	2.190 [43]	0.011 [43]
3.351	27026.8	0.37	2.092 [48]	5.620 [48]
3.351	26996.6	0.370	2.246 [49]	
3.350	27019.4	0.3701	2.184 [43]	0.010 [43]
3.300	26616.1	0.3757	2.177 (e)	0.009 (e)
3.263	26315.5	0.38	2.092 [48]	4.616
3.263	26286.2	0.380	2.238 [49]	
3.250	26212.8	0.3815	2.171 [43]	0.008 [43]
3.200	25809.5	0.3875	2.166 (e)	0.007 (e)
3.179	25640.8	0.39	2.091 [48]	3.796
3.179	25612.2	0.390	2.231 [49]	
3.179	25640.8	0.39	1.850 [56]	

(continued)

TABLE I *(Continued)*

Aluminum Nitride

eV	cm^{-1}	μm	n	k
3.150	25406.3	0.3936	2.161	0.006
3.100	25003.0	0.3999	2.156 (e)	0.005 (e)
3.100	24999.8	0.4	2.090 [48]	3.024 [48]
3.100	24971.9	0.400	2.224 [49]	
3.050	24599.7	0.4065	2.151 [43]	0.005 [43]
3.024	24390.0	0.41	2.089 [48]	2.620 [48]
3.024	24362.8	0.410	2.218 [49]	
3.000	24196.4	0.4133	2.146 [43]	0.004 [43]
2.952	23809.3	0.42	2.088 [48]	2.234 [48]
2.952	23782.7	0.420	2.212 [49]	
2.952	23809.3	0.42	1.860 [56]	
2.950	23793.2	0.4203	2.142 [43]	0.003 [43]
2.900	23389.9	0.4275	2.138 (e)	0.002 (e)
2.883	23255.6	0.43	2.087 [48]	1.868 [48]
2.883	23229.6	0.430	2.206 [49]	
2.850	22986.6	0.4350	2.135 [43]	0.002 [43]
2.818	22727.1	0.44	2.086 [48]	1.587 [48]
2.818	22701.7	0.440	2.201 [49]	
2.800	22583.3	0.4428	2.131 [43]	0.001 [43]
2.755	22222.0	0.45	2.085 [48]	1.289 [48]
2.755	22197.2	0.450	2.196 [49]	
2.750	22180.1	0.4509	2.128 [43]	0.001 [43]
2.700	21776.8	0.4592	2.124 (e)	0.001 (e)
2.695	21738.9	0.46	2.085 [48]	1.047 [48]
2.695	21714.7	0.460	2.191 [49]	
2.695	21738.9	0.46	1.870 [56]	
2.650	21373.5	0.4679	2.121 [43]	0.001 [43]
2.638	21276.4	0.47	2.084 [48]	0.842 [48]
2.638	21252.7	0.470	2.187 [49]	
2.600	20970.2	0.4769	2.118 [43]	0.000 [43]
2.583	20833.1	0.48	2.084 [48]	0.664 [48]
2.583	20809.9	0.480	2.184 [49]	
2.550	20567.0	0.4862	2.115 [43]	0.000 [43]
2.530	20408.0	0.49	2.084 [48]	0.542 [48]
2.530	20385.2	0.490	2.180 [49]	
2.500	20163.7	0.4959	2.112 [43]	0.000 [43]
2.480	19999.8	0.5	2.083 [48]	0.426 [48]
2.480	19977.5	0.500	2.177 [49]	
2.450	19760.4	0.5061	2.109 [43]	0.000 [43]
2.431	19607.7	0.51	2.083 [48]	0.277 [48]
2.431	19585.8	0.510	2.174 [49]	
2.400	19357.2	0.5166	2.106 [43]	0.000 [43]
2.384	19230.6	0.52	2.082 [48]	
2.384	19209.1	0.520	2.171 [49]	
2.350	18953.9	0.5276	2.102 [43]	0.000 [43]
2.339	18846.7	0.530	2.168 [49]	
2.300	18550.6	0.5391	2.100 [43]	0.000 [43]

TABLE I *(Continued)*

Aluminum Nitride

eV	cm^{-1}	μm	n	k
2.296	18497.7	0.540	2.166 [49]	
2.267	18281.4	0.547	2.080 [48]	
2.254	18161.4	0.550	2.163 [49]	
2.254	18181.6	0.55	1.760 [56]	
2.250	18147.3	0.5510	2.098 [43]	0.000 [43]
2.214	17837.0	0.560	2.161 [49]	
2.200	17744.1	0.5636	2.096 [43]	0.000 [43]
2.175	17524.1	0.570	2.159 [49]	
2.150	17340.8	0.5767	2.095 [43]	0.000 [43]
2.141	17271.0	0.579	2.079 [48]	
2.138	17222.0	0.580	2.157 [49]	
2.101	16930.1	0.590	2.156	
2.100	16937.5	0.5904	2.094 [43]	0.000 [43]
2.066	16647.9	0.600	2.154 [49]	
2.066	16666.5	0.60	1.700 [56]	
2.050	16534.2	0.6048	2.093 [43]	0.000 [43]
2.033	16375.0	0.610	2.153 [49]	
2.029	16366.5	0.611	2.078 [48]	
2.000	16131.0	0.6199	2.092 [43]	0.000 [43]
2.000	16110.9	0.620	2.152 [49]	
1.968	15855.2	0.630	2.150	
1.950	15727.7	0.6358	2.092 [43]	0.000 [43]
1.937	15607.4	0.640	2.149 [49]	
1.928	15552.0	0.643	2.078 [48]	
1.907	15367.3	0.650	2.147 [49]	
1.900	15324.4	0.6525	2.091 [43]	0.001 [43]
1.879	15134.5	0.660	2.146 [49]	
1.851	14908.6	0.670	2.145	
1.850	14921.1	0.6702	2.090 [43]	0.002 [43]
1.837	14814.7	0.675	2.078 [48]	
1.823	14689.3	0.680	2.144 [49]	
1.800	14517.9	0.6888	2.089 [43]	0.003 [43]
1.797	14476.4	0.690	2.144 [49]	
1.797	14492.6	0.69	1.580 [56]	
1.771	14269.6	0.700	2.143 [49]	
1.751	14124.2	0.708	2.078 [48]	
1.750	14114.6	0.7085	2.087 [43]	0.004 [43]
1.746	14068.7	0.710	2.142 [49]	
1.746	14084.4	0.71	1.630 [56]	
1.722	13873.3	0.720	2.141 [49]	
1.700	13711.3	0.7293	2.085 [43]	0.005 [43]
1.698	13683.2	0.730	2.140 [49]	
1.675	13513.4	0.74	2.077 [48]	
1.675	13498.3	0.740	2.139 [49]	
1.653	13318.3	0.750	2.138	
1.650	13308.0	0.7514	2.083 [43]	0.006 [43]

(continued)

TABLE I *(Continued)*

Aluminum Nitride

eV	cm^{-1}	μm	n	k
1.631	13143.1	0.760	2.138 [49]	
1.610	12972.4	0.770	2.137	
1.606	12953.2	0.772	2.077 [48]	
1.600	12904.8	0.7749	2.081 [43]	0.007 [43]
1.590	12806.1	0.780	2.136 [49]	
1.569	12644.0	0.790	2.136	
1.550	12501.5	0.7999	2.079 [43]	0.008 [43]
1.550	12485.9	0.800	2.135 [49]	
1.542	12437.7	0.804	2.076 [48]	
1.531	12331.8	0.810	2.135 [49]	
1.512	12181.4	0.820	2.134	
1.500	12098.2	0.8266	2.076 [43]	0.010 [43]
1.494	12034.6	0.830	2.134 [49]	
1.483	11961.6	0.836	2.075 [48]	
1.476	11891.4	0.840	2.134 [49]	
1.459	11751.5	0.850	2.133	
1.442	11614.8	0.860	2.133	
1.430	11533.9	0.867	2.075 [48]	
1.425	11481.3	0.870	2.132 [49]	
1.409	11350.8	0.880	2.132	
1.393	11223.3	0.890	2.132	
1.379	11123.4	0.899	2.074 [48]	
1.378	11098.6	0.900	2.131 [49]	
1.362	10976.6	0.910	2.131	
1.348	10857.3	0.920	2.131	
1.348	10869.5	0.92	1.460 [56]	
1.333	10740.6	0.930	2.131 [49]	
1.332	10741.0	0.931	2.073 [48]	
1.319	10626.3	0.940	2.131 [49]	
1.305	10514.5	0.950	2.130	
1.292	10404.9	0.960	2.130	
1.287	10384.1	0.963	2.073 [48]	
1.278	10297.7	0.970	2.130 [49]	
1.265	10192.6	0.980	2.130	
1.252	10089.6	0.990	2.129	
1.246	10050.2	0.995	2.072 [48]	
1.240	9988.7	1.000	2.129 [49]	
1.228	9889.8	1.010	2.129	
1.216	9792.9	1.020	2.129	
1.207	9737.0	1.027	2.072 [48]	
1.204	9697.8	1.030	2.129 [49]	
1.192	9604.6	1.040	2.129	
1.181	9513.1	1.050	2.128	
1.170	9433.9	1.06	2.072 [48]	
1.170	9423.3	1.060	2.128 [49]	
1.159	9335.3	1.070	2.128	
1.148	9248.8	1.080	2.128	

TABLE I *(Continued)*

Aluminum Nitride

eV	cm^{-1}	μm	n	k
1.137	9164.0	1.090	2.128	
1.135	9157.4	1.092	2.072 [48]	
1.127	9080.7	1.100	2.127 [49]	
1.117	8998.9	1.110	2.127	
1.107	8918.5	1.120	2.127	
1.103	8896.7	1.124	2.072 [48]	
1.097	8839.6	1.130	2.127 [49]	
1.088	8762.1	1.140	2.127	
1.078	8685.9	1.150	2.127	
1.072	8643.0	1.157	2.072 [48]	
1.069	8611.0	1.160	2.126 [49]	
1.060	8537.4	1.170	2.126	
1.051	8465.0	1.180	2.126	
1.042	8393.9	1.190	2.126	
1.033	8324.0	1.200	2.126	
1.025	8255.2	1.210	2.126	
1.016	8187.5	1.220	2.125	
1.008	8120.9	1.230	2.125	
0.9999	8055.4	1.240	2.125	
0.9919	7991.0	1.250	2.125	
0.9840	7927.6	1.260	2.125	
0.9763	7865.2	1.270	2.125	
0.9686	7803.7	1.280	2.125	
0.9611	7743.2	1.290	2.125	
0.9537	7683.7	1.300	2.125	
0.9464	7625.0	1.310	2.124	
0.9393	7567.2	1.320	2.124	
0.9322	7510.3	1.330	2.124	
0.9253	7454.3	1.340	2.124	
0.9184	7399.1	1.350	2.124	
0.9116	7344.7	1.360	2.123	
0.9050	7291.1	1.370	2.123	
0.8984	7238.2	1.380	2.123	
0.8920	7186.1	1.390	2.123	
0.8856	7134.8	1.400	2.123	
0.8793	7084.2	1.410	2.123	
0.8731	7034.3	1.420	2.122	
0.8670	6985.1	1.430	2.122	
0.8610	6936.6	1.440	2.122	
0.8551	6888.8	1.450	2.122	
0.8492	6841.6	1.460	2.122	
0.8434	6795.1	1.470	2.121	
0.8377	6749.2	1.480	2.121	
0.8321	6703.9	1.490	2.121	
0.8266	6659.2	1.500	2.120	
0.8211	6615.1	1.510	2.120	

(continued)

TABLE I *(Continued)*

Aluminum Nitride

eV	cm^{-1}	μm	n	k
0.8157	6571.5	1.520	2.119	
0.8104	6528.6	1.530	2.119	
0.8051	6486.2	1.540	2.120	
0.7999	6444.4	1.550	2.119	
0.7948	6403.0	1.560	2.119	
0.7897	6362.3	1.570	2.118	
0.7847	6322.0	1.580	2.118	
0.7798	6282.2	1.590	2.117	
0.7749	6243.0	1.600	2.117	
0.7701	6204.2	1.610	2.117	
0.7653	6165.9	1.620	2.116	
0.7606	6128.1	1.630	2.116	
0.7560	6090.7	1.640	2.116	
0.7514	6053.8	1.650	2.114	
0.7469	6017.3	1.660	2.114	
0.7424	5981.3	1.670	2.114	
0.7380	5945.7	1.680	2.114	
0.7336	5910.5	1.690	2.114	
0.7293	5875.7	1.700	2.114	
0.7251	5841.4	1.710	2.114	
0.7208	5807.4	1.720	2.114	
0.7167	5773.8	1.730	2.114	
0.7126	5740.7	1.740	2.114	
0.7085	5707.9	1.750	2.114	
0.1616	1303.2	7.67		1.086E-08 [41]
0.1579	1273.5	7.85		1.271E-08
0.1543	1244.5	8.04		1.596E-08
0.1508	1216.2	8.22		2.053E-08
0.1474	1188.5	8.41		2.681E-08
0.1440	1161.4	8.61		3.638E-08
0.1407	1135.0	8.81		4.863E-08
0.1375	1109.2	9.02		6.453E-08
0.1344	1083.9	9.23		8.562E-08
0.1313	1059.3	9.44		1.120E-07
0.1283	1035.1	9.66		1.460E-07
0.1254	1011.6	9.89		1.897E-07
0.1226	988.55	10.12		2.609E-07
0.1198	966.05	10.35		3.720E-07
0.1170	944.06	10.59		5.140E-07
0.1144	922.57	10.84		6.893E-07
0.1118	901.57	11.09		9.291E-07
0.1092	881.05	11.35		1.254E-06
0.1068	860.99	11.61		1.665E-06
0.1043	841.39	11.89		2.214E-06
0.1019	822.24	12.16		2.928E-06
0.0996	803.53	12.45		3.961E-06
0.0974	785.23	12.74		5.542E-06

TABLE I *(Continued)*

Aluminum Nitride

eV	cm^{-1}	μm	n	k
0.0951	767.36	13.03		8.169E-06
0.0930	749.89	13.34		1.102E-05
0.0909	732.82	13.65		1.406E-05
0.0888	716.14	13.96		2.033E-05
0.0868	699.84	14.29		2.917E-05
0.0848	683.91	14.62		4.115E-05
0.0829	668.34	14.96		5.822E-05
0.0810	653.13	15.31		8.514E-05
0.0791	638.26	15.67		1.293E-04
0.0773	623.73	16.03		1.945E-04
0.0756	609.54	16.41		2.796E-04
0.0739	595.66	16.79		3.754E-04
0.0722	582.10	17.18		4.652E-04
0.0705	568.85	17.58		5.686E-04
0.0689	555.90	17.99		6.595E-04
0.0674	543.25	18.41		7.701E-04
0.0658	530.88	18.84		9.159E-04
0.0643	518.80	19.28		1.293E-03
0.0629	506.99	19.72		1.909E-03
0.0614	495.45	20.18		2.987E-03
0.0600	484.17	20.65		4.857E-03
0.0587	473.15	21.13		9.321E-03
0.0573	462.38	21.63		1.646E-02
0.0560	451.86	22.13		2.474E-02
0.0547	441.57	22.65		3.459E-02
0.0535	431.52	23.17		0.043
0.0523	421.70	23.71		0.045
0.0511	412.10	24.27		0.042
0.0499	402.72	24.83		0.045
0.0488	393.55	25.41		0.041
0.0477	384.59	26.00		0.040
0.0466	375.84	26.61		0.046
0.0455	367.28	27.23		0.052
0.0445	358.92	27.86		0.049
0.0435	350.75	28.51		0.044
0.0425	342.77	29.17		0.038
0.0415	334.97	29.85		0.042
0.0406	327.34	30.55		0.054
0.0397	319.89	31.26		0.064
0.0388	312.61	31.99		0.083
0.0379	305.49	32.73		0.113
0.0370	298.54	33.50		0.171
0.0362	291.74	34.28		0.277
0.0353	285.10	35.08		0.457
0.0345	278.61	35.89		0.755
0.0338	272.27	36.73		1.276

(continued)

TABLE I *(Continued)*

Aluminum Nitride

eV	cm^{-1}	μm	n	k
0.0330	266.07	37.58		2.208
0.0322	260.02	38.46		3.481
0.0315	254.10	39.36		5.366
0.0308	248.31	40.27		10.156
0.0301	242.66	41.21		21.656
0.0294	237.14	42.17		10.903
0.0287	231.74	43.15		5.243
0.0281	226.46	44.16		2.957
0.0274	221.31	45.19		1.619
0.0268	216.27	46.24		0.875
0.0262	211.35	47.32		0.484
0.0256	206.54	48.42		0.282
0.0250	201.84	49.55		0.167
0.0245	197.24	50.70		0.108
0.0239	192.75	51.88		0.078
0.0234	188.36	53.09		0.061
0.0228	184.08	54.33		0.049
0.0223	179.89	55.59		0.041
0.0218	175.79	56.89		0.034
0.0213	171.79	58.21		0.029
0.0208	167.88	59.57		0.026
0.0203	164.06	60.95		0.023
0.0199	160.32	62.37		0.021
0.0194	156.67	63.83		0.019
0.0190	153.11	65.31		1.795E-02
0.0186	149.62	66.83		1.651E-02
0.0181	146.22	68.39		1.535E-02
0.0177	142.89	69.98		1.427E-02
0.0173	139.64	71.61		1.334E-02
0.0169	136.46	73.28		1.255E-02
0.0165	133.35	74.99		1.190E-02
0.0162	130.32	76.74		1.126E-02
0.0158	127.35	78.52		1.073E-02
0.0154	124.45	80.35		1.023E-02
0.0151	121.62	82.22		9.806E-03
0.0147	118.85	84.14		9.432E-03
0.0144	116.14	86.10		8.994E-03
0.0141	113.50	88.11		8.623E-03
0.0138	110.92	90.16		8.244E-03
0.0134	108.39	92.26		7.923E-03
0.0131	105.93	94.41		7.601E-03
0.0128	103.51	96.61		7.317E-03
0.0125	101.16	98.86		7.125E-03
0.0123	98.86	101.16		6.921E-03
0.0120	96.60	103.51		6.725E-03
0.0117	94.41	105.93		6.527E-03
0.0114	92.26	108.39		6.314E-03

TABLE I *(Continued)*

Aluminum Nitride

eV	cm^{-1}	μm	n	k
0.0112	90.16	110.92		6.145E-03
0.0109	88.10	113.50		5.956E-03
0.0107	86.10	116.15		5.729E-03
0.0104	84.14	118.85		5.554E-03
0.0102	82.22	121.62		5.377E-03
0.0100	80.35	124.45		5.203E-03
0.0097	78.52	127.35		5.028E-03
0.0095	76.74	130.32		4.838E-03
0.0093	74.99	133.35		4.679E-03
0.0091	73.28	136.46		4.515E-03
0.0089	71.61	139.64		4.343E-03
0.0087	69.98	142.89		4.193E-03
0.0085	68.39	146.22		4.078E-03
0.0083	66.83	149.62		3.963E-03
0.0081	65.31	153.11		3.836E-03
0.0079	63.83	156.68		3.719E-03
0.0077	62.37	160.32		3.604E-03
0.0076	60.95	164.06		3.491E-03
0.0074	59.57	167.88		3.375E-03
0.0072	58.21	171.79		3.244E-03
0.0071	56.89	175.79		3.134E-03
0.0069	55.59	179.89		3.032E-03
6.735E-03	54.32	184.08		2.928E-03
6.582E-03	53.09	188.37		2.835E-03
6.432E-03	51.88	192.75		2.744E-03
6.286E-03	50.70	197.24		2.657E-03
6.143E-03	49.54	201.84		2.572E-03
6.003E-03	48.42	206.54		2.469E-03
5.866E-03	47.32	211.35		2.388E-03
5.733E-03	46.24	216.27		2.310E-03
5.602E-03	45.19	221.31		2.230E-03
5.475E-03	44.16	226.46		2.160E-03
5.350E-03	43.15	231.74		2.086E-03
5.228E-03	42.17	237.14		2.024E-03
5.109E-03	41.21	242.66		1.969E-03
4.993E-03	40.27	248.31		1.891E-03
4.879E-03	39.35	254.10		1.824E-03
4.768E-03	38.46	260.02		1.755E-03
4.660E-03	37.58	266.07		1.690E-03
4.554E-03	36.73	272.27		1.640E-03
4.450E-03	35.89	278.61		1.577E-03
4.349E-03	35.08	285.10		1.527E-03
4.250E-03	34.28	291.74		1.486E-03
4.153E-03	33.50	298.54		1.439E-03
4.059E-03	32.73	305.49		1.394E-03
3.966E-03	31.99	312.61		1.343E-03

(continued)

TABLE I *(Continued)*

Aluminum Nitride

eV	cm^{-1}	μm	n	k
3.876E-03	31.26	319.89		1.296E-03
3.788E-03	30.55	327.34		1.262E-03
3.701E-03	29.85	334.97		1.217E-03
3.617E-03	29.17	342.77		1.178E-03
3.535E-03	28.51	350.75		1.146E-03
3.454E-03	27.86	358.92		1.110E-03
3.376E-03	27.23	367.28		1.079E-03
3.299E-03	26.61	375.84		1.044E-03
3.224E-03	26.00	384.59		1.004E-03
3.150E-03	25.41	393.55		9.721E-04
3.079E-03	24.83	402.72		9.353E-04
3.009E-03	24.27	412.10		9.020E-04
2.940E-03	23.71	421.70		8.724E-04
2.873E-03	23.17	431.52		8.406E-04
2.808E-03	22.65	441.57		8.131E-04
2.744E-03	22.13	451.86		7.870E-04
2.681E-03	21.63	462.38		7.622E-04
2.620E-03	21.13	473.15		7.391E-04
2.561E-03	20.65	484.17		7.133E-04
2.502E-03	20.18	495.45		6.915E-04
2.446E-03	19.72	506.99		6.732E-04
2.390E-03	19.28	518.80		6.517E-04
2.335E-03	18.84	530.89		6.337E-04
2.282E-03	18.41	543.25		6.155E-04
2.230E-03	17.99	555.91		5.946E-04
2.180E-03	17.58	568.85		5.786E-04
2.130E-03	17.18	582.10		5.591E-04
2.081E-03	16.79	595.66		5.385E-04
2.034E-03	16.41	609.54		5.232E-04
1.988E-03	16.03	623.74		5.037E-04
1.943E-03	15.67	638.26		4.878E-04
1.898E-03	15.31	653.13		4.755E-04
1.855E-03	14.96	668.35		4.622E-04
1.813E-03	14.62	683.91		4.499E-04
1.772E-03	14.29	699.84		4.372E-04
1.731E-03	13.96	716.14		4.229E-04
1.692E-03	13.65	732.83		4.116E-04
1.653E-03	13.34	749.90		3.987E-04
1.616E-03	13.03	767.36		3.841E-04
1.579E-03	12.74	785.24		3.718E-04
1.543E-03	12.45	803.53		3.597E-04
1.508E-03	12.16	822.24		3.498E-04
1.474E-03	11.88	841.40		3.416E-04
1.440E-03	11.61	861.00		3.308E-04
1.407E-03	11.35	881.05		3.213E-04
1.375E-03	11.09	901.57		3.126E-04
1.344E-03	10.84	922.57		3.025E-04

TABLE I *(Continued)*

Aluminum Nitride

eV	cm^{-1}	μm	n	k
1.313E-03	10.59	944.06		2.934E-04
1.283E-03	10.35	966.05		2.843E-04
1.254E-03	10.12	988.56		2.752E-04
1.226E-03	9.89	1011.58		2.677E-04
1.198E-03	9.66	1035.14		2.604E-04
1.170E-03	9.44	1059.26		2.532E-04
1.144E-03	9.23	1083.93		2.464E-04
1.118E-03	9.02	1109.18		2.384E-04
1.092E-03	8.81	1135.01		2.303E-04
1.068E-03	8.61	1161.45		2.228E-04
1.043E-03	8.41	1188.50		2.140E-04
1.019E-03	8.22	1216.19		2.069E-04
9.963E-04	8.04	1244.52		1.996E-04
9.736E-04	7.85	1273.51		1.926E-04
9.514E-04	7.67	1303.17		1.876E-04
9.298E-04	7.50	1333.52		1.819E-04
9.086E-04	7.33	1364.59		1.766E-04
8.879E-04	7.16	1396.37		1.719E-04
8.677E-04	7.00	1428.90		1.658E-04
8.479E-04	6.84	1462.18		1.608E-04
8.286E-04	6.68	1496.24		1.564E-04
8.098E-04	6.53	1531.09		1.513E-04
7.914E-04	6.38	1566.75		1.465E-04
7.733E-04	6.24	1604.25		1.417E-04
7.557E-04	6.10	1640.59		1.369E-04
7.385E-04	5.96	1678.81		1.331E-04
7.217E-04	5.82	1717.91		1.290E-04
7.053E-04	5.69	1757.93		1.252E-04
6.892E-04	5.56	1798.88		1.217E-04
6.735E-04	5.43	1840.78		1.179E-04
6.582E-04	5.31	1883.65		1.146E-04
6.432E-04	5.19	1927.53		1.118E-04
6.286E-04	5.07	1972.43		1.082E-04
6.143E-04	4.95	2018.37		1.050E-04
6.003E-04	4.84	2065.39		1.016E-04
5.866E-04	4.73	2113.49		9.772E-05
5.733E-04	4.62	2162.72		9.459E-05
5.602E-04	4.52	2213.10		9.139E-05
5.475E-04	4.42	2264.65		8.852E-05
5.350E-04	4.32	2317.40		8.616E-05
5.228E-04	4.22	2371.38		8.368E-05
5.109E-04	4.12	2426.62		8.131E-05
4.993E-04	4.03	2483.14		7.912E-05
4.879E-04	3.94	2540.98		7.704E-05
4.768E-04	3.85	2600.17		7.483E-05
4.660E-04	3.76	2660.73		7.250E-05

(continued)

TABLE I *(Continued)*

Aluminum Nitride

eV	cm^{-1}	μm	n	k
4.554E-04	3.67	2722.71		7.020E-05
4.450E-04	3.59	2786.13		6.829E-05
4.349E-04	3.51	2851.03		6.631E-05
4.250E-04	3.43	2917.43		6.424E-05
4.153E-04	3.35	2985.39		6.280E-05
4.059E-04	3.27	3054.93		6.135E-05
3.966E-04	3.20	3126.09		5.972E-05
3.876E-04	3.13	3198.90		5.826E-05
3.788E-04	3.05	3273.42		5.658E-05
3.701E-04	2.99	3349.66		5.485E-05
3.617E-04	2.92	3427.69		5.353E-05
3.535E-04	2.85	3507.53		5.166E-05
3.454E-04	2.79	3589.23		4.983E-05
3.376E-04	2.72	3672.83		4.856E-05
3.299E-04	2.66	3758.38		4.718E-05
3.224E-04	2.60	3845.93		4.590E-05
3.150E-04	2.54	3935.51		4.467E-05
3.079E-04	2.48	4027.18		4.329E-05
3.009E-04	2.43	4120.99		4.210E-05
2.940E-04	2.37	4216.98		4.095E-05
2.873E-04	2.32	4315.20		3.967E-05
2.808E-04	2.26	4415.72		3.860E-05
2.744E-04	2.21	4518.57		3.748E-05
2.681E-04	2.16	4623.82		3.628E-05
2.620E-04	2.11	4731.53		3.537E-05
2.561E-04	2.07	4841.74		3.446E-05
2.502E-04	2.02	4954.52		3.350E-05
2.446E-04	1.97	5069.92		3.259E-05
2.390E-04	1.93	5188.01		3.157E-05
2.335E-04	1.88	5308.86		3.063E-05
2.282E-04	1.84	5432.52		2.994E-05
2.230E-04	1.80	5559.06		2.906E-05
2.180E-04	1.76	5688.55		2.821E-05
2.130E-04	1.72	5821.05		2.751E-05
2.081E-04	1.68	5956.64		2.679E-05
2.034E-04	1.64	6095.39		2.612E-05
1.988E-04	1.60	6237.37		2.540E-05
1.943E-04	1.57	6382.65		2.444E-05
1.898E-04	1.53	6531.32		2.372E-05
1.855E-04	1.50	6683.46		2.306E-05
1.813E-04	1.46	6839.14		2.233E-05
1.772E-04	1.43	6998.44		2.172E-05
1.731E-04	1.40	7161.45		2.115E-05
1.692E-04	1.36	7328.27		2.061E-05
1.653E-04	1.33	7498.96		2.016E-05
1.616E-04	1.30	7673.64		1.962E-05
1.579E-04	1.27	7852.38		1.901E-05

TABLE I *(Continued)*

Aluminum Nitride

eV	cm^{-1}	μm	n	k
1.543E-04	1.24	8035.28		1.849E-05
1.508E-04	1.22	8222.45		1.793E-05
1.474E-04	1.19	8413.98		1.738E-05
1.440E-04	1.16	8609.96		1.693E-05
1.407E-04	1.14	8810.51		1.649E-05
1.375E-04	1.11	9015.74		1.610E-05
1.344E-04	1.08	9225.74		1.573E-05
1.313E-04	1.06	9440.64		1.529E-05

Bismuth Silicon Oxide ($Bi_{12}SiO_{20}$) Bismuth Germanium Oxide ($Bi_{12}GeO_{20}$)

E. D. PALIK
Institute for Physical Science and Technology
University of Maryland
College Park, Maryland

$Bi_{12}SiO_{20}$ (BSO) and $Bi_{12}GeO_{20}$ (BGO) are cubic crystals with space group symmetry I23 T^3, containing two molecular units per unit cell. Some of the properties making these materials of technological interest include low ultrasonic velocity, small acoustic damping up to 1 GHz, and large piezoelectric, photorefractive [1], photoelastic [2], and electrooptic (nonlinear index) [3] effects.

Although being cubic results in isotropic intensity transmission and reflection properties for linearly polarized light, both crystals are gyrotropic, showing optical activity [4], the rotation of the plane of polarization of linearly polarized light being proportional to the thickness of the crystal. Thus, the angle of rotation is given by

$$\phi = \frac{\pi d}{\lambda}(n_l - n_r), \tag{1}$$

where n_l and n_r are the indices of refraction for left and right circularly polarized light, respectively. This is similar to the optical activity of "isotropic" sugar solutions, where the activity depends on the left- and right-handedness of the microscopic molecular structure, which is left- or right-handed for any direction through the solution.

Since several of the papers examined deal with both BSO and BGO, while others deal with one or the other, we will review them from high to low photon energy with no preference. We give the n and k data in Tables I and II and Figs. 1 and 2.

Futro [5] has measured the reflectivity of BGO from 1.5 to 8.5 eV in two

HANDBOOK OF OPTICAL CONSTANTS OF SOLIDS III

Copyright © 1998 by Academic Press.
All rights of reproduction in any form reserved
ISBN 0-12-544423-0/$25.00.

steps. From 1.5 to 5.5 eV, near-normal-incidence reflectivity was measured with a Zeiss SPM-2 prism monochromator and a high-pressure xenon arc. From 5.5 to 8.5 eV a vacuum UV Hilger and Watts E766 grating monochromator was used along with a low-pressure ac discharge hydrogen lamp. An Al reference mirror was used. Although the reflectivity of BSO was also measured, no analysis of it was given. The reflectivity data were Kramers–Kronig analyzed using a suitable extrapolation for reflectivity to high frequency. The data read from a small graph of n and k (which was enlarged) are collected in Table II and Fig. 2. Near the band gap, k is much too large compared to the other direct measurements of k to be discussed. This has to do with the poor accuracy of the K-K method when $k \ll 1$. Where $k > 1$, the values of n and k are probably not good to more than two significant figures, if that.

Aldrich *et al.* [6] give several properties of BSO and BGO. Their samples were grown by the Czochralski method. Different samples showed positive and negative optical activity. For BGO the loss tangent at low frequency was determined to be 0.0035, which gives a low-frequency dielectric constant $\epsilon_0 = 40$. The band gap was found to be 3.15–3.25 eV. The index of refraction was measured by the prism minimum-deviation method from 400 to 700 nm. These data have been quoted by subsequent workers [7, 8], who have fitted a Sellmeier-type equation to the data. For BSO, the loss tangent at low frequency was 0.0015, which gives a low-frequency dielectric constant $\epsilon_0 = 56$. The band gap was 3.15–3.25 eV.

The absorption in the vicinity of the band edge of BGO and BSO has been measured in detail. There are comments to the effect that the band gaps are similar [6], the indices are similar [6], the reflectivities are similar [4], etc. Grabmaier and Oberschmid [9] studied the optical absorption near the band gap with many doped single crystals of BSO and BGO. They state that undoped BGO is yellow in color and has a band gap $E_g = 3.2$ eV. They measured the transmittance and calculated the absorption coefficient, assuming the reflectivity was given by the index of refraction analyzed by Vedam and Hennessey [7]. There was an order-of-magnitude change in the absorption coefficient as the dopants were changed. Therefore, we expect values of k to vary significantly from lab to lab, especially if the samples are not well characterized. We determined k for just the undoped samples of BSO and BGO from graphs and list its values in Tables I and II and Figs. 1 and 2. The values of k for BGO are much smaller than those of Futro in the band gap, indicating poor accuracy for the K-K method used in by Futro. [5].

Toyoda *et al.* [10, 11] studied the optical properties of the band edge of BSO as a function of temperature, attempting to fit their data with an Urbach-rule equation. Two types of faceting can be obtained from the solid–liquid interface of a growing crystal. These produce facet-core-free and facet-core samples. Although the optical differences are small, the type of sample does

affect the technical properties of interest. We read expanded graphs to get k for 293 K and list values in Table I and Fig. 1. These k data compare well with data of Grabmaier and Oberschmid.

Zengfa *et al.* [12] measured the transmittance and reflectance of a BSO sample with a thickness of 1.09 mm in the spectral region 300–550 nm, using a UN-365 UV-VIS spectrometer, and determined both n and k. The analysis of Zengfa *et al.* is not clear. They give the transmittance of a slab as

$$T = \frac{(1 - R)^2 \exp(-\alpha d)}{(1 - R^2 \exp(-2\alpha d)}, \tag{2}$$

where R must be the bulk reflectivity, which is

$$R = \frac{(n - 1)^2 + k^2}{(n + 1)^2 + k^2}. \tag{3}$$

This applies to a semi-infinite sample or to one that is wedged, so there are no multiple-reflection effects. For $k/n \ll 1$, they use

$$n = \frac{(1 + \sqrt{R})}{(1 - \sqrt{R})} \tag{4}$$

to determine n; it appears they used the measured reflectance for R. However, their sample surely had multiple-reflection effects, since it was presumably plane parallel. However, bulk reflectivity should not equal sample reflectance in transparent regions. We compare the results of Zengfa *et al.* and Toyota *et al.* in Table I. Note that in the band-gap region 3.5–3.1 eV, the k values of Zenga *et al.* [10, 11] are considerably smaller than those of Toyota *et al.* and Grabmaier and Oberschmid [9].

Tropf *et al.* [13] cite work of Gospodinov *et al.* [14], who fitted n data for BSO in the spectral region 0.48–0.7 μm with a Sellmeier-type equation of the form

$$n^2 = 2.72777 + \frac{3.01705\,\lambda^2}{\lambda^2 - (0.2661)^2}. \tag{5}$$

They also give an equation for BGO of the form

$$n^2 - 1 = \frac{4.601\,\lambda^2}{\lambda^2 - (0.242)^2} \tag{6}$$

for the spectral region 0.4–0.7 μm (citing Burattini *et al.* [8] and Vedam and Hennessey [7]). Although both of these groups try to fit the data of Al-

drich *et al.* [6] for BGO, the exact form of Eq. (6) is not given in these references. However, Burattini *et al.* do fit the data of Aldrich *et al.* and their own data with a more complicated equation discussed later. We used Eq. (5) to calculate n for BSO and give the results in Table I and Fig. 1. We defer using Eq. (6) until we discuss the BGO data of Burattini *et al.* Burattini *et al.* [8] measured n and k for BGO in the spectral region 1.2–5.0 μm. The {100} plane was the plane of the slab samples. They were ground with carborundum and polished with diamond paste. Thickness was ~200 μm, so although multiple-refection effects were present, no interference fringes were resolved. The transmittance T and the reflectance R were measured with a double-beam spectrophotometer. The reflection standard was a gold mirror. The transmittance standard was a polished Si wafer. To analyze the data, they used complicated expressions relating αd to R and T and R_1 to R and T. They defined α as the absorption coefficient, d as the sample thickness, transmittance as T, reflectance as R of the slab sample (measured quantities), and single-surface reflectivity as R_1 (reflection from a semi-infinite sample or from the front surface of a wedged sample). R_1 is of the form of Eq. (3) with the change in notation noted.

A Hertzberger-type equation of the form

$$n - n_0 = \frac{a_1}{\lambda^2 - \lambda_o^2} + \frac{a_2}{(\lambda^2 - \lambda_o^2)^2} + a_3 \lambda^2 + a_4 \lambda^4 \tag{7}$$

was used to fit the data and also data of Aldrich *et al.* [6]. The fitting parameters were $\lambda_0 = 0.1675$ μm, $n_0 = 2.4098$, $a_1 = 3.26 \times 10^{-2}$ μm^2, $a_2 = 4.69 \times 10^{-3}$ μm^4, $a_3 = -6.07 \times 10^{-3}$ μm^{-2}, $a_4 = 1.15 \times 10^{-4}$ μm^{-4}. Uncertainty (or deviation of the experimental data from the calculated) was $\Delta n = 4.23 \times 10^{-4}$. No Δk was given, but surely k is not known to four significant figures. The data are given in Table II and Fig. 2. The absorption shown is multiphonon absorption, which continues to increase to lower energy until the reststrahlen region is reached.

Wojdowski *et al.* [15, 16] measured the far-infrared reflectivity of both BSO and BGO materials. The angle of incidence was 8°. The crystals were grown by the Czochralski method. Samples were unoriented, but since the crystals are cubic, this should pose no problem. The samples were mechanically polished with corundum powder and diamond paste. They used a single-pass grating spectrometer to measure R from 50 to 900 cm^{-1} both at 300 K and near-liquid-nitrogen temperature (90 K). Although they were primarily interested in the lattice-vibration frequencies and group-theory analysis of the vibration modes, they did determine ϵ_1 and ϵ_2. A K-K analysis, not described in detail (especially the end limits), was performed to obtain ϵ_1 and ϵ_2. Although graphs of ϵ_1 and ϵ_2 were not given in the papers, Nazarewicz [17] did provide us a plot of room-temperature ϵ_1 and ϵ_2, which we enlarged. After extracting ϵ_1 and ϵ_2, we calculated n and k. These are dis-

played in Tables I and II and Figs. 1 and 2. Near the absorption lines where ϵ_1 and ϵ_2 were less than unity (and hard to read from a plot), the calculated values of k often showed sharp downward dips before rising to the peaks. A classical-oscillator model does not show such structure. It is not known whether this is an artifact or a physical phenomenon. For BGO between 700 and 800 cm^{-1}, there appears to be some residual absorption probably due to the two-phonon absorption.

Wojdowski [18] also measured the transmittance of thin evaporated films of BSO and BGO, primarily to determine vibration frequencies.

Zengfa *et al.* [12] used a Fourier-transform spectrometer to measure the reflectivity of BSO in the 50–1500 cm^{-1} region. Details of sample preparation and experimental procedure are lacking; room temperature was not defined. A K-K analysis was performed to obtain ϵ_1 and ϵ_2 and n and k. The limits of integration were not clearly discussed, especially accounting for absorption (reflection) below 50 cm^{-1} and above the band gap. Zengfa *et al.* did not cite earlier work of Wojdowski *et al.* [15] and Brody *et al.* [19]. These works might have been useful in their K-K analysis.

Examination of k indicates that the apparent resolution of Zengfa *et al.* [12] was significantly less than that of Wojdowski *et al.*, [15] and more lines were observed in the spectra of Wojdowski *et al.* For example, a triplet of lines between 535 and 610 cm^{-1} are clearly resolved by Wojdowski *et al.* but only partly resolved by Zengfa *et al.*

Although we favor the data of Wojdowski *et al.* [15] because of the higher resolution, we decided to show the n and k data of Zengfa *et al.* and Wojdowski *et al.* in Table I to compare the results for BSO. There is serious mismatch in frequencies, implying that the wave number was not carefully measured by one or the other of the groups. For most of the peaks in k the Zengfa *et al.* [12] data were on the average about 5 cm^{-1} higher than the Wojdowski *et al.* [15] data. This discrepancy points out a general problem in the calibration of spectrometers and comparing spectra of significantly different resolution. Once the spectra are shifted, so the peaks in k "agree," the magnitudes of n and k are usually within $\pm 30\%$ of each other. Such differences are to be expected, because of accuracy considerations in measuring R with a Fourier-transform spectrometer and a grating specrometer; we assume the reference mirror was an aluminum mirror in both cases.

Brody *et al.* [19] used a Fourier-transform spectrometer to measure the transmittance of thin slabs in the millimeter-wave region (15–4 cm^{-1}) for both BSO and BGO samples. Room temperature was not defined. Presumably, they used at least two thicknesses of slabs and fitted the transmittance to obtain both n and k, since channel spectra were observed. We extracted values of n and k from a graph and display them in Tables I and II and Figs. 1 and 2. Note that there are no vibration bands in this region, all of them presumably being above 15 cm^{-1}. Note that the value of n at 70 cm^{-1} is smaller than the n measured at 15 cm^{-1}. There may be another vibration

band between 70 and 15 cm^{-1}, which could account for this mismatch, or the 70 cm^{-1} data are in error due to problems with the K-K analysis.

For BGO, extrapolation to low frequency gives a dc dielectric constant $\epsilon_0 = 38.6$, in close agreeement with a loss-tangent measurement of $\epsilon_o = 40$ of Aldrich *et al.* For BSO, extrapolation to low frequency gives $\epsilon_0 = 40.7$, in poor agreement with a loss-tangent measurement of $\epsilon_0 = 56$.

REFERENCES

1. A. Grunnet-Jepsen, I. Aubrecht, and L. Solynar, Investigation of the internal field in photorefractive materials and measurement of the effective electro-optic coefficient, *J. Opt. Soc. Am. B* **12**, 921 (1995).
2. P. I. Ropot, Determination of the photoelastic constant of optically active cubic crystals by a polarization method. *Opt. Spectrosc.* **70**, 217 (1991); *Opt. Spektrosk.* **70**, 371 (1991).
3. Y. V. Shaldin and D. A. Belogurov, Dispersion of the nonlinear refractive index of gyrotropic sillenite-type crystals. *Sov. Phys. Solid State* **15**, 1846 (1974).
4. P. Hennessey and K. Vedam, Piezo- and thermo-optical properties of $Bi_{12}GeO_{20}$, I. Optical rotatory dispersion. *J. Opt. Soc. Am.* **65**, 436 (1975).
5. A. T. Futro, Analysis of reflectivity spectrum and band structure of $Bi_{12}GeO_{20}$. *J. Phys. Chem. Solids* **40**, 201 (1979).
6. R. E. Aldrich, S. L. Hou, and M. L. Harvill, Electrical and optical properties of $Bi_{12}SiO_{20}$. *J. Appl. Phys.* **42**, 493 (1971).
7. K. Vedam and P. Hennessey, Piezo- and thermo-optical properties of $Bi_{12}GeO_{20}$, II. Refractive index. *J. Opt. Soc. Am.* **65**, 442 (1975).
8. E. Burattini, G. Cappuccio, M. Grandolfo, P. Vecchia, and S.M. Efendiev, Near-infrared refractive index of bismuth germanium oxide [$Bi_{12}GeO_{20}$]. *J. Opt. Soc. Am.* **73**, 495 (1983).
9. B. C. Grabmaier and R. Oberschmid, Properties of pure and doped $Bi_{12}GeO_{20}$ and $Bi_{12}SiO_{20}$ crystals. *Phys. Status Solidi A* **96**, 199 (1986).
10. T. Toyoda, H. Nakanishi, S. Endo and T. Irie, The fitting parameters of exponential optical absorption in $Bi_{12}SiO_{20}$. *J. Phys. C: Solid State Phys.* **19**, L259 (1986).
11. T. Toyoda, S. Maruyama, H. Nakanishi, S. Endo, and T. Irie, The fundamental absorption edge in $Bi_{12}SiO_{20}$, *J. Phys. D: Appl. Phys.* **19**, 909 (1986).
12. L. Zengfa, S. Dazhao, Y. Xiaoyan, S. Sufa, and Z. Wanlin, Study of the optical properties of $Bi_{12}SiO_{20}$. *Infrared Phys.* **31**, 59 (1991).
13. W. J. Tropf, M. E. Thomas, and T. J. Harris, Properties of crystals and glasses. *In* "Handbook of Optics, Devices, Measurements & Properties" (M. Bass, ed.), Vol. 2, Chap. 33, McGraw-Hill, New York, 1995.
14. M. Gospodinov, S. Haussuhl, P. Sreshtarov, V. Tassev, and N. Petkov, Physical properties of cubic $Bi_{12}SiO_{20}$. *Bulg. J. Phys.* **15**, 140 (1988).
15. W. Wojdowski, T. Lukasiewicz, W. Nazarewicz, and J. Zmija, Infrared studies of lattice vibrations in $Bi_{12}GeO_{20}$ and $Bi_{12}SiO_{20}$ crystals. *Phys. Status Solidi B* **94**, 649 (1979).
16. W. Wojdowski, Vibrational modes in $Bi_{12}GeO_{20}$ and $Bi_{12}SiO_{20}$ crystals. *Phys. Status Solidi B* **130**, 121 (1985).
17. W. Nazarewicz, private communication, 1996.
18. W. Wojdowski, Infrared spectra of thin films of $Bi_{12}GeO_{20}$ and $Bi_{12}SiO_{20}$. *Phys. Status Solidi B* **123**, K101 (1984).
19. P. S. Brody, J. P. Sattler, and G. J. Simonis, Near-millimeter refractive indices, absorption coefficients, and electrooptic coefficients in ferroelectric and other crystals. *Ferroelectrics* **59**, 319 (1983).

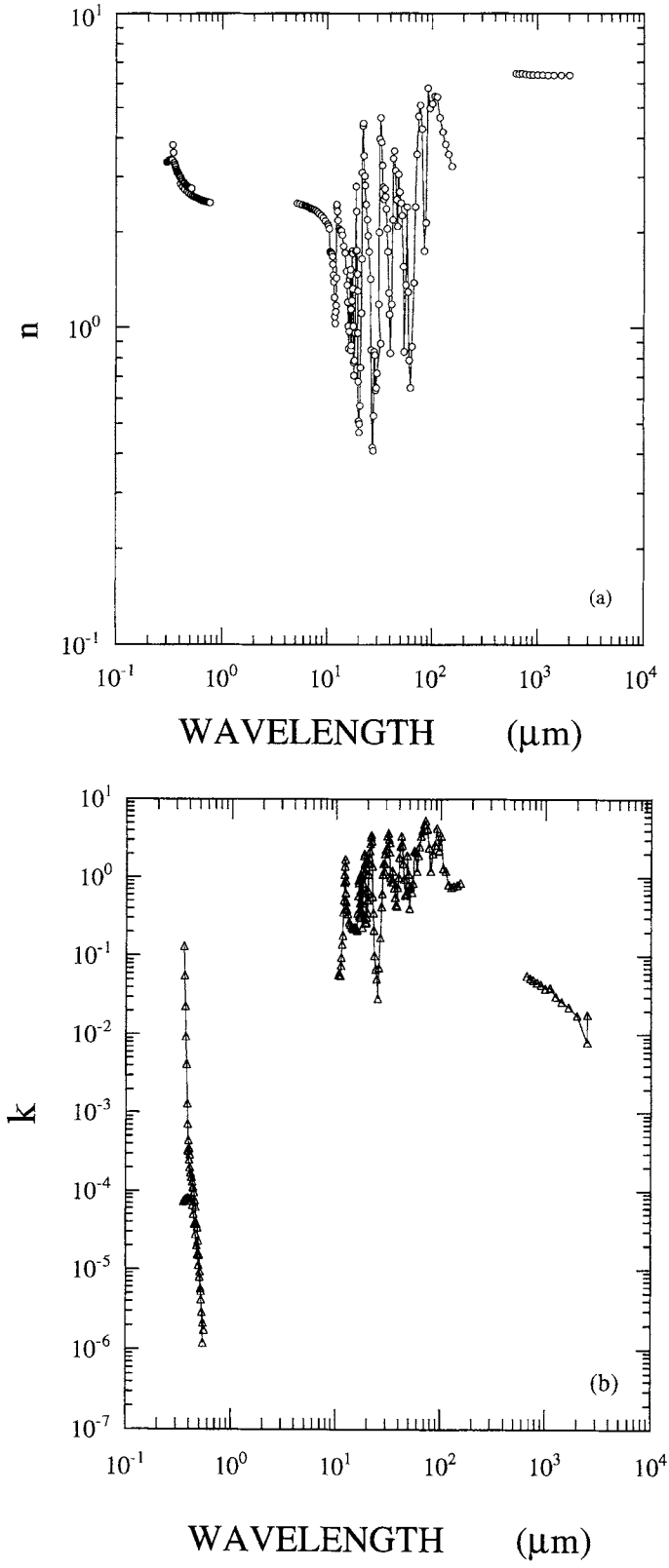

Fig. 1. (a) Log–log plot of n (○) versus wavelength in micrometers for $Bi_{12}SiO_{20}$. Some data from Toyoda *et al.* [11] and Zengfa *et al.* [12] are omitted. (b) Log–log plot of k (△) versus wavelength in micrometers for $Bi_{12}SiO_{20}$.

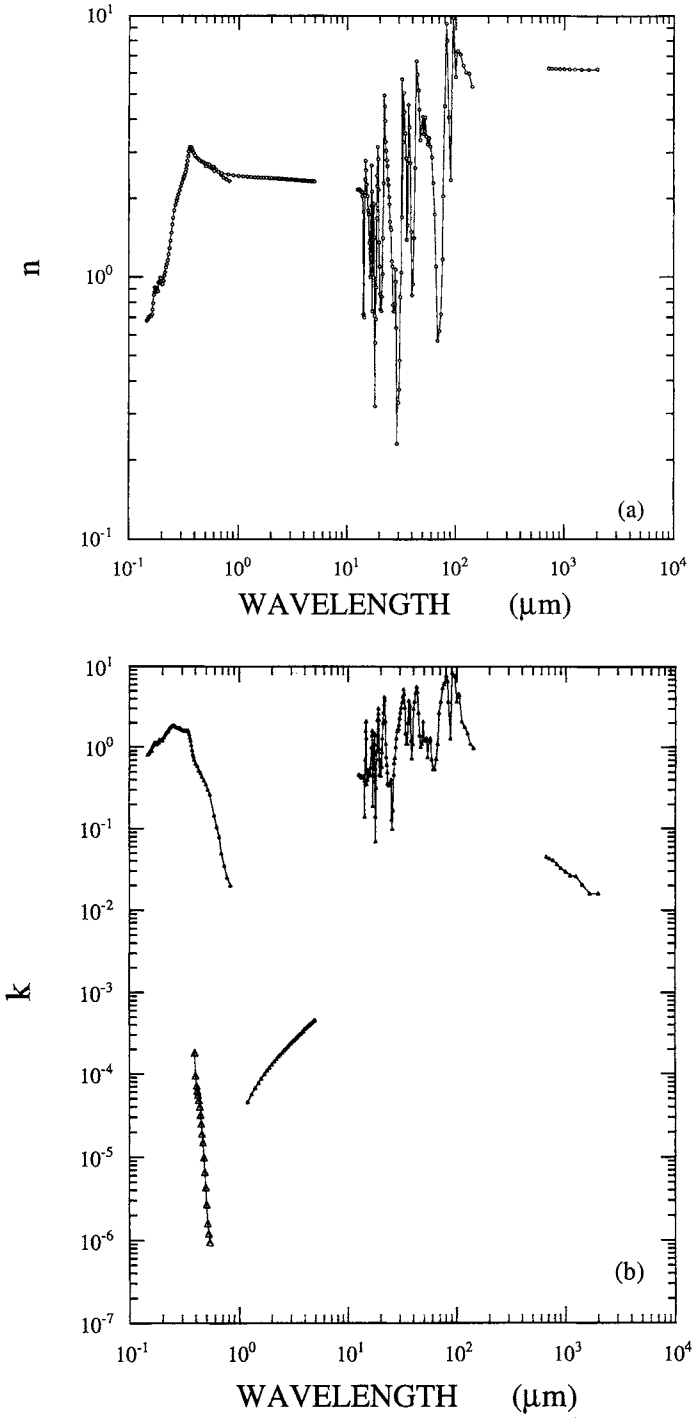

Fig. 2. (a) Log–log plot of n (○) versus wavelength in micrometers for $Bi_{12}GeO_{20}$. (b) Log–log plot of k (▲) versus wavelength in micrometers for $Bi_{12}GeO_{20}$.

TABLE I

Values of n and k for $Bi_{12}SiO_{20}$ from Various References[a]

eV	cm^{-1}	μm	n	k	n	k	k
4.133	33333	0.30	3.341[12]				
4.065	32787	0.305	3.360				
4.000	32258	0.31	3.379				
3.936	31746	0.315	3.394				
3.875	31250	0.32	3.404				
3.815	30769	0.325	3.410				
3.757	30303	0.33	3.410				
3.701	29851	0.335	3.400				
3.647	29412	0.34	3.800				
3.594	28986	0.345	3.590				
3.542	28571	0.35	3.329	7.27E-5[12]			
3.493	28169	0.355	3.280				
3.440	27778	0.36	3.224	7.59E-5			
3.397	27397	0.365	3.170				
3.351	27027	0.37	3.130	7.80E-5			
3.306	26667	0.375	3.100				
3.263	26316	0.38	3.075	7.98E-5			
3.220	25974	0.385	3.050				
3.179	25641	0.39	3.024	8.04E-5			
3.139	25316	0.395	3.005				
3.100	25000	0.40	2.983	7.97E-5	2.853[14]		
3.024	24390	0.41	2.944	7.80E-5			
2.952	23810	0.42	2.909	7.35E-5	2.787		
2.883	23256	0.43	2.880	6.50E-5			
2.818	22727	0.44	2.850	5.00E-5	2.736		
2.755	22222	0.45	2.823	3.76E-5			
2.695	21739	0.46	2.805	2.75E-5	2.695		
2.638	21277	0.47	2.789	1.98E-5			
2.583	20833	0.48	2.777	1.53E-5	2.661		
2.530	20408	0.49	2.768	1.13E-5			
2.480	20000	0.50	2.760	7.96E-6	2.634		
2.431	19608	0.51	2.759	5.68E-6			
2.384	19231	0.52		4.14E-6	2.611		
2.296	18519	0.54		2.15E-6	2.591		
2.254	18182	0.55		1.75E-6			
2.214	17857	0.56			2.574		
2.138	17241	0.58			2.559		
2.066	16667	0.60			2.546		
2.000	16129	0.62			2.535		
1.937	15625	0.64			2.525		
1.879	15152	0.66			2.516		
1.823	14706	0.68			2.508		
1.771	14286	0.70			2.501		
1.722	13889	0.72			2.494		
1.675	13514	0.74			2.489		
1.631	13158	0.76			2.483		

(continued)

[a] The references from which the values were taken are given in brackets.

TABLE I *(Continued)*

$Bi_{12}SiO_{20}$

eV	cm^{-1}	μm	n	k	n	k	k
						fcf	fc
3.5	28229	0.3542				1.3E-1[11]	1.2E-1[11]
3.45	27826	0.3594				5.6E-2	5.4E-2
3.4	27423	0.3647				2.3E-2	2.4E-2
3.35	27019	0.3701				9.4E-3	1.0E-2
3.3	26616	0.3757				4.2E-3	4.6E-3
3.25	26213	0.3815				1.3E-3	1.8E-3
3.2	25810	0.3875		3.3E-4[9]		7.1E-4	9.6E-4
3.15	25406	0.3936		3.2E-4		4.4E-4	6.3E-4
3.10	25003	0.4000		2.5E-4		3.5E-4	5.1E-4
3.05	24600	0.4065		2.0E-4		2.9E-4	4.5E-4
3.0	24196	0.4133		1.7E-4			
2.95	23793	0.4203		1.5E-4			
2.9	23390	0.4275		1.3E-4			
2.85	22987	0.4350		1.1E-4			
2.8	22583	0.4428		9.5E-5			
2.75	22180	0.4509		7.5E-5			
2.7	21777	0.4592		6.2E-5			
2.65	21374	0.4679		3.8E-5			
2.6	20970	0.4769		3.4E-5			
2.55	20567	0.4862		2.3E-5			
2.5	20164	0.4959		1.5E-5			
2.45	19760	0.5061		9.3E-6			
2.4	19357	0.5166		5.3E-6			
2.35	18954	0.5276		2.9E-6			
2.3	18551	0.5391		1.2E-6			
0.2418	1950	5.128	2.47[12]				
0.2294	1850	5.405	2.46				
0.2170	1750	5.714	2.44				
0.2046	1650	6.061	2.43				
0.1984	1600	6.250	2.42				
0.1922	1550	6.452	2.41				
0.1860	1500	6.667	2.40				
0.1798	1450	6.896	2.38				
0.1736	1400	7.143	2.37				
0.1674	1350	7.407	2.36				
0.1612	1300	7.692	2.34				
0.1550	1250	8.000	2.32				
0.1488	1200	8.333	2.29				
0.1426	1150	8.696	2.26				
0.1364	1100	9.091	2.22				
0.1302	1050	9.524	2.17				
0.1240	1000	10.00	2.12				
0.1215	980	10.20	2.09				
0.1190	960	10.42	2.05				
0.1178	950	10.53			1.73[17]	5.8E-2[17]	
0.1165	940	10.64	2.01		1.72	5.8E-2	

TABLE I *(Continued)*

$Bi_{12}SiO_{20}$

eV	cm^{-1}	μm	n	k	n	k	k
0.1153	930	10.75			1.72	5.8E-2	
0.1141	920	10.87	1.96		1.72	5.8E-2	
0.1183	910	10.99			1.70	5.6E-2	
0.1116	900	11.11	1.85		1.67	7.5E-2	
0.1103	890	11.23	1.83	4.0E-2[12]	1.58	9.5E-2	
0.1091	880	11.36	1.75	9.0E-2	1.46	1.4E-1	
0.1079	870	11.49	1.64	1.2E-1	1.39	1.8E-1	
0.1066	860	11.63	1.50	1.5E-1	1.24	3.6E-1	
0.1054	850	11.76	1.15	2.2E-1	1.08	5.1E-1	
0.1041	840	11.90	2.00	1.5E + 0	1.03	8.7E-1	
0.1038	837	11.95		2.1E + 0			
0.1035	835	11.98			1.12	1.1E + 0	
0.1029	830	12.05	3.00	1.3E + 0	1.17	1.4E + 0	
0.1023	825	12.12			1.43	1.7E + 0	
0.1017	820	12.19	2.63	3.3E-1	2.41	9.1E-1	
0.1010	815	12.27			2.45	6.3E-1	
0.1004	810	12.34	2.44	3.0E-2	2.33	4.9E-1	
0.09919	800	12.50			2.18	3.9E-1	
0.09795	790	12.66	2.24				
0.09671	780	12.82			2.05	3.4E-1	
0.09547	770	12.99	2.14				
0.09423	760	13.16			2.03	2.7E-1	
0.09299	750	13.33	2.00				
0.09175	740	13.51			2.02	2.5E-1	
0.09051	730	13.70	1.90				
0.08927	720	13.89			1.96	2.3E-1	
0.08803	710	14.08	1.79				
0.08679	700	14.29			1.80	2.2E-1	
0.08555	690	14.49	1.67				
0.08431	680	14.71			1.72	2.3E-1	
0.08307	670	14.92	1.54				
0.08183	660	15.15			1.50	2.3E-1	
0.08059	650	15.38	1.39	9.0E-2	1.36	2.2E-1	
0.07935	640	15.62	1.25	1.1E-1	1.20	2.1E-1	
0.07811	630	15.87	1.08	2.0E-1	1.01	3.5E-1	
0.07687	620	16.13	0.98	4.9E-1	0.86	5.8E-1	
0.07625	615	16.26			0.97	9.2E-1	
0.07563	610	16.39	1.11	7.8E-1	1.46	8.6E-1	
0.07501	605	16.53			1.52	3.3E-1	
0.07439	600	16.67	1.12	7.6E-1	1.14	3.1E-1	
0.07377	595	16.81			0.85	4.7E-1	
0.07315	590	16.95	1.10	1.1E + 0	0.88	6.8E-1	
0.07265	586	17.06		1.1E + 0			
0.07253	585	17.09			1.21	1.1E + 0	
0.07191	580	17.24	1.37	1.1E-1	1.74	1.0E + 0	
0.07129	575	17.39			1.71	3.5E-1	
0.07067	570	17.54	1.20	8.1E-1	1.32	2.3E-1	

(continued)

TABLE I *(Continued)*

$Bi_{12}SiO_{20}$

eV	cm^{-1}	μm	n	k	n	k	k
0.07005	565	17.70			1.01	3.5E-1	
0.06943	560	17.86	0.85	1.2E + 0	0.78	6.4E-1	
0.06881	555	18.02			0.71	8.4E-1	
0.06819	550	18.18	0.64	1.6E + 0	0.79	1.3E + 0	
0.06757	545	18.35			0.96	1.9E + 0	
0.06732	543	18.42		2.3E + 0			
0.06695	540	18.52	0.90	2.3E + 0	1.74	2.0E + 0	
0.06633	535	18.69			2.80	1.5E + 0	
0.06571	530	18.87	1.40	1.9E + 0	2.33	6.4E-1	
0.06509	525	19.05			1.75	2.6E-1	
0.06447	520	19.23	1.77	1.5E + 0	1.47	2.7E-1	
0.06410	517	19.34		1.4E + 0			
0.06385	515	19.42			1.30	3.1E-1	
0.06323	510	19.61	1.40	1.7E + 0	0.96	3.6E-1	
0.06261	505	19.80			0.68	5.1E-1	
0.06199	500	20.00	1.00	2.5E + 0	0.51	6.8E-1	
0.06137	495	20.20			0.47	1.1E + 0	
0.06075	490	20.41	0.96	3.3E + 0	0.50	1.5E + 0	
0.06013	485	20.62			0.57	1.8E + 0	
0.05951	480	20.83	1.30	4.2E + 0	0.75	2.2E + 0	
0.05914	477	20.96		5.1E + 0			
0.05889	475	21.05			1.11	2.7E + 0	
0.05827	470	21.28	2.00	3.1E + 0	1.64	3.3E + 0	
0.05763	465	21.51			3.10	3.5E + 0	
0.05703	460	21.74	5.20	1.5E + 0	4.38	2.9E + 0	
0.05641	455	21.98			4.48	1.4E + 0	
0.05579	450	22.22	5.00	4.4E-1	3.51	5.7E-1	
0.05517	445	22.47			3.02	3.5E-1	
0.05455	440	22.73	4.00	2.3E-1	2.82	2.1E-1	
0.05331	430	23.25	3.20	1.4E-1	2.45	1.0E-1	
0.05207	420	23.81	2.70	2.0E-1	2.19	6.8E-2	
0.05083	410	24.39	2.40	3.0E-1	1.95	5.1E-2	
0.04959	400	25.00	2.05	4.5E-1	1.73	2.9E-2	
0.04835	390	25.64	1.90	6.1E-1	1.42	7.1E-2	
0.04711	380	26.31	1.53	8.8E-1	0.85	1.7E-1	
0.04587	370	27.03	1.22	1.5E + 0	0.42	4.2E-1	
0.04525	365	27.40			0.41	6.1E-1	
0.04463	360	27.78	1.21	2.1E + 0	0.53	1.1E + 0	
0.04401	355	28.17			0.84	1.5E + 0	
0.04339	350	28.57	1.29	2.6E + 0	0.82	1.2E + 0	
0.04277	345	28.99			0.64	1.5E + 0	
0.04215	340	29.41	1.55	3.2E + 0	0.65	2.0E + 0	
0.04154	335	29.85			0.72	2.3E + 0	
0.04129	333	30.03		3.6E + 0			
0.04091	330	32.30	2.20	3.3E + 0	0.89	2.8E + 0	
0.04030	325	30.77			1.18	3.4E + 0	
0.03967	320	31.25	3.80	2.5E + 0	2.00	3.7E + 0	

TABLE I *(Continued)*

$Bi_{12}SiO_{20}$

eV	cm^{-1}	μm	n	k	n	k	k
0.03906	315	31.75			3.98	3.1E + 0	
0.03843	310	32.26	4.38	1.8E + 0	4.65	2.1E + 0	
0.03782	305	32.79			3.88	1.0E + 0	
0.03719	300	33.33	4.10	1.2E + 0	3.27	8.9E-1	
0.03658	295	33.90			2.79	8.9E-1	
0.03595	290	34.48	3.75	9.4E-1	2.55	1.2E + 0	
0.03534	285	35.09			2.75	8.7E-1	
0.03471	280	35.71	3.50	7.8E-1	2.60	7.3E-1	
0.03410	275	36.36			2.37	5.5E-1	
0.03347	270	37.04	2.80	7.4E-1	2.05	4.4E-1	
0.03286	265	37.74			1.73	4.3E-1	
0.03224	260	38.46	2.30	1.3E + 0	1.28	7.4E-1	
0.03162	255	39.22			1.10	1.0E + 0	
0.03100	250	40.00	1.88	2.9E + 0	0.83	1.8E + 0	
0.03062	247	40.48		3.2E + 0			
0.03038	245	40.82			1.18	2.5E + 0	
0.02976	240	41.67	2.70	2.6E + 0	2.19	3.4E + 0	
0.02914	235	42.55			3.44	2.6E + 0	
0.02852	230	43.48	3.95	1.3E + 0	3.64	1.5E + 0	
0.02790	225	44.44			3.15	9.5E-1	
0.02752	222	45.04		1.1E + 0			
0.02728	220	45.45	3.80	1.2E + 0	2.54	5.9E-1	
0.02666	215	46.51			2.09	6.2E-1	
0.02604	210	47.62	3.10	1.4E + 0	3.06	1.9E + 0	
0.02542	205	48.78			2.69	1.1E + 0	
0.02480	200	50.00	3.10	9.6E-1	2.48	4.0E-1	
0.02418	195	51.28			2.26	7.7E-1	
0.02356	190	52.63	2.20	1.3E + 0	1.55	6.4E-1	
0.02294	185	54.05			0.84	8.4E-1	
0.02232	180	55.55	1.82	2.5E + 0	1.36	2.2E + 0	
0.02170	175	57.14			2.41	2.1E + 0	
0.02108	170	58.82	1.80	2.9E + 0	1.29	1.2E + 0	
0.02046	165	60.61			0.79	1.9E + 0	
0.01984	160	62.50	1.93	4.8E + 0	0.65	2.5E + 0	
0.01922	155	64.52			0.87	3.4E + 0	
0.01860	150	66.67	1.80	6.4E + 0	1.38	4.0E + 0	
0.01798	145	68.97			2.41	4.8E + 0	
0.01736	140	71.43	3.20	4.3E + 0	3.55	5.3E + 0	
0.01674	135	74.07			4.70	4.2E + 0	
0.01612	130	76.92	6.15	3.1E + 0	5.10	2.4E + 0	
0.01562	126	79.35		2.0E + 0			
0.01550	125	80.00			4.29	1.2E + 0	
0.01488	120	83.33	5.00	3.1E + 0	1.74	2.0E + 0	
0.01426	115	86.96			2.14	2.6E + 0	
0.01364	110	90.91	4.00	4.4E + 0	5.80	4.3E + 0	
0.01302	105	95.24			4.99	2.2E + 0	
0.01240	100	100.0	5.80	3.8E + 0	5.15	3.4E + 0	

(continued)

TABLE I *(Continued)*

$Bi_{12}SiO_{20}$

eV	cm^{-1}	μm	n	k	n	k	k
0.01178	95	105.3			5.45	1.3E + 0	
0.01116	90	111.1	6.80	2.6E + 0	5.43	1.2E + 0	
0.01054	85	117.6			4.65	8.1E-1	
0.009919	80	125.0	6.70	2.1E + 0	4.19	7.4E-1	
0.009299	75	133.3			3.82	7.7E-1	
0.008679	70	142.8	6.48	2.0E + 0	3.55	7.9E-1	
0.008059	65	153.8			3.24	8.5E-1	
0.007439	60	166.7	6.28	2.0E + 0			
0.006199	50	200.0	6.00	2.4E + 0			
0.001984	16	625.0	6.450[19]				
0.001860	15	666.7	6.438	5.62E-2[19]			
0.001736	14	714.3	6.451	5.28E-2			
0.001612	13	769.2	6.415	5.01E-2			
0.001488	12	833.3	6.405	4.64E-2			
0.001364	11	909.1	6.397	4.34E-2			
0.001240	10	1000	6.390	3.89E-2			
0.001116	9	1111	6.382	3.97E-2			
0.0009919	8	1250	6.379	3.08E-2			
0.0008679	7	1428	6.378	2.61E-2			
0.0007439	6	1667	6.378	2.25E-2			
0.0006199	5	2000	6.380	1.75E-2			
0.0004959	4	2500		7.95E-3			
0.0004959	4	2500		1.79E-2			

TABLE II

Values of n and k for $Bi_{12}GeO_{20}$ from Various References[a]

eV	cm^{-1}	μm	n	k	k
8.5	68557	0.1459	0.680[5]	0.805[5]	
8.4	67750	0.1476	0.685	0.825	
8.3	66943	0.1494	0.690	0.840	
8.2	66137	0.1512	0.700	0.860	
8.1	65330	0.1531	0.703	0.880	
8.0	64524	0.1550	0.705	0.900	
7.9	63717	0.1569	0.710	0.904	
7.8	62911	0.1590	0.710	0.906	
7.7	62104	0.1610	0.710	1.00	
7.6	61298	0.1631	0.720	1.04	
7.5	60491	0.1653	0.75	1.09	
7.4	59685	0.1675	0.795	1.12	
7.3	58878	0.1698	0.85	1.13	
7.25	58475	0.1710	0.87	1.13	

[a] The references from which the values were taken are given in brackets.

TABLE II *(Continued)*

$Bi_{12}GeO_{20}$

eV	cm^{-1}	μm	n	k	k
7.2	58071	0.1722	0.91	1.12	
7.15	57668	0.1734	0.90	1.10	
7.1	57265	0.1746	0.905	1.10	
7.05	56862	0.1759	0.89	1.08	
7.0	56458	0.1771	0.875	1.10	
6.95	56055	0.1784	0.895	1.13	
6.9	55652	0.1797	0.905	1.12	
6.85	55249	0.1810	0.90	1.12	
6.8	54845	0.1823	0.89	1.13	
6.75	54442	0.1837	0.88	1.15	
6.7	54039	0.1851	0.88	1.20	
6.65	53635	0.1864	0.95	1.23	
6.6	53232	0.1879	0.96	1.21	
6.55	52829	0.1893	0.955	1.20	
6.5	52426	0.1907	0.95	1.21	
6.45	52022	0.1922	0.96	1.23	
6.4	51619	0.1937	0.995	1.23	
6.35	51216	0.1953	0.99	1.21	
6.3	50813	0.1968	0.96	1.20	
6.25	50409	0.1984	0.945	1.23	
6.2	50006	0.2000	0.935	1.26	
6.1	49199	0.2033	0.94	1.32	
6.0	48393	0.2066	0.97	1.39	
5.9	47586	0.2101	1.01	1.43	
5.8	46780	0.2138	1.04	1.49	
5.7	45973	0.2175	1.09	1.53	
5.6	45167	0.2214	1.12	1.57	
5.5	44360	0.2254	1.16	1.61	
5.4	43554	0.2296	1.22	1.69	
5.3	42747	0.2339	1.29	1.76	
5.2	41940	0.2384	1.38	1.80	
5.1	41134	0.2431	1.48	1.835	
5.0	40327	0.2480	1.59	1.85	
4.9	39521	0.2530	1.69	1.86	
4.8	38714	0.2583	1.80	1.83	
4.7	37908	0.2638	1.89	1.785	
4.6	37101	0.2695	1.955	1.75	
4.5	36295	0.2755	2.01	1.715	
4.4	35488	0.2818	2.08	1.715	
4.3	34682	0.2883	2.15	1.70	
4.2	33875	0.2952	2.23	1.665	
4.1	33068	0.3024	2.30	1.63	
4.0	32262	0.3100	2.365	1.60	
3.95	31859	0.3139	2.40	1.585	
3.9	31455	0.3179	2.435	1.58	
3.85	31052	0.3220	2.48	1.585	

(continued)

TABLE II *(Continued)*

$Bi_{12}GeO_{20}$

eV	cm^{-1}	μm	n	k	k
3.8	30649	0.3263	2.52	1.60	
3.75	30246	0.3306	2.59	1.61	
3.7	29842	0.3351	2.68	1.605	
3.65	29439	0.3397	2.78	1.605	
3.6	29036	0.3444	2.90	1.55	
3.55	28632	0.3493	3.02	1.45	
3.5	28229	0.3542	3.105	1.31	
3.45	27826	0.3594	3.135	1.20	
3.4	27423	0.3647	3.14	1.06	
3.35	27019	0.3701	3.13	0.92	
3.3	26616	0.3757	3.08	0.815	
3.25	26213	0.3815	3.02	0.77	
3.2	25810	0.3875	2.98	0.705	
3.15	25406	0.3936			1.8E-4[9]
3.1	25003	0.4000	2.91	0.63	9.5E-5
3.05	24600	0.4065			7.1E-5
3.0	24196	0.4133	2.865	0.58	6.2E-5
2.95	23793	0.4203			5.5E-5
2.9	23390	0.4275	2.83	0.52	4.8E-5
2.85	22987	0.4350			4.0E-5
2.8	22583	0.4428	2.795	0.48	3.2E-5
2.75	22180	0.4509			2.5E-5
2.7	21777	0.4592	2.765	0.435	1.9E-5
2.65	21374	0.4679			1.5E-5
2.6	20970	0.4769	2.75	0.39	9.9E-6
2.55	20567	0.4862			6.6E-6
2.5	20164	0.4959	2.73	0.35	4.3E-6
2.45	19760	0.5061			2.7E-6
2.4	19357	0.5166	2.705	0.30	1.6E-6
2.35	18954	0.5276			1.2E-6
2.3	18551	0.5391	2.695	0.265	9.4E-7
2.1	16938	0.5904	2.65	0.145	
2.0	16131	0.6199	2.585	0.105	
1.9	15324	0.6526	2.53	0.08	
1.8	14518	0.6888	2.47	0.05	
1.7	13711	0.7293	2.41	0.035	
1.6	12905	0.7749	2.37	0.025	
1.5	12098	0.8266	2.335	0.02	
3.100	25000	0.4	2.926[8]		
2.480	20000	0.5	2.651		
2.066	16667	0.6	2.549		
1.771	14286	0.7	2.499		
1.550	12500	0.8	2.472		
1.378	11111	0.9	2.454		
1.240	10000	1.0	2.442		
1.127	9091	1.1	2.434		

TABLE II *(Continued)*

$Bi_{12}GeO_{20}$

eV	cm^{-1}	μm	n	k	k
1.033	8333	1.2	2.427	4.57E-5[8]	
0.9537	7692	1.3	2.421	5.62E-5	
0.8856	7143	1.4	2.416	6.67E-5	
0.8266	6667	1.5	2.412	7.73E-5	
0.7749	6250	1.6	2.409	8.78E-5	
0.7293	5882	1.7	2.405	9.84E-5	
0.6888	5556	1.8	2.402	1.09E-4	
0.6526	5263	1.9	2.399	1.19E-4	
0.6199	5000	2.0	2.396	1.30E-4	
0.5904	4762	2.1	2.393	1.41E-4	
0.5636	4545	2.2	2.390	1.51E-4	
0.5391	4348	2.3	2.387	1.62E-4	
0.5166	4167	2.4	2.384	1.72E-4	
0.4959	4000	2.5	2.382	1.83E-4	
0.4769	3846	2.6	2.379	1.93E-4	
0.4592	3704	2.7	2.376	2.04E-4	
0.4428	3571	2.8	2.373	2.14E-4	
0.4275	3448	2.9	2.371	2.25E-4	
0.4133	3333	3.0	2.368	2.35E-4	
0.4000	3226	3.1	2.366	2.46E-4	
0.3875	3125	3.2	2.363	2.56E-4	
0.3757	3030	3.3	2.360	2.67E-4	
0.3647	2941	3.4	2.358	2.78E-4	
0.3542	2857	3.5	2.355	2.88E-4	
0.3444	2778	3.6	2.353	2.99E-4	
0.3351	2703	3.7	2.351	3.09E-4	
0.3263	2632	3.8	2.348	3.20E-4	
0.3179	2564	3.9	2.346	3.30E-4	
0.3100	2500	4.0	2.344	3.51E-4	
0.3024	2439	4.1	2.342	3.62E-4	
0.2952	2381	4.2	2.340	3.72E-4	
0.2883	2326	4.3	2.339	3.83E-4	
0.2818	2273	4.4	2.337	3.93E-4	
0.2755	2222	4.5	2.336	4.04E-4	
0.2695	2174	4.6	2.334	4.14E-4	
0.2638	2128	4.7	2.333	4.25E-4	
0.2583	2083	4.8	2.332	4.36E-4	
0.2530	2041	4.9	2.332	4.46E-4	
0.2480	2000	5.0	2.331	4.57E-4	
0.09919	800	12.50	2.17[17]	4.6E-1[17]	
0.09795	790	12.66	2.17	4.6E-1	
0.09671	780	12.82	2.17	4.6E-1	
0.09547	770	12.99	2.17	4.4E-1	
0.09423	760	13.16	2.17	4.4E-1	
0.09299	750	13.33	2.14	4.2E-1	

(continued)

TABLE II *(Continued)*

$Bi_{12}GeO_{20}$

eV	cm^{-1}	μm	n	k	k
0.09175	740	13.51	2.14	4.2E-1	
0.09051	730	13.70	2.12	4.3E-1	
0.08927	720	13.89	2.05	4.4E-1	
0.08803	710	14.08	1.78	3.9E-1	
0.08679	700	14.29	0.72	1.4E-1	
0.08617	695	14.39	0.71	7.1E-1	
0.08555	690	14.49	0.70	1.6E + 0	
0.08493	685	14.60	2.06	2.1E + 0	
0.08468	683	14.64	2.12	2.1E + 0	
0.08431	680	14.71	2.37	1.3E + 0	
0.08369	675	14.81	2.79	5.4E-1	
0.08307	670	14.92	2.57	3.5E-1	
0.08183	660	15.15	2.27	4.0E-1	
0.08059	650	15.38	2.05	4.4E-1	
0.07935	640	15.62	1.80	5.0E-1	
0.07811	630	15.87	1.74	4.6E-1	
0.07687	620	16.13	1.35	5.6E-1	
0.07563	610	16.39	1.00	1.0E + 0	
0.07501	605	16.53	1.23	1.4E + 0	
0.07439	600	16.67	1.88	1.6E + 0	
0.07377	595	16.81	2.68	4.5E-1	
0.07315	590	16.95	2.13	1.9E-1	
0.07253	585	17.09	1.03	9.8E-1	
0.07191	580	17.24	0.74	6.7E-1	
0.07129	575	17.39	1.40	1.1E + 0	
0.07104	573	17.45	1.88	1.5E + 0	
0.07067	570	17.54	1.92	8.3E-1	
0.07005	565	17.70	1.91	3.9E-1	
0.06943	560	17.86	1.42	1.4E-1	
0.06881	555	18.02	0.71	7.0E-2	
0.06819	550	18.18	0.32	3.2E-1	
0.06757	545	18.35	0.56	9.0E-1	
0.06695	540	18.52	0.69	1.4E + 0	
0.06633	535	18.69	0.91	2.2E + 0	
0.06571	530	18.87	1.68	3.0E + 0	
0.06534	527	18.98	2.45	2.6E + 0	
0.06509	525	19.05	2.24	2.2E + 0	
0.06447	520	19.23	3.15	9.5E-1	
0.06385	515	19.42	2.83	7.1E-1	
0.06323	510	19.61	2.17	4.6E-1	
0.06261	505	19.80	1.36	5.9E-1	
0.06199	500	20.00	1.10	4.5E-1	
0.06137	495	20.20	0.86	5.8E-1	
0.06075	490	20.41	0.75	8.7E-1	
0.06013	485	20.62	0.84	1.3E + 0	
0.05951	480	20.83	0.74	2.0E + 0	
0.05889	475	21.05	0.84	2.7E + 0	

TABLE II *(Continued)*

$Bi_{12}GeO_{20}$

eV	cm^{-1}	μm	n	k	k
0.05827	470	21.28	1.03	3.4E + 0	
0.05763	465	21.51	1.41	4.2E + 0	
0.05703	460	21.74	2.30	3.9E + 0	
0.05641	455	21.98	4.95	2.1E + 0	
0.05579	450	22.22	4.50	1.1E + 0	
0.05517	445	22.47	3.95	7.6E-1	
0.05455	440	22.73	3.30	6.1E-1	
0.05393	435	22.99	3.04	4.9E-1	
0.05331	430	23.25	2.81	3.6E-1	
0.05269	425	23.53	2.67	3.4E-1	
0.05207	420	23.81	2.37	3.6E-1	
0.05145	415	24.10	2.26	3.5E-1	
0.05083	410	24.39	2.03	3.7E-1	
0.05021	405	24.69	1.91	3.7E-1	
0.04959	400	25.00	1.63	4.0E-1	
0.04897	395	25.32	1.55	1.3E-1	
0.04835	390	25.64	1.52	9.9E-2	
0.04773	385	25.97	1.15	1.7E-1	
0.04711	380	26.31	1.10	4.6E-1	
0.04649	375	26.67	0.78	6.4E-1	
0.04587	370	27.03	0.74	7.4E-1	
0.04525	365	27.40	0.74	1.0E + 0	
0.04463	360	27.78	0.79	1.3E + 0	
0.04401	355	28.17	1.07	1.6E + 0	
0.04389	354	28.25	0.96	1.6E + 0	
0.04339	350	28.57	0.64	1.6E + 0	
0.04277	345	28.99	0.23	1.7E + 0	
0.04215	340	29.41	0.34	1.9E + 0	
0.04154	335	29.85	0.33	2.3E + 0	
0.04091	330	30.30	0.37	2.7E + 0	
0.04030	325	30.77	0.48	3.1E + 0	
0.03967	320	31.25	0.84	3.6E + 0	
0.03906	315	31.75	1.04	4.3E + 0	
0.03868	312	32.05	5.70	4.3E + 0	
0.03843	310	32.26	1.70	5.3E + 0	
0.03782	305	32.79	3.29	4.6E + 0	
0.03719	300	33.33	5.08	3.1E + 0	
0.03658	295	33.90	4.28	1.5E + 0	
0.03595	290	34.48	3.55	1.1E + 0	
0.03534	285	35.09	2.85	1.1E + 0	
0.03471	280	35.71	1.39	2.0E + 0	
0.03410	275	36.36	1.58	3.8E + 0	
0.03347	270	37.04	4.56	3.3E + 0	
0.03286	265	37.74	3.74	1.2E + 0	
0.03224	260	38.46	2.74	7.3E-1	
0.03162	255	39.22	1.49	1.1E + 0	

(continued)

TABLE II *(Continued)*

$Bi_{12}GeO_{20}$

eV	cm^{-1}	μm	n	k	k
0.03100	250	40.00	0.85	3.0E + 0	
0.03038	245	40.82	0.94	3.7E + 0	
0.02976	240	41.67	1.41	4.8E + 0	
0.02914	235	42.55	2.62	5.7E + 0	
0.02852	230	43.48	6.67	4.9E + 0	
0.02790	225	44.44	5.94	2.7E + 0	
0.02728	220	45.45	5.18	1.4E + 0	
0.02666	215	46.51	4.37	1.0E + 0	
0.02604	210	47.62	3.35	1.1E + 0	
0.02542	205	48.78	3.75	2.1E + 0	
0.02480	200	50.00	4.10	1.2E + 0	
0.02418	195	51.28	3.52	1.2E + 0	
0.02356	190	52.63	4.08	1.3E + 0	
0.02294	185	54.05	3.45	7.5E-1	
0.02232	180	55.55	3.22	1.2E + 0	
0.02182	176	56.82	3.41	1.3E + 0	
0.02170	175	57.14	3.40	1.2E + 0	
0.02108	170	58.82	3.16	7.1E-1	
0.02046	165	60.61	2.88	5.4E-1	
0.01984	160	62.50	2.30	5.4E-1	
0.01922	155	64.52	1.74	7.2E-1	
0.01860	150	66.67	1.10	1.1E + 0	
0.01798	145	68.97	0.57	2.7E + 0	
0.01736	140	71.43	0.62	3.7E + 0	
0.01674	135	74.07	0.72	5.5E + 0	
0.01624	131	76.34	1.17	6.2E + 0	
0.01512	130	76.92	2.05	6.1E + 0	
0.01550	125	80.00	4.51	7.8E + 0	
0.01513	122	81.97	9.35	6.7E + 0	
0.01488	120	83.33	8.00	3.7E + 0	
0.01426	115	86.96	4.08	1.3E + 0	
0.01364	110	90.91	2.36	8.5E + 0	
0.01302	105	95.24	9.83	7.7E + 0	
0.01240	100	100.0	5.81	3.7E + 0	
0.01190	96	104.2	7.27	4.6E + 0	
0.01178	95	105.3	7.31	4.5E + 0	
0.01116	90	111.1	7.10	2.1E + 0	
0.01054	85	117.6	6.43	1.8E + 0	
0.009919	80	125.0	6.06	1.5E + 0	
0.009299	75	133.3	5.98	1.1E + 0	
0.008679	70	142.8	5.33	9.8E-1	
0.001860	15	666.7		4.50E-2[19]	
0.001736	14	714.3	6.270[19]	4.26E-2	
0.001612	13	769.2	6.259	4.04E-2	
0.001488	12	833.3	6.250	3.64E-2	
0.001364	11	909.1	6.240	3.25E-2	
0.001240	10	1000	6.232	2.94E-2	

TABLE II *(Continued)*

$Bi_{12}GeO_{20}$

eV	cm^{-1}	μm	n	k	k
0.001116	9	1111	6.226	2.65E-2	
0.0009919	8	1250	6.220	2.58E-2	
0.0008679	7	1428	6.217	2.04E-2	
0.0007439	6	1667	6.210	1.59E-2	
0.0006199	5	2000	6.212	1.59E-2	

Boron Nitride (BN)

GARY L. DOLL
Materials Science Department
Timken Research
Canton, Ohio

INTRODUCTION I

The optical functions of the hexagonal and cubic phases of BN (hBN and cBN, respectively) are not nearly as well defined as those of other group III nitrides. This is due in large part to the fact that single-crystal samples either do not exist (which is the case for hexagonal boron nitride) or are extremely rare (as in the case of cubic boron nitride) [1]. Optical studies on the optically anisotropic hBN have been performed on preferentially oriented, polycrystalline samples with $\vec{E} \perp \hat{c}$ and $\vec{E} \parallel \hat{c}$ polarization. In these samples, it is difficult to obtain a complete separation of the two polarizations because the typical mosaic spread of the c-axes is greater than 20°, and because pure a-faces are not easily obtained. In this critique, we have not included experiments performed on BN films. The reasons for this are that the optical constants of these films can vary greatly with film properties such as stoichiometry, homogeneity, crystallinity, and purity, to name a few. For the most part, these types of film properties have not been correlated with optical properties that have been reported. As we shall see, the optical properties of bulk BN materials are not that well defined.

The hexagonal phase of BN is isostructural to graphite in that it is composed of planes of BN hexagons stacked along the c-axis in an ABA configuration. hBN has the space group $D_{4h}^6(\mathrm{P6_3/mmc})$, which has the irreducible representation

$$\Gamma = 2E_{2g} + A_{2u} + E_{1u} + 2B_{1g},$$

where the E_{2g} modes are Raman-active, the B_{1g} modes are silent (optically inactive), and the A_{2u} and E_{1u} modes are infrared-active. Whereas the A_{2u} modes are out-of-plane vibrations excited by light polarized parallel to the hBN c-axis ($\vec{E} \parallel \hat{c}$), the E_{1u} modes are in-plane vibrations excited by light

HANDBOOK OF OPTICAL CONSTANTS OF SOLIDS III

Copyright © 1998 by Academic Press.
All rights of reproduction in any form reserved
ISBN 0-12-544423-0/$25.00.

polarized perpendicular to the c-axis ($\vec{E} \perp \hat{c}$). The A_{2u} and E_{1u} modes are polar, which means that the longitudinal-optical or LO mode has a higher energy than the transverse-optical or TO mode.

cBN has the zincblende structure with the space group T_d^2, ($F\bar{4}3m$). Its phonon modes are of T_2 symmetry, and are polar, so that the energy of the cBN LO vibration is also higher than the TO polarization energy.

II cBN

Selected optical constants n and k for cBN taken from three sources are collected in Table I and plotted in Fig. 1. Tabulated values of the optical constants were not included in any of the sources.

Gielisse *et al.* [2] provided the first reported examination of the cBN optical constants. Although this study covered the energy range 400 to 4000 cm^{-1}, the optical constants could only be deduced from their data over the energy range 400 to 1800 cm^{-1}. In this study, Gielisse *et al.* measured the reflectivity of a collection of small single crystals compressed into compacts that were ground and polished. Their normal-incidence reflectivity was modeled using a four-parameter fit to the equations

$$\epsilon_1(\omega) = \epsilon_\infty + 4\pi\rho\omega_0^2 \frac{{\omega_0}^2 - \omega^2}{(\omega_0^2 - \omega^2)^2 + \Gamma^2\omega^2} \tag{1}$$

$$\epsilon_2(\omega) = 4\pi\rho\omega_0^2 \frac{\Gamma\omega}{(\omega_0^2 - \omega^2)^2 + \Gamma^2\omega^2}, \tag{2}$$

where ϵ_0 is the high-frequency limiting value of the dielectric constant, ω_0 is the Brillouin-zone-center, TO phonon-mode energy, $4\pi\rho$ is the strength of the resonance, Γ and is the phonon width or the damping constant. Good agreement between the calculated and measured reflectivity was found for the following parameters: $\epsilon_\infty = 4.5$, $4\pi\rho = 2.6$, $\omega_0 = 1065$ cm^{-1}, and $\Gamma = 40.5$ cm^{-1}. The static dielectric constant ϵ_0 was calculated to be 7.1 from the equation

$$\epsilon_0 = \epsilon_\infty + 4\pi\rho. \tag{3}$$

We calculated the values of $\epsilon_1(\omega)$ and $\epsilon_2(\omega)$ using the above parameters, then derived n and k by the equations

$$\begin{aligned} 2n^2 &= \sqrt{\epsilon_1^2 + \epsilon_2^2} + \epsilon_1 \\ 2k^2 &= \sqrt{\epsilon_1^2 + \epsilon_2^2} - \epsilon_1 \end{aligned} \tag{4}$$

The results are shown in Fig. 1 and listed in Table I. The energy of the LO mode was deduced to be 1340 cm^{-1} from the Lyddane–Sachs–Teller relationship $\omega_{LO} = \omega_{TO}(\epsilon_0/\epsilon_\infty)^{1/2}$.

Eremets *et al.* [3] have reported the optical properties of cBN over the energy range 500 to 28,000 cm^{-1}. Single crystals of cBN 0.45 μm thick by 150 μm square were studied in reflection and transmission, and n and k were deduced by fitting the interference fringes with equations proposed by Heavens [4]. Although n and k were neither tabulated nor shown in a form suitable for our purposes, the dielectric functions were described by a Sellmeier model that considers the contribution to $\epsilon(\omega)$ from phonons and electronic transitions. The Sellmeier model used by the authors is expressed as

$$\epsilon = \epsilon_{ph} + \epsilon_{elec} - \epsilon_\infty, \tag{5}$$

where

$$\epsilon_{elec} - 1 = \frac{\epsilon_\infty - 1}{1 - [\hbar\omega/E_0]^2}, \tag{6}$$

and ϵ_{ph} is described by Eqs. (1), (2), and (3). Using this approach, they were able to approximate the reflectance and transmittance over the measured energy range. We first calculated the dielectric functions using Eq. (5) with the parameters $\epsilon_0 = 6.8$, $\epsilon_\infty = 4.46$, $E_0 = 104{,}850$ cm^{-1}, $\omega_0 = 1055.7$ cm^{-1}, and $\Gamma = 0.005$ cm^{-1}, which were given by the authors. Eremets *et al.* also report the LO mode energy to be 1304.8 cm^{-1}. We suspect that the value of Γ given by Eremets *et al.* in [3] is incorrect, since it appears to be too small to describe phonon linewidths in these types of samples. Nevertheless, using the preceding parameters, we calculated n and k from Eq. (4). The results of this calculation are gathered in Table I and plotted in Fig. 1.

Miyata *et al.* [5] have reported the optical properties of a cBN single crystal having an area of 5 mm^2 and a thickness (d) of 0.16 mm. The sample was measured over the energy range 2 to 23 eV by reflectance and 2 to 6 eV by transmittance. In the energy range 2 to 6 eV where both R and T were measured, n and k were derived from the expressions

$$\begin{aligned} k &= \frac{\lambda}{4\pi d} \ln \frac{(1-R)^2}{T} \\ n &= \frac{R + 1 + [(R+1)^2 - (R-1)^2(1+k^2)]^{1/2}}{1-R}. \end{aligned} \tag{7}$$

To determine the optical constants from the reflectance at higher photon energy, a Kramers–Kronig relation was employed where the values of the phase-change integral were set equal to those calculated from the optical

constants in the energy region 2.5 to 5.5 eV. Their results for n and k, which we extracted from their figure, are listed in Table I and plotted in Fig. 1.

As can be seen in Fig. 1, some discrepancy exists between the data published by Gielisse *et al.* [2] and Eremets *et al.* [3] in the vicinity of the cBN IR-active phonon. Whereas Gielisse *et al.* [2] quote the energy of the TO phonon of their sample to be 1065 cm^{-1}, Eremets *et al.* [3] have determined the energy to be 1055.7 cm^{-1} for their material. One might expect this sort of discrepancy to be sample dependent. As we would expect from Eqs. (1) and (2), Fig. 1 shows us that the suspiciously low value of $\Gamma = 0.005$ cm^{-1} reported by Eremets *et al.* has a much more pronounced effect on k than on n in the region of the IR-active cBN phonon. Gielisse *et al.* [2] and Eremets *et al.* [3] derive similar values for ϵ_0 and ϵ_∞. The method used to deduce n and k from Eremets *et al.* [3] does not account for multiphonon absorption that is present at energies between 2000 cm^{-1} and 4000 cm^{-1}, so the optical constants in that energy range are not accurate. There is good agreement in the values of n derived from Eremets *et al.* [3] and Miyata *et al.* [5] where the data overlap in the energy region 2 to 3.5 eV. The onset for optical absorption was determined to be 6.1 $\pm$ 0.2 eV from Miyata *et al.* [5], and several absorption edges are also present at higher photon energies.

III hBN

The first examination of the optical properties of hBN was performed by Geick *et al.* [6] on pyrolytic hBN with a mosaic spread in the c-axis of 30°, where the c-axis is the direction normal to the BN hexagonal planes. The reflectivity was measured at near-normal incidence in $\vec{E} \perp \hat{c}$ and $\vec{E} \parallel \hat{c}$ polarizations over the energy range 300 to 2000 cm^{-1}. With this mosaic spread, a complete separation of the polarizations is not possible, but the experiment did provide first evidence for the identification of the in-plane (E_{1u}) and out-of-plane (A_{2u}) IR-active phonons in hBN. The dielectric functions were obtained from a Kramers–Kronig transformation of the reflectance data. No details of how the phase integral was extended to lower and higher energies in order to perform the transformation were given. We have calculated n and k using Eq. (4) from a digitization of their figures for ϵ_1 and ϵ_2 obtained with $\vec{E} \perp \hat{c}$ polarization. We show the results in Table II and Fig. 2. The presence of the low-frequency A_{2u} phonon near 13 μm illustrates the contribution that the crystallographic mosaic spread of the c-axis makes to the optical spectra of these types of samples. To our knowledge, there has been no optical spectrum taken on hBN samples that does not contain a mixture of these polarizations. The authors fit their dielectric functions to an oscillator model similar to Eqs. (1) and (2) but that contains contributions from both polarizations to account for the mosaic spread of the hBN crystallites. For the $\vec{E} \parallel \hat{c}$ polarization, the parameters that provided the best fit to

the data are $\epsilon_\infty = 4.10$, $\epsilon_0 = 5.09$, $\omega_{TO}^{A2u} = 783\ cm^{-1}$, $\omega_{LO}^{A2u} = 828\ cm^{-1}$, $4\pi\rho^{A2u} = 3.26 \times 10^5\ cm^{-2}$, $\Gamma^{A2u} = 8.0\ cm^{-1}$, $\omega_{TO}^{E1u} = 1510\ cm^{-1}$, $\omega_{LO}^{E1u} = 1595\ cm^{-1}$, $4\pi\rho^{E1u} = 1.04 \times 10^6\ cm^{-1}$, and $\Gamma^{E1u} = 80\ cm^{-1}$. For the $\vec{E}\perp\hat{c}$ polarization, the parameters that provided the best fit to the data are $\epsilon_\infty = 4.95$, $\epsilon_0 = 7.04$, $\omega_{TO}^{A2u} = 767\ cm^{-1}$, $\omega_{LO}^{A2u} = 778\ cm^{-1}$, $4\pi\rho^{A2u} = 1.23 \times 10^5\ cm^{-2}$, $\Gamma^{A2u} = 35.0\ cm^{-1}$, $\omega_{TO}^{E1u} = 1367\ cm^{-1}$, $\omega_{LO}^{E1u} = 1610\ cm^{-1}$, $4\pi\rho^{E1u} = 3.49 \times 10^6\ cm^{-1}$, and $\Gamma^{E1u} = 29\ cm^{-1}$. We do not display the $\vec{E}\parallel\hat{c}$ optical constants in either Fig. 2 or Table II.

Hoffman *et al.* [7] examined the $\vec{E}\perp\hat{c}$ optical reflectivity spectrum on a similar sample of pyrolytic hBN, with a mosaic spread slightly larger than that of Geick *et al.* [6] over the energy range 0.05 to 10 eV. The dielectric functions were obtained from a Kramers–Kronig transformation of the reflectance data. For purposes of integrating the phase-shift integral of the transformation, the data were extended below 0.045 eV by treating R as a constant, from 10 to 30 eV by using data from Mamy *et al.* [8], from 30 to 100 eV as $R \approx \omega^{-1}$, and thereafter as $R \approx \omega^{-4}$. We have calculated n and k using Eq. (4) from a digitization of their figures for ϵ_1 and ϵ_2, and we show the results in Table II and Fig. 2. As is evident in the figure, there is agreement in the energies of the E_{1u} and A_{2u} phonons between the two studies, but disagreement in the oscillator strengths of the vibrations. This is probably related to orientational and structural differences between the samples examined in the two studies. Another item of note is that the values of k are relatively high in the region between the ir-active phonons and the electronic band gap near 5 eV. The authors believe that this is not intrinsic to hBN, but rather is related to the rather large amounts of impurities and defects in the sample. The authors also examined the phonon region of ϵ_2 by fitting the data with an oscillator model similar to the one used by Geick *et al.* [6] for the $\vec{E}\perp\hat{c}$ polarization. The best fit to the data was achieved with the following parameters: $\omega_{TO}^{A2u} = 770\ cm^{-1}$, $4\pi\rho^{A2u} = 3.8 \times 10^4\ cm^{-2}$, $\Gamma^{A2u} = 18\ cm^{-1}$, $\omega_{TO}^{E1u} = 1383\ cm^{-1}$, $4\pi\rho^{E1u} = 7.5 \times 10^5\ cm^{-1}$, and $\Gamma^{E1u} = 30\ cm^{-1}$. Values for ϵ_∞ and ϵ_0 were not given in the paper, so a determination of the LO-mode energies from the data is not possible.

REFERENCES

1. J. H. Edgar, *in* "Properties of Group III Nitrides" (J. H. Edgar, ed.), p. 7. INSPEC, The Institute of Electrical Engineers, London, 1994.
2. P. J. Gielisse, S. S. Mitra, J. N. Plendl, R. D. Griffis, L. C. Mansur, R. Marshall, and E. A. Pascoe, *Phys. Rev.* **155**, 1039 (1967).
3. M. I. Eremets, M. Gauthier, A. Polian, J. C. Chervin, J. M. Besson, G. A. Dubitskii, and Y. Y. Semenova, *Phys. Rev. B* **52**, 8854 (1995).
4. O. S. Heavens, *Rep. Prog. Phys.* **23**, 1 (1960).
5. N. Miyata, K. Moriki, O. Mishima, M. Fujisawa, and T. Hattori, *Phys. Rev. B* **40**, 12028 (1989).
6. R. Geick, C. H. Perry, and G. Rupprecht, *Phys. Rev.* **146**, 543 (1966).
7. D. M. Hoffman, G. L. Doll, and P. C. Eklund, *Phys. Rev. B* **30**, 6052 (1984).
8. R. Mamy, J. Thomas, G. Jezequel, and J. C. Lemonnier, *J. Phys. (Paris) Lett.* **42**, 473 (1981).

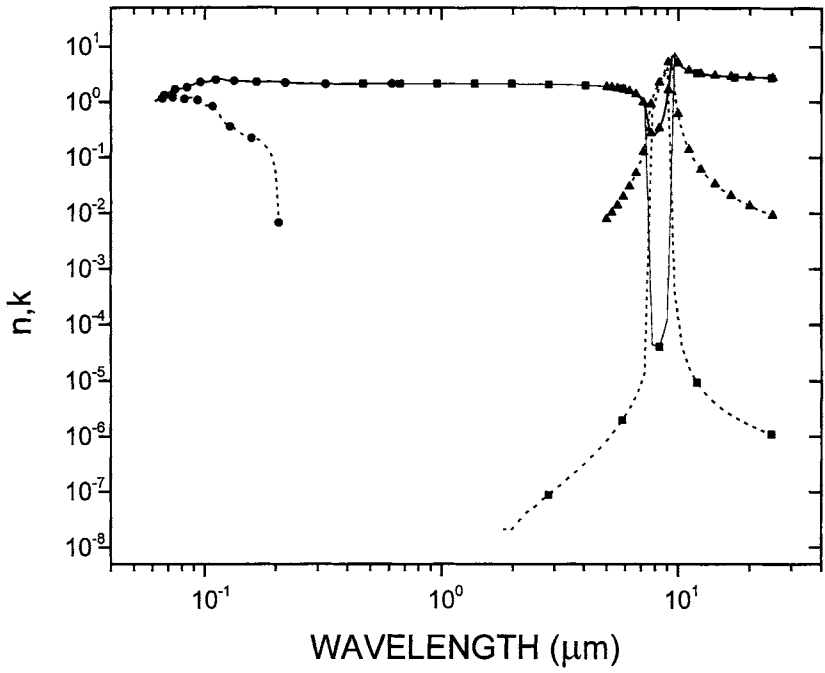

Fig. 1. Log–log plot of n (solid line) and k (dashed line) versus wavelength in micrometers for cBN. The data for n and k were derived from Gielisse *et al.* [2] (triangles), Eremets *et al.* [3] (squares), and Miyata *et al.* [5] (circles).

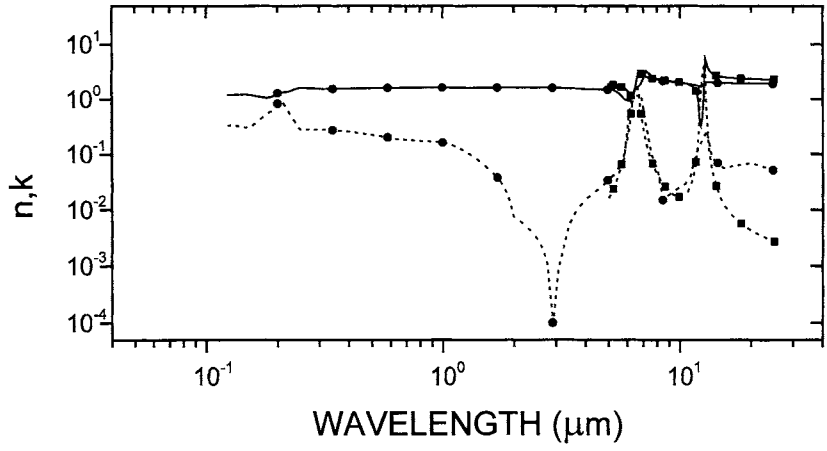

Fig. 2. Log–log plot of n (solid line) and k (dashed line) versus wavelength in micrometers for hBN obtained from $\vec{E} \perp \hat{c}$ polarization. The data for n and k were derived from Geick *et al.* [6] (squares) and Hoffman *et al.* [7] (circles).

TABLE I

Values of n and k for Cubic BN from Various References[a]

eV	cm^{-1}	μm	n	k
2.00E1	1.613E5	6.200E-2	1.0389 [5]	1.03E0 [5]
1.98E1	1.599E5	6.257E-2	1.0552	1.05E0
1.96E1	1.584E5	6.315E-2	1.0872	1.07E0
1.95E1	1.569E5	6.374E-2	1.1212	1.09E0
1.93E1	1.555E5	6.434E-2	1.1534	1.10E0
1.91E1	1.540E5	6.495E-2	1.1830	1.12E0
1.89E1	1.525E5	6.558E-2	1.2125	1.13E0
1.87E1	1.511E5	6.621E-2	1.2421	1.15E0
1.85E1	1.496E5	6.686E-2	1.2735	1.16E0
1.84E1	1.481E5	6.752E-2	1.3081	1.17E0
1.82E1	1.467E5	6.820E-2	1.3427	1.17E0
1.80E1	1.452E5	6.889E-2	1.3773	1.18E0
1.78E1	1.437E5	6.959E-2	1.4112	1.19E0
1.76E1	1.423E5	7.031E-2	1.4433	1.20E0
1.75E1	1.408E5	7.104E-2	1.4776	1.20E0
1.73E1	1.393E5	7.179E-2	1.5162	1.20E0
1.71E1	1.379E5	7.255E-2	1.5547	1.20E0
1.69E1	1.364E5	7.333E-2	1.5935	1.20E0
1.67E1	1.349E5	7.413E-2	1.6344	1.20E0
1.65E1	1.335E5	7.495E-2	1.6713	1.17E0
1.64E1	1.320E5	7.578E-2	1.6835	1.14E0
1.62E1	1.305E5	7.663E-2	1.6957	1.11E0
1.60E1	1.291E5	7.750E-2	1.7079	1.10E0
1.58E1	1.276E5	7.839E-2	1.7154	1.08E0
1.56E1	1.261E5	7.930E-2	1.7178	1.07E0
1.55E1	1.247E5	8.024E-2	1.7249	1.09E0
1.53E1	1.232E5	8.119E-2	1.7388	1.10E0
1.51E1	1.217E5	8.217E-2	1.7560	1.11E0
1.49E1	1.203E5	8.317E-2	1.7780	1.13E0
1.47E1	1.188E5	8.420E-2	1.8105	1.14E0
1.45E1	1.173E5	8.525E-2	1.8516	1.15E0
1.44E1	1.159E5	8.633E-2	1.8959	1.16E0
1.42E1	1.144E5	8.744E-2	1.9390	1.18E0
1.40E1	1.129E5	8.857E-2	1.9822	1.16E0
1.38E1	1.115E5	8.974E-2	2.0369	1.15E0
1.36E1	1.100E5	9.093E-2	2.0906	1.13E0
1.35E1	1.085E5	9.216E-2	2.1344	1.11E0
1.33E1	1.071E5	9.342E-2	2.1804	1.07E0
1.31E1	1.056E5	9.472E-2	2.2249	1.03E0
1.29E1	1.041E5	9.606E-2	2.2513	9.82E-1
1.27E1	1.027E5	9.743E-2	2.2628	9.35E-1
1.25E1	1.012E5	9.884E-2	2.2689	8.93E-1
1.24E1	9.973E4	1.003E-1	2.2648	8.60E-1
1.22E1	9.826E4	1.018E-1	2.2604	8.36E-1
1.20E1	9.679E4	1.033E-1	2.2583	8.45E-1
1.18E1	9.533E4	1.049E-1	2.2822	8.55E-1

(continued)

[a] The references from which the values were taken are given in brackets.

TABLE I *(Continued)*

Cubic BN

eV	cm^{-1}	μm	n	k
1.16E1	9.386E4	1.066E-1	2.3384	8.65E-1
1.15E1	9.239E4	1.083E-1	2.4265	8.28E-1
1.13E1	9.093E4	1.100E-1	2.4467	7.62E-1
1.11E1	8.946E4	1.118E-1	2.4702	7.19E-1
1.09E1	8.799E4	1.137E-1	2.5046	6.76E-1
1.07E1	8.653E4	1.156E-1	2.5368	5.94E-1
1.05E1	8.506E4	1.176E-1	2.5357	5.13E-1
1.04E1	8.359E4	1.197E-1	2.5046	4.38E-1
1.02E1	8.213E4	1.218E-1	2.4598	4.15E-1
1.00E1	8.066E4	1.240E-1	2.4147	3.92E-1
9.82E0	7.919E4	1.263E-1	2.3900	3.69E-1
9.64E0	7.773E4	1.287E-1	2.3733	3.57E-1
9.45E0	7.626E4	1.312E-1	2.3647	3.45E-1
9.27E0	7.479E4	1.337E-1	2.3561	3.30E-1
9.09E0	7.333E4	1.364E-1	2.3470	3.11E-1
8.91E0	7.186E4	1.392E-1	2.3362	2.91E-1
8.73E0	7.039E4	1.421E-1	2.3268	2.70E-1
8.55E0	6.893E4	1.451E-1	2.3204	2.56E-1
8.36E0	6.746E4	1.483E-1	2.3086	2.44E-1
8.18E0	6.599E4	1.516E-1	2.2960	2.32E-1
8.00E0	6.453E4	1.550E-1	2.2835	2.26E-1
7.82E0	6.306E4	1.586E-1	2.2749	2.20E-1
7.64E0	6.159E4	1.624E-1	2.2690	2.14E-1
7.45E0	6.013E4	1.663E-1	2.2687	2.08E-1
7.27E0	5.866E4	1.705E-1	2.2733	2.03E-1
7.09E0	5.720E4	1.749E-1	2.2766	1.86E-1
6.91E0	5.573E4	1.795E-1	2.2762	1.65E-1
6.73E0	5.426E4	1.843E-1	2.2782	1.45E-1
6.55E0	5.280E4	1.894E-1	2.2919	1.24E-1
6.36E0	5.133E4	1.949E-1	2.3032	9.62E-2
6.18E0	4.986E4	2.006E-1	2.2913	5.15E-2
6.00E0	4.840E4	2.067E-1	2.2692	6.72E-3
5.82E0	4.693E4	2.131E-1	2.2160	
5.64E0	4.546E4	2.200E-1	2.1981	
5.45E0	4.400E4	2.273E-1	2.1912	
5.27E0	4.253E4	2.352E-1	2.1752	
5.09E0	4.106E4	2.436E-1	2.1471	
4.91E0	3.960E4	2.526E-1	2.1286	
4.73E0	3.813E4	2.623E-1	2.1258	
4.55E0	3.666E4	2.728E-1	2.1186	
4.36E0	3.520E4	2.842E-1	2.1148	
4.18E0	3.373E4	2.965E-1	2.1073	
4.00E0	3.226E4	3.100E-1	2.0969	
3.82E0	3.080E4	3.248E-1	2.0909	
3.64E0	2.933E4	3.410E-1	2.0852	
3.55E0	2.862E4	3.490E-1	2.1111 [3]	
3.45E0	2.786E4	3.590E-1	2.0791 [5]	

TABLE I *(Continued)*

Cubic BN

eV	cm^{-1}	μm	n	k
3.30E0	2.663E4	3.760E-1	2.1110 [3]	
3.27E0	2.640E4	3.789E-1	2.0744 [5]	
3.09E0	2.493E4	4.012E-1	2.0794	
3.07E0	2.477E4	4.040E-1	2.1109 [3]	
2.91E0	2.346E4	4.263E-1	2.0815 [5]	
2.86E0	2.305E4	4.340E-1	2.1107 [3]	
2.73E0	2.200E4	4.547E-1	2.0837 [5]	
2.66E0	2.144E4	4.660E-1	2.1105 [3]	
2.55E0	2.053E4	4.871E-1	2.0935 [5]	
2.47E0	1.995E4	5.010E-1	2.1103 [3]	
2.36E0	1.907E4	5.246E-1	2.1021 [5]	
2.30E0	1.856E4	5.390E-1	2.1101 [3]	
2.18E0	1.760E4	5.683E-1	2.1109 [5]	
2.14E0	1.727E4	5.790E-1	2.1098 [3]	
2.00E0	1.613E4	6.200E-1	2.1231 [5]	
1.99E0	1.606E4	6.230E-1	2.1095 [3]	
1.85E0	1.494E4	6.690E-1	2.1091	
1.72E0	1.390E4	7.190E-1	2.1087	
1.60E0	1.293E4	7.730E-1	2.1082	
1.49E0	1.203E4	8.310E-1	2.1076	
1.39E0	1.120E4	8.930E-1	2.1069	
1.29E0	1.042E4	9.600E-1	2.1061	
1.20E0	9.690E3	1.032E0	2.1052	
1.12E0	9.015E3	1.109E0	2.1042	
1.04E0	8.387E3	1.193E0	2.1029	
9.67E-1	7.803E3	1.282E0	2.1015	
9.00E-1	7.259E3	1.378E0	2.0999	
8.37E-1	6.754E3	1.481E0	2.0979	
7.79E-1	6.283E3	1.592E0	2.0957	
7.25E-1	5.846E3	1.711E0	2.0931	
6.74E-1	5.438E3	1.839E0	2.0901 [3]	2.11E-8 [3]
6.27E-1	5.060E3	1.977E0	2.0865	2.11E-8
5.84E-1	4.707E3	2.125E0	2.0823	2.98E-8
5.43E-1	4.379E3	2.284E0	2.0774	4.21E-8
5.05E-1	4.074E3	2.455E0	2.0716	5.16E-8
4.70E-1	3.790E3	2.639E0	2.0647	6.99E-8
4.37E-1	3.526E3	2.836E0	2.0566	8.69E-8
4.07E-1	3.281E3	3.049E0	2.0468	1.13E-7
3.78E-1	3.052E3	3.277E0	2.0351	1.46E-7
3.52E-1	2.840E3	3.522E0	2.0210	1.90E-7
3.28E-1	2.642E3	3.786E0	2.0037	2.50E-7
3.05E-1	2.458E3	4.069E0	1.9825	3.33E-7
2.83E-1	2.287E3	4.374E0	1.9559	4.51E-7
2.64E-1	2.127E3	4.701E0	1.9222	6.21E-7
2.48E-1	2.000E3	5.001E0	2.8450 [2]	1.75E-2 [2]
2.47E-1	1.990E3	5.026E0	2.8440	1.74E-2
2.45E-1	1.980E3	5.051E0	2.8430	1.73E-2

(continued)

TABLE I *(Continued)*

Cubic BN

eV	cm^{-1}	μm	n	k
2.45E-1	1.979E3	5.053E0	1.8785 [3]	8.75E-7 [3]
2.44E-1	1.970E3	5.077E0	2.8420 [2]	1.72E-2 [2]
2.43E-1	1.960E3	5.103E0	2.8410	1.72E-2
2.42E-1	1.950E3	5.129E0	2.8400	1.71E-2
2.41E-1	1.940E3	5.156E0	2.8400	1.70E-2
2.39E-1	1.930E3	5.182E0	2.8390	1.69E-2
2.38E-1	1.920E3	5.209E0	2.8380	1.69E-2
2.37E-1	1.910E3	5.237E0	2.8370	1.68E-2
2.36E-1	1.900E3	5.264E0	2.8360	1.67E-2
2.34E-1	1.890E3	5.292E0	2.8350	1.67E-2
2.33E-1	1.880E3	5.320E0	2.8350	1.66E-2
2.32E-1	1.870E3	5.349E0	2.8340	1.65E-2
2.31E-1	1.860E3	5.377E0	2.8330	1.65E-2
2.29E-1	1.850E3	5.406E0	2.8320	1.64E-2
2.28E-1	1.841E3	5.432E0	1.8202 [3]	1.27E-6 [3]
2.28E-1	1.840E3	5.436E0	2.8310 [2]	1.63E-2 [2]
2.27E-1	1.830E3	5.465E0	2.8310	1.63E-2
2.26E-1	1.820E3	5.496E0	2.8300	1.62E-2
2.24E-1	1.810E3	5.526E0	2.8290	1.61E-2
2.23E-1	1.800E3	5.557E0	2.8280	1.61E-2
2.22E-1	1.790E3	5.588E0	2.8270	1.60E-2
2.21E-1	1.780E3	5.619E0	2.8270	1.59E-2
2.19E-1	1.770E3	5.651E0	2.8260	1.59E-2
2.18E-1	1.760E3	5.683E0	2.8250	1.58E-2
2.17E-1	1.750E3	5.715E0	2.8240	1.57E-2
2.16E-1	1.740E3	5.748E0	2.8240	1.57E-2
2.14E-1	1.730E3	5.781E0	2.8230	1.56E-2
2.13E-1	1.720E3	5.815E0	2.8220	1.55E-2
2.12E-1	1.713E3	5.839E0	1.7395 [3]	1.94E-6 [3]
2.12E-1	1.710E3	5.849E0	2.8210 [2]	1.55E-2 [2]
2.11E-1	1.700E3	5.883E0	2.8200	1.54E-2
2.10E-1	1.690E3	5.918E0	2.8200	1.53E-2
2.08E-1	1.680E3	5.953E0	2.8190	1.53E-2
2.07E-1	1.670E3	5.989E0	2.8180	1.52E-2
2.06E-1	1.660E3	6.025E0	2.8170	1.52E-2
2.05E-1	1.650E3	6.062E0	2.8170	1.51E-2
2.03E-1	1.640E3	6.099E0	2.8160	1.50E-2
2.02E-1	1.630E3	6.136E0	2.8150	1.50E-2
2.01E-1	1.620E3	6.174E0	2.8150	1.49E-2
2.00E-1	1.610E3	6.212E0	2.8140	1.49E-2
1.98E-1	1.600E3	6.251E0	2.8130	1.48E-2
1.98E-1	1.594E3	6.276E0	1.6215 [3]	3.16E-6 [3]
1.97E-1	1.590E3	6.290E0	2.8120 [2]	1.47E-2 [2]
1.96E-1	1.580E3	6.330E0	2.8120	1.47E-2
1.95E-1	1.570E3	6.371E0	2.8110	1.46E-2
1.93E-1	1.560E3	6.411E0	2.8100	1.46E-2
1.92E-1	1.550E3	6.453E0	2.8090	1.45E-2

TABLE I *(Continued)*

Cubic BN

eV	cm^{-1}	μm	n	k
1.91E-1	1.540E3	6.495E0	2.8090	1.44E-2
1.90E-1	1.530E3	6.537E0	2.8080	1.44E-2
1.88E-1	1.520E3	6.580E0	2.8070	1.43E-2
1.87E-1	1.510E3	6.624E0	2.8070	1.43E-2
1.86E-1	1.500E3	6.668E0	2.8060	1.42E-2
1.85E-1	1.490E3	6.713E0	2.8050	1.41E-2
1.84E-1	1.483E3	6.745E0	1.4327 [3]	5.75E-6 [3]
1.83E-1	1.480E3	6.758E0	2.8050 [2]	1.41E-2 [2]
1.82E-1	1.470E3	6.804E0	2.8040	1.40E-2
1.81E-1	1.460E3	6.851E0	2.8030	1.40E-2
1.80E-1	1.450E3	6.898E0	2.8020	1.39E-2
1.79E-1	1.440E3	6.946E0	2.8020	1.39E-2
1.77E-1	1.430E3	6.994E0	2.8010	1.38E-2
1.76E-1	1.420E3	7.044E0	2.8000	1.38E-2
1.75E-1	1.410E3	7.094E0	2.8000	1.37E-2
1.74E-1	1.400E3	7.144E0	2.7990	1.36E-2
1.72E-1	1.390E3	7.196E0	2.7980	1.36E-2
1.71E-1	1.380E3	7.248E0	2.7980	1.35E-2
1.71E-1	1.379E3	7.251E0	1.0721 [3]	1.35E-5 [3]
1.70E-1	1.370E3	7.301E0	2.7970 [2]	1.35E-2 [2]
1.69E-1	1.360E3	7.354E0	2.7960	1.34E-2
1.67E-1	1.350E3	7.409E0	2.7960	1.34E-2
1.66E-1	1.340E3	7.464E0	2.7950	1.33E-2
1.65E-1	1.330E3	7.520E0	2.7940	1.33E-2
1.64E-1	1.320E3	7.577E0	2.7940	1.32E-2
1.62E-1	1.310E3	7.635E0	2.7930	1.32E-2
1.61E-1	1.300E3	7.694E0	2.7920	1.31E-2
1.60E-1	1.290E3	7.753E0	2.7920	1.31E-2
1.59E-1	1.283E3	7.793E0		6.64E-1 [3]
1.59E-1	1.280E3	7.814E0	2.7910 [2]	1.30E-2 [2]
1.57E-1	1.270E3	7.875E0	2.7910	1.30E-2
1.56E-1	1.260E3	7.938E0	2.7900	1.29E-2
1.55E-1	1.250E3	8.001E0	2.7890	1.29E-2
1.54E-1	1.240E3	8.066E0	2.7890	1.28E-2
1.52E-1	1.230E3	8.132E0	2.7880	1.27E-2
1.51E-1	1.220E3	8.198E0	2.7870	1.27E-2
1.50E-1	1.210E3	8.266E0	2.7870	1.26E-2
1.49E-1	1.200E3	8.335E0	2.7860	1.26E-2
1.48E-1	1.194E3	8.377E0		1.98E0 [3]
1.48E-1	1.190E3	8.405E0	2.7860 [2]	1.25E-2 [2]
1.46E-1	1.180E3	8.476E0	2.7850	1.25E-2
1.45E-1	1.170E3	8.549E0	2.7840	1.24E-2
1.44E-1	1.160E3	8.622E0	2.7840	1.24E-2
1.43E-1	1.150E3	8.697E0	2.7830	1.23E-2
1.41E-1	1.140E3	8.774E0	2.7820	1.23E-2
1.40E-1	1.130E3	8.851E0	2.7820	1.23E-2
1.39E-1	1.120E3	8.930E0	2.7810	1.22E-2

(continued)

TABLE I *(Continued)*

Cubic BN

eV	cm^{-1}	μm	n	k
1.38E-1	1.111E3	9.004E0	0.0001 [3]	4.17E0 [3]
1.38E-1	1.110E3	9.011E0	2.7810 [2]	1.22E-2 [2]
1.36E-1	1.100E3	9.093E0	2.7800	1.21E-2
1.35E-1	1.090E3	9.176E0	2.7790	1.21E-2
1.34E-1	1.080E3	9.261E0	2.7790	1.20E-2
1.33E-1	1.070E3	9.348E0	2.7780	1.20E-2
1.31E-1	1.060E3	9.436E0	2.7780	1.19E-2
1.30E-1	1.050E3	9.526E0	2.7770	1.19E-2
1.29E-1	1.040E3	9.617E0	2.7770	1.18E-2
1.28E-1	1.033E3	9.678E0	7.7797 [3]	4.00E-4 [3]
1.28E-1	1.030E3	9.711E0	2.7760 [2]	1.18E-2 [2]
1.26E-1	1.020E3	9.806E0	2.7750	1.17E-2
1.25E-1	1.010E3	9.903E0	2.7750	1.17E-2
1.24E-1	1.000E3	1.000E1	2.7740	1.16E-2
1.23E-1	9.900E2	1.010E1	2.7740	1.16E-2
1.21E-1	9.800E2	1.021E1	2.7730	1.15E-2
1.20E-1	9.700E2	1.031E1	2.7720	1.15E-2
1.19E-1	9.615E2	1.040E1	4.2651 [3]	4.07E-5 [3]
1.19E-1	9.600E2	1.042E1	2.7720 [2]	1.15E-2 [2]
1.18E-1	9.500E2	1.053E1	2.7710	1.14E-2
1.17E-1	9.400E2	1.064E1	2.7710	1.14E-2
1.15E-1	9.300E2	1.076E1	2.7700	1.13E-2
1.14E-1	9.200E2	1.087E1	2.7700	1.13E-2
1.13E-1	9.100E2	1.099E1	2.7690	1.12E-2
1.12E-1	9.000E2	1.111E1	2.7690	1.12E-2
1.11E-1	8.945E2	1.118E1	3.5726 [3]	1.65E-5 [3]
1.10E-1	8.900E2	1.124E1	2.7680 [2]	1.11E-2 [2]
1.09E-1	8.800E2	1.137E1	2.7670	1.11E-2
1.08E-1	8.700E2	1.150E1	2.7670	1.11E-2
1.07E-1	8.600E2	1.163E1	2.7660	1.10E-2
1.05E-1	8.500E2	1.177E1	2.7660	1.10E-2
1.04E-1	8.400E2	1.191E1	2.7650	1.09E-2
1.03E-1	8.322E2	1.202E1	3.2627 [3]	9.35E-6 [3]
1.03E-1	8.300E2	1.205E1	2.7650 [2]	1.09E-2 [2]
1.02E-1	8.200E2	1.220E1	2.7640	1.08E-2
1.00E-1	8.100E2	1.235E1	2.7640	1.08E-2
9.92E-2	8.000E2	1.250E1	2.7630	1.08E-2
9.79E-2	7.900E2	1.266E1	2.7630	1.07E-2
9.67E-2	7.800E2	1.282E1	2.7620	1.07E-2
9.60E-2	7.742E2	1.292E1	3.0865 [3]	6.17E-6 [3]
9.55E-2	7.700E2	1.299E1	2.7620 [2]	1.06E-2 [2]
9.42E-2	7.600E2	1.316E1	2.7610	1.06E-2
9.30E-2	7.500E2	1.334E1	2.7610	1.05E-2
9.17E-2	7.400E2	1.352E1	2.7600	1.05E-2
9.05E-2	7.300E2	1.370E1	2.7600	1.05E-2
8.93E-2	7.203E2	1.389E1	2.9735 [3]	4.45E-6 [3]
8.93E-2	7.200E2	1.389E1	2.7590 [2]	1.04E-2 [2]

TABLE I *(Continued)*

Cubic BN

eV	cm^{-1}	μm	n	k
8.80E-2	7.100E2	1.409E1	2.7590	1.04E-2
8.68E-2	7.000E2	1.429E1	2.7580	1.03E-2
8.55E-2	6.900E2	1.450E1	2.7570	1.03E-2
8.43E-2	6.800E2	1.471E1	2.7570	1.03E-2
8.31E-2	6.701E2	1.493E1	2.8952 [3]	3.41E-6 [3]
8.31E-2	6.700E2	1.493E1	2.7560 [2]	1.02E-2 [2]
8.18E-2	6.600E2	1.515E1	2.7560	1.02E-2
8.06E-2	6.500E2	1.539E1	2.7550	1.01E-2
7.93E-2	6.400E2	1.563E1	2.7550	1.01E-2
7.81E-2	6.300E2	1.588E1	2.7540	1.01E-2
7.73E-2	6.234E2	1.604E1	2.8383 [3]	2.72E-6 [3]
7.69E-2	6.200E2	1.613E1	2.7540 [2]	1.00E-2 [2]
7.56E-2	6.100E2	1.640E1	2.7530	9.97E-3
7.44E-2	6.000E2	1.667E1	2.7530	9.93E-3
7.31E-2	5.900E2	1.695E1	2.7530	9.89E-3
7.19E-2	5.800E2	1.724E1	2.7954 [3]	2.24E-6 [3]
7.19E-2	5.800E2	1.725E1	2.7520 [2]	9.85E-3 [2]
7.07E-2	5.700E2	1.755E1	2.7520	9.81E-3
6.94E-2	5.600E2	1.786E1	2.7510	9.78E-3
6.82E-2	5.500E2	1.819E1	2.7510	9.74E-3
6.69E-2	5.400E2	1.852E1	2.7500	9.70E-3
6.69E-2	5.396E2	1.854E1	2.7623 [3]	1.88E-6 [3]
6.57E-2	5.300E2	1.887E1	2.7500 [2]	9.66E-3 [2]
6.45E-2	5.200E2	1.923E1	2.7490	9.62E-3
6.32E-2	5.100E2	1.961E1	2.7490	9.58E-3
6.22E-2	5.020E2	1.992E1	2.7361 [3]	1.61E-6 [3]
6.20E-2	5.000E2	2.000E1	2.7480 [2]	9.55E-3 [2]
6.07E-2	4.900E2	2.041E1	2.7480	9.51E-3
5.95E-2	4.800E2	2.084E1	2.7470	9.47E-3
5.83E-2	4.700E2	2.128E1	2.7470	9.43E-3
5.79E-2	4.670E2	2.142E1	2.7151 [3]	1.40E-6 [3]
5.70E-2	4.600E2	2.174E1	2.7460 [2]	9.40E-3 [2]
5.58E-2	4.500E2	2.223E1	2.7460	9.36E-3
5.45E-2	4.400E2	2.273E1	2.7450	9.32E-3
5.39E-2	4.345E2	2.302E1	2.6981 [3]	1.23E-6 [3]
5.33E-2	4.300E2	2.326E1	2.7450 [2]	9.28E-3 [2]
5.21E-2	4.200E2	2.381E1	2.7440	9.25E-3
5.08E-2	4.100E2	2.440E1	2.7440	9.21E-3
5.01E-2	4.043E2	2.474E1	2.6841 [3]	1.09E-6 [3]
4.96E-2	4.000E2	2.501E1	2.7440 [2]	9.17E-3 [2]

TABLE II

Values of n and k for Hexagonal BN from Various References[a]

eV	cm^{-1}	μm	n	k
1.000E1	8.066E4	1.240E-1	1.1905 [7]	3.3E-1 [7]
9.479E0	7.646E4	1.308E-1	1.1903	3.3E-1
8.985E0	7.248E4	1.380E-1	1.1949	3.2E-1
8.517E0	6.870E4	1.456E-1	1.2040	3.1E-1
8.074E0	6.512E4	1.536E-1	1.1799	3.0E-1
7.653E0	6.173E4	1.620E-1	1.1281	3.7E-1
7.255E0	5.852E4	1.709E-1	1.0819	4.4E-1
6.877E0	5.547E4	1.803E-1	1.0470	5.3E-1
6.518E0	5.258E4	1.902E-1	1.1054	6.2E-1
6.179E0	4.984E4	2.007E-1	1.2790	8.3E-1
5.857E0	4.724E4	2.117E-1	1.3301	8.4E-1
5.552E0	4.478E4	2.234E-1	1.3589	5.6E-1
5.263E0	4.245E4	2.356E-1	1.5082	4.0E-1
4.989E0	4.024E4	2.486E-1	1.5987	2.8E-1
4.729E0	3.814E4	2.622E-1	1.5810	2.8E-1
4.483E0	3.616E4	2.766E-1	1.5631	2.8E-1
4.249E0	3.427E4	2.918E-1	1.5450	2.8E-1
4.028E0	3.249E4	3.079E-1	1.5266	2.8E-1
3.818E0	3.079E4	3.248E-1	1.5193	2.7E-1
3.619E0	2.919E4	3.426E-1	1.5270	2.7E-1
3.430E0	2.767E4	3.615E-1	1.5346	2.6E-1
3.252E0	2.623E4	3.813E-1	1.5422	2.6E-1
3.082E0	2.486E4	4.023E-1	1.5496	2.5E-1
2.922E0	2.357E4	4.244E-1	1.5566	2.5E-1
2.770E0	2.234E4	4.477E-1	1.5637	2.4E-1
2.625E0	2.118E4	4.723E-1	1.5707	2.3E-1
2.489E0	2.007E4	4.983E-1	1.5778	2.2E-1
2.359E0	1.903E4	5.256E-1	1.5849	2.2E-1
2.236E0	1.804E4	5.545E-1	1.5920	2.1E-1
2.120E0	1.710E4	5.850E-1	1.5992	2.0E-1
2.009E0	1.621E4	6.172E-1	1.6049	1.9E-1
1.905E0	1.536E4	6.511E-1	1.6050	1.9E-1
1.805E0	1.456E4	6.868E-1	1.6056	1.8E-1
1.711E0	1.380E4	7.246E-1	1.6061	1.8E-1
1.622E0	1.308E4	7.644E-1	1.6067	1.8E-1
1.538E0	1.240E4	8.064E-1	1.6072	1.7E-1
1.458E0	1.176E4	8.507E-1	1.6078	1.7E-1
1.382E0	1.114E4	8.975E-1	1.6084	1.7E-1
1.310E0	1.056E4	9.468E-1	1.6090	1.7E-1
1.241E0	1.001E4	9.988E-1	1.6096	1.6E-1
1.177E0	9.492E3	1.054E0	1.6099	1.6E-1
1.116E0	8.998E3	1.112E0	1.6094	1.4E-1
1.057E0	8.529E3	1.173E0	1.6090	1.3E-1
1.002E0	8.085E3	1.237E0	1.6088	1.1E-1
9.501E-1	7.664E3	1.305E0	1.6087	9.9E-2
9.006E-1	7.265E3	1.377E0	1.6088	8.4E-2

[a] The references from which the values were taken are given in brackets.

TABLE II *(Continued)*

Hexagonal BN

eV	cm^{-1}	μm	n	k
8.537E-1	6.886E3	1.452E0	1.6093	6.9E-2
8.092E-1	6.527E3	1.532E0	1.6100	5.7E-2
7.671E-1	6.187E3	1.616E0	1.6109	4.7E-2
7.271E-1	5.865E3	1.705E0	1.6118	3.7E-2
6.893E-1	5.560E3	1.799E0	1.6128	2.7E-2
6.534E-1	5.270E3	1.898E0	1.6138	1.7E-2
6.193E-1	4.995E3	2.002E0	1.6149	7.4E-3
5.871E-1	4.735E3	2.112E0	1.6161	6.3E-3
5.565E-1	4.489E3	2.228E0	1.6173	5.3E-3
5.275E-1	4.255E3	2.351E0	1.6184	4.2E-3
5.000E-1	4.033E3	2.480E0	1.6196	3.2E-3
4.740E-1	3.823E3	2.616E0	1.6208	2.2E-3
4.493E-1	3.624E3	2.760E0	1.6142	1.1E-3
4.259E-1	3.435E3	2.912E0	1.6023	1.0E-4
4.037E-1	3.256E3	3.072E0	1.5904	8.6E-4
3.827E-1	3.087E3	3.240E0	1.5783	2.2E-3
3.627E-1	2.926E3	3.418E0	1.5661	5.4E-3
3.438E-1	2.773E3	3.606E0	1.5539	8.6E-3
3.259E-1	2.629E3	3.804E0	1.5415	1.2E-2
3.090E-1	2.492E3	4.013E0	1.5291	1.5E-2
2.929E-1	2.362E3	4.234E0	1.5166	1.8E-2
2.776E-1	2.239E3	4.467E0	1.5040	2.2E-2
2.632E-1	2.123E3	4.712E0	1.4913	2.6E-2
2.494E-1	2.012E3	4.971E0	1.4785	3.4E-2
2.480E-1	2.000E3	5.001E0	0.0337 [6]	8.3E-1 [6]
2.467E-1	1.990E3	5.026E0	0.0347	8.4E-1
2.455E-1	1.980E3	5.051E0	0.0358	8.5E-1
2.442E-1	1.970E3	5.077E0	0.0370	8.6E-1
2.430E-1	1.960E3	5.103E0	0.0382	8.7E-1
2.418E-1	1.950E3	5.129E0	0.0395	8.8E-1
2.405E-1	1.940E3	5.156E0	0.0409	8.9E-1
2.393E-1	1.930E3	5.182E0	0.0423	9.0E-1
2.380E-1	1.920E3	5.209E0	0.0439	9.2E-1
2.368E-1	1.910E3	5.237E0	0.0455	9.3E-1
2.365E-1	1.907E3	5.244E0	1.4657 [7]	4.1E-2 [7]
2.356E-1	1.900E3	5.264E0	0.0472 [6]	9.4E-1 [6]
2.343E-1	1.890E3	5.292E0	0.0491	9.5E-1
2.331E-1	1.880E3	5.320E0	0.0511	9.7E-1
2.318E-1	1.870E3	5.349E0	0.0532	9.8E-1
2.306E-1	1.860E3	5.377E0	0.0555	9.9E-1
2.294E-1	1.850E3	5.406E0	0.0579	1.0E0
2.281E-1	1.840E3	5.436E0	0.0605	1.0E0
2.269E-1	1.830E3	5.465E0	0.0633	1.0E0
2.256E-1	1.820E3	5.496E0	0.0663	1.1E0
2.244E-1	1.810E3	5.526E0	0.0696	1.1E0
2.241E-1	1.808E3	5.532E0	1.2721 [7]	5.6E-2 [7]
2.232E-1	1.800E3	5.557E0	0.0732 [6]	1.1E0 [6]

(continued)

TABLE II *(Continued)*

Hexagonal BN

eV	cm^{-1}	μm	n	k
2.219E-1	1.790E3	5.588E0	0.0771	1.1E0
2.207E-1	1.780E3	5.619E0	0.0813	1.1E0
2.194E-1	1.770E3	5.651E0	0.0860	1.2E0
2.182E-1	1.760E3	5.683E0	0.0911	1.2E0
2.170E-1	1.750E3	5.715E0	0.0967	1.2E0
2.157E-1	1.740E3	5.748E0	0.1029	1.2E0
2.145E-1	1.730E3	5.781E0	0.1098	1.2E0
2.132E-1	1.720E3	5.815E0	0.1175	1.3E0
2.125E-1	1.714E3	5.836E0	0.9780 [7]	8.3E-2 [7]
2.120E-1	1.710E3	5.849E0	0.1261 [6]	1.3E0 [6]
2.108E-1	1.700E3	5.883E0	0.1358	1.3E0
2.095E-1	1.690E3	5.918E0	0.1469	1.4E0
2.083E-1	1.680E3	5.953E0	0.1594	1.4E0
2.070E-1	1.670E3	5.989E0	0.1739	1.4E0
2.058E-1	1.660E3	6.025E0	0.1906	1.5E0
2.046E-1	1.650E3	6.062E0	0.2101	1.5E0
2.033E-1	1.640E3	6.099E0	0.2330	1.6E0
2.021E-1	1.630E3	6.136E0	0.2603	1.6E0
2.014E-1	1.624E3	6.157E0	0.9087 [7]	7.4E-1 [7]
2.008E-1	1.620E3	6.174E0	0.2930 [6]	1.7E0 [6]
1.996E-1	1.610E3	6.212E0	0.3329	1.8E0
1.984E-1	1.600E3	6.251E0	0.3821	1.8E0
1.971E-1	1.590E3	6.290E0	0.4437	1.9E0
1.959E-1	1.580E3	6.330E0	0.5220	2.0E0
1.946E-1	1.570E3	6.371E0	0.6230	2.1E0
1.934E-1	1.560E3	6.411E0	0.7549	2.2E0
1.922E-1	1.550E3	6.453E0	0.9284	2.3E0
1.909E-1	1.540E3	6.495E0	1.1541	2.4E0
1.909E-1	1.540E3	6.495E0	1.4838 [7]	1.1E0 [7]
1.897E-1	1.530E3	6.537E0	1.4357 [6]	2.4E0 [6]
1.884E-1	1.520E3	6.580E0	1.7536	2.3E0
1.872E-1	1.510E3	6.624E0	2.0515	2.1E0
1.860E-1	1.500E3	6.668E0	2.2592	1.8E0
1.847E-1	1.490E3	6.713E0	2.3459	1.5E0
1.835E-1	1.480E3	6.758E0	2.3346	1.2E0
1.822E-1	1.470E3	6.804E0	2.2666	9.6E-1
1.810E-1	1.460E3	6.851E0	2.1738	7.8E-1
1.810E-1	1.460E3	6.852E0	1.8762 [7]	1.2E0 [7]
1.798E-1	1.450E3	6.898E0	2.0746 [6]	6.5E-1 [6]
1.785E-1	1.440E3	6.946E0	1.9778	5.4E-1
1.773E-1	1.430E3	6.994E0	1.8871	4.6E-1
1.760E-1	1.420E3	7.044E0	1.8035	4.0E-1
1.748E-1	1.410E3	7.094E0	1.7270	3.5E-1
1.736E-1	1.400E3	7.144E0	1.6572	3.1E-1
1.723E-1	1.390E3	7.196E0	1.5934	2.7E-1
1.715E-1	1.384E3	7.229E0	3.2662 [7]	3.0E-1 [7]
1.711E-1	1.380E3	7.248E0	1.5348 [6]	2.4E-1 [6]

TABLE II *(Continued)*

Hexagonal BN

eV	cm^{-1}	μm	n	k
1.698E-1	1.370E3	7.301E0	1.4808	2.2E-1
1.686E-1	1.360E3	7.354E0	1.4310	2.0E-1
1.674E-1	1.350E3	7.409E0	1.3847	1.8E-1
1.661E-1	1.340E3	7.464E0	1.3415	1.7E-1
1.649E-1	1.330E3	7.520E0	1.3010	1.6E-1
1.636E-1	1.320E3	7.577E0	1.2629	1.5E-1
1.626E-1	1.311E3	7.626E0	2.5572 [7]	9.5E-2 [7]
1.624E-1	1.310E3	7.635E0	1.2270 [6]	1.4E-1 [6]
1.612E-1	1.300E3	7.694E0	1.1929	1.3E-1
1.599E-1	1.290E3	7.753E0	1.1604	1.2E-1
1.587E-1	1.280E3	7.814E0	1.1293	1.1E-1
1.575E-1	1.270E3	7.875E0	1.0995	1.1E-1
1.562E-1	1.260E3	7.938E0	1.0707	1.0E-1
1.550E-1	1.250E3	8.001E0	1.0429	9.7E-2
1.541E-1	1.243E3	8.045E0	2.3066 [7]	5.2E-2 [7]
1.537E-1	1.240E3	8.066E0	1.0159 [6]	9.2E-2 [6]
1.525E-1	1.230E3	8.132E0	0.9896	8.8E-2
1.513E-1	1.220E3	8.198E0	0.9637	8.5E-2
1.500E-1	1.210E3	8.266E0	0.9383	8.2E-2
1.488E-1	1.200E3	8.335E0	0.9133	7.9E-2
1.475E-1	1.190E3	8.405E0	0.8884	7.6E-2
1.463E-1	1.180E3	8.476E0	0.8636	7.4E-2
1.461E-1	1.178E3	8.487E0	2.1397 [7]	1.5E-2 [7]
1.451E-1	1.170E3	8.549E0	0.8387 [6]	7.2E-2 [6]
1.438E-1	1.160E3	8.622E0	0.8137	7.1E-2
1.426E-1	1.150E3	8.697E0	0.7883	6.9E-2
1.413E-1	1.140E3	8.774E0	0.7625	6.8E-2
1.401E-1	1.130E3	8.851E0	0.7361	6.7E-2
1.389E-1	1.120E3	8.930E0	0.7089	6.7E-2
1.385E-1	1.117E3	8.954E0	2.0910 [7]	1.8E-2 [7]
1.376E-1	1.110E3	9.011E0	0.6806 [6]	6.7E-2 [6]
1.364E-1	1.100E3	9.093E0	0.6510	6.7E-2
1.351E-1	1.090E3	9.176E0	0.6198	6.8E-2
1.339E-1	1.080E3	9.261E0	0.5865	6.9E-2
1.327E-1	1.070E3	9.348E0	0.5506	7.1E-2
1.314E-1	1.060E3	9.436E0	0.5115	7.4E-2
1.313E-1	1.059E3	9.446E0	2.0411 [7]	2.1E-2 [7]
1.302E-1	1.050E3	9.526E0	0.4680 [6]	7.9E-2 [6]
1.289E-1	1.040E3	9.617E0	0.4189	8.6E-2
1.277E-1	1.030E3	9.711E0	0.3619	9.8E-2
1.265E-1	1.020E3	9.806E0	0.2943	1.2E-1
1.252E-1	1.010E3	9.903E0	0.2159	1.6E-1
1.244E-1	1.004E3	9.965E0	1.9899 [7]	2.5E-2 [7]
1.240E-1	1.000E3	1.000E1	0.1460 [6]	2.3E-1 [6]
1.227E-1	9.900E2	1.010E1	0.1060	3.2E-1
1.215E-1	9.800E2	1.021E1	0.0848	4.0E-1
1.203E-1	9.700E2	1.031E1	0.0721	4.7E-1

(continued)

TABLE II *(Continued)*

Hexagonal BN

eV	cm^{-1}	μm	n	k
1.190E-1	9.600E2	1.042E1	0.0637	5.4E-1
1.180E-1	9.514E2	1.051E1	1.9374 [7]	2.9E-2 [7]
1.178E-1	9.500E2	1.053E1	0.0579 [6]	6.1E-1 [6]
1.165E-1	9.400E2	1.064E1	0.0539	6.8E-1
1.153E-1	9.300E2	1.075E1	0.0511	7.5E-1
1.141E-1	9.200E2	1.087E1	0.0494	8.2E-1
1.128E-1	9.100E2	1.099E1	0.0486	9.0E-1
1.118E-1	9.019E2	1.109E1	1.8669 [7]	3.8E-2 [7]
1.116E-1	9.000E2	1.111E1	0.0487 [6]	9.7E-1 [6]
1.103E-1	8.900E2	1.124E1	0.0499	1.1E0
1.091E-1	8.800E2	1.137E1	0.0521	1.2E0
1.079E-1	8.700E2	1.150E1	0.0559	1.3E0
1.066E-1	8.600E2	1.163E1	0.0616	1.4E0
1.060E-1	8.549E2	1.170E1	1.7817 [7]	9.8E-2 [7]
1.054E-1	8.500E2	1.177E1	0.0703 [6]	1.5E0 [6]
1.041E-1	8.400E2	1.191E1	0.0837	1.7E0
1.029E-1	8.300E2	1.205E1	0.1053	1.9E0
1.017E-1	8.200E2	1.220E1	0.1430	2.2E0
1.005E-1	8.104E2	1.234E1	1.6951 [7]	1.7E-1 [7]
1.004E-1	8.100E2	1.235E1	0.2187 [6]	2.6E0 [6]
9.918E-2	8.000E2	1.250E1	0.4147	3.3E0
9.794E-2	7.900E2	1.266E1	1.3238	4.8E0
9.670E-2	7.800E2	1.282E1	5.8255	2.9E0
9.546E-2	7.700E2	1.299E1	3.9641	5.7E-1
9.523E-2	7.682E2	1.302E1	2.0660 [7]	2.6E-1 [7]
9.422E-2	7.600E2	1.316E1	3.0979 [6]	2.5E-1 [6]
9.298E-2	7.500E2	1.334E1	2.6422	1.5E-1
9.174E-2	7.400E2	1.352E1	2.3552	9.9E-2
9.050E-2	7.300E2	1.370E1	2.1550	7.3E-2
9.027E-2	7.281E2	1.374E1	2.0118 [7]	8.3E-2 [7]
8.926E-2	7.200E2	1.389E1	2.0058 [6]	5.7E-2 [6]
8.802E-2	7.100E2	1.409E1	1.8895	4.6E-2
8.678E-2	7.000E2	1.429E1	1.7958	3.9E-2
8.557E-2	6.902E2	1.449E1	1.9709 [7]	6.9E-2 [7]
8.554E-2	6.900E2	1.450E1	1.7184 [6]	3.3E-2 [6]
8.430E-2	6.800E2	1.471E1	1.6532	2.9E-2
8.306E-2	6.700E2	1.493E1	1.5973	2.5E-2
8.182E-2	6.600E2	1.515E1	1.5489	2.3E-2
8.111E-2	6.543E2	1.529E1	1.9582 [7]	5.6E-2 [7]
8.059E-2	6.500E2	1.539E1	1.5063 [6]	2.1E-2 [6]
7.935E-2	6.400E2	1.563E1	1.4687	1.9E-2
7.811E-2	6.300E2	1.588E1	1.4350	1.7E-2
7.689E-2	6.202E2	1.613E1	1.9517 [7]	5.8E-2 [7]
7.687E-2	6.200E2	1.613E1	1.4048 [6]	1.6E-2 [6]
7.563E-2	6.100E2	1.640E1	1.3774	1.5E-2
7.439E-2	6.000E2	1.667E1	1.3525	1.4E-2
7.315E-2	5.900E2	1.695E1	1.3297	1.3E-2

TABLE II *(Continued)*

Hexagonal BN

eV	cm^{-1}	μm	n	k
7.288E-2	5.879E2	1.701E1	1.9451 [7]	6.1E-2 [7]
7.191E-2	5.800E2	1.724E1	1.3087 [6]	1.2E-2 [6]
7.067E-2	5.700E2	1.755E1	1.2895	1.2E-2
6.943E-2	5.600E2	1.786E1	1.2716	1.1E-2
6.909E-2	5.572E2	1.795E1	1.9385 [7]	6.3E-2 [7]
6.819E-2	5.500E2	1.819E1	1.2551 [6]	1.1E-2 [6]
6.695E-2	5.400E2	1.852E1	1.2396	1.0E-2
6.571E-2	5.300E2	1.887E1	1.2253	9.6E-3
6.549E-2	5.282E2	1.893E1	1.9319 [7]	6.6E-2 [7]
6.447E-2	5.200E2	1.923E1	1.2118 [6]	9.2E-3 [6]
6.323E-2	5.100E2	1.961E1	1.1992	8.8E-3
6.208E-2	5.007E2	1.998E1	1.9260 [7]	6.8E-2 [7]
6.199E-2	5.000E2	2.000E1	1.1874 [6]	8.4E-3 [6]
6.075E-2	4.900E2	2.041E1	1.1763	8.1E-3
5.951E-2	4.800E2	2.084E1	1.1658	7.7E-3
5.884E-2	4.746E2	2.107E1	1.9216 [7]	6.4E-2 [7]
5.827E-2	4.700E2	2.128E1	1.1559 [6]	7.4E-3 [6]
5.703E-2	4.600E2	2.174E1	1.1466	7.1E-3
5.579E-2	4.500E2	2.223E1	1.1377	6.9E-3
5.578E-2	4.499E2	2.223E1	1.9172 [7]	6.0E-2 [7]
5.455E-2	4.400E2	2.273E1	1.1294 [6]	6.6E-3 [6]
5.331E-2	4.300E2	2.326E1	1.1214	6.4E-3
5.287E-2	4.265E2	2.345E1	1.9128 [7]	5.6E-2 [7]
5.207E-2	4.200E2	2.381E1	1.1139 [6]	6.1E-3 [6]
5.083E-2	4.100E2	2.439E1	1.1068	5.9E-3
5.012E-2	4.043E2	2.474E1	1.9084 [7]	5.2E-2 [7]
4.959E-2	4.000E2	2.500E1	1.1000 [6]	5.7E-3 [6]
4.835E-2	3.900E2	2.565E1	1.0935	5.5E-3
4.711E-2	3.800E2	2.632E1	1.0874	5.3E-3
4.587E-2	3.700E2	2.703E1	1.0816	5.1E-3
4.463E-2	3.600E2	2.778E1	1.0760	4.9E-3
4.339E-2	3.500E2	2.858E1	1.0707	4.7E-3
4.215E-2	3.400E2	2.942E1	1.0657	4.5E-3
4.091E-2	3.300E2	3.031E1	1.0609	4.3E-3
3.967E-2	3.200E2	3.126E1	1.0563	4.2E-3
3.843E-2	3.100E2	3.226E1	1.0520	4.0E-3
3.719E-2	3.000E2	3.334E1	1.0479	3.9E-3

Cadmium Germanium Arsenide ($CdGeAs_2$)

J. C. RIFE*
Naval Research Laboratory
Washington, D.C.

$CdGeAs_2$ is a tetragonally bonded semiconductor with the chalcopyrite structure and a direct band gap of 0.57 eV at room temperature. The structure, growth, and optical and electronic properties of the chalcopyrite semiconductors have been reviewed in the book by Shay and Wernick [1]. Properties have also been summarized in the Landolt–Börnstein series [2]. The II–IV–V_2 chalcopyrite lattice is equivalent to the III–V semiconductor crystal structure, but with ordering of the II and IV components and so a doubling of the unit cell along the c-axis. The chalcopyrite lattice is typically compressed along the c-axis, leading to a crystalline electric field and birefringence with n_e ($\mathbf{E} \| \mathbf{c}$) > n_o ($\mathbf{E} \perp \mathbf{c}$) (positive uniaxial crystal). Chalcopyrite semiconductors are also optically active because of varying degrees of tetragonal distortion [3]. The $CdGeAs_2$ crystal structure, in particular, is compressed 5.6% along the c-axis. Studies of the crystalline and amorphous phases of $CdGeAs_2$ show that the amorphous phase has a density 2.5% higher [4]. The band structure of $CdGeAs_2$ has been discussed by several authors [5–7].

Since $CdGeAs_2$ has a large nonlinear coefficient due to its covalent bonding and can be phase-matched because of its birefringence, it is of great interest for second-harmonic generation. A 27% energy-conversion efficiency has been obtained in doubling the 10.6-μm CO_2 laser [8]. Fourth-harmonic generation has also been reported [9].

The optical constants, n and k, listed in Table I and plotted in Fig. 1 are derived from sources discussed in more detail later. The optical constants were taken from tables, calculated from formulae, or extracted from graphs where necessary. The table has more significant figures than justified by the

* The views presented are those of the author and do not represent the views of the Department of Defense or its components.

HANDBOOK OF OPTICAL CONSTANTS OF SOLIDS III ISBN 0-12-544423-0/$25.00.

extraction in some cases; consult the original work for the actual experimental resolution. Measurements made using polarized radiation were favored for inclusion here; in such cases, the optical constants have been given for both $\mathbf{E} \| \mathbf{c}$ and $\mathbf{E} \perp \mathbf{c}$. All measurements used were made on single crystals at room temperature, except where noted in the text. The discussion of measurements below gives references to additional work on polycrystalline or amorphous specimens.

I X-RAY TO BAND-GAP ABSORPTION EDGE

The optical constants, n and k, for the range from 10,000 to 11 eV have been calculated from the scattering factors of the elements of Henke *et al.* [10] using the compound formula and a density of 5.58 gm/cm^3 [4]. In Fig. 1, the K-edge ($1s$) transitions of As and Ge appear at 1.0 and 1.1×10^{-4} μm; the $L_{2,3}$ ($2p$) transitions of Cd at 3.3×10^{-4} μm and those of As and Ge near 1×10^{-3} μm; and the $M_{4,5}$ ($3d$) transitions of Cd at 3.0×10^{-3} μm. The calculated edges are a good approximation on the scale of Fig. 1, but the scatttering factors of the elements cannot predict the compound edge locations or structure to high degree (edge within 5 or 10 eV) because of core-level chemical shifts and bonding-dependent redistribution of the absorption at and just above the edges.

Optical constants for the 11- to 1-eV range have been taken from Goryunova *et al.* [11]. They extracted optical constants for single-crystal and amorphous samples from a Kramers-Kronig analysis of unpolarized, room-temperature reflectance data. Zlatkin *et al.* subsequently made polarized reflectance measurements from 5.5 to 1.5 eV at 195 and 100 K that showed relatively small but significant polarization-dependent structure, but they reported no optical constants [12]. Artus *et al.* made unpolarized reflectance measurements from 25 to 1.2 eV, but derived no optical constants [13]. Their data are similar to previous room-temperature results, but with more structure at lower energy, and show a smooth fall-off above 8 eV in contrast to the results of Goryunova *et al.*

II BAND-GAP ABSORPTION EDGE

Measurements of the absorption coefficient at the absorption edge have been reported by a number of authors. Isomura *et al.* give the absorption coefficient ($\alpha = 4\pi k/\lambda$) for $\mathbf{E} \| \mathbf{c}$ and $\mathbf{E} \perp \mathbf{c}$ from 0.73 to 0.5 eV and derive values of the energy gap in good agreement with those obtained using elec-

troreflectance [14]. Hong *et al.* give the absorption coefficient from 0.8 to 0.123 eV for polycrystalline and amorphous specimens [15]. Madelon *et al.* present the near-edge absorption coefficient for four temperatures from 4.2 to 260 K [16]. Bendorius *et al.* give the pressure dependence of the edge [17]. Several other absorption edge measurements of the amorphous state have also been reported [18, 19].

BAND GAP III

In the transparent gap region from the energy gap at 2.2 to 18 μm where the two-phonon lattice absorption sets in, the index of refraction for $\mathbf{E} \| \mathbf{c}$ and $\mathbf{E} \perp \mathbf{c}$ has been reported by Boyd *et al.* [20]. They determined the index by the minimum-deviation method; however, results for other individual crystals could vary slightly from their results, depending on doping. Their data have been reduced to an analog formula by Wemple *et al.* [21] and by Bhar [22]. The latter finds a good fit to a special Sellmeier form,

$$n^2 = A + \frac{B}{1 - \dfrac{C}{\lambda^2}} + \frac{D}{1 - \dfrac{E}{\lambda^2}},$$

where for n_o $(A,B,C,D,E) = (10.1064, 2.2988, 1.0872, 1.6247, 1370)$ and for n_e $(A,B,C,D,E) = (11.8018, 1.2152, 2.6971, 1.6922, 1370)$; λ is the wavelength in microns.

Absorption in the gap region is sensitive to impurities and doping. Iseler *et al.* [8] observe, for *p*-type doped crystals, a residual shoulder on the intrinsic absorption edge for wavelengths up to 5.5 μm, an absorption band near 5.5 μm due to valence-band hole transitions in the *p*-type material that disappears in going from temperatures of 300 to 77 K, and three-phonon absorption at 13.5 μm. Absorption in *n*-type crystals is a minimum at the band edge and rises from there because of free-electron intraband transitions [7]. The shoulder at 5.5 μm could present a difficulty for second-harmonic generation. In that regard, Barnes *et al.* [23] measured the temperature dependence of the absorption coefficient at 10.6 μm and the index of refraction at 5.6 μm; however, their absorption coefficient was an order of magnitude larger than that determined by Iseler *et al.* Mamedov and Osmanov [24] also observed the temperature dependence in *p*-type samples and an impurity absorption at 9.5 μm. Boyd *et al.* [20] measured the gap absorption as well, but their measurements were limited on the low-absorption side by sample size.

IV LATTICE ABSORPTION IN THE INFRARED

Transmission in the two-phonon lattice absorption region from 13 to 25 μm was measured by Boltovets *et al.* [25], but the absorption coefficient is not given. The optical constants for $\mathbf{E} \| \mathbf{c}$ and $\mathbf{E} \perp \mathbf{c}$ in the one-phonon region from 20 to 200 μm were derived by dispersion analysis from polarized reflectivity measurements by Holah *et al.* [26]. With j harmonic oscillators, the formula for the dielectric constant $\epsilon(\nu)$ is

$$\epsilon(\nu) = \epsilon_\infty + \sum_j \frac{S_j \nu^2{}_j}{(\nu^2{}_j - \nu^2 - i\nu\gamma_j},$$

where S_j is the oscillator strength, ν_j the frequency in cm^{-1}, and γ_j the damping of the jth oscillator in cm^{-1}. For $\mathbf{E} \| \mathbf{c}$, Holah *et al.* derive the two oscillators $(S_j, \nu_j, \gamma_j) = (1.06, 270, 5.6)$ and $(1.40, 203, 7.6)$ with $\epsilon_\infty = 15.4$; and for $\mathbf{E} \perp \mathbf{c}$, they give the five oscillators $(S_j, \nu_j, \gamma_j) = (1.07, 272, 4.0)$, $(0.10, 255, 4.5)$, $(1.12, 200, 12.7)$, $(0.39, 159, 4.5)$, and $(0.28, 95, 5.0)$ with $\epsilon_\infty = 15.2$. The analysis yields an ϵ_0 of 17.9 for $\mathbf{E} \| \mathbf{c}$ and 18.2 for $\mathbf{E} \perp \mathbf{c}$. Their data are given in the graph and table. Zlatkin *et al.* [27] and Goryunova *et al.* [11] previously had measured the lattice reflectivity with unpolarized light and derived the optical constants from 20 to 80 μm for single-crystal and amorphous specimens. They obtained a ϵ_∞ of 14.3 and a ϵ_0 of 18.7. More recently, Hong *et al.* reported the optical constants from unpolarized reflectance and transmission measurements from 18 to 200 μm for polycrystalline and amorphous samples [15]. The phonon frequencies have been calculated for $CdGeAs_2$ by Antropova *et al.* [28].

REFERENCES

1. J. L. Shay and J. H. Wernick, "Ternary Chalcopyrite Semiconductors: Growth, Electronic Properties, and Applications." Pergamon, New York, 1975.
2. Landolt-Börnstein, "Semiconductors—Physics of Ternary Compounds" (K.-H. Hellwege and O. Madelung, eds.), Vol. 17h. Springer-Verlag, New York, 1985.
3. G. A. Babonas, A. S. Martsinkyavichyus, and A. Yu. Shileika, *Sov. Phys. J.* **29**, 617 (1986).
4. L. Červinka, R. Hosemann, and W. Vogel, *J. Non-Cryst. Solids* **3**, 294 (1970).
5. N. A. Goryunova, A. S. Poplavnoi, Yu. I. Polygalov, and V. A. Chaldyshev, *Phys. Status Solidi* **39 B**, 9 (1970).
6. J. L. Shay and E. Buehler, *Phys. Rev. B* **3**, 2598 (1971).
7. H. Kidal, *Phys. Rev. B* **10**, 5082 (1974).
8. G. W. Iseler, H. Kildal, and N. Menyuk, *J. Electron Mater.* **7**, 737 (1978).
9. H. Kildal and G. W. Iseler, *Phys. Rev. B* **19**, 5218 (1979).
10. B. L. Henke, P. Lee, T. J. Tanaka, R. L. Shimabukuro, and B. J. Fujikawa, *At. Data Nucl. Data Tables* **27** (1982); B. L. Henke, J. C. Davis, E. M. Gullikson, and R. C. C. Perera, *Lawrence Berkeley Laboratory Report* **LBL-26259** (1988).
11. N. A. Goryunova, E. F. Gross, L. B. Zlatkin, and E. K. Ivanov, *J. Non-Cryst. Solids* **4**, 57 (1970).

12. L. B. Zlatkin, E. K. Ivanov, G. F. Karavaev, and V. A. Chaldyshev, *Sov. Phys. Semicond. (Engl. Transl.)* **5**, 1794 (1972).
13. L. Artus, Y. Bertand, C. Ance, and A. Lopez-Soler, *Solid State Commun.* **57**, 649 (1986).
14. S. Isomura, S. Takahashi, and K. Masumoto, *Jpn. J. Appl. Phys.* **16,** 1723 (1977).
15. K. S. Hong, R. F. Speyer, and R. A. Condrate, Sr., *J. Phys. Chem. Solids* **51**, 969 (1990).
16. R. Madelon, M. Shaimi, A. Hairie, E. Paumier, and B. Mercey, *Solid State Commun.* **50**, 545 (1984).
17. R. Bendorius, V. D. Prochukhan, and A. Šileika, *Phys. Status Solidi B* **53,** 745 (1972).
18. V. Vorlíček, *Phys. Status Solidi B* **67**, 731 (1975).
19. V. D. Okunev and A.G. Yurov, *Sov. Tech. Phys. Lett.* **5**(2), 64 (1979).
20. G. D. Boyd, E. Buehler, F. G. Storz, and J. H. Wernick, *IEEE J. Quantum Electron.* **QE-8**, 419 (1972).
21. S. H. Wemple, J. D. Gabbe, and G. D. Boyd, *J. Appl. Phys.* **46,** 3597 (1975).
22. G. C. Bhar, *Appl. Opt.* **15**, 305 (1976).
23. N. P. Barnes, R. C. Eckhardt, D. J. Gettemy, and L. B. Edgett, *IEEE J. Quantum Electron.* **QE-15**, 1074 (1979).
24. B. Kh. Mamedov and É. O. Osmanov, *Sov. Phys. Semicond. (Engl. Transl.)* **5**, 1120 (1972).
25. N. S. Boltovets, B. Kh. Mamedov, and É. O. Osmanov, *Sov. Phys. Semicond. (Engl. Transl.)* **4**, 499 (1970).
26. G. D. Holah, A. Miller, W. D. Dunnett, and G. W. Iseler, *Solid State Commun.* **23**, 75 (1977).
27. L. B. Zlatkin, Yu. F. Markov, A. I. Stekhanov, and M. S. Shur, *J. Phys. Chem. Solids* **31**, 567 (1970).
28. E. V. Antropova, A. A. Kopytov, and A. S. Poplavnoi, *Opt. Spectrosc.* **64**, 766 (1988).

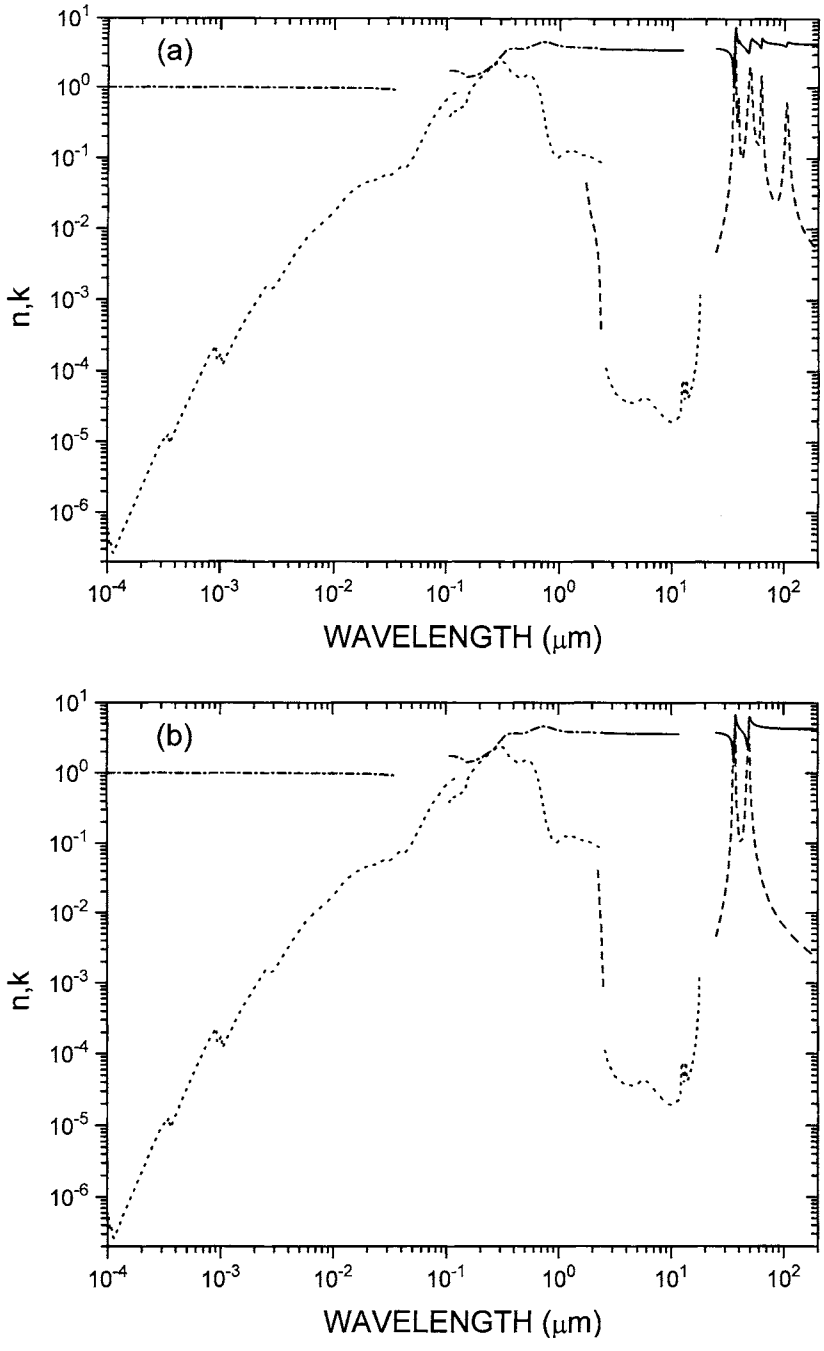

Fig. 1. (a) Log–log plot of n_o (solid line) and k_o (dashed line), $\mathbf{E} \perp \mathbf{c}$, versus wavelength for $CdGeAs_2$. (b) Log–log plot of n_e (solid line) and k_e (dashed line), $\mathbf{E} \parallel \mathbf{c}$, versus wavelength for $CdGeAs_2$. Unpolarized n (dash-dot line) and k (dotted line) are plotted on both graphs, where polarized data was not available.

TABLE I

Values of n and k for $CdGeAs_2$ Obtained from Various References[a]

eV	cm^{-1}	μm	1-n	k
			[10]	[10]
3.000E4	2.420E8	4.133E-5	1.13E-6	4.01E-8
2.010E4	1.622E8	6.167E-5	2.50E-6	9.51E-8
1.277E4	1.030E8	9.708E-5	6.02E-6	5.06E-7
1.243E4	1.003E8	9.971E-5	6.26E-6	5.57E-7
1.211E4	9.766E7	1.024E-4	6.50E-6	6.13E-7
1.179E4	9.506E7	1.052E-4	6.68E-6	3.44E-7
1.148E4	9.259E7	1.080E-4	7.21E-6	3.79E-7
1.118E4	9.017E7	1.109E-4	7.57E-6	2.81E-7
1.088E4	8.772E7	1.140E-4	8.11E-6	2.61E-7
1.060E4	8.547E7	1.170E-4	8.64E-6	2.89E-7
1.005E4	8.104E7	1.234E-4	9.66E-6	3.56E-7
8.114E3	6.545E7	1.528E-4	1.51E-5	8.02E-7
6.048E3	4.878E7	2.050E-4	2.73E-5	2.38E-6
4.053E3	3.269E7	3.059E-4	5.79E-5	1.02E-5
3.843E3	3.100E7	3.226E-4	6.38E-5	1.13E-5
3.741E3	3.018E7	3.314E-4	6.62E-5	1.25E-5
3.643E3	2.939E7	3.403E-4	6.93E-5	1.17E-5
3.548E3	2.861E7	3.495E-4	7.06E-5	1.29E-5
3.454E3	2.786E7	3.590E-4	7.74E-5	9.24E-6
3.363E3	2.712E7	3.687E-4	8.30E-5	1.02E-5
3.274E3	2.641E7	3.787E-4	8.83E-5	1.13E-5
3.023E3	2.438E7	4.102E-4	1.05E-4	1.53E-5
2.025E3	1.633E7	6.122E-4	2.29E-4	6.49E-5
1.510E3	1.218E7	8.210E-4	3.43E-4	1.64E-4
1.432E3	1.155E7	8.661E-4	3.66E-4	1.94E-4
1.394E3	1.124E7	8.895E-4	3.68E-4	2.10E-4
1.357E3	1.095E7	9.135E-4	3.56E-4	2.28E-4
1.321E3	1.066E7	9.383E-4	2.90E-4	1.38E-4
1.287E3	1.038E7	9.637E-4	3.76E-4	1.50E-4
1.253E3	1.010E7	9.897E-4	4.05E-4	1.62E-4
1.220E3	9.843E6	1.016E-3	4.07E-4	1.76E-4
1.188E3	9.579E6	1.044E-3	4.64E-4	1.20E-4
1.157E3	9.328E6	1.072E-3	5.13E-4	1.31E-4
1.012E3	8.163E6	1.225E-3	7.16E-4	2.04E-4
9.096E2	7.337E6	1.363E-3	8.92E-4	2.88E-4
7.958E2	6.418E6	1.558E-3	1.14E-3	4.36E-4
6.096E2	4.916E6	2.034E-3	1.75E-3	8.70E-4
4.922E2	3.970E6	2.519E-3	2.24E-3	1.52E-3
4.666E2	3.764E6	2.657E-3	2.24E-3	1.48E-3
4.543E2	3.664E6	2.729E-3	2.36E-3	1.44E-3
4.425E2	3.569E6	2.802E-3	2.51E-3	1.43E-3
4.308E2	3.475E6	2.878E-3	2.69E-3	1.44E-3
4.194E2	3.383E6	2.956E-3	2.88E-3	1.47E-3
4.084E2	3.294E6	3.036E-3	3.11E-3	1.52E-3
3.480E2	2.807E6	3.563E-3	4.35E-3	2.31E-3

(continued)

[a] References given in brackets.

TABLE I *(Continued)*

$CdGeAs_2$

eV	cm^{-1}	μm	1-n	k
			[10]	[10]
1.987E2	1.602E6	6.241E-3	9.12E-3	8.53E-3
1.521E2	1.227E6	8.150E-3	1.23E-2	1.27E-2
1.020E2	8.224E5	1.216E-2	2.16E-2	2.59E-2
4.959E1	4.000E5	2.500E-2	4.04E-2	5.14E-2
3.067E1	2.474E5	4.042E-2	1.11E-1	7.45E-2
2.001E1	1.614E5	6.195E-2		1.93E-1
1.492E1	1.204E5	8.308E-2		4.48E-1
9.999E0	8.065E4	1.240E-1		8.76E-1
eV	cm^{-1}	μm	n	k
			[11]	[11]
1.140E1	9.191E4	1.088E-1	1.75E0	4.03E-1
1.120E1	9.033E4	1.107E-1	1.74E0	4.30E-1
1.100E1	8.873E4	1.127E-1	1.74E0	4.16E-1
1.080E1	8.711E4	1.148E-1	1.72E0	4.28E-1
1.060E1	8.547E4	1.170E-1	1.71E0	4.41E-1
1.040E1	8.389E4	1.192E-1	1.71E0	4.54E-1
1.020E1	8.224E4	1.216E-1	1.70E0	4.67E-1
9.999E0	8.065E4	1.240E-1	1.69E0	4.66E-1
9.801E0	7.905E4	1.265E-1	1.69E0	4.79E-1
9.596E0	7.740E4	1.292E-1	1.66E0	4.92E-1
9.400E0	7.582E4	1.319E-1	1.65E0	5.05E-1
9.198E0	7.418E4	1.348E-1	1.62E0	5.18E-1
8.997E0	7.257E4	1.378E-1	1.59E0	5.17E-1
8.800E0	7.097E4	1.409E-1	1.56E0	5.57E-1
8.598E0	6.935E4	1.442E-1	1.53E0	5.83E-1
8.400E0	6.775E4	1.476E-1	1.49E0	5.83E-1
8.200E0	6.614E4	1.512E-1	1.44E0	6.49E-1
7.999E0	6.452E4	1.550E-1	1.37E0	7.57E-1
7.798E0	6.289E4	1.590E-1	1.38E0	8.51E-1
7.602E0	6.131E4	1.631E-1	1.43E0	9.58E-1
7.402E0	5.970E4	1.675E-1	1.45E0	9.85E-1
7.200E0	5.807E4	1.722E-1	1.44E0	1.05E0
7.001E0	5.647E4	1.771E-1	1.47E0	1.12E0
6.801E0	5.485E4	1.823E-1	1.50E0	1.20E0
6.598E0	5.322E4	1.879E-1	1.54E0	1.27E0
6.401E0	5.163E4	1.937E-1	1.56E0	1.33E0
6.199E0	5.000E4	2.000E-1	1.62E0	1.40E0
6.001E0	4.840E4	2.066E-1	1.66E0	1.48E0
5.799E0	4.677E4	2.138E-1	1.70E0	1.56E0
5.600E0	4.517E4	2.214E-1	1.77E0	1.65E0
5.400E0	4.355E4	2.296E-1	1.83E0	1.74E0
5.201E0	4.195E4	2.384E-1	1.90E0	1.82E0
4.999E0	4.032E4	2.480E-1	2.01E0	1.94E0
4.800E0	3.871E4	2.583E-1	2.10E0	2.04E0

TABLE I *(Continued)*

$CdGeAs_2$

eV	cm^{-1}	μm	n	k		
			[11]	[11]		
4.601E0	3.711E4	2.695E-1	2.24E0	2.15E0		
4.400E0	3.549E4	2.818E-1	2.45E0	2.27E0		
4.200E0	3.388E4	2.952E-1	2.72E0	2.34E0		
4.000E0	3.226E4	3.100E-1	3.06E0	2.37E0		
3.800E0	3.065E4	3.263E-1	3.32E0	2.28E0		
3.600E0	2.904E4	3.444E-1	3.55E0	2.01E0		
3.400E0	2.742E4	3.647E-1	3.65E0	1.73E0		
3.200E0	2.581E4	3.875E-1	3.65E0	1.61E0		
3.000E0	2.420E4	4.133E-1	3.70E0	1.47E0		
2.800E0	2.258E4	4.428E-1	3.68E0	1.37E0		
2.600E0	2.097E4	4.769E-1	3.62E0	1.41E0		
2.400E0	1.936E4	5.166E-1	3.78E0	1.51E0		
2.200E0	1.774E4	5.636E-1	4.01E0	1.45E0		
2.000E0	1.613E4	6.199E-1	4.30E0	1.14E0		
1.800E0	1.452E4	6.888E-1	4.56E0	6.55E-1		
1.600E0	1.290E4	7.749E-1	4.57E0	2.08E-1		
1.400E0	1.129E4	8.856E-1	4.28E0	1.13E-1		
1.200E0	9.681E3	1.033E0	4.01E0	1.12E-1		
9.999E-1	8.065E3	1.240E0	3.87E0	1.25E-1		
7.999E-1	6.452E3	1.550E0	3.80E0	1.11E-1		
6.001E-1	4.840E3	2.066E0	3.77E0	9.67E-2		
eV	cm^{-1}	μm	n_o	k_o	n_e	k_e
				[14]		[14]
7.309E-1	5.895E3	1.696E0		6.42E-2		
7.235E-1	5.836E3	1.714E0		4.94E-2		
7.147E-1	5.764E3	1.735E0		4.14E-2		
7.060E-1	5.694E3	1.756E0		3.55E-2		
7.000E-1	5.646E3	1.771E0		3.08E-2		
6.913E-1	5.576E3	1.794E0		2.66E-2		
6.823E-1	5.503E3	1.817E0		2.39E-2		
6.768E-1	5.458E3	1.832E0		2.19E-2		
6.689E-1	5.395E3	1.854E0		1.93E-2		
6.618E-1	5.338E3	1.873E0		1.81E-2		
6.558E-1	5.289E3	1.891E0		1.70E-2		
6.468E-1	5.217E3	1.917E0		1.55E-2		
6.401E-1	5.163E3	1.937E0		1.43E-2		
6.343E-1	5.116E3	1.955E0		1.35E-2		
6.280E-1	5.065E3	1.974E0		1.28E-2		
6.225E-1	5.021E3	1.992E0		1.19E-2		
6.157E-1	4.966E3	2.014E0		1.13E-2		
6.096E-1	4.917E3	2.034E0		1.03E-2		
6.031E-1	4.864E3	2.056E0		9.64E-3		
5.983E-1	4.825E3	2.072E0		8.93E-3		
5.926E-1	4.779E3	2.092E0		8.12E-3		

(continued)

TABLE I *(Continued)*

$CdGeAs_2$

eV	cm^{-1}	μm	n_o	k_o	n_e	k_e
				[14]		[14]
5.867E-1	4.732E3	2.113E0		7.35E-3		
5.809E-1	4.685E3	2.134E0		6.70E-3		
5.759E-1	4.645E3	2.153E0		5.71E-3		
5.705E-1	4.601E3	2.173E0		4.92E-3		
5.651E-1	4.558E3	2.194E0				5.29E-2
5.644E-1	4.552E3	2.197E0		4.80E-3		
5.602E-1	4.518E3	2.213E0				4.79E-2
5.594E-1	4.512E3	2.216E0		4.18E-3		
5.558E-1	4.483E3	2.231E0				4.45E-2
5.558E-1	4.483E3	2.231E0		3.48E-3		
5.510E-1	4.444E3	2.250E0				4.06E-2
5.490E-1	4.428E3	2.258E0		2.61E-3		
5.456E-1	4.401E3	2.272E0				3.37E-2
5.451E-1	4.397E3	2.274E0		1.91E-3		
5.410E-1	4.363E3	2.292E0				2.71E-2
5.397E-1	4.353E3	2.297E0		1.28E-3		
5.358E-1	4.322E3	2.314E0				2.12E-2
5.344E-1	4.310E3	2.320E0		6.60E-4		
5.326E-1	4.296E3	2.328E0				1.60E-2
5.314E-1	4.286E3	2.333E0		4.00E-4		
5.272E-1	4.252E3	2.352E0				1.22E-2
5.227E-1	4.216E3	2.372E0				9.35E-3
5.180E-1	4.178E3	2.394E0				7.19E-3
5.141E-1	4.147E3	2.412E0				5.25E-3
5.103E-1	4.116E3	2.430E0				3.76E-3
5.059E-1	4.080E3	2.451E0				2.80E-3
5.007E-1	4.039E3	2.476E0				2.06E-3
4.961E-1	4.001E3	2.499E0				1.47E-3
4.926E-1	3.973E3	2.517E0				9.10E-4

eV	cm^{-1}	μm	n_o	k	n_e
			[20]	[8]	[20]
5.391E-1	4.348E3	2.300E0	3.608E0		
5.166E-1	4.167E3	2.400E0	3.597E0		3.755E0
4.959E-1	4.000E3	2.500E0	3.590E0		3.732E0
4.769E-1	3.846E3	2.600E0	3.582E0	1.10E-4	3.716E0
4.592E-1	3.704E3	2.700E0	3.577E0	8.62E-5	3.703E0
4.428E-1	3.571E3	2.800E0	3.572E0	7.49E-5	3.693E0
4.275E-1	3.448E3	2.900E0	3.568E0	6.47E-5	3.685E0
4.133E-1	3.333E3	3.000E0	3.565E0	5.85E-5	3.678E0
4.000E-1	3.226E3	3.100E0	3.562E0	5.20E-5	3.671E0
3.875E-1	3.125E3	3.200E0	3.558E0	4.85E-5	3.666E0
3.647E-1	2.941E3	3.400E0	3.554E0	4.35E-5	3.657E0
3.444E-1	2.778E3	3.600E0	3.550E0	4.09E-5	3.651E0
3.263E-1	2.632E3	3.800E0	3.547E0	3.87E-5	3.645E0

TABLE I *(Continued)*

$CdGeAs_2$

eV	cm^{-1}	μm	n_o	k	n_e
			[20]	[8]	[20]
3.100E-1	2.500E3	4.000E0	3.544E0	3.73E-5	3.640E0
2.952E-1	2.381E3	4.200E0	3.542E0	3.67E-5	3.637E0
2.818E-1	2.273E3	4.400E0	3.539E0	3.63E-5	3.633E0
2.695E-1	2.174E3	4.600E0	3.537E0	3.59E-5	3.630E0
2.583E-1	2.083E3	4.800E0	3.535E0	3.63E-5	3.627E0
2.480E-1	2.000E3	5.000E0	3.534E0	3.71E-5	3.625E0
2.254E-1	1.818E3	5.500E0	3.529E0	4.17E-5	3.618E0
2.066E-1	1.667E3	6.000E0	3.525E0	4.12E-5	3.613E0
1.907E-1	1.538E3	6.500E0	3.522E0	3.76E-5	3.610E0
1.771E-1	1.429E3	7.000E0	3.520E0	3.24E-5	3.607E0
1.653E-1	1.333E3	7.500E0	3.518E0	2.84E-5	3.605E0
1.550E-1	1.250E3	8.000E0	3.516E0	2.53E-5	3.603E0
1.459E-1	1.176E3	8.500E0	3.514E0	2.28E-5	3.601E0
1.378E-1	1.111E3	9.000E0	3.512E0	2.08E-5	3.599E0
1.305E-1	1.053E3	9.500E0	3.510E0	1.97E-5	3.597E0
1.240E-1	1.000E3	1.000E1	3.508E0	1.93E-5	3.594E0
1.181E-1	9.524E2	1.050E1	3.505E0	1.98E-5	3.592E0
1.127E-1	9.091E2	1.100E1	3.503E0	2.07E-5	3.590E0
1.078E-1	8.696E2	1.150E1	3.500E0	2.23E-5	3.587E0
1.033E-1	8.333E2	1.200E1	3.498E0	2.56E-5	
1.026E-1	8.278E2	1.208E1		2.86E-5	
4.686E-1	3.779E3	1.213E1		3.33E-5	
4.647E-1	3.748E3	1.222E1		4.62E-5	
4.602E-1	3.712E3	1.226E1		5.13E-5	
4.518E-1	3.644E3	1.232E1		6.13E-5	
4.375E-1	3.529E3	1.235E1		6.91E-5	
4.287E-1	3.458E3	1.244E1		7.59E-5	
9.919E-2	8.000E2	1.250E1	3.495E0		
4.176E-1	3.368E3	1.258E1		7.54E-5	
4.089E-1	3.298E3	1.267E1		6.51E-5	
3.966E-1	3.199E3	1.275E1		5.55E-5	
3.759E-1	3.032E3	1.281E1		4.67E-5	
3.605E-1	2.908E3	1.292E1		4.18E-5	
3.403E-1	2.745E3	1.303E1		4.01E-5	
3.189E-1	2.572E3	1.314E1		4.37E-5	
2.939E-1	2.370E3	1.322E1		5.02E-5	
2.788E-1	2.249E3	1.330E1		5.97E-5	
2.658E-1	2.144E3	1.335E1		6.70E-5	
2.527E-1	2.038E3	1.341E1		7.43E-5	
2.454E-1	1.979E3	1.348E1		7.79E-5	
2.398E-1	1.934E3	1.360E1		7.52E-5	
2.322E-1	1.873E3	1.364E1		6.87E-5	
2.276E-1	1.836E3	1.366E1		6.31E-5	
2.229E-1	1.798E3	1.372E1		5.73E-5	
2.163E-1	1.745E3	1.376E1		4.99E-5	
2.080E-1	1.677E3	1.379E1		4.54E-5	

(continued)

TABLE I *(Continued)*

$CdGeAs_2$

eV	cm^{-1}	μm	n_o	k	n_e
			[20]	[8]	[20]
2.024E-1	1.632E3	1.383E1		4.22E-5	
1.968E-1	1.588E3	1.405E1		4.27E-5	
1.931E-1	1.557E3	1.443E1		4.80E-5	
1.885E-1	1.521E3	1.470E1		5.32E-5	
1.838E-1	1.483E3	1.519E1		6.43E-5	
1.818E-1	1.466E3	1.552E1		7.74E-5	
1.773E-1	1.430E3	1.596E1		1.00E-4	
1.720E-1	1.388E3	1.658E1		1.52E-4	
1.645E-1	1.327E3	1.697E1		2.26E-4	
1.606E-1	1.295E3	1.739E1		3.60E-4	
1.564E-1	1.262E3	1.764E1		5.24E-4	
1.514E-1	1.221E3	1.774E1		7.04E-4	
1.472E-1	1.187E3	1.783E1		9.41E-4	
1.434E-1	1.156E3	1.788E1		1.23E-3	

eV	cm^{-1}	μm	n_o	k_o	n_e	k_e
			[26]	[26]	[26]	[26]
4.959E-2	4.000E2	2.500E1	3.71E0	4.77E-3	3.75E0	4.70E-3
4.649E-2	3.750E2	2.667E1	3.66E0	7.00E-3	3.70E0	7.03E-3
4.339E-2	3.500E2	2.857E1	3.58E0	1.14E-2	3.62E0	1.17E-2
4.030E-2	3.250E2	3.077E1	3.42E0	2.25E-2	3.49E0	2.37E-2
3.720E-2	3.000E2	3.333E1	2.99E0	7.58E-2	3.12E0	7.92E-2
3.670E-2	2.960E2	3.378E1	2.84E0	1.05E-1	3.00E0	1.07E-1
3.620E-2	2.920E2	3.425E1	2.60E0	1.58E-1	2.82E0	1.56E-1
3.571E-2	2.880E2	3.472E1	2.23E0	2.77E-1	2.57E0	2.49E-1
3.521E-2	2.840E2	3.521E1	1.55E0	6.76E-1	2.15E0	4.75E-1
3.472E-2	2.800E2	3.571E1	1.04E0	2.14E0	1.54E0	1.23E0
3.447E-2	2.780E2	3.597E1	1.19E0	3.12E0	1.43E0	1.97E0
3.422E-2	2.760E2	3.623E1	1.71E0	4.31E0	1.61E0	2.85E0
3.397E-2	2.740E2	3.650E1	3.17E0	5.75E0	2.19E0	3.85E0
3.372E-2	2.720E2	3.676E1	6.60E0	5.53E0	3.54E0	4.78E0
3.348E-2	2.700E2	3.704E1	7.45E0	2.47E0	5.77E0	4.44E0
3.323E-2	2.680E2	3.731E1	6.58E0	1.13E0	6.67E0	2.56E0
3.298E-2	2.660E2	3.759E1	5.91E0	6.50E-1	6.29E0	1.35E0
3.273E-2	2.640E2	3.788E1	5.45E0	4.40E-1	5.82E0	8.00E-1
3.248E-2	2.620E2	3.817E1	5.11E0	3.44E-1	5.46E0	5.26E-1
3.224E-2	2.600E2	3.846E1	4.84E0	3.22E-1	5.19E0	3.75E-1
3.199E-2	2.580E2	3.876E1	4.60E0	4.02E-1	4.98E0	2.83E-1
3.174E-2	2.560E2	3.906E1	4.56E0	6.65E-1	4.82E0	2.24E-1
3.162E-2	2.550E2	3.922E1	4.73E0	7.29E-1	4.75E0	2.02E-1
3.149E-2	2.540E2	3.937E1	4.88E0	6.02E-1	4.68E0	1.84E-1
3.124E-2	2.520E2	3.968E1	4.83E0	3.14E-1	4.57E0	1.56E-1
3.100E-2	2.500E2	4.000E1	4.69E0	1.96E-1	4.48E0	1.37E-1
3.050E-2	2.460E2	4.065E1	4.47E0	1.23E-1	4.32E0	1.13E-1
3.000E-2	2.420E2	4.132E1	4.31E0	1.03E-1	4.18E0	1.02E-1

TABLE I *(Continued)*

$CdGeAs_2$

eV	cm^{-1}	μm	n_o	k_o	n_e	k_e
			[26]	[26]	[26]	[26]
2.951E-2	2.380E2	4.202E1	4.19E0	9.94E-2	4.06E0	1.01E-1
2.901E-2	2.340E2	4.274E1	4.08E0	1.06E-1	3.93E0	1.09E-1
2.852E-2	2.300E2	4.348E1	3.97E0	1.22E-1	3.80E0	1.28E-1
2.802E-2	2.260E2	4.425E1	3.86E0	1.51E-1	3.64E0	1.64E-1
2.752E-2	2.220E2	4.505E1	3.74E0	2.01E-1	3.45E0	2.33E-1
2.703E-2	2.180E2	4.587E1	3.59E0	2.88E-1	3.17E0	3.77E-1
2.653E-2	2.140E2	4.673E1	3.42E0	4.54E-1	2.76E0	7.40E-1
2.604E-2	2.100E2	4.762E1	3.24E0	7.89E-1	2.43E0	1.76E0
2.579E-2	2.080E2	4.808E1	3.21E0	1.06E0	2.65E0	2.58E0
2.554E-2	2.060E2	4.854E1	3.29E0	1.41E0	3.39E0	3.38E0
2.529E-2	2.040E2	4.902E1	3.55E0	1.77E0	4.73E0	3.69E0
2.517E-2	2.030E2	4.926E1	3.76E0	1.91E0	5.45E0	3.44E0
2.504E-2	2.020E2	4.951E1	4.02E0	1.99E0	5.98E0	2.95E0
2.480E-2	2.000E2	5.000E1	4.56E0	1.95E0	6.30E0	1.85E0
2.455E-2	1.980E2	5.051E1	4.98E0	1.64E0	6.12E0	1.14E0
2.430E-2	1.960E2	5.102E1	5.15E0	1.25E0	5.85E0	7.39E-1
2.405E-2	1.940E2	5.155E1	5.17E0	9.28E-1	5.63E0	5.12E-1
2.381E-2	1.920E2	5.208E1	5.10E0	6.90E-1	5.44E0	3.74E-1
2.356E-2	1.900E2	5.263E1	5.01E0	5.25E-1	5.30E0	2.85E-1
2.306E-2	1.860E2	5.376E1	4.83E0	3.30E-1	5.08E0	1.81E-1
2.257E-2	1.820E2	5.495E1	4.68E0	2.29E-1	4.93E0	1.25E-1
2.244E-2	1.810E2	5.525E1	4.65E0	2.12E-1	4.90E0	1.16E-1
2.232E-2	1.800E2	5.556E1	4.61E0	1.98E-1	4.87E0	1.07E-1
2.182E-2	1.760E2	5.682E1	4.49E0	1.60E-1	4.77E0	8.04E-2
2.133E-2	1.720E2	5.814E1	4.36E0	1.49E-1	4.70E0	6.29E-2
2.108E-2	1.700E2	5.882E1	4.28E0	1.57E-1	4.67E0	5.62E-2
2.083E-2	1.680E2	5.952E1	4.19E0	1.80E-1	4.64E0	5.06E-2
2.058E-2	1.660E2	6.024E1	4.07E0	2.35E-1	4.62E0	4.57E-2
2.033E-2	1.640E2	6.098E1	3.92E0	3.67E-1	4.59E0	4.16E-2
2.009E-2	1.620E2	6.173E1	3.75E0	7.24E-1	4.57E0	3.80E-2
1.984E-2	1.600E2	6.250E1	4.11E0	1.45E0	4.55E0	3.49E-2
1.959E-2	1.580E2	6.329E1	5.13E0	1.17E0	4.53E0	3.21E-2
1.934E-2	1.560E2	6.410E1	5.16E0	5.22E-1	4.52E0	2.96E-2
1.909E-2	1.540E2	6.494E1	4.98E0	2.70E-1	4.50E0	2.75E-2
1.885E-2	1.520E2	6.579E1	4.85E0	1.68E-1	4.49E0	2.55E-2
1.860E-2	1.500E2	6.667E1	4.75E0	1.18E-1	4.47E0	2.38E-2
1.835E-2	1.480E2	6.757E1	4.68E0	8.96E-2	4.46E0	2.22E-2
1.810E-2	1.460E2	6.849E1	4.63E0	7.21E-2	4.45E0	2.08E-2
1.785E-2	1.440E2	6.944E1	4.59E0	6.03E-2	4.44E0	1.95E-2
1.761E-2	1.420E2	7.042E1	4.55E0	5.19E-2	4.43E0	1.83E-2
1.736E-2	1.400E2	7.143E1	4.52E0	4.56E-2	4.42E0	1.73E-2
1.686E-2	1.360E2	7.353E1	4.47E0	3.70E-2	4.40E0	1.54E-2
1.637E-2	1.320E2	7.576E1	4.43E0	3.15E-2	4.38E0	1.38E-2
1.587E-2	1.280E2	7.813E1	4.40E0	2.78E-2	4.37E0	1.24E-2
1.537E-2	1.240E2	8.065E1	4.37E0	2.55E-2	4.36E0	1.12E-2
1.488E-2	1.200E2	8.333E1	4.34E0	2.45E-2	4.34E0	1.02E-2

(continued)

TABLE I *(Continued)*

$CdGeAs_2$

eV	cm^{-1}	μm	n_o	k_o	n_e	k_e
			[26]	[26]	[26]	[26]
1.438E-2	1.160E2	8.621E1	4.31E0	2.49E-2	4.33E0	9.25E-3
1.389E-2	1.120E2	8.929E1	4.28E0	2.77E-2	4.32E0	8.44E-3
1.364E-2	1.100E2	9.091E1	4.26E0	3.06E-2	4.32E0	8.08E-3
1.339E-2	1.080E2	9.259E1	4.24E0	3.54E-2	4.31E0	7.73E-3
1.314E-2	1.060E2	9.434E1	4.21E0	4.33E-2	4.31E0	7.40E-3
1.289E-2	1.040E2	9.615E1	4.18E0	5.72E-2	4.31E0	7.08E-3
1.265E-2	1.020E2	9.804E1	4.14E0	8.36E-2	4.30E0	6.79E-3
1.240E-2	1.000E2	1.000E2	4.08E0	1.40E-1	4.30E0	6.51E-3
1.215E-2	9.800E1	1.020E2	4.02E0	2.78E-1	4.30E0	6.24E-3
1.190E-2	9.600E1	1.042E2	4.14E0	5.59E-1	4.29E0	5.98E-3
1.178E-2	9.500E1	1.053E2	4.36E0	6.20E-1	4.29E0	5.86E-3
1.165E-2	9.400E1	1.064E2	4.55E0	5.17E-1	4.29E0	5.74E-3
1.141E-2	9.200E1	1.087E2	4.61E0	2.48E-1	4.29E0	5.51E-3
1.116E-2	9.000E1	1.111E2	4.55E0	1.26E-1	4.28E0	5.29E-3
1.091E-2	8.800E1	1.136E2	4.50E0	7.49E-2	4.28E0	5.07E-3
1.066E-2	8.600E1	1.163E2	4.46E0	5.02E-2	4.28E0	4.87E-3
1.041E-2	8.400E1	1.190E2	4.43E0	3.65E-2	4.27E0	4.67E-3
1.017E-2	8.200E1	1.220E2	4.41E0	2.82E-2	4.27E0	4.49E-3
9.919E-3	8.000E1	1.250E2	4.39E0	2.28E-2	4.27E0	4.31E-3
9.671E-3	7.800E1	1.282E2	4.38E0	1.90E-2	4.27E0	4.13E-3
9.423E-3	7.600E1	1.316E2	4.37E0	1.62E-2	4.26E0	3.97E-3
6.199E-3	5.000E1	2.000E2	4.29E0	4.98E-3	4.24E0	2.24E-3

Copper Gallium Sulfide ($CuGaS_2$)

J. C. RIFE*
Naval Research Laboratory
Washington, D.C.

$CuGaS_2$ is a tetragonally bonded semiconductor with the chalcopyrite structure and a direct band gap of 2.49 eV at room temperature. The structure, growth, and optical and electronic properties of the chalcopyrite semiconductors have been reviewed in the book by Shay and Wernick [1]. Properties have also been summarized in the Landolt–Börnstein series [2]. The I–III–VI_2 chalcopyrite lattice is equivalent to the II–VI zincblende semiconductor crystal structure but with ordering of the I and III components and so a doubling of the unit cell along the *c*-axis. The chalcopyrite lattice is typically compressed along the *c*-axis leading to a crystalline electric field and birefringence with n_e ($\mathbf{E} \| \mathbf{c}$) $> n_o$ ($\mathbf{E} \perp \mathbf{c}$), (positive uniaxial crystal). Chalcopyrite semiconductors are also optically active because of varying degrees of tetragonal distortion [3]. The $CuGaS_2$ crystal structure, in particular, is compressed 2.0% along the *c*-axis. The band structure of $CuGaS_2$ has been calculated by several authors [4–7]. $CuGaS_2$ has a band gap about 1.1 eV less than that of its analog, ZnS, which has a direct band gap of 3.6 eV in cubic form. This property is displayed by other I–III–VI_2 chalcopyrites and their analogs as well. This has been attributed to *p–d* hybridization as a result of Cu *d*-orbitals in the valence band [5, 6] and to difference in the lengths of the Cu–S and Ga–S bonds [7].

$CuGaS_2$ is promising for green-blue light emitting devices since it can be doped *p*-type and form a heterojunctions with II–VI materials, which can only be doped *n*-type [1, 8]. Stimulation at 592 nm has also been obtained from a $CuGa(S_{0.65}Se_{0.35})_2/CuAl_{0.3}Ga_{0.7}(S_{0.65}Se_{0.35})_2$ double heterostructure device pumped by the third harmonic of a Nd:YAG laser [9].

The optical constants, *n* and *k*, listed in Table I and plotted in Fig. 1 are derived from sources discussed in more detail later. The optical constants were taken from tables, calculated from formulae, or extracted from graphs

* The views presented are those of the author and do not represent the views of the Department of Defense or its components.

ISBN 0-12-544423-0/$25.00.

where necessary. The table here has more significant figures than justified in some cases; consult the original work for the actual experimental resolution. Measurements made using polarized radiation were favored for inclusion here; in such cases, the optical constants have been given for both $\mathbf{E} \| \mathbf{c}$ and $\mathbf{E} \perp \mathbf{c}$. All measurements used were made on single crystals at room temperature, except where noted in the text.

I X-RAY TO BAND-GAP ABSORPTION EDGE

The optical constants, n and k, for the range from 10,000 to 26 eV have been calculated from the scattering factors of the elements of Henke *et al.* [10] using the compound formula and a density of 4.35 gm/cm^3. In Fig. 1, the K-edge ($1s$) transitions of Ga and Cu appear at 1.2 and 1.4×10^{-4} μm and of S at 5.0×10^{-4} μm, and the $L_{2,3}$ ($2p$) transitions of Ga and Cu at 1.1 and 1.3×10^{-3} μm and of S at 7.6×10^{-3} μm. The calculated edges are a good approximation on the scale of Fig. 1, but the scattering factors of the elements cannot predict the compound edge locations or structure to high degree (edge within 5 or 10 eV) because of core-level chemical shifts and bonding-dependent redistribution of the absorption at and just above the edges. Detailed $CuGaS_2$ absorption structure at the Cu K edge has been measured by Ballal and Mande [11].

For the fundamental electronic transitions in the 26 to 2.45 eV range, here, optical constants are taken from Rife *et al.* [12]. They extracted optical constants for a single stoichiometric "yellow"/"orange" crystal sample from a Kramers–Kronig analysis of polarized, 80-K reflectance data. Other measurements in this range are the unpolarized reflectance of Ringeissen *et al.* [13] from 6 to 3.5 eV of "orange" crystals at 4.2 K and that of Hengehold and Pedrotti [14] from 11 to 2.5 eV of "green" crystals at room temperature.

II BAND-GAP ABSORPTION EDGE

Measurements of the absorption coefficient at the absorption edge have been reported by a several authors. Tell and Kasper [5] measured the absorption coefficient from 2.58 to 2.48 eV for $\mathbf{E} \perp \mathbf{c}$ at 2 K. Kobayashi *et al.* [15] measured the absorption coefficient from 2.53 to 2.40 eV for $\mathbf{E} \perp \mathbf{c}$ at 77, 213, and 293 K, removing a background likely due to a Fe impurity. Gonzalez *et al.* [16] obtained the pressure dependance of the $CuGaS_2$ edge at room temperature and zero hydrostatic pressure from 2.48 to 2.52 eV, but their absorption coefficient is lower for a given energy than that of Kobayashi *et al.*

BAND GAP III

In the transparent gap region from 0.5 to 13 μm, where the two-phonon lattice absorption sets in, the index of refraction at room temperature, the temperature derivative for $\mathbf{E}\|\mathbf{c}$ and $\mathbf{E}\perp\mathbf{c}$, and the absorption coefficient for unpolarized light have been reported by Boyd *et al.* [17]. They determined the index by the minimum-deviation method; however, results for other individual crystals could vary slightly from their results, depending on impurities or doping. Their refractive-index data have been reduced to an analog formula by Wemple *et al.* [18] and by Bhar and Ghosh [19] for 20 and 120° C and more extreme temperatures. The latter find a good fit for 20° C to a special Sellmeier form,

$$n^2 = A + \frac{B}{1 - \dfrac{C}{\lambda^2}} + \frac{D}{1 - \dfrac{E}{\lambda^2}},$$

where for n_o (A,B,C,D,E) = (3.9064, 2.3065, 0.1149, 1.5479, 738.43) and for n_e (A,B,C,D,E) = (4.3165, 1.8692, 0.1364, 1.7575, 738.43); λ is the wavelength in microns. At 120° C, these parameters are n_o (A,B,C,D,E) = (4.0984, 2.1419, 0.1225, 1.5755, 738.43) and n_e (A,B,C,D,E) = (4.4834, 1.7316, 0.1453, 1.7785, 738.43).

LATTICE ABSORPTION IN THE INFRARED IV

Several authors have studied the phonon modes of $CuGaS_2$ by transmission [20, 21] and Raman spectroscopies [20, 22]. Baars and Koschel [23] measured the polarized reflectance from 50 to 500 cm^{-1} and derived optical constants by Kramers–Kronig analysis and fitting to dispersion of a set of harmonic oscillators. Their dispersion formula for the dielectric constant $\epsilon(\nu)$ is

$$\epsilon(\nu) = \epsilon_\infty + \sum_j \frac{S_j \nu^2{}_j}{(\nu^2{}_j - \nu^2 - i\nu\gamma_j)},$$

where S_j is the oscillator strength, ν_j is the frequency in cm^{-1}, and γ_j is the damping of the jth oscillator in cm^{-1}. For $\mathbf{E}\|\mathbf{c}$, they give two oscillators out of a possible three (S_j, ν_j, γ_j) = (0.27, 364, 2.7) and (1.20, 330, 2.49) with ϵ_∞ = 6.1; and for $\mathbf{E}\perp\mathbf{c}$, they give the four oscillators out of a possible six (S_j, ν_j, γ_j) = (0.04, 387, 3.60), (0.56, 364, 3.44), (0.55, 345, 6.85), and (1.54, 259, 15.02) with ϵ_∞ = 6.2. Baars and Koschel obtained values for ϵ_0

of 7.6 for $\mathbf{E} \| \mathbf{c}$ and 8.9 for $\mathbf{E} \perp \mathbf{c}$. They observed two additional peaks in the $\mathbf{E} \perp \mathbf{c}$ reflectance at 148 and 93 cm^{-1}, but reported no oscillator parameters for them.

REFERENCES

1. J. L. Shay and J. H. Wernick, "Ternary Chalcopyrite Semiconductors: Growth, Electronic Properties, and Applications." Pergamon, New York, 1975.
2. Landolt-Börnstein, "Semiconductors—Physics of Ternary Compounds" (K.-H. Hellwege and O. Madelung, eds.), Vol. 17h. Springer-Verlag, New York, 1985.
3. G. A. Babonas, A. S. Martsinkyavichyus, and A. Yu. Shileika, *Sov. Phys. J.* **29**, 617 (1986).
4. A. S. Poplavnoi and Yu. I. Polygalov, *Inorg. Mater.* **7**, 1527 and 1531 (1971).
5. B. Tell and H. M. Kasper, *Phys. Rev.* **B 7**, 740 (1973).
6. B. Tell and P. M. Bridenbaugh, *Phys. Rev.* **B 12**, 3330 (1975).
7. J. E. Jaffe and A. Zunger, *Phys. Rev.* **B 28**, 5822 (1983).
8. H. Kukimoto, Proceedings of the Ninth International Conference on Ternary and Multinary Compounds. *Jpn. J. Appl. Phys. Suppl.* **32-3**, 10 (1993).
9. M. Yamamoto, T. Ogawa, K. Hara, J. Yoshino, and H. Kukimoto, *Jpn. J. Appl. Phys.* **33**, L624 (1994).
10. B. L. Henke, P. Lee, T. J. Tanaka, R. L. Shimabukuro, and B. J. Fujikawa, *At. Data Nucl. Data Tables* **27**, 1 (1982); B. L. Henke, J. C. Davis, E. M. Gullikson, and R. C. C. Perera, *Lawrence Berkeley Laboratory Report* **LBL-26259** (1988).
11. M. M. Ballal and C. Mande, *J. Phys. C: Solid State Phys.* **11**, 837 (1978).
12. J. C. Rife, R. N. Dexter, P. M. Bridenbaugh, and B. W. Veal, *Phys. Rev. B* **10**, 4491 (1977); J. C. Rife, Unpublished Ph.D. Thesis University of Wisconsin, Madison (1976).
13. J. Ringeissen, J. L. Regoline, and S. Lewonczuk, *Surf. Sci.* **37**, 777 (1973).
14. R. L. Hengehold and F. L. Pedrotti, *J. Appl. Phys.* **46**, 5202 (1975).
15. S. Kobayashi, N. Tsuboi, and F. Kaneko, *Jpn. J. of Appl. Phys.* **26**, 220 (1987).
16. J. Gonzalez, E. Calderon, T. Tinoco, J. P. Itie, A. Polian, and E. Moya, *J. Phys. Chem. Solids* **56**, 507 (1995).
17. G. D. Boyd, H. Kasper, and J. H. McFee, *IEEE J. Quanum Electron.* **QE-7**, 563 (1971).
18. S. H. Wemple, J. D. Gabbe, and G. D. Boyd, *J. Appl. Phys.* **46**, 3597 (1975).
19. G. C. Bhar and G.C. Ghosh, *IEEE J. Quantum Electron.* **QE-16**, 838 (1980); G. C. Bhar and G. C. Ghosh, *J. Opt. Soc. Am.* **69**, 730 (1979).
20. W. H. Koschel and M. Bettini, *Phys. Status Solidi B* **72**, 729 (1975).
21. N. V. Joshi, *J. Chem. Phys. Solids* **40**, 93 (1979).
22. J. P. van der Ziel, A. E. Meixner, H. M. Kasper, and J. A. Ditzenberger, *Phys. Rev.* **B 9**, 4286 (1974).
23. J. Baars and W. H. Koschel, *Solid State Commun.* **11** 1513 (1972).

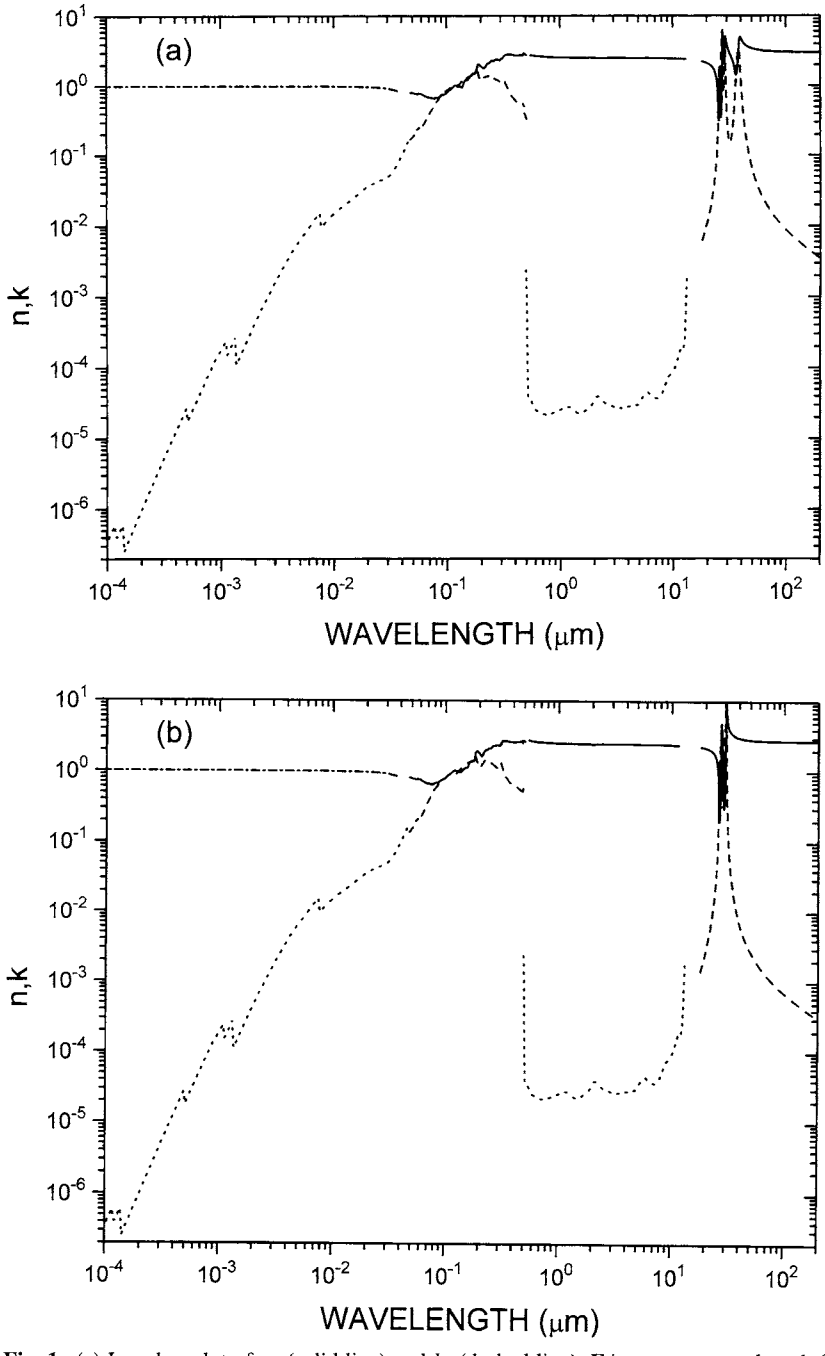

Fig. 1. (a) Log–log plot of n_o (solid line) and k_o (dashed line), $\mathbf{E} \perp \mathbf{c}$, versus wavelength for $CuGaS_2$. (b) Log–log plot of n_e (solid line) and k_e (dashed line), $\mathbf{E} \parallel \mathbf{c}$, versus wavelength for $CuGaS_2$. Unpolarized n (dash-dot line) and k (dotted line) are plotted on both graphs, where polarized data were not available.

TABLE I

Values of n and k for $CuGaS_2$ Obtained from Various References[a]

eV	cm^{-1}	μm	1-n	k
			[10]	[10]
3.000E4	2.420E8	4.133E-5	9.50E-7	1.18E-8
2.010E4	1.622E8	6.167E-5	2.09E-6	5.54E-8
1.499E4	1.209E8	8.272E-5	3.76E-6	1.68E-7
1.118E4	9.017E7	1.109E-4	6.62E-6	4.93E-7
1.088E4	8.772E7	1.140E-4	6.91E-6	5.42E-7
1.060E4	8.547E7	1.170E-4	7.21E-6	5.96E-7
1.031E4	8.319E7	1.202E-4	7.45E-6	4.01E-7
1.005E4	8.104E7	1.234E-4	7.99E-6	4.08E-7
9.778E3	7.886E7	1.268E-4	8.46E-6	4.51E-7
9.523E3	7.680E7	1.302E-4	8.94E-6	4.97E-7
9.273E3	7.479E7	1.337E-4	9.36E-6	5.47E-7
9.024E3	7.278E7	1.374E-4	9.72E-6	6.02E-7
8.787E3	7.087E7	1.411E-4	1.04E-5	2.53E-7
8.557E3	6.901E7	1.449E-4	1.10E-5	2.80E-7
8.332E3	6.720E7	1.488E-4	1.17E-5	3.10E-7
6.048E3	4.878E7	2.050E-4	2.28E-5	1.05E-6
4.053E3	3.269E7	3.059E-4	5.13E-5	4.70E-6
2.645E3	2.133E7	4.688E-4	1.15E-4	2.22E-5
2.575E3	2.077E7	4.815E-4	1.19E-4	2.44E-5
2.507E3	2.022E7	4.945E-4	1.22E-4	2.68E-5
2.441E3	1.969E7	5.079E-4	1.26E-4	1.79E-5
2.377E3	1.917E7	5.216E-4	1.38E-4	1.97E-5
2.314E3	1.867E7	5.357E-4	1.48E-4	2.17E-5
1.820E3	1.468E7	6.812E-4	2.41E-4	5.14E-5
1.394E3	1.124E7	8.895E-4	3.84E-4	1.31E-4
1.188E3	9.579E6	1.044E-3	4.60E-4	2.05E-4
1.157E3	9.328E6	1.072E-3	4.63E-4	2.21E-4
1.126E3	9.083E6	1.101E-3	4.36E-4	2.38E-4
1.096E3	8.842E6	1.131E-3	4.72E-4	1.54E-4
1.067E3	8.606E6	1.162E-3	5.24E-4	1.67E-4
1.039E3	8.382E6	1.193E-3	5.61E-4	1.81E-4
9.856E2	7.949E6	1.258E-3	6.11E-4	2.21E-4
9.596E2	7.740E6	1.292E-3	6.15E-4	2.45E-4
9.343E2	7.536E6	1.327E-3	5.14E-4	2.71E-4
9.096E2	7.337E6	1.363E-3	6.63E-4	1.12E-4
8.856E2	7.143E6	1.400E-3	7.46E-4	1.23E-4
8.622E2	6.954E6	1.438E-3	8.13E-4	1.36E-4
6.965E2	5.618E6	1.780E-3	1.36E-3	2.89E-4
5.056E2	4.078E6	2.452E-3	2.57E-3	8.41E-4
3.976E2	3.207E6	3.118E-3	3.95E-3	1.79E-3
3.045E2	2.456E6	4.072E-3	5.91E-3	3.85E-3
1.987E2	1.602E6	6.241E-3	8.80E-3	1.04E-2
1.738E2	1.402E6	7.132E-3	7.88E-3	1.40E-2
1.693E2	1.365E6	7.325E-3	6.97E-3	1.48E-2
1.648E2	1.329E6	7.523E-3	4.63E-3	1.56E-2

[a]References given in brackets.

TABLE I *(Continued)*

$CuGaS_2$

eV	cm^{-1}	μm	1-n	k		
			[10]	[10]		
1.605E2	1.294E6	7.726E-3	3.93E-3	9.64E-3		
1.563E2	1.260E6	7.935E-3	6.87E-3	1.02E-2		
1.521E2	1.227E6	8.150E-3	8.12E-3	1.07E-2		
1.262E2	1.018E6	9.824E-3	1.24E-2	1.46E-2		
1.020E2	8.224E5	1.216E-2	1.68E-2	1.94E-2		
7.602E1	6.131E5	1.631E-2	2.70E-2	2.81E-2		
4.959E1	4.000E5	2.500E-2	5.45E-2	4.28E-2		
4.006E1	3.231E5	3.095E-2	9.34E-2	5.11E-2		
3.413E1	2.753E5	3.633E-2	1.45E-1	7.28E-2		
2.987E1	2.409E5	4.151E-2		1.10E-1		
2.757E1	2.224E5	4.497E-2		1.50E-1		
2.614E1	2.108E5	4.744E-2		1.83E-1		
eV	cm^{-1}	μm	n_o	k_o	n_e	k_e
			[12]	[12]	[12]	[12]
2.590E1	2.089E5	4.787E-2	7.94E-1	1.70E-1	8.12E-1	1.37E-1
2.550E1	2.057E5	4.862E-2	7.95E-1	1.78E-1	8.08E-1	1.43E-1
2.500E1	2.016E5	4.959E-2	7.95E-1	1.85E-1	8.03E-1	1.49E-1
2.450E1	1.976E5	5.060E-2	7.92E-1	1.88E-1	7.96E-1	1.50E-1
2.400E1	1.936E5	5.166E-2	7.82E-1	1.95E-1	7.82E-1	1.64E-1
2.350E1	1.895E5	5.276E-2	7.75E-1	2.08E-1	7.77E-1	1.78E-1
2.300E1	1.855E5	5.390E-2	7.68E-1	2.19E-1	7.69E-1	1.87E-1
2.290E1	1.847E5	5.414E-2	7.64E-1	2.21E-1	7.66E-1	1.89E-1
2.280E1	1.839E5	5.438E-2	7.60E-1	2.26E-1	7.61E-1	1.94E-1
2.270E1	1.831E5	5.462E-2	7.58E-1	2.32E-1	7.60E-1	2.03E-1
2.260E1	1.823E5	5.486E-2	7.58E-1	2.38E-1	7.61E-1	2.08E-1
2.250E1	1.815E5	5.510E-2	7.60E-1	2.47E-1	7.64E-1	2.15E-1
2.240E1	1.807E5	5.535E-2	7.67E-1	2.53E-1	7.71E-1	2.18E-1
2.230E1	1.799E5	5.560E-2	7.71E-1	2.50E-1	7.72E-1	2.16E-1
2.220E1	1.791E5	5.585E-2	7.69E-1	2.51E-1	7.71E-1	2.17E-1
2.210E1	1.783E5	5.610E-2	7.67E-1	2.57E-1	7.72E-1	2.20E-1
2.200E1	1.774E5	5.635E-2	7.76E-1	2.63E-1	7.79E-1	2.21E-1
2.180E1	1.758E5	5.687E-2	7.82E-1	2.52E-1	7.75E-1	2.13E-1
2.160E1	1.742E5	5.740E-2	7.72E-1	2.53E-1	7.63E-1	2.20E-1
2.140E1	1.726E5	5.793E-2	7.74E-1	2.60E-1	7.70E-1	2.28E-1
2.120E1	1.710E5	5.848E-2	7.72E-1	2.56E-1	7.65E-1	2.23E-1
2.100E1	1.694E5	5.904E-2	7.69E-1	2.62E-1	7.64E-1	2.28E-1
2.080E1	1.678E5	5.961E-2	7.68E-1	2.61E-1	7.61E-1	2.25E-1
2.060E1	1.662E5	6.018E-2	7.60E-1	2.59E-1	7.50E-1	2.25E-1
2.040E1	1.645E5	6.077E-2	7.52E-1	2.65E-1	7.41E-1	2.32E-1
2.020E1	1.629E5	6.138E-2	7.47E-1	2.70E-1	7.35E-1	2.36E-1
2.000E1	1.613E5	6.199E-2	7.40E-1	2.73E-1	7.27E-1	2.42E-1
1.900E1	1.533E5	6.525E-2	7.07E-1	3.17E-1	6.89E-1	2.88E-1
1.800E1	1.452E5	6.888E-2	6.85E-1	3.81E-1	6.68E-1	3.55E-1
1.700E1	1.371E5	7.293E-2	6.74E-1	4.38E-1	6.59E-1	4.22E-1

(continued)

TABLE I *(Continued)*

$CuGaS_2$

eV	cm^{-1}	μm	n_o	k_o	n_e	k_e
			[12]	[12]	[12]	[12]
1.600E1	1.291E5	7.749E-2	6.62E-1	5.24E-1	6.56E-1	5.21E-1
1.500E1	1.210E5	8.265E-2	6.79E-1	6.12E-1	6.92E-1	5.96E-1
1.480E1	1.194E5	8.377E-2	6.80E-1	6.35E-1	6.92E-1	6.10E-1
1.460E1	1.178E5	8.492E-2	6.86E-1	6.59E-1	6.92E-1	6.29E-1
1.440E1	1.161E5	8.610E-2	6.95E-1	6.84E-1	6.97E-1	6.55E-1
1.420E1	1.145E5	8.731E-2	7.12E-1	7.06E-1	7.10E-1	6.77E-1
1.400E1	1.129E5	8.856E-2	7.30E-1	7.21E-1	7.23E-1	6.95E-1
1.380E1	1.113E5	8.984E-2	7.42E-1	7.28E-1	7.36E-1	7.09E-1
1.360E1	1.097E5	9.116E-2	7.46E-1	7.36E-1	7.46E-1	7.22E-1
1.340E1	1.081E5	9.252E-2	7.47E-1	7.53E-1	7.51E-1	7.37E-1
1.320E1	1.065E5	9.392E-2	7.50E-1	7.75E-1	7.58E-1	7.57E-1
1.300E1	1.049E5	9.537E-2	7.55E-1	7.98E-1	7.69E-1	7.79E-1
1.280E1	1.032E5	9.686E-2	7.66E-1	8.27E-1	7.82E-1	7.99E-1
1.260E1	1.016E5	9.840E-2	7.83E-1	8.53E-1	7.97E-1	8.19E-1
1.240E1	1.000E5	9.998E-2	8.03E-1	8.77E-1	8.13E-1	8.40E-1
1.220E1	9.840E4	1.016E-1	8.27E-1	8.97E-1	8.33E-1	8.59E-1
1.200E1	9.679E4	1.033E-1	8.50E-1	9.11E-1	8.54E-1	8.74E-1
1.180E1	9.518E4	1.051E-1	8.70E-1	9.21E-1	8.74E-1	8.87E-1
1.160E1	9.356E4	1.069E-1	8.85E-1	9.32E-1	8.93E-1	9.00E-1
1.140E1	9.195E4	1.088E-1	8.98E-1	9.51E-1	9.10E-1	9.11E-1
1.120E1	9.034E4	1.107E-1	9.21E-1	9.70E-1	9.28E-1	9.28E-1
1.100E1	8.872E4	1.127E-1	9.47E-1	9.84E-1	9.53E-1	9.44E-1
1.080E1	8.711E4	1.148E-1	9.76E-1	9.89E-1	9.89E-1	9.50E-1
1.060E1	8.550E4	1.170E-1	9.98E-1	9.84E-1	1.01E0	9.40E-1
1.040E1	8.388E4	1.192E-1	1.01E0	9.75E-1	1.02E0	9.34E-1
1.020E1	8.227E4	1.215E-1	9.99E-1	9.70E-1	1.02E0	9.28E-1
1.000E1	8.066E4	1.240E-1	9.82E-1	9.91E-1	1.01E0	9.27E-1
9.800E0	7.905E4	1.265E-1	9.73E-1	1.03E0	1.00E0	9.42E-1
9.600E0	7.743E4	1.291E-1	9.89E-1	1.06E0	9.97E-1	9.62E-1
9.400E0	7.582E4	1.319E-1	9.87E-1	1.07E0	9.77E-1	9.90E-1
9.200E0	7.421E4	1.348E-1	9.47E-1	1.13E0	9.65E-1	1.05E0
9.000E0	7.259E4	1.378E-1	9.78E-1	1.25E0	9.94E-1	1.11E0
8.800E0	7.098E4	1.409E-1	1.07E0	1.32E0	1.04E0	1.16E0
8.600E0	6.937E4	1.442E-1	1.17E0	1.33E0	1.08E0	1.19E0
8.400E0	6.775E4	1.476E-1	1.22E0	1.30E0	1.11E0	1.21E0
8.200E0	6.614E4	1.512E-1	1.21E0	1.32E0	1.12E0	1.25E0
8.000E0	6.453E4	1.550E-1	1.25E0	1.38E0	1.14E0	1.31E0
7.800E0	6.291E4	1.589E-1	1.31E0	1.42E0	1.21E0	1.42E0
7.600E0	6.130E4	1.631E-1	1.39E0	1.45E0	1.36E0	1.41E0
7.400E0	5.969E4	1.675E-1	1.47E0	1.45E0	1.40E0	1.39E0
7.200E0	5.807E4	1.722E-1	1.51E0	1.44E0	1.42E0	1.39E0
7.000E0	5.646E4	1.771E-1	1.50E0	1.50E0	1.41E0	1.50E0
6.800E0	5.485E4	1.823E-1	1.65E0	1.64E0	1.67E0	1.70E0
6.700E0	5.404E4	1.850E-1	1.80E0	1.67E0	1.88E0	1.55E0
6.600E0	5.323E4	1.878E-1	1.97E0	1.60E0	1.94E0	1.43E0
6.400E0	5.162E4	1.937E-1	2.04E0	1.29E0	1.92E0	1.22E0

TABLE I *(Continued)*

$CuGaS_2$

eV	cm^{-1}	μm	n_o	k_o	n_e	k_e
			[12]	[12]	[12]	[12]
6.200E0	5.001E4	2.000E-1	1.91E0	1.20E0	1.80E0	1.16E0
6.000E0	4.839E4	2.066E-1	1.83E0	1.20E0	1.68E0	1.22E0
5.800E0	4.678E4	2.138E-1	1.79E0	1.33E0	1.74E0	1.43E0
5.600E0	4.517E4	2.214E-1	1.92E0	1.45E0	1.94E0	1.42E0
5.500E0	4.436E4	2.254E-1	2.02E0	1.45E0	2.00E0	1.37E0
5.400E0	4.356E4	2.296E-1	2.09E0	1.40E0	2.02E0	1.35E0
5.300E0	4.275E4	2.339E-1	2.11E0	1.38E0	2.05E0	1.35E0
5.200E0	4.194E4	2.384E-1	2.15E0	1.38E0	2.10E0	1.33E0
5.100E0	4.114E4	2.431E-1	2.24E0	1.38E0	2.13E0	1.30E0
5.000E0	4.033E4	2.480E-1	2.29E0	1.29E0	2.13E0	1.28E0
4.900E0	3.952E4	2.530E-1	2.27E0	1.25E0	2.16E0	1.31E0
4.800E0	3.872E4	2.583E-1	2.28E0	1.24E0	2.25E0	1.30E0
4.700E0	3.791E4	2.638E-1	2.32E0	1.26E0	2.29E0	1.24E0
4.600E0	3.710E4	2.695E-1	2.38E0	1.21E0	2.31E0	1.21E0
4.500E0	3.630E4	2.755E-1	2.39E0	1.16E0	2.35E0	1.20E0
4.400E0	3.549E4	2.818E-1	2.38E0	1.13E0	2.37E0	1.14E0
4.300E0	3.468E4	2.883E-1	2.37E0	1.12E0	2.37E0	1.12E0
4.200E0	3.388E4	2.952E-1	2.37E0	1.19E0	2.37E0	1.11E0
4.100E0	3.307E4	3.024E-1	2.43E0	1.19E0	2.34E0	1.16E0
4.000E0	3.226E4	3.100E-1	2.49E0	1.24E0	2.48E0	1.31E0
3.900E0	3.146E4	3.179E-1	2.63E0	1.23E0	2.73E0	1.17E0
3.800E0	3.065E4	3.263E-1	2.74E0	1.14E0	2.73E0	1.00E0
3.700E0	2.984E4	3.351E-1	2.80E0	1.03E0	2.73E0	9.05E-1
3.600E0	2.904E4	3.444E-1	2.82E0	9.34E-1	2.72E0	8.25E-1
3.500E0	2.823E4	3.542E-1	2.83E0	8.50E-1	2.69E0	7.60E-1
3.400E0	2.742E4	3.646E-1	2.82E0	7.76E-1	2.68E0	7.10E-1
3.300E0	2.662E4	3.757E-1	2.81E0	6.94E-1	2.65E0	6.78E-1
3.200E0	2.581E4	3.874E-1	2.78E0	6.49E-1	2.64E0	6.56E-1
3.100E0	2.500E4	3.999E-1	2.76E0	6.19E-1	2.62E0	6.33E-1
3.000E0	2.420E4	4.133E-1	2.75E0	5.95E-1	2.63E0	6.26E-1
2.900E0	2.339E4	4.275E-1	2.74E0	5.79E-1	2.64E0	6.09E-1
2.800E0	2.258E4	4.428E-1	2.75E0	5.59E-1	2.65E0	5.85E-1
2.750E0	2.218E4	4.508E-1	2.76E0	5.48E-1	2.65E0	5.74E-1
2.700E0	2.178E4	4.592E-1	2.76E0	5.37E-1	2.69E0	5.94E-1
2.650E0	2.137E4	4.678E-1	2.76E0	5.41E-1	2.71E0	5.38E-1
2.600E0	2.097E4	4.768E-1	2.86E0	5.91E-1	2.71E0	4.69E-1
2.550E0	2.057E4	4.862E-1	2.92E0	3.94E-1	2.78E0	6.09E-1
2.500E0	2.016E4	4.959E-1	2.82E0	3.37E-1	2.73E0	4.41E-1

eV	cm^{-1}	μm	n	k
				[15]
2.400E0	1.935E4	5.167E-1		3.98E-5
2.410E0	1.944E4	5.144E-1		5.80E-5
2.420E0	1.952E4	5.123E-1		8.20E-5
2.429E0	1.959E4	5.104E-1		1.12E-4

(continued)

TABLE I *(Continued)*

$CuGaS_2$

eV	cm^{-1}	μm	n	k	
				[15]	
2.434EO	1.964E4	5.093E-1		1.46E-4	
2.438E0	1.967E4	5.085E-1		1.98E-4	
2.443E0	1.971E4	5.075E-1		2.74E-4	
2.449E0	1.975E4	5.063E-1		4.09E-4	
2.453E0	1.979E4	5.054E-1		6.03E-4	
2.458E0	1.983E4	5.044E-1		9.22E-4	
2.460E0	1.984E4	5.039E-1		1.06E-3	
2.463E0	1.987E4	5.034E-1		1.16E-3	
2.465E0	1.988E4	5.029E-1		1.20E-3	
2.468E0	1.991E4	5.023E-1		1.23E-3	
2.470E0	1.992E4	5.020E-1		1.24E-3	
2.474E0	1.995E4	5.012E-1		1.29E-3	
2.476E0	1.997E4	5.008E-1		1.35E-3	
2.478E0	1.999E4	5.004E-1		1.41E-3	
2.482E0	2.002E4	4.995E-1		1.68E-3	
2.487E0	2.006E4	4.985E-1		2.03E-3	
2.493E0	2.011E4	4.973E-1		2.60E-3	

eV	cm^{-1}	μm	n_o	k	n_e
			[17]	[17]	[17]
2.254E0	1.818E4	5.500E-1	2.763E0		2.781E0
2.101E0	1.695E4	5.529E-1		3.33E-5	
2.066E0	1.667E4	5.900E-1	2.709E0	2.64E-5	2.714E0
2.033E0	1.639E4	6.000E-1	2.698E0	2.55E-5	2.702E0
2.000E0	1.613E4	6.100E-1	2.689E0	2.50E-5	2.691E0
1.968E0	1.587E4	6.200E-1	2.680E0	2.46E-5	2.682E0
1.937E0	1.563E4	6.300E-1	2.672E0	2.42E-5	2.673E0
1.907E0	1.538E4	6.400E-1	2.664E0	2.39E-5	2.665E0
1.771E0	1.429E4	6.500E-1	2.658E0	2.35E-5	2.637E0
1.653E0	1.333E4	7.000E-1	2.629E0	2.21E-5	2.627E0
1.550E0	1.250E4	7.500E-1	2.610E0	2.18E-5	2.606E0
1.459E0	1.176E4	8.000E-1	2.593E0	2.22E-5	2.589E0
1.378E0	1.111E4	8.500E-1	2.579E0	2.30E-5	2.574E0
1.305E0	1.053E4	9.000E-1	2.568E0	2.38E-5	2.563E0
1.240E0	1.000E4	9.500E-1	2.559E0	2.48E-5	2.554E0
1.127E0	9.091E3	1.000E0	2.552E0	2.56E-5	2.546E0
1.033E0	8.333E3	1.100E0	2.541E0	2.71E-5	2.535E0
9.537E-1	7.692E3	1.200E0	2.532E0	2.78E-5	2.527E0
8.856E-1	7.143E3	1.300E0	2.526E0	2.61E-5	2.520E0
7.749E-1	6.250E3	1.400E0	2.521E0	2.33E-5	2.515E0
6.888E-1	5.556E3	1.422E0		2.26E-5	
6.199E-1	5.000E3	1.600E0	2.514E0	2.40E-5	2.507E0
5.636E-1	4.545E3	1.800E0	2.509E0	2.70E-5	2.503E0
5.166E-1	4.167E3	2.000E0	2.505E0	3.55E-5	2.449E0
4.769E-1	3.846E3	2.200E0	2.502E0	3.93E-5	2.496E0

TABLE I *(Continued)*

$CuGaS_2$

eV	cm^{-1}	μm	n_o	k	n_e
			[17]	[17]	[17]
4.428E-1	3.571E3	2.400E0	2.499E0	3.33E-5	2.493E0
4.133E-1	3.333E3	2.600E0	2.498E0	3.03E-5	2.491E0
3.875E-1	3.125E3	2.800E0	2.496E0	2.91E-5	2.489E0
3.647E-1	2.941E3	3.000E0	2.495E0	2.77E-5	2.489E0
3.444E-1	2.778E3	3.200E0	2.493E0	2.69E-5	2.487E0
3.263E-1	2.632E3	3.400E0	2.492E0	2.69E-5	2.485E0
3.100E-1	2.500E3	3.600E0	2.491E0	2.71E-5	2.484E0
2.755E-1	2.222E3	3.800E0	2.490E0	2.76E-5	2.483E0
2.480E-1	2.000E3	4.000E0	2.488E0	2.81E-5	2.482E0
2.254E-1	1.818E3	4.500E0	2.487E0	2.93E-5	2.480E0
2.066E-1	1.667E3	4.915E0		3.01E-5	
1.907E-1	1.538E3	5.000E0	2.484E0	3.17E-5	2.477E0
1.771E-1	1.429E3	5.500E0	2.480E0	4.14E-5	2.473E0
1.653E-1	1.333E3	6.000E0	2.477E0	4.51E-5	2.469E0
1.550E-1	1.250E3	6.500E0	2.474E0	3.99E-5	2.466E0
1.459E-1	1.176E3	7.000E0	2.472E0	3.72E-5	2.462E0
1.378E-1	1.111E3	7.348E0		3.67E-5	
1.305E-1	1.053E3	7.500E0	2.467E0	3.79E-5	2.458E0
1.240E-1	1.000E3	8.000E0	2.464E0	4.40E-5	2.454E0
1.181E-1	9.524E2	8.500E0	2.459E0	5.77E-5	2.449E0
1.127E-1	9.091E2	9.000E0	2.454E0	7.23E-5	2.444E0
1.078E-1	8.696E2	9.126E0		7.65E-5	
1.033E-1	8.333E2	9.500E0	2.449E0	8.12E-5	2.438E0
9.919E-2	8.000E2	1.000E1	2.443E0	9.11E-5	2.431E0
9.537E-2	7.692E2	1.050E1	2.437E0	1.09E-4	2.423E0
2.242E0	1.809E4	1.100E1	2.431E0	1.38E-4	2.418E0
2.214E0	1.786E4	1.150E1	2.428E0	1.76E-4	2.412E0
2.178E0	1.757E4	1.184E1		1.99E-4	
2.135E0	1.722E4	1.200E1	2.417E0	1.95E-4	
2.060E0	1.661E4	1.229E1		1.88E-4	
1.963E0	1.583E4	1.250E1	2.409E0	2.23E-4	
1.806E0	1.457E4	1.300E1	2.400E0	9.23E-4	
1.682E0	1.357E4	1.306E1		1.06E-3	
1.556E0	1.255E4	1.314E1		1.44E-3	
1.402E0	1.131E4	1.325E1		2.04E-3	

eV	cm^{-1}	μm	n_o	k_o	n_e	k_e
			[23]	[23]	[23]	[23]
6.199E-2	5.000E2	2.000E1	2.11E0	1.10E-2	2.21E0	2.64E-3
5.579E-2	4.500E2	2.222E1	1.87E0	2.51E-2	2.05E0	6.25E-3
5.207E-2	4.200E2	2.381E1	1.49E0	6.04E-2	1.83E0	1.39E-2
5.158E-2	4.160E2	2.404E1	1.39E0	7.24E-2	1.78E0	1.61E-2
5.108E-2	4.120E2	2.427E1	1.28E0	9.00E-2	1.73E0	1.87E-2
5.059E-2	4.080E2	2.451E1	1.13E0	1.18E-1	1.67E0	2.22E-2
5.009E-2	4.040E2	2.475E1	9.13E-1	1.73E-1	1.59E0	2.70E-2

(continued)

TABLE I *(Continued)*

$CuGaS_2$

eV	cm^{-1}	μm	n_o	k_o	n_e	k_e
			[23]	[23]	[23]	[23]
4.959E-2	4.000E2	2.500E1	5.90E-1	3.33E-1	1.50E0	3.36E-2
4.910E-2	3.960E2	2.525E1	3.35E-1	8.00E-1	1.38E0	4.37E-2
4.860E-2	3.920E2	2.551E1	3.47E-1	1.36E0	1.22E0	6.04E-2
4.798E-2	3.870E2	2.584E1	1.36E0	1.81E0	9.23E-1	1.08E-1
4.761E-2	3.840E2	2.604E1	8.78E-1	1.07E0	6.12E-1	2.03E-1
4.711E-2	3.800E2	2.632E1	3.80E-1	1.71E0	2.27E-1	7.83E-1
4.662E-2	3.760E2	2.660E1	3.65E-1	2.39E0	2.05E-1	1.39E0
4.612E-2	3.720E2	2.688E1	5.02E-1	3.21E0	2.76E-1	2.08E0
4.563E-2	3.680E2	2.717E1	1.08E0	4.62E0	6.10E-1	3.19E0
4.538E-2	3.660E2	2.732E1	2.25E0	5.78E0	1.37E0	4.22E0
4.513E-2	3.640E2	2.747E1	5.50E0	5.48E0	4.31E0	4.25E0
4.488E-2	3.620E2	2.762E1	5.85E0	2.26E0	4.35E0	1.34E0
4.439E-2	3.580E2	2.793E1	3.83E0	8.43E-1	2.71E0	3.82E-1
4.389E-2	3.540E2	2.825E1	2.60E0	1.03E0	1.77E0	3.04E-1
4.339E-2	3.500E2	2.857E1	2.13E0	2.32E0	7.17E-1	6.61E-1
4.302E-2	3.470E2	2.882E1	3.16E0	3.38E0	3.49E-1	1.54E0
4.277E-2	3.450E2	2.899E1	4.47E0	3.18E0	3.11E-1	2.04E0
4.240E-2	3.420E2	2.924E1	5.05E0	1.62E0	3.29E-1	2.78E0
4.191E-2	3.380E2	2.959E1	4.45E0	6.60E-1	4.81E-1	4.00E0
4.141E-2	3.340E2	2.994E1	3.97E0	3.67E-1	1.14E0	6.19E0
4.092E-2	3.300E2	3.030E1	3.64E0	2.50E-1	9.13E0	8.71E0
4.042E-2	3.260E2	3.067E1	3.40E0	1.94E-1	7.34E0	9.61E-1
3.992E-2	3.220E2	3.106E1	3.21E0	1.66E-1	5.65E0	3.36E-1
3.943E-2	3.180E2	3.145E1	3.06E0	1.54E-1	4.89E0	1.76E-1
3.893E-2	3.140E2	3.185E1	2.91E0	1.52E-1	4.45E0	1.11E-1
3.844E-2	3.100E2	3.226E1	2.78E0	1.58E-1	4.15E0	7.65E-2
3.794E-2	3.060E2	3.268E1	2.65E0	1.73E-1	3.95E0	5.65E-2
3.744E-2	3.020E2	3.311E1	2.52E0	1.98E-1	3.79E0	4.36E-2
3.695E-2	2.980E2	3.356E1	2.38E0	2.37E-1	3.66E0	3.48E-2
3.645E-2	2.940E2	3.401E1	2.22E0	2.97E-1	3.56E0	2.85E-2
3.596E-2	2.900E2	3.448E1	2.04E0	3.92E-1	3.48E0	2.37E-2
3.546E-2	2.860E2	3.497E1	1.83E0	5.50E-1	3.41E0	2.01E-2
3.496E-2	2.820E2	3.546E1	1.60E0	8.23E-1	3.35E0	1.73E-2
3.447E-2	2.780E2	3.597E1	1.45E0	1.26E0	3.30E0	1.50E-2
3.397E-2	2.740E2	3.650E1	1.47E0	1.82E0	3.25E0	1.32E-2
3.348E-2	2.700E2	3.704E1	1.72E0	2.44E0	3.21E0	1.17E-2
3.298E-2	2.660E2	3.759E1	2.30E0	3.06E0	3.18E0	1.04E-2
3.248E-2	2.620E2	3.817E1	3.35E0	3.39E0	3.15E0	9.34E-3
3.211E-2	2.590E2	3.861E1	4.28E0	3.11E0	3.13E0	8.64E-3
3.174E-2	2.560E2	3.906E1	4.86E0	2.39E0	3.11E0	8.02E-3
3.124E-2	2.520E2	3.968E1	4.93E0	1.47E0	3.08E0	7.28E-3
3.075E-2	2.480E2	4.032E1	4.70E0	9.15E-1	3.06E0	6.65E-3
3.025E-2	2.440E2	4.098E1	4.45E0	6.09E-1	3.04E0	6.09E-3
2.976E-2	2.400E2	4.167E1	4.25E0	4.31E-1	3.02E0	5.60E-3
2.926E-2	2.360E2	4.237E1	4.08E0	3.20E-1	3.00E0	5.16E-3
2.876E-2	2.320E2	4.310E1	3.94E0	2.47E-1	2.99E0	4.77E-3

TABLE I *(Continued)*

$CuGaS_2$

eV	cm^{-1}	μm	n_o	k_o	n_e	k_e
			[23]	[23]	[23]	[23]
2.827E-2	2.280E2	4.386E1	3.83E0	1.97E-1	2.97E0	4.42E-3
2.777E-2	2.240E2	4.464E1	3.74E0	1.60E-1	2.96E0	4.11E-3
2.728E-2	2.200E2	4.545E1	3.67E0	1.33E-1	2.95E0	3.83E-3
2.678E-2	2.160E2	4.630E1	3.60E0	1.12E-1	2.94E0	3.57E-3
2.628E-2	2.120E2	4.717E1	3.55E0	9.62E-2	2.92E0	3.34E-3
2.579E-2	2.080E2	4.808E1	3.50E0	8.33E-2	2.91E0	3.13E-3
2.529E-2	2.040E2	4.902E1	3.45E0	7.29E-2	2.90E0	2.93E-3
2.480E-2	2.000E2	5.000E1	3.41E0	6.42E-2	2.90E0	2.76E-3
1.860E-2	1.500E2	6.667E1	3.15E0	2.02E-2	2.82E0	1.37E-3
1.240E-2	1.000E2	1.000E2	3.04E0	8.74E-3	2.78E0	7.15E-4
6.199E-3	5.000E1	2.000E2	3.00E0	3.51E-3	2.76E0	3.12E-4

Gallium Selenide (GaSe)

DAVID F. EDWARDS
Tracy, California

Gallium selenide (GaSe) is a semiconductor that has recently received much attention because of its potential applications. GaSe has been proposed as the active compound for use in photovoltaic devices [1, 2], as intercalation electrodes in electrochemical lithium cells [3, 4], and as a nonlinear optical medium [5]. GaSe is also of interest because of its physical properties. The compound belongs to the family of metal chalcogens that crystallize in a layered structure. Each layer consists of four atomic sheets, Se–Ga–Ga–Se, that are bound together by strong forces, mostly covalent. The forces between layers are of the weak van der Waals type. The layer structure of GaSe is D_{3h} hexagonal symmetry with two formula units per layer unit cell [6–8]. Because of the different ways of stacking adjacent layers, GaSe crystallizes under several modifications. So far, four modifications have been proposed [9]. These are β (space group D_{6h}^4),γ (C_{3v}^5),ϵ (D_{3h}^1), and δ (C_{6v}^4). Several researchers [10, 11] question the existence of the β-structure and propose that γ-GaSe is a very rare modification [12] . The data reported in this chapter are for the ϵ-type modification. The interested reader is referred to the review paper by Fernelius [13] for an extensive compilation of the growth, structural and mechanical, thermal, electrical, and optical properties of single-crystal GaSe.

COMPLEX INDEX OF REFRACTION I

Brebner and Deverin [14] were among the first to report index-of-refraction measurements for GaSe. Their data were for a limited wavelength region in the vicinity of the band gap and for an undefined crystalline modification. Since this first report, a number of groups have reported index values using different techniques and different experimental conditions and crystalline modifications. A few developed analytical expressions that accurately represent their experimental data. Adachi and Shindo [15] used spec-

HANDBOOK OF OPTICAL CONSTANTS OF SOLIDS III

Copyright © 1998 by Academic Press.
All rights of reproduction in any form reserved
ISBN 0-12-544423-0/$25.00.

troscopic ellipsometery to measure the complex dielectric function, $\epsilon(\omega) = \epsilon_1(\omega) + i\epsilon_2(\omega)$, in the 2.0–5.0 eV photon-energy range for ϵ-GaSe. The layered structure of GaSe allows for easy cleavage with the crystallographic c-axis in the cleavage plane. From their measured data they have developed a mathematical model of the spectral dependence of $\epsilon(\omega)$ at energies below and above the fundamental absorption edge. Their model is based on the Kramers–Kronig transformation and is strongly connected with the electronic energy-band structure of the material. From their model the index of refraction, n, and extinction coefficient, k, have been calculated for selected wavelengths and are listed in Table I for light polarized perpendicular (n_o, k_o) and parallel (n_e, k_e) to the crystallographic c-axis. These data are plotted in Figs. 1 and 2, respectively. Other authors report optical measurements for this band-gap region, but only Adachi and Shindo [15] have developed a theoretical model that accurately represents their data over an extended wavelength region.

According to Adachi and Shindo [15], for light polarized perpendicular to the c-axis the complex dielectric function is the sum of the following three dispersive and one nondispersive terms. The contribution to $\epsilon(\omega)$ corresponding to the one-electron approximation for a transition from one of the three valence bands to the conduction band is

$$\epsilon(\omega) = -BX_1^{-2} ln(1 - X_1^2). \tag{1}$$

There is an additional contribution of the saddle-point exciton at this critical point given by

$$\epsilon(\omega) = B_\chi/(1 - X_1) \tag{2}$$

with

$$X_1 = (\hbar\omega + i\Gamma)/E_1. \tag{3}$$

The B's and Γ are, respectively, the strength and broadening parameters of these transitions.

The contribution to $\epsilon(\omega)$ corresponding to transitions from a second valence band to the conduction band is characterized as that of a damped harmonic oscillator,

$$\epsilon(\omega) = C/[(1 - X_3^2) - iX_3\gamma], \tag{4}$$

with

$$X_3 = \hbar\omega/E_3,$$

where C is the strength parameter and γ is the dimensionless broadening parameter. In these equations $\hbar\omega$ is the photon energy (eV), and E_1 and E_3 are the energies corresponding to critical points as resolved by the dielectric-function spectra. The B, B_χ, and C are adjustable parameters. The critical-point energies, E_1 and E_3, are adjusted to obtain better fits to the dielectric-function data. The values of these parameters are listed in Table II. To the

sum of Eqs. (1), (2), and (4) is added $\epsilon_{1\infty}$, the nondispersive term, to improve the fit. This term is assumed to arise from other higher-lying gap contributions.

The refractive index, n_o, and extinction coefficient, k_o, are obtained from the real and imaginary parts of the sum of Eqs. (1), (2), and (4) plus $\epsilon_{1\infty}$. It follows that

$$\epsilon(\omega)^{1/2} = n(\omega) + ik(\omega),$$

and

$$n(\omega) = \left(\frac{[\epsilon_1(\omega)^2 + \epsilon_2(\omega)^2]^{1/2} + \epsilon_1(\omega)}{2} \right)^{1/2}, \tag{5}$$

$$k(\omega) = \left(\frac{[\epsilon_1(\omega)^2 + \epsilon_2(\omega)^2]^{1/2} - \epsilon_1(\omega)}{2} \right)^{1/2}. \tag{6}$$

For photon energies greater than 0.1 eV the theoretical curve for n_o (n) is in good agreement with the experimental data of Adachi and Shindo [15] and those of Toullec *et al.* [16], Wasscher and Dieleman [17], and Piccioli *et al.* [18]. For photon energies below 0.1 eV the theoretical curve shows poor fit with the data of Piccioli *et al.* [18]. The reason given is that Adachi and Shindo did not take into account the reststrahlen dispersion. For this reststrahlen region the radiation field strongly interacts with the fundamental lattice vibrations [19].

An expression was also developed by Adachi and Shindo for the complex dielectric function for light polarized parallel to the c-axis. They fitted the experimental data of Toullec *et al.* [16] to a steplike absorption edge. The contribution to $\epsilon(\omega)$ for this type of transition is given by

$$\epsilon(\omega) = -AX_0^{-2}\ln(1 - X_0^2), \tag{7}$$

with

$$X_0 = (\hbar\omega + i\Gamma)/E_0,$$

where A and Γ are, respectively, the strength and broadening parameters and E_0 is the energy of the steplike edge. The extraordinary refractive indices n_e ($n\|$) and extinction coefficient k_e ($k\|$), are calculated from Eq. (7) plus the nondispersive term, $\epsilon_{1\infty}$, using Eqs. (5) and (6). The results are listed in Table I and plotted in Fig. 2.

Piccioli and co-workers [16, 18] have measured the ordinary and extraordinary optical constants for ϵ-GaSe between 0.45 and 330 μm. Three measuring techniques were used to cover this range. For the GaSe transparent region (12 to 33 μm and 70 to 330 μm) the index was determined from interference fringes produced by multiple internal reflections from the parallel faces of the sample. For the 0.45- to 0.62-μm region the index was determined from the reflectance of the sample of known thickness and which

had one face coated with aluminum. In the reststrahlen region (30–70 μm) the indices were determined from the infrared reflectance on thick samples. A Kramers–Kronig analysis of these reflectance data gives values of the transverse and longitudinal optical modes, ω_{TO} and ω_{LO}.

Piccioli and co-workers [16, 18] developed a theoretical fit of their data assuming the complex dielectric function to be a combination of electronic transitions (a polynomial development) and of lattice vibrations (a damped harmonic oscillator). Their expression as a function of wavenumber, ω, is

$$\epsilon(\omega) = A\omega^6 + B\omega^4 + C\omega^2 + \epsilon_\infty + \frac{(\omega_{LO}^2 - \omega_{TO}^2)\epsilon_\infty}{\omega_{TO}^2 - \omega^2 - i\Gamma\omega}, \tag{8}$$

where Γ is the damping of the harmonic oscillator, ω_{TO} and ω_{LO} are, respectively, the transverse and longitudinal optical-phonon wavenumbers, and A, B, C are parameters determined by a mean-square fit to the data. The index of refraction, n, and the extinction coefficient, k, are found from the real and imaginary parts of Eq. (8). Values for the parameters in Eq. (8) are given in Table III. The Piccioli *et al.* indices are listed in Table I for ϵ-GaSe as calculated using Eq. (8) and the parameters of Table III. According to Piccioli *et al.*, the calculated ordinary index of refraction reproduces the experimental results with a standard deviation of 0.002. The exception is for the band-gap region (0.619μm), where the measured n_o and k_o values deviate from those calculated by about 0.0075. Shown in Figs. 1 and 2 are the ordinary and extraordinary index of refraction and extinction coefficient, respectively, as calculated by the preceding equations. With reference to the extinction coefficient curves, it is not clear why the k values of Adachi and Shindo [15] are so much larger than those of Piccioli *et al.* One would expect the k values to decrease abruptly for photon energies below the band gap. As pointed out by Piccioli *et al.*, in the energy-gap region the transmission of the sample decreases so rapidily that important errors on the energy extreme could not be avoided. For this region their method was to measure the reflectance of a sample of known thickness and which was coated with aluminum on one face. It is not clear, but this could have a significant effect on the reflectance values and thus the smaller k values in this region.

II THERMAL COEFFICIENTS

The temperature variation of the ordinary index of refraction was measured by Antonioli *et al.* [20] for temperatures from 300 to 75 K in the 0.5- to 2.5-eV energy range. Their results are given by the expression

$$n(h\nu) = A + B(h\nu) + C(h\nu)^3, \tag{9}$$

where the phenomenological coefficients are given in Table IV for four selected temperatures. The reader is referred to the original report [20] for the complete coefficient list of 10 temperatures between 300 and 75 K. Antonioli *et al.* report the relative error for the refractive index $\Delta n/n \approx 10^{-3}$ for all the temperatures over the entire energy range investigated, with the exception of the spectral region around the exciton energy (619 nm). The 300-K values of Antionoli *et al.* are in good agreement with those of Piccioli *et al.* [18] for the 0.5- to 2.5-eV energy region.

The temperature dependence of the energy gap of ϵ-GaSe as reported by Reddy *et al.* [21] is

$$E_g = 2.137 \exp(-T \times 10^{-4}/0.61), \tag{10}$$

where T is the temperature for the range 0 to 300 K, and the energy gap, E_g, is in eV.

PRESSURE COEFFICIENT III

Gauthier *et al.* [22] have measured the refractive index of room-temperature ϵ-GaSe in the region of the direct-gap energy (1.5 to 1.9 eV) for hydrostatic pressures up to 8 GPa. They report no evidence of a phase transition, indicating that the layered structure of ϵ-GaSe is stable for this pressure range. They also found the relative variation of the index with pressure to be the same for their measured spectral region, indicating that the index dispersion does not vary significantly with pressure. From their data for the relative variation of index, the following polynomial was fit by a least-squares technique.

$$\frac{n}{n(0)} = 0.99977 + 1.8130 \times 10^{-2}p - 3.9367 \times 10^{-3}p^2 + 4.4431 \times 10^{-4}p^3 - 1.8098 \times 10^{-5}p^4, \tag{11}$$

where $n(0)$ is the atmospheric-pressure index and p is the hydrostatic pressure in GPa. They report a precision of better than 1% for $n(\lambda,p)$.

REFERENCES

1. A. Segura, J. P. Guesdon, J. M. Besson, and A. Chevy, *Rev. Phys. Appl.* **14**, 253 (1979).
2. C. Clemen, X. I. Saldana, P. Munz, and E. Butcher, *Phys. Status Solidi A* **49**, 437 (1978).
3. C. Julien and E. Hatzikkraniotis, *Mater. Lett.* **5**, 134 (1988).
4. Z. D. Kovalyuk, M. N. Pyrla, A. I. Seredyuk, and K. D. Tovstyuk, *Inorg. Mater.* **21**, 1444 (1985).
5. C. Hirliman, J. F. Morhange, M. A. Kanehisa, A. Chevy, and C. H. Brito-Cruz, *Appl. Phys. Lett.* **55**, 2307 (1989).

6. H. Hahn and G. Z. Frank, *Anorg. Allg. Chem.* **278**, 340 (1955).
7. K. Schubert, E. Dorre, and M. Kluge, *Z. Metallkd.* **46**, 216 (1955).
8. F. Jellinek and H. Hahn, *Z. Naturforsch.* **B16,** 713 (1961).
9. A. Kuhn, A. Chevy, and R. Chevalier, *Phys. Status Solidi A* **31, 469, (1975).**
10. A. Polian, K. Kunc, and A. Kuhn, *Solid State Commun.* **19,** 1079 (1976).
11. A. Gouskov, J. Camassel, and L. Gouskov, *Prog. Cryst. Growth Charact.* **5,** 323 (1982).
12. E. Finkman and A. Rizzo, *Solid State Commun.* **15,** 1841 (1974).
13. N. C. Fernelius, *Prog. Cryst. Growth Charat.* **28**, 275 (1994).
14. J. L. Brebner and J. A. Deverin, *Helv. Phys. Acta* **38,** 650 (1965).
15. S. Adachi and Y. Shindo, *J. Appl. Phys.* **71**, 428 (1992).
16. R. Le Toullec, N. Piccioli, M. Mejatty, and M. Balkanski, *Ital. Nuovo Cimento.* **38B**, 159 (1977).
17. J. O. Wasscher and J. Dieleman, *Phys. Lett.* **A39**, 279 (1972).
18. N. Piccioli, R. Le Toullec, M. Mejatty, and M. Balkanski, *Appl. Opt.* **16,** 1236 (1977).
19. See, for instance, M. Balkanski, *in* "Optical Properties of Soilds" (F. Abeles, ed.), p. 529. North-Holland Publ., Amsterdam, 1972.
20. G. Antonioli, D. Bianchi, and P. Franzosi, *Appl. Opt.* **18**, 3847 (1979).
21. R. R. Reddy, M. Ravi Kumar, and T. V. R. Rao, *Infrared Phys.* **34,** 103 (1993).
22. M. Gauthier, A. Polian, J. M. Besson, and A. Chevy, *Phys. Rev. B* **40**, 3837 (1989).

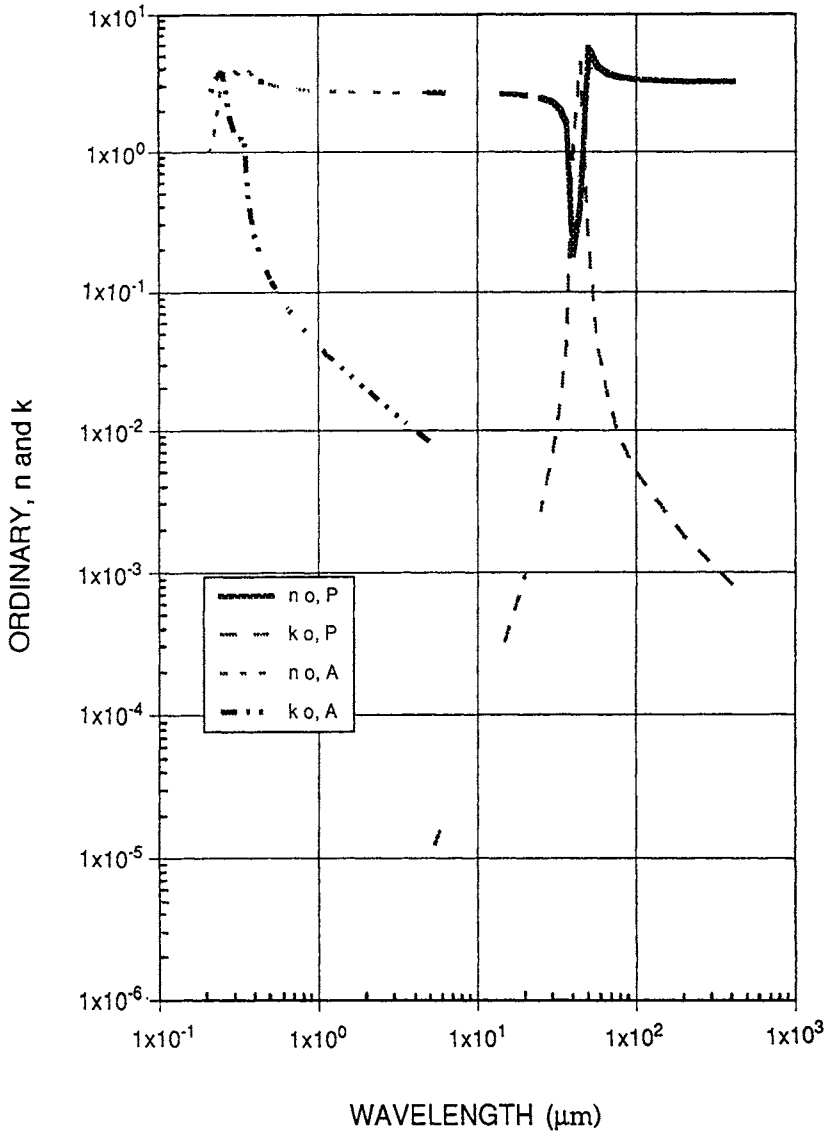

Fig. 1. Log–log plot of ordinary n_o and k_o versus wavelength in micrometers for ϵ-GaSe. The curves n_o,A and k_o,A are calculated from the sum of Eqs. (1), (2), (4), and $\epsilon_{1\infty} = 1.25$. The curves n_o,P and k_o,P are calculated from Eq. (8).

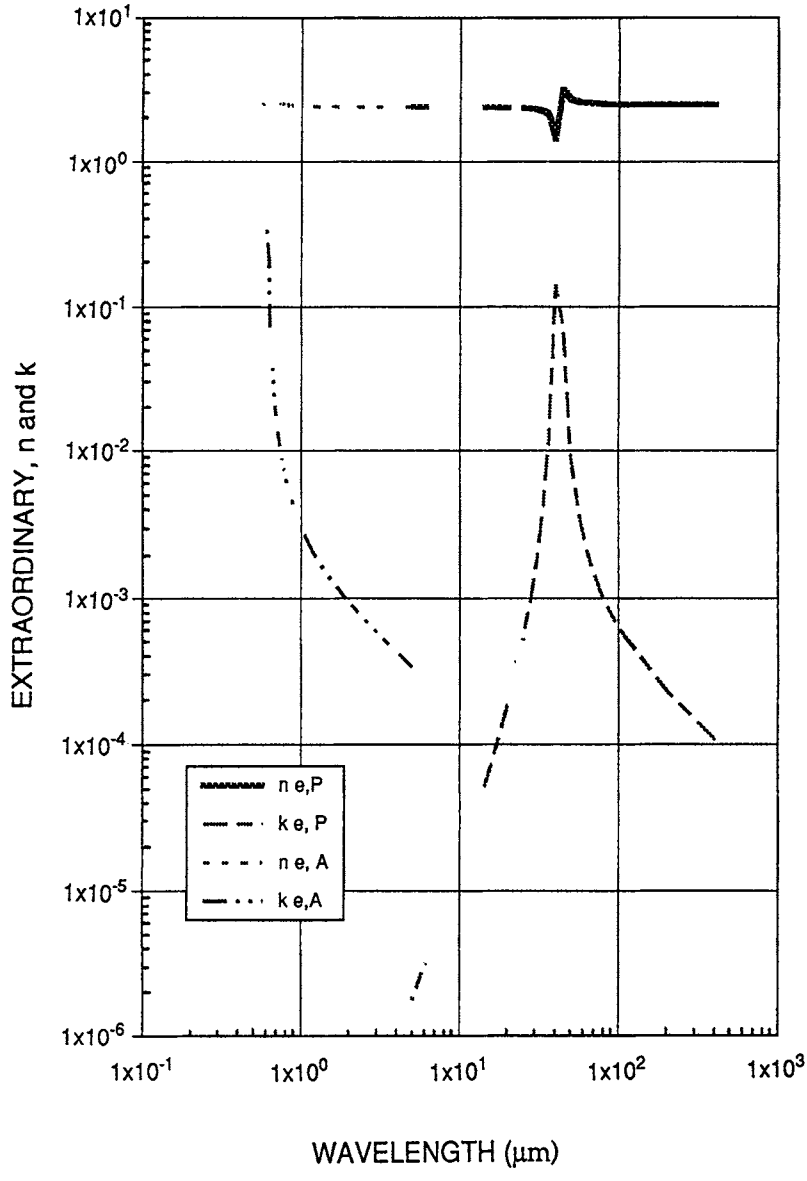

Fig. 2. Log–log plot of extraordinary n_e and k_e versus wavelength in micrometers for ϵ-GaSe. The curves n_e,A and k_e,A are calculated from the sum of Eq. (7) and $\epsilon_{1\infty} = 4.9$. The curves n_e,P and k_e,P are calculated from Eq. (8).

TABLE I

Values of n and k for ε-GaSe as Calculated from the Expressions of Adachi and Shindo [15] and Piccioli *et al.* [16, 18]

eV	cm^{-1}	μm	$n_o(P)$	$k_o(P)$	$n_e(P)$	$k_e(P)$	$n_o(A)$	$k_o(A)$	$n_e(A)$	$k_e(A)$
6.00	48309	0.207					1.00451 [15]	2.60550 [15]		
5.95	47907	0.209					1.03292	2.66138		
5.90	47504	0.211					1.06430	2.71991		
5.85	47101	0.212					1.09908	2.78124		
5.80	46699	0.214					1.13777	2.84549		
5.75	46296	0.216					1.18099	2.91279		
5.70	45894	0.218					1.22946	2.98323		
5.65	45491	0.220					1.28404	3.05683		
5.60	45089	0.222					1.34730	3.13354		
5.50	44686	0.224					1.41574	3.21320		
5.00	44283	0.226					1.49544	3.29542		
5.45	43881	0.228					1.58647	3.37957		
5.40	43478	0.230					1.69067	3.46464		
5.35	43076	0.232					1.81006	3.54905		
5.30	42673	0.234					1.94680	3.63049		
5.25	42271	0.237					2.10295	3.70570		
5.20	41868	0.239					2.28015	3.77020		
5.15	41465	0.241					2.47909	3.81818		
5.10	41063	0.244					2.69870	3.84256		
5.05	40660	0.246					2.93529	3.83555		
5.00	40258	0.248					3.18170	3.78976		
4.95	39855	0.251					3.42720	3.70010		
4.90	39453	0.253					3.65850	3.56579		
4.85	39050	0.256					3.86214	3.39166		
4.80	38647	0.259					4.02747	3.18787		
4.75	38245	0.261					4.14898	2.96771		
4.70	37842	0.264					4.22682	2.74465		

(continued)

TABLE I *(Continued)*

ϵ-GaSe

eV	cm^{-1}	μm	n_o(P)	k_o(P)	n_e(P)	k_e(P)	n_o(A)	k_o(A)	n_e(A)	k_e(A)
4.65	37440	0.267					4.26569	2.52983		
4.55	36634	0.273					4.25599	2.15190		
4.50	36232	0.276					4.22252	1.99429		
4.45	35829	0.279					4.17839	1.85759		
4.40	35427	0.282					4.12830	1.74029		
4.35	35024	0.286					4.07574	1.64041		
4.30	34622	0.289					4.02321	1.55586		
4.25	34219	0.292					3.97245	1.48466		
4.20	33816	0.296					3.92466	1.42501		
4.15	33414	0.299					3.88061	1.37539		
4.10	33011	0.303					3.84085	1.33457		
4.05	32609	0.307					3.80573	1.30168		
4.00	32206	0.311					3.77557	1.27623		
3.95	31804	0.314					3.75804	1.25832		
3.90	31401	0.318					3.73254	1.24886		
3.85	30998	0.323					3.72316	1.24886		
3.80	30596	0.327					3.72909	1.23648		
3.75	30193	0.331					3.76591	1.29431		
3.70	29791	0.336					3.86252	1.32114		
3.65	29388	0.340					4.02957	1.27878		
3.60	28986	0.345					4.17863	1.10447		
3.55	28583	0.350					4.20760	8.7237E-1		
3.50	28180	0.355					4.14411	6.8188E-1		
3.45	27778	0.360					4.04945	5.5000E-1		
3.40	27375	0.365					3.95357	4.6035E-1		

3.35	26973	0.371		3.86555	3.9730E-1
3.30	26570	0.376		3.78686	3.5091E-1
3.25	26167	0.382		3.71674	3.1529E-1
3.20	25765	0.388		3.65396	2.8692E-1
3.15	25362	0.394		3.59736	2.6364E-1
3.10	24960	0.401		3.54597	2.4405E-1
3.05	24557	0.407		3.49899	2.2724E-1
3.00	24155	0.414		3.45579	2.1258E-1
2.95	23752	0.421		3.41586	1.9962E-1
2.90	23349	0.428		3.37878	1.8804E-1
2.86	23000	0.435	3.3179		
2.85	22947	0.436		3.34421	1.7760E-1
2.84	22850	0.438	3.3064		
2.82	22725	0.440	3.2970		
2.80	22544	0.444		3.31187	1.6810E-1
2.76	22225	0.450	3.2607		
2.75	22142	0.452		3.28152	1.5942E-1
2.70	21739	0.460		3.25297	1.5143E-1
2.65	21337	0.469		3.22604	1.4404E-1
2.60	20934	0.478		3.23006	1.3718E-1
2.55	20531	0.487		3.17651	1.3079E-1
2.50	20129	0.497		3.15367	1.2481E-1
2.48	20000	0.500	3.1226		
2.45	19726	0.507		3.13198	1.1920E-1
2.40	19324	0.518		3.11136	1.1393E-1
2.35	18921	0.529		3.09173	1.0896E-1
2.30	18519	0.540		3.07303	1.0426E-1
2.26	18175	0.550	3.0336 [18]		
2.25	18116	0.552		3.05520	9.9813E-2

(continued)

TABLE I *(Continued)*

ϵ-GaSe

eV	cm^{-1}	μm	n_o(P)	k_o(P)	n_e(P)	k_e(P)	n_o(A)	k_o(A)	n_e(A)	k_e(A)
2.20	17713	0.565					3.03819		2.49335 [15]	4.1439E-1 [15]
2.15	17311	0.578					3.02194	9.1579E-2	2.54691	4.1643E-1
2.10	16908	0.591					3.00642	8.7758E-2	2.61759	4.0900E-1
2.07	16650	0.601	2.9729							
2.05	16506	0.606					2.99158	8.4114E-2	2.7182	3.7344E-1
2.00	16103	0.621					2.97738	8.0632E-2	2.8225	2.1940E-1
1.95	15700	0.637					2.96381	7.7301E-2	2.73322	7.2733E-2
1.91	15375	0.650	2.9299							
1.90	15298	0.654					2.95082	7.4110E-2	2.65709	3.7473E-2
1.85	14895	0.671					2.93838	7.1048E-2	2.60927	2.4244E-2
1.80	14493	0.690					2.92648	6.8107E-2	2.57582	1.7502E-2
1.77	14275	0.701	2.8976							
1.75	14090	0.710					2.91509	6.5278E-2	2.55064	1.3464E-2
1.70	13688	0.731					2.90418	6.2553E-2	2.53077	1.0793E-2
1.65	13325	0.750	2.8730							
1.65	13285	0.753					2.89379	5.9926E-2	2.51456	8.9065E-3
1.60	12882	0.776					2.88375	5.7389E-2	2.50101	7.5083E-3
1.55	12500	0.800	2.8537							
1.55	12480	0.801					2.87420	5.4937E-2	2.48948	6.4340E-3
1.50	12077	0.828					2.86505	5.2565E-2	2.47953	5.5848E-3
1.46	11750	0.851	2.8377	4.2147E-8						
1.45	11675	0.857					2.85631	5.0267E-2	2.47084	4.8941E-3
1.40	11272	0.887					2.84795	4.8039E-2	2.46319	4.3320E-3
1.38	11100	0.901	2.8250	5.5777E-8						
1.35	10870	0.920					2.83997	4.5875E-2	2.456396	3.8579E-3

1.31	10525	0.950	2.8145	6.0664E-8						
1.30	10467	0.955					2.83235	4.3772E-2	2.45032	3.4554E-3
1.25	10064	0.994					2.82508	4.1727E-2	2.44486	3.1095E-3
1.24	10000	1.000	2.8056	7.8850E-8		2.1073E-8				
1.20	9662	1.035					2.81815	3.9734E-2	2.43994	2.8091E-3
1.15	9259	1.080					2.81156	3.7792E-2	2.43549	2.5458E-3
1.10	8857	1.129					2.80528	3.4044E-2	2.43145	2.3131E-3
1.05	8454	1.183					2.79932	3.4044E-2	2.42778	2.1056E-3
1.0000	8052	1.242					2.79366	3.2232E-2	2.41443	1.9195E-3
0.9500	7649	1.307					2.78830	3.0459E-2	2.42138	1.7514E-3
0.9000	7246	1.380					2.78323	2.8721E-2	2.41859	1.5985E-3
0.8500	6844	1.461					2.77845	2.7015E-2	2.41605	1.4587E-3
0.8000	6441	1.553					2.77395	2.5341E-2	2.41373	1.3301E-3
0.7500	6039	1.656					2.76971	2.3695E-2	2.41161	1.2112E-3
0.7000	5636	1.774					2.76575	2.2075E-2	2.40969	1.1007E-3
0.6500	5233	1.911					2.76205	2.0479E-2	2.40794	9.9744E-4
0.6210	5000	2.000	2.7459 [18]	6.2974E-7 [18]		1.1151E-7 [18]				
0.6000	4831	2.070					2.75862	1.8906E-2	2.40636	9.0048E-4
0.5500	4428	2.258					2.75542	1.7353E-2	2.40494	8.0898E-4
0.5000	4026	2.484					2.75250	1.5818E-2	2.40366	7.2221E-4
0.4500	3623	2.760					2.74982	1.4300E-2	2.40253	6.3954E-4
0.4000	3221	3.105					2.74738	1.2796E-2	2.40153	5.6037E-4
0.3500	2818	3.549					2.74519	1.1306E-2	2.40066	4.8421E-4
0.3105	2500	4.000	2.7286	5.1258E-6	2.4045	8.9630E-7				
0.3000	2415	4.140					2.74324	9.8277E-3	2.39992	4.1059E-4
0.2500	2013	4.968					2.74153	8.3592E-3	2.39929	3.3907E-4
0.2484	2000	5.000	2.7245	1.0110E-5	2.4021	1.7703E-6				
0.2049	1650	6.061	2.7204	1.8229E-5	2.4005	3.1976E-6				
0.2000	1610	6.210					2.74005	6.8990E-3	2.39879	2.6926E-4

(continued)

TABLE I *(Continued)*

ε-GaSe

eV	cm^{-1}	μm	n_o(P)	k_o(P)	n_e(P)	k_e(P)	n_o(A)	k_o(A)	n_e(A)	k_e(A)
0.1553	1250	8.000	2.7120	4.3139E-5	2.3981	7.5976E-6				
0.1500	1208	8.280					2.73881	5.4456E-3	2.3984	2.0080E-4
0.1242	1000	10.000	2.7012	8.7524E-5	2.3956	1.5497E-5				
0.1000	805	12.420					2.73780	3.9975E-3		1.3332E-4
0.0869	700	14.286	2.6687	2.8601E-4	2.3890	5.1486E-5				
0.0776	625	16.000	2.6511	4.2644E-4	2.3856	7.7458E-5				
0.0683	550	18.182	2.6240	6.8385E-4	2.3802	1.2594E-4				
0.0652	525	19.048	2.6115	8.1808E-4	2.3777	1.5162E-4				
0.0621	500	20.000	2.5965	9.9241E-4	2.3747	1.8534E-4				
0.0500	403	24.840						2.5531E-3		6.6498E-5
0.0497	400	25.000	2.4878	2.6447E-3	2.3523	5.2160E-4				
0.0435	350	28.571	2.3616	5.3937E-3	2.3247	1.1314E-3				
0.0404	325	30.769	2.2479	8.6346E-3	2.2985	1.9113E-3				
0.0373	300	33.333	2.0525	1.5949E-2	2.2500	3.8504E-3				
0.0342	275	36.364	1.6339	4.0131E-2	2.1326	1.1290E-2				
0.0311	250	40.000	0.1824	1.0295E + 0	1.4470	1.4084E-1				
0.0279	225	44.444	0.4115	4.5493E + 0	3.1580	7.5688E-2				
0.0248	200	50.000	5.7381	2.3813E-1	2.6869	9.4049E-3				
0.0217	175	57.143	4.1270	4.0770E-2	2.5855	3.4295E-3				
0.0186	150	66.667	3.6961	1.6398E-2	2.5420	1.7213E-3				
0.0155	125	80.000	3.4979	8.5744E-3	2.5185	9.9852E-4				
0.0124	100	100.000	3.3879	5.0204E-3	2.5043	6.1952E-4				
0.0062	50	200.000	3.2826	1.7673E-3	2.4900	2.3056E-4				
0.0031	25	400.000	3.2614	8.1678E-4	2.4870	1.0776E-4				

TABLE II

Parameters Used in the Calculation of the Optical Constants for ϵ-GaSe [15] from Eqs. (1)–(4) and (7)

Parameter	Ordinary	Extraordinary
E_0(eV)		2.00
A		0.85
Γ(meV)		30
E_1(eV)	3.63	
B	2.27	
B_χ	0.17	
Γ(eV)	0.13	
E_3(eV)	4.89	
C	3.8	
γ	0.17	
$\epsilon_{1\infty}$	1.25	4.9

TABLE III

Parameters Used in the Calculation of the Optical Constants for ϵ-GaSe [16, 18] from Eq. (8)

Parameter	Ordinary		Extraordinary
ω_{LO} (cm^{-1})	254.7		245.5
ω_{TO} (cm^{-1})	213.5		237
Γ (cm^{-1})	3		2.8
ϵ_∞	7.443		5.76
A (cm^6)		$6.105\ 10^{-27}$	
B (cm^4)		$1.8564\ 10^{-18}$	
C (cm^2)		$4.0499\ 10^{-9}$	

TABLE IV

Coefficients of the Thermal Dependence of the Refractive Index Dispersion Relation [20] to be Used in Eq. (9)

T(K)	A	B (eV^{-1})	C (eV^{-3})
300	2.716	0.04053	0.01986
225	2.709	0.04059	0.01916
150	2.702	0.04116	0.01831
75	2.697	0.04186	0.01774

Gallium Telluride (GaTe)

DAVID F. EDWARDS
Tracy, California

Gallium telluride, GaTe, is a layered semiconductor belonging to the III–VI metal-chalcogen family of GaS, GaSe, and GaTe. The crystal structure of GaTe, however, is considerably more complex than the structures of GaS and GaSe. These layered crystals are made up of weakly interacting two-dimensional sheets, each four atoms thick, which, when stacked in a variety of ways, give the full three-dimensional structure. Two modifications, one stable and the other metastable, have been reported for GaTe [1]. The stable modification, α-GaTe, has a monoclinic structure with space group C_{2h}^3 – C2/m. The metastable modification, β-GaTe, is hexagonal with space group D_{6h}^4 – C6/mmc. The hexagonal phase converts to the monoclinic phase at high temperatures. Only the stable modification, α-GaTe, is of interest here.

The crystal structure of monoclinic α-GaTe is shown in Fig. 1 [2]. The crystallographic *abc*-axes are indicated. The coordinate axes *(xyz)* are not shown, but the *a* and *b* axes are in the *x* and *y* directions, respectively. The easy cleavage plane for these layered crystals is the *x*–*y* plane with *z* normal to this plane.

Girlanda *et al.* [3] have measured the reflectance of a freshly cleaved α-GaTe sample at the fundamental absorption edge using light polarized in different directions inside the *x*–*y* plane. They report reflection spectra for $\mathbf{E}\perp\mathbf{b}$ and $\mathbf{E}\parallel\mathbf{b}$ for the 2–6 eV photon-energy range. They also measured the reflectance for unpolarized radiation in the same energy region. Unfortunately, insufficient data are given to allow the determination of *n* and *k*. However, their reflectance spectra do show appreciable variation for the two polarizations, both in intensity and in the energies of the main peaks at the absorption edge. These variations are strong evidence of the expected polarization dependence of *n* and *k* for a monoclinic crystal.

Levêque *et al.* [4] have made similar measurements of the reflectance of α-GaTe in the 2.5- to 26-eV energy range using polarized synchrotron radiation. Their measurements were for normal and oblique incidence on a freshly cleaved surface. Two reflectance curves permit the determination of

HANDBOOK OF OPTICAL CONSTANTS OF SOLIDS III

Copyright © 1998 by Academic Press.
All rights of reproduction in any form reserved
ISBN 0-12-544423-0/$25.00.

the complex refractive-index tensor from which they extract the three complex refractive indices relative to the *xyz* crystallographic directions. Given in Table I are the n and k values for three polarizations ($\mathbf{E}\|\mathbf{x}$, $\mathbf{E}\|\mathbf{y}$, $\mathbf{E}\|\mathbf{z}$) resulting from their measurements and analysis. The n and k values are plotted in Figs. 2 and 3, respectively, as functions of the wavelength.

This work is particularly interesting because they have deduced three different dielectric constants of a biaxial crystal only from reflectance measurements. A total of eight reflectance curves were needed ($\mathbf{E}\|\mathbf{a}$, $\mathbf{E}\perp\mathbf{a}$, $\mathbf{E}\|\mathbf{b}$, $\mathbf{E}\perp\mathbf{b}$, for two angles of incidence). They also show that their results are consistent with the Kramers–Kronig relations. They do note, however, that their method has inherent systematic errors because of neglecting the nondiagonal terms of the dielectric tensor.

Grasso *et al.* [5] have measured the optical constants of room-temperature α-GaTe in the spectral region of the energy gap (1.0 to 6.0 eV). The real and imaginary parts of the complex refractive index (n,k) were obtained from the normal incidence reflectivity spectrum using a rapidly converging Kramers–Kronig transform. For these measurements it is assumed unpolarized light and cleaved *xy*-surfaces were used. The room temperature n and k values are listed in Table II and are shown in Figs. 4 and 5, respectively.

Tatsuyama *et al.* [6] have also measured the room-temperature optical constants of α-GaTe using reflectance and transmittance measurements on single crystals. The samples were cleaved along the easy planes, and the radiation was unpolarized and near normal incidence. Their measurements were in a narrow spectral region about the energy gap (1.7 eV). The absorption coefficient was calculated from the relation

$$\alpha = \frac{1}{d} \ln \frac{(1-R)^2 + \sqrt{(1-R)^4 + T^2R^2}}{2T},$$

where d is the sample thickness, R the reflectance, and T the transmittance. The extinction coefficient, k, has been calculated using

$$k = \frac{\lambda\alpha}{4\pi},$$

where λ is the wavelength. Tatsuyama *et al.* obtained their index of refraction values from the reflectance assuming k is small:

$$n = \frac{1+\sqrt{R}}{1-\sqrt{R}}.$$

The Tatsuyama *et al.* n and k values are listed in Table II. The spectral dependence of n and k is given in Figs. 4 and 5, respectively. Tatsuyama *et al.*

also report absorption values (and thus k values) for sample temperature of 77 K for the 1.5- to 2.0-eV spectral region.

Brebner *et al.* [7] and Grandolfo *et al.* [8] also report absorption-coefficient data for the 1.7-eV spectral region. Both groups used unpolarized light on samples cleaved along the x–y plane.

Mead and Genzel [9] report room-temperature, far-infrared optical constants (n,k) of α-GaTe for $\mathbf{E}\perp\mathbf{b}$ for the 50- to 350-cm^{-1} frequency region. Their measuring technique was that of asymmetric Fourier transform spectroscopy. They point out that the great advantage of this technique is that both the real and imaginary parts of the index of refraction can be measured directly in a single experiment. Their measurements were on the $(\bar{2}01)$ cleavage plane. The crystal structure of α-GaTe allows 33 degrees of freedom to be assigned to the phonon modes. It is therefore expected that the n and k spectra would be highly structured as shown in Figs. 4 and 5. The spectra show three strong reststrahlen bands with peaks at 146, 160, and 200 cm^{-1}. Weaker bands are noted at 89, 103, 115, 126, and 216 cm^{-1}. Mead and Genzel suggest that the missing infrared-active lattice modes may be too weak to detect. n and k values as read from Figs. 4 and 5 are listed in Table II.

REFERENCES

1. S. A. Semiletov and V. A. Vlasov, *Kristallografia* **8**, 877 (1963); *Sov. Phys. Crystallogr.* **8**, 704 (1964).
2. W. B. Pearson, *Acta Crystallogr.* **17**, 1 (1964).
3. R. Girlanda, V. Grasso, G. Mondio, and E. Doni, *Solid State Commun.* **57**, 253 (1986).
4. G. Levêque, C. G. Olson, and D. W. Lynch, *J. Phys. (Paris)* **45**, 1699 (1984).
5. V. Grasso, G. Mondio, and G. Saitta, *Phys. Lett.* **64A**, 95 (1973).
6. C. Tatsuyama, Y. Watanabe, C. Hamaguchi, and J. Nakai, *J. Phys. Soc. Jpn.* **29**, 150 (1970).
7. J. L. Brebner, G. Fischer, and E. Mooser, *J. Phys. Chem. Solids* **23**, 1417 (1962).
8. M. Grandolfo, E. Gratton, F. Anfosso Somma, and P. Vecchia, *Phys. Status Solidi B* **48**, 729 (1971).
9. D. G. Mead and L. Genzel, *Infrared Phys.* **18**, 555 (1978).

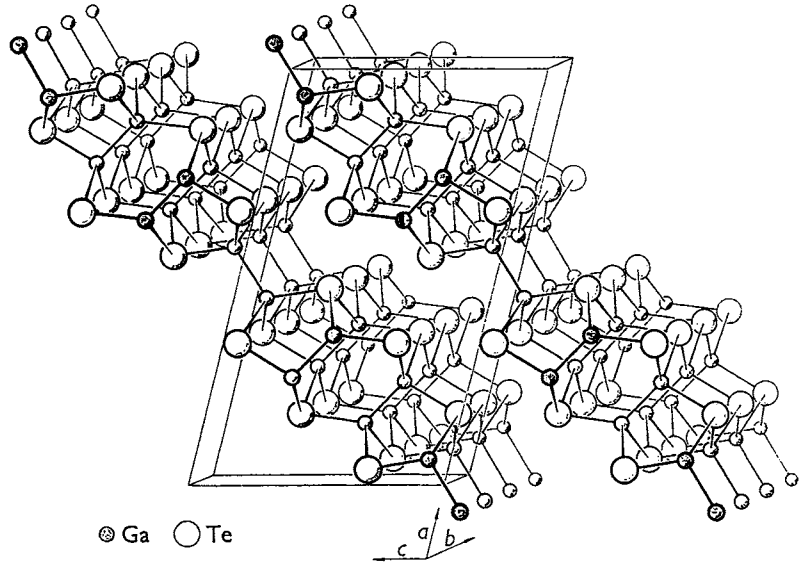

Fig. 1. The GaTe structure (monoclinic), after Pearson [2].

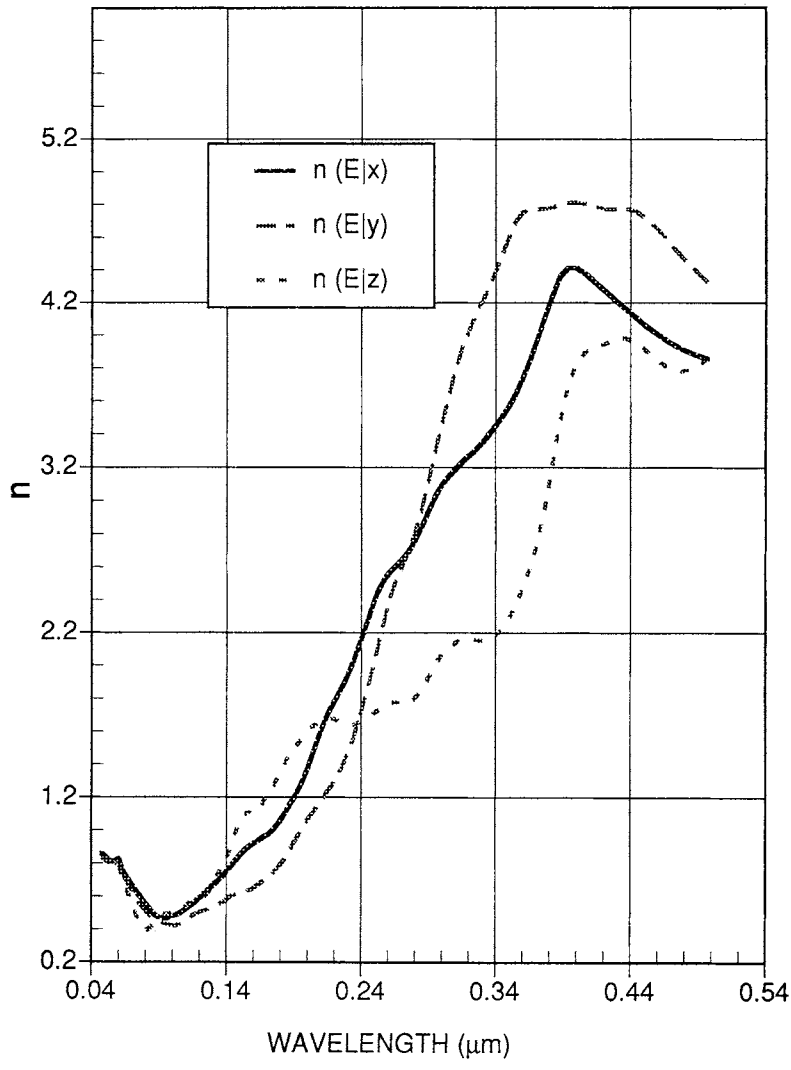

Fig. 2. Plot of n versus wavelength in microns as calculated by Levêque *et al.* [4].

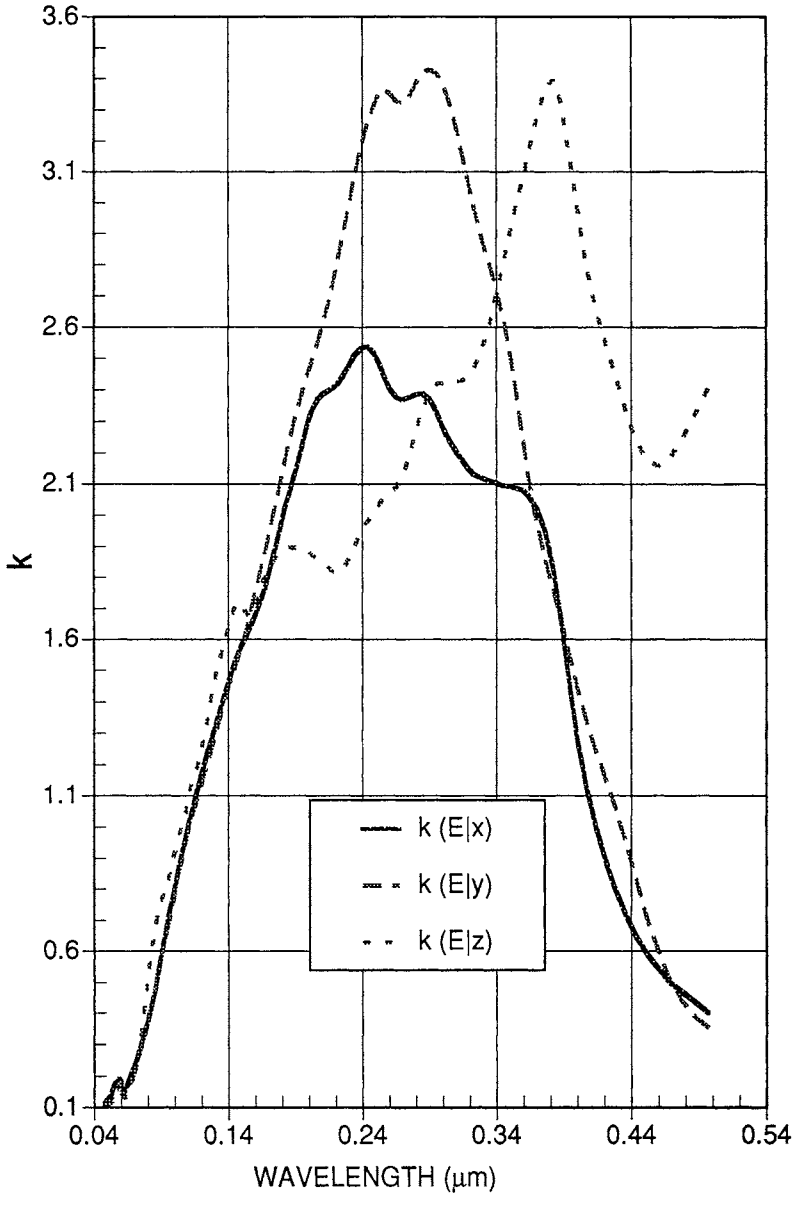

Fig. 3. Plot of k versus wavelength in microns as calculated by Levêque *et al.* [4].

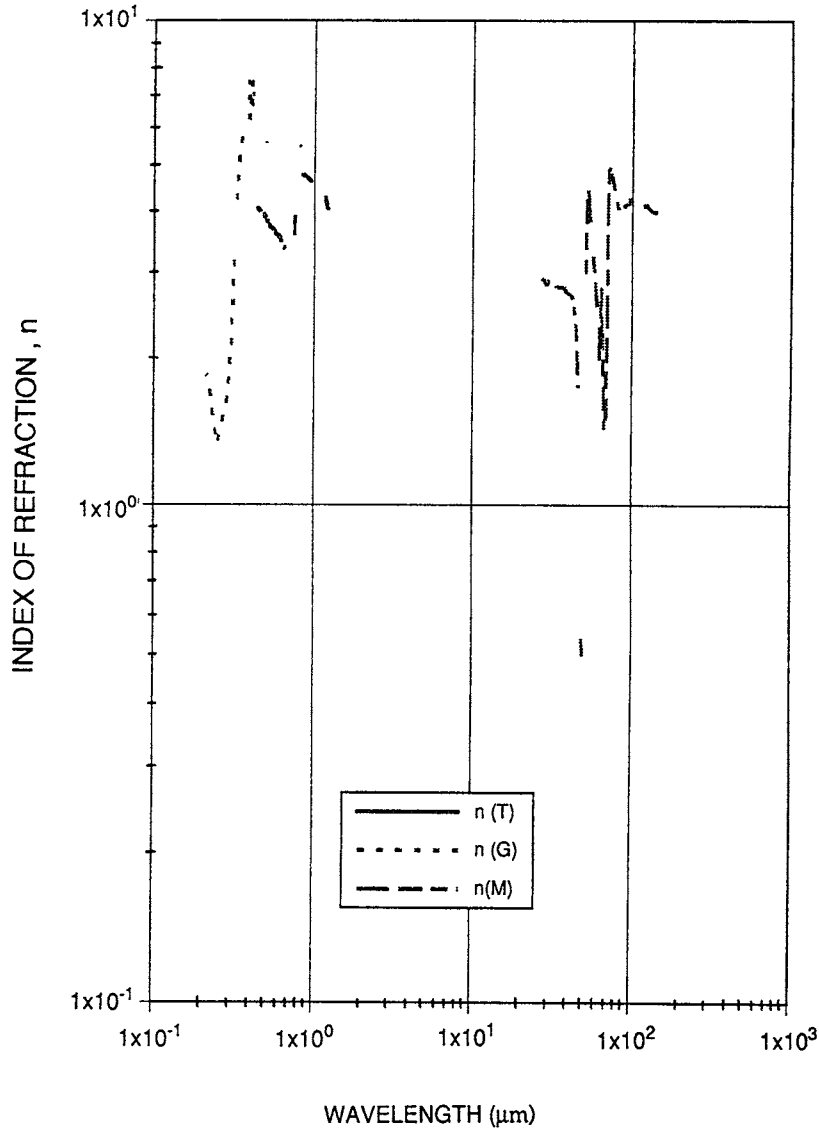

Fig. 4. Log–log plot of n versus wavelength (micrometers). The curve $n(T)$ is from Tatsuyama *et al.* [6], curve n (G) from Grasso *et al.* [5], and curve $n(M)$ from Mead and Genzel [9].

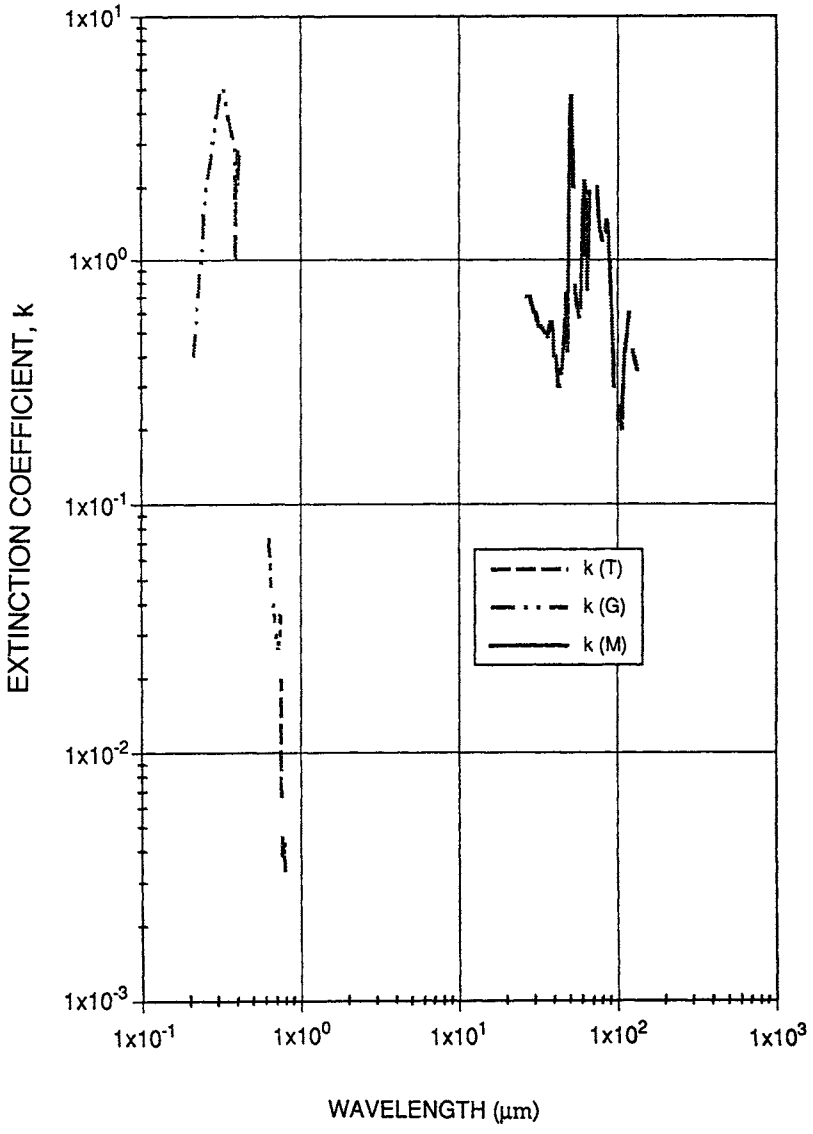

Fig. 5. Log–log plot of k versus wavelength (micrometers). The curve $k(T)$ is from Tatsuyama *et al.* [6], curve $k(G)$ from Grasso *et al.* [5], and curve $k(M)$ from Mead and Genzel [9].

TABLE I

Values of n and k for GaTe as Calculated by Levêque *et al.* [4]

eV	cm^{-1}	μm	n(E∥x)	n(E∥y)	n(E∥z)	k(E∥x)	k(E∥y)	k(E∥z)
26.10	210145	0.0476	0.8587	0.8579	0.8336	0.1100	0.1081	0.0933
25.80	207729	0.0481	0.8552	0.8547	0.8294	0.1128	0.1103	0.0939
25.50	205314	0.0487	0.8513	0.8507	0.8255	0.1161	0.1128	0.0986
25.20	202899	0.0493	0.8475	0.8466	0.8211	0.1196	0.1164	0.1004
24.90	200483	0.0499	0.8438	0.8436	0.8173	0.1231	0.1202	0.1051
24.60	198068	0.0505	0.8399	0.8412	0.8133	0.1266	0.1232	0.1064
24.30	195652	0.0511	0.8358	0.8386	0.8096	0.1301	0.1249	0.1098
24.00	193237	0.0518	0.8308	0.8344	0.8036	0.1330	0.1255	0.1069
23.80	191626	0.0522	0.8265	0.8300	0.7981	0.1354	0.1260	0.1096
23.60	190016	0.0526	0.8211	0.8245	0.7920	0.1394	0.1280	0.1131
23.40	188406	0.0531	0.8166	0.8192	0.7850	0.1449	0.1314	0.1145
23.20	186795	0.0535	0.8133	0.8144	0.7786	0.1515	0.1363	0.1207
23.00	185185	0.0540	0.8114	0.8116	0.7725	0.1584	0.1420	0.1226
22.80	183575	0.0545	0.8117	0.8104	0.7672	0.1653	0.1469	0.1320
22.60	181965	0.0550	0.8133	0.8095	0.7652	0.1702	0.1505	0.1399
22.40	180354	0.0554	0.8146	0.8084	0.7648	0.1735	0.1532	0.1448
22.20	178744	0.0559	0.8154	0.8065	0.7633	0.1758	0.1554	0.1458
22.00	177134	0.0565	0.8157	0.8037	0.7585	0.1773	0.1582	0.1481
21.90	176329	0.0567	0.8150	0.8021	0.7562	0.1779	0.1603	0.1516
21.80	175523	0.0570	0.8140	0.8011	0.7528	0.1786	0.1627	0.1502
21.70	174718	0.0572	0.8130	0.8006	0.7501	0.1806	0.1655	0.1579
21.60	173913	0.0575	0.8124	0.8007	0.7481	0.1824	0.1680	0.1579
21.50	173108	0.0578	0.8123	0.8014	0.7469	0.1852	0.1709	0.1666
21.40	172303	0.0580	0.8132	0.8033	0.7469	0.1878	0.1735	0.1677
21.30	171498	0.0583	0.8162	0.8070	0.7485	0.1901	0.1752	0.1751
21.20	170692	0.0586	0.8199	0.8118	0.7530	0.1902	0.1741	0.1777
21.10	169887	0.0589	0.8235	0.8153	0.7563	0.1870	0.1691	0.1756
21.00	169082	0.0591	0.8231	0.8143	0.7555	0.1821	0.1629	0.1737
20.90	168277	0.0594	0.8194	0.8101	0.7535	0.1804	0.1600	0.1777
20.80	167472	0.0597	0.8179	0.8084	0.7551	0.1831	0.1609	0.1822
20.70	166667	0.0600	0.8228	0.8120	0.7652	0.1814	0.1589	0.1855
20.60	165862	0.0603	0.8288	0.8134	0.7763	0.1776	0.1502	0.1732
20.50	165056	0.0606	0.8287	0.8080	0.7743	0.1653	0.1399	0.1588
20.40	164251	0.0609	0.8194	0.7973	0.7650	0.1551	0.1337	0.1506
20.30	163446	0.0612	0.8076	0.7867	0.7560	0.1523	0.1330	0.1479
20.20	162641	0.0615	0.7994	0.7794	0.7516	0.1541	0.1341	0.1492
20.10	161836	0.0618	0.7948	0.7732	0.7475	0.1542	0.1337	0.1421
20.00	161031	0.0621	0.7887	0.7656	0.7386	0.1518	0.1333	0.1376
19.90	160225	0.0624	0.7794	0.7574	0.7304	0.1514	0.1341	0.1381
19.80	159420	0.0627	0.7711	0.7495	0.7223	0.1538	0.1362	0.1354
19.60	157810	0.0634	0.7576	0.7356	0.7046	0.1601	0.1420	0.1355
19.40	156200	0.0640	0.7469	0.7236	0.6874	0.1667	0.1484	0.1354
19.20	154589	0.0647	0.7366	0.7120	0.6694	0.1732	0.1550	0.1411
19.00	152979	0.0654	0.7268	0.7010	0.6528	0.1799	0.1623	0.1481
18.70	150564	0.0664	0.7120	0.6854	0.6286	0.1909	0.1729	0.1600
18.40	148148	0.0675	0.6982	0.6685	0.6038	0.2028	0.1847	0.1756
18.10	145733	0.0686	0.6843	0.6525	0.5791	0.2149	0.1972	0.1890

(continued)

TABLE I *(Continued)*

Gallium Telluride

eV	cm^{-1}	μm	n(E‖x)	n(E‖y)	n(E‖z)	k(E‖x)	k(E‖y)	k(E‖z)
17.80	143317	0.0698	0.6705	0.6350	0.5526	0.2276	0.2112	0.2083
17.50	140902	0.0710	0.6553	0.6181	0.5254	0.2416	0.2267	0.2305
17.20	138486	0.0722	0.6406	0.5998	0.4978	0.2569	0.2442	0.2562
16.90	136071	0.0735	0.6251	0.5828	0.4698	0.2738	0.2641	0.2866
16.60	133655	0.0748	0.6102	0.5659	0.4443	0.2924	0.2851	0.3284
16.30	131240	0.0762	0.5944	0.5488	0.4224	0.3118	0.3086	0.3667
16.00	128824	0.0776	0.5791	0.5335	0.4019	0.3336	0.3338	0.4191
15.70	126409	0.0791	0.5633	0.5176	0.3927	0.3570	0.3604	0.4777
15.40	123994	0.0806	0.5470	0.5024	0.3916	0.3812	0.3896	0.5319
15.10	121578	0.0823	0.5281	0.4882	0.3977	0.4083	0.4215	0.5828
14.80	119163	0.0839	0.5093	0.4771	0.4099	0.4415	0.4551	0.6342
14.50	116747	0.0857	0.4929	0.4664	0.4270	0.4795	0.4891	0.6752
14.20	114332	0.0875	0.4789	0.4567	0.4421	0.5215	0.5246	0.7173
13.90	111916	0.0894	0.4705	0.4474	0.4655	0.5666	0.5621	0.7549
13.60	109501	0.0913	0.4670	0.4393	0.4810	0.6136	0.6022	0.7778
13.30	107085	0.0934	0.4651	0.4339	0.4891	0.6578	0.6437	0.8086
13.00	104670	0.0955	0.4635	0.4287	0.4932	0.7074	0.6855	0.8339
12.70	102254	0.0978	0.4737	0.4228	0.4936	0.7572	0.7313	0.8770
12.40	99839	0.1002	0.4765	0.4201	0.5066	0.7997	0.7821	0.9220
12.10	97424	0.1026	0.4808	0.4221	0.5183	0.8520	0.8355	0.9576
11.80	95008	0.1053	0.4919	0.4287	0.5233	0.9065	0.8906	0.9989
11.50	92593	0.1080	0.5077	0.4408	0.5284	0.9600	0.9461	1.0495
11.20	90177	0.1109	0.5263	0.4581	0.5463	1.0123	0.9989	1.1081
10.90	87762	0.1139	0.5459	0.4764	0.5738	1.0645	1.0472	1.1569
10.60	85346	0.1172	0.5672	0.4920	0.5891	1.1177	1.0931	1.1948
10.30	82931	0.1206	0.5915	0.5036	0.5913	1.1737	1.1409	1.2524
10.00	80515	0.1242	0.6195	0.5126	0.6038	0.2286	1.1945	1.3335
9.80	78905	0.1267	0.6386	0.5196	0.6269	1.2660	1.2347	1.3946
9.60	77295	0.1294	0.6585	0.5288	0.6600	1.3041	1.2776	1.4541
9.40	75684	0.1321	0.6789	0.5408	0.7032	1.3437	1.3223	1.5103
9.20	74074	0.1350	0.7016	0.5552	0.7510	1.3863	1.3673	1.5572
9.00	72464	0.1380	0.7279	0.5710	0.7981	1.4293	1.4127	1.6014
8.80	70853	0.1411	0.7568	0.5885	0.8499	1.4731	1.4579	1.6527
8.60	69243	0.1444	0.7903	0.6052	0.9236	1.5168	1.5018	1.7018
8.40	67633	0.1479	0.8274	0.6179	1.0160	1.5564	1.5466	1.7204
8.20	66023	0.1515	0.8623	0.6256	1.0842	1.5908	1.5976	1.6982
8.00	64412	0.1553	0.8919	0.6328	1.1117	1.6254	1.6599	1.6772
7.85	63205	0.1582	0.9105	0.6425	1.1087	1.6536	1.7147	1.6775
7.70	61997	0.1613	0.9267	0.6591	1.1033	1.6862	1.7714	1.7127
7.55	60789	0.1645	0.9424	0.6773	1.1280	1.7249	1.8284	1.7690
7.40	59581	0.1678	0.9585	0.6973	1.1803	1.7693	1.8886	1.8100
7.25	58374	0.1713	0.9765	0.7195	1.2296	1.8235	1.9533	1.8329
7.10	57166	0.1749	1.0025	0.7459	1.2752	1.8869	2.0235	1.8612
6.95	55958	0.1787	1.0412	0.7788	1.3345	1.9558	2.0996	1.8870
6.80	54750	0.1826	1.0919	0.8224	1.3993	2.0224	2.1799	1.8977
6.65	53543	0.1868	1.1476	0.8780	1.4547	2.0863	2.2580	1.8974
6.50	52335	0.1911	1.2083	0.9400	1.5054	2.1536	2.3296	1.8960

TABLE I *(Continued)*

Gallium Telluride

eV	cm^{-1}	μm	n(E‖x)	n(E‖y)	n(E‖z)	k(E‖x)	k(E‖y)	k(E‖z)
6.40	51530	0.1941	1.2546	0.9823	1.5376	2.2017	2.3748	1.8923
6.30	50725	0.1971	1.3085	1.0246	1.5697	2.2522	2.4189	1.8901
6.20	49919	0.2003	1.3742	1.0661	1.6023	2.3019	2.4626	1.8830
6.10	49114	0.2036	1.4509	1.1059	1.6285	2.3422	2.5077	1.8690
6.00	48309	0.2070	1.5323	1.1449	1.6474	2.3703	2.5569	1.8563
5.90	47504	0.2105	1.6112	1.1854	1.6642	2.3857	2.6105	1.8477
5.80	46699	0.2141	1.6823	1.2266	1.6784	2.3948	2.6692	1.8346
5.70	45894	0.2179	1.7455	1.2707	1.6799	2.4038	2.7370	1.8200
5.60	45089	0.2218	1.8032	1.3227	1.6685	2.4186	2.8132	1.8151
5.50	44283	0.2258	1.8631	1.3856	1.6504	2.4442	2.8982	1.8267
5.40	43478	0.2300	1.9349	1.4638	1.6387	2.4768	2.9892	1.8599
5.30	42673	0.2343	2.0220	1.5616	1.6425	2.5085	3.0830	1.9008
5.20	41868	0.2388	2.1247	1.6812	1.6594	2.5317	3.1719	1.9419
5.10	41063	0.2435	2.2398	1.8200	1.6821	2.5379	3.2497	1.9758
5.00	40258	0.2484	2.3581	1.9742	1.7061	2.5198	3.3129	2.0088
4.92	39614	0.2524	2.4443	2.1126	1.7278	2.4857	3.3529	2.0340
4.84	38969	0.2566	2.5136	2.2606	1.7500	2.4435	3.3658	2.0569
4.76	38325	0.2609	2.5639	2.3973	1.7702	2.4017	3.3523	2.0755
4.68	37681	0.2654	2.5995	2.5056	1.7790	2.3747	3.3265	2.0913
4.60	37037	0.2700	2.6352	2.5910	1.7727	2.3679	3.3206	2.1246
4.52	36393	0.2748	2.6843	2.6800	1.7733	2.3749	3.3419	2.1845
4.44	35749	0.2797	2.7515	2.7953	1.7979	2.3847	3.3828	2.2609
4.36	35105	0.2849	2.8380	2.9463	1.8521	2.3881	3.4187	2.3368
4.28	34461	0.2902	2.9374	3.1242	1.9301	2.3703	3.4315	2.3922
4.20	33816	0.2957	3.0323	3.3155	2.0134	2.3284	3.4150	2.4208
4.15	33414	0.2993	3.0824	3.4392	2.0606	2.2924	3.3888	2.4225
4.10	33011	0.3029	3.1224	3.5616	2.0942	2.2577	3.3508	2.4207
4.05	32609	0.3067	3.1574	3.6829	2.1188	2.2273	3.0009	2.4230
4.00	32206	0.3105	3.1912	3.7991	2.1420	2.2013	3.2371	2.4281
3.95	31804	0.3144	3.2254	3.9067	2.1585	2.1767	3.1624	2.4309
3.90	31401	0.3185	3.2573	3.9992	2.1607	2.1526	3.0787	2.4392
3.85	30998	0.3226	3.2863	4.0799	2.1577	2.1338	3.0007	2.4639
3.80	30596	0.3268	3.3174	4.1561	2.1556	2.1227	2.9245	2.5019
3.75	30193	0.3312	3.3560	4.2296	2.1557	2.1161	2.8540	2.5542
3.70	29791	0.3357	3.4007	4.3082	2.1628	2.1090	2.7874	2.6229
3.65	29388	0.3403	3.4509	4.3980	2.1843	2.1027	2.7187	2.7069
3.60	28986	0.3450	3.5059	4.4972	2.2255	2.0953	2.6353	2.8005
3.55	28583	0.3499	3.5676	4.6022	2.2885	2.0911	2.5298	2.8973
3.50	28180	0.3549	3.6418	4.6942	2.3701	2.0872	2.3926	2.9918
3.45	27778	0.3600	3.7334	4.7519	2.4684	2.0792	2.2350	3.0855
3.40	27375	0.3653	3.8408	4.7693	2.5853	2.0563	2.0863	3.1819
3.35	26973	0.3707	3.9631	4.7716	2.7357	2.0170	1.9631	3.2854
3.30	26570	0.3764	4.1017	4.7731	2.9479	1.9482	1.8574	3.3743
3.25	26167	0.3822	4.2437	4.7813	3.2152	1.8326	1.7621	3.3955
3.20	25765	0.3881	4.3586	4.7988	3.4862	1.6639	1.6638	3.3207
3.15	25362	0.3943	4.4142	4.8135	3.7052	1.4651	1.5535	3.1632
3.10	24960	0.4006	4.4098	4.8105	3.8428	1.2777	1.4404	2.9714

(continued)

TABLE I *(Continued)*

Gallium Telluride

eV	cm^{-1}	μm	n(E ∥ x)	n(E ∥ y)	n(E ∥ z)	k(E ∥ x)	k(E ∥ y)	k(E ∥ z)
3.05	24557	0.4072	4.3723	4.8002	3.9061	1.1235	1.3372	2.7917
3.00	24155	0.4140	4.3245	4.7845	3.9287	0.9986	1.2407	2.6541
2.95	23752	0.4210	4.2730	4.7744	3.9483	0.8902	1.1550	2.5489
2.90	23349	0.4283	4.2180	4.7734	3.9733	0.8002	1.0641	2.4507
2.85	22947	0.4358	4.1662	4.7747	3.9833	0.7208	0.9584	2.3406
2.80	22544	0.4436	4.1110	4.7605	3.9565	0.6490	0.8339	2.2410
2.75	22142	0.4516	4.0550	4.7146	3.9028	0.5921	0.7078	2.1765
2.70	21739	0.4600	4.0072	4.6486	3.8418	0.5432	0.5983	2.1576
2.65	21337	0.4687	3.9565	4.5694	3.7956	0.4988	0.5065	2.1843
2.60	20934	0.4777	3.9146	4.4836	3.7807	0.4671	0.4374	2.2424
2.55	20531	0.4871	3.8821	4.4033	3.8013	0.4357	0.3881	2.3181
2.50	20129	0.4968	3.8546	4.3293	3.8583	0.4009	0.3520	2.4024

TABLE II

Values of n and k for α-GaTe as Given by Grasso *et al.* [5], Tatsuyama *et al.* [6], and Mead and Genzel [9]

eV	cm^{-1}	μm	n [6]	k [6]	n [5]	k [5]	n [9]	k [9]
5.900	47504	0.211			1.93			
5.850	47101	0.212				0.40		
5.800	46699	0.214			1.86	0.42		
5.700	45894	0.218			1.80	0.50		
5.600	45089	0.222			1.75	0.56		
5.500	44283	0.226			1.70	0.65		
5.400	43478	0.230			1.62	0.77		
5.300	42673	0.234			1.54	0.90		
5.200	41868	0.239			1.47	1.03		
5.100	41063	0.244			1.40	1.25		
5.000	40258	0.248			1.33	1.57		
4.900	39452	0.253			1.34	1.75		
4.800	38647	0.259			1.40	2.00		
4.700	37842	0.264			1.46	2.25		
4.600	37037	0.270			1.50	2.42		
4.500	36232	0.276			1.56	2.73		
4.400	35427	0.282			1.58	3.05		
4.300	34622	0.289			1.68	3.40		
4.200	33816	0.296			1.83	3.80		
4.100	33011	0.303			2.14	4.20		
4.000	32206	0.311			2.70	4.65		
3.900	31401	0.318			3.28	5.05		
3.850	30998	0.323				5.15		
3.800	30596	0.327			4.10	5.14		
3.700	29791	0.336			5.00	4.70		
3.600	28986	0.345			5.43	4.20		
3.500	28180	0.355			5.80	3.78		
3.400	27375	0.365			5.94	3.45		
3.300	26570	0.376			6.03	3.16		
3.250	26167	0.382				3.00		
3.200	25765	0.388			6.16	2.95		
3.100	24960	0.401			6.50	2.83		
3.000	24155	0.414			7.00	2.70		
3.100	24960	0.401			7.55	2.00		
3.200	25765	0.388			7.55	1.00		
2.850	22947	0.436	4.12					
2.850	22947	0.436			7.70			
2.800	22544	0.444	4.07					
2.760	22222	0.450	4.05					
2.710	21820	0.458	4.01					
2.700	21739	0.460			6.75	0.15		
2.670	21498	0.465	3.97					
2.650	21337	0.469				0.08		
2.600	20934	0.478	3.98					
2.600	20934	0.478			6.10	0.08		

(continued)

TABLE II *(Continued)*

Gallium Telluride

eV	cm^{-1}	μm	n [6]	k [6]	n [5]	k [5]	n [9]	k [9]
2.560	20612	0.485	3.96					
2.540	20451	0.489	3.92					
2.500	20129	0.497	3.89					
2.500	20129	0.497			5.62	0.10		
2.500	20129	0.497			5.60			
2.470	19887	0.503	3.85					
2.440	19646	0.509	3.82					
2.400	19324	0.518	3.80					
2.400	19324	0.518			5.30	0.10		
2.370	19082	0.524	3.76					
2.350	18921	0.529	3.73					
2.310	18599	0.538	3.71					
2.300	18519	0.540			5.10	0.14		
2.280	18357	0.545	3.70					
2.230	17955	0.557	3.67					
2.200	17713	0.565			4.96	0.20		
2.190	17633	0.567	3.64					
2.160	17391	0.575	3.60					
2.130	17150	0.583	3.59					
2.100	16908	0.591			4.87	0.30		
2.090	16828	0.594	3.58					
2.060	16586	0.603	3.56					
2.020	16264	0.615	3.53					
2.010	16184	0.618	3.50					
2.000	16103	0.621	3.48					
2.000	16103	0.621			4.80	0.45		
1.985	15982	0.626		7.87E-02				
1.980	15942	0.627	3.44					
1.970	15862	0.630		7.32E-02				
1.953	15725	0.636		6.73E-02				
1.940	15620	0.640		6.22E-02				
1.925	15499	0.645		5.49E-02				
1.920	15459	0.647	3.38					
1.910	15378	0.650	3.36					
1.910	15378	0.650		5.10E-02				
1.900	15298	0.654		4.68E-02				
1.900	15298	0.654			4.72	0.55		
1.865	15016	0.666		4.08E-02				
1.850	14895	0.671	3.30					
1.850	14895	0.671		4.01E-02				
1.832	14750	0.678		3.78E-02				
1.825	14694	0.681		3.57E-02				
1.811	14581	0.686		3.38E-02				
1.800	14493	0.690			4.60	0.80		
1.797	14469	0.691		3.19E-02				
1.790	14412	0.694	3.33					
1.785	14372	0.696		3.05E-02				

TABLE II *(Continued)*

Gallium Telluride

eV	cm^{-1}	μm	n [6]	k [6]	n [5]	k [5]	n [9]	k [9]
1.770	14251	0.702		2.90E-02				
1.760	14171	0.706	3.31					
1.760	14171	0.706		2.78E-02				
1.750	14090	0.710			4.52			
1.745	14050	0.712		2.66E-02				
1.734	13961	0.716		2.62E-02				
1.725	13889	0.720		2.64E-02				
1.720	13849	0.722	3.31					
1.717	13824	0.723		2.73E-02				
1.710	13768	0.726		2.89E-02				
1.705	13728	0.728		3.01E-02				
1.700	13688	0.731	3.25					
1.700	13688	0.731		3.08E-02				
1.700	13688	0.731				1.25		
1.700	13688	0.731			4.75			
1.695	13647	0.733		3.32E-02				
1.687	13583	0.736		3.57E-02				
1.680	13527	0.739		3.65E-02				
1.675	13486	0.741		2.95E-02				
1.670	13446	0.744	3.28					
1.670	13446	0.744		2.01E-02				
1.664	13398	0.746		1.16E-02				
1.660	13366	0.748		7.14E-03				
1.653	13309	0.751		6.58E-03				
1.650	13285	0.753	3.33					
1.644	13237	0.755		6.01E-03				
1.642	13221	0.756	3.60					
1.638	13188	0.758	3.90					
1.638	13188	0.758		4.83E-03				
1.630	13124	0.762		3.64E-03				
1.622	13060	0.766	4.34					
1.622	13060	0.766		3.05E-03				
1.618	13027	0.768	4.60					
1.615	13003	0.769		1.84E-03				
1.606	12931	0.773		1.85E-03				
1.600	12882	0.776	4.72					
1.600	12882	0.776		2.47E-03				
1.600	12882	0.776			5.43	0.95		
1.595	12842	0.779		3.72E-03				
1.588	12786	0.782		4.36E-03				
1.580	12721	0.786		4.38E-03				
1.570	12641	0.791		3.34E-03				
1.560	12560	0.796	4.71					
1.550	12480	0.801			5.49			
1.500	12077	0.828			5.48	0.65		
1.470	11836	0.845	4.78					

(continued)

TABLE II *(Continued)*

Gallium Telluride

eV	cm^{-1}	μm	n [6]	k [6]	n [5]	k [5]	n [9]	k [9]
1.420	11433	0.875	4.75					
1.400	11272	0.887			5.44	0.50		
1.370	11031	0.907	4.72					
1.300	10467	0.955	4.63					
1.300	10467	0.955			5.38	0.37		
1.240	9984	1.002	4.57					
1.200	9662	1.035			5.32	0.30		
1.120	9018	1.109	4.42					
1.100	8857	1.129			5.25	0.26		
1.060	8535	1.172	4.28					
1.020	8213	1.218	4.06					
1.000	8052	1.242			5.20	0.25		
4.66E-02	375	26.667						0.70
4.60E-02	370	27.027					2.90	0.70
4.53E-02	365	27.397					2.92	0.70
4.47E-02	360	27.778					2.92	0.70
4.41E-02	355	28.169					2.90	0.70
4.35E-02	350	28.571					2.85	0.66
4.28E-02	345	28.986					2.83	0.64
4.22E-02	340	29.412					2.85	0.62
4.16E-02	335	29.851					2.88	0.60
4.10E-02	330	30.303					2.90	0.60
4.04E-02	325	30.769					2.90	0.58
3.97E-02	320	31.250					2.90	0.56
3.91E-02	315	31.746					2.88	0.53
3.85E-02	310	32.258					2.85	0.53
3.79E-02	305	32.787					2.84	0.53
3.73E-02	300	33.333					2.82	0.52
3.66E-02	295	33.898					2.80	0.52
3.60E-02	290	34.483					2.80	0.50
3.54E-02	285	35.088					2.80	0.50
3.48E-02	280	35.714					2.80	0.50
3.42E-02	275	36.364					2.80	0.48
3.35E-02	270	37.037					2.80	0.52
3.29E-02	265	37.736						0.55
3.29E-02	265	37.736					2.80	
3.23E-02	260	38.462					2.75	0.55
3.17E-02	255	39.216					2.71	0.50
3.11E-02	250	40.000					2.73	0.40
3.04E-02	245	40.816					2.72	0.40
2.98E-02	240	41.667					2.70	0.35
2.92E-02	235	42.553					2.65	0.30
2.86E-02	230	43.478						0.30
2.86E-02	230	43.478					2.55	
2.79E-02	225	44.444					2.40	0.34
2.73E-02	220	45.455					2.13	0.40
2.67E-02	215	46.512					1.75	0.52

TABLE II *(Continued)*

Gallium Telluride

eV	cm^{-1}	μm	n [6]	k [6]	n [5]	k [5]	n [9]	k [9]
2.61E-02	210	47.619						0.72
2.61E-02	210	47.619					1.20	
2.56E-02	206	48.544						0.42
2.55E-02	205	48.780					0.54	0.63
2.48E-02	200	50.000					0.50	3.40
2.43E-02	196	51.020						4.66
2.42E-02	195	51.282					3.00	4.68
2.36E-02	190	52.632					4.45	2.00
2.35E-02	189	52.910					4.45	
2.30E-02	185	54.054					4.15	0.78
2.24E-02	180	55.556					3.65	0.65
2.17E-02	175	57.143						0.58
2.17E-02	175	57.143					3.25	
2.11E-02	170	58.824					3.00	0.63
2.05E-02	165	60.606					2.50	1.60
2.01E-02	162	61.728						2.10
1.99E-02	160	62.500					1.94	2.00
1.93E-02	155	64.516					2.80	0.75
1.86E-02	150	66.667					1.75	1.90
1.83E-02	147	68.027					1.43	
1.80E-02	145	68.966						3.95
1.80E-02	145	68.966					1.50	
1.74E-02	140	71.429					4.90	3.10
1.70E-02	137	72.993					5.00	
1.68E-02	135	74.074					4.80	2.00
1.61E-02	130	76.923					4.45	1.35
1.55E-02	125	80.000						1.20
1.55E-02	125	80.000					4.20	
1.49E-02	120	83.333					4.00	1.30
1.45E-02	117	85.470						1.45
1.44E-02	116	86.207					3.96	
1.43E-02	115	86.957					4.00	1.40
1.37E-02	110	90.909					4.15	0.80
1.30E-02	105	95.238					4.14	0.30
1.28E-02	103	97.087					4.27	
1.24E-02	100	100.000					4.25	0.22
1.22E-02	98	102.041						0.25
1.18E-02	95	105.263					4.00	0.21
1.17E-02	94	106.383						0.20
1.12E-02	90	111.111					3.95	0.40
1.06E-02	85	117.647						0.60
1.06E-02	85	117.647					4.10	
1.02E-02	82	121.951					4.15	
9.94E-03	80	125.000					4.10	0.42
9.32E-03	75	133.333					4.00	0.35
8.69E-03	70	142.857					4.00	

Iron Pyrite (FeS_2)

E. D. PALIK
Institute for Physical Science and Technology
University of Maryland
College Park, Maryland

Iron pyrite is called "fool's gold" because to the untrained prospector, it looks very much like gold. However, comparison of the optical constants in the visible spectral region easily distinguishes between the two materials. While the reflectivity $R = \sim 0.40$ at 3 eV for both Au and FeS_2, it rises rapidly to $R = 0.97$ at 1.6 eV for Au and continues to rise into the near IR, while for FeS_2 it rises to a peak $R = 0.65$ at 1.6 eV, then drops to $R = 0.44$ at 0.5 eV. This gives the characteristic yellow color, but this color should be brighter for Au and duller for FeS_2.

Iron pyrite is a cubic semiconductor of space group symmetry class Pa3 (T_h^6). The optic irreducible representation is

$$A_g(\mathrm{R}) + 2A_u(0) + E_g(\mathrm{R}) + 2E_u(0) + 5F_u(\mathrm{IR}), \tag{1}$$

where we define R, Raman; IR, infrared; 0, silent. This predicts 33 optic modes. There is an additional F_u triply degenerate acoustic mode to complete the total irreducible representation.

The far-IR lattice-vibration region has been studied by Verble and Wallis [1] and Lutz *et al.* [2, 3]. Verble and Wallis measured the reflectivity (at an undesignated room temperature) of a natural single-crystal sample in the region 190–660 cm^{-1} with a Perkin-Elmer Model 301 spectrophotometer. An aluminum mirror served as a reference standard. Both Kramers–Kronig (K-K) and Lorentz-oscillator-model analyses were performed. The K-K analysis gave a small, nearly constant $k = \sim 0.2$ above 460 to 650 cm^{-1}, which the Lorentz-oscillator model ignored. Although five F_u IR modes were expected, only four were observed. The Lorentz-oscillator model gives

$$\begin{aligned} n^2 - k^2 = \epsilon_{\mathrm{R}} &= \epsilon_\infty + \sum_j \frac{4\pi \rho_j \omega_j^2 (\omega_j^2 - \omega^2)}{(\omega_j^2 - \omega^2)^2 + (\gamma_j \omega_j \omega)^2} \\ 2nk = \epsilon_{\mathrm{I}} &= \sum_j \frac{4\pi \rho_j \omega_j^2 \omega}{(\omega_j^2 - \omega^2)^2 + (\gamma_j \omega_j \omega)^2}. \end{aligned} \tag{2}$$

HANDBOOK OF OPTICAL CONSTANTS OF SOLIDS III

Copyright © 1998 by Academic Press.
All rights of reproduction in any form reserved
ISBN 0-12-544423-0/$25.00.

We can just as well define the damping parameter as $\Gamma_j = \gamma_j\ \omega_j$, so Γ_j has units of cm^{-1} and signifies the FWHM of the jth absorption line. The angular frequency is ω; the oscillator strength is ρ; ω_j is the jth resonant frequency. The fitting parameters are given in Table I for Verble and Wallis [1]. The calculated values of n and k are listed in Table II.

Lutz *et al.* [3] performed similar reflectivity measurements (at an undesignated room temperature) with a Fourier-transform spectrometer in the spectral range 30–700 cm^{-1}. Polycrystalline FeS_2 samples were prepared by heating stoichiometric mixtures of the elements in evacuated fused-quartz tubes at high temperature. Such samples were hot pressed and polished; some natural crystalline samples were also used. There were considerable differences in the two sets of reflectivity data. For the natural crystals they determined oscillator parameters, some of which were similar to and some drastically different from those found by Verble and Wallis. Because we are suspicious of how well a Fourier-transform spectrometer can measure R, we will not use these data; we do list the fitting parameters for the natural crystal in Table I for Lutz *et al.* [3]. Note the difference in notation by Verble and Wallis [1] and Lutz *et al.* [3] regarding Γ and γ. However, Lutz *et al.* [3] did measure all five IR modes in transmittance using powdered material in a CsI matrix, while Verble and Wallis could not find one mode in reflectivity in the vicinity of 422 cm^{-1}.

Toward the near IR we could find no measurements of index of refraction n up to the the vicinity of the fundamental indirect band gap at $E_g = \sim 0.7$ eV. Therefore, we have to extrapolate the Lorentz-oscillator-model results [1] up to 0.5 eV.

The various natural crystals and deposited thin films used by the many researchers must have had significantly different properties, since there were significant differences in n and k.

We summarize some of the papers [4–10], and list others [11–14] for the reader's further interest.

Ferrer *et al.* [4]: Natural samples and flash-evaporated films on a glass substrate; Cary Model 2415 spectrophotometer at normal incidence; both R and T measured in spectral region 0.5–5.5 eV; K-K analysis; room temperature not specified; peak $R = 0.53$ at 1.7 eV. K-K analysis is notorious for giving inaccurate values of k when k is small (less than a few tenths).

There have been numerous measurements of the extinction coefficient k in the band-gap region. Ferrer *et al.* [4] noticed significant variations among these works when they attempted to fit the absorption coefficient α (cm^{-1}) with a formula of the form

$$(\alpha\ h\ \nu)^n = B\ (h\ \nu - E_o), \tag{3}$$

where ν is the frequency in Hz; for direct transitions $E_o = E_g$; for indirect transitions $E_o = E_g + E_p$, with E_p being the associated phonon energy; and $n = \frac{1}{2}, \frac{1}{3}, 2, \frac{2}{3}$ for allowed and forbidden indirect transitions and allowed and

forbidden direct transitions, respectively. This n is not to be confused with the index of refraction. Equation (3) was derived for parabolic conduction and valence bands. They analyzed their own data and could not definitely decide between allowed and forbidden indirect. When they noted that the several sets of data of other workers gave drastically different values of E_g and n (direct and indirect, allowed and forbidden), they concluded that Eq. (3) is not applicable for FeS_2 because the bands are rather flat. We include in Table II some data of Ferrer *et al.* that hint that the band gap $E_g = 1.1$ eV and is allowed indirect.

Bither *et al.* [5]: Samples grown by high-pressure reaction of high-purity reactants (Fe,S) pelleted first at room temperature and then inserted into an anvil press that could be heated; near-normal-incidence reflectivity measured in spectral region 0.5–5.0 eV; Perkin-Elmer 112 monochromator; as-grown crystal faces; room temperature was 300 K; K-K analysis using an extrapolation formula to high frequency; peak $R = 0.62$ at 1.7 eV. Also, the reflectance was measured as a function of angle of incidence (θ), and n and k were directly computed. However, it is not clear which set of data are given in the figures, and no comparisons are made of the two sets of data.

Schlegel and Wachter [6]: Natural crystals; reflectivity measured in the IR spectral region 0.03–0.5 eV; thin-film transmittance measured from 0.03 to 1.1 eV and showed peculiar constant level of absorption with $\alpha = \sim 1.4 \times 10^3$ cm^{-1} from 0.06 to 0.8 eV; also, lowest lattice mode showed a splitting (277, 290 cm^{-1}); this was not seen by Verble and Wallis and Lutz *et al.;* reflectivity also measured from 0.5 to 12 eV; K-K analysis used, but extrapolation method not mentioned; peak $R = 0.53$ at 1.7 eV.

Kou and Seehra [7]: Two thin-film natural samples of low and high resistivity; low-resistivity sample showed free-carrier absorption; high-resistivity sample showed a constant background absorption below the band gap; spectral region was 0.7–1.0 eV; residual absorption was presumably subtracted out on α (cm^{-1}) versus (eV) plot. The formula used was

$$I_t/I_o = \frac{(1 - R^2)\exp(-\alpha d).}{1 - R^2\exp(-2\,\alpha\, d)} \tag{4}$$

This formula contains multiple-reflection effects but does not show interference fringes. Since R was nearly constant at $R = 0.43$ in the narrow spectral region covered, and if $R^2\exp(-2\,\alpha\, d) \ll 1$, one can measure the optical density $D_o = \log_{10}(I_t/I_o)$ and from this obtain

$$\alpha\, d = 2.303\, D_o - 4.606\log_{10}(1 - R). \tag{5}$$

Since D_o varies rapidly with wavelength in the band-gap region, its absorption in the first term is superimposed on a nearly constant second term. This second term is computed to be ~ 125 cm^{-1} for $d = 90$ μm and $R = 0.43$. The observed absorption is 720 cm^{-1}. For a second film with $d = 150$ μm,

the calculated value is 75 cm^{-1}, but a background absorption of 400 cm^{-1} was measured. Kuo and Seehra do not directly say that the observed constant absorption is this constant term. Also, thin films with $d = 90$ μm and $d = 150$ μm give somewhat different values of α after the background absorption is subtracted. For example, at 0.8 eV, $(\alpha h\nu) = 5.5$ for $d = 90$ μm and 4.0 for 150 μm. This is unusual.

We have occasionally noticed that workers will subtract off a background absorption at the k or α level. This is not quite proper. Linear optics suggests that the dielectric constants are additive; for example, a Drude model described by $\epsilon(D)$ can be added to a Lorentz model described by $\epsilon(L)$, and can be added to a constant-background lattice model described by ϵ_∞. When tempted to make such a subtraction at the k level, the worker should actually calculate the error introduced by adding or subtracting k's instead of ϵ_I's.

However, we have elected to include the k data in Table II for the $d = 150$ μm sample for comparison with other data to be discussed next. It will be obvious that the materials must vary to produce such variations in n and k [4, 7–9].

Yang *et al.* [8]: Synthetic single crystals grown by chemical-vapor-transport method; thin plates made by diamond-saw cutting and polishing down to 30 μm; transmission near normal incidence measured with a Bruker model IFS 120HR in the spectral region 0.8–1.3 eV; room temperature was 300 K. Data analysis was similar to that of Kou and Seehra [7]. Since the absorption was about a factor of 5 smaller than measured by Kuo and Seehra, and the spectral region was somewhat wider, we choose to present these band-edge data in Table II. Analysis was done with the indirect-allowed-transition model similar to the method of Kuo and Seehra. However, Yang *et al.* had variations in absorption for samples of different thickness (like Kuo and Seehra). They did estimate that $E_g = 0.93$ eV at 300 K.

Suga *et al.* [9]: Natural crystals polished and etched; p-polarized reflectivity spectrum using a 1-m Seya-Namioka monochromator attached to the beam line of a 0.4-GeV electron storage ring; 3000–400 Å; with additional, presumably new, unpublished data of Sato in the region 0.3–4 eV; room temperature not specified; peak $R = 0.64$ at 1.7 eV.

Sato [10]: Thin films made by a chemical vapor-transport reaction; surfaces etched; double-beam refectivity spectrometer in the spectral region 0.5–4.4 eV; K-K analysis using the VUV data of Suga *et al.;* room temperature not specified; peak $R = 0.54$ at 1.7 eV.

We finally choose the data of Suga *et al.* because they used natural crystals; there was no free-carier absorption below E_g as was the case with the data of Sato; also below E_g, $n = 5.0$ at 0.5 eV, above (but approaching) the value $n = 4.617$ of Verble and Wallis. The reflection peak near 1.7 eV is the highest at $R = \sim 0.64$ compared to $R = \sim 0.54$ for Sato and ~ 0.53 for

Ferrer *et al.* There is a proverb saying that bigger (reflectivity) is better, especially in the interband region where strong transitions give peaks in R; these peaks can be supressed by native oxides and poorly prepared surfaces.

Because of the possible use of FeS_2 as a solar-energy material, several methods of growing it economically have been tried. These include polycrystal films made from powdered FeS_2 heated in a fused-quartz ampule with a detailed heating cycle for days [11]; spray pyrolysis deposition on a hot fused-quartz plate utilizing solutions of ferric salts and sulfo-organic compounds [12, 13]; iron films made by flash evaporation on a glass substrate were placed into vacuum sealed glass ampules with sulfur with temperatures as high as 500 K applied for many hours [14]. There were signficant differences in the band-gap data of such thin films, and we cannot use the optical constants obtained from such samples. Unfortunately, even the natural crystals seem to vary in their optical constants, suggesting other impurity and structure problems.

In all these papers the n and k data were presented in small graphs which were enlarged by photocopying and then read. We estimate that n and k are uncertain to $\pm 10\%$ when read this way; this is above and beyond the experimental uncertainties seldom discussed in the various papers.

There are data for the temperature dependence of the band gap [8, 15], but they are not of direct interest here. No data could be found above 25 eV. However, Suguiro [16] measured the K x-ray absorption edge of S in FeS_2 near 2472 eV with some structure observed. No absolute values of absorption coefficient were determined.

Lastly, the data in Table II are plotted in Fig. 1.

REFERENCES

1. J. L. Verble and R. F. Wallis, Infrared studies of lattice vibrations in iron pyrite. *Phys. Rev.* **182**, 783 (1969).
2. H. D. Lutz, G. Schneider, and G. Kliche, Far-infrared reflection spectra, TO- and LO-phonon frequencies, coupled and decoupled plasmon-phonon modes, dielectric constants, and effective dynamical charges of manganese, iron, and platinum group pyrite type compounds. *J. Phys. Chem. Solids* **46**, 437 (1985).
3. H. D. Lutz, G. Kliche, and H. Haeuseler, Far-infrared reflection spectra, optical and dielectric constants, and effective charges of the pyrite type compounds FeS_2, MnS_2, $MnSe_2$ and $MnTe_2$. *Z. Naturforsch.* **36a**, 184 (1981).
4. I. J. Ferrer, D. M. Nevskaia, C. de las Heras, and C. Sanchez, About the band gap nature of FeS_2 as determined from optical and photo-electrochemical measurements. *Solid State Commun.* **74**, 913 (1990).
5. T. A. Bither, R. J. Bouchard, W. H. Cloud, P. C. Donohue, and W. J. Siemons, Transition metal pyrite dichalcogenides. High-pressure synthesis and correlation of properties. *Inorg. Chem.* **7**, 2208 (1968).
6. A. Schlegel and P. Wachter, Optical properties, phonons and electronic structure of iron pyrite (FeS_2). *J. Phys. C: Solid State Phys.* **9**, 3363 (1976).

7. W. W. Kou and M. S. Seehra, Optical absorption in iron pyrite (FeS_2). *Phys. Rev. B* **18**, 7062 (1978).
8. T.-R. Yang, J.-T. Yu, J.-K. Huang, S.-H. Chen, M.-Y. Tsay, and Y.-S. Huang, Optical-absorption study of synthetic pyrite FeS_2 single crystals. *J. Appl. Phys.* **77**, 1710 (1995).
9. S. Suga, K. Inoue, M. Taniguchi, S. Shin, M. Seki, K. Sato, and T. Teranishi, Vacuum ultraviolet reflectance spectra and band structures of pyrites (FeS_2, CoS_2 and NiS_2) and NiO measured with synchrotron radiation. *J. Phys. Soc. Jpn.* **52**, 1848 (1983).
10. K. Sato, Reflectivity spectra and optical constants of pyrites (FeS_2, CoS_2 and NiS_2) between 0.2 and 4.4 eV. *J. Phys. Soc. Jpn.* **53**, 1617 (1984).
11. A. Ennaoui, S. Fiechter, H. Goslowsky, and H. Tributsch, Photoactive synthetic polycrystalline pyrite (FeS_2). *J. Electrochem. Soc.* **132**, 1579 (1985).
12. A. K. Abass, Z. A. Ahmed, and R. E. Tahir, Interband transitions of chemically deposited pyrite FeS_2 films in the fundamental absorption region between 1 and 3.8 eV. *Phys. Status Solidi A* **97**, 243 (1986).
13. A. K. Abass, Z. A. Ahmed, and R. E. Tahir, Absorption edge measurements in chemically deposited pyrite FeS_2 thin layers. *J. Appl. Phys.* **61**, 2339 (1987).
14. I. J. Ferrer and C. Sanchez, Characterization of FeS_2 thin films prepared by thermal sulfidation of flash evaporated iron. *J. Appl. Phys.* **70**, 641 (1991).
15. M. S. Seehra and S. S. Seehra, Temperature dependence of the band gap of FeS_2. *Phys. Rev. B* **19**, 6620 (1979).
16. C. Sugiura, Sulfur K x-ray absorption spectra of FeS, FeS_2, and Fe_2S_3. *J. Chem. Phys.* **74**, 215 (1981).

TABLE I

Lorentz-Oscillator-Model Parameters Obtained from Fitting Measured Reflectivities from Verble and Wallis [1] and Lutz *et al.* [3][a]

	ω_j (cm^{-1})		ρ_j		Γ_j (cm^{-1})	
j	[1]	[3]	[1]	[3]	[1]	[3]
1	293	293	0.0258	0.027	1.46	2.78
2	348	348	0.065	0.033	1.95	0.83
3	402	401	0.27	0.255	5.23	3.97
4	415	412	0.022	0.026	9.13	13.93
5		422		0.00079		10.04

[a] $\epsilon_\infty = 21.32$ [1]; 19.80 [3].

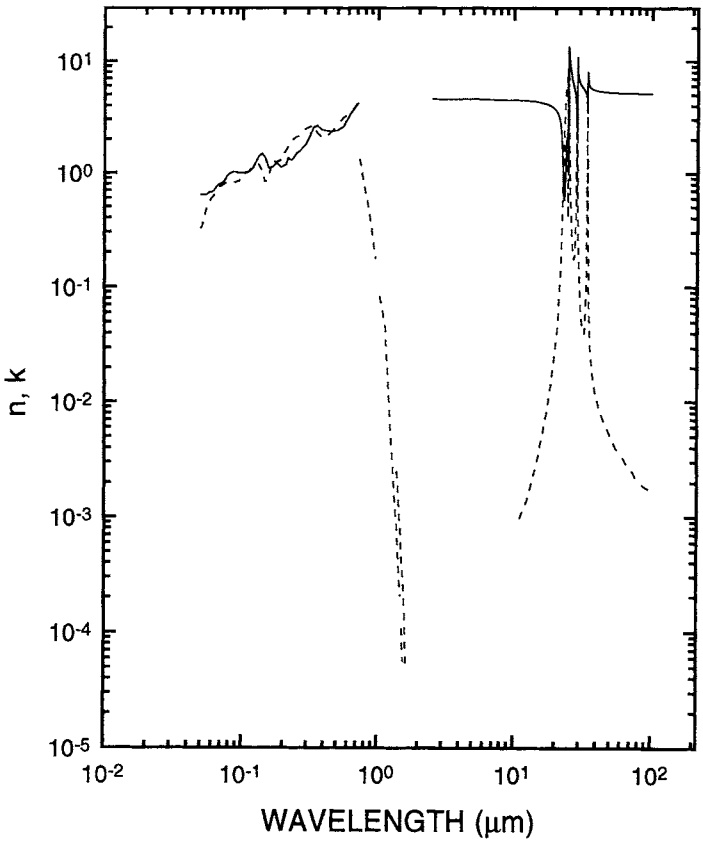

Fig. 1. Log–log plot of n (—) and k (----) versus wavelength in micrometers for iron pyrite.

TABLE II

Values of n and k for Iron Pyrite Obtained from Various References[a]

eV	cm−1	μm	n	k	k	k
25.0	201600.	0.04959	0.64[9]	3.2E-1[9]		
24.5	197600.	0.05061	0.64	3.4E-1		
24.0	193600.	0.05166	0.64	3.8E-1		
23.5	189500.	0.05276	0.64	4.1E-1		
23.0	185500.	0.05391	0.64	4.6E-1		
22.5	181500.	0.05510	0.65	4.9E-1		
22.0	177400.	0.05636	0.66	5.2E-1		
21.5	173400.	0.05767	0.68	5.6E-1		
21.0	169400.	0.05904	0.68	5.9E-1		
20.5	165300.	0.06048	0.68	6.1E-1		
20.0	161300.	0.06199	0.70	6.3E-1		
19.5	157300.	0.06358	0.73	6.7E-1		
19.0	153200.	0.06525	0.77	7.0E-1		
18.5	149200.	0.06702	0.79	7.3E-1		
18.0	145200.	0.06888	0.80	7.6E-1		
17.5	141100.	0.07085	0.82	7.8E-1		
17.0	137100.	0.07293	0.84	8.0E-1		
16.5	133100.	0.07514	0.89	8.1E-1		
16.0	129000.	0.07749	0.95	8.2E-1		
15.5	125000.	0.0800	0.99	8.3E-1		
15.0	121000.	0.08265	1.00	8.3E-1		
14.5	116900.	0.08551	1.02	8.3E-1		
14.0	112900.	0.08856	1.02	8.3E-1		
13.5	108900.	0.09184	1.01	8.4E-1		
13.0	104800.	0.09537	1.00	8.6E-1		
12.5	100800.	0.09919	1.00	9.2E-1		
12.0	96780.	0.1003	1.00	9.8E-1		
11.5	92750.	0.1078	1.02	1.01E0		
11.0	88720.	0.1127	1.04	1.06E0		
10.5	84690.	0.1181	1.10	1.12E0		
10.0	80650.	0.1240	1.23	1.19E0		
9.5	76620.	0.1305	1.41	1.21E0		
9.0	72570.	0.1378	1.48	1.02E0		
8.5	68560.	0.1459	1.38	8.3E-1		
8.0	64520.	0.1550	1.10	9.6E-1		
7.5	60490.	0.1653	1.13	1.27E0		
7.0	56460.	0.1771	1.23	1.25E0		
6.5	52420.	0.1907	1.12	1.30E0		
6.0	48390.	0.2066	1.18	1.60E0		
5.75	46380.	0.2156	1.37	1.73E0		
5.5	44360.	0.2254	1.30	1.81E0		
5.25	42340.	0.2362	1.36	2.02E0		
5.0	40330.	0.2480	1.49	2.10E0		
4.75	38310.	0.2610	1.56	2.15E0		
4.5	36290.	0.2755	1.68	2.32E0		
4.25	34280.	0.2917	1.80	2.50E0		

[a] References given in brackets.

TABLE II *(Continued)*

Iron Pyrite

eV	cm−1	μm	n	k	k	k
4.0	32260.	0.3100	2.12	2.60E0		
3.75	30240.	0.3306	2.59	2.65E0		
3.5	28230.	0.3542	2.65	2.24E0		
3.25	26210.	0.3815	2.44	2.08E0		
3.0	24200.	0.4133	2.38	2.10E0		
2.75	22180.	0.4508	2.35	2.34E0		
2.5	20160.	0.4959	2.40	2.67E0		
2.25	18150.	0.5510	2.60	3.12E0		
2.0	16130.	0.6199	3.38	3.46E0		
1.75	14110.	0.7085	4.20	4.30E0		
1.7	13710.	0.7293			1.33E0[4]	
1.6	12900.	0.7749			8.63E-1	
1.5	12100.	0.8265	6.65	4.09E0	5.92E-1	
1.4	11290.	0.8856			3.52E-1	
1.3	10480.	0.9537			1.74E-1	
1.25	10080.	0.9919	5.90	1.0E0		
1.2	9678.	1.033			8.22E-2	
1.1	8872.	1.127			4.48E-2	
1.02	8227.	1.215			8.25E-3[8]	
1.00	8065.	1.240	5.45	5.1E-1	5.82E-3	
0.98	7904.	1.265			3.82E-3	
0.96	7743.	1.291			2.60E-3	
0.94	7581.	1.319			1.71E-3	
0.92	7420.	1.348			1.21E-3	
0.90	7257.	1.378			8.79E-4	2.5E-3[7]
0.88	7098.	1.409			6.02E-4	1.9E-3
0.86	6936.	1.442			3.20E-4	1.2E-3
0.84	6775.	1.476			2.02E-4	7.0E-4
0.83	6694.	1.494				5.2E-4
0.82	6614.	1.512			1.07E-4	4.1E-4
0.80	6452.	1.550			5.56E-5	2.6E-4
0.78	6291.	1.589				1.4E-4
0.76	6130.	1.631				4.9E-5
0.75	6049.	1.653	5.12			
0.74	5968.	1.675				2.7E-6
0.4959	4000.	2.500	4.60[1]			
0.4339	3500.	2.857	4.60			
0.3719	3000.	3.333	4.60			
0.3097	2500.	4.000	4.59			
0.2480	2000.	5.000	4.59			
0.1860	1500.	6.667	4.57			
0.1240	1000.	10.00	4.51			
0.1116	900.	11.11	4.49	9.76E-4[1]		
0.0991	800.	12.50	4.44	1.38E-3		
0.0867	700.	14.28	4.37	2.58E-3		
0.08183	660.	15.15	4.32	3.52E-3		
0.08059	650.	15.38	4.30	3.78E-3		

(continued)

TABLE II *(Continued)*

Iron Pyrite

eV	cm−1	μm	n	k	k	k
0.07935	640.	15.62	4.29	4.26E-3		
0.07811	630.	15.87	4.27	4.68E-3		
0.07687	620.	16.13	4.25	5.07E-3		
0.07563	610.	19.39	4.23	5.61E-3		
0.07439	600.	16.67	4.21	6.25E-3		
0.07315	590.	16.95	4.18	7.04E-3		
0.07191	580.	17.24	4.15	7.87E-3		
0.07067	570.	17.54	4.12	9.00E-3		
0.06943	560.	17.86	4.08	1.03E-2		
0.06819	550.	18.18	4.04	1.19E-2		
0.06695	540.	18.52	3.99	1.39E-2		
0.06571	530.	18.87	3.93	1.64E-2		
0.06447	520.	19.23	3.86	1.97E-2		
0.06323	510.	19.61	3.77	2.41E-2		
0.06199	500.	25.00	3.67	3.03E-2		
0.06075	490.	20.41	3.54	3.91E-2		
0.05951	480.	20.83	3.37	5.26E-2		
0.05827	470.	21.28	3.14	7.50E-2		
0.05703	460.	21.74	2.79	1.17E-1		
0.05579	450.	22.22	2.22	2.20E-1		
0.05455	440.	22.73	1.01	7.96E-1		
0.05393	435.	22.99	0.612	1.81E0		
0.05331	430.	23.25	0.584	2.78E0		
0.05269	425.	23.53	0.706	3.80E0		
0.05207	420.	23.81	1.10	5.00E0		
0.05182	418.	23.92	1.44	5.49E0		
0.05158	416.	24.04	1.88	5.82E0		
0.05145	415.	24.10	2.03	5.89E0		
0.05133	414.	24.15	2.08	5.97E0		
0.05108	412.	24.27	2.00	6.44E0		
0.05083	410.	24.39	2.08	7.40E0		
0.05058	408.	24.51	2.58	8.74E0		
0.05034	406.	24.63	3.84	10.4E0		
0.05021	405.	24.69	5.01	11.4E0		
0.05009	404.	24.75	6.81	12.2E0		
0.04997	403.	24.81	9.31	12.3E0		
0.04984	402.	24.87	11.9	11.0E0		
0.04972	401.	24.94	13.5	8.50E0		
0.04959	400.	25.00	13.6	6.09E0		
0.04947	399.	25.06	13.1	4.36E0		
0.04935	398.	25.12	12.3	3.21E0		
0.04910	396	25.25	11.0	1.93E0		
0.04835	390.	25.64	8.69	7.06E-1		
0.04711	380.	26.31	7.05	2.81E-1		
0.04587	370.	27.02	6.15	1.73E-1		
0.04463	360.	27.78	5.22	1.96E-1		
0.04389	354.	28.25	3.76	6.11E-1		

TABLE II *(Continued)*

Iron Pyrite

eV	cm−1	μm	n	k	k	k
0.04364	352.	28.41	2.45	1.83E0		
0.04352	351.	28.49	2.15	3.40E0		
0.04339	350.	28.57	2.67	5.37E-1		
0.04327	349.	28.65	4.65	7.69E0		
0.04315	348.	28.73	9.63	7.60E0		
0.04302	347.	28.82	10.9	3.30E0		
0.04290	346.	28.90	9.70	1.47E0		
0.04401	345.	28.98	8.82	8.24E-1		
0.04265	344.	29.07	8.24	5.32E-1		
0.04240	342.	29.24	7.54	2.85E-1		
0.04215	340.	29.41	7.13	1.86E-1		
0.04091	330.	30.30	6.26	6.58E-2		
0.03967	320.	31.25	5.90	4.33E-2		
0.03843	310.	32.26	5.61	3.95E-2		
0.03720	300.	33.33	5.10	9.26E-2		
0.03695	298.	33.56	4.82	1.65E-1		
0.03670	296.	33.78	4.18	4.61E-1		
0.03657	295.	33.90	3.52	1.11E0		
0.03645	294.	34.01	3.45	3.30E0		
0.03633	293.	34.13	7.23	4.52E-1		
0.03620	292.	34.25	8.05	1.42E0		
0.03608	291.	34.36	7.28	5.40E-1		
0.03596	290.	34.48	6.83	2.81E-1		
0.03571	288.	34.72	6.38	1.21E-1		
0.03546	286.	34.96	6.16	7.13E-2		
0.03472	280.	35.71	5.86	3.09E-2		
0.03348	270.	37.04	5.66	1.74E-2		
0.03224	260.	38.46	5.56	1.29E-2		
0.03100	250.	40.00	5.48	1.04E-2		
0.02976	240.	41.67	5.43	8.68E-3		
0.02852	230.	43.48	5.38	7.43E-3		
0.02728	220.	45.45	5.34	6.47E-3		
0.02604	210.	47.62	5.31	5.69E-3		
0.02490	200.	50.00	5.28	5.07E-3		
0.02356	190.	52.63	5.26	4.47E-3		
0.02232	180.	55.56	5.24	3.91E-3		
0.02108	170.	58.82	5.22	3.52E-3		
0.01984	160.	62.50	5.20	3.24E-3		
0.01860	150.	66.67	5.19	2.76E-3		
0.01736	140.	71.43	5.18	2.58E-3		
0.01612	130.	76.92	5.16	2.18E-3		
0.01488	120.	83.33	5.15	1.95E-3		
0.01364	110.	90.91	5.14	1.80E-3		
0.01240	100.	100.0	5.14	1.69E-3		

Silicon (Si) Revisited (1.1–3.1 eV)

JON GEIST
Olney, Maryland

THE INDEX OF REFRACTION OF SILICON IN THE VISIBLE AND VERY NEAR IR I

Introduction A

At room temperature, the extinction coefficient, k, of nominally pure, single-crystal silicon increases from less than 10^{-6} at the onset of the indirect transition to almost 1 at 370 nm. On the other hand, the real part of the index of refraction, n, of silicon at room temperature varies by less than a factor of 2 over the same spectral range.

Transmission measurements are the most accurate way to determine $k \ll 1$, but they require impractically thin samples for wavelengths less than about 550 nm. More accurate values of k can be deduced from reflectance or ellipsometric measurements below this wavelength. Only reflectance and ellipsometric measurements can be used to measure n except at the longest wavelengths of this spectral region because of the large values of the absorption coefficient $\alpha = 4\ \pi\ k/\lambda$ over most of the region.

The extinction-coefficient data will be considered first, then the index data. But first, a few generalizations about the data to be discussed can be made. All of the measurements discussed here were carried out at nominal room temperature, but very few authors reported the exact temperature, so corrections among the different data sets for small differences in measurement temperature are not possible. All of the authors used single-crystal material that was pure enough to preclude extrinsic effects in the spectral region of their measurements. All authors were concerned with the effect of surface films, surface roughness, and surface damage, and most attempted to minimize or correct for the effects of these imperfections in the measured data. On the other hand, there was no consensus at all about how to do this.

HANDBOOK OF OPTICAL CONSTANTS OF SOLIDS III

Copyright © 1998 by Academic Press.
All rights of reproduction in any form reserved
ISBN 0-12-544423-0/$25.00.

B Extinction Coefficient

A large number of references report k spectra for nominally pure, single-crystal silicon at room temperature, but the agreement among most of these spectra is very poor. In fact, just two of these, the room-temperature data of Jellison [1] and Weakliem and Redfield [2], have been selected as having a satisfactory combination of range and accuracy over the spectral region of interest here. Furthermore, an analytic model was used to summarize the data of Jellison [1] and Weakliem and Redfield [2]. This model is given by

$$k(h\nu) = f(h\nu)\ [1.23985 \times 10^{-4}\ \text{cm eV}/h\nu][g(h\nu)/h\nu]/4\pi \tag{1}$$

$$g(h\nu) = \sum_{i=1}^{2} \sum_{j=-1}^{1} \{C_{i,j}[L(h\nu - \epsilon_1 + jd\epsilon_i)]^2\} + C_3[2L(h\nu - \epsilon_3)]^{N+dN\,h\nu} \tag{2}$$

$$f(h\nu) = \exp\{K_4 L(h\nu - \epsilon_4) + K_5 L(h\nu - \epsilon_5)\} \tag{3}$$

$$L(\epsilon) = (\epsilon + |\epsilon|)/2eV, \tag{4}$$

where $j = 0$ is not used in the sum over j, $|\epsilon|$ indicates the absolute value of ϵ, $h\nu$ is the photon energy = 1.23985 μm eV/λ, λ is the vacuum wavelength, and the values of the parameters in Eqs. (1)–(4) are given in Table I.

This model is an extension of the fit of $g(h\nu)$ that was reported by Geist *et al.* [3] to the absorption-coefficient data of Weakliem and Redfield [2]. The terms under the double sum in Eq. (2) describe the onset of the indirect (phonon-assisted) transition in silicon according to quantum band theory as described in by Macfarlane *et al.* [4]. The C_3 term in Eq. (2) is an empirical term to describe the effect of the nonparabolic nature of the bands away from the silicon band edge. The function $f(h\nu)$ is an empirical correction factor that was fitted to the ratio of the data of Jellison [1] to the values calculated from $g(h\nu)$ for photon energies greater than those used to adjust the parameters in $g(h\nu)$.

The k values calculated from the model given in Eqs. (1)–(4) are shown in Fig. 1 over the range from 370 to 1170 nm. (The kink between 1000 and 1100 nm is real, as discussed by Macfarlane *et al.* [4].) The model fits the data of Jellison [1] and Weakliem and Redfield [2] very well from 390 to 1130 nm, considering that k(390 nm)/k(1130 nm) > 35,000. The quality of the fit over this range is shown in Fig. 2, which plots the ratio of the reported data points to those calculated from the model.

A few other data sets are also plotted in Fig. 2 as consistency checks. Note that the temperature coefficient of k is of the order of 0.5%/K at room temperature between 400 and 800 nm [9]. Thus, the major differences in Fig. 2, are not due to the use of different temperatures for nominal room temperature by the authors of the different references, although some of the smaller differences might be.

The data of Weakliem and Redfield [2] were chosen for fitting for a number of reasons. First, three different sample thicknesses (5.50, 249, and 797 μm) were used in the transmission measurements reported therein. This has the virtue of covering a large range of extinction coefficient and also of providing a good consistency check on the k values in spectral regions where the transmission measurements overlap. Second, it was already shown by Geist *et al.* [3] that the data of Weakliem and Redfield [2] agree well with the data of Macfarlane *et al.* [4] (not shown in Fig. 2) at the longer wavelengths, and with a single high-accuracy datum point at 633 nm [5] that is shown in Fig. 2. Another virtue of this data set is that tabulated numerical values were available to the author [10]. Finally, note that the two thinner samples were measured at 297 K, and the thickest sample was measured at 299 K.

A portion of a second data set [6] of k data that was derived from transmission measurements is also shown in Fig. 2 as a consistency check on the model fit to the data of Weakliem and Redfield [2]. The points shown in Fig. 2 for these data were read from an enlarged copy of a different version of Fig. 11 by Gentile *et al.* [11]. Notice that the k data of Vol'fson and Subashiev [6] differ from the model by a uniform $3.4 \pm 0.5\%$ over the spectral region for which the data of Vol'fson and Subashiev [6] are plotted. This is consistent with a 3.4% error between the sample-thickness measurements upon which the two data sets were based.

The consistency of Eqs. (1)–(4) with the data of Vol'fson and Subashiev [6] is important because the agreement between the k values derived from the 5.50-μm-thick sample and the 249-μm-thick sample used by Weakliem and Redfield [2] is not as good as might be desired. The consistency also shows that fitting a function that is based on physical principles to the data tends to ignore the less-accurate data points.

The data of Jellison [1] were chosen for fitting for a number of reasons. First, the two-channel, polarization-modulation ellipsometric technique on which these data were based is more accurate for $k < 1$ than more conventional ellipsometric techniques such as rotating-analyzer ellipsometry. Second, these data were corrected for the presence of a thin native-oxide layer on the silicon surface. Third, Jellison [1] includes a careful uncertainty analysis that estimates about 1, 4, and 10% uncertainties at 400, 500, and 600 nm, respectively. Finally, these data agree with the high-accuracy datum point at 633 nm [5] mentioned earlier and with another high-accuracy datum point that was also based on transmission measurements using samples of different thicknesses (4.80, 5.93, 8.80, and 10.82 μm) at 546 nm [7] within the uncertainties estimated in [1, 5, 7]. This level of agreement tends to confirm the choice of the data from Jellison [1] based on the first three reasons. A final virtue of this data set is that tabulated numerical values were published in Jellison [1].

A portion of another set [8] of k data is also shown in Fig. 2 as a consistency check of the model around 400 nm. These k values were obtained in a

very different way: from a Kramers–Kronig analysis of reflectance data. These k values also include a correction for the effect of the native oxide. The rapid increase of the difference between that data points of Philipp [8] and the data points of Jellison [1] with increasing wavelength is not considered a problem with the latter, since a Kramers–Kronig analysis is not well suited to determining the smaller k values at the longer wavelengths.

Notice that the data of Jellison [1] and Weakliem and Redfield [2] agree very well in the center of their overlap region. Such agreement is usually considered a good sign of consistency. However, the agreement between the data sets of Jellison [1] and Weakliem and Redfield [2] in the overlap region may be fortuitous. Actually, the data of Jellison [1] were normalized to agree with another data set [12] that does not agree well with that of Weakliem and Redfield [2], but the normalization was carried out in a spectral region where the data of Dash and Newman [12] do not agree with those of Weakliem and Redfield [2], either. Therefore, the agreement at 633 nm might be a coincidence that has no bearing on the actual uncertainty of either data set in the overlap region. The independent agreement of both data sets with the high-accuracy datum point from Geist *et al.* [5] at 633 nm suggests that the data from Jellison [1] and Weakliem and Redfield [2] are indeed reliable in the overlap region.

The author knows of no other data set covering this spectral region that is comparable to that of Jellison [1] and Weakliem and Redfield [2] with respect to the virtues just mentioned. In fact, most of the k values in other data sets differ so much from the data shown in Fig. 2 that they would not even show up in Fig. 2.

Plus or minus 10% should be a very conservative uncertainty on k from this model over the 400 to 1130 nm spectral region, whereas $\pm$ 5% would appear to be a reasonable estimated one-standard-deviation equivalent uncertainty where such is required.

Before turning attention to n, note that the k values given in Table III at the end of this section are quite different from those given in by Edwards [13]. Also, note that the k values in Table III are not the data points reported by Jellison [1] and Weakliem and Redfield [2], but the values calculated from the model of Eqs. (1)–(4). Finally, note that k decreases so rapidly with increasing wavelength in this spectral region that great care is needed during interpolation of the data in Table III to avoid incurring significant errors. This is particularly so at the ends of the table. For this reason, it is probably safer to calculate k values from Eqs. (1)–(4) directly rather than to try to interpolate them from Table III.

C Real Part of the Index of Refraction

The choice among the various sets of n data is not as straightforward as was the case with the k data. Nevertheless, a model was fitted to the room-

temperature data in Jellison [1] and to three room-temperature data points from Edwards [13]. The model is given by

$$n(h\nu) = y(h\nu)z(h\nu) \tag{5}$$

$$z(h\nu) = N_0 + h\nu(N_1 + h\nu(N_2 + h\nu(N_3 + h\nu N_4))) \tag{6}$$

$$y(h\nu) = \exp\{y_6(h\nu)[K_{61} + y_6(h\nu)K_{62}] + y_7(h\nu)[K_{71} + y_7(h\nu)K_{72}]\} \tag{7}$$

$$y_m(h\nu) = 2L(h\nu - \epsilon_m), \tag{8}$$

where $m = 6, 7$, the function $L(\epsilon)$ is defined in Eq. (4), and the values of the parameters needed in Eqs. (5)–(8) are given in Table II. The model fits the n data of Jellison [1] and Edwards [13] reasonably well from 390 to 1200 nm, as shown in Fig. 3 [14]. This figure plots the ratio of the reported data points to those calculated from the model.

A few other data sets are also plotted in Fig. 3 as consistency checks. Note that the temperature coefficient of n is of the order of 0.025%/K at room temperature [9]. Thus the major differences in Fig. 3 are not due to the use of different temperatures as nominal room temperature by the authors of the different references, although the smaller differences might be.

The data of Jellison [1] were chosen partially because the quality of these data had already been established in connection with the selection of the k data, but also because they are recent, and they agree well at 546.1 nm with the value reported in by Taft [7]. The latter value has been characterized by Aspnes and Studna [14] as "most probably, the best data" among the more than 15 data points (ranging from 4.004 to 4.151) that have been reported at this wavelength.

Three data points between 1100 and 1200 nm were selected from Edwards [13] because these are derived from measurements of the angle of minimum deviation, which should be considerably more accurate than ellipsometric or reflectance measurements. Data points from two other widely referenced [8, 14] index spectra are also shown in Fig. 3 for comparison. Ellipsometric measurements were used by Aspnes and Studna [14], whereas a Kramers–Kronig analysis of reflectance measurements was used by Philipp [8].

The model of Eqs. (5)–(8) was fitted only to the plus signs in Fig. 3. The plus signs below 900 nm are from Jellison [1] and those above 1100 nm are from Edwards [13]. Jellison [1] estimated the uncertainty of the data used in Fig. 3 at less than 0.6% between 400 and 800 nm. Therefore, the model of Eqs. (5)–(8) fits the data from Jellison [1] to well within the estimated uncertainty of the data except near 400 nm and at wavelengths longer than 800 nm, where the error in the fit approaches the estimated error.

Since the two other spectra [8, 14] included in Fig. 3 have very similar shapes, it is somewhat disconcerting that the spectrum from Jellison [1] has a different shape below about 550 nm. On the other hand, Jellison [1] agrees better with Taft [7] at 546.1 nm, and Jellison [1] devoted a significant amount of time to estimating and reporting the uncertainties in his measurements. In

light of (i) the small but not negligible inconsistencies among the data shown in Fig. 3, (ii) the uncertainty estimate provided by Jellison [1], and (iii) the lack of good coverage over an extended region from about 800 to 1100 nm, a conservative uncertainty estimate might be $\pm 1\%$ for wavelengths greater than 550 nm, and $+1$–2% for shorter wavelengths. It is not possible to assign a convincing "one-standard-deviation equivalent" uncertainty for the model of Eqs. (5)–(8) in light of the inconsistencies shown in the data in Fig. 3.

Table III contains n and k data calculated from Eqs. (1)–(8) at 0.05-eV intervals from 1.10 to 3.10 eV. Data about the variation of n and k with temperature at different wavelengths can be found elsewhere [2, 9, 15]. Finally, note that Gentile *et al.* [11] review a wider variety of k data, but reaches similar conclusions to those given here.

ACKNOWLEDGEMENT

The author thanks T. R. Gentile for providing a preprint of the appendix reviewing k data in Gentile *et al.* [11], a different version of Fig. 11 in Gentile *et al.* [11], a computer disk containing data keyed from Jellison [1], and other useful information about the data reviewed by Gentile *et al.* [11].

REFERENCES

1. G. E. Jellison Jr., Optical functions of silicon determined by two-channel polarization modulation ellipsometry. *Opt. Mater.* **1**, 41–47 (1992).
2. H. A. Weakliem and D. Redfield, Temperature dependence of the optical properties of silicon. *J. Appl. Phys.* **50**, 1491–1493 (1979).
3. J. Geist, A. Migdall, and H. P. Baltes, Analytic representation of the silicon absorption coefficient in the indirect transition region. *Appl. Opt.* **27**, 3777–3779 (1988).
4. G. G. Macfarlane, T. P. McLean, J. E. Quarington, and V. Roberts, Fine structure in the absorption-edge spectrum of silicon. *Phys. Rev.* **111**, 1245–1254 (1958); G. G. Macfarlane, P. T. McLean, J. E. Quarington, and V. Roberts, Exiton and phonon effects in the absorption spectra of germanium and silicon. *J. Phys. Chem. Solids* **8**, 388–392 (1959).
5. J. Geist, A. R. Schaefer, J.-F. Song, Y. H. Wang, and E. F. Zalewski, An accurate value for the absorption coefficient of silicon at 633 nm. *J. Res. Natl. Inst. Stand. Technol.* **95**, 549–558 (1990).
6. A. A. Vol'fson and V. K. Subashiev, Fundamental absorption edge of silicon heavily doped with donor or acceptor impurities. *Sov. Phys. Semicond. (Engl. Transl.)* **1**, 327–332 (1967), which includes a pure-silicon reference.
7. E. A. Taft, The optical constants of silicon and dry oxygen oxides of silicon at 5461 Å. *J. Electrochem. Soc.* **125**, 968–971 (1978).
8. H. R. Philipp, Influence of oxide layers on the determination of the optical properties of silicon. *J. Appl. Phys.* **43**, 2835–2839 (1972); H. R. Philipp personal communication, 1979.
9. G. E. Jellison, Jr. and F. A. Modine, Optical functions of silicon at elevated temperatures. *J. Appl. Phys.* **76**, 3758–3761 (1994).
10. H. A. Weakliem personal communication, 1979.
11. T. R. Gentile, J. M. Houston, and C. L. Cromer, Realization of a scale of absolute spectral

response using the National Institute of Standards and Technology high-accuracy cyrogenic radiometer. *Appl. Opt.* **35**, 4392–4403 (1996).
12. W. C. Dash and R. Newman, Intrinsic optical absorption spectra in single-crystal germanium and silicon at 77° K and 300° K. *Phys. Rev.* **99**, 1151–1155 (1955).
13. D. F. Edwards, Silicon (Si). *in* "Handbook of Optical Constants of Solids" (E. D. Palik, ed.), pp. 547–569. Academic Press, Orlando, Florida, 1985.
14. D. E. Aspnes and A. A. Studna, Dielectric functions and optical parameters of Si, Ge, GaP, GaAs, GaSb, InP, InAs, and InSb from 1.5 to 6.0 eV. *Phys. Rev. B* **27**, 985–1009 (1983).
15. G. E. Jellison, Jr., and D. H. Lowndes, Optical absorption coefficients of silicon at 1.152 μ at elevated temperatures. *Appl. Phys. Lett.* **41**, 594–596 (1982).

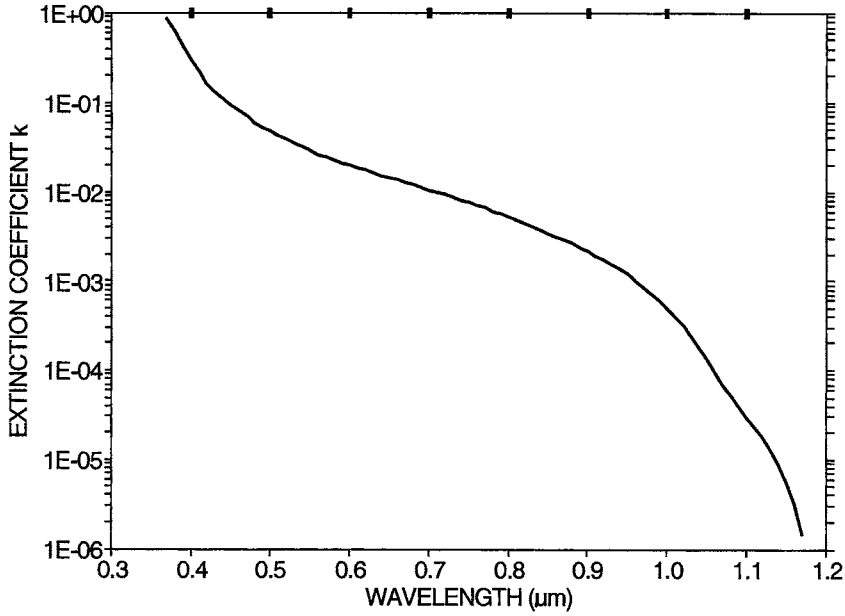

Fig. 1. The extinction coefficient of a pure silicon crystal at room temperature from 370 to 1170 nm as calculated from Eqs. (1)–(4) to represent the data of Jellison [1] and Weakliem and Redfield [2].

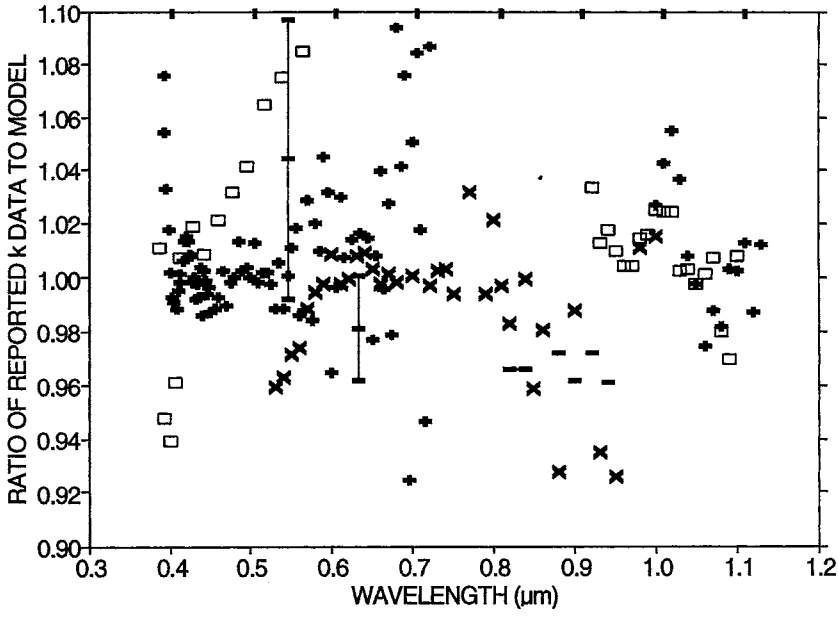

Fig. 2. The ratio of the k values reported by some different authors to the k values calculated from Eqs. (1)–(4) at the same wavelengths: plus signs below 800 nm from Jellison [1], x's from Weakliem and Redfield [2]; plus signs and open boxes above 800 nm also from Weakliem and Redfield [2]; 633-nm data point with error bars from Giest *et al.* [5]; minus signs from Vol'fson and Subashiev [6]; 546-nm data point with error bars from Taft [7]; open boxes below 600 nm from Philipp [8].

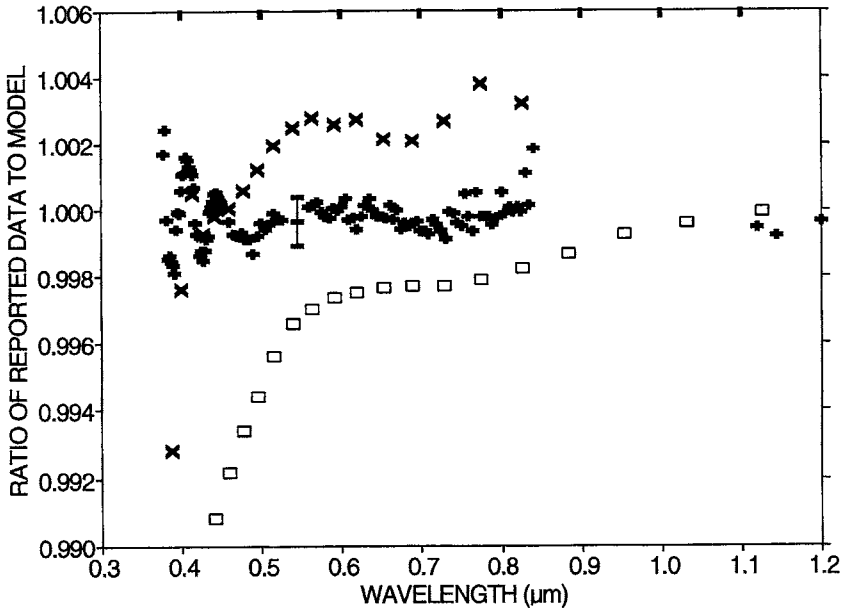

Fig. 3. The ratio of the n values reported by some different authors to the n values calculated from Eqs. (5)–(8) at the same wavelengths: plus signs below 900 nm from Jellison [1]; plus signs above 1100 nm from Edwards [13]; 546-nm data point with error bars from Taft [7]; open boxes from Philipp [8]; and x's from Aspnes and Studna [14].

TABLE I

Parameters for Use in Eqs. (1)–(4) to Describe the Extinction Coefficient of Pure Silicon at Room Temperature from 400 to 1180 nm

Parameter	Value
ϵ_1	1.09969 eV
$d\epsilon_1$	0.0583148 eV
$C_{1,-1}$	5030.02 cm^{-1} eV
$C_{1,+1}$	483.916 cm^{-1} eV
ϵ_2	(not used)
$d\epsilon_2$	0.0220161 eV
$C_{2,-2}$	1634.30 cm^{-1} eV
$C_{2,+2}$	79.4079 cm^{-1} eV
ϵ_3	1.40985 eV
C_3	1046.08 cm^{-1} eV
N	0.394122
dN	1.23084 eV^{-1}
ϵ_4	2.15362 eV
K_4	0.210102
ϵ_5	2.95893 eV
K_5	1.03681

TABLE II

Parameters for Use in Eqs. (5)–(8) to Describe the Index of Refraction of Pure Silicon at Room Temperature from 390 to 1200 nm

Parameter	Value
N_0	3.76289
N_1	−1.02862
N_2	1.19270
N_3	−0.504529
N_4	0.0909420
ϵ_6	2.74717 eV
K_{61}	0.00891406
K_{62}	0.0292730
ϵ_7	2.97648 eV
K_{71}	−0.0012589
K_{72}	0.197000

TABLE III

Values of n and k for Silicon Obtained from Various References

eV	cm^{-1}	μm	n	k
3.10	25000	0.4000	5.5832	2.96E-01
3.05	24600	0.4065	5.3834	2.40E-01
3.00	24200	0.4133	5.2195	1.96E-01
2.95	23790	0.4203	5.0855	1.62E-01
2.90	23390	0.4275	4.9647	1.40E-01
2.85	22990	0.4350	4.8544	1.21E-01
2.80	22580	0.4428	4.7539	1.05E-01
2.75	22180	0.4509	4.6627	9.19E-02
2.70	21780	0.4592	4.5828	8.05E-02
2.65	21370	0.4679	4.5085	7.08E-02
2.60	20970	0.4769	4.4394	6.25E-02
2.55	20570	0.4862	4.3749	5.54E-02
2.50	20160	0.4959	4.3149	4.92E-02
2.45	19760	0.5061	4.2589	4.39E-02
2.40	19360	0.5166	4.2068	3.93E-02
2.35	18950	0.5276	4.1582	3.52E-02
2.30	18550	0.5391	4.1128	3.16E-02
2.25	18150	0.5510	4.0704	2.84E-02
2.20	17740	0.5636	4.0307	2.56E-02
2.15	17340	0.5767	3.9936	2.31E-02
2.10	16940	0.5904	3.9588	2.10E-02
2.05	16530	0.6048	3.9261	1.91E-02
2.00	16130	0.6199	3.8953	1.73E-02
1.95	15730	0.6358	3.8662	1.57E-02
1.90	15320	0.6526	3.8388	1.41E-02
1.85	14920	0.6702	3.8127	1.26E-02
1.80	14520	0.6888	3.7880	1.12E-02
1.75	14110	0.7085	3.7644	9.92E-03
1.70	13710	0.7293	3.7419	8.65E-03
1.65	13310	0.7514	3.7204	7.45E-03
1.60	12900	0.7749	3.6999	6.30E-03
1.55	12500	0.7999	3.6801	5.22E-03
1.50	12100	0.8266	3.6611	4.21E-03
1.45	11690	0.8551	3.6429	3.29E-03
1.40	11290	0.8856	3.6254	2.47E-03
1.35	10890	0.9184	3.6087	1.75E-03
1.30	10490	0.9537	3.5926	1.11E-03
1.25	10080	0.9919	3.5773	5.87E-04
1.20	9679	1.033	3.5628	2.21E-04
1.15	9275	1.078	3.5491	5.55E-05
1.10	8872	1.127	3.5362	1.39E-05

Silicon (Si) Revisited (1.4–6.0 eV)

DAVID F. EDWARDS
Tracy, California

Adachi [1, 2] has developed a method for the calculation of the complex dielectric function, $\epsilon(\omega) = \epsilon_1(\omega) + i\,\epsilon_2(\omega)$, of Si based on a simplified model of the energy-band structure of the material. This model covers the optical response of Si over the entire range of photon energies (0–6.0 eV) and is based on the Kramers–Kronig transformation. The calculation takes into account the effects of interband transitions at the major energy–band critical points and indirect band gap. The model relies on the measured critical point energies of Lautenschlager *et al.* [3]. This group measured the dielectric function of Si by ellipsometry in the 1.7- to 5.7-eV photon-energy range. For the Adachi model the strength and damping parameters were adjusted to optimize the fit to experimental data. The experimental data of Aspens and Studna [4] were used for the fit of the $\epsilon_2(\omega)$ calculation. These experimental data were obtained from spectroscopic ellipsometry. For the $\epsilon_1(\omega)$ calculation the experimental data of Philipp and Ehrenreich [5] were used for energies below 1.5 eV and those in the 1.5- to 6.0-eV range from Aspens and Studna [4]. In order to improve the $\epsilon_1(\omega)$ fit, the nondispersive term, $\epsilon_{1\infty}$, was added to the sum of the dispersive terms. The spectral dependence of the refractive index, n, and the extinction coefficient, k, were calculated from the real and imaginary parts of $\epsilon(\omega)$. The details of these calculations are given later.

Overall, the continuous analytical functions for n and k are in satisfactory agreement with experiment concerning the simplicity of the model and complexity of the problem. The calculated k values appear to be about 9–10% too small in the energy region greater than about 4.27 eV. The fit of the calculated n values is much better for energies less than 3.38 eV than for energies greater than this value. For purpose of this review article, only n and k values in the 3.0- to 6.0 eV-range are tabulated. The 1.10- to 3.1-eV data of Geist (included in this volume) appear to give a more accurate fit to experimental data.

For the interband transitions, E_1, along the $\langle 111 \rangle$ direction of the Brillouin zone (near 3.4 eV), the contributions to ϵ_2 are

HANDBOOK OF OPTICAL CONSTANTS OF SOLIDS III

Copyright © 1998 by Academic Press.
All rights of reproduction in any form reserved
ISBN 0-12-544423-0/$25.00.

$$\begin{aligned} \epsilon_2(\omega) &= \pi\chi_1^{-2}[B_1 - B_{11}(E_1 - \hbar\omega)^{0.5} \quad (\hbar\omega < E_1) \\ &= \pi B_1 \chi_1^{-2} \qquad\qquad\qquad\quad (\hbar\omega \geq E_1), \end{aligned} \tag{1}$$

where $\chi_1 = \hbar\omega/E_1$.

The contribution of the E_1 transition to $\epsilon_1(\omega)$ is

$$\epsilon_1(\omega) = -B_1\chi_1^{-2}\ln|1 - \chi_1^2|. \tag{2}$$

The B's are the strength parameters. The numerical parameters used in the calculations are listed in Table I.

At the $\langle 100 \rangle$ edge of the Brillouin zone (near 4.3 eV), the E_2 transition has two contributions to the dielectric function . The first is characterized by a damped harmonic oscillator,

$$\epsilon_2(\omega) = C\chi_2\gamma/[(1 - \chi_2^2)^2 + \chi_2^2\gamma^2] \tag{3}$$

and

$$\epsilon_1(\omega) = C(1 - \chi_2^2)/[(1 - \chi_2^2)^2 + \chi_2^2\gamma^2] \tag{4}$$

with

$$\chi_2 = \hbar\omega/E_2,$$

where C and γ are, respectively, the strength and damping parameters of the oscillator.

The second contribution for the E_2 transition is

$$\epsilon_2(\omega) = \pi F\chi_2^{-2}H(\chi_{cl} - 1) \tag{5}$$

with

$$\chi_1 = \hbar\omega/E_1$$

and

$$\epsilon_1(\omega) = -F\chi_2^{-2}/\ln\left|\frac{1 - \chi_{cl}^2}{1 - \chi_2^2}\right|. \tag{6}$$

Here F is the strength parameter and

$$\begin{aligned} H(y) &= 1 \text{ for } y \geq 0 \\ &= 0 \text{ for } y < 0. \end{aligned}$$

The E_1' transitions near 5.3 eV are to a higher valence band. They are assumed by Adachi to be of the form of damped harmonic oscillators:

$$\epsilon_2(\omega) = C_a\gamma_a\chi_a/[1 - \chi_a^2)^2 + \chi_a^2\gamma_a^2] \tag{7}$$

$$\epsilon_1(\omega) = C_a(1 - \chi_a^2)/[(1 - \chi_a^2)^2 + \chi_a^2\gamma_a^2], \tag{8}$$

with

$$\chi_a = \hbar\omega/E_a,$$

where E_a is the energy of the oscillator.

The contribution of the indirect transition to $\epsilon_2(\omega)$ is

$$\epsilon_2(\omega) = \frac{D}{\hbar\omega^2}(\hbar\omega - E_g^{id} \pm \hbar\omega_q)^2 H(1 - \chi_g), \tag{9}$$

with

$$\chi_g = (E_g^{id} \pm \hbar\omega_q)/\hbar\omega,$$

where D is the direct-transition strength parameter and $\hbar\omega_q$ is the phonon energy associated with the indirect transition. Adachi states that there is no contribution of the indirect transition to $\epsilon_1(\omega)$.

The nondispersive term, $\epsilon_{1\infty}(= 1.8$ eV), is added to the sum of Eqs. (2), (4), (6), and (8) for the final summation of the $\epsilon_1(\omega)$.

The complex refractive index, $n^*(\omega)$, is

$$n^*(\omega) = n(\omega) + ik(\omega) = \epsilon(\omega)^{1/2}, \tag{10}$$

where n and k are, respectively, the real refractive index and the extinction coefficient. From Eq. (10), the optical constants are

$$n(\omega) = \left(\frac{(\epsilon_1(\omega)^2 + \epsilon_2(\omega)^2)^{1/2} + \epsilon_1(\omega)}{2}\right)^{1/2} \tag{11}$$

$$k(\omega) = \left(\frac{(\epsilon_1(\omega)^2 + \epsilon_2(\omega)^2)^{1/2} - \epsilon_1(\omega)}{2}\right)^{1/2}. \tag{12}$$

Listed in Table II are n and k values for the energy range 3.0 to 6.0 eV (0.207 to 0.414 μm) as calculated from Eqs. (11) and (12) and the parameters of Table I.

REFERENCES

1. S. Adachi, *Phys. Rev. B* **38**, 12966 (1988).
2. S. Adachi, *J. Appl. Phys.* **66**, 3224 (1989).
3. P. Lautenschlager, N. Garriga, L. Viña, and M. Cardona, *Phys. Rev. B* **36**, 4821 (1987).
4. D. E. Aspens and A. A. Studna, *Phys. Rev. B* **27** 985 (1983).
5. H. R. Philipp and H. J. Ehrenreich, *Phys. Rev.* **129**, 1550 (1963).

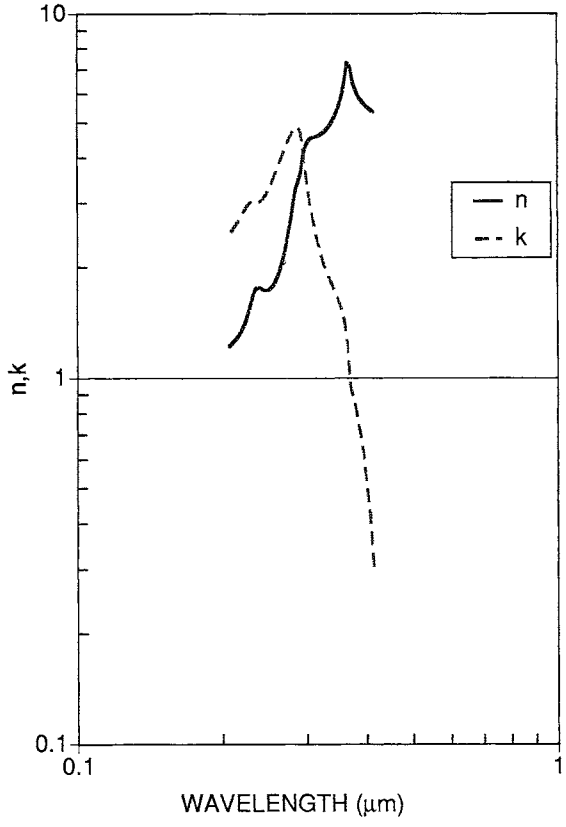

Fig. 1. Log–log plot of n and k versus wavelength in microns for silicon as calculated from Eqs. (1)–(12).

TABLE 1

Parameters Used in the Calculation of $n(\omega)$ and $k(\omega)$ (at room temperature)

E_1(eV)	3.38
B_1	5.22
B_{11} ($eV^{-0.5}$)	7.47
E_2(eV)	4.27
C	3.01
γ	0.127
F	3.51
$\Gamma[E_2]$ (eV)	0.04
E_a (eV)	5.32
C_a	0.21
γ_a	0.089
E_g^{ID}(eV)	1.12
D	0.89
$\epsilon_{1\infty}$	1.8

TABLE II

Values of n and k for Silicon Calculated from Eqs. (1)–(12)

eV	cm^{-1}	μm	n	k
6.00	48309	0.2070	1.2215	2.4570
5.95	47907	0.2087	1.2338	2.4961
5.90	47504	0.2105	1.2472	2.5373
5.85	47101	0.2123	1.2622	2.5808
5.80	46699	0.2141	1.2791	2.6269
5.75	46296	0.2160	1.2987	2.6758
5.70	45894	0.2179	1.3217	2.7275
5.65	45491	0.2198	1.3494	2.7819
5.60	45089	0.2218	1.3835	2.8386
5.55	44686	0.2238	1.4259	2.8958
5.50	44283	0.2258	1.4785	2.9506
5.45	43881	0.2279	1.5418	2.9974
5.40	43478	0.2300	1.6127	3.0292
5.35	43076	0.2321	1.6813	3.0403
5.30	42673	0.2343	1.7337	3.0333
5.25	42271	0.2366	1.7600	3.0216
5.20	41868	0.2388	1.7624	3.0214
5.15	41465	0.2412	1.7516	3.0421
5.10	41063	0.2435	1.7385	3.0847
5.05	40660	0.2459	1.7300	3.1459
5.00	40258	0.2484	1.7297	3.2220
4.95	39855	0.2509	1.7388	3.3103
4.90	39452	0.2535	1.7583	3.4092
4.85	39050	0.2561	1.7888	3.5180
4.80	38647	0.2588	1.8318	3.6365
4.75	38245	0.2615	1.8893	3.7647
4.70	37842	0.2643	1.9641	3.9025
4.65	37440	0.2671	2.0601	4.0490
4.60	37037	0.2700	2.1823	4.2024
4.55	36634	0.2730	2.3365	4.3582
4.50	36232	0.2760	2.5280	4.5085
4.45	35829	0.2791	2.7588	4.6407
4.40	35427	0.2823	3.0209	4.7384
4.35	35024	0.2855	3.2832	4.7922
4.30	34622	0.2888	3.4479	4.8588
4.25	34219	0.2922	3.6423	4.6901
4.20	33816	0.2957	4.0828	4.0766
4.15	33414	0.2993	4.3189	3.6196
4.10	33011	0.3029	4.4468	3.2317
4.05	32609	0.3067	4.5097	2.9100
4.00	32206	0.3105	4.5401	2.6504
3.95	31804	0.3144	4.5611	2.4436
3.90	31401	0.3185	4.5874	2.2789
3.85	30998	0.3226	4.6281	2.1460
3.80	30596	0.3268	4.6890	2.0366
3.75	30193	0.3312	4.7742	1.9436

(continued)

TABLE 2 *(Continued)*

Silicon

eV	cm^{-1}	μm	n	k
3.70	29791	0.3357	4.8877	1.8616
3.65	29388	0.3403	5.0349	1.7859
3.60	28986	0.3450	5.2236	1.7122
3.55	28583	0.3499	5.4679	1.6359
3.50	28180	0.3549	5.7966	1.5505
3.45	27778	0.3600	6.2842	1.4427
3.40	27375	0.3653	7.2958	1.2577
3.35	26973	0.3707	7.0864	0.9453
3.30	26570	0.3764	6.3887	0.8896
3.25	26167	0.3822	6.0408	0.8075
3.20	25765	0.3881	5.8121	0.7171
3.15	25362	0.3943	5.6458	0.6215
3.10	24960	0.4006	5.5186	0.5210
3.05	24557	0.4072	5.4189	0.4156
3.00	24155	0.4140	5.3399	0.3050

Silicon–Germanium Alloys (Si_xGe_{1-x}) Revisited

J. HUMLÍČEK
Masaryk University, Faculty of Science
Department of Solid State Physics
Brno, Czech Republic

Silicon and germanium form a continuous series of crystalline alloys, Si_xGe_{1-x}. Their optical constants have been compiled for three compositions x ($\approx$ 0.80, 0.50, and 0.25) in *HOC II* [1]. Optical constants of both constituents are available in the critiques of Potter (Ge, [2]) and Edwards (Si, [3]). Recently, the silicon-rich alloys from the range $1 < x < 0.75$ have become important in silicon-based thin-film structures. Very thin epitaxial alloy layers of a few tens of nanometers can accomodate the silicon—substrate lattice constant, resulting in appreciable strain that influences the optical response [4]. Thicker films are (at least partly) relaxed. Most of the recent work not covered by Humlíček *et al.* [1] has been done on the epitaxial films.

In the present critique we (i) compile a comprehensive database for $x \approx 0.80$ from the x-ray to the far-infrared region, including data taken on the relaxed films, and (ii) provide narrowly spaced, interpolated data over the compositions, within the spectral range from UV to NIR. In Table I we list n and k data obtained for the compositions equal or close to $x = 0.80$. The spectra from several sources are plotted in Fig. 1. In the x-ray region, the data were calculated using the Henke model [5, 6]. The calculation is based on the data for pure Si and Ge, and on the assumption of independent contributions of the atomic cross-sections of both constituents. The only input for the particular alloy composition x consisted in the density of 2.93 g/cm^3, obtained by linear interpolation between $x = 1$ and $x = 0$. Let us note that the model does not take into account the valence-band structure of the alloy, resulting in the loss of accuracy with decreasing photon energy. In the UV range, we use the results of reflectance measurements [7], discussed in detail by Humlíček *et al.* [1]. The range of fundamental interband transitions has been covered by several spectroellipsometric studies [4, 8, 9]. The main problem influencing the accuracy of the optical data consists in the

HANDBOOK OF OPTICAL CONSTANTS OF SOLIDS III

Copyright © 1998 by Academic Press.
All rights of reproduction in any form reserved
ISBN 0-12-544423-0/$25.00.

quality of sample surfaces. A significant improvement might be obtained with the high-quality (relaxed) epitaxial layers, with an appropriate procedure for the removal of the influence of substrate and overlayer [4]. We have selected data of Pickering and Carline [4] and Humlíček *et al.* [8] for the two entries of Table I; they are in a fairly good agreement. We expect the thin-film data of Pickering and Carline [4] to be more reliable, especially for the low extinction at the lowest photon energies; consequently, we display also values of k below 0.3 reported by Pickering and Carline [4]. The low extinction values obtained on bulk samples are considered to be unreliable [1] in the results of Humlíček *et al.* [8] and are therefore skipped in Table I. At the band edge, we include the k data resulting from an interpolation scheme using the gap and phonon energy as functions of the concentration [1]. The parametrization used the absorption measurements of Braunstein *et al.* [10]. We complement the extinction data with the values of refractive index obtained using the Kramers–Kronig transformation of the ellipsometric data above the edge [11]. It should be noted that the latter work corrects the erroneous results obtained for the refractive index found elsewhere [12, 13], where n has been related to the position of the indirect band gap. The rich spectral structure due to lattice vibrations in the infrared changes very strongly with the alloy composition and displays both first- and higher-order phonon processes [1]. We therefore complement the data of Table I by the plot of the absorption coefficient of silicon-rich alloys [14] shown in Fig. 2. Besides a number of multiphonon bands and an extrinsic, oxygen-related band at $\sim$1100 cm^{-1}, two distinct absorption peaks at $\sim$400 and $\sim$500 cm^{-1} reveal the "Ge–Si" and "Si–Si" vibrations [15], respectively. They represent a convenient fingerprint of alloying in the optical constants of the Si-rich materials.

In Fig. 3 we plot n and k data obtained from the databases of others [7, 8, 10, 11] by linear interpolation over compositions with steps of 0.1. The concentration dependence is fairly smooth in the whole spectral interval, except for k in the range of the indirect band gap (because of the crossover of the conduction-band minima for $x \approx 0.15$ [10]). Consequently, the corresponding data in Table II are expected to provide a reasonable basis for intermediate compositions.

REFERENCES

1. J. Humlíček, F. Lukeš, and E. Schmidt, *in* "Handbook of Optical Constants of Solids II" (E. D. Palik, ed.), p. 607. Academic Press, San Diego, 1991.
2. R. F. Potter, *in* "Handbook of Optical Constants of Solids" (E. D. Palik, ed.), p. 465. Academic Press, Orlando, Florida, 1985.
3. D. F. Edwards, *in* "Handbook of Optical Constants of Solids" (E. D. Palik, ed.), p. 465. Academic Press, Orlando, Florida, 1985.
4. C. Pickering and R. T. Carline, *J. Appl. Phys.* **75**, 4642 (1994); C. Pickering, private information, 1994.
5. B. L. Henke, P. Lee, T. J. Tanaka, R. L. Shimobukuro, and B. K. Fujikama, *At. Data Nucl. Data Tables* **27**, 1 (1982).

6. B. L. Henke, J. C. Davis, E. M. Gullikson, and R. C. C. Perera, *Lawrence Berkeley Laboratory Report No.* **LBL–26259** (1988).
7. E. Schmidt, *Phys. Status. Solidi* **27**, 57 (1968).
8. J. Humlíček, M. Garriga, M. I. Alonso, and M. Cardona, *J. Appl. Phys.* **65**, 2827 (1989).
9. G. E. Jellison Jr., T. E. Haynes, and H. H. Burke, *Opt. Mater.* **2**, 105 (1993).
10. R. Braunstein, A. R. Moore, and F. Herman, *Phys. Rev.* **109**, 695 (1958).
11. J. Humlíček, A. Roeseler, T. Zettler, M. G. Kekoua, and E. Khoutsishvili, *Appl. Opt.* **31**, 90 (1992).
12. J. J. Miceli and D. P. Naughton, *Appl. Opt.* **27**, 500 (1988).
13. D. P. Naughton, J. J. Miceli, and D. T. Moore, *Appl. Opt.* **27**, 505 (1988).
14. M. Lorenc and J. Humlíček, unpublished data, 1996.
15. G. M. Zinger, I. P. Ipatova, and A. V. Subashiev, *Sov. Phys. Semicond. (Engl. Transl.)* **11**, 383 (1977).

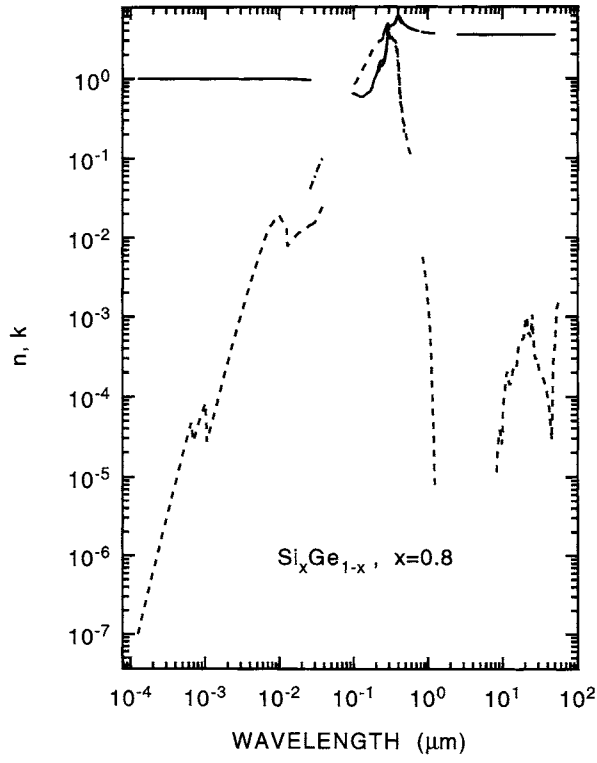

Fig. 1. Log–log plot of n (solid lines) and k (dashed lines) versus wavelength in microns for Si_xGe_{1-x}, $x = 0.8$.

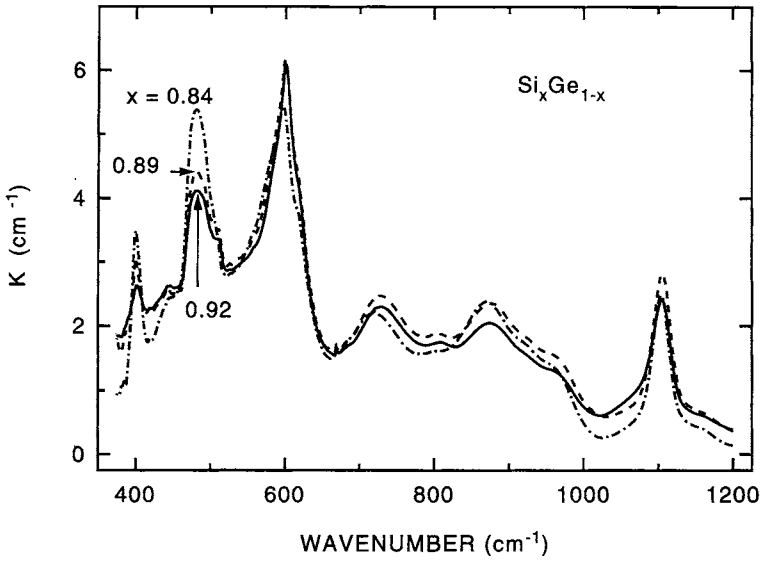

Fig. 2. Linear/linear plot of absorption coefficient for three compositions x of Si_xGe_{1-x} versus wavenumber.

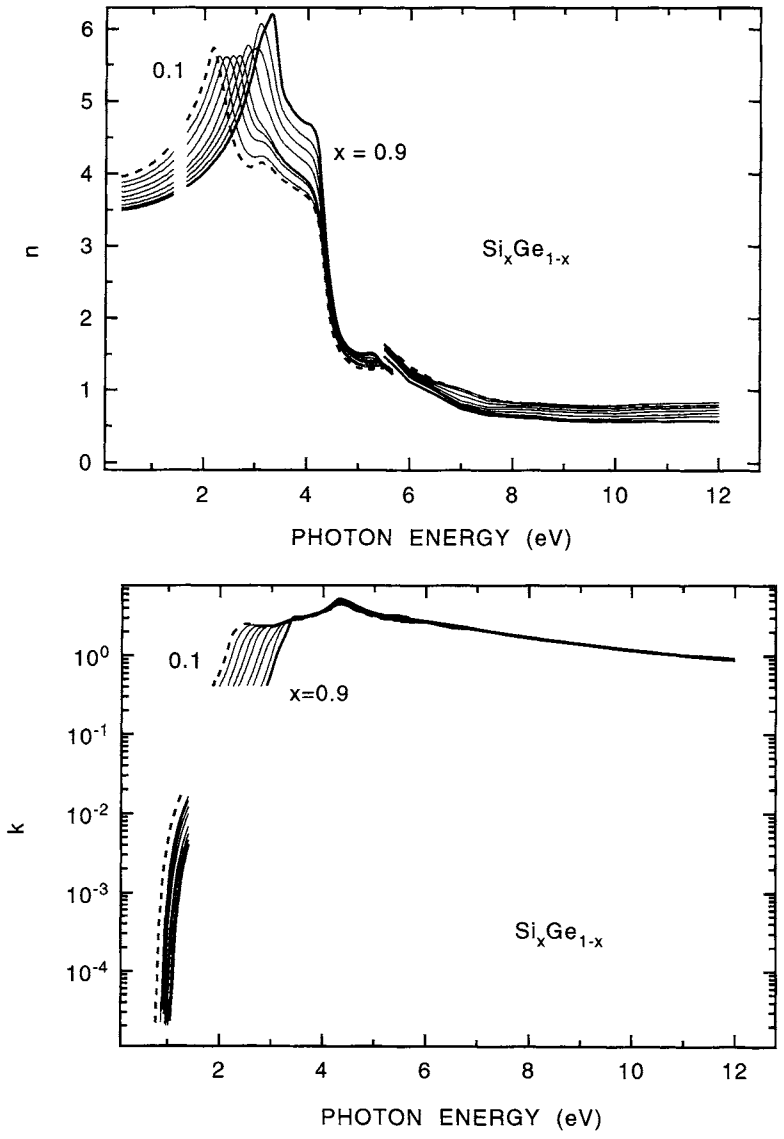

Fig. 3. Optical constants for Si_xGe_{1-x} with the composition $x = 0.1$ (dashed lines), 0.2, . . ., 0.8 in steps of 0.1 (thin solid lines) and 0.9 (solid lines). Linear–linear plot of n versus photon energy. Log–linear plot of k versus photon energy.

TABLE 1

Values of n and k for Si_xGe_{1-x}, $x \approx 0.80$, from Various References[a]

eV	cm^{-1}	Å	n	n	k	k
9918.	79,990,000	1.25	0.99999418 [5, 6]		1.001E-07 [5, 6]	
3306.	26,660,000	3.75	0.9999461		6.569E-06	
1983.	15,990,000	6.25	0.999869		4.122E-05	
1416.	11,420,000	8.75	0.999762		5.731E-05	
1102.	8,888,000	11.2	0.999622		3.470E-05	
901.7	7,272,000	13.7	0.999398		6.973E-05	
762.9	6,153,000	16.2	0.999140		1.268E-04	
661.2	5,333,000	18.7	0.99884		2.109E-04	
583.4	4,705,000	21.2	0.99851		3.259E-04	
522.0	4,210,000	23.7	0.99814		4.761E-04	
472.3	3,809,000	26.2	0.99775		6.615E-04	
431.2	3,478,000	28.7	0.99733		8.898E-04	
396.7	3,199,000	31.2	0.99689		1.156E-03	
367.3	2,962,000	33.7	0.99642		1.474E-03	
342.0	2,758,000	36.2	0.99594		1.844E-03	
319.9	2,580,000	38.7	0.99546		2.274E-03	
300.5	2,424,000	41.2	0.99497		2.767E-03	
283.3	2,285,000	43.7	0.99451		3.312E-03	
268.0	2,162,000	46.2	0.99407		3.901E-03	
254.3	2,051,000	48.7	0.99364		4.522E-03	
241.8	1,950,000	51.2	0.99321		5.207E-03	
206.8	1,668,000	59.9	0.99199		8.090E-03	
180.7	1,457,000	68.6	0.99191		1.170E-02	
160.4	1,294,000	77.2	0.99327		1.414E-02	
144.2	1,163,000	85.9	0.99374		1.680E-02	
131.0	1,057,000	94.6	0.99707		1.915E-02	
120.0	968,300	103.	0.999334		1.813E-02	
110.7	893,400	111.	0.99877		1.596E-02	
102.8	829,100	120.	0.99771		1.503E-02	
95.9	773,500	129.	0.999833		7.868E-03	
89.8	725,000	137.	0.99570		8.488E-03	
84.5	682,100	146.	0.99285		9.095E-03	
79.8	644,000	155.	0.99045		9.698E-03	
75.6	610,000	163.	0.9882		1.029E-02	
71.8	579,300	172.	0.9860		1.088E-02	
68.3	551,600	181.	0.9839		1.142E-02	
65.2	526,500	189.	0.9817		1.167E-02	
62.4	503,500	198.	0.9793		1.193E-02	
59.8	482,400	207.	0.9768		1.221E-02	
57.4	463,100	215.	0.9741		1.251E-02	
55.2	445,200	224.	0.9713		1.284E-02	
53.1	428,600	233.	0.9683		1.322E-02	
51.2	413,300	241.	0.9653		1.362E-02	

[a] The reference from which the values were extracted is given in brackets next to the first value. The nominal alloy compositions are: $x = 0.80$ [5, 6], $x = 0.803$ [7], $x = 0.782$ [8], $x = 0.805$ [4], $x = 0.782$ [10,11], $x = 0.80$ [14].

TABLE I *(Continued)*

Si_xGe_{1-x}, $x \approx 0.80$

eV	cm^{-1}	Å	n	n	k	k
49.4	399,000	250.	0.9623		1.402E-02	
47.8	385,600	259.	0.9592		1.428E-02	
12.8	103,200	0.09686	0.64 [7]		0.78 [7]	
12.2	98,420	0.1016	0.65		0.84	
11.3	91,910	0.1088	0.63		0.92	
10.5	85,470	0.1170	0.61		1.04	
9.80	79,050	0.1265	0.60		1.20	
8.99	72,560	0.1378	0.60		1.40	
8.20	66,130	0.1512	0.65		1.63	
7.79	62,890	0.1590	0.67		1.76	
7.00	56,460	0.1771	0.77		2.18	
6.80	54,850	0.1823	0.87		2.30	
6.59	53,220	0.1879	0.95		2.38	
6.40	51,620	0.1937	1.02		2.45	
6.19	50,000	0.2000	1.08		2.57	
6.00	48,400	0.2066	1.18		2.71	
5.70	45,970	0.2175	1.40		2.89	
5.62	45,320	0.2206	1.27 [8]		3.06 [8]	
5.56	44,840	0.2230	1.30		3.08	
5.49	44,360	0.2254	1.35		3.11	
5.44	43,870	0.2279	1.40		3.13	
5.37	43,390	0.2305	1.44		3.13	
5.32	42,900	0.2331	1.47		3.14	
5.26	42,420	0.2357	1.48		3.15	
5.20	41,940	0.2384	1.48		3.18	
5.13	41,450	0.2412	1.48		3.23	
5.08	40,970	0.2441	1.48		3.29	
5.02	40,480	0.2470	1.49		3.37	
4.99	40,320	0.2480		1.520 [4]		3.412 [4]
4.95	40,000	0.2500	1.51		3.45	
4.94	39,920	0.2505		1.540		3.491
4.89	39,510	0.2531	1.53	1.568	3.55	3.581
4.83	39,030	0.2562	1.57	1.599	3.66	3.673
4.79	38,710	0.2583		1.641		3.770
4.78	38,550	0.2594	1.61		3.78	
4.74	38,300	0.2611		1.687		3.878
4.72	38,060	0.2627	1.68		3.93	
4.69	37,900	0.2638		1.741		4.003
4.66	37,580	0.2661	1.76		4.08	
4.64	37,500	0.2667		1.824		4.140
4.59	37,090	0.2696	1.87	1.929	4.26	4.287
4.54	36,610	0.2731	2.03	2.085	4.46	4.447
4.49	36,290	0.2756		2.269		4.610
4.48	36,130	0.2768	2.26		4.66	
4.44	35,880	0.2787		2.522		4.769
4.41	35,640	0.2805	2.56		4.84	
4.39	35,480	0.2818		2.826		4.885

(continued)

TABLE I *(Continued)*

Si_xGe_{1-x}, $x \approx 0.80$

eV	cm^{-1}	Å	n	n	k	k
4.35	35,160	0.2844	2.96		4.98	
4.34	35,080	0.2851		3.172		4.967
4.29	34,670	0.2884	3.48	3.586	4.97	4.864
4.23	34,190	0.2924	3.93	3.927	4.73	4.683
4.19	33,870	0.2952		4.188		4.427
4.18	33,710	0.2966	4.20		4.40	
4.14	33,460	0.2988		4.314		4.175
4.12	33,230	0.3009	4.33		4.11	
4.09	33,060	0.3024		4.394		3.957
4.06	32,740	0.3054	4.40		3.88	
4.04	32,660	0.3062		4.441		3.771
3.99	32,250	0.3100	4.44	4.470	3.69	3.616
3.94	31,770	0.3147	4.47	4.488	3.55	3.496
3.89	31,450	0.3180		4.509		3.393
3.87	31,290	0.3196	4.51		3.42	
3.84	31,040	0.3221		4.538		3.305
3.81	30,810	0.3246	4.54		3.32	
3.79	30,640	0.3263		4.569		3.228
3.75	30,320	0.3298	4.59		3.24	
3.74	30,240	0.3307		4.594		3.161
3.69	29,830	0.3351	4.64	4.629	3.16	3.100
3.63	29,350	0.3406	4.69	4.668	3.10	3.050
3.59	29,030	0.3444		4.717		3.014
3.57	28,870	0.3463	4.75		3.05	
3.54	28,620	0.3493		4.774		2.983
3.52	28,390	0.3522	4.82		3.01	
3.49	28,220	0.3543		4.859		2.956
3.45	27,900	0.3583	4.94		2.98	
3.44	27,820	0.3594		4.959		2.923
3.39	27,410	0.3647	5.09	5.090	2.95	2.895
3.34	26,930	0.3712	5.29	5.264	2.89	2.840
3.29	26,610	0.3758		5.458		2.749
3.28	26,450	0.3780	5.55		2.76	
3.24	26,210	0.3815		5.660		2.587
3.21	25,970	0.3851	5.82		2.52	
3.19	25,800	0.3875		5.846		2.342
3.15	25,480	0.3924	6.01		2.17	
3.14	25,400	0.3937		5.997		2.048
3.09	25,000	0.4000	6.11	6.089	1.73	1.686
3.03	24,510	0.4079	6.04	6.044	1.30	1.311
2.99	24,190	0.4133		5.897		1.000
2.97	24,030	0.4161	5.86		0.95	
2.94	23,790	0.4203		5.708		0.776
2.91	23,550	0.4246	5.64		0.73	
2.89	23,380	0.4276		5.518		0.638
2.86	23,060	0.4335	5.44		0.56	
2.84	22,980	0.4351		5.352		0.535

TABLE I *(Continued)*

Si_xGe_{1-x}, $x \approx 0.80$

eV	cm^{-1}	Å	n	n	k	k
2.79	22,580	0.4429	5.26	5.209	0.44	0.461
2.74	22,090	0.4525	5.11	5.078	0.37	0.394
2.69	21,770	0.4593		4.967		0.346
2.68	21,610	0.4626	4.97		0.30	
2.64	21,370	0.4679		4.857		0.299
2.61	21,130	0.4732	4.85			
2.59	20,960	0.4769		4.766		0.271
2.55	20,640	0.4843	4.75			
2.54	20,560	0.4863		4.705		0.254
2.49	20,160	0.4960	4.65	4.645		0.237
2.43	19,680	0.5081	4.57	4.568		0.210
2.39	19,350	0.5167		4.492		0.187
2.37	19,190	0.5210	4.49			
2.34	18,950	0.5277		4.418		0.166
2.31	18,710	0.5344	4.41			
2.29	18,540	0.5391		4.348		0.149
2.25	18,220	0.5486	4.35			
2.24	18,140	0.5511		4.288		0.135
2.19	17,740	0.5636	4.29	4.236		0.124
2.13	17,260	0.5794	4.23	4.191		0.116
2.09	16,930	0.5905		4.148		0.108
2.08	16,770	0.5961	4.18			
2.04	16,530	0.6049		4.107		0.100
2.01	16,290	0.6138	4.13			
1.99	16,120	0.6200		4.066		0.091
1.95	15,800	0.6326	4.08			
1.90	15,320	0.6526	4.04			
1.84	14,840	0.6738	4.00			
1.78	14,350	0.6965	3.97			
1.72	13,870	0.7208	3.93			
1.65	13,380	0.7469	3.90			
1.40	11,290	0.8856	3.75 [10, 11]		4.63E-03 [10, 11]	
1.38	11,130	0.8984	3.74		4.19E-03	
1.35	10,960	0.9117	3.73		3.77E-03	
1.33	10,800	0.9253	3.72		3.37E-03	
1.31	10,640	0.9393	3.72		2.99E-03	
1.30	10,480	0.9537	3.71		2.62E-03	
1.28	10,320	0.9686	3.70		2.27E-03	
1.26	10,160	0.9840	3.70		1.95E-03	
1.23	10,000	0.9999	3.69		1.64E-03	
1.21	9,840	1.016	3.68		1.36E-03	
1.20	9,679	1.033	3.68		1.10E-03	
1.18	9,517	1.050	3.67		8.68E-04	
1.16	9,356	1.068	3.67		6.60E-04	
1.13	9,195	1.087	3.66		4.80E-04	
1.12	9,033	1.107	3.65		3.29E-04	
1.10	8,872	1.127	3.65		2.08E-04	

(continued)

TABLE I *(Continued)*

Si_xGe_{1-x}, $x \approx 0.80$

eV	cm^{-1}	Å	n	n	k	k
1.08	8,711	1.148	3.64		1.20E-04	
1.05	8,549	1.169	3.64		6.56E-05	
1.03	8,388	1.192	3.63		4.01E-05	
1.02	8,227	1.215	3.63		2.15E-05	
0.1000	8,065	1.239	3.62		8.44E-06	
0.9800	7,904	1.265	3.62		1.30E-06	
0.1488	1,200	8.330			1.05E-05 [14]	
0.1438	1,160	8.620			1.92E-05	
0.1388	1,120	8.930			3.18E-05	
0.1339	1,080	9.260			3.77E-05	
0.1289	1,040	9.620			2.78E-05	
0.1240	1,000	10.00			3.22E-05	
0.1190	960	10.42			9.31E-05	
0.1141	920	10.87			1.27E-04	
0.1091	880	11.36			1.91E-04	
0.1042	840	11.90			1.84E-04	
0.09919	800	12.50			1.41E-04	
0.09421	760	13.16			1.59E-04	
0.08926	720	13.89			2.15E-04	
0.08557	690	14.49			2.37E-04	
0.08184	660	15.15			2.21E-04	
0.07687	620	16.13			3.63E-04	
0.07192	580	17.24			5.00E-04	
0.06942	560	17.86			5.17E-04	
0.06447	520	19.23			5.30E-04	
0.06075	490	20.41			9.45E-04	
0.05826	470	21.28			9.21E-04	
0.05580	450	22.22			6.06E-04	
0.05330	430	23.26			5.97E-04	
0.05145	415	24.10			5.55E-04	
0.05022	405	24.69			9.63E-04	
0.04897	395	25.32			8.23E-04	
0.04711	380	26.32			4.42E-04	
0.04463	360	27.78			2.91E-04	
0.04214	340	29.42			2.85E-04	
0.03720	300	33.33			1.88E-04	
0.03224	260	38.46			1.24E-04	
0.02728	220	45.45			2.84E-05	
0.02480	200	50.00			4.28E-04	
0.02232	180	55.55			1.49E-03	

TABLE II

Values of n and k for Si_xGe_{1-x}, Interpolated for Various x[a]

eV	cm^{-1}	μm	n	k	n	k
			$x = 0.90$		$x = 0.70$	
12.00	96,780	0.1033	0.57 [7]	0.88 [7]	0.68 [7]	0.87 [7]
11.00	88,720	0.1127	0.57	1.01	0.66	0.98
10.00	80,650	0.1240	0.57	1.19	0.64	1.16
9.00	72,580	0.1378	0.58	1.42	0.65	1.39
8.00	64,520	0.1550	0.63	1.72	0.70	1.67
7.00	56,450	0.1771	0.74	2.19	0.79	2.16
6.00	48,390	0.2066	1.12	2.74	1.20	2.71
5.00	40,320	0.2480	1.52 [8]	3.45 [8]	1.47 [8]	3.35 [8]
4.90	39,520	0.2530	1.54	3.62	1.51	3.50
4.80	38,710	0.2583	1.60	3.83	1.58	3.69
4.70	37,900	0.2638	1.69	4.09	1.68	3.91
4.60	37,100	0.2695	1.88	4.43	1.84	4.18
4.50	36,290	0.2755	2.24	4.80	2.12	4.49
4.40	35,480	0.2818	2.81	5.11	2.60	4.79
4.30	34,680	0.2883	3.66	5.21	3.36	4.86
4.20	33,870	0.2952	4.43	4.66	3.98	4.45
4.10	33,060	0.3024	4.64	4.09	4.22	3.99
4.00	32,260	0.3100	4.69	3.72	4.31	3.67
3.90	31,450	0.3179	4.74	3.48	4.36	3.44
3.80	30,640	0.3263	4.80	3.32	4.42	3.28
3.70	29,840	0.3351	4.89	3.18	4.49	3.14
3.60	29,030	0.3444	5.01	3.10	4.57	3.04
3.50	28,220	0.3542	5.24	3.09	4.68	2.97
3.40	27,420	0.3647	5.87	2.94	4.86	2.91
3.30	26,610	0.3757	6.21	2.07	5.14	2.80
3.20	25,810	0.3875	6.05	1.46	5.45	2.52
3.10	25,000	0.4000	5.87	0.99	5.67	2.10
3.00	24,190	0.4133	5.59	0.62	5.72	1.65
2.90	23,390	0.4275	5.28		5.68	1.21
2.80	22,580	0.4428	5.02		5.50	0.79
2.70	21,770	0.4592	4.82		5.24	0.52
2.60	20,970	0.4769	4.65		5.00	
2.50	20,160	0.4959	4.50		4.82	
2.40	19,350	0.5166	4.37		4.64	
2.30	18,550	0.5391	4.27		4.50	
2.20	17,740	0.5636	4.18		4.38	
2.10	16,930	0.5904	4.09		4.28	
2.00	16,130	0.6199	4.02		4.19	
1.90	15,320	0.6526	3.95		4.11	
1.80	14,510	0.6888	3.90		4.04	
1.70	13,710	0.7293	3.84		3.98	
1.40	11,290	0.8856	3.72 [11]	4.03E-03 [10]	3.81 [11]	5.50E-03 [10]

(continued)

[a] The references from which the dataset for interpolation was taken are given in brackets next to the first value.

TABLE II *(Continued)*

Si_xGe_{1-x}

eV	cm^{-1}	μm	n	k	n	k
			$x = 0.90$		$x = 0.70$	
1.38	11,130	0.8984	3.71	3.59E-03	3.80	5.02E-03
1.36	10,960	0.9117	3.70	3.18E-03	3.79	4.56E-03
1.32	10,640	0.9393	3.69	2.42E-03	3.77	3.68E-03
1.30	10,480	0.9537	3.68	2.07E-03	3.77	3.28E-03
1.28	10,320	0.9686	3.67	1.74E-03	3.76	2.89E-03
1.26	10,160	0.9840	3.67	1.44E-03	3.75	2.52E-03
1.24	10,000	0.9999	3.66	1.17E-03	3.74	2.17E-03
1.22	9,840	1.016	3.65	9.17E-04	3.73	1.84E-03
1.20	9,679	1.033	3.65	6.97E-04	3.73	1.54E-03
1.18	9,517	1.050	3.64	5.07E-04	3.72	1.26E-03
1.16	9,356	1.068	3.64	3.49E-04	3.72	1.01E-03
1.14	9,195	1.087	3.63	2.23E-04	3.71	7.80E-04
1.12	9,033	1.107	3.62	1.31E-04	3.70	5.83E-04
1.10	8,872	1.127	3.62	7.14E-05	3.70	4.16E-04
1.08	8,711	1.148	3.61	4.24E-05	3.69	2.80E-04
1.06	8,549	1.169	3.61	2.32E-05	3.69	1.78E-04
			$x = 0.60$		$x = 0.50$	
12.00	96,780	0.1033	0.73 [7]	0.88 [7]	0.77 [7]	0.88 [7]
11.00	88,720	0.1127	0.71	0.99	0.75	0.99
10.00	80,650	0.1240	0.68	1.15	0.72	1.15
9.00	72,580	0.1378	0.70	1.38	0.73	1.37
8.00	64,520	0.1550	0.74	1.64	0.77	1.63
7.00	56,450	0.1771	0.81	2.14	0.85	2.12
6.00	48,390	0.2066	1.21	2.70	1.23	2.68
5.00	40,320	0.2480	1.44 [8]	3.29 [8]	1.43 [8]	3.17 [8]
4.90	39,520	0.2530	1.48	3.44	1.47	3.32
4.80	38,710	0.2583	1.55	3.61	1.54	3.48
4.70	37,900	0.2638	1.65	3.81	1.63	3.66
4.60	37,100	0.2695	1.80	4.07	1.77	3.89
4.50	36,290	0.2755	2.05	4.36	2.01	4.16
4.40	35,480	0.2818	2.50	4.65	2.41	4.42
4.30	34,680	0.2883	3.21	4.72	3.04	4.47
4.20	33,870	0.2952	3.79	4.36	3.56	4.17
4.10	33,060	0.3024	4.03	3.94	3.80	3.81
4.00	32,260	0.3100	4.13	3.63	3.90	3.53
3.90	31,450	0.3179	4.19	3.41	3.97	3.32
3.80	30,640	0.3263	4.25	3.24	4.03	3.17
3.70	29,840	0.3351	4.31	3.11	4.09	3.05
3.60	29,030	0.3444	4.38	3.01	4.15	2.95
3.50	28,220	0.3542	4.46	2.93	4.23	2.88
3.40	27,420	0.3647	4.59	2.86	4.34	2.80
3.30	26,610	0.3757	4.76	2.77	4.47	2.70
3.20	25,810	0.3875	4.94	2.63	4.60	2.58
3.10	25,000	0.4000	5.14	2.51	4.69	2.47

TABLE II *(Continued)*

			Si_xGe_{1-x}			
eV	cm^{-1}	μm	n	k	n	k
			$x = 0.60$		$x = 0.50$	
3.00	24,190	0.4133	5.43	2.30	4.82	2.41
2.90	23,390	0.4275	5.72	1.86	5.06	2.32
2.80	22,580	0.4428	5.72	1.26	5.38	2.06
2.60	20,970	0.4769	5.23	0.54	5.51	1.01
2.50	20,160	0.4959	5.03		5.26	0.68
2.40	19,350	0.5166	4.80		5.03	0.46
2.30	18,550	0.5391	4.64		4.83	
2.20	17,740	0.5636	4.50		4.65	
2.10	16,930	0.5904	4.38		4.50	
2.00	16,130	0.6199	4.28		4.39	
1.90	15,320	0.6526	4.19		4.29	
1.80	14,510	0.6888	4.12		4.20	
1.70	13,710	0.7293	4.05		4.12	
1.40	11,290	0.8856	3.88 [11]	6.78E-03 [10]	3.99 [11]	9.86E-03 [10]
1.38	11,130	0.8984	3.87	6.24E-03	3.98	9.14E-03
1.36	10,960	0.9117	3.86	5.71E-03	3.97	8.43E-03
1.34	10,800	0.9253	3.85	5.20E-03	3.96	7.75E-03
1.32	10,640	0.9393	3.84	4.70E-03	3.95	7.09E-03
1.30	10,480	0.9537	3.84	4.23E-03	3.94	6.44E-03
1.28	10,320	0.9686	3.83	3.78E-03	3.92	5.82E-03
1.26	10,160	0.9840	3.82	3.34E-03	3.91	5.22E-03
1.24	10,000	0.9999	3.81	2.93E-03	3.90	4.65E-03
1.22	9,840	1.016	3.80	2.53E-03	3.90	4.11E-03
1.20	9,679	1.033	3.80	2.17E-03	3.89	3.59E-03
1.18	9,517	1.050	3.79	1.82E-03	3.88	3.09E-03
1.16	9,356	1.068	3.78	1.50E-03	3.87	2.63E-03
1.14	9,195	1.087	3.78	1.21E-03	3.86	2.20E-03
1.12	9,033	1.107	3.77	9.52E-04	3.85	1.80E-03
1.10	8,872	1.127	3.76	7.20E-04	3.84	1.44E-03
1.08	8,711	1.148	3.76	5.20E-04	3.84	1.12E-03
1.06	8,549	1.169	3.75	3.54E-04	3.83	8.31E-04
1.04	8,388	1.192	3.75	2.23E-04	3.82	5.86E-04
1.02	8,227	1.215	3.74	1.29E-04	3.81	3.85E-04
1.00	8,065	1.239	3.73	7.58E-05	3.81	2.29E-04
0.9800	7,904	1.265	3.73	4.34E-05	3.80	1.21E-04
0.9600	7,743	1.291	3.72	2.12E-05	3.80	6.01E-05
			$x = 0.40$		$x = 0.30$	
12.00	96,780	0.1033	0.80 [7]	0.89 [7]	0.83 [7]	0.90 [7]
11.00	88,720	0.1127	0.78	0.99	0.82	0.99
10.00	80,650	0.1240	0.75	1.14	0.78	1.13
9.00	72,580	0.1378	0.76	1.37	0.78	1.36
8.00	64,520	0.1550	0.79	1.63	0.82	1.64
7.00	56,450	0.1771	0.92	2.11	0.99	2.09
6.00	48,390	0.2066	1.24	2.64	1.26	2.60

(continued)

TABLE II *(Continued)*

Si_xGe_{1-x}

eV	cm^{-1}	μm	n	k	n	k
			$x = 0.40$		$x = 0.30$	
5.00	40,320	0.2480	1.41 [8]	3.20 [8]	1.37 [8]	3.19 [8]
4.90	39,520	0.2530	1.46	3.34	1.42	3.33
4.80	38,710	0.2583	1.52	3.50	1.48	3.49
4.70	37,900	0.2638	1.61	3.68	1.57	3.68
4.50	36,290	0.2755	1.98	4.18	1.92	4.18
4.40	35,480	0.2818	2.39	4.45	2.33	4.47
4.30	34,680	0.2883	3.02	4.51	2.98	4.52
4.20	33,870	0.2952	3.53	4.21	3.49	4.22
4.10	33,060	0.3024	3.78	3.86	3.73	3.87
4.00	32,260	0.3100	3.88	3.58	3.84	3.59
3.90	31,450	0.3179	3.95	3.37	3.91	3.38
3.80	30,640	0.3263	4.01	3.22	3.96	3.23
3.70	29,840	0.3351	4.07	3.09	4.02	3.10
3.60	29,030	0.3444	4.13	2.98	4.08	2.99
3.50	28,220	0.3542	4.21	2.90	4.14	2.90
3.40	27,420	0.3647	4.30	2.82	4.23	2.81
3.30	26,610	0.3757	4.42	2.71	4.33	2.71
3.20	25,810	0.3875	4.52	2.58	4.41	2.58
3.10	25,000	0.4000	4.57	2.47	4.44	2.46
3.00	24,190	0.4133	4.64	2.42	4.46	2.40
2.90	23,390	0.4275	4.79	2.40	4.53	2.40
2.80	22,580	0.4428	5.05	2.32	4.69	2.41
2.70	21,770	0.4592	5.40	2.06	4.97	2.35
2.60	20,970	0.4769	5.60	1.60	5.31	2.14
2.50	20,160	0.4959	5.56	1.06	5.55	1.71
2.40	19,350	0.5166	5.34	0.68	5.60	1.22
2.30	18,550	0.5391	5.10	0.46	5.43	0.78
2.20	17,740	0.5636	4.91		5.19	0.52
2.10	16,930	0.5904	4.73		4.98	
2.00	16,130	0.6199	4.60		4.82	
1.90	15,320	0.6526	4.46		4.67	
1.80	14,510	0.6888	4.36		4.55	
1.70	13,710	0.7293	4.27		4.44	
1.40	11,290	0.8856	4.06 [11]	1.21E-02 [10]	4.18 [11]	1.43E-02 [10]
1.38	11,130	0.8984	4.05	1.13E-02	4.16	1.34E-02
1.36	10,960	0.9117	4.04	1.04E-02	4.15	1.25E-02
1.34	10,800	0.9253	4.03	9.64E-03	4.14	1.16E-02
1.32	10,640	0.9393	4.02	8.87E-03	4.12	1.07E-02
1.30	10,480	0.9537	4.01	8.12E-03	4.11	9.83E-03
1.28	10,320	0.9686	3.99	7.39E-03	4.10	9.00E-03
1.26	10,160	0.9840	3.98	6.69E-03	4.09	8.19E-03
1.24	10,000	0.9999	3.97	6.01E-03	4.08	7.41E-03
1.22	9,840	1.016	3.97	5.36E-03	4.06	6.66E-03
1.20	9,679	1.033	3.96	4.74E-03	4.05	5.94E-03
1.18	9,517	1.050	3.95	4.15E-03	4.04	5.25E-03

TABLE II *(Continued)*

Si_xGe_{1-x}

eV	cm^{-1}	μm	n	k	n	k
			$x = 0.40$		$x = 0.30$	
1.16	9,356	1.068	3.94	3.59E-03	4.03	4.60E-03
1.14	9,195	1.087	3.93	3.06E-03	4.03	3.97E-03
1.12	9,033	1.107	3.92	2.57E-03	4.02	3.39E-03
1.10	8,872	1.127	3.91	2.11E-03	4.01	2.84E-03
1.08	8,711	1.148	3.91	1.70E-03	4.00	2.34E-03
1.04	8,388	1.192	3.89	9.90E-04	3.98	1.46E-03
1.02	8,227	1.215	3.88	7.04E-04	3.98	1.09E-03
1.00	8,065	1.239	3.88	4.67E-04	3.97	7.71E-04
0.9800	7,904	1.265	3.87	2.82E-04	3.96	5.07E-04
0.9600	7,743	1.291	3.87	1.51E-04	3.95	3.02E-04
0.9400	7,582	1.318	3.86	7.21E-05	3.94	1.58E-04
0.9200	7,420	1.347	3.85	3.31E-05	3.94	7.37E-05
			$x = 0.20$		$x = 0.10$	
12.00	96,780	0.1033	0.83 [7]	0.91 [7]	0.79 [7]	0.94 [7]
11.00	88,720	0.1127	0.82	1.00	0.78	1.04
10.00	80,650	0.1240	0.79	1.15	0.77	1.20
9.00	72,580	0.1378	0.80	1.38	0.79	1.41
8.00	64,520	0.1550	0.83	1.65	0.83	1.69
7.00	56,450	0.1771	1.02	2.09	1.01	2.12
6.00	48,390	0.2066	1.29	2.59	1.33	2.61
5.00	40,320	0.2480	1.35 [8]	3.10 [8]	1.31 [8]	3.09 [8]
4.90	39,520	0.2530	1.39	3.24	1.34	3.22
4.80	38,710	0.2583	1.45	3.40	1.40	3.38
4.70	37,900	0.2638	1.53	3.58	1.48	3.57
4.60	37,100	0.2695	1.66	3.80	1.59	3.80
4.50	36,290	0.2755	1.87	4.07	1.79	4.09
4.40	35,480	0.2818	2.28	4.37	2.22	4.42
4.30	34,680	0.2883	2.92	4.40	2.90	4.43
4.20	33,870	0.2952	3.40	4.10	3.38	4.10
4.10	33,060	0.3024	3.63	3.75	3.59	3.75
4.00	32,260	0.3100	3.72	3.49	3.68	3.48
3.90	31,450	0.3179	3.78	3.29	3.74	3.29
3.80	30,640	0.3263	3.83	3.14	3.78	3.14
3.70	29,840	0.3351	3.89	3.02	3.83	3.02
3.60	29,030	0.3444	3.94	2.91	3.88	2.91
3.50	28,220	0.3542	4.00	2.82	3.93	2.82
3.40	27,420	0.3647	4.08	2.74	4.00	2.73
3.30	26,610	0.3757	4.16	2.64	4.08	2.63
3.20	25,810	0.3875	4.22	2.51	4.13	2.50
3.10	25,000	0.4000	4.24	2.39	4.15	2.38
3.00	24,190	0.4133	4.23	2.32	4.12	2.30
2.90	23,390	0.4275	4.25	2.33	4.09	2.29
2.80	22,580	0.4428	4.32	2.36	4.13	2.33
2.70	21,770	0.4592	4.47	2.40	4.22	2.39

(continued)

TABLE II *(Continued)*

Si_xGe_{1-x}

eV	cm^{-1}	μm	n	k	n	k
			$x = 0.20$		$x = 0.10$	
2.60	20,970	0.4769	4.74	2.41	4.37	2.45
2.50	20,160	0.4959	5.12	2.27	4.64	2.50
2.40	19,350	0.5166	5.44	1.92	5.06	2.39
2.30	18,550	0.5391	5.61	1.42	5.38	2.09
2.20	17,740	0.5636	5.47	0.88	5.72	1.60
2.10	16,930	0.5904	5.22	0.58	5.58	0.95
1.90	15,320	0.6526	4.85		5.08	0.49
1.80	14,510	0.6888	4.72		4.93	
1.70	13,710	0.7293	4.61		4.78	
1.40	11,290	0.8856	4.30 [11]	1.62E-02 [10]	4.45 [11]	2.65E-02 [10]
1.38	11,130	0.8984	4.29	1.52E-02	4.44	2.51E-02
1.36	10,960	0.9117	4.27	1.42E-02	4.42	2.38E-02
1.34	10,800	0.9253	4.25	1.32E-02	4.40	2.24E-02
1.32	10,640	0.9393	4.23	1.22E-02	4.38	2.11E-02
1.30	10,480	0.9537	4.22	1.13E-02	4.36	1.98E-02
1.28	10,320	0.9686	4.20	1.04E-02	4.34	1.86E-02
1.26	10,160	0.9840	4.19	9.47E-03	4.32	1.73E-02
1.24	10,000	0.9999	4.18	8.61E-03	4.31	1.61E-02
1.22	9,840	1.016	4.16	7.78E-03	4.29	1.49E-02
1.20	9,679	1.033	4.15	6.98E-03	4.28	1.38E-02
1.18	9,517	1.050	4.14	6.21E-03	4.26	1.27E-02
1.16	9,356	1.068	4.13	5.48E-03	4.25	1.16E-02
1.14	9,195	1.087	4.12	4.78E-03	4.24	1.05E-02
1.12	9,033	1.107	4.11	4.12E-03	4.22	9.49E-03
1.10	8,872	1.127	4.09	3.50E-03	4.21	8.51E-03
1.08	8,711	1.148	4.08	2.92E-03	4.20	7.56E-03
1.06	8,549	1.169	4.07	2.39E-03	4.19	6.66E-03
1.04	8,388	1.192	4.06	1.90E-03	4.17	5.80E-03
1.02	8,227	1.215	4.05	1.46E-03	4.16	4.99E-03
1.00	8,065	1.239	4.04	1.08E-03	4.15	4.23E-03
0.9800	7,904	1.265	4.04	7.48E-04	4.14	3.53E-03
0.9600	7,743	1.291	4.03	4.78E-04	4.13	2.88E-03
0.9400	7,582	1.318	4.02	2.72E-04	4.12	2.29E-03
0.9200	7,420	1.347	4.01	1.33E-04	4.12	1.76E-03
0.9000	7,259	1.377	4.00	6.07E-05	4.11	1.31E-03
0.8800	7,098	1.408	3.99	2.22E-05	4.10	9.15E-04

Silver Chloride (AgCl), Silver Bromide (AgBr), Silver Iodide (AgI)

MASATO TAZAWA
National Industrial Research Institute of Nagoya
Nagoya, Japan
and
ARMAND HADNI
Université Henri Poincaré, Nancy
Vandœuvre-les-Nancy, France

AgCl (CUBIC) I

The optical constants from the visible to the UV region were determined in the energy range 2–21 eV by means of reflectivity measurements at room temperature and a Kramers–Kronig (K-K) analysis by White and Straley in 1968 [1]. They were revised in 1974 [2]. The purpose of the revision was to eliminate an unphysical negative dip in the absorption edge occurring at 3.2 eV and caused by an inadequate fitting. Their apparatus consisted of a McPherson model 225 1-m VUV scanning monochromator and a slightly modified Tropel S-2 reflectometer. The K-K analysis was based on reflectivity values over four energy regions: (1) From 0.0 to 3.0 eV, the reflectivity was computed from literature values of the index of refraction [3, 4]. (2) From 3.1 to 14.0 eV, the experimentally determined values of the reflectivity were least-square fitted in four subregions. (3) From 14.1 to 21.1 eV, the experimentally determined values of the reflectivity were fitted to an exponential curve. (4) Beyond 21.1 eV, the reflectivity was inferred by using the extrapolation formula

$$\ln R(E) = -A \ln(E/E_f) + \ln R_f,$$

where E and R are the photon energy and the reflectivity, respectively, f denotes the last-measured data point, and A is an energy-independent, adjustable parameter. They used $A = 2.027$ and $E_f = 21.1$ eV.

Carrera and Brown [5] have also given the optical constants from 3.5 to

Copyright © 1998 by Academic Press.
All rights of reproduction in any form reserved
ISBN 0-12-544423-0/$25.00.

6.7 eV and from 30 to 240 eV at room, liquid-nitrogen, and liquid-helium temperatures. They observed the transmission of two thin films with a different thickness, deposited by vacuum evaporation onto a thin, transparent substrate of Formvar (polyvinyl formal resin) or Lucite (methyl methacrylate resin). In order to obtain the extinction coefficient k, they used the following expressions:

$$D_2 - D_1 = \alpha(t_2 - t_1)/2.303$$
$$k = \lambda\alpha/4\pi = (hc/4\pi E)\alpha,$$

where D and t are the optical density and the thickness, α is the absorption coefficient in cm^{-1}, E is the photon energy, and λ is the wavelength. They obtained the refractive index n by means of a K-K analysis using their own k values and those of White and Straley [1]. In the UV range, a Cary model 14R spectrophotometer was used, and in the extreme UV range, a modified Hilger-Watts E580 was used with the synchrotron radiation from the 240-MeV electron storage ring of the University of Wisconsin.

The optical constants in the mid-IR region were obtained by Tilton et al. [4] with a 31° prism of silver chloride used at the minimum deviation, and a Perkin-Elmer infrared spectrometer equipped with a calibrated screw for operation of the Littrow mirror. These optical constants were used by White and co-workers [1, 2]. Tilton *et al.* [4] determined the refractive index from 578 nm to 20.56 μm. The extinction coefficients were not obtained.

Hadni *et al.* [6] measured the far-IR reflectivity of a single crystal at room temperature, 80 K, and 25 K by means of a grating spectrometer. The optical constants shown in Table IV were obtained by a K-K analysis. They also gave the parameter values of the Lorentz oscillators by fitting the reflectivity with two Lorentz oscillators. Table I gives these parameters, and

$$(n + ik)^2 = \epsilon_{RV} + \sum_{j=1}^{2} \frac{4\pi\rho_j\nu_j^2}{\nu_j^2 - \nu^2 - i\nu\nu_0\delta_j}.$$

Two Lorentz oscillators were needed, and the stronger one corresponds to the one-phonon transition to the transverse optic mode with a wave vector $q = 0$ and the other one, about 10 times weaker, corresponds to a two-phonon addition process, probably TA + TO.

Values of n and k from these various references are listed in Table IV, and the data are plotted in Fig. 1.

II AgBr (CUBIC)

The optical constants in the UV range were first obtained by Carrera and Brown [5] at room temperature and at liquid-nitrogen and liquid-helium tem-

peratures. Their experimental method was the same one used for AgCl. The optical constants are, however, limited between 4 and 6.8 eV, probably because of the lack of a wide enough range for the K-K analysis.

White [7] also reported the optical constants between 3 and 16 eV at room temperature. The method was the same as in the case of AgCl.

In the mid-IR region, McCarthy [8] measured a refractive index of 2.167 and 2.162 at 9.93 and 12.67 μm, respectively, at 313 K.

In the far-IR region, Hadni *et al.* [6] reported the optical constants determined by a K-K analysis at room temperature (shown in Table V), 80 K, and 25 K. The experimental procedure was the same as in the case of AgCl, but the samples were not single crystals; they were pellets. Two Lorentz oscillators were also needed for AgBr; the stronger one corresponds to the TO mode and the weaker one to the TA + TO mode (see Table II).

Values of n and k from these various references are listed in Table V, and the data are plotted in Fig. 2.

β-AgI (HEXAGONAL), STABLE FOR $T < T_c = 147°$ C III

Ageev *et al.* [9] have obtained the optical constants of polycrystalline samples prepared by treating, in iodine vapor at room temperature, thin films of silver deposited by vacuum evaporation on glass substrates. To find the optical constants averaged over the random arrangement of crystallites in the film, they measured both transmission and reflection between 1000 and 370 nm using an SF-4 spectrophotometer. They gave the optical constants between 370 and 460 nm.

Bedikyan *et al.* [10] reported the dielectric constant in the region extending from 2.7 to 4.0 eV at 90, 293, and 393 K. Their β-AgI films (2H polytype) were prepared by treating in iodine vapor thin Ag films evaporated in vacuum onto a quartz substrate, and they were textured with a preferred orientation of the c-axis perpendicular to the substrate. The optical constants were determined by measuring the transmission (perhaps in normal incidence) of the films over a wide spectral range (0.22–1.2 μm), then treating the measured data by means of a K-K analysis. The error in the determination of n and k should amount to 0.1 for n and 0.02 for k. However, the optical constants that are said to have been "determined" are shown neither in tables nor in figures.

Cochrane [11] has also measured the absorption coefficient and the refractive index of single crystals at 293 K. He used single crystals of β-AgI grown by the slow evaporation of either an HI solution saturated with AgI, or a KI solution saturated with AgI. Although there were impurities of potassium and sodium, detected by spectrochemical analysis and flame photometry, no differences were observed in the optical behavior of crystals obtained by the two methods. Platelike specimens were prepared by cleaving

prism-shaped single crystals perpendicular to the *c*-axis with a razor blade. The absorption coefficients were determined from transmission measurements at normal incidence in the wavelength range 200–750 nm carried out in a Perkin-Elmer PE 350 spectrophotometer.

In the far-IR, Hadni *et al.* [6] reported the effective optical constants shown in Table VI obtained by K-K analysis. The experiment was the same one as in the case of AgCl, except that the samples were not single crystals, but pellets. Two Lorentz oscillators were also needed for AgI at room temperature (Table III); the stronger one corresponds to the TO mode and the weaker one to the TA + LA mode, an addition process that is IR-active.

Funke and Jost [12] also reported the optical constants in the frequency range from 8.5×10^{11} to 6×10^{12} Hz using Fourier spectrophotometry. The samples, which were prepared by reaction of silver with iodine in the dark at about 170°C, were probably polycrystalline. The reflectivity and transmission measurements were carried out with the spectrophotometers LR 100 (using a lamellar grating interferometer) and FS 720 (using a Michelson interferometer). The resultant optical constants are said to be accurate within 2%.

Values of n and k from these various references are listed in Table VI, and the data are plotted in Fig. 3.

IV α-AgI (CUBIC), STABLE FOR $T > T_c = 147°$ C

It is well known since the pioneering work of Strock[13] that the dc conductivity of AgI, which is very small at room temperature (β-AgI), increases dramatically at the phase transition when the cubic phase occurs for $T > T_c$, with values comparable to those found in aqueous solutions of electrolytes. The AgI is the archetype of superionic conductors with applications to solid-state batteries. The far-IR and mid-IR spectra are known [12, 14–16], but the optical constants have only been published in terms of dynamic conductivity between 10 and 250 cm^{-1}.

REFERENCES

1. J. J. White III and J. W. Straley, *J. Opt. Soc. Am.* **58**, 759 (1968).
2. R. S. Bauer, W. E. Spicer, and J. J. White III, *J. Opt. Soc. Am.* **64**, 830 (1974).
3. H. Schröter, *Z. Phys.* **67**, 24 (1931).
4. L. W. Tilton, E. K. Plyler, and R. E. Stephens, *J. Opt. Soc. Am.* **40**, 540 (1950).
5. N. J. Carrera and F. C. Brown, *Phys. Rev. B* **4**, 3651 (1971).
6. A. Hadni, J. Claudel, and P. Strimer, *Appl. Opt.* **7**, 1159 (1968).
7. J. J. White III, *J. Opt. Soc. Am.* **62**, 212 (1972).
8. D. E. McCarthy, *Appl. Opt.* **12**, 409 (1973).
9. L. A. Ageev, V. K. Miloslavskii, and I. N. Shklyarevskii, *Opt. Spectrosc.* **31**, 561 (1971).
10. L. D. Bedikyan, V. K. Miloslavskii, and L. A. Ageev, *Opt. Spectrosc.* **47**, 225 (1979).
11. G. Cochrane, *J. Phys. D* **7**, 748 (1974).

12. K. Funke and A. Jost, *Ber. Bunsen-Ges. Phys. Chem.* **75**, 436 (1971).
13. L. W. Strock, *Z. Phys. Chem. B* **25**, 411 (1934).
14. W. Jost, K. Funke, and A. Jost, *Z. Naturforsch. A* **25**, 983 (1970).
15. P. Brüesch, S. Strässler, and H. R. Zeller, *Phys. Status Solidi A* **31**, 217 (1975).
16. G. Burns, F. H. Dacol, and M. W. Shafer, *Phys. Rev. B* **16**, 1416 (1977).

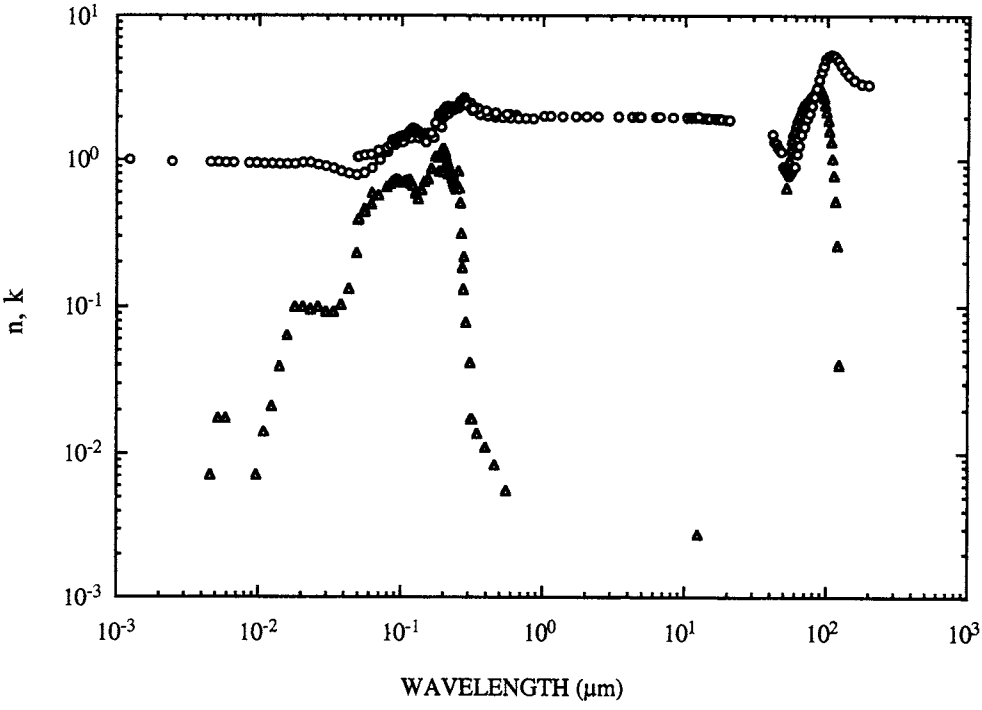

Fig. 1. Log–log plot of n (open circles) and k (open triangles) versus wavelength in micrometers for silver chloride.

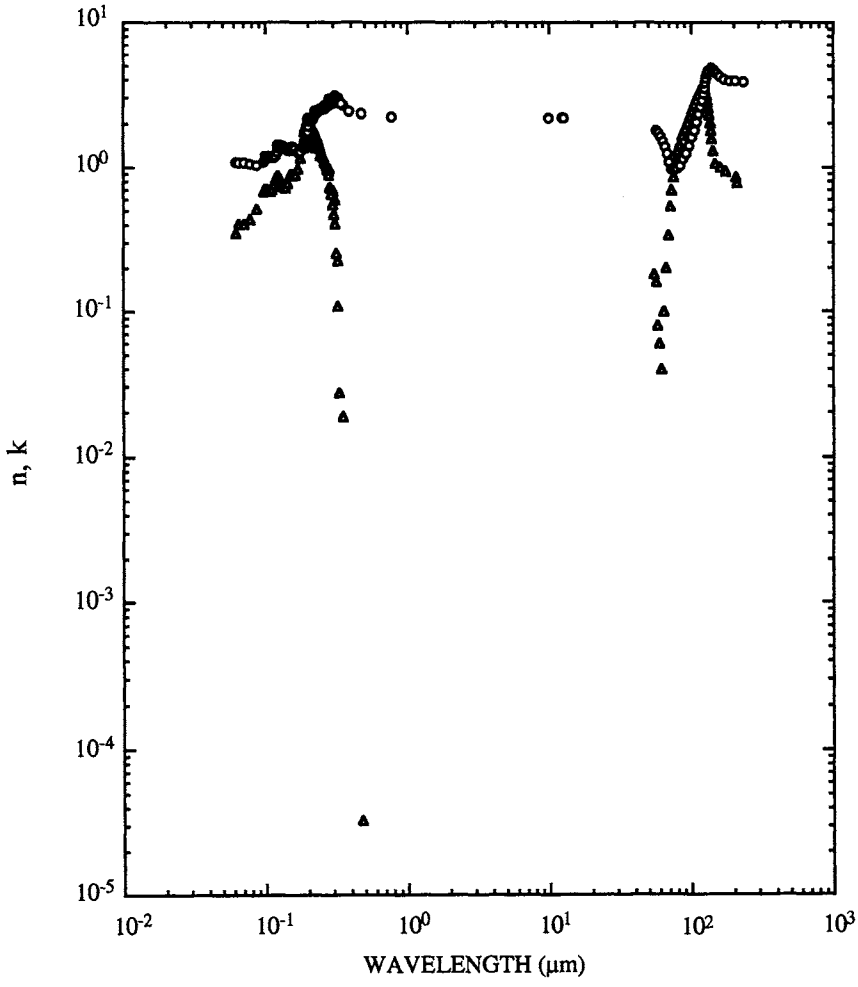

Fig. 2. Log–log plot of n (open circles) and k (open triangles) versus wavelength in micrometers for silver bromide.

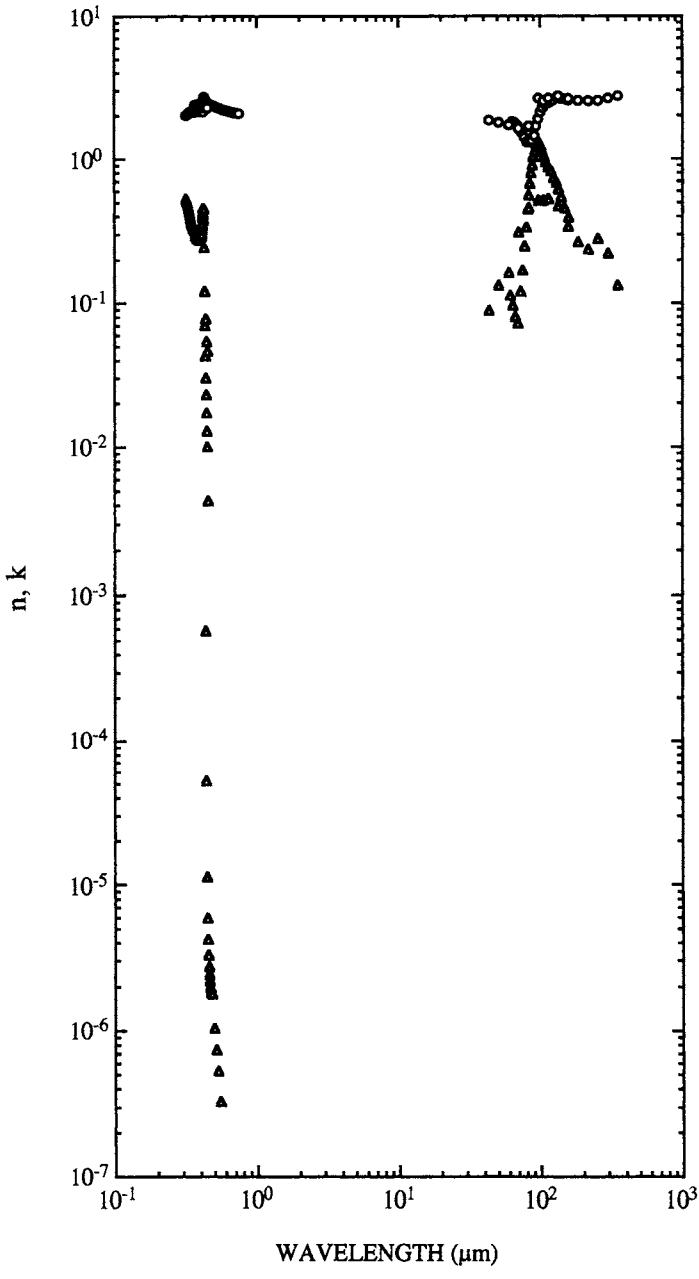

Fig. 3. Log–log plot of n (open circles) and k (open triangles) versus wavelength in micrometers for silver iodide.

TABLE I

Lorentz Oscillators Analysis of AgCl

T(K)	$\nu_1(cm^{-1})$	ρ_1	δ_1	$\nu_2(cm^{-1})$	ρ_2	δ_2	ϵ_{RV}
290	105	0.56	0.33	138	0.05	0.20	3.9
80	114	0.45	0.05	141	0.04	0.15	3.9
25	119	0.43	0.03	142	0.03	0.15	3.9

TABLE II

Lorentz Oscillators Analysis of AgBr

T(K)	$\nu_1(cm^{-1})$	ρ_1	δ_1	$\nu_2(cm^{-1})$	ρ_2	δ_2	ϵ_{RV}
290	79	0.61	0.32	105	0.020	0.25	4.5
80	84	0.52	0.10	120	0.015	0.20	4.5
25	85	0.48	0.028	122	0.010	0.20	4.5

TABLE III

Lorentz Oscillators Analysis of AgI

T(K)	$\nu_1(cm^{-1})$	ρ_1	δ_1	$\nu_2(cm^{-1})$	ρ_2	δ_2	ϵ_{RV}
290	103	0.14	0.36	80	0.01	0.10	4.91
80	106	0.14	0.10				4.91
25	106	0.14	0.04				4.91

TABLE IV

Values of n and k Obtained from Various References for AgCl[a]

eV	cm^{-1}	μm	n	k
1000.	8065000.	0.001240	1.000 [5]	0.000 [5]
504.3	4068000.	0.002458	0.967	0.000
270.7	2183000.	0.004581	0.961	0.007
239.0	1928000.	0.005188	0.961	0.018
211.0	1702000.	0.005876	0.954	0.018
186.3	1503000.	0.006654	0.954	0.000
145.3	1172000.	0.008535	0.947	0.000
128.3	1035000.	0.009666	0.947	0.007
113.3	913400.	0.01095	0.941	0.014
100.0	806500.	0.01240	0.941	0.021
88.30	712200.	0.01404	0.934	0.039
77.96	628800.	0.01590	0.934	0.064
68.84	555200.	0.01801	0.934	0.099
60.78	490200.	0.02040	0.954	0.099
53.67	432900.	0.02310	0.954	0.096
47.39	382200.	0.02616	0.921	0.099
41.84	337500.	0.02963	0.901	0.092
36.95	298000.	0.03356	0.868	0.092
32.62	263100.	0.03801	0.829	0.103
28.80	232300.	0.04304	0.803	0.131
25.43	205100.	0.04875	0.783	0.230
25.00	201600.	0.04959	1.044 [2]	0.386 [2]
24.60	198400.	0.05041	1.051	0.395
22.46	181100.	0.05521	0.809 [5]	0.461 [5]
22.36	180400.	0.05545	1.072 [2]	0.441 [2]
20.13	162300.	0.06161	1.086	0.497
19.83	159900.	0.06253	0.875 [5]	0.592 [5]
17.89	144300.	0.06931	1.156 [2]	0.568 [2]
17.51	141200.	0.07082	0.993 [5]	
15.65	126200.	0.07921	1.204 [2]	0.648 [2]
15.46	124700.	0.08020	1.132 [5]	
14.76	119000.	0.08401	1.267 [2]	0.684 [2]
14.31	115400.	0.08664	1.371	0.703
13.86	111800.	0.08943	1.336	0.720
13.65	110100.	0.09083	1.270 [5]	
13.42	108200.	0.09241	1.392 [2]	0.734 [2]
12.97	104600.	0.09560	1.427	0.731
12.52	101000.	0.09901	1.455	0.703
12.08	97390.	0.1027	1.462	0.698
12.05	97210.	0.1029	1.329 [5]	
11.63	93780.	0.1066	1.469 [2]	0.712 [2]
11.18	90180.	0.1109	1.524	0.726
10.73	86570.	0.1155	1.594	0.728
10.64	85830.	0.1165	1.415 [5]	
10.29	82960.	0.1205	1.664 [2]	0.662 [2]

(continued)

[a] References are indicated in brackets.

TABLE IV *(Continued)*

AgCl

eV	cm^{-1}	μm	n	k
9.840	79360.	0.1260	1.636	0.588
9.397	75790.	0.1319	1.421 [5]	
9.390	75750.	0.1320	1.573 [2]	0.538 [2]
8.940	72140.	0.1386	1.510	0.621
8.500	68530.	0.1459	1.517	0.703
8.297	66920.	0.1494	1.329 [5]	
8.050	64930.	0.1540	1.524 [2]	0.734 [2]
7.600	61320.	0.1631	1.531	0.869
7.326	59090.	0.1692	1.428 [5]	
7.160	57710.	0.1733	1.810 [2]	1.062 [2]
6.772	54620.	0.1831	2.075 [5]	1.044 [5]
6.710	54110.	0.1850	2.019	0.836
6.684	53910.	0.1855	2.053	1.044
6.596	53200.	0.1880	2.039	1.070
6.509	52500.	0.1905	2.053	1.122
6.469	52170.	0.1917	1.691	
6.421	51790.	0.1931	2.082	1.174
6.333	51080.	0.1958	2.131	1.200
6.260	50500.	0.1980	1.984 [2]	0.828 [2]
6.246	50370.	0.1985	2.202 [5]	1.200 [5]
6.158	49670.	0.2013	2.273	1.165
6.070	48960.	0.2043	2.309	1.122
5.982	48250.	0.2072	2.351	1.044
5.895	47540.	0.2103	2.351	0.974
5.810	46890.	0.2133	2.095 [2]	0.800 [2]
5.807	46840.	0.2135	2.344 [5]	0.922 [5]
5.719	46130.	0.2168	2.344	0.870
5.712	46070.	0.2171	2.205	
5.632	45420.	0.2202	2.337	0.835
5.544	44710.	0.2236	2.337	0.791
5.456	44010.	0.2272	2.330	0.748
5.370	43290.	0.2310	2.227 [2]	0.789 [2]
5.368	43300.	0.2310	2.323 [5]	0.713 [5]
5.281	42590.	0.2348	2.316	0.687
5.193	41880.	0.2388	2.309	0.652
5.105	41180.	0.2429	2.287	0.626
5.043	40680.	0.2458	2.284	
5.018	40470.	0.2471	2.280	0.635
4.930	39760.	0.2515	2.301	0.652
4.920	39680.	0.2520	2.332 [2]	0.836 [2]
4.842	39050.	0.2561	2.422	0.635
4.754	38350.	0.2608	2.564	0.504
4.739	38220.	0.2616	2.547	
4.667	37640.	0.2657	2.599	0.313
4.579	36930.	0.2708	2.571	0.183
4.491	36220.	0.2761	2.507	0.130
4.470	36070.	0.2772	2.715 [2]	0.218 [2]

TABLE IV *(Continued)*

AgCl

eV	cm^{-1}	μm	n	k
4.453	35920.	0.2784	2.448 [5]	
4.316	34810.	0.2873	2.422 [5]	0.078 [5]
4.030	32460.	0.3080	2.471 [2]	0.041 [2]
3.965	31980.	0.3127	2.287 [5]	0.017 [5]
3.932	31710.	0.3153	2.211	
3.877	31270.	0.3198	2.259	0.017
3.580	28860.	0.3465	2.276 [2]	0.014 [2]
3.472	28000.	0.3571	2.073 [5]	
3.130	25280.	0.3960	2.186 [2]	0.011 [2]
3.065	24720.	0.4045	2.020 [5]	
2.707	21830.	0.4581	1.987	
2.680	21640.	0.4621	2.123 [2]	0.008 [2]
2.390	19280.	0.5188	1.974 [5]	
2.240	18040.	0.5545	2.081 [2]	0.006 [2]
2.145	17300.	0.5780	2.069 [4]	
2.110	17020.	0.5876	1.961 [5]	
1.926	15530.	0.6438	2.055 [4]	
1.863	15030.	0.6654	1.948 [5]	
1.645	13270.	0.7536	1.948	
1.453	11720.	0.8535	1.941	
1.222	9860.	1.014	2.022 [4]	
1.098	8857.	1.129	2.018	
0.9050	7299.	1.370	2.012	
0.7293	5882.	1.700	2.008	
0.6138	4950.	2.020	2.006	
0.5102	4115.	2.430	2.004	
0.3657	2950.	3.390	2.001	
0.2924	2358.	4.240	1.999	
0.2684	2165.	4.620	1.998	
0.2546	2053.	4.870	1.998	
0.1981	1597.	6.260	1.994	
0.1925	1553.	6.440	1.994	
0.1873	1511.	6.620	1.993	
0.1508	1217.	8.220	1.988	
0.1199	967.1	10.34	1.979	
0.1124	906.6	11.03	1.975	
0.1081	871.8	11.47	1.973	
0.1045	843.2	11.86	1.971	
0.09379	756.4	13.22	1.963	
0.08658	698.3	14.32	1.956	
0.08277	667.6	14.98	1.951	
0.07560	609.8	16.40	1.940	
0.07336	591.7	16.90	1.936	
0.07134	575.4	17.38	1.932	
0.06966	561.8	17.80	1.928	
0.06827	550.7	18.16	1.925	
0.06262	505.1	19.80	1.909	

(continued)

TABLE IV *(Continued)*

AgCl

eV	cm^{-1}	μm	n	k
0.06030	486.4	20.56	1.901	
0.03000	241.7	41.38	1.506 [6]	
0.02920	235.7	42.42	1.343	
0.02830	228.2	43.83	1.302	
0.02750	221.8	45.08	1.221	
0.02680	215.9	46.32	1.180	
0.02600	209.9	47.64	1.140	
0.02510	202.8	49.32	0.895	
0.02450	197.6	50.60	0.855	
0.02390	192.7	51.88		0.640 [6]
0.02370	191.3	52.28	0.814	
0.02330	188.3	53.10		0.840
0.02300	185.7	53.85	0.773	
0.02280	184.3	54.27		1.000
0.02230	180.2	55.48		1.200
0.02220	179.4	55.75	0.814	
0.02190	177.0	56.49		1.400
0.02160	174.6	57.27	0.855	
0.02150	173.8	57.54		1.560
0.02100	169.8	58.91		1.620
0.02080	167.9	59.57	0.895	
0.02060	166.1	60.19		1.800
0.02010	162.1	61.69		1.960
0.02010	161.9	61.76	1.099	
0.01950	157.7	63.43		2.080
0.01940	156.7	63.80	1.262	
0.01900	153.2	65.26		2.240
0.01870	151.2	66.14	1.506	
0.01850	149.2	67.03		2.400
0.01790	144.0	69.42	1.709	
0.01770	143.1	69.86		2.500
0.01720	138.5	72.21	1.954	
0.01710	137.9	72.51		2.600
0.01650	133.5	74.92		2.740
0.01640	132.5	75.45	2.116	
0.01590	128.6	77.74		2.840
0.01580	127.4	78.50	2.401	
0.01540	124.2	80.52		3.000
0.01520	122.6	81.55	2.767	
0.01490	120.6	82.94		3.160
0.01470	118.3	84.56	3.174	
0.01440	116.1	86.11		3.300
0.01410	113.5	88.11	3.622	
0.01380	111.3	89.86		3.180
0.01350	109.1	91.64	4.070	
0.01340	108.1	92.54		2.980
0.01310	105.6	94.74	4.477	

TABLE IV *(Continued)*

AgCl

eV	cm^{-1}	μm	n	k
0.01300	104.8	95.38		2.740
0.01280	103.2	96.88		2.440
0.01270	102.4	97.67	4.965	
0.01250	100.8	99.20		2.180
0.01210	97.58	102.5		1.900
0.01210	97.22	102.9	5.209	
0.01190	96.37	103.8		1.600
0.01150	93.15	107.4		1.340
0.01150	92.46	108.2	5.291	
0.01130	91.53	109.3		1.020
0.01100	89.11	112.2		0.780
0.01080	87.30	114.5	5.169	
0.01070	86.69	115.3		0.520
0.01040	83.87	119.2		0.260
0.01030	82.94	120.6	4.884	
0.01000	81.05	123.4		0.040
0.009800	78.97	126.6	4.517	
0.009200	74.60	134.0	4.151	
0.008700	70.24	142.4	3.866	
0.008000	64.29	155.6	3.581	
0.007000	56.75	176.2	3.378	
0.006300	50.80	196.9	3.337	

TABLE V

Values of n and k Obtained from Various References for AgBr[a]

eV	cm^{-1}	μm	n	k
20.00	161300.	0.06199	1.083 [7]	0.350 [7]
19.05	153600.	0.06509	1.075	0.406
17.46	140800.	0.07101	1.075	0.406
15.87	128000.	0.07811	1.052	0.438
14.29	115200.	0.08679	1.036	0.519
12.70	102400.	0.09764	1.091	0.681
12.40	100000.	0.1000	1.200	0.710
12.38	99860.	0.1001	1.130	0.713
12.06	97300.	0.1028	1.177	0.706
11.75	94740.	0.1055	1.200	0.694
11.43	92180.	0.1085	1.192	0.688
11.11	89620.	0.1116	1.169	0.713
10.79	87060.	0.1149	1.169	0.763
10.48	84500.	0.1184	1.200	0.831
10.16	81940.	0.1220	1.278	0.869
10.10	81460.	0.1228	1.430	0.880
9.841	79370.	0.1260	1.364	0.844
9.524	76810.	0.1302	1.418	0.788
9.206	74250.	0.1347	1.403	0.744
8.889	71690.	0.1395	1.348	0.725
8.571	69130.	0.1446	1.309	0.775
8.254	66570.	0.1502	1.317	0.881
8.100	65330.	0.1531	1.380	0.900
7.937	64010.	0.1562	1.387	0.881
7.619	61450.	0.1627	1.348	0.888
7.302	58890.	0.1698	1.270	0.975
6.984	56330.	0.1775	1.286	1.163
6.667	53770.	0.1860	1.379	1.369
6.596	53200.	0.1880	1.423 [5]	1.773 [5]
6.506	52470.	0.1906	1.508	1.864
6.416	51750.	0.1933	1.569	1.918
6.349	51210.	0.1953	1.590 [7]	1.569 [7]
6.326	51020.	0.1960	1.654 [5]	2.018 [5]
6.236	50300.	0.1988	1.754	2.082
6.200	50010.	0.2000	2.170 [7]	1.650 [7]
6.146	49570.	0.2017	1.915 [5]	2.091 [5]
6.056	48850.	0.2047	2.078	2.055
6.032	48650.	0.2060	2.018 [7]	1.588 [7]
5.966	48120.	0.2078	2.162 [5]	1.927 [5]
5.876	47400.	0.2110	2.169	1.864
5.787	46670.	0.2143	2.185	1.827
5.714	46090.	0.2170	2.135 [7]	1.406 [7]
5.697	45950.	0.2176	2.215 [5]	1.809 [5]
5.607	45220.	0.2211	2.239	1.791
5.517	44500.	0.2247	2.315	1.718
5.500	44360.	0.2254	2.440 [7]	1.400 [7]

[a] References are indicated in brackets.

TABLE V *(Continued)*

AgBr

eV	cm^{-1}	μm	n	k
5.427	43770.	0.2285	2.354 [5]	1.655 [5]
5.397	43530.	0.2297	2.346 [7]	1.369 [7]
5.337	43050.	0.2323	2.400 [5]	1.600 [5]
5.247	42320.	0.2363	2.446	1.527
5.157	41600.	0.2404	2.462	1.436
5.079	40970.	0.2441	2.509 [7]	1.213 [7]
5.067	40870.	0.2447	2.477 [5]	1.355 [5]
4.978	40150.	0.2491	2.500	1.273
4.888	39420.	0.2537	2.500	1.200
4.798	38700.	0.2584	2.515	1.164
4.762	38410.	0.2604	2.618 [7]	1.094 [7]
4.708	37970.	0.2634	2.531 [5]	1.091 [5]
4.618	37250.	0.2685	2.546	1.036
4.528	36520.	0.2738	2.600	0.964
4.444	35850.	0.2790	2.805 [7]	0.944 [7]
4.438	35800.	0.2794	2.685 [5]	0.891 [5]
4.400	35490.	0.2818	2.930 [7]	0.980 [7]
4.348	35070.	0.2851	2.731 [5]	0.727 [5]
4.258	34350.	0.2912	2.731	0.655
4.169	33620.	0.2974	2.739	0.555
4.127	33290.	0.3004	2.961 [7]	0.694 [7]
4.079	32900.	0.3040	2.754 [5]	0.473 [5]
4.000	32260.	0.3100	3.090 [7]	0.600 [7]
3.989	32170.	0.3108	2.808 [5]	0.409 [5]
3.899	31450.	0.3180	2.900	0.255
3.810	30730.	0.3255	2.984 [7]	0.225 [7]
3.809	30720.	0.3255	2.892 [5]	0.109 [5]
3.719	30000.	0.3334	2.839	0.027
3.629	29270.	0.3416	2.723	0.000
3.492	28170.	0.3550	2.649 [7]	0.019 [7]
3.175	25610.	0.3906	2.416	0.000
2.600	20970.	0.4769	2.330	0.000
1.587	12800.	0.7811	2.205	
0.1249	1008.	9.926	2.167 [8]	
0.1000	806.5	12.40	2.174 [7]	
0.09795	790.0	12.66	2.162 [8]	
0.02254	181.8	55.01		0.180 [6]
0.02184	176.1	56.77		0.160
0.02180	176.1	56.79	1.787 [6]	
0.02119	170.9	58.51		0.080
0.02100	169.7	58.93	1.727	
0.02054	165.7	60.36		0.060
0.02020	162.9	61.39	1.627	
0.01994	160.9	62.17		0.040
0.01950	157.2	63.61	1.506	
0.01925	155.2	64.42		0.100

(continued)

TABLE V *(Continued)*

AgBr

eV	cm^{-1}	μm	n	k
0.01880	152.0	65.79	1.386	
0.01855	149.6	66.84		0.200
0.01820	147.2	67.93	1.245	
0.01790	144.4	69.27		0.340
0.01770	142.8	70.03	1.084	
0.01735	140.0	71.45		0.540
0.01700	136.7	73.15	0.964	
0.01695	136.7	73.14		0.700
0.01645	132.7	75.35		0.860
0.01620	130.3	76.75	0.964	
0.01596	128.7	77.71		1.100
0.01550	125.1	79.94	0.984	
0.01546	124.7	80.22		1.300
0.01491	120.2	83.17		1.440
0.01480	119.0	84.03	1.024	
0.01436	115.8	86.34		1.660
0.01410	113.4	88.18	1.145	
0.01371	110.6	90.42		1.840
0.01340	108.2	92.42	1.245	
0.01316	106.2	94.19		2.020
0.01280	102.9	97.18	1.406	
0.01262	101.7	98.29		2.240
0.01222	98.53	101.5		2.440
0.01220	98.50	101.5	1.606	
0.01177	94.91	105.4		2.700
0.01170	94.50	105.8	1.787	
0.01147	92.49	108.1		2.900
0.01130	91.30	109.5	2.028	
0.01107	89.28	112.0		3.140
0.01100	88.50	113.0	2.309	
0.01072	86.46	115.7		3.380
0.01060	85.30	117.2	2.590	
0.01030	83.20	120.2	2.851	
0.01022	82.44	121.3		3.500
0.01010	81.20	123.2	3.173	
0.009919	80.00	125.0	3.454	
0.009872	79.62	125.6		3.360
0.009869	79.60	125.6	3.775	
0.009720	78.40	127.6	4.076	
0.009623	77.61	128.8		3.060
0.009500	76.80	130.2	4.378	
0.009473	76.41	130.9		2.800
0.009400	75.60	132.3	4.619	
0.009374	75.60	132.3		2.560
0.009274	74.80	133.7		2.300
0.009075	73.19	136.6		2.020
0.008975	72.39	138.1		1.800

TABLE V *(Continued)*

AgBr

eV	cm^{-1}	μm	n	k
0.008900	71.60	139.7	4.819	
0.008875	71.58	139.7		1.580
0.008676	69.97	142.9		1.300
0.008500	68.40	146.2	4.639	
0.008376	67.56	148.0		1.060
0.008100	65.50	152.7	4.418	
0.007800	62.70	159.5	4.197	
0.007728	62.33	160.4		1.000
0.007200	58.30	171.5	3.996	
0.007080	57.10	175.1		0.940
0.006600	53.50	186.9	3.916	
0.006000	48.70	205.3	3.916	
0.005983	48.26	207.2		0.860
0.005883	47.45	210.7		0.780
0.005300	42.60	234.7	3.855	

TABLE VI

Values of n and k Obtained from Various References for AgI[a]

eV	cm^{-1}	μm	n	k
3.900	31460.	0.3179	2.001 [10]	0.535 [10]
3.860	31130.	0.3212	2.015	0.519
3.820	30810.	0.3246	2.029	0.505
3.780	30490.	0.3280	2.048	0.486
3.740	30170.	0.3315	2.074	0.460
3.700	29840.	0.3351	2.100	0.438
3.660	29520.	0.3387	2.112	0.414
3.620	29200.	0.3425	2.117	0.390
3.580	28880.	0.3463	2.125	0.367
3.540	28550.	0.3502	2.123	0.356
3.500	28230.	0.3542	2.123	0.344
3.460	27910.	0.3583	2.122	0.335
3.420	27590.	0.3625	2.125	0.327
3.380	27260.	0.3668	2.129	0.322
3.356	27070.	0.3694	2.377 [9]	0.296 [9]
3.340	26940.	0.3712	2.133 [10]	0.319 [10]
3.310	26700.	0.3746	2.138	0.316
3.270	26380.	0.3791	2.144	0.313
3.260	26300.	0.3803	2.391 [9]	0.284 [9]
3.230	26050.	0.3838	2.149 [10]	0.312 [10]
3.190	25730.	0.3887	2.148	0.310
3.182	25660.	0.3897	2.394 [9]	0.279 [9]
3.150	25410.	0.3936	2.153 [10]	0.309 [10]

(continued)

[a] References are indicated in brackets.

TABLE VI *(Continued)*

AgI

eV	cm^{-1}	μm	n	k
3.110	25080.	0.3987	2.169	0.307
3.102	25020.	0.3997	2.385 [9]	0.275 [9]
3.070	24760.	0.4038	2.194 [10]	0.303 [10]
3.030	24440.	0.4092	2.227	0.301
3.028	24430.	0.4094	2.391 [9]	0.292 [9]
3.013	24300.	0.4115	2.382	0.307
3.000	24200.	0.4132	2.388	0.328
2.990	24120.	0.4146	2.160 [10]	0.356 [10]
2.983	24060.	0.4156	2.400 [9]	0.353 [9]
2.969	23940.	0.4176	2.427	0.399
2.958	23860.	0.4191	2.474	0.425
2.950	23790.	0.4203	2.121 [10]	0.457 [10]
2.942	23730.	0.4215	2.547 [9]	0.417 [9]
2.927	23610.	0.4235	2.621	0.381
2.910	23470.	0.4260	2.284 [10]	0.453 [10]
2.907	23450.	0.4265	2.706 [9]	0.245 [9]
2.887	23290.	0.4294	2.703	0.122
2.875	23190.	0.4312	2.496 [11]	
2.870	23150.	0.4320	2.430 [10]	0.121 [10]
2.868	23130.	0.4324	2.653 [9]	0.071 [9]
2.848	22970.	0.4353	2.588	0.043
2.839	22900.	0.4370		5.8E-04 [11]
2.830	22830.	0.4381	2.366 [10]	0.078 [10]
2.829	22820.	0.4382	2.538 [9]	0.030 [9]
2.818	22730.	0.4400		5.3E-05 [11]
2.810	22670.	0.4412	2.500 [9]	0.023 [9]
2.797	22560.	0.4430		1.1E-05 [11]
2.792	22520.	0.4441	2.474 [9]	0.017 [9]
2.790	22500.	0.4444	2.290 [10]	0.055 [10]
2.776	22390.	0.4470		6.0E-06 [11]
2.773	22370.	0.4471	2.459 [9]	0.013 [9]
2.755	22220.	0.4500		4.3E-06 [11]
2.755	22220.	0.4500	2.444 [9]	0.010 [9]
2.750	22180.	0.4508	2.261 [10]	0.046 [10]
2.746	22150.	0.4515	2.441 [11]	
2.735	22060.	0.4530		3.3E-06 [11]
2.720	21940.	0.4559	2.424 [9]	0.004 [9]
2.715	21900.	0.4570		2.8E-06 [11]
2.695	21740.	0.4600		2.4E-06
2.685	21660.	0.4618	2.394 [9]	
2.676	21580.	0.4630		2.2E-06 [11]
2.657	21430.	0.4670		2.0E-06
2.638	21280.	0.4700		1.8E-06
2.600	20970.	0.4769	2.378 [11]	
2.583	20830.	0.4800		1.8E-06
2.496	20130.	0.4970		1.0E-06
2.468	19910.	0.5023	2.327	

TABLE VI *(Continued)*

AgI

eV	cm^{-1}	μm	n	k
2.415	19480.	0.5130		7.5E-07
2.350	18950.	0.5277	2.280	
2.339	18870.	0.5300		5.3E-07
2.254	18180.	0.5500		3.3E-07
2.242	18080.	0.5530	2.241	
2.143	17290.	0.5784	2.202	
2.053	16560.	0.6038	2.171	
1.971	15890.	0.6292	2.145	
1.894	15280.	0.6546	2.122	
1.823	14710.	0.6799	2.102	
1.758	14180.	0.7053	2.086	
1.697	13690.	0.7307	2.076	
1.653	13330.	0.7500	2.067	
0.02857	230.4	43.41	1.842 [12]	0.090 [12]
0.02432	196.1	50.99	1.782	0.134
0.02070	167.0	59.89	1.708	0.163
0.02015	162.5	61.53		0.113 [6]
0.01959	158.0	63.29	1.806 [6]	
0.01935	156.1	64.08		0.097
0.01885	152.0	65.79	1.766	
0.01855	149.6	66.85		0.081
0.01810	146.0	68.49	1.706	
0.01780	143.5	69.67		0.073
0.01762	142.1	70.36	1.619 [12]	0.312 [12]
0.01736	140.0	71.43	1.605 [6]	
0.01704	137.5	72.75		0.121 [6]
0.01671	134.8	74.18	1.505	
0.01654	133.4	74.95		0.169
0.01607	129.6	77.16	1.405	
0.01594	128.6	77.78		0.250
0.01549	124.9	80.04		0.339
0.01542	124.4	80.39	1.304	
0.01514	122.1	81.90		0.452
0.01500	121.0	82.65	1.678 [12]	0.460 [12]
0.01499	120.9	82.72		0.565 [6]
0.01478	119.2	83.89	1.304 [6]	
0.01474	118.9	84.13		0.677
0.01444	116.4	85.88		0.798
0.01418	114.4	87.41	1.345	
0.01414	114.0	87.71		0.903
0.01394	112.4	88.97		1.032
0.01364	110.0	90.91	1.445	
0.01354	109.2	91.61		1.129
0.01329	107.2	93.28	1.686	
0.01328	107.1	93.33		1.242

(continued)

TABLE VI *(Continued)*

AgI

eV	cm^{-1}	μm	n	k
0.01293	104.3	95.87		1.339
0.01285	103.6	96.53	1.886	
0.01277	103.0	97.08	2.644 [12]	0.520 [12]
0.01253	101.1	98.93		1.282 [6]
0.01240	100.0	100.0	2.107 [6]	
0.01228	99.06	101.0		1.210
0.01198	96.63	103.5		1.121
0.01195	96.40	103.7	2.268	
0.01178	95.04	105.2	2.525 [12]	0.520 [12]
0.01163	93.80	106.6		1.032 [6]
0.01146	92.40	108.2	2.388 [6]	
0.01138	91.78	109.0		0.952
0.01093	88.14	113.5		0.879
0.01087	87.69	114.0	2.644 [12]	0.535 [12]
0.01081	87.20	114.7	2.448 [6]	
0.01043	84.10	118.9		0.823 [6]
0.01022	82.40	121.4	2.528	
0.009976	80.46	124.3		0.742
0.009524	76.82	130.2		0.686
0.009423	76.00	131.6	2.689	
0.009255	74.65	134.0	2.733 [12]	0.475 [12]
0.009224	74.39	134.4		0.621 [6]
0.008927	72.00	138.9	2.629 [6]	
0.008823	71.16	140.5		0.548
0.008431	68.00	147.1	2.609	
0.008321	67.12	149.0		0.460
0.007935	64.00	156.3	2.549	
0.007879	63.55	157.4	2.614 [12]	0.342 [12]
0.007820	63.07	158.5		0.395 [6]
0.006707	54.10	184.8	2.540 [12]	0.267 [12]
0.005710	46.05	217.1	2.525	0.238
0.004861	39.21	255.1	2.540	0.282
0.004138	33.38	299.6	2.644	0.223
0.003523	28.41	352.0	2.733	0.134

Silver Gallium Selenide ($AgGaSe_2$)
Silver Gallium Sulfide ($AgGaS_2$)

LUIS ARTÚS
Instituto Jaime Almera
Consejo Superior de Investigaciones Cientificas (C.S.I.C.)
Barcelona, SPAIN

$AgGaS_2$ and $AgGaSe_2$ are I–III–VI_2 compounds that belong to the chalcopyrite family. All these compounds have space-group symmetry $I\bar{4}2d$, and they are considered as derived from II–VI binary zincblende semiconductors. In ideal chalcopyrite crystals, the c parameter of the unit cell should be twice the a parameter, and the anions should be at equal distance from both cations, ocupying positions $(\frac{1}{4}, \frac{1}{4}, \frac{1}{8})$ and their equivalent positions in the unit cell. However, two important structural anomalies take place in real ternary chalcopyrite compounds. One is the so-called tetrahedral distortion, which takes into account the displacement of the anions toward the smaller cations; it is characterized by the parameter u, defined as

$$u = \tfrac{1}{4} + (d_{AC}{}^2 - d_{BC}{}^2)/a,$$

where d_{AC} and d_{BC} stand for the distances existing between the anions and cations I and III, respectively. The second structural change corresponds to the tetragonal compression that makes the c parameter different from twice the a parameter. This tetragonal compression is measured by the parameter $\mu = c/2a$. For $AgGaS_2$ these structural parameters take the values $u = 0.304$ and $\mu = 0.894$, whereas for $AgGaSe_2$ the values are $u = 0.276$ and $\mu = 0.896$ [1].

In the II–VI zincblende compounds, the fundamental gap corresponds to transitions occurring at the center of the Brillouin zone between the threefold-degenerate Γ_{15} level, which constitutes the top of the valence band, and the nondegenerate Γ_1 level, which constitutes the bottom of the conduction band. In the $AgGaS_2$ and $AgGaSe_2$ chalcopyrite compounds, because of the existence of the tetragonal crystal field, the threefold degeneracy of the Γ_{15} level is lifted in such a way that a nondegenerate Γ_4 level lies above a doubly degenerate Γ_5 level. If the spin–orbit interaction is taken into account, Γ_5

HANDBOOK OF OPTICAL CONSTANTS OF SOLIDS III

Copyright © 1998 by Academic Press.
All rights of reproduction in any form reserved
ISBN 0-12-544423-0/$25.00.

splits into Γ_6 and Γ_7, whereas Γ_4 and Γ_1 convert into Γ_7 and Γ_6, respectively. So, three structures can be observed in the fundamental-gap region in the optical spectra of the $AgGaS_2$ and $AgGaSe_2$ chalcopyrite compounds. The first one corresponds to transitions that occur at the fundamental gap between Γ_7 and Γ_6 levels, and it is labeled the A transition. The two other structures are due to transitions ocurring between Γ_6 and Γ_6 levels (B transition) and between Γ_7 and Γ_6 levels (C transition).

I OPTICAL PROPERTIES OF $AgGaSe_2$

For $AgGaSe_2$, these three structures A, B, and C have been measured at 5 K by means of reflectivity at near-normal incidence to take place at 1.804, 2.00, and 2.27 eV, respectively [2]. Taking into account the excitonic character of the A transition, the measurement of the fundamental excitonic state, as well as of its first excited state, allowed the determination of the gap value of $AgGaSe_2$ at liquid-helium temperatures to be $E_g = 1.824$ eV [2]. A similar value of $E_g = 1.830$ eV has been reported by other authors [3]. The pressure dependence of the band gap was found to be 5.3 meV/kbar with an atmospheric-pressure band-gap value of 1.80 eV at 300 K by means of absorption measurements under hydrostatic pressure [4]. An anomalous dependence of the band gap on temperature was found between 5 and 300 K [5]. So, a positive temperature coefficient $+1.0 \times 10^{-4}$ eV K^{-1} was found between 5 and 70 K, whereas a negative temperature coefficient of -1.4×10^{-4} eV K^{-1} was found between 110 and 300 K. This anomalous behavior of the band gap with temperature is related to the hybridization between the *d* orbitals of Ag and the Se *p* orbitals that takes place in the $AgGaSe_2$ compound.

At energies higher than the fundamental band gap, only unpolarized reflectivity measurements performed at room temperature from 1.2 to 25 eV [6] and polarized wavelength-modulated reflectivity performed at room temperature and 10 K up to 5.5 eV [7] have been reported. To estimate the *n* and *k* values in this energy region, a Kramers–Kronig analysis from the unpolarized reflectivity data reported up to 25 eV [6] has been carried out. At higher energies, we used the extrapolation suggested by Cardona and Greenaway [8], who consider a minus fourth-power reflectivity dependence of the energy. For the low-energy end, we have fitted an analytical curve to the monotonically decreasing reflectivity data measured below the band gap, which has been extrapolated to zero energy. The values of the refractive indices obtained by using this extrapolation are consistent with the values of the refractive indices obtained experimentally in the transparent region [9]. The values obtained for *n* and *k* from the fundamental-band-gap energy up to 25 eV are listed in Table I.

Optical absorption on thin films of thickness between 250 and 750 nm in the range 3.0–1.5 eV were reported [10], and the corresponding values of the extinction coefficient k in this energy range are listed in Table I. To read the values of the absorption coefficient from the graph displayed by Murthy *et al.* [10], we have digitized the curve. Hereafter, the same procedure has been carried out to obtain the data from the different reported graphs. Soliman [11] measured the transmittance and reflectance of thin films with different thickness in the range 0.5–2.0 μm and, from these experimental data, he calculated n and k by means of Murmann's formulae. The reported data have been listed in Table I.

Experimental measurements of n or k have been reported in the transparent region of this compound. Boyd *et al.* [9] determined accurately the refractive indices by measuring the minimum-deviation angle on a prism of angle close to 20° cut from the crystal boule. They measured n_o and n_e values in the range 0.725–13.5 μm with four decimal figures as shown in Table I. According to these authors, the presence of imperfections in their samples precludes obtaining reliable absolute values of the absorption-coefficient dispersion, and they could only determine relative variations of the absorption coefficient with wavelength. Consequently, the corresponding k values are not listed in Table I.

We have fitted the measured values of Boyd *et al.* [9] to the modified Sellmeier-type dispersion formula [12] of the form

$$n^2 = A + \frac{B}{\lambda^2 - C} + \frac{D\lambda^2}{E\lambda^2 - 1}.$$

The fit has been performed using the 43 reported experimental points. When the wavelengths are expressed in micrometers, the following parameters for the n_o and n_e dispersions in the range 0.725–13.5 μm are obtained:

A_o =	1.002933	A_e =	1.000687
B_o =	8.596864E03	B_e =	1.308038E04
C_o =	−2.523862E03	C_e =	−3.035824E03
D_o =	1.399621E01	D_e =	4.860614
E_o =	5.725267	E_e =	3.512771

Here, the subindices o or e denote ordinary or extraordinary rays, respectively. The RMS deviation of the measured refractive indices and the values calculated from the preceeding dispersion formula are 0.48% and 0.70% for n_o and n_e, respectively.

Catella *et al.* [13] performed polarized mid-IR transmission in the region below the band gap on several different samples. The values of the extinction coefficient k listed in Table I are obtained from their transmission curves for ordinary and extraordinary rays in the range 0.73–2.6 μm.

Reflectivity measurements in the reststrahlen region have been reported

by several authors [14–16]. Kanellis and Kampas [14] calculated from the polarized reflectivity data, using the classical dispersion theory, the n and k dispersion curves from 400 to 10 cm^{-1} for both polarizations. The values they obtained are listed in Table I.

The data of Table I are plotted in Figs. 1a and b for $AgGaSe_2$.

II OPTICAL PROPERTIES OF $AgGaS_2$

The three electronic transitions near the fundamental gap have been found to be at 2.679, 2.91, and 2.94 eV for A, B, and C transitions, respectively, from reflectivity measurements at 5 K [17]. The differences found in the gap values reported for this compound are greater than usual, which can be explained taking into account that $AgGaS_2$ crystals are frequently found to be nonstoichiometric. Some authors [18] have observed variation of the color of the crystals depending on their proximity to the stoichiometric composition. At liquid-helium temperature, excitonic behavior has been found by several authors, who reported values of about 2.72 eV for the fundamental gap [17, 19, 20]. A fundamental-band-gap value of 2.70 eV at room temperature and a pressure dependence of this gap of 2.2 meV/kbar were found by absorption measurements under hydrostatic pressure [4]. As happens for the $AgGaSe_2$ compound, the $AgGaS_2$ crystals also present an anomalous behavior of the fundamental band gap with temperature: The temperature coefficient was positive up to 80 K with a value of 1.0×10^{-4} eV K^{-1}, whereas from 110 K to room temperature the coefficient was found to be -2.2×10^{-4} eV K^{-1} [5].

At energies higher than the fundamental gap, unpolarized reflectivity measurements at room temperature from 1.2 up to 25 eV [6] and to 10 eV [21] have been reported, as well as polarized reflectivity at 80 K up to 7 eV [22]. By applying a Kramers–Kronig analysis to the reflectivity data [6] using the extrapolations discussed earlier, the n and k dispersions from 25 eV to the band-gap energy have been calculated, and their values are listed in Table II. Absorption measurements on polycrystalline $AgGaS_2$ at room temperature have been performed up to about 7 eV [23]. The values of the extinction coefficient k obtained from these measurements are listed in Table II.

In the transparent region, the indices n_o and n_e were measured in the range 0.49–13.0 μm by the minimum-deviation-angle method on a prism of angle close to 30° cut from the crystal boule [24]. The values are given in Table II. Absorption-coefficient measurements were also performed up to 12.5 μm, but according to the authors, the presence of cracks and voids in the crystal made absolute values unreliable, and consequently, only relative variations are meaningful.

We have fitted the measured values of Boyd *et al.* [24] to the modified

Sellmeier-type dispersion formula mentioned earlier. The fit has been performed using the 50 reported experimental points. The following parameters have been obtained for the n_o and n_e dispersions in the range 0.49–13.0 μm when the wavelength is in micrometers:

A_o =	0.966201	A_e =	1.000010
B_o =	2.689302E03	B_e =	3.372195E03
C_o =	−9.541617E02	C_e =	−1.061937E03
D_o =	1.903090E01	D_e =	1.007695E01
E_o =	9.426157	E_e =	7.290825

The RMS deviation between the measured refractive indices and the values calculated from the dispersion formula are 3.7% and 0.97% for n_o and n_e, respectively.

The existence of optical activity in a non-enantiomorphous crystal was first demonstrated by Hobden [25] by taking advantage of the unusual property that, for the $AgGaS_2$ crystal, the birefringence changes sign at 4974 Å. So, the accidental isotropy of the crystal at this wavelength allowed its optical activity to be seen without the difficulties arising from the presence of birefringence. Measurement of n_o and n_e by the prism method for six different wavelengths in the transparent region up to 0.67 μm was also reported in this paper, the measured values being close to those obtained by Boyd *et al.* [24].

Chemla *et al.* [26] measured the transmission of the crystal in the range 0.5–13.0 μm for ordinary and extraordinary rays. The extinction coefficients k listed in Table II have been obtained from these transmission curves. The temperature dependence of the refractive indices of $AgGaS_2$ crystals was determined by Bhar *et al.* [27] by means of the classical minimum-deviation technique controlling the prism temperature from room temperature up to 90° C. The nondispersive value of the thermooptic coefficient dn/dT was found to be 15.5×10^{-5}/°C in the temperature range studied.

In the reststrahlen region, polarized reflectivity measurements were performed from 400 to 40 cm^{-1} by Holah *et al.* [28]. By using the classical dispersion theory, they calculated the n and k dispersion curves throughout this range. The corresponding values are listed in Table II.

The data in Table II are plotted in Figs. 2a and b for $AgGaS_2$.

REFERENCES

1. H. W. Spiess, V. Haeberln, G. Brandt, A. Rauber, and J. Schneider, *Phys. Status Solidi B* **62**, 183 (1974).
2. L. Artús, Y. Bertrand, and C. Ance, *J. Phys. C: Solid State Phys.* **19**, 5937 (1986).
3. B. Tell and H. M. Kasper, *Phys. Rev. B* **4**, 4455 (1971).
4. A. Jayaraman, V. Narayanamurti, H. M. Kasper, M. A. Chin, and R. G. Maines, *Phys. Rev. B* **14**, 3516 (1976).
5. L. Artús and Y. Bertrand, *Solid State Commun.* **61**, 733 (1987).

6. L. Artús, Y. Bertrand, and A. López-Soler, *J. Phys. C: Solid State Phys.* **20**, 111 (1987).
7. B. Sermage and G. Fishman, *Inst. Phys. Confer. Ser.* **35**, 139 (1977).
8. M. Cardona and D. L. Greenaway, *Phys. Rev.* **133**, 1685 (1964).
9. G. D. Boyd, H. M. Kasper, J. H. McFee, and F. G. Storz, *IEEE J. Quantum Electron.* **8**, 900 (1972).
10. Y. S. Murthy, B. S. Naidu, and P. J. Reddy, *Vacuum* **41**, 1448 (1990).
11. H. S. Soliman, *J. Phys. D: Appl. Phys.* **28**, 764 (1995).
12. F. Zernike, *J. Opt. Soc. Am.* **54**, 1215 (1964).
13. G. C. Catella, L. R. Shiozawa, J. R. Hietanen, R. C. Eckardt, R. K. Route, R. S. Feigelson, D. G. Cooper, and C. L. Marquardt, *Appl. Opt.* **32**, 3948 (1993).
14. G. Kanellis and K. Kampas, *J. Phys.(Paris)* **38**, 833 (1977).
15. A. Miller, G. D. Holah, W. D. Dunnett, and G. Iseler, *Phys. Status Solidi B* **78**, 569 (1976).
16. J. Camassel, L. Artús and J. Pascual, *Phys. Rev. B* **41**, 5717 (1990).
17. L. Artús and Y. Bertrand, *J. Phys. C: Solid State Phys.* **20**, 1365 (1987).
18. P. Korczak and C. Staff, *J. Cryst. Growth* **41**, 146 (1974).
19. B. Tell and H. M. Kasper, *Phys. Rev. B* **6**, 3008 (1972).
20. P. Yu, W. J. Anderson, and Y. S. Park, *Solid State Commun.* **13**, 1883 (1973).
21. R. L. Hengehold and F. L. Pedrotti, *J. Appl. Phys.* **46**, 5202 (1975).
22. J. Austinat, H. Nelkowski, and W. Scrittenlacher, *Solid State Commun.* **37**, 285 (1981).
23. H. V. Campe, *J. Phys. Chem. Solids* **44**, 1019 (1983).
24. G. D. Boyd, H. Kasper, and J. H. McFee, *IEEE J. Quantum Electron* **7**, 563 (1971).
25. M. V. Hobden, *Nature (London)* **216**,678 (1967); M. V. Hobden, *Acta Crystallogr. A* **24**, 676 (1968).
26. D. S. Chemla, P. J. Kupecek, D. S. Robertson, and R. C. Smith, *Opt. Commun.* **3**, 29 (1971).
27. G. C. Bhar, D. K. Ghosh, P. S. Ghosh, and D. Schmitt, *Appl. Opt.* **22**, 2492 (1983).
28. G. D. Holah, J. S. Webb, and H. Montgomery, *J. Phys. C: Solid State Phys.* **7**, 3875 (1974).

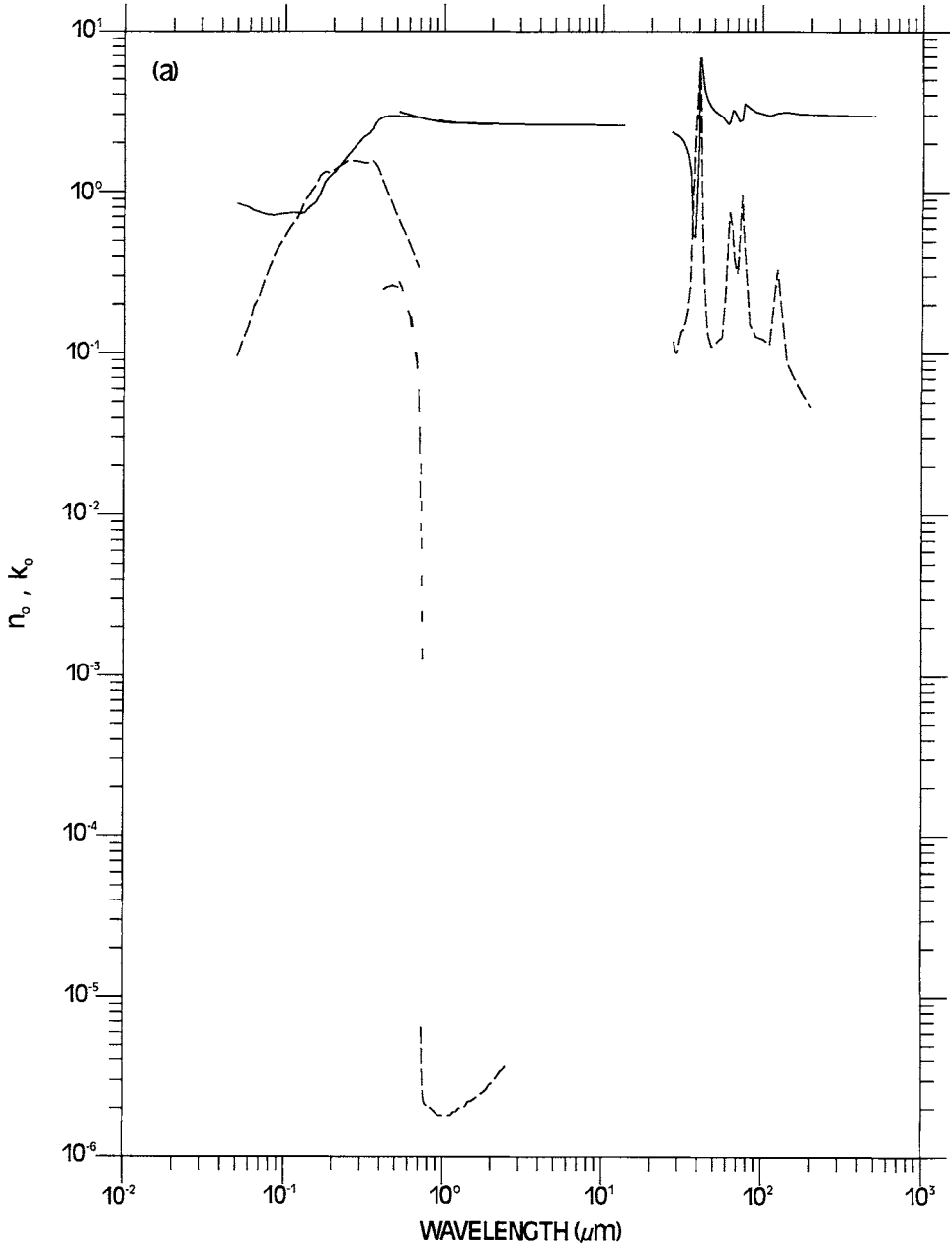

Fig. 1. (a) Log–log plot of n_o (solid line) and k_o (dashed line) versus wavelength in micrometers for silver gallium selenide ($AgGaSe_2$).

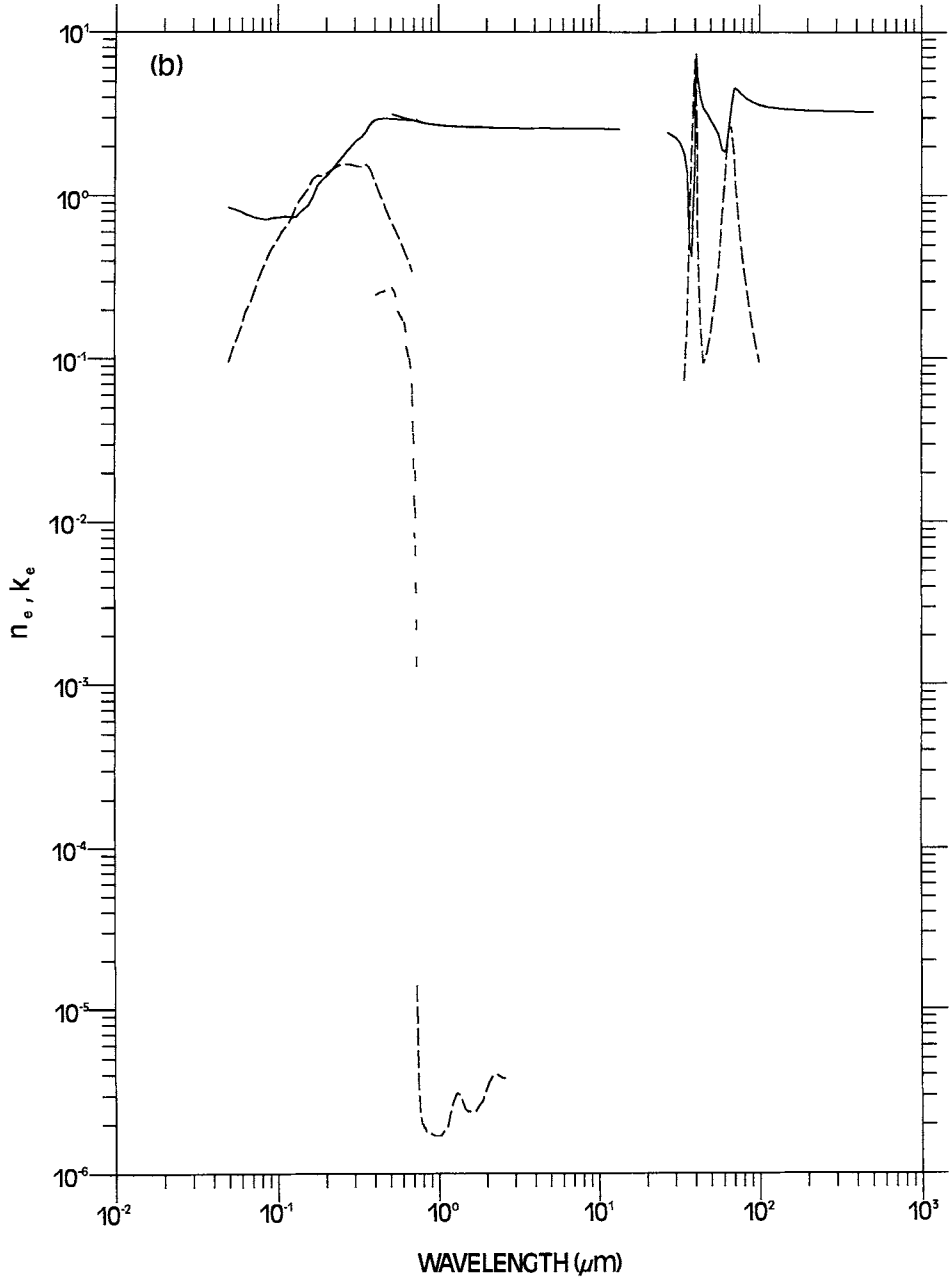

Fig. 1. (b) Log–log plot of n_e (solid line) and k_e (dashed line) versus wavelength in micrometers for silver gallium selenide ($AgGaSe_2$).

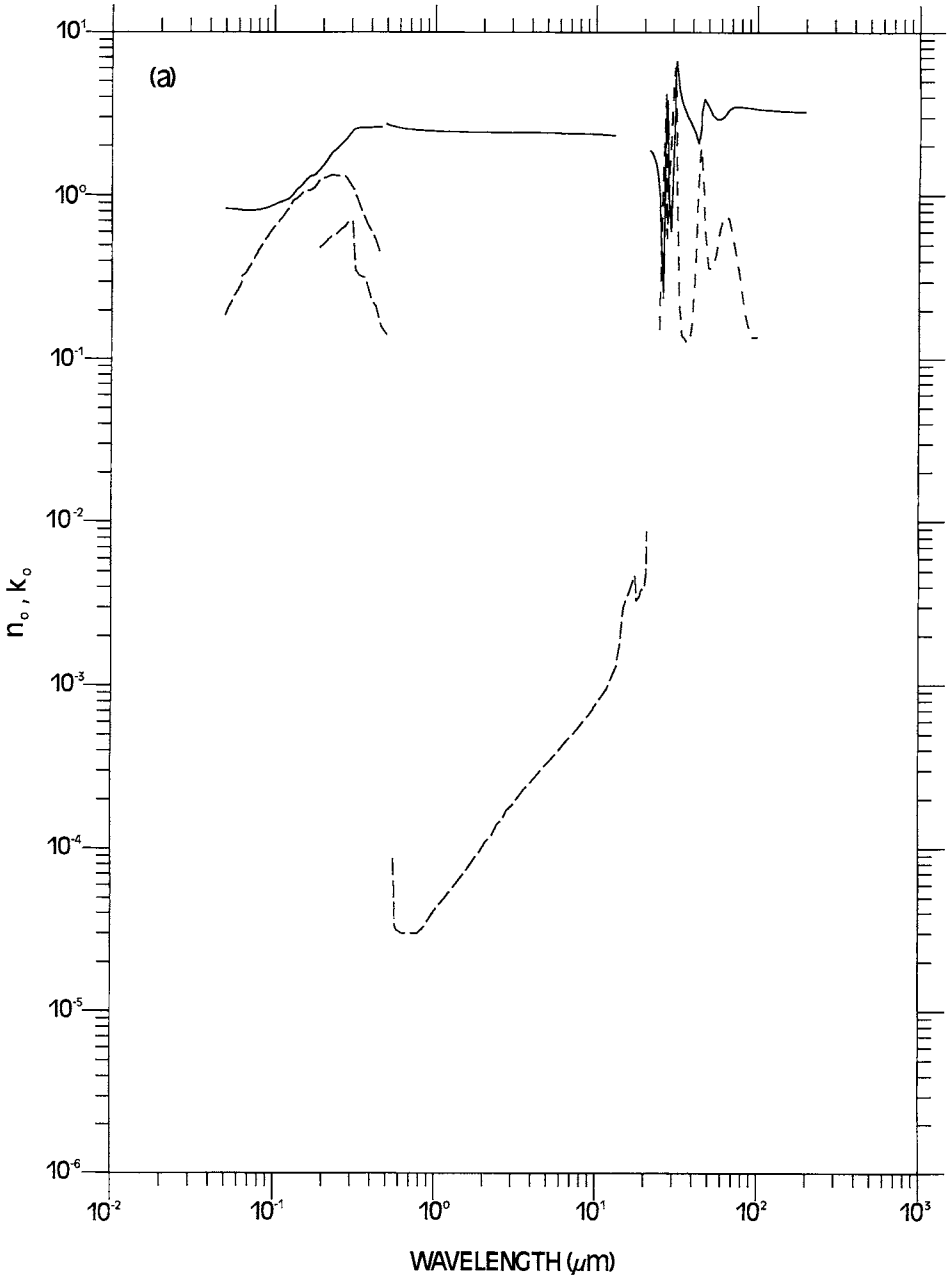

Fig. 2. (a) Log–log plot of n_o (solid line) and k_o (dashed line) versus wavelength in micrometers for silver gallium sulfide ($AgGaS_2$).

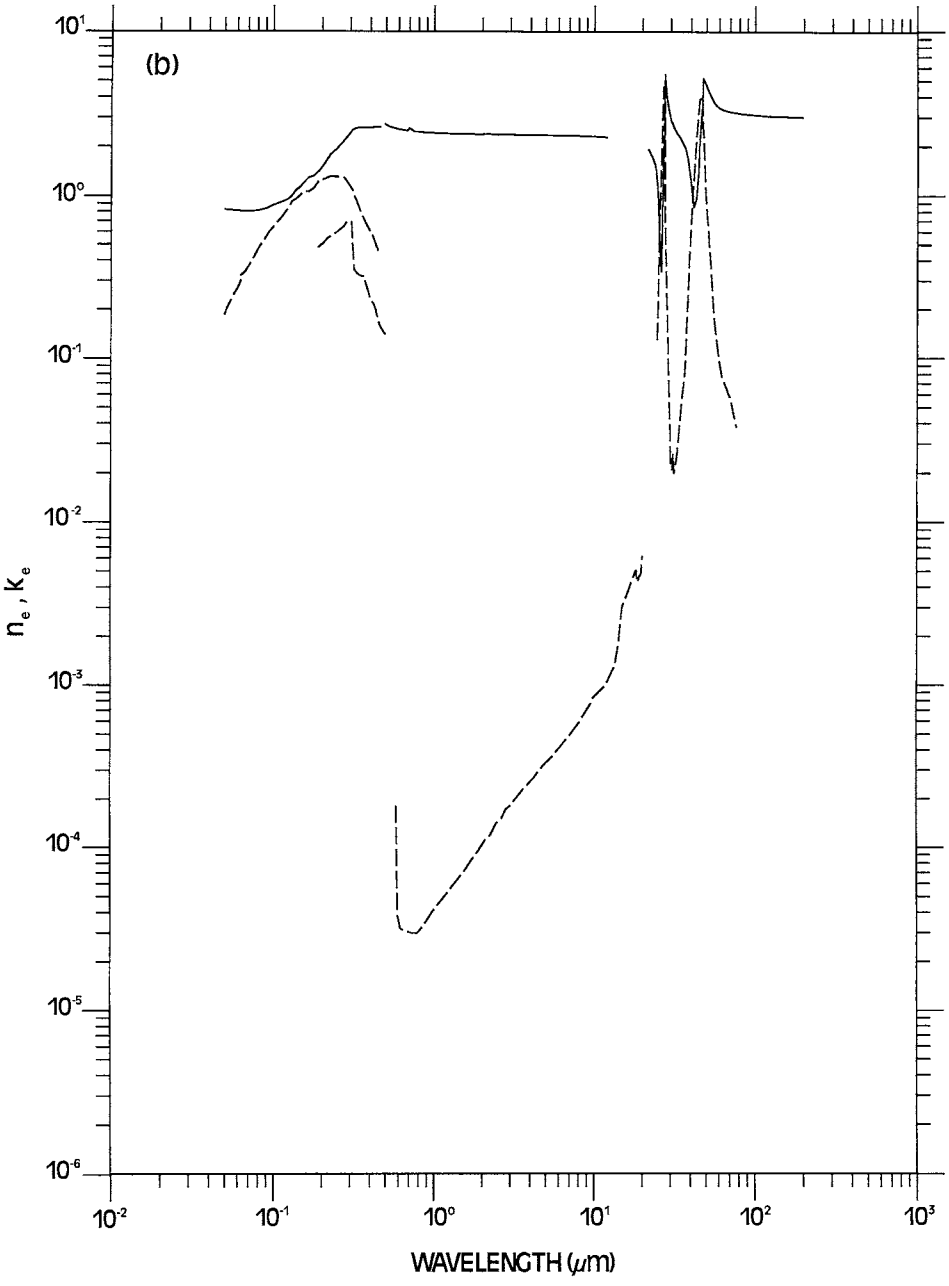

Fig. 2. (b) Log–log plot of n_e (solid line) and k_e (dashed line) versus wavelength in micrometers for silver gallium sulfide ($AgGaS_2$).

TABLE I

Values of n and k for $AgGaSe_2$ Obtained from Various References[a]

eV	cm^{-1}	μm	n	k
25.0	2.016E5	0.04959	0.845 [6]	0.095 [6]
24.0	1.936E5	0.05166	0.835	0.106
23.0	1.855E5	0.05390	0.824	0.119
22.0	1.774E5	0.05636	0.812	0.133
21.0	1.694E5	0.05904	0.799	0.151
20.5	1.653E5	0.06048	0.791	0.160
19.0	1.532E5	0.06358	0.768	0.195
18.0	1.452E5	0.06889	0.748	0.227
17.5	1.411E5	0.07085	0.739	0.248
17.0	1.371E5	0.07293	0.732	0.270
16.0	1.290E5	0.07749	0.721	0.321
15.5	1.250E5	0.07997	0.721	0.345
15.0	1.210E5	0.08266	0.716	0.372
14.5	1.169E5	0.08555	0.715	0.405
14.0	1.129E5	0.08856	0.719	0.437
13.5	1.089E5	0.09184	0.725	0.467
13.0	1.049E5	0.09537	0.730	0.495
12.5	1.008E5	0.09919	0.731	0.527
12.0	9.679E4	0.1033	0.734	0.564
11.5	9.275E4	0.1078	0.739	0.605
11.0	8.872E4	0.1127	0.743	0.643
10.5	8.469E4	0.1181	0.738	0.681
10.0	8.066E4	0.1240	0.731	0.749
9.50	7.662E4	0.1305	0.738	0.852
9.00	7.259E4	0.1378	0.784	0.933
8.50	6.856E4	0.1459	0.825	1.010
8.00	6.452E4	0.1550	0.864	1.097
7.50	6.049E4	0.1653	0.965	1.252
7.00	5.646E4	0.1771	1.146	1.324
6.50	5.243E4	0.1907	1.247	1.311
6.00	4.839E4	0.2066	1.341	1.378
5.50	4.436E4	0.2254	1.493	1.470
5.00	4.032E4	0.2478	1.683	1.553
4.50	3.630E4	0.2755	1.911	1.552
4.00	3.226E4	0.3100	2.175	1.512
3.90	3.146E4	0.3179	2.211	1.501
3.80	3.065E4	0.3263	2.253	1.502
3.70	2.984E4	0.3351	2.298	1.514
3.60	2.904E4	0.3444	2.372	1.543
3.50	2.823E4	0.3542	2.438	1.546
3.40	2.742E4	0.3647	2.602	1.508
3.30	2.662E4	0.3757	2.712	1.442
3.20	2.581E4	0.3874	2.804	1.353
3.10	2.500E4	0.3999	2.868	1.243
3.00	2.420E4	0.4133	2.905	1.141
2.90	2.339E4	0.4275	2.925	1.047

(continued)

[a] References shown in brackets.

TABLE I *(Continued)*

$AgGaSe_2$

eV	cm^{-1}	μm	n	k
2.80	2.258E4	0.4428	2.938	0.964
2.70	2.178E4	0.4592	2.951	0.885
2.60	2.097E4	0.4769	2.952	0.804
2.50	2.016E4	0.4960	2.943	0.732
2.40	1.936E4	0.5166	2.933	0.672
2.30	1.855E4	0.5391	2.927	0.616
2.20	1.774E4	0.5636	2.918	0.563
2.10	1.694E4	0.5904	2.917	0.507
2.00	1.613E4	0.6199	2.905	0.451
1.90	1.532E4	0.6526	2.889	0.400
1.80	1.452E4	0.6888	2.894	0.345
3.02	2.436E4	0.4105		0.247 [10]
2.93	2.363E4	0.4232		0.252
2.84	2.291E4	0.4366		0.257
2.75	2.218E4	0.4509		0.259
2.65	2.137E4	0.4679		0.262
2.55	2.057E4	0.4862		0.259
2.48	2.000E4	0.4999		0.257
2.40	1.936E4	0.5166		0.254
2.33	1.879E4	0.5321		0.245
2.26	1.823E4	0.5486		0.226
2.19	1.766E4	0.5661		0.196
2.14	1.726E4	0.5794		0.186
2.09	1.686E4	0.5932		0.179
2.04	1.645E4	0.6078		0.167
2.00	1.613E4	0.6199		0.142
1.95	1.573E4	0.6358		0.119
1.90	1.532E4	0.6526		0.103
1.85	1.492E4	0.6702		0.088
1.80	1.452E4	0.6888		0.066
1.79	1.444E4	0.6927		0.056
1.78	1.436E4	0.6965		0.041
1.76	1.420E4	0.7045		0.028
1.75	1.412E4	0.7085		0.016
1.74	1.403E4	0.7126		0.011
1.73	1.395E4	0.7167		0.008
2.398	1.934E4	0.517	3.124 [11]	0.276 [11]
2.300	1.855E4	0.539	3.089	0.255
2.218	1.789E4	0.559	3.058	0.219
2.138	1.724E4	0.580	3.028	0.204
2.070	1.669E4	0.599	2.999	0.190
2.009	1.621E4	0.617	2.974	0.168
1.937	1.563E4	0.640	2.943	0.133
1.884	1.520E4	0.658	2.922	0.108
1.829	1.475E4	0.678	2.898	0.084
1.771	1.429E4	0.700	2.872	0.040

TABLE I *(Continued)*

$AgGaSe_2$

eV	cm^{-1}	μm	n	k		
1.720	1.387E4	0.721	2.850	0.019		
1.676	1.351E4	0.740	2.831	0.001		
1.636	1.319E4	0.758	2.812			
1.554	1.253E4	0.798	2.781			
1.481	1.195E4	0.837	2.754			
1.382	1.115E4	0.897	2.727			
1.309	1.056E4	0.947	2.710			
1.216	9.804E3	1.020	2.690			
1.128	9.099E3	1.099	2.674			
1.033	8.333E3	1.200	2.661			
0.9530	7.686E3	1.301	2.651			
0.8856	7.143E3	1.400	2.644			
0.8260	6.662E3	1.501	2.639			
0.7739	6.242E3	1.602	2.634			
0.7280	5.872E3	1.703	2.631			
0.6872	5.543E3	1.804	2.629			
0.6512	5.252E3	1.904	2.625			
0.6199	5.000E3	2.000	2.624			
eV	cm^{-1}	μm	n_o	k_o	n_e	k_e
1.710	1.379E4	0.725	2.8452 [9]		2.8932 [9]	
1.653	1.333E4	0.750	2.8191		2.8415	
1.550	1.250E4	0.800	2.7849		2.7866	
1.459	1.177E4	0.850	2.7598		2.7522	
1.378	1.111E4	0.900	2.7406		2.7275	
1.306	1.053E4	0.950	2.7552		2.7085	
1.240	1.000E4	1.00	2.7132		2.6934	
1.127	9.091E3	1.10	2.6942		2.6712	
1.033	8.333E3	1.20	2.6806		2.6554	
0.9537	7.692E3	1.30	2.6705		2.6438	
0.8856	7.143E3	1.40	2.6624		2.6347	
0.7749	6.250E3	1.60	2.6516		2.6224	
0.6889	5.556E3	1.80	2.6432		2.6131	
0.6119	5.000E3	2.00	2.6376		2.6071	
0.5635	4.545E3	2.20	2.6336		2.6027	
0.5166	4.167E3	2.40	2.6304		2.5992	
0.4768	3.846E3	2.60	2.6286		2.5968	
0.4428	3.571E3	2.80	2.6261		2.5943	
0.4132	3.333E3	3.00	2.6245		2.5925	
0.3875	3.125E3	3.20	2.6231		2.5912	
0.3646	2.941E3	3.40	2.6221		2.5899	
0.3444	2.778E3	3.60	2.6213		2.5889	
0.3263	2.632E3	3.80	2.6200		2.5876	
0.3100	2.500E3	4.00	2.6189		2.5863	
0.2755	2.222E3	4.50	2.6166		2.5840	
0.2480	2.000E3	5.00	2.6144		2.5819	

(continued)

TABLE I *(Continued)*

$AgGaSe_2$

eV	cm^{-1}	μm	n_o	k_o	n_e	k_e
0.2254	1.818E3	5.50	2.6128		2.5800	
0.2067	1.667E3	6.00	2.6113		2.5784	
0.1907	1.538E3	6.50	2.6094		2.5765	
0.1772	1.429E3	7.00	2.6070		2.5743	
0.1653	1.333E3	7.50	2.6049		2.5723	
0.1550	1.250E3	8.00	2.6032		2.5704	
0.1458	1.176E3	8.50	2.6009		2.5681	
0.1377	1.111E3	9.00	2.5988		2.5659	
0.1306	1.053E3	9.50	2.5964		2.5635	
0.1240	1.000E3	10.0	2.5939		2.5608	
0.1181	9.524E2	10.5	2.5917		2.5585	
0.1127	9.091E2	11.0	2.5890		2.5555	
0.1078	8.696E2	11.5	2.5868		2.5536	
0.1033	8.333E2	12.0	2.5837		2.5505	
0.09919	8.000E2	12.5	2.5805		2.5473	
0.09537	7.692E2	13.0	2.5771		2.5439	
0.09184	7.407E2	13.5	2.5731		2.5404	
1.692	1.364E4	0.733		6.5E-06 [13]		1.4E-05 [13]
1.680	1.355E4	0.738		4.0E-06		1.0E-05
1.666	1.344E4	0.744		2.9E-06		5.5E-06
1.655	1.335E4	0.749		2.5E-06		3.7E-06
1.644	1.326E4	0.754		2.3E-06		2.9E-06
1.631	1.316E4	0.760		2.2E-06		2.5E-06
1.606	1.295E4	0.772		2.1E-06		2.2E-06
1.581	1.276E4	0.784		2.1E-06		2.0E-06
1.560	1.258E4	0.795		2.0E-06		2.0E-06
1.538	1.241E4	0.806		2.0E-06		1.9E-06
1.518	1.224E4	0.817		2.0E-06		1.9E-06
1.496	1.206E4	0.829		2.0E-06		1.8E-06
1.474	1.189E4	0.841		2.0E-06		1.8E-06
1.325	1.068E4	0.936		1.8E-06		1.7E-06
1.204	9.709E3	1.03		1.8E-06		1.7E-06
1.159	9.346E3	1.07		1.8E-06		1.8E-06
1.097	8.850E3	1.13		1.8E-06		1.9E-06
1.060	8.547E3	1.17		1.9E-06		2.3E-06
1.016	8.197E3	1.22		1.9E-06		2.7E-06
0.9763	7.874E3	1.27		2.0E-06		3.0E-06
0.9465	7.634E3	1.31		2.0E-06		3.1E-06
0.9117	7.353E3	1.36		2.0E-06		3.0E-06
0.8793	7.092E3	1.41		2.1E-06		2.7E-06
0.8551	6.897E3	1.45		2.2E-06		2.5E-06
0.8266	6.667E3	1.50		2.2E-06		2.4E-06
0.7749	6.250E3	1.60		2.3E-06		2.4E-06
0.7336	5.917E3	1.69		2.4E-06		2.4E-06
0.6966	5.618E3	1.78		2.5E-06		2.6E-06
0.6595	5.319E3	1.88		2.6E-06		2.8E-06

TABLE I *(Continued)*

$AgGaSe_2$

eV	cm^{-1}	μm	n_o	k_o	n_e	k_e
0.6274	5.076E3	1.97		2.8E-06		3.2E-06
0.5990	4.831E3	2.07		2.9E-06		3.6E-06
0.5713	4.608E3	2.17		3.1E-06		3.9E-06
0.5367	4.329E3	2.31		3.4E-06		4.0E-06
0.5166	4.167E3	2.40		3.5E-06		3.9E-06
0.4959	4.000E3	2.50		3.7E-06		3.8E-06
0.4787	3.861E3	2.59		3.8E-06		3.8E-06
46.00E-3	371	26.95	2.348 [14]		2.420 [14]	
44.76E-3	361	27.70	2.317	0.118 [14]	2.389	
43.52E-3	351	28.49	2.280	0.102	2.354	
42.28E-3	341	29.33	2.247	0.100	2.307	
41.04E-3	331	30.21	2.191	0.122	2.277	
39.80E-3	321	31.15	2.114	0.137	2.201	
38.56E-3	311	32.15	2.024	0.141	2.107	
37.32E-3	301	33.22	1.870	0.159	1.961	
36.08E-3	291	34.36	1.697	0.188	1.784	0.073 [14]
34.72E-3	280	35.71	1.351	0.269	1.389	0.145
33.48E-3	270	37.04	0.544	0.913	0.488	0.658
32.36E-3	261	38.31	0.528	2.410	0.422	2.150
31.12E-3	251	39.84	1.826	4.744	1.519	5.197
30.87E-3	249	40.16	3.655	5.637	4.264	6.776
30.50E-3	246	40.65	6.862	5.770	7.291	4.945
30.00E-3	242	41.32	6.850	2.657	5.912	1.982
29.88E-3	241	41.49	6.124	1.403	5.324	0.572
28.64E-3	231	43.29	4.226	0.282	3.960	0.171
27.40E-3	221	45.25	3.690	0.132	3.425	0.093
26.04E-3	210	47.62	3.361	0.110	3.135	0.109
24.80E-3	200	50.00	3.169	0.112	2.879	0.138
23.56E-3	190	52.63	3.054	0.120	2.639	0.205
22.19E-3	179	55.87	2.935	0.126	2.376	0.342
21.08E-3	170	58.82	2.748	0.229	1.911	0.741
20.33E-3	164	60.98	2.642	0.456	1.854	1.115
19.84E-3	160	62.50	2.747	0.752	1.928	1.746
19.09E-3	154	64.94	3.225	0.613	2.644	2.591
18.47E-3	149	67.11	3.133	0.381	3.341	2.621
17.73E-3	143	69.93	2.872	0.317	4.493	1.784
17.36E-3	140	71.43	2.744	0.408	4.523	1.160
16.61E-3	134	74.63	2.799	0.959	4.348	0.723
16.12E-3	130	76.92	3.541	0.550	4.192	0.501
14.88E-3	120	83.33	3.304	0.152	3.926	0.280
13.64E-3	110	90.91	3.135	0.127	3.730	0.158
12.40E-3	100	100.0	3.053	0.123	3.581	0.095
11.16E-3	90.0	111.1	2.969	0.113	3.497	
9.919E-3	80.0	125.0	3.095	0.335	3.444	
8.679E-3	70.0	142.9	3.119	0.088	3.387	
7.439E-3	60.0	166.7	3.051	0.064	3.349	

(continued)

TABLE I *(Continued)*

$AgGaSe_2$

eV	cm^{-1}	μm	n_o	k_o	n_e	k_e
6.199E-3	50.0	200.0	3.028	0.047	3.317	
4.959E-3	40.0	250.0	3.005		3.298	
3.720E-3	30.0	333.3	2.988		3.285	
2.480E-3	20.0	500.0	2.971		3.260	

TABLE II

Values of *n* and *k* for $AgGaS_2$ Obtained from Various References[a]

eV	cm^{-1}	μm	n	k
25.0	2.016E5	0.04959	0.827 [6]	0.185 [6]
24.0	1.936E5	0.05166	0.822	0.206
23.0	1.855E5	0.05390	0.822	0.222
22.0	1.774E5	0.05636	0.816	0.245
21.0	1.694E5	0.05904	0.815	0.264
20.0	1.613E5	0.06199	0.810	0.291
19.5	1.573E5	0.06358	0.807	0.306
19.0	1.532E5	0.06226	0.805	0.321
18.5	1.492E5	0.06702	0.803	0.341
18.0	1.452E5	0.06889	0.805	0.360
17.5	1.411E5	0.07085	0.807	0.374
17.0	1.371E5	0.07293	0.805	0.396
16.5	1.331E5	0.07514	0.808	0.416
16.0	1.290E5	0.07749	0.810	0.439
15.5	1.250E5	0.08000	0.813	0.464
15.0	1.210E5	0.08266	0.819	0.491
14.5	1.169E5	0.08555	0.826	0.515
14.0	1.129E5	0.08856	0.832	0.545
13.5	1.089E5	0.09184	0.842	0.577
13.0	1.049E5	0.09537	0.858	0.610
12.5	1.009E5	0.09919	0.874	0.637
12.0	9.679E4	0.1033	0.886	0.669
11.6	9.356E4	0.1069	0.900	0.698
11.0	8.872E4	0.1127	0.917	0.742
10.5	8.469E4	0.1181	0.934	0.790
10.0	8.066E4	0.1240	0.958	0.846
9.50	7.662E4	0.1305	1.008	0.925
9.00	7.259E4	0.1378	1.083	0.955
8.50	6.856E4	0.1459	1.126	1.007
8.00	6.452E4	0.1550	1.213	1.063
7.50	6.049E4	0.1653	1.292	1.058
7.00	5.646E4	0.1771	1.317	1.110
6.50	5.243E4	0.1907	1.415	1.240
6.00	4.839E4	0.2066	1.564	1.266

[a] References given in brackets.

TABLE II *(Continued)*

$AgGaS_2$

eV	cm^{-1}	μm	n	k
5.50	4.436E4	0.2254	1.784	1.314
5.00	4.033E4	0.2478	1.939	1.305
4.50	3.630E4	0.2755	2.173	1.283
4.00	3.226E4	0.3100	2.515	1.080
3.90	3.146E4	0.3179	2.542	1.006
3.80	3.065E4	0.3263	2.569	0.944
3.70	2.984E4	0.3351	2.578	0.875
3.60	2.904E4	0.3444	2.590	0.820
3.50	2.823E4	0.3542	2.589	0.766
3.40	2.742E4	0.3647	2.590	0.717
3.30	2.662E4	0.3757	2.587	0.672
3.20	2.581E4	0.3874	2.586	0.634
3.10	2.500E4	0.3999	2.586	0.600
3.00	2.420E4	0.4133	2.597	0.566
2.90	2.339E4	0.4275	2.609	0.518
2.80	2.258E4	0.4428	2.601	0.468
2.75	2.218E4	0.4509	2.601	0.450
2.70	2.178E4	0.4592	2.606	0.429
6.54	5.275E4	0.1896		0.479 [23]
6.29	5.073E4	0.1971		0.496
6.06	4.888E4	0.2046		0.510
5.80	4.678E4	0.2138		0.539
5.55	4.476E4	0.2234		0.559
5.31	4.283E4	0.2335		0.569
5.05	4.073E4	0.2455		0.590
4.80	3.871E4	0.2583		0.620
4.56	3.678E4	0.2719		0.643
4.32	3.484E4	0.2870		0.693
4.06	3.275E4	0.3054		0.687
3.91	3.154E4	0.3171		0.350
3.71	2.992E4	0.3342		0.329
3.51	2.831E4	0.3532		0.320
3.41	2.750E4	0.3636		0.320
3.32	2.678E4	0.3735		0.291
3.20	2.581E4	0.3875		0.258
3.11	2.508E4	0.3987		0.235
2.90	2.339E4	0.4275		0.208
2.70	2.178E4	0.4592		0.158
2.50	2.016E4	0.4959		0.141

eV	cm^{-1}	μm	n_o	k_o	n_e	k_e
2.531	2.041E4	0.490	2.7148 [24]		2.7287 [24]	
2.480	2.000E4	0.500	2.6916		2.6867	
2.362	1.905E4	0.525	2.6503		2.6239	
2.254	1.818E4	0.550	2.6190		2.5834	
2.156	1.739E4	0.575	2.5944		2.5537	

(continued)

TABLE II *(Continued)*

$AgGaS_2$

eV	cm^{-1}	μm	n_o	k_o	n_e	k_e
2.067	1.667E4	0.600	2.5748		2.5303	
1.984	1.600E4	0.625	2.5577		2.5116	
1.908	1.539E4	0.650	2.5437		2.4961	
1.837	1.482E4	0.675	2.5310		2.4824	
1.772	1.429E4	0.700	2.5205		2.5706	
1.653	1.333E4	0.750	2.5049		2.4540	
1.550	1.250E4	0.800	2.4909		2.4395	
1.459	1.177E4	0.850	2.4802		2.4279	
1.377	1.111E4	0.900	2.4716		2.4192	
1.306	1.053E4	0.950	2.4644		2.4118	
1.240	1.000E4	1.00	2.4582		2.4053	
1.127	9.091E3	1.10	2.4486		2.3954	
1.033	8.333E3	1.20	2.4414		2.3881	
0.9537	7.692E3	1.30	2.4359		2.3819	
0.8856	7.143E3	1.40	2.4315		2.3781	
0.8266	6.667E3	1.50	2.4280		2.3745	
0.7749	6.250E3	1.60	2.4252		2.3716	
0.6889	5.556E3	1.80	2.4206		2.3670	
0.6199	5.000E3	2.00	2.4164		2.3637	
0.5635	4.545E3	2.20	2.4161		2.3684	
0.5166	4.167E3	2.40	2.4119		2.3583	
0.4768	3.846E3	2.60	2.4102		2.3567	
0.4428	3.571E3	2.80	2.4094		2.3559	
0.4132	3.333E3	3.00	2.4080		2.3545	
0.3875	3.125E3	3.20	2.4068		2.3534	
0.3646	2.941E3	3.40	2.4062		2.3522	
0.3444	2.778E3	3.60	2.4046		2.3511	
0.3263	2.632E3	3.80	2.4024		2.3491	
0.3100	2.500E3	4.00	2.4024		2.3488	
0.2755	2.222E3	4.50	2.4003		2.3461	
0.2480	2.000E3	5.00	2.3955		2.3419	
0.2254	1.818E3	5.50	2.3938		2.3401	
0.2067	1.667E3	6.00	2.3908		2.3369	
0.1907	1.538E3	6.50	2.3874		2.3334	
0.1772	1.429E3	7.00	2.3827		2.3291	
0.1653	1.333E3	7.50	2.3787		2.3252	
0.1550	1.250E3	8.00	2.3757		2.3219	
0.1458	1.176E3	8.50	2.3699		2.3163	
0.1377	1.111E3	9.00	2.3663		2.3121	
0.1306	1.053E3	9.50	2.3606		2.3064	
0.1240	1.000E3	10.0	2.3548		2.3012	
0.1181	9.524E2	10.5	2.3486		2.2948	
0.1127	9.091E2	11.0	2.3417		2.2880	
0.1078	8.696E2	11.5	2.3329		2.2789	
0.1033	8.333E2	12.0	2.3266		2.2716	
0.09919	8.000E2	12.5	2.3177			
0.09537	7.692E2	13.0	2.3076			

TABLE II *(Continued)*

$AgGaS_2$

eV	cm^{-1}	μm	n_o	k_o	n_e	k_e
2.522	2.034E4	0.4916	2.700 [25]		2.710 [25]	
2.472	1.994E4	0.5016	2.683		2.676	
2.270	1.831E4	0.5461	2.619		2.585	
2.145	1.730E4	0.5780	2.587		2.546	
2.110	1.702E4	0.5876	2.579		2.537	
1.857	1.498E4	0.6678	2.529		2.481	
2.234	1.802E4	0.555		8.6E-05 [26]		
2.175	1.754E4	0.570		3.3E-05		
2.112	1.704E4	0.587		3.1E-05		1.8E-04 [26]
2.070	1.669E4	0.599		3.1E-05		3.9E-05
1.990	1.605E4	0.623		3.0E-05		3.2E-05
1.887	1.522E4	0.657		3.0E-05		3.1E-05
1.705	1.376E4	0.727		3.0E-05		3.0E-05
1.556	1.255E4	0.797		3.0E-05		3.0E-05
1.425	1.149E4	0.870		3.3E-05		3.3E-05
1.328	1.071E4	0.934		3.7E-05		3.7E-05
1.241	1.001E4	0.999		4.1E-05		4.1E-05
1.042	8.403E3	1.19		5.1E-05		5.1E-05
0.8920	7.194E3	1.39		6.2E-05		6.2E-05
0.7897	6.369E3	1.57		7.2E-05		7.2E-05
0.7045	5.682E3	1.76		8.5E-05		8.5E-05
0.6424	5.181E3	1.93		9.6E-05		9.6E-05
0.5904	4.762E3	2.10		1.1E-04		1.1E-04
0.5414	4.367E3	2.29		1.2E-04		1.2E-04
0.5020	4.049E3	2.47		1.4E-04		1.4E-04
0.4643	3.745E3	2.67		1.5E-04		1.5E-04
0.4382	3.534E3	2.83		1.7E-04		1.7E-04
0.4119	3.322E3	3.01		1.8E-04		1.8E-04
0.4092	3.300E3	3.03		1.8E-04		1.8E-04
0.3397	2.740E3	3.65		2.3E-04		2.3E-04
0.2931	2.364E3	4.23		2.7E-04		2.7E-04
0.2545	2.053E3	4.87		3.2E-04		3.2E-04
0.2266	1.828E3	5.47		3.6E-04		3.6E-04
0.2030	1.637E3	6.11		4.1E-04		4.1E-04
0.1851	1.493E3	6.70		4.6E-04		4.6E-04
0.1694	1.366E3	7.32		5.0E-04		5.1E-04
0.1566	1.263E3	7.92		5.5E-04		5.7E-04
0.1461	1.178E3	8.49		6.0E-04		6.3E-04
0.1364	1.100E3	9.09		6.5E-04		7.0E-04
0.1292	1.042E3	9.60		7.0E-04		7.7E-04
0.1252	1.010E3	9.90		7.4E-04		8.3E-04
0.1042	8.403E2	11.9		9.6E-04		1.0E-03
0.09184	7.407E2	13.5		1.3E-03		1.3E-03
0.08670	6.993E2	14.3		1.8E-03		1.8E-03

(continued)

TABLE II *(Continued)*

$AgGaS_2$

eV	cm^{-1}	μm	n_o	k_o	n_e	k_e
0.08266	6.667E2	15.0		3.0E-03		3.0E-03
0.07005	5.650E2	17.7		4.7E-03		
0.06927	5.587E2	17.9		3.3E-03		
0.06739	5.435E2	18.4		3.4E-03		5.1E-03
0.06595	5.319E2	18.8		3.5E-03		4.3E-03
0.06457	5.208E2	19.2		3.8E-03		4.6E-03
0.06293	5.076E2	19.7		3.9E-03		4.8E-03
0.06168	4.975E2	20.1		3.9E-03		6.2E-03
0.05990	4.831E2	20.7		4.9E-03		
0.05932	4.785E2	20.9		8.7E-03		
57.41E-3	463	21.60	1.875 [28]		1.931 [28]	
56.28E-3	454	22.03	1.826		1.870	
55.05E-3	444	22.52	1.759		1.792	
53.81E-3	434	23.04	1.665		1.721	
52.45E-3	423	23.64	1.522		1.591	
51.21E-3	413	24.21	1.319		1.439	
49.84E-3	402	24.88	1.010	0.152 [28]	1.112	0.131 [28]
48.73E-3	393	25.45	0.471	0.475	0.568	0.554
47.36E-3	382	26.18	0.237	1.507	0.340	1.838
46.12E-3	372	26.88	1.721	3.329	1.819	4.605
45.75E-3	369	27.10	3.029	4.177	2.063	4.645
45.13E-3	364	27.47	3.810	1.513	5.526	3.417
45.01E-3	363	27.55	3.674	0.546	5.185	0.870
43.77E-3	353	28.33	0.988	1.082	3.868	0.257
42.40E-3	342	29.24	0.605	2.250	3.200	0.079
41.16E-3	332	30.12	1.398	4.421	2.856	0.023
40.17E-3	324	30.86	3.580	6.061	2.696	0.021
39.92E-3	322	31.06	5.690	5.554	2.625	0.026
39.30E-3	317	31.55	6.652	2.394	2.550	0.020
38.81E-3	313	31.95	5.846	0.866	2.498	0.021
37.69E-3	304	32.89	4.408	0.246	2.377	0.026
36.33E-3	293	34.13	3.721	0.139	2.268	0.038
34.96E-3	282	35.46	3.362	0.134	2.100	0.058
33.72E-3	272	36.76	3.059	0.125	1.969	0.083
32.48E-3	262	38.17	2.842	0.126	1.694	0.198
31.24E-3	252	39.68	2.617	0.172	1.305	0.504
29.88E-3	241	41.49	2.345	0.374	0.855	1.227
28.76E-3	232	43.10	2.060	1.090	0.964	2.216
27.77E-3	224	44.64	2.550	1.947	1.416	3.374
27.52E-3	222	45.05	3.195	1.850	2.013	3.831
26.53E-3	214	46.73	3.897	1.020	3.419	4.050
26.16E-3	211	47.39	3.801	0.637	5.216	2.657
24.92E-3	201	49.75	3.502	0.364	4.695	0.912
23.56E-3	190	52.63	3.091	0.358	4.110	0.435
22.32E-3	180	55.56	2.938	0.437	3.679	0.187
21.08E-3	170	58.82	2.915	0.619	3.458	0.111

TABLE II ***(Continued)***

$AgGaS_2$

eV	cm^{-1}	μm	n_o	k_o	n_e	k_e
19.84E-3	160	62.50	3.048	0.754	3.353	0.077
18.60E-3	150	66.67	3.332	0.723	3.292	0.065
17.48E-3	141	70.92	3.473	0.546	3.241	0.056
16.12E-3	130	76.92	3.482	0.345	3.193	0.038
14.88E-3	120	83.33	3.454	0.203	3.153	
13.64E-3	110	90.91	3.420	0.135	3.129	
12.40E-3	100	100.0	3.373	0.136	3.104	
11.16E-3	90	111.1	3.333		3.069	
9.919E-3	80	125.0	3.300		3.051	
8.679E-3	70	142.9	3.276		3.048	
7.439E-3	60	166.7	3.248		3.031	
6.323E-3	51	196.1	3.230		3.017	

Zinc Arsenide (Zn_3As_2)

J. MISIEWICZ and K. JEZIERSKI
Institute of Physics
Technical University of Wroclaw
Wroclaw, Poland

Zinc arsenide, Zn_3As_2, is a member of the II–V group of semiconducting compounds [1]. It posseses a tetragonal unit cell described by $I4_1cd \equiv C_{4v}^{12}$ symmetry. Optical properties of this material are not intensively studied, mainly because of the relatively high and temperature-independent concentration of holes in the range of $10^{17}cm^{-3}$, which results in a very limited range of possible applications of Zn_3As_2 in semiconductor devices.

Infrared optical processes are dominated by strong absorption when the photon energy decreases below 0.8 eV [2]. Within this energy region there are very intense intraband and defect-related transitions observed even at 5 K by Sujak-Cyrul *et al.* [3]. Within the 0.9–1 eV energy range, a strong increase of absorption connected with the fundamental absorption edge is observed by Misiewicz and Pawlikowski [2]. Above an energy of 1 eV, absorption was investigated only on polycrystalline thin films [4]. Żdanowicz and Pawlikowski [5] determined a refractive index equal to 3.85 from interference fringes observed in transmission spectra for polycrystalline Zn_3As_2 thin films within the wavelength range 3–20 μm. The values of extinction coefficient given in Table I for energies smaller than 1.5 eV are derived directly from the absorption coefficient determined by means of transmission measurements [2–4].

The reflectivity spectrum for Zn_3As_2 measured within the energy range 1–5 eV is presented elsewhere [6]. The high-energy spectrum up to 12 eV was published by Sobolev *et al.* [7]. Zivitz and Stevenson [8] presented reflectivity obtained by using a glow-discharge lamp source (up to 20 eV) and a synchrotron radiation source (up to 30 eV) utilizing polycrystal samples. These spectra covered the whole energy range from 1 eV up to 30 eV, and from them one spectrum was constructed in order to perform the Kramers–Kronig analysis. It was necessary to reject the reflectivity data for the synchrotron-radiation source, because for these data negative values of the extinction coefficient for high energies were obtained. Therefore, the values

HANDBOOK OF OPTICAL CONSTANTS OF SOLIDS III

Copyright © 1998 by Academic Press.
All rights of reproduction in any form reserved
ISBN 0-12-544423-0/$25.00.

of n and k given in Table I covered the energy range up to 20 eV. In the Kramers–Kronig calculations [9] the values of extinction coefficient below 1.5 eV were assumed to be equal to those known from the experiment [2–4]. The spectra of n and k for unpolarized light over a wide spectral range are presented in Fig. 1.

The measured optical spectra of Zn_3As_2 showed anisotropy, which was observed by Misiewicz *et al.* for the fundamental absorption edge [10] and in the reflectivity spectra within the visible and ultraviolet energy range [11]. The measurements were performed at room temperature by using x-ray oriented Zn_3As_2 single crystals obtained from a gas-transport growth method. The double grating Carl-Zeiss GDM-1000 monochromator equipped with linear polarizers from Carl-Zeiss and a Hamamatsu photomultiplier were utilized. Within the 0.9–1.0 eV energy range, a HgCdTe-based detector was used. The determined values of n_e, n_o and k_e, k_o are also included in Table I and presented in Figs. 2 and 3.

REFERENCES

1. E. K. Arushanov, *Prog. Cryst. Growth Charact.* **25**, 131 (1992).
2. J. Misiewicz and J. M. Pawlikowski, *Solid State Commun.* **32**, 687 (1979).
3. B. Sujak-Cyrul, B. Kolodka, J. Misiewicz, and J. M. Pawlikowski, *J. Phys. Chem. Solids* **43**, 1045 (1982).
4. B. Kołodka, J. Misiewicz, and J. M. Pawlikowski, *Acta Phys. Pol.* **A62**, 63 (1982).
5. W. Żdanowicz and J. M. Pawlikowski, *Acta Phys. Pol.* **A38**, 11 (1970).
6. J. Misiewicz, J. Wróbel, B. Sujak-Cyrul, and F. Królicki, *Opt. Appl.* **10**, 75 (1980).
7. V. V. Sobolev, N. N. Syrbu, T.A. Zjubina, and I. A. Ugai, *Fiz. Tekh. Poluprovadn. (Leningrad.)* **5**, 327 (1971).
8. M. Zivitz and J. R. Stevenson, *Phys. Rev. B* **10**, 2457 (1974).
9. K. Jezierski, *J. Phys. C: Solid State Phys.* **17**, 475 (1984).
10. J. Misiewicz, J. M. Wróbel, and K. Jezierski, *Solid State Commun.* **86**, 509 (1993).
11. J. Misiewicz, J. Wróbel, and K. Jezierski, *J. Phys. C: Solid State Phys.* **17**, 3091 (1984).

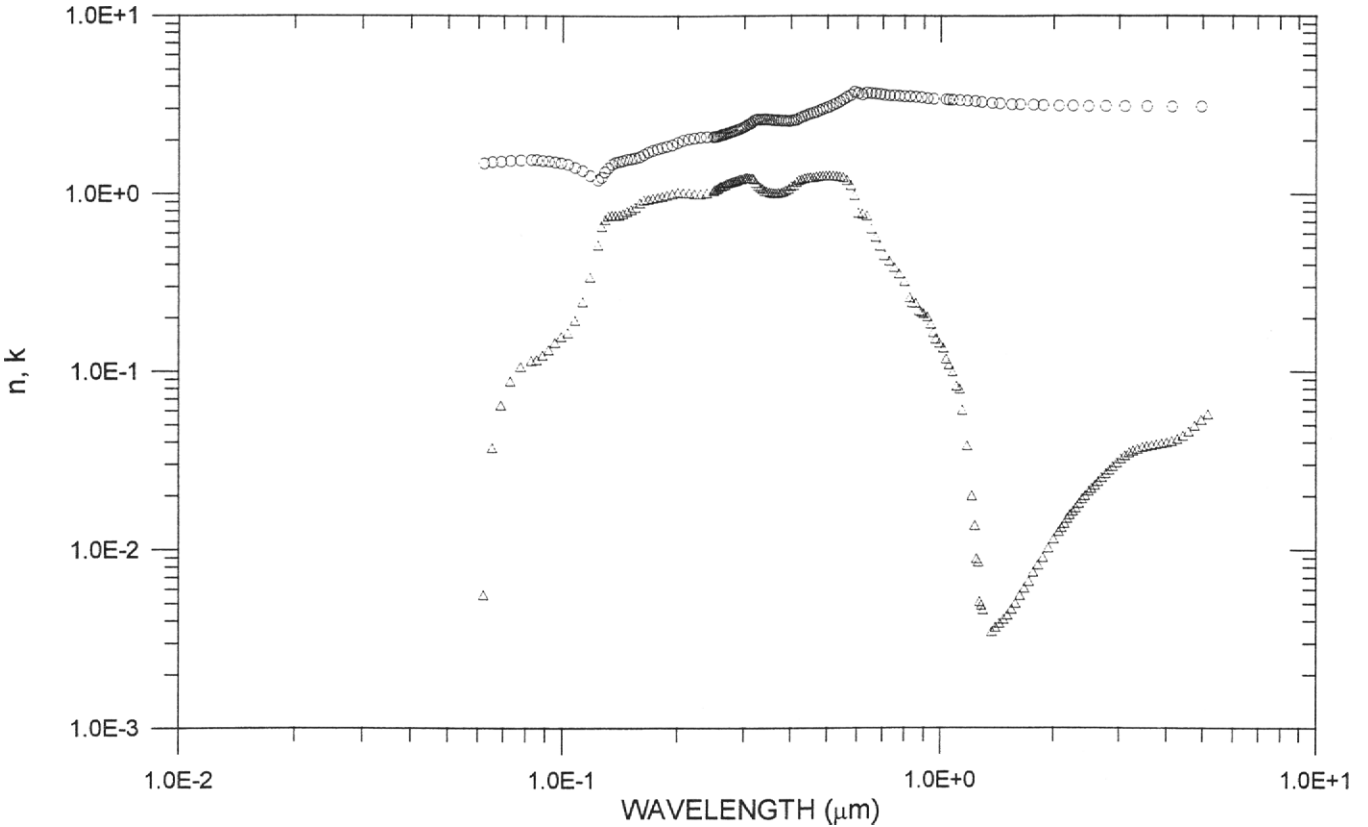

Fig. 1. Log–log plot of n (circles) and k (triangles) versus wavelength in micrometers for zinc arsenide (Zn_3As_2). Data are for unpolarized light for monocrystal samples [2, 6–8] and for polycrystal samples [4].

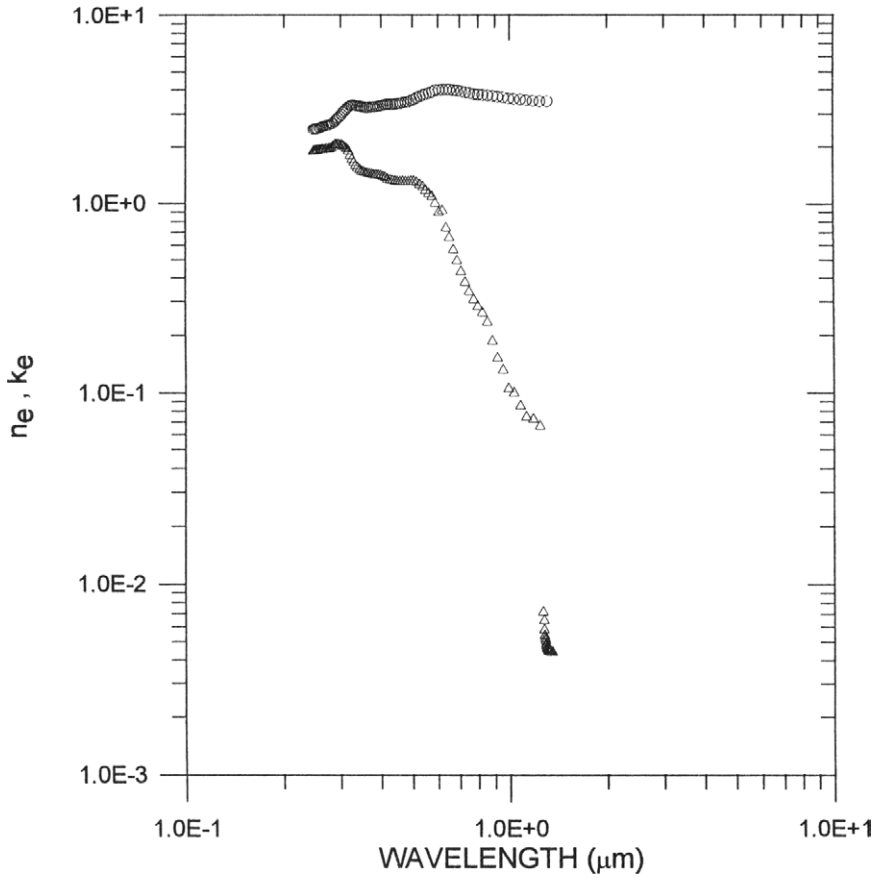

Fig. 2. Log–log plot of n_e (circles) and k_e (triangles) versus wavelength in micrometers for zinc arsenide (Zn_3As_2).

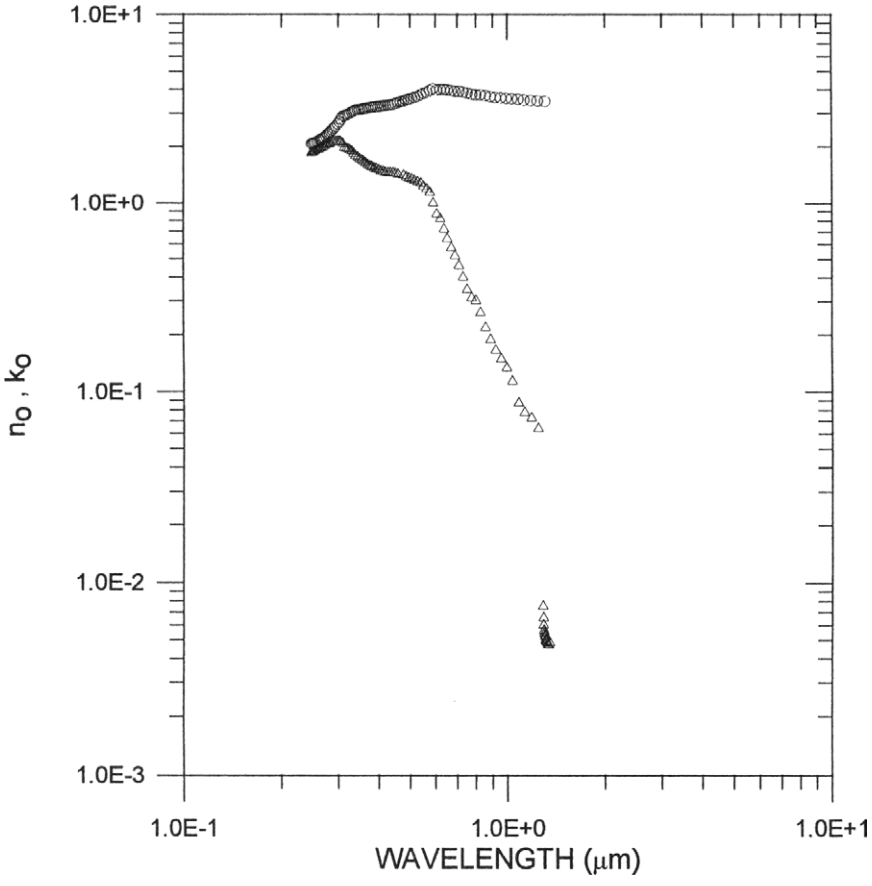

Fig. 3. Log–log plot of n_o (circles) and k_o (triangles) versus wavelength in micrometers for zinc arsenide (Zn_3As_2).

TABLE I

Values of n and k Obtained from Various References for Zinc Arsenide[a]

eV	cm^{-1}	μm	n	k
20	161,300	0.06199	1.4921 [8]	0.0056 [8]
19	153,200	0.06526	1.51	0.0372
18	145,200	0.06888	1.522	0.0646
17	137,100	0.07293	1.537	0.0885
16	129,000	0.07749	1.552	0.107
15	121,000	0.08266	1.562	0.115
14.5	116,900	0.08551	1.554	0.117
14	112,900	0.08856	1.544	0.124
13.5	108,900	0.09184	1.53	0.133
13	104,900	0.09537	1.514	0.146
12.5	100,800	0.09919	1.497	0.157
12	96,780	0.1033	1.466	0.165
11.5	92,750	0.1078	1.408	0.195
11	88,720	0.1127	1.351	0.248
10.5	84,690	0.1181	1.271	0.341
10	80,650	0.1240	1.199 [7]	0.516 [7]
9.8	79,040	0.1265	1.238	0.658
9.6	77,430	0.1292	1.331	0.718
9.4	75,810	0.1319	1.401	0.753
9.2	74,200	0.1348	1.467	0.763
9	72,590	0.1378	1.505	0.758
8.8	70,980	0.1409	1.526	0.761
8.6	69,360	0.1442	1.544	0.776
8.4	67,750	0.1476	1.564	0.796
8.2	66,140	0.1512	1.582	0.816

8	64,520	0.1550	1.594	0.843				
7.8	62,910	0.1590	1.626	0.89				
7.6	61,300	0.1631	1.674	0.922				
7.4	59,680	0.1675	1.723	0.938				
7.2	58,070	0.1722	1.764	0.945				
7	56,460	0.1771	1.796	0.955				
6.8	54,850	0.1823	1.829	0.97				
6.6	53,230	0.1879	1.862	0.985				
6.4	51,620	0.1937	1.898	1.005				
6.2	50,010	0.2000	1.952	1.023				
6	48,390	0.2066	2.002	1.018				
5.8	46,780	0.2138	2.039	1.012				
5.6	45,170	0.2214	2.066	1.004				
5.4	43,550	0.2296	2.087	1.006				
5.2	41,940	0.2384	2.099	1.012				
eV	cm^{-1}	μm	n_e	k_e	n_o	k_o	n	k
5	40,330	0.2480	2.49 [11]	1.931 [11]	2.072 [11]	1.885 [11]	2.105 [6]	1.048 [6]
4.95	39,920	0.2505	2.495	1.937	2.077	1.896	2.116	1.062
4.9	39,520	0.2530	2.503	1.943	2.087	1.918	2.117	1.068
4.85	39,120	0.2556	2.511	1.948	2.102	1.935	2.123	1.091
4.8	38,710	0.2583	2.526	1.959	2.12	1.958	2.144	1.106
4.75	38,310	0.2610	2.544	1.963	2.144	1.976	2.161	1.111
4.7	37,910	0.2638	2.56	1.967	2.167	1.993	2.171	1.119
4.65	37,500	0.2666	2.577	1.971	2.191	2.011	2.177	1.129
4.6	37,100	0.2695	2.595	1.975	2.218	2.029	2.197	1.152
4.55	36,700	0.2725	2.614	1.978	2.243	2.047	2.219	1.161

(continued)

[a] References given in brackets.

TABLE I *(Continued)*

Zinc Arsenide

eV	cm^{-1}	μm	n_e	k_e	n_o	k_o	n	k
4.5	36,290	0.2755	2.627	1.983	2.279	2.077	2.241	1.17
4.45	35,890	0.2786	2.639	1.994	2.323	2.09	2.259	1.174
4.4	35,490	0.2818	2.66	2.019	2.359	2.108	2.279	1.184
4.35	35,080	0.2850	2.687	2.042	2.4	2.126	2.297	1.189
4.3	34,680	0.2883	2.736	2.077	2.453	2.15	2.314	1.201
4.25	34,280	0.2917	2.802	2.093	2.515	2.16	2.339	1.215
4.2	33,880	0.2952	2.863	2.087	2.571	2.163	2.367	1.222
4.15	33,470	0.2988	2.916	2.082	2.631	2.171	2.394	1.229
4.1	33,070	0.3024	2.99	2.086	2.712	2.176	2.429	1.239
4.05	32,660	0.3061	3.064	2.055	2.789	2.149	2.467	1.239
4	32,260	0.3100	3.126	2.024	2.881	2.114	2.503	1.233
3.95	31,860	0.3139	3.193	1.989	2.921	2.016	2.535	1.229
3.9	31,460	0.3179	3.274	1.935	2.93	1.998	2.6	1.219
3.85	31,050	0.3220	3.329	1.839	2.965	1.978	2.636	1.159
3.8	30,650	0.3263	3.339	1.751	3.002	1.949	2.639	1.122
3.75	30,250	0.3306	3.335	1.682	3.047	1.924	2.636	1.097
3.7	29,840	0.3351	3.327	1.625	3.084	1.874	2.648	1.078
3.65	29,440	0.3397	3.306	1.576	3.106	1.828	2.64	1.048
3.6	29,040	0.3444	3.3	1.548	3.124	1.792	2.638	1.041
3.55	28,630	0.3493	3.28	1.509	3.138	1.758	2.632	1.027
3.5	28,230	0.3542	3.268	1.497	3.154	1.73	2.627	1.022
3.45	27,830	0.3594	3.26	1.482	3.172	1.702	2.623	1.017
3.4	27,420	0.3647	3.255	1.475	3.188	1.673	2.614	1.015
3.35	27,020	0.3701	3.261	1.47	3.203	1.644	2.609	1.02
3.3	26,620	0.3757	3.263	1.458	3.212	1.619	2.601	1.027
3.25	26,210	0.3815	3.267	1.454	3.228	1.598	2.595	1.041

3.2	25,810	0.3875	3.285	1.452	3.237	1.572	2.597	1.058
3.15	25,410	0.3936	3.298	1.44	3.247	1.554	2.587	1.075
3.1	25,000	0.4000	3.32	1.434	3.26	1.535	2.606	1.112
3.05	24,600	0.4065	3.34	1.417	3.269	1.518	2.609	1.128
3	24,200	0.4133	3.36	1.4	3.285	1.505	2.634	1.177
2.95	23,790	0.4203	3.373	1.375	3.296	1.486	2.677	1.207
2.9	23,390	0.4275	3.379	1.359	3.302	1.481	2.718	1.22
2.85	22,990	0.4350	3.388	1.349	3.325	1.485	2.751	1.231
2.8	22,580	0.4428	3.4	1.338	3.35	1.477	2.801	1.249
2.75	22,180	0.4509	3.409	1.329	3.382	1.473	2.843	1.244
2.7	21,780	0.4592	3.421	1.33	3.411	1.46	2.874	1.248
2.65	21,370	0.4679	3.443	1.333	3.446	3.453	2.909	1.258
2.6	20,970	0.4769	3.47	1.332	3.49	1.439	2.955	1.271
2.55	20,570	0.4862	3.496	1.332	3.529	1.414	3.007	1.277
2.5	20,160	0.4959	3.541	1.338	3.566	1.392	3.058	1.275
2.45	19,760	0.5061	3.585	1.333	3.601	1.37	3.106	1.276
2.4	19,360	0.5166	3.656	1.326	3.644	1.353	3.174	1.281
2.35	18,950	0.5276	3.716	1.287	3.69	1.331	3.237	1.268
2.3	18,550	0.5391	3.773	1.25	3.752	1.305	3.312	1.265
2.25	18,150	0.5510	3.823	1.201	3.814	1.262	3.402	1.249
2.2	17,740	0.5636	3.869	1.156	3.871	1.221	3.514	1.205
2.15	17,340	0.5767	3.924	1.111	3.973	1.168	3.598	1.129
2.1	16,940	0.5904	4.001	1.027	4.043	1.019	3.738	0.993
2.05	16,530	0.6048	4.015	0.915	3.993	0.888	3.676	0.786
2	16,130	0.6199	4.029	0.939	4.018	0.837	3.616	0.779
1.95	15,730	0.6358	4.03	0.757	4.016	0.736	3.688	0.761
1.9	15,320	0.6526	4.041	0.672	3.992	0.653	3.677	0.641
1.85	14,920	0.6702	4.018	0.576	3.961	0.584	3.65	0.576

(continued)

TABLE I *(Continued)*

Zinc Arsenide

eV	cm^{-1}	μm	n_e	k_e	n_o	k_o	n	k
1.8	14,520	0.6888	3.984	0.504	3.934	0.529	3.641	0.513
1.75	14,110	0.7085	3.947	0.441	3.919	0.47	3.6	0.454
1.7	13,710	0.7293	3.907	0.388	3.882	0.409	3.579	0.423
1.65	13,310	0.7514	3.864	0.346	3.853	0.352	3.559	0.389
1.6	12,900	0.7749	3.829	0.314	3.788	0.319	3.547	0.359
1.55	12,500	0.7999	3.793	0.289	3.77	0.309	3.535	0.325
1.5	12,100	0.8266	3.777	0.268	3.757	0.266	3.523	0.263 [4]
1.48	11,940	0.8377						0.247
1.45	11,690	0.8551	3.761	0.239	3.724	0.223	3.51	0.245
1.42	11,450	0.8731						0.222
1.4	11,290	0.8856	3.748	0.19	3.689	0.193	3.499	0.218
1.38	11,130	0.8984						0.214
1.35	10,890	0.9184	3.693	0.155	3.653	0.17	3.458	0.205
1.32	10,650	0.9393						0.187
1.3	10,480	0.9537	3.676	0.134	3.626	0.152	3.432	0.167
1.28	10,320	0.9686						0.154
1.25	10,080	0.9919	3.63	0.1071	3.599	0.136		0.146
1.22	9,840	1.016						0.137
1.2	9,678	1.033	3.602	0.102	3.582	0.116	3.399	0.119
1.18	9,517	1.051					3.392	0.11
1.15	9,275	1.078	3.584	0.087	3.556	0.089	3.38	0.101
1.12	9,033	1.107						8.37E-2
1.1	8,870	1.127	3.547	0.076	3.52	0.079	3.368	8.07E-2
1.08	8,711	1.148						6.12E-2
1.05	8,469	1.181	3.529	0.074	3.502	0.074	3.352	3.85E-2
1.02	8,227	1.216						2.03E-2

1	8,005	1.240	3.511	0.068	3.484	0.065	3.317	1.38E-2 [2]
0.99	7,985	1.252						8.97E-3
0.98	7,904	1.265		7.3E-3 [10]				8.63E-3
0.975	7,864	1.272		6.58E-3				
0.9725	7,844	1.275		5.88E-3				
0.97	7,824	1.278		5.49E-3				5.19E-3
0.9675	7,803	1.282		5.30E-3				
0.965	7,783	1.285		5.16E-3		7.7E-3 [10]		
0.9625	7,763	1.288		4.97E-3		6.66E-3		
0.96	7,743	1.291		4.88E-3		6.11E-3	3.283	4.93E-3
0.9575	7,723	1.295		4.74E-3		5.72E-3		
0.955	7,702	1.298		4.70E-3		5.53E-3		
0.9525	7,682	1.302		4.66E-3		5.39E-3		
0.95	7,662	1.305	3.502	4.62E-3	3.475	5.30E-3		4.67E-3
0.9475	7,642	1.309		4.58E-3		5.15E-3		
0.945	7,622	1.312		4.56E-3		5.06E-3		
0.9425	7,602	1.316		4.55E-3		5.02E-3		
0.94	7,582	1.319		4.51E-3		4.98E-3		
0.935	7,541	1.326		4.50E-3		4.91E-3		
0.93	7,501	1.333		4.51E-3		4.83E-3		
0.925	7,461	1.340		4.48E-3		4.80E-3		
0.92	7,420	1.348		4.50E-3		4.93E-3		

eV	cm^{-1}	μm	n	k
0.9	7,259	1.378	3.246 [2]	3.51E-3 [2]
0.88	7,098	1.409		3.70E-3
0.86	6,936	1.442	3.227	3.90E-3

(continued)

TABLE I *(Continued)*

Zinc Arsenide

eV	cm^{-1}	μm	n	k
0.84	6,775	1.476		4.11E-3
0.82	6,614	1.512		4.33E-3
0.8	6,452	1.550	3.202	4.69E-3
0.78	6,291	1.589		5.06E-3
0.76	6,130	1.631	3.188	5.58E-3
0.74	5,968	1.675		6.13E-3
0.72	5,807	1.722		6.71E-3
0.7	5,646	1.771	3.17	7.54E-3
0.68	5,485	1.823		8.27E-3
0.66	5,323	1.879	3.159	9.11E-3
0.64	5,162	1.937		1.03E-2
0.62	5,001	2.000		1.16E-2
0.6	4,839	2.066	3.144	1.27E-2
0.59	4,759	2.101		1.34E-2
0.58	4,678	2.138		1.41E-2
0.57	4,597	2.175		1.51E-2
0.56	4,517	2.214		1.58E-2
0.55	4,436	2.254	3.133	1.66E-2
0.54	4,355	2.296		1.73E-2
0.53	4,275	2.339		1.83E-2
0.52	4,194	2.384		1.94E-2
0.51	4,113	2.431		2.03E-2
0.5	4,033	2.480	3.124	2.14E-2
0.49	3,952	2.530		2.23E-2
0.48	3,871	2.583		2.32E-2
0.47	3,791	2.638		2.43E-2

TABLE I *(Continued)*

Zinc Arsenide

eV	cm^{-1}	μm	n	k
0.46	3,710	2.695		2.56E-2
0.45	3,629	2.755	3.117	2.68E-2
0.44	3,549	2.818		2.81E-2
0.43	3,468	2.883		2.95E-2
0.42	3,387	2.952		3.10E-2
0.41	3,307	3.024		3.26E-2
0.4	3,226	3.100	3.113	3.40E-2
0.39	3,145	3.179		3.52E-2
0.38	3,065	3.263		3.61E-2
0.37	2,984	3.351		3.69E-2
0.36	2,904	3.444		3.77E-2
0.35	2,823	3.542	3.113	3.83E-2
0.34	2,742	3.647		3.86E-2
0.33	2,662	3.757		3.92E-2
0.32	2,581	3.875		3.95E-2
0.31	2,501	3.999		4.01E-2
0.3	2,419	4.133	3.109	4.08E-2
0.29	2,339	4.275		4.18E-2
0.28	2,258	4.428		4.37E-2
0.27	2,178	4.592		4.60E-2
0.26	2,097	4.769		4.97E-2
0.25	2,016	4.959	3.103	5.37E-2
0.24	1,936	5.166		5.75E-2

Zinc Phosphide (Zn_3P_2)

J. MISIEWICZ and K. JEZIERSKI
Institute of Physics
Technical University of Wroclaw
Wroclaw, Poland

Zn_3P_2 belongs to the group of II–V semiconducting compounds [1]. It possesses the tetragonal crystal structure described by $P4_2/nmc \equiv D_{4h}^{15}$ space symmetry group. The unit cell of Zn_3P_2 is characterized by the dimensions ratio $c/a \approx \sqrt{2}$ and consists of 40 atoms. The crystal structure of Zn_3P_2 may be regarded as a Na_2O lattice (or anti-fluoride lattice) in which one-quarter of the metal sites are vacant. The main interest of this material arises from its very high photoconductivity within the solar spectrum [2]. Compared to the well-known semiconductors, the number of papers for Zn_3P_2 is limited. The optical properties of this compound were measured over a wide range of photon energies from 3 meV up to 11 eV. The measurements were performed for unpolarized light and for Zn_3P_2 samples with c-axis parallel to the surface, so the results are mixed with both components, $E \| c$ and $E \perp c$. Therefore, the optical constants tabulated later as n and k should be regarded as the average ones. Only within the energy range of 1.35–5 eV were measurements done for the polarizations $E \| c$ and $E \perp c$, so n_e, k_e as well as n_o, k_o could be tabulated.

In the far-infrared region of 30–400 cm^{-1} the reflectivity measurements were performed by Misiewicz *et al.* [3] by using a Bruker model 113 V Fourier interferometer at room and low temperatures. High-quality Zn_3P_2 single crystals with high resistivity and hole concentrations of $\sim 10^{13} cm^{-3}$ were used. To determine the refractive index n and extinction coefficient k the measured spectra were analyzed with the help of a classical oscillator model [4]. The use of the oscillator model gives us the set of parameters that characterize zone center transverse lattice modes in Zn_3P_2 by the formulas

$$\epsilon_1(\omega) = \epsilon_\infty + \sum_{i=1}^{18} \frac{f_i \, \omega_{Ti}^2 (\omega_{Ti}^2 - \omega^2)}{(\omega_{Ti}^2 - \omega^2)^2 + \Gamma_i^2 \omega^2} \tag{1}$$

HANDBOOK OF OPTICAL CONSTANTS OF SOLIDS III

Copyright © 1998 by Academic Press.
All rights of reproduction in any form reserved
ISBN 0-12-544423-0/$25.00.

$$\epsilon_2(\omega) = \sum_{i=1}^{18} \frac{f_i\, \omega_{Ti}^2\, \Gamma_i\, \omega}{(\omega_{Ti}^2 - \omega^2)^2 + \Gamma_i^2 \omega^2}, \tag{2}$$

where ϵ_1 and ϵ_2 are average values of the dielectric constants, ω_{Ti} is the transverse-mode frequency, f_i is the oscillator strength, and Γ_i is the damping parameter. Parameters obtained by Misiewicz *et al.* [4] for room temperature and 10 K are given in Table I. Phonon frequencies determined from the classical oscillator model correspond well with those observed in Raman-scattering experiments [5, 6]. Frequencies of 16 longitudinal optical phonons are determined and shown elsewhere [5]. The n and k values obtained with Eqs. (1) and (2) within the range 30–400 cm^{-1} are presented in Table II. These data are very close to the ones obtained by Kramers–Kronig analysis of reflectivity spectra [3].

The knowledge of the osillator strengths enables us to determine the static dielectric constant, which is given by

$$\epsilon_S = \epsilon_\infty + \sum_{i=1}^{N} f_i. \tag{3}$$

The value of ϵ_∞ was assumed to be equal to 11 $\pm$ 1.5 in accordance with the data obtained for monocrystals and thin films [7–12]. The value of ϵ_S determined from Eq. 3 was equal to 33 (at 300 K) and was within the range of values determined from electrical measurements for Zn_3P_2 grown by different methods [13].

Within the 380–1200 cm^{-1} wave-number range, where there are multiphonon transitions, the optical-constant measurements were carried out with both the Fourier interferometer and Beckman spectrometer [3, 5]. The transmission spectrum within the 400–750 cm^{-1} wave-number range was presented by Radautsan *et al.* [14]. For energies smaller than 0.2 eV (1600 cm^{-1}) a strong absorption increase is observed in high-concentration Zn_3P_2 samples ($p \geq 10^{17}$ cm^{-3}) [15]. Within the 0.2–1.3 eV energy range, optical constants do not vary much. The refractive index for this range was found equal to 3.3 $\pm$ 0.1 [7–9]. The fundamental absorption edge for bulk Zn_3P_2 was investigated from 1.3 to 1.6 eV elsewhere [8, 9, 16–19]. Data presented in these papers are in good agreement, except for results published by Sobolev and Syrbu [19]. For energy higher than 1.6 eV, only transmission data for thin films are available [8–12]. The high-quality thin films of Zn_3P_2 with thicknesses below 0.5 μm were obtained by thermal vacuum evaporation onto the glass substrate. A standard optical system was used in the optical measurements.

The values of extinction coefficient given in Table II for energies smaller than 1.6 eV are derived directly from the absorption coefficient determined by means of transmission measurements [5, 15]. High-quality Zn_3P_2 single

crystals of two types, with hole concentrations higher than 10^{17} cm^{-3} and lower than 10^{16} cm^{-3}, were used in the measurements. The transmission was measured with high-resolution spectrometers, according to the wavenumber range: with a GDM 1000 from 0.77 to 1.3 μm, with a Carry II from 1.2 to 2.5 μm, and with a Beckman spectrophotometer from 2.5 to 10 μm.

In the visible and ultraviolet regions the values of n and k are provided by Kramers–Kronig analysis of the reflectivity spectra for single crystals of Zn_3P_2. The published reflectivity spectra were measured within different energy ranges, namely by Sobolev and Syrbu [19] within the energy range of 1–12 eV, by Misiewicz and Jezierski [20] within the 4–11 eV energy range, by Fagen [8] from 1.4 to 5 eV, by Jezierski *et al.* [21] from 2.2 to 5.8 eV, and by Misiewicz *et al.* [7] from 1.2 to 5.2 eV. The values of reflectivity presented by Sobolev and Syrbu [19] are much smaller than those reported by Misiewicz and Jezierski [20], especially for energies higher than 3.5 eV. This difference is related to the quality of the samples. Therefore, the Kramers–Kronig analysis was performed only for the spectrum with higher reflectivity values [20]. The n and k values are given in Table II for energies greater than 5 eV.

For the lower energies K-K analysis was based on the reflectivity spectrum chosen from the spectra published by Jezierski *et al.* [21]. The chosen spectrum was characterized by the highest reflectivity value ($R = 0.524$) at the second maximum. This value indicates a good-quality sample with a well-prepared surface. The surface preparation involved polishing with aluminum-oxide powder of decreasing grain size (1.0, 0.3, and 0.05 μm) and etching in 1% bromine–methanol solution [21]. It is worthwhile to notice that the highest value obtained by Fagen ($R = 0.5$ at the second peak) [8] is very close to that just mentioned. The values from K-K analysis for the spectrum chosen from those measured by Jezierski *et al.* [21] are tabulated for the energy range 1.93–5.7 eV.

For energies lower than 2.2 eV, the reflectivity was calculated by K-K analysis [22] from a knowledge of the absorption coefficient in this range. For energies lower than 1.93 eV, the n values given in Table II were characteristic of the K-K analysis of the reflectivity spectra measured down to 1.2 eV, for example, the spectrum given by Misiewicz *et al.* [7]. These values of n are decreasing to the value 3.32 with decreasing energy. The spectra for n and k for unpolarized light over a wide spectral range are presented in Fig. 1.

The measured optical spectra of Zn_3P_2 showed anisotropy, which was observed for the fundamental absorption edge [16, 18] and in the reflectivity spectra within the visible and ultraviolet energy range [23]. The measurements were performed at room temperature by using x-ray oriented Zn_3P_2 single crystals obtained from a gas-transport growth method. A double-grating Carl-Zeiss GDM-1000 monochromator equipped with linear polarizers from Carl-Zeiss and a Hamamatsu photomultiplier were utilized. Within the 0.9–1.0 eV energy range, a HgCdTe-based detector was used. The de-

termined values of n_e, n_o and k_e, k_o are also included in Table II and presented in Figs. 2 and 3.

The small birefringence in Zn_3P_2 was measured within the 0.5–1.44 eV energy range [24, 25]. The birefringence value increased from 0.0156 at 0.5 eV, through 0.0165 at 1.1 eV and 0.0176 at 1.30 eV, up to 0.0200 at 1.44 eV.

REFERENCES

1. E. K. Arushanov, *Prog. Cryst. Growth Charact.* **25**, 131 (1992).
2. J. M. Pawlikowski, *Rev. Solid State Sci.* **2**, 581 (1988); J. Misiewicz, L. Bryja, K. Jezierski, J. Szatkowski, N. Mirowska, Z. Gumienny, and E. Placzek-Popko, *Microelectron. J.* **25**, 23 (1994).
3. J. Misiewicz, J. M. Wróbel, and B. P. Clayman, *Solid State Commun.* **66**, 747 (1988).
4. J. Misiewicz, A. Lemiec, K. Jezierski, J. M. Wróbel, and B. P. Clayman, *Infrared Phys. Technol.* **35**, 775 (1994).
5. J. Misiewicz, *J. Phys. Condens. Matter* **1**, 9283 (1989).
6. G. Pangilinan, R. Sooryakumar, and J. Misiewicz, *Phys. Rev. B* **44**, 2582 (1991).
7. J. Misiewicz, J. Wróbel, and B. Sujak-Cyrul, *Opt. Appl.* **10**, 75 (1980).
8. E. A. Fagen, *J. Appl. Phys.* **50**, 6505 (1979).
9. L. Żdanowicz, W. Żdanowicz, D. Petelenz, and K. Kloc, *Acta Phys. Pol.* **A57**, 159 (1980).
10. K. R. Murali, B. S. V. Gopalam, and J. Sabhanadri, *Thin Solid Films* **136**, 275 (1986).
11. J. L. Deiss, B. Elidrissi, M. Robino, and R. Weil, *Appl. Phys. Lett.* **49**, 969 (1986).
12. A. Weber, P. Sutter, and H. von Kanel, *J. Appl. Phys.* **75**, 7448 (1994).
13. A. Subrahmanyam, K. R. Murali, B. S. V. Gopalam, and J. Sobhanadri, *Phys. Status Solidi A* **88**, 681 (1985).
14. R. S. Radautsan, N. N. Syrbu, J. J. Nebola, and K. J. Volodina, *Sov. Phys. Solid State* **19**, 1290 (1977).
15. J. Misiewicz, *J. Phys. Chem. Solids* **50**, 1013 (1988).
16. V. Munoz, D. Decroix, A. Chery, and J. M. Besson, *J. Appl. Phys.* **60**, 3282 (1986).
17. J. M. Pawlikowski, J. Misiewicz, and N. Mirowska, *J. Phys. Chem. Solids* **40**, 1027 (1979).
18. J. Misiewicz, *J. Phys. Condens. Matter* **2**, 2053 (1990).
19. V. V. Sobolev and N. N. Syrbu, *Phys. Status Solidi B* **64**, 423 (1974).
20. J. Misiewicz and K. Jezierski, *Solid State Commun.* **70**, 465 (1989).
21. K. Jezierski, J. Misiewicz, and F. Królicki, *Phys. Status Solidi A* **112**, K135 (1989).
22. K. Jezierski, *J. Phys. C: Solid State Phys.* **17**, 475 (1984).
23. J. Misiewicz, J. Wróbel, and K. Jezierski, *J. Phys. C: Solid State Phys.* **17**, 3091 (1984).
24. J. Misiewicz and J. A. Gaj, *Phys Status Solidi B* **105**, K23 (1981).
25. J. Misiewicz, N. Mirowska, and Z. Gumienny, *Phys. Status Solidi A* **83**, K51 (1984).

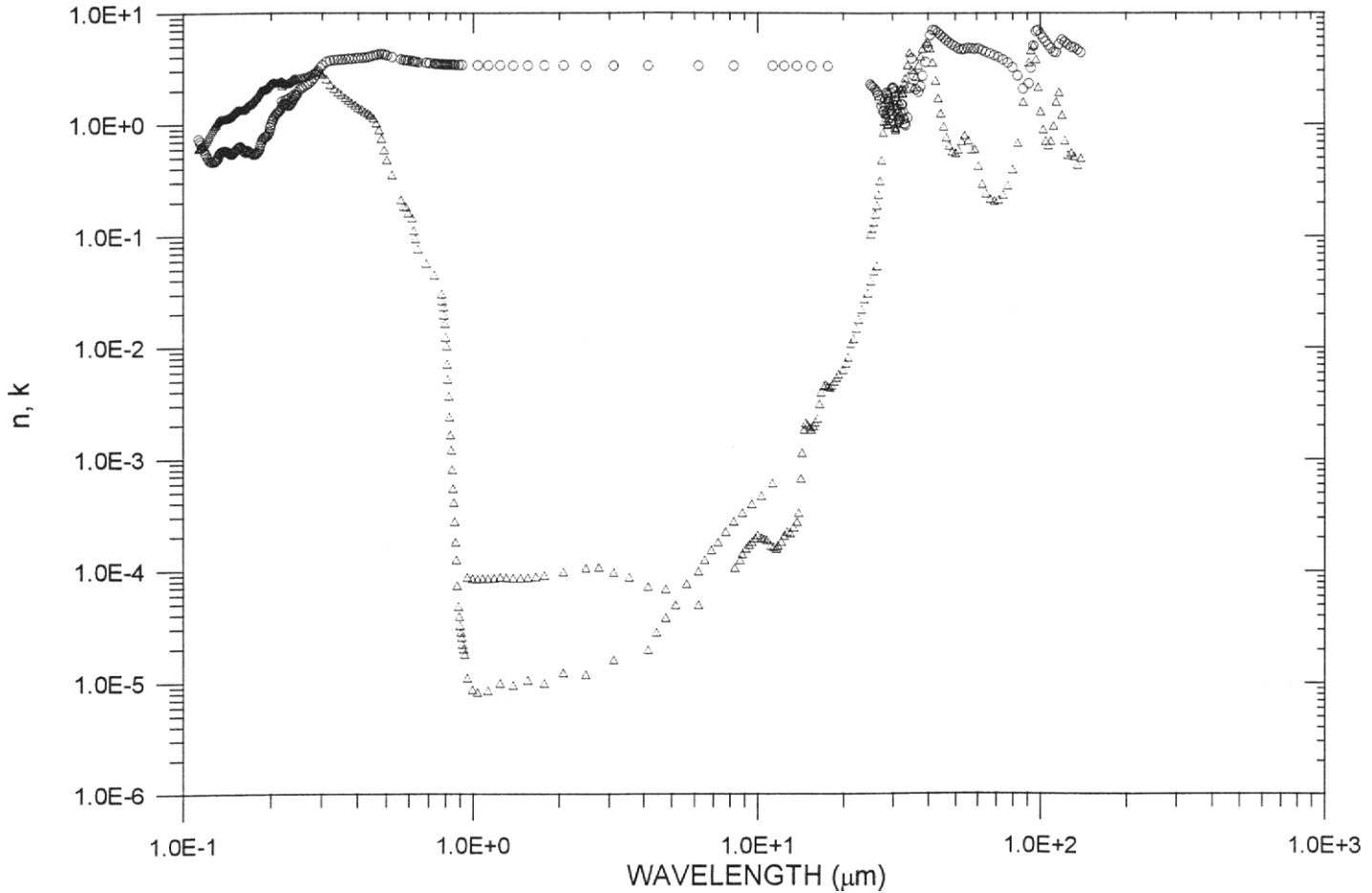

Fig. 1. Log–log plot of n (circles) and k (triangles) versus wavelength in micrometers for zinc phosphide.

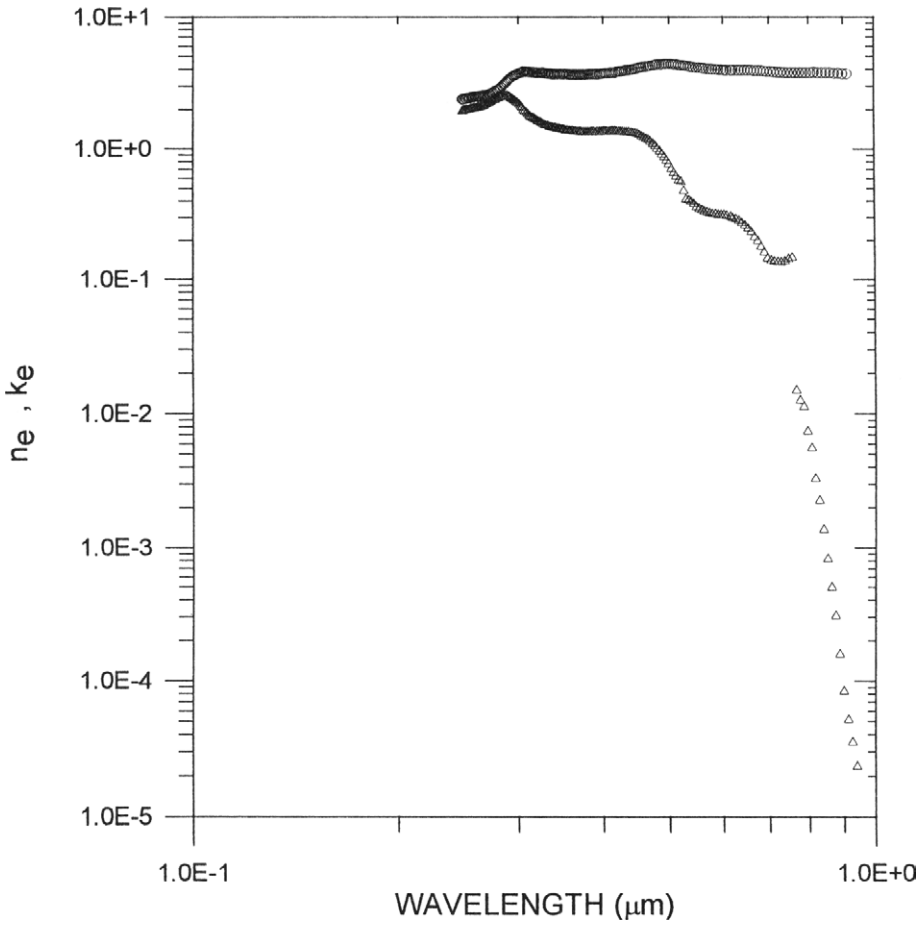

Fig. 2. Log–log plot of n_e (circles) and k_e (triangles) versus wavelength in micrometers for zinc phosphide.

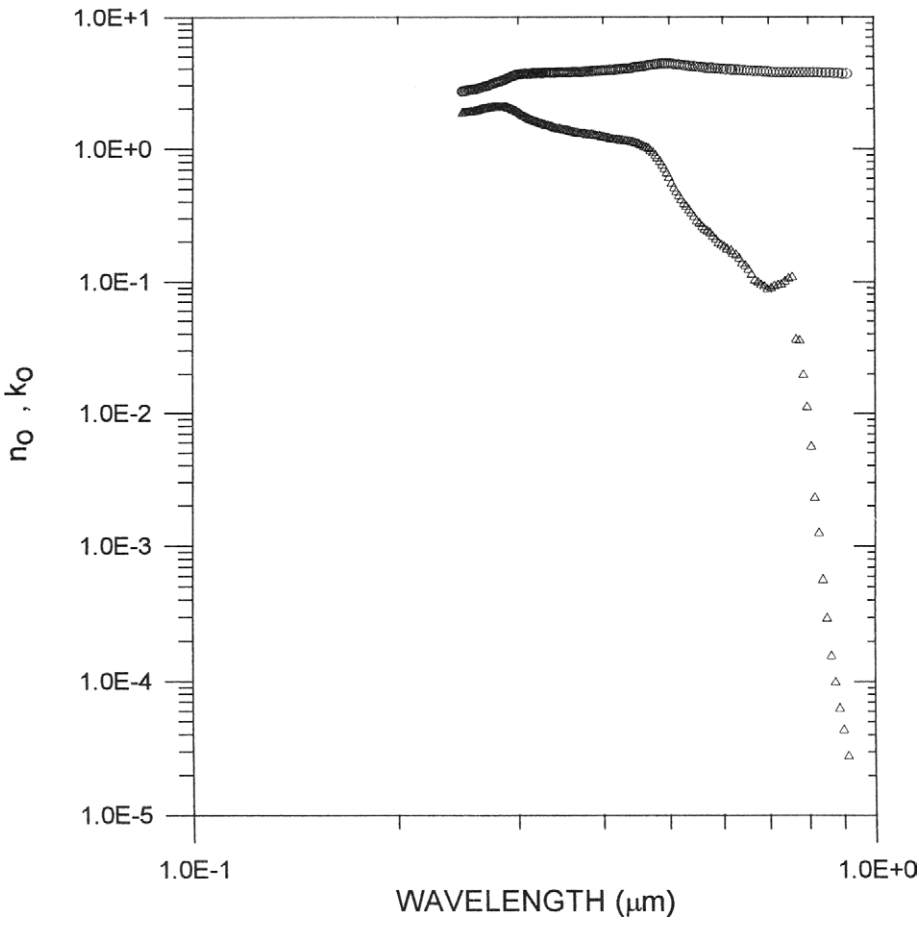

Fig. 3. Log–log plot of n_o (circles) and k_o (triangles) versus wavelength in micrometers for zinc phosphide.

TABLE I

Values of the Oscillator Parameters Obtained from a Fit to the Zn_3P_2 Reflectivity Spectrum in the Reststrahlen Region from Misiewicz *et al.* [4]

	10 K			300 K		
i	ω_{Ti} (cm^{-1})	f_i	Γ_i (cm^{-1})	ω_{Ti} (cm^{-1})	f_i	Γ_i (cm^{-1})
1	46	10.32	5.5	40	3.2	5.39
2	48	0.01	0.36	44	4.16	4.09
3	52	2.2	3.54	48	5.79	6.99
4	62	0.27	1.21	64	0.35	2.88
5	70	0.27	1.06	70	0.18	5.51
6	77	0.11	1.02	77	0.09	3.11
7	89	1.54	3.56	86	1.12	5.35
8	105	0.19	2.59	105	0.15	5.96
9	112	0.23	2.76	112	0.23	18.9
10	171	0.39	4.2	169	0.13	9.37
11	184	0.68	4.96	184	0.57	20.4
12	252	4.86	9.15	246	6.03	24.1
13	287	1.06	6.01	287	0.61	7.11
14	302	0.02	1.7	—	—	—
15	314	0.11	2.61	310	0.08	7.37
16	331	0.03	4.33	331	0.03	7.91
17	341	0.2	8.06	337	0.14	11.1
18	357	0.1	7.75	353	0.1	10.5

TABLE II

Values of n and k Obtained from Various References for Zinc Phosphide[a]

eV	cm^{-1}	μm	n	k
11	88,720	0.1127	0.739 [20]	0.615 [20]
10.9	87,910	0.1137	0.702	0.626
10.8	87,110	0.1148	0.665	0.637
10.7	86,300	0.1159	0.629	0.657
10.6	85,490	0.1170	0.601	0.671
10.5	84,690	0.1181	0.564	0.696
10.4	83,880	0.1192	0.538	0.721
10.3	83,070	0.1204	0.511	0.756
10.2	82,270	0.1216	0.493	0.788
10.1	81,460	0.1228	0.472	0.831
10	80,650	0.1240	0.469	0.872
9.9	79,850	0.1252	0.464	0.912
9.8	79,040	0.1265	0.467	0.949
9.7	78,230	0.1278	0.47	0.987
9.65	77,830	0.1285	0.473	1.005
9.6	77,430	0.1292	0.476	1.025
9.55	77,030	0.1298	0.48	1.045
9.5	76,620	0.1305	0.489	1.07
9.45	76,220	0.1312	0.505	1.087
9.4	75,810	0.1319	0.523	1.108
9.35	75,410	0.1326	0.55	1.11
9.3	75,010	0.1333	0.56	1.11
9.25	74,610	0.1340	0.569	1.111
9.2	74,200	0.1348	0.575	1.112
9.15	73,800	0.1355	0.578	1.113

(continued)

[a] References given in brackets.

TABLE II *(Continued)*

Zinc Phosphide

eV	cm^{-1}	μm	n	k
9.1	73,400	0.1362	0.581	1.115
9.05	72,990	0.1370	0.582	1.119
9	72,590	0.1378	0.582	1.122
8.95	72,190	0.1385	0.58	1.127
8.9	71,780	0.1393	0.579	1.133
8.85	71,380	0.1401	0.578	1.14
8.8	70,980	0.1409	0.575	1.146
8.75	70,570	0.1417	0.571	1.154
8.7	70,170	0.1425	0.566	1.163
8.65	69,770	0.1433	0.56	1.173
8.6	69,360	0.1442	0.551	1.19
8.55	68,960	0.1450	0.548	1.206
8.5	68,560	0.1459	0.546	1.227
8.45	68,150	0.1467	0.548	1.246
8.4	67,750	0.1476	0.551	1.268
8.35	67,350	0.1485	0.561	1.287
8.3	66,940	0.1494	0.568	1.305
8.25	66,540	0.1503	0.58	1.321
8.2	66,140	0.1512	0.591	1.335
8.15	65,730	0.1521	0.608	1.346
8.1	65,330	0.1531	0.619	1.348
8.05	64,930	0.1540	0.624	1.35
8	64,520	0.1550	0.631	1.353
7.95	64,120	0.1560	0.635	1.353
7.9	63,720	0.1569	0.634	1.351
7.85	63,310	0.1579	0.624	1.344
7.8	62,910	0.1590	0.603	1.36

7.75	62,510	0.1600	0.597	1.377		
7.7	62,100	0.1610	0.587	1.389		
7.65	61,700	0.1621	0.572	1.41		
7.6	61,300	0.1631	0.564	1.446		
7.55	60,890	0.1642	0.578	1.473		
7.5	60,490	0.1653	0.583	1.488		
7.45	60,090	0.1664	0.587	1.501		
7.4	59,680	0.1675	0.581	1.511		
7.35	59,280	0.1687	0.569	1.53		
7.3	58,880	0.1698	0.561	1.555		
7.25	58,470	0.1710	0.553	1.582		
7.2	58,070	0.1722	0.546	1.614		
7.15	57,670	0.1734	0.542	1.65		
7.1	57,260	0.1746	0.543	1.686		
7.05	56,860	0.1759	0.545	1.723		
7	56,460	0.1771	0.546	1.764		
6.95	56,050	0.1784	0.554	1.807		
6.9	55,650	0.1797	0.563	1.855		
6.85	55,250	0.1810	0.582	1.903		
6.8	54,850	0.1823	0.605	1.96		
6.75	54,440	0.1837	0.654	2.007		
6.7	54,040	0.1851	0.701	2.024		
6.65	53,640	0.1864	0.732	2.035		
6.6	53,230	0.1879	0.751	2.051		
eV	cm^{-1}	μm	n	k	n	k
6.55	52,830	0.1893	0.769	2.069		
6.5	52,420	0.1907	0.778	2.091		
6.45	52,020	0.1922	0.783	2.126		
6.4	51,620	0.1937	0.798	2.175		
6.35	51,210	0.1953	0.825	2.223		

(continued)

TABLE II *(Continued)*

Zinc Phosphide

eV	cm^{-1}	μm	n	k	n	k
6.3	50,810	0.1968	0.862	2.294		
6.25	50,410	0.1984	0.942	2.337		
6.2	50,010	0.2000	1.004	2.355		
6.15	49,600	0.2016	1.062	2.363		
6.1	49,200	0.2033	1.113	2.372		
6.05	48,800	0.2049	1.168	2.384		
6	48,390	0.2066	1.221	2.375		
5.95	47,990	0.2084	1.259	2.355		
5.9	47,590	0.2101	1.271	2.355		
5.85	47,180	0.2119	1.29	2.371		
5.8	46,780	0.2138	1.321	2.391		
5.75	46,380	0.2156	1.363	2.423		
5.7	45,970	0.2175	1.435	2.425		
5.687	45,870	0.218			1.616 [21]	2.225 [21]
5.65	45,570	0.2194	1.496	2.405		
5.6	45,170	0.2214	1.528	2.365		
5.55	44,760	0.2234	1.539	2.342		
5.535	44,640	0.224			1.651	2.307
5.5	44,360	0.2254	1.531	2.308		
5.45	43,960	0.2275	1.493	2.315		
5.438	43,860	0.228			1.691	2.35
5.4	43,550	0.2296	1.476	2.363		
5.344	43,100	0.232			1.726	2.403
5.35	43,150	0.2317	1.486	2.429		
5.3	42,750	0.2339	1.524	2.484		
5.254	42,380	0.236			1.78	2.458
5.25	42,340	0.2362	1.579	2.551		
5.2	41,940	0.2384	1.666	2.57		

5.166	41,670	0.24			1.843	2.506		
5.15	41,540	0.2407	1.731	2.572				
5.1	41,130	0.2431	1.789	2.579				
5.061	40,820	0.245			1.93	2.568		
5.05	40,730	0.2455	1.85	2.573				
eV	cm^{-1}	μm	n_e	k_e	n_o	k_o	n	k
5	40,330	0.2480	2.388 [23]	1.988 [23]	2.692 [23]	1.879 [23]		
4.98	40,170	0.2490	2.399	2	2.705	1.891		
4.96	40,000	0.2500	2.408	2.009	2.72	1.896	2.024 [21]	2.608 [21]
4.94	39,840	0.2510	2.417	2.017	2.732	1.899		
4.92	39,680	0.2520	2.426	2.026	2.743	1.904		
4.9	39,520	0.2530	2.429	2.036	2.758	1.906		
4.88	39,360	0.2541	2.443	2.051	2.765	1.91		
4.86	39,200	0.2551	2.457	2.059	2.772	1.917	2.102	2.637
4.84	39,040	0.2562	2.467	2.068	2.782	1.92		
4.82	38,880	0.2572	2.478	2.077	2.789	1.927		
4.8	38,710	0.2583	2.487	2.086	2.8	1.938		
4.78	38,550	0.2594	2.497	2.095	2.81	1.944		
4.769	38,460	0.26					2.185	2.669
4.76	38,390	0.2605	2.505	2.104	2.82	1.956		
4.74	38,230	0.2616	2.513	2.117	2.832	1.967		
4.72	38,070	0.2627	2.523	2.13	2.846	1.979		
4.7	37,910	0.2638	2.534	2.142	2.859	1.991		
4.68	37,750	0.2649	2.538	2.149	2.881	2.007	2.252	2.714
4.66	37,580	0.2661	2.545	2.168	2.903	2.011		
4.64	37,420	0.2672	2.548	2.192	2.918	2.02		
4.62	37,260	0.2684	2.552	2.219	2.936	2.033		
4.6	37,100	0.2695	2.573	2.245	2.958	2.042		
4.592	37,040	0.27					2.325	2.78
4.58	36,940	0.2707	2.573	2.272	2.985	2.053		

(continued)

TABLE II *(Continued)*

Zinc Phosphide

eV	cm^{-1}	μm	n_e	k_e	n_o	k_o	n	k
4.56	36,780	0.2719	2.604	2.299	3.009	2.056		
4.54	36,620	0.2731	2.609	2.33	3.029	2.062		
4.52	36,460	0.2743	2.648	2.361	3.057	2.07		
4.509	36,370	0.275					2.447	2.858
4.5	36,290	0.2755	2.682	2.395	3.085	2.073		
4.48	36,130	0.2768	2.723	2.419	3.111	2.075		
4.46	35,970	0.2780	2.746	2.444	3.147	2.074		
4.44	35,810	0.2792	2.794	2.472	3.168	2.07		
4.428	35,710	0.28					2.58	2.928
4.42	35,650	0.2805	2.828	2.505	3.192	2.068		
4.4	35,490	0.2818	2.888	2.525	3.215	2.072		
4.38	35,330	0.2831	2.939	2.553	3.243	2.072		
4.36	35,170	0.2844	3.014	2.573	3.271	2.073		
4.35	35,080	0.285					2.784	3.009
4.34	35,000	0.2857	3.085	2.575	3.298	2.073		
4.32	34,840	0.2870	3.15	2.581	3.334	2.076		
4.3	34,680	0.2883	3.222	2.584	3.374	2.07		
4.28	34,520	0.2897	3.307	2.573	3.41	2.055		
4.275	34,480	0.29					3.017	3.004
4.26	34,360	0.2910	3.381	2.539	3.442	2.043		
4.24	34,200	0.2924	3.44	2.502	3.475	2.026		
4.22	34,040	0.2938	3.536	2.457	3.529	1.997		
4.203	33,900	0.295					3.217	2.915
4.2	33,880	0.2952	3.572	2.425	3.544	1.98		
4.18	33,710	0.2966	3.619	2.376	3.569	1.963		
4.16	33,550	0.2980	3.656	2.329	3.599	1.935		
4.14	33,390	0.2995	3.698	2.29	3.625	1.905		
4.133	33,330	0.3					3.378	2.81

4.12	33,230	0.3009	3.748	2.239	3.645	1.872		
4.1	33,070	0.3024	3.769	2.177	3.658	1.844		
4.08	32,910	0.3039	3.799	2.121	3.659	1.805		
4.06	32,750	0.3054	3.871	2.031	3.688	1.776		
4.04	32,580	0.3069	3.847	1.984	3.692	1.761		
4.02	32,420	0.3084	3.827	1.941	3.688	1.736		
4	32,260	0.31	3.828	1.885	3.696	1.713	3.645	2.548
3.98	32,100	0.3115	3.832	1.831	3.704	1.684		
3.96	31,940	0.3131	3.814	1.801	3.703	1.672		
3.94	31,780	0.3147	3.802	1.773	3.708	1.655		
3.92	31,620	0.3163	3.797	1.746	3.708	1.636		
3.9	31,450	0.3179	3.788	1.725	3.709	1.629		
3.88	31,290	0.3195	3.791	1.69	3.723	1.611		
3.875	31,250	0.32					3.751	2.271
3.86	31,130	0.3212	3.784	1.657	3.732	1.584		
3.84	30,970	0.3229	3.774	1.637	3.722	1.567		
3.82	30,810	0.3246	3.771	1.619	3.724	1.565		
3.8	30,650	0.3263	3.765	1.588	3.731	1.548		
3.78	30,490	0.3280	3.755	1.564	3.737	1.533		
3.76	30,330	0.3297	3.744	1.547	3.737	1.52		
3.757	30,300	0.33					3.775	2.078
3.74	30,160	0.3315	3.73	1.533	3.738	1.512		
3.72	30,000	0.3333	3.722	1.516	3.742	1.498		
3.7	29,840	0.3351	3.711	1.507	3.745	1.492		
3.68	29,680	0.3369	3.702	1.494	3.753	1.477		
3.66	29,520	0.3388	3.704	1.484	3.758	1.458		
3.647	29,410	0.34					3.793	1.943
3.64	29,360	0.3406	3.698	1.476	3.757	1.451		
3.62	29,200	0.3425	3.7	1.458	3.767	1.435		
3.6	29,040	0.3444	3.692	1.455	3.765	1.43		
3.58	28,870	0.3463	3.687	1.449	3.769	1.423		

(continued)

TABLE II *(Continued)*

Zinc Phosphide

eV	cm^{-1}	μm	n_e	k_e	n_o	k_o	n	k
3.56	28,710	0.3483	3.689	1.44	3.771	1.412		
3.542	28,570	0.35					3.821	1.837
3.54	28,550	0.3502	3.682	1.43	3.772	1.408		
3.52	28,390	0.3522	3.68	1.419	3.779	1.397		
3.5	28,230	0.3542	3.675	1.412	3.784	1.388		
3.48	28,070	0.3563	3.672	1.406	3.789	1.379		
3.46	27,910	0.3583	3.667	1.405	3.792	1.373		
3.444	27,780	0.36					3.85	1.733
3.44	27,750	0.3604	3.667	1.398	3.8	1.36		
3.42	27,580	0.3625	3.665	1.395	3.8	1.351		
3.4	27,420	0.3647	3.665	1.39	3.805	1.342		
3.38	27,260	0.3668	3.67	1.381	3.813	1.327		
3.36	27,100	0.3690	3.667	1.381	3.811	1.324		
3.351	27,030	0.37					3.87	1.641
3.34	26,940	0.3712	3.666	1.38	3.814	1.32		
3.32	26,780	0.3734	3.667	1.377	3.813	1.32		
3.3	26,620	0.3757	3.671	1.373	3.83	1.318		
3.28	26,450	0.378	3.671	1.373	3.837	1.297		
3.263	26,320	0.38					3.886	1.558
3.26	26,290	0.3803	3.674	1.37	3.841	1.295		
3.24	26,130	0.3827	3.674	1.372	3.844	1.293		
3.22	25,970	0.385	3.676	1.378	3.853	1.296		
3.2	25,810	0.3875	3.682	1.378	3.865	1.286		
3.18	25,650	0.3899	3.692	1.377	3.878	1.275	3.914	1.483
3.16	25,490	0.3924	3.697	1.38	3.887	1.27		
3.14	25,330	0.3949	3.706	1.386	3.895	1.265		
3.12	25,160	0.3974	3.715	1.383	3.907	1.253		
3.1	25,000	0.4	3.722	1.387	3.913	1.246	3.935	1.411

3.08	24,840	0.4025	3.736	1.389	3.921	1.236		
3.06	24,680	0.4052	3.749	1.388	3.93	1.231		
3.04	24,520	0.4078	3.756	1.386	3.941	1.22		
3.024	24,390	0.41					3.954	1.356
3.02	24,360	0.4105	3.764	1.391	3.951	1.207		
3	24,200	0.4133	3.78	1.403	3.958	1.204		
2.98	24,030	0.4161	3.782	1.409	3.969	1.192		
2.96	23,870	0.4189	3.873	1.389	3.977	1.19		
2.952	23,810	0.42					3.981	1.304
2.94	23,710	0.4217	3.876	1.382	3.988	1.187		
2.92	23,550	0.4246	3.881	1.378	4	1.18		
2.9	23,390	0.4275	3.898	1.378	4.011	1.177		
2.883	23,250	0.43					4.013	1.254
2.88	23,230	0.4305	3.92	1.376	4.028	1.171		
2.86	23,070	0.4335	3.941	1.375	4.044	1.169		
2.84	22,910	0.4366	3.97	1.37	4.063	1.157		
2.82	22,740	0.4397	3.997	1.362	4.081	1.15		
2.818	22,730	0.44					4.069	1.207
2.8	22,580	0.4428	4.027	1.354	4.105	1.139		
2.78	22,420	0.4460	4.058	1.342	4.123	1.125		
2.76	22,260	0.4492	4.091	1.33	4.147	1.117		
2.755	22,220	0.45					4.145	1.139
2.74	22,100	0.4525	4.137	1.31	4.177	1.1		
2.72	21,940	0.4558	4.169	1.276	4.203	1.078		
2.7	21,780	0.4592	4.188	1.245	4.216	1.055		
2.695	21,740	0.46					4.215	1.031
2.68	21,610	0.4626	4.211	1.225	4.241	1.044		
2.66	21,540	0.4661	4.244	1.206	4.28	1.023		
2.64	21,290	0.4696	4.282	1.169	4.301	0.988		
2.638	21,280	0.47					4.265	0.889
2.62	21,130	0.4732	4.311	1.126	4.331	0.959		
2.6	20,970	0.4769	4.338	1.081	4.358	0.915		

(continued)

TABLE II *(Continued)*

Zinc Phosphide

eV	cm^{-1}	μm	n_e	k_e	n_o	k_o	n	k
2.583	20,830	0.48					4.275	0.748
2.58	20,810	0.4806	4.357	1.034	4.378	0.872		
2.56	20,650	0.4843	4.369	0.983	4.393	0.821		
2.54	20,490	0.4881	4.379	0.933	4.401	0.768		
2.53	20,410	0.49					4.226	0.59
2.52	20,320	0.4920	4.388	0.891	4.405	0.723		
2.5	20,160	0.4959	4.397	0.841	4.408	0.673		
2.48	20,000	0.4999	4.4	0.788	4.402	0.62	4.166	0.482
2.46	19,840	0.5040	4.398	0.727	4.389	0.563		
2.44	19,680	0.5081	4.384	0.678	4.369	0.523		
2.42	19,520	0.5123	4.364	0.635	4.343	0.487		
2.4	19,360	0.5166	4.344	0.594	4.322	0.454		
2.384	19,230	0.52					4.032	0.356
2.38	19,200	0.5209	4.313	0.579	4.299	0.425		
2.36	19,030	0.5254	4.3	0.495	4.276	0.397		
2.34	18,870	0.5299	4.276	0.424	4.251	0.378		
2.32	18,710	0.5344	4.237	0.418	4.232	0.354		
2.3	18,550	0.5391	4.2	0.408	4.211	0.337		
2.28	18,390	0.5438	4.175	0.392	4.189	0.316		
2.26	18,230	0.5486	4.152	0.368	4.17	0.294		
2.24	18,070	0.5535	4.121	0.358	4.15	0.282		
2.22	17,900	0.5585	4.096	0.349	4.131	0.265		
2.214	17,860	0.56					3.846	0.214 [15]
2.2	17,740	0.5636	4.075	0.342	4.11	0.253		
2.18	17,580	0.5687	4.051	0.337	4.089	0.246		
2.16	17,420	0.5740	4.032	0.332	4.075	0.238	3.786	0.185
2.14	17,260	0.5794	4.013	0.327	4.065	0.224		
2.13	17,180	0.5821					3.76	0.183

2.12	17,100	0.5848	4	0.327	4.046	0.213		
2.1	16,940	0.5904	3.988	0.321	4.031	0.2		
2.09	16,860	0.5932					3.731	0.161
2.08	16,780	0.5961	3.978	0.322	4.016	0.194		
2.06	16,610	0.6019	3.97	0.321	4.001	0.188		
2.04	16,450	0.6078	3.965	0.316	3.986	0.18		
2.03	16,370	0.6108					3.701	0.146
2.02	16,290	0.6158	3.958	0.311	3.975	0.175		
2	16,130	0.6199	3.954	0.305	3.961	0.167	3.681	0.113
1.98	15,970	0.6262	3.949	0.299	3.949	0.163		
1.97	15,890	0.6294					3.649	0.095
1.96	15,810	0.6326	3.948	0.291	3.942	0.154		
1.94	15,650	0.6391	3.948	0.279	3.929	0.141		
1.93	15,570	0.6424					3.611	0.077
1.92	15,490	0.6458	3.944	0.267	3.918	0.136		
1.9	15,320	0.6526	3.941	0.254	3.907	0.127		
1.88	15,160	0.6595	3.938	0.238	3.895	0.117		
1.86	15,000	0.6666	3.93	0.218	3.879	0.105		
1.84	14,840	0.6738	3.921	0.203	3.862	0.102		
1.82	14,680	0.6812	3.911	0.184	3.849	0.097		
1.81	14,600	0.6850					3.576 [7]	0.057
1.8	14,520	0.6888	3.895	0.166	3.834	0.094		
1.78	14,360	0.6965	3.875	0.149	3.82	0.089		
1.76	14,200	0.7045	3.851	0.143	3.803	0.091	3.534	
1.74	14,030	0.7126	3.831	0.141	3.793	0.095		
1.72	13,870	0.7208	3.817	0.14	3.782	0.096		
1.7	13,710	0.7293	3.802	0.139	3.773	0.098	3.503	0.045
1.68	13,550	0.7380	3.784	0.141	3.764	0.103	3.489	
1.66	13,390	0.7469	3.776	0.148	3.761	0.109	3.477	
1.64	13,230	0.7560	3.771	0.152	3.759	0.111	3.47	
1.62	13,070	0.7653	3.768	1.53E-2 [18]	3.761	3.72E-2 [18]	3.466	

(continued)

TABLE II *(Continued)*

Zinc Phosphide

eV	cm^{-1}	μm	n_e	k_e	n_o	k_o	n	k
1.6	12,900	0.7749	3.767	1.29E-2	3.759	3.64E-2	3.462	3.02E-2
1.59	12,820	0.7798						2.61E-2
1.58	12,740	0.7847	3.77	1.16E-2	3.762	2.0E-2	3.459	2.31E-2
1.57	12,660	0.7897						1.95E-2
1.56	12,580	0.7948	3.78	7.59E-3	3.763	1.14E-2	3.458	1.64E-2
1.55	12,500	0.7999						1.24E-2
1.54	12,420	0.8051	3.793	5.7E-3	3.765	5.7E-3	3.457	1.03E-2
1.53	12,340	0.8104						7.09E-3
1.52	12,260	0.8157	3.798	3.37E-3	3.768	2.34E-3	3.455	5.19E-3
1.51	12,180	0.8211						3.66E-3
1.5	12,100	0.8266	3.793	2.3E-3	3.762	1.28E-3	3.452	2.37E-3
1.49	12,020	0.8321						1.65E-3
1.48	11,940	0.8377	3.787	1.4E-3	3.751	5.73E-4	3.448	1.20E-3
1.47	11,860	0.8434						8.05E-4
1.46	11,780	0.8492	3.779	8.45E-4	3.743	3.01E-4	3.441	5.41E-4
1.45	11,690	0.8551						4.08E-4
1.44	11,610	0.8610	3.767	5.14E-4	3.733	1.58E-4	3.429	2.74E-4
1.43	11,530	0.8670	0.867					1.79E-4
1.42	11,450	0.8731	3.755	3.13E-4	3.723	1.01E-4		1.25E-4
1.41	11,370	0.8793	0.8793					7.35E-5
1.4	11,290	0.8856	3.743	1.62E-4	3.712	6.41E-5	3.42	4.79E-5
1.39	11,210	0.8920	0.892					3.90E-5
1.38	11,130	0.8984	3.729	8.58E-5	3.702	4.43E-5		3.22E-5
1.37	11,050	0.9050	0.905					2.81E-5
1.36	10,970	0.9117	3.709	5.29E-5	3.69	2.83E-5	3.408	2.54E-5
1.35	10,890	0.9184	0.9184					2.19E-5
1.34	10,810	0.9253		3.61E-5				1.99E-5
1.33	10,730	0.9322	0.9322					1.78E-5

eV	cm^{-1}	μm	n	k	k
1.3	10,480	0.9537		1.1E-5 [15]	8.7E-5 [15]
1.25	10,080	0.9919		8.68E-6	8.44E-5
1.2	9,678	1.033	3.397 [7]	8.22E-6	8.39E-5
1.15	9,275	1.078			8.49E-5
1.1	8,872	1.127	3.387	8.52E-6	8.52E-5
1.05	8,469	1.181			8.55E-5
1	8,065	1.240	3.376	9.87E-6	8.68E-5
0.95	7,662	1.305			8.62E-5
0.9	7,260	1.378	3.367	9.43E-6	8.55E-5
0.85	6,856	1.459			8.59E-5
0.8	6,452	1.550	3.358	1.05E-5	8.63E-5
0.75	6,049	1.653			8.81E-5
0.7	5,646	1.771	3.35	9.87E-6	9.02E-5
0.6	4,839	2.066	3.344	1.23E-5	9.65E-5
0.5	4,033	2.480	3.338	1.18E-5	1.05E-4
0.45	3,629	2.755			1.07E-4
0.4	3,226	3.100	3.334	1.60E-5	9.62E-5
0.35	2,823	3.542			8.74E-5
0.3	2,420	4.133	3.33	1.97E-5	7.23E-5
0.28	2,258	4.428		2.82E-5	
0.26	2,097	4.769		3.79E-5	6.83E-5
0.24	1,936	5.166		4.93E-5	
0.22	1,774	5.636		7.62E-5	
0.2	1,613	6.199	3.327	9.87E-5	4.93E-5
0.19	1,532	6.525		1.25E-4	
0.18	1,452	6.888		1.53E-4	
0.17	1,371	7.293		1.80E-4	
0.16	1,290	7.749		2.22E-4	
0.15	1,209	8.266	3.325	2.76E-4	

(continued)

TABLE II *(Continued)*

Zinc Phosphide

eV	cm^{-1}	μm	n	k	k
0.1488	1,200	8.332			1.06E-4 [5]
0.1426	1,150	8.695			1.25E-4
0.1401	1,130	8.850			1.41E-4
0.14	1,129	8.856		3.31E-4	
0.1364	1,100	9.090			1.59E-4
0.1327	1,070	9.343			1.71E-4
0.1302	1,050	9.523			1.82E-4
0.13	1,048	9.537		3.95E-4	
0.1265	1,020	9.801			1.95E-4
0.1240	1,000	9.999			2.07E-4
0.1203	970	10.31			1.97E-4
0.12	968	10.33		4.69E-4	
0.1178	950	10.52			1.93E-4
0.1153	930	10.75			1.88E-4
0.1116	900	11.11			1.68E-4
0.11	887.2	11.27	3.324	6.10E-4	
0.1091	880	11.36			1.63E-4
0.1066	860	11.63			1.57E-4
0.1054	850	11.76			1.68E-4
0.1029	830	12.05		1.82E-4 [5]	
0.1004	810	12.35	3.324	2.06E-4	
0.0979	790	12.66		2.22E-4	
0.0955	770	12.98		2.17E-4	
0.0930	750	13.33		2.44E-4	
0.0905	730	13.70	3.324	2.73E-4	
0.0893	720	13.88		3.31E-4	
0.0880	710	14.09		6.73E-4	

0.0868	700	14.28		1.14E-3	
0.0855	690	14.50		1.85E-3	
0.0843	680	14.71		2.11E-3	
0.0831	670	14.92		2.02E-3	
0.0818	660	15.16		1.93E-3	
0.0806	650	15.38	3.324	1.84E-3	
0.0794	640	15.61		1.99E-3	
0.0781	630	15.87		2.15E-3	
0.0769	620	16.12		2.31E-3	
0.0756	610	16.40		3.13E-3	
0.0744	600	16.66		3.98E-3	
0.0732	590	16.94		4.58E-3	
0.0719	580	17.24		4.66E-3	
0.0707	570	17.54	3.323	4.46E-3	
0.0694	560	17.86		4.41E-3	
0.0682	550	18.18		4.63E-3	
0.0670	540	18.51		5.01E-3	
0.0657	530	18.87		5.41E-3	
0.0645	520	19.22		5.81E-3	
0.0620	500	20.00		6.36E-3	
0.0608	490	20.39		7.30E-3	
0.0595	480	20.84		8.29E-3	
0.0583	470	21.27		1.10E-2	
0.0570	460	21.75		1.21E-2	
0.0558	450	22.22		1.50E-2	
0.0546	440	22.71		1.81E-2	
0.0533	430	23.26		2.22E-2	
0.0521	420	23.80		2.75E-2	
0.0508	410	24.41		3.11E-2	
0.04959	400	25.00	2.276 [4]	0.105 [4]	3.98E-2 [5]
0.04897	395	25.32	2.212	0.118	

(continued)

TABLE II *(Continued)*

Zinc Phosphide

eV	cm^{-1}	μm	n	k	k
0.04835	390	25.64	2.139	0.135	4.90E-2
0.04773	385	25.98	2.053	0.158	
0.04711	380	26.32	1.951	0.189	5.45E-2
0.04649	375	26.67	1.825	0.236	
0.04587	370	27.03	1.665	0.316	
0.04525	365	27.40	1.463	0.48	
0.04463	360	27.78	1.302	0.85	
0.04439	358	27.93	1.334	1.063	
0.04414	356	28.09	1.473	1.255	
0.04389	354	28.25	1.699	1.333	
0.04364	352	28.41	1.887	1.243	
0.04339	350	28.57	1.918	1.089	
0.04315	348	28.73	1.826	1.002	
0.04290	346	28.90	1.697	1.022	
0.04265	344	29.07	1.598	1.141	
0.04240	342	29.24	1.586	1.325	
0.04215	340	29.41	1.699	1.501	
0.04191	338	29.58	1.911	1.568	
0.04166	336	29.76	2.097	1.475	
0.04141	334	29.94	2.156	1.322	
0.04116	332	30.12	2.147	1.205	
0.04092	330	30.30	2.112	1.072	
0.04067	328	30.49	1.982	0.946	
0.04042	326	30.67	1.792	0.899	
0.04017	324	30.86	1.592	0.928	
0.03992	322	31.06	1.402	1.023	
0.03968	320	31.25	1.239	1.178	
0.03943	318	31.44	1.121	1.384	

0.03918	316	31.64	1.07	1.629
0.03893	314	31.84	1.111	1.888
0.03868	312	32.05	1.282	2.095
0.03844	310	32.25	1.514	2.087
0.03819	308	32.46	1.506	1.918
0.03794	306	32.68	1.3	1.916
0.03769	304	32.89	1.123	2.087
0.03744	302	33.11	1.027	2.332
0.03720	300	33.33	0.994	2.606
0.03658	295	33.89	1.151	3.413

eV	cm^{-1}	μm	n	k
0.03596	290	34.48	2.123	4.425
0.03534	285	35.08	3.91	3.107
0.03472	280	35.71	2.766	2.172
0.03410	275	36.36	2.067	2.676
0.03348	270	37.03	1.965	3.396
0.03286	265	37.73	2.199	4.108
0.03234	260	38.34	2.728	4.796
0.03162	255	39.21	3.638	5.372
0.03100	250	39.99	4.978	5.531
0.03038	245	40.81	6.358	4.858
0.02976	240	41.66	7.045	3.598
0.02914	235	42.55	7.017	2.48
0.02852	230	43.47	6.702	1.732
0.02790	225	44.44	6.339	1.264
0.02728	220	45.45	6.004	0.967
0.02666	215	46.51	5.709	0.775
0.02604	210	47.61	5.449	0.652
0.02542	205	48.77	5.217	0.581

(continued)

TABLE II *(Continued)*

Zinc Phosphide

eV	cm^{-1}	μm	n	k
0.02480	200	49.99	5.005	0.56
0.02418	195	51.28	4.823	0.6
0.02356	190	52.62	4.716	0.711
0.02294	185	54.05	4.767	0.809
0.02232	180	55.55	4.858	0.725
0.02170	175	57.14	4.799	0.599
0.02108	170	58.82	4.759	0.605
0.02046	165	60.60	4.787	0.429
0.01984	160	62.49	4.63	0.297
0.01922	155	64.51	4.472	0.243
0.01860	150	66.66	4.322	0.219
0.01798	145	68.96	4.169	0.21
0.01736	140	71.42	4.003	0.215
0.01674	135	74.06	3.81	0.236
0.01612	130	76.91	3.567	0.287
0.01550	125	79.99	3.235	0.4
0.01488	120	83.32	2.738	0.69
0.01426	115	86.95	2.096	1.588
0.01364	110	90.90	2.329	3.618
0.01339	108	92.60	3.203	4.646
0.01314	106	94.36	5.063	5.162
0.01289	104	96.19	6.885	3.851
0.01265	102	98.01	6.965	2.173
0.01240	100	99.99	6.445	1.307
0.01215	98	102.0	5.944	0.904
0.01190	96	104.2	5.523	0.716
0.01165	94	106.4	5.151	0.654
0.01141	92	108.7	4.794	0.711

0.01116	90	111.1	4.457	0.973
0.01091	88	113.6	4.409	1.602
0.01066	86	116.3	5.253	1.949
0.01041	84	119.1	5.724	1.226
0.01017	82	121.9	5.493	0.722
0.00992	80	125.0	5.181	0.536
0.00967	78	128.2	4.924	0.559
0.00942	76	131.6	4.9	0.52
0.00917	74	135.2	4.665	0.434
0.00893	72	138.8	4.436	0.504
0.00868	70	142.8	4.331	0.62
0.00843	68	147.1	4.182	0.614
0.00818	66	151.6	3.852	0.819
0.00794	64	156.1	4.19	1.371
0.00769	62	161.2	4.22	0.807
0.00744	60	166.6	3.731	0.783
0.00719	58	172.4	3.244	1.041
0.00694	56	178.6	2.778	1.606
0.00670	54	185.0	2.56	2.549
0.00645	52	192.2	2.853	3.685
0.00620	50	200.0	3.804	4.696
0.00595	48	208.4	5.223	4.949
0.00570	46	217.5	6.082	4.734
0.00546	44	227.1	7.621	4.604
0.00521	42	238.0	8.142	3.008
0.00496	40	250.0	8.186	2.444
0.00471	38	263.2	8.279	1.522
0.00446	36	278.0	7.881	0.874
0.00422	34	293.8	7.493	0.562
0.00397	32	312.3	7.196	0.395
0.00372	30	333.3	6.97	0.295

Zinc Germanium Phosphide ($ZnGeP_2$)

J. C. RIFE*
Naval Research Laboratory
Washington, D.C.

$ZnGeP_2$ is a tetragonally bonded semiconductor with the chalcopyrite structure and an effective direct band gap of 2.34 eV at room temperature. The structure, growth, and optical and electronic properties of the chalcopyrite semiconductors have been reviewed in the book by Shay and Wernick [1]. Properties have also been summarized in the Landolt-Börnstein series [2]. The II–IV–V_2 chalcopyrite lattice is equivalent to the III–V semiconductor crystal structure, but with ordering of the II and IV components and so a doubling of the unit cell along the c-axis. The chalcopyrite lattice is typically compressed along the c-axis, leading to a crystalline electric field and birefringence with n_e $(\mathbf{E} \| \mathbf{c}) > n_o$ $(\mathbf{E} \perp \mathbf{c})$, (positive uniaxial crystal). Chalcopyrite semiconductors are also optically active because of varying degrees of tetragonal distortion [3]. The $ZnGeP_2$ crystal structure, in particular, is compressed 2.0% along the c-axis. The $ZnGeP_2$ band gap was given earlier as only an effective direct one at 2.34 eV because, in fact, the lowest-energy electronic transition to the conduction-band minimum is at 1.99 eV at 300 K [4]. That is the weak "pseudodirect" band gap due to the fact that the III–V analog, GaP, has an indirect gap, and the indirect gap is folded to the zone center in the band structure of $ZnGeP_2$. The band structure of $ZnGeP_2$ has been calculated by several authors [5–7].

$ZnGeP_2$ is the most promising material for optical parametric oscillation, where tunable, mid-infrared light is generated from a shorter-wavelength pump laser. This is because $ZnGeP_2$ has a large nonlinear coefficient due to its covalent bonding, can be phase-matched because of its birefringence, has a wide transparency range (0.6 to 13 μm), and can sustain higher pumping powers because of its high thermal conductivity. Attempts to maximize performance by minimizing absorption in the band gap due to defects and im-

* The views presented are those of the author and do not represent the views of the Department of Defense or its components.

HANDBOOK OF OPTICAL CONSTANTS OF SOLIDS III
ISBN 0-12-544423-0/$25.00.

purities are referenced later. Useful second-harmonic generation in $ZnGeP_2$ is limited by its insufficient birefringence.

The optical constants, n and k, listed in Table I and plotted in Fig. 1 are derived from sources discussed in more detail later. The optical constants were taken from tables, calculated from formulae, or extracted from graphs where necessary. The table here has more significant figures than justified in some cases; consult the original work for the actual experimental resolution. Measurements made using polarized radiation were favored for inclusion here; in such cases, the optical constants have been given for both $\mathbf{E} \| \mathbf{c}$ and $\mathbf{E} \perp \mathbf{c}$. All measurements used were made on single crystals at room temperature, except where noted in the text. The following discussion of measurements gives references to additional work on polycrystalline or amorphous specimens.

I X-RAY TO BAND-GAP ABSORPTION EDGE

The optical constants, n and k, for the range from 10,000 to 20 eV have been calculated from the scattering factors of the elements of Henke *et al.* [8] using the compound formula and a density of 4.17 gm/cm^3. In Fig. 1, the K-edge ($1s$) transitions of Ge and Zn appear at 1.1 and 1.3×10^{-4} μm and of P at 5.8×10^{-4} μm; the $L_{2,3}$ ($2p$) transitions of Ge and Zn at 1.0 and 1.2×10^{-3} μm and of P at 9.1×10^{-3} μm; and the $M_{4,5}$ ($3d$) transitions of Ge at 4.1×10^{-2} μm. The calculated edges are a good approximation on the scale of Fig. 1, but the scatttering factors of the elements cannot predict the compound edge locations or structure to high degree (edge within 5 or 10 eV) because of core-level chemical shifts and bonding-dependent redistribution of the absorption at and just above the edges.

Optical constants for the fundamental electronic transitions in the 20 to 2.2 eV range are from Rife *et al.* [9]. They extracted optical constants for single-crystal samples from a Kramers–Kronig analysis of polarized, 80-K temperature reflectance data. De Alvarez and co-workers measured the reflectance from 2 to 5.5 eV at 5 and 300 K and compared with theory, but reported no optical constants [6].

II BAND-GAP ABSORPTION EDGE

Measurements of the absorption coefficient at the absorption edge have been reported by a number of authors with considerable scatter in the data, probably because of the variation of crystal quality and the psuedodirect gap. Isomura and Masumoto [10] give the absorption coefficient ($\alpha = 4\pi k/\lambda$) at

300, 207, and 99 K for unpolarized light from 2.1 to 0.9 eV. Gorban *et al.* show the absorption edge from 2.2 to 1.7 eV at 293 and 80 K, the lower temperature revealing pseudodirect transitions at 2.168 and 2.086 eV [11]. Bendorius *et al.* give the pressure dependence [12].

BAND GAP III

In the transparent gap region from 0.6 to 13 μm, where the two-phonon lattice absorption sets in, the index of refraction for $\mathbf{E} \| \mathbf{c}$ and $\mathbf{E} \perp \mathbf{c}$ has been reported by Boyd *et al.* [13]. They determined the index by the minimum deviation method; however, results for other individual crystals could vary slightly from their results, depending on doping. Their data have been reduced to an analog formula by Wemple *et al.* [14] and by Bhar and Ghosh [15]. At 20° C, the latter find a good fit to a special Sellmeier form,

$$n^2 = A + \frac{B}{1 - \dfrac{C}{\lambda^2}} + \frac{D}{1 - \dfrac{E}{\lambda^2}},$$

where for n_o (A, B, C, D, E) = (4.4733, 5.2658, 0.1338, 1.4909, 662.55) and for n_e (A, B, C, D, E) = (4.6332, 5.3422, 0.1426, 1.4580, 662.55); λ is the wavelength in microns. At 70° C, they find that n_o (A, B, C, D, E) = (4.4492, 5.3338, 0.1353, 1.4736, 662.55) and n_e (A, B, C, D, E) = (4.5717, 5.4513, 0.1435, 1.4262, 662.55). Bhar and Ghosh have also published the temperature dependence of the Sellmeier coefficients for temperatures as high as 400° C and low as −180° C [16].

Absorption in the gap region is sensitive to impurities and doping. Boyd *et al.* [17] measured absorption of high-quality samples in the gap. They observed a large shoulder between 0.6 and 3 μm that has since been attributed to defects. Considerable effort has been expended in the study of this absorption and methods for its reduction, since it is the primary limitation in optical parametric oscillator applications [18–21].

LATTICE ABSORPTION IN THE INFRARED IV

Poplavnoi [22] has reviewed infrared absorption and Raman scattering in $ZnGeP_2$ and a number of other II–IV–V_2 semiconductors. The optical constants in the infrared have been determined by a number of authors from polarized reflectance and transmittance measurements. Most recently, Voitsekhovskii *et al.* [23] have derived a set of harmonic oscillators that match

their data for both polarizations over the 10 to 600 cm^{-1} range and consider the overall picture of the dielectric characteristics in that range complete. Their results compare well with the previous work above 200 cm^{-1} of Miller *et al.* [24] and Markov *et al.* [25], but they find additional modes at 120 and 142 cm^{-1} and measure absorption in the 10 to 120 cm^{-1} range due to free-carrier absorption arising from impurities. Their formula for the dielectric constant $\epsilon(\nu)$ is

$$\epsilon(\nu) = \epsilon_\infty + \sum \frac{S_j \nu^2_j}{(\nu^2_j - \nu^2 - i\nu\gamma_j)},$$

where S_j is the oscillator strength, ν_j is the frequency in cm^{-1}, and γ_j is the damping of the jth oscillator in cm^{-1}. For $\mathbf{E} \| \mathbf{c}$, Voitsekhovskii *et al.* give the three oscillators (S_j, ν_j, γ_j) = (0.48, 397, 7.4), (1.15, 345, 5.5), and (0.02, 120, 0.55) with $\epsilon_\infty = 9.96$; for $\mathbf{E} \perp \mathbf{c}$ they give the five oscillators (S_j, ν_j, γ_j) = (0.50, 386, 3.0), (0.64, 368, 2.3), (0.34, 327, 6.0), (0.18, 202, 4.3), and (0.025, 141.5, 0.72), with $\epsilon_\infty = 9.73$. They determine ϵ_0 (at 13 cm^{-1}) to be 11.6 for $\mathbf{E} \| \mathbf{c}$ and 11.4 for $\mathbf{E} \perp \mathbf{c}$.

REFERENCES

1. J. L. Shay and J. H. Wernick, "Ternary Chalcopyrite Semiconductors: Growth, Electronic Properties, and Applications." Pergamon, New York, 1975.
2. Landolt-Börnstein, "Semiconductors—Physics of Ternary Compounds" (K.-H. Hellwege and O. Madelung, eds.), Vol. 17h, Springer-Verlag, New York, 1985.
3. G. A. Babonas, A. S. Martsinkyavichyus, and A. Yu. Shileika, *Sov. Phys. J.* **29**, 617 (1986).
4. A. Shileika, *Surf. Sci.* **37**, 730 (1973).
5. A. S. Poplavnoi and Y. I. Polygalov, *Sov. Phys. J.* **13**, 766 and 849 (1970).
6. C. V. de Alvarez and M. L. Cohen, *Phys. Rev. Lett.* **20**, 979 (1973); C. V. de Alvarez, M. L. Cohen, S. E. Kohn, Y. Petroff, and Y. R. Shen, *Phys. Rev. B* **10**, 5175 (1974).
7. J. E. Jaffe and A. Zunger, *Phys. Rev. B* **30**, 741 (1984).
8. B. L. Henke, P. Lee, T. J. Tanaka, R. L. Shimabukuro, and B. J. Fujikawa, *At. Data Nucl. Data Tables* **27**, 1 (1982); B. L. Henke, J. C. Davis, E. M. Gullikson, and R. C. C. Perera, *Lawrence Berkeley Laboratory Report* **LBL-26259** (1988).
9. J. C. Rife, R. N. Dexter, P. M. Bridenbaugh, and B. W. Veal, *Phys. Rev. B* **10**, 4491 (1977); J. C. Rife, Unpublished Ph.D. Thesis, University of Wisconsin, Madison (1976).
10. S. Isomura and K. Masumoto, *Phys. Status Solidi A* **13**, 223 (1972).
11. I. S. Gorban, V. A. Goryna, V. V. Lugovskii, and I. I. Tychina, *Sov. Phys. Solid State* **16**, 1029 (1974).
12. R. Bendorius, V. D. Prochukhan, and A. Šileika, *Phys. Status Solidi B* **53**, 745 (1972).
13. G. D. Boyd, E. Buehler, and F. G. Storz, *Appl. Phys. Lett.* **18**, 301 (1970).
14. S. H. Wemple, J. D. Gabbe, and G. D. Boyd, *J. Appl. Phys.* **46**, 3597 (1975).
15. G. C. Bhar and G. Ghosh, *J. Opt. Soc. Am.* **69**, 730 (1979).
16. G. C. Bhar and G. C. Ghosh, *IEEE J. Quantum Electron.* **QE-16**, 838 (1980).
17. G. D. Boyd, E. Buehler, F. G. Storz, and J. H. Wernick, *IEEE J. Quantum Electron.* **QE-8**, 419 (1972).
18. P. G. Schunemann, P. J. Drevinsky, M. C. Ohmer, W. C. Mitchel, and N. C. Fernelius, *Mater. Res. Soc. Symp.* **354**, 729 (1995).

19. M. H. Rakowsky, W. J. Lauderdale, R. A. Mantz, R. Pandey, and P. J. Drevinsky, *Mater. Res. Soc. Symp.* **354**, 735 (1995).
20. V. N. Brudnyi, V. A. Novikov, and E. A. Popova, *Sov. Phys. J.* **29**, 679 (1986).
21. Yu.V. Rud, *Sov. Phys. Semicond. (Engl. Transl.)* **28**, 633 (1994); *Fiz. Tekh. Poluprovodn. (St. Petersburg)* **28**, 1105 (1994).
22. A. S. Poplavnoi, *Sov. Phys. J.* **29**, 587 (1986).
23. V. V. Voitsekhovskii, A. A. Volkov, G. A. Komandin, and Yu. A. Shakir, *Sov. Phys. Solid State* **37**, 1198 (1995); *Fiz. Tverd. Tela (St. Petersburg)* **37**, 2199 (1995).
24. A. Miller, G. D. Holah, and W. C. Clark, *J. Phys. Chem. Solids,* **35**, 685 (1974).
25. Yu. F. Markov, V. S. Grigoreva, B. S. Zadokhin, and T. V. Rybakova, *Opt. Spectrosc.* **36**, 93 (1974).

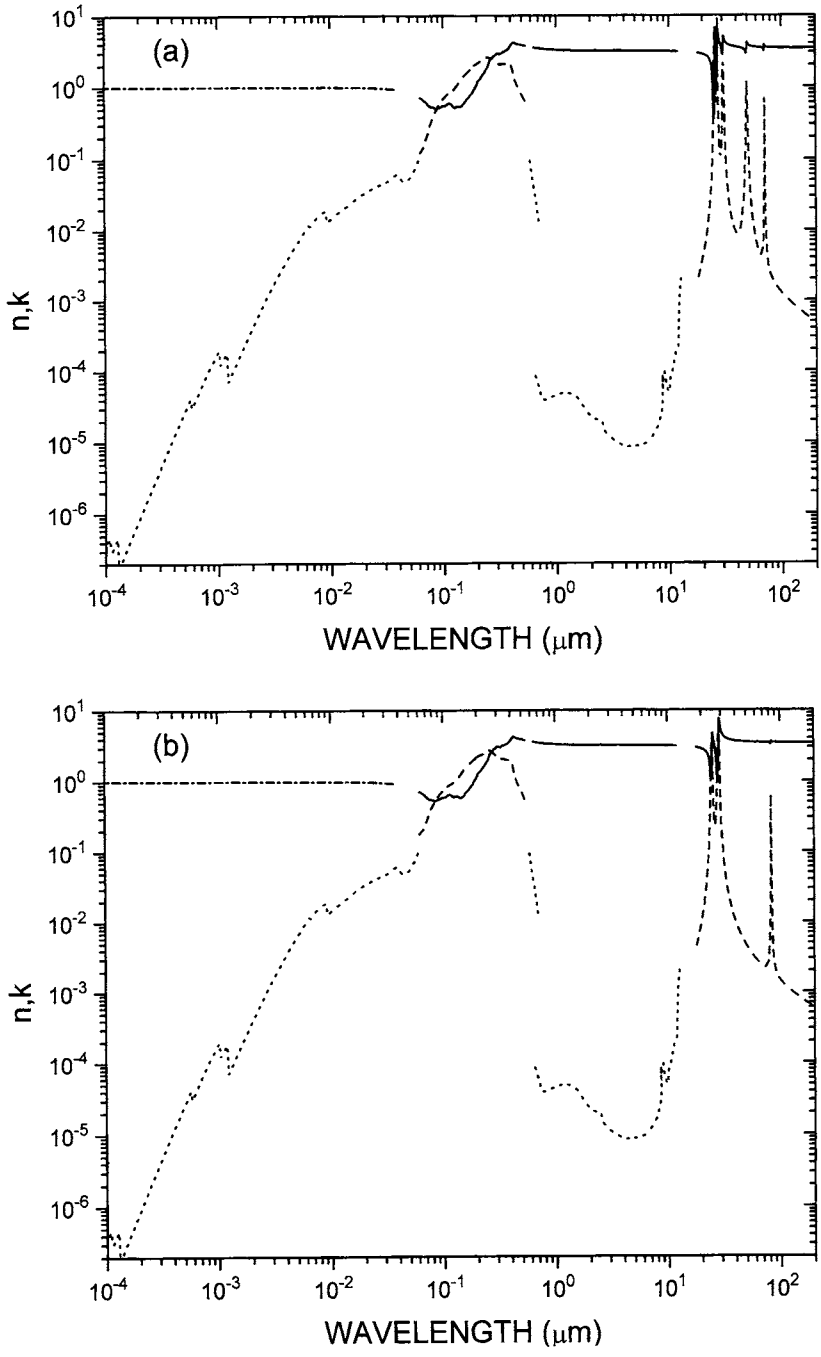

Fig. 1. (a) Log–log plot of n_o (solid line) and k_o (dashed line), $\mathbf{E} \perp \mathbf{c}$, versus wavelength for $ZnGeP_2$. (b) Log–log plot of n_e (solid line) and k_e (dashed line), $\mathbf{E} \parallel \mathbf{c}$, versus wavelength for $ZnGeP_2$. Unpolarized n (dash-dot line) and k (dotted line) are plotted on both graphs, where polarized data was not available.

TABLE I

Values of n and k for $ZnGeP_2$ Obtained from Various References[a]

eV	cm^{-1}	μm	1−n	k
			[8]	[8]
3.000E4	2.420E8	4.133E-5	8.90E-7	1.24E-8
2.010E4	1.622E8	6.167E-5	1.97E-6	5.76E-8
1.211E4	9.766E7	1.024E-4	5.36E-6	3.79E-7
1.179E4	9.506E7	1.052E-4	5.60E-6	4.18E-7
1.148E4	9.259E7	1.080E-4	5.84E-6	4.60E-7
1.118E4	9.017E7	1.109E-4	6.02E-6	3.35E-7
1.088E4	8.772E7	1.140E-4	6.44E-6	3.07E-7
1.060E4	8.547E7	1.170E-4	6.85E-6	3.38E-7
1.031E4	8.319E7	1.202E-4	7.21E-6	3.73E-7
1.005E4	8.104E7	1.234E-4	7.57E-6	4.13E-7
9.778E3	7.886E7	1.268E-4	7.81E-6	4.59E-7
9.523E3	7.680E7	1.302E-4	7.93E-6	1.75E-7
9.273E3	7.479E7	1.337E-4	8.88E-6	1.94E-7
9.024E3	7.278E7	1.374E-4	9.42E-6	2.15E-7
8.114E3	6.545E7	1.528E-4	1.19E-5	3.24E-7
6.048E3	4.878E7	2.050E-4	2.16E-5	9.88E-7
4.053E3	3.269E7	3.059E-4	4.88E-5	4.44E-6
2.314E3	1.867E7	5.357E-4	1.41E-4	3.42E-5
2.253E3	1.818E7	5.502E-4	1.47E-4	3.76E-5
2.194E3	1.770E7	5.651E-4	1.50E-4	4.13E-5
2.136E3	1.723E7	5.804E-4	1.51E-4	3.07E-5
2.080E3	1.678E7	5.961E-4	1.67E-4	3.38E-5
2.025E3	1.633E7	6.122E-4	1.79E-4	3.71E-5
1.593E3	1.285E7	7.784E-4	2.82E-4	8.58E-5
1.394E3	1.124E7	8.895E-4	3.41E-4	1.32E-4
1.287E3	1.038E7	9.637E-4	3.66E-4	1.69E-4
1.253E3	1.010E7	9.897E-4	3.63E-4	1.83E-4
1.220E3	9.843E6	1.016E-3	3.37E-4	1.98E-4
1.188E3	9.579E6	1.044E-3	3.81E-4	1.24E-4
1.157E3	9.328E6	1.072E-3	4.16E-4	1.34E-4
1.126E3	9.083E6	1.101E-3	4.41E-4	1.45E-4
1.096E3	8.842E6	1.131E-3	4.60E-4	1.56E-4
1.067E3	8.606E6	1.162E-3	4.73E-4	1.69E-4
1.039E3	8.382E6	1.193E-3	4.69E-4	1.83E-4
1.012E3	8.163E6	1.225E-3	4.28E-4	7.13E-5
9.856E2	7.949E6	1.258E-3	5.47E-4	7.81E-5
9.596E2	7.740E6	1.292E-3	6.04E-4	8.55E-5
7.958E2	6.418E6	1.558E-3	9.71E-4	1.66E-4
5.932E2	4.785E6	2.090E-3	1.81E-3	4.53E-4
3.976E2	3.207E6	3.118E-3	3.81E-3	1.68E-3
2.965E2	2.391E6	4.182E-3	6.04E-3	3.93E-3
2.040E2	1.646E6	6.077E-3	8.50E-3	1.04E-2
1.442E2	1.163E6	8.597E-3	5.77E-3	1.79E-2
1.404E2	1.133E6	8.829E-3	4.75E-3	1.83E-2
1.367E2	1.103E6	9.068E-3	2.64E-3	1.86E-2

(continued)

[a] References given in brackets.

TABLE I *(Continued)*

$ZnGeP_2$

eV	cm^{-1}	μm	1−n	k		
1.331E2	1.074E6	9.313E-3	2.68E-3	1.28E-2		
1.296E2	1.045E6	9.565E-3	5.50E-3	1.34E-2		
1.262E2	1.018E6	9.824E-3	6.72E-3	1.40E-2		
9.927E1	8.006E5	1.249E-2	1.22E-2	1.92E-2		
7.402E1	5.970E5	1.675E-2	1.95E-2	2.77E-2		
4.959E1	4.000E5	2.500E-2	3.57E-2	4.09E-2		
3.413E1	2.753E5	3.633E-2	7.63E-2	5.71E-2		
3.323E1	2.680E5	3.731E-2	7.94E-2	5.94E-2		
3.236E1	2.610E5	3.832E-2	8.13E-2	6.11E-2		
3.151E1	2.541E5	3.935E-2	8.31E-2	6.08E-2		
3.067E1	2.474E5	4.042E-2	8.52E-2	5.85E-2		
2.987E1	2.409E5	4.151E-2		5.33E-2		
2.908E1	2.346E5	4.263E-2		4.99E-2		
2.831E1	2.284E5	4.379E-2		4.79E-2		
2.757E1	2.224E5	4.497E-2		4.78E-2		
2.684E1	2.165E5	4.619E-2		4.86E-2		
2.614E1	2.108E5	4.744E-2		4.97E-2		
2.413E1	1.946E5	5.139E-2		5.75E-2		
2.227E1	1.796E5	5.567E-2		7.19E-2		
2.001E1	1.614E5	6.195E-2		1.10E-1		
eV	cm^{-1}	μm	n_o	k_o	n_e	k_e
			[9]	[9]	[9]	[9]
1.995E1	1.609E5	6.215E-2	7.06E-1	1.22E-1	7.03E-1	1.76E-1
1.975E1	1.593E5	6.277E-2	7.01E-1	1.25E-1	7.05E-1	1.77E-1
1.950E1	1.573E5	6.358E-2	6.94E-1	1.28E-1	6.97E-1	1.81E-1
1.925E1	1.553E5	6.441E-2	6.82E-1	1.31E-1	6.89E-1	1.86E-1
1.900E1	1.533E5	6.525E-2	6.71E-1	1.39E-1	6.81E-1	1.93E-1
1.875E1	1.512E5	6.612E-2	6.61E-1	1.44E-1	6.73E-1	1.97E-1
1.850E1	1.492E5	6.702E-2	6.45E-1	1.52E-1	6.60E-1	2.03E-1
1.825E1	1.472E5	6.793E-2	6.34E-1	1.65E-1	6.48E-1	2.13E-1
1.800E1	1.452E5	6.888E-2	6.25E-1	1.76E-1	6.40E-1	2.22E-1
1.775E1	1.432E5	6.985E-2	6.13E-1	1.85E-1	6.26E-1	2.29E-1
1.750E1	1.411E5	7.085E-2	6.01E-1	1.97E-1	6.11E-1	2.43E-1
1.725E1	1.391E5	7.187E-2	5.88E-1	2.07E-1	5.99E-1	2.59E-1
1.700E1	1.371E5	7.293E-2	5.66E-1	2.23E-1	5.80E-1	2.72E-1
1.675E1	1.351E5	7.402E-2	5.53E-1	2.47E-1	5.66E-1	2.99E-1
1.650E1	1.331E5	7.514E-2	5.42E-1	2.70E-1	5.61E-1	3.22E-1
1.625E1	1.311E5	7.630E-2	5.34E-1	2.95E-1	5.48E-1	3.41E-1
1.600E1	1.290E5	7.749E-2	5.30E-1	3.20E-1	5.44E-1	3.72E-1
1.575E1	1.270E5	7.872E-2	5.27E-1	3.42E-1	5.45E-1	3.96E-1
1.550E1	1.250E5	7.999E-2	5.24E-1	3.64E-1	5.44E-1	4.16E-1
1.525E1	1.230E5	8.130E-2	5.22E-1	3.85E-1	5.39E-1	4.38E-1
1.500E1	1.210E5	8.265E-2	5.20E-1	4.04E-1	5.38E-1	4.60E-1
1.450E1	1.170E5	8.550E-2	5.00E-1	4.54E-1	5.29E-1	5.11E-1
1.425E1	1.149E5	8.700E-2	5.01E-1	4.86E-1	5.26E-1	5.42E-1

TABLE I *(Continued)*

$ZnGeP_2$

eV	cm^{-1}	μm	n_o	k_o	n_e	k_e
1.400E1	1.129E5	8.856E-2	5.04E-1	5.14E-1	5.35E-1	5.74E-1
1.375E1	1.109E5	9.017E-2	5.10E-1	5.43E-1	5.46E-1	5.99E-1
1.350E1	1.089E5	9.184E-2	5.17E-1	5.66E-1	5.55E-1	6.18E-1
1.325E1	1.069E5	9.357E-2	5.15E-1	5.90E-1	5.53E-1	6.40E-1
1.300E1	1.049E5	9.537E-2	5.22E-1	6.20E-1	5.60E-1	6.69E-1
1.275E1	1.028E5	9.724E-2	5.33E-1	6.47E-1	5.70E-1	6.95E-1
1.250E1	1.008E5	9.918E-2	5.43E-1	6.66E-1	5.80E-1	7.15E-1
1.225E1	9.881E4	1.012E-1	5.44E-1	6.84E-1	5.83E-1	7.34E-1
1.200E1	9.681E4	1.033E-1	5.43E-1	7.12E-1	5.84E-1	7.58E-1
1.175E1	9.479E4	1.055E-1	5.51E-1	7.43E-1	5.88E-1	7.92E-1
1.150E1	9.276E4	1.078E-1	5.63E-1	7.70E-1	6.03E-1	8.22E-1
1.125E1	9.074E4	1.102E-1	5.78E-1	7.92E-1	6.21E-1	8.47E-1
1.100E1	8.873E4	1.127E-1	5.89E-1	8.04E-1	6.37E-1	8.61E-1
1.075E1	8.673E4	1.153E-1	5.88E-1	8.14E-1	6.43E-1	8.71E-1
1.050E1	8.467E4	1.181E-1	5.77E-1	8.31E-1	6.36E-1	8.81E-1
1.025E1	8.264E4	1.210E-1	5.54E-1	8.47E-1	6.19E-1	9.04E-1
9.999E0	8.065E4	1.240E-1	5.28E-1	9.00E-1	6.05E-1	9.45E-1
9.747E0	7.862E4	1.272E-1	5.13E-1	9.58E-1	6.00E-1	9.96E-1
9.501E0	7.663E4	1.305E-1	5.25E-1	1.02E0	6.08E-1	1.04E0
9.253E0	7.463E4	1.340E-1	5.35E-1	1.07E0	6.13E-1	1.08E0
8.997E0	7.257E4	1.378E-1	5.34E-1	1.12E0	5.99E-1	1.12E0
8.750E0	7.057E4	1.417E-1	5.31E-1	1.19E0	5.83E-1	1.18E0
8.498E0	6.854E4	1.459E-1	5.41E-1	1.27E0	5.79E-1	1.27E0
8.249E0	6.653E4	1.503E-1	5.65E-1	1.35E0	5.96E-1	1.36E0
7.999E0	6.452E4	1.550E-1	6.02E-1	1.43E0	6.26E-1	1.46E0
7.749E0	6.250E4	1.600E-1	6.40E-1	1.51E0	6.75E-1	1.54E0
7.501E0	6.050E4	1.653E-1	6.85E-1	1.59E0	7.24E-1	1.62E0
7.251E0	5.848E4	1.710E-1	7.23E-1	1.67E0	7.67E-1	1.70E0
7.001E0	5.647E4	1.771E-1	7.79E-1	1.77E0	8.28E-1	1.80E0
6.950E0	5.605E4	1.784E-1	7.93E-1	1.78E0	8.41E-1	1.82E0
6.900E0	5.565E4	1.797E-1	8.03E-1	1.80E0	8.54E-1	1.84E0
6.850E0	5.525E4	1.810E-1	8.11E-1	1.82E0	8.69E-1	1.86E0
6.801E0	5.485E4	1.823E-1	8.17E-1	1.84E0	8.83E-1	1.88E0
6.749E0	5.444E4	1.837E-1	8.28E-1	1.87E0	8.95E-1	1.90E0
6.702E0	5.405E4	1.850E-1	8.45E-1	1.89E0	9.06E-1	1.92E0
6.652E0	5.365E4	1.864E-1	8.65E-1	1.92E0	9.21E-1	1.95E0
6.602E0	5.325E4	1.878E-1	8.85E-1	1.94E0	9.44E-1	1.98E0
6.550E0	5.283E4	1.893E-1	9.05E-1	1.96E0	9.68E-1	2.00E0
6.502E0	5.244E4	1.907E-1	9.26E-1	1.99E0	9.90E-1	2.02E0
6.451E0	5.203E4	1.922E-1	9.46E-1	2.01E0	1.01E0	2.03E0
6.401E0	5.163E4	1.937E-1	9.67E-1	2.03E0	1.03E0	2.05E0
6.352E0	5.123E4	1.952E-1	9.89E-1	2.05E0	1.05E0	2.07E0
6.300E0	5.081E4	1.968E-1	1.01E0	2.07E0	1.08E0	2.09E0
6.249E0	5.040E4	1.984E-1	1.04E0	2.10E0	1.10E0	2.12E0
6.199E0	5.000E4	2.000E-1	1.06E0	2.12E0	1.13E0	2.14E0
6.150E0	4.960E4	2.016E-1	1.10E0	2.15E0	1.15E0	2.16E0
6.102E0	4.921E4	2.032E-1	1.14E0	2.17E0	1.19E0	2.19E0

(continued)

TABLE I *(Continued)*

$ZnGeP_2$

eV	cm^{-1}	μm	n_o	k_o	n_e	k_e
6.051E0	4.880E4	2.049E-1	1.19E0	2.17E0	1.24E0	2.20E0
6.001E0	4.840E4	2.066E-1	1.21E0	2.16E0	1.27E0	2.19E0
5.949E0	4.798E4	2.084E-1	1.23E0	2.17E0	1.29E0	2.20E0
5.901E0	4.760E4	2.101E-1	1.24E0	2.18E0	1.30E0	2.20E0
5.851E0	4.719E4	2.119E-1	1.25E0	2.19E0	1.32E0	2.22E0
5.799E0	4.677E4	2.138E-1	1.26E0	2.22E0	1.34E0	2.24E0
5.751E0	4.638E4	2.156E-1	1.29E0	2.24E0	1.36E0	2.25E0
5.700E0	4.598E4	2.175E-1	1.32E0	2.27E0	1.38E0	2.27E0
5.651E0	4.558E4	2.194E-1	1.35E0	2.29E0	1.40E0	2.30E0
5.600E0	4.517E4	2.214E-1	1.38E0	2.31E0	1.43E0	2.32E0
5.550E0	4.476E4	2.234E-1	1.42E0	2.32E0	1.47E0	2.34E0
5.501E0	4.437E4	2.254E-1	1.44E0	2.34E0	1.50E0	2.35E0
5.450E0	4.396E4	2.275E-1	1.47E0	2.35E0	1.53E0	2.37E0
5.400E0	4.355E4	2.296E-1	1.50E0	2.37E0	1.55E0	2.39E0
5.351E0	4.316E4	2.317E-1	1.53E0	2.40E0	1.58E0	2.41E0
5.301E0	4.275E4	2.339E-1	1.55E0	2.43E0	1.61E0	2.44E0
5.249E0	4.234E4	2.362E-1	1.60E0	2.46E0	1.65E0	2.47E0
5.201E0	4.195E4	2.384E-1	1.65E0	2.48E0	1.69E0	2.49E0
5.151E0	4.155E4	2.407E-1	1.70E0	2.49E0	1.74E0	2.51E0
5.100E0	4.114E4	2.431E-1	1.75E0	2.50E0	1.78E0	2.53E0
5.050E0	4.073E4	2.455E-1	1.78E0	2.52E0	1.82E0	2.55E0
4.999E0	4.032E4	2.480E-1	1.82E0	2.54E0	1.87E0	2.57E0
4.950E0	3.992E4	2.505E-1	1.87E0	2.58E0	1.90E0	2.60E0
4.901E0	3.953E4	2.530E-1	1.93E0	2.62E0	1.96E0	2.65E0
4.851E0	3.912E4	2.556E-1	2.01E0	2.65E0	2.04E0	2.68E0
4.800E0	3.871E4	2.583E-1	2.11E0	2.66E0	2.12E0	2.71E0
4.750E0	3.831E4	2.610E-1	2.22E0	2.67E0	2.22E0	2.73E0
4.700E0	3.791E4	2.638E-1	2.32E0	2.62E0	2.35E0	2.72E0
4.651E0	3.751E4	2.666E-1	2.38E0	2.54E0	2.43E0	2.66E0
4.601E0	3.711E4	2.695E-1	2.40E0	2.51E0	2.50E0	2.62E0
4.550E0	3.670E4	2.725E-1	2.44E0	2.49E0	2.56E0	2.58E0
4.500E0	3.630E4	2.755E-1	2.49E0	2.48E0	2.61E0	2.54E0
4.450E0	3.589E4	2.786E-1	2.56E0	2.46E0	2.65E0	2.51E0
4.400E0	3.549E4	2.818E-1	2.62E0	2.40E0	2.71E0	2.48E0
4.350E0	3.509E4	2.850E-1	2.64E0	2.36E0	2.77E0	2.46E0
4.301E0	3.469E4	2.883E-1	2.68E0	2.33E0	2.82E0	2.39E0
4.250E0	3.428E4	2.917E-1	2.71E0	2.31E0	2.85E0	2.35E0
4.200E0	3.388E4	2.952E-1	2.76E0	2.29E0	2.89E0	2.33E0
4.151E0	3.348E4	2.987E-1	2.82E0	2.26E0	2.95E0	2.30E0
4.100E0	3.307E4	3.024E-1	2.85E0	2.18E0	2.99E0	2.23E0
4.050E0	3.267E4	3.061E-1	2.87E0	2.12E0	3.03E0	2.17E0
4.000E0	3.226E4	3.100E-1	2.86E0	2.08E0	3.03E0	2.10E0
3.950E0	3.186E4	3.139E-1	2.85E0	2.06E0	3.02E0	2.05E0
3.900E0	3.146E4	3.179E-1	2.84E0	2.05E0	3.01E0	2.03E0
3.850E0	3.106E4	3.220E-1	2.84E0	2.05E0	2.99E0	2.01E0
3.800E0	3.065E4	3.263E-1	2.85E0	2.06E0	2.99E0	2.02E0
3.750E0	3.025E4	3.306E-1	2.88E0	2.09E0	3.01E0	2.06E0

TABLE I *(Continued)*

$ZnGeP_2$

eV	cm^{-1}	μm	n_o	k_o	n_e	k_e
3.700E0	2.984E4	3.351E-1	2.93E0	2.10E0	3.08E0	2.07E0
3.650E0	2.944E4	3.397E-1	3.00E0	2.08E0	3.13E0	2.03E0
3.600E0	2.904E4	3.444E-1	3.01E0	2.04E0	3.17E0	1.99E0
3.551E0	2.864E4	3.492E-1	3.02E0	2.05E0	3.16E0	1.96E0
3.500E0	2.823E4	3.542E-1	3.07E0	2.08E0	3.18E0	1.98E0
3.450E0	2.782E4	3.594E-1	3.13E0	2.06E0	3.23E0	1.98E0
3.401E0	2.743E4	3.646E-1	3.18E0	2.04E0	3.27E0	1.96E0
3.350E0	2.702E4	3.701E-1	3.21E0	2.04E0	3.31E0	1.96E0
3.300E0	2.662E4	3.757E-1	3.24E0	2.05E0	3.34E0	1.96E0
3.250E0	2.621E4	3.815E-1	3.32E0	2.11E0	3.40E0	1.99E0
3.200E0	2.581E4	3.874E-1	3.43E0	2.09E0	3.48E0	1.99E0
3.150E0	2.541E4	3.936E-1	3.55E0	2.09E0	3.58E0	1.98E0
3.100E0	2.501E4	3.999E-1	3.69E0	2.05E0	3.69E0	1.96E0
3.050E0	2.460E4	4.065E-1	3.84E0	1.97E0	3.82E0	1.94E0
3.000E0	2.420E4	4.133E-1	3.99E0	1.86E0	3.97E0	1.84E0
2.950E0	2.379E4	4.203E-1	4.11E0	1.65E0	4.12E0	1.68E0
2.900E0	2.339E4	4.275E-1	4.11E0	1.45E0	4.19E0	1.49E0
2.850E0	2.299E4	4.350E-1	4.09E0	1.29E0	4.16E0	1.29E0
2.800E0	2.258E4	4.428E-1	4.00E0	1.16E0	4.11E0	1.18E0
2.750E0	2.218E4	4.508E-1	3.97E0	1.09E0	4.07E0	1.05E0
2.700E0	2.178E4	4.592E-1	3.90E0	1.01E0	4.02E0	9.74E-1
2.650E0	2.138E4	4.678E-1	3.88E0	9.73E-1	3.97E0	9.08E-1
2.600E0	2.097E4	4.768E-1	3.86E0	9.18E-1	3.95E0	8.54E-1
2.550E0	2.057E4	4.862E-1	3.84E0	8.64E-1	3.91E0	7.87E-1
2.500E0	2.017E4	4.959E-1	3.83E0	8.06E-1	3.88E0	7.49E-1
2.450E0	1.976E4	5.060E-1	3.81E0	7.36E-1	3.87E0	7.01E-1
2.400E0	1.936E4	5.166E-1	3.75E0	6.92E-1	3.85E0	6.33E-1
2.350E0	1.895E4	5.276E-1	3.73E0	6.58E-1	3.79E0	5.71E-1
2.300E0	1.855E4	5.390E-1	3.70E0	6.27E-1	3.76E0	5.42E-1

eV	cn^{-1}	μm	n	k
				[10]
2.109E0	1.701E4	5.880E-1		9.36E-2
1.997E0	1.610E4	6.210E-1		4.94E-2
1.867E0	1.506E4	6.640E-1		2.64E-2
1.749E0	1.410E4	7.090E-1		1.13E-2

eV	cm^{-1}	μm	n_o	k	n_e
			[13]	[17]	[13]
1.937E0	1.563E4	6.400E-1	3.505E0		3.580E0
1.879E0	1.515E4	6.600E-1	3.476E0	7.78E-5	3.547E0
1.823E0	1.471E4	6.800E-1	3.448E0	6.73E-5	3.516E0
1.771E0	1.429E4	7.000E-1	3.423E0	5.72E-5	3.489E0
1.653E0	1.333E4	7.500E-1	3.373E0	3.94E-5	3.432E0
1.550E0	1.250E4	8.000E-1	3.336E0	3.92E-5	3.392E0

(continued)

TABLE I *(Continued)*

$ZnGeP_2$

eV	cm^{-1}	μm	n_o	k	n_e
1.459E0	1.176E4	8.500E-1	3.306E0	4.10E-5	3.359E0
1.378E0	1.111E4	9.000E-1	3.283E0	4.29E-5	3.334E0
1.305E0	1.053E4	9.500E-1	3.264E0	4.46E-5	3.312E0
1.240E0	1.000E4	1.000E0	3.248E0	4.62E-5	3.295E0
1.127E0	9.091E3	1.100E0	3.223E0	4.84E-5	3.269E0
1.033E0	8.333E3	1.200E0	3.205E0	4.89E-5	3.249E0
9.537E-1	7.692E3	1.300E0	3.192E0	4.79E-5	3.235E0
8.856E-1	7.143E3	1.400E0	3.182E0	4.54E-5	3.224E0
7.749E-1	6.250E3	1.600E0	3.167E0	3.71E-5	3.208E0
6.888E-1	5.556E3	1.800E0	3.156E0	2.76E-5	3.197E0
6.199E-1	5.000E3	2.000E0	3.149E0	2.18E-5	3.189E0
5.636E-1	4.545E3	2.200E0	3.143E0	2.05E-5	3.183E0
5.166E-1	4.167E3	2.400E0	3.139E0	1.98E-5	3.178E0
4.769E-1	3.846E3	2.600E0	3.136E0	1.42E-5	3.175E0
4.428E-1	3.571E3	2.800E0	3.133E0	1.22E-5	3.172E0
4.133E-1	3.333E3	3.000E0	3.130E0	1.12E-5	3.169E0
3.875E-1	3.125E3	3.200E0	3.128E0	1.04E-5	3.167E0
3.647E-1	2.941E3	3.400E0	3.126E0	9.85E-6	3.165E0
3.444E-1	2.778E3	3.600E0	3.126E0	9.36E-6	3.163E0
3.263E-1	2.632E3	3.800E0	3.124E0	8.87E-6	3.162E0
3.100E-1	2.500E3	4.000E0	3.122E0	8.45E-6	3.161E0
2.952E-1	2.381E3	4.200E0	3.121E0	8.50E-6	3.160E0
2.755E-1	2.222E3	4.500E0	3.119E0	8.57E-6	3.156E0
2.638E-1	2.128E3	4.700E0	3.117E0	8.61E-6	3.154E0
2.480E-1	2.000E3	5.000E0	3.115E0	8.68E-6	3.153E0
2.254E-1	1.818E3	5.500E0	3.113E0	9.00E-6	3.152E0
2.066E-1	1.667E3	6.000E0	3.110E0	9.33E-6	3.148E0
1.907E-1	1.538E3	6.500E0	3.106E0	1.07E-5	3.145E0
1.771E-1	1.429E3	7.000E0	3.104E0	1.20E-5	3.142E0
1.653E-1	1.333E3	7.500E0	3.099E0	1.48E-5	3.138E0
1.550E-1	1.250E3	8.000E0	3.096E0	1.82E-5	3.135E0
1.459E-1	1.176E3	8.500E0	3.092E0	2.91E-5	3.131E0
1.441E-1	1.162E3	8.603E0		5.57E-5	
1.419E-1	1.144E3	8.739E0		9.10E-5	
1.378E-1	1.111E3	9.000E0	3.088E0	8.94E-5	3.127E0
1.354E-1	1.092E3	9.157E0		7.21E-5	
1.305E-1	1.053E3	9.500E0	3.084E0	5.55E-5	3.123E0
1.255E-1	1.012E3	9.879E0		4.94E-5	
1.245E-1	1.004E3	9.962E0		6.50E-5	
1.240E-1	1.000E3	1.000E1	3.079E0	7.18E-5	3.118E0
1.181E-1	9.524E2	1.050E1	3.074E0	9.75E-5	3.114E0
1.150E-1	9.276E2	1.078E1			1.20E-4
1.127E-1	9.091E2	1.100E1	3.069E0	1.47E-4	3.109E0
1.099E-1	8.865E2	1.128E1		1.81E-4	
1.078E-1	8.696E2	1.150E1	3.062E0	1.94E-4	3.101E0
1.043E-1	8.410E2	1.189E1		2.10E-4	
1.038E-1	8.368E2	1.195E1		2.43E-4	

TABLE I *(Continued)*

$ZnGeP_2$

eV	cm^{-1}	μm	n_o	k	n_e	
1.033E-1	8.333E2	1.200E1	3.055E0	3.89E-4	3.095E0	
1.021E-1	8.237E2	1.214E1		8.97E-4		
1.006E-1	8.110E2	1.233E1		1.34E-3		
9.871E-2	7.962E2	1.256E1		1.83E-3		
9.747E-2	7.862E2	1.272E1		1.23E-3		
eV	cm^{-1}	μm	n_o	k_o	n_e	k_e
			[23]	[23]	[23]	[23]
6.819E-2	5.500E2	1.818E1	2.92E0	2.15E-3	2.95E0	4.57E-3
6.199E-2	5.000E2	2.000E1	2.82E0	4.30E-3	2.85E0	9.61E-3
5.579E-2	4.500E2	2.222E1	2.57E0	1.29E-2	2.58E0	3.35E-2
4.959E-2	4.000E2	2.500E1	3.81E-1	1.17E0	2.33E0	3.36E0
4.922E-2	3.970E2	2.519E1	3.62E-1	1.89E0	4.07E0	3.19E0
4.885E-2	3.940E2	2.538E1	4.52E-1	2.68E0	4.67E0	1.70E0
4.835E-2	3.900E2	2.564E1	9.64E-1	4.27E0	4.14E0	7.14E-1
4.786E-2	3.860E2	2.591E1	5.80E0	5.59E0	3.67E0	4.01E-1
4.736E-2	3.820E2	2.618E1	4.76E0	9.12E-1	3.33E0	2.81E-1
4.687E-2	3.780E2	2.646E1	3.05E0	5.88E-1	3.05E0	2.36E-1
4.637E-2	3.740E2	2.674E1	1.23E0	1.92E0	2.77E0	2.33E-1
4.587E-2	3.700E2	2.703E1	2.22E0	5.87E0	2.46E0	2.71E-1
4.563E-2	3.680E2	2.717E1	7.67E0	6.71E0	2.28E0	3.13E-1
4.513E-2	3.640E2	2.747E1	6.37E0	6.48E-1	1.80E0	4.99E-1
4.463E-2	3.600E2	2.778E1	5.15E0	2.37E-1	1.17E0	1.11E0
4.414E-2	3.560E2	2.809E1	4.59E0	1.40E-1	9.71E-1	2.29E0
4.364E-2	3.520E2	2.841E1	4.24E0	1.08E-1	1.32E0	3.71E0
4.315E-2	3.480E2	2.874E1	3.98E0	1.02E-1	2.91E0	5.66E0
4.240E-2	3.420E2	2.924E1	3.63E0	1.36E-1	7.30E0	2.27E0
4.191E-2	3.380E2	2.959E1	3.36E0	2.22E-1	6.10E0	8.01E-1
4.141E-2	3.340E2	2.994E1	2.98E0	5.10E-1	5.39E0	4.03E-1
4.092E-2	3.300E2	3.030E1	2.87E0	1.63E0	4.97E0	2.44E-1
4.054E-2	3.270E2	3.058E1	4.36E0	2.14E0	4.75E0	1.81E-1
4.017E-2	3.240E2	3.086E1	4.94E0	9.53E-1	4.58E0	1.40E-1
3.968E-2	3.200E2	3.125E1	4.55E0	3.27E-1	4.41E0	1.04E-1
3.918E-2	3.160E2	3.165E1	4.29E0	1.60E-1	4.28E0	8.11E-2
3.868E-2	3.120E2	3.205E1	4.12E0	9.54E-2	4.18E0	6.51E-2
3.819E-2	3.080E2	3.247E1	4.01E0	6.43E-2	4.10E0	5.36E-2
3.769E-2	3.040E2	3.289E1	3.92E0	4.69E-2	4.03E0	4.49E-2
3.720E-2	3.000E2	3.333E1	3.86E0	3.60E-2	3.97E0	3.83E-2
3.100E-2	2.500E2	4.000E1	3.50E0	8.75E-3	3.63E0	1.02E-2
2.790E-2	2.250E2	4.444E1	3.38E0	1.48E-2	3.56E0	6.64E-3
2.752E-2	2.220E2	4.505E1	3.35E0	1.82E-2	3.55E0	6.33E-3
2.703E-2	2.180E2	4.587E1	3.31E0	2.62E-2	3.54E0	5.96E-3
2.604E-2	2.100E2	4.762E1	3.14E0	9.37E-2	3.53E0	5.29E-3
2.554E-2	2.060E2	4.854E1	2.92E0	3.26E-1	3.52E0	5.00E-3
2.504E-2	2.020E2	4.951E1	3.64E0	1.17E0	3.51E0	4.72E-3
2.455E-2	1.980E2	5.051E1	3.93E0	2.44E-1	3.51E0	4.47E-3

(continued)

TABLE I *(Continued)*

$ZnGeP_2$

eV	cm^{-1}	μm	n_o	k_o	n_e	k_e
2.405E-2	1.940E2	5.155E1	3.74E0	7.86E-2	3.50E0	4.23E-3
2.356E-2	1.900E2	5.263E1	3.64E0	3.83E-2	3.50E0	4.01E-3
2.306E-2	1.860E2	5.376E1	3.59E0	2.30E-2	3.49E0	3.81E-3
2.257E-2	1.820E2	5.495E1	3.55E0	1.56E-2	3.49E0	3.62E-3
2.207E-2	1.780E2	5.618E1	3.53E0	1.14E-2	3.48E0	3.44E-3
2.157E-2	1.740E2	5.747E1	3.51E0	8.88E-3	3.48E0	3.27E-3
2.108E-2	1.700E2	5.882E1	3.49E0	7.19E-3	3.47E0	3.12E-3
2.058E-2	1.660E2	6.024E1	3.48E0	6.03E-3	3.47E0	2.97E-3
2.009E-2	1.620E2	6.173E1	3.47E0	5.21E-3	3.46E0	2.83E-3
1.959E-2	1.580E2	6.329E1	3.45E0	4.66E-3	3.46E0	2.70E-3
1.909E-2	1.540E2	6.494E1	3.44E0	4.39E-3	3.45E0	2.58E-3
1.860E-2	1.500E2	6.667E1	3.42E0	4.67E-3	3.45E0	2.48E-3
1.810E-2	1.460E2	6.849E1	3.39E0	7.66E-3	3.45E0	2.38E-3
1.754E-2	1.415E2	7.067E1	3.51E0	7.02E-1	3.44E0	2.29E-3
1.736E-2	1.400E2	7.143E1	3.60E0	3.97E-2	3.44E0	2.27E-3
1.686E-2	1.360E2	7.353E1	3.48E0	5.34E-3	3.43E0	2.23E-3
1.637E-2	1.320E2	7.576E1	3.46E0	3.16E-3	3.43E0	2.29E-3
1.587E-2	1.280E2	7.813E1	3.44E0	2.48E-3	3.42E0	2.62E-3
1.562E-2	1.260E2	7.937E1	3.44E0	2.28E-3	3.41E0	3.16E-3
1.513E-2	1.220E2	8.197E1	3.43E0	2.00E-3	3.35E0	1.39E-2
1.463E-2	1.180E2	8.475E1	3.43E0	1.80E-3	3.52E0	1.31E-2
1.413E-2	1.140E2	8.772E1	3.42E0	1.64E-3	3.46E0	2.86E-3
1.364E-2	1.100E2	9.091E1	3.42E0	1.50E-3	3.45E0	1.95E-3
1.314E-2	1.060E2	9.434E1	3.41E0	1.39E-3	3.44E0	1.64E-3
1.240E-2	1.000E2	1.000E2	3.41E0	1.24E-3	3.43E0	1.42E-3
6.199E-3	5.000E1	2.000E2	3.39E0	4.76E-4	3.41E0	5.85E-4

Aluminum Oxide (Al_2O_3) Revisited

WILLIAM J. TROPF and MICHAEL E. THOMAS
Applied Physics Laboratory
The Johns Hopkins University
Laurel, Maryland

In a previous volume of this series, Gervais [1] reviewed the optical properties of aluminum oxide. We extend his chapter by providing additional information, much of it recent. Table I gives the anisotropic optical constants of aluminum oxide from 0 to 116 eV.

The hexagonal (rhombohedral) form of aluminum oxide is variously called α-Al_2O_3, alumina (usually applied to the non-fully-dense polycrystalline ceramic), corundum (mineral name), ruby (red [chromium containing] corundum), or sapphire (blue corundum; also frequently used to denote the pure, synthetic crystal). It is a hard, stable material melting at 2319 K. The space group is $R\bar{3}c$ (or D_{3d}^6) with six formula units per unit cell. Room-temperature cell dimensions are 4.759 Å (a-axis) and 12.989 Å (c-axis), giving an x-ray density of 3.987 g/cm^2. Atomic coordinates are as follows: aluminum atoms occupy the 12(c) sites at 0, 0, 0.347 (with point symmetry 3 or C_3) and the oxygen atoms occupy 18(e) sites at 0.306, 0, $\frac{1}{4}$ (with point symmetry 2 or C_2).

Aluminum oxide is a negative, uniaxial crystal transparent from 0.145 to 5.0 μm (ordinary ray) and 0.147 to 5.2 μm (extraordinary ray). Optical anisotropy is small from the extreme ultraviolet through the infrared, becoming larger in the microwave region. Optical-quality crystalline aluminum oxide (or "sapphire") is made by several techniques including Czochralski growth, flame fusion (Verneuil method), the heat-exchanger method (HEM), and the edge-defined, film-fed growth (EFG) techniques. The high mechanical and dielectric strength of aluminum oxide make it a desirable laser host material. Chromium- and titanium-doped aluminum oxide are common solid-state laser-gain media.

Gervais [1] used a compilation of optical constants for amorphous aluminum oxide [2] that do not contain information on the anisotropy of the crystalline state. We supplement this information with single-crystal and polarization measurements as discussed in the following.

Tomiki *et al.* [3] provided the complex dielectric constant, determined

Copyright © 1998 by Academic Press.
All rights of reproduction in any form reserved
ISBN 0-12-544423-0/$25.00.

from a Kramers–Kronig analysis, in digital form with three decimal places. About 600 points were provided for both principal values, covering the range from 6.2 to 119 eV for the real component and above 9 to 119 eV for the imaginary component. Reflectance-measurement accuracy is better than 2.2% ($E > 7.3$ eV) and less accurate at higher energy [4]; therefore, the second decimal place of n and k is uncertain. The complex refractive index (n and k) values determined from selected points of these data are listed in Table I.

Harman *et al.* [5] used Tomiki's data to represent the optical constants of aluminum oxide from 1 to 30 eV using the classical oscillator model with 13 modes. The model reproduces the imaginary refractive index well, but agreement with the real refractive index is poor.

French *et al.* [6] provided the complex refractive index of the ordinary ray of crystalline aluminum oxide determined from an average of several measurements. Optical constants were determined from a Kramers–Kronig analysis of reflectance (to 42 eV, resolution 0.01 to 0.1 eV) and electron-energy-loss (to 140 eV, resolution approximately 0.7 eV) spectra. Optical constants above 119 eV are taken from the electron-energy-loss data, and selected reflectance-measurement values (below 42 eV) are provided in Table I.

Aluminum oxide has a direct band gap of 8.8 eV. Excitonic absorption leads up to the absorption peaks at 9 and 13 eV, which are maxima in the interband transitions between the upper valence band of oxygen ($2p^6$) to the conduction band of triply ionized aluminum ($3s + 3p$ states). Other features at higher frequencies include a plasma oscillation peaking near 25 eV and transitions from oxygen ($2s^2$) to aluminum ($3p$ states) in the 33 to 45 eV region. At higher energies, photoabsorption by the inner core electrons, beginning at the $L_{2,3}$ edge, dominate the spectrum.

Tomiki *et al.* [4] also give the temperature dependence of exciton absorption at the UV edge of the transparent region (8.5–9.0 eV) between 10 and 297 K and fit their measurements to an Urbach rule formulation:

$$\beta(E, T) = \beta_0 \exp(-\sigma_s(T)(E_0 - E)/k_B T), \tag{1a}$$

where $\beta(E, T)$ is the absorption coefficient as a function of energy (E) and temperature (T), and k_B is Boltzmann's constant. The slope parameter $\sigma_s(T)$ is given by

$$\sigma_s(T) = \sigma_{s0}(2k_B T/E_{s0}) \tanh(E_{s0}/2k_B T). \tag{1b}$$

Constants of Eq. (1) are $\beta_0 = 3.87 \times 10^7$ cm^{-1}, $E_0 = 9.314$ eV, $\sigma_{s0} = 0.672$, and $E_{s0} = 33.79$ meV for the ordinary ray (or $\mathbf{E} \perp c$-axis) and $\beta_0 = 1.117 \times 10^7$ cm^{-1}, $E_0 = 9.249$ eV, $\sigma_{s0} = 0.505$, and $E_{s0} = 31.87$ meV for the extraordinary ray (or $\mathbf{E} \parallel c$-axis). The ordinary-ray results agree well with the measurement of Thomas *et al.* [7] near the edge of transparency. Values of the imaginary part of the refractive index between 8.5 and 9.0 eV given in Table I are calculated from this equation using Tomiki's constants.

At energy lower than 8.5 eV, aluminum oxide continues to exhibit considerable absorption due to trace impurities and defects. Innocenzi *et al.* [8] review prior measurements and present chemical analyses and laser-calorimetry absorption data on several aluminum-oxide crystals grown by the Czochralski method. They found that the absorption coefficient between 0.9 and 8.5 eV could be represented by a "weak-absorption-tail" model of the form

$$\beta(E) = \beta_0 \cdot 10^{E/E_0}, \tag{2}$$

where $\beta_0 = 3.13 \times 10^{-5}$ cm^{-1} and $E_0 = 1.7$ eV. Evans [9] performed a similar absorption study using transmission measurements. This work studied aluminum-oxide crystals grown by different techniques and included optical anisotropy. Evans identified the major spectral features as trace impurities and oxygen vacancies (F and F^+ centers). Single-crystal aluminum oxide has very low ultraviolet and visible scatter loss.

Chandrasekharan and Damany [10] measured the ultraviolet birefringence of aluminum oxide between 3.9 and 8.7 eV. The birefringence ($n_e - n_o$) is zero at 0.1426 μm, rises rapidly to -0.0010 at 0.147 μm, has a minimum value of -0.0013 at 0.1595 μm, then slowly falls to -0.0010 near 0.223 μm. Their results generally agree with whose of Tomiki given in Table I and closely match the refractive index and direct birefringence measurements of Jeppesen [11].

Refractive-index data for aluminum oxide in the transparent region are given by several sources [11–15]; measurements [11, 12] are given in Table I. Unfortunately, the preponderance of measurements is for the ordinary ray. Jeppesen [11] measured near-ultraviolet and visible refractive indices at 24° C between 0.25 and 0.7 μm, and Malitson [12] determined the ordinary-ray refractive index between 0.26 and 5.6 μm at 24° C. Malitson [12] and Malitson and Dodge [13] give the refractive index in the form of a Sellmeier-type dispersion formula,

$$n^2(\lambda) - 1 = \sum_i \frac{A_i \lambda^2}{\lambda^2 - \lambda_i^2}, \tag{3}$$

based on minimum-dispersion prism measurements, where the constants A_i and λ_i are given in Table II. Malitson (private communication, 7/11/96) gives the accuracy of the dispersion equation as $\pm 2 \times 10^{-5}$ over the 0.2 to 5.5 μm range.

Harman *et al.* [5] made ellipsometric measurements of both principal values of the dielectric constant of single-crystal aluminum oxide between 1.2 and 5.4 eV. They provide their data as a dispersion equation that agrees reasonably well with the values in Table I (differences in third decimal place).

DeFranzo and Pazol [14] measured the ordinary- and extraordinary-ray refractive index in the visible from 20 to 295 K for aluminum-oxide crystals

grown with the HEM and EFG techniques. The HEM crystal exhibited consistently higher refractive index, between 0.0015 and 0.0020 throughout the measurement range. The indices of both materials appear lower than the measurements of Malitson [12].

Several references give the temperature dependence of the refractive index of aluminum oxide [11, 12, 14–19]. These values are tabulated in Table III. Note that Jeppesen [11] and Feldman *et al.* [17] determined $dn_e/dT > dn_o/dT$, while DeFranzo and Pazol [14] obtained $dn_e/dT < dn_o/dT$. The many dn_o/dT values generally agree, although differences may be 20% or more.

Dodge *et al.* [20] measured the birefringent refractive index of ruby (Al_2O_3 with 0.062% Cr_2O_3 by weight) in the visible. Results are very close to those of Jeppesen [11] for pure aluminum oxide. As the concentration of Cr_2O_3 increases, both refractive indices rise, as shown by the measurements of Mandarino [21]. Wilson [22] measured the temperature coefficient of the refractive index of ruby at 0.633 μm and found $dn_e/dT > dn_o/dT$, in agreement with the measurement of Jeppesen [11].

At the infrared edge of transparency, loss rises because of multiphonon absorption. Several measurements of this loss have been made [23–26]. In aluminum oxide, the absorption falls exponentially with increasing frequency. Deutsch [23] models the absorption coefficient, $\beta(\nu)$, as

$$\beta(\nu) = \beta_0 \exp(-\gamma\nu/\nu_{LO}), \tag{4}$$

where ν is frequency (usually in wave numbers), β_0 is a normalizing constant, ν_{LO} is the maximum longitudinal optical frequency of the material, and γ is another constant (typically between 4 and 5). For aluminum oxide, Deutsch [23], and Thomas and co-workers [24, 25] determined these constants as given in Table IV. Multiphonon-absorption data given in Table I come from measurements by Thomas and co-workers [24, 25] and Gervais *et al.* [26]. Thomas *et al.* [24] gives a multiphonon-absorption model covering all temperatures to the melt.

Harrington *et al.* [27] measured infrared absorption coefficients of aluminum-oxide crystals at HF and DF multiline wavelengths using laser calorimetry. Measured absorption coefficients at DF laser wavelengths (nominally at 3.8μm or 2630 cm^{-1}) were 2.4×10^{-2} and 2.5×10^{-2} cm^{-1} for crystals from Crystal Systems (HEM growth method) and Union Carbide (Czochralski growth), respectively. These values are essentially the intrinsic multiphonon absorption. At HF laser wavelengths (nominally at 2.7 μm or 3700 cm^{-1}), absorption coefficients were 3.4×10^{-3} and 2.6×10^{-3} cm^{-1} for the same samples, far above the intrinsic levels. Aluminum oxide can exhibit significant absorption due to hydrogen, resulting in an OH^- vibrational band peaking at 3278 cm^{-1} [28].

The fundamental lattice vibrations have been studied by Barker [29], Gervais and co-workers [26, 30], and Hoffmann [31]. All model the complex

refractive index in the reststrahlen region. Barker gives the optical modes of aluminum oxide as

$$\Gamma = 2A_{1g}(\mathrm{R}) + 2A_{1u}(-) + 3A_{2g}(-) + 2A_{2u}(\mathrm{IR},\mathbf{E} \parallel \mathbf{c}) + 5E_g(\mathrm{R}) + 4E_u(\mathrm{IR},\mathbf{E} \perp \mathbf{c}), \quad (5)$$

and Table V summarizes measured locations of the infrared-active modes. Porto and Krishnan [32] make the following assignments to the Raman-active modes: A_{1g} vibrations at 418 and 645 cm^{-1} and E_g vibrations at 378, 432, 451, 578, and 751 cm^{-1}.

Refractive indices for the region of fundamental lattice vibrations given in Table I are calculated by the method of Gervais and co-workers [26, 30], essentially duplicating the results reported in 1991 [1]. Real refractive index is calculated over the 200 to 1400 cm^{-1} interval and at 100 cm^{-1} for comparison to low-frequency measurements. The imaginary index is calculated between 200 and 1000 cm^{-1} to avoid regions of multiphonon absorption, which are not represented by this model.

Barker [29] gives a classical oscillator model for the far-infrared optical constants of aluminum oxide, and Harman *et al.* [5] give a refined model based on reanalysis of Barker's reflectance data.

Below 300 cm^{-1}, absorption arises from the red wing of the one-phonon resonances and from multiphonon difference bands. Several measurements of the real refractive index and absorption coefficient [33–38] cover the 5–200 cm^{-1} region. Values from these references are given in Table I.

Low-frequency measurements (1 MHz) of Fontella *et al.* [39], made by the method of substitution, give the static dielectric constant as $\epsilon_o = 9.395 \pm 0.005$ (or $n_o = 3.065 \pm 0.001$) for the ordinary ray ($\mathbf{E} \perp \mathbf{c}$) and $\epsilon_e = 11.589 \pm 0.005$ (or $n_e = 3.404 \pm 0.001$) for the extraordinary ray ($\mathbf{E} \parallel \mathbf{c}$). These values agree well with extrapolated values from Russell and Bell [33], Loewenstein *et al.* [34], Roberts and Coon [37], and Grischkowsky *et al.* [38].

Figures 1 and 2 shows a composite of the principal values of the complex refractive index of aluminum oxide taken from all of the data sources.

ACKNOWLEDGMENTS

We thank Professor T. Tomiki, University of Ryukyus (retired), for graciously providing digital data from his measurements. We acknowledge and greatly appreciate the information provided by Mr. I. H. Malitson, (NBS, retired) on refractive-index measurements and dispersion equations. We also thank Dr. R. H. French and Mr. D. J. Jones of DuPont Company for reanalyzing their measurements and providing their data in digital form.

REFERENCES

1. F. Gervais, Aluminum oxide (Al_2O). *in* "Handbook of Optical Constants of Solids II," (E. D. Palik, ed.), pp. 761–775. Academic Press, San Diego, 1991.
2. H.-J. Hagemann, W. Gudat, and C. Kunz, Optical constants from the far infrared to the

x-ray region: Mg, Al, Cu, Ag, Au, Bi, C, and Al_2O_3. *J. Opt. Soc. Am.* **65**, 742–744 (1975); H.-J. Hagemann, W. Gudat, and C. Kunz, Optical constants from the far infrared to the x-ray region: Mg, Al, Cu, Ag, Au, Bi, C, and Al_2O_3, *DESY* **SR-74/7** (Hamburg, 1974).

3. T. Tomiki, Y. Ganaha, T. Futemma, T. Shikenbaru, Y. Aiura, M. Yuri, S. Sato, H. Fututani, H. Kato, T. Miyahara, J. Tamashiro, and A. Yonesu, Anisotropic optical spectra of α-Al_2O_3 single crystals in the vacuum ultraviolet region. II. Spectra of optical constants. *J. Phys. Soc. Jpn.* **62**, 1372–1387 (1993).
4. T. Tomiki, Y. Ganaha, T. Shikenbaru, T. Futemma, M. Yuri, Y. Aiura, S. Sato, H. Fukutani, H. Kato, T. Miyahara, A. Yonesu, and J. Tamashiro, Anisotropic optical spectra of α-Al_2O single crystals in the vacuum ultraviolet region. I. Spectra of absorption tail and reflectivity. *J. Phys. Soc. Jpn.* **62**, 573–584 (1993).
5. A. K. Harman, S. Ninomiya, and S. Adachi, Optical constants of sapphire (α-Al_2O_3) single crystals. *J. Appl. Phys.* **76**, 8032–8036 (1994).
6. R. H. French, H. Müllejans, and D. J. Jones, Optical properties of aluminum oxide determined from vacuum ultraviolet and electron energy loss spectroscopies. *J. Am. Ceram. Soc.* submitted.
7. M. E. Thomas, W. J. Tropf, and S. L. Gilbert, Vacuum-ultraviolet characterization of sapphire, ALON, and spinel near the band gap. *Opt. Eng.* **32**, 1340–1343 (1993).
8. M. E. Innocenzi, R. T. Swimm, M. Bass, R. H. French, A. B. Villaverde, and M. R. Kokta, Room-temperature optical absorption in undoped α-Al_2O_3. *J. Appl. Phys.* **67**, 7542–7546 (1990).
9. B. D. Evans, Optical transmission in undoped crystalline α-Al_2O_3 grown by several techniques. *J.Appl. Phys.* **70**, 3995–3997 (1991).
10. V. Chandrasekharan and H. Damany, Birefringence of sapphire, magnesium fluoride, and quartz in the vacuum ultraviolet, and retardation plates. *Appl. Opt.* **7**, 939–941 (1968); V. Chandrasekharan and H. Damany, Anomalous dispersion of birefringence of sapphire and magnesium fluoride in the vacuum ultraviolet. *Appl. Opt.* **8**, 671–675 (1969).
11. M. A. Jeppesen, Some optical, thermo-optical, and piezo-optical properties of synthetic sapphire. *J. Opt. Soc. Am.* **48**, 629–632 (1958).
12. I. H. Malitson, Refraction and dispersion of synthetic sapphire. *J. Opt. Soc. Am.* **52**, 1377–1379 (1962); I. H. Malitson, F. V. Murphy, and W. S. Rodney, Refractive index of synthetic sapphire. *J. Opt. Soc. Am.* **48**, 72–73 (1958).
13. I. H. Malitson and M. J. Dodge, Refractive index and birefringence of synthetic sapphire. *J. Opt. Soc. Am.* **62**, 1405 (1972); the cited dispersion equation is given in M. J. Dodge, Refractive index. *in* "Handbook of Laser Science and Technology, Volume IV, Optical Material: Part 2" (M. J. Weber, ed.), CRC Press, Boca Raton, Florida, 1986.
14. A. C. DeFranzo and B. G. Pazol, Index of refraction measurements on sapphire at low temperatures and visible wavelengths. *Appl. Opt.* **32**, 2224–2234 (1993).
15. J. Tapping and M. L. Reilly, Index of refraction of sapphire between 24 and 1060°C for wavelengths of 633 and 799 nm. *J. Opt. Soc. Am. A* **3**, 610–616 (1986).
16. E. S. Zouboulis and M. Grimsditch, Refractive index and elastic properties of single-crystal corundum (α-Al_2O_3) up to 2100 K. *J. Appl. Phys.* **70**, 772–776 (1991).
17. A. Feldman, D. Horowitz, R. M. Walker, and M. J. Dodge, "Optical Materials Characterization Final Technical Report, February 1, 1978–September 30, 1978," NBS Technical Note 993, February 1979.
18. V. I. Bukatyi, Yu. V. Goncharov, V. N. Krasnopevtsev, A. M. Shaiduk, V. P. Lushev, A. A. Pavlenko, and M. G. Potapov, Study of the temperature dependence of the refractive index of sapphire. *Opt. Spectrosc.* **56**, 283–285 (1984).
19. C. H. Lange and D. D. Duncan, Temperature coefficient of refractive index for candidate optical windows. *SPIE Proc.* **1326**, 71–78 (1990).
20. M. J. Dodge, I. H. Malitson, and A. I. Mahan, A special method for precise refractive index measurement of uniaxial optical media. *Appl. Opt.* **8**, 1703–1705 (1969).

21. J. A. Mandarino, Refraction, absorption, and biabsorption in synthetic ruby. *Am. Mineral.* **44**, 961–973 (1959).
22. K. E. Wilson, Thermo-optics of nonlinear crystals and laser materials. Ph.D. Dissertation, University of Southern California, Los Angeles (January 1980).
23. T. F. Deutsch, Absorption coefficient of infrared laser window materials. *J. Phys. Chem. Solids* **34**, 2091–2104 (1973); also see T. F. Deutsch, Laser window materials—An overview. *J. Electron. Mater.* **4**, 663–719 (1975).
24. M. E. Thomas, R. I. Joseph, and W. J. Tropf, Infrared transmission properties of sapphire, spinel, yttria, and ALON as a function of temperature and frequency. *Appl. Opt.* **27**, 239–245 (1988).
25. M. E. Thomas, Infrared properties of the extraordinary ray multiphonon processes in sapphire. *Appl. Opt.* **28**, 3277–3278 (1989).
26. F. Gervais, D. Billard, and B. Piriou, High temperature phonon self-energy: An application to infrared spectra of corundum Al_2O_3. *Rev. Int. Haut. Temp. Refract.* **12**, 58–62 (1975).
27. J. A. Harrington, D. A. Gregory, and W. F. Ott, Infrared absorption in chemical laser window materials. *Appl. Opt.* **15**, 1953–1959 (1976).
28. T. J. Turner and J. H. Crawford, V Centers in single crystal Al_2O_3. *Solid State Commun.* **17**, 167–169 (1975).
29. A. S. Barker, Infrared lattice vibrations and dielectric dispersion in corundum. *Phys. Rev.* **132**, 1474–1481 (1963).
30. F. Gervais and B. Piriou, Anharmonicity in several-polar-mode crystals: Adjusting phonon self-energy of LO and TO modes in Al_2O_3 and TiO_2 to fit infrared reflectivity. *J. Phys. C* **7**, 2374–2386 (1974).
31. C. Hoffmann, Optical constants of infrared active phonons as a function of temperature. Masters Essay, The Johns Hopkins University, Baltimore, Maryland (1988).
32. S. P. S. Porto and R. S. Krishnan, Raman effect of corundum. *J. Chem Phys.* **47**, 1009–1012 (1967).
33. E. E. Russell and E. E. Bell, Optical constants of sapphire in the far infrared. *J. Opt. Soc. Am.* **57**, 543–544 (1967).
34. E. V. Loewenstein, D. R. Smith, and R. L. Morgan, Optical constants of far infrared materials 2: Crystalline solids. *Appl. Opt.* **12**, 398–406 (1973).
35. W. B. Cook and S. Perkowitz, Temperature dependence of the far-infrared ordinary-ray optical constants of sapphire. *Appl. Opt.* **24**, 1773–1775 (1985).
36. V. P. Bystrov, Yu. G. Goncharov, G. V. Kozlov, and A. F. Kupriyanenko, Dielectric properties of optical crystals at submillimeter wavelengths. *Sov. Phys. Tech. Phys. (Engl. Transl.)* **31** 1206–1207 (1986).
37. S. Roberts and D. D. Coon, Far-infrared properties of quartz and sapphire. *J. Opt. Soc. Am.* **52**, 1023–1029 (1962).
38. D. Grischkowsky, S. Keiding, M. van Exter, and C. Fattinger, Far-infrared time-domain spectroscopy with terahertz beams of dielectrics and semiconductors. *J. Opt. Soc. Am. B* **7**, 2006–2015 (1990).
39. J. Fontella, C. Andeen, and D. Schuele, Low-frequency dielectric constants of α-quartz, sapphire, MgF_2, and MgO. *J. Appl. Phys.* **45**, 2852–2854 (1974).

NOTE ADDED IN PROOF

Temperature-dependence of the ultraviolet absorption edge, based on exciton and band locations, is given by French, *et al.*, [40] from 0 K to the melt.

40. R. H. French, D. J. Jones, and S. Loughin, Interband electronic structure of α-alumina up to 2167 K. *J. Am. Ceram. Soc.* **77**, 412-422 (1994).

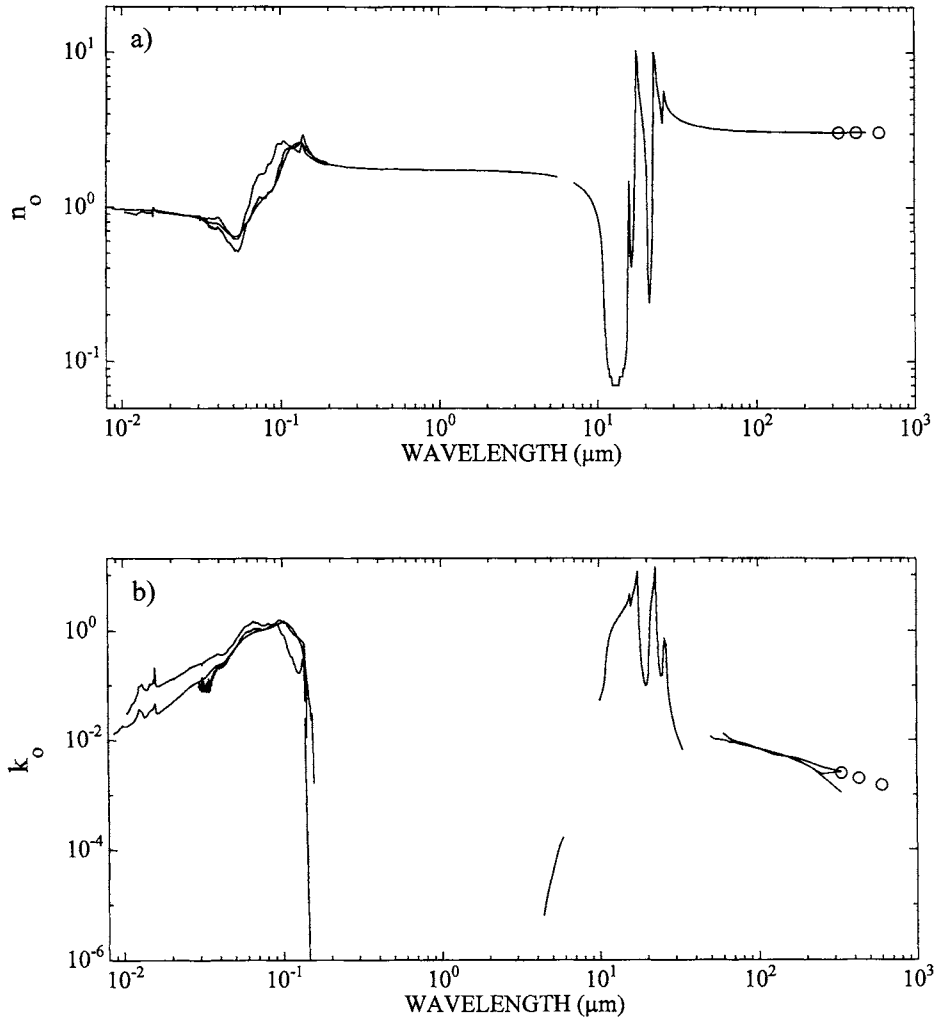

Fig. 1. (a) Log–log plot of the ordinary-ray index of refraction n_o versus wavelength in micrometers for aluminum oxide. (b) Log–log plot of the ordinary-ray extinction coefficient k_o versus wavelength in micrometers for aluminum oxide. Lines are data sets of many points; scattered data are indicated by circles.

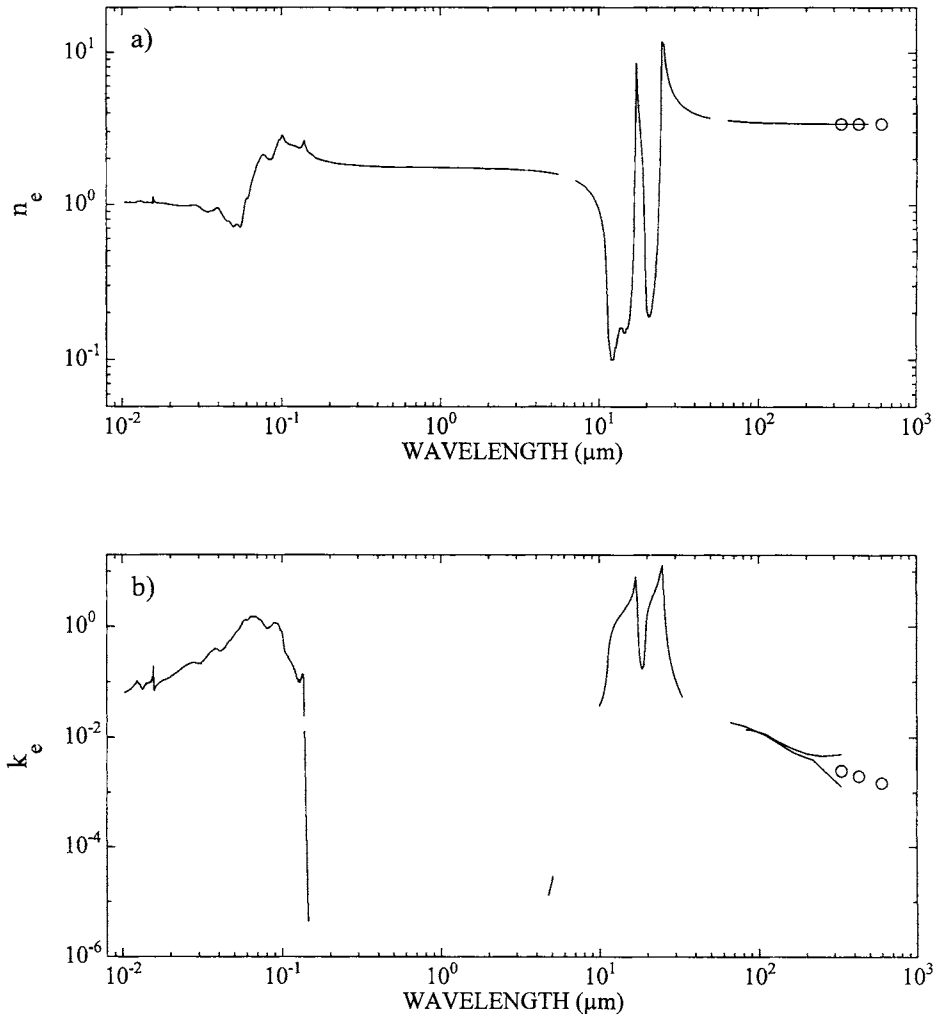

Fig. 2. (a) Log–log plot of the extraordinary-ray index of refraction n_e versus wavelength in micrometers for aluminum oxide. (b) Log–log plot of the extraordinary-ray extinction coefficient k_e versus wavelength in micrometers for aluminum oxide. Lines are data sets of many points; scattered data are indicated by circles.

TABLE I

Values of n and k for Aluminum Oxide (Al_2O_3) from Various References[a]

eV	cm^{-1}	μm	n_o	k_o	n_e	k_e
142.000	1145298	0.008731	0.975 [6]	0.0130 [6]		
141.020	1137394	0.008792	0.975	0.0135		
140.040	1129490	0.008854	0.975	0.0138		
139.000	1121102	0.008920	0.975	0.0139		
138.030	1113278	0.008982	0.975	0.0140		
137.050	1105374	0.009047	0.975	0.0141		
136.010	1096986	0.009116	0.975	0.0143		
135.040	1089162	0.009181	0.974	0.0145		
134.000	1080774	0.009253	0.974	0.0147		
133.020	1072870	0.009321	0.974	0.0150		
132.040	1064966	0.009390	0.973	0.0156		
131.010	1056659	0.009464	0.973	0.0161		
130.030	1048754	0.009535	0.973	0.0165		
129.050	1040850	0.009608	0.973	0.0168		
128.010	1032462	0.009686	0.973	0.0170		
127.040	1024639	0.009760	0.973	0.0174		
126.000	1016250	0.009840	0.973	0.0182		
125.020	1008346	0.009917	0.974	0.0182		
124.050	1000523	0.009995	0.974	0.0178		
123.010	992135	0.010079	0.973	0.0177		
122.030	984231	0.010160	0.973	0.0177		
121.060	976407	0.010242	0.973	0.0177		
120.020	968019	0.010330	0.972	0.0177		
119.897	967027	0.01034			1.035 [3]	0.063 [3]
118.800	958179	0.01044	0.972 [6]	0.0178 [6]		
118.691	957300	0.01045			1.037	0.064
118.182	953195	0.01049	0.929 [3]	0.031 [3]		
118.081	952380	0.01050			1.035	0.064
117.577	948315	0.01055	0.928	0.032		
117.477	947508	0.01055			1.035	0.065
116.967	943395	0.01060	0.927	0.032		
116.868	942597	0.01061			1.035	0.066
116.363	938523	0.01066	0.927	0.033		
116.265	937733	0.01066			1.034	0.066
115.453	931184	0.01074	0.925	0.034		
115.356	930402	0.01075			1.034	0.068
114.546	923868	0.01082	0.924	0.036		
114.441	923022	0.01083			1.034	0.069
113.936	918949	0.01088	0.923	0.036		
113.842	918190	0.01089			1.033	0.069
113.032	911657	0.01097	0.921	0.038		
112.929	910827	0.01098			1.033	0.070
112.122	904318	0.01106	0.919	0.040		
112.021	903503	0.01107			1.033	0.071
111.217	897018	0.01115	0.918	0.042		

[a] References given in brackets.

TABLE I *(Continued)*

Aluminum Oxide (Al_2O_3)

eV	cm^{-1}	μm	n_o	k_o	n_e	k_e
111.108	896139	0.01116			1.032	0.072
110.307	889679	0.01124	0.918	0.045		
110.199	888808	0.01125	0.918	0.045	1.031	0.073
108.692	876653	0.01141	0.916	0.046	1.030	0.076
107.776	869265	0.01150	0.914	0.048	1.030	0.077
106.874	861990	0.01160	0.912	0.049	1.028	0.079
105.961	854626	0.01170	0.909	0.051	1.028	0.082
105.054	847311	0.01180	0.907	0.054	1.029	0.085
104.145	839979	0.01191	0.904	0.058	1.029	0.087
103.235	832640	0.01201	0.902	0.062	1.030	0.089
102.020	822840	0.01215	0.900	0.068	1.031	0.093
101.113	815525	0.01226	0.895	0.072	1.032	0.098
100.206	808209	0.01237	0.892	0.088	1.040	0.104
99.299	800894	0.01249	0.906	0.098	1.050	0.100
98.082	791078	0.01264	0.913	0.099	1.052	0.094
97.175	783763	0.01276	0.918	0.102	1.053	0.090
96.269	776456	0.01288	0.922	0.102	1.053	0.088
95.051	766632	0.01304	0.931	0.107	1.054	0.084
94.142	759300	0.01317	0.940	0.101	1.052	0.078
93.236	751993	0.01330	0.942	0.094	1.048	0.074
92.025	742226	0.01347	0.939	0.087	1.039	0.074
91.119	734918	0.01361	0.935	0.087	1.034	0.078
90.204	727539	0.01374	0.936	0.086	1.031	0.082
89.294	720199	0.01389	0.932	0.083	1.030	0.086
88.083	710432	0.01408	0.925	0.085	1.031	0.093
87.178	703132	0.01422	0.922	0.087	1.033	0.092
86.268	695793	0.01437	0.915	0.094	1.032	0.095
85.055	686009	0.01458	0.920	0.105	1.033	0.095
84.149	678702	0.01473	0.925	0.104	1.032	0.096
83.239	671362	0.01490	0.922	0.108	1.031	0.100
82.028	661595	0.01511	0.923	0.107	1.032	0.099
81.116	654239	0.01528	0.917	0.115	1.025	0.109
79.996	645206	0.01550	0.929	0.130	1.043	0.118
79.934	644706	0.01551	0.929	0.129	1.042	0.117
79.903	644456	0.01552	0.930	0.129	1.043	0.117
79.846	643996	0.01553	0.931	0.127	1.043	0.115
79.784	643496	0.01554	0.930	0.126	1.042	0.114
79.723	643004	0.01555	0.931	0.124	1.041	0.113
79.661	642504	0.01556	0.930	0.122	1.038	0.112
79.600	642012	0.01558	0.927	0.119	1.035	0.112
79.539	641520	0.01559	0.923	0.115	1.030	0.113
79.483	641069	0.01560	0.916	0.113	1.025	0.117
79.422	640577	0.01561	0.907	0.114	1.018	0.124
79.361	640085	0.01562	0.893	0.120	1.017	0.137
79.300	639593	0.01563	0.881	0.133	1.017	0.155
79.239	639101	0.01565	0.874	0.157	1.030	0.176
79.178	638609	0.01566	0.883	0.183	1.056	0.186

(continued)

TABLE I *(Continued)*

Aluminum Oxide (Al_2O_3)

eV	cm^{-1}	μm	n_o	k_o	n_e	k_e
79.118	638125	0.01567	0.906	0.206	1.088	0.183
79.057	637633	0.01568	0.939	0.214	1.116	0.161
78.997	637149	0.01569	0.968	0.200	1.116	0.124
78.936	636657	0.01571	0.978	0.175	1.108	0.108
78.876	636173	0.01572	0.976	0.157	1.089	0.102
78.816	635689	0.01573	0.965	0.151	1.081	0.107
78.756	635205	0.01574	0.959	0.157	1.083	0.115
78.691	634681	0.01576	0.964	0.165	1.092	0.114
78.631	634197	0.01577	0.976	0.166	1.100	0.107
78.571	633713	0.01578	0.989	0.162	1.104	0.094
78.511	633229	0.01579	0.997	0.150	1.099	0.082
78.452	632753	0.01580	0.998	0.134	1.091	0.074
78.387	632229	0.01582	0.993	0.125	1.083	0.071
78.328	631753	0.01583	0.990	0.120	1.076	0.070
78.268	631269	0.01584	0.986	0.117	1.070	0.070
78.209	630793	0.01585	0.982	0.114	1.066	0.071
78.145	630277	0.01587	0.979	0.111	1.063	0.071
78.086	629801	0.01588	0.977	0.110	1.060	0.072
78.027	629325	0.01589	0.975	0.109	1.058	0.073
77.963	628809	0.01590	0.973	0.107	1.056	0.073
77.905	628341	0.01591	0.972	0.107	1.054	0.074
77.846	627865	0.01593	0.970	0.106	1.053	0.075
77.782	627349	0.01594	0.968	0.105	1.051	0.075
77.724	626881	0.01595	0.967	0.104	1.050	0.076
77.661	626373	0.01596	0.966	0.103	1.049	0.076
77.602	625897	0.01598	0.965	0.103	1.048	0.076
77.539	625389	0.01599	0.964	0.103	1.047	0.077
77.481	624921	0.01600	0.963	0.102	1.046	0.077
77.100	621849	0.01608	0.958	0.100		
77.000	621042	0.01610			1.040	0.080
76.501	617017	0.01621	0.952	0.098	1.036	0.083
75.901	612178	0.01634	0.947	0.098		
75.499	608936	0.01642			1.031	0.087
75.002	604927	0.01653	0.942	0.099	1.029	0.088
74.398	600056	0.01667	0.939	0.100	1.026	0.091
74.101	597660	0.01673	0.938	0.100	1.025	0.092
73.499	592805	0.01687	0.935	0.100	1.024	0.094
72.001	580723	0.01722	0.930	0.104	1.022	0.099
71.101	573464	0.01744	0.928	0.106	1.020	0.100
70.199	566189	0.01766	0.926	0.108	1.019	0.103
68.999	556510	0.01797	0.923	0.111	1.017	0.105
68.101	549267	0.01821	0.921	0.114	1.015	0.107
66.900	539581	0.01853	0.920	0.117	1.013	0.110
65.999	532314	0.01879	0.918	0.120	1.012	0.111
65.101	525071	0.01905	0.917	0.123	1.009	0.113
64.201	517812	0.01931	0.915	0.126	1.007	0.115
63.001	508133	0.01968	0.915	0.130	1.003	0.119

TABLE I *(Continued)*

Aluminum Oxide (Al_2O_3)

eV	cm^{-1}	μm	n_o	k_o	n_e	k_e
62.101	500874	0.01997	0.913	0.131	0.999	0.122
61.200	493607	0.02026	0.911	0.134	0.997	0.126
60.001	483937	0.02066	0.911	0.136	0.995	0.130
59.100	476670	0.02098	0.905	0.139	0.992	0.135
58.201	469419	0.02130	0.903	0.143	0.990	0.139
56.999	459724	0.02175	0.900	0.148	0.986	0.144
56.099	452465	0.02210	0.897	0.152	0.983	0.149
55.200	445214	0.02246	0.895	0.157	0.980	0.155
54.000	435536	0.02296	0.892	0.164	0.977	0.164
53.101	428285	0.02335	0.890	0.169	0.976	0.171
52.200	421018	0.02375	0.888	0.174	0.977	0.178
51.000	411339	0.02431	0.884	0.182	0.976	0.185
50.099	404072	0.02475	0.881	0.188	0.976	0.193
49.200	396822	0.02520	0.879	0.196	0.977	0.199
48.000	387143	0.02583	0.878	0.207	0.979	0.207
47.100	379884	0.02632	0.879	0.216	0.980	0.212
46.199	372617	0.02684	0.880	0.223	0.982	0.217
45.000	362947	0.02755	0.881	0.230	0.985	0.222
44.099	355680	0.02812	0.881	0.236	0.988	0.224
43.200	348429	0.02870	0.880	0.241	0.989	0.221
42.000	338750	0.02952	0.882 [3]	0.249 [3]	0.983	0.215
			0.859 [6]	0.098 [6]		
41.100	331491	0.03017	0.875 [3]	0.252 [3]	0.967	0.214
40.200	324232	0.03084	0.882	0.256	0.960	0.216
39.000	314554	0.03179	0.859	0.269	0.931	0.235
38.100	307295	0.03254	0.854	0.282	0.916	0.252
37.200	300036	0.03333	0.851	0.297	0.906	0.274
36.000	290357	0.03444	0.849	0.316	0.894	0.309
35.100	283098	0.03532	0.851	0.329	0.900	0.338
34.200	275839	0.03625	0.846	0.339	0.907	0.356
33.000	266161	0.03757	0.842	0.361	0.916	0.390
32.100	258902	0.03862	0.843	0.379	0.941	0.396
31.200	251643	0.03974	0.859	0.387	0.950	0.380
30.000	241964	0.04133	0.841	0.367	0.901	0.360
29.100	234705	0.04261	0.800	0.379	0.858	0.384
28.302	228269	0.04381	0.764	0.400	0.814	0.416
27.984	225704	0.04431	0.749	0.411	0.798	0.439
27.673	223196	0.04480	0.731	0.427	0.787	0.465
27.369	220744	0.04530	0.716	0.448	0.780	0.490
27.072	218349	0.04580	0.706	0.472	0.778	0.512
27.013	217873	0.04590	0.605 [6]	0.317 [6]		
26.891	216889	0.04611	0.596	0.328		
26.799	216147	0.04626	0.592	0.335		
26.780	215994	0.04630	0.703 [3]	0.492 [3]	0.776	0.534
26.738	215655	0.04637	0.590 [6]	0.344 [6]		
26.616	214671	0.04658	0.593	0.353		
26.496	213703	0.04679	0.698 [3]	0.508 [3]	0.776	0.550

(continued)

TABLE I *(Continued)*

Aluminum Oxide (Al_2O_3)

eV	cm^{-1}	μm	n_o	k_o	n_e	k_e
26.494	213687	0.04680	0.593 [6]	0.359 [6]		
26.311	212211	0.04712	0.594	0.369		
26.219	211469	0.04729	0.590	0.371		
26.217	211453	0.04729	0.691 [3]	0.519 [3]	0.772	0.562
26.127	210727	0.04745	0.590 [6]	0.376 [6]		
26.005	209743	0.04768	0.584	0.380		
25.944	209251	0.04779	0.676 [3]	0.538 [3]	0.760	0.575
25.914	209009	0.04784	0.582 [6]	0.386 [6]		
25.700	207283	0.04824	0.575	0.396		
25.676	207089	0.04829	0.666 [3]	0.556 [3]	0.744	0.595
25.609	206549	0.04841	0.572 [6]	0.399 [6]		
25.425	205065	0.04877	0.560	0.419		
25.414	204976	0.04879	0.652 [3]	0.578 [3]	0.730	0.625
25.303	204081	0.04900	0.559 [6]	0.426 [6]		
25.212	203347	0.04918	0.557	0.431		
25.158	202911	0.04928	0.640 [3]	0.604 [3]	0.723	0.655
25.120	202605	0.04936	0.552 [6]	0.438 [6]		
24.907	200887	0.04978	0.545	0.461		
24.906	200879	0.04978	0.629 [3]	0.633 [3]	0.717	0.688
24.815	200145	0.04996	0.544 [6]	0.465 [6]		
24.723	199403	0.05015	0.540	0.474		
24.659	198887	0.05028	0.622 [3]	0.667 [3]	0.717	0.725
24.601	198419	0.05040	0.536 [6]	0.481 [6]		
24.510	197685	0.05059	0.531	0.495		
24.418	196943	0.05078	0.621 [3]	0.698 [3]	0.725	0.756
24.418	196943	0.05078	0.529 [6]	0.500 [6]		
24.204	195217	0.05123	0.522	0.537		
24.180	195023	0.05128	0.620 [3]	0.728 [3]	0.733	0.782
24.113	194483	0.05142	0.524 [6]	0.542 [6]		
24.021	193741	0.05162	0.523	0.558		
23.948	193152	0.05177	0.620 [3]	0.758 [3]	0.739	0.804
23.930	193007	0.05181	0.527 [6]	0.564 [6]		
23.808	192023	0.05208	0.527	0.577		
23.720	191313	0.05227	0.622 [3]	0.785 [3]	0.742	0.825
23.716	191281	0.05228	0.526 [6]	0.581 [6]		
23.502	189555	0.05276	0.524	0.608		
23.496	189507	0.05277	0.618 [3]	0.817 [3]	0.741	0.845
23.411	188821	0.05296	0.523 [6]	0.616 [6]		
23.319	188079	0.05317	0.520	0.627		
23.277	187740	0.05327	0.619 [3]	0.851 [3]	0.734	0.868
23.228	187345	0.05338	0.517 [6]	0.638 [6]		
23.106	186361	0.05366	0.515	0.663		
23.061	185998	0.05376	0.622 [3]	0.890 [3]	0.724	0.898
23.014	185619	0.05387	0.517 [6]	0.678 [6]		
22.922	184877	0.05409	0.522	0.695		
22.849	184288	0.05426	0.631 [3]	0.927 [3]	0.714	0.938
22.800	183893	0.05438	0.527 [6]	0.707 [6]		

TABLE I *(Continued)*

Aluminum Oxide (Al_2O_3)

eV	cm^{-1}	μm	n_o	k_o	n_e	k_e
22.709	183159	0.05460	0.529	0.720		
22.642	182619	0.05476	0.642 [3]	0.962 [3]	0.709	0.985
22.617	182417	0.05482	0.531 [6]	0.734 [6]		
22.526	181683	0.05504	0.535	0.752		
22.438	180973	0.05526	0.653 [3]	1.000 [3]	0.712	1.039
22.404	180699	0.05534	0.543 [6]	0.766 [6]		
22.312	179957	0.05557	0.546	0.786		
22.238	179360	0.05575	0.668 [3]	1.039 [3]	0.723	1.098
22.220	179215	0.05580	0.554 [6]	0.797 [6]		
22.129	178481	0.05603	0.560	0.815		
22.041	177771	0.05625	0.690 [3]	1.077 [3]	0.747	1.158
22.007	177497	0.05634	0.574 [6]	0.828 [6]		
21.915	176755	0.05658	0.581	0.848		
21.847	176207	0.05675	0.716 [3]	1.110 [3]	0.784	1.217
21.824	176021	0.05681	0.593 [6]	0.854 [6]		
21.702	175037	0.05713	0.602	0.874		
21.658	174682	0.05725	0.742 [3]	1.142 [3]	0.834	1.266
21.610	174295	0.05737	0.614 [6]	0.885 [6]		
21.518	173553	0.05762	0.625	0.896		
21.471	173174	0.05775	0.772 [3]	1.170 [3]	0.892	1.300
21.427	172819	0.05786	0.636 [6]	0.907 [6]		
21.305	171835	0.05820	0.655	0.918		
21.287	171690	0.05824	0.803 [3]	1.196 [3]	0.948	1.321
21.213	171093	0.05845	0.665 [6]	0.923 [6]		
21.122	170359	0.05870	0.675	0.934		
21.107	170238	0.05874	0.839 [3]	1.216 [3]	1.003	1.331
21.000	169375	0.05904	0.691 [6]	0.946 [6]		
20.929	168802	0.05924	0.871 [3]	1.226 [3]	1.051	1.326
20.908	168633	0.05930	0.703 [6]	0.950 [6]		
20.816	167891	0.05956	0.714	0.961		
20.755	167399	0.05974	0.895 [3]	1.237 [3]	1.083	1.313
20.725	167157	0.05982	0.729 [6]	0.965 [6]		
20.603	166173	0.06018	0.743	0.973		
20.584	166020	0.06023	0.917 [3]	1.245 [3]	1.095	1.304
20.511	165431	0.06045	0.756 [6]	0.974 [6]		
20.420	164697	0.06072	0.770	0.987		
20.415	164657	0.06073	0.932 [3]	1.258 [3]	1.098	1.310
20.328	163955	0.06099	0.787 [6]	0.978 [6]		
20.249	163318	0.06123	0.948 [3]	1.276 [3]	1.099	1.333
20.085	161995	0.06173	0.966	1.298	1.111	1.368
20.084	161987	0.06173	0.793 [6]	0.978 [6]		
19.992	161245	0.06202	0.800	0.983		
19.925	160705	0.06223	0.986 [3]	1.318 [3]	1.134	1.406
19.840	160019	0.06249	0.815 [6]	0.997 [6]		
19.767	159430	0.06272	1.007 [3]	1.343 [3]	1.169	1.448
19.748	159277	0.06278	0.820 [6]	0.992 [6]		
19.657	158543	0.06307	0.821	0.998		

(continued)

TABLE I *(Continued)*

Aluminum Oxide (Al_2O_3)

eV	cm^{-1}	μm	n_o	k_o	n_e	k_e
19.611	158172	0.06322	1.034 [3]	1.372 [3]	1.218	1.481
19.565	157801	0.06337	0.824 [6]	1.010 [6]		
19.473	157059	0.06367	0.833	1.025		
19.458	156938	0.06372	1.068 [3]	1.397 [3]	1.273	1.505
19.382	156325	0.06397	0.843 [6]	1.033 [6]		
19.307	155720	0.06422	1.106 [3]	1.422 [3]	1.331	1.515
19.290	155583	0.06427	0.850 [6]	1.039 [6]		
19.199	154849	0.06458	0.861	1.058		
19.158	154518	0.06472	1.152 [3]	1.443 [3]	1.384	1.515
19.138	154357	0.06478	0.873 [6]	1.066 [6]		
19.016	153373	0.06520	0.891	1.071		
19.012	153341	0.06521	1.201 [3]	1.452 [3]	1.429	1.510
18.954	152873	0.06541	0.901 [6]	1.079 [6]		
18.893	152381	0.06562	0.912	1.083		
18.868	152179	0.06571	1.247 [3]	1.456 [3]	1.468	1.507
18.832	151889	0.06584	0.923 [6]	1.084 [6]		
18.771	151397	0.06605	0.932	1.087		
18.726	151034	0.06621	1.292 [3]	1.449 [3]	1.504	1.504
18.680	150663	0.06637	0.951 [6]	1.093 [6]		
18.588	149921	0.06670	0.967	1.087		
18.587	149913	0.06671	1.330 [3]	1.441 [3]	1.540	1.508
18.497	149187	0.06703	0.974 [6]	1.082 [6]		
18.449	148800	0.06720	1.364 [3]	1.430 [3]	1.582	1.507
18.375	148203	0.06747	0.993 [6]	1.087 [6]		
18.313	147703	0.06770	1.392 [3]	1.420 [3]	1.623	1.504
18.283	147461	0.06781	0.998 [6]	1.080 [6]		
18.191	146719	0.06816	1.014	1.092		
18.180	146630	0.06820	1.417 [3]	1.412 [3]	1.666	1.502
18.100	145985	0.06850	1.017 [6]	1.077 [6]		
18.048	145566	0.06870	1.442 [3]	1.407 [3]	1.710	1.492
18.008	145243	0.06885	1.028 [6]	1.093 [6]		
17.947	144751	0.06908	1.036	1.091		
17.918	144517	0.06920	1.469 [3]	1.401 [3]	1.757	1.483
17.886	144259	0.06932	1.044 [6]	1.094 [6]		
17.825	143767	0.06956	1.056	1.097		
17.790	143485	0.06969	1.496 [3]	1.395 [3]	1.804	1.459
17.764	143275	0.06980	1.064 [6]	1.091 [6]		
17.703	142783	0.07004	1.069	1.088		
17.664	142469	0.07019	1.525 [3]	1.388 [3]	1.839	1.428
17.642	142291	0.07028	1.073 [6]	1.085 [6]		
17.581	141799	0.07052	1.077	1.084		
17.540	141469	0.07069	1.554 [3]	1.373 [3]	1.865	1.401
17.520	141307	0.07077	1.080 [6]	1.086 [6]		
17.459	140815	0.07102	1.087	1.093		
17.417	140476	0.07119	1.579 [3]	1.358 [3]	1.884	1.376
17.398	140323	0.07126	1.102 [6]	1.102 [6]		
17.337	139831	0.07151	1.112	1.094		

TABLE I *(Continued)*

Aluminum Oxide (Al_2O_3)

eV	cm^{-1}	μm	n_o	k_o	n_e	k_e
17.296	139501	0.07168	1.601 [3]	1.338 [3]	1.904	1.364
17.276	139339	0.07177	1.112 [6]	1.082 [6]		
17.184	138597	0.07215	1.130	1.098		
17.177	138541	0.07218	1.616 [3]	1.316 [3]	1.927	1.348
17.123	138105	0.07241	1.139 [6]	1.087 [6]		
17.093	137863	0.07254	1.140	1.080		
17.059	137589	0.07268	1.626 [3]	1.299 [3]	1.952	1.337
17.032	137371	0.07280	1.145 [6]	1.079 [6]		
16.970	136871	0.07306	1.154	1.077		
16.943	136653	0.07318	1.636 [3]	1.284 [3]	1.985	1.324
16.909	136379	0.07332	1.153 [6]	1.062 [6]		
16.848	135887	0.07359	1.156	1.063		
16.828	135726	0.07368	1.640 [3]	1.265 [3]	2.019	1.299
16.787	135395	0.07386	1.165 [6]	1.063[6]		
16.726	134903	0.07413	1.159	1.045		
16.715	134814	0.07418	1.639 [3]	1.256 [3]	2.046	1.268
16.665	134411	0.07440	1.154 [6]	1.042 [6]		
16.604	133919	0.07467	1.641 [3]	1.251 [3]	2.071	1.239
16.604	133919	0.07467	1.158 [6]	1.050 [6]		
16.543	133427	0.07495	1.155	1.042		
16.494	133032	0.07517	1.643 [3]	1.247 [3]	2.090	1.203
16.482	132935	0.07522	1.150 [6]	1.041 [6]		
16.391	132201	0.07564	1.155 [3]	1.050 [3]		
16.385	132153	0.07567	1.646	1.245	2.104	1.170
16.299	131459	0.07607	1.148 [6]	1.042 [6]		
16.279	131298	0.07616	1.647 [3]	1.242 [3]	2.116	1.137
16.207	130717	0.07650	1.144 [6]	1.052 [6]		
16.173	130443	0.07666	1.648 [3]	1.246 [3]	2.122	1.100
16.116	129983	0.07693	1.149 [6]	1.062 [6]		
16.085	129733	0.07708	1.148	1.060		
16.068	129596	0.07716	1.651 [3]	1.249 [3]	2.125	1.068
15.994	128999	0.07752	1.144 [6]	1.064 [6]		
15.965	128765	0.07766	1.652 [3]	1.255 [3]	2.120	1.033
15.902	128257	0.07797	1.145 [6]	1.075 [6]		
15.864	12795	10.07816	1.656 [3]	1.267 [3]	2.112	1.005
15.841	127765	0.07827	1.148 [6]	1.085 [6]		
15.763	127136	0.07866	1.661 [3]	1.277 [3]	2.100	0.979
15.750	127031	0.07872	1.157 [6]	1.091 [6]		
15.664	126338	0.07915	1.668 [3]	1.293 [3]	2.085	0.957
15.658	126289	0.07918	1.146 [6]	1.083 [6]		
15.566	125547	0.07965	1.680 [3]	1.314 [3]	2.065	0.941
15.566	125547	0.07965	1.140 [6]	1.102 [6]		
15.475	124813	0.08012	1.142	1.125		
15.470	124773	0.08015	1.699 [3]	1.335 [3]	2.047	0.933
15.383	124071	0.08060	1.147 [6]	1.145 [6]		
15.374	123999	0.08065	1.728 [3]	1.356 [3]	2.030	0.928
15.292	123337	0.08108	1.166 [6]	1.174 [6]		

(continued)

TABLE I *(Continued)*

Aluminum Oxide (Al_2O_3)

eV	cm^{-1}	μm	n_o	k_o	n_e	k_e
15.280	123241	0.08114	1.763 [3]	1.367 [3]	2.014	0.929
15.200	122595	0.08157	1.176 [6]	1.181 [6]		
15.187	122490	0.08164	1.802 [3]	1.372 [3]	2.003	0.935
15.139	122103	0.08190	1.192 [6]	1.199 [6]		
15.095	121748	0.08214	1.838 [3]	1.364 [3]	1.995	0.940
15.047	121361	0.08240	1.205 [6]	1.196 [6]		
15.004	121014	0.08263	1.866 [3]	1.353 [3]	1.987	0.946
14.956	120627	0.08290	1.222 [6]	1.218 [6]		
14.914	120289	0.08313	1.892 [3]	1.340 [3]	1.982	0.954
14.864	119885	0.08341	1.243 [6]	1.214 [6]		
14.825	119571	0.08363	1.909 [3]	1.321 [3]	1.978	0.963
14.773	119151	0.08393	1.246 [6]	1.214 [6]		
14.737	118861	0.08413	1.919 [3]	1.310 [3]	1.974	0.974
14.681	118409	0.08445	1.263 [6]	1.224 [6]		
14.651	118167	0.08463	1.924 [3]	1.301 [3]	1.970	0.987
14.565	117474	0.08513	1.933	1.303	1.971	1.004
14.529	117183	0.08534	1.265 [6]	1.220 [6]		
14.480	116788	0.08563	1.942 [3]	1.302 [3]	1.975	1.022
14.437	116441	0.08588	1.271 [6]	1.233 [6]		
14.396	116111	0.08612	1.950 [3]	1.306 [3]	1.981	1.041
14.376	115949	0.08624	1.270 [6]	1.234 [6]		
14.315	115457	0.08661	1.271	1.246		
14.314	115449	0.08662	1.961 [3]	1.315 [3]	1.989	1.061
14.254	114965	0.08698	1.276 [6]	1.258 [6]		
14.232	114788	0.08712	1.977 [3]	1.327 [3]	2.003	1.086
14.193	114473	0.08736	1.274 [6]	1.262 [6]		
14.151	114135	0.08762	2.001 [3]	1.338 [3]	2.023	1.109
14.132	113981	0.08773	1.274 [6]	1.279 [6]		
14.071	113489	0.08811	2.024 [3]	1.343 [3]	2.047	1.131
14.071	113489	0.08811	1.285 [6]	1.304 [6]		
14.010	112997	0.08850	1.295	1.319		
13.992	112852	0.08861	2.049 [3]	1.351 [3]	2.081	1.152
13.949	112505	0.08888	1.307 [6]	1.335 [6]		
13.914	112223	0.08911	2.076 [3]	1.357 [3]	2.117	1.164
13.888	112013	0.08928	1.320 [6]	1.349 [6]		
13.837	111602	0.08960	2.105 [3]	1.361 [3]	2.155	1.171
13.827	111521	0.08967	1.330 [6]	1.359 [6]		
13.766	111029	0.09007	1.338	1.369		
13.760	110981	0.09011	2.132 [3]	1.363 [3]	2.193	1.172
13.704	110529	0.09047	1.343 [6]	1.383 [6]		
13.685	110376	0.09060	2.164 [3]	1.372 [3]	2.228	1.169
13.643	110037	0.09088	1.355 [6]	1.408 [6]		
13.610	109771	0.09110	2.199 [3]	1.376 [3]	2.265	1.165
13.582	109545	0.09129	1.375 [6]	1.434 [6]		
13.536	109174	0.09160	2.246 [3]	1.384 [3]	2.294	1.153
13.521	109053	0.09170	1.394 [6]	1.452 [6]		
13.463	108586	0.09209	2.292 [3]	1.376 [3]	2.325	1.150

TABLE I *(Continued)*

Aluminum Oxide (Al_2O_3)

eV	cm^{-1}	μm	n_o	k_o	n_e	k_e
13.460	108561	0.09211	1.413 [6]	1.469 [6]		
13.399	108069	0.09253	1.435	1.491		
13.390	107997	0.09260	2.346 [3]	1.373 [3]	2.351	1.143
13.338	107577	0.09296	1.461 [6]	1.513 [6]		
13.319	107424	0.09309	2.402 [3]	1.350 [3]	2.389	1.147
13.277	107085	0.09338	1.494 [6]	1.538 [6]		
13.248	106851	0.09359	2.454 [3]	1.319 [3]	2.432	1.137
13.216	106593	0.09381	1.538 [6]	1.560 [6]		
13.178	106287	0.09408	2.499 [3]	1.278 [3]	2.473	1.122
13.155	106101	0.09425	1.578 [6]	1.563 [6]		
13.109	105730	0.09458	2.534 [3]	1.232 [3]	2.517	1.104
13.094	105609	0.09469	1.604 [6]	1.556 [6]		
13.040	105174	0.09508	2.560 [3]	1.186 [3]	2.560	1.078
13.033	105117	0.09513	1.632 [6]	1.561 [6]		
12.972	104625	0.09558	2.581 [3]	1.142 [3]	2.603	1.044
12.972	104625	0.09558	1.670 [6]	1.573 [6]		
12.911	104133	0.09603	1.708	1.574		
12.905	104085	0.09608	2.596 [3]	1.096 [3]	2.639	0.999
12.850	103641	0.09649	1.745 [6]	1.572 [6]		
12.838	103545	0.09658	2.605 [3]	1.052 [3]	2.661	0.948
12.789	103149	0.09695	1.789 [6]	1.569 [6]		
12.772	103012	0.09708	2.609 [3]	1.010 [3]	2.664	0.901
12.728	102657	0.09741	1.816 [6]	1.548 [6]		
12.707	102488	0.09757	2.607 [3]	0.972 [3]	2.661	0.871
12.667	102165	0.09788	1.840 [6]	1.536 [6]		
12.643	101972	0.09807	2.600 [3]	0.939 [3]	2.663	0.855
12.606	101673	0.09835	1.886 [6]	1.533 [6]		
12.579	101456	0.09857	2.592 [3]	0.912 [3]	2.679	0.848
12.545	101181	0.09883	1.903 [6]	1.499 [6]		
12.516	100948	0.09906	2.584 [3]	0.892 [3]	2.710	0.835
12.484	100689	0.09932	1.895 [6]	1.470 [6]		
12.453	100439	0.09956	2.577 [3]	0.876 [3]	2.757	0.808
12.422	100189	0.09981	1.905 [6]	1.472 [6]		
12.391	99939.4	0.1001	2.571 [3]	0.867 [3]	2.790	0.758
12.361	99697.4	0.1003	1.918 [6]	1.476 [6]		
12.330	99447.4	0.1006	2.578 [3]	0.864 [3]	2.822	0.702
12.300	99205.4	0.1008	1.943 [6]	1.486 [6]		
12.269	98955.4	0.1011	2.589 [3]	0.854 [3]	2.838	0.629
12.239	98713.4	0.1013	1.975 [6]	1.493 [6]		
12.209	98471.4	0.1016	2.601 [3]	0.844 [3]	2.826	0.557
12.178	98221.4	0.1018	1.999 [6]	1.493 [6]		
12.149	97987.5	0.1021	2.622 [3]	0.834 [3]	2.808	0.498
12.117	97729.4	0.1023	2.048 [6]	1.504 [6]		
12.090	97511.7	0.1026	2.651 [3]	0.812 [3]	2.775	0.447
12.056	97237.4	0.1028	2.100 [6]	1.499 [6]		
12.032	97043.9	0.1030	2.667 [3]	0.776 [3]	2.745	0.409
11.995	96745.4	0.1034	2.129 [6]	1.478 [6]		

(continued)

TABLE I *(Continued)*

Aluminum Oxide (Al_2O_3)

eV	cm^{-1}	μm	n_o	k_o	n_e	k_e
11.974	96576.1	0.1035	2.678 [3]	0.743 [3]	2.706	0.380
11.934	96253.4	0.1039	2.177 [6]	1.469 [6]		
11.917	96116.3	0.1040	2.687 [3]	0.708 [3]	2.680	0.362
11.873	95761.4	0.1044	2.227 [6]	1.446 [6]		
11.860	95656.6	0.1045	2.687 [3]	0.673 [3]	2.651	0.345
11.812	95269.4	0.1050	2.254 [6]	1.410 [6]		
11.804	95204.9	0.1050	2.691 [3]	0.639 [3]	2.624	0.336
11.751	94777.5	0.1055	2.288 [6]	1.380 [6]		
11.748	94753.3	0.1055	2.678 [3]	0.604 [3]	2.610	0.328
11.693	94309.7	0.1060	2.677	0.580	2.587	0.317
11.690	94285.5	0.1061	2.307 [6]	1.344 [6]		
11.638	93866.1	0.1065	2.668 [3]	0.548 [3]	2.570	0.315
11.629	93793.5	0.1066	2.324 [6]	1.314 [6]		
11.584	93430.5	0.1070	2.655 [3]	0.523 [3]	2.565	0.311
11.568	93301.5	0.1072	2.362 [6]	1.285 [6]		
11.531	93003.0	0.1075	2.645 [3]	0.502 [3]	2.552	0.300
11.507	92809.5	0.1077	2.366 [6]	1.241 [6]		
11.477	92567.5	0.1080	2.638 [3]	0.479 [3]	2.541	0.295
11.446	92317.5	0.1083	2.357 [6]	1.210 [6]		
11.425	92148.1	0.1085	2.620 [3]	0.457 [3]	2.535	0.286
11.385	91825.5	0.1089	2.380 [6]	1.191 [6]		
11.373	91728.7	0.1090	2.613 [3]	0.441 [3]	2.517	0.280
11.324	91333.5	0.1095	2.397 [6]	1.162 [6]		
11.321	91309.3	0.1095	2.593 [3]	0.423 [3]	2.515	0.280
11.270	90898.0	0.1100	2.586	0.413	2.510	0.271
11.263	90841.5	0.1101	2.400 [6]	1.131 [6]		
11.219	90486.6	0.1105	2.575 [3]	0.397 [3]	2.503	0.263
11.202	90349.5	0.1107	2.405 [6]	1.105 [6]		
11.169	90083.3	0.1110	2.564 [3]	0.383 [3]	2.495	0.255
11.141	89857.5	0.1113	2.412 [6]	1.080 [6]		
11.119	89680.1	0.1115	2.549 [3]	0.370 [3]	2.487	0.250
11.079	89357.5	0.1119	2.427 [6]	1.051 [6]		
11.069	89276.8	0.1120	2.538 [3]	0.362 [3]	2.481	0.244
11.020	88881.6	0.1125	2.526	0.354	2.471	0.241
11.018	88865.5	0.1125	2.415 [6]	1.020 [6]		
10.972	88494.4	0.1130	2.515 [3]	0.350 [3]	2.475	0.236
10.957	88373.5	0.1132	2.392 [6]	1.005 [6]		
10.924	88107.3	0.1135	2.510 [3]	0.345 [3]	2.461	0.228
10.896	87881.5	0.1138	2.408 [6]	0.998 [6]		
10.876	87720.2	0.1140	2.502 [3]	0.338 [3]	2.463	0.226
10.835	87389.5	0.1144	2.423 [6]	0.982 [6]		
10.829	87341.1	0.1145	2.494 [3]	0.337 [3]	2.454	0.219
10.782	86962.0	0.1150	2.500	0.336	2.457	0.214
10.774	86897.5	0.1151	2.431 [6]	0.962 [6]		
10.735	86582.9	0.1155	2.499 [3]	0.325 [3]	2.448	0.205
10.713	86405.5	0.1157	2.453 [6]	0.936 [6]		
10.689	86211.9	0.1160	2.503 [3]	0.314 [3]	2.444	0.200

TABLE I *(Continued)*

Aluminum Oxide (Al_2O_3)

eV	cm^{-1}	μm	n_o	k_o	n_e	k_e
10.652	85913.5	0.1164	2.438 [6]	0.908 [6]		
10.644	85849.0	0.1165	2.505 [3]	0.294 [3]	2.439	0.195
10.598	85478.0	0.1170	2.485	0.279	2.435	0.192
10.591	85421.5	0.1171	2.420 [6]	0.895 [6]		
10.553	85115.0	0.1175	2.487 [3]	0.273 [3]	2.437	0.184
10.509	84760.1	0.1180	2.476	0.256	2.427	0.175
10.500	84687.5	0.1181	2.449 [6]	0.871 [6]		
10.465	84405.2	0.1185	2.458 [3]	0.251 [3]	2.422	0.171
10.438	84187.5	0.1188	2.430 [6]	0.851 [6]		
10.421	84050.4	0.1190	2.458 [3]	0.252 [3]	2.415	0.169
10.378	83703.6	0.1195	2.458	0.242	2.415	0.168
10.377	83695.5	0.1195	2.422 [6]	0.845 [6]		
10.292	83009.9	0.1205	2.441 [3]	0.218 [3]	2.417	0.157
10.286	82961.5	0.1205	2.439 [6]	0.831 [6]		
10.249	82663.1	0.1210	2.437 [3]	0.210 [3]	2.409	0.147
10.207	82324.4	0.1215	2.427	0.198	2.405	0.143
10.194	82219.5	0.1216	2.444 [6]	0.815 [6]		
10.166	81993.7	0.1220	2.411 [3]	0.192 [3]	2.402	0.138
10.133	81727.5	0.1224	2.454 [6]	0.802 [6]		
10.124	81654.9	0.1225	2.406 [3]	0.190 [3]	2.401	0.130
10.083	81324.2	0.1230	2.395	0.184	2.393	0.122
10.072	81235.5	0.1231	2.452 [6]	0.792 [6]		
10.043	81001.6	0.1235	2.386 [3]	0.182 [3]	2.385	0.119
10.011	80743.5	0.1238	2.464 [6]	0.783 [6]		
10.002	80670.9	0.1240	2.378 [3]	0.179 [3]	2.380	0.117
9.962	80348.3	0.1245	2.370	0.177	2.376	0.113
9.951	80255.6	0.1246	2.476 [6]	0.770 [6]		
9.923	80033.8	0.1249	2.362 [3]	0.175 [3]	2.369	0.112
9.890	79763.6	0.1254	2.475 [6]	0.762 [6]		
9.883	79711.1	0.1255	2.356 [3]	0.174 [3]	2.369	0.112
9.844	79396.6	0.1260	2.348	0.173	2.370	0.107
9.829	79271.6	0.1261	2.491 [6]	0.754 [6]		
9.806	79090.1	0.1264	2.343 [3]	0.172 [3]	2.363	0.100
9.767	78778.8	0.1269	2.510 [6]	0.739 [6]		
9.767	78775.5	0.1269	2.335 [3]	0.171 [3]	2.353	0.100
9.729	78469.1	0.1274	2.328	0.172	2.350	0.103
9.706	78286.8	0.1277	2.514 [6]	0.726 [6]		
9.691	78162.6	0.1279	2.319 [3]	0.175 [3]	2.348	0.108
9.653	77856.1	0.1284	2.314	0.180	2.357	0.106
9.645	77794.0	0.1285	2.528 [6]	0.716 [6]		
9.616	77557.7	0.1289	2.310 [3]	0.185 [3]	2.351	0.098
9.584	77302.0	0.1294	2.548 [6]	0.701 [6]		
9.579	77259.2	0.1294	2.306 [3]	0.192 [3]	2.347	0.097
9.543	76968.9	0.1299	2.310	0.196	2.338	0.101
9.523	76809.2	0.1302	2.559 [6]	0.686 [6]		
9.506	76670.5	0.1304	2.303 [3]	0.199 [3]	2.342	0.109
9.470	76380.1	0.1309	2.302	0.209	2.347	0.111

(continued)

TABLE I *(Continued)*

Aluminum Oxide (Al_2O_3)

eV	cm^{-1}	μm	n_o	k_o	n_e	k_e
9.462	76317.2	0.1310	2.569 [6]	0.675 [6]		
9.434	76089.7	0.1314	2.301 [3]	0.218 [3]	2.350	0.112
9.401	75824.4	0.1319	2.588 [6]	0.665 [6]		
9.399	75807.4	0.1319	2.298 [3]	0.233 [3]	2.351	0.116
9.371	75578.4	0.1323	2.600 [6]	0.658 [6]		
9.363	75517.1	0.1324	2.307 [3]	0.257 [3]	2.362	0.116
9.340	75332.4	0.1327	2.613 [6]	0.652 [6]		
9.328	75234.8	0.1329	2.335 [3]	0.272 [3]	2.355	0.121
9.310	75086.4	0.1332	2.624 [6]	0.645 [6]		
9.293	74952.5	0.1334	2.346 [3]	0.282 [3]	2.375	0.133
9.279	74839.6	0.1336	2.636 [6]	0.640 [6]		
9.259	74678.3	0.1339	2.377 [3]	0.303 [3]	2.390	0.133
9.249	74593.6	0.1341	2.648 [6]	0.636 [6]		
9.224	74396.0	0.1344	2.429 [3]	0.310 [3]	2.403	0.136
9.218	74347.6	0.1345	2.665 [6]	0.632 [6]		
9.190	74121.8	0.1349	2.477 [3]	0.294 [3]	2.430	0.137
9.188	74101.6	0.1349	2.690 [6]	0.625 [6]		
9.157	73855.6	0.1354	2.518 [3]	0.270 [3]	2.448	0.134
9.157	73854.8	0.1354	2.725 [6]	0.613 [6]		
9.126	73608.8	0.1359	2.765	0.592		
9.123	73581.4	0.1359	2.563 [3]	0.237 [3]	2.488	0.130
0.096	73362.8	0.1363	2.807 [6]	0.563 [6]		
9.090	73315.2	0.1364	2.604 [3]	0.184 [3]	2.526	0.107
9.065	73116.8	0.1368	2.845 [6]	0.526 [6]		
9.057	73049.1	0.1369	2.621 [3]	0.117 [3]	2.562	0.076
9.035	72870.0	0.1372	2.878 [6]	0.482 [6]		
9.024	72782.9	0.1374	2.619 [3]	0.052 [3]	2.603	0.024
9.004	72624.0	0.1377	2.907 [6]	0.430 [6]		
8.991	72516.7	0.1379	2.605 [3]	0.025 [4]	2.616	0.013 [4]
8.974	72378.0	0.1382	2.929 [6]	0.372 [6]		
8.959	72258.6	0.1384	2.572 [3]	0.012 [4]	2.618	7.64E-03
8.943	72132.0	0.1386	2.942 [6]	0.310 [6]		
8.927	72000.5	0.1389	2.526 [3]	5.81E-03 [4]	2.590	4.37E-03
8.913	71886.0	0.1391	2.943 [6]	0.246 [6]		
8.895	71742.4	0.1394	2.489 [3]	2.79E-03 [4]	2.549	2.51E-03
8.882	71639.2	0.1396	2.933 [6]	0.183 [6]		
8.863	71484.3	0.1399	2.449 [3]	1.34E-03 [4]	2.511	1.44E-03
8.852	71393.2	0.1401	2.912 [6]	0.125 [6]		
8.832	71234.3	0.1404	2.417 [3]	6.60E-04 [4]	2.474	8.37E-04
8.821	71147.2	0.1406	2.881 [6]	0.075 [6]		
8.801	70984.3	0.1409	2.392 [3]	3.25E-04 [4]	2.447	4.88E-04
8.791	70901.2	0.1410	2.841 [6]	0.037 [6]		
8.770	70734.3	0.1414	2.357 [3]	1.60E-04 [4]	2.419	2.84E-04
8.760	70654.4	0.1415	2.797 [6]	0.011 [6]		
8.739	70484.2	0.1419		7.85E-05 [4]	2.398	1.66E-04
8.730	70408.4	0.1420	2.753 [6]	0.0 [6]		
8.708	70234.2	0.1424	2.326 [3]	3.86E-05 [4]	2.375	9.66E-05

TABLE I *(Continued)*

Aluminum Oxide (Al_2O_3)

eV	cm^{-1}	μm	n_o	k_o	n_e	k_e
8.648	69750.3	0.1434	2.279	9.78E-06	2.336	3.40E-05
8.588	69266.3	0.1444	2.246	2.48E-06	2.273	1.20E-05
8.529	68790.5	0.1454	2.242	6.41E-07	2.247	4.28E-06
8.471	68322.7	0.1464	2.231		2.225	
8.414	67862.9	0.1474	2.210		2.207	
8.358	67411.3	0.1483	2.188		2.195	
8.302	66959.6	0.1493	2.174		2.183	
8.193	66080.5	0.1513	2.150		2.161	
8.034	64798.1	0.1543	2.127		2.125	
7.932	63975.4	0.1563	2.105		2.102	
7.832	63168.8	0.1583	2.081		2.083	
7.735	62386.5	0.1603	2.070		2.053	
7.687	61999.3	0.1613	2.059		2.040	
7.663	61805.8	0.1618			2.033	
7.593	61241.2	0.1633	2.044			
7.547	60870.2	0.1643	2.037		2.013	
7.457	60144.3	0.1663	2.020			
7.435	59966.8	0.1668			2.000	
7.412	59781.3	0.1673	2.014			
7.325	59079.6	0.1693	1.995		1.988	
7.250	58474.7	0.1710	1.986			
7.219	58224.7	0.1717			1.977	
7.198	58055.3	0.1722	1.975			
7.116	57394.0	0.1742	1.969		1.970	
7.076	57071.3	0.1752	1.967			
7.016	56587.4	0.1767			1.962	
6.996	56426.1	0.1772	1.962			
6.918	55797.0	0.1792	1.953		1.953	
6.880	55490.5	0.1802	1.947			
6.824	55038.8	0.1817			1.948	
6.805	54885.6	0.1822	1.940			
6.731	54288.7	0.1842	1.933		1.938	
6.695	53998.4	0.1852	1.930			
6.624	53425.7	0.1872	1.930		1.929	
6.554	52861.2	0.1892	1.929		1.922	
6.469	52175.6	0.1917	1.936		1.919	
6.386	51506.2	0.1942	1.930		1.918	
6.305	50852.9	0.1966	1.924		1.915	
6.226	50215.7	0.1991	1.920		1.908	
6.1993	50000.0	0.2000	1.91271 [13]		1.90163 [13]	
5.6357	45454.5	0.2200	1.87817		1.86774	
5.1661	41666.7	0.2400	1.85446		1.84453	
4.8890	39432.2	0.2536	1.844 [11]		1.834 [11]	
4.7687	38461.5	0.2600	1.8376		1.8280	
4.6752	37707.4	0.26520	1.83360 [12]		1.82411 [13]	
4.4280	35714.3	0.2800	1.8242 [11]		1.8149 [11]	
4.4225	35669.7	0.28035	1.82427 [12]		1.81490 [13]	

(continued)

TABLE I *(Continued)*

Aluminum Oxide (Al_2O_3)

eV	cm^{-1}	μm	n_o	k_o	n_e	k_e
4.2848	34559.0	0.28936	1.81949		1.81021	
4.1784	33700.7	0.29673	1.81595		1.80674	
4.1328	33333.3	0.3000	1.8147 [11]		1.8056 [11]	
4.1034	33096.1	0.30215	1.81351 [12]		1.80437 [13]	
3.9612	31948.9	0.3130	1.80906		1.80005	
3.7571	30303.0	0.3300	1.8035 [11]		1.7947 [11]	
3.7105	29926.7	0.33415	1.80184 [12]		1.79293 [13]	
3.5770	28850.0	0.34662	1.79815		1.78940	
3.4340	27696.9	0.36105	1.79450		1.78579	
3.3967	27396.1	0.36502	1.7935 [11]		1.7849 [11]	
			1.79358 [12]		1.78488 [13]	
3.1739	25599.0	0.39064	1.78826		1.77970	
3.0640	24712.3	0.40466	1.78582		1.77730	
			1.78571 [11]		1.77724 [11]	
2.8448	22944.7	0.43583	1.78110		1.77275	
			1.78120 [12]		1.77279 [13]	
2.5505	20570.6	0.48613	1.77547 [11]		1.76724 [11]	
2.2705	18312.7	0.54607	1.77067		1.76254	
			1.77078 [12]		1.76258 [13]	
2.1489	17332.2	0.576960	1.76884		1.76069	
2.1411	17269.2	0.57907	1.76871		1.76057	
2.1039	16969.3	0.5893	1.76808 [11]		1.75999 [11]	
1.9257	15531.6	0.64385	1.76547 [12]		1.75739 [13]	
			1.76538 [11]		1.75734 [11]	
1.8892	15237.4	0.65628	1.76485		1.75682	
1.7950	14477.6	0.69072	1.76351		1.75549	
1.7549	14153.9	0.70652	1.76303 [12]		1.75500 [13]	
1.4550	11735.4	0.85212	1.75885		1.75090	
1.3862	11180.7	0.89440	1.75796		1.74994	
1.2228	9862.1	1.01398	1.75547		1.74794 [12]	
1.0985	8860.1	1.12866	1.75339		1.74549 [13]	
0.9068	7313.8	1.36728	1.74936		1.74148	
0.8887	7168.2	1.39506	1.74888		1.74101	
0.8106	6538.0	1.52952	1.74660		1.73874	
0.7323	5906.0	1.6932	1.74368		1.73584	
0.7254	5850.9	1.70913	1.74340		1.73555	
0.6838	5515.5	1.81307	1.74144		1.73362	
0.6325	5101.8	1.9601	1.73833		1.73074	
0.5760	4645.5	2.1526	1.73444		1.72670	
0.5512	4445.8	2.24929	1.73231		1.72455	
0.5332	4300.3	2.32542	1.73057		1.72279	
0.5087	4102.7	2.4374	1.72783		1.72011	
0.3822	3082.7	3.2439	1.70437		1.69688	
0.3795	3061.1	3.2668	1.70356		1.69612	
0.3754	3027.9	3.3026	1.70231		1.69491	
0.3723	3002.7	3.3303	1.70140		1.69397	
0.3623	2922.3	3.422	1.69818		1.69077	

TABLE I *(Continued)*

Aluminum Oxide (Al_2O_3)

eV	cm^{-1}	μm	n_o	k_o	n_e	k_e
0.3535	2851.4	3.5070	1.69504		1.68772	
0.3345	2697.8	3.7067	1.68746		1.68021	
0.3100	2500.0	4.000	1.67523 [13]	1.30E-06 [26]	1.66825	
0.2976	2400.0	4.167	1.66777	2.60E-06	1.66094	
0.2914	2350.0	4.2553	1.66371 [12]		1.65690	
0.2852	2300.0	4.348	1.65920 [13]	5.78E-06	1.65257	
0.2824	2278.0	4.3898	1.65714	6.29E-06 [24]	1.65056	
0.2728	2200.0	4.545	1.64928	1.12E-05 [26]	1.64289	
0.2705	2181.0	4.5830	1.64732	1.24E-05 [24]	1.64099	
0.2616	2110.0	4.7393	1.63894	2.03E-05 [25]	1.63284	1.32E-05 [25]
0.2604	2100.0	4.762	1.63769	2.99E-05 [26]	1.63163	
0.2585	2085.0	4.7962	1.63579	2.29E-05 [24]	1.62978	
0.2503	2018.6	4.954	1.62665 [12]		1.62102	
0.2480	2000.0	5.000	1.62403 [13]	3.76E-05 [26]	1.61839	
0.2465	1988.0	5.0302	1.62223	3.96E-05 [24]	1.61664	
0.2460	1984.0	5.0403	1.62162	3.85E-05 [25]	1.61605	2.73E-05
0.2452	1978.0	5.0556	1.62070	4.17E-05	1.61516	2.93E-05
0.2410	1943.4	5.1456	1.61514 [12]		1.60983	
0.2356	1900.0	5.263	1.60775 [13]	6.53E-05 [26]	1.60266	
0.2346	1892.0	5.2854	1.60631	6.98E-05 [24]	1.60127	
0.2318	1869.5	5.349	1.60202 [12]		1.59727	
0.2288	1845.4	5.419	1.59735		1.59277	
0.2232	1800.0	5.556	1.58808	1.20E-04 [26]	1.58375	
0.2227	1796.0	5.5679	1.58721	1.22E-04 [24]	1.58291	
0.2223	1793.1	5.577	1.58638		1.58230	
0.2108	1700.0	5.882		2.14E-04 [26]		
0.2107	1699.0	5.8858		1.69E-04 [24]		
0.1984	1600.0	6.250		5.82E-04 [26]		
0.1860	1500.0	6.667		1.50E-03		
0.1736	1400.0	7.143	1.459 [30]	3.60E-03	1.44 [26]	
0.1674	1350.0	7.407	1.42		1.41	
0.1612	1300.0	7.692	1.38		1.38	
0.1550	1250.0	8.000	1.34		1.34	
0.1488	1200.0	8.333	1.29		1.29	
0.1426	1150.0	8.696	1.22		1.23	
0.1364	1100.0	9.091	1.14		1.16	
0.1302	1050.0	9.524	1.03		1.06	
0.1240	1000.0	10.00	0.88	0.053 [30]	0.94	0.037 [26]
0.1227	990.0	10.10	0.84	0.057	0.90	0.039
0.1215	980.0	10.20	0.80	0.062	0.87	0.042
0.1203	970.0	10.31	0.75	0.068	0.83	0.045
0.1190	960.0	10.42	0.70	0.075	0.79	0.049
0.1178	950.0	10.53	0.64	0.084	0.74	0.054
0.1165	940.0	10.64	0.57	0.097	0.69	0.061
0.1153	930.0	10.75	0.48	0.117	0.64	0.069
0.1141	920.0	10.87	0.38	0.153	0.57	0.081
0.1128	910.0	10.99	0.27	0.224	0.49	0.098

(continued)

TABLE I *(Continued)*

Aluminum Oxide (Al_2O_3)

eV	cm^{-1}	μm	n_o	k_o	n_e	k_e
0.1116	900.0	11.11	0.18	0.344	0.39	0.128
0.1103	890.0	11.24	0.14	0.468	0.28	0.192
0.1091	880.0	11.36	0.12	0.579	0.18	0.312
0.1079	870.0	11.49	0.10	0.680	0.14	0.440
0.1066	860.0	11.63	0.09	0.774	0.12	0.553
0.1054	850.0	11.76	0.09	0.864	0.11	0.655
0.1041	840.0	11.90	0.08	0.951	0.10	0.750
0.1029	830.0	12.05	0.08	1.04	0.10	0.840
0.1017	820.0	12.20	0.08	1.12	0.10	0.927
0.1004	810.0	12.35	0.07	1.21	0.10	1.01
0.09919	800.0	12.50	0.07	1.29	0.11	1.09
0.09795	790.0	12.66	0.07	1.38	0.12	1.18
0.09671	780.0	12.82	0.07	1.47	0.12	1.26
0.09547	770.0	12.99	0.07	1.57	0.13	1.34
0.09423	760.0	13.16	0.07	1.66	0.14	1.42
0.09299	750.0	13.33	0.07	1.77	0.15	1.50
0.09175	740.0	13.51	0.07	1.87	0.16	1.58
0.09051	730.0	13.70	0.08	1.99	0.16	1.66
0.08927	720.0	13.89	0.08	2.11	0.16	1.75
0.08803	710.0	14.08	0.08	2.24	0.16	1.85
0.08679	700.0	14.29	0.08	2.39	0.15	1.96
0.08555	690.0	14.49	0.09	2.55	0.15	2.08
0.08431	680.0	14.71	0.09	2.74	0.15	2.22
0.08307	670.0	14.93	0.10	2.96	0.16	2.37
0.08183	660.0	15.15	0.12	3.24	0.16	2.55
0.08059	650.0	15.38	0.16	3.66	0.17	2.75
0.07935	640.0	15.63	0.58	4.56	0.19	3.00
0.07811	630.0	15.87	1.48	2.77	0.23	3.32
0.07687	620.0	16.13	0.47	3.56	0.29	3.74
0.07563	610.0	16.39	0.41	4.28	0.41	4.36
0.07439	600.0	16.67	0.49	5.10	0.73	5.43
0.07315	590.0	16.95	0.75	6.30	2.37	7.85
0.07191	580.0	17.24	1.69	8.61	8.50	3.27
0.07067	570.0	17.54	10.26	11.28	5.36	0.678
0.06943	560.0	17.86	9.10	1.53	3.96	0.313
0.06819	550.0	18.18	6.55	0.507	3.11	0.206
0.06695	540.0	18.52	5.28	0.255	2.45	0.174
0.06571	530.0	18.87	4.46	0.158	1.84	0.186
0.06447	520.0	19.23	3.82	0.115	1.13	0.278
0.06323	510.0	19.61	3.24	0.099	0.34	0.932
0.06199	500.0	20.00	2.64	0.106	0.21	1.64
0.06075	490.0	20.41	1.83	0.163	0.19	2.17
0.05951	480.0	20.83	0.38	1.03	0.19	2.64
0.05827	470.0	21.28	0.24	2.62	0.20	3.10
0.05703	460.0	21.74	0.32	4.16	0.23	3.61
0.05579	450.0	22.22	0.73	6.68	0.28	4.19
0.05455	440.0	22.73	10.08	14.01	0.36	4.91

TABLE I *(Continued)*

Aluminum Oxide (Al_2O_3)

eV	cm^{-1}	μm	n_o	k_o	n_e	k_e
0.05331	430.0	23.26	8.57	0.764	0.52	5.88
0.05207	420.0	23.81	6.36	0.257	0.89	7.38
0.05083	410.0	24.39	5.36	0.152	2.16	10.22
0.04959	400.0	25.00	4.64	0.156	11.82	12.96
0.04835	390.0	25.64	3.53	0.732	11.36	2.26
0.04711	380.0	26.32	5.64	0.552	8.54	0.804
0.04587	370.0	27.03	4.77	0.097	7.18	0.422
0.04463	360.0	27.78	4.44	4.55E-02	6.36	0.264
0.04339	350.0	28.57	4.23	2.83E-02	5.82	0.182
0.04215	340.0	29.41	4.08	1.97E-02	5.42	0.133
0.04092	330.0	30.30	3.95	1.45E-02	5.11	0.101
0.03968	320.0	31.25	3.85	1.10E-02	4.87	7.99E-02
0.03844	310.0	32.26	3.77	8.55E-03	4.67	6.44E-02
0.03720	300.0	33.33	3.69	6.68E-03	4.51	5.30E-02
0.03596	290.0	34.48	3.63		4.37	
0.03472	280.0	35.71	3.57		4.25	
0.03348	270.0	37.04	3.52		4.15	
0.03224	260.0	38.46	3.48		4.06	
0.03100	250.0	40.00	3.43		3.98	
0.02976	240.0	41.67	3.40		3.91	
0.02852	230.0	43.48	3.36		3.85	
0.02728	220.0	45.45	3.33		3.79	
0.02604	210.0	47.62	3.30		3.74	
0.02480	200.0	50.00	3.260 [34]	0.0117 [35]		
0.02480	200.0	50.00	3.28 [26]		3.70	
0.02356	190.0	52.63	3.241 [34]	0.0103		
0.02232	180.0	55.56	3.218	0.0103		
0.02187	176.4	56.69	3.2113 [33]			
0.02124	171.3	58.38	3.2018			
0.02108	170.0	58.82	3.198 [34]	0.0100		
0.02062	166.3	60.13	3.1921 [33]	0.0130 [33]		
0.02000	161.3	62.00	3.1854			
0.01984	160.0	62.50	3.180 [34]	0.00975 [35]		
0.01937	156.2	64.02	3.1795 [33]		3.6042 [33]	
0.01875	151.2	66.14	3.1696	0.0104 [33]	3.5856	0.0189 [33]
0.01860	150.0	66.67	3.164 [34]	0.0101 [34]		
0.01811	146.1	68.45	3.1623 [33]		3.5746	
0.01749	141.1	70.87	3.1549		3.5612	
0.01736	140.0	71.43	3.149 [34]	0.0091		
0.01687	136.1	73.48	3.1485 [33]	0.0092 [33]	3.5508	0.0173
0.01624	131.0	76.34	3.1422		3.5375	
0.01612	130.0	76.92	3.136 [34]	0.00898 [35]		
0.01562	126.0	79.37	3.1357 [33]		3.5279	
0.01499	120.9	82.71	3.1304	0.0085 [33]	3.5185	0.0158
0.01488	120.0	83.33	3.125 [34]	0.0080 [34]	3.524 [34]	0.0139 [34]
0.01437	115.9	86.28	3.1249 [33]		3.5081 [33]	
0.01375	110.9	90.17	3.1198		3.4998	

(continued)

TABLE I *(Continued)*

Aluminum Oxide (Al_2O_3)

eV	cm^{-1}	μm	n_o	k_o	n_e	k_e
0.01364	110.0	90.91	3.114 [34]	0.0074	3.502 [34]	0.0137
0.01312	105.8	94.52	3.1249 [33]	0.0074 [33]	3.5081 [33]	0.0134 [33]
0.01250	100.8	99.21	3.1198		3.4993	
0.01240	100.0	100.0	3.105 [34]	0.0069 [34]	3.485 [34]	0.0127 [34]
			3.12 [30]	0.0070 [35]	3.42 [26]	
0.01188	95.8	104.4	3.1147 [33]		3.4908 [33]	
0.01125	90.7	110.3	3.1019	0.0063 [33]	3.4689	0.0111 [33]
0.01116	90.0	111.1	3.097 [34]	0.0065 [34]	3.470 [34]	0.0115 [34]
0.01063	85.7	116.7	3.0982 [33]		3.4625 [33]	
0.00999	80.6	124.1	3.0941		3.4569	
0.00992	80.0	125.0	3.090 [34]	0.0058	3.455 [34]	0.0093
0.00937	75.6	132.3	3.0906 [33]	0.0052 [33]	3.4510 [33]	0.0080 [33]
0.00875	70.6	141.6	3.0870		3.4440	
0.00868	70.0	142.9	3.085 [34]	0.0052 [34]	3.445 [34]	0.0076 [34]
0.00812	65.5	152.7	3.0843 [33]		3.4391 [33]	
0.00750	60.5	165.3	3.0822	0.0047 [33]	3.4334	0.0053 [33]
0.00744	60.0	166.7	3.080 [34]	0.0044 [34]	3.436 [34]	0.0062 [34]
0.00687	55.4	180.5	3.0795 [33]		3.4294 [33]	
0.00625	50.4	198.4	3.0770		3.4260	
0.00620	50.0	200.0	3.076 [34]	0.0035	3.428 [34]	0.0051
0.00563	45.4	220.3	3.0752 [33]	0.0030 [33]	3.4232 [33]	0.0039 [33]
0.00500	40.3	248.1	3.0740		3.4187	
0.00496	40.0	250.0	3.072 [34]	0.0024 [34]	3.420 [34]	0.0046 [34]
0.00438	35.3	283.3	3.0720 [33]		3.4163 [33]	
0.00374	30.2	331.1	3.0704	0.0011 [33]	3.4234	0.0013 [33]
0.00372	30.0	333.3	3.069 [34]	0.0027 [34]	3.415 [34]	0.0050 [34]
0.00372	30.0	333.3	3.06 [36]	0.0025 [36]	3.40 [36]	0.0025 [36]
0.00312	25.2	396.8	3.0698 [33]		3.4129 [33]	
0.00289	23.3	428.6	3.06 [36]	0.0020	3.40 [36]	0.0020
0.00250	20.2	495.0	3.0688 [33]		3.4111 [33]	
0.00207	16.7	600.0	3.05 [36]	0.0015	3.39 [36]	0.0015
0	0	∞	3.068 [34]		3.406 [34]	
			3.067 [33]		3.408 [33]	
			3.066 [39]		3.404 [39]	

TABLE II

Sellmeier Dispersion Equation Constants for Aluminum Oxide

Term (Eq. [4])	Malitson [12] o-ray	Malitson and Dodge [13] o-ray	Malitson and Dodge [13] e-ray
λ_1	0.06144821	0.0726631	0.0740298
λ_2	0.1106997	0.1193242	0.1216529
λ_3	17.92656	18.028251	20.072248
A_1	1.023798	1.4313493	1.5039759
A_2	1.058264	0.65054713	0.55069141
A_3	5.280792	5.3414021	6.5927379
Temperature:	24° C	20° C	20° C
Wavelength:	0.26–5.5 μm	0.2–5.5 μm	0.2–5.5 μm

[a] Corrects error of Ref. [13].

TABLE III

Thermo-optical Coefficients of Aluminum Oxide

Wavelength (μm)	dn/dT (10^{-6}/K) o-ray	dn/dT (10^{-6}/K) e-ray	Temperature (°C)	Reference
~0.26	20		24	[12]
0.4047	14.1		24	[12]
0.4579	11.7	12.8	20	[17]
0.475	16	12	22	[14]
0.4358	13.9		24	[12]
0.502	16	12	22	[14]
0.5145	16.5		27	[16]
0.5461	13.1		24	[12]
	13.7		20–700	[18]
0.552	14	12	22	[14]
0.5770	13.1		24	[12]
0.5791	13.1		24	[12]
	14.0		20–700	[18]
0.5893	13.6	14.7	50	[11]
0.603	14	11	22	[12]
0.633	12.8		24	[15]
	11.7		24	[19]
	13.0[a]	14.2[a]	30–45	[22]
0.6438	12.8		24	[12]
0.651	13	12	22	[14]
0.701	13	9.7	22	[14]
0.7065	12.6		24	[12]
0.799	12.4		24	[15]
~4	10		24	[12]

[a] Ruby measurement.

TABLE IV

Constants for Infrared Absorption Coefficient of Aluminum Oxide

	Model parameters			
Orientation	β_0 (cm^{-1})	γ	ν_{LO} (cm^{-1})	Reference
o-ray	55222	5.03	900	[23]
o-ray	94778	5.28	914	[24]
e-ray	33523	4.73	871	[25]

TABLE V

Transverse (and Longitudinal) Optical Phonon Frequencies in Aluminum Oxide

Mode	Barker [29]	Gervais [26,30]	Hoffmann [31]
E_u (**E** $\perp$ **c**)	385 (388)	384.6 (387.7)	384
E_u (**E** $\perp$ **c**)	442 (480)	439.3 (482)	439
E_u (**E** $\perp$ **c**)	569 (625)	569.5 (630.5)	568
E_u (**E** $\perp$ **c**)	635 (900)	635 (908)	633
A_{1g} (**E** $\parallel$ **c**)	400 (512)	399.5 (514)	—
A_{1g} (**E** $\parallel$ **c**)	583 (871)	584 (886.5)	—

Barium Fluoride (BaF_2)

MICHAEL E. THOMAS and WILLIAM J. TROPF
Applied Physics Laboratory
The Johns Hopkins University
Laurel, Maryland

Barium fluoride is a general-purpose optical window material that offers a wide range of transparency, from the ultraviolet to the long-wave infrared (0.15 to 12 μm), with low reflectance loss and low dispersion. This combination of broad transparency and low dispersion is rare in optical window materials used in infrared systems. It allows experimenters to conveniently perform initial system alignment in the visible and then switch to the IR with only minor correction of the optical components. Furthermore, barium fluoride has good surface hardness (Knoop scale 78 kg/mm^2), and it is not attacked by water vapor, though immersion in water causes surface damage. It has moderate flexure strength (27 MPa) and is very brittle, requiring careful handling. Thus, barium fluoride is better suited for laboratory than to field work. It is also a relatively inexpensive single-crystal material that is readily available from a number of vendors.

Barium fluoride is a cubic crystal with the fluorite structure, space group Fm3m (O_h^5), with four formula units per unit cell. The lattice constant is 6.2001 Å, giving a theoretical density of 4.886 g/cm^3. The atomic arrangement is barium atoms occupy the 4(a) sites (m3m or O_h symmetry), and the fluorine atoms occupy the 8(c) sites ($\bar{4}$3m or T_d symmetry). Melting point is 1641 K.

Ultraviolet reflectance of bulk BaF_2 was measured by Ganin *et al.* [1] up to 20 eV at room temperature and liquid-helium temperature. Rubloff [2] has measured the room-temperature reflectance up to 36 eV. Unfortunately, these measurements are not reduced to optical constants. However, similar measurements from 10 to 33 eV by Nisar and Robin [3] have been reduced to optical constants utilizing the Kramers–Kronig relation. Thin-film optical constant data is available from transmittance and reflectance measurements by Zukic *et al.* [4], but only between 0.12 and 0.2 μm. These results extend the Nisar and Robin data set down to 6.2 eV. These data are listed in Table I and plotted in Fig. 1.

The Urbach tail represents absorption below the band gap, defining the

HANDBOOK OF OPTICAL CONSTANTS OF SOLIDS III

Copyright © 1998 by Academic Press.
All rights of reproduction in any form reserved
ISBN 0-12-544423-0/$25.00.

end of transparency. The room-temperature absorption coefficient was determined from transmission measurements by Tomiki and Miyata [5] in the spectral range from 9.1 to 9.35 eV and fitted to the functional form

$$\beta_{abs}(E,T) = \beta_{U0}\exp[\sigma_s(T)(E - E_g)/k_BT], \tag{1}$$

where β_{abs} is the absorption coefficient (typically in units of cm^{-1}); β_{U0} is a scaling coefficient (in units of cm^{-1}), E_g is the band-gap energy at absolute zero temperature, typically given in electron volts; k_B is Boltzmann's constant; and T is temperature in Kelvins. The exponential factor $\sigma_s(T)$ is given by the equation

$$\sigma_s(T) = \sigma_0 \frac{2k_BT}{E_p} \tanh \frac{E_p}{2k_BT}, \tag{2}$$

where E_p is an effective acoustic-phonon energy of the material. The Urbach tail parameters for BaF_2 are $\beta_{U0} = 4.17 \times 10^8$ cm^{-1}, $E_g = 10.162$ eV, $\sigma_0 = 0.58$, and $E_p = 0.04$ eV. The room-temperature values for k in Table I and Fig. 1 for this spectral region are generated using Eqs. (1) and (2).

The room-temperature (25° C) index of refraction from the ultraviolet to the infrared (0.27 to 10.3 μm) has been measured by Malitson [6] using a prism and the minimum-deviation technique. A Sellmeier model of the form

$$n^2(\lambda,T) = 1 + \sum_i \frac{\lambda^2 \Delta\epsilon_i(T)}{\lambda^2 - \lambda_i^2(T)} \tag{3}$$

is used to accurately represent the data (± 0.00002). Model parameters are listed in Table II. A comprehensive analysis on a variety of data sets was perfomed by Li [7]. A Sellmeier formula was also generated covering the range from 0.15 to 15 μm at $T = 20°$ C. The Li model parameters are also listed in Table II. Because the Sellmeier model has a physical basis, the extrapolation to higher frequencies beyond the experimental limit is justified. The values for n in Table I and Fig. 1 for the spectral region from 650 to 67,000 cm^{-1} are generated by the preceding formula. A temperature-dependent Sellmeier model covering the range from 100 to 450 K has been developed by Tropf [8]. Room-temperature thermo-optic coefficients, measured at different wavelengths, are listed in Table III [6, 9–13]. Notice that the thermo-optic coefficients are negative. This gives BaF_2 some athermal performance as an optical element. An athermal material has the property that

$$\frac{d(n(T)L(T))}{dT} = 0.$$

The value of the optical-path derivative as given above for BaF_2 is 7.5×10^{-6} nL per Kelvin at visible and near-infrared wavelengths. Thus, BaF_2 is useful for optical designs that require insensitivity to temperature.

Laser-calorimetry data [14] at DF (3.8 μm) and HF (2.7 μm) laser wavelengths indicate low-level absorption in roughly the middle of the transparency range of BaF_2. Material obtained from Adolf Meller had absorption-coefficient values of 2.0×10^{-4} cm^{-1} at the DF laser wavelength and 1.4×10^{-4} cm^{-1} at the HF laser wavelength. Material obtained from Optovac had absorption-coefficient values of 2.0×10^{-3} cm^{-1} at the DF laser wavelength and 1.8×10^{-3} cm^{-1} at the HF laser wavelength. The lowest values are listed in Table I and plotted in Fig. 1. The low-level absorption and the near-athermal performance of BaF_2 make it a candidate window material for high-power laser applications.

The multiphonon absorption (multiple-quanta lattice vibrations) edge marks the end of infrared transparency. Absorption-coefficient measurements by Deutsch [15] are represented by the simple formula

$$\beta_{abs}(\nu) = \beta_0 \exp\left(-\gamma \frac{\nu}{\nu_0}\right), \tag{4}$$

where for BaF_2, $\beta_0 = 49.641$ cm^{-1} and $\nu_0/\gamma = 75.9$ cm^{-1} at room temperature. The values of k in the spectral range from 800 to 1250 cm^{-1} in Table I and Fig. 1 are obtained from this formula. The data cover the three-phonon to four-phonon regions. Temperature-dependent experimental data on the absorption coefficient are described in Lipson *et al.* [16]. A temperature-dependent multiphonon model has been developed by Thomas *et al.* [17] and applied to BaF_2. Measurements in the two-phonon region are reported by Kaiser *et al.* [18]. The experimental results are listed in Table I and plotted in Fig. 1.

The one-phonon (one-quantum fundamental lattice vibrations) region is opaque and therefore characterized by reflectance measurements. A room-temperature reflectance measurement is reported by Kaiser *et al.* [18]. Temperature-dependent data are available from Hoffmann [19]. The classical-oscillator model is often used to fit the reflectance data and then to derive the optical constants. The classical-oscillator model is expressed in terms of the relative permittivity, $\epsilon_r(\nu,T)$, as given by[1]

$$\epsilon_r(\nu,T) = \epsilon_\infty(T) + \sum_i \frac{\Delta\epsilon_i(T)\nu_i^2(T)}{\nu_i^2(T) - \nu^2 + j\Gamma_i(\nu,T)\nu}, \tag{5}$$

where $\Delta\epsilon_i$, Γ_i, and ν_i are the ith-mode strength, line width, and long-wavelength transverse optical frequency, ν_{TO}, respectively. The sum on i is over all transverse optical modes. For BaF_2, there is only one allowed

[1] The expression uses the engineering convention for a time harmonic field of $\exp(-j\omega t)$. To convert to the convention commonly used in the *HOC* series, use $i = -j$.

infrared-active vibrational mode based on group theory of a perfect lattice. This is formally stated as

$$\Gamma = F_{1u}(\mathrm{IR}) + F_{2g}(\mathrm{R}).$$

The first mode is infrared active (mode 1 in Table IV), and the second mode is Raman active (241 cm^{-1} [20]). Table IV lists the classical-oscillator-model parameters used to fit the experimental data. More than one mode is needed to account for impurities and defects in real materials. Also, the high-frequency edge of the reflectance spectrum must include two-phonon contributions (see mode 4, Hoffmann [19], in Table IV). The n and k values in Table I and Fig. 1 are generated by Eq. (5) and the parameters from Hoffmann [19].

Below ν_{TO}, the index of refraction, n, is determined by extrapolation of the classical-oscillator model with reasonable accuracy. The absorption coefficient has been measured by Bosomworth [21]. Table I and Fig. 1 list and display the resulting values.

The static-dielectric constant data is the sum of all the strengths of higher frequency oscillators, including vibrational and electronic. Using Eq. (5), the static dielectric constant, $\epsilon_s(T) = \epsilon_r'(0,T)$, becomes

$$\epsilon_s(T) = \epsilon_\infty(T) + \sum_i \Delta\epsilon_i(T). \tag{6}$$

Based on the parameters listed in Table IV, we expect the value of ϵ_s to be between 6.73 and 7.63. Experimental results, obtained from capacitance bridges operating from 1 kHz to 1 MHz, produce values from 7.28 to 7.36, with most results closer to the higher value [13, 22–24]. The corresponding refractive index value is $n_s = 2.71$. Because the static dielectric constant predicted by the Hoffmann [19] parameters is close to the experimental result, his model parameters are used in the calculations of n in Table I and Fig. 1 below ν_{TO}. The static-index values are located incorrectly at 1×10^4 μm; however, there is little difference in the value of n_s at the measured wavelength and the plotted wavelength.

Whenever possible, physically based models are used to represent experimental measurements in Table I and Fig. 1. The models tend to reduce noise and allow interpolation and extrapolation to obtain meaningful results where no experimental data exist. In some case, the models discussed in this section also allow temperature-dependent data to be obtained.

REFERENCES

1. V. A. Ganin, M. G. Karin, V. K. Sidorin, K. K. Sidorin, N. V. Starostin, G. P. Startsev, and M. P. Shepilov, Optical constants and energy-band structure of fluorite-type crystals. *Sov. Phys. Solid State* **16**, 2313–2318 (1975).
2. G. W. Rubloff, Far-infrared reflectance spectra and the electronic structure of ionic crystals. *Phys. Rev. B* **5**, 662–684 (1972).

3. M. Nisar and S. Robin, Far ultraviolet electronic spectra of SrF_2 and BaF_2. *Pak. J. Sci. Ind. Res.* **17**, 49–54 (1974).
4. M. Zukic, D. G. Torr, J. F. Spann, and M. R. Torr, Vacuum ultraviolet thin films. 1: Optical constants of BaF_2, CaF_2, LaF_3, MgF_2, Al_2O_3, HfO_2 and SiO_2 thin films. *Appl. Opt.* **29**, 4284–4292 (1990).
5. T. Tomiki and T. Miyata, Optical studies of alkali fluorides and alkaline earth fluorides in VUV region. *J. Phys. Soc. Jpn.* **27**, 658–678 (1969).
6. I. H. Malitson, Refractive properties of barium fluoride. *J. Opt. Soc. Am.* **54**, 628–632 (1964).
7. H. H. Li, Refractive index of alkaline earth halides and its wavelength and temperature derivatives. *J. Phys. Chem. Ref. Data* **9**, 161–289 (1980).
8. W. J. Tropf, Temperature-dependent refractive index models for BaF_2, CaF_2, MgF_2, SrF_2, LiF, NaF, KCl, ZnS and ZnSe. *Opt. Eng.* **34**, 1369–1373 (1995).
9. A. Feldman, D. Horowitz, R. M. Walker, and M. J. Dodge, "Optical Materials Characterization Final Technical Report, February 1, 1978–September 30, 1978," NBS Technical Note 993, February 1979.
10. H. G. Lipson, Y. F. Tsay, B. Bendow, and P. A. Ligor, Temperature dependence of the refractive index of alkaline earth fluorides. *Appl. Opt.* **15**, 2352–2354 (1976).
11. Y. F. Tsay, H. G. Lipson, and P. A. Ligor, The temperature variation of the thermo-optic coefficient of CaF_2. *J. Appl. Phys.* **48**, 1953–1955 (1977).
12. R. J. Harris, G. T. Johnson, G. A. Kepple, P. C. Krok, and H. Mukai, Infrared thermooptic coefficient measurement of polycrystalline ZnSe, ZnS, CdTe, CaF_2 and BaF_2, single crystal KCl, and TI-20 glass. *Appl. Opt.* **16**, 436–438 (1977).
13. M. Wintersgill, J. Fontanella, C. Andeen, and D. Schuele, The temperature variation of the dielectric constant of "pure" CaF_2, SrF_2, BaF_2, and MgO. *J. Appl. Phys.* **50**, 8259–8261 (1979).
14. J. A. Harrington, D. A. Gregory, and W. F. Otto, Jr., Infrared absorption in chemical laser window materials. *Appl. Opt.* **15**, 1953–1959 (1976).
15. T. F. Deutsch, Absorption coefficient of infrared laser window materials. *J. Phys. Chem. Solids* **34**, 2091–2104 (1973).
16. H. G. Lipson, B. Bendow, N. E. Massa, and S. S. Mitra, Multiphonon infrared absorption in the transparent regime of alkaline-earth fluorides. *Phys. Rev. B* **13**, 2614–2619 (1976).
17. M. E. Thomas, R. I. Joseph, and W. J. Tropf, Infrared transmission properties of sapphire, spinel, yttria and ALON as a function of temperature and frequency. *Appl. Opt.* **27**, 239 (1988); M. E. Thomas, Temperature dependence of the complex index of refraction. *In* "Handbook of Optical Constants of Solids II" (E. D. Palik, ed.), pp. 177–201. Academic Press, Orlando, Florida, 1991; M. E. Thomas, A computer code for modeling optical properties of window materials, in Window and Dome Technologies and Materials. *Proc. of SPIE* **1112**, 260–267 (1989).
18. W. Kaiser, W. G. Spitzer, R. H. Kaiser, and L. E. Howarth, Infrared properties of CaF_2, SrF_2, and BaF_2. *Phys. Rev.* **127**, 1950–1954 (1962).
19. C. E. Hoffmann, Optical constants of infrared active phonons as a function of frequency and temperature. M.S. Thesis, Johns Hopkins University, Baltimore, Maryland (1988).
20. I. Richman, Longitudinal optical phonons in CaF_2, SrF_2 and BaF_2. *J. Chem. Phys.* **41**, 2836–2837 (1966).
21. D. R. Bosomworth, Far-infrared optical properties of CaF_2, SrF_2, BaF_2, and CdF_2. *Phys. Rev.* **157**, 709–715 (1967).
22. K. V. Rao and A. Smakula, Dielectric properties of alkaline earth fluoride single crystals. *J. Appl. Phys.* **37**, 319–323 (1965).
23. C. Andeen, J. Fontanella, and D. Schuele, Low-frequency dielectric constants of the alkaline earth fluorides by the method of substitution. *J. Appl. Phys.* **42**, 2216–2219 (1971).
24. G. A. Samara, Temperature and pressure dependence of the dielectric properties of PbF_2 and the alkaline-earth fluorides. *Phys. Rev. B* **13**, 4529–4544 (1976).

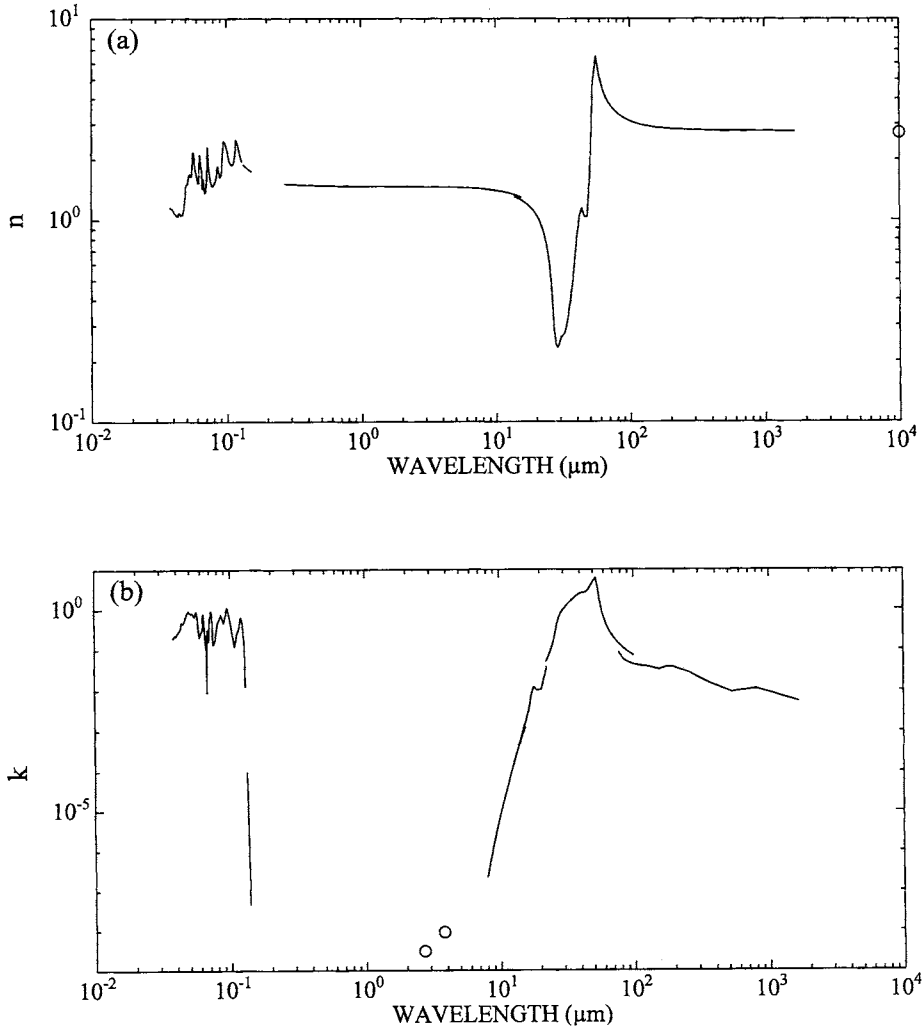

Fig. 1. (a) Log–log plot of the room-temperature index of refraction, n, for BaF_2 versus wavelength in microns. (b) Log–log plot of the room-temperature extinction coefficient, k, for BaF_2 versus wavelength in microns. Isolated data points are indicated with a symbol.

TABLE I

Values of n and k for BaF_2 from Various References[a]

eV	cm^{-1}	μm	n	k
32.91	265400	0.03767	1.149 [3]	0.1900 [3]
31.71	255800	0.03910	1.134	0.2208
31.42	253500	0.03946	1.130	0.2263
31.20	251600	0.03974	1.118	0.2138
30.35	244800	0.04086	1.084	0.2436
29.97	241700	0.04137	1.077	0.2614
28.91	233100	0.04289	1.040	0.3217
28.71	231600	0.04318	1.043	0.3344
28.60	230700	0.04335	1.044	0.3767
28.52	230000	0.04348	1.046	0.4149
28.40	229100	0.04365	1.052	0.4468
28.22	227600	0.04393	1.081	0.4727
27.47	221600	0.04514	1.074	0.4452
27.27	219900	0.04547	1.056	0.4568
27.07	218300	0.04580	1.054	0.4885
26.81	216200	0.04625	1.063	0.5393
26.46	213400	0.04686	1.058	0.6116
25.75	207700	0.04816	1.153	0.7983
25.55	206100	0.04853	1.196	0.8265
25.35	204500	0.04891	1.251	0.8610
25.22	203400	0.04916	1.323	0.9051
25.03	201900	0.04954	1.440	0.9275
24.72	199400	0.05016	1.479	0.8579
24.51	197700	0.05059	1.507	0.8247
24.18	195000	0.05128	1.517	0.8062
24.02	193700	0.05162	1.561	0.7774
23.89	192700	0.05189	1.604	0.8146
23.73	191400	0.05225	1.649	0.8438
23.52	189700	0.05271	1.680	0.8169
23.34	188200	0.05313	1.686	0.7727
22.91	184700	0.05413	1.638	0.7006
22.66	182800	0.05471	1.659	0.6882
22.48	181300	0.05515	1.702	0.7341
22.14	178600	0.05600	2.116	0.8357
22.03	177700	0.05627	2.163	0.8987
21.86	176300	0.05671	2.155	0.8533
21.76	175500	0.05698	2.123	0.7893
21.66	174700	0.05724	2.072	0.7178
21.58	174100	0.05744	2.031	0.6405
21.49	173400	0.05768	1.972	0.5627
21.43	172800	0.05786	1.926	0.4945
21.34	172100	0.05811	1.870	0.4196
21.26	171400	0.05833	1.825	0.3641
21.15	170600	0.05861	1.781	0.2973
20.86	168300	0.05943	1.685	0.2063
20.23	163100	0.06130	1.527	0.2784

(continued)

[a] References given in brackets.

TABLE I *(Continued)*

Barium Fluoride

eV	cm^{-1}	μm	n	k
19.97	161100	0.06208	1.529	0.3039
19.79	159700	0.06264	2.096	0.3464
19.73	159200	0.06283	2.102	0.3943
19.71	159000	0.06290	2.094	0.4627
19.65	158500	0.06309	2.073	0.5899
19.65	158500	0.06310	2.073	0.6628
19.64	158400	0.06314	2.068	0.7318
19.56	157700	0.06340	2.014	0.7757
19.44	156800	0.06377	1.953	0.7318
19.37	156300	0.06399	1.917	0.6568
19.25	155300	0.06439	1.805	0.4843
19.14	154300	0.06479	1.813	0.3468
19.05	153600	0.06509	1.812	0.2730
18.96	153000	0.06538	1.726	0.2107
18.86	152100	0.06573	1.504	0.1616
18.76	151300	0.06608	1.433	0.1349
18.52	149400	0.06693	1.597	0.0961
18.48	149100	0.06708	1.582	0.0543
18.40	148400	0.06739	1.523	0.0086
18.33	147900	0.06763	1.473	0.0611
18.32	147732	0.06769	1.462	0.1209
18.31	147764	0.06773	1.457	0.1668
18.30	147600	0.06775	1.456	0.2168
18.29	147500	0.06779	1.446	0.2674
18.24	147100	0.06797	1.417	0.3101
18.09	145900	0.06855	1.363	0.2612
18.05	145600	0.06869	1.365	0.2027
17.94	144700	0.06910	1.372	0.1651
17.80	143600	0.06965	1.381	0.2058
17.72	142900	0.06998	1.427	0.2497
17.67	142500	0.07018	1.457	0.3108
17.63	142200	0.07034	1.474	0.3856
17.61	142000	0.07041	1.480	0.4522
17.59	141800	0.07050	1.489	0.5121
17.54	141400	0.07070	1.508	0.5679
17.43	140600	0.07114	1.622	0.6246
17.29	139500	0.07171	2.288	0.6744
17.22	138900	0.07199	2.246	0.7235
17.21	138800	0.07203	2.241	0.7717
17.21	138800	0.07203	2.241	0.8344
17.20	138800	0.07204	2.239	0.8843
17.14	138300	0.07233	2.105	0.9368
16.98	137000	0.07301	1.885	0.9063
16.94	136600	0.07318	1.855	0.8525
16.86	136000	0.07354	1.820	0.7332
16.72	134800	0.07416	1.737	0.4620
16.63	134100	0.07456	1.686	0.2532

TABLE I *(Continued)*

Barium Fluoride

eV	cm^{-1}	μm	*n*	*k*
16.61	134000	0.07464	1.676	0.1981
16.48	132900	0.07522	1.619	0.1388
16.32	131600	0.07596	1.550	0.1405
16.04	129400	0.07729	1.481	0.1644
15.86	127900	0.07820	1.467	0.2023
15.73	126800	0.07884	1.477	0.2521
15.61	125900	0.07940	1.485	0.3047
15.43	124400	0.08037	1.507	0.4231
15.26	123000	0.08127	1.526	0.4748
15.07	121600	0.08225	1.551	0.5121
14.96	120700	0.08287	1.586	0.5555
14.81	119400	0.08374	1.639	0.5974
14.59	117700	0.08498	1.814	0.6492
14.50	116900	0.08553	1.845	0.7024
14.42	116300	0.08600	1.845	0.7457
14.22	114700	0.08721	1.755	0.6855
14.00	112900	0.08856	1.645	0.5621
13.89	112000	0.08925	1.633	0.5027
13.76	111000	0.09013	1.655	0.4675
13.63	109900	0.09096	1.675	0.5213
13.57	109500	0.09134	1.684	0.5859
13.29	107200	0.09326	2.210	0.7223
13.25	106900	0.09356	2.366	0.7724
13.21	106500	0.09388	2.415	0.8294
13.18	106300	0.09410	2.428	0.8841
13.11	105700	0.09460	2.457	1.001
12.98	104700	0.09552	2.443	1.113
12.86	103800	0.09638	2.427	1.052
12.81	103300	0.09678	2.416	0.9956
12.77	103000	0.09708	2.399	0.9291
12.71	102500	0.09755	2.367	0.8661
12.65	102100	0.09799	2.337	0.7979
12.57	101300	0.09867	2.291	0.7258
12.51	100900	0.09909	2.269	0.6605
12.41	100100	0.09987	2.230	0.5781
12.34	99540	0.1005	2.203	0.506
12.25	98760	0.1013	2.161	0.4437
12.15	97960	0.1021	2.094	0.3779
12.05	97210	0.1029	2.033	0.3087
11.96	96420	0.1037	1.982	0.2574
11.78	95010	0.1053	1.928	0.2154
11.48	92600	0.1080	1.882	0.121
11.31	91200	0.1097	1.873	0.1532
11.04	89010	0.1123	1.908	0.2276
10.94	88230	0.1133	1.932	0.2623
10.80	87140	0.1148	2.133	0.2967
10.66	86000	0.1163	2.491	0.3385

(continued)

TABLE I *(Continued)*

Barium Fluoride

eV	cm^{-1}	μm	n	k
10.54	85040	0.1176	2.465	0.3917
10.46	84400	0.1185	2.447	0.4592
10.41	83960	0.1191	2.417	0.5208
10.38	83720	0.1195	2.398	0.5806
10.27	82800	0.1208	2.328	0.6321
10.12	81650	0.1225	2.236	0.5717
10.07	81190	0.1232	2.199	0.5121
10.01	80700	0.1239	2.163	0.4417
9.953	80260	0.1246	2.132	0.3712
9.891	79750	0.1254	2.094	0.3053
9.850	79440	0.1259	2.075	0.2423
9.771	78810	0.1269	2.038	0.1713
9.716	78370	0.1276	2.013	0.1095
9.646	77800	0.1285	1.980	0.06145
9.590	77350	0.1293	1.954	0.01223
9.321	75180	0.1330	1.882 [4]	
9.357	75470	0.1325		9.759E-5 [5]
9.287	74910	0.1335		2.589E-5
9.218	74350	0.1345		7.004E-6
9.214	74320	0.1346	1.873	
9.150	73800	0.1355		1.932E-6
9.137	73690	0.1357	1.857	
9.083	73260	0.1365		5.431E-7
9.017	72730	0.1375		1.555E-7
8.975	72390	0.1381	1.834	
8.952	72200	0.1385		4.535E-8
8.808	71040	0.1408	1.815	
8.697	70150	0.1426	1.800	
8.538	68860	0.1452	1.782	
8.396	67710	0.1477	1.767	
8.099	65320	0.1531	1.741	
8.266	66670	0.15	1.678 [7]	
6.199	50000	0.20	1.557	
4.959	40000	0.25	1.519	
4.133	33330	0.30	1.501	
4.592	37037	0.27	1.51031 [6]	
3.874	31250	0.32	1.49636	
3.350	27027	0.37	1.48821	
2.952	23809	0.42	1.48301	
2.637	21276	0.47	1.47946	
2.384	19230	0.52	1.47691	
2.175	17543	0.57	1.47503	
1.999	16129	0.62	1.47358	
1.850	14925	0.67	1.47245	
1.722	13888	0.72	1.47153	
1.610	12987	0.77	1.47078	
1.512	12195	0.82	1.47016	

TABLE I *(Continued)*

Barium Fluoride

eV	cm^{-1}	μm	n	k
1.425	11494	0.87	1.46963	
1.347	10869	0.92	1.46917	
1.278	10309	0.97	1.46877	
1.215	9803	1.02	1.46842	
1.158	9345	1.07	1.46811	
1.107	8928	1.12	1.46783	
1.059	8547	1.17	1.46757	
1.016	8196	1.22	1.46733	
0.976	7874	1.27	1.46710	
0.939	7575	1.32	1.46689	
0.904	7299	1.37	1.46669	
0.873	7042	1.42	1.46651	
0.843	6802	1.47	1.46632	
0.815	6578	1.52	1.46615	
0.789	6369	1.57	1.46598	
0.765	6172	1.62	1.46581	
0.742	5988	1.67	1.46565	
0.720	5813	1.72	1.46549	
0.700	5649	1.77	1.46533	
0.681	5494	1.82	1.46517	
0.663	5347	1.87	1.46501	
0.645	5208	1.92	1.46485	
0.629	5076	1.97	1.46470	
0.613	4950	2.02	1.46454	
0.598	4830	2.07	1.46438	
0.584	4716	2.12	1.46422	
0.571	4608	2.17	1.46406	
0.558	4504	2.22	1.46390	
0.546	4405	2.27	1.46374	
0.534	4310	2.32	1.46358	
0.523	4219	2.37	1.46341	
0.512	4132	2.42	1.46325	
0.501	4048	2.47	1.46308	
0.492	3968	2.52	1.46291	
0.482	3891	2.57	1.46273	
0.473	3816	2.62	1.46256	
0.464	3745	2.67	1.46238	
0.459	3704	2.70		3.03E-9 [14]
0.455	3676	2.72	1.46220	
0.447	3610	2.77	1.46202	
0.439	3541	2.82	1.46184	
0.432	3484	2.87	1.46165	
0.424	3424	2.92	1.46146	
0.417	3367	2.97	1.46127	
0.410	3311	3.02	1.46107	
0.403	3257	3.07	1.46088	
0.397	3205	3.12	1.46068	

(continued)

TABLE I *(Continued)*

Barium Fluoride

eV	cm^{-1}	μm	n	k
0.391	3154	3.17	1.46047	
0.385	3105	3.22	1.46027	
0.379	3058	3.27	1.46006	
0.373	3012	3.32	1.45985	
0.367	2967	3.37	1.45964	
0.362	2923	3.42	1.45942	
0.357	2881	3.47	1.45920	
0.352	2840	3.52	1.45898	
0.347	2801	3.57	1.45876	
0.342	2762	3.62	1.45853	
0.337	2724	3.67	1.45830	
0.333	2688	3.72	1.45806	
0.328	2652	3.77	1.45783	
0.326	2632	3.80		9.07E-9 [14]
0.324	2617	3.82	1.45759	
0.320	2583	3.87	1.45734	
0.316	2551	3.92	1.45710	
0.312	2518	3.97	1.45685	
0.308	2487	4.02	1.45660	
0.304	2457	4.07	1.45634	
0.300	2427	4.12	1.45608	
0.297	2398	4.17	1.45582	
0.293	2369	4.22	1.45556	
0.290	2341	4.27	1.45529	
0.287	2314	4.32	1.45502	
0.283	2288	4.37	1.45475	
0.280	2262	4.42	1.45447	
0.277	2237	4.47	1.45419	
0.274	2212	4.52	1.45391	
0.271	2188	4.57	1.45362	
0.268	2164	4.62	1.45333	
0.265	2141	4.67	1.45304	
0.262	2118	4.72	1.45274	
0.259	2096	4.77	1.45244	
0.257	2074	4.82	1.45214	
0.254	2053	4.87	1.45183	
0.252	2032	4.92	1.45153	
0.249	2012	4.97	1.45121	
0.246	1992	5.02	1.45090	
0.244	1972	5.07	1.45058	
0.242	1953	5.12	1.45026	
0.239	1934	5.17	1.44993	
0.237	1915	5.22	1.44960	
0.235	1897	5.27	1.44927	
0.233	1879	5.32	1.44893	
0.230	1862	5.37	1.44860	
0.228	1845	5.42	1.44825	

TABLE I *(Continued)*

Barium Fluoride

eV	cm^{-1}	μm	n	k
0.226	1828	5.47	1.44791	
0.224	1811	5.52	1.44756	
0.222	1795	5.57	1.44721	
0.220	1779	5.62	1.44685	
0.218	1763	5.67	1.44649	
0.216	1748	5.72	1.44613	
0.214	1733	5.77	1.44576	
0.213	1718	5.82	1.44540	
0.211	1703	5.87	1.44502	
0.209	1689	5.92	1.44465	
0.207	1675	5.97	1.44427	
0.205	1661	6.02	1.44388	
0.204	1647	6.07	1.44350	
0.202	1633	6.12	1.44311	
0.200	1620	6.17	1.44271	
0.199	1607	6.22	1.44232	
0.197	1594	6.27	1.44192	
0.196	1582	6.32	1.44151	
0.194	1569	6.37	1.44110	
0.193	1557	6.42	1.44069	
0.191	1545	6.47	1.44028	
0.190	1533	6.52	1.43986	
0.188	1522	6.57	1.43944	
0.187	1510	6.62	1.43901	
0.185	1499	6.67	1.43858	
0.184	1488	6.72	1.43815	
0.183	1477	6.77	1.43772	
0.181	1466	6.82	1.43728	
0.180	1455	6.87	1.43683	
0.179	1445	6.92	1.43638	
0.177	1434	6.97	1.43593	
0.176	1424	7.02	1.43548	
0.175	1414	7.07	1.43502	
0.174	1404	7.12	1.43456	
0.172	1394	7.17	1.43409	
0.171	1385	7.22	1.43363	
0.170	1375	7.27	1.43315	
0.169	1366	7.32	1.43268	
0.168	1356	7.37	1.43220	
0.167	1347	7.42	1.43171	
0.165	1338	7.47	1.43122	
0.164	1329	7.52	1.43073	
0.163	1321	7.57	1.43024	
0.162	1312	7.62	1.42974	
0.161	1303	7.67	1.42923	
0.160	1295	7.72	1.42873	
0.159	1287	7.77	1.42822	

(continued)

TABLE I *(Continued)*

Barium Fluoride

eV	cm^{-1}	μm	n	k
0.158	1278	7.82	1.42770	
0.157	1270	7.87	1.42718	
0.156	1262	7.92	1.42666	
0.155	1254	7.97	1.42613	
0.155	1250.0	8.0	1.4259 [7]	2.225E-7 [15]
0.146	1176.5	8.5	1.4204	6.228E-7
0.138	1111.1	9.0	1.4145	1.560E-6
0.131	1052.6	9.5	1.4082	3.558E-6
0.124	1000.0	10.0	1.4014	7.494E-6
0.118	952.4	10.5	1.3942	1.474E-5
0.113	909.1	11.0	1.3865	2.731E-5
0.108	869.6	11.5	1.3783	4.805E-5
0.103	833.3	12.0	1.3697	8.082E-5
0.100	800.0	12.5	1.3604	0.000131
0.095	769.2	13.0	1.3506	0.000204
0.0919	740.7	13.5	1.3402	0.000308
0.0886	714.3	14.0	1.3292	0.000453
0.09016	727.2	13.75	1.3040 [19]	0.000400 [18]
0.08740	704.9	14.19	1.2921	0.00057
0.08530	688.0	14.53	1.2821	0.00077
0.08363	674.5	14.83	1.2735	0.00098
0.08209	662.1	15.10	1.2650	0.00123
0.07894	636.7	15.71	1.2455	0.00177
0.07780	627.5	15.94	1.2377	0.00223
0.07660	617.8	16.92	1.2289	0.00270
0.07577	611.1	16.36	1.2226	0.00301
0.07396	596.5	16.76	1.2077	0.00441
0.07318	590.2	16.94	1.2008	0.00546
0.07242	584.1	17.12	1.1939	0.00666
0.07168	578.1	17.29	1.1867	0.00805
0.07068	570.1	17.54	1.1767	0.00936
0.06991	563.9	17.73	1.1685	0.01038
0.06908	557.2	17.94	1.1593	0.01159
0.06828	550.7	18.16	1.1498	0.01196
0.06745	544.0	18.38	1.1395	0.01145
0.06591	531.6	18.81	1.1190	0.01019
0.06528	526.5	18.99	1.1099	0.01003
0.06391	515.5	19.40	1.0888	0.01026
0.06270	505.7	19.77	1.0682	0.01027
0.06094	491.5	20.34	1.0348	0.01023
0.05998	483.8	20.67	1.0145	0.01131
0.05943	479.3	20.86	1.0019	0.01275
0.05855	472.2	21.18	0.9806	0.01703
0.05739	462.9	21.60	0.9501	0.02099
0.05673	457.6	21.85	0.9311	0.02337
0.05599	451.6	22.14	0.9010	0.02939
0.05564	448.8	22.28	0.8967	0.03298

TABLE I *(Continued)*

Barium Fluoride

eV	cm^{-1}	μm	n	k
0.05543	447.1	22.36	0.8895	0.03795
0.05455	440	22.37	0.8579	0.05890 [19]
0.05331	430	23.26	0.8074	0.0694
0.05207	420	23.81	0.7483	0.0834
0.05083	410	24.39	0.6778	0.1032
0.04959	400	25.00	0.5922	0.1334
0.04835	390	25.64	0.4873	0.1845
0.04711	380	26.32	0.3691	0.2801
0.04587	370	27.03	0.2800	0.4304
0.04463	360	27.78	0.2411	0.5931
0.04339	350	28.57	0.2325	0.7473
0.04215	340	29.41	0.2426	0.8911
0.04091	330	30.30	0.2603	1.020
0.03967	320	31.25	0.2672	1.147
0.03843	310	32.26	0.2725	1.296
0.03719	300	33.33	0.2940	1.463
0.03595	290	34.48	0.3367	1.644
0.03471	280	35.71	0.4014	1.835
0.03347	270	37.04	0.4902	2.040
0.03223	260	38.46	0.6235	2.260
0.03099	250	40.00	0.8233	2.4592
0.02975	240	41.67	1.0499	2.568
0.02851	230	43.48	1.139	2.609
0.02727	220	45.45	1.036	2.869
0.02603	210	47.62	1.038	3.590
0.02479	200	50.00	1.636	4.911
0.02355	190	52.63	4.894	6.135
0.02231	180	55.56	6.461	2.095
0.02107	170	58.82	5.168	0.787
0.01983	160	62.50	4.431	0.4251
0.01859	150	66.67	3.987	0.2735
0.01735	140	71.43	3.690	0.1935
0.01611	130	76.92	3.477	0.1449
0.01599	128.94	77.55	3.458 [19]	0.0875 [20]
0.01590	128.23	77.99	3.446	0.0846
0.01576	127.13	78.66	3.427	0.0801
0.01556	125.50	79.68	3.400	0.0751
0.01538	124.01	80.64	3.377	0.0708
0.01523	122.81	81.42	3.359	0.0667
0.01505	121.40	82.37	3.338	0.0644
0.01489	120.12	83.25	3.320	0.0600
0.01446	116.66	85.72	3.273	0.0549
0.01398	112.78	88.67	3.226	0.0512
0.01337	107.86	92.71	3.172	0.0480
0.01275	102.86	97.22	3.123	0.0448
0.01211	97.65	102.4	3.078	0.0428
0.01137	91.67	109.1	3.031	0.0409

(continued)

TABLE I *(Continued)*

Barium Fluoride

eV	cm^{-1}	μm	n	k
0.01063	85.77	116.6	2.991	0.0395
0.01003	80.87	123.6	2.961	0.0385
0.00949	76.53	130.7	2.937	0.0390
0.00877	70.71	141.4	2.909	0.0347
0.00799	64.46	155.1	2.881	0.0326
0.00712	57.45	174.1	2.855	0.0373
0.00643	51.89	192.7	2.837	0.0374
0.00484	39.00	256.4	2.803	0.0272
0.00414	33.40	299.4	2.792	0.0203
0.00330	26.59	376.2	2.781	0.0141
0.00234	18.90	529	2.772	0.0090
0.00155	12.50	800	2.766	0.0108
0.00074	6.00	1666.7	2.763	0.0053
0.0	0	∞	2.713 [13]	0.0

TABLE II

Room-temperature Sellmeier Model Parameters

ith mode		$\Delta\epsilon_i$	λ_i
Malitson model [6]			
	1	0.643356	0.057789
	2	0.506762	0.10968
	3	3.8261	46.3864
Li model [7]			
	1	0.33973	0.0
	2	0.81070	0.10065
	3	0.19652	29.87
	4	4.52469	63.82

TABLE III

Thermo-optical Coefficients of Barium Fluoride

Wavelength (μm)	dn/dT (10^{-6}/K)	Measurement temperature (°C)	Reference
0.3250	−15.6	37	[11]
0.4047	−15.0	15–55	[6]
0.4416	−16.3	37	[11]
0.4579	−15.6	20	[9]
0.5461	−15.2	15–55	[6]
0.6328	−16.0	20	[9]
	−16.7	37	[10, 11]
	−16.4	25–65	[12]
0.6563	−15.2	15–55	[6]
0.7679	−15.5	15–55	[6]
1.15	−16.2	20	[9]
	−17.1	37	[10, 11]
	−16.8	25–65	[12]
3.39	−15.9	20	[9]
	−16.8	37	[10, 11]
	−16.3	25–65	[12]
10.6	−14.5	20	[9]
∞	290	7–47	[13]

TABLE IV

Room-Temperature Classical Oscillator Model Parameters

Mode number i	ν_i (cm^{-1})	$\Delta\epsilon_i$	Γ_i/ν_i	Reference
1	184	4.5	0.020	[18]
2	278	0.07	0.30	
$\epsilon_\infty = 2.16$				
1	188	4.5	0.069	[19]
2	236	0.96	0.21	
3	278	0.015	0.15	
4	328	0.014	0.125	
$\epsilon_\infty = 2.141$				

Calcium Carbonate, Calcite ($CaCO_3$)

WILLIAM J. TROPF
Applied Physics Laboratory
The Johns Hopkins University
Laurel, Maryland

Calcite (or calcspar) is the mineral name of the low-pressure, hexagonal form of calcium carbonate, $CaCO_3$. (Orthorhombic aragonite [high-pressure form] and the rare hexagonal mineral vaterite are isomorphs found in nature.) Calcite is the principal constituent of limestone, marble, and chalk. The mineral Iceland spar is a pure, colorless, optical-quality form of calcite. The outstanding optical feature of calcite is its very high (negative) birefringence, making it a useful material for polarizers. Calcite is soft (3 on the Mohs scale) and dissociates into calcium oxide and carbon dioxide above 1170 K.

Crystalline calcite has a hexagonal (rhombohedral) structure, the space group is $R\bar{3}c$ (or D_{3d}^6), and the lattice dimensions are $a = 4.9900$ and $c = 17.060$. The unit cell contains six formula units (30 atoms), giving a theoretical density of 2.711 g/cm^3. Calcium atoms occupy 6(b) sites (with $\bar{3}$ or $C_{3i}[S_6]$ point symmetry), carbon atoms are in the 6(a) sites (32 or D_3 point symmetry), and the oxygen atoms are in the 18(e) sites (C_2 point symmetry).

Ultraviolet optical constants of calcite were determined from a Kramers–Kronig analysis of reflectance measurements by Kondo *et al.* [1] from 5 to 12 eV and from polarized reflection measurements by Uzan *et al.* [2] from 6 to 9.5 eV. There are considerable differences in the two results, but they agree on the basic features. The ordinary ray is dominated by a strong absorption peak near 8 eV, while the extraordinary-ray absorption becomes strong near 9.5 eV. The ordinary-ray absorption is explained by Kondo as arising from a transition from the A_1' state to an excited E' state of the carbonate radical. Values in Table I from 6.7 to 11.7 eV are from the measurements of Kondo *et al.* [1] with an additional value at 10.2 eV from variable-angle reflection measurements of Stéphan *et al.* [3].

Uzan *et al.* [4] also determined the absorption coefficients in the 6.5–7.3 eV region from transmission measurements of thin samples. These data are also included in Table I.

Copyright © 1998 by Academic Press.
All rights of reproduction in any form reserved
ISBN 0-12-544423-0/$25.00.

Smakula [5] summarizes the available refractive-index values. The accurate data listed in Table I are nearly a century old and come primarily from minimum-deviation prism measurements by Martens (0.2–0.77 μm, measured at 18° C [6]), by Gifford (measured at 15° C [7]), and by Carvallo (0.62–2.32 μm, measured at 20° C [8, 9]), supplemented by a single-wavelength measurement of Barbaron (0.55 μm, 18° C [10]). A standard Sellmeier dispersion equation of the form

$$n^2(\lambda) - 1 = \sum_i \frac{A_i \lambda^2}{\lambda^2 - \lambda_i^2} \tag{1}$$

can be used to represent the refractive index in the transparent region. Values of the constants A_i and λ_i are given by Ramachandran [11] and Tropf *et al.* [12] and are listed in Table II. These dispersion formulae are based on the data cited earlier, but are accurate only to the third decimal place. A few sources [10, 13, 14] give the temperature dependence of the refractive index. All measurements are in the ultraviolet or visible spectral regions. Table III lists the values of dn/dT with references. Ramachandran [11] also gives a temperature-dependent dispersion relationship based on these data.

The fundamental infrared and Raman spectra of calcite have been extensively studied. Optical modes of calcite are

$$\begin{aligned} \Gamma = {} & A_{1g}(\mathrm{R}) + 3A_{2g}(-) + 2A_{1u}(-) + 3A_{2u}(\mathrm{IR},\mathbf{E} \parallel \mathbf{c}) \\ & + 4E_g(\mathrm{R}) + 5E_u(\mathrm{IR},\mathbf{E} \perp \mathbf{c}), \end{aligned} \tag{2}$$

where the Raman frequencies are given by Porto *et al.* [15] as a A_{1g} vibration at 1088 cm^{-1} and E_g vibrations at 156, 283, 714, and 1432 cm^{-1}. Infrared-active modes have been extensively studied using reflection and emission measurements [16–23], including determination of temperature dependence [16], and measurements made at oblique angles with respect to the principal axes [20]. Table IV summarizes the location of the infrared-active optical modes measured by several authors. Of special interest are the classical-oscillator dispersion models of Hellwege *et al.* [19] and Long *et al.* [22], which can be used to calculate optical constants. Model calculations from Long *et al.* [22] are used to provide the optical constants given in Table I from 0 to 2500 cm^{-1}. Selected results of a Kramers–Kronig analysis of reflectivity [24] near several of the optical modes are also included in Table I.

Measurements made in the submillimeter region [25] given in Table I agree well with low-frequency model results [22]. The microwave (10 GHz) impedance measurement of Demau [26] gives the low-frequency dielectric constant as $\epsilon_o = 8.680$ ($n_o = 2.946$) and $\epsilon_e = 8.307$ ($n_e = 2.882$).

Figures 1 and 2 show a composite of the principal values of the complex refractive index of calcite taken from all of the data sources.

REFERENCES

1. S. Kondo, H. Yamashita, and K. Nakamura, Optical properties of calcite in the vacuum ultraviolet. *J. Phys. Soc. Jpn.* **34**, 711–714 (1973).
2. E. Uzan, H. Damany, and V. Chandrasekharan, Optical properties of calcite in the Schumann region. *Opt. Commun.* **1**, 221–222 (1969).
3. G. Stéphan, Y. Le Calvez, and S. Robin, A method to determine the complex refractive indices of an absorbing uniaxial crystal. *C. R. Acad. Sci. (Paris)* **265**, 281–284 (1967).
4. E. Uzan, H. Damany, and V. Chandrasekharan, Determination of the absorption indices of calcite in the dichroic region. *Opt. Commun.* **2**, 273–275 (1969); also see J. Schellman, V. Chandrasekharan, H. Damany, and J. Romand, Dichroic absorption of calcite in the Schumann region. *C. R. Acad. Sci. (Paris)* **260**, 117–120 (1965).
5. A. Smakula, "Single Crystals: Growth, Production, and Application," p. 400, Springer-Verlag, Berlin, 1962; also see B. H. Billings, Optics. *In* "American Institute of Physics Handbook," (D. E. Gray, ed.), 3rd Ed. McGraw-Hill, New York, 1972. Note: several typographic errors occur in these references.
6. F. F. Martens, On the dispersion of ultraviolet light. *Ann. Phys. (Leipzig)* **7**, 603–640 (1901).
7. J. W. Gifford, The refractive indices of fluorite, quartz, and calcite. *Proc. R. Soc. London* **70**, 329–340 (1902).
8. E. Carvallo, Precise measurement of the infrared dispersion of Iceland spar. *C. R. Acad. Sci (Paris)* **126**, 950–953 (1898).
9. E. Carvallo, On the unusual dispersion of Iceland spar. *J. Phys. Radium* **9**, 465–479 (1900).
10. M. Barbaron, Optical constants of calcite at low temperatures. *C. R. Acad. Sci (Paris)* **229**, 875–876 (1949).
11. G. N. Ramachandran, Birefringence of crystals and its temperature variation, Part I: Calcite and aragonite. *Proc. Indian Acad. Sci. B* **A26**, 77–92 (1947).
12. W. J. Tropf, M. E. Thomas, and T. Harris, Properties of crystals and glasses. *in* "Optical Society of America Handbook of Optics" (M. Bass, ed.), 2nd Ed. McGraw-Hill, New York, 1994.
13. F. J. Micheli, On the influence of temperature on ultraviolet dispersion of fluorite, rock salt, quartz, and calcite. *Ann. Phys. (Leipzig)* **7**, 772–790 (1902).
14. J. O. Reed, On the influence of temperature on the refraction and dispersion of single crystals and glasses. *Ann. Phys. Chem. (Leipzig)* **65**, 707–744 (1898).
15. S. P. S. Porto, J. A. Giordmaine, and T. C. Damen, Depolarization of raman scattering in calcite. *Phys. Rev.* **147**, 608–611 (1966).
16. T. Sakuria and T. Sato, Temperature dependence of vibrational spectra in calcite by means of emissivity measurement. *Phys. Rev. B* **4**, 583–591 (1971).
17. P. J. Ring, Dispersion analysis of the isomorphs sodaniter and calcite. *Infrared Phys.* **12**, 237–249 (1972).
18. R. K. Vincent, Emission polarization study on quartz and calcite. *Appl. Opt.* **11**, 1942–1945 (1972).
19. K. H. Hellwege, W. Lesch, M. Plihal, and G. Schaack, Two phonon absorption spectra and dispersion of phonon branches in crystals of the calcite structure. *Z. Phys.* **232**, 61–86 (1970).
20. R. Frech and H. Nichols, Infrared reflectivity of calcite: Oblique phonons. *Phys. Rev. B* **17**, 2275–2779 (1978).
21. C. Pastorek and J. C. Declus, Infrared vibrational intensities, dipole derivatives, and charge flux parameters for BF_3, CO_3^{2-}, and NO_3^-. *J. Phys. Chem.* **83**, 1379–1385 (1979).
22. L. L. Long, M. R. Querry, R. J. Bell, and R. W. Alexander, Optical properties of calcite and gypsum in crystalline and powdered form in the infrared and far-infrared. *Infrared Phys.* **34**, 191–201 (1993).
23. E. V. Antropova and A. S. Poplavnoi, Optical properties of calcite-structure crystals in the infrared region. *Opt. Spectrosc.* **79**, 445–449 (1995).

24. F. Matossi and V. Hohler, Optical constants of calcite in the region of fundamental frequencies. *Z. Naturforsch.* **22A**, 1516–1524 (1967).
25. V. P. Bystrov, Yu. G. Goncharov, G. V. Kozlov, and A. F. Kupriyanenko, Dielectric properties of optical crystals at submillimeter wavelengths. *Sov. Phys. Tech. Phys. (Engl. Transl.)* **31**, 1206–1207 (1986).
26. C. Demau, Measurement of the dielectric constants and dielectric anisotropies of various crystals at X-band. *J. Phys. (Paris)* **24,** 284–285 (1963).

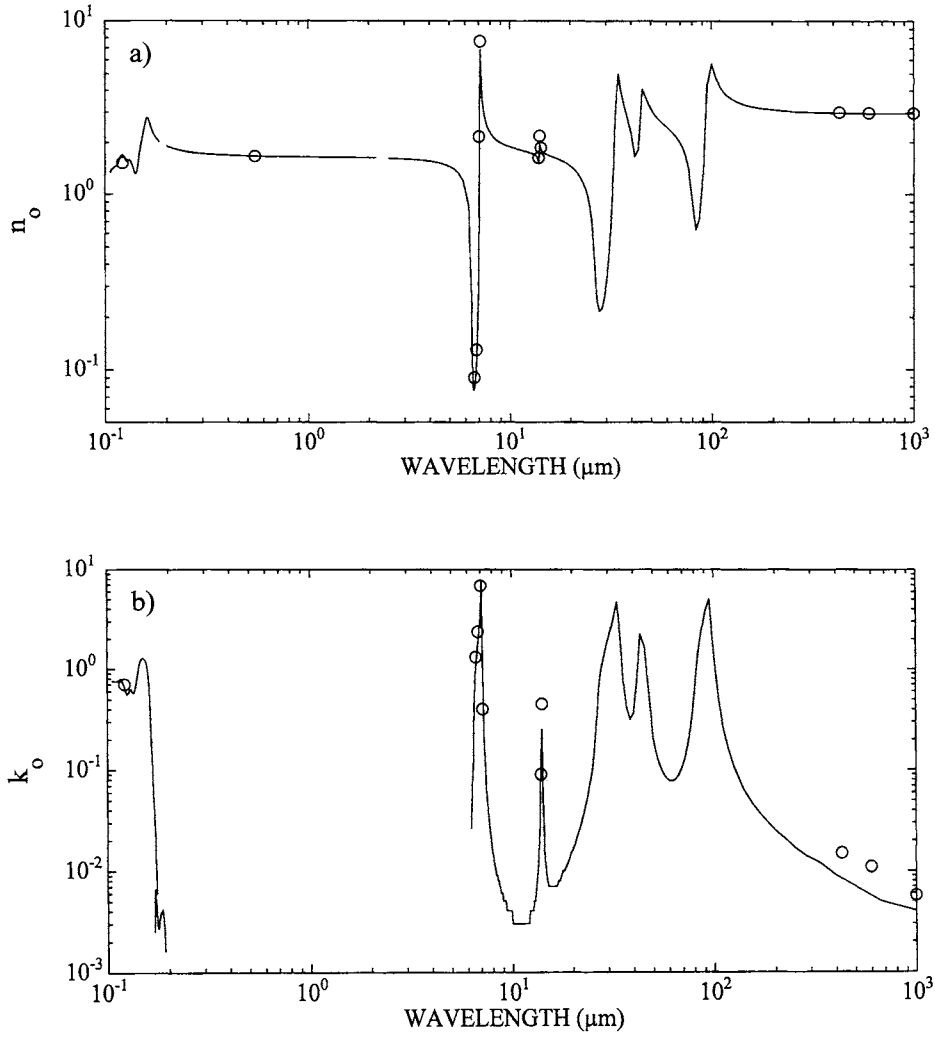

Fig. 1. (a) Log–log plot of the ordinary-ray index of refraction n_o versus wavelength in micrometers for calcium carbonate (calcite). (b) Log–log plot of the ordinary-ray extinction coefficient, k_o versus wavelength in micrometers for calcium carbonate (calcite). Lines are data sets of many points; scattered data are indicated by circles.

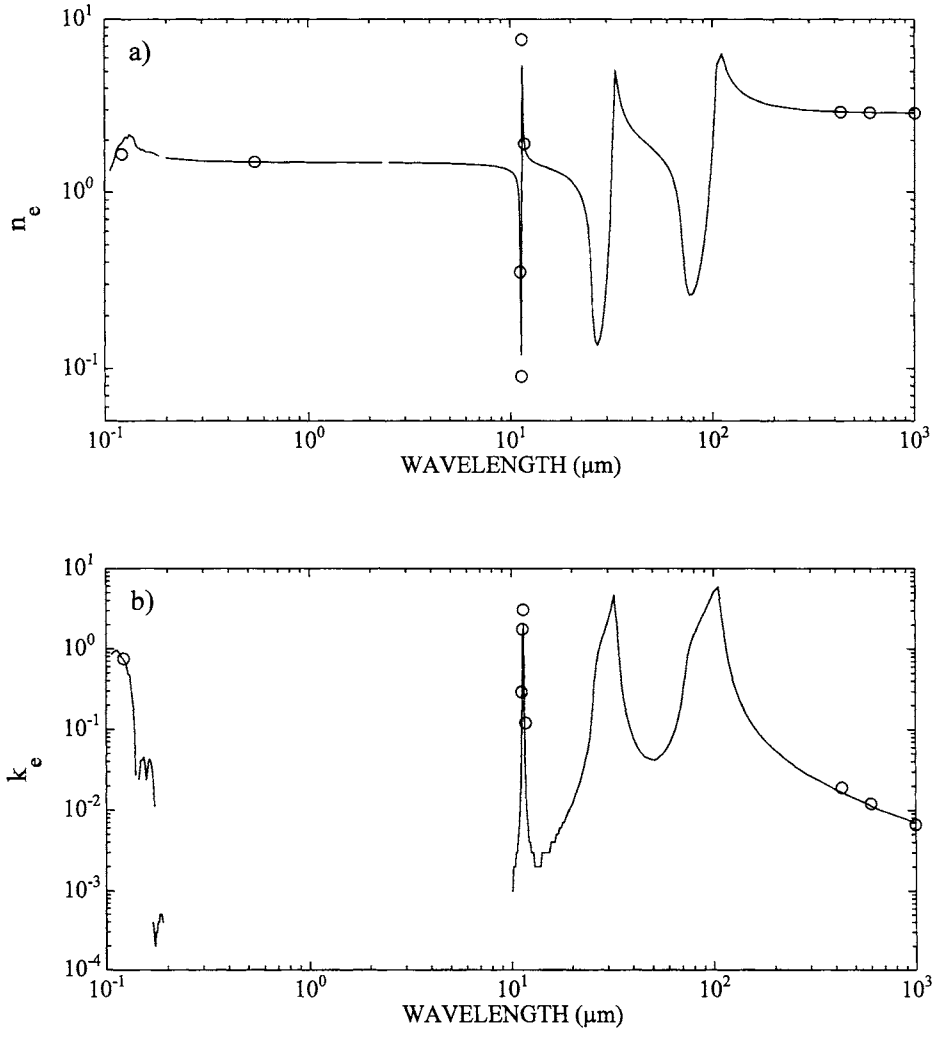

Fig. 2. (a) Log–log plot of the extraordinary-ray index of refraction n_e versus wavelength in micrometers for calcium carbonate (calcite). (b) Log–log plot of the extraordinary-ray extinction coefficient k_e versus wavelength in micrometers for calcium carbonate (calcite). Lines are data sets of many points; scattered data are indicated by circles.

TABLE I

Values of n and k for Calcium Carbonate (Calcite) from Various References[a]

eV	cm^{-1}	μm	n_o	k_o	n_e	k_e
11.7000	94366.1	0.1060	1.34 [1]	0.751 [1]	1.33 [1]	0.846 [1]
11.6000	93559.6	0.1069	1.36	0.757	1.35	0.867
11.5000	92753.0	0.1078	1.39	0.757	1.38	0.887
11.4000	91946.5	0.1088	1.40	0.754	1.41	0.906
11.3000	91139.9	0.1097	1.42	0.752	1.45	0.922
11.2000	90333.4	0.1107	1.43	0.752	1.49	0.939
11.1000	89526.8	0.1117	1.44	0.754	1.55	0.949
11.0000	88720.3	0.1127	1.45	0.759	1.60	0.959
10.9000	87913.7	0.1137	1.46	0.767	1.67	0.957
10.8000	87107.2	0.1148	1.49	0.777	1.75	0.927
10.7000	86300.6	0.1159	1.51	0.789	1.80	0.889
10.6000	85494.1	0.1170	1.56	0.787	1.84	0.854
10.5000	84687.5	0.1181	1.62	0.765	1.86	0.817
10.4000	83881.0	0.1192	1.66	0.729	1.89	0.780
10.3000	83074.4	0.1204	1.68	0.689	1.91	0.751
10.2000	82267.9	0.1216	1.69	0.644	1.94	0.732
10.1962	82236.8	0.1216	1.51 [3]	0.70 [3]	1.65 [3]	0.75 [3]
10.1000	81461.3	0.1228	1.67 [1]	0.606 [1]	1.97 [1]	0.707 [1]
10.0000	80654.8	0.1240	1.65	0.573	2.01	0.678
9.9000	79848.3	0.1252	1.60	0.555	2.06	0.632
9.8000	79041.7	0.1265	1.56	0.566	2.09	0.553
9.7000	78235.2	0.1278	1.54	0.599	2.07	0.484
9.6000	77428.6	0.1292	1.54	0.628	2.06	0.478
9.5000	76622.1	0.1305	1.57	0.632	2.10	0.464
9.4000	75815.5	0.1319	1.58	0.600	2.15	0.370
9.3000	75009.0	0.1333	1.55	0.581	2.14	0.283
9.2000	74202.4	0.1348	1.51	0.578	2.12	0.223
9.1000	73395.9	0.1362	1.45	0.605	2.10	0.175
9.0000	72589.3	0.1378	1.39	0.662	2.09	0.109
8.9000	71782.8	0.1393	1.33	0.742	2.04	0.027
8.8000	70976.2	0.1409	1.31	0.847	1.95	
8.7000	70169.7	0.1425	1.34	1.002	1.85	
8.6000	69363.1	0.1442	1.44	1.126	1.81	0.024
8.5000	68556.6	0.1459	1.58	1.204	1.80	0.030
8.4000	67750.0	0.1476	1.74	1.252	1.79	0.041
8.3000	66943.5	0.1494	1.90	1.273	1.77	0.041
8.2000	66136.9	0.1512	2.05	1.265	1.76	0.043
8.1000	65330.4	0.1531	2.21	1.236	1.75	0.045
8.0000	64523.8	0.1550	2.37	1.182	1.75	0.037
7.9000	63717.3	0.1569	2.54	1.045	1.73	0.024
7.8000	62910.7	0.1590	2.73	0.843	1.71	0.031
7.7000	62104.2	0.1610	2.78	0.588	1.70	0.039
7.6000	61297.6	0.1631	2.74	0.307	1.70	0.042
7.5000	60491.1	0.1653	2.61	0.132	1.70	0.040
7.4000	59684.6	0.1675	2.46	0.067	1.70	0.032

(continued)

[a] References given in brackets.

TABLE I *(Continued)*

Calcium Carbonate (Calcite)

eV	cm^{-1}	μm	n_o	k_o	n_e	k_e
7.3364	59171.6	0.1690		0.0025 [4]		0.0004 [4]
7.3000	58878.0	0.1698	2.34	0.035 [1]	1.69	0.022 [1]
7.2506	58479.5	0.1710		0.0066 [4]		0.0003 [4]
7.2000	58071.5	0.1722	2.26	0.018 [1]	1.68	0.011 [1]
7.1668	57803.5	0.1730		0.0041 [4]		0.0002 [4]
7.1000	57264.9	0.1746	2.20	0.006 [1]	1.67	
7.0849	57142.9	0.1750		0.0029 [4]		0.0003
7.0048	56497.2	0.1770		0.0027		0.0003
7.0000	56458.4	0.1771	2.14		1.66	
6.9265	55865.9	0.1790		0.0033		0.0004
6.9000	55651.8	0.1797	2.09		1.64	
6.8500	55248.6	0.1810		0.0037		0.0004
6.8000	54845.3	0.1823	2.05		1.63	
6.7751	54644.8	0.1830		0.0039		0.0005
6.7019	54054.1	0.1850		0.0041		0.0005
6.7000	54038.7	0.1851	2.02		1.62	
6.6302	53475.9	0.1870		0.0036		0.0005
6.5601	52910.1	0.1890		0.0027		0.0004
6.4914	52356.0	0.1910		0.0016		0.0004
6.2307	50253.8	0.19899			1.57796 [6]	
6.1965	49977.5	0.20009	1.90284 [6]		1.57649	
6.0637	48906.9	0.20447	1.88242		1.57081	
5.9546	48027.0	0.20821	1.86733		1.56640	
5.9074	47646.3	0.20988	1.8608110 [7]			
5.8739	47375.9	0.21108	1.85692 [6]		1.56327	
5.7815	46630.9	0.21445	1.84558		1.55976	
			1.8458240 [7]		1.5599225 [7]	
5.6501	45570.5	0.21944	1.8307980		1.5551219	
5.6496	45566.4	0.21946	1.83075 [6]		1.55496 [6]	
5.5351	44642.9	0.22400	1.81890		1.55105	
5.4736	44147.6	0.22651	1.8130351 [7]		1.5491444 [7]	
5.3651	43272.2	0.23110	1.8023942		1.5455001	
5.3606	43235.8	0.23129	1.80233 [6]		1.54541 [6]	
5.1063	41184.5	0.24281	1.78111		1.53782	
5.0692	40885.4	0.24459	1.7796645 [7]		1.5373101 [7]	
4.9528	39946.8	0.25033	1.76968 [6]		1.53358 [6]	
4.8185	38863.3	0.25731	1.7605000 [7]		1.5301212 [7]	
4.8184	38862.6	0.25732	1.76038 [6]		1.53005 [6]	
4.7107	37993.9	0.26320	1.75343		1.52736	
4.6331	37367.8	0.26761	1.74864		1.52547	
4.5107	36381.1	0.27487	1.7415041 [7]		1.5226617	
			1.74139 [6]		1.52261 [6]	
4.4023	35506.3	0.28164	1.73538		1.52018	
4.2553	34320.9	0.29137	1.72774		1.51705	
4.0862	32957.5	0.30342	1.7195881 [7]		1.5136464 [7]	
4.0225	32443.6	0.30823	1.71657 [6]		1.51240 [6]	
3.9703	32022.5	0.31228	1.71425		1.51140	

TABLE I *(Continued)*

Calcium Carbonate (Calcite)

eV	cm^{-1}	μm	n_o	k_o	n_e	k_e
3.7539	30276.9	0.33029	1.7051544 [7]		1.5074581 [7]	
3.6428	29380.8	0.34036	1.70078 [6]		1.50562 [6]	
3.4565	27878.3	0.35870	1.69297		1.50267	
3.4339	27695.8	0.36107	1.6931606 [7]		1.5022352 [7]	
3.1435	25354.0	0.39442	1.68397 [6]		1.49810 [6]	
3.1296	25241.8	0.39617	1.6832956 [7]		1.4977742 [7]	
3.0227	24379.2	0.41019	1.68014 [6]		1.49640 [6]	
2.8564	23038.0	0.43407	1.67552		1.49430	
			1.6755174 [7]		1.4942419 [7]	
2.8077	22645.6	0.44159	1.67423 [6]		1.49373 [6]	
2.6502	21375.2	0.46783	1.67024		1.49190	
2.5504	20569.8	0.48615	1.66785		1.49074	
2.5504	20569.8	0.48615	1.6678308 [7]		1.4907407 [7]	
2.4377	19661.6	0.50861	1.66527 [6]		1.48956 [6]	
2.3526	18974.9	0.52701	1.6634145 [7]		1.4887055 [7]	
2.3226	18732.6	0.53383	1.66277 [6]		1.48841 [6]	
2.3175	18691.6	0.5350	1.662671 [8]		1.488421 [8]	
2.2708	18315.0	0.5460	1.66193 [10]		1.48840 [10]	
2.2704	18311.7	0.54610	1.66168 [6]		1.48793 [6]	
2.2113	17834.8	0.56070	1.66046		1.48736	
2.2112	17834.5	0.56071	1.6604550 [7]		1.4873449 [7]	
2.1039	16969.0	0.58931	1.658369 [8]		1.486449 [8]	
			1.65835 [6]		1.48640 [6]	
			1.6583551 [7]		1.4863915 [7]	
2.0138	16242.5	0.6157			1.485677 [8]	
1.9748	15927.6	0.62784	1.65592 [6]		1.48529 [6]	
1.9566	15780.8	0.6337			1.485200 [8]	
1.9256	15530.8	0.64388	1.65504		1.48490 [6]	
1.8991	15317.2	0.6529			1.484722 [8]	
1.8891	15236.8	0.65630	1.65437		1.48459 [6]	
			1.6543988 [7]		1.4845685 [7]	
1.8483	14907.6	0.6708	1.653688 [8]		1.484331 [8]	
			1.65367 [6]		1.48426 [6]	
1.8420	14856.6	0.6731			1.484283 [8]	
1.7840	14388.5	0.6950	1.652581 [8]		1.483834 [8]	
1.7548	14153.1	0.70656	1.6520702 [7]		1.4835315 [7]	
1.7256	13917.9	0.7185	1.651581 [8]		1.483396 [8]	
1.6676	13449.9	0.7435	1.650611		1.482976	
1.6144	13020.8	0.7680	1.649741		1.482607	
1.6139	13016.8	0.76824	1.64974 [6]		1.48259 [6]	
			1.6497403 [7]		1.4825523 [7]	
1.6079	12968.5	0.7711	1.649650 [8]		1.482566 [8]	
1.5596	12578.6	0.7950	1.6488640 [7]		1.4821645 [7]	
1.5485	12489.1	0.8007	1.648687 [8]		1.482156 [8]	
1.4893	12012.0	0.8325	1.647724		1.481756	
1.4299	11532.7	0.8671	1.646759		1.481365	
1.3705	11053.4	0.9047	1.645784		1.480984	

(continued)

TABLE I *(Continued)*

Calcium Carbonate (Calcite)

eV	cm^{-1}	μm	n_o	k_o	n_e	k_e
1.3106	10570.8	0.9460	1.644800		1.480602	
1.2506	10086.7	0.9914	1.643798		1.480221	
1.1902	9599.7	1.0417	1.642762		1.479849	
1.1299	9113.3	1.0973	1.641675		1.479477	
1.0696	8626.6	1.1592	1.640511		1.479096	
1.0090	8138.0	1.2288	1.639262		1.478704	
0.9738	7854.2	1.2732	1.638487			
0.9486	7651.1	1.3070	1.637894		1.478312	
0.9396	7578.6	1.3195	1.637670			
0.9060	7307.3	1.3685	1.636809			
0.8883	7164.4	1.3958	1.636366		1.477891	
0.8720	7032.8	1.4219	1.635898			
0.8382	6760.4	1.4792	1.634901			
0.8281	6679.1	1.4972	1.634571		1.477441	
0.8044	6487.6	1.5414	1.633811			
0.7707	6216.2	1.6087	1.632611			
0.7679	6193.5	1.6146			1.476950	
0.7373	5947.1	1.6815	1.631266			
0.7090	5718.5	1.7487			1.476381	
0.7039	5677.3	1.7614	1.629741			
0.6707	5409.2	1.8487	1.628002			
0.6496	5239.7	1.9085			1.475733	
0.6372	5139.5	1.9457	1.626023			
0.6039	4870.7	2.0531	1.623717			
0.5905	4762.4	2.0998			1.474919	
0.5709	4604.3	2.1719	1.620995			
0.5334	4302.4	2.3243			1.473918	
0.4959	4000.0	2.500	1.614 [22]		1.473 [22]	
0.4649	3750.0	2.667	1.609		1.472	
0.4339	3500.0	2.857	1.603		1.472	
0.4030	3250.0	3.077	1.596		1.470	
0.3720	3000.0	3.333	1.586		1.469	
0.3410	2750.0	3.636	1.572		1.467	
0.3100	2500.0	4.000	1.550		1.465	
0.2790	2250.0	4.444	1.515		1.462	
0.2480	2000.0	5.000	1.448		1.457	
0.2356	1900.0	5.263	1.401		1.455	
0.2232	1800.0	5.556	1.326		1.452	
0.2108	1700.0	5.882	1.190		1.448	
0.1984	1600.0	6.250	0.853	0.026 [22]	1.443	
0.1922	1550.0	6.452	0.233	0.174	1.441	
0.1909	1540.0	6.494	0.107	0.437	1.440	
0.1897	1530.0	6.536	0.084	0.650	1.440	
0.1885	1520.0	6.579	0.077	0.836	1.439	
0.1872	1510.0	6.623	0.077	1.015	1.438	
			0.09 [24]	1.31 [24]		
0.1860	1500.0	6.667	0.079 [22]	1.197 [22]	1.438	

TABLE I *(Continued)*

Calcium Carbonate (Calcite)

eV	cm^{-1}	μm	n_o	k_o	n_e	k_e
0.1847	1490.0	6.711	0.086	1.389	1.437	
0.1835	1480.0	6.757	0.096	1.601	1.436	
0.1823	1470.0	6.803	0.112	1.842	1.436	
			0.13 [24]	2.35 [24]		
0.1810	1460.0	6.849	0.136 [22]	2.130 [22]	1.435	
0.1798	1450.0	6.897	0.176	2.489	1.434	
0.1785	1440.0	6.944	0.248	2.970	1.433	
0.1773	1430.0	6.993	0.402	3.687	1.433	
0.1761	1420.0	7.042	0.864	4.960	1.432	
			2.16 [24]	6.85 [24]		
0.1748	1410.0	7.092	3.878 [22]	7.485 [22]	1.431	
0.1736	1400.0	7.143	6.865	1.869	1.430	
			7.67 [24]	0.40 [24]		
0.1723	1390.0	7.194	4.969 [22]	0.553 [22]	1.429	
0.1711	1380.0	7.246	4.109	0.273	1.428	
0.1699	1370.0	7.299	3.622	0.166	1.427	
0.1686	1360.0	7.353	3.306	0.113	1.426	
0.1674	1350.0	7.407	3.081	0.083	1.425	
0.1661	1340.0	7.463	2.912	0.063	1.424	
0.1649	1330.0	7.519	2.780	0.050	1.423	
0.1637	1320.0	7.576	2.674	0.041	1.422	
0.1624	1310.0	7.634	2.587	0.034	1.421	
0.1612	1300.0	7.692	2.513	0.029	1.420	
0.1599	1290.0	7.752	2.451	0.025	1.418	
0.1587	1280.0	7.813	2.396	0.022	1.417	
0.1575	1270.0	7.874	2.349	0.019	1.416	
0.1562	1260.0	7.937	2.307	0.017	1.414	
0.1550	1250.0	8.000	2.270	0.015	1.413	
0.1537	1240.0	8.065	2.237	0.014	1.411	
0.1525	1230.0	8.130	2.207	0.012	1.410	
0.1513	1220.0	8.197	2.180	0.011	1.408	
0.1500	1210.0	8.264	2.155	0.010	1.406	
0.1488	1200.0	8.333	2.132	0.009	1.404	
0.1475	1190.0	8.403	2.111	0.009	1.402	
0.1463	1180.0	8.475	2.092	0.008	1.400	
0.1451	1170.0	8.547	2.074	0.008	1.398	
0.1438	1160.0	8.621	2.057	0.007	1.396	
0.1426	1150.0	8.696	2.041	0.007	1.394	
0.1413	1140.0	8.772	2.027	0.006	1.391	
0.1401	1130.0	8.850	2.013	0.006	1.388	
0.1389	1120.0	8.929	2.000	0.006	1.385	
0.1376	1110.0	9.009	1.988	0.005	1.382	
0.1364	1100.0	9.091	1.976	0.005	1.379	
0.1351	1090.0	9.174	1.965	0.005	1.375	
0.1339	1080.0	9.259	1.955	0.005	1.372	
0.1327	1070.0	9.346	1.945	0.004	1.367	
0.1314	1060.0	9.434	1.935	0.004	1.363	

(continued)

TABLE I *(Continued)*

Calcium Carbonate (Calcite)

eV	cm^{-1}	μm	n_o	k_o	n_e	k_e
0.1302	1050.0	9.524	1.926	0.004	1.358	
0.1289	1040.0	9.615	1.917	0.004	1.352	
0.1277	1030.0	9.709	1.908	0.004	1.346	
0.1265	1020.0	9.804	1.900	0.004	1.339	
0.1252	1010.0	9.901	1.892	0.004	1.331	
0.1240	1000.0	10.000	1.885	0.003	1.323	0.001 [22]
0.1227	990.0	10.101	1.877	0.003	1.312	0.001
0.1215	980.0	10.204	1.870	0.003	1.300	0.002
0.1203	970.0	10.309	1.863	0.003	1.286	0.002
0.1190	960.0	10.417	1.856	0.003	1.269	0.002
0.1178	950.0	10.526	1.849	0.003	1.247	0.003
0.1165	940.0	10.638	1.842	0.003	1.219	0.003
0.1153	930.0	10.753	1.836	0.003	1.181	0.004
0.1141	920.0	10.870	1.829	0.003	1.126	0.006
0.1128	910.0	10.989	1.822	0.003	1.038	0.010
0.1116	900.0	11.111	1.816	0.003	0.873	0.020
0.1103	890.0	11.236	1.810	0.003	0.368	0.106
0.1103	890.0	11.236			0.35 [24]	0.29 [24]
0.1091	880.0	11.364	1.803	0.003	0.120 [22]	1.373 [22]
					0.09 [24]	1.75 [24]
0.1079	870.0	11.494	1.797	0.003	5.387 [22]	2.064 [22]
					7.62 [24]	3.06 [24]
0.1066	860.0	11.628	1.790	0.003	2.288 [22]	0.052 [22]
0.1054	850.0	11.765	1.783	0.003	1.913	0.018
					1.90 [24]	0.12 [24]
0.1041	840.0	11.905	1.777	0.003	1.760 [22]	0.009 [22]
0.1029	830.0	12.048	1.770	0.003	1.676	0.006
0.1017	820.0	12.195	1.762	0.004	1.621	0.004
0.1004	810.0	12.346	1.755	0.004	1.583	0.004
0.0992	800.0	12.500	1.747	0.004	1.554	0.003
0.0979	790.0	12.658	1.738	0.004	1.531	0.003
0.0967	780.0	12.821	1.729	0.005	1.513	0.003
0.0955	770.0	12.987	1.718	0.005	1.497	0.002
0.0942	760.0	13.158	1.705	0.007	1.483	0.002
0.0930	750.0	13.333	1.688	0.009	1.470	0.002
0.0917	740.0	13.514	1.663	0.013	1.459	0.002
0.0905	730.0	13.699	1.619	0.028	1.448	0.002
0.0893	720.0	13.889	1.505	0.133	1.439	0.002
			1.62 [24]	0.09 [24]		
0.0880	710.0	14.085	1.951 [22]	0.251 [22]	1.429	0.003
			2.18 [24]	0.45 [24]		
0.0868	700.0	14.286	1.828 [22]	0.038 [22]	1.420	0.003
			1.86 [24]			
0.0855	690.0	14.493	1.772 [22]	0.016	1.411	0.003
0.0843	680.0	14.706	1.743	0.010	1.402	0.003
0.0831	670.0	14.925	1.723	0.008	1.393	0.003
0.0818	660.0	15.152	1.707	0.007	1.385	0.003

TABLE I *(Continued)*

Calcium Carbonate (Calcite)

eV	cm^{-1}	μm	n_o	k_o	n_e	k_e
0.0806	650.0	15.385	1.693	0.007	1.376	0.003
0.0794	640.0	15.625	1.680	0.007	1.366	0.004
0.0781	630.0	15.873	1.668	0.007	1.357	0.004
0.0769	620.0	16.129	1.656	0.007	1.347	0.004
0.0756	610.0	16.393	1.643	0.007	1.336	0.004
0.0744	600.0	16.667	1.630	0.007	1.326	0.005
0.0732	590.0	16.949	1.617	0.008	1.314	0.005
0.0719	580.0	17.241	1.604	0.008	1.302	0.006
0.0707	570.0	17.544	1.589	0.009	1.289	0.006
0.0694	560.0	17.857	1.574	0.010	1.275	0.007
0.0682	550.0	18.182	1.557	0.010	1.260	0.007
0.0670	540.0	18.519	1.540	0.011	1.243	0.008
0.0657	530.0	18.868	1.520	0.012	1.225	0.009
0.0645	520.0	19.231	1.500	0.013	1.206	0.010
0.0632	510.0	19.608	1.477	0.015	1.184	0.011
0.0620	500.0	20.000	1.452	0.016	1.160	0.012
0.0608	490.0	20.408	1.424	0.018	1.132	0.014
0.0595	480.0	20.833	1.393	0.021	1.101	0.016
0.0583	470.0	21.277	1.357	0.024	1.066	0.019
0.0570	460.0	21.739	1.317	0.027	1.024	0.022
0.0558	450.0	22.222	1.271	0.032	0.975	0.027
0.0546	440.0	22.727	1.217	0.038	0.916	0.033
0.0533	430.0	23.256	1.152	0.046	0.843	0.041
0.0521	420.0	23.810	1.073	0.057	0.750	0.055
0.0508	410.0	24.390	0.974	0.074	0.623	0.079
0.0496	400.0	25.000	0.843	0.102	0.434	0.138
0.0484	390.0	25.641	0.662	0.157	0.204	0.366
0.0471	380.0	26.316	0.404	0.318	0.144	0.664
0.0459	370.0	27.027	0.248	0.659	0.136	0.928
0.0446	360.0	27.778	0.217	0.990	0.147	1.198
0.0434	350.0	28.571	0.225	1.314	0.173	1.501
0.0422	340.0	29.412	0.260	1.669	0.226	1.874
0.0409	330.0	30.303	0.335	2.096	0.339	2.385
0.0397	320.0	31.250	0.496	2.667	0.648	3.205
0.0384	310.0	32.258	0.934	3.535	2.118	4.672
0.0372	300.0	33.333	2.713	4.689	5.076	2.060
0.0360	290.0	34.483	4.971	2.212	3.818	0.563
0.0347	280.0	35.714	3.946	0.761	3.152	0.264
0.0335	270.0	37.037	3.230	0.414	2.778	0.157
0.0322	260.0	38.462	2.726	0.318	2.533	0.107
0.0310	250.0	40.000	2.252	0.363	2.356	0.079
0.0298	240.0	41.667	1.656	0.765	2.217	0.062
0.0285	230.0	43.478	1.815	2.227	2.102	0.052
0.0273	220.0	45.455	4.071	1.703	2.000	0.046
0.0248	200.0	50.000	3.137	0.209	1.810	0.042
0.0242	195.0	51.282	2.991	0.161	1.761	0.042
0.0236	190.0	52.632	2.872	0.130	1.710	0.043

(continued)

TABLE I *(Continued)*

Calcium Carbonate (Calcite)

eV	cm^{-1}	μm	n_o	k_o	n_e	k_e
0.0229	185.0	54.054	2.770	0.110	1.656	0.046
0.0223	180.0	55.556	2.679	0.096	1.598	0.049
0.0217	175.0	57.143	2.595	0.087	1.533	0.053
0.0211	170.0	58.824	2.514	0.081	1.461	0.060
0.0205	165.0	60.606	2.433	0.078	1.377	0.068
0.0198	160.0	62.500	2.350	0.078	1.278	0.081
0.0192	155.0	64.516	2.260	0.081	1.156	0.101
0.0186	150.0	66.667	2.159	0.088	1.000	0.134
0.0180	145.0	68.966	2.040	0.102	0.785	0.201
0.0174	140.0	71.429	1.891	0.125	0.490	0.387
0.0167	135.0	74.074	1.691	0.170	0.304	0.774
0.0161	130.0	76.923	1.395	0.269	0.261	1.153
0.0155	125.0	80.000	0.931	0.577	0.265	1.523
0.0149	120.0	83.333	0.630	1.386	0.297	1.922
0.0143	115.0	86.957	0.730	2.374	0.364	2.389
0.0136	110.0	90.909	1.323	3.737	0.499	2.988
0.0130	105.0	95.238	4.336	5.036	0.803	3.842
0.0124	100.0	100.00	5.677	1.508	1.733	5.206
0.0118	95.0	105.26	4.651	0.520	5.471	5.800
0.0112	90.0	111.11	4.107	0.263	6.273	1.850
0.0105	85.0	117.65	3.790	0.160	5.088	0.715
0.00992	80.0	125.00	3.585	0.108	4.408	0.379
0.00930	75.0	133.33	3.441	0.079	3.994	0.236
0.00868	70.0	142.86	3.334	0.060	3.718	0.161
0.00806	65.0	153.85	3.252	0.047	3.521	0.117
0.00744	60.0	166.67	3.188	0.038	3.374	0.089
0.00682	55.0	181.82	3.136	0.031	3.261	0.069
0.00620	50.0	200.00	3.094	0.025	3.172	0.055
0.00558	45.0	222.22	3.059	0.021	3.102	0.044
0.00496	40.0	250.00	3.031	0.017	3.045	0.035
0.00434	35.0	285.71	3.007	0.014	2.999	0.028
0.00372	30.0	333.33	2.988	0.012	2.962	0.023
0.00310	25.0	400.00	2.973	0.009	2.932	0.018
0.00289	23.3	428.57	2.987 [25]	0.015 [25]	2.915 [25]	0.019 [25]
0.00248	20.0	500.00	2.961 [22]	0.007 [22]	2.909 [22]	0.014 [22]
0.00207	16.7	600.00	2.968 [25]	0.011 [25]	2.888 [25]	0.012 [25]
0.00186	15.0	666.67	2.952 [22]	0.005 [22]	2.892 [22]	0.010 [22]
0.00124	10.0	1000.0	2.945	0.004	2.880	0.007
			2.950 [25]	0.0057 [25]	2.862 [25]	0.0066 [25]
0.000620	5.0	2000.0	2.941 [22]	0.002 [22]	2.873 [22]	0.003 [22]
0.000372	3.0	3333.3	2.946 [26]	0.0 [26]	2.883 [26]	0.0 [26]
0	0.0	∞	2.940 [22]	0.0 [22]	2.871 [22]	0.0 [22]

TABLE II

Sellmeier Dispersion Equation Constants for Calcite

	Ramachandran [11]		Tropf [12]	
Term [Eq. (1)]	n_o	n_e	n_o	n_e
λ_1	0.0500	0.0500	0.0588	0.07897
λ_2	0.1000	0.1000	0.141	0.142
λ_3	0.1535	0.1535	0.197	11.468
λ_4	6.7	11.3	7.005	—
A_1	0.43257	0.45899	0.8559	1.0856
A_2	0.82932	0.69835	0.8391	0.0988
A_3	0.43376	0.02680	0.0009	0.317
A_4	0.61855	0.30018	0.6845	—
Range (μm)	0.2–2.1		0.2–2.2	

TABLE III

Thermo-optical Coefficients of Calcite (in Vacuum)

Wavelength (μm)	dn_o/dT (10^{-6}/K)	dn_e/dT (10^{-6}/K)	Temperature[a] (°C)	Reference
0.211	20.0		$\overline{T} = 61.5$	[13]
0.214	18.8	24.3	$\overline{T} = 61.5$	[13]
0.219	16.7	23.5	$\overline{T} = 61.5$	[13]
0.224	15.0		$\overline{T} = 61.5$	[13]
0.226		20.8	$\overline{T} = 61.5$	[13]
0.231	12.5	22.0	$\overline{T} = 61.5$	[13]
0.257	8.1	17.6	$\overline{T} = 61.5$	[13]
0.274	6.4	16.3	$\overline{T} = 61.5$	[13]
0.288	5.4	15.7	$\overline{T} = 61.5$	[13]
0.298	4.7	15.3	$\overline{T} = 61.5$	[13]
0.313	3.8		$\overline{T} = 61.5$	[13]
0.325	3.4	14.4	$\overline{T} = 61.5$	[13]
0.340	2.7	13.7	$\overline{T} = 61.5$	[13]
0.361	2.4	13.4	$\overline{T} = 61.5$	[13]
0.436	1.44	11.92	$\overline{T} = 57.1$	[14]
0.441	2.1	12.1	$\overline{T} = 61.5$	[13]
0.467	2.0		$\overline{T} = 61.5$	[13]
	1.34	11.79	$\overline{T} = 57.1$	[14]
0.480	1.8	11.8	$\overline{T} = 61.5$	[13]
0.508	1.7	11.3	$\overline{T} = 61.5$	[13]
0.546	0.5	12.0	−100 to 18	[10]
0.589	1.2	11.1	$\overline{T} = 61.5$	[13]
	0.78	10.94	$\overline{T} = 57.1$	[14]
0.643	0.9	10.8	$\overline{T} = 61.5$	[13]
0.656	0.71	10.62	$\overline{T} = 57.1$	[14]

[a] $\overline{T}$ is the mean measurement temperature.

TABLE IV

Transverse (and Longitudinal) Optical Phonon Frequencies in Calcite ($CaCO_3$)

Mode	Hellwege [19]	Long [22]	Pastorek [21]
E_u (**E**⊥**c**)	102(123)	104.1	
E_u (**E**⊥**c**)	223(239)	223.3	
E_u (**E**⊥**c**)	297(381)	295.6	
E_u (**E**⊥**c**)	712(715)	713.2	711.9(713.2)
E_u (**E**⊥**c**)	1407(1599)	1406.8	1408(1551.5)
A_{2u} (**E**∥**c**)	92(136)	94.6	
A_{2u} (**E**∥**c**)	303(387)	304.9	
A_{2u} (**E**∥**c**)	872(890)	870.8	869.8(887.4)

Cesium Bromide (CsBr)

W. J. MOORE
Naval Research Laboratory
Washington, D.C.

Values for the room-temperature refractive index, n, and the extinction coefficient, k, for CsBr presented in Fig. 1 and Table I are based on measurements by Dianov and Irisova [1] at 2.31 mm, Geick [2] from 275 to 31 μm, Rodney and Spindler [3] from 39 to 0.36 μm, Matthews [4] near 0.2 μm, Eby *et al.* [5] from 0.19 to 0.11 μm, Cardona *et al.* [6] from 1.77×10^{-2} to 7.3×10^{-3} μm, and Henke and co-workers [7, 8] from 0.124 to 4.13×10^{-5} μm.

Data are quoted, in most cases, as presented in these references with suitable unit conversion and standardization. Exceptions include the region 0.2 to 55 μm, where the values from Rodney and Spindler [3] and those of Geick [2] are presented as combined and critiqued by Li [9]. Refractive indices and extinction coefficients in the region 0.124 to 4.13×10^{-5} μm were calculated from atomic scattering coefficients of the component materials. The optical-density data of Eby *et al.* [5] in the region 0.11 to 0.19 μm have been scaled to compensate for uncertainty in sample thickness. Where data were originally published as an x–y plot only, we have scanned and digitized these plots in order to provide tabulated results.

The plotted results of Fig. 1 contain all points tabulated in the original references and a high data point density for the scanned x–y plots. Data points tabulated in Table I include only the minimum point density that adequately reproduces the structure apparent in the original.

Additional data at room temperature can be found in Vergnat *et al.* [10], Jones *et al.* [11], and Plyler and Phelps [12]. Low-temperature data and the temperature coefficient of n near room temperature can be found in Dianov and Irisova [1], Vergnat *et al.* [10], Havinga and Bosman [13], Selvarajan *et al.* [14], and Li [9].

At very long wavelengths the "2 mm" result of Dianov and Irisova [1] is an early example of a technique later generalized for simultaneous acquisition of a range of frequencies and known as dispersive Fourier-transform-

HANDBOOK OF OPTICAL CONSTANTS OF SOLIDS III

Copyright © 1998 by Academic Press.
All rights of reproduction in any form reserved
ISBN 0-12-544423-0/$25.00.

spectroscopy. In the Dianov and Irisova application the source was a monochromatic microwave oscillator at 2.31 mm [15] feeding a Michelson interferometer in a hybrid waveguide/optical configuration. The sinusoidal interference pattern due to moving one mirror was measured with no sample, then again with the sample in the moving mirror arm. The refractive index was determined from the shift in phase between the two measurements. The samples used were described only as crystals with no comment on purity.

Vergnat *et al.* [10] found refractive indices and extinction coefficients for the Cs halides at 290, 80, and 25 K from analysis of reflection measurements in the 200 to 1000 μm spectral region. Their static value for n at 290 K was 2.56, which equals Dianov and Irisova's 2-mm interferometric value at 300 K. The CsBr sample used was a single crystal.

In the reststrahlen region Geick [2] determined n and k by analyzing measurement of transmission and reflection of CsBr samples ranging from 0.2 μm to 1 cm thick. Samples from 0.2 to 2.5 μm thick were vacuum deposited onto cellulose-acetate films. Those with thicknesses from 25 μm to 1 cm were cut from thicker commercial samples or used as received.

Rodney and Spindler [3] measured the refractive index of CsBr prisms by the minimum-deviation method from 0.365 to 39.22 μm. The results were quoted to six significant figures. Two samples, grown by different organizations, were studied. Differences between the two sets of refractive-index data were described as "several units in the fifth decimal," that is, less than $\pm 0.007\%$. These data overlap those of Geick [2] in the 31 to 39.22 micron range. At 31 μm Geick gets $n = 1.606$, while Rodney and Spindler's result interpolates to 1.60546. Agreement is better than 0.04%. However, at 39 μm Geick gets $n = 1.565$, while Rodney and Spindler's data interpolates to 1.56144; agreement here has dropped to 0.23%. Li [9] critiqued these results and recommended an analytic expression of the Sellmeier form as accurate to five places in the region 0.21 to 55 μm at 293 K:

$$n^2 = 1.14600 + \frac{1.26628\,\lambda^2}{\lambda^2 - (0.120)^2} + \frac{0.01137\,\lambda^2}{\lambda^2 - (0.146)^2} + \frac{0.00975\,\lambda^2}{\lambda^2 - (0.16)^2} + \frac{0.00672\,\lambda^2}{\lambda^2 - (0.173)^2} + \frac{0.34557\,\lambda^2}{\lambda^2 - (0.187)^2} + \frac{3.76339\,\lambda^2}{\lambda^2 - (136.05)^2}. \quad (1)$$

This equation yields 1.60613 and 1.56486 at 31 and 39 μm, respectively; these values are slightly increased over the Rodney and Spindler results in the long-wavelength region but blend smoothly with those of Geick. Data points in Fig. 1 and Table I were calculated with Eq. (1).

Plyler and Phelps [12] have measured transmission in the region 0.32 to 38 μm. The samples were grown from the melt using highly purified charge material. We have extracted extinction coefficients from these data and find values not exceeding 1×10^{-5} at all wavelengths between 0.32 and 24 μm. This value is believed to be at the limit of the absorption measuring capability of their experiment and so should be taken as an upper limit to k only.

Matthews [4] has measured transmission of good-quality crystalline CsBr throughout its transparent spectral range. We have scanned and digitized his plots in the near ultraviolet, converted to approximate extinction coefficient, and tabulated and plotted the result to indicate the onset of opacity as energy increases in that region.

Eby *et al.* [5] have measured optical density in the 0.11 to 0.19 μm region of thin films of alkali halides evaporated in vacuum onto LiF substrates. Reflection and substrate effects were minimized by tabulating the difference in optical density of films with estimated thicknesses of 100 and 1000 Å. Data were presented as a plot of optical density versus energy. The CsBr plot has been scanned and digitized. Because there was no accurate thickness determination, the conversion from optical density to extinction coefficient has an undetermined scaling factor. The raw results calculated with their estimates of sample thickness fall below the extinction coefficients calculated from the atomic scattering coefficients of the constituent Cs and Br with cooperative effects neglected. Considerable structure attributed to exciton absorption was found in these spectra. Consequently, they contain useful data but are complicated by the scaling uncertainty. The Eby *et al.* extinction-coefficient data in Fig. 1 and in Table I have been scaled by a factor of 5 in order to bring the absorption by the crystal above that expected for the constituent atoms.

Cardona *et al.* [6] have studied absorption by Cs and Rb halides evaporated in vacuum onto carbon foils supported by a copper grid in the spectral region from 1.77×10^{-2} to 7.3×10^{-3} μm. Sample thickness was measured to an accuracy of about 20% by a quartz oscillator. These data were presented as absorption coefficient versus energy. The CsBr plot was scanned and digitized as described earlier.

At wavelengths shorter than 7.3×10^{-3} μm we have only the calculation of n and k based on atomic scattering factors for the constituent atoms published by Henke and co-workers [7, 8]. The calculation is described in the CsI critique by Eldridge [16] and on the Lawrence Berkeley Laboratory Internet Web site www-cxro.lbl.gov/optical_constants. Agreement between calculated values for extinction coefficient and those measured by Cardona *et al.* [6] is quite good, typically within the 20% error in sample-thickness determination.

ACKNOWLEDGMENTS

The contributions of K. Matthews of Crystran, Ltd. who provided unpublished near-ultraviolet transmission spectra, and W. R. Hunter, who calculated n and k from atomic scattering factors, are gratefully acknowledged.

REFERENCES

1. E. M. Dianov and N. A. Irisova, *Sov. Phys. Solid State* **8**, 1807 (1967).
2. R. Geick, *Z. Phys.* **163**, 499 (1961).
3. W. S. Rodney and R. J. Spindler, *J. Res. NBS* **51**, 123 (1953).

4. "Crystran Ltd. Handbook." Crystran, Poole, U.K.; K. Matthews, private communication, 1996.
5. J. E. Eby, K. J. Teegarden, and D. B. Dutton, *Phys. Rev.* **116**, 1099 (1959).
6. M. Cardona, R. Haensel, D. W. Lynch, and B. Sonntag, *Phys. Rev. B* **2**, 1117 (1970).
7. B. L. Henke, E. M. Gullikson, and J. C. Davis, *At. Data Nucl. Data Tables* **54**, 181 (1993).
8. E. M. Gullikson, private communication, 1996.
9. H. H. Li, *J. Phys. Chem. Ref. Data* **5**, 329 (1976).
10. P. Vergnat, J. Claudel, A. Hadni, P. Strimer, and F. Vermillard, *J. Phys. (Paris)* **30**, 723 (1969).
11. G. O. Jones, D. H. Martin, P. A. Mawer, and C. H. Perry, *Proc. R. Soc. London A* **261**, 10 (1961).
12. E. K. Plyler and F. P. Phelps, *J. Opt. Soc. Am.* **41**, 209 (1951).
13. E. E. Havinga and A. J. Bosman, *Phys. Rev.* **140**, A292 (1965).
14. A. Selvarajan, J. L. Swedberg, A. G. DeBell, and W. L. Wolfe, *Appl. Opt.* **18**, 3116 (1979).
15. E. A. Vinogradov, E. M. Dianov, and N. A. Irisova, *Radio Eng. Electron. Phys.* **10**, 1547 (1965).
16. J. E. Eldridge, *in* "Handbook of Optical Constants of Solids II" (E. D. Palik, ed.), p. 851. Academic Press, Orlando, Florida, 1991.

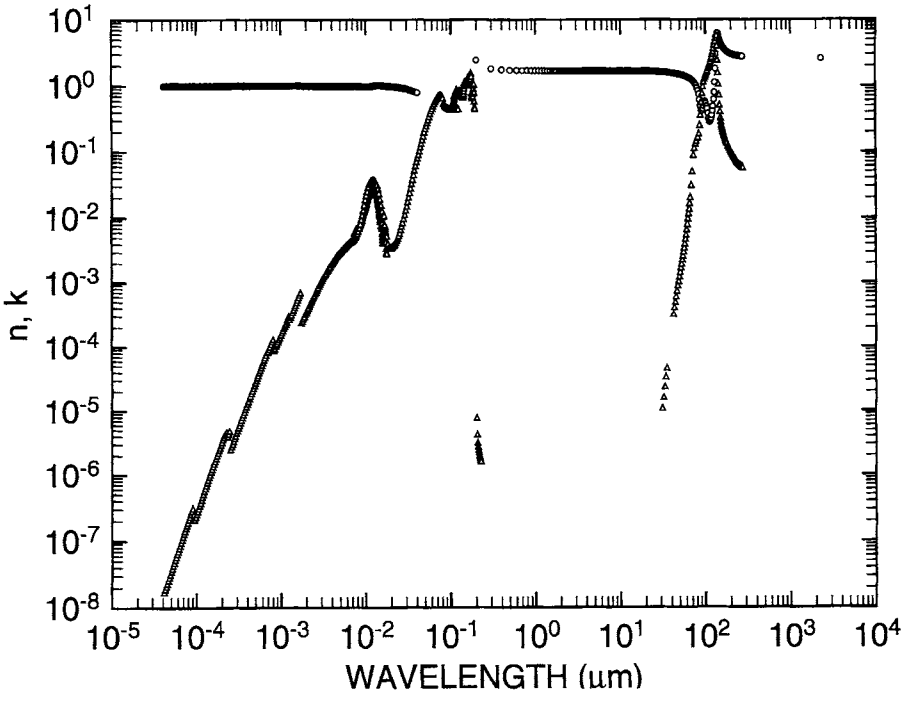

Fig. 1. Log–log plot of n (circles) and k (triangles) versus wavelength in micrometers for cesium bromide.

TABLE I

Values of n and k for Cesium Bromide from Various References[a]

eV	cm^{-1}	μm	n	k
3.000E4	2.420E8	4.13E-5	1.00 [7, 8]	1.74E-8 [7, 8]
2.556E4	2.061E8	4.85E-5	1.00	3.19E-8
2.178E4	1.757E8	5.69E-5	1.00	5.82E-8
1.856E4	1.497E8	6.68E-5	1.00	1.06E-7
1.624E4	1.310E8	7.64E-5	1.00	1.74E-7
1.421E4	1.146E8	8.73E-5	1.00	2.84E-7
1.384E4	1.116E8	8.96E-5	1.00	3.13E-7
1.312E4	1.058E8	9.45E-5	1.00	2.09E-7
1.211E4	9.766E7	1.02E-4	1.00	2.83E-7
1.031E4	8.319E7	1.20E-4	1.00	5.13E-7
8.787E3	7.087E7	1.41E-4	1.00	9.29E-7
7.487E3	6.039E7	1.66E-4	1.00	1.66E-6
6.381E3	5.147E7	1.94E-4	1.00	2.95E-6
5.735E3	4.625E7	2.16E-4	1.00	4.28E-6
5.018E3	4.047E7	2.47E-4	1.00	4.86E-6
4.885E3	3.940E7	2.54E-4	1.00	2.52E-6
4.510E3	3.638E7	2.75E-4	1.00	3.37E-6
3.843E3	3.100E7	3.23E-4	1.00	6.02E-6
3.274E3	2.641E7	3.79E-4	1.00	1.07E-5
2.790E3	2.250E7	4.44E-4	1.00	1.88E-5
2.377E3	1.917E7	5.22E-4	1.00	3.3E-5
2.025E3	1.633E7	6.12E-4	1.00	5.73E-5
1.820E3	1.468E7	6.81E-4	1.00	8.22E-5
1.636E3	1.319E7	7.58E-4	1.00	1.1E-4
1.551E3	1.251E7	7.99E-4	1.00	1.3E-4
1.510E3	1.218E7	8.21E-4	1.00	8.77E-5
1.394E3	1.124E7	8.90E-4	1.00	1.11E-4
1.287E3	1.038E7	9.64E-4	1.00	1.41E-4
1.096E3	8.842E6	1.13E-3	1.00	2.27E-4
9.096E2	7.337E6	1.36E-3	1.00	3.4E-4
7.958E2	6.418E6	1.56E-3	1.00	5.3E-4
7.345E2	5.924E6	1.69E-3	1.00	6.98E-4
7.154E2	5.770E6	1.73E-3	1.00	2.36E-4
6.602E2	5.325E6	1.88E-3	1.00	2.96E-4
5.625E2	4.537E6	2.20E-3	1.00	4.69E-4
4.793E2	3.865E6	2.59E-3	1.00	7.24E-4
4.084E2	3.294E6	3.04E-3	1.00	1.1E-3
3.480E2	2.807E6	3.56E-3	1.00	1.6E-3
2.965E2	2.391E6	4.18E-3	1.00	2.25E-3
2.526E2	2.037E6	4.91E-3	1.00	2.96E-3
2.152E2	1.736E6	5.76E-3	0.99	3.69E-3
1.834E2	1.479E6	6.76E-3	0.99	4.38E-3
1.648E2	1.329E6	7.52E-3	0.99	5.06E-3

(continued)

[a] Tabulation of n and k as a function of photon energy (electron volts), wave number (inverse centimeters), and wavelength (microns). References for the data are given in brackets and apply to all data below the brackets until a new reference appears.

TABLE I *(Continued)*

Cesium Bromide

eV	cm^{-1}	μm	n	k
1.521E2	1.227E6	8.15E-3	0.99	6.3E-3
1.367E2	1.103E6	9.07E-3	0.98	1.1E-2
1.262E2	1.018E6	9.82E-3	0.98	1.88E-2
1.165E2	9.398E5	1.06E-2	0.98	2.93E-2
1.047E2	8.446E5	1.18E-2	0.99	3.71E-2
9.407E1	7.587E5	1.32E-2	1.00	3.41E-2
8.920E1	7.194E5	1.39E-2	1.01	2.76E-2
8.457E1	6.821E5	1.47E-2	1.03	1.92E-2
8.020E1	6.468E5	1.55E-2	1.00	1.26E-2
7.402E1	5.970E5	1.68E-2	1.00	7.87E-3
7.017E1	5.659E5	1.77E-2	0.99	5.33E-3
6.652E1	5.365E5	1.86E-2	0.98	3.47E-3
6.306E1	5.086E5	1.97E-2	0.98	3.5E-3
5.518E1	4.450E5	2.25E-2	0.96	4.27E-3
4.702E1	3.792E5	2.64E-2	0.93	7.53E-3
4.340E1	3.500E5	2.86E-2	0.91	1.12E-2
4.006E1	3.231E5	3.10E-2	0.89	1.76E-2
3.698E1	2.982E5	3.35E-2	0.86	2.8E-2
3.413E1	2.753E5	3.63E-2	0.83	4.48E-2
3.151E1	2.541E5	3.94E-2	0.80	7.13E-2
2.908E1	2.346E5	4.26E-2		1.04E-1
2.684E1	2.165E5	4.62E-2		1.53E-1
2.478E1	1.998E5	5.00E-2		2.26E-1
2.287E1	1.845E5	5.42E-2		3.09E-1
1.949E1	1.572E5	6.36E-2		5.39E-1
1.660E1	1.339E5	7.47E-2		7.23E-1
1.574E1	1.270E5	7.88E-2		7.14E-1
1.492E1	1.204E5	8.31E-2		5.54E-1
1.341E1	1.082E5	9.24E-2		4.66E-1
1.080E1	8.710E4	1.15E-1		4.42E-1
1.174E1	9.470E4	1.06E-1		4.42E-1
1.695E2	1.367E6	7.316E-3		5.850E-3 [6]
1.684E2	1.358E6	7.362E-3		5.930E-3
1.673E2	1.350E6	7.409E-3		5.940E-3
1.663E2	1.341E6	7.457E-3		6.020E-3
1.656E2	1.335E6	7.489E-3		6.080E-3
1.634E2	1.318E6	7.587E-3		6.240E-3
1.624E2	1.310E6	7.636E-3		6.500E-3
1.645E2	1.327E6	7.538E-3		6.120E-3
1.616E2	1.304E6	7.670E-3		6.750E-3
1.613E2	1.301E6	7.687E-3		6.760E-3
1.606E2	1.295E6	7.722E-3		6.510E-3
1.599E2	1.289E6	7.756E-3		6.360E-3
1.588E2	1.281E6	7.808E-3		6.520E-3
1.577E2	1.272E6	7.861E-3		6.640E-3

(continued)

TABLE I *(Continued)*

Cesium Bromide

eV	cm^{-1}	μm	n	k
1.567E2	1.264E6	7.914E-3		6.760E-3
1.556E2	1.255E6	7.969E-3		6.890E-3
1.545E2	1.246E6	8.024E-3		6.940E-3
1.534E2	1.238E6	8.080E-3		7.030E-3
1.524E2	1.229E6	8.136E-3		7.120E-3
1.513E2	1.220E6	8.194E-3		7.180E-3
1.502E2	1.212E6	8.252E-3		7.240E-3
1.492E2	1.203E6	8.311E-3		7.330E-3
1.481E2	1.195E6	8.371E-3		7.430E-3
1.474E2	1.189E6	8.412E-3		7.510E-3
1.467E2	1.183E6	8.452E-3		7.590E-3
1.460E2	1.177E6	8.493E-3		7.710E-3
1.453E2	1.172E6	8.535E-3		7.790E-3
1.442E2	1.163E6	8.598E-3		7.930E-3
1.431E2	1.154E6	8.662E-3		8.120E-3
1.421E2	1.146E6	8.727E-3		8.350E-3
1.410E2	1.137E6	8.793E-3		8.580E-3
1.403E2	1.131E6	8.838E-3		8.800E-3
1.392E2	1.123E6	8.905E-3		9.120E-3
1.382E2	1.114E6	8.974E-3		9.450E-3
1.371E2	1.106E6	9.043E-3		9.950E-3
1.360E2	1.097E6	9.114E-3		1.040E-2
1.350E2	1.089E6	9.185E-3		1.090E-2
1.339E2	1.080E6	9.258E-3		1.130E-2
1.328E2	1.071E6	9.333E-3		1.180E-2
1.318E2	1.063E6	9.408E-3		1.230E-2
1.307E2	1.054E6	9.484E-3		1.280E-2
1.297E2	1.046E6	9.562E-3		1.320E-2
1.286E2	1.037E6	9.641E-3		1.360E-2
1.275E2	1.029E6	9.721E-3		1.410E-2
1.265E2	1.020E6	9.803E-3		1.460E-2
1.254E2	1.012E6	9.886E-3		1.520E-2
1.251E2	1.009E6	9.914E-3		1.530E-2
1.240E2	1.000E6	9.999E-3		1.600E-2
1.229E2	9.911E5	1.009E-2		1.670E-2
1.219E2	9.833E5	1.017E-2		1.740E-2
1.208E2	9.747E5	1.026E-2		1.820E-2
1.198E2	9.662E5	1.035E-2		1.920E-2
1.186E2	9.569E5	1.045E-2		2.000E-2
1.176E2	9.488E5	1.054E-2		2.110E-2
1.166E2	9.407E5	1.063E-2		2.200E-2
1.156E2	9.320E5	1.073E-2		2.270E-2
1.145E2	9.234E5	1.083E-2		2.340E-2
1.134E2	9.149E5	1.093E-2		2.430E-2
1.123E2	9.058E5	1.104E-2		2.500E-2
1.113E2	8.977E5	1.114E-2		2.590E-2

(continued)

TABLE I *(Continued)*

Cesium Bromide

eV	cm^{-1}	μm	n	k
1.103E2	8.896E5	1.124E-2		2.678E-2
1.091E2	8.803E5	1.136E-2		2.750E-2
1.085E2	8.749E5	1.143E-2		2.780E-2
1.073E2	8.658E5	1.155E-2		2.780E-2
1.063E2	8.576E5	1.166E-2		2.770E-2
1.060E2	8.547E5	1.170E-2		2.770E-2
1.053E2	8.489E5	1.178E-2		2.820E-2
1.042E2	8.403E5	1.190E-2		2.880E-2
1.031E2	8.313E5	1.203E-2		2.960E-2
1.020E2	8.230E5	1.215E-2		3.010E-2
1.010E2	8.143E5	1.228E-2		2.980E-2
9.991E1	8.058E5	1.241E-2		2.920E-2
9.879E1	7.968E5	1.255E-2		2.810E-2
9.770E1	7.880E5	1.269E-2		2.670E-2
9.664E1	7.794E5	1.283E-2		2.490E-2
9.589E1	7.734E5	1.293E-2		2.460E-2
9.515E1	7.675E5	1.303E-2		2.400E-2
9.443E1	7.616E5	1.313E-2		2.290E-2
9.372E1	7.559E5	1.323E-2		2.250E-2
9.301E1	7.502E5	1.333E-2		2.390E-2
9.232E1	7.446E5	1.343E-2		2.420E-2
9.090E1	7.331E5	1.364E-2		2.210E-2
8.939E1	7.210E5	1.387E-2		1.860E-2
9.776E1	7.885E5	1.268E-2		1.282E-2
8.831E1	7.123E5	1.404E-2		1.630E-2
8.756E1	7.062E5	1.416E-2		1.520E-2
8.682E1	7.003E5	1.428E-2		1.340E-2
8.574E1	6.916E5	1.446E-2		1.120E-2
8.469E1	6.831E5	1.464E-2		1.340E-2
8.394E1	6.770E5	1.477E-2		1.050E-2
8.327E1	6.716E5	1.489E-2		8.950E-3
8.184E1	6.601E5	1.515E-2		1.000E-2
8.146E1	6.570E5	1.522E-2		8.950E-3
8.035E1	6.481E5	1.543E-2		7.270E-3
7.968E1	6.427E5	1.556E-2		8.290E-3
7.892E1	6.365E5	1.571E-2		6.020E-3
7.822E1	6.309E5	1.585E-2		4.740E-3
7.749E1	6.250E5	1.600E-2		4.190E-3
7.677E1	6.192E5	1.615E-2		4.390E-3
7.606E1	6.135E5	1.630E-2		5.050E-3
7.537E1	6.079E5	1.645E-2		5.870E-3
7.464E1	6.020E5	1.661E-2		6.950E-3
7.407E1	5.974E5	1.674E-2		7.240E-3
7.336E1	5.917E5	1.690E-2		7.400E-3
7.302E1	5.889E5	1.698E-2		6.880E-3
7.263E1	5.858E5	1.707E-2		6.040E-3

(continued)

TABLE I *(Continued)*

Cesium Bromide

eV	cm^{-1}	μm	n	k
7.229E1	5.831E5	1.715E-2		6.320E-3
7.154E1	5.770E5	1.733E-2		4.440E-3
7.117E1	5.741E5	1.742E-2		3.480E-3
7.081E1	5.711E5	1.751E-2		3.010E-3
7.013E1	5.656E5	1.768E-2		2.880E-3
1.134E1	9.149E4	1.093E-1		5.69E-1 [5]
1.124E1	9.066E4	1.103E-1		6.25E-1
1.115E1	8.993E4	1.112E-1		6.79E-1
1.105E1	8.913E4	1.122E-1		7.28E-1
1.095E1	8.834E4	1.132E-1		7.75E-1
1.086E1	8.757E4	1.142E-1		8.12E-1
1.076E1	8.681E4	1.152E-1		8.40E-1
1.066E1	8.598E4	1.163E-1		8.64E-1
1.056E1	8.518E4	1.174E-1		8.79E-1
1.047E1	8.446E4	1.184E-1		8.70E-1
1.038E1	8.368E4	1.195E-1		8.44E-1
1.027E1	8.285E4	1.207E-1		8.23E-1
1.008E1	8.130E4	1.230E-1		8.17E-1
9.887E0	7.974E4	1.254E-1		8.35E-1
9.793E0	7.899E4	1.266E-1		8.42E-1
9.694E0	7.819E4	1.279E-1		8.48E-1
9.596E0	7.740E4	1.292E-1		8.45E-1
9.501E0	7.663E4	1.305E-1		8.13E-1
9.400E0	7.582E4	1.319E-1		7.80E-1
9.357E0	7.547E4	1.325E-1		7.71E-1
9.260E0	7.468E4	1.339E-1		7.81E-1
9.211E0	7.429E4	1.346E-1		7.79E-1
9.110E0	7.348E4	1.361E-1		7.54E-1
9.017E0	7.273E4	1.375E-1		7.23E-1
8.920E0	7.194E4	1.390E-1		6.97E-1
8.825E0	7.117E4	1.405E-1		6.78E-1
8.725E0	7.037E4	1.421E-1		7.16E-1
8.676E0	6.998E4	1.429E-1		7.63E-1
8.628E0	6.959E4	1.437E-1		8.33E-1
8.580E0	6.920E4	1.445E-1		9.25E-1
8.533E0	6.882E4	1.453E-1		1.02E0
8.486E0	6.845E4	1.461E-1		1.10E0
8.389E0	6.766E4	1.478E-1		1.17E0
8.338E0	6.725E4	1.487E-1		1.16E0
8.244E0	6.649E4	1.504E-1		1.10E0
8.146E0	6.570E4	1.522E-1		1.04E0
7.953E0	6.414E4	1.559E-1		1.02E0
7.852E0	6.333E4	1.579E-1		1.12E0
7.759E0	6.258E4	1.598E-1		1.28E0
7.711E0	6.219E4	1.608E-1		1.34E0

(continued)

TABLE I *(Continued)*

Cesium Bromide

eV	cm^{-1}	μm	n	k
7.663E0	6.180E4	1.618E-1		1.35E0
7.565E0	6.101E4	1.639E-1		1.24E0
7.469E0	6.024E4	1.660E-1		1.12E0
7.420E0	5.984E4	1.671E-1		1.10E0
7.323E0	5.907E4	1.693E-1		1.17E0
7.225E0	5.828E4	1.716E-1		1.38E0
7.175E0	5.787E4	1.728E-1		1.52E0
7.130E0	5.750E4	1.739E-1		1.56E0
7.081E0	5.711E4	1.751E-1		1.39E0
7.033E0	5.672E4	1.763E-1		1.05E0
6.981E0	5.631E4	1.776E-1		7.90E-1
6.884E0	5.552E4	1.801E-1		6.64E-1
6.835E0	5.513E4	1.814E-1		6.56E-1
6.738E0	5.435E4	1.840E-1		7.78E-1
6.691E0	5.397E4	1.853E-1		9.14E-1
6.644E0	5.359E4	1.866E-1		1.04E0
6.595E0	5.319E4	1.880E-1		1.07E0
6.546E0	5.280E4	1.894E-1		8.00E-1
6.512E0	5.252E4	1.904E-1		5.86E-1
6.464E0	5.214E4	1.918E-1		4.81E-1
6.414E0	5.173E4	1.933E-1		4.52E-1
6.138E0	4.950E4	2.020E-1		7.86E-6 [4]
6.075E0	4.900E4	2.041E-1		4.29E-6
6.013E0	4.850E4	2.062E-1		3.21E-6
5.949E0	4.798E4	2.084E-1		2.78E-6
5.887E0	4.748E4	2.106E-1		2.49E-6
5.826E0	4.699E4	2.128E-1		2.27E-6
5.764E0	4.649E4	2.151E-1		2.08E-6
5.700E0	4.598E4	2.175E-1		1.96E-6
5.638E0	4.548E4	2.199E-1		1.83E-6
5.575E0	4.496E4	2.224E-1		1.72E-6
5.513E0	4.446E4	2.249E-1		1.62E-6
6.199E0	5.000E4	0.2	2.4393 [9]	
4.133E0	3.333E4	0.3	1.8048	
3.100E0	2.500E4	0.4	1.7357	
2.480E0	2.000E4	0.5	1.7095	
2.066E0	1.667E4	0.6	1.6964	
1.771E0	1.429E4	0.7	1.6888	
1.550E0	1.250E4	0.8	1.6840	
1.378E0	1.111E4	0.9	1.6808	
1.240E0	1.000E4	1.0	1.6785	
6.199E-1	5.000E3	2.0	1.6711	
4.133E-1	3.333E3	3.0	1.6695	
3.100E-1	2.500E3	4.0	1.6687	

(continued)

TABLE I *(Continued)*

Cesium Bromide

eV	cm^{-1}	μm	n	k
2.480E-1	2.000E3	5.0	1.6679	
2.066E-1	1.667E3	6.0	1.6671	
1.771E-1	1.429E3	7.0	1.6662	
1.550E-1	1.250E3	8.0	1.6653	
1.378E-1	1.111E3	9.0	1.6642	
1.240E-1	1.000E3	10	1.6630	
1.127E-1	9.091E2	11	1.6617	
1.033E-1	8.333E2	12	1.6602	
9.537E-2	7.692E2	13	1.6587	
8.856E-2	7.143E2	14	1.6570	
8.266E-2	6.667E2	15	1.6552	
7.749E-2	6.250E2	16	1.6532	
7.293E-2	5.882E2	17	1.6511	
6.888E-2	5.556E2	18	1.6489	
6.526E-2	5.263E2	19	1.6465	
6.199E-2	5.000E2	20	1.6440	
5.904E-2	4.762E2	21	1.6413	
5.636E-2	4.545E2	22	1.6385	
5.391E-2	4.348E2	23	1.6356	
5.166E-2	4.167E2	24	1.6324	
4.959E-2	4.000E2	25	1.6292	
4.769E-2	3.846E2	26	1.6258	
4.592E-2	3.704E2	27	1.6222	
4.428E-2	3.571E2	28	1.6184	
4.275E-2	3.448E2	29	1.6145	
4.133E-2	3.333E2	30	1.6104	
4.000E-2	3.226E2	31	1.6061	
3.875E-2	3.125E2	32	1.6017	
3.757E-2	3.030E2	33	1.5970	
3.647E-2	2.941E2	34	1.5922	
3.542E-2	2.857E2	35	1.5871	
3.444E-2	2.778E2	36	1.5819	
3.351E-2	2.703E2	37	1.5764	
3.263E-2	2.632E2	38	1.5708	
3.179E-2	2.564E2	39	1.5649	
3.100E-2	2.500E2	40	1.5587	
3.024E-2	2.439E2	41	1.5524	
2.952E-2	2.381E2	42	1.5457	
2.883E-2	2.326E2	43	1.5389	
2.818E-2	2.273E2	44	1.5317	
2.755E-2	2.222E2	45	1.5243	
2.695E-2	2.174E2	46	1.5166	
2.638E-2	2.128E2	47	1.5085	
2.583E-2	2.083E2	48	1.5002	
2.530E-2	2.041E2	49	1.4916	
2.480E-2	2.000E2	50	1.4826	

(continued)

TABLE I *(Continued)*

Cesium Bromide

eV	cm^{-1}	μm	n	k
2.431E-2	1.961E2	51	1.4732	
2.384E-2	1.923E2	52	1.4635	
2.339E-2	1.887E2	53	1.4534	
2.296E-2	1.852E2	54	1.4429	
2.254E-2	1.818E2	55	1.4320	
4.000E-2	3.226E2	31	1.606 [2]	1.10E-5 [2]
3.875E-2	3.125E2	32	1.601	1.62E-5
3.757E-2	3.030E2	33	1.597	2.37E-5
3.647E-2	2.941E2	34	1.592	3.38E-5
3.542E-2	2.857E2	35	1.587	4.65E-5
3.444E-2	2.778E2	36	1.582	
3.351E-2	2.703E2	37	1.577	
3.263E-2	2.632E2	38	1.571	
3.179E-2	2.564E2	39	1.565	
3.100E-2	2.500E2	40	1.558	
3.024E-2	2.439E2	41	1.552	
2.952E-2	2.381E2	42	1.546	3.23E-4
2.883E-2	2.326E2	43	1.539	4.07E-4
2.818E-2	2.273E2	44	1.532	5.00E-4
2.755E-2	2.222E2	45	1.524	6.10E-4
2.695E-2	2.174E2	46	1.516	7.40E-4
2.638E-2	2.128E2	47	1.508	9.00E-4
2.583E-2	2.083E2	48	1.500	1.05E-3
2.530E-2	2.041E2	49	1.491	1.23E-3
2.480E-2	2.000E2	50	1.482	1.45E-3
2.431E-2	1.961E2	51	1.472	1.70E-3
2.384E-2	1.923E2	52	1.462	1.97E-3
2.339E-2	1.887E2	53	1.451	2.29E-3
2.296E-2	1.852E2	54	1.440	2.65E-3
2.254E-2	1.818E2	55	1.429	3.10E-3
2.214E-2	1.786E2	56	1.417	3.55E-3
2.175E-2	1.754E2	57	1.405	4.10E-3
2.138E-2	1.724E2	58	1.390	4.85E-3
2.101E-2	1.695E2	59	1.380	5.60E-3
2.066E-2	1.667E2	60	1.365	6.70E-3
2.033E-2	1.639E2	61	1.350	8.13E-3
2.000E-2	1.613E2	62	1.330	9.73E-3
1.968E-2	1.587E2	63	1.315	1.16E-2
1.937E-2	1.563E2	64	1.300	1.37E-2
1.907E-2	1.538E2	65	1.285	1.66E-2
1.879E-2	1.515E2	66	1.270	2.04E-2
1.823E-2	1.471E2	68	1.240	3.13E-2
1.771E-2	1.429E2	70	1.200	5.07E-2
1.722E-2	1.389E2	72	1.160	8.93E-2
1.675E-2	1.351E2	74	1.110	1.15E-1

(continued)

TABLE I *(Continued)*

Cesium Bromide

eV	cm^{-1}	μm	n	k
1.631E-2	1.316E2	76	1.060	1.34E-1
1.590E-2	1.282E2	78	1.000	1.46E-1
1.550E-2	1.250E2	80	0.924	1.61E-1
1.512E-2	1.220E2	82	0.842	1.68E-1
1.476E-2	1.190E2	84	0.744	1.90E-1
1.442E-2	1.163E2	86	0.618	2.57E-1
1.409E-2	1.136E2	88	0.497	3.64E-1
1.378E-2	1.111E2	90	0.426	5.69E-1
1.348E-2	1.087E2	92	0.416	7.80E-1
1.319E-2	1.064E2	94	0.449	9.80E-1
1.292E-2	1.042E2	96	0.495	1.15E0
1.265E-2	1.020E2	98	0.551	1.29E0
1.240E-2	1.000E2	100	0.579	1.39E0
1.216E-2	9.804E1	102	0.541	1.49E0
1.192E-2	9.615E1	104	0.491	1.59E0
1.170E-2	9.434E1	106	0.449	1.68E0
1.148E-2	9.259E1	108	0.382	1.82E0
1.127E-2	9.091E1	110	0.321	1.93E0
1.107E-2	8.929E1	112	0.287	2.06E0
1.088E-2	8.772E1	114	0.284	2.16E0
1.069E-2	8.621E1	116	0.299	2.31E0
1.051E-2	8.475E1	118	0.323	2.51E0
1.033E-2	8.333E1	120	0.359	2.72E0
1.016E-2	8.197E1	122	0.417	3.00E0
9.999E-3	8.065E1	124	0.490	3.27E0
9.840E-3	7.937E1	126	0.622	3.70E0
9.686E-3	7.813E1	128	0.801	4.18E0
9.537E-3	7.692E1	130	1.13	4.70E0
9.393E-3	7.576E1	132	1.80	5.27E0
9.253E-3	7.463E1	134	3.00	6.00E0
9.117E-3	7.353E1	136	4.89	5.74E0
8.984E-3	7.246E1	138	6.24	4.01E0
8.856E-3	7.143E1	140	6.10	2.47E0
8.731E-3	7.042E1	142	5.72	1.59E0
8.610E-3	6.944E1	144	5.29	1.07E0
8.492E-3	6.849E1	146	5.07	7.39E-1
8.377E-3	6.757E1	148	4.81	5.20E-1
8.266E-3	6.667E1	150	4.59	4.14E-1
8.157E-3	6.579E1	152	4.38	3.31E-1
8.051E-3	6.494E1	154	4.23	2.90E-1
7.948E-3	6.410E1	156	4.11	2.58E-1
7.847E-3	6.329E1	158	3.99	2.38E-1
7.749E-3	6.250E1	160	3.88	2.21E-1
7.653E-3	6.173E1	162	3.78	2.06E-1
7.560E-3	6.098E1	164	3.69	1.95E-1
7.469E-3	6.024E1	166	3.61	1.83E-1

(continued)

TABLE I *(Continued)*

Cesium Bromide

eV	cm^{-1}	μm	n	k
7.380E-3	5.952E1	168	3.54	1.74E-1
7.293E-3	5.882E1	170	3.47	1.66E-1
7.208E-3	5.814E1	172	3.42	1.59E-1
7.126E-3	5.747E1	174	3.36	1.53E-1
7.045E-3	5.682E1	176	3.32	1.47E-1
6.965E-3	5.618E1	178	3.28	1.42E-1
6.888E-3	5.556E1	180	3.24	1.37E-1
6.702E-3	5.405E1	185	3.16	1.24E-1
6.526E-3	5.263E1	190	3.10	1.14E-1
6.358E-3	5.128E1	195	3.05	1.07E-1
6.199E-3	5.000E1	200	3.00	9.98E-2
6.048E-3	4.878E1	205	2.97	9.45E-2
5.904E-3	4.762E1	210	2.94	8.94E-2
5.767E-3	4.651E1	215	2.92	8.49E-2
5.636E-3	4.545E1	220	2.90	8.11E-2
5.510E-3	4.444E1	225	2.88	7.72E-2
5.391E-3	4.348E1	230	2.86	7.42E-2
5.276E-3	4.255E1	235	2.85	7.05E-2
5.166E-3	4.167E1	240	2.83	6.83E-2
5.061E-3	4.082E1	245	2.82	6.61E-2
4.959E-3	4.000E1	250	2.80	6.44E-2
4.862E-3	3.922E1	255	2.79	6.27E-2
4.769E-3	3.846E1	260	2.78	6.15E-2
4.679E-3	3.774E1	265	2.77	6.04E-2
4.592E-3	3.704E1	270	2.77	5.89E-2
4.509E-3	3.636E1	275	2.76	5.77E-2
5.367E-4	4.329E0	2.31E3	2.56 [1]	

Cesium Chloride (CsCl)

JOHN E. ELDRIDGE
Department of Physics
University of British Columbia
Vancouver, British Columbia, Canada

The room-temperature values of n and k tabulated here (Table I, Fig. 1) were obtained from the following works and references therein: In the far-infrared region, the reststrahlen values of n from 10 to 245 cm^{-1} and values of k from 100 to 245 cm^{-1} are from Shimizu *et al.* [1]; these are supplemented with values of k from 75 to 98 cm^{-1}, just below the peak, from Vergnat *et al.* [2]. In the transparent region from 250 cm^{-1} (40 μm) to 55,556 cm^{-1} (0.18 μm), values of n have been calculated by Li [3], who used the results of Wulff and co-workers [4–6] as the basis for the data generation; finally, in the low-energy x-ray region from 100 eV (12.4 nm) to 2000 eV (0.62 nm), *calculated* values of n and k are from Henke *et al.* [7].

Cesium chloride, which has cubic symmetry Pm3m (O_h^1), is very hygroscopic and highly soluble in water (1.62 g/cm^3). It is, therefore, an unsatisfactory material for making optical parts, despite its broad transparent range. Because of this, very few measurements of the refractive index or extinction coefficient have been made.

The far-infrared reststrahlen data were obtained by Shimizu *et al.* [1] by measuring the near-normal-incidence reflectivity of single crystals. These were polished with 0.3 μm particle size alumina dissolved in ethyl alcohol. After polishing, the samples were cleaned with methyl alcohol. The n and k data presented here were obtained after a Kramers–Kronig analysis. The measured reflectivity was higher than that obtained by Vergnat *et al.* [2], who used a pressed-powder sample, and for this reason was considered the more accurate. However, the high- and low-frequency extrapolations required for the Kramers–Kronig analysis were obviously in error, since the values of k just below the reststrahlen peak are negative. For this reason we have substituted the k values from Vergnat *et al.* [2], which were obtained from a Lorentz-oscillator fit to the reflectivity, in this small region. For the same reason one can see a discontinuity in Table I in going from the low-accuracy n data in the high-frequency wing of the restrahlen peak at 245 cm^{-1}, from

HANDBOOK OF OPTICAL CONSTANTS OF SOLIDS III

Copyright © 1998 by Academic Press.
All rights of reproduction in any form reserved
ISBN 0-12-544423-0/$25.00.

Shimuzu *et al.* [1], to the more accurate data of Li [3] at 250 cm^{-1}. The lowest-frequency n value, of 2.67 at 10 cm^{-1}, however, compares well with $\sqrt{\epsilon_s}$, equal to 2.64, where ϵ_s is the static dielectric constant with a value of 6.95 measured by Lowndes and Martin [8]. These same authors measured ω_T, the frequency of the zero-wave-vector transverse-optic (TO) phonon, to be 99.5 $\pm$ 0.5 cm^{-1}, in good agreement with the ~99.5 cm^{-1} frequency of the maximum value of the product nk (since $\epsilon_2 = 2nk$) using the values presented here.

The absorption in the wings of the reststrahlen band, away from the TO mode at ω_T, is due to two- and higher-phonon sum and difference processes by which the TO mode can relax when energy and momentum are conserved, producing broad structure in these regions. This absorption has been calculated by Shimizu *et al.* [9], but the agreement is not very satisfactory.

In the wide transparent region from 40 μm (250 cm^{-1}) to 0.18 μm (55,556 cm^{-1}), Li [3] has tabulated accurate values of n. He found only four sets of refractive-index data in the literature but considered the three works by Wulff and co-workers [4–6] to be sufficiently reliable to be used as the basis for the reference-data generation. These were corrected to 293 K, the chosen reference temperature. Using the infrared absorption peak at 100.5 μm (99.5 cm^{-1}, as mentioned earlier) plus the four measured absorption peaks in the vacuum ultraviolet [10–12] at 0.119 μm (10.42 eV), 0.137 μm (9.05 eV), 0.145 μm (8.55 eV), and 0.162 μm (7.65 eV), Li fitted the Wulff data to a dispersion equation of the Sellmeier type,

$$n^2 = 1.33013 + \frac{0.98369\lambda^2}{\lambda^2 - (0.119)^2} + \frac{0.00009\lambda^2}{\lambda^2 - (0.137)^2} + \frac{0.00018\lambda^2}{\lambda^2 - (0.145)^2} + \frac{0.30914\lambda^2}{\lambda^2 - (0.162)^2} + \frac{4.320\lambda^2}{\lambda^2 - (100.5)^2}, \quad (1)$$

where λ is in units of micrometers. In practical use the contributions of the third and fourth terms are small and can be neglected. Values from Eq. (1) are listed in Table I, although to greater accuracy than warranted by the experiment for the purpose of smoothness and internal comparison. Wulff's measurements of minimum deviation were performed on prismatic crystal specimens suspended in organic solutions. Uncertainties of 0.0001 were quoted.

No values of k above the far-infrared reststrahlen region have been found, nor values of n beyond Wulff's measurements [4–6]. Many studies of total absorption at energies above the transparent region have been performed, usually through thin films, which yield spectra of the absorption coefficient μ either in arbitrary or in absolute units. Those performed before 1977 have been summarized by Haelbich *et al.* [13]. In particular, Teegarden and Baldini [14] give μ in arbitrary units at 10 K between 7.4 and 12 eV, whereas

Saito *et al.* [15] continue this region up to 24 eV at room temperature. Cardona *et al.* [16] give μ in absolute units from 70 to 190 eV. They made the thin films, from 10 to 1000 nm thick, by *in situ* evaporation and measured the thickness to an accuracy of $\pm 20\%$ by an oscillating quartz. These spectra contain the same features as would the k spectra and can be used to obtain an approximate value of k, since the true absorption coefficient α is related to k through $\alpha = 4\pi k\nu$, where ν is in wave numbers (cm^{-1}), whereas μ was obtained without correcting for the surface reflectivity. Values of k obtained using this relationship are within 50% of those calculated from Henke *et al.* [7]. μ in arbitrary units is given by Iguchi *et al.* [17] from 200 to 280 eV. The absorption at the Cl K edge at 2.8 kV is given by Kiyono and Sugiura [18] and the Cl L edges at 5 kV by the same authors [19].

For several materials, good agreement has been found previously in the soft x-ray region between experimental values and those calculated using the atomic scattering factors of Henke *et al.* [7]. We have therefore tabulated the calculated values of n and k for CsCl between 100 eV and 2000 eV. In scattering theory, the complex refractive index is given as

$$n = 1 - \delta - ik, \tag{2}$$

where

$$\delta = \frac{r_0\lambda^2}{2\pi} N f_1 \tag{3}$$

$$k = \frac{r_0\lambda^2}{2\pi} N f_2. \tag{4}$$

Here $r_0 = e^2/mc^2$, the classical electron radius, equal to 2.814×10^{-13} cm; λ is the wavelength; N is the density of molecules per unit volume, equal in this case to 14.26×10^{21} CsCl molecules per cm^3; and f_1 and f_2 are the sum of the individual Cs and Cl atomic scattering factors, which are listed elsewhere [7].

REFERENCES

1. H. Shimizu, Y. Ohbayashi, K. Yamamoto, K. Abe, M. Midorikawa, and Y. Ishibashi, *J. Phys. Soc. Jpn.* **39**, 448 (1975).
2. P. P. Vergnat, J. Claudel, A. Hadni, P. Strimer, and F. Vermillard, *J. Phys. (Paris)* **30**, 723 (1969).
3. H. H. Li, *J. Phys. Chem. Ref. Data* **5**, 329 (1976).
4. P. Wulff and D. Schaller, *Z. Kristallogr.* **87**, 43 (1934).
5. P. Wulff and T. F. Anderson, *Z. Phys.* **94**, 28 (1935).
6. P. Wulff and A. Heigl, *Z. Kristallogr.* **77**, 84 (1931).
7. B. L. Henke, P. Lee, T. J. Tanaka, R. L. Shimabukuro, and B. K. Fujukawa, *in* "Low Energy X-Ray Diagnostics-1981," (D. T. Attwood and B. L. Henke, eds.), AIP Conf. Proc. No. 75, p. 340. American Institute of Physics, New York, 1981.
8. R. P. Lowndes and D. H. Martin, *Proc. R. Soc. London A.* **308**, 473 (1969).

9. H. Shimizu, Y. Ohbayashi, K. Yamamoto, K. Abe, and Y. Ishibashi, *J. Phys. Soc. Jpn.* **40**, 1684 (1976).
10. R. Hilsch and R. W. Pohl, *Z. Phys.* **59**, 812 (1930).
11. E. G. Schneider and H. M. O'Brian, *Phys. Rev.* **51**, 293 (1937).
12. G. N. Ramachandran, *Proc. Indian Acad. Sci. Sect. A* **25A**, 481 (1947).
13. R. P. Haelbich, M. Iwan, and E. E. Koch, "Physik Daten-Physics Data," p. 152. Fachinformation Zentrum, Karlsruhe, Germany, 1977.
14. K. Teegarden and G. Baldini, *Phys. Rev.* **155**, 896 (1967).
15. H. Saito, S. Saito, R. Onaka, and B. Ikeo, *J. Phys. Soc. Jpn.* **24**, 1095 (1968).
16. M. Cardona, R. Haensel, D. W. Lynch, and B. Sonntag, *Phys. Rev. B* **2**, 1117 (1970).
17. Y. Iguchi, T. Sagawa, S. Sato, M. Watanabe, H. Yamashita, A. Ejiri, M. Sasonuma, S. Nakai, M. Nakamura, A. Yamaguchi, Y. Nakai, and T. Oshio, *Solid State Commun.* **6**, 575 (1968).
18. S. Kiyono and C. Sugiura, *Sci. Rep. Tohoku Univ.* **30**, 9 (1965).
19. C. Sugiura and S. Kiyono, *Technol. Rep. Tohoku Univ.* **35**, 119 (1970).

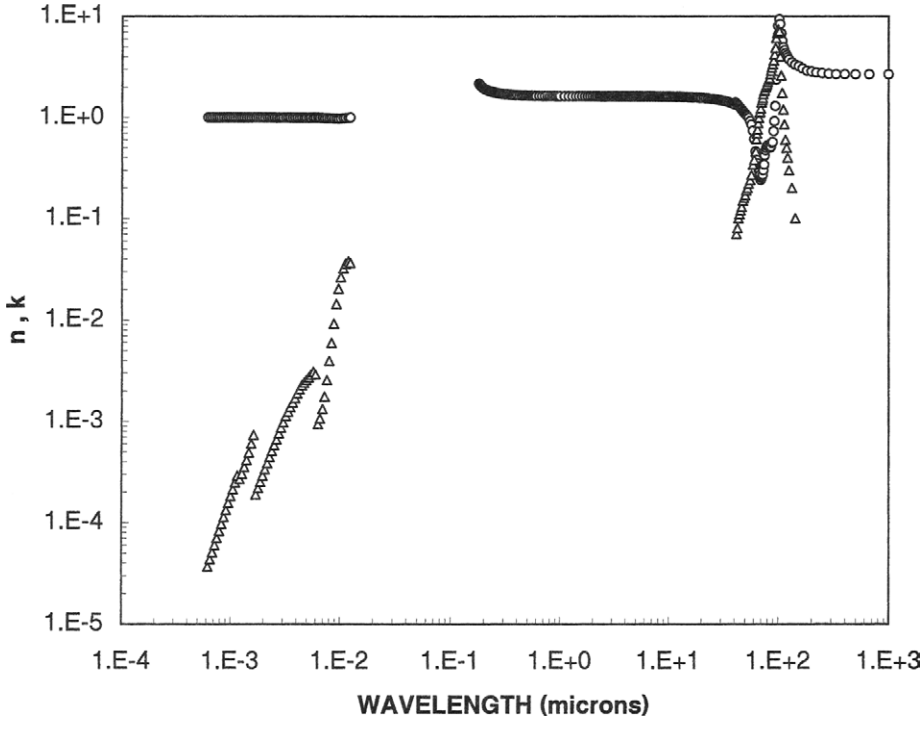

Fig. 1. Log–log plot of n (○) and k (△) versus wavelength in micrometers for cesium chloride.

TABLE I

Values of n and k for Cesium Chloride from Various References[a]

eV	cm^{-1}	nm	n	k
2000	16131000	0.620	0.99984 [7]	3.67 E-5 [7]
1905	15365000	0.651	0.99982	4.33 E-5
1815	14639000	0.683	0.99980	5.09 E-5
1730	13953000	0.717	0.99979	5.99 E-5
1648	13292000	0.752	0.99977	7.02 E-5
1570	12663000	0.790	0.99974	8.26 E-5
1496	12066000	0.829	0.99972	9.69 E-5
1426	11501000	0.869	0.99970	1.13 E-4
1358	10953000	0.913	0.99967	1.33 E-4
1294	10437000	0.958	0.99964	1.56 E-4
1233	9944700	1.006	0.99962	1.83 E-4
1175	9476900	1.055	0.99959	2.13 E-4
1119	9025300	1.108	0.99957	2.49 E-4
1067	8605900	1.162	0.99956	2.90 E-4
1016	8194500	1.220	0.99956	2.70 E-4
968	7807400	1.281	0.99949	3.03 E-4
923	7444400	1.343	0.99944	3.53 E-4
879	7089600	1.411	0.99941	4.14 E-4
838	6758900	1.480	0.99938	4.91 E-4
798	6436300	1.554	0.99939	6.01 E-4
760	6129800	1.631	0.99950	7.33 E-4
725	5847500	1.710	1.00036	1.90 E-4
690	5565200	1.797	0.99951	2.19 E-4
658	5307100	1.884	0.99932	2.52 E-4
627	5057100	1.977	0.99918	2.91 E-4
597	4815100	2.077	0.99905	3.35 E-4
569	4589300	2.179	0.99892	3.85 E-4
542	4371500	2.288	0.99879	4.43 E-4
516	4161800	2.403	0.99865	5.09 E-4
492	3968200	2.520	0.99850	5.80 E-4
469	3782700	2.644	0.99836	6.61 E-4
447	3605300	2.774	0.99820	7.59 E-4
426	3435900	2.910	0.99803	8.64 E-4
406	3274600	3.054	0.99787	9.76 E-4
386	3113300	3.212	0.99769	1.13 E-3
368	2968100	3.369	0.99750	1.24 E-3
351	2831000	3.532	0.99732	1.38 E-3
334	2693900	3.712	0.99710	1.53 E-3
318	2564800	3.899	0.99688	1.70 E-3
303	2443800	4.092	0.99666	1.88 E-3
289	2330900	4.290	0.99644	2.07 E-3
275	2218000	4.509	0.99622	2.27 E-3
262	2113200	4.732	0.99600	2.41 E-3

(continued)

[a] Tabulation of n and k as a function of photon energy (electron volts), wave number (inverse centimeters), and wavelength (nm or μm). References for the data are given in brackets and apply to all data below the brackets until a new reference appears.

TABLE I *(Continued)*

Cesium Chloride

eV	cm^{-1}	nm	n	k
250	2016400	4.959	0.99574	2.56 E-3
238	1919600	5.209	0.99545	2.72 E-3
227	1830900	5.462	0.99518	2.88 E-3
216	1742100	5.740	0.99501	3.07 E-3
206	1661500	6.019	0.99553	2.90 E-3
196	1580800	6.326	0.99391	9.37 E-4
187	1508200	6.630	0.99208	1.06 E-3
178	1435700	6.965	0.99023	1.32 E-3
170	1371100	7.293	0.98836	1.76 E-3
162	1306600	7.653	0.98609	2.55 E-3
154	1242100	8.051	0.98337	3.93 E-3
147	1185600	8.434	0.98065	5.96 E-3
140	1129200	8.856	0.97762	9.20 E-3
133	1072700	9.322	0.97520	1.44 E-2
127	1024300	9.763	0.97485	2.03 E-2
121	975920	10.25	0.97647	2.65 E-2
115	927530	10.78	0.98048	3.22 E-2
110	887200	11.27	0.98551	3.58 E-2
104	838810	11.92	0.99318	3.76 E-2
100	806550	12.40	0.99848	3.65 E-2
eV	cm^{-1}	μm	n	k
6.888	55556	0.180	2.16918 [3]	
6.738	54348	0.184	2.09684	
6.595	53191	0.188	2.04273	
6.458	52083	0.192	2.00270	
6.326	51020	0.196	1.96580	
6.199	50000	0.200	1.93711	
6.078	49020	0.204	1.91275	
5.961	48077	0.208	1.89176	
5.848	47170	0.212	1.87345	
5.740	46296	0.216	1.85730	
5.636	45455	0.220	1.84294	
5.535	44643	0.224	1.83008	
5.438	43860	0.228	1.81848	
5.344	43103	0.232	1.80797	
5.254	42373	0.236	1.79839	
5.166	41667	0.240	1.78963	
5.081	40984	0.244	1.78158	
4.999	40323	0.248	1.77416	
4.920	39683	0.252	1.76731	
4.843	39063	0.256	1.76095	
4.769	38462	0.260	1.75504	
4.696	37879	0.264	1.74953	
4.626	37313	0.268	1.74438	
4.558	36765	0.272	1.73957	
4.492	36232	0.276	1.73505	
4.428	35714	0.280	1.73080	
4.366	35211	0.284	1.72681	

TABLE I *(Continued)*

Cesium Chloride

eV	cm^{-1}	μm	n	k
4.305	34722	0.288	1.72305	
4.246	34247	0.292	1.71949	
4.189	33784	0.296	1.71613	
4.133	33333	0.300	1.71295	
4.000	32258	0.310	1.70570	
3.875	31250	0.320	1.69931	
3.757	30303	0.330	1.69364	
3.647	29412	0.340	1.68859	
3.542	28571	0.350	1.68407	
3.444	27778	0.360	1.68000	
3.351	27027	0.370	1.67631	
3.263	26316	0.38	1.67297	
3.179	25641	0.39	1.66993	
3.100	25000	0.40	1.66714	
2.952	23810	0.42	1.66225	
2.818	22727	0.44	1.65810	
2.695	21739	0.46	1.65453	
2.583	20833	0.48	1.65146	
2.480	20000	0.50	1.64878	
2.384	19231	0.52	1.64643	
2.296	18519	0.54	1.64435	
2.214	17857	0.56	1.64252	
2.138	17241	0.58	1.64088	
2.066	16667	0.60	1.63941	
1.937	15625	0.64	1.63690	
1.823	14706	0.68	1.63484	
1.722	13889	0.72	1.63313	
1.631	13158	0.76	1.63169	
1.550	12500	0.80	1.63047	
1.476	11905	0.84	1.62942	
1.409	11364	0.88	1.62852	
1.348	10870	0.92	1.62773	
1.292	10417	0.96	1.62704	
1.240	10000	1.00	1.62643	
1.127	9091	1.10	1.62518	
1.033	8333	1.20	1.62423	
0.954	7692	1.30	1.62348	
0.886	7143	1.40	1.62288	
0.827	6667	1.50	1.62239	
0.775	6250	1.60	1.62198	
0.729	5882	1.70	1.62162	
0.689	5556	1.80	1.62132	
0.653	5263	1.90	1.62105	
0.620	5000	2.00	1.62082	
0.590	4762	2.10	1.62060	
0.564	4545	2.20	1.62041	
0.539	4348	2.30	1.62023	

(continued)

TABLE I *(Continued)*

Cesium Chloride

eV	cm^{-1}	μm	n	k
0.517	4167	2.40	1.62006	
0.496	4000	2.50	1.61990	
0.4769	3846	2.6	1.61975	
0.4592	3704	2.7	1.61961	
0.4428	3571	2.8	1.61947	
0.4275	3448	2.9	1.61934	
0.4133	3333	3.0	1.61921	
0.4000	3226	3.1	1.61908	
0.3875	3125	3.2	1.61895	
0.3757	3030	3.3	1.61882	
0.3647	2941	3.4	1.61870	
0.3542	2857	3.5	1.61857	
0.3444	2778	3.6	1.61845	
0.3351	2703	3.7	1.61832	
0.3263	2632	3.8	1.61820	
0.3179	2564	3.9	1.61807	
0.3100	2500	4.0	1.61795	
0.3024	2439	4.1	1.61782	
0.2952	2381	4.2	1.61769	
0.2883	2326	4.3	1.61756	
0.2818	2273	4.4	1.61743	
0.2755	2222	4.5	1.61729	
0.2695	2174	4.6	1.61716	
0.2638	2128	4.7	1.61702	
0.2583	2083	4.8	1.61688	
0.2530	2041	4.9	1.61674	
0.2480	2000	5.0	1.61660	
0.2384	1923	5.2	1.61631	
0.2296	1852	5.4	1.61601	
0.2214	1786	5.6	1.61570	
0.2138	1724	5.8	1.61538	
0.2066	1667	6.0	1.61505	
0.2000	1613	6.2	1.61471	
0.1937	1563	6.4	1.61436	
0.1879	1515	6.6	1.61401	
0.1823	1471	6.8	1.61364	
0.1771	1429	7.0	1.61326	
0.1722	1389	7.2	1.61287	
0.1675	1351	7.4	1.61248	
0.1631	1316	7.6	1.61207	
0.1590	1282.0	7.8	1.61165	
0.1550	1250.0	8.0	1.61122	
0.1512	1219.5	8.2	1.61078	
0.1476	1190.5	8.4	1.61032	
0.1442	1162.8	8.6	1.60986	
0.1409	1136.4	8.8	1.60939	
0.1378	1111.1	9.0	1.60890	

TABLE I *(Continued)*

Cesium Chloride

eV	cm^{-1}	μm	n	k
0.1348	1087.0	9.2	1.60841	
0.1319	1063.8	9.4	1.60790	
0.1292	1041.7	9.6	1.60738	
0.1265	1020.4	9.8	1.60685	
0.1240	1000.0	10.0	1.60631	
0.1192	961.5	10.4	1.60520	
0.1148	925.9	10.8	1.60404	
0.1107	892.9	11.2	1.60283	
0.1069	862.1	11.6	1.60158	
0.1033	833.3	12.0	1.60028	
0.1000	806.5	12.4	1.59893	
0.0969	781.3	12.8	1.59754	
0.0939	757.6	13.2	1.59609	
0.0912	735.3	13.6	1.59460	
0.0886	714.3	14.0	1.59306	
0.0861	694.4	14.4	1.59147	
0.0838	675.7	14.8	1.58983	
0.0816	657.9	15.2	1.58814	
0.0795	641.0	15.6	1.58640	
0.0775	625.0	16.0	1.58460	
0.0756	609.8	16.4	1.58276	
0.0738	595.2	16.8	1.58086	
0.0721	581.4	17.2	1.57891	
0.0704	568.2	17.6	1.57690	
0.0689	555.6	18.0	1.57484	
0.0674	543.5	18.4	1.57272	
0.0659	531.9	18.8	1.57055	
0.0646	520.8	19.2	1.56832	
0.0633	510.2	19.6	1.56604	
0.0620	500.0	20.0	1.56369	
0.0590	476.2	21.0	1.55758	
0.05636	454.5	22.0	1.55108	
0.05391	434.8	23.0	1.54418	
0.05166	416.7	24.0	1.53688	
0.04959	400.0	25.0	1.52915	
0.04769	384.6	26.0	1.52098	
0.04592	370.4	27.0	1.51235	
0.04428	357.1	28.0	1.50323	
0.04275	344.8	29.0	1.49361	
0.04133	333.3	30.0	1.48346	
0.04000	322.6	31.0	1.47275	
0.03875	312.5	32.0	1.46146	
0.03757	303.0	33.0	1.44954	
0.03647	294.1	34.0	1.43698	
0.03542	285.7	35.0	1.42372	
0.03444	277.8	36.0	1.40973	
0.03351	270.3	37.0	1.39495	

(continued)

TABLE I *(Continued)*

Cesium Chloride

eV	cm^{-1}	μm	n	k
0.03263	263.2	38.0	1.37935	
0.03179	256.4	39.0	1.36285	
0.03100	250.0	40.0	1.34539	
0.03038	245.0	40.82	1.41 [1]	0.07 [1]
0.02976	240.0	41.67	1.38	0.80
0.02914	235.0	42.55	1.35	0.10
0.02852	230.0	43.48	1.31	0.11
0.02790	225.0	44.44	1.27	0.12
0.02728	220.0	45.45	1.24	0.13
0.02666	215.0	46.51	1.20	0.15
0.02604	210.0	47.62	1.16	0.16
0.02542	205.0	48.78	1.12	0.17
0.02480	200.0	50.00	1.09	0.19
0.02418	195.0	51.28	1.06	0.20
0.02356	190.0	52.63	1.03	0.22
0.02294	185.0	54.05	0.99	0.24
0.02232	180.0	55.56	0.92	0.27
0.02170	175.0	57.14	0.85	0.34
0.02108	170.0	58.82	0.74	0.38
0.02046	165.0	60.61	0.61	0.46
0.01984	160.0	62.50	0.46	0.61
0.01959	158.0	63.29	0.42	0.69
0.01934	156	64.10	0.38	0.76
0.01909	154	64.94	0.35	0.88
0.01885	152	65.79	0.33	0.99
0.01860	150	66.67	0.30	1.11
0.01835	148	67.57	0.29	1.14
0.01810	146	68.49	0.27	1.22
0.01785	144	69.44	0.24	1.41
0.01761	142	70.42	0.25	1.49
0.01736	140	71.43	0.26	1.56
0.01711	138	72.46	0.27	1.70
0.01686	136	73.53	0.30	1.83
0.01661	134	74.63	0.34	1.87
0.01637	132	75.76	0.42	1.98
0.01612	130	76.92	0.472	2.06
0.01587	128	78.13	0.499	2.14
0.01562	126	79.37	0.519	2.25
0.01537	124	80.65	0.529	2.37
0.01513	122	81.97	0.520	2.44
0.01488	120	83.33	0.505	2.67
0.01463	118	84.75	0.502	2.90
0.01438	116	86.21	0.512	3.13
0.01413	114	87.72	0.559	3.36
0.01389	112	89.29	0.57	3.66
0.01364	110	90.91	0.73	4.20
0.01339	108	92.59	0.92	4.89

TABLE I *(Continued)*

Cesium Chloride

eV	cm^{-1}	μm	n	k
0.01314	106	94.34	1.30	6.11
0.01289	104	96.15	2.37	6.87
0.01277	103	97.09	3.04	7.03
0.01265	102	98.04	4.20	7.40
0.01252	101	99.01	5.32	7.38
0.01240	100	100.0	8.02	7.10
0.01227	99	101.0	8.75	5.10
0.01215	98	102.0	9.35	4.00 [2]
0.01203	97	103.1	8.90	3.19
0.01190	96	104.2	8.40	2.60
0.01165	94	106.4	6.79	1.75
0.01141	92	108.7	5.72	1.20
0.01116	90	111.1	4.96	0.85
0.01091	88	113.6	4.62	0.60
0.01066	86	116.3	4.31	0.50
0.01041	84	119.0	4.12	0.40
0.01017	82	122.0	3.93	0.30
0.00992	80	125.0	3.74	0.20
0.00930	75	133.3	3.51	0.10
0.00868	70	142.9	3.32	
0.00806	65	153.8	3.21	
0.00744	60	166.7	3.05	
0.00682	55	181.8	2.90	
0.00620	50	200.0	2.86	
0.00558	45	222.2	2.79	
0.00496	40	250.0	2.75	
0.00434	35	285.7	2.71	
0.00372	30	333.3	2.69	
0.00310	25	400.0	2.68	
0.00248	20	500.0	2.67	
0.00186	15	666.7	2.67	
0.00124	10	1000.0	2.67	

Cesium Fluoride (CsF)

JOHN E. ELDRIDGE
Department of Physics
University of British Columbia
Vancouver, British Columbia, Canada

Cesium fluoride has cubic symmetry Fm3m (O_h^5), with the NaCl structure, which consists of two interpenetrating face-centered cubic lattices, one of Na and one of Cl. It is extremely hygroscopic and soluble in water (3.67 g/cm^3) and is, therefore, a very unsatisfactory material for making optical parts and consequently has been little studied. Only one measurement of refractive index has been found, and no measurements of extinction coefficient.

The room-temperature values of n and k tabulated here (Table I, Fig. 1) were *calculated* and are taken from two references [1, 2]. Li [1] used the one refractive-index datum point together with several other input data as the basis for the generation of his dispersion equation of the Sellmeier type, for n throughout the wide transparent region,

$$n^2 = 1.60 + \frac{0.56\lambda^2}{\lambda^2 - (0.121)^2} + \frac{5.92\lambda^2}{\lambda^2 - (78.74)^2}, \tag{1}$$

where λ is in units of micrometers. The one refractive-index measurement was made by Spangenberg [3] for a single spectral line, the sodium D line at a wavelength of 0.5893 μm, using the immersion method. He gave two values for n, one for α-CsF (equal to 1.478, and this is the one used by Li [1]), and one for β-CsF. [The α phase is the NaCl structure mentioned earlier, which is stable at elevated temperatures. The β phase is the CsCl structure, which consists of two interpenetrating cubic lattices of Cs and Cl, one displaced from the other by the vector 0.5, 0.5, 0.5. This phase of CsF is stable only at normal temperatures.] The other input data include the 78.74-μm wavelength (127 cm^{-1}) of the zero-wave-vector transverse optic (TO) phonon, which resonates in the far-infrared region and was measured by Lowndes and Martin [4], and the value of 8.08 for the static dielectric constant ϵ_s, and 2.16 for the high-frequency dielectric constant ϵ_∞, measured

HANDBOOK OF OPTICAL CONSTANTS OF SOLIDS III

Copyright © 1998 by Academic Press.
All rights of reproduction in any form reserved
ISBN 0-12-544423-0/$25.00.

by the same authors [4]. This value of ϵ_s predicts a low-frequency value of n, given by $\sqrt{\epsilon_s}$, of 2.84. In the second term of Eq. 1 the 0.121 μm is the average wavelength of the three peaks observed in the ultraviolet by Schneider and O'Brian [5]. Values from Eq. 1 are listed in Table I, although to far greater accuracy than warranted by the experiments, for the purpose of smoothness and internal comparison. Because of the paucity of input data, only the values of n between 0.3 μm and 2 μm are recommended; those outside this range are classified by Li as provisional.

Several studies of total absorption at energies above the transparent region have been performed, usually through thin films, which yield spectra of the absorption coefficient μ either in arbitrary or in absolute units. Those performed before 1977 have been summarized by Haelbich *et al.* [6]. In particular, Watanabe *et al.* [7] give μ in arbitrary units at room temperature between 8 and 32 eV. Cardona *et al.* [8] give μ in absolute units from 70 to 190 eV. They made the thin films, from 10 to 1000 nm thick, by *in situ* evaporation and measured the thickness to an accuracy of $\pm 20\%$ by an oscillating quartz. These spectra contain the same features as would the k spectra and can be used to obtain an approximate value of k, since the true absorption coefficient α is related to k through $\alpha = 4\pi k\nu$, where ν is in wave numbers (cm^{-1}), whereas μ was obtained without correcting for the surface reflectivity. Values of k obtained using this relationship are within 50% of those calculated from Henke *et al.* [2] (see below and Table I). μ in arbitrary units is given by Vinogradov *et al.* [9] from 680 to 720 eV. The absorption at the Cl L edges near 5 keV is given by Sugiura and Kiyono [10].

For several materials, good agreement has been found previously in the soft x-ray region between experimental values and those calculated using the atomic scattering factors of Henke *et al.* [2]. We have therefore tabulated the *calculated* values of n and k for CsF between 100 and 2000 eV. In scattering theory, the complex refractive index is given as

$$n = 1 - \delta - ik, \tag{2}$$

where

$$\delta = \frac{r_0\lambda^2}{2\pi} N f_1 \tag{3}$$

$$k = \frac{r_0\lambda^2}{2\pi} N f_2. \tag{4}$$

Here $r_0 = e^2/mc^2$, the classical electron radius, equal to 2.814×10^{-13} cm; λ is the wavelength; N is the density of molecules per unit volume, equal in this case to 16.31×10^{21} CsF molecules per cm^3; and f_1 and f_2 are the sum of the individual Cs and F atomic scattering factors, which are listed by Henke *et al.* [2].

REFERENCES

1. H. H. Li, *J. Phys. Chem. Ref. Data* **5**, 329 (1976).
2. B. L. Henke, P. Lee, T. J. Tanaka, R. L. Shimabukuro, and B. K. Fujukawa, *in* "Low Energy X-Ray Diagnostics-1981" (D. T. Attwood and B. L. Henke, eds.), AIP Conf. Proc. No. 75, p. 340. American Institute of Physics, New York, 1981.
3. K. Spangenberg, *Z. Kristallogr.* **57**, 494 (1923).
4. R. P. Lowndes and D. H. Martin, *Proc. R. Soc. London A.* **308**, 473 (1969).
5. E. G. Schneider and H. M. O'Brian, *Phys. Rev.* **51**, 293 (1937).
6. R. P. Haelbich, M. Iwan, and E. E. Koch, "Physik Daten-Physics Data," p. 152. Fachinformation Zentrum, Karlsruhe, Germany, 1977.
7. M. Watanabe, H. Nishida, and A. Ejiri, "Vacuum Ultraviolet Radiation Physics" (E. E. Koch, R. Haensel, and C. Kunz, eds.), p. 370. Pergamon-Vieweg, Braunschweig, Germany, 1974.
8. M. Cardona, R. Haensel, D. W. Lynch, and B. Sonntag, *Phys. Rev. B* **2**, 1117 (1970).
9. A. S. Vinogradov, T. M. Zimkina, and Yu. F. Mal'tsev, *Sov. Phys. Solid State* **11**, 2721 (1970).
10. C. Sugiura and S. Kiyono, *Technol. Rep. Tohoku Univ.* **35**, 119 (1970).

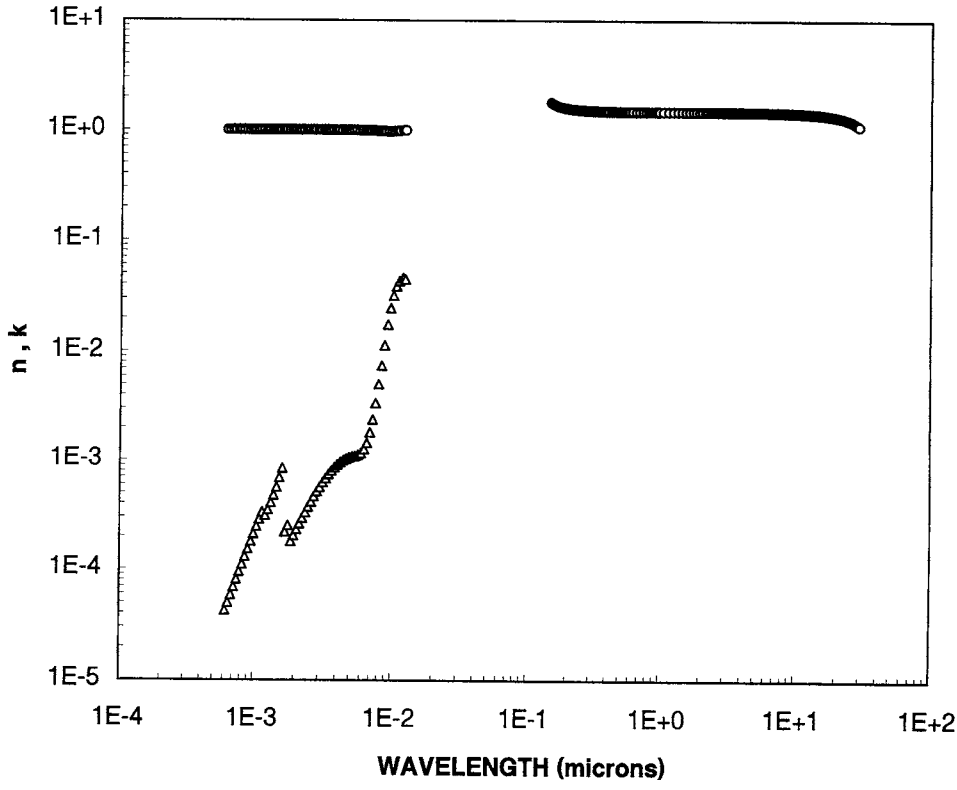

Fig. 1. Log–log plot of n (○) and k (△) versus wavelength in micrometers for cesium fluoride.

TABLE I

Values of n and k for Cesium Fluoride from Various References[a]

eV	cm^{-1}	nm	n	k
2000	16131000	0.620	0.99983 [2]	4.21 E-5 [2]
1905	15365000	0.651	0.99982	4.96 E-5
1815	14639000	0.683	0.99980	5.84 E-5
1730	13953000	0.717	0.99978	6.88 E-5
1648	13292000	0.752	0.99976	8.07 E-5
1570	12663000	0.790	0.99974	9.49 E-5
1496	12066000	0.829	0.99971	1.11 E-5
1426	11501000	0.869	0.99969	1.30 E-4
1358	10953000	0.913	0.99966	1.53 E-4
1294	10437000	0.958	0.99964	1.79 E-4
1233	9944700	1.006	0.99961	2.10 E-4
1175	9476900	1.055	0.99959	2.45 E-4
1119	9025300	1.108	0.99957	2.86 E-4
1067	8605900	1.162	0.99957	3.33 E-4
1016	8194500	1.220	0.99958	3.10 E-4
968	7807400	1.281	0.99951	3.49 E-4
923	7444400	1.343	0.99947	4.06 E-4
879	7089600	1.411	0.99944	4.76 E-4
838	6758900	1.480	0.99943	5.64 E-4
798	6436300	1.554	0.99946	6.90 E-4
760	6129800	1.631	0.99962	8.43 E-4
725	5847500	1.710	1.00064	2.19 E-4
690	5565200	1.797	0.99977	2.51 E-4
658	5307100	1.884	0.99952	1.79 E-4
627	5057100	1.977	0.99936	2.03 E-4
597	4815100	2.077	0.99923	2.30 E-4
569	4589300	2.179	0.99910	2.60 E-4
542	4371500	2.288	0.99897	2.93 E-4
516	4161800	2.403	0.99883	3.30 E-4
492	3968200	2.520	0.99869	3.69 E-4
469	3782700	2.644	0.99855	4.11 E-4
447	3605300	2.774	0.99839	4.63 E-4
426	3435900	2.910	0.99822	5.13 E-4
406	3274600	3.054	0.99805	5.63 E-4
386	3113300	3.212	0.99784	6.23 E-4
368	2968100	3.369	0.99763	6.80 E-4
351	2831000	3.532	0.99740	7.38 E-4
334	2693900	3.712	0.99714	7.98 E-4
318	2564800	3.899	0.99685	8.57 E-4
303	2443800	4.092	0.99655	9.09 E-4
289	2330900	4.290	0.99621	9.57 E-4
275	2218000	4.509	0.99580	1.00 E-3
262	2113200	4.732	0.99536	1.03 E-3

[a] Tabulation of n and k as a function of photon energy (electron volts), wave number (inverse centimeters), and wavelength (nm or μm). References for the data are given in brackets and apply to all data below the brackets until a new reference appears.

TABLE I *(Continued)*

Cesium Fluoride

eV	cm^{-1}	nm	*n*	*k*
250	2016400	4.959	0.99485	1.06 E-3
238	1919600	5.209	0.99423	1.08 E-3
227	1830900	5.462	0.99353	1.09 E-3
216	1742100	5.740	0.99265	1.12 E-3
206	1661500	6.019	0.99164	1.16 E-3
196	1580800	6.326	0.99037	1.26 E-3
187	1508200	6.630	0.98894	1.44 E-3
178	1435700	6.965	0.98710	1.80 E-3
170	1371100	7.293	0.98510	2.36 E-3
162	1306600	7.653	0.98261	3.34 E-3
154	1242100	8.051	0.97956	5.02 E-3
147	1185600	8.434	0.97648	7.45 E-3
140	1129200	8.856	0.97303	1.13 E-2
133	1072700	9.322	0.97028	1.74 E-2
127	1024300	9.763	0.96988	2.44 E-2
121	975920	10.25	0.97174	3.17 E-2
115	927530	10.78	0.97633	3.85 E-2
110	887200	11.27	0.98210	4.28 E-2
104	838810	11.92	0.99089	4.54 E-2
100	806550	12.40	0.99700	4.45 E-2
eV	cm^{-1}	μm	*n*	*k*
8.265	66667	0.150	1.78976 [1]	
8.051	64935	0.154	1.75027	
7.847	63291	0.158	1.71878	
7.653	61728	0.162	1.69310	
7.469	60241	0.166	1.67177	
7.293	58824	0.170	1.65378	
7.125	57471	0.174	1.63840	
6.965	56180	0.178	1.62513	
6.812	54945	0.182	1.61356	
6.666	53763	0.186	1.60338	
6.525	52632	0.190	1.59438	
6.391	51546	0.194	1.58635	
6.262	50505	0.198	1.57916	
6.138	49505	0.202	1.57269	
6.018	48544	0.206	1.56682	
5.904	47619	0.210	1.56150	
5.793	46729	0.214	1.55664	
5.687	45872	0.218	1.55219	
5.585	45045	0.222	1.54810	
5.486	44248	0.226	1.54434	
5.390	43478	0.230	1.54086	
5.298	42735	0.234	1.53764	
5.209	42017	0.238	1.53465	

(continued)

TABLE I *(Continued)*

Cesium Fluoride

eV	cm^{-1}	μm	n	k
5.123	41322	0.242	1.53187	
5.040	40650	0.246	1.52927	
4.959	40000	0.250	1.52684	
4.881	39370	0.254	1.52457	
4.805	38760	0.258	1.52245	
4.732	38168	0.262	1.52045	
4.661	37594	0.266	1.51857	
4.592	37037	0.270	1.51679	
4.525	36496	0.274	1.51512	
4.460	35971	0.278	1.51354	
4.396	35461	0.282	1.51205	
4.335	34965	0.286	1.51063	
4.275	34483	0.290	1.50929	
4.217	34014	0.294	1.50802	
4.160	33557	0.298	1.50681	
4.065	32787	0.305	1.50483	
3.936	31746	0.315	1.50228	
3.815	30769	0.325	1.50000	
3.701	29851	0.335	1.49797	
3.594	28986	0.345	1.49614	
3.492	28169	0.355	1.49449	
3.397	27397	0.365	1.49299	
3.306	26667	0.375	1.49162	
3.220	25974	0.385	1.49038	
3.139	25316	0.395	1.48924	
3.024	24390	0.41	1.48771	
2.883	23256	0.43	1.48593	
2.755	22222	0.45	1.48440	
2.638	21277	0.47	1.48308	
2.530	20408	0.49	1.48194	
2.431	19608	0.51	1.48093	
2.339	18868	0.53	1.48004	
2.254	18182	0.55	1.47925	
2.175	17544	0.57	1.47855	
2.101	16949	0.59	1.47792	
2.000	16129	0.62	1.47709	
1.878	15152	0.66	1.47616	
1.771	14286	0.70	1.47539	
1.675	13514	0.74	1.47474	
1.589	12821	0.78	1.47419	
1.512	12195	0.82	1.47371	
1.442	11628	0.86	1.47330	
1.378	11111	0.90	1.47293	
1.319	10638	0.94	1.47261	
1.265	10204	0.98	1.47233	
1.181	9524	1.05	1.47190	

TABLE I *(Continued)*

Cesium Fluoride

eV	cm^{-1}	μm	n	k
1.078	8696	1.15	1.47140	
0.9918	8000	1.25	1.47099	
0.9184	7407	1.35	1.47064	
0.8550	6897	1.45	1.47035	
0.7999	6452	1.55	1.47008	
0.7514	6061	1.65	1.46984	
0.7085	5714	1.75	1.46961	
0.6702	5405	1.85	1.46940	
0.6358	5128	1.95	1.46919	
0.6048	4878	2.05	1.46899	
0.5767	4651	2.15	1.46880	
0.5510	4444	2.25	1.46860	
0.5276	4255	2.35	1.46840	
0.5060	4082	2.45	1.46821	
0.4862	3922	2.55	1.46801	
0.4678	3774	2.65	1.46781	
0.4508	3636	2.75	1.46760	
0.4350	3509	2.85	1.46739	
0.4203	3390	2.95	1.46718	
0.4065	3279	3.05	1.46697	
0.3936	3175	3.15	1.46674	
0.3815	3077	3.25	1.46652	
0.3701	2985	3.35	1.46629	
0.3594	2899	3.45	1.46605	
0.3492	2817	3.55	1.46581	
0.3397	2740	3.65	1.46556	
0.3306	2667	3.75	1.46531	
0.3220	2597	3.85	1.46505	
0.3139	2532	3.95	1.46478	
0.3061	2469	4.05	1.46451	
0.2987	2410	4.15	1.46424	
0.2917	2353	4.25	1.46395	
0.2850	2299	4.35	1.46366	
0.2786	2247	4.45	1.46337	
0.2725	2198	4.55	1.46307	
0.2666	2151	4.65	1.46276	
0.2610	2105	4.75	1.46244	
0.2556	2062	4.85	1.46212	
0.2505	2020	4.95	1.46180	
0.2431	1961	5.10	1.46129	
0.2339	1887	5.30	1.46060	
0.2254	1818	5.50	1.45988	
0.2175	1754	5.70	1.45913	
0.2101	1695	5.90	1.45836	
0.2032	1639	6.10	1.45756	
0.1968	1587	6.3	1.45673	

(continued)

TABLE I *(Continued)*

Cesium Fluoride

eV	cm^{-1}	μm	n	k
0.1907	1538	6.5	1.45588	
0.1850	1493	6.7	1.45499	
0.1797	1449	6.9	1.45408	
0.1746	1408	7.1	1.45315	
0.1698	1370	7.3	1.45218	
0.1653	1333	7.5	1.45119	
0.1610	1299	7.7	1.45017	
0.1569	1266	7.9	1.44911	
0.1531	1235	8.1	1.44804	
0.1494	1205	8.3	1.44693	
0.1459	1176	8.5	1.44579	
0.1425	1149	8.7	1.44463	
0.1393	1124	8.9	1.44343	
0.1362	1099	9.1	1.44221	
0.1333	1075	9.3	1.44095	
0.1305	1053	9.5	1.43967	
0.1278	1031	9.7	1.43835	
0.1252	1010	9.9	1.43701	
0.1215	980.4	10.2	1.43494	
0.1170	943.4	10.6	1.43206	
0.1127	909.1	11.0	1.42907	
0.1088	877.2	11.4	1.42594	
0.1051	847.5	11.8	1.42269	
0.1016	819.7	12.2	1.41931	
0.09840	793.7	12.6	1.41580	
0.09537	769.2	13.0	1.41215	
0.09252	746.3	13.4	1.40836	
0.08984	724.6	13.8	1.40444	
0.08731	704.2	14.2	1.40037	
0.08492	684.9	14.6	1.39616	
0.08265	666.7	15.0	1.39180	
0.08051	649.4	15.4	1.38729	
0.07847	632.9	15.8	1.38263	
0.07653	617.3	16.2	1.37781	
0.07469	602.4	16.6	1.37283	
0.07293	588.2	17.0	1.36769	
0.07125	574.7	17.4	1.36239	
0.06965	561.8	17.8	1.35691	
0.06812	549.5	18.2	1.35126	
0.06666	537.6	18.6	1.34542	
0.06525	526.3	19.0	1.33941	
0.06391	515.5	19.4	1.33220	
0.06262	505.1	19.8	1.32681	
0.06048	487.8	20.5	1.31513	
0.05767	465.1	21.5	1.29734	
0.05510	444.4	22.5	1.27814	

TABLE I *(Continued)*

Cesium Fluoride

eV	cm^{-1}	μm	n	k
0.05276	425.5	23.5	1.25743	
0.05060	408.2	24.5	1.23508	
0.04862	392.2	25.5	1.21094	
0.04678	377.4	26.5	1.18483	
0.04508	363.6	27.5	1.15655	
0.04350	350.9	28.5	1.12584	
0.04203	339.0	29.5	1.09242	

Beta-Gallium Oxide (β-Ga_2O_3)

DAVID F. EDWARDS
Tracy, California

Gallium oxide, Ga_2O_3, has been shown [1] to exist in five phases; only one phase, called β-Ga_2O_3, is stable. At one time crystals of β-Ga_2O_3 doped with small amounts of Cr^{3+} ions were believed to have important applications as a MASER material [2, 3]. More recently the semiconductor industry has focused attention on the anodic oxide on GaAs made up of amorphous Ga_2O_3 and As_2O_3 [4]. β-Ga_2O_3 crystals also have interesting scientific properties. They can be either insulators or conductors, depending on the growth conditions. For either condition the crystals are layered material similar to GaSe and GaTe, also in this volume.

The crystal structure of the stable phase, β-Ga_2O_3, is monoclinic with lattice parameters of $a = 12.23$ Å, $b = 3.04$ Å, $c = 5.80$ Å, and $\alpha = 103.7°$ [5]. Geller [6] has determined that the most probable space group of β-Ga_2O_3 is C_{2h}^3 – C 2/m with four Ga_2O_3 molecules per unit cell.

The four metastable phases of Ga_2O_3 have been designated by Roy *et al.* [1] as α-, γ-, δ-, and ϵ-. The α-Ga_2O_3 has been identified to be hexagonal, analogous to α-Al_2O_3. The γ-Ga_2O_3 was originally reported by Böhm [7] to be analogous to γ-Al_2O_3 with the spinel structure (O_h^7 – Fd3m). Roy *et al.* were not able to confirm this relationship. The structure of δ-Ga_2O_3 is body centered cubic with space group T_h^7—Ia3. Large particles of this crystalline phase were found to be birefringent with an apparent index of refraction of about 1.8. The structure of ϵ-Ga_2O_3 could not be determined by Roy *et al.*, but they report its symmetry to be lower than hexagonal or tetragonal.

Single crystals of β-Ga_2O_3 have been grown by the Verneuil technique [8], the chemical transport method [9], and the vapor-phase reaction method [10]. The most extensive optical measurements on relatively large single crystals of β-Ga_2O_3 have been reported by Matsumoto *et al.* [10]. Their single-crystal platelets of β-Ga_2O_3 were grown by vapor-phase Ga/HCl/O_2/Ar reaction and were insulators [11]. The crystalline platelets consisted of layers parallel to the (100) direction. The major cleavage plane is (100), and the secondary one is (001). β-Ga_2O_3, being monoclinic and thus biaxial, has a triaxial ellipsoidal refractive-index surface. Based on their index mea-

HANDBOOK OF OPTICAL CONSTANTS OF SOLIDS III

Copyright © 1998 by Academic Press.
All rights of reproduction in any form reserved
ISBN 0-12-544423-0/$25.00.

surements Matsumoto *et al.* speculate as to the orientation of the principal dielectric axes (X , Y , Z) with respect to the crystallographic axes (*a*, *b*, *c*). They conclude that the *b*-axis is parallel to the Z-axis, and the *a*- and *c*-axes are approximately parallel to X and Y, respectively. They assume the electric polarization to be the easiest when the electric vector of the incident light is parallel to the (100) plane. They identify this condition as that for measuring the largest index. Their conclusions for the three indices are as follows: n_z for $\mathbf{E} \| \mathbf{b}$, n_y for $\mathbf{E} \| \mathbf{c}$, and n_x for $\mathbf{E} \perp \mathbf{b}$ and $\mathbf{c}$. The platelet orientations allowed only n_y and n_z measurements; no measurements of n_x were possible. The expected anisotropy between n_y and n_z appears to be small and could not be distinguished because of experimental error.

Matsumoto *et al.* [10] determined the refractive indices from the interference fringes produced by the multiple internal reflections in the thin platelets. These are called channel spectra. As noted by this writer [12], special care must be exercised in using channel spectra for the visible and near infrared because of the very large fringe order and the difficulty in its determination. For the channel-spectra technique the flatness, wedge, and platelet thickness can be the determining factors in the accuracy of the index values. For the Matsumoto *et al.* data the accuracy of the index values is limited by the approximately 5% accuracy of their platelet-thickness measurement.

The indices of refraction, n_y and n_z, as reported by Matsumoto *et al.*, are shown in Fig. 1. These data are listed in Table I as read from the figure. The solid curve in the figure is the least-squares fit of these combined data. The formulas given next, were used for the calculated average values listed in the table. For convenience, separate formulas are given for the ultraviolet and visible regions.

Ultraviolet (2775 Å $\leq \lambda \leq$ 3025 Å):

$$n_{uv} = -2.6396 + 9.7307/\lambda^4 + 4.0975 \times 10^7/\lambda^2,$$

where λ is in angstrom units.

Visible (3050 Å $\leq \lambda \leq$ 6900 Å):

$$n_{vis} = 1.3168 + 0.5179/\lambda^4 + 4.2114 \times 10^6/\lambda^2.$$

No vaccum UV determination of n and k could be found in the literature. The far-infrared reflection spectrum of sintered polycrystalline β-Ga_2O_3 showed weak reststrahlen bands, but no analysis could be done to obtain n and k [4]. A rough estimate of the dielectric constant, ϵ_0, can be made using the Clausius–Mossotti equation,

$$\frac{M}{\rho}\left(\frac{\epsilon - 1}{\epsilon + 2}\right) = \frac{4\pi}{3} N_0 \alpha,$$

where M is the molecular weight, ρ the density, N_0 Avogadro's constant, and α the total polarizability per molecule. For β-Ga_2O_3, $\alpha = 8.80$ Å^3 [13], yielding the approximate value for the dielectric constant $\epsilon_0 = 7.9$.

REFERENCES

1. R. Roy, V. G. Hill, and E. F. Osborn, *J. Am. Chem. Soc.* **74**, 719 (1952).
2. C. Kikuchi, University of Michigan, Willow Run Laboratory, private communication (1960).
3. M. Peter and A. L. Schawlow, *Bull. Am. Phys. Soc. Ser. II,* **5**, 158 (1960).
4. E. D. Palik, N. Ginsburg, R. T. Holm, and J. W. Gibson, *J. Vac. Sci. Technol.* **15**, 1488 (1978); and references therein.
5. J. A. Kohn, G. Katz, and J. D. Broder, *Am. Miner.* **42**, 398 (1975).
6. S. Geller, *J. Chem. Phys.* **33**, 676 (1960).
7. J. Böhm, *Angew. Chem.* **53**, 131 (1940).
8. A. B. Chase, *J. Am. Ceram. Soc.* **47**, 470 (1964).
9. H. Juskowiak and A. Pajaczkowska, *J. Mater. Sci.* **21**, 3430 (1986).
10. T. Matsumoto, M. Aoki, A. Kinoshita, and T. Aono, *Jpn. J. Appl. Phys.* **13**, 737 and 1578 (1974).
11. M. R. Lorenz, J. F. Woods, and R. J. Gambino, *J. Phys. Chem. Solids* **28**, 403 (1967).
12. D. F. Edwards, *in* "Handbook of Optical Constants of Solids," (E. D. Palik, ed.), p. 547. Academic Press, Orlando, Florida, 1985.
13. R. D. Shannon, M. A. Subraminian, T. H. Allik, H. Kimura, M. R. Kokta, M. H. Randels, and G. R. Rossman, *J. Appl. Phys.* **67**, 3798 (1990).

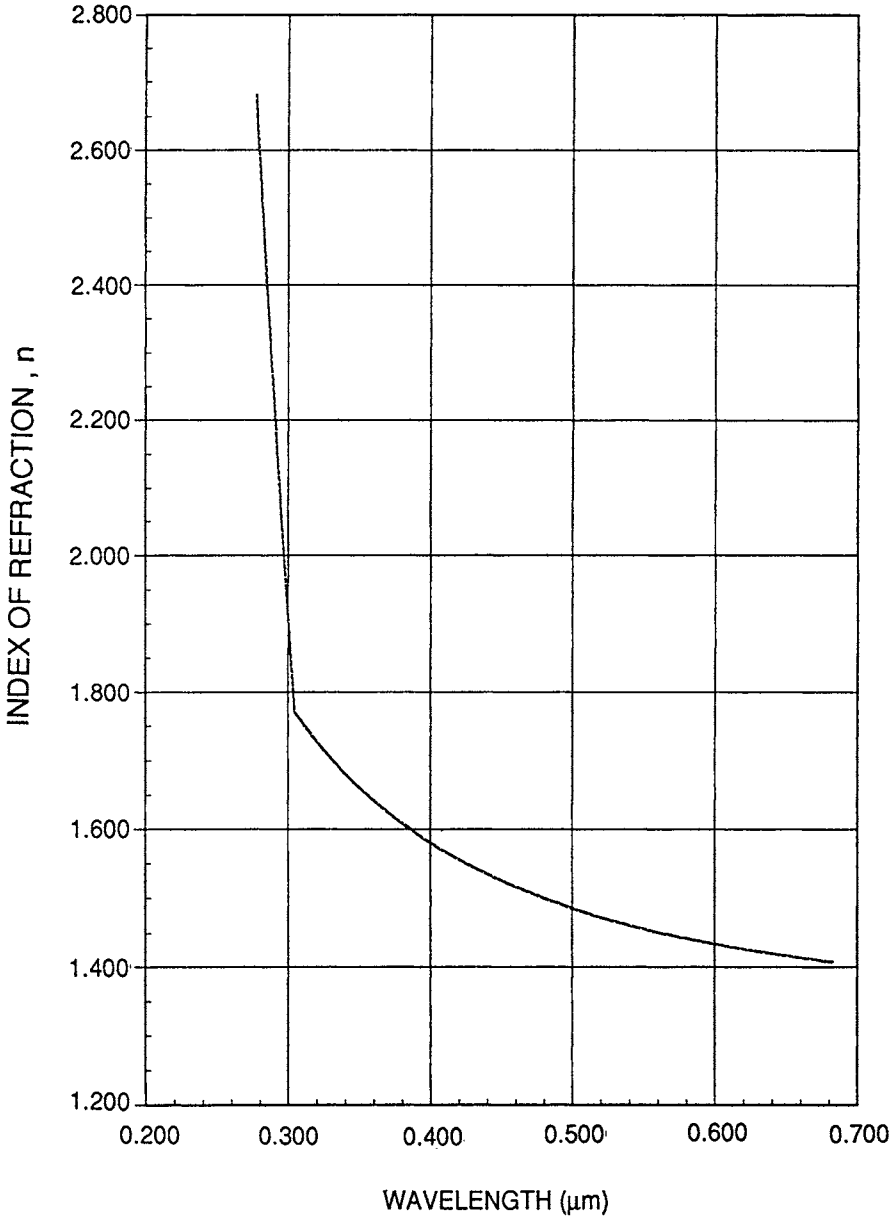

Fig. 1. Average values of index of refraction n versus wavelength in micrometers for β-Ga_2O_3.

TABLE I

Values of Index of Refraction n for β-Ga_2O_3 from Ref. [10]

eV	cm^{-1}	Å	n_{calc}	n_y	n_z
4.4757	36036	2775	2.6814		2.7750 [10]
4.4357	35714	2800	2.5868		
4.3965	35398	2825	2.4947		
4.3579	35088	2850	2.4050	2.5250 [10]	2.4000
4.3200	34783	2875	2.3177	2.0250	
4.2828	34483	2900	2.2326		
4.2462	34188	2925	2.1496		
4.2102	33898	2950	2.0688		
4.1748	33613	2975	1.9900		
4.1400	33333	3000	1.9132	1.8600	
4.1058	33058	3025	1.8382		1.9750
4.0721	32787	3050	1.7695		
4.0390	32520	3075	1.7622		
4.0065	32258	3100	1.7550		
3.9744	32000	3125	1.7480	1.6650	1.7100
3.9429	31746	3150	1.7412		
3.9118	31496	3175	1.7346		
3.8813	31250	3200	1.7281		
3.8512	31008	3225	1.7217		
3.8215	30769	3250	1.7155	1.7300	
3.7924	30534	3275	1.7094		
3.7636	30303	3300	1.7035		
3.7353	30075	3325	1.6977		
3.7075	29851	3350	1.6921		1.6250
3.6800	29630	3375	1.6865		
3.6529	29412	3400	1.6811	1.7700	
3.6263	29197	3425	1.6758		
3.6000	28986	3450	1.6706		
3.5741	28777	3475	1.6656		
3.5486	28571	3500	1.6606		
3.5234	28369	3525	1.6557		
3.4986	28169	3550	1.6510		
3.4741	27972	3575	1.6463	1.7250	
3.4500	27778	3600	1.6418		
3.4262	27586	3625	1.6373		
3.4027	27397	3650	1.6329		
3.3796	27211	3675	1.6286		
3.3568	27027	3700	1.6244		
3.3342	26846	3725	1.6203		
3.3120	26667	3750	1.6163		
3.2901	26490	3775	1.6123		
3.2684	26316	3800	1.6084		
3.2471	26144	3825	1.6046		
3.2260	25974	3850	1.6009		
3.2052	25806	3875	1.5973		
3.1846	25641	3900	1.5937		
3.1643	25478	3925	1.5902		

(continued)

TABLE I *(Continued)*

β-Ga_2O_3

eV	cm^{-1}	Å	n_{calc}	n_y	n_z
3.1443	25316	3950	1.5867		
3.1245	25157	3975	1.5833		
3.1050	25000	4000	1.5800		
3.0857	24845	4025	1.5768		
3.0667	24691	4050	1.5736		
3.0479	24540	4075	1.5704		
3.0293	24390	4100	1.5673		1.6000
3.0109	24242	4125	1.5643		
2.9928	24096	4150	1.5613		
2.9749	23952	4175	1.5584		
2.9571	23810	4200	1.5555	1.5300	
2.9396	23669	4225	1.5527		
2.9224	23529	4250	1.5500		
2.9053	23392	4275	1.5472		
2.8884	23256	4300	1.5446		
2.8717	23121	4325	1.5419		
2.8552	22989	4350	1.5394		
2.8389	22857	4375	1.5368		
2.8227	22727	4400	1.5343		
2.8068	22599	4425	1.5319		
2.7910	22472	4450	1.5295		
2.7754	22346	4475	1.5271		
2.7600	22222	4500	1.5248		
2.7448	22099	4525	1.5225		
2.7297	21978	4550	1.5202		
2.7148	21858	4575	1.5180		
2.7000	21739	4600	1.5158		
2.6854	21622	4625	1.5137		
2.6710	21505	4650	1.5116	1.4750	
2.6567	21390	4675	1.5095		
2.6426	21277	4700	1.5074		
2.6286	21164	4725	1.5054		
2.6147	21053	4750	1.5035		
2.6010	20942	4775	1.5015		1.5250
2.5875	20833	4800	1.4996		
2.5741	20725	4825	1.4977	1.5700	
2.5608	20619	4850	1.4958		
2.5477	20513	4875	1.4940		
2.5347	20408	4900	1.4922		
2.5218	20305	4925	1.4904		
2.5091	20202	4950	1.4887		
2.4965	20101	4975	1.4870		
2.4840	20000	5000	1.4853		
2.4716	19900	5025	1.4836		
2.4594	19802	5050	1.4819		
2.4473	19704	5075	1.4803		
2.4353	19608	5100	1.4787		

TABLE I *(Continued)*

β-Ga_2O_3

eV	cm^{-1}	Å	n_{calc}	n_y	n_z
2.4234	19512	5125	1.4771		
2.4117	19417	5150	1.4756		
2.4000	19324	5175	1.4741		
2.3885	19231	5200	1.4725		
2.3770	19139	5225	1.4711		
2.3657	19048	5250	1.4696		
2.3545	18957	5275	1.4681		1.5700
2.3434	18868	5300	1.4667		
2.3324	18779	5325	1.4653		
2.3215	18692	5350	1.4639		
2.3107	18605	5375	1.4626		
2.3000	18519	5400	1.4612		
2.2894	18433	5425	1.4599	1.4900	
2.2789	18349	5450	1.4586		
2.2685	18265	5475	1.4573		
2.2582	18182	5500	1.4560		
2.2480	18100	5525	1.4548		
2.2378	18018	5550	1.4535		1.4500
2.2278	17937	5575	1.4523		
2.2179	17857	5600	1.4511		
2.2080	17778	5625	1.4499	1.4750	
2.1982	17699	5650	1.4487		
2.1885	17621	5675	1.4476		
2.1789	17544	5700	1.4464		
2.1694	17467	5725	1.4453		
2.1600	17391	5750	1.4442		
2.1506	17316	5775	1.4431		
2.1414	17241	5800	1.4420		
2.1322	17167	5825	1.4409		
2.1231	17094	5850	1.4399		
2.1140	17021	5875	1.4388		
2.1051	16949	5900	1.4378		
2.0962	16878	5925	1.4368		
2.0874	16807	5950	1.4358		
2.0787	16736	5975	1.4348		
2.0700	16667	6000	1.4338		
2.0614	16598	6025	1.4328		
2.0529	16529	6050	1.4319	1.4250	
2.0444	16461	6075	1.4309		
2.0361	16393	6100	1.4300		
2.0278	16327	6125	1.4291		
2.0195	16260	6150	1.4281		
2.0113	16194	6175	1.4272		
2.0032	16129	6200	1.4264		
1.9952	16064	6225	1.4255		
1.9872	16000	6250	1.4246		
1.9793	15936	6275	1.4238		

(continued)

TABLE I *(Continued)*

β-Ga_2O_3

eV	cm^{-1}	Å	n_{calc}	n_y	n_z
1.9714	15873	6300	1.4229		
1.9636	15810	6325	1.4221	1.3050	
1.9559	15748	6350	1.4212		
1.9482	15686	6375	1.4204		1.4300
1.9406	15625	6400	1.4196		
1.9331	15564	6425	1.4188		
1.9256	15504	6450	1.4180		
1.9181	15444	6475	1.4172		
1.9108	15385	6500	1.4165		
1.9034	15326	6525	1.4157		
1.8962	15267	6550	1.4150		
1.8890	15209	6575	1.4142		
1.8818	15152	6600	1.4135		
1.8747	15094	6625	1.4128		1.3650
1.8677	15038	6650	1.4120		
1.8607	14981	6675	1.4113		
1.8537	14925	6700	1.4106	1.3600	
1.8468	14870	6725	1.4099		
1.8400	14815	6750	1.4092		
1.8332	14760	6775	1.4086		
1.8265	14706	6800	1.4079		
1.8198	14652	6825	1.4072		

Lead Fluoride (PbF_2)

MÁRCIA A. F. DESTRO and ALVARO J. DAMIÃO
Instituto de Estudos Avançados—CTA
São José dos Campos, SP, Brasil

Lead fluoride is a transparent insulator over a wide range of the optical spectrum from the ultraviolet to the middle infrared. It has a medium refractive index in the visible (1.77) and a low index in the infrared (1.63), when compared to other transparent materials. It is an electronic insulator with a large energy band gap, $E_g = 5.84$ eV at 298 K [1]. The melting point is 1095 K [2].

Lead fluoride can be found in two different crystalline structures, the cubic fluorite structure (space group Fm3m—O_h^5, β-phase) or in an orthorhombic structure (space group Pmnb—V_{2h}^{16}, α-phase). Sample preparation is very important when studying PbF_2, as even the grinding process can affect the crystalline structure and its transition temperature. For a strain-free material the initial temperature of α- to β-PbF_2 transformation is 328° C, and the heat necessary to this transformation is 1630 J/mol [3]. The transition temperature around 600 K, is controversial, probably because of kinetic effects [4]. Both phases exhibit relatively high ionic conductivity, and the cubic phase becomes a "superionic" conductor at high temperature, where its conductivity attains at $\geq$800 K what seems to be one of the highest values for any known solid ionic conductor [5, 6].

Three main approaches appear in the literature for studying optical properties of PbF_2:

Crystal [7–9]
Superionic conductor at high temperatures [1, 10, 11]
Thin films [12, 13]

With these approaches, part of the data was obtained using crystals and part using thin films, depending mainly on the technique used and on the specific application.

Eijkelenkamp [14] used the diffuse-reflection technique to ascertain the positions of optical transitions of finely grained powders for α- and β-PbF_2,

HANDBOOK OF OPTICAL CONSTANTS OF SOLIDS III

Copyright © 1998 by Academic Press.
All rights of reproduction in any form reserved
ISBN 0-12-544423-0/$25.00.

between 3 and 7 eV, and he showed some results of heat treatment on α-PbF_2 powder.

The index of refraction of β-PbF_2 at $\lambda = 589.3$ nm increases linearly with pressure, as well as the strain, with a slope of 7.76×10^{-4}/kbar up to 4.8 kbar, when a irreversible phase transformation to α-PbF_2 occurs [15].

When the crystal is heated at $T_c \cong 700$ K, well below the melting temperature 1095 K, an ionic disorder occurs. About 40% of the fluorine ions leave their normal sites in the anion sublattice, and the crystal becomes a superionic conductor. This disorder manifests itself in the Raman scattering and in the temperature dependence of the lattice constant [10]. Hayes *et al.* [11] carried out a Raman study of disorder in PbF_2 at high temperatures, and Kosacki and Zalibowski [10] made measurements of temperature and frequency dependence of the dielectric constant and dielectric loss function. In their article a figure shows the temperature dependence of dielectric constant ϵ' for PbF_2 crystals at the frequencies of 1 kHz, 10 kHz, 100 kHz, and 0.5 MHz.

Moss and Peacock [16] measured the transmission of cut and polished 6.7-mm-thick specimens using a Leiss double monochromator fitted with NaCl, KBr, or CsI prisms. A diagram in their article shows the results, corrected for surface losses.

Findley *et al.* [1] obtained, at near-normal incidence, the absolute reflectance spectra of polished β-PbF_2 crystal 3 mm thick from 4 to 10 eV, in the vicinity of the fundamental absorption edge, at temperatures between 298 and 800 K. There are three figures in their paper showing the reflectance and the imaginary part ϵ_2 of the dielectric response at three temperatures, 298, 613, and 773 K.

The optical data are presented in Table I, for crystals and thin films. They were obtained by a variety of optical techniques. Special attention must be paid to the fact that the sample preparation process can change the crystalline structure and its transition temperature; then the data presented on Table I are not exclusive for α- or β-phase, but most probably a mixture of the two phases.

Malitson and Dodge [8] and Jones [2] measured the refractive index of lead-fluoride prisms by means of the minimum-deviation method. Malitson and Dodge [8] used a synthetic prism at 20° C from 0.28 to 11.9 μm. Jones [2] used a prism with an angle of approximately 62.5° and faces approximately 3×3 cm^2, the room temperature varying between 17.5 and 19.5° C, and showed the transmission for a 1-cm-thick crystal, from UV to near IR regions (200 to 1000 nm) for a clear specimen, after 6-hour exposure to light from a Hg arc and to neutron bombardment.

Dodge [17], using the Malitson and Dodge data [8], obtained the parameters of a Sellmeier dispersion equation. The fitting range of λ is 0.3 to 11.9 μm:

$$n^2 = 1 + \sum_i \frac{A_i \lambda^2}{\lambda^2 - \lambda_i^2}. \quad (1)$$

$\lambda_1 = 0.00034911$ $\lambda_2 = 0.17144455$ $\lambda_3 = 0.28125513$ $\lambda_4 = 796.67469$
$A_1 = 0.66959342$ $A_2 = 1.3086319$ $A_3 = 0.01670641$ $A_4 = 2007.8865$

These calculated data are listed in Table I.

Aurora *et al.* [5] measured the temperature variation of the coefficients of linear thermal expansion and optical length for PbF_2 crystals, using an interferometer with a He–Ne laser over the temperature range of 300–1300 K. They calculated the temperature variation of the molecular polarizability, energy band gap, refractive-index variation with density, and the strain-polarizability parameter. This information was obtained to verify the applicability of this material for laser windows and other optical components.

Beaumont *et al.* [7] presented the optical constants of PbF_2 between its fundamental absorption edge at 5.7 eV and 130 eV, obtained from reflectivity and transmission measurements. For the reflectivity experiments (8–60 eV), they used polished single crystals with cubic structure and evaporated films that were thick enough to make negligible the interference effects due to reflections from the rear surface. The reflectivity was Kramers–Kronig analyzed. Transmission measurements (16–130 eV) were obtained from evaporated thin films on a zapon substrate. The reflectivity (above 8 eV) and transmission data presented were obtained with synchrotron radiation from NINA, the electron synchrotron at Daresbury laboratory. Beaumont *et al.* showed figures for the reflection spectrum at 77 K (2–30 eV), the real and imaginary parts of the dielectric constant (2–30 eV), the absorption coefficient at 77 K (2–30 eV) and at 290 K (30–130 eV) measured on evaporated thin films, and a single-crystal XPS spectrum (0–32 eV). It was found that absorption coefficients obtained from the K-K analysis of the reflectivity data agreed with those obtained from transmission measurements in the photon energy region where the spectra overlapped. Selected data of Beaumont *et al.* [7] are listed in Table I.

Axe *et al.* [9] made infrared reflectivity measurements between 10 and 150 μm at room temperature on samples of cubic (probably single) crystal 2 inches in length cut and polished using standard metallographic procedures. The reflectivity was measured by a point-by-point comparison with an aluminized surface in a Perkin-Elmer model 301 spectrometer. The measurements were corrected for the reflectivity of the aluminum but not for the off-axis configuration (the angle of incidence was 9°). The reflectivity was fitted with an oscillator model and by Kramers–Kronig analysis.The n and k values listed in Table I were obtained from our reading of a graph of Axe *et al.* [9]. The low-frequency dielectric constants were determined by measuring the capacitance of sample disks of material several millimeters thick in a conventional Schering bridge circuit.

Harrington *et al.* [18] used calorimetry to measure the absorption of low-loss thin dielectric films to be used as antireflection and enhanced-reflection coatings at the common IR laser wavelengths. The absorption coefficients were measured in film–bar combination (film with $\lambda/2$ at 5.3 μm thick, at one end of the KCl bar) using a conventional vacuum calorimeter and a CO_2 laser delivering approximately 5 W of cw power. The fractional power αL absorbed by the films was obtained directly from the temperature–time curves using a three-slope calculation. Using this fractional power, the extinction coefficient k, defined by $N = n - ik$, where N is the complex index of refraction, is computed for the film. Finally, the absorption coefficient α is obtained from $k = \alpha\lambda/4\pi$.

Pulker [12] reviewed the basic optical properties of the main dielectric materials in the form of single thin films to help the design of optical thin-film multilayers. Besides optical data, information is also presented on their preparation, structure, and mechanical properties. When the starting material was PbF_2, using a resistive evaporation (boat) at a temperature of 850° C, the information obtained was as follows: a β-PbF_2 film structure, with a packing density of 0.91, when substrate temperature (T_s) was 30° C, having a good transmittance ($\alpha < 10^{-3}$ cm^{-1}) from 0.25 to 17 μm and refractive index (T_s = 30° C) of 1.98 for 0.3 μm and 1.75 for 0.55 μm. The film was soft, and it had a compressive stress for thicknesses smaller than 0.1 μm, and a tensile stress for thicknesses larger than 0.1 μm.

Bennett *et al.* [19] critically investigated the technique for determining the optical constants of a metal by overcoating it with a dielectric film of known optical constants. They measured the thickness, transmittances, reflectances, and wavelengths of the interference maxima and minima for samples of lead fluoride on quartz and lead fluoride on aluminum. There were appreciable changes with time in the optical constants of lead fluoride films deposited on a substrate at room temperature. However, when the substrate was heated to 80° C, the change in k with time was from 0.008 to 0.007. Evaporation rates of about 100 Å/min were used with a pressure of about 10^{-5} torr and a coating distance of 46 cm. By mounting the substrates on a turntable rotating at 65 rpm, films 9000 Å in thickness could be formed. The thickness of the lead-fluoride film was determined by a multiple-beam interferometric technique using fringes of equal chromatic order. All absolute reflectance and transmittance measurements were made using the NOTS absolute reflectometer. The refractive index n was determined from the measured wavelengths of the interference maxima and minima in transmission produced by the lead fluoride film on fused quartz. Data from Bennett *et al.* [19] are listed in Table I.

Destro *et al.* [13, 20, 21] studied the optical and crystalline properties of PbF_2 thin films as a function of the substrate temperature during deposition, keeping other evaporation conditions as constant as possible. The films were evaporated on a BK7 Schott glass substrate. The residual

pressure of the chamber was 10^{-5} torr, and the crucible was made of tungsten and coated with aluminum oxide (Al_2O_3). A typical current of 100 A and a voltage of 5 V were employed. A Varian bell-jar evaporation system was used, and the substrate was heated by IR light. The thickness, $\approx$800 nm, was measured using a quartz monitor. The deposition rate varied from 0.5 to 0.75 nm/s. After the film deposition, the vacuum chamber was opened in the presence of N_2, when the sample reached room temperature. Some of the samples were obtained while the substrate holder was rotating, but the majority were obtained with the substrate holder standing still. The optical-characterization techniques used were channel spectra, guided modes, ellipsometry [13, 20], and envelope [21]. A Perkin-Elmer Lambda 9 spectrophotometer coupled to a computer was used for the spectral measurements. Using the same points of the maxima and minima, it was possible to obtain n, k, and the thickness of these thin films with the envelope technique. A Gaertner L117 ellipsometer was used to obtain the ellipsometric results; the data were reduced by the program described by McCrakin [22]. The coupling of the light to the film through a prism was used to obtain the guided-modes results. The He–Ne and argon laser beams were combined to obtain the measurements at five different wavelengths. A Rigaku's Bragg–Brentano x-ray diffractometer was used to verify the occurrence of changes in the crystalline phase and the existence of a preferential crystalline direction as a function of substrate temperature. A figure in Destro *et al.* [13] shows the change in the preferential orientation from β-PbF_2 $\langle 111 \rangle$ to β-PbF_2 $\langle 200 \rangle$, when the temperature increased. The parameters of Cauchy dispersion equations for thin films around 760 nm thick, measured with guided-modes technique [20], using λ in the range 400 to 650 nm, are

$$\begin{gathered} n = A + B\lambda^{-2} + C\lambda^{-4} \\ A = 1.726 \qquad B = 1.157 \times 10^4 \qquad C = 3.774 \times 10^8, \end{gathered} \tag{2}$$

and measured with the envelope technique [21], using λ in the range 400 to 800 nm, are

$$A = 1.7 \qquad B = 1.9 \times 10^4 \qquad C = -4.0 \times 10^8.$$

Data of Destro and co-workers [13, 21] are listed in Table I.

Baumeister *et al.* [23] measured the index of refraction of a single-layer PbF_2 film, $\lambda/4$ optically thick, at 16 μm. They obtained identical transmittance for thin films of the ZnSe and the PbF_2 on germanium substrates and from knowledge of the substrate index n_s, of the air n_0, and of the coating (ZnSe) n_2. They found the index of the second coating (PbF_2) using the relation $n_1 n_2 = n_0 n_s$. The thin films were made in a Balzer BA-500 chamber using a thermal heated platinum boat. The evaporation run started at pressures in the range of $1\text{–}3 \times 10^{-6}$ torr, the optimum evaporation rate was

found to be about 0.1 μm/min, and the chamber temperature was 100–150° C. Data of Baumeister *et al.* [23] are listed in Table I.

Bezuidenhout *et al.* [24] report on the optical, structural, and chemical properties of vacuum evaporated thin films of PbF_2 on Schott K-50 glass, quartz glass, silicon, germanium and sapphire discs as substrates, with the growth rate between 1 and 2 nm/s. The pressure during evaporation was below 2×10^{-6} torr, and the substrate temperature was 150° C. The layer thickness was obtained by measurements of fringe dislocation over a step (interferometric method), and the optical properties were calculated on the turning points of reflectance and transmittance spectra, which were measured with a Beckman UV 5270 from 0.7 to 2.0 μm and a Perkin-Elmer 983 from 2.0 to 12 μm. Data of Bezuidenhout *et al.* [24] are listed in Table I.

Sankur [25] compared thin-film optical data, refractive index, and extinction coefficient, obtained from reflectance and transmittance spectral analysis. The films were prepared by e-beam, pulsed, and cw laser deposition. For cw evaporation Sankur found that the refractive index, for 632.8 nm, is independent of the evaporation rate between 0.1 and 100 Å/s. The source material was a mixture of α- and β-PbF_2 in pellet form. The films were grown on glass and low-conductivity Si substrate at room temperature at pressures of 2×10^{-7} torr. Data of Sankur [25] are listed in Table I.

Many of the n and k data in Table I are plotted in Fig. 1.

REFERENCES

1. P. R. Findley, Z. Wu, and W. C. Walker, *Phys. Rev. B* **28**, 4761 (1983).
2. D. A. Jones, *Proc. Phys. Soc. (London) B* **68**, 165 (1955).
3. J. P. Auffredic, R. Couple and D. Louër, *J. Mater. Sci.* **20**, 2119 (1985).
4. O. K. Nikol'skaya and L. N. Dem'yantes, *Inorg. Mater.* **30**, 1097 (1994).
5. T. S. Aurora, S. M. Day, and D. O. Pederson, *J. Appl. Phys.* **76**, 2122 (1994).
6. S. Palchoudhuri and G. K. Bichile, *Solid State Commun.* **69**, 271 (1989).
7. J. H. Beaumont, A. J. Bourdillon, and J. Bordas, *J. Phys. C* **10**, 761 (1977).
8. I. H. Malitson and M. J. Dodge, *J. Opt. Soc. Am.* **59**, 500A (1969).
9. J. D. Axe, J. W. Gaglianello, and J. E. Scardefield, *Phys. Rev.* **139**, A1211 (1965).
10. I. Kosacki and K. Zalibowski, *Phys. Status Solidi A* **108**, 765 (1988).
11. W. Hayes, A. J. Rushworth, J. F. Ryan, R. J. Elliot, and W. G. Kleppmann, *J. Phys. C* **10**, L111 (1977).
12. H. K. Pulker, *Appl. Opt.* **18**, 1969 (1979).
13. M. A. F. Destro, R. A. Stempniak, and A. J. Damião, *Appl. Opt.* **32**, 7106 (1993).
14. A. J. H. Eijkelenkamp, *Phys. Status Solidi B* **76**, 153 (1976).
15. E. D. D. Schmidt and K. Vedam, *J. Phys. Chem. Solids* **27**, 1563 (1966).
16. T. S. Moss and A. G. Peacock, *Infrared Phys.* **1**, 104 (1961).
17. M. J. Dodge, *in* "CRC Handbook of Laser Science and Technology" (M. J. Weber, ed.), Vol 4, Optical Materials, Part 2: Properties, CRC Press, Boca Raton, Florida, 1986.
18. J. A. Harrington, M. Braunstein, and E Rudisill, *Appl. Opt.* **16**, 2843 (1977).
19. J. M. Bennett, E. J. Ashley, and H. E. Bennett, *Appl. Opt.* **4**, 961 (1965).
20. M. A. F. Destro, Propriedades Ópticas e Cristalinas de Filmes Finos de Fluoreto de Chumbo. M. S. Thesis, Instituto Tecnológico de Aeronáutica—CTA, São José dos Campos—SP, Brazil, 1991 (in Portuguese).

21. M. A. F. Destro and A. J. Damião, Techical Report, Instituto de Estudos Avaçados—CTA, IEAv/RP-002/95, February 1995 (in Portuguese).
22. F. L. McCrakin, "A FORTRAN program for analysis of ellipsometer measurements," U.S. Natl. Bur. Stand. Tech. Note 479, Washington, D.C., 1969.
23. P. Baumeister, J. Pritts, D. Lees, and D. F. Edwards, *Appl. Opt.* **18**, 3127 (1979).
24. D. F. Bezuidenhout, B. Theron, and R. Pretorius, *S. Afr. J. Phys.* **10**, 23 (1987).
25. H. Sankur, *Appl. Opt.* **25**, 1962 (1986).

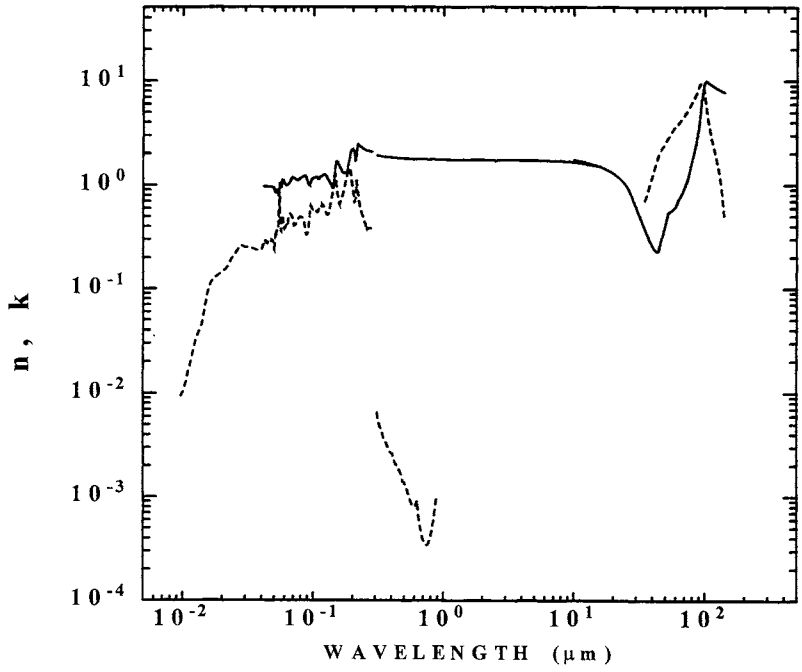

Fig. 1. Log–log plot of n (———) and k (-------) versus wavelength in micrometers for lead fluoride.

TABLE I

Values of *n* and *k* for Lead Fluoride Obtained from Various References[a, b, c]

eV	cm^{-1}	μm	n	k
130	1048512	0.0095373		9.11E-3 [7]
128	1032381	0.0096863		9.40E-3
126	1016250	0.0098401		9.79E-3
124	1000119	0.0099988		1.01E-2
122	983988	0.010163		1.06E-2
120	967857	0.010332		1.15E-2
118	951726	0.010507		1.24E-2
116	935595	0.010688		1.32E-2
114	919464	0.010876		1.47E-2
112	903333	0.011070		1.63E-2
110	887202	0.011271		1.79E-2
108	871071	0.011480		1.96E-2
106	854940	0.011697		2.19E-2
104	838809	0.011922		2.42E-2
102	822679	0.012155		2.71E-2
100	806548	0.012398		3.01E-2
98	790417	0.012652		3.32E-2
96	774286	0.012915		3.54E-2
94	758155	0.013190		3.78E-2
92	742024	0.013477		4.04E-2
90	725893	0.013776		4.27E-2
88	709762	0.014089		4.76E-2
86	693631	0.014417		5.74E-2
84	677500	0.014760		6.58E-2
82	661369	0.015120		7.82E-2
80	645238	0.015498		9.00E-2
78	629107	0.015895		1.06E-1
76	612976	0.016314		1.14E-1
74	596845	0.016755		1.19E-1
72	580714	0.017220		1.25E-1
70	564583	0.017712		1.30E-1
68	548452	0.018233		1.32E-1
66	532321	0.018786		1.37E-1
64	516190	0.019373		1.40E-1
62	500059	0.019998		1.46E-1
60	483929	0.020664		1.52E-1
58	467798	0.021377		1.54E-1
56	451767	0.022140		1.67E-1 [7]
54	435536	0.022960		1.84E-1
52	419405	0.023843		2.01E-1
50	403274	0.024797		2.15E-1
48	387143	0.025830		2.25E-1
46	371012	0.026953		2.57E-1

[a] Measured on thin films.
[b] Not at room temperature.
[c] References are indicated in brackets.

TABLE I *(Continued)*

PbF_2

eV	cm^{-1}	μm	n	k
44	354881	0.028178		2.61E-1
42	338750	0.029520		2.47E-1
40	322619	0.030996		2.54E-1
38	306488	0.032628		2.47E-1
36	290357	0.034440		2.45E-1
34	274226	0.036466		2.32E-1
32	258095	0.038745		2.37E-1
30	241964	0.041328		2.30E-1
30.0	241964	0.041328	0.963 [7][b]	2.95E-1 [7][b]
29.0	233899	0.042753	0.963	2.95E-1
28	225833	0.044280		2.47E-1 [7]
28.0	225833	0.044280	0.963	2.95E-1 [7][b]
27.0	217768	0.045920	0.958	2.97E-1
26.5	213735	0.046787	0.958	2.97E-1
26	209702	0.047687		2.71E-1 [7]
26.0	209702	0.047687	0.958	2.97E-1 [7][b]
25.5	205670	0.048622	0.953	2.98E-1
25.0	201637	0.049594	0.942	2.81E-1
24.8	200024	0.049994	0.926	2.42E-1
24.6	198411	0.050400	0.873	2.51E-1
24.4	196798	0.050814	0.823	2.97E-1
24.2	195184	0.051234	0.848	3.59E-1
24	193571	0.051660		2.94E-1 [7]
24.0	193571	0.051660	0.872	3.61E-1 [7][b]
23.8	191958	0.052095	0.845	3.66E-1
23.6	190345	0.052536	0.871	4.24E-1
23.4	188732	0.052985	0.888	3.99E-1
23.2	187119	0.053442	0.851	3.93E-1
23.0	185506	0.053907	0.746	4.55E-1
22.8	183893	0.054379	0.780	6.40E-1
22.6	182280	0.054861	0.956	7.84E-1
22.4	180667	0.055351	1.17	4.25E-1
22.2	179054	0.055849	1.05 [7][b]	3.45E-1 [7][b]
22.0	177440	0.056357	0.963	3.58E-1
21.8	175827	0.056874	0.880	4.54E-1
21.6	174214	0.057401	1.03	5.97E-1
21.4	172601	0.057937	1.16	5.10E-1
21.2	170988	0.058484	1.12	4.23E-1
21.0	169375	0.059041	1.07	3.87E-1
20.8	167762	0.059608	1.05	3.79E-1
20.6	166149	0.060187	1.02	3.81E-1
20.4	164536	0.060777	0.993	3.97E-1
20.2	162923	0.061379	0.990	4.13E-1
20.0	161309	0.061993	1.00	4.39E-1
19.8	159696	0.062619	1.00	4.14E-1
19.6	158083	0.063258	0.988	4.09E-1

(continued)

TABLE I *(Continued)*

PbF_2

eV	cm^{-1}	μm	n	k
19.4	156470	0.063910	1.01	4.84E-1
19.2	154857	0.064576	1.02	5.04E-1
19.0	153244	0.065255	1.03	5.29E-1
18.5	149211	0.067019	1.12	5.33E-1
18.0	145179	0.068881	1.18	4.95E-1
17.5	141146	0.070849	1.16	4.07E-1
17.0	137113	0.072932	1.11	4.11E-1
16.5	133080	0.075143	1.10	4.53E-1
16.0	129048	0.077491	1.12	4.89E-1
15.5	125015	0.079990	1.16	4.99E-1
15.0	120982	0.082657	1.19	4.84E-1
14.8	119369	0.083774	1.20	4.65E-1
14.6	117756	0.084921	1.23	4.18E-1
14.4	116143	0.086101	1.22	3.67E-1
14.2	114530	0.087313	1.20	3.33E-1
14.0	112917	0.088561	1.14	3.23E-1
13.8	111304	0.089844	1.09	3.30E-1
13.6	109690	0.091166	1.02	3.81E-1
13.4	108077	0.092526	0.969	4.58E-1
13.2	106464	0.093928	0.982	5.34E-1
13.0	104851	0.095373	1.05	6.28E-1
12.8	103238	0.096863	1.14	6.12E-1
12.6	101625	0.098401	1.15	5.69E-1
12.4	100012	0.099988	1.17	5.52E-1
12.2	98399	0.10163	1.17 [7][b]	5.55E-1 [7][b]
12.0	96786	0.10332	1.18	5.62E-1
11.8	95173	0.10507	1.21	5.63E-1
11.6	93559	0.10688	1.19	5.35E-1
11.4	91946	0.10876	1.13	5.37E-1
11.2	90333	0.11070	1.12	6.21E-1
11.0	88720	0.11271	1.23	6.48E-1
10.8	87107	0.11480	1.20	5.90E-1
10.6	85494	0.11697	1.22	6.53E-1
10.4	83881	0.11922	1.26	6.26E-1
10.2	82268	0.12155	1.27	5.94E-1
10.0	80655	0.12398	1.26	5.52E-1
9.8	79042	0.12651	1.20	5.09E-1
9.6	77429	0.12915	1.13	5.05E-1
9.4	75815	0.13190	1.10	5.44E-1
9.2	74202	0.13477	1.04	6.34E-1
9.0	72589	0.13776	0.983	7.52E-1
8.8	70976	0.14089	0.894	8.94E-1
8.7	70170	0.14251	0.939	1.06E0
8.6	69363	0.14417	1.06	1.21E0
8.5	68556	0.14586	1.26	1.26E0
8.4	67750	0.14760	1.46	1.32E0

TABLE I *(Continued)*

PbF_2

eV	cm^{-1}	μm	n	k
8.3	66943	0.14938	1.62	1.10E0
8.2	66137	0.15120	1.72	8.71E-1
8.1	65330	0.15307	1.66	8.12E-1
8.0	64524	0.15498	1.60	7.47E-1
7.8	62911	0.15895	1.52	6.52E-1
7.6	61298	0.16314	1.39	7.05E-1
7.4	59684	0.16755	1.31	7.97E-1
7.2	58071	0.17220	1.29	9.30E-1
7.0	56458	0.17712	1.27	1.10E0
6.8	54845	0.18233	1.34	1.26E0
6.7	54039	0.18505	1.51	1.38E0
6.6	53232	0.18786	1.66	1.44E0
6.5	52426	0.19075	1.86	1.50E0
6.4	51619	0.19373	2.08	1.24E0
6.3	50812	0.19680	2.2	1.02E0
6.2	50006	0.19998	2.19	9.01E-1
6.1	49199	0.20325	2.15 [7][b]	7.90E-1 [7][b]
6.0	48393	0.20664	2.15	6.51E-1
5.9	47586	0.21014	1.71	5.83E-1
5.8	46779	0.21377	1.66	1.08E0
5.7	45973	0.21752	2.50	8.78E-1
5.6	45167	0.22140	2.44	7.75E-1
5.4	43554	0.22960	2.33	5.99E-1
5.2	41940	0.23843	2.24	4.89E-1
5.0	40327	0.24797	2.17	4.41E-1
4.8	38714	0.25830	2.13	3.73E-1
4.6	37101	0.26953	2.10	3.96E-1
4.4	35488	0.28178	2.08	3.79E-1
4.2	33875	0.29520	2.06	3.58E-1
4.0	32262	0.30996	2.05	3.40E-1
4.133	33333	0.30	1.9366 [17]	
4.015	32383	0.3088	1.915 [19][a]	6.5E-3 [19][a]
3.889	31368	0.3188	1.887	4.6E-3
3.714	29958	0.3338	1.882	4.8E-3
3.581	28885	0.3462	1.854	3.7E-3
3.542	28571	0.35	1.8542 [17]	
3.401	27435	0.3645	1.849 [19][a]	3.5E-3
3.254	26247	0.3810	1.826 [19][a]	2.6E-3
3.100	25000	0.40	1.8180 [17]	
3.065	24722	0.4045	1.824 [19][a]	2.6E-3
3.064	24712	0.40466	1.8155 [2][b]	
		0.412	1.7922 [21][a]	4.6E-4 [21][a]
2.959	23866	0.419	1.793 [13][a]	
2.906	23441	0.4266	1.804 [19][a]	1.8E-3 [19][a]
2.856	23039	0.43404	1.8023 [2][b]	
		0.444	1.7800 [21][a]	2.7E-4 [21][a]

(continued)

TABLE I *(Continued)*

PbF_2

eV	cm^{-1}	μm	n	k
2.773	22364	0.44715	1.7974	
2.755	22222	0.45	1.7964 [17]	
2.749	22173	0.451	1.781 [13][a]	
2.716	21906	0.4565	1.801 [19][a]	2.1E-3 [19][a]
2.650	21376	0.46781	1.7907 [2][b]	
2.602	20986	0.4765	1.7841 [13][a]	
		0.479	1.7689 [21][a]	2.2E-4 [21][a]
2.583	20834	0.47999	1.7872 [2][b]	
2.550	20571	0.48613	1.7856	
2.543	20509	0.4876	1.787 [19][a]	1.4E-3 [19][a]
2.541	20492	0.488	1.7809 [13][a]	
2.535	20450	0.489	1.771 [13][a]	
2.519	20317	0.49219	1.7841 [2][b]	
2.497	20141	0.4965	1.7789 [13][a]	
2.480	20000	0.50	1.7822 [17]	
2.438	19663	0.50858	1.7803 [2][b]	
2.410	19436	0.5145	1.7749 [13][a]	
		0.525	1.7571 [21][a]	5.7E-5 [21][a]
2.349	18950	0.5277	1.785 [19][a]	1.4E-3 [19][a]
2.317	18692	0.535	1.761 [13][a]	
2.270	18313	0.54607	1.7729 [2][b]	
2.254	18182	0.55	1.7722 [17]	
2.171	17510	0.5711	1.771 [19][a]	6.0E-4
		0.580	1.7462 [21][a]	4.1E-5 [21][a]
2.110	17019	0.58756	1.7665 [2][b]	
2.105	16978	0.58900	1.7663	
2.103	16961	0.58959	1.7663	
2.098	16920	0.591	1.751 [13][a]	
2.066	16667	0.60	1.7649 [17]	
1.981	15977	0.6259	1.764 [19][a]	9.0E-4 [19][a]
1.959	15803	0.6328	1.7570 [13][a]	~0 [13][a]
1.959	15803	0.6328	1.76 [25][a]	
1.926	15532	0.64385	1.7599 [2][b]	
1.907	15385	0.65	1.7593 [17]	
		0.651	1.7357 [21][a]	~0 [21][a]
1.889	15237	0.65628	1.7587 [2][b]	
1.873	15106	0.662	1.743 [13][a]	
1.857	14974	0.66781	1.7577 [2][b]	
1.795	14477	0.69075	1.7558	
1.789	14430	0.6930	1.758 [19][a]	3.0E-4 [19][a]
1.771	14286	0.70	1.7550 [17]	
1.755	14154	0.70652	1.7545 [2][b]	
		0.735	1.7267 [21][a]	2.3E-4 [21][a]
1.653	13333	0.75	1.77 [24][a]	
1.653	13333	0.75	1.7516 [17]	
1.642	13245	0.755	1.740 [13][a]	

TABLE I *(Continued)*

PbF_2

eV	cm^{-1}	μm	n	k
1.595	12862	0.7775	1.753 [19][a]	2.0E-4 [19][a]
1.550	12500	0.80	1.7488 [17]	
1.550	12500	0.8	1.75 [24][a]	
1.459	11765	0.85	1.79	
1.459	11765	0.85	1.7465 [17]	
1.399	11285	0.8861	1.748 [19][a]	~0 [19][a]
1.378	11111	0.9	1.77 [24][a]	
1.378	11111	0.90	1.7445 [17]	
1.305	10526	0.95	1.7429	
1.240	10000	1.0	1.77 [24][a]	
1.240	10000	1.00	1.7415 [17]	
1.203	9699	1.031	1.744 [19][a]	~0
1.181	9524	1.05	1.7403 [17]	
1.127	9091	1.1	1.72 [24][a]	
1.127	9091	1.10	1.73921 [17]	
1.078	8696	1.15	1.7383	
1.033	8333	1.2	1.72 [24][a]	
1.033	8333	1.20	1.7374 [17]	
1.002	8084	1.237	1.743 [19][a]	~0
0.992	8000	1.25	1.7366 [17]	
0.954	7692	1.3	1.73 [24][a]	
0.954	7692	1.30	1.7360 [17]	
0.918	7407	1.35	1.7353	
0.886	7143	1.4	1.74 [24][a]	
0.886	7143	1.40	1.7347 [17]	
0.855	6897	1.45	1.7342	
0.827	6667	1.5	1.73 [24][a]	
0.827	6667	1.50	1.7337 [17]	
0.802	6472	1.545	1.742 [19][a]	~0
0.800	6452	1.55	1.7332 [17]	
0.775	6250	1.6	1.72 [24][a]	
0.775	6250	1.60	1.7328 [17]	
0.751	6061	1.65	1.7324	
0.729	5882	1.70	1.7320	
0.708	5714	1.75	1.7316	
0.689	5556	1.8	1.75 [24][a]	
0.689	5556	1.80	1.7312 [17]	
0.670	5405	1.85	1.7308	
0.653	5263	1.90	1.7305	
0.636	5128	1.95	1.7302 [17]	
0.620	5000	2.0	1.77 [24][a]	
0.620	5000	2.00	1.7298 [17]	
0.605	4878	2.05	1.7295	
0.602	4859	2.058	1.740 [19][a]	~0 [19][a]
0.590	4762	2.10	1.7292 [17]	
0.577	4651	2.15	1.7289	

(continued)

TABLE I *(Continued)*

PbF_2

eV	cm^{-1}	μm	n	k
0.564	4545	2.20	1.7285	
0.551	4444	2.25	1.7282	
0.539	4348	2.30	1.7279	
0.528	4255	2.35	1.7276	
0.517	4167	2.40	1.7273	
0.506	4082	2.45	1.7270	
0.4959	4000	2.50	1.7267	
0.4959	4000	2.5	1.7 [24][a]	
0.4862	3922	2.55	1.7264 [17]	
0.4769	3846	2.60	1.7261	
0.4679	3774	2.65	1.7258	
0.4592	3704	2.70	1.7255	
0.4509	3636	2.75	1.7252	
0.4428	3571	2.80	1.7249	
0.4350	3509	2.85	1.7246	
0.4275	3448	2.90	1.7243	
0.4203	3390	2.95	1.7239	
0.4133	3333	3.00	1.7236	
0.4133	3333	3.0	1.7 [24][a]	
0.4016	3239	3.087	1.740 [19][a]	~0
0.3875	3125	3.20	1.7223 [17]	
0.3647	2941	3.40	1.7210	
0.3444	2778	3.60	1.7196	
0.3263	2632	3.80	1.7181	
0.3100	2500	4.0	1.7 [24][a]	
0.3100	2500	4.00	1.7166 [17]	
0.2952	2381	4.20	1.7150	
0.2818	2273	4.40	1.7134	
0.2695	2174	4.60	1.7117	
0.2583	2083	4.80	1.7099	
0.2480	2000	5.0	1.7 [24][a]	
0.2480	2000	5.00	1.7080 [17]	
0.2339	1887	5.3		2.5E-4 [18][a]
0.2254	1818	5.50	1.7031	
0.2066	1667	6.00	1.6977	
0.2008	1620	6.174	1.740 [19][a]	
0.1907	1538	6.50	1.6918 [17]	
0.1771	1429	7.00	1.6854	
0.1653	1333	7.50	1.6786	
0.1550	1250	8.0	1.7 [24][a]	
0.1550	1250	8.00	1.6712 [17]	
0.1459	1176	8.50	1.6634	
0.1378	1111	9.00	1.6550	
0.1305	1053	9.5	1.69 [24][a]	
0.1305	1053	9.50	1.6461 [17]	
0.1240	1000	10.0	1.6367	

TABLE I *(Continued)*

PbF_2

eV	cm^{-1}	μm	n	k
0.1240	1000	10.0	1.73 [9]	
0.1181	952.4	10.5	1.6268 [17]	
0.1170	943.4	10.6	1.63 [23][a]	
0.1127	909.1	11.0	1.6163 [17]	
0.1078	869.6	11.5	1.6052	
0.1042	840.3	11.9	1.5960	
0.08266	666.7	15.0	1.58 [9]	
0.07749	625.0	16.0	1.5 [23][a]	
0.06199	500.0	20.0	1.41 [9]	
0.04959	400.0	25.0	1.00	
0.04133	333.3	30.0	0.707	
0.03542	285.7	35.0		0.707 [9]
0.03100	250.0	40.0		1.22
0.02917	235.3	42.5	0.157	1.59
0.02755	222.2	45.0	0.248	2.02
0.02610	210.5	47.5	0.331	2.26
0.02480	200.0	50.0	0.402	2.48
0.02362	190.5	52.5	0.537	2.79
0.02254	181.8	55.0	0.558	3.13
0.02156	173.9	57.5	0.581	3.44
0.02066	166.7	60.0	0.615	3.66
0.01984	160.0	62.5	0.710	3.87
0.01907	153.8	65.0	0.797 [9]	4.10 [9]
0.01837	148.1	67.5	0.845	4.44
0.01771	142.9	70.0	0.961	4.68
0.01710	137.9	72.5	1.05	5.01
0.01653	133.3	75.0	1.20	5.43
0.01600	129.0	77.5	1.51	5.81
0.01550	125.0	80.0	1.66	6.31
0.01503	121.2	82.5	2.00	6.75
0.01459	117.6	85.0	2.30	7.40
0.01417	114.3	87.5	2.96	8.11
0.01378	111.1	90.0	3.74	8.95
0.01340	108.1	92.5	5.08	9.64
0.01305	105.3	95.0	7.06	9.99
0.01272	102.6	97.5	8.69	8.69
0.01240	100.0	100.0	10.3	6.87
0.01210	97.56	102.5	10.1	5.36
0.01181	95.24	105.0	9.69	4.23
0.01153	93.02	107.5	9.46	3.54
0.01127	90.91	110.0	9.29	3.04
0.01102	88.89	112.5	9.13	2.71
0.01078	86.96	115.0	8.97	2.43
0.01055	85.11	117.5	8.82	2.18
0.01033	83.33	120.0	8.64	1.91
0.01012	81.63	122.5	8.48	1.71

(continued)

TABLE I *(Continued)*

PbF_2

eV	cm^{-1}	μm	n	k
0.009919	80.00	125.0	8.36	1.53
0.009724	78.43	127.5	8.23	1.34
0.009537	76.92	130.0	8.12	1.17
0.009184	74.07	135.0	7.95	0.849
0.008856	71.43	140.0	7.83	0.511
0.008551	68.97	145.0	7.75	0.226

Lithium Tantalate ($LiTaO_3$)

FRANÇOIS GERVAIS
Laboratoire d'Electrodynamique des Matériaux Avancés
Faculté des Sciences & Techniques, Université François Rabelais
Tours, France

and

VICENTE FONSECA
Centre de Recherches sur la Physique des Hautes Températures
Centre National de la Recherche Scientifique
Orléans, France

$LiTaO_3$ crystallizes in the pseudo-ilmenite 3m structure. It was found to be ferroelectric by Matthias and Remeika in 1949 [1]. The Curie temperature is ~890 K. Although the spontaneous polarization is not as large as in the parent compound $LiNbO_3$, there are many possible technical applications of $LiTaO_3$ related to the large electro-optic coefficient [2]. High-quality single crystals may be grown by the Czochralski pulling method. The system is uniaxial, and optical properties measured on a single crystal are, therefore, anisotropic. The anisotropy of the refractive index in the visible region, mainly related to the anisotropy of the oxygen polarizability, is surprisingly small, ~0.2% in the visible region. In the millimeter-wave range, the anisotropy remains small (~2%) also. These small anisotropies are related to the fact that the structure of $LiTaO_3$ derives from the cubic perovskite structure. However, at intermediate frequencies, the anisotropy of the structure induces very different lattice dynamical properties and band structure, so that the spectra of the index of refraction n and extinction coefficient k are very different for the polarizations parallel and perpendicular to the ferroelectric c axis.

The availability of synchrotron-radiation sources allowed the first measurements of optical response of this material at high energies, as well as for many other materials in the past 20 years. Reflection spectra in the op-

HANDBOOK OF OPTICAL CONSTANTS OF SOLIDS III

Copyright © 1998 by Academic Press.
All rights of reproduction in any form reserved
ISBN 0-12-544423-0/$25.00.

tical range 2–35 eV were obtained with the aid of the storage ring at the Stoughton Synchrotron Radiation Center of the University of Wisconsin. Data were published by Mamedov and co-workers [3, 4], but they are, unfortunately, restricted to a single surface orientation, for the crystal cut perpendicular to the ferroelectric (FE) c-axis. Measurements parallel to the ferroelectric axis would be highly desirable to complement the data. The purpose of the measurements was to study the electronic excitations in relation to partial hybridization of atomic orbitals, but not properly to determine the optical constants n and k which are not displayed in the papers. Only the maxima of the imaginary part of the dielectric response $\epsilon = n - ik$ are discussed. In the absence of other studies devoted to the specific measurement of these spectra, we have attempted to extract information useful for the present purpose from reflectivity. This was done by Kramers–Kronig (K-K) analysis. But, by doing so, and even after proper extrapolation of low-frequency data, we realized that the absorption coefficient (or the imaginary part of the dielectric function, or the imaginary part of the inverse dielectric function equally well) found by K-K inversion is negative below 34,000 cm^{-1} (see also Fig. 3 of Mamedov [4]), which is obviously meaningless physically. We made, therefore, the slightest correction of all the data (-2.5%) to recover physically reasonable values, viz., the real part of the dielectric response which tends towards unity at infinite frequency and positive values of the imaginary part everywhere. The minimum correction according to these criteria gives the results of n and k listed in Table I. Whereas the accuracy of the highest k values is little affected by this correction, the accuracy of lowest values is poor. New measurements are, therefore, highly desirable. Indices n are less affected by the uncertainty.

Absorption in the range 3.2–4.7 eV was measured by Kase and Ohi [5]. The deduced k values ($k = \alpha/4\pi\sigma$, where α is the absorption coefficient and σ the wave number) are much more accurate than the estimation in this region by K-K analysis for the reasons given earlier. Note that a slight shift of the band edge is found by comparing the values of Mamedov [3] and these data.

The indices of refraction of $LiTaO_3$ prisms measured over its entire range of transmission (0.4 to 4 μm) and for both principal directions are reported by Bond [6]. Results are listed in Tables I and II. Note that one value, 2.0299, in Table IV of Bond [6] does not extrapolate to neighboring values and is most likely a misprint.

The earliest set of measurements in the infrared complemented by data processing was performed by Barker *et al.* [7] in 1970. Several single crystals cut parallel or perpendicular to the FE axis from boules grown by the Czochralski pulling technique were used. Infrared reflection measurements were performed with a prism spectrometer. Complementary transmission measurements performed on 30- and 147-μm-thick thin slabs made use of a Michelson interferometer. Gervais and Servoin [7, 8] also remeasured the

spectra with a prism spectrometer. The same authors [9–11] later performed a complete study of the temperature dependence of infrared reflectivity, including both sides of the ferroelectric–paraelectric (FE-PE) phase transition, with a modern Fourier-transform infrared spectrometer. These spectra were obtained on single crystals also cut from Czochralski-grown boules. Unfortunately, in none of these studies were the spectra of n and k given explicitly.

In single crystals, the dielectric function $\epsilon = n - ik$ can be modeled. As soon as a dielectric-function model fits the infrared reflectivity, one may deduce the optical constants more accurately than with a K-K analysis. The absorption coefficient is extremely high in the atomic-vibration region, because of the large polar character of the vibrations in such a ferroelectric crystal. The penetration depth of the infrared radiation is found to be less than 1 μm at a peak, corresponding to a normal vibration mode. As a result, the infrared beam in these narrow spectral regions probes the surface of the sample rather than the bulk. The result is then very sensitive to the alterations of the crystal surface. Conversely, far from normal modes, the penetration depth of the infrared beam is much larger. Disorder or alteration of the sample surface increases mode damping and, therefore, lowers the reflectivity. Fitting the spectra can minimize the spurious effects of the surface by comparison with a K-K analysis because the damping coefficient is then averaged over a wide spectral range (with larger penetration depth on an average) in the former case instead of being determined near the mode frequency, where disorder may alter the result.

Barker *et al.* [7] fitted their spectra with the usual dielectric-function model

$$\epsilon = \epsilon_\infty + \sum_j \Delta\epsilon_j \frac{\Omega_{j\mathrm{TO}}^2}{\Omega_{j\mathrm{TO}}^2 - \omega^2 + i\gamma_{j\mathrm{TO}}\omega}. \tag{1}$$

ϵ_∞ is the high-frequency dielectric constant; $\Delta\epsilon_j$, $\Omega_{j\mathrm{TO}}$, and $\gamma_{j\mathrm{TO}}$ are the oscillator strength, the frequency, and the damping of the jth TO (transverse optic) mode, respectively.

A factorization over poles and zeroes of the dielectric response in the form

$$\epsilon = \epsilon_\infty \prod_j \frac{\Omega_{j\mathrm{LO}}^2 - \omega^2 + i\gamma_{j\mathrm{LO}}\omega}{\Omega_{j\mathrm{LO}}^2 - \omega^2 + i\gamma_{j\mathrm{TO}}\omega} \tag{2}$$

was preferred by others [7–11]. Here the index LO refers to longitudinal optic modes. The reason invoked by the authors is that in systems that are highly polar and where the Coulombic field splits the polar modes into transverse and longitudinal components (the later being possibly twice more energetic than the former), phonons can have very different decays, and then dampings can be very different. Conversely, identical dampings are implicitly assumed for the TO and LO components by the model Eq. (1). Results

deduced from the fit to the reflectivity data with the dielectric-function model Eq. (2) are compared to K-K transformed data of Barker *et al.* [7] and from Servoin [11] in Table I. Data are given for the electric field of infrared radiation polarized perpendicular to the crystal c-axis (ordinary ray). The overall agreement is good.

The situation for the polarization parallel to the FE c-axis is more complicated. Indeed, neither model, Eq. (1) or (2), is able to fit the data correctly. This is why some authors [7–11] introduced a phonon self-energy function that yields in practice a frequency dependence of the damping function of certain modes (including the soft FE mode) to get a good fit to reflectivity data. But this procedure introduces many more fitting parameters and is, therefore, questionable. At least, it is nonstandard. Here we preferred to adopt a compromise and fitted with the general model Eq. (2), by just adding an overdamped mode at low frequency to take account of the bump that develops at low frequency on heating [10–12]. Results are satisfactory. They are compared with K-K analyses in Table II.

Lowest-frequency values of k in Tables I and II are those of Barker [7], deduced from absorption-coefficient measurements in thin slabs.

Much of the n and k data in Table I and II is plotted in Figs. 1 and 2.

As mentioned earlier, the temperature dependence of infrared reflection spectra has been studied in detail elsewhere [10–12]. In particular, it was shown that, whereas a soft vibrational mode is observed on approaching the temperature of the FE-PE phase transition, the soft mode alone does not explain the behavior of the dielectric constant. A soft mode assumes a displacive-type phase transition, whereas a discrepancy of ϵ_0 measured in the very far infrared and in the radio-frequency range is rather indicative of an order–disorder-type phase transition. These experimental observations were, therefore, understood in terms of a crossover from displacive to order–disorder behavior in a model for ferroelectrics proposed by Müller and co-workers [13].

REFERENCES

1. B. T. Matthias and J. P. Remeika, *Phys. Rev.* **76**, 1886 (1949).
2. P. V. Lenzo, E. H. Turner, E. G. Spencer, and A. A. Balman, *Appl. Phys. Lett.* **8**, 81 (1966).
3. A. M. Mamedov, *Ferroelectrics* **45**, 55 (1982).
4. A. M. Mamedov, M. A. Osman, and L. C. Hajieva, *Appl. Phys. A* **34**, 189 (1984).
5. S. Kase and K. Ohi, *Ferroelectrics* **8**, 419 (1974).
6. W. L. Bond, *J. Appl. Phys.* **36**, 1674 (1965).
7. A. S. Barker, A. A. Ballman, and J. A. Ditzenberger, *Phys. Rev. B* **2**, 4233 (1970).
8. F. Gervais and J. L. Servoin, *Phys. Rev. B* **15**, 4532 (1977).
9. J. L. Servoin and F. Gervais, *Appl. Opt.* **16**, 2952 (1977).
10. J. L. Servoin and F. Gervais, *Solid State Commun.* **31**, 387 (1979).
11. J. L. Servoin, Ph.D. Thesis, University of Orléans, France (1980).
12. F. Gervais, *in* "Infrared and Millimeter Waves," (K. J. Button, ed.), Vol. 8, p. 279. Academic Press, New York, 1983.
13. K. A. Müller, Y. Luspin, J. L. Servoin, and F. Gervais, *J. Phys. Lett.* **43**, 537 (1982).

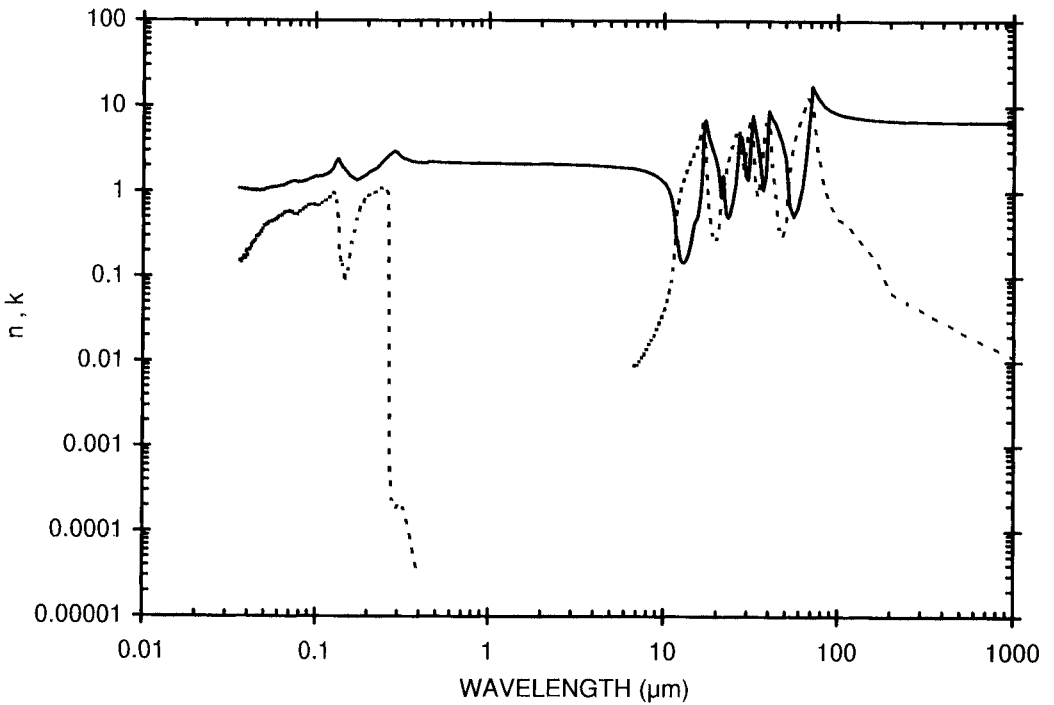

Fig. 1. Log–log plot of $n_\perp$ (—) and $k_\perp$ (---) versus wavelength in micrometers for lithium tantalate.

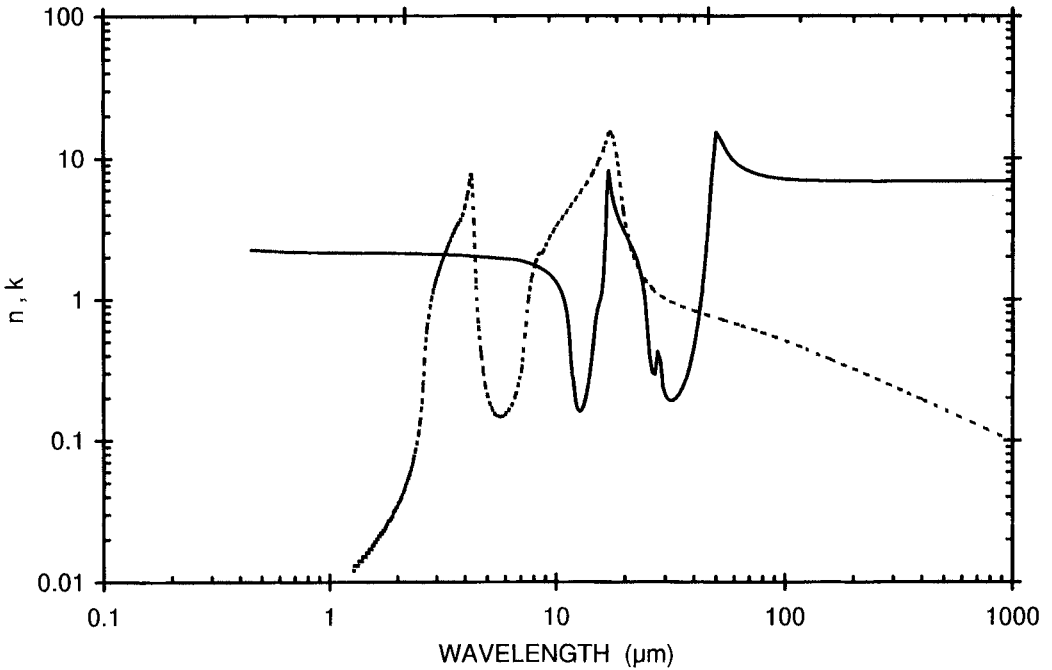

Fig. 2. Log–log plot of $n_{\|}$ (—) and $k_{\|}$ (---) versus wavelength in micrometers for lithium tantalate.

TABLE I

Values of $n_\perp$ and $k_\perp$ for Lithium Tantalate from Various References

eV	cm ^{1}	μm	$n_\perp$	$k_\perp$	$n_\perp$	$k_\perp$	$n_\perp$	$k_\perp$
35.0	282000	0.03546	1.082 [3]	0.145 [3]				
34.8	281000	0.03559	1.080	0.147				
34.7	280000	0.03571	1.080	0.149				
34.6	279000	0.03584	1.080	0.152				
34.5	278000	0.03597	1.080	0.154				
34.3	277000	0.03610	1.082	0.155				
34.2	276000	0.03623	1.083	0.155				
34.1	275000	0.03636	1.084	0.155				
34.0	274000	0.03650	1.085	0.152				
33.8	273000	0.03663	1.082	0.149				
33.7	272000	0.03676	1.075	0.148				
33.6	271000	0.03690	1.070	0.154				
33.5	270000	0.03704	1.070	0.158				
33.4	269000	0.03717	1.072	0.159				
33.2	268000	0.03731	1.070	0.159				
33.1	267000	0.03745	1.068	0.160				
33.0	266000	0.03759	1.065	0.161				
32.9	265000	0.03774	1.062	0.164				
32.7	264000	0.03788	1.061	0.169				
32.6	263000	0.03802	1.061	0.173				
32.5	262000	0.03817	1.063	0.176				
32.4	261000	0.03831	1.070	0.177				
32.2	260000	0.03846	1.068	0.168				
32.1	259000	0.03861	1.057	0.162				

(continued)

TABLE I *(Continued)*

Lithium Tantalate

eV	cm^{-1}	μm	$n_\perp$	$k_\perp$	$n_\perp$	$k_\perp$	$n_\perp$	$k_\perp$
32.0	258000	0.03876	1.047	0.173				
31.9	257000	0.03891	1.044	0.182				
31.7	256000	0.03906	1.045	0.193				
31.6	255000	0.03922	1.054	0.203				
31.5	254000	0.03937	1.067	0.197				
31.4	253000	0.03953	1.068	0.189				
31.2	252000	0.03968	1.063	0.180				
31.1	251000	0.03984	1.048	0.174				
31.0	250000	0.04000	1.037	0.197				
30.9	249000	0.04016	1.045	0.201				
30.7	248000	0.04032	1.047	0.204				
30.6	247000	0.04049	1.051	0.204				
30.5	246000	0.04065	1.051	0.201				
30.4	245000	0.04082	1.046	0.199				
30.3	244000	0.04098	1.038	0.202				
30.1	243000	0.04115	1.034	0.209				
30.0	242000	0.04132	1.032	0.216				
29.9	241000	0.04149	1.033	0.222				
29.8	240000	0.04167	1.035	0.229				
29.6	239000	0.04184	1.046	0.233				
29.5	238000	0.04202	1.043	0.218				
29.4	237000	0.04219	1.023	0.231				
29.3	236000	0.04237	1.036	0.247				
29.1	235000	0.04255	1.043	0.243				
29.0	234000	0.04274	1.045	0.237				
28.9	233000	0.04292	1.039	0.231				
28.8	232000	0.04310	1.021	0.236				

28.6	231000	0.04329	1.021	0.254
28.5	230000	0.04348	1.028	0.263
28.4	229000	0.04367	1.039	0.261
28.3	228000	0.04386	1.036	0.254
28.1	227000	0.04405	1.028	0.265
28.0	226000	0.04425	1.040	0.263
27.9	225000	0.04444	1.024	0.259
27.8	224000	0.04464	1.015	0.272
27.6	223000	0.04484	1.023	0.293
27.5	222000	0.04505	1.035	0.291
27.4	221000	0.04525	1.040	0.287
27.3	220000	0.04545	1.038	0.282
27.2	219000	0.04566	1.024	0.280
27.0	218000	0.04587	1.025	0.298
26.9	217000	0.04608	1.029	0.295
26.8	216000	0.04630	1.018	0.300
26.7	215000	0.04651	1.022	0.318
26.5	214000	0.04673	1.031	0.309
26.4	213000	0.04695	1.013	0.317
26.3	212000	0.04717	1.020	0.333
26.2	211000	0.04739	1.029	0.342
26.0	210000	0.04762	1.040	0.338
25.9	209000	0.04785	1.039	0.332
25.8	208000	0.04808	1.027	0.342
25.7	207000	0.04831	1.038	0.344
25.5	206000	0.04854	1.026	0.343
25.4	205000	0.04878	1.033	0.361
25.3	204000	0.04902	1.034	0.354
25.2	203000	0.04926	1.021	0.367
25.0	202000	0.04950	1.024	0.389
24.9	201000	0.04975	1.045	0.394

(continued)

TABLE I *(Continued)*

Lithium Tantalate

eV	cm^{-1}	μm	$n_\perp$	$k_\perp$	$n_\perp$	$k_\perp$	$n_\perp$	$k_\perp$
24.8	200000	0.05000	1.051	0.388				
24.7	199000	0.05025	1.041	0.399				
24.5	198000	0.05051	1.061	0.406				
24.4	197000	0.05076	1.060	0.400				
24.3	196000	0.05102	1.059	0.408				
24.2	195000	0.05128	1.072	0.419				
24.1	194000	0.05155	1.080	0.412				
23.9	193000	0.05181	1.076	0.408				
23.8	192000	0.05208	1.074	0.413				
23.7	191000	0.05236	1.073	0.424				
23.6	190000	0.05263	1.089	0.434				
23.4	189000	0.05291	1.098	0.426				
23.3	188000	0.05319	1.092	0.420				
23.2	187000	0.05348	1.091	0.432				
23.1	186000	0.05376	1.101	0.434				
22.9	185000	0.05405	1.104	0.432				
22.8	184000	0.05435	1.101	0.434				
22.7	183000	0.05464	1.105	0.443				
22.6	182000	0.05495	1.112	0.441				
22.4	181000	0.05525	1.109	0.440				
22.3	180000	0.05556	1.112	0.447				
22.2	179000	0.05587	1.116	0.449				
22.1	178000	0.05618	1.118	0.451				
21.9	177000	0.05650	1.120	0.452				
21.8	176000	0.05682	1.120	0.454				
21.7	175000	0.05714	1.123	0.465				
21.6	174000	0.05747	1.133	0.460				

21.4	173000	0.05780	1.128	0.455
21.3	172000	0.05814	1.124	0.462
21.2	171000	0.05848	1.122	0.470
21.1	170000	0.05882	1.127	0.481
21.0	169000	0.05917	1.136	0.485
20.8	168000	0.05952	1.137	0.478
20.7	167000	0.05988	1.131	0.494
20.6	166000	0.06024	1.144	0.502
20.5	165000	0.06061	1.152	0.495
20.3	164000	0.06098	1.145	0.506
20.2	163000	0.06135	1.158	0.510
20.1	162000	0.06173	1.163	0.510
20.0	161000	0.06211	1.165	0.510
19.8	160000	0.06250	1.164	0.518
19.7	159000	0.06289	1.178	0.518
19.6	158000	0.06329	1.172	0.518
19.5	157000	0.06369	1.181	0.527
19.3	156000	0.06410	1.181	0.516
19.2	155000	0.06452	1.164	0.531
19.1	154000	0.06494	1.175	0.549
19.0	153000	0.06536	1.187	0.559
18.8	152000	0.06579	1.199	0.560
18.7	151000	0.06623	1.206	0.561
18.6	150000	0.06667	1.208	0.567
18.5	149000	0.06711	1.224	0.573
18.3	148000	0.06757	1.232	0.570
18.2	147000	0.06803	1.235	0.576
18.1	146000	0.06849	1.252	0.580
18.0	145000	0.06897	1.261	0.573
17.9	144000	0.06944	1.260	0.570
17.7	143000	0.06993	1.269	0.579

(continued)

TABLE I *(Continued)*

Lithium Tantalate

eV	cm^{-1}	μm	$n_\perp$	$k_\perp$	$n_\perp$	$k_\perp$	$n_\perp$	$k_\perp$
17.6	142000	0.07042	1.284	0.572				
17.5	141000	0.07092	1.285	0.563				
17.4	140000	0.07143	1.287	0.570				
17.2	139000	0.07194	1.300	0.570				
17.1	138000	0.07246	1.306	0.562				
17.0	137000	0.07299	1.308	0.557				
16.9	136000	0.07353	1.311	0.554				
16.7	135000	0.07407	1.316	0.550				
16.6	134000	0.07463	1.316	0.541				
16.5	133000	0.07519	1.312	0.538				
16.4	132000	0.07576	1.312	0.536				
16.2	131000	0.07634	1.310	0.526				
16.1	130000	0.07692	1.296	0.525				
16.0	129000	0.07752	1.280	0.535				
15.9	128000	0.07813	1.276	0.552				
15.7	127000	0.07874	1.285	0.565				
15.6	126000	0.07937	1.290	0.569				
15.5	125000	0.08000	1.293	0.573				
15.4	124000	0.08065	1.294	0.578				
15.3	123000	0.08130	1.295	0.583				
15.1	122000	0.08197	1.296	0.589				
15.0	121000	0.08264	1.297	0.597				
14.9	120000	0.08333	1.297	0.608				
14.8	119000	0.08403	1.304	0.618				
14.6	118000	0.08475	1.306	0.628				
14.5	117000	0.08547	1.321	0.648				
14.4	116000	0.08621	1.335	0.636				

14.3	115000	0.08696	1.326	0.644
14.1	114000	0.08772	1.332	0.667
14.0	113000	0.08850	1.353	0.668
13.9	112000	0.08929	1.356	0.674
13.8	111000	0.09009	1.369	0.688
13.6	110000	0.09091	1.391	0.691
13.5	109000	0.09174	1.395	0.684
13.4	108000	0.09259	1.410	0.699
13.3	107000	0.09346	1.423	0.696
13.1	106000	0.09434	1.426	0.698
13.0	105000	0.09524	1.447	0.701
12.9	104000	0.09615	1.448	0.705
12.8	103000	0.09709	1.468	0.710
12.6	102000	0.09804	1.489	0.709
12.5	101000	0.09901	1.501	0.694
12.4	100000	0.1000	1.504	0.688
12.3	99000	0.1010	1.515	0.680
12.2	98000	0.1020	1.501	0.671
12.0	97000	0.1031	1.500	0.682
11.9	96000	0.1042	1.507	0.690
11.8	95000	0.1053	1.516	0.691
11.7	94000	0.1064	1.512	0.689
11.5	93000	0.1075	1.508	0.702
11.4	92000	0.1087	1.510	0.729
11.3	91000	0.1099	1.529	0.740
11.2	90000	0.1111	1.542	0.750
11.0	89000	0.1124	1.554	0.765
10.9	88000	0.1136	1.573	0.776
10.8	87000	0.1149	1.590	0.785
10.7	86000	0.1163	1.598	0.803
10.5	85000	0.1176	1.625	0.819

(continued)

TABLE I *(Continued)*

Lithium Tantalate

eV	cm^{-1}	μm	$n_\perp$	$k_\perp$	$n_\perp$	$k_\perp$	$n_\perp$	$k_\perp$
10.4	84000	0.1190	1.659	0.837				
10.3	83000	0.1205	1.672	0.855				
10.2	82000	0.1220	1.722	0.870				
10.0	81000	0.1235	1.759	0.903				
9.92	80000	0.1250	1.812	0.927				
9.79	79000	0.1266	1.915	0.958				
9.67	78000	0.1282	2.031	0.936				
9.55	77000	0.1299	2.157	0.889				
9.42	76000	0.1316	2.270	0.763				
9.30	75000	0.1333	2.344	0.628				
9.17	74000	0.1351	2.411	0.418				
9.05	73000	0.1370	2.222	0.214				
8.93	72000	0.1389	2.117	0.171				
8.80	71000	0.1408	2.027	0.123				
8.68	70000	0.1429	1.917	0.136				
8.55	69000	0.1449	1.906	0.138				
8.43	68000	0.1471	1.826	0.081				
8.31	67000	0.1493	1.746	0.105				
8.18	66000	0.1515	1.704	0.103				
8.06	65000	0.1538	1.621	0.121				
7.94	64000	0.1563	1.576	0.149				
7.81	63000	0.1587	1.503	0.200				
7.69	62000	0.1613	1.487	0.250				
7.56	61000	0.1639	1.447	0.277				
7.44	60000	0.1667	1.427	0.335				
7.32	59000	0.1695	1.393	0.372				
7.19	58000	0.1724	1.355	0.470				

7.07	57000	0.1754	1.379	0.537	
6.94	56000	0.1786	1.385	0.590	
6.82	55000	0.1818	1.430	0.669	
6.70	54000	0.1852	1.453	0.700	
6.57	53000	0.1887	1.484	0.752	
6.45	52000	0.1923	1.526	0.795	
6.32	51000	0.1961	1.558	0.824	
6.20	50000	0.2000	1.616	0.877	
6.08	49000	0.2041	1.675	0.899	
5.95	48000	0.2083	1.719	0.909	
5.83	47000	0.2128	1.754	0.927	
5.70	46000	0.2174	1.795	0.952	
5.58	45000	0.2222	1.830	0.984	
5.46	44000	0.2273	1.897	1.053	
5.33	43000	0.2326	2.007	1.096	
5.21	42000	0.2381	2.118	1.089	
5.08	41000	0.2439	2.236	1.082	
4.96	40000	0.2500	2.349	1.053	
4.84	39000	0.2564	2.470	1.007	
4.71	38000	0.2632	2.590	0.940	
4.59	37000	0.2703	2.720	0.837	5.1E-04 [5]
4.46	36000	0.2778	2.836	0.697	2.3E-04
4.34	35000	0.2857	2.957	0.496	1.9E-04
4.22	34000	0.2941	2.896	0.173	1.9E-04
4.09	33000	0.3030	2.686	0.002	2.0E-04
3.97	32000	0.3125	2.558		2.0E-04
3.84	31000	0.3226	2.428		1.8E-04
3.72	30000	0.3333	2.398		1.5E-04
3.60	29000	0.3448	2.330		1.1E-04
3.47	28000	0.3571	2.256		7.9E-05
3.35	27000	0.3704	2.232		5.4E-05

(continued)

TABLE I *(Continued)*

Lithium Tantalate

eV	cm^{-1}	μm	$n_\perp$	$k_\perp$	$n_\perp$	$k_\perp$	$n_\perp$	$k_\perp$
3.22	26000	0.3846	2.197			3.8E-05		
3.10	25000	0.4000	2.183					
2.98	24000	0.4167	2.161					
2.85	23000	0.4348	2.155					
2.73	22000	0.4545	2.155					
2.60	21000	0.4762	2.134					
2.48	20000	0.5000	2.130					
2.755	22222	0.45			2.2420 [6]			
2.480	20000	0.50			2.2160			
2.066	16667	0.60			2.1834			
1.771	14286	0.70			2.1652			
1.550	12500	0.80			2.1538			
1.378	11111	0.90			2.1454			
1.240	10000	1.00			2.1391			
1.033	8333	1.20			2.1305			
0.8856	7143	1.40			2.1236			
0.7749	6250	1.60			2.1174			
0.6888	5556	1.80			2.1120			
0.6199	5000	2.00			2.1066			
0.5636	4545	2.20			2.1009			
0.5166	4167	2.40			2.0951			
0.4769	3846	2.60			2.0891			
0.4428	3571	2.80			2.0825			
0.4133	3333	3.00			2.0755			
0.3875	3125	3.20			2.0680			
0.3647	2941	3.40			2.0601			
0.3444	2778	3.60			2.0513			

0.3263	2632	3.80			2.0424	
0.3100	2500	4.00			2.0335	
0.2108	1700	5.882	1.879 [7]			
0.2095	1690	5.917	1.875			
0.2083	1680	5.952	1.872			
0.2071	1670	5.988	1.868			
0.2058	1660	6.024	1.864			
0.2046	1650	6.061	1.861			
0.2033	1640	6.098	1.857			
0.2021	1630	6.135	1.854			
0.2009	1620	6.173	1.850			
0.1996	1610	6.211	1.847			
0.1984	1600	6.250	1.843	0.001 [7]		
0.1971	1590	6.289	1.839	0.002		
0.1959	1580	6.329	1.836	0.003		
0.1947	1570	6.369	1.832	0.004		
0.1934	1560	6.410	1.828	0.005		
0.1922	1550	6.452	1.825	0.006		
0.1909	1540	6.494	1.821	0.007		
0.1897	1530	6.536	1.818	0.007		
0.1885	1520	6.579	1.814	0.008		
0.1872	1510	6.623	1.810	0.009		
0.1860	1500	6.667	1.807	0.009		
0.1847	1490	6.711	1.803	0.009	1.887 [11]	0.008 [11]
0.1835	1480	6.757	1.799	0.009	1.882	0.008
0.1823	1470	6.803	1.796	0.008	1.877	0.009
0.1810	1460	6.849	1.792	0.006	1.872	0.009
0.1798	1450	6.897	1.786	0.003	1.867	0.009
0.1785	1440	6.944	1.779	0.003	1.862	0.009
0.1773	1430	6.993	1.773	0.003	1.856	0.009
0.1761	1420	7.042	1.766	0.004	1.850	0.009

(continued)

TABLE I *(Continued)*

Lithium Tantalate

eV	cm^{-1}	μm	$n_\perp$	$k_\perp$	$n_\perp$	$k_\perp$	$n_\perp$	$k_\perp$
0.1748	1410	7.092	1.760	0.005	1.845	0.010		
0.1736	1400	7.143	1.753	0.006	1.839	0.010		
0.1723	1390	7.194	1.747	0.007	1.833	0.010		
0.1711	1380	7.246	1.740	0.009	1.826	0.010		
0.1699	1370	7.299	1.733	0.010	1.820	0.011		
0.1686	1360	7.353	1.727	0.012	1.813	0.011		
0.1674	1350	7.407	1.720	0.014	1.806	0.011		
0.1661	1340	7.463	1.714	0.015	1.799	0.011		
0.1649	1330	7.519	1.707	0.017	1.792	0.012		
0.1637	1320	7.576	1.700	0.018	1.785	0.012		
0.1624	1310	7.634	1.694	0.019	1.777	0.012		
0.1612	1300	7.692	1.687	0.019	1.769	0.012		
0.1599	1290	7.752	1.680	0.019	1.760	0.013		
0.1587	1280	7.813	1.673	0.016	1.752	0.013		
0.1575	1270	7.874	1.663	0.014	1.743	0.014		
0.1562	1260	7.937	1.654	0.015	1.734	0.014		
0.1550	1250	8.000	1.644	0.017	1.724	0.014		
0.1537	1240	8.065	1.634	0.019	1.715	0.015		
0.1525	1230	8.130	1.624	0.021	1.704	0.015		
0.1513	1220	8.197	1.614	0.024	1.694	0.016		
0.1500	1210	8.264	1.604	0.026	1.683	0.016		
0.1488	1200	8.333	1.594	0.029	1.672	0.017		
0.1475	1190	8.403	1.584	0.031	1.660	0.017		
0.1463	1180	8.475	1.574	0.033	1.648	0.018		
0.1451	1170	8.547	1.564	0.034	1.635	0.018		
0.1438	1160	8.621	1.554	0.034	1.621	0.019		
0.1426	1150	8.696	1.543	0.033	1.608	0.020		

0.1413	1140	8.772	1.533	0.027	1.593	0.020		
0.1401	1130	8.850	1.521	0.010	1.578	0.021		
0.1389	1120	8.929	1.502	0.005	1.562	0.022		
0.1376	1110	9.009	1.482	0.008	1.546	0.023		
0.1364	1100	9.091	1.461	0.014	1.528	0.024		
0.1351	1090	9.174	1.440	0.024	1.510	0.025		
0.1339	1080	9.259	1.418	0.034	1.491	0.026		
0.1327	1070	9.346	1.395	0.046	1.471	0.027		
0.1314	1060	9.434	1.371	0.058	1.450	0.029		
0.1302	1050	9.524	1.345	0.070	1.427	0.030		
0.1289	1040	9.615	1.318	0.082	1.403	0.032		
0.1277	1030	9.709	1.289	0.091	1.378	0.033		
0.1265	1020	9.804	1.258	0.099	1.352	0.035		
0.1252	1010	9.901	1.234	0.109	1.323	0.037		
0.1240	1000	10.00	1.215	0.121	1.293	0.040		
0.1227	990	10.10	1.195	0.133	1.260	0.042	1.200 [a]	0.007 [a]
0.1215	980	10.20	1.173	0.144	1.225	0.045	1.173	0.048
0.1203	970	10.31	1.148	0.154	1.188	0.049	1.144	0.035
0.1190	960	10.42	1.121	0.161	1.147	0.053	1.095	0.052
0.1178	950	10.53	1.092	0.165	1.102	0.058	1.058	0.078
0.1165	940	10.64	1.059	0.166	1.053	0.063	1.036	0.089
0.1153	930	10.75	1.022	0.161	0.999	0.070	0.956	0.101
0.1141	920	10.87	0.979	0.146	0.939	0.078	0.919	0.094
0.1128	910	10.99	0.862	0.184	0.870	0.089	0.840	0.113
0.1116	900	11.11	0.740	0.200	0.792	0.104	0.779	0.129
0.1103	890	11.24	0.658	0.192	0.700	0.125	0.706	0.141
0.1091	880	11.36	0.600	0.187	0.589	0.161	0.587	0.153
0.1079	870	11.49	0.466	0.216	0.457	0.229	0.442	0.225
0.1066	860	11.63	0.315	0.315	0.335	0.362	0.321	0.371
0.1054	850	11.76	0.272	0.505	0.285	0.520	0.281	0.533
0.1041	840	11.90	0.239	0.628	0.269	0.632	0.282	0.636

(continued)

[a] Best fit of model Eq. (2) to reflectivity data of Ref. [11].

TABLE I *(Continued)*

Lithium Tantalate

eV	cm^{-1}	μm	$n_\perp$	$k_\perp$	$n_\perp$	$k_\perp$	$n_\perp$	$k_\perp$
0.1029	830	12.05	0.207	0.748	0.227	0.733	0.243	0.719
0.1017	820	12.20	0.194	0.879	0.189	0.853	0.196	0.829
0.1004	810	12.35	0.180	1.001	0.167	0.978	0.166	0.953
0.09919	800	12.50	0.180	1.120	0.155	1.100	0.151	1.074
0.09795	790	12.66	0.180	1.238	0.150	1.220	0.140	1.189
0.09671	780	12.82	0.183	1.354	0.148	1.339	0.132	1.306
0.09547	770	12.99	0.194	1.473	0.149	1.458	0.126	1.430
0.09423	760	13.16	0.207	1.589	0.152	1.580	0.128	1.557
0.09299	750	13.33	0.221	1.708	0.159	1.706	0.135	1.685
0.09175	740	13.51	0.235	1.829	0.168	1.837	0.145	1.819
0.09051	730	13.70	0.246	1.960	0.183	1.974	0.162	1.958
0.08927	720	13.89	0.260	2.113	0.203	2.119	0.189	2.105
0.08803	710	14.08	0.304	2.274	0.232	2.274	0.225	2.251
0.08679	700	14.29	0.357	2.442	0.274	2.436	0.269	2.405
0.08555	690	14.49	0.433	2.605	0.331	2.601	0.324	2.562
0.08431	680	14.71	0.501	2.761	0.396	2.758	0.386	2.715
0.08307	670	14.93	0.572	2.944	0.445	2.914	0.441	2.864
0.08183	660	15.15	0.652	3.131	0.468	3.104	0.472	3.034
0.08059	650	15.38	0.684	3.420	0.490	3.366	0.485	3.256
0.07935	640	15.63	0.815	3.800	0.543	3.715	0.503	3.586
0.07811	630	15.87	1.040	4.362	0.660	4.174	0.598	4.030
0.07687	620	16.13	1.695	5.012	0.899	4.796	0.826	4.605
0.07563	610	16.39	3.027	5.438	1.433	5.684	1.286	5.381
0.07439	600	16.67	4.495	4.884	2.897	6.878	2.424	6.397
0.07315	590	16.95	5.479	3.548	6.462	6.308	5.256	6.423
0.07191	580	17.24	5.383	2.098	6.992	2.713	6.593	3.712
0.07067	570	17.54	4.778	1.234	5.750	1.257	5.869	1.889

0.06943	560	17.86	4.287	0.822	4.831	0.736	5.080	1.130
0.06819	550	18.18	3.801	0.571	4.179	0.503	4.459	0.726
0.06695	540	18.52	3.363	0.376	3.680	0.382	3.954	0.451
0.06571	530	18.87	2.978	0.322	3.268	0.316	3.440	0.281
0.06447	520	19.23	2.609	0.340	2.903	0.281	2.977	0.243
0.06323	510	19.61	2.298	0.372	2.557	0.270	2.592	0.273
0.06199	500	20.00	2.008	0.443	2.204	0.283	2.256	0.323
0.06075	490	20.41	1.698	0.498	1.806	0.334	1.894	0.378
0.05951	480	20.83	1.309	0.713	1.296	0.505	1.455	0.508
0.05827	470	21.28	1.030	1.215	0.867	1.230	0.949	0.998
0.05703	460	21.74	1.307	1.299	1.542	1.289	1.458	1.365
0.05579	450	22.22	0.819	1.376	0.810	1.260	0.894	1.230
0.05455	440	22.73	0.624	1.847	0.541	1.831	0.560	1.784
0.05331	430	23.26	0.604	2.383	0.498	2.348	0.469	2.334
0.05207	420	23.81	0.748	2.873	0.545	2.844	0.527	2.857
0.05083	410	24.39	0.994	3.339	0.678	3.341	0.673	3.384
0.04959	400	25.00	1.354	3.714	0.865	3.861	0.913	3.943
0.04835	390	25.64	1.791	4.129	1.212	4.567	1.350	4.598
0.04711	380	26.32	2.650	4.537	2.213	5.416	2.289	5.277
0.04587	370	27.03	4.144	3.916	4.398	4.970	4.339	5.135
0.04463	360	27.78	3.991	2.009	4.442	2.650	4.755	2.608
0.04339	350	28.57	2.658	1.725	2.908	1.945	3.118	1.732
0.04215	340	29.41	1.448	2.630	1.546	2.857	1.725	2.576
0.04092	330	30.30	1.714	4.258	1.398	4.644	1.405	4.223
0.03968	320	31.25	3.979	5.776	3.141	7.097	3.054	6.689
0.03844	310	32.26	5.468	3.144	7.877	3.970	7.339	3.971
0.03720	300	33.33	4.736	1.561	5.614	1.255	5.553	1.303
0.03596	290	34.48	3.415	1.081	3.859	0.875	3.832	0.730
0.03472	280	35.71	2.037	1.411	2.060	1.338	1.942	1.142
0.03348	270	37.04	1.048	3.226	1.058	3.487	1.079	3.228
0.03224	260	38.46	2.081	5.458	1.569	6.282	1.436	5.666

(continued)

TABLE I *(Continued)*

Lithium Tantalate

eV	cm^{-1}	μm	$n_\perp$	$k_\perp$	$n_\perp$	$k_\perp$	$n_\perp$	$k_\perp$
0.03100	250	40.00	5.409	5.824	8.997	8.705	5.581	7.540
0.02976	240	41.67	5.967	3.231	7.365	2.041	7.966	3.011
0.02852	230	43.48	5.538	2.043	6.450	0.921	6.248	1.143
0.02728	220	45.45	4.732	1.537	5.017	0.376	4.861	0.642
0.02604	210	47.62	4.285	1.164	3.855	0.293	3.762	0.501
0.02480	200	50.00	2.595	0.829	2.531	0.406	2.364	0.557
0.02356	190	52.63	0.883	2.352	0.705	1.797	0.896	1.976
0.02232	180	55.56	1.159	4.311	0.515	3.796	0.409	3.787
0.02108	170	58.82	1.596	5.845	0.653	5.655	0.443	5.665
0.01984	160	62.50	2.461	7.855	1.137	8.124	0.881	8.340
0.01860	150	66.67	6.245	10.345	3.288	12.701	4.150	12.382
0.01736	140	71.43	11.762	7.685	17.429	10.457	12.580	10.900
0.01612	130	76.92	11.076	2.801	12.825	1.876	13.134	3.878
0.01488	120	83.33	9.729	1.158	10.319	0.780	10.668	1.620
0.01364	110	90.91	8.426	0.670	9.077	0.443	9.331	1.123
0.01240	100	100.0	7.904	0.483	8.331	0.289	8.662	0.925
0.01116	90	111.1		0.433 [b]	7.834	0.204	8.198	0.746
0.009919	80	125.0		0.321	7.482	0.151	7.902	0.618
0.008679	70	142.9		0.226	7.222	0.115	7.657	0.486
0.007439	60	166.7		0.156	7.026	0.088	7.454	0.416
0.006199	50	200.0			6.878	0.067	7.308	0.366
0.004959	40	250.0			6.767	0.050	7.239	0.337
0.003720	30	333.3			6.686	0.036	7.211	0.290
0.002480	20	500.0			6.631	0.023	7.210	0.207
0.001240	10	1000.0			6.599	0.011		

[b] Calculated from absorption coefficient of Ref. [7].

TABLE II

Values of $n_\parallel$ and $k_\parallel$ for Lithium Tantalate from Various References

eV	cm^{-1}	μm	$n_\parallel$	$k_\parallel$	$n_\parallel$	$k_\parallel$	$n_\parallel$	$k_\parallel$
2.755	22222	0.45	2.2468 [6]					
2.480	20000	0.50	2.2205					
2.066	16667	0.60	2.1878					
1.771	14286	0.70	2.1696					
1.550	12500	0.80	2.1578					
1.378	11111	0.90	2.1493					
1.240	10000	1.00	2.1432					
1.033	8333	1.20	2.1341					
0.8856	7143	1.40	2.1273					
0.7749	6250	1.60	2.1213					
0.6888	5556	1.80	2.1170					
0.6199	5000	2.00	2.1115					
0.5636	4545	2.20	2.1053					
0.5166	4167	2.40	2.0993					
0.4769	3846	2.60	2.0936					
0.4428	3571	2.80	2.0871					
0.4133	3333	3.00	2.0799					
0.3875	3125	3.20	2.0727					
0.3647	2941	3.40	2.0649					
0.3444	2778	3.60	2.0561					
0.3263	2632	3.80	2.0473					
0.3100	2500	4.00	2.0377					
0.2108	1700	5.882			1.932 [7]			
0.2095	1690	5.917			1.929			
0.2083	1680	5.952			1.925			

(continued)

TABLE II *(Continued)*

Lithium Tantalate

eV	cm^{-1}	μm	$n_{\parallel}$	$k_{\parallel}$	$n_{\parallel}$	$k_{\parallel}$	$n_{\parallel}$	$k_{\parallel}$
0.2071	1670	5.988			1.921			
0.2058	1660	6.024			1.918			
0.2046	1650	6.061			1.914			
0.2033	1640	6.098			1.910			
0.2021	1630	6.135			1.905			
0.2009	1620	6.173			1.900			
0.1996	1610	6.211			1.895			
0.1984	1600	6.250			1.890			
0.1971	1590	6.289			1.885			
0.1959	1580	6.329			1.880			
0.1947	1570	6.369			1.875			
0.1934	1560	6.410			1.870			
0.1922	1550	6.452			1.866			
0.1909	1540	6.494			1.861			
0.1897	1530	6.536			1.856			
0.1885	1520	6.579			1.851			
0.1872	1510	6.623			1.846			
0.1860	1500	6.667			1.841			
0.1847	1490	6.711			1.837		1.905 [a]	0.012 [a]
0.1835	1480	6.757			1.832		1.900	0.012
0.1823	1470	6.803			1.827		1.895	0.013
0.1810	1460	6.849			1.822		1.890	0.013
0.1798	1450	6.897			1.817		1.885	0.013
0.1785	1440	6.944			1.812		1.880	0.013
0.1773	1430	6.993			1.808		1.875	0.013
0.1761	1420	7.042			1.803		1.870	0.014
0.1748	1410	7.092			1.798		1.864	0.014

[a] Best fit of model Eq. (2) to reflectivity data of Ref. [11].

0.1736	1400	7.143	1.793	1.858	0.014
0.1723	1390	7.194	1.788	1.853	0.014
0.1711	1380	7.246	1.783	1.846	0.015
0.1699	1370	7.299	1.778	1.840	0.015
0.1686	1360	7.353	1.773	1.834	0.015
0.1674	1350	7.407	1.768	1.827	0.015
0.1661	1340	7.463	1.763	1.820	0.016
0.1649	1330	7.519	1.758	1.813	0.016
0.1637	1320	7.576	1.752	1.806	0.016
0.1624	1310	7.634	1.747	1.799	0.017
0.1612	1300	7.692	1.741	1.791	0.017
0.1599	1290	7.752	1.735	1.783	0.017
0.1587	1280	7.813	1.729	1.775	0.018
0.1575	1270	7.874	1.716	1.766	0.018
0.1562	1260	7.937	1.704	1.757	0.019
0.1550	1250	8.000	1.691	1.748	0.019
0.1537	1240	8.065	1.680	1.738	0.020
0.1525	1230	8.130	1.668	1.729	0.020
0.1513	1220	8.197	1.656	1.718	0.021
0.1500	1210	8.264	1.645	1.708	0.021
0.1488	1200	8.333	1.634	1.697	0.022
0.1475	1190	8.403	1.622	1.685	0.022
0.1463	1180	8.475	1.611	1.673	0.023
0.1451	1170	8.547	1.599	1.661	0.023
0.1438	1160	8.621	1.587	1.648	0.024
0.1426	1150	8.696	1.576	1.634	0.025
0.1413	1140	8.772	1.564	1.620	0.026
0.1401	1130	8.850	1.551	1.606	0.027
0.1389	1120	8.929	1.539	1.590	0.027
0.1376	1110	9.009	1.526	1.574	0.028
0.1364	1100	9.091	1.513	1.557	0.029

(continued)

TABLE II *(Continued)*

Lithium Tantalate

eV	cm^{-1}	μm	$n_{\parallel}$	$k_{\parallel}$	$n_{\parallel}$	$k_{\parallel}$	$n_{\parallel}$	$k_{\parallel}$
0.1351	1090	9.174			1.499		1.539	0.031
0.1339	1080	9.259			1.484		1.520	0.032
0.1327	1070	9.346			1.465		1.501	0.033
0.1314	1060	9.434			1.436		1.480	0.034
0.1302	1050	9.524			1.412		1.458	0.036
0.1289	1040	9.615			1.389		1.435	0.037
0.1277	1030	9.709			1.366		1.410	0.039
0.1265	1020	9.804			1.343		1.383	0.041
0.1252	1010	9.901			1.319		1.355	0.043
0.1240	1000	10.00	1.275 [11]		1.293		1.325	0.046
0.1227	990	10.10	1.208		1.264		1.293	0.049
0.1215	980	10.20	1.176		1.230		1.258	0.052
0.1203	970	10.31	1.143		1.177		1.221	0.055
0.1190	960	10.42	1.112		1.153		1.180	0.059
0.1178	950	10.53	1.068		1.144		1.135	0.064
0.1165	940	10.64	1.030	0.011 [11]	1.122	0.002 [7]	1.087	0.070
0.1153	930	10.75	0.978	0.003	1.066	0.042	1.032	0.077
0.1141	920	10.87	0.920	0.023	0.992	0.055	0.972	0.086
0.1128	910	10.99	0.853	0.031	0.920	0.068	0.903	0.097
0.1116	900	11.11	0.799	0.042	0.871	0.038	0.824	0.112
0.1103	890	11.24	0.713	0.048	0.841	0.006	0.732	0.134
0.1091	880	11.36	0.605	0.063	0.788	0.001	0.621	0.169
0.1079	870	11.49	0.462	0.120	0.672	0.001	0.488	0.234
0.1066	860	11.63	0.336	0.246	0.522	0.023	0.358	0.362
0.1054	850	11.76	0.265	0.394	0.403	0.117	0.293	0.525
0.1041	840	11.90	0.237	0.521	0.293	0.225	0.267	0.652
0.1029	830	12.05	0.201	0.631	0.233	0.377	0.227	0.768

0.1017	820	12.20	0.168	0.755	0.191	0.500	0.192	0.900
0.1004	810	12.35	0.150	0.879	0.152	0.621	0.173	1.033
0.09919	800	12.50	0.141	1.000	0.137	0.762	0.164	1.164
0.09795	790	12.66	0.137	1.116	0.127	0.886	0.160	1.294
0.09671	780	12.82	0.135	1.234	0.122	1.007	0.161	1.424
0.09547	770	12.99	0.136	1.354	0.121	1.137	0.165	1.556
0.09423	760	13.16	0.142	1.478	0.138	1.258	0.172	1.692
0.09299	750	13.33	0.153	1.605	0.152	1.369	0.184	1.834
0.09175	740	13.51	0.169	1.735	0.162	1.486	0.200	1.984
0.09051	730	13.70	0.189	1.869	0.172	1.609	0.224	2.142
0.08927	720	13.89	0.211	2.011	0.188	1.745	0.257	2.313
0.08803	710	14.08	0.241	2.168	0.215	1.883	0.303	2.496
0.08679	700	14.29	0.290	2.336	0.247	2.028	0.368	2.691
0.08555	690	14.49	0.359	2.502	0.289	2.182	0.459	2.896
0.08431	680	14.71	0.438	2.677	0.341	2.343	0.577	3.098
0.08307	670	14.93	0.537	2.852	0.407	2.516	0.713	3.287
0.08183	660	15.15	0.656	3.008	0.487	2.691	0.836	3.465
0.08059	650	15.38	0.698	3.152	0.567	2.852	0.919	3.682
0.07935	640	15.63	0.717	3.419	0.597	3.088	0.986	4.014
0.07811	630	15.87	0.781	3.822	0.663	3.443	1.112	4.537
0.07687	620	16.13	0.964	4.458	0.858	3.911	1.440	5.350
0.07563	610	16.39	1.577	5.375	1.263	4.640	2.401	6.618
0.07439	600	16.67	3.338	6.328	2.407	5.274	5.687	7.585
0.07315	590	16.95	5.713	4.842	4.436	5.134	8.143	3.503
0.07191	580	17.24	5.925	2.732	5.212	3.122	6.638	1.320
0.07067	570	17.54	5.248	1.514	4.722	2.070	5.529	0.685
0.06943	560	17.86	4.592	1.044	4.335	1.484	4.814	0.434
0.06819	550	18.18	4.133	0.779	3.888	1.116	4.311	0.312
0.06695	540	18.52	3.738	0.608	3.609	0.943	3.932	0.244
0.06571	530	18.87	3.408	0.537	3.337	0.809	3.627	0.203
0.06447	520	19.23	3.156	0.524	3.070	0.735	3.372	0.178

(continued)

TABLE II *(Continued)*

Lithium Tantalate

eV	cm^{-1}	μm	$n_{\parallel}$	$k_{\parallel}$	$n_{\parallel}$	$k_{\parallel}$	$n_{\parallel}$	$k_{\parallel}$
0.06323	510	19.61	2.981	0.513	2.914	0.711	3.150	0.162
0.06199	500	20.00	2.816	0.487	2.773	0.672	2.949	0.152
0.06075	490	20.41	2.649	0.457	2.643	0.621	2.763	0.148
0.05951	480	20.83	2.493	0.439	2.507	0.583	2.584	0.146
0.05827	470	21.28	2.331	0.424	2.383	0.525	2.408	0.149
0.05703	460	21.74	2.173	0.417	2.207	0.486	2.230	0.155
0.05579	450	22.22	2.006	0.419	2.019	0.473	2.044	0.165
0.05455	440	22.73	1.831	0.426	1.836	0.478	1.845	0.181
0.05331	430	23.26	1.635	0.441	1.633	0.496	1.623	0.206
0.05207	420	23.81	1.407	0.458	1.429	0.528	1.363	0.249
0.05083	410	24.39	1.118	0.511	1.134	0.521	1.041	0.334
0.04959	400	25.00	0.710	0.660	0.725	0.733	0.646	0.560
0.04835	390	25.64	0.457	1.072	0.465	1.119	0.387	0.991
0.04711	380	26.32	0.347	1.446	0.394	1.531	0.302	1.400
0.04587	370	27.03	0.324	1.798	0.415	1.864	0.294	1.773
0.04463	360	27.78	0.410	2.124	0.529	2.118	0.424	2.083
0.04339	350	28.57	0.399	2.215	0.513	2.211	0.368	2.126
0.04215	340	29.41	0.256	2.482	0.358	2.476	0.237	2.446
0.04092	330	30.30	0.217	2.817	0.323	2.818	0.203	2.779
0.03968	320	31.25	0.211	3.137	0.329	3.164	0.192	3.112
0.03844	310	32.26	0.203	3.487	0.381	3.529	0.191	3.458
0.03720	300	33.33	0.220	3.865	0.460	3.892	0.198	3.829
0.03596	290	34.48	0.247	4.280	0.553	4.279	0.211	4.240
0.03472	280	35.71	0.293	4.750	0.669	4.713	0.235	4.706
0.03348	270	37.04	0.356	5.302	0.844	5.232	0.273	5.248
0.03224	260	38.46	0.476	5.980	1.119	5.794	0.338	5.902
0.03100	250	40.00	0.720	6.835	1.546	6.449	0.450	6.723

0.02976	240	41.67	1.179	7.901	2.176	7.017	0.659	7.809
0.02852	230	43.48	2.088	9.176	2.818	7.678	1.107	9.354
0.02728	220	45.45	3.886	10.580	4.044	8.653	2.294	11.765
0.02604	210	47.62	7.019	10.982	6.104	8.727	6.685	15.217
0.02480	200	50.00	10.181	9.309	7.970	7.654	15.148	10.271
0.02356	190	52.63	11.441	6.088	8.955	6.460	13.288	4.126
0.02232	180	55.56	10.919	3.643	9.902	4.964	11.150	2.352
0.02108	170	58.82	9.839	2.296	9.387	2.934	9.830	1.667
0.01984	160	62.50	8.906	1.685	8.906	2.242	8.969	1.330
0.01860	150	66.67	8.256	1.431	8.425	1.629	8.374	1.138
0.01736	140	71.43	7.850	1.301	7.915	1.261	7.945	1.017
0.01612	130	76.92	7.548	1.168	7.607	1.020	7.630	0.932
0.01488	120	83.33	7.345	1.102	7.311	0.812	7.396	0.868
0.01364	110	90.91	7.181	1.014	7.052	0.660	7.222	0.814
0.01240	100	100.0	7.089	0.964	6.793	0.575	7.093	0.764
0.01116	90	111.1	7.018	0.882		0.566 [b]	7.001	0.713
0.009919	80	125.0	6.952	0.793		0.419	6.937	0.658
0.008679	70	142.9	6.933	0.695		0.284	6.894	0.598
0.007439	60	166.7	6.895	0.611		0.161	6.867	0.531
0.006199	50	200.0	6.879	0.512			6.852	0.457
0.004959	40	250.0	6.858	0.415			6.845	0.375
0.003720	30	333.3	6.849	0.309			6.843	0.288
0.002480	20	500.0	6.862	0.223			6.843	0.195
0.001240	10	1000.0					6.844	0.098

[b] Calculated from absorption coefficient of Ref. [7].

Potassium Iodide (KI)

MICHAEL E. THOMAS
Applied Physics Laboratory
The Johns Hopkins University
Laurel, Maryland

Potassium iodide offers a wide range of transparency, from the ultraviolet to the far infrared (0.25 to 38 μm). It is a soft material (Knoop scale 5 kg/mm^2) that is easily scratched, and it is highly hygroscopic. It has a flexure strength less than that of KBr (11 MPa). These mechanical properties limit the general utility of this optical material.

Potassium iodide is a cubic crystal with the sodium-chloride structure, space group Fm3m (O_h^5), with four formula units per unit cell. The lattice constant is 7.06555 Å, giving a theoretical density of 3.126 g/cm^3. The atomic arrangement is potassium atoms occupy the 4(a) sites and the iodine atoms occupy the 4(b) sites (both sites with m3m or O_h symmetry). Melting point is 954 K.

Ultraviolet reflectance of bulk KI was measured by Blechschmidt *et al.* [1] from 12 to 27 eV at room temperature. A Kramers–Kronig analysis yielded the optical constants in this spectral range. Tomiki *et al.* [2] measured the room-temperature (295 K) reflectance from 5 to 9 eV. Unfortunately, only the imaginary part of the permittivity was published. To complete the data set for this review, a Hilbert transform of the imaginary part of the permittivity was numerically computed to obtain the real part. The result was checked against the measured reflectance for validation. Knowing the permittivity, the optical constants were obtained. These data are listed in Table I and plotted in Fig. 1.

The Urbach tail represents absorption below the band gap, defining the end of bulk transparency. The room-temperature absorption coefficient was determined from transmission measurements by Tomiki *et al.* [3] in the spectral range from 5.0 to 5.4 eV and fitted to the functional form

$$\beta_{\text{abs}}(E,T) = \beta_{\text{U0}}\exp[\sigma_{\text{s}}(T)(E - E_{\text{g}})/k_{\text{B}}T], \tag{1}$$

where β_{abs} is the absorption coefficient (typically in units of cm^{-1}); β_{U0} is a scaling coefficient in units of cm^{-1}; E_{g} is the band-gap energy at absolute-

HANDBOOK OF OPTICAL CONSTANTS OF SOLIDS III

Copyright © 1998 by Academic Press.
All rights of reproduction in any form reserved
ISBN 0-12-544423-0/$25.00.

zero temperature, typically given in units of eV; k_B is Boltzmann's constant; and T is temperature in Kelvins. The exponential factor $\sigma_s(T)$ is given by the equation

$$\sigma_s(T) = \sigma_0 \frac{2k_B T}{E_P} \tanh \frac{E_P}{2k_B T}, \tag{2}$$

where E_p is an effective acoustic-phonon energy of the material. The Urbach tail parameters for KI are $\beta_{U0} = 6.0 \times 10^9$ cm^{-1}, $E_g = 5.890$ eV, $\sigma_0 = 0.83$, and $E_p = 0.0045$ eV. Additional measurements of the Urbach edge covering the temperature range from 300 to 900 K are reported by Matienssen [4]. The room-temperature (295 K) values for k in Table I and Fig. 1 for this spectral region are generated using Eqs. (1) and (2).

The room-temperature (20° C) index of refraction from the ultraviolet to the far infrared (0.25 to 50 μm) has been determined by Li [5] using data from a variety of different sources. A Sellmeier model of the form

$$n^2(\lambda,T) = 1 + \sum_i \frac{\lambda^2 \Delta\epsilon_i(T)}{\lambda^2 - \lambda_i^2(T)} \tag{3}$$

is used to represent the data accurately. A Sellmeier model determined from a single consistent data sets at 311 K and 339 K is reported by Ramachandran [6]. Model parameters are listed in Table II. Because the Sellmeier model has a physical basis, the extrapolation to higher frequencies beyond the experimental limit is justified. The values for n in Table I and Fig. 1 for the spectral regions indicated are generated by the Sellmeier formula. Experimental results are reported by Korth [7] from 0.55 to 29 μm at a temperature of 311 K. Experimental results in the visible region are reported by Lowndes and Martin [8] at temperatures of 2 and 290 K. Near-room-temperature thermo-optic coefficients measured at different wavelengths are listed in Table III [7, 9, 10]. Notice that the thermo-optic coefficients at wavelengths longer than 0.3 μm are negative. This gives KI some athermal performance as an optical element. An athermal material has the property that

$$\frac{d(n(T)L(T))}{dT} = 0.$$

The value of the optical-path derivative as given above for KI is $15.7 \times 10^{-6} nL$ per Kelvin at visible and near-infrared wavelengths. Thus, KI is useful for optical designs in the far infrared that require some insensitivity to temperature.

The multiphonon absorption (multiple-quanta lattice vibrations) edge marks the end of infrared transparency. Absorption-coefficient measurements are represented by the simple formula [11]

$$\beta_{abs}(\nu) = \beta_0 \exp\left(-\gamma \frac{\nu}{\nu_0}\right), \tag{4}$$

where for KI, $\beta_0 = 4294\ cm^{-1}$ and $\nu_0/\gamma = 35.1\ cm^{-1}$ at room temperature. The values of k in the spectral range from 225 to 500 cm^{-1} in Table I and Fig. 1 are obtained from this formula. The data cover the three-phonon to four-phonon regions. Temperature-dependent data on the absorption coefficient are described in Li [11]. A temperature-dependent multiphonon model has been developed by Thomas *et al.* [12] and applied to KI. Measurements in the two-phonon region are reported by Berg and Bell [13] and Pai *et al.* [14]. These results are listed in Table I and plotted in Fig. 1.

The one-phonon (one-quanta fundamental lattice vibrations) region is opaque and therefore characterized by reflectance measurements. Room-temperature reflectance measurement is reported by Berg and Bell [13]. Room-temperature measurement using a dispersive Fourier transform spectrometer is reported by Pai *et al.* [14]. The classical-oscillator model is often used to fit the reflectance data and then to derive the optical constants. The classical-oscillator model is expressed in terms of the relative permittivity, $\epsilon_r(\nu,T)$, as[1]

$$\epsilon_r(\nu,T) = \epsilon_\infty(T) + \sum_i \frac{\Delta\epsilon_i(T)\nu_i^2(T)}{\nu_i^2(T) - \nu^2 + j\Gamma_i(\nu,T)\nu}, \tag{5}$$

where $\Delta\epsilon_i(T)$, $\Gamma_i(\nu,T)$, and $\nu_i(T)$ are the ith-mode strength, line width, and long-wavelength transverse optical frequency, ν_{TO}, respectively. The sum on i is over all transverse optical modes. For KI, there is only one allowed infrared active vibrational mode based on group theory of a perfect lattice. This is formally stated as

$$\Gamma = F_{1u}(\text{IR}).$$

The mode is infrared active (mode 1 in Table IV). Table IV lists the classical-oscillator-model parameters used to fit the experimental data [15]. More than one mode is needed to account for impurities and defects in real materials. Also, the high-frequency edge of the reflectance spectrum must include two-phonon contributions (see mode 2 in Table IV). A complete theoretical description of the infrared properties of KI is given by Hardy and Karo [16]. Unfortunately, the value of ϵ_∞ used by Hadni *et al.* [15] is not consistent with the value from the Sellmeier model mentioned previously. For this reason the joining of the Sellmeier model and the one-phonon model is not smooth. Good agreement with the static dielectric constant is obtained. The n and k values in Table I and Fig. 1 come from Berg and Bell [13] and Pai *et al.* [14].

[1] The expression uses the engineering convention for a time harmonic field of $\exp(-j\omega t)$. To convert to the convention commonly used in the *HOC* series use $i = -j$.

Below ν_{TO}, the index of refraction, n, and the extinction coefficient, k, have been measured by Berg and Bell [13], and Pai *et al* [13]. Table I and Fig. 1 list and display the resulting values.

The static-dielectric-constant data is the sum of all the strengths of higher-frequency oscillators including vibrational and electronic. Using Eq. (5), the static dielectric constant, $\epsilon_s(T) = \epsilon_r'(0,T)$, becomes

$$\epsilon_s(T) = \epsilon_\infty(T) + \sum_i \Delta\, \epsilon_i(T). \tag{6}$$

Based on the parameters listed in Table IV, we expect the value of ϵ_s to be 5.11. Experimental results, obtained from capacitance bridges operating from 1 kHz to 1 MHz, microwave techniques, or reflection measurements using a Fourier transform spectrometer produce values from 5.00 to 5.12, with the best results closer to the higher value [5, 10, 13, 16, 17]. The representative refractive index value is $n_s = 2.256$. The static-index values incorrectly are located at 1×10^4 μm in Fig. 1; however, there is little difference in the value of n_s at the measured wavelength and the plotted wavelength.

Whenever possible, physically based models are used to represent experimental measurements in Table I and Fig. 1. The models tend to reduce noise and allow interpolation and extrapolation to obtain meaningful results where no experimental data exists. In some case, the models discussed in this section also allow temperature-dependent data to be obtained.

REFERENCES

1. D. Blechschmidt, R. Klucker and M. Skibowski, Dielectric properties of KCl, KBr, and KI single crystals in the extreme ultraviolet up to 35 eV. *Phys. Status Solidi* **36**, 625–634 (1959).
2. T. Tomiki, T. Miyata, and H. Tsukamoto, Temperature dependence of the fundamental spectra of potassium-halides in the Schumann ultraviolet (4.4–13.5 eV), *J. Phys. Soc. Jpn.* **35**, 495–507 (1973).
3. T. Tomiki, T. Mayata, and H. Tsukamoto, The Urbach rule for the sodium- and potassium-halides. *Z. Naturforsch.* **29A**, 145–157 (1974).
4. W. Martienssen, The optical absorption edge in ionic crystals. *J. Phys. Chem. Solids* **8**, 294–296 (1959).
5. H. H. Li, Refractive index of alkali halides and its wavelength and temperature derivatives. *J. Phys. Chem. Ref. Data* **5**, 329–528 (1976).
6. G. N. Ramachandran, Thermo-optic behavior of solids V. Alkali halides. *Proc. Indian Acad. Sci. Sect. A* **25**, 481–497 (1947).
7. K. Korth, Dispersion measurements on potassium bromide and potassium iodide in the infrared region. *Z. Phys.* **84**, 677–685 (1933).
8. R. P. Lowndes and D. H. Martin, Dielectric dispersion and the structures of ionic lattices. *Proc. R. Soc. London A* **308**, 473–496 (1969).
9. H. Harting, The optical aspect of some crystals and their representation by the Hartmann equation. *Z. Instrum.* **63**, 125–131 (1943).
10. R. P. Lowndes and D. H. Martin, Dielectric constants of ionic crystals and their variations with temperature and pressure. *Proc. R. Soc. London A* **316**, 351–375 (1970).

11. H. H. Li, The infrared absorption coefficient of alkali halides. *Int. J. Thermophys.* **1**, 97–134 (1980).
12. M. E. Thomas, R. I. Joseph, and W. J. Tropf, Infrared transmission properties of sapphire, spinel, yttria and ALON as a function of temperature and frequency. *Appl. Opt.* **27**, 239–245 (1988); M. E. Thomas, Temperature dependence of the complex didex of refraction. *in* "Handbook of Optical Constants of Solids II" (E. D. Palik, ed.), Chap 8, pp. 177–201. Orlando, Florida, Academic Press, 1991; M. E. Thomas, A computer code for modeling optical properties of window materials, in window and dome technologies and materials. *Proc. of SPIE* **1112**, 260–267 (1989).
13. J. I. Berg and E. E. Bell, Far-infrared optical constants of KI. *Phys. Rev.* **B 4**, 3572–3580 (1971).
14. K. F. Pai, T. J. Parker, N. E. Tornberg, R. P. Lowndes and W. G. Chambers, Determination of the complex refractive indices of solids in the far-infrared by dispersive fourier transform spectroscopy-I. Alkali halides. *Infrared Phys.* **18**, 199–214 (1978).
15. A. Hadni, J. Claudel, G. Morlet, and P. Strimer, Transmission and reflection spectra of pure and doped potassium iodide at low temperatures. *Appl. Opt.* **7**, 161–165 (1968).
16. J. R. Hardy and A. M. Karo, Theoretical study of the long-wavelength optical properties of NaCl, KCl, KBr and KI. *Phys. Rev.* **B 26**, 3327–3337 (1982).
17. C. Demau, Measurement of the dielectric constants and dielectric anisotropies of various crystals at X-band. *J. Phys. (Paris)* **24**, 284–285 (1963).

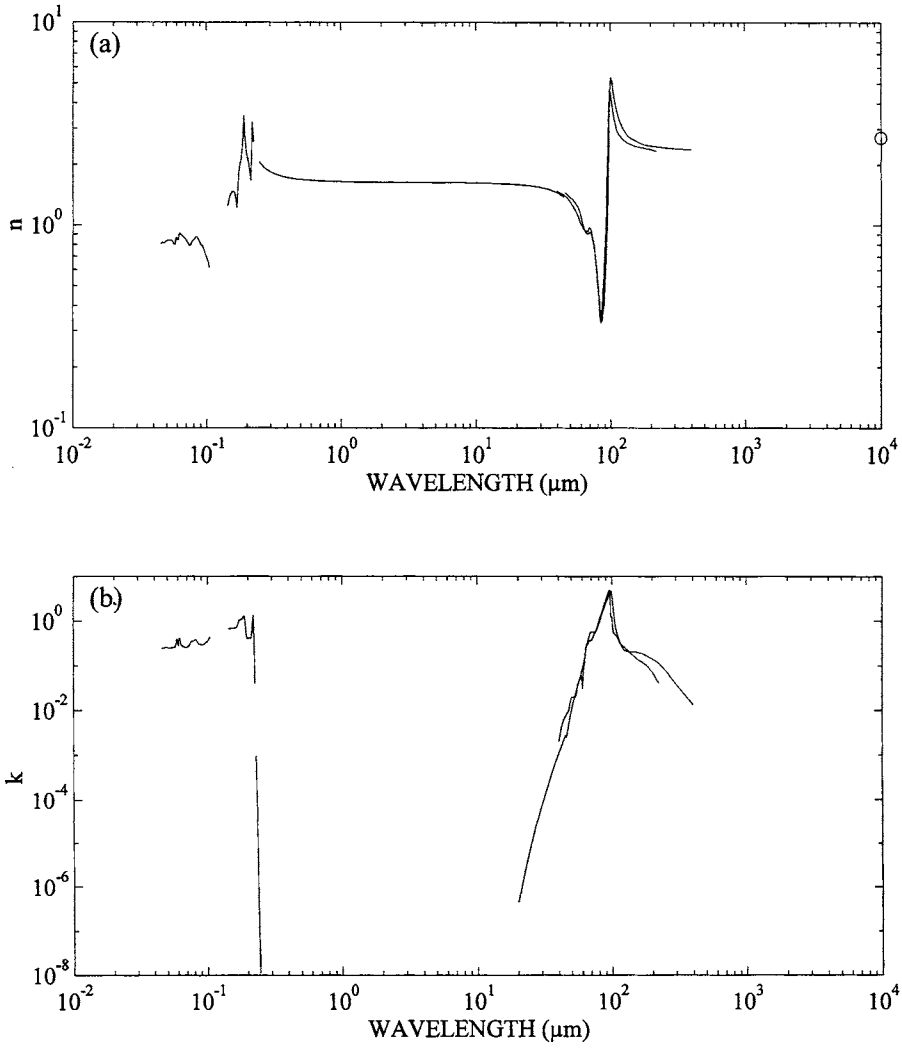

Fig. 1. (a) Log–log plot of the room-temperature index of refraction, n, for KI versus wavelength in micrometers. (b) Log–log plot of the room-temperature extinction coefficient, k, for KI versus wavelength in micrometers. Isolated data points are indicated with a symbol.

TABLE I

Values of n and k for Potassium Iodide from Various References[a]

eV	cm^{-1}	μm	n	k
27.34	220500	0.04536	0.8020 [1]	0.2474 [1]
26.65	214900	0.04653	0.8210	0.2464
26.07	210200	0.04757	0.8122	0.2507
25.76	207800	0.04813	0.8097	0.2548
25.27	203800	0.04907	0.8198	0.2614
24.84	200400	0.04991	0.8314	0.2547
24.52	197700	0.05057	0.8339	0.2500
24.10	194400	0.05145	0.8370	0.2467
23.51	189600	0.05275	0.8403	0.2487
22.88	184600	0.05419	0.8412	0.2519
22.28	179700	0.05565	0.8296	0.2546
21.81	175900	0.05684	0.8029	0.2591
21.61	174300	0.05738	0.8002	0.2693
21.49	173300	0.05769	0.7988	0.2904
21.39	172500	0.05796	0.7976	0.3102
21.32	172000	0.05815	0.8043	0.3314
21.26	171500	0.05831	0.8147	0.3475
21.27	171500	0.05830	0.8140	0.3651
21.12	170400	0.05869	0.8379	0.3959
20.89	168500	0.05934	0.8655	0.3807
20.81	167800	0.05958	0.8618	0.3653
20.78	167600	0.05965	0.8605	0.3451
20.64	166500	0.06008	0.8532	0.3067
20.53	165600	0.06040	0.8476	0.2746
20.48	165200	0.06054	0.8456	0.3082
20.50	165400	0.06048	0.8465	0.3306
20.42	164700	0.06071	0.8432	0.3545
20.20	163000	0.06137	0.8427	0.3973
20.10	162100	0.06169	0.8585	0.4219
19.99	161300	0.06201	0.8858	0.4050
19.96	161000	0.06212	0.8947	0.3873
19.81	159800	0.06259	0.9048	0.3420
19.79	159600	0.06265	0.9056	0.3275
19.75	159300	0.06277	0.9071	0.3139
19.64	158400	0.06314	0.9091	0.3020
19.52	157400	0.06352	0.9044	0.2898
19.31	155700	0.06421	0.8963	0.2772
19.07	153800	0.06503	0.8871	0.2677
17.97	145000	0.06899	0.8556	0.2527
16.94	136600	0.07319	0.8016	0.2775
16.86	136000	0.07355	0.7965	0.2906
16.80	135500	0.07382	0.7933	0.3061
16.64	134200	0.07452	0.7871	0.3193
16.60	133900	0.07470	0.7856	0.3411
16.26	131100	0.07627	0.8013	0.3458

(continued)

[a] References given in brackets.

TABLE I *(Continued)*

Potassium Iodide

eV	cm^{-1}	μm	n	k
15.95	128600	0.07775	0.8240	0.3532
15.72	126800	0.07889	0.8339	0.3590
15.59	125700	0.07954	0.8395	0.3648
15.53	125300	0.07983	0.8419	0.3745
15.15	122200	0.08186	0.8612	0.3898
15.08	121600	0.08222	0.8653	0.3798
15.02	121200	0.08252	0.8682	0.3708
14.77	119100	0.08393	0.8750	0.3394
14.65	118200	0.08463	0.8683	0.3280
14.36	115800	0.08635	0.8523	0.3039
13.65	110100	0.09081	0.7963	0.2951
13.27	107000	0.09343	0.7838	0.2996
12.66	102100	0.09790	0.7115	0.3367
12.60	101600	0.09838	0.7066	0.3403
12.42	100200	0.09984	0.6936	0.3507
12.00	96780	0.1033	0.6457	0.4120
11.92	96180	0.1040	0.6369	0.4264
11.84	95480	0.1047	0.6137	0.4411
8.610	69440	0.1440	1.242 [2]	0.675 [2]
8.486	68440	0.1461	1.281	0.684
8.362	67440	0.1483	1.369	0.6879
8.238	66440	0.1505	1.410	0.6841
8.114	65440	0.1528	1.437	0.683
7.990	64440	0.1552	1.456	0.6875
7.866	63440	0.1576	1.464	0.6895
7.742	62440	0.1601	1.459	0.6985
7.618	61440	0.1628	1.436	0.7025
7.494	60440	0.1654	1.343	0.7254
7.370	59440	0.1682	1.215	0.8313
7.246	58440	0.1711	1.431	1.003
7.122	57440	0.1741	1.777	1.061
6.998	56440	0.1772	1.961	1.069
6.874	55440	0.1804	2.069	1.101
6.750	54440	0.1837	2.318	1.206
6.626	53440	0.1871	2.742	1.298
6.502	52440	0.1907	3.449	0.9769
6.378	51440	0.1944	2.659	0.4732
6.254	50440	0.1982	2.284	0.3918
6.130	49440	0.2023	2.159	0.4171
6.006	48440	0.2064	2.055	0.4087
5.882	47440	0.2108	1.848	0.4104
5.758	46440	0.2153	1.655	0.76
5.634	45440	0.2201	3.219	1.3
5.510	44440	0.2250	2.583	0.040
5.391	43480	0.230	2.391 [5]	0.00095 [3]
5.344	43100	0.232	2.325	0.00021

TABLE I *(Continued)*

Potassium Iodide

eV	cm^{-1}	μm	*n*	*k*
5.298	42740	0.234	2.272	4.8E-5
5.254	42370	0.236	2.229	1.1E-5
5.209	42020	0.238	2.192	2.7E-6
5.166	41670	0.240	2.161	6.6E-7
5.123	41320	0.242	2.133	1.7E-7
5.081	40980	0.244	2.109	4.3E-8
5.040	40650	0.246	2.087	1.3E-8
4.959	40000	0.25	2.0493	
3.542	28571	0.35	1.7595	
2.755	22222	0.45	1.6979	
2.254	18182	0.55	1.6723	
1.907	15385	0.65	1.6589	
1.653	13333	0.75	1.6509	
1.458	11765	0.85	1.6457	
1.305	10526	0.95	1.6422	
1.181	9523.8	1.05	1.6396	
1.078	8695.7	1.15	1.6377	
0.9990	8000	1.25	1.6363	
0.9184	7407.4	1.35	1.6351	
0.8551	6896.6	1.45	1.6342	
0.7999	6451.6	1.55	1.6335	
0.7514	6060.6	1.65	1.6328	
0.7085	5714.3	1.75	1.6323	
0.6702	5405.4	1.85	1.6319	
0.6358	5128.2	1.95	1.6315	
0.6048	4878	2.05	1.6312	
0.5510	4444.4	2.25	1.6306	
0.5061	4081.6	2.45	1.6302	
0.4679	3773.6	2.65	1.6298	
0.4350	3508.8	2.85	1.6295	
0.4065	3278.7	3.05	1.6292	
0.3815	3076.9	3.25	1.6289	
0.3594	2898.6	3.45	1.6287	
0.3397	2739.7	3.65	1.6285	
0.3220	2597.4	3.85	1.6282	
0.3061	2469.1	4.05	1.628	
0.2917	2352.9	4.25	1.6278	
0.2786	2247.2	4.45	1.6276	
0.2666	2150.5	4.65	1.6274	
0.2556	2061.9	4.85	1.6272	
0.2455	1980.2	5.05	1.6270	
0.2362	1904.8	5.25	1.6268	
0.2275	1834.9	5.45	1.6266	
0.2194	1769.9	5.65	1.6264	
0.2119	1709.4	5.85	1.6262	
0.2049	1652.9	6.05	1.6259	

(continued)

TABLE I *(Continued)*

Potassium Iodide

eV	cm^{-1}	μm	n	k
0.1984	1600.0	6.25	1.6257	
0.1922	1550.4	6.45	1.6255	
0.1864	1503.8	6.65	1.6253	
0.1810	1459.9	6.85	1.6250	
0.1759	1418.4	7.05	1.6248	
0.1710	1379.3	7.25	1.6245	
0.1664	1342.3	7.45	1.6242	
0.1621	1307.2	7.65	1.6240	
0.1579	1273.9	7.85	1.6237	
0.1540	1242.2	8.05	1.6234	
0.1503	1212.1	8.25	1.6231	
0.1467	1183.4	8.45	1.6229	
0.1433	1156.1	8.65	1.6226	
0.1401	1129.9	8.85	1.6223	
0.1370	1105.0	9.05	1.6219	
0.1340	1081.1	9.25	1.6216	
0.1312	1058.2	9.45	1.6213	
0.1285	1036.3	9.65	1.6210	
0.1259	1015.2	9.85	1.6206	
0.1234	995.02	10.05	1.6203	
0.1210	975.61	10.25	1.6199	
0.1186	956.94	10.45	1.6196	
0.1164	938.97	10.65	1.6192	
0.1143	921.66	10.85	1.6188	
0.1122	904.98	11.05	1.6185	
0.1102	888.89	11.25	1.6181	
0.1083	873.36	11.45	1.6177	
0.1064	858.37	11.65	1.6173	
0.1046	843.88	11.85	1.6169	
0.1029	829.88	12.05	1.6164	
0.1012	816.33	12.25	1.6160	
0.09959	803.21	12.45	1.6156	
0.09801	790.51	12.65	1.6152	
0.09649	778.21	12.85	1.6147	
0.09501	766.28	13.05	1.6142	
0.09357	754.72	13.25	1.6138	
0.09218	743.49	13.45	1.6133	
0.09083	732.6	13.65	1.6128	
0.08952	722.02	13.85	1.6124	
0.08824	711.74	14.05	1.6119	
0.08701	701.75	14.25	1.6114	
0.08580	692.04	14.45	1.6108	
0.08463	682.59	14.65	1.6103	
0.08349	673.4	14.85	1.6098	
0.08238	664.45	15.05	1.6093	
0.08025	647.25	15.45	1.6082	

TABLE I *(Continued)*

Potassium Iodide

eV	cm^{-1}	μm	*n*	*k*		
0.07822	630.91	15.85	1.6071			
0.07630	615.38	16.25	1.6059			
0.07446	600.6	16.65	1.6047			
0.07272	586.51	17.05	1.6035			
0.07105	573.07	17.45	1.6022			
0.06946	560.22	17.85	1.6009			
0.06794	547.95	18.25	1.5996			
0.06648	536.19	18.65	1.5982			
0.06508	524.93	19.05	1.5968			
0.06374	514.14	19.45	1.5954			
0.06246	503.78	19.85	1.5939			
0.06199	500.0	20.0	1.5933	4.448E-7 [11]		
0.05904	476.1	21.0	1.5894	9.203E-7		
0.05636	454.5	22.0	1.5853	1.786E-6		
0.05391	434.8	23.0	1.5809	3.279E-6		
0.05166	416.7	24.0	1.5762	5.734E-6		
0.04959	400.0	25.0	1.5712	9.602E-6		
0.04769	384.6	26.0	1.5660	1.548E-5		
0.04592	370.4	27.0	1.5604	2.412E-5		
0.04428	357.1	28.0	1.5545	3.646E-5		
0.04275	344.8	29.0	1.5483	5.364E-5		
0.04133	333.3	30.0	1.5417	7.699E-5		
0.03999	322.6	31.0	1.5347	0.000109		
0.03874	312.5	32.0	1.5273	0.000149		
0.03757	303.0	33.0	1.5195	0.000201		
0.03647	294.1	34.0	1.5112	0.000267		
0.03542	285.7	35.0	1.5024	0.000349		
0.03444	277.8	36.0	1.4931	0.000450		
0.03351	270.3	37.0	1.4832	0.000573		
0.03263	263.2	38.0	1.4727	0.000720		
0.03179	256.4	39.0	1.4615	0.000896		
0.03100	250.0	40.0	1.4497	0.00110		
eV	cm^{-1}	μm	*n*	*k*	*n*	*k*
0.03024	243.9	41.0	1.4370	0.00134		
0.02952	238.1	42.0	1.4235	0.00163		
0.02883	232.6	43.0	1.4090	0.00195		
0.02818	227.3	44.0	1.3935	0.00232		
0.02755	222.2	45.0	1.3769	0.00274		
0.03100	250	40.0			1.47 [14]	0.002 [14]
0.02976	240	41.7			1.45	0.004
0.02852	230	43.5			1.43	0.006
0.02728	220	45.5	1.454 [13]	0.002 [13]	1.40	0.008
0.02666	215	46.5	1.437	0.004		
0.02604	210	47.6	1.424	0.005	1.37	0.01

(continued)

TABLE I *(Continued)*

Potassium Iodide

eV	cm^{-1}	μm	n	k	n	k
0.02542	205	48.8	1.400	0.007	1.34	0.015
0.02480	200	50.0	1.380	0.010	1.31	0.02
0.02418	195	51.3		0.014	1.28	0.02
0.02356	190	52.6	1.338	0.019	1.24	0.02
0.02331	188	53.2			1.23	0.02
0.02306	186	53.8			1.21	0.02
0.02294	185	54.1	1.305	0.027		
0.02281	184	54.4			1.19	0.025
0.02257	182	55.0			1.18	0.03
0.02232	180	55.6	1.272	0.035	1.16	0.04
0.02207	178	56.2			1.14	0.04
0.02182	176	56.8			1.13	0.045
0.02170	175	57.1	1.234	0.048		
0.02157	174	57.5			1.10	0.05
0.02133	172	58.1			1.08	0.05
0.02108	170	58.8	1.174	0.066	1.05	0.06
0.02083	168	59.5			1.02	0.05
0.02058	166	60.2			1.01	0.03
0.02046	165	60.6	1.083	0.092		
0.02033	164	61.0			1.00	0.07
0.02009	162	61.7			0.98	0.1
0.01984	160	62.5	0.984	0.149	0.96	0.15
0.01959	158	63.3	0.960	0.235	0.95	0.2
0.01934	156	64.1	0.938	0.275	0.94	0.26
0.01909	154	64.9	0.922	0.308	0.94	0.28
0.01885	152	65.8	0.912	0.342	0.93	0.31
0.01860	150	66.7	0.905	0.393	0.93	0.33
0.01835	148	67.6	0.904	0.453	0.93	0.35
0.01810	146	68.5	0.908	0.530	0.95	0.37
0.01785	144	69.4	0.915	0.558	0.97	0.36
0.01761	142	70.4	0.919	0.568	0.97	0.37
0.01736	140	71.4	0.913	0.564	0.95	0.4
0.01711	138	72.5	0.894	0.560	0.91	0.45
0.01686	136	73.5	0.862	0.564	0.86	0.5
0.01661	134	74.6	0.825	0.573	0.81	0.54
0.01637	132	75.8	0.778	0.593	0.75	0.59
0.01612	130	76.9	0.709	0.634	0.71	0.67
0.01587	128	78.1	0.615	0.710	0.64	0.77
0.01562	126	79.4	0.535	0.813	0.57	0.92
0.01537	124	80.6	0.464	0.942	0.49	1.11
0.01513	122	82.0	0.399	1.100	0.43	1.26
0.01488	120	83.3	0.351	1.277	0.38	1.42
0.01463	118	84.7	0.330	1.485	0.34	1.6
0.01438	116	86.2	0.340	1.714	0.38	1.87
0.01413	114	87.7	0.369	2.001	0.48	2.27
0.01389	112	89.3	0.425	2.342	0.59	2.75

TABLE I *(Continued)*

Potassium Iodide

eV	cm^{-1}	μm	n	k	n	k
0.01364	110	90.9	0.528	2.718	0.75	3.28
0.01339	108	92.6	0.682	3.169	1.03	3.96
0.01314	106	94.3	0.961	3.787	1.66	4.51
0.01289	104	96.2	1.597	4.387	2.92	4.88
0.01265	102	98.0	3.692	4.788	4.62	1.24
0.01240	100	100.0	5.371	3.770	4.54	1.24
0.01215	98	102.0	5.177	2.302	4.09	0.58
0.01190	96	104.2	4.742	1.168	3.72	0.51
0.01166	94	106.4	4.313	0.732	3.39	0.48
0.01141	92	108.7	3.976	0.543	3.16	0.45
0.01116	90	111.1	3.706	0.439	2.97	0.39
0.01091	88	113.6	3.503	0.359	2.88	0.33
0.01066	86	116.3	3.342	0.300	2.80	0.3
0.01042	84	119.1	3.197	0.254	2.75	0.28
0.01017	82	122.0	3.064	0.228	2.69	0.27
0.00992	80	125.0	2.974	0.213	2.65	0.25
0.00930	75	133.3	2.788	0.202	2.57	0.21
0.00868	70	142.9	2.694	0.203	2.51	0.17
0.00806	65	153.9	2.625	0.200	2.46	0.14
0.00744	60	166.7	2.555	0.187	2.44	0.12
0.00682	55	181.8	2.504	0.164	2.41	0.1
0.00620	50	200.0	2.475	0.139	2.38	0.07
0.00558	45	222.2	2.453	0.113	2.33	0.04
0.00496	40	250.0	2.433	0.077		
0.00434	35	285.7	2.409	0.046		
0.00372	30	333.3	2.390	0.026		
0.00310	25	400.0	2.372	0.013		
0.0	0	∞	2.256 [15]			

TABLE II

Room-Temperature Sellmeier Model Parameters

ith Mode	$\Delta\epsilon_i$	λ_i
Li model, $T = 293$ K, 0.25–50 μm [5]		
1	0.47285	0.0
2	0.41222	0.129
3	0.44163	0.175
4	0.16076	0.187
5	0.33571	69.44
6	1.92474	98.04
Ramachandran model, $T = 339$ K, 0.253–0.615 μm [6]		
1	0.4532	0.0
2	0.2150	0.1290
3	0.8027	0.1805
4	0.1780	0.2190
Ramachandran model, $T = 311$ K, 4.0–29.0 μm [6]		
1	1.6499	0.0
2	2.530	102.0

TABLE III

Thermo-optical Coefficients of Potassium Iodide

Wavelength (μm)	dn/dT (10^{-6}/K)	Measurement Temperature (°C)	Reference
0.24828	131	20	[9]
0.25365	102	20	[9]
0.26537	42	20	[9]
0.28936	0	20	[9]
0.54	−50	38	[7]
0.33415	−22	20	[9]
1.08303	−43	20	[9]
5.0	−45	20	[5]
10.0	−44	20	[5]
∞	373	27	[10]

TABLE IV

Room-Temperature Classical Oscillator-Model Parameters

Mode number i	ν_i [cm^{-1}]	$\Delta\epsilon_i$	Γ_i/ν_i	Reference
1	102	2.136	0.084	[15]
2	316	0.276	0.3	
		$\epsilon_\infty = 2.7$		

Potassium Niobate ($KNbO_3$)

IVAN BIAGGIO
Nonlinear Optics Laboratory
Institute of Quantum Electronics
Swiss Federal Institute of Technology
Zürich, Switzerland

Potassium niobate is a perovskite ferroelectric crystal with orthorhombic structure and space group Bmm2 at room temperature. Upon cooling from the high-temperature cubic phase, it undergoes a series of phase transitions to a tetragonal, orthorhombic, and rhombohedral phase at temperatures of 418, 203, and $-50°$ C, respectively. On heating, the orthorhombic-to-tetragonal phase transition takes place at 223° C. The orthorhombic nonprimitive unit cell contains twice as many atoms as the cubic phase primitive cell. The orthorhombic crystallographic a-axis is oriented along the (101) direction derived from the cube of the ideal perovskite structure, the b-axis is along (010), and the c-axis is along $(\bar{1}01)$. The $+c$-axis is, by definition, parallel to the spontaneous polarization. The corresponding lattice parameters are $a_o = 0.56896$ nm, $b_o = 0.39692$ nm, and $c_o = 0.57256$ nm [1, 2]. With this choice of crystallographic axes, the space group is labeled Bmm2, because the b-face of the orthorhombic unit cell is centered. It is important to note that the refractive indices in the visible spectral range obey $n_b > n_a > n_c$, and that, although this is the convention most often used in the optics literature relating to $KNbO_3$, another convention has been proposed [3, 4] and is sometimes used. In this alternative convention the a and b axes are interchanged with respect to the definition used here and the space group is labeled Amm2.

Index matching for second-harmonic generation is possible through angle and temperature tuning for fundamental wavelengths longer than 850 nm and up to a few micrometers [5].

The UV and band-edge data has been measured by Wiesendanger [6] up to a photon energy of 10 eV. Wiesendanger used single-domain crystals grown from a top-seeded, flux-growth technique, and poled a few degrees below the orthorhombic–tetragonal phase transition (poling of the crystal is performed by application of an electric field and makes sure that the ferro-

Copyright © 1998 by Academic Press.
All rights of reproduction in any form reserved
ISBN 0-12-544423-0/$25.00.

electric polarization is oriented in the same direction throughout the crystal sample). Vacuum-ultraviolet reflectivity was measured with polarized light at near-normal incidence in the range between 3 and 10 eV. Reproducibility of the reflectance values for each polarization was better than 0.01. Anisotropy effects are observed especially in the low-energy part below 7 eV, with differences in reflectivity up to 0.12. Above 7 eV these differences are less marked. The optical constants were derived from the measured reflectivity spectra by Kramers–Kronig analysis for every polarization. For the Kramers–Kronig analysis the data had to be extrapolated. Details of the extrapolation affected the absolute values of the optical constants but had little influence on the positions of the different peaks or on the relative magnitudes of the optical constants for different light polarizations. We take the (n, k) data directly from the plots published by Wiesendanger. Note that the k values are slightly too high in the low-energy region around 3.5 eV, especially for k_b. This is apparent when comparing to the band-edge absorption measurements presented later.

Mamedov and Gadzhieva [7] measured UV reflectivity up to a photon energy of 35 eV. We do not use their data here because it is not clear what the polarization of their light source was. Qualitatively, the structure they observe below 10 eV is similar to the measurements of Wiesendanger. Above 10 eV, the reflectivity slowly decreases, with a not-well-pronounced, strongly broadened maximum around 17 eV, which has a reflectivity more than 5 times smaller than the peaks observed below 10 eV.

Wiesendanger [6] also studied the band-edge absorption with polarized light in the energy range from 3.1 to 3.3 eV and found an Urbach-rule behavior, with the absorption coefficient α increasing exponentially with the photon energy. The slopes of the $\ln(\alpha)$ versus photon energy lines were the same for all polarization of the light, but the absorption for light polarized along b was approximately twice the absorption observed for light polarized along a or c. The latter was found to be 100 cm^{-1} at a photon energy of 3.31 eV. The data presented in the table is Wiesendanger's Urbach-rule fit to his absorption measurements.

Montemezzani *et al.* [8] measured the transmittivity of thin $KNbO_3$ crystals in a UV spectrophotometer between 3.2 and 3.5 eV for light polarized along the c- and the b-axis. The samples were prepared by gluing $KNbO_3$ platelets with polished a face onto fused-silica substrates using polymethyl methacrylate (PMMA) and subsequently polishing the crystals to final thicknesses of 25 and 70 μm. They obtained absorption-coefficient values with a precision of about 10% and observed the deviation from the Urbach-rule behavior for light energies higher than 3.3 eV. The results for the two samples were within the 10% error margin. The data we present in Tables IV–VI are the average of the data of both samples. Wiesendanger has shown that at the band edge the absorption for a- and c-polarized light is equal within experimental uncertainty. Therefore, we use the data measured by Montemezzani *et al.* with c-polarized light also in the table for k_a.

The refractive-index data in the wavelength range 400–3400 nm were measured by Zysset *et al.* [9] at six different temperatures between 22 and 180° C. The refractive indices were measured for the three light polarizations using the minimum-deviation technique and three different prisms. The prisms were obtained from high-optical-quality boules of nominally pure $KNbO_3$ grown by the top-seeded-solution technique [10]. All prisms had the *c*-axis oriented parallel to the apex of the prism. Two of them had the *b*-axis in the prism-bisecting plane, and a third one the *a*-axis. This allowed the measurement of n_a in one prism, measurements of n_b in two prisms, and measurements of n_c in all three samples. The orientation of the prisms was controlled by x-ray scattering to better than 30 arcmin, and the process of fabricating the prisms introduced an error of less than 30 arcmin. The refractive indices were measured at 22 different wavelengths between 404.66 and 3400 nm. The maximum error for a single data point was estimated to be ±0.0003. The scattering of the experimental data of the various samples was within the error margin. The data were fitted with a two-term Sellmeier oscillator model with an IR correction term:

$$n^2 - 1 = S_1 \frac{\lambda^2 \lambda_1^2}{\lambda^2 - \lambda_1^2} + S_2 \frac{\lambda^2 \lambda_2^2}{\lambda_2 - \lambda_2^2} - D\lambda^2, \tag{1}$$

where n is the refractive index at vacuum wavelength λ, S_i, λ_i are the strengths and wavelengths of the two UV oscillators, and D is the coefficient of an IR correction term. The term $-D\lambda^2$ is the limiting form of the complete oscillator term $S_{IR}/(\lambda_{IR}^{-2} - \lambda^{-2})$ when $\lambda << \lambda_{IR}$. The simplified form is enough to fit the refractive indices over the 400–3400 nm range with the required accuracy. The IR term gives a small correction of less than 0.1 in the visible, but dominates the dispersion for wavelengths longer than 2μm. The refractive indices calculated with Eq. (1) and the parameters in Table I have a maximum error of ±0.00025, or approximately 0.01% of the index values. In Table I we list the Sellmeier coefficients to be used to calculate the three principal refractive indices at 22° C using Eq. (1). We refer to Zysset *et al.* [9] for the high-temperature data.

Jundt *et al.* [11] refitted the complete data set of Zysset *et al.* using an ad hoc dispersion formula that gives the refractive index at all wavelengths between 400 and 3400 nm and at all temperatures in the orthorhombic phase:

$$\begin{aligned} n^2 - 1 = {} & (S_1 + b_1 F + b_2 G) \frac{\lambda^2 \lambda_1^2}{\lambda^2 - (\lambda_1 + b_3 F + b_4 G)^2} \\ & + (S_2 + b_5 F) \frac{\lambda^2 \lambda_2^2}{\lambda^2 - (\lambda_2 + b_6 F)^2} - (D + b_7 F)\lambda^2 + b_8 F \lambda^4, \end{aligned} \tag{2}$$

with $F = (\vartheta + 273.15)^2 - (22 + 273.15)^2$ and $G = \vartheta - 22$, where ϑ is the crystal temperature in °C. This expression gives the $KNbO_3$ refractive indi-

ces over the whole temperature range as accurately as the Sellmeier fits using Eq. (1). The parameters are given in Table II.

Note that in Zysset *et al.* [9] and Jundt *et al.* [11] the oscillator energies in electron volts are given, rather than their wavelength in nanometers, and that in these two publications different conversion factors were used to transform from the fitted wavelengths to the energy in electron volts given in Tables I and V. These conversion factors are given in the table footnotes.

Absorption losses in the visible and near infrared have been measured in high-quality $KNbO_3$ samples by Busse *et al.* [12] and are generally around 3% per centimeter at a wavelength of 500 nm for light polarized parallel to the *c*-axis, and less than 0.5% per centimeter between 800 and 1064 nm for light polarization along the *b*-axis. We did not find precise absorption data in the spectral range from 1 to 10 μm, but from a transmission measurement performed in 1-mm-thick plates in our laboratory, we know that the absorption remains low up to a wavelength of $\sim$5 μm. At wavelengths longer than 5 μm the transmission of the sample decreases, and it becomes less than 1% (corresponding to an absorption coefficient of approximately 45 cm^{-1}, or $k = 3 \times 10^{-3}$) at wavelengths longer than 8 μm.

The optical phonon reflection branches have been measured at optical frequencies between 100 and 1000 cm^{-1} by Bozinis and Hurrell [13] and by Fontana *et al.* [14]. Fontana *et al.* fitted the reflectivity $R = |(n + ik) - 1|^2/|(n + ik) + 1|^2$ with the factorized form of the dielectric function $\epsilon = (n + ik)^2$:

$$\epsilon(\omega) = \epsilon_\infty \prod_{i=1}^{4} \frac{\Omega^2(\mathrm{LO}_i) - \omega^2 + i\,\omega\,\gamma(\mathrm{LO}_i)}{\Omega^2(\mathrm{TO}_i) - \omega^2 + i\,\omega\,\gamma(\mathrm{TO}_i)}, \tag{3}$$

where ϵ_∞ is the dielectric constant at optical frequencies, and Ω,γ are the frequencies and dampings of the transversal optical (TO) and longitudinal optical (LO) vibrational modes.

Fontana *et al.* [14] do not state explicitly the value of ϵ_∞ they used in their fit and only measured the reflectivity spectrum for light polarized along the *b*-axis at room temperature. Bozinis and Hurrell give spectra for all light polarizations, but their data are less precise, and they do not explicitly derive the dielectric constant from it.

We used Eq. (3) to fit the *b*-polarization data of Fontana *et al.* [14] and the *a*- and *c*-polarization data of Bozinis and Hurrell [13]. For all fits we imposed the constraint that the limiting values of the dielectric constant at low and high frequencies correspond to the independently determined values. That is, we fixed $\epsilon(\lambda = 1.5\mu\mathrm{m})$ to the values given by Zysset *et al.* [9] (at 1.5 μm $n_a = 2.1992$, $n_b = 2.2341$, $n_c = 2.1029$) and $\epsilon(\omega = 0)$ to the clamped values of the dielectric constants determined by Zgonik *et al.* [15] ($\epsilon_a = 34 \pm 2$, $\epsilon_b = 780 \pm 22$, $\epsilon_c = 24 \pm 2$). These are the values of the dielectric constant at electric-field frequencies where the optical vibrational modes contribute to the polarization but the acoustic modes do not.

The parameters obtained from the fit and from the published data of Fontana *et al.* [14] and Bozinis and Hurrell [13] are given in Table III. From the dielectric function calculated from Eq. (3) we then obtain the values of n and k for wavelengths longer than 10 μm. In the tables for (n_a,k_a) and (n_c,k_c) we give a reference to the work of Bozinis and Hurrell for the data in this spectral range. This refers to the original reflectivity data from which the optical constants were extracted.

The fit for the *b*-polarized, room-temperature reflectivity data of Fontana *et al.* was good and could reproduce their experimental data within the scatter of the data points. The experimental data points in the measurements of Bozinis and Hurrell have a larger uncertainty. Moreover, their data below $\sim 300\ cm^{-1}$ suffer from poor precision and calibration uncertainty. Their measured reflectivity values at low frequency are too low when compared to the clamped dielectric permittivity values [15]. Because of this, a fit to the Bozinis and Hurrell [13] data below $300\ cm^{-1}$ was not possible. The parameters characterizing the two oscillators found in this range were taken from the published frequency values of Bozinis and Hurrell, and only their linewidth was fitted whenever this led to a better fit of the data above $300\ cm^{-1}$. The parameters given in Table III for *a*- and *c*-polarizations should not be used to calculate the dielectric constant at frequencies between 100 and $300\ cm^{-1}$. Although the limiting value for low frequency is correct, the resonance structure between 100 and $300 cm^{-1}$ is not well determined. For these reasons we do not give any (n_a,k_a) and (n_c,k_c) data for frequencies in this spectral range. We estimate the accuracy of n and k determined by the foregoing method to be approximately $\pm 10\%$ for *b*-polarization. The accuracy for *a*- and *c*-polarization is lower, approximately $\pm 20\%$. The accuracy is expected to be worse whenever k or n peaks at a narrow resonance.

REFERENCES

1. L. Katz and H. D. Megaw, The structure of potassium niobate at room temperature: The solution of a pseudosymmetric structure by Fourier methods. *Acta Crystallogr.* **22**, 639–648 (1967).
2. U. J. Flückiger, Darstellung und Eigenschaften von reinen und dotierten, eindomänigen $KNbO_3$ Kristallen. Ph. D. Dissertation, University of Zurich, Zurich (1976).
3. D. A. Roberts, Simplified characterization of uniaxial and biaxial nonlinear optical crystals: A plea for standardization of nomenclature and conventions. *IEEE J. Quantum Electron.* **28**, 2057–2074 (1992).
4. D. A. Roberts and T. R. Meeker, Proposed revisions for the polar orthorhombic class, *in* IEEE/ANSI Std 176. *IEEE Transactions on Ultrasonics and Frequency Control* **39**, 165–166 (1992).
5. I. Biaggio, P. Kerkoc, L.-S. Wu, and P. Günter, Refractive indices of orthorhombic $KNbO_3$. II. Phase matching configurations for nonlinear-optical interactions. *J. Opt. Soc. Am. B* **9**, 507–517 (1992).
6. E. Wiesendanger, Dielectric, mechanical, and optical properties of orthorhombic $KNbO_3$. *Ferroelectrics* **6**, 263–281 (1974).
7. A. M. Mamedov and L. S. Gadzhieva, Optical properties of potassium niobate in the fundamental absorption region. *Sov. Phys. Solid State* **26**, 1732–1733 (1984).

8. G. Montemezzani, P. Rogin, M. Zgonik, and P. Günter, Interband photorefractive effects: Theory and experiments in $KNbO_3$. *Phys. Rev. B* **49**, 2484–2502 (1994).
9. B. Zysset, I. Biaggio, and P. Günter, Refractive indices of orthorhombic $KNbO_3$. I. Dispersion and temperature dependence. *J. Opt. Soc. Am. B* **9**, 380–386 (1992).
10. J. Hulliger, R. Gutmann, and H. Wüest, Growth of large size $KNbO_3$ crystals and epitaxial layers of $KTa_{1-x}Nb_xO_3$. *J. Cryst. Growth* **128**, 897–902 (1993).
11. D. H. Jundt, P. Günter, and B. Zysset, A temperature-dependent dispersion equation for $KNbO_3$. *Nonlinear Opt.* **4**, 341–345 (1993).
12. L. E. Busse, L. Goldberg, and M. R. Surette, Absorption losses in MgO-doped and undoped potassium niobate. *J. Appl. Phys.* **75**, 1102–1110 (1994).
13. D. G. Bozinis and J. P. Hurrell, Optical modes and dielectric properties of ferroelectric orthorhombic $KNbO_3$. *Phys. Rev. B* **13**, 3109–3120 (1976).
14. M. D. Fontana, G. Métrat, J. L. Servoin, and F. Gervais, Infrared spectroscopy in $KNbO_3$ through the successive ferroelectric phase transitions. *J. Phys. C: Solid State Phys.* **16**, 483–514 (1984).
15. M. Zgonik, R. Schlesser, I. Biaggio, E. Voit, J. Tcherry, and P. Günter, Material constants of $KNbO_3$ relevant for electro- and acousto-optics, *J. Appl. Phys.* **74**, 1287–1297 (1993).

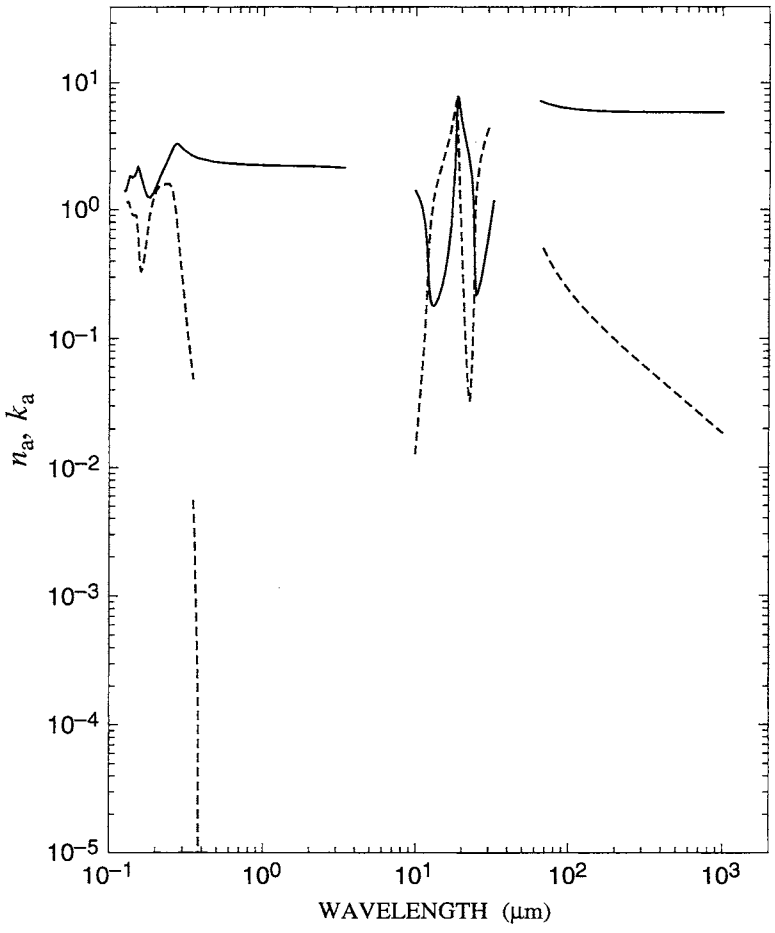

Fig. 1. Log–log plot of n_a (———) and k_a (- - - -) versus wavelength in micrometers for potassium niobate.

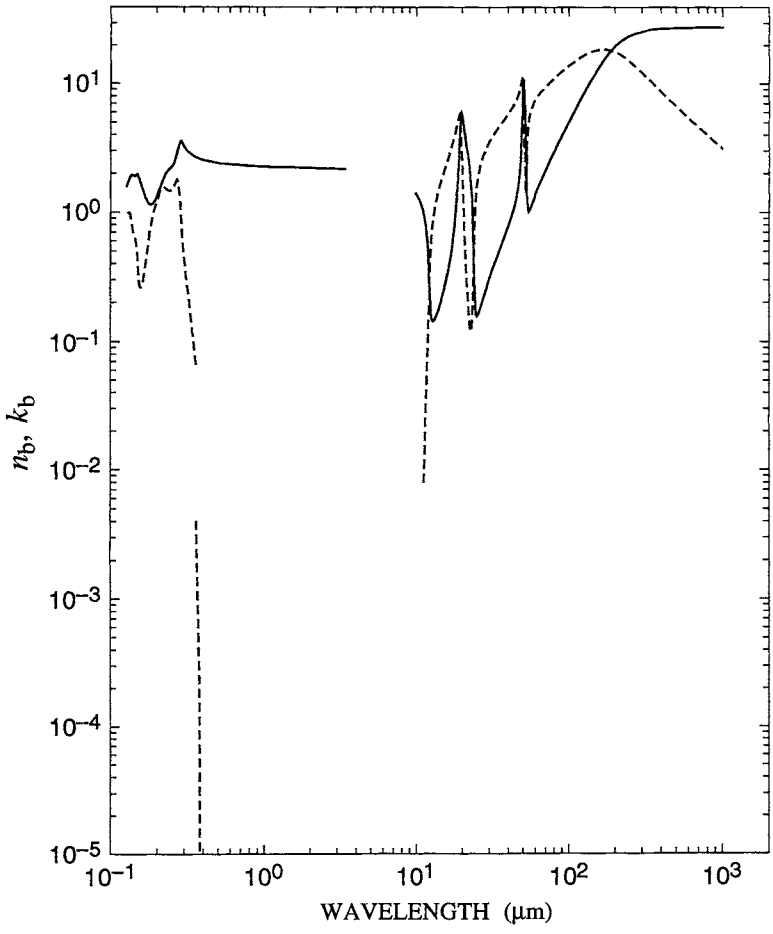

Fig. 2. Log–log plot of n_b (———) and k_b (- - - -) versus wavelength in micrometers for potassium niobate.

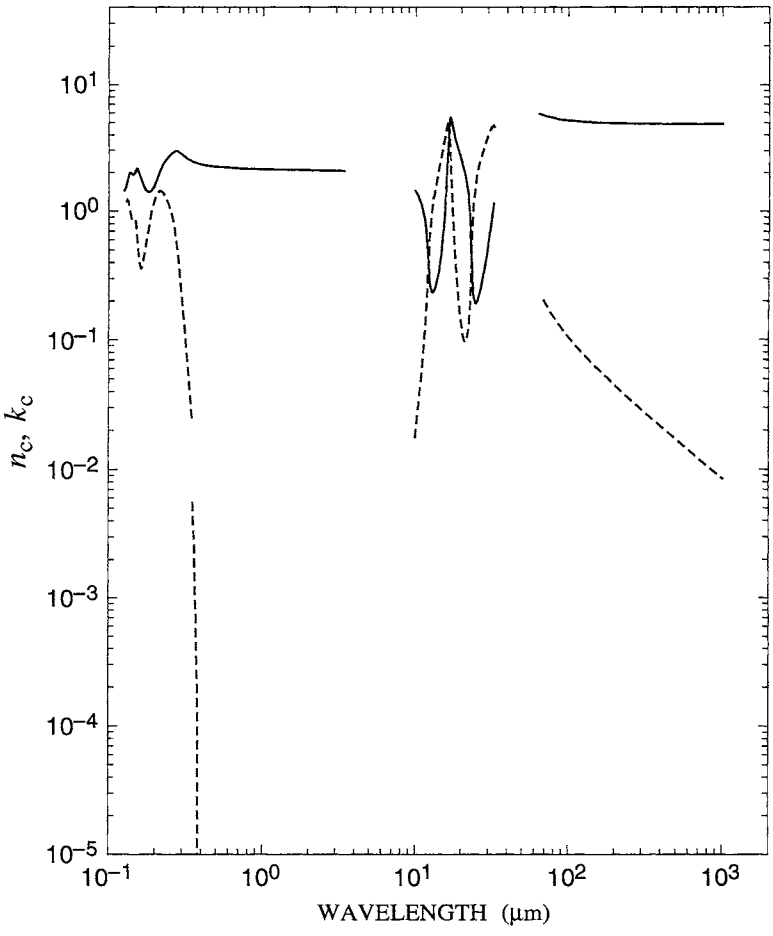

Fig. 3. Log–log plot of n_c (———) and k_c (- - - -) versus wavelength in micrometers for potassium niobate.

TABLE I

Parameters to Calculate the 22°C Refractive Indices in the Spectral range from 0.4 μm to 3.4 μm from Eq. (1).[a]

Parameter	n_a	n_b	n_c
S_1 [μm^{-2}]	20.05519	19.37347	16.0917
S_2 [μm^{-2}]	149.8408	135.4992	165.4431
E_1 [eV]	4.802660	4.545782	4.857787
E_2 [eV]	9.604319	9.049686	10.356684
D [μm^{-2}]	0.02517432	0.02845018	0.01943289

[a] $\lambda_i = (1.23986\ \mu m\ eV) / E_i$.

TABLE II

Parameters to Calculate the Refractive Indices in the Spectral Range from 0.4 μm to 3.4 μm from Eq. (2).[a]

Parameter	n_a	n_b	n_c
S_1 [μm^{-2}]	17.381	19.456	16.086
S_2 [μm^{-2}]	142.40	134.95	166.258
E_1 [eV]	4.7288	4.5492	4.8553
E_2 [eV]	9.1082	9.0392	10.3834
D [μm^{-2}]	0.02513	0.02837	0.01939
b_1 [μm^{-2}]	-2.018×10^{-5}	-5.263×10^{-5}	-3.267×10^{-5}
b_2 [μm^{-2}]	-1.32×10^{-3}	-1.65×10^{-3}	-2.8×10^{-3}
b_3 [μm]	1.231×10^{-7}	2.38×10^{-7}	1.89×10^{-7}
b_4 [μm]	-1.82×10^{-5}	-6.78×10^{-5}	-2.48×10^{-5}
b_5 [μm^{-2}]	0.9017×10^{-4}	2.0536×10^{-4}	1.990×10^{-4}
b_6 [μm]	0.796×10^{-7}	1.767×10^{-7}	1.75×10^{-7}
b_7 [μm^{-2}]	-5.58×10^{-9}	-12.2×10^{-9}	-2.7×10^{-9}
b_8 [μm^{-4}]	-4.4×10^{-10}	-3.3×10^{-10}	-5.7×10^{-10}

[a] $\lambda = (1.239852\ \mu m\ eV) / E$.

TABLE III

Parameters to Calculate the Dielectric Function from Eq. (3)[a]

Parameter	ϵ_a [b]	ϵ_b [c]	ϵ_c [b]
ϵ_∞	5.0753	5.2717	4.6065
$\Omega(TO_1)$	187.0	198.5	190.0
$\Omega(TO_2)$	243.0	53.0	267.8
$\Omega(TO_3)$	262.9	—	290.0
$\Omega(TO_4)$	537.1	512.1	601.5
$\Omega(LO_1)$	190.0	189.7	193.0
$\Omega(LO_2)$	254.0	420.1	429.9
$\Omega(LO_3)$	412.7	—	296.0
$\Omega(LO_4)$	833.9	822.3	824.8
$\gamma(TO_1)$	3.0	5.1	3.0
$\gamma(TO_2)$	25.0	61.5	15.1
$\gamma(TO_3)$	26.6	—	14.0
$\gamma(TO_4)$	22.3	27.1	33.1
$\gamma(LO_1)$	3.0	2.8	3.0
$\gamma(LO_2)$	12.0	4.8	8.4
$\gamma(LO_3)$	4.6	—	3.0
$\gamma(LO_4)$	27.1	17.6	31.0

[a] The frequencies Ω and γ have units [cm^{-1}].

[b] Eq. (3) is valid between 300 and 1000 cm^{-1} with an accuracy of ~20%.

[c] Eq. (3) is valid between 0 and 1000 cm^{-1} with an accuracy of ~10%.

TABLE IV

Values for n_a and k_a for Potassium Niobate Obtained from Various References

eV	cm^{-1}	μm	n_a	k_a
10.0	80655	0.1240	1.43 [6]	0.89 [6]
9.9	79849	0.1252	1.40	0.93
9.8	79042	0.1265	1.39	0.99
9.7	78236	0.1278	1.42	1.06
9.6	77429	0.1292	1.47	1.11
9.5	76623	0.1305	1.55	1.14
9.4	75816	0.1319	1.64	1.16
9.3	75010	0.1333	1.72	1.14
9.2	74203	0.1348	1.80	1.10
9.1	73396	0.1362	1.83	1.03
9.0	72590	0.1378	1.81	0.97
8.9	71783	0.1393	1.79	0.93
8.8	70977	0.1409	1.79	0.91
8.7	70170	0.1425	1.80	0.90
8.6	69364	0.1442	1.83	0.90
8.5	68557	0.1459	1.87	0.91
8.4	67751	0.1476	1.93	0.91
8.3	66944	0.1494	2.01	0.89
8.2	66137	0.1512	2.12	0.81
8.1	65331	0.1531	2.15	0.64
8.0	64524	0.1550	2.07	0.46
7.9	63718	0.1569	1.94	0.37
7.8	62911	0.1590	1.82	0.34
7.7	62105	0.1610	1.72	0.34
7.6	61298	0.1631	1.62	0.35
7.5	60492	0.1653	1.54	0.37
7.4	59685	0.1675	1.47	0.41
7.3	58878	0.1698	1.40	0.46
7.2	58072	0.1722	1.34	0.53
7.1	57265	0.1746	1.29	0.61
7.0	56459	0.1771	1.26	0.71
6.9	55652	0.1797	1.24	0.81
6.8	54846	0.1823	1.24	0.91
6.7	54039	0.1851	1.26	1.00
6.6	53233	0.1879	1.28	1.08
6.5	52426	0.1907	1.32	1.16
6.4	51619	0.1937	1.37	1.23
6.3	50813	0.1968	1.43	1.31
6.2	50006	0.2000	1.50	1.38
6.1	49200	0.2033	1.58	1.45
6.0	48393	0.2066	1.67	1.50
5.9	47587	0.2101	1.76	1.54
5.8	46780	0.2138	1.85	1.57
5.7	45974	0.2175	1.95	1.57
5.6	45167	0.2214	2.05	1.58

TABLE IV *(Continued)*

$KNbO_3$

eV	cm^{-1}	μm	n_a	k_a
5.5	44360	0.2254	2.14	1.58
5.4	43554	0.2296	2.23	1.59
5.3	42747	0.2339	2.33	1.59
5.2	41941	0.2384	2.45	1.60
5.1	41134	0.2431	2.58	1.60
5.0	40328	0.2480	2.75	1.56
4.9	39521	0.2530	2.92	1.48
4.8	38715	0.2583	3.07	1.35
4.7	37908	0.2638	3.19	1.17
4.6	37101	0.2695	3.27	0.96
4.5	36295	0.2755	3.27	0.75
4.4	35488	0.2818	3.21	0.55
4.3	34682	0.2883	3.12	0.41
4.2	33875	0.2952	3.03	0.31
4.1	33069	0.3024	2.94	0.23
4.0	32262	0.3100	2.86	0.17
3.9	31456	0.3179	2.79	0.13
3.8	30649	0.3263	2.73	0.10
3.7	29843	0.3351	2.67	0.07
3.6	29036	0.3444	2.63	0.06
3.5	28229	0.3542	2.59	0.05
3.4	27423	0.3647	2.55	0.03
3.54	28552	0.3502		5.46E-3 [8]
3.50	28229	0.3542		4.18E-3
3.45	27826	0.3594		2.54E-3
3.40	27423	0.3647		1.33E-3
3.35	27020	0.3701		6.11E-4
3.30	26616	0.3757		2.49E-4
3.30	26616	0.3757		2.19E-4 [6]
3.25	26213	0.3815		6.96E-5
3.20	25810	0.3875		2.22E-5
3.15	25406	0.3936		7.05E-6
3.10	25003	0.3999		2.25E-6
3.05	24600	0.4065		7.15E-7
3.00	24197	0.4133		2.28E-7
3.351	27027	0.370	2.5386 [9]	
3.263	26316	0.380	2.5103	
3.179	25641	0.390	2.4859	
3.100	25000	0.400	2.4646	
3.024	24390	0.410	2.4459	
2.952	23810	0.420	2.4293	
2.883	23256	0.430	2.4145	
2.818	22727	0.440	2.4012	

(continued)

TABLE IV *(Continued)*

$KNbO_3$

eV	cm^{-1}	μm	n_a	k_a
2.755	22222	0.450	2.3892	
2.695	21739	0.460	2.3783	
2.638	21277	0.470	2.3684	
2.583	20833	0.480	2.3594	
2.530	20408	0.490	2.3511	
2.480	20000	0.500	2.3434	
2.431	19608	0.510	2.3364	
2.384	19231	0.520	2.3298	
2.339	18868	0.530	2.3238	
2.296	18519	0.540	2.3181	
2.254	18182	0.550	2.3129	
2.214	17857	0.560	2.3080	
2.175	17544	0.570	2.3034	
2.138	17241	0.580	2.2991	
2.101	16949	0.590	2.2950	
2.066	16667	0.600	2.2912	
2.000	16129	0.620	2.2842	
1.937	15625	0.640	2.2780	
1.879	15152	0.660	2.2723	
1.823	14706	0.680	2.2673	
1.771	14286	0.700	2.2627	
1.722	13889	0.720	2.2585	
1.675	13514	0.740	2.2547	
1.631	13158	0.760	2.2512	
1.590	12821	0.780	2.2479	
1.550	12500	0.800	2.2449	
1.512	12195	0.820	2.2422	
1.476	11905	0.840	2.2396	
1.442	11628	0.860	2.2372	
1.409	11364	0.880	2.2350	
1.378	11111	0.900	2.2329	
1.348	10870	0.920	2.2309	
1.319	10638	0.940	2.2290	
1.292	10417	0.960	2.2273	
1.265	10204	0.980	2.2256	
1.240	10000	1.0	2.2240	
1.127	9091	1.1	2.2172	
1.033	8333	1.2	2.2117	
0.9537	7692	1.3	2.2070	
0.8856	7143	1.4	2.2029	
0.8266	6667	1.5	2.1992	
0.7749	6250	1.6	2.1958	
0.7293	5882	1.7	2.1925	
0.6888	5556	1.8	2.1893	
0.6525	5263	1.9	2.1862	
0.6199	5000	2.0	2.1832	

TABLE IV *(Continued)*

$KNbO_3$

eV	cm^{-1}	μm	n_a	k_a
0.5636	4545	2.2	2.1770	
0.5166	4167	2.4	2.1706	
0.4769	3846	2.6	2.1640	
0.4428	3571	2.8	2.1571	
0.4133	3333	3.0	2.1498	
0.3875	3125	3.2	2.1421	
0.3647	2941	3.4	2.1340	
0.1364	1100	9.091	1.60 [13]*	
0.1240	1000	10.00	1.39	
0.1178	950	10.53	1.23	0.03 [13]*
0.1116	900	11.11	0.99	0.06
0.1054	850	11.76	0.56	0.18
0.1017	820	12.20	0.25	0.54
0.09919	800	12.50	0.19	0.81
0.09299	750	13.33	0.18	1.38
0.08679	700	14.29	0.22	1.95
0.08059	650	15.38	0.31	2.67
0.07439	600	16.67	0.58	3.82
0.07191	580	17.24	0.88	4.63
0.06943	560	17.86	1.77	6.02
0.06819	550	18.18	3.09	7.02
0.06757	545	18.35	4.36	7.38
0.06695	540	18.52	6.11	7.06
0.06571	530	18.87	7.85	3.75
0.06447	520	19.23	6.76	1.59
0.06199	500	20.00	4.87	0.43
0.05951	480	20.83	3.78	0.15
0.05703	460	21.74	2.96	0.05
0.05455	440	22.73	2.18	0.03
0.05207	420	23.81	1.14	0.13
0.04959	400	25.00	0.22	1.49
0.04711	380	26.32	0.26	2.46
0.04463	360	27.78	0.37	3.28
0.04215	340	29.41	0.54	4.13
0.03967	320	31.25	0.85	5.14
0.03720	300	33.33	1.51	6.46
0.01240	100	100.00	6.26	0.24
0.006199	50	200.00	5.93	0.10
0	0		5.83 [15]	

* The reflectivity data from which n and k were derived are from Ref. [13].

TABLE V

Values for n_b and k_b for Potassium Niobate Obtained from Various References

eV	cm^{-1}	μm	n_b	k_b
10.0	80655	0.1240	1.55 [6]	0.88 [6]
9.9	79849	0.1252	1.56	0.91
9.8	79042	0.1265	1.58	0.93
9.7	78236	0.1278	1.61	0.95
9.6	77429	0.1292	1.65	0.97
9.5	76623	0.1305	1.70	0.99
9.4	75816	0.1319	1.77	1.00
9.3	75010	0.1333	1.84	0.98
9.2	74203	0.1348	1.90	0.94
9.1	73396	0.1362	1.94	0.85
9.0	72590	0.1378	1.95	0.78
8.9	71783	0.1393	1.93	0.72
8.8	70977	0.1409	1.92	0.68
8.7	70170	0.1425	1.91	0.65
8.6	69364	0.1442	1.91	0.63
8.5	68557	0.1459	1.92	0.62
8.4	67751	0.1476	1.96	0.55
8.3	66944	0.1494	1.96	0.46
8.2	66137	0.1512	1.92	0.37
8.1	65331	0.1531	1.84	0.30
8.0	64524	0.1550	1.75	0.27
7.9	63718	0.1569	1.67	0.26
7.8	62911	0.1590	1.60	0.26
7.7	62105	0.1610	1.52	0.27
7.6	61298	0.1631	1.46	0.29
7.5	60492	0.1653	1.39	0.32
7.4	59685	0.1675	1.33	0.36
7.3	58878	0.1698	1.28	0.41
7.2	58072	0.1722	1.23	0.47
7.1	57265	0.1746	1.19	0.54
7.0	56459	0.1771	1.17	0.61
6.9	55652	0.1797	1.15	0.70
6.8	54846	0.1823	1.15	0.79
6.7	54039	0.1851	1.15	0.87
6.6	53233	0.1879	1.17	0.95
6.5	52426	0.1907	1.19	1.03
6.4	51619	0.1937	1.22	1.10
6.3	50813	0.1968	1.27	1.16
6.2	50006	0.2000	1.32	1.23
6.1	49200	0.2033	1.38	1.31
6.0	48393	0.2066	1.46	1.39
5.9	47587	0.2101	1.54	1.48
5.8	46780	0.2138	1.64	1.53
5.7	45974	0.2175	1.74	1.56
5.6	45167	0.2214	1.85	1.57
5.5	44360	0.2254	1.94	1.55

TABLE V *(Continued)*

$KNbO_3$

eV	cm^{-1}	μm	n_b	k_b
5.4	43554	0.2296	2.03	1.52
5.3	42747	0.2339	2.10	1.49
5.2	41941	0.2384	2.15	1.47
5.1	41134	0.2431	2.18	1.47
5.0	40328	0.2480	2.23	1.48
4.9	39521	0.2530	2.29	1.52
4.8	38715	0.2583	2.39	1.59
4.7	37908	0.2638	2.55	1.69
4.6	37101	0.2695	2.81	1.78
4.5	36295	0.2755	3.16	1.70
4.4	35488	0.2818	3.46	1.34
4.3	34682	0.2883	3.57	0.84
4.2	33875	0.2952	3.39	0.55
4.1	33069	0.3024	3.20	0.41
4.0	32262	0.3100	3.06	0.31
3.9	31456	0.3179	2.95	0.24
3.8	30649	0.3263	2.87	0.19
3.7	29843	0.3351	2.80	0.14
3.6	29036	0.3444	2.74	0.11
3.5	28229	0.3542	2.69	0.08
3.4	27423	0.3647	2.64	0.06
3.43	27665	0.3615		3.99E-3 [8]
3.40	27423	0.3647		2.81E-3
3.35	27020	0.3701		1.24E-3
3.30	26616	0.3757		4.63E-4
3.30	26616	0.3757		4.39E-4 [6]
3.25	26213	0.3815		1.40E-4
3.20	25810	0.3875		4.44E-5
3.15	25406	0.3936		1.41E-5
3.10	25003	0.3999		4.50E-6
3.05	24600	0.4065		1.43E-6
3.00	24197	0.4133		4.57E-7
3.3509	27027	0.370	2.6646 [9]	
3.2627	26316	0.380	2.6253	
3.1791	25641	0.390	2.5919	
3.0996	25000	0.400	2.5633	
3.0240	24390	0.410	2.5384	
2.9520	23810	0.420	2.5167	
2.8834	23256	0.430	2.4974	
2.8178	22727	0.440	2.4802	
2.7552	22222	0.450	2.4649	
2.6953	21739	0.460	2.4510	
2.6380	21277	0.470	2.4385	

(continued)

TABLE V *(Continued)*

$KNbO_3$

eV	cm^{-1}	μm	n_b	k_b
2.5830	20833	0.480	2.4271	
2.5303	20408	0.490	2.4167	
2.4797	20000	0.500	2.4072	
2.4311	19608	0.510	2.3984	
2.3843	19231	0.520	2.3903	
2.3393	18868	0.530	2.3828	
2.2960	18519	0.540	2.3759	
2.2543	18182	0.550	2.3695	
2.2140	17857	0.560	2.3634	
2.1752	17544	0.570	2.3578	
2.1377	17241	0.580	2.3526	
2.1014	16949	0.590	2.3476	
2.0664	16667	0.600	2.3430	
1.9997	16129	0.620	2.3346	
1.9373	15625	0.640	2.3270	
1.8785	15152	0.660	2.3203	
1.8233	14706	0.680	2.3142	
1.7712	14286	0.700	2.3087	
1.7220	13889	0.720	2.3037	
1.6755	13514	0.740	2.2991	
1.6314	13158	0.760	2.2949	
1.5895	12821	0.780	2.2911	
1.5498	12500	0.800	2.2875	
1.5120	12195	0.820	2.2843	
1.4760	11905	0.840	2.2812	
1.4417	11628	0.860	2.2784	
1.4089	11364	0.880	2.2757	
1.3776	11111	0.900	2.2733	
1.3477	10870	0.920	2.2709	
1.3190	10638	0.940	2.2687	
1.2915	10417	0.960	2.2667	
1.2651	10204	0.980	2.2647	
1.2398	10000	1.0	2.2629	
1.1271	9091	1.1	2.2549	
1.0332	8333	1.2	2.2485	
0.9537	7692	1.3	2.2431	
0.8856	7143	1.4	2.2384	
0.8266	6667	1.5	2.2341	
0.7749	6250	1.6	2.2302	
0.7293	5882	1.7	2.2265	
0.6888	5556	1.8	2.2229	
0.6525	5263	1.9	2.2194	
0.6199	5000	2.0	2.2159	
0.5636	4545	2.2	2.2089	
0.5166	4167	2.4	2.2018	
0.4769	3846	2.6	2.1944	
0.4428	3571	2.8	2.1867	

TABLE V *(Continued)*

$KNbO_3$

eV	cm^{-1}	μm	n_b	k_b
0.4133	3333	3.0	2.1785	
0.3875	3125	3.2	2.1699	
0.3647	2941	3.4	2.1608	
0.1364	1100	9.091	1.60 [14]	
0.1240	1000	10.00	1.38	
0.1178	950	10.53	1.23	
0.1116	900	11.11	1.01	
0.1054	850	11.76	0.65	0.06 [14]
0.09919	800	12.50	0.16	0.61
0.09299	750	13.33	0.15	1.17
0.08679	700	14.29	0.19	1.66
0.08059	650	15.38	0.27	2.20
0.07439	600	16.67	0.43	2.92
0.07191	580	17.24	0.56	3.33
0.06943	560	17.86	0.81	3.90
0.06695	540	18.52	1.43	4.77
0.06447	520	19.23	3.76	5.69
0.06323	510	19.61	5.71	4.33
0.06199	500	20.00	5.69	2.14
0.05951	480	20.83	4.01	0.56
0.05703	460	21.74	2.82	0.21
0.05455	440	22.73	1.82	0.12
0.05207	420	23.81	0.42	0.42
0.04959	400	25.00	0.16	1.68
0.04711	380	26.32	0.18	2.33
0.04463	360	27.78	0.23	2.85
0.04215	340	29.41	0.28	3.33
0.03967	320	31.25	0.35	3.80
0.03720	300	33.33	0.43	4.29
0.03472	280	35.71	0.54	4.82
0.03224	260	38.46	0.68	5.44
0.02976	240	41.67	0.89	6.23
0.02728	220	45.45	1.31	7.44
0.02604	210	47.62	1.95	8.67
0.02480	200	50.00	7.63	11.0
0.02455	198	50.51	10.7	7.57
0.02418	195	51.28	7.99	2.34
0.02356	190	52.63	2.42	1.88
0.02232	180	55.56	1.04	5.78
0.01984	160	62.50	1.55	7.99
0.01736	140	71.43	2.23	9.65
0.01488	120	83.33	3.26	11.5
0.01240	100	100.00	5.02	13.8
0.009919	80	125.00	8.35	16.6
0.006199	50	200.00	19.6	17.8
0	0		27.9 [15]	

(continued)

TABLE VI

Values for n_c and k_c for Potassium Niobate Obtained from Various References

eV	cm^{-1}	μm	n_c	k_c
10.0	80655	0.1240	1.44 [6]	0.92 [6]
9.9	79849	0.1252	1.44	0.98
9.8	79042	0.1265	1.45	1.02
9.7	78236	0.1278	1.48	1.07
9.6	77429	0.1292	1.53	1.13
9.5	76623	0.1305	1.62	1.19
9.4	75816	0.1319	1.71	1.22
9.3	75010	0.1333	1.81	1.20
9.2	74203	0.1348	1.89	1.15
9.1	73396	0.1362	1.96	1.06
9.0	72590	0.1378	1.99	0.97
8.9	71783	0.1393	1.97	0.90
8.8	70977	0.1409	1.94	0.85
8.7	70170	0.1425	1.92	0.83
8.6	69364	0.1442	1.91	0.84
8.5	68557	0.1459	1.93	0.85
8.4	67751	0.1476	1.98	0.86
8.3	66944	0.1494	2.06	0.83
8.2	66137	0.1512	2.14	0.74
8.1	65331	0.1531	2.15	0.60
8.0	64524	0.1550	2.08	0.48
7.9	63718	0.1569	1.98	0.41
7.8	62911	0.1590	1.88	0.37
7.7	62105	0.1610	1.79	0.36
7.6	61298	0.1631	1.71	0.36
7.5	60492	0.1653	1.65	0.38
7.4	59685	0.1675	1.58	0.42
7.3	58878	0.1698	1.53	0.46
7.2	58072	0.1722	1.47	0.51
7.1	57265	0.1746	1.44	0.57
7.0	56459	0.1771	1.42	0.64
6.9	55652	0.1797	1.40	0.72
6.8	54846	0.1823	1.40	0.80
6.7	54039	0.1851	1.41	0.88
6.6	53233	0.1879	1.43	0.97
6.5	52426	0.1907	1.46	1.05
6.4	51619	0.1937	1.50	1.12
6.3	50813	0.1968	1.55	1.18
6.2	50006	0.2000	1.61	1.25
6.1	49200	0.2033	1.69	1.31
6.0	48393	0.2066	1.79	1.37
5.9	47587	0.2101	1.89	1.41
5.8	46780	0.2138	2.01	1.43
5.7	45974	0.2175	2.12	1.42
5.6	45167	0.2214	2.23	1.40
5.5	44360	0.2254	2.33	1.37

TABLE VI *(Continued)*

$KNbO_3$

eV	cm^{-1}	μm	n_c	k_c
5.4	43554	0.2296	2.42	1.32
5.3	42747	0.2339	2.51	1.27
5.2	41941	0.2384	2.59	1.21
5.1	41134	0.2431	2.67	1.14
5.0	40328	0.2480	2.74	1.07
4.9	39521	0.2530	2.81	1.00
4.8	38715	0.2583	2.87	0.91
4.7	37908	0.2638	2.92	0.80
4.6	37101	0.2695	2.95	0.67
4.5	36295	0.2755	2.97	0.55
4.4	35488	0.2818	2.93	0.43
4.3	34682	0.2883	2.87	0.33
4.2	33875	0.2952	2.80	0.24
4.1	33069	0.3024	2.72	0.17
4.0	32262	0.3100	2.66	0.12
3.9	31456	0.3179	2.60	0.09
3.8	30649	0.3263	2.54	0.06
3.7	29843	0.3351	2.49	0.04
3.6	29036	0.3444	2.45	0.03
3.5	28229	0.3542	2.41	0.02
3.4	27423	0.3647	2.38	0.002
3.54	28552	0.3502		5.46E-3 [8]
3.50	28229	0.3542		4.18E-3
3.45	27826	0.3594		2.54E-3
3.40	27423	0.3647		1.33E-3
3.35	27020	0.3701		6.11E-4
3.30	26616	0.3757		2.49E-4
3.30	26616	0.3757		2.19E-4 [6]
3.25	26213	0.3815		6.96E-5
3.20	25810	0.3875		2.22E-5
3.15	25406	0.3936		7.05E-6
3.10	25003	0.3999		2.25E-6
3.05	24600	0.4065		7.15E-7
3.00	24197	0.4133		2.28E-7
3.351	27027	0.370	2.3761 [9]	
3.263	26316	0.380	2.3536	
3.179	25641	0.390	2.3342	
3.100	25000	0.400	2.3172	
3.024	24390	0.410	2.3023	
2.952	23810	0.420	2.2890	
2.883	23256	0.430	2.2771	
2.818	22727	0.440	2.2664	

(continued)

TABLE VI *(Continued)*

$KNbO_3$

eV	cm^{-1}	μm	n_c	k_c
2.755	22222	0.450	2.2568	
2.695	21739	0.460	2.2481	
2.638	21277	0.470	2.2401	
2.583	20833	0.480	2.2328	
2.530	20408	0.490	2.2261	
2.480	20000	0.500	2.2199	
2.431	19608	0.510	2.2142	
2.384	19231	0.520	2.2090	
2.339	18868	0.530	2.2041	
2.296	18519	0.540	2.1995	
2.254	18182	0.550	2.1953	
2.214	17857	0.560	2.1913	
2.175	17544	0.570	2.1875	
2.138	17241	0.580	2.1841	
2.101	16949	0.590	2.1808	
2.066	16667	0.600	2.1777	
2.000	16129	0.620	2.1720	
1.937	15625	0.640	2.1669	
1.879	15152	0.660	2.1624	
1.823	14706	0.680	2.1583	
1.771	14286	0.700	2.1545	
1.722	13889	0.720	2.1511	
1.675	13514	0.740	2.1480	
1.631	13158	0.760	2.1452	
1.590	12821	0.780	2.1425	
1.550	12500	0.800	2.1401	
1.512	12195	0.820	2.1378	
1.476	11905	0.840	2.1358	
1.442	11628	0.860	2.1338	
1.409	11364	0.880	2.1320	
1.378	11111	0.900	2.1303	
1.348	10870	0.920	2.1287	
1.319	10638	0.940	2.1271	
1.292	10417	0.960	2.1257	
1.265	10204	0.980	2.1244	
1.240	10000	1.0	2.1231	
1.127	9091	1.1	2.1175	
1.033	8333	1.2	2.1130	
0.9537	7692	1.3	2.1092	
0.8856	7143	1.4	2.1059	
0.8266	6667	1.5	2.1029	
0.7749	6250	1.6	2.1001	
0.7293	5882	1.7	2.0974	
0.6888	5556	1.8	2.0949	
0.6525	5263	1.9	2.0924	
0.6199	5000	2.0	2.0899	

TABLE VI *(Continued)*

$KNbO_3$

eV	cm^{-1}	μm	n_c	k_c
0.5636	4545	2.2	2.0849	
0.5166	4167	2.4	2.0797	
0.4769	3846	2.6	2.0744	
0.4428	3571	2.8	2.0689	
0.4133	3333	3.0	2.0630	
0.3875	3125	3.2	2.0568	
0.3647	2941	3.4	2.0503	
0.1364	1100	9.091	1.61 [13]*	
0.1240	1000	10.00	1.42	0.02 [13]*
0.1178	950	10.53	1.28	0.04
0.1116	900	11.11	1.07	0.07
0.1054	850	11.76	0.70	0.16
0.09919	800	12.50	0.26	0.74
0.09299	750	13.33	0.25	1.42
0.08679	700	14.29	0.35	2.18
0.08059	650	15.38	0.78	3.43
0.07563	610	16.39	3.47	5.14
0.07687	620	16.13	2.13	4.85
0.07439	600	16.67	5.10	4.28
0.07315	590	16.95	5.53	2.59
0.07191	580	17.24	5.08	1.49
0.06943	560	17.86	4.09	0.61
0.06695	540	18.52	3.41	0.31
0.06447	520	19.23	2.92	0.19
0.06199	500	20.00	2.50	0.13
0.05951	480	20.83	2.09	0.10
0.05703	460	21.74	1.63	0.10
0.05455	440	22.73	0.98	0.18
0.05207	420	23.81	0.23	0.99
0.04959	400	25.00	0.19	1.77
0.04711	380	26.32	0.23	2.41
0.04463	360	27.78	0.31	3.05
0.04215	340	29.41	0.46	3.76
0.01240	100	100.00	5.21	0.10
0.006199	50	200.00	4.97	0.04
0	0		4.90 [15]	

* The reflectivity data from which n and k were derived are from Ref. [13].

Rubidium Bromide (RbBr)

IVAN OHLÍDAL
Department of Solid State Physics
Faculty of Sciences
Masaryk University Brno
Brno, Czech Republic

and

MILOSLAV OHLÍDAL
Institute of Physical Engineering
Technical University
Brno, Czech Republic

Single crystals of rubidium bromide exhibit the cubic structure of NaCl (O_h^5-Fm3m space group).

Rubidium bromide is a hygroscopic material similar to the other rubidium halides. Surfaces of optical components fabricated from RbBr crystals must be prepared with great care. Roughness of the surfaces of the RbBr components achieved by the usual polishing procedures causes a considerable decrease in transmittance of these components, at shorter wavelengths in particular [1]. This is probably caused by the fact that these procedures cause surface roughness that is characterized by relatively large values of the heights of the surface irregularities [1]. In practice the spectral region 0.25–40 μm can be considered as the region of transparency of RbBr.

So far, only four sets of optical-constant data have been published for RbBr in the literature. Three of these sets are summarized in this work. The room-temperature values of the refractive index n and the extinction coefficient k tabulated here (see Table I and Fig. 1) were obtained from the following papers: the 54.05 μm (0.02294 eV) to 0.21 μm (5.904 eV) values of n are calculated using the dispersion formula published in the Li paper [2]; the 0.656 μm (1.890 eV) to 0.486 μm (2.551 eV) values of n are from Sprockhoff [3]; and 222.2 μm (45 cm^{-1}) to 50.00 μm (200 cm^{-1}) values of n and k were presented by Pai *et al.*[4].

Copyright © 1998 by Academic Press.
All rights of reproduction in any form reserved
ISBN 0-12-544423-0/$25.00.

The Li formula employed for calculating the refractive-index data of RbBr in the region 54.00 μm $\geq \lambda \geq$ 0.21 μm was constructed in the form

$$n^2 = 1.45931 + \frac{0.16301\,\lambda^2}{\lambda^2 - (0.123)^2} + \frac{0.29841\,\lambda^2}{\lambda^2 - (0.146)^2} + \frac{0.17198\,\lambda^2}{\lambda^2 - (0.155)^2} + \frac{0.12186\,\lambda^2}{\lambda^2 - (0.178)^2} + \frac{0.13039\,\lambda^2}{\lambda^2 - (0.191)^2} + \frac{2.520\,\lambda^2}{\lambda^2 - (114.29)^2}, \tag{1}$$

where λ is in micrometers.

The values of n calculated by means of the Li formula (see Table I) correspond to the RbBr single crystal because this formula was obtained on the basis of the important Kublitzky refractive-index data [5]. The primary Kublitzky data were measured for prisms formed with the RbBr single crystal by means of the method of minimum deviation at selected wavelengths in the spectral region 0.578 μm $\geq \lambda \geq$ 0.219 μm [5]. Li constructed his formula of the Sellmeier type in such a way that the wavelengths of the ultraviolet absorption peaks and the wavelength of the fundamental infrared absorption peak λ_I found by direct measurements are included in this formula. The values of the adjustable parameters of the formula mentioned (e.g., 0.16301) were sought by fitting the Kublitzky data by means of the least-squares method [2]. This means that the values of the refractive index n can be calculated using the Li dispersion formula at wavelengths beyond the Kublitzky's data in both directions, that is, at wavelengths belonging to the near-UV and the IR regions.

On the basis of the Kublitzky data, Radhakrishnan [6] also derived the following empirical dispersion formula expressing the spectral dependence of the refractive index n of the RbBr single crystal in the region 0.546 μm $\geq \lambda \geq$ 0.219 μm:

$$n^2 = 1.4500 + \frac{0.2000\,\lambda^2}{\lambda^2 - 0.015129} + \frac{0.3651\,\lambda^2}{\lambda^2 - 0.022650} + \frac{0.3224\,\lambda^2}{\lambda^2 - 0.033124}, \tag{2}$$

λ is also in micrometers.

This formula gives wavelengths of ultraviolet absorption peaks that agree closely with those obtained by direct measurements [7, 8] but gives no information concerning the infrared absorption peak. Extrapolated values of n for the long wavelengths, that is, for the IR wavelengths, as given by the Radhakrishnan formula have large uncertainties in contrast to those given by the Li formula expressed with Eq. (1). This means that the Radhakrish-

nan dispersion formula is not an adequate one for use in a wide wavelength range, that is, in both the mid-IR and the far-IR regions in particular. Thus, the Radhakrishnan formula only correlates the dispersion in both the visible and the near UV with absorption bands in the UV region.

Sprockhoff [3] measured the values of n of RbBr using the method of minimum deviation as well. He determined the refractive-index value of the RbBr single crystal at the following wavelengths: 0.486, 0.589 and 0.656 μm (see Table I).

The errors of the refractive-index data calculated using Eq. (1) are dependent on wavelength. (The greatest and/or smallest errors in n are equal to $\pm$ 0.02 in the regions 0.21–0.22 μm and 40.00–60.00 μm and/or $\pm$ 0.002 in the region 0.40–1.50 μm.) In the Sprockhoff and Kublitzky data the errors of the values of n can be estimated as $\pm$ 0.001.

Pai *et al.* [4] determined the spectral dependences of n and k characterizing RbBr bulk samples (i.e., single crystals) by means of amplitude and phase reflection measurements made by dispersive Fourier transform spectroscopy in the region 222.2 μm $\geq \lambda \geq$ 50 μm. The errors in the optical constants n and k evaluated in this way are also dependent on wavelength. (The greatest and/or smallest errors in both n and k are equal to $\pm$ 0.10 and/or $\pm$ 0.01 at the wavelength of about 116 μm and/or in the interval 93 μm $\geq \lambda \geq$ 50 μm [4].) Spectral dependences of n and k in the vicinity of the maximum value of k at the wavelength of the fundamental infrared absorption peak λ_I are related to the TO phonon mode. The fine structures in the curves of n and k in the far-IR region may be caused by multiple-phonon absorption processes. In the visible there is very good agreement between the refractive-index data calculated using the Li formula [2] and measured by Kublitzky [5] on one side and those presented by Sprockhoff [3] on the other side (see Table I). Similarly, one can see a relatively good agreement between the values of n calculated by means of the Li formula and those determined by Pai *et al.* [4] in the region 54.00 μm $\geq \lambda \geq$ 50.00 μm (see Table I). Both the facts mentioned give support for the correctness and reliability of the optical-constant data presented for the RbBr single crystal in this paper.

From Eq. (1) and the spectral dependence of k determined by Pai *et al.* [4], one can see that there is a good agreement between the value of λ_I used in the Li formula [2] and that implied by the data of Pai *et al.*

It should be noted that in the parts of the IR region in which RbBr is a weakly absorbing material ($k \leq 0.1$), more precise values of k can be determined by transmittance measurements of sufficiently thin RbBr slabs than by means of the experimental techniques used by Pai *et al.* [4]. Thus far, these measurements of the transmittance of the RbBr slabs have not been performed in the IR region. Unfortunately, measurements enabling us to evaluate the values of the extinction coefficient k of the RbBr single crystals or RbBr thin films in the UV region have not been carried out, either.

The optical-constant data presented here are the room-temperature

data, as pointed out earlier. However, strictly speaking, there are small differences at temperatures corresponding to the data summarized. Namely, the refractive-index data obtained by means of the Li dispersion formula [2], the values of n determined by Sprockhoff [3] and the values of n and k published by Pai *et al.* [4] correspond to 293 K, 298 K, and 300 K, respectively. Both the Radhakrishnan formula [6] and the Kublitzky data correspond to 308 K. This means that at first Li reduced the Kublitzky refractive-index data from 308 to 293 K to obtain his formula in the form presented. He performed these corrections by using empirical parameters to construct a formula for dn/dT, enabling him to carry out the mentioned corrections of the Kublitzky values of n [2] (dn/dT denotes the derivative of the refractive index with respect to temperature T).

In conclusion, it is possible to state that the optical-constant data summarized here represent the best values of the refractive index n characterizing the RbBr single crystal in the region 222.2 μm $\geq \lambda \geq$ 0.21 μm and the best values of the extinction coefficient k of the same material in the region 222.2 μm $\geq \lambda \geq$ 50 μm.

REFERENCES

1. D. E. McCarthy, *Appl. Opt.* **7**, 1243 (1968).
2. H. H. Li, J. Phys. *Chem. Ref. Data* **5**, 329 (1976).
3. M. Sprockhoff, *Neues Jahrb. Mineral. Geol. Palaeontol., Beilageband* **18**, 117 (1904).
4. K. F. Pai, T. J. Parker, N. E. Tornberg, R. P. Lowndes, and W. G. Chambers, *Infrared Phys.* **18**, 199 (1978).
5. A. Kublitzky, *Ann. Phys.* **20**, 793 (1934).
6. T. Radhakrishnan, *Proc. Indian Acad. Sci. Sect. A* **27**, 165 (1948).
7. R. Hilsch and R. W. Pohl, *Z. Phys.* **59**, 812 (1930).
8. E. G. Schneider and H. M. O'Bryan, *Phys. Rev.* **51**, 293 (1937).

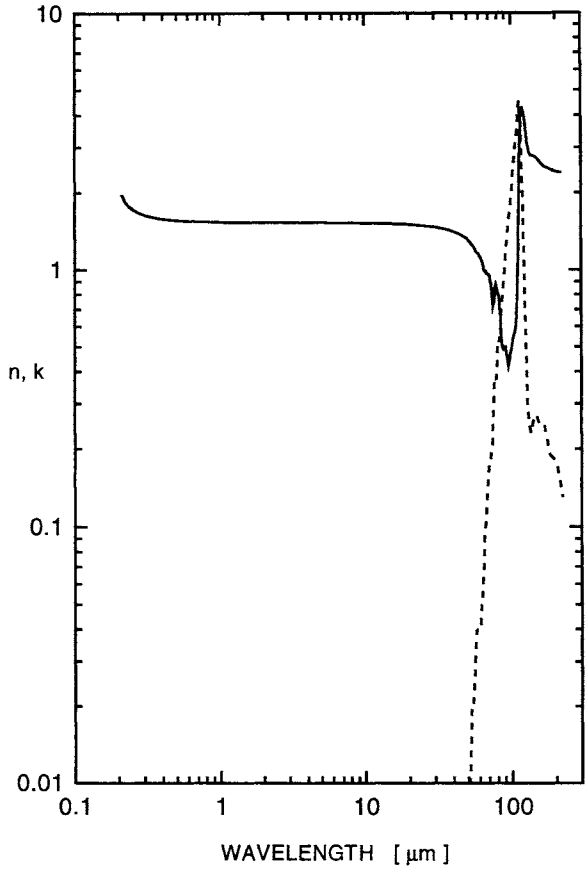

Fig. 1. Log–log plot of n (solid line) and k (dashed line) versus wavelength in micrometers for RbBr.

TABLE I

Values of n and k for Rubidium Bromide as Obtained from Various References[a]

eV	cm^{-1}	μm	n	k
5.904	47,620	0.210	1.962 [2]	
5.848	47,170	0.212	1.936	
5.794	46,730	0.214	1.913	
5.740	46,300	0.216	1.893	
5.687	45,870	0.218	1.875	
5.636	45,450	0.220	1.858	
5.585	45,050	0.222	1.844	
5.535	44,640	0.224	1.830	
5.486	44,250	0.226	1.818	
5.438	43,860	0.228	1.807	
5.391	43,480	0.230	1.796	
5.344	43,100	0.232	1.787	
5.299	42,740	0.234	1.777	
5.254	42,370	0.236	1.769	
5.209	42,020	0.238	1.761	
5.166	41,670	0.240	1.754	
5.123	41,320	0.242	1.747	
5.081	40,980	0.244	1.740	
5.040	40,650	0.246	1.734	
4.999	40,320	0.248	1.728	
4.959	40,000	0.250	1.722	
4.920	39,680	0.252	1.717	
4.881	39,370	0.254	1.712	
4.843	39,060	0.256	1.707	
4.806	38,760	0.258	1.703	
4.769	38,460	0.260	1.698	
4.732	38,170	0.262	1.694	
4.696	37,880	0.264	1.690	
4.661	37,590	0.266	1.686	
4.626	37,310	0.268	1.683	
4.592	37,040	0.270	1.679	
4.558	36,760	0.272	1.676	
4.525	36,500	0.274	1.673	
4.492	36,230	0.276	1.669	
4.460	35,970	0.278	1.666	
4.428	35,710	0.280	1.664	
4.397	35,460	0.282	1.661	
4.366	35,210	0.284	1.658	
4.335	34,970	0.286	1.655	
4.305	34,720	0.288	1.653	
4.275	34,480	0.290	1.651	
4.246	34,250	0.292	1.648	
4.217	34,010	0.294	1.646	
4.189	33,780	0.296	1.644	
4.161	33,560	0.298	1.642	

(continued)

[a] References given in brackets.

TABLE I *(Continued)*

Rubidium Bromide

eV	cm^{-1}	μm	n	k
4.133	33,330	0.300	1.640	
4.065	32,790	0.305	1.635	
4.000	32,260	0.310	1.630	
3.936	31,750	0.315	1.626	
3.875	31,250	0.320	1.622	
3.815	30,770	0.325	1.618	
3.757	30,300	0.330	1.615	
3.701	29,850	0.335	1.612	
3.647	29,410	0.340	1.609	
3.594	28,990	0.345	1.606	
3.542	28,570	0.350	1.603	
3.493	28,170	0.355	1.601	
3.444	27,780	0.360	1.598	
3.397	27,400	0.365	1.596	
3.351	27,030	0.370	1.594	
3.306	26,670	0.375	1.592	
3.263	26,320	0.380	1.590	
3.220	25,970	0.385	1.588	
3.179	25,640	0.390	1.587	
3.139	25,320	0.395	1.585	
3.100	25,000	0.400	1.583	
3.024	24,390	0.410	1.580	
2.952	23,810	0.420	1.578	
2.883	23,260	0.430	1.575	
2.818	22,730	0.440	1.573	
2.755	22,220	0.450	1.571	
2.695	21,740	0.460	1.569	
2.638	21,280	0.470	1.567	
2.583	20,830	0.480	1.566	
2.551	20,580	0.486	1.565 [3]	
2.530	20,410	0.490	1.564 [2]	
2.480	20,000	0.500	1.563	
2.431	19,610	0.510	1.561	
2.384	19,230	0.520	1.560	
2.339	18,870	0.530	1.559	
2.296	18,520	0.540	1.558	
2.254	18,180	0.550	1.557	
2.214	17,860	0.560	1.556	
2.175	17,540	0.570	1.555	
2.138	17,240	0.580	1.554	
2.105	16,980	0.589	1.553 [3]	
2.101	16,950	0.590	1.553 [2]	
2.066	16,670	0.600	1.552	
2.000	16,130	0.620	1.551 [2]	
1.937	15,630	0.640	1.550	
1.890	15,240	0.656	1.548 [3]	

(continued)

TABLE I *(Continued)*

Rubidium Bromide

eV	cm^{-1}	μm	n	k
1.879	15,150	0.660	1.548 [2]	
1.823	14,710	0.680	1.547	
1.771	14,290	0.700	1.546	
1.722	13,890	0.720	1.546	
1.675	13,510	0.740	1.545	
1.631	13,160	0.760	1.544	
1.590	12,820	0.780	1.543	
1.550	12,500	0.800	1.543	
1.512	12,200	0.820	1.542	
1.476	11,900	0.840	1.542	
1.442	11,630	0.860	1.541	
1.409	11,360	0.880	1.541	
1.378	11,110	0.900	1.540	
1.348	10,870	0.920	1.540	
1.319	10,640	0.940	1.539	
1.292	10,420	0.960	1.539	
1.265	10,200	0.980	1.539	
1.240	10,000	1.00	1.538	
1.181	9,524	1.05	1.538	
1.127	9,091	1.10	1.537	
1.078	8,696	1.15	1.537	
1.033	8,333	1.20	1.536	
0.9919	8,000	1.25	1.536	
0.9537	7,692	1.30	1.535	
0.9184	7,407	1.35	1.535	
0.8856	7,143	1.40	1.535	
0.8551	6,897	1.45	1.535	
0.8266	6,667	1.50	1.534	
0.7749	6,250	1.60	1.534	
0.7293	5,882	1.70	1.534	
0.6888	5,556	1.80	1.533	
0.6526	5,263	1.90	1.533	
0.6199	5,000	2.00	1.533	
0.5636	4,545	2.20	1.532	
0.5166	4,167	2.40	1.532	
0.4769	3,846	2.60	1.532	
0.4428	3,571	2.80	1.532	
0.4133	3,333	3.00	1.532	
0.3542	2,857	3.50	1.531	
0.3100	2,500	4.00	1.531	
0.2755	2,222	4.50	1.530	
0.2480	2,000	5.00	1.530	
0.2066	1,667	6.00	1.529	
0.1771	1,429	7.00	1.528	
0.1550	1,250	8.00	1.527	
0.1378	1,111	9.00	1.526	

TABLE I *(Continued)*

Rubidium Bromide

eV	cm^{-1}	μm	n	k
0.1240	1,000	10.0	1.525	
0.1127	909.1	11.0	1.524	
0.1033	833.3	12.0	1.522	
0.09537	769.2	13.0	1.521	
0.08856	714.3	14.0	1.519	
0.08266	666.7	15.0	1.517	
0.07999	645.2	15.5	1.516	
0.07749	625.0	16.0	1.515	
0.07514	606.1	16.5	1.514	
0.07293	588.2	17.0	1.513	
0.07085	571.4	17.5	1.511	
0.06888	555.6	18.0	1.510	
0.06702	540.5	18.5	1.509	
0.06526	526.3	19.0	1.508	
0.06358	512.8	19.5	1.506	
0.06199	500.0	20.0	1.505	
0.06048	487.8	20.5	1.504	
0.05904	476.2	21.0	1.502	
0.05767	465.1	21.5	1.501	
0.05636	454.5	22.0	1.499	
0.05510	444.4	22.5	1.498	
0.05391	434.8	23.0	1.496	
0.05276	425.5	23.5	1.495	
0.05166	416.7	24.0	1.493	
0.05061	408.2	24.5	1.491	
0.04959	400.0	25.0	1.489	
0.04862	392.2	25.5	1.488	
0.04769	384.6	26.0	1.486	
0.04679	377.4	26.5	1.484	
0.04592	370.4	27.0	1.482	
0.04509	363.6	27.5	1.480	
0.04428	357.1	28.0	1.478	
0.04350	350.9	28.5	1.476	
0.04275	344.8	29.0	1.474	
0.04203	339.0	29.5	1.471	
0.04133	333.3	30.0	1.469	
0.04065	327.9	30.5	1.467	
0.04000	322.6	31.0	1.465	
0.03936	317.5	31.5	1.462	
0.03875	312.5	32.0	1.460	
0.03815	307.7	32.5	1.457	
0.03757	303.0	33.0	1.455	
0.03701	298.5	33.5	1.452	
0.03647	294.1	34.0	1.449	
0.03594	289.9	34.5	1.446	
0.03542	285.7	35.0	1.444	

(continued)

TABLE I *(Continued)*

Rubidium Bromide

eV	cm^{-1}	μm	n	k
0.03493	281.7	35.5	1.441	
0.03444	277.8	36.0	1.438	
0.03397	274.0	36.5	1.435	
0.03351	270.3	37.0	1.432	
0.03306	266.7	37.5	1.429	
0.03263	263.2	38.0	1.425	
0.03220	259.7	38.5	1.422	
0.03179	256.4	39.0	1.419	
0.03139	253.2	39.5	1.415	
0.03100	250.0	40.0	1.412	
0.03061	246.9	40.5	1.408	
0.03024	243.9	41.0	1.405	
0.02988	241.0	41.5	1.401	
0.02952	238.1	42.0	1.397	
0.02917	235.3	42.5	1.393	
0.02883	232.6	43.0	1.389	
0.02850	229.9	43.5	1.385	
0.02818	227.3	44.0	1.381	
0.02786	224.7	44.5	1.376	
0.02755	222.2	45.0	1.372	
0.02725	219.8	45.5	1.368	
0.02695	217.4	46.0	1.363	
0.02666	215.1	46.5	1.358	
0.02638	212.8	47.0	1.354	
0.02610	210.5	47.5	1.349	
0.02583	208.3	48.0	1.344	
0.02556	206.2	48.5	1.338	
0.02530	204.1	49.0	1.333	
0.02505	202.0	49.5	1.328	
0.02480	200	50.00	1.322	
			1.31 [4]	0.01 [4]
0.02418	195	51.28	1.308 [2]	
			1.29 [4]	0.01 [4]
0.02356	190	52.63	1.291 [2]	
			1.27 [4]	0.02 [4]
0.02294	185	54.05	1.272 [2]	
			1.25 [4]	0.02 [4]
0.02232	180	55.56	1.22	0.03
0.02170	175	57.14	1.18	0.04
0.02108	170	58.82	1.16	0.04
0.02046	165	60.61	1.13	0.04
0.02009	162	61.73	1.11	0.05
0.01984	160	62.50	1.09	0.05
0.01959	158	63.29	1.07	0.06
0.01934	156	64.10	1.04	0.07
0.01909	154	64.94	1.00	0.09

TABLE I *(Continued)*

Rubidium Bromide

eV	cm^{-1}	μm	n	k
0.01885	152	65.79	0.99	0.10
0.01860	150	66.67	0.99	0.11
0.01835	148	67.57	0.97	0.13
0.01810	146	68.49	0.96	0.14
0.01785	144	69.44	0.96	0.17
0.01761	142	70.42	0.95	0.18
0.01736	140	71.43	0.91	0.18
0.01711	138	72.46	0.88	0.20
0.01686	136	73.53	0.80	0.21
0.01661	134	74.63	0.72	0.27
0.01637	132	75.76	0.75	0.36
0.01612	130	76.92	0.84	0.38
0.01587	128	78.13	0.87	0.37
0.01562	126	79.37	0.84	0.44
0.01537	124	80.65	0.81	0.53
0.01513	122	81.97	0.78	0.52
0.01488	120	83.33	0.69	0.56
0.01463	118	84.75	0.55	0.67
0.01438	116	86.21	0.50	0.76
0.01413	114	87.72	0.49	0.86
0.01389	112	89.29	0.50	0.99
0.01364	110	90.91	0.50	1.14
0.01339	108	92.59	0.45	1.30
0.01314	106	94.34	0.42	1.46
0.01289	104	96.15	0.44	1.61
0.01265	102	98.04	0.47	1.76
0.01240	100	100.0	0.49	1.99
0.01215	98.0	102.0	0.54	2.33
0.01190	96.0	104.2	0.56	2.68
0.01165	94.0	106.4	0.59	3.05
0.01141	92.0	108.7	0.73	3.46
0.01116	90.0	111.1	1.25	4.12
0.01091	88.0	113.6	2.66	4.56
0.01066	86.0	116.3	4.26	3.31
0.01041	84.0	119.0	4.27	1.95
0.01017	82.0	122.0	4.08	1.17
0.00992	80.0	125.0	3.62	0.52
0.00967	78.0	128.2	3.12	0.29
0.00942	76.0	131.6	2.87	0.25
0.00917	74.0	135.1	2.78	0.23
0.00893	72.0	138.9	2.78	0.25
0.00868	70.0	142.9	2.76	0.27
0.00843	68.0	147.1	2.73	0.27
0.00806	65.0	153.8	2.65	0.25
0.00744	60.0	166.7	2.53	0.25
0.00682	55.0	181.8	2.47	0.19
0.00620	50.0	200.0	2.41	0.18
0.00558	45.0	222.2	2.39	0.13

Rubidium Iodide (RbI)

IVAN OHLÍDAL and DANIEL FRANTA
Department of Solid State Physics
Faculty of Sciences
Masaryk University Brno
Brno, Czech Republic

Single crystals of rubidium iodide exhibit the cubic structure of NaCl (O_h^5-Fm3m space group).

Rubidium iodide crystals are widely used for manufacturing various optical components employed especially in the infrared region. This is due to the fact that RbI crystals exhibit a broad range of transparency from the near UV (0.24 μm) to the far IR (64 μm).

RbI is the most hygroscopic material of the rubidium halides. Considerable care has to be devoted to preparing surfaces of the optical components fabricated from RbI crystals, since these surfaces play an important role in their transparency properties. The gradual decrease in transmittance at shorter wavelengths is due to surface scattering that is caused by roughness of the surfaces of the components prepared by usual procedures of polishing, and not by absorption or scattering within the material itself [1]. This is probably caused by the fact that usual polishing procedures yield roughness of surfaces of the RbI components, exhibiting relatively large values of the heights of the surface irregularities.

There are few data of the optical constants available for RbI, similar to the other rubidium halides. The room-temperature values of the refractive index n and the extinction coefficient k tabulated here (see Table I and Fig. 1) were obtained from the following papers: the 0.25 μm (4.959 eV) to 0.18 μm (6.888 eV) results are from the paper of Baldini and Rigaldi [2]; the 0.26 μm (4.769 eV) to 0.23 μm (5.391 eV) values of n and k are obtained on the basis of measurements presented in the article of Fröhlich *et al.* [3]; the 64 μm (0.01937 eV) to 0.24 μm (5.166 eV) refractive-index data were calculated by means of the dispersion formula presented in the paper of Li [4]; the 0.656 μm (1.890 eV) to 0.486 μm (2.551 eV) values of n are from the paper of Sprockhoff [5]; and the 222.2 μm (45 cm^{-1}) to 52.63 μm (190 cm^{-1}) values of n and k were published by Pai *et al.* [6].

Copyright © 1998 by Academic Press.
All rights of reproduction in any form reserved
ISBN 0-12-544423-0/$25.00.

The values of n and k presented by Baldini and Rigaldi [2] were obtained by interpreting spectral dependences of the reflectances and transmittance of a RbI thin film with the thickness of 0.042 μm (the error of the thickness was ± 0.003 μm). The RbI film was prepared by sublimation onto a fused-silica plate in the vacuum chamber employed simultaneously for the optical measurements (temperature of the fused-silica substrate during the deposition of the RbI film is not specified in the paper of Baldini and Rigaldi [2], but one can assume that it was about room temperature). Thus, the spectral dependences of both the reflectances R and R' of the film for incidence of light from the ambient side and the substrate side, respectively, could be measured together with the transmittance T of the film corresponding to incidence of light from the ambient side in the spectral region of interest ($R \neq R'$ and $T = T'$, if the film under investigation is absorbing, where T' denotes the transmittance of the film corresponding to incidence of light from the substrate side). The authors measured the values of these three different optical quantities, that is, the values of R, R' and T, at selected wavelengths at near-normal incidence of light. They then determined the value of the thickness and the values of n and k by solving the three equations expressing R, R', and T by means of a numerical procedure at the wavelengths of interest without any auxiliary measurements [2]. The spectral dependences of the optical constants of the RbI film determined in this way correspond to absorption caused by excitons in this region. Uncertainty of the optical-constant data was reported to be about 1%. It should be noted that the wavelengths of the ultraviolet absorption peaks derived from the work by Baldini and Rigaldi [2] are inconsistent with those observed for bulk material of RbI [7, 8].

In the region $0.260\ \mu\text{m} \geq \lambda \geq 0.230\ \mu\text{m}$, we calculated the values of the refractive index n and extinction coefficient k by means of the values of parameters characterizing resonances on the lower exciton–polariton branch in RbI single crystals evaluated with three-photon difference-frequency generation (TP-DFG) by Fröhlich *et al.* [3]. Namely, as a modern method of nonlinear optical spectroscopy, the TP-DFG method opens up new possibilities to study elementary excitations in solids and, moreover, in the corresponding spectral region this method allows the determination of the spectral dependences of the optical constants of thick bulk samples of the single crystals in a reliable way. Therefore, the values of positions and widths of the resonance peaks (i.e., the values of the parameters characterizing resonances) determined for the RbI single crystal by the TP-DFG method at room temperature in the paper of Fröhlich *et al.* [3] were used to calculate the spectral dependences of n and k of RbI for the region of the exponential tail of the excitonic absorption edge, that is, for the region mentioned earlier. Equations enabling us to carry out these calculations are introduced in the paper mentioned [3]. Unfortunately, uncertainties in the values of the parameters determined with the TP-DFG method (and needed for calculating n and k)

are not introduced in the paper of Fröhlich *et al.*, and so it is not possible to estimate an accuracy of the optical constants calculated. Thus, it is impossible to compare the values of n and k determined by Baldini and Rigaldi [2] with those calculated on the basis of the TP-DFG method in an exact way. In spite of this fact, it is evident that there are nonnegligible differences between the Baldini and Rigaldi data and the data calculated. This statement is especially true for the region $0.238\ \mu m \geq \lambda \geq 0.230\ \mu m$ (see Table I). One can expect that the values of n and k calculated on the basis of the TP-DFG measurements are more reliable than those determined by Baldini and Rigaldi. The values of the optical constants obtained by Baldini and Rigaldi are probably influenced by defects frequently occurring in thin solid films. The RbI thin film studied by Baldini and Rigaldi probably exhibited polycrystalline structure (structure of this film was not examined), and thus the defects such as columnar structure, impurities, and roughness of the boundaries could considerably affect the correctness of the data presented. This conclusion is also supported by the fact that the wavelengths of the ultraviolet absorption peaks corresponding to the Baldini and Rigaldi data are inconsistent with those observed for the RbI single crystals in direct measurements [7, 8].

In the region $64.00\ \mu m \geq \lambda \geq 0.24\ \mu m$, that is, in the region of transparency of RbI, the refractive-index data obtained on the basis of the Li results [4] are introduced. This author employed the important refractive-index data published by Kublitzky [9] to obtain the following empirical dispersion formula for the refractive index of RbI:

$$n^2 = 1.60563 + \frac{0.00947\lambda^2}{\lambda^2 - (0.120)^2} + \frac{0.01073\lambda^2}{\lambda^2 - (0.134)^2} + \frac{0.00136\lambda^2}{\lambda^2 - (0.156)^2} + \frac{0.41864\lambda^2}{\lambda^2 - (0.179)^2} + \frac{0.41771\lambda^2}{\lambda^2 - (0.187)^2} + \frac{0.13707\lambda^2}{\lambda^2 - (0.223)^2} + \frac{2.36091\lambda^2}{\lambda^2 - (132.45)^2}, \quad (1)$$

λ denotes the wavelengths in micrometers.

Thus, this formula of the Sellmeier type was utilized for calculating the values of n within the spectral region of transparency of RbI [4]. These refractive-index values correspond to the RbI single crystal, since Kublitzky [9] measured the values of n characterizing RbI prisms by the method of minimum deviation at selected wavelengths in the spectral region $0.578\ \mu m \geq \lambda \geq 0.254\ \mu m$.

Sprockhoff [5] also measured the values of n of RbI by means of the method of minimum deviation. He determined the refractive-index values of the single crystal for the following three wavelengths: 0.486, 0.589, and 0.656 μm (see Table I).

The uncertainties of the refractive-index values determined by means of Eq. (1) are dependent on wavelength. (The smallest and/or greatest uncertainties in n are equal to ± 0.002 in the region $1.5\ \mu\text{m} \geq \lambda \geq 0.4\ \mu\text{m}$ and/or ± 0.02 in regions $0.25\ \mu\text{m} \geq \lambda \geq 0.24\ \mu\text{m}$ and $64\ \mu\text{m} \geq \lambda \geq 50\ \mu\text{m}$). The errors of n in Sprockhoff's measurements can be estimated as ± 0.001.

One can see that the values of n determined using Eq. (1) agree very well with those calculated on the basis of the TP-DFG measurements. Similarly, there is a very good agreement between values of n determined by means of Eq. (1) and those measured by Sprockhoff. These facts gives significant support for the correctness and reliability of the n values of bulk RbI presented here for both the visible and the region 0.23–0.38 μm. It should be noted that in the region $0.546\ \mu\text{m} \geq \lambda \geq 0.25\ \mu\text{m}$ by treating the Kublitzky data, Radhakrishnan [10] obtained the empirical dispersion formula of the Sellmeier type expressing the spectral dependence of n of the RbI single crystal in the following form:

$$n^2 = 1.6017 + \frac{0.01749\lambda^2}{\lambda^2 - 0.015625} + \frac{0.83466\lambda^2}{\lambda^2 - 0.033489} + \frac{0.13917\lambda^2}{\lambda^2 - 0.049729}, \tag{2}$$

λ is also in micrometers.

This formula yields the wavelengths of three ultraviolet absorption peaks, which agree with those studied for bulk material by direct measurements [7, 8] but gives no information concerning the infrared absorption peak. Thus, the Radhakrishnan formula [10] can not be used to calculate the values of n in a wide spectral region. Namely, the extrapolated refractive-index values for the IR wavelengths using this formula have large uncertainties compared to those obtained using the Li formula [4]. This is caused by the fact that Radhakrishnan only correlated his formula with the wavelengths of the absorption peaks in the UV region found in the independent way, while Li performed the correlation of his formula not only with these ultraviolet wavelengths, but also with the wavelength of the fundamental infrared absorption peak λ_I found by direct measurements. This fact enables us to use the Li formula in the IR region in which RbI is a nonabsorbing material. It should be noted that the values of the adjustable parameters of both the empirical dispersion formulas mentioned (e.g., the value of 0.00947 in the Li formula) were found by fitting the Kublitzky data [9] by means of the least-squares method.

Pai *et al.* [6] determined the spectral dependences of n and k characterizing RbI bulk samples (i.e., the single crystals) using amplitude and phase reflection measurements made by dispersive Fourier transform spectroscopy in the region $222.2\ \mu\text{m} \geq \lambda \geq 52.63\ \mu\text{m}$. The errors of n and k determined in this way are also dependent on wavelength. (The greatest and/or smallest

errors in both n and k are equal to ± 0.13 and/or ± 0.01 at the wavelength of about 132 μm and/or in the interval 106 μm $\geq \lambda \geq$ 54 μm [6].) Spectral dependences of n and k in the vicinity of the maximum value of k at the wavelength of the fundamental infrared absorption peak λ_I are related to one-photon absorption, corresponding to the TO phonon mode. The fine structures of the curves expressing the spectral dependences of n and k in the region 60–90 μm may be caused by multiple-phonon processes of absorption. In the region 64.52 μm $\geq \lambda \geq$ 52.63 μm, very good agreement exists between the refractive-index data presented by Pai *et al.* [6] and those calculated using the Li formula [4] (see Table I). This agreement again gives support for the correctness and reliability of the n and k values of bulk RbI introduced for the infrared region here. However, it is necessary to point out that more precise values of k will be able to be determined using transmittance measurements of sufficiently thin RbI slabs in the intervals of the infrared region in which RbI is weakly absorbing ($k \leq 0.1$), if these measurements are ever performed.

From Eq. (1) and the spectral dependence of k determined by Pai *et al.* [6], one can see that there is relatively good agreement between the value of λ_I used in the Li formula and that implied by the data of Pai *et al.*

The optical-constant data presented in this paper are the room-temperature data, as emphasized earlier. However, strictly speaking there are small differences at temperatures corresponding to the data summarized. Namely, Baldini and Rigaldi's data [2] and the data derived from the TP-DFG measurements [3] correspond to 298 K. Li's values of n [4], Sprockhoff's values of n [5], and the data of Pai *et al.* [6] correspond to 293, 298, and 300 K, respectively. Both the Radhakrishnan formula [10] and the Kublitzky measurements were for 309 K. Thus, to obtain his formula in the form presented at first, Li [4] reduced the Kublitzky data of n from 309 to 293 K by using empirical parameters enabling him to construct a dn/dT formula that was employed for the corrections mentioned (dn/dT denotes the derivative of the refractive index n with respect to temperature T).

In conclusion, one can state that the data of n and k summarized in this work represent the best values of these optical constants characterizing bulk RbI in the spectral region 222.2 μm $\geq \lambda \geq$ 0.23 μm (i.e., these data consist of the data based on the TP-DFG method, the Li data [4], the Sprockhoff [5] values of n, and the data of Pai *et al.* [6]). The data of n and k presented by Baldini and Rigaldi [2] can serve as the values of the optical constants of RbI usable for applications in the first approximation.

REFERENCES

1. D. E. McCarthy, *Appl. Opt.* **7**, 1243 (1968).
2. G. Baldini and L. Rigaldi, *J. Opt. Soc. Am.* **69**, 495 (1970).
3. D. Fröhlich, P. Köhler, W. Nieswand, and T. Rappen, *Phys. Rev. B* **43**, 12590 (1991).
4. H. H. Li, *J. Phys. Chem. Ref. Data* **5**, 329 (1976).

5. M. Sprockhoff, *Neues Jahrb. Mineral. Geol. Palaeontol., Beilageband* **18**, 117 (1904).
6. K. F. Pai, T. J. Parker, N. E. Tornberg, R. P. Lowndes, and W. G. Chambers, *Infrared Phys.* **18**, 199 (1978).
7. R. Hilsch and R. W. Pohl, *Z. Phys.* **59**, 812 (1930).
8. E. G. Schneider and H. M. O'Bryan, *Phys. Rev.* **51**, 293 (1937).
9. A. Kublitzky, *Ann. Phys.* **20**, 793 (1934).
10. T. Radhakrishnan, *Proc. Indian Acad. Sci. Sect. A* **27**, 165 (1948).

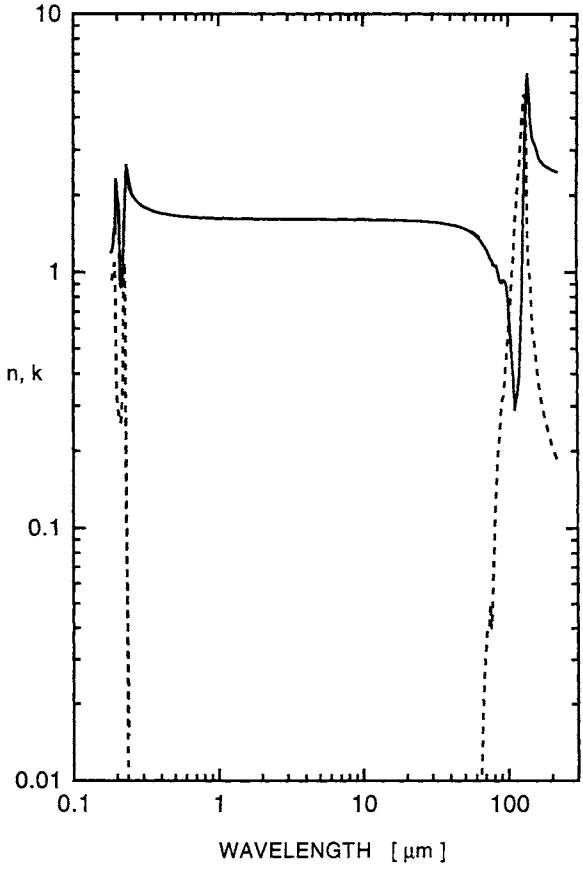

Fig. 1. Log–log plot of n (solid line) and k (dashed line) versus wavelength in micrometers for RbI.

TABLE I

Values of n and k for Rubidium Iodide as Obtained from Various References[a]

eV	cm^{-1}	μm	n	k
6.888	55,560	0.180	1.193 [2]	0.857 [2]
6.812	54,950	0.182	1.199	0.884
6.738	54,350	0.184	1.215	0.928
6.666	53,760	0.186	1.254	0.986
6.595	53,190	0.188	1.318	1.040
6.526	52,630	0.190	1.412	1.054
6.458	52,090	0.192	1.494	1.096
6.391	51,550	0.194	1.415	0.953
6.326	51,020	0.196	2.299	0.509
6.262	50,510	0.198	2.153	0.339
6.199	50,000	0.200	1.998	0.314
6.138	49,500	0.202	1.903	0.298
6.078	49,020	0.204	1.830	0.286
6.019	48,540	0.206	1.706	0.277
5.961	48,080	0.208	1.032	0.267
5.904	47,620	0.210	0.896	0.257
5.848	47,170	0.212	0.873	0.262
5.794	46,730	0.214	0.883	0.281
5.740	46,300	0.216	0.925	0.326
5.687	45,870	0.218	1.000	0.423
5.636	45,460	0.220	1.172	0.627
5.585	45,050	0.222	1.432	0.978
5.535	44,640	0.224	1.706	1.096
5.486	44,250	0.226	1.984	0.951
5.438	43,860	0.228	2.262	0.469
5.391	43,480	0.230	2.488	0.112
			2.636 [3]	0.270 [3]
5.344	43,100	0.232	2.540 [2]	0.069 [2]
			2.461 [3]	0.0751 [3]
5.299	42,740	0.234	2.497 [2]	0.046 [2]
			2.355 [3]	0.0213 [3]
5.254	42,370	0.236	2.419 [2]	0.028 [2]
			2.280 [3]	0.0062 [3]
5.209	42,020	0.238	2.343 [2]	0.015 [2]
			2.223 [3]	0.0018 [3]
5.166	41,670	0.240	2.272 [2]	
			2.177 [3]	
			2.155 [4]	
5.123	41,320	0.242	2.220 [2]	
			2.140 [3]	
			2.123 [4]	
5.081	40,980	0.244	2.171 [2]	
			2.108 [3]	
			2.094 [4]	

(continued)

[a] References given in brackets.

TABLE I *(Continued)*

Rubidium Iodide

eV	cm^{-1}	μm	n	k
5.040	40,650	0.246	2.131 [2]	
			2.081 [3]	
			2.070 [4]	
4.999	40,320	0.248	2.092 [2]	
			2.057 [3]	
			2.048 [4]	
4.959	40,000	0.250	2.059 [2]	
			2.036 [3]	
			2.028 [4]	
4.920	39,680	0.252	2.017 [3]	
			2.010 [4]	
4.881	39,370	0.254	2.000 [3]	
			1.994 [4]	
4.843	39,060	0.256	1.984 [3]	
			1.979 [4]	
4.806	38,760	0.258	1.970 [3]	
			1.966 [4]	
4.769	38,460	0.260	1.957 [3]	
			1.953 [4]	
4.732	38,170	0.262	1.941	
4.696	37,880	0.264	1.930	
4.661	37,590	0.266	1.920	
4.626	37,310	0.268	1.910	
4.592	37,040	0.270	1.901	
4.558	36,760	0.272	1.893	
4.525	36,500	0.274	1.885	
4.492	36,230	0.276	1.877	
4.460	35,970	0.278	1.870	
4.428	35,710	0.280	1.863	
4.397	35,460	0.282	1.856	
4.366	35,210	0.284	1.850	
4.335	34,970	0.286	1.844	
4.305	34,720	0.288	1.838	
4.275	34,480	0.290	1.833	
4.246	34,250	0.292	1.828	
4.217	34,010	0.294	1.823	
4.189	33,780	0.296	1.818	
4.161	33,560	0.298	1.813	
4.133	33,330	0.300	1.809	
4.065	32,790	0.305	1.798	
4.000	32,260	0.310	1.789	
3.936	31,750	0.315	1.780	
3.875	31,250	0.320	1.772	
3.815	30,770	0.325	1.765	
3.757	30,300	0.330	1.758	
3.701	29,850	0.335	1.752	

TABLE I *(Continued)*

Rubidium Iodide

eV	cm^{-1}	μm	n	k
3.647	29,410	0.340	1.746	
3.594	28,990	0.345	1.741	
3.542	28,570	0.350	1.736	
3.493	28,170	0.355	1.731	
3.444	27,780	0.360	1.727	
3.397	27,400	0.365	1.722	
3.351	27,030	0.370	1.718	
3.306	26,670	0.375	1.715	
3.263	26,320	0.380	1.711	
3.220	25,970	0.385	1.708	
3.179	25,640	0.390	1.705	
3.139	25,320	0.395	1.702	
3.100	25,000	0.400	1.699	
3.024	24,390	0.410	1.694	
2.952	23,810	0.420	1.689	
2.883	23,260	0.430	1.685	
2.818	22,730	0.440	1.681	
2.755	22,220	0.450	1.677	
2.695	21,740	0.460	1.674	
2.638	21,280	0.470	1.671	
2.583	20,830	0.480	1.668	
2.551	20,580	0.486	1.667 [5]	
2.530	20,410	0.490	1.665 [4]	
2.480	20,000	0.500	1.663	
2.431	19,610	0.510	1.661	
2.384	19,230	0.520	1.659	
2.339	18,870	0.530	1.657	
2.296	18,520	0.540	1.655	
2.254	18,180	0.550	1.653	
2.214	17,860	0.560	1.652	
2.175	17,540	0.570	1.650	
2.138	17,240	0.580	1.649	
2.105	16,980	0.589	1.647 [5]	
2.101	16,950	0.590	1.647 [4]	
2.066	16,670	0.600	1.646	
2.000	16,130	0.620	1.644	
1.937	15,625	0.640	1.642	
1.890	15,240	0.656	1.640 [5]	
1.879	15,150	0.660	1.640 [4]	
1.823	14,710	0.680	1.638	
1.771	14,290	0.700	1.637	
1.722	13,890	0.720	1.635	
1.675	13,510	0.740	1.634	
1.631	13,160	0.760	1.633	
1.590	12,820	0.780	1.632	
1.550	12,500	0.800	1.631	

(continued)

TABLE I *(Continued)*

Rubidium Iodide

eV	cm^{-1}	μm	n	k
1.512	12,200	0.820	1.630	
1.476	11,900	0.840	1.629	
1.442	11,630	0.860	1.628	
1.409	11,360	0.880	1.627	
1.378	11,110	0.900	1.627	
1.348	10,870	0.920	1.626	
1.319	10,640	0.940	1.625	
1.292	10,420	0.960	1.625	
1.265	10,200	0.980	1.624	
1.240	10,000	1.00	1.624	
1.181	9,524	1.05	1.623	
1.127	9,091	1.10	1.622	
1.078	8,696	1.15	1.621	
1.033	8,333	1.20	1.620	
0.9919	8,000	1.25	1.620	
0.9537	7,692	1.30	1.619	
0.9184	7,407	1.35	1.619	
0.8856	7,143	1.40	1.618	
0.8551	6,897	1.45	1.618	
0.8266	6,667	1.50	1.617	
0.7749	6,250	1.60	1.617	
0.7293	5,882	1.70	1.616	
0.6888	5,556	1.80	1.616	
0.6526	5,263	1.90	1.616	
0.6199	5,000	2.00	1.615	
0.5637	4,545	2.20	1.615	
0.5166	4,167	2.40	1.614	
0.4769	3,846	2.60	1.614	
0.4428	3,571	2.80	1.614	
0.4133	3,333	3.00	1.613	
0.3542	2,857	3.50	1.613	
0.3100	2,500	4.00	1.613	
0.2755	2,222	4.50	1.612	
0.2480	2,000	5.00	1.612	
0.2066	1,667	6.00	1.611	
0.1771	1,429	7.00	1.611	
0.1550	1,250	8.00	1.610	
0.1378	1,111	9.00	1.609	
0.1240	1,000	10.0	1.609	
0.1127	909.1	11.0	1.608	
0.1033	833.3	12.0	1.607	
0.09537	769.2	13.0	1.606	
0.08856	714.3	14.0	1.604	
0.08266	666.7	15.0	1.603	
0.07999	645.2	15.5	1.602	
0.07749	625.0	16.0	1.602	

TABLE I *(Continued)*

Rubidium Iodide

eV	cm^{-1}	μm	n	k
0.07514	606.1	16.5	1.601	
0.07293	588.2	17.0	1.600	
0.07085	571.4	17.5	1.600	
0.06888	555.6	18.0	1.599	
0.06702	540.5	18.5	1.598	
0.06526	526.3	19.0	1.597	
0.06358	512.8	19.5	1.596	
0.06199	500.0	20.0	1.596	
0.06048	487.8	20.5	1.595	
0.05904	476.2	21.0	1.594	
0.05767	465.1	21.5	1.593	
0.05636	454.5	22.0	1.592	
0.05510	444.4	22.5	1.591	
0.05391	434.8	23.0	1.590	
0.05276	425.5	23.5	1.589	
0.05166	416.7	24.0	1.588	
0.05061	408.2	24.5	1.587	
0.04959	400.0	25.0	1.585	
0.04862	392.2	25.5	1.584	
0.04769	384.6	26.0	1.583	
0.04679	377.4	26.5	1.582	
0.04592	370.4	27.0	1.581	
0.04509	363.6	27.5	1.579	
0.04428	357.1	28.0	1.578	
0.04350	350.9	28.5	1.577	
0.04275	344.8	29.0	1.575	
0.04203	339.0	29.5	1.574	
0.04133	333.3	30.0	1.573	
0.04065	327.9	30.5	1.571	
0.04000	322.6	31.0	1.570	
0.03936	317.5	31.5	1.568	
0.03875	312.5	32.0	1.567	
0.03815	307.7	32.5	1.565	
0.03757	303.0	33.0	1.563	
0.03701	298.5	33.5	1.562	
0.03647	294.1	34.0	1.560	
0.03594	289.9	34.5	1.558	
0.03542	285.7	35.0	1.557	
0.03493	281.7	35.5	1.555	
0.03444	277.8	36.0	1.553	
0.03397	274.0	36.5	1.551	
0.03351	270.3	37.0	1.549	
0.03306	266.7	37.5	1.548	
0.03263	263.2	38.0	1.546	
0.03220	259.7	38.5	1.544	
0.03179	256.4	39.0	1.542	

(continued)

TABLE I *(Continued)*

Rubidium Iodide

eV	cm^{-1}	μm	n	k
0.03139	253.2	39.5	1.540	
0.03100	250.0	40.0	1.537	
0.03061	246.9	40.5	1.535	
0.03024	243.9	41.0	1.533	
0.02988	241.0	41.5	1.531	
0.02952	238.1	42.0	1.529	
0.02917	235.3	42.5	1.526	
0.02883	232.6	43.0	1.524	
0.02850	229.9	43.5	1.522	
0.02818	227.3	44.0	1.519	
0.02786	224.7	44.5	1.517	
0.02755	222.2	45.0	1.514	
0.02725	219.8	45.5	1.512	
0.02695	217.4	46.0	1.509	
0.02666	215.1	46.5	1.506	
0.02638	212.8	47.0	1.504	
0.02610	210.5	47.5	1.501	
0.02583	208.3	48.0	1.498	
0.02556	206.2	48.5	1.495	
0.02530	204.1	49.0	1.492	
0.02505	202.0	49.5	1.489	
0.02480	200.0	50.0	1.486	
0.02455	198.0	50.5	1.483	
0.02431	196.1	51.0	1.480	
0.02407	194.2	51.5	1.477	
0.02384	192.3	52.0	1.473	
0.02362	190.5	52.5	1.470	
0.02356	190.0	52.63	1.46 [6]	
0.02339	188.7	53.0	1.466 [4]	
0.02317	186.9	53.5	1.463	
0.02296	185.2	54.0	1.459	
0.02294	185.0	54.05	1.46 [6]	
0.02275	183.5	54.5	1.456 [4]	
0.02254	181.8	55.0	1.452	
0.02234	180.2	55.5	1.448	
0.02232	180.0	55.56	1.44 [6]	
0.02214	178.6	56.0	1.445 [4]	
0.02194	177.0	56.5	1.441	
0.02175	175.4	57.0	1.437	
0.02170	175.0	57.14	1.43 [6]	0.01 [6]
0.02156	173.9	57.5	1.433 [4]	
0.02138	172.4	58.0	1.428	
0.02119	170.9	58.5	1.424	
0.02108	170.0	58.82	1.41 [6]	0.01 [6]
0.02101	169.5	59.0	1.420 [4]	
0.02084	168.1	59.5	1.416	

TABLE I *(Continued)*

Rubidium Iodide

eV	cm^{-1}	μm	n	k
0.02066	166.7	60.0	1.411	
0.02049	165.3	60.5	1.406	
0.02046	165.0	60.61	1.39 [6]	0.01 [6]
0.02033	163.9	61.0	1.402 [4]	
0.02016	162.6	61.5	1.397	
0.02000	161.3	62.0	1.392	
0.01984	160.0	62.50	1.387	
			1.37 [6]	0.01 [6]
0.01968	158.7	63.0	1.382 [4]	
0.01953	157.5	63.5	1.377	
0.01937	156.3	64.0	1.372	
0.01922	155	64.52	1.34 [6]	0.01 [6]
0.01860	150	66.67	1.30	0.02
0.01798	145	68.97	1.27	0.03
0.01736	140	71.43	1.23	0.04
0.01711	138	72.46	1.21	0.04
0.01686	136	73.53	1.18	0.04
0.01661	134	74.63	1.16	0.05
0.01637	132	75.76	1.13	0.04
0.01612	130	76.92	1.12	0.04
0.01587	128	78.13	1.10	0.06
0.01562	126	79.37	1.07	0.08
0.01537	124	80.65	1.06	0.10
0.01513	122	81.97	1.06	0.14
0.01488	120	83.34	1.06	0.16
0.01463	118	84.75	1.02	0.20
0.01438	116	86.21	0.98	0.22
0.01413	114	87.72	0.94	0.24
0.01389	112	89.29	0.91	0.29
0.01364	110	90.91	0.91	0.32
0.01339	108	92.59	0.93	0.33
0.01314	106	94.34	0.93	0.37
0.01289	104	96.15	0.92	0.43
0.01265	102	98.04	0.88	0.49
0.01240	100	100.0	0.79	0.57
0.01215	98.0	102.0	0.64	0.67
0.01190	96.0	104.2	0.55	0.78
0.01165	94.0	106.4	0.46	0.93
0.01141	92.0	108.7	0.37	1.12
0.01116	90.0	111.1	0.29	1.38
0.01091	88.0	113.6	0.32	1.67
0.01066	86.0	116.3	0.34	2.05
0.01041	84.0	119.0	0.40	2.48
0.01017	82.0	122.0	0.56	3.08
0.00992	80.0	125.0	0.83	3.93
0.00967	78.0	128.2	1.52	4.93

(continued)

TABLE I *(Continued)*

Rubidium Iodide

eV	cm^{-1}	μm	n	k
0.00942	76.0	131.6	4.26	4.80
0.00917	74.0	135.1	5.89	2.41
0.00893	72.0	138.9	4.97	1.07
0.00868	70.0	142.9	3.80	0.94
0.00843	68.0	147.1	3.33	0.59
0.00818	66.0	151.5	3.19	0.52
0.00794	64.0	156.3	3.04	0.44
0.00769	62.0	161.3	2.87	0.38
0.00744	60.0	166.7	2.73	0.33
0.00682	55.0	181.8	2.60	0.26
0.00620	50.0	200.0	2.51	0.21
0.00558	45.0	222.2	2.46	0.18

Sodium Nitrate ($NaNO_3$)

EDWARD D. PALIK
Institute for Physical Science and Technology

and

R. KHANNA
Department of Chemistry and Biochemistry
University of Maryland
College Park, Maryland

Sodium nitrate ($NaNO_3$) is isomorphic with $CaCO_3$ (calcite). Unlike calcite, $NaNO_3$ is water soluble and, hence, not particularly suitable as an industrial birefringent material. The interest in $NaNO_3$ is principally due to an order–disorder phase transition it undergoes in the temperature range 150 to 276° C. In the room-temperature phase sodium nitrate is a trigonal crystal with space group symmmetry R3c (D_{3d}). The unit cell contains two $NaNO_3$ formula units; the two NO_3^- ions are oriented in planes perpendicular to the optic axis. Above the phase transition, the NO_3^- ions are randomly oriented in the same plane.

The optical characteristics of $NaNO_3$ have been determined from the vacuum UV (95,000 cm^{-1}) to the far IR (10 cm^{-1}). The values of n(o), k(o), n(e) and k(e) specifying the ordinary and extraordinary optical constants obtained in this critique are listed in Table I and plotted in Fig. 1.

The ultraviolet region has been studied by Uzan *et al.* [1] and Yamashita [2]. Measurements of reflectivity were made as a function of angle of incidence with *s*- and *p*-polarized light [1]. The sample was mechanically polished with the *c*-axis presumably in the plane. The polarized reflectivity was measured on a cleaved (1011) surface at normal incidence and treated by Kramers–Kronig (K-K) analysis by Yamashita [2]. Although we prefer the angle-of-incidence technique with polarized light, the sample, being mechanically polished, presents several problems depending on the depth of damage, the crystal orientation within the optical skin depth $\delta = 1/\alpha = \lambda/4\pi k$, and the effect of water on the surface while the sample is being prepared and inserted into the vacuum spectrometer. In fact, Yamashita demon-

Copyright © 1998 by Academic Press.
All rights of reproduction in any form reserved
ISBN 0-12-544423-0/$25.00.

strated for reflectivity results with mechanical polishing that there was a significant variation in R, with R(polished) always smaller than R(cleaved). However, his analysis for the cleaved surface was more complicated. The sample had the c-axis at 43°49′ to the surface, so with normal incidence one can measure $\mathbf{E}\perp\mathbf{c}$ directly but not $\mathbf{E}\parallel\mathbf{c}$, only $\mathbf{E}\parallel\mathbf{c}'$, where $\mathbf{c}'$ is a direction in the surface containing the plane of incidence, the c-axis and the c'-axis. It was then necessary to use K-K analysis and the equation for the dielectric ellipsoid (with both real and imaginary parts) to obtain ϵ(e); ϵ(o) was directly measured.

Because there is folklore saying that bigger (reflectivity) is better, we choose to exhibit the data of Yamashita [2] in Table I. Plots of the real and imaginary plots of ϵ(o) and ϵ(e) were expanded and read. This can be done at best to two significant figures, but we give n(o), k(o) and n(e), k(e) to three or four figures to show trends and structures in the spectrum. The absolute values are surely uncertain to $\pm 10\%$ and even more for small values of k.

There do not seem to be any measurements of the refractive indices throughout the visible. The refractive indices reported in the "CRC Handbook of Chemistry and Physics" [3], presumably for the Na D line, are n(o) = 1.587 and n(e) = 1.336. There is little or no absorption and, consequently, no significant dispersion in the visible region. We include these two values in Table I.

We could find no measurements of n(o) or n(e) in the vis–near IR spectral region that might be fitted with a Sellmeier-type dispersion equation.

Greenberg and Hallgren [4] measured the near-IR (2–15 μm) transmittance of films grown in the interstices of a fine-mesh platinum screen; we assume the sample was polycrystalline. They observed several weak bands in the 3–6 μm region, which they assigned as overtone or combination bands. They also assigned fundamental bands at $\nu_3 = 1400\ \text{cm}^{-1}$, $\nu_2 = 833\ \text{cm}^{-1}$, and $\nu_4 = 719\ \text{cm}^{-1}$. Just above the melting point an additional weak absorption line at $1047\ \text{cm}^{-1}$ was assigned to ν_1, which is inactive in the room-temperature crystal phase. The ν notation refers to the internal vibration modes of the NO_3^- molecule. Because of the lack of information on sample thickness, these data could not be used to obtained the optical constants.

Frech and Nichols [5] measured the (ordinary) reflectance of the strong vibration band at 7.1 μm. This oscillator makes a significant contribution to the reflectance, whereas the weak band at $833\ \text{cm}^{-1}$ is probably too weak to show up in reflection. Interestingly, Frech and Nichols assume a classical oscillator with a frequency-dependent damping constant to explain a sharp dip in the reststrahlen peak at $1448\ \text{cm}^{-1}$. They found $\omega_T = 1356\ \text{cm}^{-1}$ and $\omega_L = 1468\ \text{cm}^{-1}$ and used $\epsilon_\infty = 2.518$, which corresponds to $n(\text{o})^2$ at 0.5890 μm as given in Table I. We calculated n(o) and k(o) using a classical oscillator model with the frequency-dependent damping constant given by Frech and Nicols [5]. Our calculation did not quite reproduce the measured reflectivity, giving a peak reflectivity of 0.86 compared to the measured value of 0.80. Therefore, we only give n and k to 2–3 figures. The values of n(o)

were extrapolated from 1700 up to 10,000 cm^{-1}. We also extrapolated n(o) to somewhat lower frequency to note how it blended into the lower-frequency data of Brehat and Wyncke [6], to be discussed later.

The far-infrared region 10–600 cm^{-1} has been studied by Brehat and Wyncke [6]. $NaNO_3$ crystals were grown by the Bridgman method. Several plates of (1010) orientation were mechanically polished. Both $\mathbf{E} \| \mathbf{c}$ (A_{2u} modes) and $\mathbf{E} \| \mathbf{a}$ (E_u modes) were measured; here $\mathbf{E} \| \mathbf{a}$ is equivalent to $\mathbf{E} \perp \mathbf{c}$. Measurements were made at temperatures from 10 to 549 K. Room-temperature spectra were shown at 299 K for A_{2u} modes and 303 K for E_u modes. Infrared reflectivity was measured at a 10° angle of incidence with a grating spectrometer. In addition, transmission measurements were made at 7–18 cm^{-1} using a monochromatic spectrometer with a tunable electron-beam, backward-wave oscillator [7]. A factorized form of the dielectric function was used to fit the reflectivity:

$$\epsilon(\omega) = \epsilon_\infty \frac{(\omega - i\gamma_{LR})}{(\omega - i\gamma_{TR})} \prod_j \frac{(\omega_{Lj}^2 - \omega^2 + i\omega\gamma_{Lj})}{(\omega_{Tj}^2 - \omega^2 + i\omega\gamma_{Tj})}, \tag{1}$$

Here, ω_j and γ_j are the frequencies and damping constants of the transverse and longitudinal polar lattice mode j, ϵ_∞ is the high-frequency dielectric constant, and γ_{TR} and γ_{LR} are damping factors for a relaxation mode assumed to be at $\omega = 0$. Although the Lorentz model is often used for several independent oscillators, a dielectric function of the form of Eq. (1) is sometimes used when the Lorentz model does not fit the reflectivity data well. One appears to be adding more adjustable parameters to obtain a better fit. Much more-detailed models are discussed by Gervais and Piriou [8] and Berreman and Unterwald [9]. The fitting parameters are listed in Table II; here we have obtained the relaxation parameters at 300 K from a graph showing their temperature dependence by Brehat and Wyncke [6]. Equation (1) at $\omega = 0$ gives the dc dielectric constants as $\epsilon(0)\perp = 5.96$ and $\epsilon(0)\| = 8.51$. We have calculated n(o,⊥), k(o,⊥), n(e,∥), k(e,∥) and list the data in Table I. The n and k for the three transmittance measurements are listed at 9.3, 13.3, and 17.3 cm^{-1} for comparison with the oscillator model; here $T = 26°$ C for (o) and $T = 30°$ C for (e).

The drastic mismatch in n(o) near 1000 cm^{-1} from Frech and Nichols [5] and Brehat and Wyncke [6] is due to the fact that Brehat and Wynke omitted the strong oscillator near 1400 cm^{-1} [5] from their model given in Eq. (1). In principle, the reader can do this to obtain somewhat better n(o) data in this spectral region.

REFERENCES

1. E. Uzan, H. Damany, and V. Chandrasekharan, Proprietes optique du nitrate de sodium dans la region de Schumann. *Opt. Commun.* **2**, 84 (1970).
2. H. Yamashita, Optical properties of sodium nitrate in the vacuum ultraviolet region. *J. Phys. Soc. Jpn.* **33**, 1407 (1972).

3. R. C. Weast, ed., "CRC Handbook of Chemistry and Physics," 53rd Ed., The Chemical Rubber Co., Cleveland, Ohio, 1972.
4. G. Greenberg and L. J. Hallgren, Infrared absorption spectra of alkali metal nitrates and nitrites above and below the melting point. *J. Chem. Phys.* **33**, 900 (1960).
5. R. Frech and H. Nichols, Anomalous infrared reflectivity minimum in $NaNO_3$. *Phys. Rev. B* **19**, 1243 (1979).
6. F. Brehat and B. Wyncke, Analysis of the temperature-dependent infrared active lattice modes in the ordered phase of sodium nitrate. *J. Phys. C: Solid State Phys.* **18**, 4247 (1985).
7. B. Wyncke, F. Brehat, and G. V. Kozlov, Low-frequency dielectric response function of sodium nitrate. *Phys. Status Solidi B* **129**, 531 (1985).
8. F. Gervais and B. Piriou, Temperature dependence of transverse- and longitudinal-optic modes in TiO_2 (rutile). *Phys. Rev. B* **10**, 1646 (1974).
9. D. W. Berreman and F. C. Unterwald, Adjusting poles and zeroes of dielectric dispersion to fit reststrahlen of $PrCl_3$ and $LaCl_3$. *Phys. Rev.* **174**, 791 (1968).

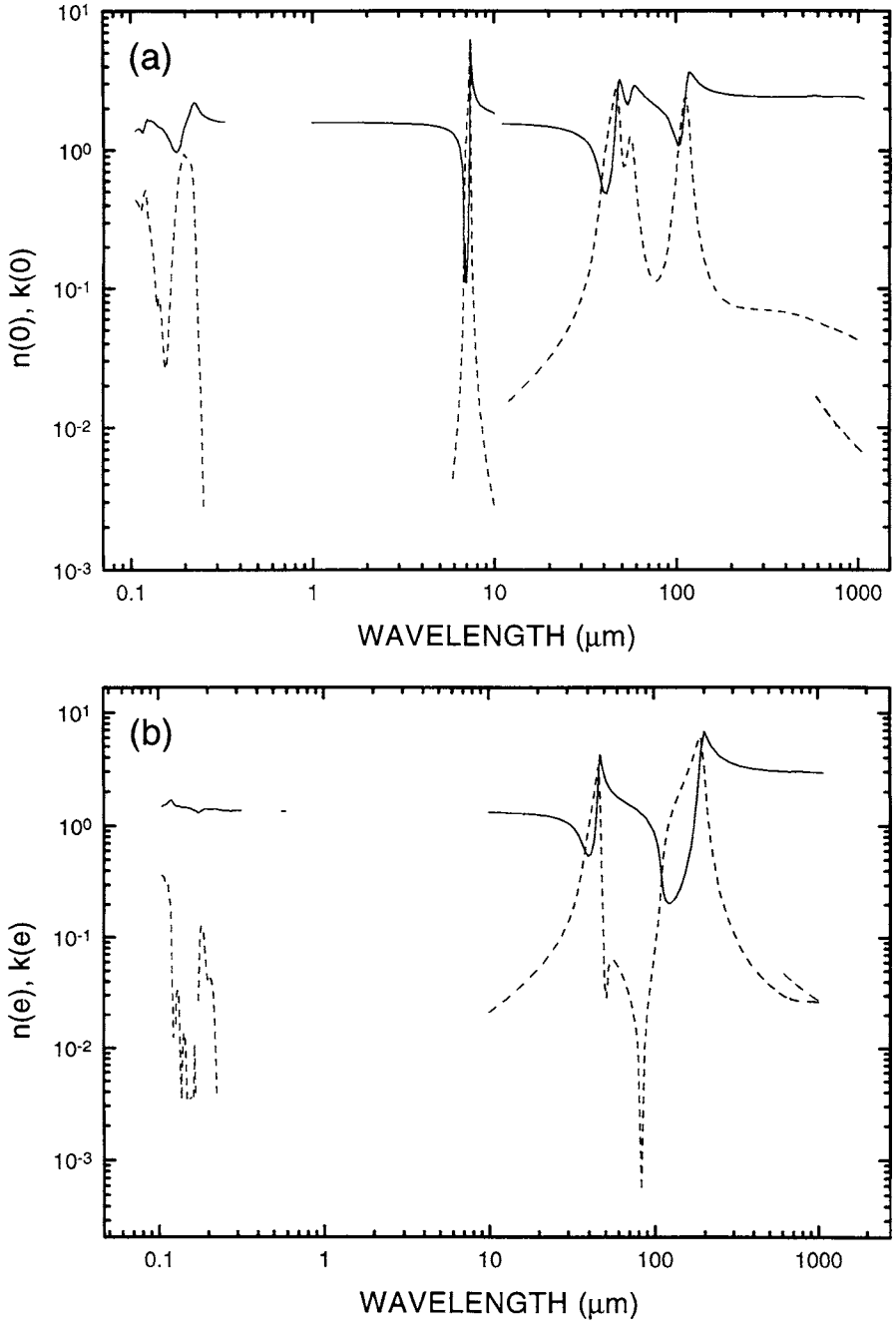

Fig. 1. (a) Log–log plot of n(o) (solid line) and k(o) (dashed line) versus wavelength in micrometers for sodium nitrate. (b) Log–log plot of n(e) (solid line) and k(e) (dashed line) versus wavelength in micrometers for sodium nitrate.

TABLE I

Values of n and k for Sodium Nitrate as Obtained from Various References[a]

eV	cm^{-1}	μm	n(o)	k(o)	n(e)	k(e)
11.8	95170	0.1051	1.374 [2]	4.36E-1 [2]	1.480 [2]	3.61E-1 [2]
11.7	94370	0.1060	1.388	4.33E-1	1.490	3.62E-1
11.6	93560	0.1069	1.404	4.28E-1	1.503	3.59E-1
11.5	92750	0.1078	1.413	4.22E-1	1.514	3.53E-1
11.4	91950	0.1088	1.421	4.11E-1	1.522	3.41E-1
11.3	91140	0.1097	1.424	4.00E-1	1.531	3.26E-1
11.2	90330	0.1107	1.424	3.86E-1	1.541	3.08E-1
11.1	89530	0.1117	1.420	3.69E-1	1.546	3.00E-1
11.0	88720	0.1127	1.403	3.59E-1	1.556	3.02E-1
10.9	87910	0.1137	1.380	3.69E-1	1.579	3.10E-1
10.8	87110	0.1148	1.344	4.09E-1	1.609	3.01E-1
10.7	86300	0.1159	1.341	4.47E-1	1.627	2.45E-1
10.6	85490	0.1170	1.393	4.80E-1	1.642	2.19E-1
10.5	84690	0.1181	1.454	5.05E-1	1.659	2.08E-1
10.4	83880	0.1192	1.516	5.19E-1	1.688	1.71E-1
10.3	83070	0.1204	1.578	5.10E-1	1.681	9.51E-2
10.2	82270	0.1216	1.638	4.30E-1	1.646	3.64E-2
10.1	81460	0.1228	1.660	3.55E-1	1.621	2.46E-2
10.0	80650	0.1240	1.646	3.15E-1	1.587	1.25E-2
9.9	79850	0.1252	1.639	2.95E-1	1.552	
9.8	79040	0.1265	1.635	2.75E-1	1.519	
9.7	78240	0.1278	1.631	2.51E-1	1.506	1.65E-2
9.6	77430	0.1292	1.627	2.24E-1	1.490	3.02E-2
9.5	76620	0.1305	1.619	1.94E-1	1.490	3.35E-2
9.4	75820	0.1319	1.609	1.77E-1	1.490	3.02E-2
9.3	75010	0.1333	1.594	1.50E-1	1.486	3.02E-2
9.2	74200	0.1348	1.576	1.26E-1	1.483	1.68E-2
9.1	73400	0.1362	1.553	1.11E-1	1.473	6.79E-3
9.0	72590	0.1378	1.525	8.84E-2	1.459	3.43E-3
8.9	71780	0.1393	1.495	7.35E-2	1.449	6.89E-3
8.8	70980	0.1409	1.475	8.13E-2	1.445	1.03E-2
8.7	70170	0.1425	1.458	8.57E-2	1.445	1.38E-2
8.6	69360	0.1442	1.454	7.90E-2	1.445	1.38E-2
8.5	68560	0.1459	1.447	6.90E-2	1.445	1.03E-2
8.4	67750	0.1476	1.436	6.09E-2	1.445	6.91E-3
8.3	66940	0.1494	1.411	4.60E-2	1.442	3.46E-3
8.2	66140	0.1512	1.386	3.60E-2	1.438	
8.1	65330	0.1531	1.356	2.94E-2	1.435	
8.0	64520	0.1550	1.330	2.63E-2	1.428	3.50E-3
7.9	63720	0.1569	1.292	2.70E-2	1.417	3.53E-3
7.8	62910	0.1590	1.257	3.18E-2	1.403	3.56E-3
7.7	62100	0.1610	1.217	4.10E-2	1.382	
7.6	61300	0.1631	1.176	6.37E-2	1.371	3.64E-3
7.5	60490	0.1653	1.130	8.84E-2	1.363	1.09E-2
7.4	59680	0.1675	1.076	1.39E-1	1.360	3.86E-3

[a] References given in brackets.

TABLE I *(Continued)*

Sodium Nitrate

eV	cm^{-1}	μm	n(o)	k(o)	n(e)	k(e)
7.3	58880	0.1698	1.031	1.84E-1	1.349	3.70E-3
7.2	58070	0.1722	1.001	2.49E-1	1.311	
7.1	57260	0.1746	0.991	3.22E-1	1.300	2.69E-2
7.0	56460	0.1771	0.973	3.95E-1	1.301	6.14E-2
6.9	55650	0.1797	0.969	4.89E-1	1.319	1.09E-1
6.8	54850	0.1823	0.987	5.87E-1	1.347	1.26E-1
6.7	54040	0.1851	1.029	6.85E-1	1.369	1.24E-1
6.6	53230	0.1879	1.092	7.64E-1	1.386	1.11E-1
6.5	52430	0.1907	1.204	8.42E-1	1.399	8.57E-2
6.4	51620	0.1937	1.319	8.78E-1	1.405	6.40E-2
6.3	50810	0.1968	1.446	9.43E-1	1.404	4.62E-2
6.2	50010	0.2000	1.519	8.98E-1	1.396	3.93E-2
6.1	49200	0.2033	1.618	8.89E-1	1.393	4.30E-2
6.0	48390	0.2066	1.705	8.70E-1	1.393	4.30E-2
5.9	47590	0.2101	1.804	8.58E-1	1.393	3.94E-2
5.8	46780	0.2138	1.941	8.24E-1	1.396	3.22E-2
5.7	45970	0.2175	2.075	7.46E-1	1.400	2.14E-2
5.6	45170	0.2214	2.174	5.74E-1	1.400	1.07E-2
5.5	44360	0.2254	2.212	3.38E-1	1.396	3.57E-3
5.4	43550	0.2296	2.147	1.74E-1	1.385	
5.3	42750	0.2339	2.046	8.06E-2	1.378	
5.2	41940	0.2384	1.952	3.58E-2	1.371	
5.1	41130	0.2431	1.881	2.12E-2	1.367	
5.0	40330	0.2480	1.822	1.09E-2	1.363	
4.9	39520	0.2530	1.783	2.80E-3	1.361	
4.8	38710	0.2583	1.740		1.360	
4.7	37910	0.2638	1.717		1.356	
4.6	37100	0.2695	1.688		1.352	
4.5	36290	0.2755	1.667		1.352	
4.4	35490	0.2818	1.652		1.352	
4.3	34680	0.2883	1.640		1.356	
4.2	33880	0.2952	1.624		1.360	
4.1	33070	0.3024	1.615		1.363	
4.0	32260	0.3100	1.612		1.363	
2.105	16980	0.5890	1.587 [3]		1.336 [3]	
1.240	10000	1.000	1.584 [5]			
1.116	9000	1.111	1.583			
0.9919	8000	1.250	1.582			
0.8679	7000	1.429	1.581			
0.7439	6000	1.667	1.579			
0.6199	5000	2.000	1.576			
0.4959	4000	2.500	1.569			
0.4339	3500	2.857	1.562			
0.3720	3000	3.333	1.552			

(continued)

TABLE I *(Continued)*

Sodium Nitrate

eV	cm^{-1}	μm	n(o)	k(o)	n(e)	k(e)
0.3472	2800	3.571	1.544			
0.3224	2600	3.846	1.535			
0.2976	2400	4.167	1.521			
0.2728	2200	4.545	1.501			
0.2480	2000	5.000	1.466			
0.2356	1900	5.263	1.438			
0.2232	1800	5.556	1.396			
0.2108	1700	5.882	1.33	4.4E-3 [5]		
0.2046	1650	6.061	1.27	6.3E-3		
0.1984	1600	6.250	1.19	9.8E-3		
0.1922	1550	6.452	1.05	1.8E-2		
0.1860	1500	6.667	0.77	4.3E-2		
0.1847	1490	6.711	0.66	5.8E-2		
0.1835	1480	6.757	0.51	8.6E-2		
0.1823	1470	6.803	0.29	1.8E-1		
0.1820	1468	6.812	0.24	2.4E-1		
0.1818	1466	6.821	0.20	2.8E-1		
0.1815	1464	6.831	0.17	3.4E-1		
0.1813	1462	6.840	0.15	4.0E-1		
0.1810	1460	6.849	0.14	4.6E-1		
0.1808	1458	6.859	0.13	5.1E-1		
0.1805	1456	6.868	0.12	5.6E-1		
0.1804	1455	6.873	0.12	5.9E-1		
0.1803	1454	6.878	0.12	6.1E-1		
0.1802	1453	6.882	0.12	6.4E-1		
0.1800	1452	6.887	0.13	6.6E-1		
0.1799	1451	6.892	0.14	6.8E-1		
0.1798	1450	6.897	0.15	7.1E-1		
0.1797	1449	6.901	0.18	7.3E-1		
0.1795	1448	6.906	0.21	7.6E-1		
0.1794	1447	6.911	0.21	7.8E-1		
0.1793	1446	6.916	0.18	8.0E-1		
0.1792	1445	6.920	0.15	8.2E-1		
0.1790	1444	6.925	0.13	8.4E-1		
0.1789	1443	6.930	0.12	8.6E-1		
0.1788	1442	6.935	0.12	8.9E-1		
0.1785	1440	6.944	0.11	9.3E-1		
0.1779	1435	6.969	0.11	1.1E0		
0.1773	1430	6.993	0.11	1.2E0		
0.1767	1425	7.018	0.11	1.3E0		
0.1761	1420	7.042	0.12	1.4E0		
0.1754	1415	7.067	0.13	1.5E0		
0.1748	1410	7.092	0.14	1.7E0		
0.1742	1405	7.117	0.16	1.8E0		
0.1736	1400	7.143	0.18	2.0E0		
0.1723	1390	7.194	0.24	2.4E0		

TABLE I *(Continued)*

Sodium Nitrate

eV	cm^{-1}	μm	n(o)	k(o)	n(e)	k(e)
0.1711	1380	7.246	0.38	3.0E0		
0.1699	1370	7.299	0.77	4.1E0		
0.1692	1365	7.326	1.34	5.0E0		
0.1686	1360	7.353	2.97	6.1E0		
0.1680	1355	7.380	6.20	4.8E0		
0.1674	1350	7.407	6.07	2.0E0		
0.1668	1345	7.435	5.10	9.5E-1		
0.1661	1340	7.463	4.45	5.6E-1		
0.1649	1330	7.519	3.69	2.7E-1		
0.1637	1320	7.576	3.27	1.6E-1		
0.1624	1310	7.634	2.99	1.1E-1		
0.1612	1300	7.692	2.80	7.8E-2		
0.1587	1280	7.813	2.54	4.7E-2		
0.1562	1260	7.937	2.38	3.1E-2		
0.1537	1240	8.065	2.27	2.3E-2		
0.1513	1220	8.197	2.18	1.7E-2		
0.1488	1200	8.333	2.12	1.3E-2		
0.1364	1100	9.091	1.95	5.3E-3		
0.1240	1000	10.00	1.86	2.8E-3		
0.1240	1000	10.00	1.558 [6]	1.26E-2 [6]	1.322 [6]	2.11E-2 [6]
0.1116	900	11.11	1.552	1.42E-2	1.317	2.38E-2
0.09919	800	12.59	1.544	1.63E-2	1.310	2.74E-2
0.08679	700	14.29	1.532	1.93E-2	1.300	3.23E-2
0.07439	600	16.67	1.512	2.38E-2	1.283	3.98E-2
0.06199	500	20.00	1.475	3.15E-2	1.251	5.24E-2
0.05951	480	20.83	1.464	3.38E-2	1.242	5.61E-2
0.05703	460	21.74	1.451	3.65E-2	1.231	6.05E-2
0.05455	440	22.73	1.435	3.98E-2	1.218	6.57E-2
0.05207	420	23.81	1.417	4.37E-2	1.202	7.20E-2
0.04959	400	25.00	1.394	4.87E-2	1.182	7.99E-2
0.04835	390	25.64	1.380	5.18E-2	1.170	8.47E-2
0.04711	380	26.32	1.364	5.52E-2	1.157	9.01E-2
0.04587	370	27.03	1.347	5.93E-2	1.142	9.64E-2
0.04463	360	27.78	1.327	6.40E-2	1.125	1.04E-1
0.04339	350	28.57	1.304	6.97E-2	1.105	1.13E-1
0.04215	340	29.41	1.277	7.66E-2	1.082	1.23E-1
0.04091	330	30.30	1.245	8.52E-2	1.055	1.36E-1
0.03968	320	31.25	1.207	9.62E-2	1.022	1.53E-1
0.03843	310	32.26	1.160	1.11E-1	0.981	1.75E-1
0.03720	300	33.33	1.102	1.31E-1	0.931	2.05E-1
0.03595	290	34.48	1.027	1.60E-1	0.867	2.48E-1
0.03472	280	35.71	0.929	2.06E-1	0.786	3.16E-1
0.03347	270	37.04	0.796	2.88E-1	0.688	4.29E-1
0.03224	260	38.46	0.630	4.56E-1	0.591	6.18E-1
0.03100	250	40.00	0.504	7.58E-1	0.538	8.97E-1

(continued)

TABLE I *(Continued)*

Sodium Nitrate

eV	cm^{-1}	μm	n(o)	k(o)	n(e)	k(e)
0.02976	240	41.67	0.486	1.15E0	0.558	1.28E0
0.02852	230	43.48	0.591	1.65E0	0.717	1.86E0
0.02790	225	44.44	0.729	1.97E0	0.946	2.31E0
0.02728	220	45.45	1.000	2.35E0	1.549	2.95E0
0.02697	217.5	45.98	1.236	2.56E0	2.256	3.27E0
0.02666	215	46.51	1.581	2.75E0	3.406	3.12E0
0.02635	212.5	47.06	2.067	2.83E0	4.188	2.02E0
0.02604	210	47.62	2.633	2.68E0	4.006	9.89E-1
0.02573	207.5	48.19	3.065	2.24E0	3.590	4.75E-1
0.02542	205	48.78	3.199	1.71E0	3.237	2.31E-1
0.02480	200	50.00	2.933	1.01E0	2.762	3.66E-2
0.02418	195	51.28	2.560	7.63E-1	2.468	2.85E-2
0.02356	190	52.63	2.262	7.78E-1	2.269	5.30E-2
0.02294	185	54.05	2.120	9.87E-1	2.123	6.17E-2
0.02232	180	55.56	2.290	1.25E0	2.011	6.34E-2
0.02170	175	57.14	2.711	1.21E0	1.921	6.18E-2
0.02108	170	58.82	2.916	8.34E-1	1.845	5.85E-2
0.02046	165	60.61	2.843	5.14E-1	1.780	5.43E-2
0.01984	160	62.50	2.700	3.33E-1	1.721	4.96E-2
0.01860	150	66.67	2.449	1.79E-1	1.617	3.95E-2
0.01736	140	71.43	2.260	1.26E-1	1.520	2.86E-2
0.01612	130	76.92	2.097	1.12E-1	1.418	1.62E-2
0.01550	125	80.00	2.015	1.15E-1	1.362	8.93E-3
0.01488	120	83.33	1.924	1.27E-1	1.298	5.46E-4
0.01426	115	86.96	1.815	1.51E-1	1.226	9.60E-3
0.01364	110	90.91	1.674	2.01E-1	1.139	2.27E-2
0.01240	100	100.0	1.187	6.25E-1	0.887	6.97E-2
0.01209	97.5	102.6	1.081	9.52E-1	0.794	9.24E-2
0.01178	95	105.3	1.111	1.39E0	0.680	1.27E-1
0.01147	92.5	108.1	1.352	1.90E0	0.533	1.90E-1
0.01116	90	111.1	1.943	2.38E0	0.364	3.27E-1
0.01085	87.5	114.3	2.962	2.40E0	0.258	5.41E-1
0.01054	85	117.6	3.634	1.62E0	0.219	7.50E-1
0.01023	82.5	121.2	3.588	9.13E-1	0.206	9.45E-1
0.009919	80	125.0	3.371	5.48E-1	0.204	1.13E0
0.009299	75	133.3	3.030	2.62E-1	0.223	1.52E0
0.008679	70	142.9	2.827	1.62E-1	0.273	1.98E0
0.008059	65	153.8	2.699	1.18E-1	0.378	2.58E0
0.007439	60	166.7	2.611	9.58E-2	0.648	3.51E0
0.007129	57.5	173.9	2.578	8.88E-2	0.986	4.24E0
0.006819	55	181.8	2.550	8.36E-2	1.816	5.31E0
0.006509	52.5	190.5	2.526	7.98E-2	4.348	6.20E0
0.006199	50	200.0	2.504	7.69E-2	6.773	3.33E0
0.005889	47.5	210.5	2.487	7.48E-2	5.842	1.30E0
0.005573	45	222.2	2.471	7.33E-2	4.995	6.55E-1
0.004959	40	250.0	2.447	7.14E-2	4.079	2.58E-1

TABLE I *(Continued)*

Sodium Nitrate

eV	cm^{-1}	μm	n(o)	k(o)	n(e)	k(e)
0.004339	35	285.7	2.431	7.04E-2	3.616	1.35E-1
0.003720	30	333.3	2.421	6.94E-2	3.342	8.09E-2
0.003100	25	400.0	2.417	6.74E-2	3.165	5.31E-2
0.002480	20	500.0	2.418	6.31E-2	3.047	3.74E-2
0.002145	17.3	578.0	2.47 [7]	1.62E-2 [7]	3.00 [7]	5.33E-2 [7]
0.001860	15	666.7	2.424 [6]	5.51E-2 [6]	2.968 [6]	2.84E-2 [6]
0.001649	13.3	751.9	2.45 [7]	1.02E-2 [7]	2.98 [7]	3.69E-2 [7]
0.001240	10	1000	2.432 [6]	4.18E-2 [6]	2.919 [6]	2.43E-2 [6]
0.001153	9.3	1075	2.35 [7]	6.18E-3 [7]	2.90 [7]	2.60E-2 [7]

TABLE II

Coupled Oscillator Parameters from Brehat and Wyncke [6]

	ϵ_∞	ω_T (cm^{-1})	γ_T (cm^{-1})	ω_L (cm^{-1})	γ_L (cm^{-1})	γ_{TR} (cm^{-1})	γ_{LR} (cm^{-1})
A_{2u}	1.8	51.5	4.5	90	5	3.5	3.6
		214	8	262.5	37		
E_u	2.5	87	8	98.5	9	26.5	29.4
		175.5	19	184.5	19		
		209	14	257.5	25		

Strontium Fluoride (SrF_2)

MICHAEL E. THOMAS
Applied Physics Laboratory
The Johns Hopkins University
Laurel, Maryland

Strontium fluoride offers a wide range of transparency, from the ultraviolet to the long-wave infrared (0.13 to 11 μm), with low reflectance loss and low dispersion. This combination of broad transparency and low dispersion is rare in optical-window materials used in infrared systems. Like BaF_2, it allows experimenters to conveniently perform initial system alignment in the visible and then switch to the IR with only minor correction of the optical components. Furthermore, strontium fluoride has good surface hardness (Knoop scale 150 kg/mm^2) and is not hygroscopic. It has a flexure strength between those of CaF_2 (90 MPa) and BaF_2 (27 MPa).

Strontium fluoride is a cubic crystal with the fluorite structure, space group Fm3m (O_h^5), with four formula units per unit cell. The lattice constant is 5.7996 Å, giving a theoretical density of 4.277 g/cm^3. The atomic arrangement is strontium atoms occupy the 4(a) sites (m3m or O_h symmetry), and the fluorine atoms occupy the 8(c) sites ($\bar{4}$3m or T_d symmetry). Melting point is 1750 K.

Ultraviolet reflectance of bulk SrF_2 was measured by Ganin *et al.* [1] up to 20 eV at room temperature and liquid-helium temperature. Rubloff [2] measured the room-temperature reflectance up to 36 eV. Unfortunately, these measurements are not reduced to optical constants. However, similar measurements from 10 to 36 eV by Nisar and Robin [3] have been reduced to optical constants using the Kramers–Kronig relation. These data are listed in Table I and plotted in Fig. 1.

The Urbach tail represents absorption below the band gap, defining the end of transparency. The room-temperature absorption coefficient was determined from transmission measurements by Tomiki and Miyata [4] in the spectral range from 9.5 to 9.8 eV and fitted to the functional form

$$\beta_{\text{abs}}(E, T) = \beta_{\text{U0}} \exp[\sigma_s(T)(E - E_g)/k_B T], \tag{1}$$

where β_{abs} is the absorption coefficient (typically in units of cm^{-1}), β_{U0} is

HANDBOOK OF OPTICAL CONSTANTS OF SOLIDS III

Copyright © 1998 by Academic Press.
All rights of reproduction in any form reserved
ISBN 0-12-544423-0/$25.00.

a scaling coefficient (in units of cm^{-1}), E_g is the band-gap energy at absolute zero temperature (typically given in units of eV), k_B is Boltzmann's constant, and T is temperature in Kelvins. The exponential factor $\sigma_s(T)$ is given by the equation

$$\sigma_s(T) = \sigma_0 \frac{2k_B T}{E_p} \tanh \frac{E_p}{2k_B T}, \tag{2}$$

where E_p is an effective acoustic-phonon energy of the material. The Urbach tail parameters for SrF_2 are $\beta_{U0} = 1.35 \times 10^9$ cm^{-1}, $E_g = 10.670$ eV, $\sigma_0 = 0.60$, and $E_p = 0.044$ eV. The room-temperature (295 K) values for k in Table I and Fig. 1 for this spectral region are generated using Eqs. (1) and (2).

The room-temperature (25° C) index of refraction from the ultraviolet to the infrared (0.22 to 11.5 μm) has been measured by Feldman *et al.* [5] using a prism and the minimum-deviation technique. A Sellmeier model of the form

$$n^2(\lambda, T) = 1 + \sum_i \frac{\lambda^2 \Delta\epsilon_i(T)}{\lambda^2 - \lambda_i^2(T)} \tag{3}$$

is used to represent the data accurately. Model parameters are listed in Table II. A comprehensive analysis on a variety of data sets was performed by Li [6]. A Sellmeier formula was also generated covering the range from 0.15 to 14 μm at $T = 20°$ C. The Li model parameters are also listed in Table II. Because the Sellmeier model has a physical basis, the extrapolation to higher frequencies beyond the experimental limit is justified. The values for n in Table I and Fig. 1 for the spectral regions indicated are generated by the appropriate formula. A temperature-dependent Sellmeier model covering the range from 100 to 450 K has been developed by Tropf [7]. Near-room-temperature thermo-optic coefficients measured at different wavelengths are listed in Table III [5, 8–10]. Notice that the thermo-optic coefficients are negative. This gives SrF_2 some athermal performance as an optical element. An athermal material has the property that

$$\frac{d(n(T)L(T))}{dT} = 0.$$

The value of the optical-path derivative as given earlier for SrF_2 is 6.9×10^{-6} nL per Kelvin at visible and near infrared wavelengths. Thus, SrF_2 is useful for optical designs that require insensitivity to temperature.

Laser-calorimetry data [11] at DF (3.8 μm) and HF (2.7 μm) laser wavelengths indicate low-level absorption in roughly the middle of the transparency range of SrF_2. Material obtained from Optovac had absorption-

coefficient values of 2.0×10^{-4} cm^{-1} at the DF laser wavelength and 1.4×10^{-4} cm^{-1} at the HF laser wavelength. The corresponding k values are listed in Table I and plotted in Fig. 1. The low-level absorption and the near athermal performance of SrF_2 make it a candidate window material for high-power laser applications.

The multiphonon absorption (multiple-quanta lattice vibrations) edge marks the end of infrared transparency. Absorption-coefficient measurements by Deutsch [12] are represented by the simple formula

$$\beta_{abs}(\nu) = \beta_0 \exp\left(-\gamma \frac{\nu}{\nu_0}\right), \tag{4}$$

where for SrF_2, $\beta_0 = 22{,}548$ cm^{-1} and $\nu_0/\gamma = 90.4$ cm^{-1} at room temperature. The values of k in the spectral range from 820 to 1300 cm^{-1} in Table I and Fig. 1 are obtained from this formula. The data cover the three-phonon to four-phonon regions. Temperature-dependent experimental data on the absorption coefficient is described in Lipson *et al.* [13]. A temperature-dependent multiphonon model has been developed by Thomas *et al.* [14] and applied to SrF_2. Measurements in the two-phonon region are reported by Kaiser *et al.* [15]. The experimental results are listed in Table I and plotted in Fig. 1.

The one-phonon (one-quanta fundamental lattice vibrations) region is opaque and therefore characterized by reflectance measurements. A room-temperature reflectance measurement is reported by Kaiser *et al.* [15]. The classical-oscillator model is often used to fit the reflectance data and then to derive the optical constants. The classical-oscillator model is expressed in terms of the relative permittivity, $\epsilon_r(\nu,T)$, as given by[1]

$$\epsilon_r(\nu,T) = \epsilon_\infty(T) + \sum_i \frac{\Delta\epsilon_i(T)\nu_i^2(T)}{\nu_i^2(T) - \nu^2 + j\Gamma_i(\nu,T)\nu}, \tag{5}$$

where $\Delta\epsilon_i(T)$, $\Gamma_i(\nu,T)$ and $\nu_i(T)$ are the ith-mode strength, linewidth, and long-wavelength transverse optical frequency, ν_{TO}, respectively. The sum on i is over all transverse optical modes. For SrF_2, there is only one allowed infrared-active vibrational mode based on group theory of a perfect lattice. This is formally stated as

$$\Gamma = F_{1u}(\mathrm{IR}) + F_{2g}(\mathrm{R}).$$

The first mode is infrared active (mode 1 in Table IV), and the second mode is Raman active (286 cm^{-1} [16]). Table IV lists the classical-oscillator model parameters used to fit the experimental data. More than one mode is needed

[1] The expression uses the engineering convention for a time harmonic field of $\exp(-j\omega t)$. To convert to the convention commonly used in the *HOC* series, use $i = -j$.

to account for impurities and defects in real materials. Also, the high-frequency edge of the reflectance spectrum must include two-phonon contributions (see mode 2 in Table IV). Unfortunately, the value of ϵ_∞ used by Kaiser *et al.* is not consistent with the value from the Sellmeier models mentioned previously, and the same is true for the static dielectric constant. For this reason the model parameters have been modified to agree with these limiting values and still match the reflectance spectrum. These modified values are listed in Table IV. The n and k values in Table I and Fig. 1 are generated by Eq. (5) and the modified parameters in Table IV.

Below ν_{TO}, the index of refraction, n, is determined by extrapolation of the classical-oscillator model with reasonable accuracy. The absorption coefficient has been measured by Bosomworth [17]. Table I and Fig. 1 list and display the resulting values. The values are above the one-phonon red wing because multiphonon difference bands are also included in this spectral region.

The static-dielectric-constant data is the sum of all the strengths of higher-frequency oscillators including vibrational and electronic. Using Eq. (5), the static dielectric constant, $\epsilon_s(T) = \epsilon_r'(0,T)$, becomes

$$\epsilon_s(T) = \epsilon_\infty(T) + \sum_i \Delta\epsilon_i(T). \tag{6}$$

Based on the parameters listed in Table IV, we expect the value of ϵ_s to be between 6.14 and 6.5. Experimental results, obtained from capacitance bridges operating from 1 kHz to 1 MHz, produce values from 6.45 to 6.48, with most results closer to the higher value [18–21]. The corresponding refractive index value is $n_s = 2.543$. The static-index values incorrectly are located at 1×10^4 μm; however, there is little difference in the value of n_s at the measured wavelength and the plotted wavelength.

Whenever possible, physically based models are used to represent experimental measurements in Table I and Fig. 1. The models tend to reduce noise and allow interpolation and extrapolation to obtain meaningful results where no experimental data exists. In some case, the models discussed in this section also allow temperature-dependent data to be obtained.

REFERENCES

1. V. A. Ganin, M. G. Karin, V. K. Sidorin, K. K. Sidorin, N. V. Starostin, G. P. Startsev, and M. P. Shepilov, Optical constants and energy-band structure of fluorite-type crystals. *Sov. Phys. Solid State* **16**, 2313–2318 (1975).
2. G. W. Rubloff, Far-infrared reflectance spectra and the electronic structure of ionic crystals. *Phys. Rev. B* **5**, 662–684 (1972).
3. M. Nisar and S. Robin, Far ultraviolet electronic spectra of SrF_2 and BaF_2. *Pak. J. Sci. Ind. Res.* **17**, 49–54 (1974).
4. T. Tomiki and T. Miyata, Optical studies of alkali fluorides and alkaline earth fluorides in VUV region. *J. Phys. Soc. Jpn.* **27**, 658–678 (1969).

5. A. Feldman, D. Horowitz, R. M. Walker, and M. J. Dodge, Optical Materials Characterization Final Technical Report, February 1, 1978–September 30, 1978. *NBS Technical Note* **993** (February 1979).
6. H. H. Li, Refractive index of alkaline earth halides and its wavelength and temperature derivatives. *J. Phys. Chem. Ref. Data* **9**, 161–289 (1980).
7. W. J. Tropf, Temperature-dependent refractive index models for BaF_2, CaF_2, MgF_2, SrF_2, LiF, NaF, KCl, ZnS and ZnSe. *Opt. Eng.* **34**, 1369–1373 (1995).
8. Y. F. Tsay, H. G. Lipson, and P. A. Ligor, The temperature variation of the thermo-optic coefficient of CaF_2. *J. Appl. Phys.* **48**, 1953–1955 (1977).
9. H. G. Lipson, Y. F. Tsay, B. Bendow, and P. A. Ligor, Temperature dependence of the refractive index of alkaline earth fluorides. *Appl. Opt.* **15**, 2352–2354 (1976).
10. M. Wintersgill, J. Fontanella, C. Andeen, and D. Schuele, The temperature variation of the dielectric constant of "pure" CaF_2, SrF_2, BaF_2, and MgO. *J. Appl. Phys.* **50**, 8259–8261 (1979).
11. J. A. Harrington, D. A. Gregory, and W. F. Otto, Jr., Infrared absorption in chemical laser window materials. *Appl. Opt.* **15**, 1953–1959 (1976).
12. T. F. Deutsch, Absorption coefficient of infrared laser window materials. *J. Phys. Chem. Solids* **34**, 2091–2104 (1973).
13. H. G. Lipson, B. Bendow, N. E. Massa, and S. S. Mitra, Multiphonon infrared absorption in the transparent regime of alkaline-earth fluorides. *Phys. Rev. B* **13**, 2614–2619 (1976).
14. M. E. Thomas, R. I. Joseph, and W. J. Tropf, Infrared transmission properties of sapphire, spinel, yttria and ALON as a function of temperature and frequency. *Appl. Opt.* **27**, 239–245 (1988); M. E. Thomas, Temperature dependence of the complex index of refraction, *in* "Handbook of Optical Constants of Solids II" (E. D. Palik ed.), Chap. 8, pp. 177–201. Academic Press, Orlando, Florida, 1991; M. E. Thomas, A computer code for modeling optical properties of window materials, in window and dome technologies and materials. *Proc. of SPIE* **1112**, 260–267 (1989).
15. W. Kaiser, W. G. Spitzer, R. H. Kaiser, and L. E. Howarth, Infrared properties of CaF_2, SrF_2, and BaF_2. *Phys. Rev.* **127**, 1950–1954 (1962).
16. I. Richman, Longitudinal optical phonons in CaF_2, SrF_2 and BaF_2. *J. Chem. Phys.* **41**, 2836–2837 (1966).
17. D. R. Bosomworth, Far-infrared optical properties of CaF_2, SrF_2, BaF_2, and CdF_2. *Phys. Rev.* **157**, 709–715 (1967).
18. K. V. Rao and A. Smakula, Dielectric properties of alkaline earth fluoride single crystals. *J. Appl. Phys.* **37**, 319–323 (1965).
19. C. Andeen, J. Fontanella, and D. Schuele, Low-frequency dielectric constants of the alkaline earth fluorides by the method of substitution. *J. Appl. Phys.* **42**, 2216–2219 (1971).
20. G. A. Samara, Temperature and pressure dependence of the dielectric properties of PbF_2 and the alkaline-earth fluorides. *Phys. Rev. B* **13**, 4529–4544 (1976).
21. M. Wintersgill, J. Fontanella, C. Andeen, and D. Schuele, The temperature variation of the dielectric constant of "pure" CaF_2, SrF_2, BaF_2, and MgO. *J. Appl. Phys.* **50**, 8259–8261 (1979).

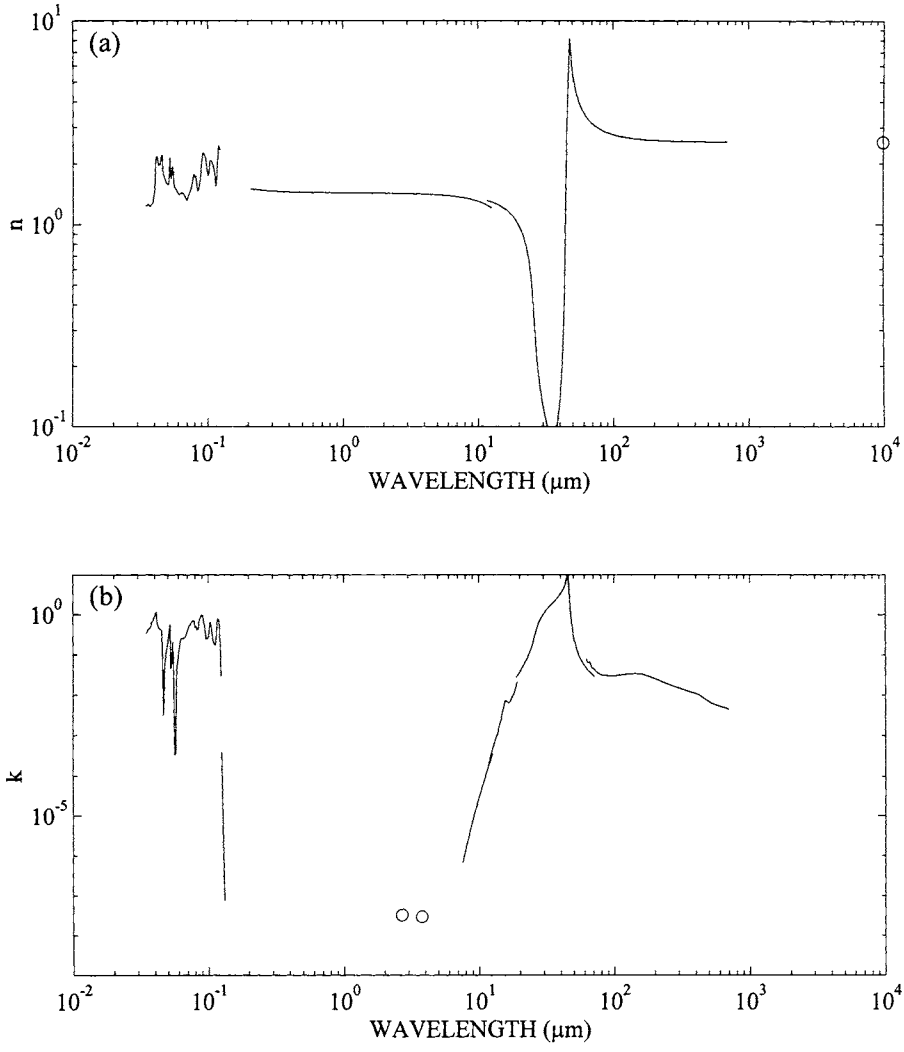

Fig. 1. (a) Log–log plot of the room-temperature index of refraction, n, for SrF_2 versus wavelength in microns. (b) Log–log plot of the room-temperature extinction coefficient, k, for SrF_2 versus wavelength in microns. Isolated data points are indicated with a symbol.

TABLE I

Values of n and k for Strontium Fluoride from Various References[a]

eV	cm^{-1}	μm	n	k
35.90	289500	0.03454	1.242	0.3412 [3]
35.24	284300	0.03518	1.236	0.3963
34.94	281800	0.03549	1.261	0.4173
34.58	278900	0.03586	1.266	0.4291
33.63	271200	0.03687	1.236	0.4696
33.15	267300	0.03740	1.225	0.5356
32.97	265900	0.03761	1.237	0.5875
32.72	263900	0.03789	1.261	0.6360
32.12	259000	0.03861	1.272	0.6871
31.98	257900	0.03878	1.274	0.7286
31.84	256800	0.03894	1.293	0.7873
31.21	251700	0.03973	1.407	0.9057
31.03	250300	0.03996	1.448	0.9605
30.90	249200	0.04013	1.480	1.011
30.74	248000	0.04033	1.536	1.064
30.68	247400	0.04042	1.584	1.115
30.39	245100	0.04080	1.991	1.150
30.33	244700	0.04087	2.051	1.112
30.30	244400	0.04092	2.075	1.063
30.26	244100	0.04097	2.102	1.007
30.21	243600	0.04104	2.137	0.9336
30.13	243000	0.04115	2.154	0.8745
30.06	242500	0.04124	2.146	0.8165
29.97	241700	0.04137	2.143	0.7493
29.86	240800	0.04152	2.150	0.6764
29.76	240000	0.04167	2.158	0.6196
29.64	239000	0.04184	2.149	0.5502
28.85	232700	0.04298	1.951	0.4337
28.58	230500	0.04338	1.971	0.4471
28.35	228700	0.04373	1.976	0.4198
28.15	227000	0.04405	1.969	0.4257
27.68	223300	0.04479	2.180	0.4002
27.43	221200	0.04520	2.193	0.1579
27.33	220400	0.04537	2.197	0.07584
27.05	218200	0.04584	2.007	0.00311
26.77	215900	0.04632	1.773	0.00451
26.47	213500	0.04684	1.748	0.03753
26.15	210900	0.04742	1.702	0.07288
25.26	203700	0.04909	1.604	0.1530
25.01	201700	0.04957	1.589	0.1877
24.56	198100	0.05048	1.568	0.2835
24.42	196900	0.05078	1.565	0.3399
24.20	195200	0.05124	1.613	0.5235
24.10	194400	0.05145	1.789	0.5621

(continued)

[a] References given in brackets.

TABLE I *(Continued)*

Strontium Fluoride

eV	cm^{-1}	μm	n	k
23.99	193500	0.05169	2.013	0.5311
23.93	193000	0.05180	2.110	0.4473
23.77	191700	0.05217	2.123	0.0440
23.50	189500	0.05276	1.746	0.0500
23.20	187100	0.05344	1.680	0.1000
22.92	184900	0.05409	1.820	0.2068
22.75	183500	0.05449	1.910	0.1012
22.64	182600	0.05476	1.925	0.0427
22.44	181000	0.05525	1.813	0.00551
22.13	178500	0.05603	1.592	0.00033
21.77	175600	0.05695	1.523	0.00037
21.54	173700	0.05756	1.499	0.02126
21.28	171700	0.05825	1.477	0.05195
20.96	169000	0.05916	1.447	0.0827
20.20	162900	0.06139	1.403	0.2047
19.71	159000	0.06291	1.434	0.2516
19.46	157000	0.06370	1.431	0.2553
19.17	154600	0.06468	1.431	0.2538
18.86	152100	0.06575	1.419	0.2518
18.45	148800	0.06718	1.387	0.2706
18.21	146900	0.06808	1.364	0.3070
17.76	143300	0.06980	1.319	0.3907
17.59	141900	0.07049	1.319	0.4455
17.43	140600	0.07114	1.348	0.4962
17.26	139200	0.07185	1.383	0.5240
17.03	137400	0.07280	1.411	0.5437
16.83	135800	0.07365	1.437	0.5801
16.34	131800	0.07590	1.536	0.6662
16.13	130100	0.07687	1.607	0.6928
15.92	128400	0.07790	1.709	0.6637
15.76	127200	0.07865	1.766	0.6845
15.71	126700	0.07892	1.764	0.6449
15.69	126500	0.07903	1.764	0.5219
15.64	126200	0.07925	1.762	0.4731
15.42	124400	0.08042	1.704	0.5124
15.20	122600	0.08155	1.737	0.4517
15.15	122200	0.08186	1.706	0.4011
14.80	119400	0.08378	1.501	0.4348
14.63	118000	0.08472	1.452	0.5763
14.57	117500	0.08508	1.466	0.6442
14.38	116000	0.08623	1.520	0.7740
14.27	115100	0.08688	1.564	0.8387
14.19	114500	0.08736	1.601	0.8853
14.07	113500	0.08814	1.677	0.9228
14.00	112900	0.08855	1.736	0.9694
13.74	110800	0.09022	2.055	0.9530

TABLE I *(Continued)*

Strontium Fluoride

eV	cm^{-1}	μm	n	k
13.60	109700	0.09116	2.185	0.8583
13.53	109200	0.09160	2.225	0.8077
13.43	108300	0.09231	2.245	0.6814
13.38	107900	0.09269	2.254	0.6182
13.31	107300	0.09317	2.241	0.5482
13.11	105800	0.09454	2.206	0.3949
12.84	103500	0.09658	2.105	0.2394
12.34	99540	0.1005	1.738	0.2703
12.28	99020	0.1010	1.759	0.3342
12.24	98760	0.1013	1.770	0.3888
12.19	98360	0.1017	1.786	0.4590
12.14	97930	0.1021	1.803	0.5389
12.09	97540	0.1025	1.818	0.6044
12.02	96930	0.1032	1.991	0.6413
11.92	96120	0.1040	2.059	0.5856
11.87	95700	0.1045	2.060	0.5012
11.81	95240	0.1050	2.060	0.4392
11.71	94440	0.1059	2.062	0.3726
11.58	93390	0.1071	2.029	0.3015
11.45	92320	0.1083	2.006	0.2424
11.32	91270	0.1096	1.973	0.1942
11.09	89460	0.1118	1.857	0.1697
10.91	88010	0.1136	1.691	0.2072
10.84	87460	0.1143	1.620	0.2625
10.79	87060	0.1149	1.582	0.3263
10.76	86770	0.1152	1.554	0.3936
10.72	86430	0.1157	1.545	0.4574
10.67	86050	0.1162	1.572	0.6011
10.64	85830	0.1165	1.623	0.6730
10.58	85330	0.1172	1.766	0.7409
10.52	84860	0.1178	1.925	0.8018
10.30	83060	0.1204	2.415	0.6704
10.29	83000	0.1205	2.423	0.6066
10.27	82840	0.1207	2.443	0.5469
10.25	82630	0.1210	2.446	0.4814
10.24	82570	0.1211	2.441	0.4262
10.21	82360	0.1214	2.426	0.3630
10.17	82040	0.1219	2.402	0.2947
10.15	81900	0.1221	2.394	0.2326
10.10	81460	0.1228	2.370	0.1654
10.05	81070	0.1234	2.335	0.1017
10.01	80750	0.1238	2.315	0.0293
9.879	79680	0.1255	1.746 [6]	0.0003826 [4]
9.801	79050	0.1265	1.735	8.702E-5
9.724	78430	0.1275	1.725	2.026E-5
9.649	77820	0.1285	1.716	4.823E-6

(continued)

TABLE I *(Continued)*

Strontium Fluoride

eV	cm^{-1}	μm	n	k
9.574	77220	0.1295	1.707	1.174E-6
9.501	76630	0.1305	1.699	2.922E-7
9.429	76050	0.1315	1.691	7.428E-8
8.266	66670	0.150	1.594	
7.085	57140	0.175	1.534	
6.199	50000	0.200	1.504	
5.510	44440	0.225	1.486	
5.904	47619	0.21	1.49513 [5]	
4.959	40000	0.25	1.47336	
3.999	32258	0.31	1.45725	
3.542	28571	0.35	1.45131	
3.024	24390	0.41	1.44556	
2.755	22222	0.45	1.44309	
2.431	19608	0.51	1.44029	
2.254	18182	0.55	1.43906	
2.032	16393	0.61	1.43740	
1.907	15384	0.65	1.43675	
1.746	14084	0.71	1.43560	
1.653	13333	0.75	1.43527	
1.531	12346	0.81	1.43435	
1.362	10989	0.91	1.43343	
1.228	9901.0	1.01	1.43269	
1.117	9009.0	1.11	1.43206	
1.025	8264.5	1.21	1.43151	
0.9464	7633.6	1.31	1.43100	
0.8793	7092.2	1.41	1.43051	
0.8211	6622.5	1.51	1.43003	
0.7701	6211.2	1.61	1.42956	
0.7251	5847.9	1.71	1.42909	
0.6850	5524.9	1.81	1.42861	
0.6491	5235.6	1.91	1.42812	
0.6168	4975.1	2.01	1.42761	
0.5876	4739.3	2.11	1.42709	
0.5610	4524.9	2.21	1.42656	
0.5367	4329.0	2.31	1.42601	
0.5145	4149.4	2.41	1.42544	
0.4940	3984.1	2.51	1.42485	
0.4750	3831.4	2.61	1.42424	
0.4590	3703.7	2.70		3.20E-8 [11]
0.4575	3690.0	2.71	1.42361	
0.4412	3558.7	2.81	1.42296	
0.4261	3436.4	2.91	1.42228	
0.4119	3322.3	3.01	1.42159	
0.3987	3215.4	3.11	1.42087	
0.3862	3115.3	3.21	1.42013	
0.3746	3021.1	3.31	1.41937	

TABLE I *(Continued)*

Strontium Fluoride

eV	cm^{-1}	μm	n	k
0.3636	2932.5	3.41	1.41858	
0.3532	2849.0	3.51	1.41778	
0.3434	2770.1	3.61	1.41694	
0.3342	2695.4	3.71	1.41609	
0.3260	2631.6	3.80		2.90E-8 [11]
0.3254	2624.7	3.81	1.41521	
0.3171	2557.5	3.91	1.41430	
0.3092	2493.8	4.01	1.41337	
0.3017	2433.1	4.11	1.41242	
0.2945	2375.3	4.21	1.41144	
0.2877	2320.2	4.31	1.41044	
0.2811	2267.6	4.41	1.40941	
0.2749	2217.3	4.51	1.40835	
0.2689	2169.2	4.61	1.40727	
0.2633	2123.1	4.71	1.40617	
0.2578	2079.0	4.81	1.40503	
0.2525	2036.7	4.91	1.40388	
0.2475	1996.0	5.01	1.40269	
0.2426	1956.9	5.11	1.40148	
0.2380	1919.4	5.21	1.40024	
0.2335	1883.2	5.31	1.39898	
0.2292	1848.4	5.41	1.39768	
0.2250	1814.9	5.51	1.39636	
0.2210	1782.5	5.61	1.39502	
0.2171	1751.3	5.71	1.39364	
0.2134	1721.2	5.81	1.39223	
0.2098	1692.1	5.91	1.39080	
0.2063	1663.9	6.01	1.38934	
0.2029	1636.7	6.11	1.38785	
0.1997	1610.3	6.21	1.38633	
0.1965	1584.8	6.31	1.38478	
0.1934	1560.1	6.41	1.38320	
0.1905	1536.1	6.51	1.38159	
0.1876	1512.9	6.61	1.37995	
0.1848	1490.3	6.71	1.37828	
0.1821	1468.4	6.81	1.37658	
0.1794	1447.2	6.91	1.37485	
0.1769	1426.5	7.01	1.37308	
0.1744	1406.5	7.11	1.37128	
0.1720	1387.0	7.21	1.36946	
0.1696	1368.0	7.31	1.36759	
0.1673	1349.5	7.41	1.36570	
0.1651	1331.6	7.51	1.36377	
0.1629	1314.1	7.61	1.36181	
0.1608	1297.0	7.71	1.35981	
0.1588	1280.4	7.81	1.35778	

(continued)

TABLE I *(Continued)*

Strontium Fluoride

eV	cm^{-1}	μm	n	k
0.1567	1264.2	7.91	1.35572	
0.1548	1248.4	8.01	1.35362	
0.1531	1234.6	8.1	1.3517 [6]	1.7035E-6 [12]
0.1442	1162.8	8.6	1.3405	4.11E-6
0.1363	1098.9	9.1	1.3283	8.58E-6
0.1292	1041.7	9.6	1.3151	1.71E-5
0.1228	990.1	10.1	1.3800	3.17E-5
0.1170	943.4	10.6	1.2854	5.58E-5
0.1117	900.9	11.1	1.2686	9.36E-5
0.1069	862.1	11.6	1.2505	0.0150
0.10609	855.7	11.69	1.3156	0.000173 [15]
0.10037	809.5	12.35	1.3002	0.000361
0.09776	788.5	12.68	1.2921	0.000502
0.09526	768.3	13.02	1.2835	0.000631
0.09346	753.8	13.27	1.2768	0.000780
0.09161	738.9	13.53	1.2695	0.000955
0.08967	723.2	13.83	1.2611	0.00120
0.08838	712.8	14.03	1.2552	0.00159
0.08485	684.4	14.61	1.2373	0.00252
0.08200	661.4	15.12	1.2206	0.00432
0.07944	640.7	15.61	1.2035	0.00719
0.07867	634.5	15.76	1.1979	0.00702
0.07795	628.7	15.91	1.1926	0.00708
0.07686	619.9	16.13	1.1840	0.00682
0.07584	611.7	16.35	1.1756	0.00644
0.07463	601.9	16.61	1.1649	0.00619
0.07280	587.2	17.03	1.1474	0.00693
0.06859	553.2	18.08	1.0991	0.0107
0.06486	523.1	19.12	1.0442	0.0206
0.06447	520	19.23	1.038[2]	0.0297[2]
0.06323	510	19.61	1.015	0.0331
0.06199	500	20.00	0.991	0.0370
0.06075	490	20.41	0.964	0.0416
0.05951	480	20.83	0.934	0.0470
0.05827	470	21.28	0.901	0.0535
0.05703	460	21.74	0.864	0.0612
0.05579	450	22.22	0.822	0.0708
0.05455	440	22.73	0.774	0.0826
0.05331	430	23.26	0.719	0.0977
0.05207	420	23.81	0.655	0.118
0.05083	410	24.39	0.578	0.146
0.04959	400	25.00	0.486	0.189
0.04835	390	25.64	0.380	0.261
0.04711	380	26.32	0.282	0.378
0.04587	370	27.03	0.219	0.519
0.04463	360	27.78	0.181	0.660

[2] Results obtained from modified classical-oscillator parameters in Table IV.

TABLE I *(Continued)*

Strontium Fluoride

eV	cm^{-1}	μm	n	k
0.04339	350	28.57	0.156	0.800
0.04215	340	29.41	0.137	0.940
0.04092	330	30.30	0.122	1.087
0.03968	320	31.25	0.110	1.243
0.03844	310	32.26	0.0998	1.413
0.03720	300	33.33	0.0925	1.602
0.03596	290	34.48	0.0881	1.818
0.03472	280	35.71	0.0876	2.071
0.03348	270	37.04	0.0923	2.379
0.03224	260	38.46	0.106	2.770
0.03100	250	40.00	0.136	3.304
0.02976	240	41.67	0.208	4.121
0.02852	230	43.48	0.448	5.668
0.02728	220	45.45	3.166	10.930
0.02604	210	47.62	8.167	1.012
0.02480	200	50.00	5.525	0.272
0.02356	190	52.63	4.534	0.136
0.02232	180	55.56	3.994	0.0855
0.02108	170	58.82	3.648	0.0594
0.01984	160	62.50	3.406	0.0445
0.01860	150	66.67	3.227	0.0349
0.01736	140	71.43	3.090	0.0282
0.01995	160.9	62.14	3.426	0.0792 [17]
0.01993	160.7	62.21	3.422	0.0766
0.01989	160.4	62.34	3.415	0.0746
0.01980	159.7	62.63	3.399	0.0725
0.01969	158.8	62.96	3.383	0.0687
0.01948	157.1	63.66	3.349	0.0643
0.01921	154.9	64.55	3.309	0.0620
0.01876	151.3	66.10	3.248	0.0650
0.01860	150.0	66.67	3.227	0.0593
0.01849	149.2	67.04	3.214	0.0550
0.01837	148.2	67.50	3.199	0.0509
0.01815	146.4	68.32	3.173	0.0472
0.01781	143.7	69.60	3.136	0.0454
0.01748	141.0	70.94	3.102	0.0436
0.01721	138.8	72.03	3.076	0.0416
0.01701	137.2	72.89	3.057	0.0385
0.01670	134.7	74.26	3.029	0.0362
0.01589	128.2	78.02	2.964	0.0329
0.01531	123.5	80.99	2.922	0.0315
0.01482	119.5	83.66	2.890	0.0306
0.01370	110.5	90.51	2.825	0.0295
0.01299	104.8	95.42	2.790	0.0294
0.01235	99.6	100.4	2.761	0.0298
0.01172	94.5	105.8	2.735	0.0304

(continued)

TABLE I *(Continued)*

Strontium Fluoride

eV	cm^{-1}	μm	n	k
0.01102	88.9	112.5	2.710	0.0312
0.01044	84.2	118.8	2.690	0.0318
0.00978	78.9	126.8	2.670	0.0331
0.00924	74.5	134.2	2.655	0.0333
0.00872	70.3	142.2	2.642	0.0335
0.00824	66.5	150.4	2.630	0.0330
0.00769	62.0	161.3	2.618	0.0327
0.00720	58.1	172.2	2.608	0.0304
0.00664	53.6	186.6	2.598	0.0275
0.00595	48.0	208.4	2.587	0.0239
0.00534	43.1	232.1	2.578	0.0204
0.00481	38.8	258.0	2.571	0.0176
0.00359	29.0	344.8	2.559	0.0127
0.00293	23.7	422.7	2.554	0.0101
0.00239	19.3	519.0	2.550	0.0062
0.00178	14.4	697.0	2.547	0.0045
0.0	0.0	∞	2.543 [21]	0.0

TABLE II

Room-Temperature Sellmeier Model Parameters

ith mode	$\Delta\epsilon_i$	λ_i
Feldman *et al.* model		
1	0.67805894	0.05628989
2	0.37140533	0.10801027
3	3.8484723	34.649040
Li model		
1	0.33973	0.0
2	0.70970	0.09597
3	0.1788	26.03
4	3.8796	45.60

TABLE III

Thermo-optical Coefficients of Strontium Fluoride

Wavelength (μm)	dn/dT (10^{-6}/K)	Measurement temperature (°C)	Reference
0.3250	−10.8	37	[8]
0.4416	−11.6	37	[8]
0.4579	−12.0	20	[5]
0.6328	−12.4	20	[5]
	−12.0	37	[8, 9]
1.15	−12.6	20	[5]
	−12.7	37	[8, 9]
3.39	−12.4	20	[5]
	−13.0	37	[8, 9]
10.6	−9.8	20	[5]
∞	265	7–47	[10]

TABLE IV

Room-Temperature Classical Oscillator Model Parameters

Mode number i	ν_i (cm^{-1})	$\Delta\epsilon_i$	Γ_i/ν_i	Reference
1	217	4.0	0.0170	[16]
2	316	0.07	0.25	
$\epsilon_\infty = 2.07$				
Modified				
1	217	4.3	0.017	[see text]
2	360	0.6	0.25	
$\epsilon = 2.05$				

Orthorhombic Sulfur (α-S)

KIRK A. FULLER
Department of Atmospheric Science
Colorado State University
Fort Collins, Colorado

HARRY D. DOWNING
Department of Physics and Astronomy
Stephen F. Austin State University
Nacogdoches, Texas

MARVIN R. QUERRY
Department of Physics
University of Missouri
Kansas City, Missouri

OVERVIEW I

Although elemental sulfur has a high propensity for catenation and, therefore, occurs in a wide variety of molecular allotropes [1], the only completely stable molecule in the solid phase is cyclo-octasulfur. The cyclo-S_8 molecules also constitute a large fraction of the melt throughout the liquid phase, although helical molecules are more prevalent at temperatures above about 498 K [2].

Cyclo-octasulfur is frequently referred to as λ sulfur (λ-S). From λ-S, strongly birefringent orthorhombic crystals or weakly birefringent monoclinic crystals may be assimilated. These two crystallographic allotropes are known as α- and β-S, respectively. At room temperature, α-S is the only thermodynamically stable modification of the element. Pure β-S may be very long-lived below about 198 K, and it tends to convert only slowly to the orthorhombic modification between 200 K and about 366 K, [3, 4]. The longest-lived transient polymorph of sulfur is a polymeric form known as μ-S, which can be preserved for several years, but is unstable against x-rays and sunlight [5]. μ-S is composed of long helical molecules that dominate

HANDBOOK OF OPTICAL CONSTANTS OF SOLIDS III

Copyright © 1998 by Academic Press.
All rights of reproduction in any form reserved
ISBN 0-12-544423-0/$25.00.

the more viscous, high-temperature melt and is insoluble in carbon disulfide. All other modifications convert to α-S with half-lives ranging from a few seconds to more than a year.

Terrestrially, native sulfur is found in sedimentary formations in association with gypsum and limestone, and it is produced by volcanic and fumarolic activity (such as at Yellowstone National Park). Pure sulfur is almost nonexisting in Earth's atmosphere. Extraterrestrially, an abundance of elemental sulfur is expected to occur in the clouds of Venus [6]. Elemental sulfur also is generally believed to exist, at least in small regions, on the surface of the Jovian moon Io [7], and possibly in the polar regions of Mercury [8].

The morphology of both natural and synthetic specimens of α-S ranges from cryptocrystalline masses or fine-grained aggregates to large crystals of well-formed basal pinachoidal or dipyramidal habits. The λ-S molecules are weakly held in the crystals almost exclusively by van der Waals forces [9]. Crystalline sulfur is a soft, brittle material, and is difficult to polish. The crystals display poor cleavage and tend to fracture conchoidally. Sulfur also is a poor conductor of heat, and thermal expansion from handling may result in fracturing or spallation of a specimen.

In part because of the instability of allotropes other than α-sulfur, related optical data are sparse and a comprehensive review of their optical constants is not possible now. Therefore, data for α-S, along with some discussion of the optical properties of liquid sulfur, are presented in this review. Furthermore, α-S's poor cleavage, difficulties in polishing, and the sensitivity of its bulk morphology and optical properties to thermodynamic history and trace impurities have resulted in limited consistency of measurements from one study to another.

In particular, the primary crystal data tabulated here are restricted to refractive-index measurements with polarization components along the *a*- and *b*-axes, and thus exclude polarization with components along the *c*-axis of the α-S crystal. As such, they are the only polarimetric measurements on sulfur that are available throughout the UV–mid-IR. It must be remembered, however, that near-normal-incidence reflectance R and corresponding refractive index n are significantly higher when the incident radiant flux has its electric field aligned with the *c*-axis. The absorption index can display a strong polarization dependence, as well. In order to give some understanding of how the optical constants of more general orientations may differ from the *a*- and *b*-axis data displayed in the graph, values of n and k for cryptocrystalline or amorphous samples are included as supplemental data in our tabulations, where possible.

Reviews of the optical and thermodynamic properties are given by Fuller and co-workers [10, 11], Moses and Nash [7], Young [12], Stuedel [2], and Meyer [1, 5, 13]. Although the literature on the spectral features of α-S is somewhat extensive, it certainly is not comprehensive. A considerable amount of work has been published on the transmission spectra of this allo-

trope in the infrared [14–23]. Sasson *et al.* [24] measured the visible and near-IR reflectance of unpolarized light from polycrystalline melt–freeze samples in which the *c*-axis of the crystallites tended to align normal to the substrates onto which they were frozen. Kurrelmeyer [25] and Spear and Adams [26] measured the absorption coefficient in the visible region, while investigating the photoconductivity of α-S. Its reflectance spectrum was studied with unpolarized UV light by Cook and Spear [27] and polarimetrically by Emerald *et al.* [28]. Sulfur absorbs too strongly in the UV region to permit detailed measurements of transmittance spectra. Although most references just cited pertain to single orthorhombic crystals, there also have been measurements of the optical properties of powdered (orthorhombic) and molten sulfur [24, 29–33]. Because of its weak absorption of radiant flux throughout much of the visible and infrared, powdered sulfur has found use as a diffuse reflectance standard in those spectral regions.

The IR absorption spectrum of α-S displays bands of attenuation centered around the following wave-number positions: 191, 243, 435, 470, 509, 549, 584, 618, 659, 679, 711, 845, 903, and 936 cm^{-1} [21], as well as 986, 1050, and 1298 cm^{-1} [16–18]. The bands at 191, 243, and 470 cm^{-1} are relatively strong and correspond, respectively, to the E_1, B_2, and E_1 irreducible representations of the S_8 molecule. The remaining bands listed are combinations and overtones that are rather weak, with the exception of the feature at 845 cm^{-1}, which is of moderate strength. (Care should be taken with regard to spectra of crystals grown in CS_2 solutions. Such specimens will possess solvent inclusions, and the strong ν_3 fundamental of CS_2, which occurs at about 1510 cm^{-1}, has been mistaken for a combination band of λ-S.)

For information on the absorption spectrum of sulfur in the far IR, the low-temperature studies of Gautier and Debeau [22] and Anderson and Boczar [23] are recommended, although one cannot glean information on the optical constants in this region, because insufficient detail was provided regarding their samples. In the intermediate infrared Barrow [27] investigated some effects of birefringence on the transmittance of α-S over the 1500–700 cm^{-1} range. Bernstein and Powling [16] and Srb and Vaško [19] also provided absorption spectra for α-S over the 1600–400 cm^{-1} and 1800–400 cm^{-1} regions, respectively.

Fuller *et al.* [10] measured the near-normal specular reflectance $R_\perp$ and $R_\parallel$ of the (111) plane of an orthorhombic sulfur crystal at room temperature with respective polarizations having projections perpendicular and parallel to the *c*-axis of the crystal. The reflectance R_C, in unpolarized radiation, of a cryptocrystalline melt freeze was also obtained. Note that the subscript is a capital "C" and does not refer to a crystallographic axis, but rather to the cryptocrystalline nature of the sample. Optical constants were determined from Kramers–Kronig phase-shift analysis of the reflectance data, although *k* was too small to be determined accurately throughout much of the range. The scatter in the reflectance data was on the order of 0.5% or less. It was

concluded that over the range 5000–180 cm^{-1}, the near-normal-incidence reflectance of the (111) face of an α-S crystal in unpolarized radiation is about 0.11 ± 0.005, that the corresponding values of n are around 1.99 ± 0.05, and that the reflectance and refractive index, respectively, do not fall below 0.097 ± 0.003 and 1.90 ± 0.03 or rise above 0.148 ± 0.004 and 2.25 ± 0.03 as the polarization of the incident beam is varied. These limits correspond to the extrema encountered at the endpoints of regions of anomalous dispersion. Over most of the spectrum, it was observed that $R_\perp \approx 0.100 \pm 0.002$, $R_C \approx 0.112 \pm 0.002$, $R_\parallel \approx 0.125 \pm 0.002$, $n_\perp \approx 1.92 \pm 0.01$, $n_C \approx 2.00 \pm 0.01$, and $n_\parallel \approx 2.09 \pm 0.01$.

Fuller *et al.* [10] found that scattering from the microcrystallites that were formed in the frozen-melt sample as it cooled to room temperature (a large fraction of this material probably underwent a transition from β-S to α-S) led to a noticeable contribution to an *apparent* reflectance by backscattered radiation. As the sequence of λ-S bands beginning with those centered near 936 and 903 cm^{-1} is approached, there is a corresponding increase in $k(\nu)$ that attenuates the internally scattered radiation before a detectable amount emerges from the sample, and the average reflectance below 1000 cm^{-1} drops by about 2% from its value at higher energies. The scatter in n_C was not observed to be more than about 1.5%, even in the raw data, where problems associated with volume scattering occurred.

The general decrease in the transmittance of α-S below 1000 cm^{-1} along with a window in the region of 760 cm^{-1} can be easily seen in the published spectra of the element. The role of multiple scattering in the foregoing context is exemplified in the diffuse reflectance spectra of Nash [32], where the influence of the increased k values beginning near 1000 cm^{-1} and the 760 cm^{-1} window is particularly strong. Similar structure appears in diffuse spectra at about 1300 cm^{-1}. Such features are important in helping to determine the abundance of sulfur on the surfaces of solar-system bodies.

II EXTRAPOLATION TO DIFFERENT TEMPERATURES

Wong [34] measured the IR reflectance of molten sulfur from 2 to 22μm at 423 and 473 K. By paralleling R_C to Wong's data, estimates of this reflectance were obtained over domains that extended out to 5000 cm^{-1}. Based on these extrapolations, n_C was found to range between 2.00 and 2.01. The density of α-S at room temperature is about 2.07 g/cm^3. One can use this and the density of the melt at around 423 K, which is about 1.78 g/cm^3 [13, 35], to obtain, via the Lorentz–Lorenz equation, approximations of refractive indices at this temperature based on one's knowledge of these indices at room temperature. This leads to values for n_C of between 1.84 and 1.85

at 423 K. (Because the optical properties of cryptocrystalline and amorphous sulfur are not expected to differ significantly, the subscript C is used in describing amorphous sulfur, as well.) Upon correcting R_C for the contribution of backscatter attributed to the granularities in the microcrystalline sample, estimated to be about 2%, the refractive index of what would constitute *solid* amorphous λ-sulfur at 300 K and 5000 cm^{-1} is found to be 1.99, giving a refractive index $n_C \approx 1.83$ for liquid (amorphous) λ-S at 423 K. Wong [34] has found the melt at 423 K to have a refractive index of 1.81 ± 0.02 throughout most of the 5000–450 cm^{-1} region. Sasson and Arakawa [33] conducted studies similar to ours over the 25,000 to 5000 cm^{-1} interval and determined n_C (5000) for the melt to be 1.84 ± 0.01 at a temperature of 428 K.

The Lorentz–Lorenz formula is only an approximation when applied to solids or liquids [36, 37]; furthermore, it is being applied here to a temperature regime in which a crystalline material of strong birefringence transforms to a liquid and, therefore, amorphous structure. The formula has been used successfully, however, in the study of water [38] and has produced excellent results when applied to sulfuric-acid solutions of varying concentration [39]. Furthermore, in view of the weak intermolecular coupling between λ-S molecules in both the solid and liquid phases, it is quite likely that the polarizabilities of the molecule, which are ultimately responsible for the refractive index of the bulk material, are very nearly the same in either phase. Support for this latter argument is found in the results of a study conducted by Robertson *et al.* [40] on the optical constants of solid NH_3.

If the thermal expansion coefficient of α-S is assumed to be no larger than about 20×10^{-5}/K from room temperature [3, 13], down to about 100 K, then the change in refractive index is expected to be only on the order of a few hundredths of a percent.

THE TABULATED DATA III

For this critique, values for n and k in the far-UV–x-ray region were calculated with the Henke model [41]. A density of 2.07 g/cm^3 was assumed, and crystallographic orientation was neglected even though ⊥ is specified in Table I.

The data of Emerald *et al.* [28] was chosen for the UV. They measured the reflectance for polarization parallel to the *a*- and *b*-axes for up to 12 eV, from which the optical constants were obtained with Kramers–Kronig analysis. Professor Zallen kindly provided original figures [28], from which the numerical values were extracted by scanning. To maintain consistency with data at lower energies, values presented here for n and k in the UV are simple averages of those obtained for the two polarizations. The variation of optical properties with polarization is illustrated by a peak reflectance at 9.5 eV,

which dominated the spectra of Cook and Spear [27], but was not nearly as strong and occurred at a somewhat lower energy in the work reported by Emerald *et al.*

The orientation of the polycrystalline samples in the measurements made by Sasson *et al.* [24] are compatible with the UV work of Emerald *et al.* [28], and their values for n have been selected for tabulation in the visible to near-IR. The high transparency of sulfur in the vis–near-IR coupled with scattering losses from their samples prevented Sasson *et al.* from obtaining k values for α-S. The slight mismatch in the values of n reported by Emerald *et al.* and by Sasson *et al.* is believed to be due to some variation in crystal orientation in the polycrystalline samples of Sasson *et al.* In view of the previous discussion on extrapolation to other temperatures, one may reasonably expect to estimate n_C in the visible via the Lorentz–Lorenz approximation.

Spear and Adams [26] measured the absorption coefficient ($\alpha = 4\pi k\nu$) of the near-UV absorption edge using unpolarized light incident on thin sections taken from single crystals. Further into the visible, values for k are taken from the early work of Kurrelmeyer, who measured the absorption coefficient for unpolarized light incident along the c-axis. A baseline absorbance of zero was forced at 0.700 μm, rendering data for $\lambda > 0.600$ μm questionable. The measurements of Sasson and Arakawa [33] are used for the near IR, although this latter work dealt with the low-temperature melt, and it is unclear how similar the k-values are to those for the room-temperature solid; they likely provide an upper bound. It is worth noting that the absorption edge seen in these works is responsible for the characteristic yellow color of sulfur. Because of preferential absorption of shorter wavelengths, the light emerging from sulfur at room temperature appears yellow. As the temperature rises, thermal broadening of the band centered at about 4 eV carries the absorption edge further into the visible, and the hue darkens. Conversely, the absorption edge recedes into the UV with decreasing temperature, rendering sulfur crystals colorless below about $-50°$ C.

Further into the IR, the n-values obtained by Fuller *et al.* [10] for incident irradiance normal to the (111) crystal plane and with polarization perpendicular to the c-axis are used. The refractive indices were obtained from Kramers–Kronig analysis, and data were also collected for the orthogonal polarization and for a cryptocrystalline melt freeze. By far the most prominent features in the reflectance spectra of Fuller *et al.* are the bands centered near 190 and 240 cm^{-1}, respectively. Because of extrapolations beyond experimental range that are required by K-K analysis, it is difficult to be sure of the uncertainty in k below 250 cm^{-1}, but based on several different extrapolations, $k(190)$ was not found to change by more than about ± 0.01 and $k(240)$ varied by no more than about ± 0.003. A strong dependence on polarization of the band at 240 cm^{-1} was observed, and the E_1 band at

190 cm^{-1} appears only as a shoulder on what is a very strong B_2 absorption in the case of $\perp$ or *ab* polarization.

The band arising from the ν_5 fundamental at 470 cm^{-1} was easily distinguished in all spectra. Values of $k(470)$ were found to range between 0.016 ($k_{\parallel}$) and 0.019 ($k_{\perp}$). Rather than lying somewhere between $k_{\parallel}$ and $k_{\perp}$, the value of k_C was found to be 0.023. This anomalously high value is attributed to both particle-size effects and experimental uncertainty.

The most important combination band appearing in the transmittance and diffuse reflectance spectra of α-S is the $\nu_{10} + \nu_3$ combination, which is centered at about 845 cm^{-1}. As calculated from transmission spectra of various authors, peak values of $k(845)$ 0.001 to 0.004.

All other absorption bands are quite weak. Their influence on R and n is on the order of at most 0.3%, and any k values obtained via the Kramers–Kronig relations from such faint structures are quite unreliable. Above 675 cm^{-1} numerical values for k were obtained by electronically scanning graphs presented in Barrow's paper. Unpolarized light incident on the (110) plane was used because the transmission of the band at 845 cm^{-1} was too low at the desired polarization to allow the absorption index to be extracted. After correcting for reflection losses with the use of measurements made by Fuller *et al.*, values for k were taken from the spectra of Srb and Vaško between 675 and 500 cm^{-1}. Below 500 cm^{-1}, the k values provided by Fuller *et al.* [10] are used, but supplemental values are also provided from the Srb and Vaško's work between 450 and 410 cm^{-1}.

Data for optical constants in the far IR are not available, though work is planned for this region. In view of mm–far-IR instrumentation planned by NASA, there are additional features, especially absorption at around 74 cm^{-1}, that warrant investigation.

To provide some idea of the optical constants associated with more arbitrary polarizations or crystallographic orientations, those of the melt freeze are included in the tabulated values. Attention is called to the differences between the two sets of data at energies below about 250 cm^{-1}.

Crystal structure [42] and electric-vector polarization are discussed in the caption of Fig. 1.

ACKNOWLEDGMENTS

We are grateful to Dr. W. R. Hunter (SFA, Inc., 1401 McCormick Dr., Largo, MD 20774) for calculation of n and k in the far-UV–x-ray region, and we also wish to thank Philip Gabriel for his assistance in electronically scanning many of the graphs from which the tabulated data were obtained.

REFERENCES

1. B. Meyer, Elemental sulfur. *Chem. Rev.* **76**, 367–388 (1976).
2. R. Stuedel, Homocyclic sulfur molecules. *Top. Curr. Chem.* **102**, 147–176 (1981).

3. E. D. Eastman and W. C. McGavock, Heat capacity and entropy of rhombic and monoclinic sulfur. *J. Am. Chem. Soc.* **59**, 145–151 (1937).
4. E. D. West, Heat capacity of sulfur from 25 to 450K, the heats and temperatures of transition and fusion. *J. Am. Chem. Soc.* **81**, 29–37 (1959).
5. B. Meyer, Solid allotropes of sulfur. *Chem. Rev.* **64**, 429–451 (1964).
6. A. T. Young, Venus cloud microphysics. *Icarus* **56**, 568–577 (1983).
7. J. I. Moses and D. B. Nash, Phase transformations and the spectral reflectance of solid sulfur: Can metastable sulfur allotropes exist on Io? *Icarus* **89**, 277–304 (1991).
8. A. L. Sprague, D. M. Hunten, and K. Lodders, Sulfur at Mercury, elemental at the poles and sulfides in the regolith. *Icarus* **118**, 211–215 (1995).
9. A. R. Adams and W. E. Spear, Charge transport in orthorhombic sulphur crystals. *J. Phys. Chem. Solids* **25**, 1113–1118 (1964).
10. K. A. Fuller, H. D. Downing, and M. R. Querry, Infrared optical properties of orthorhombic sulfur. *Appl. Opt.* **30**, 4081–4093 (1991).
11. K. A. Fuller, Elemental sulfur and its optical properties in the infrared. M. S. Thesis, Stephen F. Austin State University, Nacogdoches, Texas (1984).
12. A. T. Young, No sulfur flows on Io. *Icarus* **58**, 197–226 (1984).
13. B. Meyer, "Sulfur, Energy and Environment." Elsevier, New York, 1979.
14. W. W. Coblentz, Optical notes. *Phys. Rev.* **19**, 89–97 (1904).
15. R. B. Barnes, Measurements in the long wavelength infrared from 20 μm to 135 μm. *Phys. Rev.* **39**, 562–575 (1932).
16. H. J. Bernstein and J. Powling, The vibrational spectra and structure of inorganic molecules. II. Sulfur S_8, sulfur chloride S_2Cl_2, phosphorous P_4. *J. Chem. Phys.* **18**, 1018–1023 (1950).
17. G. M. Barrow, The infrared spectra of oriented rhombic sulfur crystals with polarized radiation. *J. Chem. Phys.* **21**, 219–222 (1953).
18. V. D. Neff and T. H. Walnut, Effect of temperature on the intensity and structure of bands in the infrared spectrum of rhombic sulfur. *J. Chem. Phys.* **35**, 1723–1729 (1961).
19. I. Srb and A. Vaško, Remark on the infrared spectrum of rhombic sulfur. *J. Chem. Phys.* **37**, 1892–1893 (1962).
20. C. E. MacNeill, Infrared transmittance of rhombic sulfur. *J. Opt. Soc. Am.* **53**, 398–399 (1963).
21. D. W. Scott, J. P. McCullough, and F. H. Kruse, Vibrational assignment and force constants of S_8 from a normal coordinate treatment. *J. Mol. Spectrosc.* **13**, 313–320 (1964).
22. G. Gautier and M. Debeau, Spectres vibration d'un monocristal de soufre orthorhombique. *Spectrochim. Acta Part A* **30**, 1193–1198 (1974).
23. A. Anderson and P. G. Boczar, Far infrared spectrum of orthorhombic sulfur. *Chem. Phys. Lett.* **43**, 506–511 (1976).
24. R. Sasson, R. Wright, E. T. Arakawa, B. N. Khare, and C. Sagan, Optical properties of solid and liquid sulfur at visible and infrared wavelengths. *Icarus* **64**, 368–374 (1985).
25. B. Kurrelmeyer, The photoelectric conductivity of sulphur. *Phys. Rev.* **30**, 893–910 (1927).
26. W. E. Spear and A. R. Adams, Photogeneration of charge carriers and related optical properties in orthorhombic sulphur. *J. Chem. Phys. Solids* **27**, 281–289 (1966).
27. B. E. Cook and W. E. Spear, The optical properties of orthorhombic sulphur in the vacuum ultraviolet. *J. Phys. Chem. Solids* **30**, 1125–1134 (1969).
28. R. L. Emerald, R. E. Drews, and R. Zallen, Polarization-dependent optical properties of orthorhombic sulfur in the ultraviolet. *Phys. Rev. B* **14**, 808–813 (1976).
29. B. Meyer, M. Gouterman, D. Jensen, T. Oommen, and T. Stroyer-Hansen, The spectrum of sulfur and its allotropes. *Adv. Chem. Ser.* **110**, 53–72 (1972).
30. N. M. Nelson, D. C. Pieri, S. M. Bologa, D. B. Nash, and C. Sagan, The reflection spectrum of liquid sulfur: Implications for Io. *Icarus* **56**, 409–413 (1983).
31. J. Gradie and J. Veverka, Photometric properties of sulfur. *Icarus* **58**, 227–245 (1984).

32. D. B. Nash, Mid-infrared reflectance spectra (2.3–22μm) of sulfur, gold, KBr, MgO, and Halon. *Appl. Opt.* **25**, 2427–2433 (1986).
33. R. Sasson and E. T. Arakawa, Temperature dependence of index of refraction, reflection, and extinction coefficient of liquid sulfur in the 0.4–2.0 μm wavelength range. *Appl. Opt.* **25**, 2675–2680 (1986).
34. M. Wong, The infrared optical constants of molten sulfur at 150° and 200°C. M. S. Thesis Stephen F. Austin State University, Nacogdoches, Texas, (1984).
35. A. M. Kellas, The determination of the molecular complexity of liquid sulphur. *J. Chem. Soc.* **113**, 903–922 (1918).
36. L. Brillouin, "Wave Propagation and Group Velocity," Academic Press, New York, 1960.
37. J. D. Jackson, "Classical Electrodynamics," 2nd Ed. Wiley, New York, 1975.
38. L. W. Pinkley, P. P. Sethna, and D. Williams, Optical constants of water in the infrared: Influence of temperature. *J. Opt. Soc. Am.* **67**, 494–499 (1977).
39. L. W. Pinkley and D. Williams, The infrared optical constants of sulfuric acid at 250K. *J. Opt. Soc. Am.* **66**, 122–124 (1976).
40. C. W. Robertson, H. D. Downing, B. Curnutte, and D. Williams, Optical constants of solid ammonia in the infrared. *J. Opt. Soc. Am.* **65**, 432–435 (1975).
41. B. L. Henke, E. M. Gullikson, and J. C. Davis, X-ray interactions: Photoabsorption, scattering, transmission, and reflection at E = 50-30000 eV, Z = 1-92. *At. Data Nucl. Data Tables* **54**, 181 (1993).
42. A. S. Cooper, W. L. Bond, and S. C. Abrahams, The lattice and molecular constants in orthorhombic sulfur. *Acta Crystallogr.* **14**, 1008 (1961).

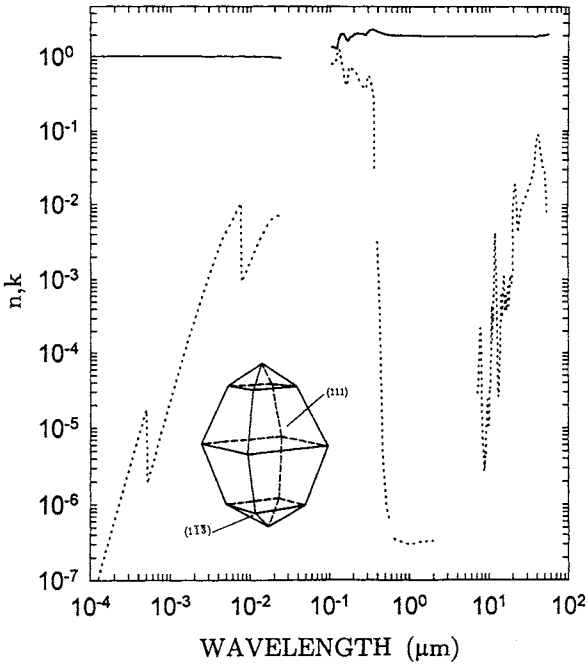

Fig. 1. Log–log plot of n (———) and k (- - - -) versus wavelength in micrometers for α-S. The symmetry of the orthorhombic crystals is F*ddd* with lattice constants of Cooper *et al.* [42]

$$a : b : c = 10.46 : 12.87 : 24.49.$$

The c-axis of the orthorhombic crystal lies along the length of the crystal. The *ab*-plane contains the middle horizontal parallelogram shown in the figure, with the a-axis lying along the diagonal that extends out of the plane of the figure. The primary tabulated data (columns 4 and 5) involve incident radiation with electric vector contained in the *ab*-plane. The direction of incidence for the primary data is along the c-axis for the UV-VIS region and perpendicular to it in the IR.

TABLE I

Values for *n* and *k* for Orthorhombic Sulfur Obtained from Various References[a]

eV	cm^{-1}	μm	$n_{\perp}$	$k_{\perp}$	n_{supp}	k_{supp}
.300E + 05	.242E + 09	.413E-04	1.000 [41]	.123E-08 [41]		
.292E + 05	.236E + 09	.425E-04	1.000	.137E-08		
.284E + 05	.229E + 09	.436E-04	1.000	.153E-08		
.277E + 05	.223E + 09	.448E-04	1.000	.171E-08		
.270E + 05	.217E + 09	.460E-04	1.000	.190E-08		
.263E + 05	.212E + 09	.472E-04	1.000	.212E-08		
.256E + 05	.206E + 09	.485E-04	1.000	.236E-08		
.249E + 05	.201E + 09	.498E-04	1.000	.263E-08		
.242E + 05	.195E + 09	.512E-04	1.000	.293E-08		
.236E + 05	.190E + 09	.526E-04	1.000	.327E-08		
.230E + 05	.185E + 09	.540E-04	1.000	.364E-08		
.224E + 05	.180E + 09	.554E-04	1.000	.406E-08		
.218E + 05	.176E + 09	.569E-04	1.000	.452E-08		
.212E + 05	.171E + 09	.585E-04	1.000	.503E-08		
.206E + 05	.167E + 09	.601E-04	1.000	.560E-08		
.201E + 05	.162E + 09	.617E-04	1.000	.624E-08		
.196E + 05	.158E + 09	.633E-04	1.000	.695E-08		
.191E + 05	.154E + 09	.651E-04	1.000	.773E-08		
.186E + 05	.150E + 09	.668E-04	1.000	.860E-08		
.181E + 05	.146E + 09	.686E-04	1.000	.957E-08		
.176E + 05	.142E + 09	.705E-04	1.000	.107E-07		
.171E + 05	.138E + 09	.774E-04	1.000	.118E-07		
.167E + 05	.135E + 09	.743E-04	1.000	.132E-07		
.162E + 05	.131E + 09	.764E-04	1.000	.147E-07		
.158E + 05	.128E + 09	.784E-04	1.000	.163E-07		
.154E + 05	.124E + 09	.805E-04	1.000	.181E-07		
.150E + 05	.121E + 09	.827E-04	1.000	.201E-07		
.146E + 05	.118E + 09	.850E-04	1.000	.224E-07		
.142E + 05	.115E + 09	.878E-04	1.000	.248E-07		
.138E + 05	.112E + 09	.896E-04	1.000	.276E-07		
.135E + 05	.109E + 09	.920E-04	1.000	.307E-07		
.131E + 05	.106E + 09	.945E-04	1.000	.341E-07		
.128E + 05	.103E + 09	.971E-04	1.000	.378E-07		
.124E + 05	.100E + 09	.997E-04	1.000	.420E-07		
.121E + 05	.976E + 08	.102E-03	1.000	.467E-07		
.118E + 05	.951E + 08	.105E-03	1.000	.518E-07		
.115E + 05	.926E + 08	.108E-03	1.000	.575E-07		
.112E + 05	.901E + 08	.111E-03	1.000	.639E-07		
.109E + 05	.878E + 08	.114E-03	1.000	.709E-07		
.106E + 05	.855E + 08	.117E-03	1.000	.787E-07		
.103E + 05	.832E + 08	.120E-03	1.000	.873E-07		
.100E + 05	.810E + 08	.123E-03	1.000	.967E-07		
.978E + 04	.789E + 08	.127E-03	1.000	.107E-06		
.952E + 04	.768E + 08	.130E-03	1.000	.119E-06		
.927E + 04	.748E + 08	.134E-03	1.000	.132E-06		

(continued)

[a] References given in brackets.

TABLE I *(Continued)*

Orthorhombic Sulfur

eV	cm^{-1}	μm	$n_\perp$	$k_\perp$	n_{supp}	k_{supp}
.903E + 04	.728E + 08	.137E-03	1.000	.146E-06		
.879E + 04	.709E + 08	.141E-03	1.000	.162E-06		
.856E + 04	.690E + 08	.145E-03	1.000	.180E-06		
.833E + 04	.672E + 08	.149E-03	1.000	.199E-06		
.811E + 04	.654E + 08	.153E-03	1.000	.221E-06		
.790E + 04	.637E + 08	.157E-03	1.000	.245E-06		
.769E + 04	.620E + 08	.161E-03	1.000	.271E-06		
.749E + 04	.604E + 08	.166E-03	1.000	.301E-06		
.729E + 04	.588E + 08	.170E-03	1.000	.333E-06		
.710E + 04	.573E + 08	.175E-03	1.000	.369E-06		
.691E + 04	.558E + 08	.179E-03	1.000	.409E-06		
.673E + 04	.543E + 08	.184E-03	1.000	.453E-06		
.655E + 04	.529E + 08	.189E-03	1.000	.502E-06		
.638E + 04	.515E + 08	.194E-03	1.000	.556E-06		
.621E + 04	.501E + 08	.200E-03	1.000	.616E-06		
.605E + 04	.488E + 08	.205E-03	1.000	.682E-06		
.589E + 04	.475E + 08	.211E-03	1.000	.755E-06		
.573E + 04	.463E + 08	.216E-03	1.000	.835E-06		
.558E + 04	.450E + 08	.222E-03	1.000	.924E-06		
.544E + 04	.438E + 08	.228E-03	1.000	.102E-05		
.529E + 04	.427E + 08	.234E-03	1.000	.113E-05		
.515E + 04	.416E + 08	.241E-03	1.000	.125E-05		
.502E + 04	.405E + 08	.247E-03	1.000	.138E-05		
.489E + 04	.394E + 08	.254E-03	1.000	.153E-05		
.476E + 04	.384E + 08	.261E-03	1.000	.169E-05		
.463E + 04	.374E + 08	.268E-03	1.000	.187E-05		
.451E + 04	.364E + 08	.275E-03	1.000	.207E-05		
.439E + 04	.354E + 08	.282E-03	1.000	.228E-05		
.428E + 04	.345E + 08	.290E-03	1.000	.252E-05		
.416E + 04	.336E + 08	.298E-03	1.000	.278E-05		
.405E + 04	.327E + 08	.306E-03	1.000	.307E-05		
.395E + 04	.318E + 08	.314E-03	1.000	.339E-05		
.384E + 04	.310E + 08	.323E-03	1.000	.374E-05		
.374E + 04	.302E + 08	.331E-03	1.000	.413E-05		
.364E + 04	.294E + 08	.340E-03	1.000	.455E-05		
.355E + 04	.286E + 08	.350E-03	1.000	.502E-05		
.345E + 04	.279E + 08	.359E-03	1.000	.553E-05		
.336E + 04	.271E + 08	.369E-03	1.000	.609E-05		
.327E + 04	.264E + 08	.379E-03	1.000	.671E-05		
.319E + 04	.257E + 08	.389E-03	1.000	.738E-05		
.310E + 04	.250E + 08	.399E-03	1.000	.812E-05		
.302E + 04	.244E + 08	.410E-03	1.000	.893E-05		
.294E + 04	.237E + 08	.421E-03	1.000	.982E-05		
.287E + 04	.231E + 08	.433E-03	1.000	.108E-04		
.279E + 04	.225E + 08	.444E-03	1.000	.119E-04		
.272E + 04	.219E + 08	.456E-03	1.000	.130E-04		

TABLE I *(Continued)*

Orthorhombic Sulfur

eV	cm^{-1}	μm	$n_\perp$	$k_\perp$	n_{supp}	k_{supp}
.264E + 04	.213E + 08	.469E-03	1.000	.143E-04		
.258E + 04	.208E + 08	.481E-03	1.000	.157E-04		
.251E + 04	.202E + 08	.495E-03	1.000	.172E-04		
.244E + 04	.197E + 08	.508E-03	1.000	.186E-05		
.238E + 04	.192E + 08	.522E-03	1.000	.207E-05		
.231E + 04	.187E + 08	.536E-03	1.000	.230E-05		
.225E + 04	.182E + 08	.550E-03	1.000	.255E-05		
.219E + 04	.177E + 08	.565E-03	1.000	.282E-05		
.214E + 04	.172E + 08	.580E-03	1.000	.313E-05		
.208E + 04	.168E + 08	.596E-03	1.000	.346E-05		
.203E + 04	.163E + 08	.612E-03	1.000	.383E-05		
.197E + 04	.159E + 08	.629E-03	1.000	.423E-05		
.192E + 04	.155E + 08	.646E-03	1.000	.467E-05		
.187E + 04	.151E + 08	.663E-03	1.000	.516E-05		
.182E + 04	.147E + 08	.681E-03	1.000	.570E-05		
.177E + 04	.143E + 08	.700E-03	1.000	.630E-05		
.173E + 04	.139E + 08	.719E-03	1.000	.695E-05		
.168E + 04	.136E + 08	.738E-03	1.000	.766E-05		
.164E + 04	.132E + 08	.758E-03	1.000	.844E-05		
.159E + 04	.128E + 08	.778E-03	1.000	.930E-05		
.155E + 04	.125E + 08	.799E-03	1.000	.102E-04		
.151E + 04	.122E + 08	.821E-03	1.000	.113E-04		
.147E + 04	.119E + 08	.843E-03	1.000	.125E-04		
.143E + 04	.115E + 08	.866E-03	1.000	.137E-04		
.139E + 04	.112E + 08	.890E-03	1.000	.152E-04		
.136E + 04	.109E + 08	.914E-03	1.000	.167E-04		
.132E + 04	.107E + 08	.938E-03	1.000	.185E-04		
.129E + 04	.104E + 08	.964E-03	1.000	.204E-04		
.125E + 04	.101E + 08	.990E-03	1.000	.225E-04		
.122E + 04	.984E + 07	.102E-02	1.000	.248E-04		
.119E + 04	.958E + 07	.104E-02	1.000	.274E-04		
.116E + 04	.933E + 07	.107E-02	1.000	.303E-04		
.113E + 04	.908E + 07	.110E-02	1.000	.334E-04		
.110E + 04	.884E + 07	.113E-02	1.000	.369E-04		
.107E + 04	.861E + 07	.116E-02	1.000	.407E-04		
.104E + 04	.838E + 07	.119E-02	1.000	.449E-04		
.101E + 04	.816E + 07	.123E-02	1.000	.496E-04		
.985E + 03	.795E + 07	.126E-02	1.000	.547E-04		
.959E + 03	.774E + 07	.129E-02	1.000	.603E-04		
.934E + 03	.753E + 07	.133E-02	1.000	.665E-04		
.910E + 03	.734E + 07	.136E-02	0.999	.733E-04		
.886E + 03	.714E + 07	.140E-02	0.999	.808E-04		
.862E + 03	.695E + 07	.144E-02	0.999	.891E-04		
.840E + 03	.677E + 07	.148E-02	0.999	.981E-04		
.817E + 03	.659E + 07	.152E-02	0.999	.108E-03		
.796E + 03	.642E + 07	.156E-02	0.999	.119E-03		

(continued)

TABLE I *(Continued)*

Orthorhombic Sulfur

eV	cm^{-1}	μm	$n_{\perp}$	$k_{\perp}$	n_{supp}	k_{supp}
.775E + 03	.625E + 07	.160E-02	0.999	.131E-03		
.755E + 03	.609E + 07	.164E-02	0.999	.144E-03		
.735E + 03	.592E + 07	.169E-02	0.999	.159E-03		
.715E + 03	.577E + 07	.173E-02	0.999	.175E-03		
.696E + 03	.562E + 07	.178E-02	0.999	.192E-03		
.678E + 03	.547E + 07	.183E-02	0.999	.210E-03		
.660E + 03	.532E + 07	.188E-02	0.999	.231E-03		
.643E + 03	.518E + 07	.193E-02	0.999	.255E-03		
.626E + 03	.505E + 07	.198E-02	0.999	.279E-03		
.609E + 03	.492E + 07	.203E-02	0.999	.306E-03		
.593E + 03	.479E + 07	.209E-02	0.999	.335E-03		
.578E + 03	.466E + 07	.215E-02	0.999	.367E-03		
.563E + 03	.454E + 07	.220E-02	0.999	.402E-03		
.548E + 03	.442E + 07	.226E-02	0.999	.440E-03		
.533E + 03	.430E + 07	.232E-02	0.999	.480E-03		
.519E + 03	.419E + 07	.239E-02	0.999	.525E-03		
.506E + 03	.408E + 07	.245E-02	0.998	.573E-03		
.492E + 03	.397E + 07	.252E-02	0.998	.625E-03		
.479E + 03	.387E + 07	.259E-02	0.998	.683E-03		
.467E + 03	.376E + 07	.266E-02	0.998	.746E-03		
.454E + 03	.366E + 07	.273E-02	0.998	.814E-03		
.442E + 03	.357E + 07	.280E-02	0.998	.887E-03		
.431E + 03	.347E + 07	.288E-02	0.998	.965E-03		
.419E + 03	.338E + 07	.296E-02	0.998	.105E-02		
.408E + 03	.329E + 07	.304E-02	0.998	.114E-02		
.398E + 03	.321E + 07	.312E-02	0.998	.124E-02		
.387E + 03	.312E + 07	.320E-02	0.998	.135E-02		
.377E + 03	.304E + 07	.329E-02	0.997	.146E-02		
.367E + 03	.296E + 07	.338E-02	0.997	.157E-02		
.357E + 03	.288E + 07	.347E-02	0.997	.170E-02		
.348E + 03	.281E + 07	.356E-02	0.997	.183E-02		
.339E + 03	.273E + 07	.366E-02	0.997	.198E-02		
.330E + 03	.266E + 07	.376E-02	0.997	.214E-02		
.321E + 03	.259E + 07	.386E-02	0.997	.231E-02		
.313E + 03	.252E + 07	.397E-02	0.997	.249E-02		
.305E + 03	.246E + 07	.407E-02	0.997	.269E-02		
.297E + 03	.239E + 07	.418E-02	0.997	.291E-02		
.289E + 03	.233E + 07	.430E-02	0.997	.314E-02		
.281E + 03	.227E + 07	.441E-02	0.997	.339E-02		
.274E + 03	.221E + 07	.453E-02	0.997	.361E-02		
.267E + 03	.215E + 07	.465E-02	0.996	.381E-02		
.259E + 03	.209E + 07	.478E-02	0.996	.401E-02		
.253E + 03	.204E + 07	.491E-02	0.996	.422E-02		
.246E + 03	.198E + 07	.504E-02	0.996	.444E-02		
.240E + 03	.193E + 07	.518E-02	0.996	.467E-02		
.233E + 03	.188E + 07	.532E-02	0.996	.491E-02		

TABLE I *(Continued)*

Orthorhombic Sulfur

eV	cm^{-1}	μm	$n_{\perp}$	$k_{\perp}$	n_{supp}	k_{supp}
.227E + 03	.183E + 07	.546E-02	0.996	.517E-02		
.221E + 03	.178E + 07	.561E-02	0.996	.544E-02		
.215E + 03	.174E + 07	.576E-02	0.996	.573E-02		
.210E + 03	.169E + 07	.592E-02	0.996	.606E-02		
.204E + 03	.165E + 07	.608E-02	0.996	.646E-02		
.199E + 03	.160E + 07	.624E-02	0.997	.688E-02		
.193E + 03	.156E + 07	.641E-02	0.997	.732E-02		
.188E + 03	.152E + 07	.658E-02	0.997	.778E-02		
.183E + 03	.148E + 07	.676E-02	0.998	.825E-02		
.179E + 03	.144E + 07	.694E-02	0.998	.873E-02		
.174E + 03	.140E + 07	.713E-02	0.999	.924E-02		
.169E + 03	.137E + 07	.733E-02	1.001	.978E-02		
.165E + 03	.133E + 07	.752E-02	1.004	.103E-01		
.161E + 03	.129E + 07	.773E-02	1.006	.928E-03		
.156E + 03	.126E + 07	.793E-02	1.001	.988E-03		
.152E + 03	.123E + 07	.815E-02	1.000	.105E-02		
.148E + 03	.119E + 07	.837E-02	0.999	.112E-02		
.144E + 03	.116E + 07	.860E-02	0.998	.120E-02		
.140E + 03	.113E + 07	.883E-02	0.997	.128E-02		
.137E + 03	.110E + 07	.907E-02	0.996	.138E-02		
.133E + 03	.108E + 07	.931E-02	0.996	.147E-02		
.130E + 03	.105E + 07	.957E-02	0.995	.157E-02		
.126E + 03	.102E + 07	.982E-02	0.994	.168E-02		
.123E + 03	.991E + 06	.101E-01	0.994	.179E-02		
.120E + 03	.965E + 06	.104E-01	0.993	.191E-02		
.117E + 03	.940E + 06	.106E-01	0.992	.204E-02		
.113E + 03	.915E + 06	.109E-01	0.991	.218E-02		
.110E + 03	.890E + 06	.112E-01	0.991	.231E-02		
.108E + 03	.867E + 06	.115E-01	0.990	.246E-02		
.105E + 03	.844E + 06	.118E-01	0.989	.264E-02		
.102E + 03	.822E + 06	.122E-01	0.988	.283E-02		
.993E + 02	.801E + 06	.125E-01	0.988	.303E-02		
.966E + 02	.779E + 06	.128E-01	0.987	.321E-02		
.941E + 02	.759E + 06	.132E-01	0.986	.340E-02		
.916E + 02	.739E + 06	.135E-01	0.985	.361E-02		
.892E + 02	.719E + 06	.139E-01	0.984	.382E-02		
.869E + 02	.701E + 06	.143E-01	0.983	.403E-02		
.846E + 02	.682E + 06	.147E-01	0.982	.426E-02		
.823E + 02	.664E + 06	.151E-01	0.981	.449E-02		
.802E + 02	.647E + 06	.155E-01	0.980	.474E-02		
.781E + 02	.630E + 06	.159E-01	0.979	.497E-02		
.760E + 02	.613E + 06	.163E-01	0.977	.519E-02		
.740E + 02	.597E + 06	.168E-01	0.976	.546E-02		
.721E + 02	.582E + 06	.172E-01	0.975	.575E-02		
.702E + 02	.566E + 06	.177E-01	0.973	.597E-02		
.683E + 02	.551E + 06	.182E-01	0.972	.618E-02		

(continued)

TABLE I *(Continued)*

Orthorhombic Sulfur

eV	cm^{-1}	μm	$n_\perp$	$k_\perp$	n_{supp}	k_{supp}
.665E + 02	.536E + 06	.186E-01	0.970	.637E-02		
.648E + 02	.523E + 06	.191E-01	0.968	.653E-02		
.631E + 02	.509E + 06	.197E-01	0.967	.665E-02		
.614E + 02	.495E + 06	.202E-01	0.965	.673E-02		
.598E + 02	.482E + 06	.207E-01	0.963	.688E-02		
.582E + 02	.469E + 06	.213E-01	0.960	.699E-02		
.567E + 02	.457E + 06	.219E-01	0.958	.693E-02		
.557E + 02	.449E + 06	.225E-01	0.955	.693E-02		
.537E + 02	.433E + 06	.231E-01	0.953	.693E-02		
.523E + 02	.422E + 06	.237E-01	0.950	.686E-02		
.118E + 02	.952E + 05	.105E + 00	1.340 [28]	.795E + 00 [28]		
.117E + 02	.944E + 05	.106E + 00	1.344	.793E + 00		
.116E + 02	.936E + 05	.107E + 00	1.352	.789E + 00		
.115E + 02	.928E + 05	.108E + 00	1.358	.783E + 00		
.114E + 02	.920E + 05	.109E + 00	1.359	.778E + 00		
.113E + 02	.911E + 05	.110E + 00	1.358	.775E + 00		
.112E + 02	.903E + 05	.111E + 00	1.352	.771E + 00		
.111E + 02	.895E + 05	.112E + 00	1.348	.770E + 00		
.110E + 02	.887E + 05	.113E + 00	1.338	.775E + 00		
.109E + 02	.879E + 05	.114E + 00	1.332	.782E + 00		
.108E + 02	.871E + 05	.115E + 00	1.326	.798E + 00		
.107E + 02	.863E + 05	.116E + 00	1.318	.815E + 00		
.106E + 02	.855E + 05	.117E + 00	1.308	.834E + 00		
.105E + 02	.847E + 05	.118E + 00	1.296	.853E + 00		
.104E + 02	.839E + 05	.119E + 00	1.281	.880E + 00		
.103E + 02	.831E + 05	.120E + 00	1.272	.930E + 00		
.102E + 02	.823E + 05	.122E + 00	1.272	.101E + 01		
.101E + 02	.815E + 05	.123E + 00	1.301	.109E + 01		
.100E + 02	.806E + 05	.124E + 00	1.358	.116E + 01		
.990E + 01	.798E + 05	.125E + 00	1.432	.121E + 01		
.980E + 01	.790E + 05	.126E + 00	1.503	.124E + 01		
.970E + 01	.782E + 05	.128E + 00	1.599	.125E + 01		
.960E + 01	.774E + 05	.129E + 00	1.705	.125E + 01		
.950E + 01	.766E + 05	.131E + 00	1.802	.122E + 01		
.940E + 01	.758E + 05	.132E + 00	1.877	.117E + 01		
.930E + 01	.750E + 05	.133E + 00	1.947	.112E + 01		
.920E + 01	.742E + 05	.135E + 00	2.009	.106E + 01		
.910E + 01	.734E + 05	.136E + 00	2.040	.986E + 00		
.900E + 01	.726E + 05	.138E + 00	2.047	.914E + 00		
.890E + 01	.718E + 05	.139E + 00	2.045	.851E + 00		
.880E + 01	.710E + 05	.141E + 00	2.049	.807E + 00		
.870E + 01	.702E + 05	.142E + 00	2.061	.778E + 00		
.860E + 01	.694E + 05	.144E + 00	2.079	.742E + 00		
.850E + 01	.686E + 05	.146E + 00	2.089	.692E + 00		
.840E + 01	.678E + 05	.148E + 00	2.078	.635E + 00		
.830E + 01	.669E + 05	.149E + 00	2.044	.577E + 00		

TABLE I *(Continued)*

Orthorhombic Sulfur

eV	cm^{-1}	μm	$n_{\perp}$	$k_{\perp}$	n_{supp}	k_{supp}
.820E + 01	.661E + 05	.151E + 00	2.005	.526E + 00		
.810E + 01	.653E + 05	.153E + 00	1.962	.484E + 00		
.800E + 01	.645E + 05	.155E + 00	1.907	.450E + 00		
.790E + 01	.637E + 05	.157E + 00	1.848	.423E + 00		
.780E + 01	.629E + 05	.159E + 00	1.790	.405E + 00		
.770E + 01	.621E + 05	.161E + 00	1.737	.399E + 00		
.760E + 01	.613E + 05	.163E + 00	1.692	.423E + 00		
.750E + 01	.605E + 05	.165E + 00	1.659	.473E + 00		
.740E + 01	.597E + 05	.168E + 00	1.648	.534E + 00		
.730E + 01	.589E + 05	.170E + 00	1.672	.593E + 00		
.720E + 01	.581E + 05	.172E + 00	1.723	.653E + 00		
.710E + 01	.573E + 05	.175E + 00	1.782	.702E + 00		
.700E + 01	.565E + 05	.177E + 00	1.833	.727E + 00		
.690E + 01	.556E + 05	.180E + 00	1.868	.725E + 00		
.680E + 01	.548E + 05	.182E + 00	1.883	.709E + 00		
.670E + 01	.540E + 05	.185E + 00	1.891	.684E + 00		
.660E + 01	.532E + 05	.188E + 00	1.903	.670E + 00		
.650E + 01	.524E + 05	.191E + 00	1.923	.672E + 00		
.640E + 01	.516E + 05	.194E + 00	1.951	.678E + 00		
.630E + 01	.508E + 05	.197E + 00	1.984	.680E + 00		
.620E + 01	.500E + 05	.200E + 00	2.018	.667E + 00		
.610E + 01	.492E + 05	.203E + 00	2.043	.655E + 00		
.600E + 01	.484E + 05	.207E + 00	2.063	.643E + 00		
.590E + 01	.476E + 05	.210E + 00	2.085	.623E + 00		
.580E + 01	.468E + 05	.214E + 00	2.097	.592E + 00		
.570E + 01	.460E + 05	.218E + 00	2.103	.566E + 00		
.560E + 01	.452E + 05	.221E + 00	2.102	.541E + 00		
.550E + 01	.444E + 05	.225E + 00	2.101	.515E + 00		
.540E + 01	.436E + 05	.230E + 00	2.096	.487E + 00		
.530E + 01	.428E + 05	.234E + 00	2.087	.461E + 00		
.520E + 01	.419E + 05	.238E + 00	2.082	.438E + 00		
.510E + 01	.411E + 05	.243E + 00	2.077	.421E + 00		
.500E + 01	.403E + 05	.248E + 00	2.076	.410E + 00		
.490E + 01	.395E + 05	.253E + 00	2.074	.403E + 00		
.480E + 01	.387E + 05	.258E + 00	2.062	.393E + 00		
.470E + 01	.379E + 05	.264E + 00	2.042	.378E + 00		
.460E + 01	.371E + 05	.269E + 00	2.015	.363E + 00		
.450E + 01	.363E + 05	.275E + 00	1.985	.356E + 00		
.440E + 01	.355E + 05	.282E + 00	1.990	.370E + 00		
.430E + 01	.347E + 05	.288E + 00	2.065	.435E + 00		
.420E + 01	.339E + 05	.295E + 00	2.150	.516E + 00		
.410E + 01	.331E + 05	.302E + 00	2.217	.552E + 00		
.400E + 01	.323E + 05	.310E + 00	2.275	.539E + 00		
.390E + 01	.315E + 05	.318E + 00	2.322	.498E + 00		
.380E + 01	.306E + 05	.326E + 00	2.353	.435E + 00		
.370E + 01	.298E + 05	.335E + 00	2.380	.370E + 00		

(continued)

TABLE I *(Continued)*

Orthorhombic Sulfur

eV	cm^{-1}	μm	$n_{\perp}$	$k_{\perp}$	n_{supp}	k_{supp}
.360E + 01	.290E + 05	.344E + 00	2.395	.313E + 00		
.350E + 01	.282E + 05	.354E + 00	2.376	.249E + 00		
.344E + 01	.277E + 05	.360E + 00	2.360	.287E-01		
.340E + 01	.274E + 05	.365E + 00	2.339			
.330E + 01	.266E + 05	.376E + 00	2.293			
.320E + 01	.258E + 05	.387E + 00	2.247			
.315E + 01	.254E + 05	.394E + 00	2.230	.313E-02 [26]		
.292E + 01	.236E + 05	.425E + 00	2.160	.338E-03		
.277E + 01	.223E + 05	.448E + 00	2.130	.356E-04		
.263E + 01	.212E + 05	.471E + 00	2.090	.375E-05		
.248E + 01	.200E + 05	.500E + 00	2.030 [24]	.174E-05 [25]		
.243E + 01	.197E + 05	.510E + 00	2.020	.122E-05		
.238E + 01	.192E + 05	.520E + 00	2.020	.931E-06		
.234E + 01	.189E + 05	.530E + 00	2.010	.844E-06		
.230E + 01	.185E + 05	.540E + 00	2.010	.752E-06		
.225E + 01	.182E + 05	.550E + 00	2.000	.711E-06		
.221E + 01	.179E + 05	.560E + 00	2.000	.668E-06		
.218E + 01	.175E + 05	.570E + 00	1.990	.624E-06		
.214E + 01	.172E + 05	.580E + 00	1.990	.600E-06		
.210E + 01	.169E + 05	.590E + 00	1.980	.587E-06		
.207E + 01	.167E + 05	.600E + 00	1.990			
.191E + 01	.154E + 05	.650E + 00	1.980	.350E-06 [33]		
.177E + 01	.143E + 05	.700E + 00	1.970	.330E-06		
.165E + 01	.133E + 05	.750E + 00	1.970	.330E-06		
.155E + 01	.125E + 05	.800E + 00	1.960	.320E-06		
.146E + 01	.118E + 05	.850E + 00	1.955	.312E-06		
.138E + 01	.111E + 05	.900E + 00	1.950	.305E-06		
.130E + 01	.105E + 05	.950E + 00	1.950	.298E-06		
.124E + 01	.100E + 05	.100E + 01	1.950	.290E-06		
.118E + 01	.952E + 04	.105E + 01	1.947	.294E-06		
.113E + 01	.909E + 04	.110E + 01	1.945	.298E-06		
.108E + 01	.870E + 04	.115E + 01	1.942	.301E-06		
.103E + 01	.833E + 04	.120E + 01	1.940	.305E-06		
.992E + 00	.800E + 04	.125E + 01	1.940	.309E-06		
.954E + 00	.769E + 04	.130E + 01	1.940	.312E-06		
.918E + 00	.741E + 04	.135E + 01	1.940	.316E-06		
.886E + 00	.714E + 04	.140E + 01	1.940	.320E-06		
.855E + 00	.690E + 04	.145E + 01	1.940	.321E-06		
.827E + 00	.667E + 04	.150E + 01	1.940	.322E-06		
.800E + 00	.645E + 04	.155E + 01	1.940	.323E-06		
.775E + 00	.625E + 04	.160E + 01	1.940	.323E-06		
.751E + 00	.606E + 04	.165E + 01	1.940	.324E-06		
.729E + 00	.588E + 04	.170E + 01	1.940	.325E-06		
.709E + 00	.571E + 04	.175E + 01	1.940	.326E-06		
.689E + 00	.556E + 04	.180E + 01	1.940	.327E-06		
.670E + 00	.540E + 04	.185E + 01	1.940	.328E-06		

TABLE I *(Continued)*

Orthorhombic Sulfur

eV	cm^{-1}	μm	$n_\perp$	$k_\perp$	n_{supp}	k_{supp}
.653E + 00	.526E + 04	.190E + 01	1.940	.328E-06		
.636E + 00	.513E + 04	.195E + 01	1.940	.329E-06		
.620E + 00	.500E + 04	.200E + 01	1.926 [10]		2.003 [10]	
.558E + 00	.450E + 04	.222E + 01	1.926		2.003	
.496E + 00	.400E + 04	.250E + 01	1.926		2.003	
.434E + 00	.350E + 04	.286E + 01	1.926		2.003	
.372E + 00	.300E + 04	.333E + 01	1.926		2.003	
.310E + 00	.250E + 04	.400E + 01	1.926		2.003	
.248E + 00	.200E + 04	.500E + 01	1.926		2.003	
.186E + 00	.150E + 04	.667E + 01	1.926		2.003	
.185E + 00	.149E + 04	.671E + 01	1.925		2.003	
.184E + 00	.148E + 04	.676E + 01	1.925		2.003	
.182E + 00	.147E + 04	.680E + 01	1.925		2.003	
.181E + 00	.146E + 04	.685E + 01	1.925		2.003	
.180E + 00	.145E + 04	.690E + 01	1.925		2.003	
.178E + 00	.144E + 04	.694E + 01	1.925		2.003	
.177E + 00	.143E + 04	.699E + 01	1.925		2.003	
.176E + 00	.142E + 04	.704E + 01	1.925		2.003	
.175E + 00	.141E + 04	.709E + 01	1.924		2.003	
.174E + 00	.140E + 04	.714E + 01	1.924	.288E-04 [17]	2.003	
.173E + 00	.140E + 04	.717E + 01	1.924	.303E-04	2.003	
.172E + 00	.139E + 04	.719E + 01	1.924	.315E-04	2.003	
.172E + 00	.138E + 04	.722E + 01	1.924	.329E-04	2.003	
.171E + 00	.138E + 04	.725E + 01	1.924	.356E-04	2.003	
.170E + 00	.138E + 04	.727E + 01	1.924	.374E-04	2.003	
.170E + 00	.137E + 04	.730E + 01	1.924	.396E-04	2.002	
.169E + 00	.136E + 04	.733E + 01	1.924	.429E-04	2.002	
.169E + 00	.136E + 04	.735E + 01	1.924	.465E-04	2.002	
.168E + 00	.136E + 04	.738E + 01	1.924	.554E-04	2.002	
.167E + 00	.135E + 04	.741E + 01	1.924	.660E-04	2.002	
.167E + 00	.134E + 04	.743E + 01	1.923	.790E-04	2.002	
.166E + 00	.134E + 04	.746E + 01	1.923	.926E-04	2.002	
.166E + 00	.134E + 04	.749E + 01	1.923	.108E-03	2.002	
.165E + 00	.133E + 04	.752E + 01	1.923	.127E-03	2.002	
.164E + 00	.132E + 04	.755E + 01	1.922	.148E-03	2.002	
.164E + 00	.132E + 04	.758E + 01	1.921	.166E-03	2.002	
.163E + 00	.132E + 04	.761E + 01	1.921	.192E-03	2.002	
.162E + 00	.131E + 04	.763E + 01	1.920	.211E-03	2.002	
.162E + 00	.130E + 04	.766E + 01	1.921	.217E-03	2.002	
.161E + 00	.130E + 04	.769E + 01	1.921	.218E-03	2.002	
.161E + 00	.130E + 04	.772E + 01	1.921	.216E-03	2.002	
.160E + 00	.129E + 04	.775E + 01	1.922	.213E-03	2.002	
.159E + 00	.128E + 04	.778E + 01	1.923	.206E-03	2.002	
.159E + 00	.128E + 04	.781E + 01	1.923	.184E-03	2.002	
.158E + 00	.128E + 04	.784E + 01	1.924	.158E-03	2.002	
.157E + 00	.127E + 04	.787E + 01	1.926	.132E-03	2.002	

(continued)

TABLE I *(Continued)*

Orthorhombic Sulfur

eV	cm^{-1}	μm	$n_\perp$	$k_\perp$	n_{supp}	k_{supp}
.157E + 00	.126E + 04	.791E + 01	1.926	.101E-03	2.002	
.156E + 00	.126E + 04	.794E + 01	1.927	.771E-04	2.002	
.156E + 00	.126E + 04	.797E + 01	1.927	.624E-04	2.002	
.155E + 00	.125E + 04	.800E + 01	1.927	.457E-04	2.002	
.154E + 00	.124E + 04	.803E + 01	1.927	.329E-04	2.002	
.154E + 00	.124E + 04	.806E + 01	1.927	.258E-04	2.002	
.153E + 00	.124E + 04	.810E + 01	1.927	.187E-04	2.002	
.153E + 00	.123E + 04	.813E + 01	1.927	.154E-04	2.002	
.152E + 00	.122E + 04	.816E + 01	1.927	.132E-04	2.002	
.151E + 00	.122E + 04	.820E + 01	1.927	.110E-04	2.002	
.151E + 00	.122E + 04	.823E + 01	1.927	.979E-05	2.002	
.150E + 00	.121E + 04	.826E + 01	1.927	.815E-05	2.002	
.149E + 00	.120E + 04	.830E + 01	1.927	.734E-05	2.002	
.149E + 00	.120E + 04	.833E + 01	1.927	.610E-05	2.002	
.148E + 00	.120E + 04	.837E + 01	1.927	.584E-05	2.002	
.147E + 00	.119E + 04	.840E + 01	1.927	.506E-05	2.002	
.147E + 00	.118E + 04	.844E + 01	1.927	.508E-05	2.002	
.146E + 00	.118E + 04	.848E + 01	1.927	.429E-05	2.002	
.146E + 00	.118E + 04	.851E + 01	1.927	.433E-05	2.002	
.145E + 00	.117E + 04	.855E + 01	1.927	.435E-05	2.002	
.144E + 00	.116E + 04	.858E + 01	1.927	.357E-05	2.002	
.144E + 00	.116E + 04	.862E + 01	1.927	.277E-05	2.002	
.143E + 00	.116E + 04	.866E + 01	1.927	.343E-05	2.002	
.143E + 00	.115E + 04	.870E + 01	1.927	.279E-05	2.002	
.142E + 00	.114E + 04	.873E + 01	1.927	.317E-05	2.002	
.141E + 00	.114E + 04	.877E + 01	1.927	.302E-05	2.002	
.141E + 00	.114E + 04	.881E + 01	1.927	.367E-05	2.002	
.140E + 00	.113E + 04	.885E + 01	1.927	.319E-05	2.002	
.140E + 00	.112E + 04	.889E + 01	1.927	.431E-05	2.002	
.139E + 00	.112E + 04	.893E + 01	1.927	.449E-05	2.002	
.138E + 00	.112E + 04	.897E + 01	1.927	.456E-05	2.002	
.138E + 00	.111E + 04	.901E + 01	1.927	.482E-05	2.002	
.137E + 00	.110E + 04	.905E + 01	1.927	.464E-05	2.002	
.136E + 00	.110E + 04	.909E + 01	1.927	.547E-05	2.002	
.136E + 00	.110E + 04	.913E + 01	1.927	.690E-05	2.002	
.135E + 00	.109E + 04	.917E + 01	1.927	.812E-05	2.002	
.134E + 00	.108E + 04	.922E + 01	1.927	.872E-05	2.002	
.134E + 00	.108E + 04	.926E + 01	1.927	.102E-04	2.002	
.133E + 00	.108E + 04	.930E + 01	1.927	.109E-04	2.002	
.133E + 00	.107E + 04	.935E + 01	1.927	.133E-04	2.002	
.132E + 00	.106E + 04	.939E + 01	1.927	.152E-04	2.002	
.131E + 00	.106E + 04	.943E + 01	1.927	.175E-04	2.002	
.131E + 00	.106E + 04	.948E + 01	1.927	.207E-04	2.002	
.130E + 00	.105E + 04	.952E + 01	1.927	.214E-04	2.002	
.130E + 00	.104E + 04	.957E + 01	1.927	.233E-04	2.002	
.129E + 00	.104E + 04	.961E + 01	1.927	.234E-04	2.002	

TABLE I *(Continued)*

Orthorhombic Sulfur

eV	cm^{-1}	μm	$n_{\perp}$	$k_{\perp}$	n_{supp}	k_{supp}
.128E + 00	.104E + 04	.966E + 01	1.927	.223E-04	2.002	
.128E + 00	.103E + 04	.971E + 01	1.927	.187E-04	2.002	
.127E + 00	.102E + 04	.976E + 01	1.927	.156E-04	2.002	
.126E + 00	.102E + 04	.980E + 01	1.927	.135E-04	2.002	
.126E + 00	.102E + 04	.985E + 01	1.927	.107E-04	2.001	
.125E + 00	.101E + 04	.990E + 01	1.927	.118E-04	2.001	
.125E + 00	.100E + 04	.995E + 01	1.927	.124E-04	2.001	
.124E + 00	.100E + 04	.100E + 02	1.927	.130E-04	2.001	
.123E + 00	.995E + 03	.101E + 02	1.927	.260E-04	2.001	
.123E + 00	.990E + 03	.101E + 02	1.927	.304E-04	2.001	
.122E + 00	.985E + 03	.101E + 02	1.926	.331E-04	2.001	
.122E + 00	.980E + 03	.102E + 02	1.926	.289E-04	2.001	
.121E + 00	.975E + 03	.103E + 02	1.926	.349E-04	2.001	
.120E + 00	.970E + 03	.103E + 02	1.926	.395E-04	2.001	
.120E + 00	.965E + 03	.104E + 02	1.926	.433E-04	2.000	
.119E + 00	.960E + 03	.104E + 02	1.926	.579E-04	2.000	
.118E + 00	.955E + 03	.105E + 02	1.926	.912E-04	2.000	
.118E + 00	.950E + 03	.105E + 02	1.926	.161E-03	1.999	
.117E + 00	.945E + 03	.106E + 02	1.926	.296E-03	1.998	
.116E + 00	.940E + 03	.106E + 02	1.926	.430E-03	1.998	
.116E + 00	.935E + 03	.107E + 02	1.926	.434E-03	2.000	
.115E + 00	.930E + 03	.108E + 02	1.925	.315E-03	2.001	
.115E + 00	.925E + 03	.108E + 02	1.926	.198E-03	2.002	
.114E + 00	.920E + 03	.109E + 02	1.926	.150E-03	2.003	
.113E + 00	.915E + 03	.109E + 02	1.926	.157E-03	2.003	
.113E + 00	.910E + 03	.110E + 02	1.926	.262E-03	2.002	
.112E + 00	.905E + 03	.111E + 02	1.926	.312E-03	2.001	
.112E + 00	.900E + 03	.111E + 02	1.926	.280E-03	2.001	
.111E + 00	.895E + 03	.112E + 02	1.926	.301E-03	2.002	
.110E + 00	.890E + 03	.112E + 02	1.926	.420E-03	2.003	
.110E + 00	.885E + 03	.113E + 02	1.926	.607E-03	2.001	
.109E + 00	.880E + 03	.114E + 02	1.926	.848E-03	1.999	
.108E + 00	.875E + 03	.114E + 02	1.926	.102E-02	1.997	
.108E + 00	.870E + 03	.115E + 02	1.926	.119E-02	1.996	
.107E + 00	.865E + 03	.116E + 02	1.925	.131E-02	1.995	
.107E + 00	.860E + 03	.116E + 02	1.924	.167E-02	1.994	
.106E + 00	.855E + 03	.117E + 02	1.924	.237E-02	1.995	
.105E + 00	.850E + 03	.118E + 02	1.924	.334E-02	1.995	
.105E + 00	.845E + 03	.118E + 02	1.924	.419E-02	1.997	
.104E + 00	.840E + 03	.119E + 02	1.925	.307E-02	1.998	
.104E + 00	.835E + 03	.120E + 02	1.926	.220E-02	2.000	
.103E + 00	.830E + 03	.121E + 02	1.926	.149E-02	2.003	
.102E + 00	.825E + 03	.121E + 02	1.926	.109E-02	2.004	
.102E + 00	.820E + 03	.122E + 02	1.926	.810E-03	2.005	
.101E + 00	.815E + 03	.123E + 02	1.926	.647E-03	2.005	
.100E + 00	.810E + 03	.124E + 02	1.926	.486E-03	2.005	

(continued)

TABLE I *(Continued)*

Orthorhombic Sulfur

eV	cm^{-1}	μm	$n_\perp$	$k_\perp$	n_{supp}	k_{supp}
.998E-01	.805E + 03	.124E + 02	1.926	.297E-03	2.005	
.992E-01	.800E + 03	.125E + 02	1.926	.200E-03	2.005	
.986E-01	.795E + 03	.126E + 02	1.926	.141E-03	2.005	
.979E-01	.790E + 03	.127E + 02	1.926	.103E-03	2.005	
.973E-01	.785E + 03	.127E + 02	1.926	.716E-04	2.004	
.967E-01	.780E + 03	.128E + 02	1.925	.442E-04	2.004	
.961E-01	.775E + 03	.129E + 02	1.925	.296E-04	2.004	
.955E-01	.770E + 03	.130E + 02	1.925	.257E-04	2.004	
.949E-01	.765E + 03	.131E + 02	1.925	.262E-04	2.004	
.942E-01	.760E + 03	.132E + 02	1.925	.269E-04	2.004	
.936E-01	.755E + 03	.132E + 02	1.924	.344E-04	2.004	
.930E-01	.750E + 03	.133E + 02	1.924	.422E-04	2.004	
.924E-01	.745E + 03	.134E + 02	1.924	.525E-04	2.004	
.918E-01	.740E + 03	.135E + 02	1.924	.695E-04	2.004	
.911E-01	.735E + 03	.136E + 02	1.923	.964E-04	2.004	
.905E-01	.730E + 03	.137E + 02	1.923	.134E-03	2.004	
.899E-01	.725E + 03	.138E + 02	1.923	.201E-03	2.004	
.893E-01	.720E + 03	.139E + 02	1.923	.425E-03	2.004	
.887E-01	.715E + 03	.140E + 02	1.923	.593E-03	2.004	
.880E-01	.710E + 03	.141E + 02	1.922	.612E-03	2.004	
.874E-01	.705E + 03	.142E + 02	1.921	.502E-03	2.004	
.868E-01	.700E + 03	.143E + 02	1.920	.447E-03	2.004	
.862E-01	.695E + 03	.144E + 02	1.919	.306E-03 [19]	2.003	
.856E-01	.690E + 03	.145E + 02	1.919	.364E-03	2.003	
.849E-01	.685E + 03	.146E + 02	1.919	.478E-03	2.003	
.843E-01	.680E + 03	.147E + 02	1.919	.569E-03	2.003	
.837E-01	.675E + 03	.148E + 02	1.918	.671E-03	2.002	
.831E-01	.670E + 03	.149E + 02	1.918	.872E-03	2.001	
.825E-01	.665E + 03	.150E + 02	1.919	.103E-02	2.000	
.818E-01	.660E + 03	.151E + 02	1.920	.111E-02	1.999	
.812E-01	.655E + 03	.153E + 02	1.922	.994E-03	1.998	
.806E-01	.650E + 03	.154E + 02	1.924	.666E-03	1.998	
.800E-01	.645E + 03	.155E + 02	1.927	.440E-03	2.001	
.794E-01	.640E + 03	.156E + 02	1.930	.368E-03	2.004	
.787E-01	.635E + 03	.158E + 02	1.931	.373E-03	2.009	
.781E-01	.630E + 03	.159E + 02	1.933	.443E-03	2.013	
.775E-01	.625E + 03	.160E + 02	1.933	.560E-03	2.013	
.769E-01	.620E + 03	.161E + 02	1.932	.609E-03	2.013	
.763E-01	.615E + 03	.163E + 02	1.931	.524E-03	2.016	
.756E-01	.610E + 03	.164E + 02	1.930	.409E-03	2.019	
.750E-01	.605E + 03	.165E + 02	1.930	.378E-03	2.019	
.744E-01	.600E + 03	.167E + 02	1.930	.401E-03	2.019	
.738E-01	.595E + 03	.168E + 02	1.930	.494E-03	2.016	
.732E-01	.590E + 03	.170E + 02	1.930	.705E-03	2.014	
.725E-01	.585E + 03	.171E + 02	1.929	.801E-03	2.012	
.719E-01	.580E + 03	.172E + 02	1.929	.628E-03	2.010	

TABLE I *(Continued)*

Orthorhombic Sulfur

eV	cm^{-1}	μm	$n_{\perp}$	$k_{\perp}$	n_{supp}	k_{supp}
.713E-01	.575E + 03	.174E + 02	1.928	.485E-03	2.009	
.707E-01	.570E + 03	.175E + 02	1.927	.443E-03	2.007	
.701E-01	.565E + 03	.177E + 02	1.926	.476E-03	2.009	
.694E-01	.560E + 03	.179E + 02	1.925	.650E-03	2.010	
.688E-01	.555E + 03	.180E + 02	1.924	.936E-03	2.008	
.682E-01	.550E + 03	.182E + 02	1.924	.113E-02	2.006	
.676E-01	.545E + 03	.184E + 02	1.923	.108E-02	2.007	
.670E-01	.540E + 03	.185E + 02	1.923	.986E-03	2.009	
.663E-01	.535E + 03	.187E + 02	1.923	.907E-03	2.007	
.657E-01	.530E + 03	.189E + 02	1.923	.880E-03	2.004	
.651E-01	.525E + 03	.190E + 02	1.923	.966E-03	2.003	
.645E-01	.520E + 03	.192E + 02	1.923	.107E-02	2.003	
.639E-01	.515E + 03	.194E + 02	1.923	.113E-02	2.003	
.632E-01	.510E + 03	.196E + 02	1.923	.120E-02	2.002	
.626E-01	.505E + 03	.198E + 02	1.923	.125E-02	2.002	
.620E-01	.500E + 03	.200E + 02	1.922	.900E-02 [10]	2.002	.130E-02 [19]
.614E-01	.495E + 03	.202E + 02	1.921	.102E-01	2.001	.133E-02
.608E-01	.490E + 03	.204E + 02	1.920	.114E-01	2.001	.134E-02
.601E-01	.485E + 03	.206E + 02	1.921	.137E-01	1.995	.460E-02 [10]
.595E-01	.480E + 03	.208E + 02	1.921	.159E-01	1.990	.920E-02
.589E-01	.475E + 03	.210E + 02	1.924	.172E-01	1.995	.160E-01
.583E-01	.470E + 03	.213E + 02	1.927	.186E-01	2.000	.229E-01
.576E-01	.465E + 03	.215E + 02	1.931	.176E-01	2.016	.194E-01
.570E-01	.460E + 03	.217E + 02	1.934	.166E-01	2.033	.160E-01
.564E-01	.455E + 03	.220E + 02	1.935	.137E-01	2.027	.800E-02
.558E-01	.450E + 03	.222E + 02	1.936	.108E-01	2.021	.181E-02 [19]
.552E-01	.445E + 03	.225E + 02	1.935	.835E-02	2.016	.205E-02
.545E-01	.440E + 03	.227E + 02	1.934	.590E-02	2.011	.253E-02
.539E-01	.435E + 03	.230E + 02	1.931	.505E-02	2.011	.278E-02
.533E-01	.430E + 03	.233E + 02	1.929	.420E-02	2.011	.263E-02
.527E-01	.425E + 03	.235E + 02	1.928	.470E-02	2.010	.242E-02
.521E-01	.420E + 03	.238E + 02	1.927	.520E-02	2.009	.207E-02
.514E-01	.415E + 03	.241E + 02	1.926	.585E-02	2.009	.173E-02
.508E-01	.410E + 03	.244E + 02	1.925	.650E-02	2.008	.169E-02
.502E-01	.405E + 03	.247E + 02	1.925	.725E-02	2.008	
.496E-01	.400E + 03	.250E + 02	1.925	.800E-02	2.008	
.490E-01	.395E + 03	.253E + 02	1.925	.835E-02	2.008	
.483E-01	.390E + 03	.256E + 02	1.925	.870E-02	2.008	
.477E-01	.385E + 03	.260E + 02	1.924	.915E-02	2.007	
.471E-01	.380E + 03	.263E + 02	1.924	.960E-02	2.007	
.465E-01	.375E + 03	.267E + 02	1.924	.995E-02	2.007	
.459E-01	.370E + 03	.270E + 02	1.924	.103E-01	2.007	
.452E-01	.365E + 03	.274E + 02	1.924	.108E-01	2.007	
.446E-01	.360E + 03	.278E + 02	1.924	.113E-01	2.006	
.440E-01	.355E + 03	.282E + 02	1.923	.117E-01	2.005	
.434E-01	.350E + 03	.286E + 02	1.923	.121E-01	2.004	

(continued)

TABLE I *(Continued)*

Orthorhombic Sulfur

eV	cm^{-1}	μm	$n_\perp$	$k_\perp$	n_{supp}	k_{supp}
.428E-01	.345E + 03	.290E + 02	1.923	.126E-01	2.003	
.421E-01	.340E + 03	.294E + 02	1.923	.132E-01	2.002	
.415E-01	.335E + 03	.299E + 02	1.923	.136E-01	2.000	
.409E-01	.330E + 03	.303E + 02	1.922	.139E-01	1.999	
.403E-01	.325E + 03	.308E + 02	1.921	.146E-01	1.998	
.397E-01	.320E + 03	.312E + 02	1.921	.152E-01	1.998	
.391E-01	.315E + 03	.318E + 02	1.921	.159E-01	1.996	
.384E-01	.310E + 03	.323E + 02	1.920	.167E-01	1.994	
.378E-01	.305E + 03	.328E + 02	1.919	.178E-01	1.993	
.372E-01	.300E + 03	.333E + 02	1.919	.188E-01	1.992	
.366E-01	.295E + 03	.339E + 02	1.918	.201E-01	1.990	
.360E-01	.290E + 03	.345E + 02	1.917	.214E-01	1.988	
.353E-01	.285E + 03	.351E + 02	1.916	.232E-01	1.986	
.347E-01	.280E + 03	.357E + 02	1.915	.250E-01	1.984	
.341E-01	.275E + 03	.364E + 02	1.912	.286E-01	1.980	
.335E-01	.270E + 03	.370E + 02	1.909	.321E-01	1.976	
.329E-01	.265E + 03	.377E + 02	1.906	.422E-01	1.971	.600E-03 [10]
.322E-01	.260E + 03	.385E + 02	1.902	.524E-01	1.966	.120E-02
.316E-01	.255E + 03	.392E + 02	1.911	.657E-01	1.955	.162E-01
.310E-01	.250E + 03	.400E + 02	1.919	.789E-01	1.944	.313E-01
.304E-01	.245E + 03	.408E + 02	1.939	.844E-01	1.969	.458E-01
.298E-01	.240E + 03	.417E + 02	1.958	.900E-01	1.993	.603E-01
.291E-01	.235E + 03	.425E + 02	1.975	.810E-01	2.013	.451E-01
.285E-01	.230E + 03	.435E + 02	1.993	.720E-01	2.033	.299E-01
.279E-01	.225E + 03	.444E + 02	1.997	.587E-01	2.020	.158E-01
.273E-01	.220E + 03	.455E + 02	2.001	.455E-01	2.006	.160E-02
.267E-01	.215E + 03	.465E + 02	1.998	.388E-01	1.991	.145E-02
.260E-01	.210E + 03	.476E + 02	1.995	.322E-01	1.976	.130E-02
.254E-01	.205E + 03	.488E + 02	1.999	.318E-01	1.964	.281E-01
.248E-01	.200E + 03	.500E + 02	2.003	.315E-01	1.951	.550E-01
.242E-01	.195E + 03	.513E + 02	2.016	.233E-01	1.968	.843E-01
.236E-01	.190E + 03	.526E + 02	2.028	.150E-01	1.985	.114E + 00
.229E-01	.185E + 03	.540E + 02	2.037	.750E-02	2.080	0.912E-01
.223E-01	.180E + 03	.556E + 02	2.046		2.176	.686E-01

Cubic Thallium(I) Halides

WILLIAM J. TROPF
Applied Physics Laboratory
The Johns Hopkins University
Laurel, Maryland

Most of the univalent thallium [thallium(I) or thallous] halides have the cubic cesium-chloride structure (space group Pm3m or O_h^5). Exceptions are thallium fluoride and the low-temperature (below 170° C) form of thallium iodide, which are both orthorhombic. Cubic forms of the thallium(I) halides are important optical materials because of their high refractive index, far-infrared transparency, relative insolubility in water, and moderate strength. Thallium halides are miscible in all concentrations; eutectic mixtures are typically used to improve composition homogeneity [1]. The cubic eutectic mixtures of thallium-halide crystals with the designations KRS-5 and KRS-6[1] are especially important. The usual composition of KRS-5 is 54.3 mole-percent TlI and of KRS-6 is 70.2 mole percent TlCl, with the balance being thallium bromide for both. Single crystals of pure and mixed thallous halides are grown by the Stockbarger technique. Table I summarizes the physical properties of thallous-halide crystals.

THALLIUM CHLORIDE I

Thallium chloride has a direct band gap of 3.4 eV [1]. Unlike most materials, the band gap increases with temperature, by about 0.02 eV from 0 to 200 K. Optical constants in the region of fundamental electronic absorption from the band gap to about 20 eV were determined by Hinson and Stevenson [2] and Frandon and LaHaye [3] from Kramers–Krönig analyses of reflection and energy-loss spectra, respectively. Absorption immediately above the band gap has been determined from transmission measurements by Martienssen [4] and Tutihasi [5]. These results are given in Table II.

[1] KRS is an abbreviation for the German term Kristalle aus dem *S*chmeltzfluß, or crystal from the fused melt.

Copyright © 1998 by Academic Press.
All rights of reproduction in any form reserved
ISBN 0-12-544423-0/$25.00.

Strong absorption begins with exciton formation at the band gap followed by interband transitions between the valence band of chlorine and the conduction band of thallium. A thallium-valence-electron plasma oscillation occurs around 7.2 eV and a chlorine $4p$ electron plasma resonance occurs near 12.4 eV.

Smakula [6] reports low-level absorption at the ultraviolet and infrared edges of transparency.

Refractive index in the visible transparent region has been measured by Barth [7] (method unknown, probably index matching), Schröter [8] (minimum-deviation method), and Takahei and Kobayashi [9] (prism refraction method). Barth's data are lower that those from other sources by 0.015 to 0.020. The later two references give dispersion equations only. McCarthy [10] gives interferometrically measured refractive indices in the infrared at 45° C, which have been corrected to room temperature (20° C) by adding 0.006. The dispersion equation of Schröter [8] is

$$\frac{n^2(\lambda)-1}{n^2(\lambda)+2} = 0.47856 + \frac{0.07858}{\lambda^2 - 0.08277} - 0.00881\lambda^2 \tag{1}$$

for the 0.435 to 0.660 μm range, and the dispersion equation of Takahei and Kobayashi [9] is

$$n^2(\lambda) = (2.146)^2 + \frac{1.780}{(\lambda/0.2651)^2 - 1} + \frac{0.0778}{(\lambda/0.3532)^2 - 1} \tag{2}$$

for the 0.390 to 0.635 μm range. Wavelengths are in micrometers in both cases. Table II has the data of Barth and McCarthy and selected calculated values from the dispersion equations.

The temperature change of the refractive index due to electronic absorption, dn_∞/dT, of thallium chloride is determined by Takahei and Kobayashi [9] to be -154×10^{-6}/K over the interval 40 to 300 K and as -194×10^{-6}/K by Shanker and Sundaraj [11] (using $n_\infty = 2.146$). This latter dn/dT value was used to correct the McCarthy data (see earlier discussion) to room temperature.

Low-level infrared absorption of thallium chloride, up to the region of fundamental lattice vibration absorption, was measured by Hidaka *et al.* [12]. They model the absorption coefficient in the 500 to 1100 cm^{-1} region with the equation

$$\beta(\nu) = \beta_0 \exp(-\nu/\nu_0) \tag{3}$$

with $\beta_0 = 6$ cm^{-1}, $\nu_0 = 100$ cm^{-1}, and ν is in wave numbers.

Infrared reflection measurements have been made by Mitsuishi *et al.* [13], Lowndes [14], and Claudel *et al.* [15]. Thallium chloride, like the other cubic thallous halides, has only a single (degenerate) Raman-inactive, infrared-

active optical mode (F_{1u}). Lowndes uses a model of the complex refractive index (n) of the form

$$n^2(\nu) = \epsilon(\nu) = \epsilon_\infty \frac{\nu_{LO}^2 - \nu^2 - i\gamma_{LO}\nu}{\nu_{TO}^2 - \nu^2 - i\gamma_{TO}\nu}, \tag{4}$$

where the transverse and longitudinal frequencies of thallium chloride are $\nu_{TO} = 62\ cm^{-1}$ and $\nu_{LO} = 173\ cm^{-1}$, with widths of $\gamma_{TO} = 7.7\ cm^{-1}$ and $\gamma_{LO} = 20\ cm^{-1}$, and $\epsilon_\infty = 4.60$.

Claudel *et al.* [15] used a classical oscillator model of the form

$$n^2(\nu) = \epsilon(\nu) = \epsilon_\infty + \sum_j \frac{4\pi\rho_j\nu_{TOj}^2}{\nu_{TOj}^2 - \nu^2 - i\gamma_j\nu} \tag{5}$$

with two far-infrared modes to represent their data. Their model parameters are $\rho_1 = 2.20$, $\rho_2 = 0.05$, $\nu_{TO1} = 63\ cm^{-1}$, $\nu_{TO2} = 120\ cm^{-1}$, $\gamma_1 = 0.08$, $\gamma_2 = 0.6$, and $\epsilon_\infty = 4.4$. Both models, which generally agree within 10%, are used to calculate the optical constants given in Table II.

The room-temperature, low-frequency (1–100 kHz) dielectric constant was measured as $\epsilon_0 = 32.7 \pm 0.2$ (or $n = 5.72 \pm 0.02$) by Lowndes [16], $\epsilon_0 = 32.4 \pm 0.1$ (or $n = 5.70 \pm 0.01$) by Lowndes and Martin [17], and $\epsilon_0 = 32.3 \pm 0.2$ (or $n = 5.68 \pm 0.02$) by Samara [18] using capacitance techniques. The low-frequency dielectric constant has a large, negative temperature dependence: $d\epsilon_0/dT = -0.012\ K^{-1}$ [16–18] and $d\epsilon_0/dT = -0.01216\ K^{-1}$ [11] (or $dn/dT = -0.0011\ K^{-1}$).

Table II gives all the optical-constant data for thallium chloride and Fig. 1 shows the data graphically.

THALLIUM BROMIDE II

Thallium bromide has a direct band gap of 3.0 eV [1]. Like thallium chloride, the band gap increases with temperature, by about 0.02 eV from 0 to 200 K. Optical constants in the region of fundamental electronic absorption from the band gap to about 20 eV were determined by Hinson and Stevenson [2] and Frandon and LaHaye [3] from a Kramers–Kronig analysis of reflection and energy-loss spectra, respectively. These results are given in Table III.

Strong absorption begins with exciton formation at the band gap followed by interband transitions between the valence band of bromine and the conduction band of thallium. A thallium-valence-electron plasma oscillation occurs around 6.7 eV and bromine 4p electron plasma resonance occurs near 11.8 eV.

Smakula [6] reports low-level absorption at the ultraviolet and infrared edges of transparency.

Refractive index in the visible transparent region has been measured by Barth [7], Schröter [8], and Takahei and Kobayashi [9]. Barth's data is lower that the other sources by 0.020. The latter two references give dispersion equations only. McCarthy [10] gives refractive indices in the infrared at 45° C which have been corrected to room temperature (20° C) by adding 0.006. The dispersion equation of Schröter [8] is

$$\frac{n^2(\lambda) - 1}{n^2(\lambda) + 2} = 0.48484 + \frac{0.10279}{\lambda^2 - 0.090000} - 0.0047896\lambda^2 \qquad (6)$$

for the 0.435 to 0.660 μm range, and the dispersion equation of Takahei and Kobayashi [9] is

$$n^2(\lambda) = (2.273)^2 + \frac{2.582}{(\lambda/0.2736)^2 - 1} + \frac{0.0789}{(\lambda/0.3986)^2 - 1} \qquad (7)$$

for the 0.390 to 0.635 μm range. Wavelengths are in micrometers in both cases. Table III has the data of Barth and McCarthy and selected calculated values from the dispersion equations.

The temperature change of the refractive index due to electronic absorption, dn_∞/dT, of thallium bromide is determined by Takahei and Kobayashi [9] to be -180×10^{-6}/K over the interval 40 to 300 K and as -229×10^{-6}/K by Shanker and Sundaraj [11] (using $n_\infty = 2.27$). This latter dn/dT value was used to correct the McCarthy data (see above) to room temperature.

Infrared reflection measurements have been made by Mitsuishi *et al.* [13], Lowndes [14], and Claudel *et al.* [15]. Lowndes uses the model of the complex refractive index (n) given by Eq. (4) with the transverse and longitudinal frequencies of thallium bromine are $\nu_{TO} = 47$ cm^{-1} and $\nu_{LO} = 116$ cm^{-1}, with widths are $\gamma_{TO} = 4.0$ cm^{-1} and $\gamma_{LO} = 17.5$ cm^{-1}, and $\epsilon_\infty = 5.15$. Claudel *et al.* [15] uses the classical oscillator model of Eq. (5) with two far-infrared modes to represent their data. Their model parameters are $\rho_1 = 1.98$, $\rho_2 = 0.02$, $\nu_{TO1} = 47.5$ cm^{-1}, $\nu_{TO2} = 137.5$ cm^{-1}, $\gamma_1 = 0.10$, $\gamma_2 = 0.5$, and $\epsilon_\infty = 5.4$. Both models give similar results, with agreement typically 20%. The Lowndes model is used to calculate the optical constants given in Table III.

Pai *et al.* [19] measured the room-temperature complex dielectric constant of thallium bromide between 22 and 190 cm^{-1} using dispersive Fourier transform spectroscopy. These data are also given in Table III.

The room-temperature, low-frequency (1–100 kHz) dielectric constant of thallium bromide was measured as $\epsilon_0 = 30.6 \pm 0.2$ (or $n = 5.53 \pm 0.01$) by Lowndes [16] and Lowndes and Martin [17], and $\epsilon_0 = 30.0 \pm 0.2$ (or

$n = 5.48 \pm 0.02$) by Samara [18] using capacitance techniques. The low-frequency dielectric constant has a large, negative temperature dependence: $d\epsilon_0/dT = -0.013\ K^{-1}$ [16, 17], $d\epsilon_0/dT = -0.011\ K^{-1}$ [18], and $d\epsilon_0/dT = -0.01295\ K^{-1}$ [11] (or $dn/dT \approx -0.0012\ K^{-1}$).

Table III gives all the optical constant data for thallium bromide and Fig. 2 shows the data graphically.

THALLIUM IODIDE III

Little is known about the optical properties of thallium iodide. Thallium iodide is orthorhombic at room temperature and 1 atmosphere (see Table I) and does not revert to the cubic (CsCl) structure until temperature is raised to 170° C or pressure to 5000 atm. The orthorhombic form (space group Cmcm or D_{2h}^{17}) has four molecules per unit cell. The thallium and iodide atoms both occupy 4(c) sites (C_{2v} symmetry). The band gap of thallium iodide is 2.7 eV (orthorhombic structure) or about 2.1–2.2 eV for the cubic structure (extrapolated from pressure-dependent absorption measurements [20]).

Optical constants in the region of fundamental electronic absorption from the band gap to about 22 eV were determined by Frandon and LaHaye [3] from a Kramers–Kronig analysis of an energy-loss spectrum of a thin film of thallium iodide measured in transmission. The authors state that the measured crystals (TlCl, TlBr, and TlI) all have cubic symmetry. Most likely the thallium iodide film is orthorhombic (optical constants are consistent with the band gap) and polycrystalline. These results are given in Table IV.

Barth [7] measured the refractive index (method unknown) of metastable cubic thallium iodide at room temperature by quickly cooling and carefully handling the crystals. (Note that comparison of Barth's measurements of the refractive index of TlCl and TlBr, made at the same time, are lower than those of other researchers; see above). His values are given in Table IV.

Unpolarized infrared reflection measurements of orthorhombic TlI were made by Claudel *et al.* [15], probably with a polycrystalline sample. They used the classical-oscillator model of Eq. (5) with two far-infrared modes to represent their data. The model parameters are $\rho_1 = 1.12$, $\rho_2 = 0.05$, $\nu_{TO1} = 51\ cm^{-1}$, $\nu_{TO2} = 90\ cm^{-1}$, $\gamma_1 = 0.02$, $\gamma_2 = 0.5$, and $\epsilon_\infty = 6.1$. These results indicate that the optical modes of different crystallographic directions are very similar. This model was used to provide the far-infrared optical constants in Table IV.

Samara [18] measured the room-temperature, low-frequency (10 kHz) dielectric constant of polycrystalline orthorhombic thallium iodide as $\epsilon_0 = 21.2 \pm 0.2$ (or $n = 4.60 \pm 0.02$) and extrapolated the dielectric constant of cubic thallium iodide as $\epsilon_0 = 29.6 \pm 0.5$ (or $n = 5.44 \pm 0.05$) from its

pressure variation using a capacitance technique. Von Hippel [21] gives $\epsilon_0 = 21.8$ (1 kHz–10 MHz) for (orthorhombic) TlI at 25° C and $\epsilon_0 = 37.3$ (10 MHz) for (cubic) TlI at 193° C. Note that the orthorhombic values agree well with the value of 20.9 obtained from the model of Claudel *et al.* [15].

Table IV gives all the optical-constant data for thallium iodide, and Fig. 3 shows the data graphically.

IV MIXED THALLOUS HALIDES KRS-5 AND KRS-6

The mixed crystals KRS-5 and KRS-6 are less studied than TlCl and TlBr, but more optically important. Optical properties of these materials were originally studied by Barth [7], and later they were developed in Germany during World War II (see Hettner and Leisegang [22]). Further study of these mixtures improved optical uniformity by accurately finding the eutectic compositions [23]. The actual composition of some measured materials given later may differ from the eutectic mixture and have different optical constants.

Takahei and Kobayashi [9] measured low-temperature reflectance of pure and mixed crystals of TlCl–TlBr and derived dispersion equations for several mixtures at different temperatures. Their results give the band gap of KRS-6 as 3.25 eV. Absorption-edge measurements of Smakula [6] and room-temperature reflectance measurements of Tropf [24] indicate a band gap of ≈2.45–2.50 eV for KRS-5.

Tropf [24] measured the absorption coefficient of KRS-5 at the visible edge of transparency between 20 and 209° C and fit his data to an Urbach-rule model of the form

$$\beta(\nu, T) = \beta_0 \exp\left(-\sigma_s hc(\nu_g - \nu)/k_B T\right), \tag{8}$$

where $\beta(\nu,T)$ is the absorption coefficient as a function of wave number (ν) and temperature (T). Fixed quantities are Planck's constant (h), Boltzmann's constant (k_B), and the speed of light (c). Material-dependent parameters are the slope parameter, $\sigma_s = 0.9418$, a constant over the measured temperature range; $\beta_0 = 1.8063\ \text{cm}^{-1}$; and $\nu_g = 17{,}474\ \text{cm}^{-1}$.

The only measurement of room-temperature visible absorption of KRS-6 are the absorption-edge transmission and laser-calorimetry measurements of Mori and Izawa [25]. Their measurements are included in Table VI and were fitted to the sum of two exponential absorption edges with absorption coefficient, $\beta(\nu)$, each having the form

$$\beta(\nu) = \beta_0 \exp(\nu/\nu_0), \tag{9}$$

where $\beta_0 = 1 \times 10^{-34}\ \text{cm}^{-1}$ and $\nu_0 = 301.3\ \text{cm}^{-1}$ for the fundamental absorption-edge component and $\beta_0 = 5.62 \times 10^{-6}\ \text{cm}^{-1}$ and $\nu_0 = 2258.3$

cm^{-1} for the weak-absorption-tail component. These two components combine to model the absorption edge from 15,000 to 25,000 cm^{-1}, with fundamental absorption dominating above 23,000 cm^{-1}. (Extrapolated values to 26,600 cm^{-1} are given in Table VI.)

The KRS-5 Urbach-edge model of Tropf [24], Eq. (8), gives room-temperature (295 K) constants $\beta_0 = 2.5 \times 10^{-35}$ cm^{-1} and $\nu_0 = 217.7$ cm^{-1}, when recast into the form of Eq. (9). These values were used to calculate the imaginary part of the refractive index of KRS-5 at the electronic absorption edge between 17,000 and 19,000 cm^{-1} (2.10 to 2.35 eV).

The refractive index of KRS-5 was measured using the minimium-deviation method by Hettner and Leisegang [22] for a composition 56 mol % TlI, by Tilton *et al.* [26] for compositions of 58 and 58.3 mol % TlI, and at three near-ambient temperatures by Rodney and Malitson [27] for a composition of 54.3 mol % thallium iodide. Barth [7] also provided data for several TlBr-TlI mixtures including 50 and 60 mol % thallium iodide. Rodney and Malitson's measurements at 25° C are given in Table V. Tilton *et al.* provide a dispersion equation and Rodney and Malitson give a five-term Sellmeier equation for their data. Tropf [24] developed this equally accurate three-term Sellmeier dispersion equation based on the Rodney and Malitson 25° C measurements (0.57 to 39.4 μm):

$$n^2(\lambda) - 1 = \frac{3.7442390\lambda^2}{\lambda^2 - (0.2079603)^2} + \frac{0.9189162\lambda^2}{\lambda^2 - (0.3765643)^2} + \frac{12.5444602\lambda^2}{\lambda^2 - (165.6525518)^2}. \tag{10}$$

Wavelength (λ) is in micrometers. He also gives three-term Sellmeier models for their data at 19 and 31° C, as well as a less-accurate, temperature-dependent Sellmeier model.

The refractive index of KRS-6 was measured using the minimum-deviation method by Hettner and Leisegang [22] for a highly noneutectic composition, 60 mol % TlCl (which will have a higher index) and by Takahei and Kobayashi [9] for a composition with 68 mol % TlCl. The dispersion equation of Takahei and Kobayashi is

$$n^2(\lambda) = (2.186)^2 + \frac{1.877}{(\lambda/0.2828)^2 - 1} + \frac{0.0296}{(\lambda/0.3748)^2 - 1} \tag{11}$$

for the 0.390 to 0.635 μm range; wavelengths are in micrometers. The data of Hettner and Leisegang and calculations from the visible-wavelength dispersion equation of Takahei and Kobayashi are given in Table IV.

Barth [7] used a Lorentz–Lorenz molar-refractivity formulation to estimate the visible refractive index of mixed TlBr–TlI crystals of various com-

positions. Craig [28] later refined Barth's calculation and obtained a good fit to his data.

Rodney and Malitson [27] give dn/dT for KRS-5 as -254×10^{-6}/K at 0.577 μm, decreasing to -233×10^{-6}/K at 11.025 μm, and to -154×10^{-6}/K at 39.38 μm. Tropf [24] measured an average dn/dT for KRS-5 as -232×10^{-6}/K over the 700–1000 cm^{-1} (10–14.3 μm) spectral range and the temperature interval of 22 to 209° C, consistent with the Rodney and Malitson results. The temperature change of the refractive index due to electronic absorption, dn_∞/dT, of KRS-6 (68 mol % TlCl) was determined by Takahei and Kobayashi [9] to be -160×10^{-6}/K over the interval 40 to 300 K. Afanas'ev and Nosov [29] give $dn/dT = -254 \times 10^{-6}$/K for KRS-5 and $dn/dT = -234 \times 10^{-6}$/K for KRS-6 at 0.633 μm.

Absorption of KRS-5 and KRS-6 in the transparent region has been extensively studied, primarily for infrared fibers. Available data includes the laser-calorimetry measurements of Harrington *et al.* [30] on crystalline KRS-5 at HF and DF laser wavelengths; transmission measurements on long polycrystalline KRS-5 fibers at 10.6 μm by Harrington and Standlee [31]; laser calorimetry at 1, 5, and 10 μm by Belousov *et al.* [32] on crystalline KRS-5 and KRS-6; carbon-monoxide laser calorimetry measurements of Nosov *et al.* [33] on crystalline KRS-5 and KRS-6; and differential-spectrophotometry measurements of Hidaka *et al.* [12] on crystalline KRS-5. This last set of measurements covers a broad spectral range (500–1150 cm^{-1}) and is included in Table V. Typical measured infrared absorption coefficients in the transparent range of these materials are on the order of 10^{-3} to 10^{-5}/cm.

Absorption at the infrared edge of transparency was measured by Smakula [6] and by Dianov *et al.* [34] for both KRS-5 and KRS-6, and for KRS-5 alone by Hidaka *et al.* [12] and by Tropf [24]. The infrared absorption coefficient, $\beta(\nu)$, can also be modeled as a exponential edge using Eq. (3). For KRS-5 at room temperature, Hidaka *et al.* give $\beta_0 = 5400$ and $\nu_0 = 25$ cm^{-1}; Dianov *et al.* give $\beta_0 = 20700$ and $\nu_0 = 25$ cm^{-1}; and Tropf gives $\beta_0 = 7700$ and $\nu_0 = 27.1$ cm^{-1}. For KRS-6, Dianov *et al.* give $\beta_0 = 10810$ and $\nu_0 = 43$ cm^{-1}. Values of the imaginary refractive index at the infrared absorption edge in Tables IId and IIe come from Tropf [24] and Dianov *et al.* [34] for KRS-5 and KRS-6, respectively. (Note: Dianov *et al.* also gives model parameters for the visible absorption edges of KRS-5 and KRS-6. These values appear to be in error.)

There is little data on optical constants of KRS-5 and KRS-6 in the region of fundamental optical absorption. The reflectance measurements of Mitsuishi *et al.* [13] were fit to a the dispersion model of Eq. (4), and the following parameters provided a good fit: for KRS-5, $\nu_{TO} = 43$ cm^{-1}, $\nu_{LO} = 103$ cm^{-1}, $\gamma_{TO} = 7$ cm^{-1}, $\gamma_{LO} = 25$ cm^{-1}, and $\epsilon_\infty = 5.66$; for KRS-6, $\nu_{TO} = 58$ cm^{-1}, $\nu_{LO} = 149$ cm^{-1}, $\gamma_{TO} = 8$ cm^{-1}, $\gamma_{LO} = 35$ cm^{-1}, and $\epsilon_\infty = 4.85$. These values were used to calculate far-infrared optical constants given in Tables V and VI.

The room-temperature, low-frequency (measurement method unknown, accuracy of 2% or better) dielectric constants of KRS-5 (58 mol % TlI) and KRS-6 (60 mol % TlCl[2]) are given by von Hippel [21] as $\epsilon_0 = 32.5$ (or $n = 5.70$) for frequencies from 10 kHz to 10 MHz and $\epsilon_0 = 31.8$ (or $n = 5.64$) at 100 kHz, respectively. Von Hippel also gives $d\epsilon_0/dT = -0.0091\ K^{-1}$ for KRS-5 at 1 MHz and $d\epsilon_0/dT = -0.0075\ K^{-1}$ for KRS-6 at 10 MHz.

Tables V and VI give all the optical constant data for KRS-5 and KRS-6, respectively. Figures 4 and 5 shows the same data graphically.

REFERENCES

1. C. W. Jurgensen and H. G. Drickamer, High-pressure studies of the absorption edges of three thallous halides. *Phys. Rev. B* **30**, 7202–7205 (1984).
2. D. C. Hinson and J. R. Stevenson, Optical constants of TlCl and TlBr with a comparison of the Kramers-Krönig and "two-angle" methods of data analysis. *Phys. Rev.* **159,** 711–716 (1967).
3. J. Frandon and B. LaHaye, Electron loss characteristics of TlCl, TlBr, TlI and calculated optical constants from 3 to 25 eV. *J. Phys (Paris)* **33**, 229–235 (1972).
4. W. Martienssen, The optical absorption edge in ionic crystals. *J. Phys. Chem. Solids* **8**, 294–296 (1959).
5. S. Tutihasi, Ultraviolet absorption in thallous halides. *J. Phys. Chem. Solids* **12**, 344–348 (1960).
6. A. Smakula, Synthetic crystals and polarizing materials. *Opt. Acta* **9**, 205–222 (1962).
7. T. F. W. Barth, Optical properties of mixed crystals. *Am. J. Sci.* **219**, 135–146 (1930); also see T. Barth, Some new immersion melts of high refraction. *Am. Mineral.* **14**, 358–361 (1929).
8. H. Schröter, On the refractive indices of some heavy-metal halides in the visible and calculation of interpolation formulas for dispersion. *Z. Phys.* **67**, 24–36 (1931).
9. K. Takahei and K. Kobayashi, Reflectivity spectra of TlCl-TlBr mixed crystals, *J. Phys. Soc. Jpn.* **43**, 891–898 (1977).
10. D. E. McCarthy, Refractive index measurements of TlBr and TlCl in the IR. *Appl. Opt.* **4**, 878–879 (1965).
11. J. Shanker and R. Sundaraj, Dielectric and anharmonic behavior of silver halides, thallous halides, alkaline earth fluorides, and lead fluoride crystals. *Phys. Status Solidi B* **115**, 67–74 (1968).
12. T. Hidaka, T. Morikawa, and J. Shimada, Spectroscopic small loss measurements on infrared transparent materials. *Appl. Opt.* **19**, 3763–3766 (1980).
13. A. Mitsuishi, Y. Yamada, and H. Yoshinaga, Reflection measurements on reststrahlen crystals in the far-infrared region. *J. Opt. Soc. Am.* **52**, 14–16 (1962).
14. R. P. Lowndes, Anharmonicity in the silver and thallium halides: Far-infrared dielectric response. *Phys. Rev. B* **6**, 1490–1498 (1972).
15. J. Claudel, A. Handi, P. Strimer, and P. Vergnat, Absorption spectra and reflection of the thallium halides in the far infrared at low temperatures. *J. Phys. Chem. Solids* **29**, 1539–1544 (1968).
16. R. P. Lowndes, Anharmonicity in the silver and thallium halides: Low-frequency dielectric response. *Phys. Rev. B* **6**, 4667–4674 (1972).
17. R. P. Lowndes and D. H. Martin, Dielectric constants of ionic crystals and their variations with temperature and pressure. *Proc. R. Soc. (London) A* **316**, 351–375 (1970).

[2] Composition of 60% TlBr, 40% TlCl stated; this is undoubtedly an error. Molar percentage assumed corresponding to the composition of this era.

18. G. A. Samara, Temperature and pressure dependence of the dielectric constants of the thallous halides. *Phys. Rev.* **165**, 959–969 (1968).
19. K. F. Pai, T. J. Parker, N. E. Tornberg, and R. P. Lowndes, Determination of the complex refractive indices of solids in the far-infrared by dispersive fourier transform spectroscopy—II. Pseudo-displacement ferroelectrics. *Infrared Phys.* **18**, 327–336 (1978).
20. J. C. Zahner and H. G. Drickamer, The effect of pressure on the absorption edge in heavy-metal halides. *J. Phys. Chem. Solids* **11**, 92–96 (1959).
21. A. R. von Hippel, ed., "Dielectric Materials and Applications." Wiley, New York, 1954.
22. G. Hettner and G. Leisegang, Dispersion of mixed crystals TlBr-TlI (KRS 5) and TlCl-TlBr (KRS 6) in the infrared. *Optik* **3**, 305–314 (1948).
23. A. Smakula, J. Kalnajs, and V. Sils, Inhomogeneity of thallium halide mixed crystals and its elimination. *J. Opt. Soc. Am.* **43**, 698–701 (1953).
24. A. Z. Tropf, M. E. Thomas, and W. J. Tropf, Optical properties of KRS-5. To be published in *Proc. SPIE* **3060** (1997).
25. H. Mori and T. Izawa, A new loss mechanism in ultralow loss optical fiber materials. *J. Appl. Phys.* **51**, 2270–2271 (1980).
26. L. W. Tilton, K. Plyler, and R. E. Stephens, Refractive indices of thallium bromide-iodide crystals for visible and infrared radiant energy. *J. Res. Natl. Bur. Stand. (U.S.)* **43**, 81–86 (1949).
27. W. S. Rodney, and I. H. Malitson, Refraction and dispersion of thallium bromide iodide. *J. Opt. Soc. Am.* **46**, 956–961 (1956).
28. H. Craig, A simple model for refractive indices in mixed crystals and glasses. *Geochim. Comochim. Acta* **56**, 3001–3006 (1992).
29. I. I. Afanas'ev and V. B. Nosov, Temperature increments of the refractive indices of certain single crystals. *Sov. J. Opt. Technol.* **46**, 281–283 (1979).
30. J. A. Harrington, D. A. Gregory, and W. F. Otto, Jr., Infrared absorption in chemical laser window materials. *Appl. Opt.* **15**, 1953–1959 (1976).
31. J. A. Harrington and A. G. Standlee, Attenuation at 10.6 mm in loaded and unloaded polycrystalline KRS-5 fibers. *Appl. Opt.* **22**, 3073–3078 (1983).
32. A. P. Belousov, E. M. Dianov, I. S. Lisitskii, T. M. Nesterova, V. G. Plotnichenko, and V. K. Sysoev, Single crystals of thallium halides with optical losses below 10 dB/km. *Sov. J. Quantum Electron.* **12**, 496–497 (1982).
33. V. B. Nosov, G. T. Petrovskii, M. V. Serzhantova, and A. V. Shatilov, Calorimetric measurements of the volume and surface absorption of IR materials in the 5-6 mm spectral region. *Sov. J. Opt. Technol.* **56**, 238–240 (1989).
34. E. M. Dianov, N. S. Lisitskii, V. G. Plotnichenko, V. B. Sulimov, and V. K. Sysoev, Evaluation of minimum possible optical losses in thallium halides. *Opt. Spectrosc.* **56**, 281–283 (1984); also see E. M. Dianov, N. S. Lisitsky, V. G. Plotnichenko, V. K. Sysoev, V. B. Sulimov, and L. N. Butvina, Evaluation of optical loss minima in thallium halide crystals. *Fiber Integr. Opt.* **5**, 125–133 (1985). (Note error in Table 1 of the latter reference.)

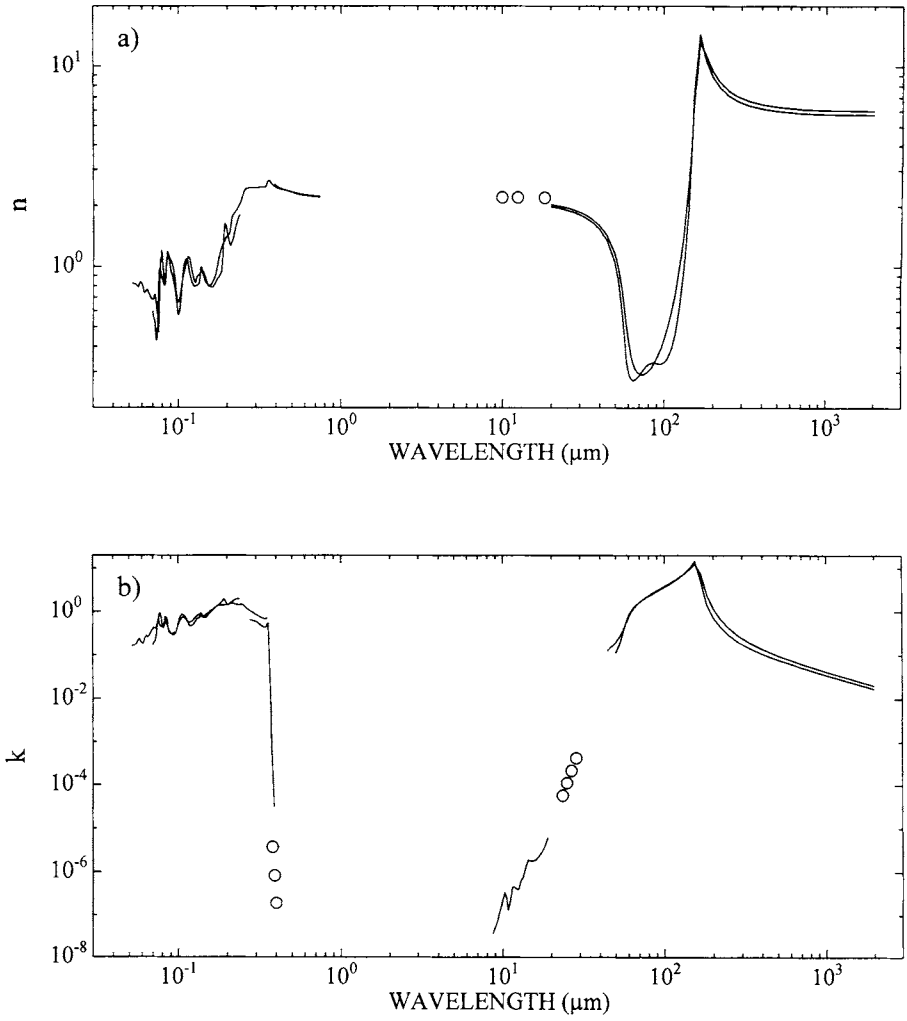

Fig. 1. (a) Log–log plot of the index of refraction n versus wavelength in micrometers for thallium(I) chloride. (b) Log–log plot of the extinction coefficient k versus wavelength in micrometers for thallium(I) chloride. Lines are data sets of many points; scattered data are indicated by circles.

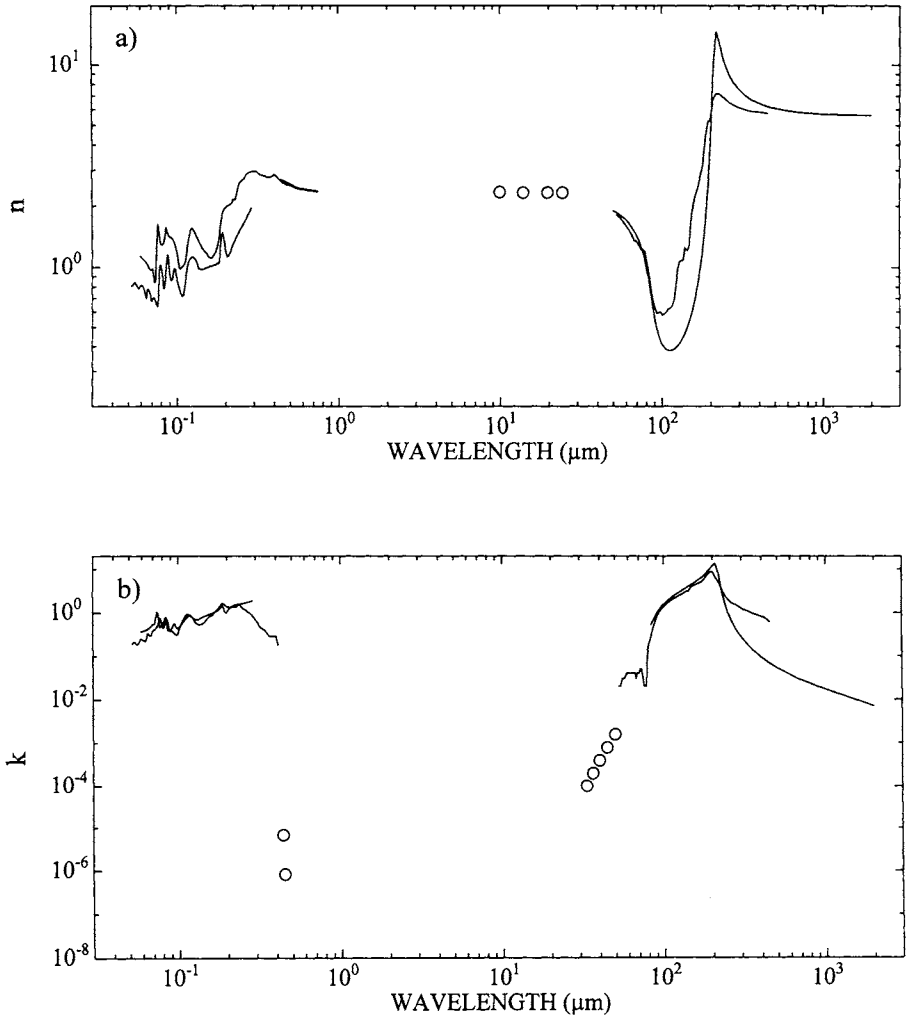

Fig. 2. (a) Log–log plot of the index of refraction n versus wavelength in micrometers for thallium(I) bromide. (b) Log–log plot of the extinction coefficient k versus wavelength in micrometers for thallium(I) bromide. Lines are data sets of many points; scattered data are indicated by circles.

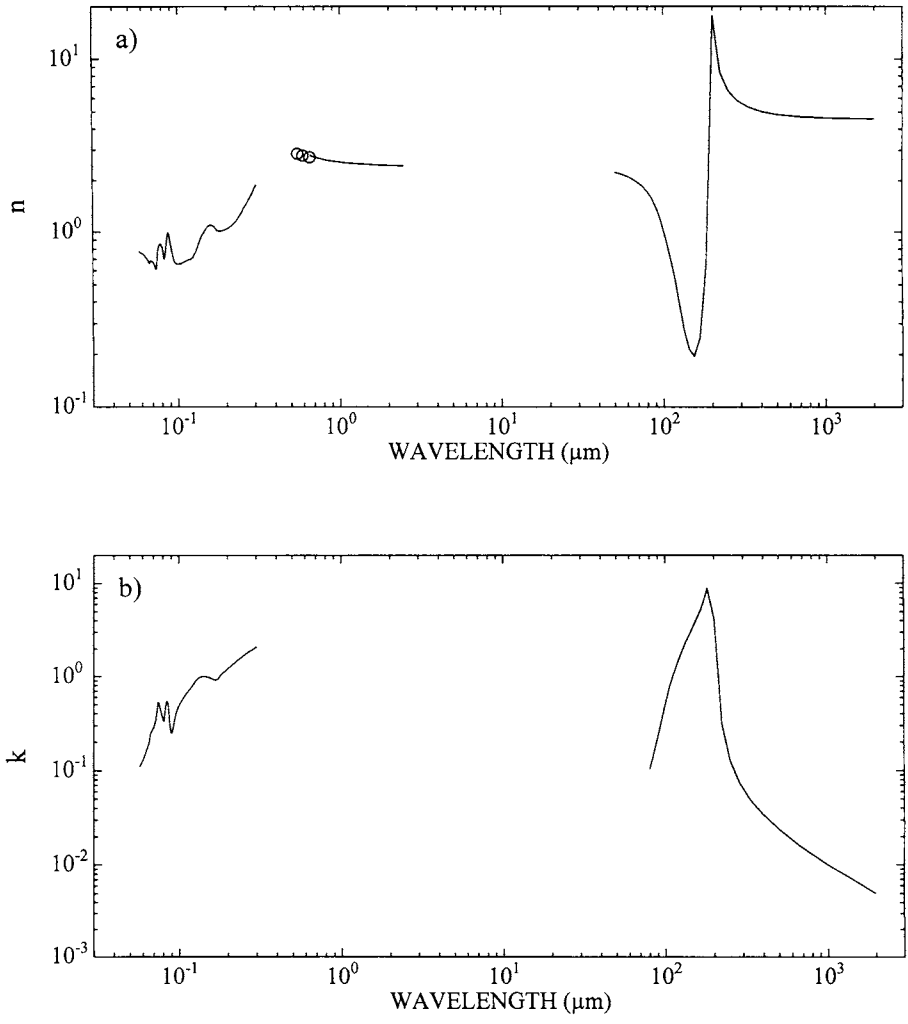

Fig. 3. (a) Log–log plot of the index of refraction n versus wavelength in micrometers for thallium(I) iodide. (b) Log–log plot of the extinction coefficient k versus wavelength in micrometers for thallium(I) iodide. Lines are data sets of many points; scattered data are indicated by circles.

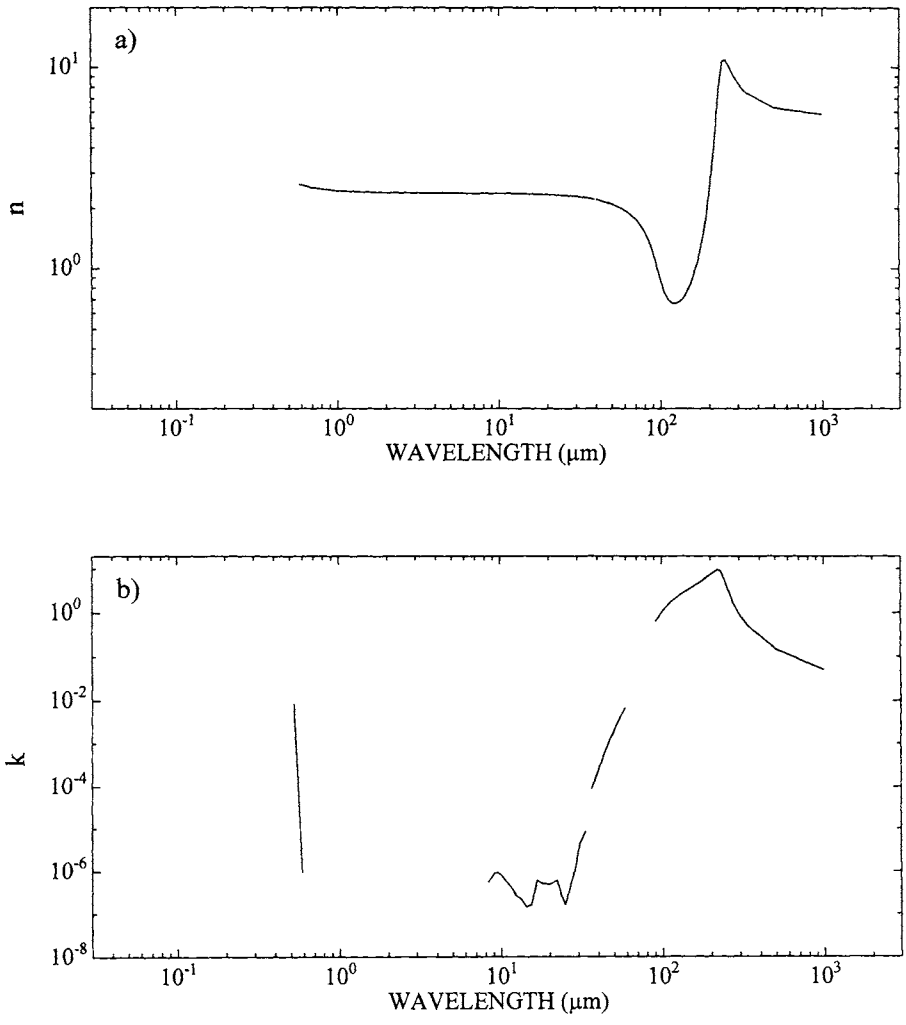

Fig. 4. (a) Log–log plot of the index of refraction n versus wavelength in micrometers for KRS-5. (b) Log–log plot of the extinction coefficient k versus wavelength in micrometers for KRS-5.

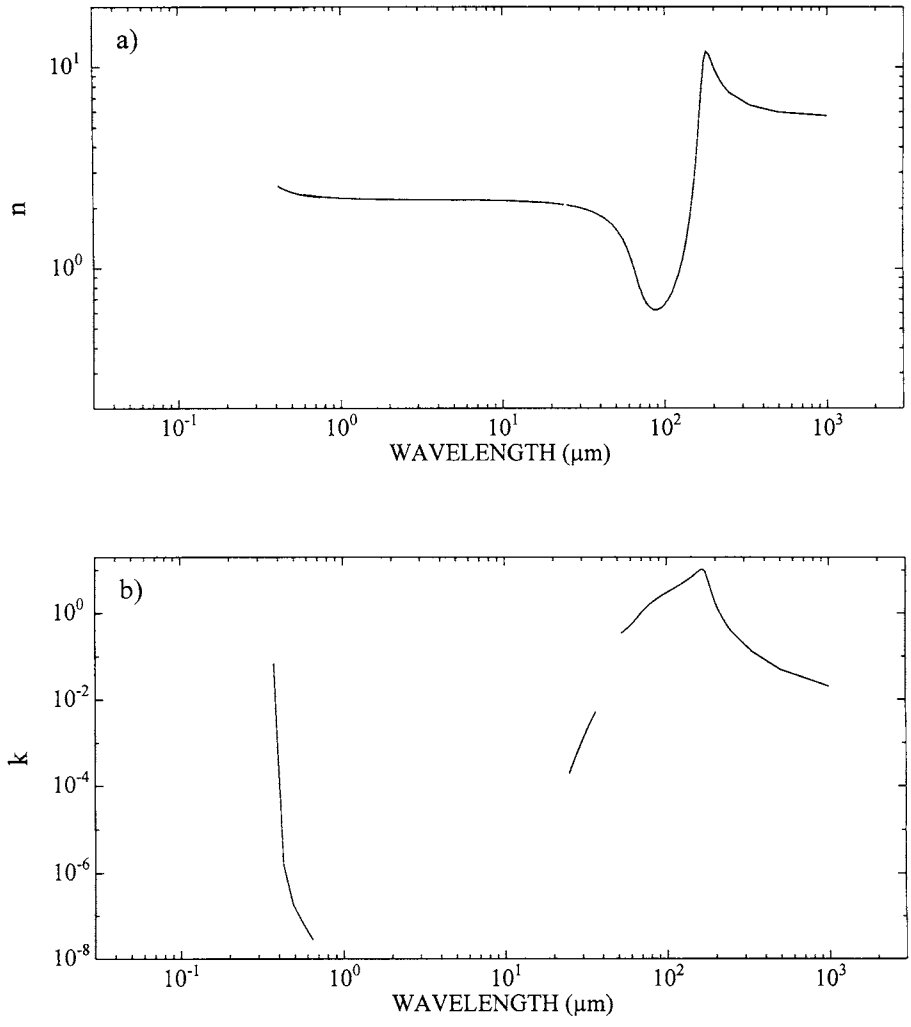

Fig. 5. (a) Log–log plot of the index of refraction n versus wavelength in micrometers for KRS-6. (b) Log–log plot of the extinction coefficient k versus wavelength in micrometers for KRS-6.

TABLE 1

Properties of Pure and Mixed Thallium(I) Halides

Material	Crystal Structure and Space Group	Lattice Constants (Å)	Density (g/cm^3)	Melting Point (°C)
TlF	Orthorhombic: Fmmm	$a = 5.495$; $b = 6.080$; $c = 5.180$	8.573	326
TlCl	Cubic: Pm3m	$a = 3.84247$	7.020	430.2
TlCl–TlBr	Cubic: Pm3m	$a = 3.88946$	7.142	422.9
TlBr	Cubic: Pm3m	$a = 3.98588$	7.455	460.5
TlBr–TlI	Cubic: Pm3m	$a = 4.11826$	7.365	413.9
TlI	Cubic: Pm3m	$a = 4.2099$[a]	7.373	441.8
TlI	Orthorhombic: Cmcm	$a = 4.582$; $b = 12.92$; $c = 5.251$	7.079	~170[b]

[a] extrapolated to room temperature and pressure.
[b] Phase change from orthorhombic to cubic.

TABLE II

Values of *n* and *k* for Thallium Chloride from Various References

eV	cm^{-1}	μm	*n*	*k*	*n*	*k*
23.800	191958.4	0.05209	0.821 [3]	0.162 [3]		
23.600	190345.3	0.05254	0.821	0.162		
23.400	188732.2	0.05299	0.822	0.164		
23.200	187119.1	0.05344	0.820	0.165		
23.000	185506.0	0.05391	0.817	0.167		
22.800	183892.9	0.05438	0.814	0.169		
22.600	182279.9	0.05486	0.810	0.173		
22.400	180666.8	0.05535	0.804	0.180		
22.200	179053.7	0.05585	0.798	0.189		
22.000	177440.6	0.05636	0.791	0.203		
21.800	175827.5	0.05687	0.787	0.221		
21.600	174214.4	0.05740	0.805	0.234		
21.400	172601.3	0.05794	0.825	0.234		
21.200	170988.2	0.05848	0.831	0.222		
21.000	169375.1	0.05904	0.830	0.206		
20.800	167762.0	0.05961	0.820	0.194		
20.600	166148.9	0.06019	0.805	0.183		
20.400	164535.8	0.06078	0.779	0.180		
20.200	162922.7	0.06138	0.752	0.193		
20.000	161309.6	0.06199	0.736	0.219		
19.800	159696.5	0.06262	0.739	0.244		
19.600	158083.4	0.06326	0.750	0.262		
19.400	156470.3	0.06391	0.762	0.274		
19.200	154857.2	0.06458	0.767	0.264		
19.000	153244.1	0.06526	0.747	0.257		
18.800	151631.0	0.06595	0.729	0.266		
18.600	150017.9	0.06666	0.716	0.286		

TABLE II *(Continued)*

Thallium Chloride

eV	cm^{-1}	μm	n	k	n	k
18.400	148404.8	0.06738	0.702	0.309		
18.200	146791.7	0.06812	0.693	0.332		
18.000	145178.6	0.06888	0.685	0.356		
17.900	144372.1	0.06927	0.683	0.370		
17.800	143565.5	0.06965	0.681	0.383	0.596 [2]	0.173 [2]
17.700	142759.0	0.07005	0.681	0.399	0.579	0.171
17.600	141952.5	0.07045	0.688	0.411	0.561	0.176
17.500	141145.9	0.07085	0.703	0.422	0.550	0.189
17.400	140339.4	0.07126	0.714	0.426	0.547	0.197
17.300	139532.8	0.07167	0.722	0.420	0.538	0.203
17.200	138726.3	0.07208	0.718	0.411	0.516	0.208
17.100	137919.7	0.07251	0.700	0.408	0.484	0.212
17.000	137113.2	0.07293	0.676	0.417	0.449	0.229
16.900	136306.6	0.07336	0.644	0.437	0.429	0.272
16.800	135500.1	0.07380	0.617	0.465	0.434	0.329
16.700	134693.5	0.07424	0.592	0.485	0.458	0.422
16.600	133887.0	0.07469	0.559	0.517	0.505	0.518
16.500	133080.4	0.07514	0.490	0.596	0.633	0.643
16.400	132273.9	0.07560	0.471	0.665	0.778	0.710
16.300	131467.3	0.07606	0.486	0.742	0.898	0.622
16.200	130660.8	0.07653	0.627	0.846	0.953	0.544
16.100	129854.2	0.07701	0.803	0.910	0.974	0.501
16.000	129047.7	0.07749	0.908	0.900	0.967	0.474
15.900	128241.1	0.07798	1.079	0.795	0.946	0.457
15.800	127434.6	0.07847	1.152	0.755	0.924	0.445
15.700	126628.0	0.07897	1.199	0.695	0.904	0.445
15.600	125821.5	0.07948	1.172	0.555	0.884	0.449
15.500	125014.9	0.07999	1.109	0.456	0.864	0.457
15.400	124208.4	0.08051	1.021	0.431	0.846	0.468
15.300	123401.8	0.08104	0.963	0.422	0.830	0.480
15.200	122595.3	0.08157	0.894	0.443	0.816	0.505
15.100	121788.8	0.08211	0.853	0.465	0.803	0.545
15.000	120982.2	0.08266	0.829	0.507	0.804	0.637
14.900	120175.7	0.08321	0.824	0.560	0.818	0.749
14.800	119369.1	0.08377	0.844	0.630	0.906	0.657
14.700	118562.6	0.08434	0.980	0.743	0.984	0.580
14.600	117756.0	0.08492	1.105	0.706	1.045	0.528
14.500	116949.5	0.08551	1.181	0.660	1.086	0.489
14.400	116142.9	0.08610	1.180	0.557	1.104	0.454
14.300	115336.4	0.08670	1.151	0.431	1.111	0.421
14.200	114529.8	0.08731	1.134	0.370	1.111	0.394
14.100	113723.3	0.08793	1.108	0.332	1.108	0.371
14.000	112916.7	0.08856	1.058	0.320	1.102	0.353
13.900	112110.2	0.08920	1.012	0.318	1.095	0.335
13.800	111303.6	0.08984	0.982	0.315	1.082	0.321
13.700	110497.1	0.09050	0.951	0.312	1.066	0.312
13.600	109690.5	0.09117	0.925	0.308	1.048	0.303

(continued)

TABLE II *(Continued)*

Thallium Chloride

eV	cm^{-1}	μm	n	k	n	k
13.500	108884.0	0.09184	0.903	0.307	1.029	0.296
13.400	108077.4	0.09253	0.881	0.310	1.006	0.290
13.300	107270.9	0.09322	0.857	0.314	0.981	0.287
13.200	106464.3	0.09393	0.834	0.319	0.950	0.285
13.100	105657.8	0.09465	0.810	0.326	0.915	0.290
13.000	104851.2	0.09537	0.782	0.320	0.874	0.299
12.900	104044.7	0.09611	0.753	0.311	0.820	0.310
12.800	103238.1	0.09686	0.710	0.318	0.762	0.323
12.700	102431.6	0.09763	0.671	0.346	0.719	0.348
12.600	101625.1	0.09840	0.628	0.380	0.690	0.379
12.500	100818.5	0.09919	0.593	0.426	0.671	0.429
12.400	100012.0	0.09999	0.573	0.489	0.665	0.479
12.300	99205.4	0.1008	0.576	0.576	0.667	0.525
12.200	98398.9	0.1016	0.592	0.657	0.681	0.564
12.100	97592.3	0.1025	0.621	0.721	0.697	0.600
12.000	96785.8	0.1033	0.666	0.767	0.734	0.634
11.900	95979.2	0.1042	0.712	0.807	0.771	0.667
11.800	95172.7	0.1051	0.771	0.843	0.807	0.697
11.700	94366.1	0.1060	0.837	0.852	0.844	0.719
11.600	93559.6	0.1069	0.912	0.839	0.878	0.732
11.500	92753.0	0.1078	0.980	0.815	0.908	0.737
11.400	91946.5	0.1088	1.025	0.798	0.937	0.732
11.300	91139.9	0.1097	1.049	0.769	0.964	0.716
11.200	90333.4	0.1107	1.075	0.738	0.991	0.692
11.100	89526.8	0.1117	1.085	0.699	1.024	0.652
11.000	88720.3	0.1127	1.087	0.654	1.056	0.615
10.900	87913.7	0.1137	1.086	0.604	1.086	0.578
10.800	87107.2	0.1148	1.033	0.584	1.114	0.544
10.700	86300.6	0.1159	0.987	0.566	1.115	0.511
10.600	85494.1	0.1170	0.949	0.552	1.107	0.483
10.500	84687.5	0.1181	0.912	0.551	1.082	0.462
10.400	83881.0	0.1192	0.878	0.559	1.041	0.458
10.300	83074.4	0.1204	0.852	0.572	0.993	0.462
10.200	82267.9	0.1216	0.829	0.589	0.952	0.469
10.100	81461.3	0.1228	0.817	0.610	0.917	0.481
10.000	80654.8	0.1240	0.803	0.641	0.885	0.497
9.900	79848.3	0.1252	0.793	0.675	0.858	0.516
9.800	79041.7	0.1265	0.795	0.701	0.838	0.547
9.700	78235.2	0.1278	0.798	0.728	0.828	0.599
9.600	77428.6	0.1292	0.800	0.757	0.859	0.652
9.500	76622.1	0.1305	0.802	0.785	0.885	0.675
9.400	75815.5	0.1319	0.807	0.813	0.899	0.682
9.300	75009.0	0.1333	0.813	0.838	0.905	0.691
9.200	74202.4	0.1348	0.825	0.867	0.911	0.714
9.100	73395.9	0.1362	0.882	0.863	0.920	0.780
9.000	72589.3	0.1378	0.985	0.910	0.938	0.785
8.900	71782.8	0.1393	0.987	0.862	0.948	0.774

TABLE II *(Continued)*

Thallium Chloride

eV	cm^{-1}	μm	n	k	n	k
8.800	70976.2	0.1409	0.942	0.780	0.953	0.742
8.700	70169.7	0.1425	0.910	0.759	0.941	0.719
8.600	69363.1	0.1442	0.876	0.783	0.919	0.708
8.500	68556.6	0.1459	0.850	0.815	0.896	0.711
8.400	67750.0	0.1476	0.832	0.843	0.868	0.724
8.300	66943.5	0.1494	0.819	0.871	0.842	0.755
8.200	66136.9	0.1512	0.810	0.899	0.818	0.792
8.100	65330.4	0.1531	0.808	0.926	0.798	0.833
8.000	64523.8	0.1550	0.799	0.964	0.793	0.876
7.900	63717.3	0.1569	0.792	1.004	0.800	0.923
7.800	62910.7	0.1590	0.790	1.049	0.808	0.977
7.700	62104.2	0.1610	0.785	1.085	0.820	1.034
7.600	61297.6	0.1631	0.785	1.124	0.837	1.081
7.500	60491.1	0.1653	0.799	1.172	0.857	1.124
7.400	59684.6	0.1675	0.813	1.217	0.878	1.184
7.300	58878.0	0.1698	0.831	1.268	0.908	1.248
7.200	58071.5	0.1722	0.850	1.317	0.955	1.303
7.100	57264.9	0.1746	0.866	1.365	1.014	1.347
7.000	56458.4	0.1771	0.877	1.422	1.085	1.382
6.900	55651.8	0.1797	0.897	1.492	1.148	1.402
6.800	54845.3	0.1823	0.917	1.572	1.205	1.400
6.700	54038.7	0.1851	0.944	1.654	1.254	1.395
6.600	53232.2	0.1879	1.142	1.779	1.293	1.392
6.500	52425.6	0.1907	1.482	1.941	1.324	1.396
6.400	51619.1	0.1937	1.623	1.802	1.339	1.407
6.300	50812.5	0.1968	1.587	1.618	1.395	1.411
6.200	50006.0	0.2000	1.475	1.403	1.410	1.415
6.100	49199.4	0.2033	1.377	1.418	1.431	1.441
6.000	48392.9	0.2066	1.296	1.497	1.454	1.499
5.900	47586.3	0.2101	1.270	1.594	1.580	1.560
5.800	46779.8	0.2138	1.320	1.684	1.735	1.594
5.700	45973.2	0.2175	1.369	1.734	1.798	1.548
5.600	45166.7	0.2214	1.460	1.810	1.834	1.499
5.500	44360.1	0.2254	1.557	1.875	1.868	1.472
5.400	43553.6	0.2296	1.648	1.927	1.906	1.449
5.300	42747.0	0.2339	1.727	1.952	1.957	1.439
5.200	41940.5	0.2384	1.801	1.966	2.020	1.441
5.100	41133.9	0.2431			2.100	1.447
5.000	40327.4	0.2480			2.207	1.444
4.900	39520.9	0.2530			2.325	1.402
4.800	38714.3	0.2583			2.408	1.262
4.700	37907.8	0.2638			2.428	1.178
4.600	37101.2	0.2695			2.438	1.112
4.500	36294.7	0.2755		0.634 [5]	2.449	1.053
4.400	35488.1	0.2818		0.630	2.458	0.997
4.300	34681.6	0.2883		0.621	2.453	0.941
4.200	33875.0	0.2952		0.602	2.450	0.884

(continued)

TABLE II *(Continued)*

Thallium Chloride

eV	cm^{-1}	μm	n	k	n	k
4.100	33068.5	0.3024		0.572	2.451	0.835
4.000	32261.9	0.3100		0.534	2.454	0.789
3.900	31455.4	0.3179		0.497	2.461	0.747
3.800	30648.8	0.3263		0.462	2.468	0.711
3.700	29842.3	0.3351		0.434	2.467	0.683
3.600	29035.7	0.3444		0.436	2.474	0.683
3.500	28229.2	0.3542		0.531	2.633	0.703
						0.495 [4]
3.480	28067.9	0.3563		0.533		0.433
3.460	27906.6	0.3583		0.424		0.324
3.440	27745.3	0.3604		0.212		0.210
3.420	27583.9	0.3625		0.0890		0.111
3.400	27422.6	0.3647		0.0412	2.656	0.0590
3.380	27261.3	0.3668		0.0187		0.0248
3.360	27100.0	0.3690		0.0083		0.00961
3.340	26938.7	0.3712		0.0039		0.00401
3.320	26777.4	0.3734		0.0019		0.00153
3.300	26616.1	0.3757		0.0009	2.550	5.73E-4
3.280	26454.8	0.3780		0.0004		2.91E-4
3.263	26315.8	0.3800				3.74E-6 [6]

eV	cm^{-1}	μm	n	n	n	k
3.200	25809.5	0.3875			2.49	3.03E-5 [4]
3.179	25641.0	0.3900		2.5474 [9]		8.25E-7 [6]
3.100	25003.0	0.4000		2.5050	2.46	1.91E-7
3.024	24390.2	0.4100		2.4714		
3.000	24196.4	0.4133		2.4618	2.42	
2.844	22935.8	0.436	2.4112 [8]	2.4079	2.400 [7]	
2.271	18315.0	0.546	2.2856	2.2826	2.270	
2.145	17301.0	0.578	2.2681	2.2640	2.253	
2.105	16977.9	0.589	2.2629	2.2586	2.247	
1.907	15384.6	0.650	2.2402	2.2345	2.223	
1.653	13333.3	0.750	2.2155	2.2094	2.198	

eV	cm^{-1}	μm	n	k	n	k
0.1426	1150.0	8.696		3.51E-8 [12]		
0.1333	1075.0	9.302		7.41E-8		
0.1302	1050.0	9.524		1.13E-7		
0.1271	1025.0	9.756		1.58E-7		
0.1240	1000.0	10.00	2.199 [10]	2.41E-7		
0.1209	975.0	10.26		3.45E-7		
0.1178	950.0	10.53		2.62E-7		
0.1147	925.0	10.81		1.32E-7		
0.1116	900.0	11.11		2.25E-7		
0.1085	875.0	11.43		4.56E-7		
0.1054	850.0	11.76		4.68E-7		

TABLE II *(Continued)*

Thallium Chloride

eV	cm^{-1}	μm	n	k	n	k
0.1023	825.0	12.12		4.23E-7		
0.0994	802.0	12.47	2.197			
0.0992	800.0	12.50		4.05E-7		
0.0961	775.0	12.90		6.34E-7		
0.0930	750.0	13.33		7.57E-7		
0.0899	725.0	13.79		1.22E-6		
0.0868	700.0	14.29		1.86E-6		
0.0837	675.0	14.81		1.84E-6		
0.0806	650.0	15.38		1.81E-6		
0.0775	625.0	16.00		1.91E-6		
0.0744	600.0	16.67		2.31E-6		
0.0713	575.0	17.39		2.86E-6		
0.0682	550.0	18.18		3.93E-6		
0.0676	545.0	18.35	2.188			
0.06509	525.0	19.05		6.23E-6		
0.06199	500.0	20.00	2.029 [14]		1.979 [15]	
0.05889	475.0	21.05	2.015		1.966	
0.05579	450.0	22.22	2.000		1.950	
0.05269	425.0	23.53	1.981		1.930	5.71E-5 [6]
0.04959	400.0	25.00	1.959		1.907	1.11E-4
0.04649	375.0	26.67	1.931		1.878	2.16E-4
0.04339	350.0	28.57	1.896		1.843	4.24E-4
0.04030	325.0	30.77	1.852		1.797	
0.03720	300.0	33.33	1.794		1.736	
0.03410	275.0	36.36	1.715		1.654	
0.03100	250.0	40.00	1.604		1.537	
0.02790	225.0	44.44	1.437	0.128 [14]	1.358	
0.02480	200.0	50.00	1.157	0.196	1.049	0.113 [15]
0.02356	190.0	52.63	0.984	0.255	0.848	0.171
0.02232	180.0	55.56	0.751	0.372	0.563	0.321
0.02108	170.0	58.82	0.498	0.635	0.334	0.687
0.02046	165.0	60.61	0.414	0.817	0.295	0.882
0.01984	160.0	62.50	0.362	1.003	0.278	1.066
0.01922	155.0	64.52	0.330	1.187	0.273	1.240
0.01860	150.0	66.67	0.310	1.369	0.276	1.410
0.01798	145.0	68.97	0.299	1.553	0.283	1.579
0.01736	140.0	71.43	0.293	1.741	0.293	1.748
0.01674	135.0	74.07	0.291	1.936	0.305	1.921
0.01612	130.0	76.92	0.295	2.140	0.317	2.099
0.01550	125.0	80.00	0.302	2.358	0.327	2.286
0.01488	120.0	83.33	0.313	2.593	0.332	2.489
0.01426	115.0	86.96	0.331	2.850	0.334	2.714
0.01364	110.0	90.91	0.354	3.136	0.331	2.973
0.01302	105.0	95.24	0.387	3.458	0.329	3.275
0.01240	100.0	100.0	0.432	3.829	0.333	3.636
0.01178	95.0	105.3	0.495	4.267	0.350	4.073
0.01116	90.0	111.1	0.588	4.798	0.390	4.615

(continued)

TABLE II *(Continued)*

Thallium Chloride

eV	cm^{-1}	μm	n	k	n	k
0.01054	85.0	117.6	0.731	5.466	0.469	5.312
0.00992	80.0	125.0	0.974	6.349	0.625	6.259
0.00930	75.0	133.3	1.443	7.599	0.968	7.666
0.00868	70.0	142.9	2.573	9.521	1.955	10.087
0.00806	65.0	153.8	6.400	12.135	7.200	14.464
0.00744	60.0	166.7	13.222	7.565	14.443	5.057
0.00682	55.0	181.8	11.316	2.509	10.692	1.481
0.00620	50.0	200.0	9.433	1.150	8.841	0.716
0.00558	45.0	222.2	8.303	0.649	7.807	0.428
0.00496	40.0	250.0	7.575	0.410	7.151	0.284
0.00434	35.0	285.7	7.077	0.277	6.703	0.200
0.00372	30.0	333.3	6.722	0.194	6.383	0.146
0.00310	25.0	400.0	6.464	0.138	6.150	0.107
0.00248	20.0	500.0	6.277	0.098	5.980	0.078
0.00186	15.0	666.7	6.143	0.067	5.859	0.055
0.00124	10.0	1000.0	6.053	0.042	5.778	0.035
0.00062	5.0	2000.0	6.001	0.020	5.731	0.017
0.0	0.0		5.985	0.000	5.716	0.000
			5.72 [16]		5.68 [18]	

TABLE III

Values of *n* and k for Thallium Bromide from Various References

eV	cm^{-1}	μm	n	k	n	k
23.800	191958.4	0.05209	0.804 [3]	0.188 [3]		
23.600	190345.3	0.05254	0.807	0.197		
23.400	188732.2	0.05299	0.811	0.205		
23.200	187119.1	0.05344	0.821	0.212		
23.000	185506.0	0.05391	0.830	0.214		
22.800	183892.9	0.05438	0.836	0.209		
22.600	182279.9	0.05486	0.837	0.198		
22.400	180666.8	0.05535	0.828	0.191		
22.200	179053.7	0.05585	0.821	0.188		
22.000	177440.6	0.05636	0.813	0.188		
21.800	175827.5	0.05687	0.803	0.191		
21.600	174214.4	0.05740	0.791	0.201		
21.400	172601.3	0.05794	0.782	0.217		
21.200	170988.2	0.05848	0.787	0.238		
21.000	169375.1	0.05904	0.800	0.248	1.135 [2]	0.369 [2]
20.900	168568.5	0.05932	0.805	0.247	1.131	0.368
20.800	167762.0	0.05961	0.809	0.245	1.127	0.369
20.700	166955.4	0.05990	0.812	0.243	1.123	0.369
20.600	166148.9	0.06019	0.813	0.241	1.120	0.371
20.500	165342.3	0.06048	0.813	0.238	1.115	0.373
20.400	164535.8	0.06078	0.810	0.235	1.111	0.375
20.300	163729.2	0.06108	0.807	0.232	1.106	0.377

TABLE III *(Continued)*

Thallium Bromide

eV	cm^{-1}	μm	n	k	n	k
20.200	162922.7	0.06138	0.803	0.230	1.102	0.378
20.100	162116.2	0.06168	0.798	0.228	1.097	0.380
20.000	161309.6	0.06199	0.792	0.227	1.093	0.382
19.900	160503.1	0.06230	0.784	0.225	1.088	0.385
19.800	159696.5	0.06262	0.775	0.225	1.082	0.388
19.700	158890.0	0.06294	0.765	0.225	1.077	0.390
19.600	158083.4	0.06326	0.752	0.231	1.072	0.394
19.500	157276.9	0.06358	0.736	0.242	1.067	0.397
19.400	156470.3	0.06391	0.718	0.256	1.063	0.400
19.300	155663.8	0.06424	0.706	0.274	1.058	0.404
19.200	154857.2	0.06458	0.702	0.300	1.052	0.410
19.100	154050.7	0.06491	0.725	0.323	1.046	0.415
19.000	153244.1	0.06526	0.758	0.333	1.040	0.421
18.900	152437.6	0.06560	0.773	0.329	1.032	0.426
18.800	151631.0	0.06595	0.782	0.325	1.025	0.433
18.700	150824.5	0.06630	0.781	0.316	1.016	0.440
18.600	150017.9	0.06666	0.775	0.306	1.008	0.446
18.500	149211.4	0.06702	0.768	0.297	0.999	0.453
18.400	148404.8	0.06738	0.761	0.294	0.991	0.463
18.300	147598.3	0.06775	0.751	0.293	0.983	0.473
18.200	146791.7	0.06812	0.738	0.295	0.976	0.482
18.100	145985.2	0.06850	0.723	0.301	0.973	0.496
18.000	145178.6	0.06888	0.706	0.317	0.970	0.511
17.900	144372.1	0.06927	0.680	0.343	0.970	0.525
17.800	143565.5	0.06965	0.678	0.364	0.973	0.538
17.700	142759.0	0.07005	0.686	0.382	0.982	0.551
17.600	141952.5	0.07045	0.696	0.397	0.983	0.545
17.500	141145.9	0.07085	0.701	0.398	0.972	0.543
17.400	140339.4	0.07126	0.704	0.400	0.939	0.549
17.300	139532.8	0.07167	0.704	0.403	0.903	0.566
17.200	138726.3	0.07208	0.701	0.410	0.866	0.597
17.100	137919.7	0.07251	0.694	0.420	0.843	0.674
17.000	137113.2	0.07293	0.688	0.433	0.841	0.772
16.900	136306.6	0.07336	0.680	0.446	0.850	0.860
16.800	135500.1	0.07380	0.671	0.462	0.916	0.958
16.700	134693.5	0.07424	0.661	0.482	1.054	1.033
16.600	133887.0	0.07469	0.647	0.509	1.211	0.996
16.500	133080.4	0.07514	0.650	0.524	1.392	0.914
16.400	132273.9	0.07560	0.635	0.586	1.543	0.787
16.300	131467.3	0.07606	0.651	0.629	1.622	0.694
16.200	130660.8	0.07653	0.693	0.671	1.591	0.554
16.100	129854.2	0.07701	0.795	0.723	1.510	0.478
16.000	129047.7	0.07749	0.925	0.748	1.431	0.462
15.900	128241.1	0.07798	0.997	0.713	1.378	0.469
15.800	127434.6	0.07847	1.016	0.653	1.342	0.481
15.700	126628.0	0.07897	1.024	0.593	1.313	0.494
15.600	125821.5	0.07948	1.018	0.537	1.303	0.510

(continued)

TABLE III *(Continued)*

Thallium Bromide

eV	cm^{-1}	μm	n	k	n	k
15.500	125014.9	0.07999	0.992	0.497	1.293	0.531
15.400	124208.4	0.08051	0.968	0.465	1.291	0.555
15.300	123401.8	0.08104	0.938	0.446	1.290	0.581
15.200	122595.3	0.08157	0.878	0.458	1.296	0.611
15.100	121788.8	0.08211	0.813	0.486	1.308	0.651
15.000	120982.2	0.08266	0.784	0.533	1.329	0.705
14.900	120175.7	0.08321	0.795	0.579	1.368	0.756
14.800	119369.1	0.08377	0.815	0.628	1.420	0.790
14.700	118562.6	0.08434	0.863	0.667	1.477	0.755
14.600	117756.0	0.08492	0.935	0.699	1.549	0.649
14.500	116949.5	0.08551	0.992	0.683	1.566	0.491
14.400	116142.9	0.08610	1.064	0.645	1.529	0.418
14.300	115336.4	0.08670	1.148	0.576	1.488	0.395
14.200	114529.8	0.08731	1.152	0.524	1.464	0.388
14.100	113723.3	0.08793	1.129	0.460	1.444	0.390
14.000	112916.7	0.08856	1.075	0.412	1.428	0.391
13.900	112110.2	0.08920	1.017	0.395	1.420	0.390
13.800	111303.6	0.08984	0.960	0.384	1.412	0.389
13.700	110497.1	0.09050	0.912	0.398	1.407	0.388
13.600	109690.5	0.09117	0.876	0.425	1.403	0.387
13.500	108884.0	0.09184	0.861	0.451	1.395	0.383
13.400	108077.4	0.09253	0.864	0.484	1.387	0.377
13.300	107270.9	0.09322	0.872	0.519	1.378	0.367
13.200	106464.3	0.09393	0.887	0.549	1.368	0.355
13.100	105657.8	0.09465	0.920	0.564	1.356	0.343
13.000	104851.2	0.09537	0.966	0.566	1.337	0.334
12.900	104044.7	0.09611	0.984	0.527	1.316	0.324
12.800	103238.1	0.09686	0.981	0.496	1.293	0.318
12.700	102431.6	0.09763	0.976	0.463	1.265	0.315
12.600	101625.1	0.09840	0.940	0.443	1.233	0.313
12.500	100818.5	0.09919	0.902	0.433	1.198	0.310
12.400	100012.0	0.09999	0.861	0.432	1.161	0.323
12.300	99205.4	0.1008	0.838	0.443	1.120	0.360
12.200	98398.9	0.1016	0.815	0.456	1.072	0.401
12.100	97592.3	0.1025	0.797	0.481	1.026	0.450
12.000	96785.8	0.1033	0.780	0.511	0.992	0.494
11.900	95979.2	0.1042	0.761	0.544	0.985	0.525
11.800	95172.7	0.1051	0.744	0.580	0.987	0.550
11.700	94366.1	0.1060	0.729	0.616	0.997	0.573
11.600	93559.6	0.1069	0.719	0.655	1.003	0.595
11.500	92753.0	0.1078	0.719	0.697	1.009	0.618
11.400	91946.5	0.1088	0.724	0.742	1.015	0.642
11.300	91139.9	0.1097	0.732	0.799	1.024	0.669
11.200	90333.4	0.1107	0.762	0.844	1.035	0.697
11.100	89526.8	0.1117	0.811	0.897	1.051	0.726
11.000	88720.3	0.1127	0.862	0.928	1.082	0.757
10.900	87913.7	0.1137	0.912	0.938	1.146	0.800

TABLE III *(Continued)*

Thallium Bromide

eV	cm^{-1}	μm	n	k	n	k
10.800	87107.2	0.1148	0.960	0.935	1.217	0.837
10.700	86300.6	0.1159	1.015	0.909	1.285	0.861
10.600	85494.1	0.1170	1.044	0.892	1.342	0.881
10.500	84687.5	0.1181	1.070	0.870	1.395	0.892
10.400	83881.0	0.1192	1.089	0.848	1.455	0.892
10.300	83074.4	0.1204	1.101	0.827	1.499	0.867
10.200	82267.9	0.1216	1.115	0.805	1.538	0.827
10.100	81461.3	0.1228	1.124	0.784	1.553	0.784
10.000	80654.8	0.1240	1.127	0.766	1.559	0.737
9.900	79848.3	0.1252	1.125	0.747	1.547	0.687
9.800	79041.7	0.1265	1.121	0.728	1.522	0.642
9.700	78235.2	0.1278	1.112	0.713	1.489	0.606
9.600	77428.6	0.1292	1.096	0.702	1.459	0.579
9.500	76622.1	0.1305	1.078	0.693	1.432	0.563
9.400	75815.5	0.1319	1.061	0.688	1.407	0.550
9.300	75009.0	0.1333	1.037	0.691	1.381	0.540
9.200	74202.4	0.1348	1.008	0.709	1.360	0.537
9.100	73395.9	0.1362	0.985	0.726	1.339	0.536
9.000	72589.3	0.1378	0.983	0.747	1.319	0.541
8.900	71782.8	0.1393	0.981	0.768	1.297	0.546
8.800	70976.2	0.1409	0.978	0.789	1.273	0.553
8.700	70169.7	0.1425	0.976	0.808	1.249	0.573
8.600	69363.1	0.1442	0.978	0.823	1.231	0.593
8.500	68556.6	0.1459	0.982	0.840	1.214	0.616
8.400	67750.0	0.1476	0.986	0.857	1.198	0.653
8.300	66943.5	0.1494	0.990	0.875	1.188	0.692
8.200	66136.9	0.1512	0.995	0.891	1.177	0.730
8.100	65330.4	0.1531	0.999	0.904	1.161	0.768
8.000	64523.8	0.1550	1.004	0.917	1.141	0.801
7.900	63717.3	0.1569	1.006	0.931	1.124	0.837
7.800	62910.7	0.1590	1.008	0.947	1.116	0.861
7.700	62104.2	0.1610	1.012	0.964	1.108	0.876
7.600	61297.6	0.1631	1.014	0.983	1.111	0.913
7.500	60491.1	0.1653	1.017	1.005	1.127	0.966
7.400	59684.6	0.1675	1.022	1.026	1.145	1.023
7.300	58878.0	0.1698	1.028	1.045	1.162	1.083
7.200	58071.5	0.1722	1.027	1.074	1.186	1.141
7.100	57264.9	0.1746	1.032	1.108	1.219	1.203
7.000	56458.4	0.1771	1.049	1.152	1.257	1.268
6.900	55651.8	0.1797	1.042	1.223	1.321	1.337
6.800	54845.3	0.1823	1.056	1.262	1.429	1.419
6.700	54038.7	0.1851	1.279	1.404	1.607	1.592
6.600	53232.2	0.1879	1.443	1.446	1.736	1.643
6.500	52425.6	0.1907	1.476	1.294	1.844	1.611
6.400	51619.1	0.1937	1.396	1.078	1.905	1.531
6.300	50812.5	0.1968	1.313	1.001	1.946	1.452
6.200	50006.0	0.2000	1.188	1.033	1.972	1.387

(continued)

TABLE III *(Continued)*

Thallium Bromide

eV	cm^{-1}	μm	n	k	n	k
6.100	49199.4	0.2033	1.129	1.136	1.989	1.370
6.000	48392.9	0.2066	1.133	1.246	2.003	1.354
5.900	47586.3	0.2101	1.159	1.332	2.019	1.339
5.800	46779.8	0.2138	1.190	1.399	2.039	1.369
5.700	45973.2	0.2175	1.240	1.443	2.061	1.401
5.600	45166.7	0.2214	1.288	1.479	2.139	1.383
5.500	44360.1	0.2254	1.329	1.502	2.155	1.343
5.400	43553.6	0.2296	1.374	1.530	2.152	1.364
5.300	42747.0	0.2339	1.421	1.554	2.281	1.495
5.200	41940.5	0.2384	1.464	1.576	2.478	1.550
5.100	41133.9	0.2431	1.506	1.597	2.601	1.428
5.000	40327.4	0.2480	1.548	1.620	2.651	1.313
4.900	39520.9	0.2530	1.590	1.643	2.689	1.238
4.800	38714.3	0.2583	1.645	1.680	2.726	1.191
4.700	37907.8	0.2638	1.698	1.718	2.776	1.141
4.600	37101.2	0.2695	1.747	1.755	2.860	1.056
4.500	36294.7	0.2755	1.805	1.801	2.904	0.991
4.400	35488.1	0.2818	1.874	1.850	2.936	0.918
4.300	34681.6	0.2883	1.957	1.900	2.952	0.836
4.200	33875.0	0.2952			2.955	0.742
4.100	33068.5	0.3024			2.960	0.649
4.000	32261.9	0.3100			2.970	0.576
3.900	31455.4	0.3179			2.913	0.482
3.800	30648.8	0.3263			2.858	0.441
3.700	29842.3	0.3351			2.843	0.417
3.600	29035.7	0.3444			2.825	0.387
3.500	28229.2	0.3542			2.795	0.339
3.400	27422.6	0.3647			2.760	0.291
3.300	26616.1	0.3757			2.767	0.284
3.200	25809.5	0.3875			2.790	0.285
3.100	25003.0	0.4000			2.857	0.289
3.000	24196.4	0.4133			2.819	0.180
2.900	23389.9	0.4275			2.709	
2.818	22727.3	0.4400			6.8E-6 [6]	
2.800	22583.3	0.4428			2.637	
2.755	22222.2	0.4500			8.2E-7	
2.700	21776.8	0.4592			2.580	
2.600	20970.2	0.4769			2.539	

eV	cm^{-1}	μm	n	n	n	n
2.844	22935.8	0.436	2.7111 [8]	2.6917 [9]	2.652 [7]	
2.271	18315.0	0.546	2.4744	2.4743	2.452	
2.145	17301.0	0.578	2.4448	2.4462	2.424	
2.105	16977.9	0.589	2.4364	2.4380	2.418	
1.907	15384.6	0.650	2.4001	2.4021	2.384	
1.653	13333.3	0.750	2.3634	2.3652	2.350	

TABLE III *(Continued)*

Thallium Bromide

eV	cm^{-1}	μm	n	k	n	k
0.1242	1002.0	9.98	2.343 [10]			
0.0889	717.0	13.95	2.326			
0.0627	506.0	19.76	2.326			
0.0508	410.0	24.39	2.326			
0.0372	300.0	33.33				0.0001 [6]
0.0341	275.0	36.36				0.0002
0.0310	250.0	40.00				0.00039
0.0279	225.0	44.44				0.00077
0.0248	200.0	50.00			1.907 [15]	0.00155
0.0236	190.0	52.63	1.82 [19]	0.02 [19]	1.861	
0.0229	185.0	54.05	1.78	0.02	1.835	
0.0223	180.0	55.56	1.74	0.03	1.805	
0.0217	175.0	57.14	1.70	0.03	1.772	
0.0211	170.0	58.82	1.64	0.04	1.736	
0.0205	165.0	60.61	1.58	0.04	1.695	
0.0198	160.0	62.50	1.53	0.04	1.648	
0.0192	155.0	64.52	1.46	0.04	1.595	
0.0186	150.0	66.67	1.38	0.04	1.533	
0.0183	148.0	67.57	1.35	0.03	1.506	
0.0181	146.0	68.49	1.36	0.04	1.477	
0.0179	144.0	69.44	1.35	0.04	1.446	
0.0176	142.0	70.42	1.33	0.04	1.413	
0.0174	140.0	71.43	1.30	0.05	1.378	
0.0171	138.0	72.46	1.28	0.05	1.340	
0.0169	136.0	73.53	1.25	0.04	1.300	
0.0166	134.0	74.63	1.23	0.03	1.256	
0.0164	132.0	75.76	1.23	0.02	1.209	
0.0161	130.0	76.92	1.21	0.02	1.158	
0.0159	128.0	78.13	1.20	0.02	1.102	
0.0156	126.0	79.37	1.14	0.10	1.043	
0.0154	124.0	80.65	1.05	0.18	0.978	
0.0151	122.0	81.97	0.99	0.22	0.910	
0.0149	120.0	83.33	0.91	0.28	0.838	0.519 [15]
0.0146	118.0	84.75	0.82	0.35	0.765	0.587
0.0144	116.0	86.21	0.75	0.44	0.695	0.667
0.0141	114.0	87.72	0.69	0.55	0.631	0.760
0.0139	112.0	89.29	0.65	0.68	0.577	0.862
0.0136	110.0	90.91	0.62	0.82	0.531	0.971
0.0134	108.0	92.59	0.59	0.93	0.495	1.083
0.0131	106.0	94.34	0.59	1.03	0.466	1.196
0.0129	104.0	96.15	0.60	1.13	0.443	1.311
0.0126	102.0	98.04	0.60	1.24	0.425	1.428
0.0124	100.0	100.00	0.58	1.36	0.411	1.545
0.0122	98.0	102.04	0.58	1.46	0.400	1.665
0.0119	96.0	104.17	0.59	1.55	0.392	1.787
0.0117	94.0	106.38	0.60	1.67	0.386	1.912
0.0114	92.0	108.70	0.62	1.80	0.383	2.041

(continued)

TABLE III *(Continued)*

Thallium Bromide

eV	cm^{-1}	μm	n	k	n	k
0.0112	90.0	111.11	0.62	1.92	0.381	2.174
0.0109	88.0	113.64	0.63	2.02	0.381	2.313
0.0107	86.0	116.28	0.65	2.11	0.384	2.457
0.0104	84.0	119.05	0.69	2.19	0.388	2.610
0.0102	82.0	121.95	0.79	2.33	0.394	2.770
0.0099	80.0	125.00	0.97	2.46	0.403	2.941
0.0097	78.0	128.21	1.07	2.59	0.414	3.124
0.0094	76.0	131.58	1.08	2.72	0.428	3.321
0.0092	74.0	135.14	1.08	2.96	0.446	3.535
0.0089	72.0	138.89	1.25	3.10	0.469	3.768
0.0087	70.0	142.86	1.21	3.14	0.497	4.026
0.0084	68.0	147.06	1.26	3.73	0.533	4.313
0.0082	66.0	151.52	1.73	4.11	0.579	4.637
0.0079	64.0	156.25	2.05	4.34	0.639	5.009
0.0077	62.0	161.29	2.26	4.63	0.719	5.441
0.0074	60.0	166.67	2.47	4.85	0.830	5.956
0.0072	58.0	172.41	2.81	5.18	0.990	6.585
0.0069	56.0	178.57	3.16	6.13	1.235	7.379
0.0067	54.0	185.19	4.21	7.13	1.647	8.427
0.0064	52.0	192.31	5.17	8.44	2.429	9.879
0.0062	50.0	200.00	5.37	8.68	4.233	11.932
0.0060	48.0	208.33	6.73	6.55	9.167	13.595
0.0057	46.0	217.39	7.19	5.10	14.658	8.314
0.0055	44.0	227.27	7.19	3.64	13.099	3.386
0.0052	42.0	238.10	6.96	2.51	11.137	1.673
0.0050	40.0	250.00	6.77	1.99	9.808	0.974
0.0047	38.0	263.16	6.50	1.66	8.891	0.627
0.0045	36.0	277.78	6.34	1.53	8.226	0.431
0.0042	34.0	294.12	6.19	1.34	7.722	0.309
0.0040	32.0	312.50	6.08	1.16	7.329	0.229
0.0037	30.0	333.33	5.98	1.08	7.015	0.174
0.0035	28.0	357.14	5.90	0.95	6.758	0.134
0.0032	26.0	384.62	5.85	0.87	6.546	0.105
0.0030	24.0	416.67	5.82	0.77	6.369	0.083
0.0027	22.0	454.55	5.76	0.60	6.220	0.066
0.00248	20.0	500.00			6.095	0.053
0.00186	15.0	666.67			5.860	0.030
0.00124	10.0	1000.0			5.711	0.017
0.00062	5.0	2000.0			5.628	0.007
0.0	0.0		5.53 [16]		5.601	0.0
			5.53 [15]		5.48 [18]	

TABLE IV

Values of n and k Obtained for Polycrystalline Orthorhombic (and Cubic as Noted) Thallium Iodide

eV	cm^{-1}	μm	n	k
21.500	173407.8	0.05767	0.775 [3]	0.110 [3]
21.200	170988.2	0.05848	0.768	0.115
21.000	169375.1	0.05904	0.763	0.120
20.800	167762.0	0.05961	0.759	0.125
20.600	166148.9	0.06019	0.755	0.130
20.400	164535.8	0.06078	0.751	0.135
20.200	162922.7	0.06138	0.745	0.141
20.000	161309.6	0.06199	0.738	0.147
19.800	159696.5	0.06262	0.730	0.153
19.600	158083.4	0.06326	0.722	0.161
19.400	156470.3	0.06391	0.713	0.169
19.200	154857.2	0.06458	0.704	0.180
19.000	153244.1	0.06526	0.691	0.192
18.800	151631.0	0.06595	0.676	0.213
18.600	150017.9	0.06666	0.662	0.235
18.400	148404.8	0.06738	0.678	0.253
18.200	146791.7	0.06812	0.683	0.261
18.000	145178.6	0.06888	0.681	0.268
17.800	143565.5	0.06965	0.675	0.278
17.600	141952.5	0.07045	0.669	0.291
17.400	140339.4	0.07126	0.662	0.310
17.200	138726.3	0.07208	0.645	0.335
17.000	137113.2	0.07293	0.613	0.381
16.800	135500.1	0.07380	0.616	0.456
16.600	133887.0	0.07469	0.742	0.530
16.500	133080.4	0.07514	0.788	0.529
16.400	132273.9	0.07560	0.809	0.517
16.300	131467.3	0.07606	0.823	0.496
16.200	130660.8	0.07653	0.836	0.474
16.100	129854.2	0.07701	0.845	0.453
16.000	129047.7	0.07749	0.852	0.431
15.900	128241.1	0.07798	0.855	0.411
15.800	127434.6	0.07847	0.852	0.395
15.700	126628.0	0.07897	0.842	0.382
15.600	125821.5	0.07948	0.830	0.368
15.500	125014.9	0.07999	0.818	0.352
15.400	124208.4	0.08051	0.806	0.335
15.300	123401.8	0.08104	0.774	0.333
15.200	122595.3	0.08157	0.730	0.364
15.100	121788.8	0.08211	0.704	0.408
15.000	120982.2	0.08266	0.710	0.453
14.900	120175.7	0.08321	0.730	0.490
14.800	119369.1	0.08377	0.769	0.524
14.700	118562.6	0.08434	0.823	0.539
14.600	117756.0	0.08492	0.880	0.539

(continued)

TABLE IV *(Continued)*

Orthorhombic (and Cubic as Noted) Thallium Iodide

eV	cm^{-1}	μm	n	k
14.500	116949.5	0.08551	0.927	0.524
14.400	116142.9	0.08610	0.964	0.493
14.300	115336.4	0.08670	0.988	0.437
14.200	114529.8	0.08731	0.988	0.365
14.100	113723.3	0.08793	0.963	0.314
14.000	112916.7	0.08856	0.928	0.287
13.900	112110.2	0.08920	0.895	0.267
13.800	111303.6	0.08984	0.862	0.252
13.700	110497.1	0.09050	0.831	0.249
13.600	109690.5	0.09117	0.802	0.258
13.500	108884.0	0.09184	0.769	0.270
13.400	108077.4	0.09253	0.741	0.290
13.300	107270.9	0.09322	0.724	0.308
13.200	106464.3	0.09393	0.706	0.329
13.100	105657.8	0.09465	0.686	0.353
13.000	104851.2	0.09537	0.673	0.376
12.900	104044.7	0.09611	0.666	0.395
12.800	103238.1	0.09686	0.661	0.414
12.700	102431.6	0.09763	0.657	0.432
12.600	101625.1	0.09840	0.656	0.449
12.500	100818.5	0.09919	0.657	0.465
12.400	100012.0	0.09999	0.658	0.479
12.300	99205.4	0.1008	0.658	0.493
12.200	98398.9	0.1016	0.658	0.508
12.100	97592.3	0.1025	0.658	0.522
12.000	96785.8	0.1033	0.659	0.536
11.900	95979.2	0.1042	0.660	0.549
11.800	95172.7	0.1051	0.662	0.563
11.700	94366.1	0.1060	0.665	0.576
11.600	93559.6	0.1069	0.668	0.589
11.500	92753.0	0.1078	0.671	0.603
11.400	91946.5	0.1088	0.673	0.617
11.300	91139.9	0.1097	0.676	0.632
11.200	90333.4	0.1107	0.679	0.647
11.100	89526.8	0.1117	0.681	0.663
11.000	88720.3	0.1127	0.684	0.678
10.900	87913.7	0.1137	0.688	0.690
10.800	87107.2	0.1148	0.692	0.702
10.700	86300.6	0.1159	0.696	0.714
10.600	85494.1	0.1170	0.698	0.728
10.500	84687.5	0.1181	0.698	0.746
10.400	83881.0	0.1192	0.698	0.764
10.300	83074.4	0.1204	0.700	0.780
10.200	82267.9	0.1216	0.706	0.799
10.100	81461.3	0.1228	0.712	0.818
10.000	80654.8	0.1240	0.718	0.837
9.900	79848.3	0.1252	0.732	0.861

TABLE IV *(Continued)*

Orthorhombic (and Cubic as Noted) Thallium Iodide

eV	cm^{-1}	μm	n	k
9.800	79041.7	0.1265	0.746	0.884
9.700	78235.2	0.1278	0.760	0.908
9.600	77428.6	0.1292	0.780	0.924
9.500	76622.1	0.1305	0.799	0.940
9.400	75815.5	0.1319	0.823	0.955
9.300	75009.0	0.1333	0.847	0.965
9.200	74202.4	0.1348	0.870	0.975
9.100	73395.9	0.1362	0.892	0.983
9.000	72589.3	0.1378	0.913	0.992
8.900	71782.8	0.1393	0.938	0.996
8.800	70976.2	0.1409	0.957	0.996
8.700	70169.7	0.1425	0.976	0.996
8.600	69363.1	0.1442	0.994	0.995
8.500	68556.6	0.1459	1.012	0.994
8.400	67750.0	0.1476	1.031	0.992
8.300	66943.5	0.1494	1.048	0.987
8.200	66136.9	0.1512	1.064	0.982
8.100	65330.4	0.1531	1.077	0.976
8.000	64523.8	0.1550	1.088	0.970
7.900	63717.3	0.1569	1.093	0.961
7.800	62910.7	0.1590	1.096	0.952
7.700	62104.2	0.1610	1.095	0.942
7.600	61297.6	0.1631	1.090	0.931
7.500	60491.1	0.1653	1.081	0.922
7.400	59684.6	0.1675	1.066	0.919
7.300	58878.0	0.1698	1.050	0.918
7.200	58071.5	0.1722	1.027	0.926
7.100	57264.9	0.1746	1.016	0.949
7.000	56458.4	0.1771	1.011	0.977
6.900	55651.8	0.1797	1.010	1.010
6.800	54845.3	0.1823	1.012	1.041
6.700	54038.7	0.1851	1.014	1.071
6.600	53232.2	0.1879	1.016	1.100
6.500	52425.6	0.1907	1.020	1.129
6.400	51619.1	0.1937	1.026	1.158
6.300	50812.5	0.1968	1.034	1.189
6.200	50006.0	0.2000	1.042	1.219
6.100	49199.4	0.2033	1.051	1.246
6.000	48392.9	0.2066	1.060	1.273
5.900	47586.3	0.2101	1.074	1.307
5.800	46779.8	0.2138	1.088	1.341
5.700	45973.2	0.2175	1.102	1.375
5.600	45166.7	0.2214	1.116	1.409
5.500	44360.1	0.2254	1.141	1.450
5.400	43553.6	0.2296	1.167	1.488
5.300	42747.0	0.2339	1.199	1.527
5.200	41940.5	0.2384	1.233	1.567

(continued)

TABLE IV *(Continued)*

Orthorhombic (and Cubic as Noted) Thallium Iodide

eV	cm^{-1}	μm	n	k
5.100	41133.9	0.2431	1.269	1.609
5.000	40327.4	0.2480	1.311	1.654
4.900	39520.9	0.2530	1.363	1.704
4.800	38714.3	0.2583	1.412	1.751
4.700	37907.8	0.2638	1.457	1.795
4.600	37101.2	0.2695	1.512	1.847
4.500	36294.7	0.2755	1.572	1.891
4.400	35488.1	0.2818	1.633	1.927
4.300	34681.6	0.2883	1.713	1.982
4.200	33875.0	0.2952	1.796	2.040
4.100	33068.5	0.3024	1.882	2.078
2.271	18315.0	0.546	2.85† [7]	
2.105	16977.9	0.589	2.78†	
1.907	15384.6	0.650	2.72†	
1.90	15324.4	0.653	2.790 [3]	
1.80	14517.9	0.689	2.740	
1.70	13711.3	0.729	2.700	
1.60	12904.8	0.775	2.660	
1.50	12098.2	0.827	2.620	
1.40	11291.7	0.886	2.590	
1.30	10485.1	0.954	2.570	
1.20	9678.6	1.033	2.540	
1.10	8872.0	1.127	2.520	
1.00	8065.5	1.240	2.500	
0.90	7258.9	1.378	2.490	
0.80	6452.4	1.550	2.470	
0.70	5645.8	1.771	2.450	
0.60	4839.3	2.066	2.440	
0.50	4032.7	2.480	2.430	
0.0248	200.0	50.00	2.230 [15]	
0.0242	195.0	51.28	2.216	
0.0236	190.0	52.63	2.200	
0.0229	185.0	54.05	2.183	
0.0223	180.0	55.56	2.164	
0.0217	175.0	57.14	2.143	
0.0211	170.0	58.82	2.120	
0.0205	165.0	60.61	2.093	
0.0198	160.0	62.50	2.064	
0.0192	155.0	64.52	2.031	
0.0186	150.0	66.67	1.993	
0.0180	145.0	68.97	1.950	
0.0174	140.0	71.43	1.900	
0.0167	135.0	74.07	1.842	
0.0161	130.0	76.92	1.774	
0.0155	125.0	80.00	1.693	0.104 [15]
0.0149	120.0	83.33	1.597	0.135
0.0143	115.0	86.96	1.482	0.180

† Cubic thallium iodide

TABLE IV *(Continued)*

Orthorhombic (and Cubic as Noted) Thallium Iodide

eV	cm^{-1}	μm	n	k
0.0136	110.0	90.91	1.344	0.248
0.0130	105.0	95.24	1.182	0.353
0.0124	100.0	100.0	1.005	0.512
0.0118	95.0	105.3	0.834	0.734
0.0112	90.0	111.1	0.679	1.008
0.0105	85.0	117.6	0.526	1.342
0.0099	80.0	125.0	0.385	1.770
0.0093	75.0	133.3	0.278	2.314
0.0087	70.0	142.9	0.214	3.008
0.0081	65.0	153.8	0.196	3.950
0.0074	60.0	166.7	0.251	5.444
0.0068	55.0	181.8	0.656	8.853
0.0062	50.0	200.0	17.685	4.132
0.0056	45.0	222.2	8.373	0.316
0.0050	40.0	250.0	6.584	0.128
0.0043	35.0	285.7	5.779	0.074
0.0037	30.0	333.3	5.320	0.048
0.0031	25.0	400.0	5.029	0.034
0.0024	20.0	500.0	4.836	0.024
0.0018	15.0	666.7	4.706	0.016
0.0012	10.0	1000.0	4.623	0.010
0.00062	5.0	2000.0	4.576	0.005
0.0	0.0		4.561	0.0
			4.60 [18]	
			5.44† [18]	

TABLE V

Values of n and k for KRS-5 from Various References

eV	cm^{-1}	μm	n	k
2.3557	19000.0	0.5263		8.38E-3 [24]
2.2937	18500.0	0.5405		8.66E-4
2.2317	18000.0	0.5556		8.95E-5
2.1697	17500.0	0.5714		9.26E-6
2.1489	17332.2	0.57696	2.62758 [27]	4.33E-6
2.1413	17270.7	0.57902	2.62505	3.27E-6
2.1077	17000.0	0.5882		9.59E-7
1.9257	15531.6	0.64385	2.56454	
1.7949	14477.0	0.69075	2.53470	
1.4550	11735.4	0.85212	2.47448	
1.3862	11180.7	0.8944	2.46470	
1.2228	9862.1	1.01398	2.44416	
1.1697	9434.0	1.0600		8.44E-11 [31]
1.0985	8860.1	1.12866	2.43090	

(continued)

TABLE V *(Continued)*

KRS-5

eV	cm^{-1}	μm	n	k
0.90679	7313.7	1.3673	2.41385	
0.88878	7168.5	1.395	2.41242	
0.81061	6538.0	1.52952	2.40658	
0.73225	5906.0	1.6932	2.40143	
0.72540	5850.7	1.7092	2.40105	
0.68384	5515.5	1.81308	2.39851	
0.62933	5075.9	1.9701	2.39553	
0.53322	4300.7	2.3252	2.39076	
0.36266	2925.0	3.4188	2.38386	
0.29118	2348.5	4.258	2.38142	
0.22380	1805.1	5.54		3.53E-10
0.18527	1494.3	6.692	2.37680	
0.14878	1200.0	8.333		5.64E-7 [12]
0.14258	1150.0	8.696		7.00E-7
0.13638	1100.0	9.091		8.97E-7
0.13018	1050.0	9.524		9.25E-7
0.12750	1028.4	9.724	2.37132	
0.12399	1000.0	10.000		8.24E-7
0.11779	950.0	10.526		6.35E-7
0.11697	943.4	10.60		4.22E-9 [31]
0.11236	906.2	11.035	2.36857	
0.11159	900.0	11.111		5.03E-7 [12]
0.10539	850.0	11.765		3.67E-7
0.09919	800.0	12.500		2.58E-7
0.09299	750.0	13.333		2.18E-7
0.08679	700.0	14.286		1.48E-7
0.08676	699.8	14.29	2.36023	
0.08277	667.6	14.98	2.35824	
0.08059	650.0	15.385		1.58E-7
0.08009	646.0	15.48	2.35667	
0.07439	600.0	16.667		6.13E-7
0.07126	574.7	17.40	2.35022	
0.06827	550.7	18.16	2.34755	
0.06819	550.0	18.182		5.05E-7
0.06199	500.0	20.000		4.95E-7
0.06027	486.1	20.57	2.33816	
0.05690	458.9	21.79	2.33290	
0.05579	450.0	22.222		6.13E-7
0.05448	439.4	22.76	2.32851	
0.05269	425.0	23.529		2.88E-7
0.05205	419.8	23.82	2.32338	
0.04959	400.0	25.00		1.64E-7
0.04928	397.5	25.16	2.31696	
0.04774	385.1	25.97	2.31260	
0.04656	375.5	26.63	2.30902	
0.04339	350.0	28.571		1.01E-6
0.04159	335.5	29.81	2.28988	

TABLE V *(Continued)*

KRS-5

eV	cm^{-1}	μm	n	k
0.04030	325.0	30.769		4.39E-6
0.03911	315.5	31.70	2.27730	
0.03757	303.0	33.00	2.26821	
0.03720	300.0	33.333		8.49E-6
0.03596	290.0	34.48	2.25740	
0.03410	275.0	36.364		8.75E-5 [24]
0.03301	266.2	37.56	2.23243	1.25E-4
0.03148	253.9	39.38	2.21621	2.06E-4
0.03100	250.0	40.00	2.21 [13]	2.42E-4
0.02976	240.0	41.67	2.19	3.64E-4
0.02852	230.0	43.48	2.17	5.49E-4
0.02728	220.0	45.45	2.15	8.30E-4
0.02604	210.0	47.62	2.13	1.26E-3
0.02480	200.0	50.00	2.10	1.91E-3
0.02356	190.0	52.63	2.06	2.91E-3
0.02232	180.0	55.56	2.02	4.44E-3
0.02108	170.0	58.82	1.97	6.80E-3
0.01984	160.0	62.50	1.91	
0.01860	150.0	66.67	1.83	
0.01736	140.0	71.43	1.73	
0.01612	130.0	76.92	1.60	
0.01587	128.0	78.13	1.56	
0.01562	126.0	79.37	1.53	
0.01537	124.0	80.65	1.49	
0.01513	122.0	81.97	1.45	
0.01488	120.0	83.33	1.41	
0.01463	118.0	84.75	1.36	
0.01438	116.0	86.21	1.31	
0.01413	114.0	87.72	1.26	
0.01389	112.0	89.29	1.21	
0.01364	110.0	90.91	1.15	0.63 [13]
0.01339	108.0	92.59	1.09	0.69
0.01314	106.0	94.34	1.03	0.75
0.01289	104.0	96.15	0.98	0.83
0.01265	102.0	98.04	0.92	0.92
0.01240	100.0	100.0	0.87	1.01
0.01215	98.0	102.0	0.82	1.12
0.01190	96.0	104.2	0.78	1.23
0.01165	94.0	106.4	0.75	1.35
0.01141	92.0	108.7	0.72	1.47
0.01116	90.0	111.1	0.70	1.59
0.01091	88.0	113.6	0.69	1.73
0.01066	86.0	116.3	0.68	1.86
0.01041	84.0	119.0	0.67	2.00
0.01017	82.0	122.0	0.67	2.15
0.00992	80.0	125.0	0.67	2.30
0.00967	78.0	128.2	0.68	2.46

(continued)

TABLE V *(Continued)*

KRS-5

eV	cm^{-1}	μm	n	k
0.00942	76.0	131.6	0.69	2.64
0.00917	74.0	135.1	0.70	2.82
0.00893	72.0	138.9	0.72	3.01
0.00868	70.0	142.9	0.75	3.22
0.00843	68.0	147.1	0.78	3.45
0.00818	66.0	151.5	0.83	3.70
0.00794	64.0	156.3	0.88	3.97
0.00769	62.0	161.3	0.96	4.28
0.00744	60.0	166.7	1.05	4.63
0.00719	58.0	172.4	1.18	5.03
0.00694	56.0	178.6	1.35	5.49
0.00670	54.0	185.2	1.59	6.04
0.00645	52.0	192.3	1.95	6.71
0.00620	50.0	200.0	2.52	7.52
0.00595	48.0	208.3	3.48	8.48
0.00570	46.0	217.4	5.22	9.42
0.00546	44.0	227.3	8.11	9.42
0.00521	42.0	238.1	10.70	7.09
0.00496	40.0	250.0	10.92	4.20
0.00471	38.0	263.2	10.08	2.46
0.00446	36.0	277.8	9.21	1.54
0.00422	34.0	294.1	8.50	1.03
0.00397	32.0	312.5	7.95	0.72
0.00372	30.0	333.3	7.51	0.53
0.00248	20.0	500.0	6.30	0.15
0.00124	10.0	1000.0	5.83	0.05
0.0	0.0		5.70	0.0
			5.70 [21]	

TABLE VI

Values of n and k for KRS-6 from Various References

eV	cm^{-1}	μm	n	k
3.3000	26616.1	0.3757		0.0697 [25]
3.2000	25809.5	0.3875		0.00493
3.1000	25003.0	0.4000		0.000349
3.0508	24606.0	0.4064		9.46E-5
3.0240	24390.2	0.4100	2.5754 [9]	4.66E-5
2.9771	24012.0	0.4165	2.5516	1.35E-5
2.9559	23840.9	0.4194	2.5417	7.71E-6
2.8955	23353.3	0.4282	2.5155	1.56E-6
2.8437	22935.8	0.4360	2.4951	
2.5407	20491.8	0.4880	2.4021	1.90E-7
2.4098	19436.3	0.5145	2.3716	1.26E-7

TABLE VI *(Continued)*

KRS-6

eV	cm^{-1}	μm	*n*	*k*
2.2708	18315.0	0.5460	2.3437	
2.1821	17599.4	0.5682	2.3280	6.16E-8
2.1451	17301.0	0.5780	2.3218	
2.1039	16969.3	0.5893	2.3154	
			2.3367 [22]	
2.0664	16666.7	0.6000	2.3294	
1.9160	15453.6	0.6471	2.2884 [9]	2.71E-08
1.9075	15384.6	0.650	2.2873	
1.7712	14285.7	0.700	2.2982 [22]	
			2.2708 [9]	
1.6531	13333.3	0.750	2.2582	
1.5498	12500.0	0.80	2.2660 [22]	
1.3776	11111.1	0.90	2.2510	
1.2399	10000.0	1.00	2.2404	
1.1697	9434.0	1.06		6.77E-10 [32]
1.1271	9090.9	1.10	2.2321	
1.0332	8333.3	1.20	2.2255	
0.9537	7692.3	1.30	2.2212	
0.8856	7142.9	1.40	2.2176	
0.8266	6666.7	1.50	2.2148	
0.7749	6250.0	1.60	2.2124	
0.7293	5882.4	1.70	2.2103	
0.6888	5555.6	1.80	2.2086	
0.6526	5263.2	1.90	2.2071	
0.6199	5000.0	2.00	2.2059	
0.5636	4545.5	2.20	2.2039	
0.5166	4166.7	2.40	2.2024	
0.4769	3846.2	2.60	2.2011	
0.4428	3571.4	2.80	2.2001	
0.4133	3333.3	3.00	2.1990	
0.3542	2857.1	3.50	2.1972	
0.3100	2500.0	4.00	2.1956	
0.2755	2222.2	4.50	2.1942	
0.2480	2000.0	5.00	2.1928	
0.2238	1805.1	5.54		6.17E-10
0.2066	1666.7	6.00	2.1900	
0.1771	1428.6	7.00	2.1870	
0.1550	1250.0	8.00	2.1839	
0.1378	1111.1	9.00	2.1805	
0.1240	1000.0	10.00	2.1767	
0.1170	943.4	10.60		1.18E-09
0.1127	909.1	11.00	2.1723	
0.10332	833.3	12.00	2.1674	
0.09537	769.2	13.00	2.1620	
0.08856	714.3	14.00	2.1563	
0.08266	666.7	15.00	2.1504	
0.07749	625.0	16.00	2.1442	

(continued)

TABLE VI *(Continued)*

KRS-6

eV	cm^{-1}	μm	n	k
0.07293	588.2	17.00	2.1377	
0.06888	555.6	18.00	2.1309	
0.06526	526.3	19.00	2.1236	
0.06199	500.0	20.00	2.1154	
0.05904	476.2	21.00	2.1067	
0.05636	454.5	22.00	2.0976	
0.05391	434.8	23.00	2.0869	
0.05166	416.7	24.00	2.0752	
0.04959	400.0	25.00	2.07 [13]	1.96E-4 [34]
0.04649	375.0	26.67	2.05	3.74E-4
0.04339	350.0	28.57	2.03	7.17E-4
0.04030	325.0	30.77	2.00	1.38E-3
0.03720	300.0	33.33	1.96	2.68E-3
0.03410	275.0	36.36	1.91	5.22E-3
0.03100	250.0	40.00	1.83	
0.02976	240.0	41.67	1.80	
0.02852	230.0	43.48	1.76	
0.02728	220.0	45.45	1.71	
0.02604	210.0	47.62	1.65	
0.02480	200.0	50.00	1.58	
0.02356	190.0	52.63	1.49	0.34 [13]
0.02232	180.0	55.56	1.39	0.40
0.02108	170.0	58.82	1.25	0.49
0.01984	160.0	62.50	1.09	0.62
0.01959	158.0	63.29	1.06	0.65
0.01934	156.0	64.10	1.02	0.69
0.01909	154.0	64.94	0.99	0.73
0.01885	152.0	65.79	0.95	0.77
0.01860	150.0	66.67	0.92	0.82
0.01835	148.0	67.57	0.89	0.87
0.01810	146.0	68.49	0.85	0.93
0.01785	144.0	69.44	0.82	0.99
0.01761	142.0	70.42	0.79	1.05
0.01736	140.0	71.43	0.77	1.12
0.01711	138.0	72.46	0.74	1.19
0.01686	136.0	73.53	0.72	1.26
0.01661	134.0	74.63	0.70	1.33
0.01637	132.0	75.76	0.69	1.41
0.01612	130.0	76.92	0.67	1.48
0.01587	128.0	78.13	0.66	1.56
0.01562	126.0	79.37	0.65	1.64
0.01537	124.0	80.65	0.64	1.73
0.01513	122.0	81.97	0.63	1.81
0.01488	120.0	83.33	0.63	1.90
0.01463	118.0	84.75	0.62	1.99
0.01438	116.0	86.21	0.62	2.09
0.01413	114.0	87.72	0.62	2.18

TABLE VI *(Continued)*

KRS-6

eV	cm^{-1}	μm	n	k
0.01389	112.0	89.29	0.62	2.28
0.01364	110.0	90.91	0.62	2.39
0.01339	108.0	92.59	0.63	2.49
0.01314	106.0	94.34	0.63	2.61
0.01289	104.0	96.15	0.64	2.73
0.01265	102.0	98.04	0.65	2.85
0.01240	100.0	100.0	0.66	2.98
0.01215	98.0	102.0	0.68	3.12
0.01190	96.0	104.2	0.69	3.26
0.01165	94.0	106.4	0.71	3.42
0.01141	92.0	108.7	0.74	3.58
0.01116	90.0	111.1	0.76	3.76
0.01091	88.0	113.6	0.80	3.95
0.01066	86.0	116.3	0.84	4.16
0.01041	84.0	119.0	0.89	4.39
0.01017	82.0	122.0	0.94	4.64
0.00992	80.0	125.0	1.02	4.92
0.00967	78.0	128.2	1.10	5.23
0.00942	76.0	131.6	1.22	5.58
0.00917	74.0	135.1	1.36	5.97
0.00893	72.0	138.9	1.56	6.44
0.00868	70.0	142.9	1.82	6.98
0.00843	68.0	147.1	2.20	7.62
0.00818	66.0	151.5	2.76	8.38
0.00794	64.0	156.3	3.65	9.27
0.00769	62.0	161.3	5.15	10.18
0.00744	60.0	166.7	7.59	10.61
0.00719	58.0	172.4	10.55	9.33
0.00694	56.0	178.6	12.00	6.42
0.00670	54.0	185.2	11.64	3.96
0.00645	52.0	192.3	10.75	2.50
0.00620	50.0	200.0	9.91	1.66
0.00595	48.0	208.3	9.20	1.16
0.00570	46.0	217.4	8.63	0.85
0.00546	44.0	227.3	8.17	0.63
0.00521	42.0	238.1	7.78	0.49
0.00496	40.0	250.0	7.47	0.38
0.00372	30.0	333.3	6.46	0.13
0.00248	20.0	500.0	5.97	0.05
0.00124	10.0	1000.0	5.73	0.02
0.0	0.0		5.66	0.0
			5.63 [21]	

Yttrium Aluminum Garnet ($Y_3Al_5O_{12}$)

WILLIAM J. TROPF
Applied Physics Laboratory
The Johns Hopkins University
Laurel, Maryland

Yttrium aluminum garnet (YAG or yttrogarnet), is a synthetic, nonmagnetic material with the chemical formula $Y_3Al_5O_{12}$ or $Y_3Al_2(AlO_4)_3$. It is a host medium for rare-earth-doped, solid-state lasers, a low-loss material for acoustic devices, and a gemstone. YAG crystals have body-centered cubic crystalline structure with space group Ia3d (or O_h^{10}). The unit cell has an edge dimension of 12.008 Å [1] and contains eight formula units, giving a theoretical density of 4.554 g/cm^3. The yttrium atoms occupy the 24(c) sites (222 or D_2 point symmetry), aluminum(1) atoms occupy the 16(a) sites ($\bar{3}$ or $C_{3i}[S_6]$ point symmetry), aluminum(2) atoms occupy the 24(d) sites ($\bar{4}$ or S_4 point symmetry), and the oxygen atoms occupy the 96(h) sites (1 or C_1 point symmetry). YAG undergoes a phase change at 2193 K.

Optical constants above the electronic band gap have been extensively studied by Tomiki *et al.* [2–5] using Kramers–Kronig analyses of reflectance spectra. Professor Tomiki provided approximately 750 values of the complex dielectric constant at 297 K [4], from the band edge at 6.4 eV to 116 eV, in digital form with three decimal places. Selected values of the complex refractive index (n and k) determined from these data are given in Table I.

Yttrium aluminum garnet has a direct band gap at 6.5 eV. The lowest-energy feature in the electronic absorption is excitonic absorption (see later discussion). Interband transitions from the upper valence band of oxygen ($2p^6$) to the conduction bands of yttria ($4d$ + $5s$ states) dominate the structure from 7 to 15 eV. Optical constants between 15 and 26 eV are mainly due to interband transitions from the oxygen valence bands to conduction bands of yttrium ($5d$ + $6s$ levels) and aluminum ($3s$ + $3p$ levels). The valence electrons form a plasma oscillation centered at 23.4 eV.

Inner-core yttria electron transitions occur in the 26 to 35 eV region. At energies above 29.3 eV, absorption is mainly due to transitions from oxygen ($2s^2$) bands to the aluminum ($3p$) conduction band. Plasma oscillations from

HANDBOOK OF OPTICAL CONSTANTS OF SOLIDS III

Copyright © 1998 by Academic Press.
All rights of reproduction in any form reserved
ISBN 0-12-544423-0/$25.00.

the full bands of yttria ($4p^6$) and oxygen ($2s^2$) peak near 36.2 eV. At higher energies, yttria and aluminum electron transitions dominate, especially the prominent aluminum $L_{2,3}$ transitions near 77 eV.

Tomiki *et al.* [3, 5] determined the temperature dependence of exciton absorption between 10 and 297 K from transmission measurements (6.5–7.0 eV) and fitted their data to an Urbach-rule formulation,

$$\beta(E, T) = \beta_0 \exp(-\sigma_s(T)(E_0 - E)/k_B T), \tag{1a}$$

where $\beta(E,T)$ is the absorption coefficient as a function of energy (E) and temperature (T), and k_B is Boltzmann's constant. The slope parameter $\sigma_s(T)$ is given by

$$\sigma_s(T) = \sigma_{s0}\ (2kT/E_{s0}) \tanh(E_{s0}/2kT). \tag{1b}$$

Constants of Eq. (1) are $\beta_0 = 4.093 \times 10^5$ cm^{-1}, $E_0 = 7.047$ eV, $\sigma_{s0} = 0.558$, and $E_{s0} = 36.5$ meV [5]. Values of the imaginary part of the refractive index between 6.4 and 6.6 eV given in Table I are calculated from this equation.

Slack *et al.* [6] measured YAG absorption at 300 K in the vicinity of the Urbach absorption edge. Imaginary index values between 4.5 and 6.6 eV in Table I are taken from his measurements. Values below 6.4 eV are dominated by extrinsic absorption but are similar to those reported by Tomiki *et al.* [2, 3, 5].

Refractive-index measurements in the transparent region are surprisingly sparse. The most comprehensive data set, covering 0.4 to 4.0 μm, is the minimum-deviation prism measurement of Bond [7]. Other measurements (primarily from interferometric techniques) are those of Shchavelev *et al.* [8], McCollum *et al.* [9], and Wilson [10], which are restricted to the visible. Data given in Table I are from Bond [7], Shchavelev *et al.* [8], and McCollum *et al.* [9],

Several sources give Sellmeier dispersion relationships for YAG in the form

$$n^2(\lambda) - 1 = \sum_i \frac{A_i \lambda^2}{\lambda^2 - \lambda_i^2}, \tag{2}$$

where the constants A_i and λ_i are given in Table II. These dispersion formulas are either based on the data of Bond (see [2, 11]) or on visible measurements [12, 13]. Several sources give the temperature dependence of the refractive index [14–16]. All are restricted to the visible or near infrared. Table III lists values of dn/dT with references.

Absorption from the infrared edge of transparency through the region of fundamental lattice vibrations was measured by Slack *et al.* [6] and DeShazer *et al.* [17]. Imaginary-refractive-index values from 840 to 2350 cm^{-1} derived from these measurements are included in Table I.

The fundamental infrared lattice vibrations are studied by Hurrell *et al.* [18], Thirumavalavan *et al.* [19], Gledhill *et al.* [20], and Hofmeister and Campbell [21]. Hurrell *et al.* give the optical irreducible representation as

$$\Gamma = 5A_{1u}(-) + 3A_{1g}(R) + 5A_{2u}(-) + 5A_{2g}(-) + 10E_u(-) + 8E_g(R) + 14F_{1g}(-) + 17F_{1u}(IR) + 14F_{2g}(R) + 16F_{2u}(-) \quad (3)$$

and make the following assignments to the Raman-active modes: A_{1g} vibrations at 373, 561, and 783 cm^{-1}; E_g vibrations at 162, 310, 340, 403, 531, 537, 714, and 758 cm^{-1}; and 11 of 14 F_{2g} modes located at 144, 218, 243, 259, 296, 408, 436, 544, 690, 719, and 857 cm^{-1}. Table IV summarizes measured locations of the infrared-active modes from several sources.

Optical constants in Table I for the region of fundamental lattice vibrations are derived from the models of Gledhill *et al.* [20] and Hofmeister and Campbell [21]. Gledhill *et al.* measured room-temperature reflectivity and fitted the data to a dispersion model of the form

$$n^2(\nu) = \epsilon(\nu) = \epsilon_\infty \sum_j \frac{\nu_{\mathrm{LO}_j}^2 - \nu^2 - i\gamma_{\mathrm{LO}_j}\nu}{\nu_{\mathrm{TO}_j}^2 - \nu^2 - i\gamma_{\mathrm{TO}_j}\nu}, \quad (4)$$

where ν_{TO} and ν_{LO} are the transverse and longitudinal infrared-active optical mode frequencies, γ_{TO} and γ_{LO} are the respective mode widths, and ϵ_∞ the high-frequency (electronic) contribution to the dielectric constant. Hofmeister and Campbell also made reflectivity measurements, preformed a Kramers–Krönig analysis on their data, and fit the resulting optical constants to a Lorentzian (classical) oscillator model of the form

$$n^2(\nu) = \epsilon(\nu) = \epsilon_\infty + \sum_j \frac{f_j \nu_{\mathrm{TO}_j}^2}{\nu_{\mathrm{TO}_j}^2 - \nu^2 - i\gamma_j\nu}, \quad (5)$$

where ν_{TO} is transverse infrared-active optical mode frequency, γ is the mode width, f is the oscillator strength, and ϵ_∞ the high-frequency (electronic) contribution to the dielectric constant. These models were used to calculate the real index between 200 and 2350 cm^{-1} and the imaginary index between 200 and 835 cm^{-1} (or to 1000 cm^{-1} for [21]).

Real refractive index and absorption coefficient below 100 cm^{-1} for Nd-doped YAG were measured by Zhan and Coleman [22] using channeled-spectrum (interference) technique, who also provide a Sellmeier-type dispersion relationship for this regime,

$$n^2 = 9.42 + \frac{0.983\,\nu_0^2}{\nu_0^2 - \nu^2}, \quad (6)$$

where ν is in wave numbers, and ν_0 is the lowest-frequency infrared-active vibration (set to 123 cm^{-1}). In Table I, real-refractive-index values are cal-

culated from this equation, and the imaginary values are derived from the measured absorption coefficient.

The low-frequency (1 MHz) dielectric constant was determined by Shannon *et al.* [23] as $\epsilon = 10.60 \pm 0.05$ (giving $n = 3.26 \pm 0.01$) using a parallel-plate capacitance technique. This value is included in Table I, as well as limiting values from the infrared models of Gledhill *et al.* [20] and Hofmeister and Campbell [21], and the refractive-index model of Zhan and Coleman [22] based on Eq. (6).

Figure 1 shows a composite of the complex refractive index of yttrium aluminum garnet.

ACKNOWLEDGMENT

The author thanks Professor T. Tomiki, University of Ryukyus (retired), for graciously providing digital data from his measurements.

REFERENCES

1. H. S. Yoder and M. L. Keith, Complete substitution of aluminum for silicon: The systems $3MnO \times Al_2O_3 \cdot 3SiO_2 - 3Y_2O_3 \cdot 5Al_2O_3$. *Am. Mineral.* **36**, 519–533 (1951).
2. T. Tomiki, J. Tamashiro, M. Hiraoka, N. Hirata, and T. Futemma, A determination of the spectra of $Y_3Al_5O_{12}$ (YAG)—Reflectivity and intrinsic tail absorptivity in VUV region. *J. Phys. Soc. Jpn.* **57**, 4429–4433 (1988).
3. T. Tomiki, F. Fukudome, M. Kaminao, M. Fujisawa, Y. Tanahara, and T. Futemma, Optical spectra of $Y_3Al_5O_{12}$ (YAG) single crystals in the vacuum ultraviolet region. *J. Phys. Soc. Jpn.* **58**, 1801–1810 (1989).
4. T. Tomiki, Y. Ganaha, T. Shikenbaru, T. Futemma, M. Yuri, Y. Aiura, H. Fukutani, H. Kato, J. Tamashiro, T. Miyahara, and A. Yonesu, Optical spectra of $Y_3Al_5O_{12}$(YAG) single crystals in the vacuum ultraviolet region. II. *J. Phys. Soc. Jpn.* **62**, 1388–1400 (1993).
5. T. Tomiki, Y. Isa, Y. Kadekawa, Y. Ganaha, N. Toyokawa, T. Miyazato, M. Miyazato, T. Kohatsu, H. Shimabukuro, and J. Tamashiro, Optical absorption of single crystals of $Y_3Al_5O_{12}$ and $Y_3Al_5O_{12}$:Nd^{3+} in the UV fundamental absorption edge region. *J. Phys. Soc. Jpn.* **65**, 1106–1113 (1996).
6. G. A. Slack, D. W. Oliver, R. M Chrenko, and S. Roberts, Optical absorption of $Y_3Al_5O_{12}$ from 10− to 55,000 cm^{-1} wave numbers. *Phys. Rev.* **177**, 1308–1314 (1969).
7. W. L. Bond, Measurement of the refractive index of several crystals. *J. Appl. Phys.* **36**, 1674–1677 (1965).
8. O. S. Shchavelev, V. A. Babkina, and Z. S. Mal'tseva, Thermo-optic properties, expansion coefficient and refractive index of yttrium aluminum garnet. *Sov. J. Opt. Technol.* **40**, 623–624 (1973).
9. B. C. McCollum, W. R. Bekebrede, M. Kestigian, and A. B. Smith, Refractive index measurements on magnetic garnet films. *Appl. Phys. Lett.* **23**, 702–703 (1973).
10. K. E. Wilson, Thermo-optics of nonlinear crystals and laser materials. Ph.D. Dissertation, University of Southern California, Los Angeles (January 1980).
11. W. J. Tropf, M. E. Thomas, and T. J. Harris, Properties of crystals and glasses, *in* "Optical Society of America Handbook of Optics" (M. Bass, ed.), 2nd Ed., Chap. 33, McGraw-Hill, New York, 1994.
12. S. H. Wemple and W. J. Tabor, Refractive index behavior of garnets. *J. Appl. Phys.* **44**, 1395–1396 (1973).

13. E. V. Zharikov, Yu. S. Privis, P. A. Studenikin, V. A. Chikov, V. D. Shigorin, and I. A. Shcherbakov, Temperature-wise measurements of refractive indices of rare-earth garnets. *Sov. Phys. Crystallogr.* **34**, 712–714 (1989).
14. J. D. Foster and L. M. Osterink, Index of refraction and expansion thermal coefficients of Nd:YAG. *Appl. Opt.* **7**, 2428–2429 (1968).
15. D. D. Young, K. C. Jungling, T. L. Williamson, and E. R. Nichols, Holographic interferometry measurement of the thermal refractive index coefficient and thermal expansion coefficient of Nd:YAG and Nd:YALO. *IEEE J. Quantum Electon.* **QE-8**, 720–721 (1972).
16. P. R. Stoddart, P. E. Ngoepe, P. M. Mjwara, J. D. Comins, and G. A. Saunders, High-temperature elastic constants of yttrium aluminum garnet. *J. Appl. Phys.* **73**, 7298–7301 (1993).
17. L. G. DeShazer, S. C. Rand, and B. A. Wechsler, Laser crystals, *in* "CRC Handbook of Laser Science and Technology," (M. J. Weber, ed.), Vol. 5. pp. 281–338, CRC Press, Boca Raton, Florida, 1988.
18. J. P. Hurrell, S. P. S. Porto, I. F. Chang, S. S. Mitra, and R. P. Bauman, Optical phonons of yttrium aluminum garnet. *Phys. Rev.* **173**, 851–856 (1968).
19. M. Thirumavalavan, J. Kumar, F. D. Gnanam, and P. Ramasamy, Vibrational spectra of $Y_3Al_5O_{12}$ crystals grown from Ba- and Pb-based Flux systems. *Infrared Phys.* **26**, 101–103 (1986).
20. G. A. Gledhill, P. M. Nikolić, A. Hamilton, S. Stojilković, V. Blagojević, P. Mihajlović, and S. Djurić, FIR optical properties of single crystal $Y_3Al_5O_{12}$ (YAG). *Phys. Status Solidi B* **163**, K123–K128 (1991).
21. A. M. Hofmeister and K. R. Campbell, Infrared Spectroscopy of yttrium aluminum, yttrium gallium, and yttrium iron garnets. *J. Appl. Phys.* **72**, 638–646 (1992).
22. Y. Zhan and P. D. Coleman, Far-IR properties of $Y_3Al_5O_{12}$, $LiYF_4$, $Cs_2NaDyCl_6$, and Rb_2NaYF_6. *Appl. Opt.* **23**, 548–551 (1984).
23. R. D. Shannon, M. A. Subramanian, T. H. Allik, H. Kimura, M. R. Kokta, M. H. Randles, and G. R. Rossman, Dielectric constants of yttrium and rare-earth garnets, the polarizability of gallium oxide, and the oxide additive rule. *J. Appl. Phys.* **67**, 3798–3802 (1990).

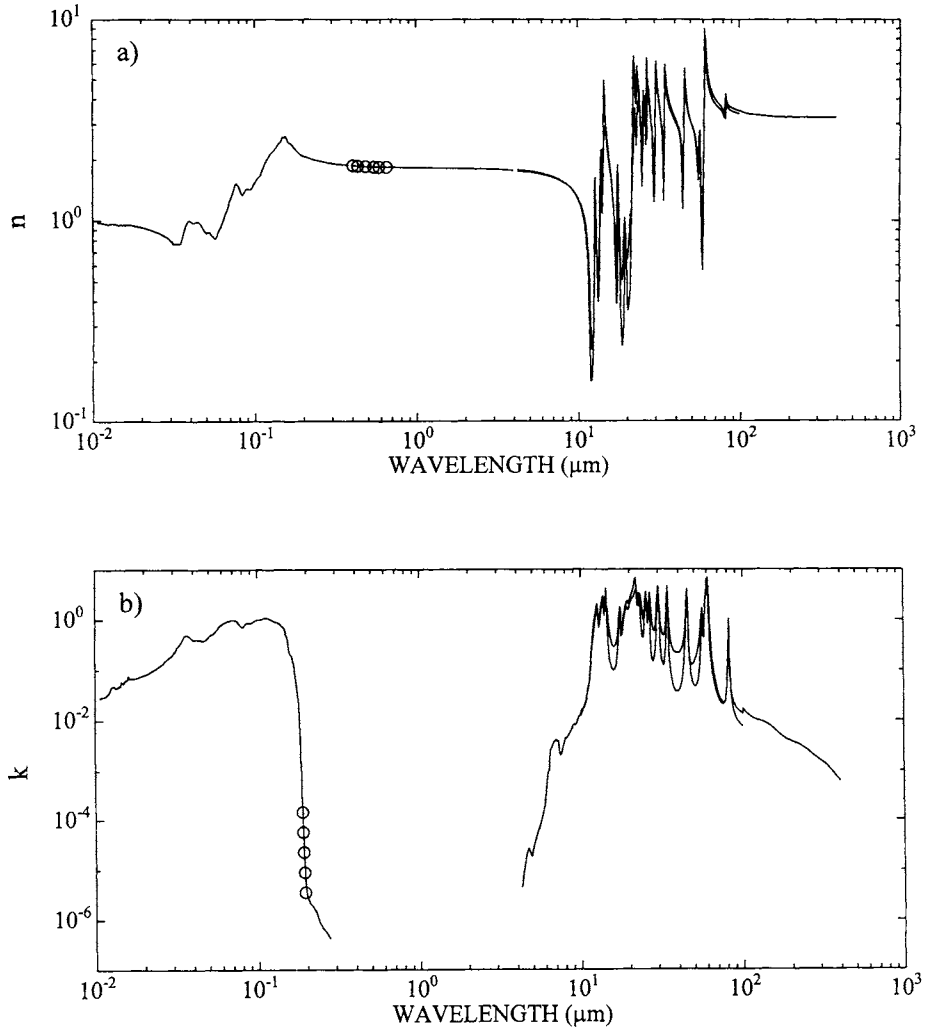

Fig. 1. (a) Log–log plot of the index of refraction n versus wavelength in micrometers for yttrium aluminum garnet. (b) Log–log plot of the extinction coefficient k versus wavelength in micrometers for yttrium aluminum garnet. Lines are data sets of many points; scattered data are indicated by circles.

TABLE I

Values of *n* and *k* for Yttrium Aluminum Garnet (YAG) from Various References

eV	cm^{-1}	μm	*n*	*k*	*n*	*k*
115.982	935451	0.01069	0.978 [4]	0.028 [4]		
114.758	925578	0.01080	0.977	0.028		
113.539	915747	0.01092	0.976	0.028		
112.315	905874	0.01104	0.975	0.029		
111.098	896059	0.01116	0.974	0.029		
109.877	886211	0.01128	0.973	0.029		
108.654	876347	0.01141	0.972	0.029		
107.439	866547	0.01154	0.971	0.030		
106.416	858296	0.01165	0.969	0.030		
105.403	850126	0.01176	0.967	0.030		
104.593	843593	0.01185	0.966	0.032		
103.571	835350	0.01197	0.965	0.033		
102.552	827131	0.01209	0.963	0.033		
101.535	818929	0.01221	0.961	0.035		
100.523	810766	0.01233	0.959	0.038		
99.506	802564	0.01246	0.958	0.041		
98.998	798466	0.01252	0.959	0.043		
98.487	794345	0.01259	0.959	0.044		
97.981	790264	0.01265	0.960	0.046		
97.473	786167	0.01272	0.961	0.046		
96.962	782045	0.01279	0.962	0.047		
96.456	777964	0.01285	0.962	0.047		
95.941	773810	0.01292	0.962	0.047		
95.439	769761	0.01299	0.963	0.048		
94.928	765640	0.01306	0.964	0.049		
94.422	761559	0.01313	0.965	0.049		
93.914	757461	0.01320	0.966	0.048		
93.404	753348	0.01327	0.966	0.047		
92.894	749235	0.01335	0.965	0.046		
92.388	745154	0.01342	0.965	0.045		
91.875	741016	0.01349	0.964	0.044		
91.367	736919	0.01357	0.962	0.044		
90.858	732813	0.01365	0.961	0.044		
90.348	728700	0.01372	0.959	0.045		
89.844	724635	0.01380	0.959	0.046		
89.333	720514	0.01388	0.958	0.046		
88.827	716432	0.01396	0.958	0.047		
88.315	712303	0.01404	0.957	0.048		
87.808	708214	0.01412	0.956	0.049		
87.301	704124	0.01420	0.956	0.048		
86.794	700035	0.01428	0.954	0.048		
86.286	695938	0.01437	0.950	0.048		
85.773	691800	0.01446	0.948	0.054		
85.266	687711	0.01454	0.951	0.059		
84.759	683622	0.01463	0.954	0.058		
84.252	679533	0.01472	0.955	0.058		
83.740	675403	0.01481	0.956	0.056		

(continued)

TABLE I *(Continued)*

Yttrium Aluminum Garnet (YAG)

eV	cm^{-1}	μm	n	k	n	k
83.234	671322	0.01490	0.954	0.055		
82.723	667201	0.01499	0.952	0.055		
82.218	663128	0.01508	0.950	0.056		
81.709	659022	0.01517	0.948	0.058		
81.201	654925	0.01527	0.947	0.061		
80.688	650787	0.01537	0.949	0.064		
80.182	646706	0.01546	0.951	0.065		
79.672	642593	0.01556	0.951	0.064		
79.163	638488	0.01566	0.951	0.064		
78.646	634318	0.01576	0.949	0.063		
78.160	630398	0.01586	0.945	0.068		
77.641	626212	0.01597	0.947	0.074		
77.153	622276	0.01607	0.953	0.076		
76.633	618082	0.01618	0.957	0.072		
76.116	613912	0.01629	0.957	0.069		
75.605	609791	0.01640	0.955	0.068		
75.097	605693	0.01651	0.955	0.068		
74.586	601572	0.01662	0.954	0.068		
74.078	597475	0.01674	0.953	0.068		
73.573	593402	0.01685	0.953	0.067		
73.061	589272	0.01697	0.952	0.068		
72.553	585175	0.01709	0.951	0.068		
71.946	580279	0.01723	0.950	0.068		
71.334	575343	0.01738	0.949	0.068		
70.723	570415	0.01753	0.948	0.069		
70.115	565511	0.01768	0.948	0.069		
69.502	560567	0.01784	0.946	0.069		
68.892	555647	0.01800	0.944	0.070		
68.281	550719	0.01816	0.943	0.071		
67.751	546444	0.01830	0.942	0.072		
67.150	541597	0.01846	0.941	0.072		
66.849	539169	0.01855	0.940	0.073		
66.249	534330	0.01872	0.939	0.073		
65.649	529491	0.01889	0.938	0.075		
65.050	524659	0.01906	0.936	0.076		
64.451	519828	0.01924	0.935	0.076		
63.851	514989	0.01942	0.934	0.078		
63.251	510150	0.01960	0.933	0.078		
62.650	505302	0.01979	0.932	0.078		
62.048	500447	0.01998	0.929	0.080		
61.449	495616	0.02018	0.928	0.081		
60.849	490776	0.02038	0.926	0.083		
60.251	485953	0.02058	0.926	0.082		
59.648	481090	0.02079	0.921	0.083		
59.049	476259	0.02100	0.919	0.086		
58.450	471427	0.02121	0.917	0.088		
57.850	466588	0.02143	0.916	0.088		

TABLE I *(Continued)*

Yttrium Aluminum Garnet (YAG)

eV	cm^{-1}	μm	n	k	n	k
57.249	461741	0.02166	0.913	0.090		
56.650	456909	0.02189	0.911	0.092		
56.049	452062	0.02212	0.909	0.094		
55.450	447231	0.02236	0.906	0.096		
54.851	442400	0.02260	0.904	0.098		
54.251	437560	0.02285	0.901	0.100		
53.650	432713	0.02311	0.898	0.101		
53.051	427882	0.02337	0.895	0.104		
52.449	423026	0.02364	0.893	0.106		
51.851	418203	0.02391	0.889	0.109		
51.250	413356	0.02419	0.886	0.112		
50.650	408517	0.02448	0.882	0.116		
50.051	403685	0.02477	0.879	0.118		
49.450	398838	0.02507	0.875	0.122		
48.850	393999	0.02538	0.871	0.126		
48.251	389167	0.02570	0.867	0.129		
47.650	384320	0.02602	0.863	0.133		
47.050	379481	0.02635	0.859	0.138		
46.450	374642	0.02669	0.854	0.143		
45.849	369794	0.02704	0.849	0.148		
45.250	364963	0.02740	0.844	0.153		
44.650	360124	0.02777	0.838	0.160		
44.051	355292	0.02815	0.834	0.167		
43.450	350445	0.02854	0.829	0.173		
42.850	345606	0.02893	0.823	0.181		
42.249	340758	0.02935	0.818	0.188		
41.650	335927	0.02977	0.808	0.190		
41.051	331096	0.03020	0.793	0.207		
40.449	326241	0.03065	0.790	0.228		
39.850	321409	0.03111	0.773	0.230		
39.249	316562	0.03159	0.768	0.264		
38.650	311731	0.03208	0.772	0.285		
38.050	306892	0.03258	0.772	0.303		
37.450	302052	0.03311	0.770	0.323		
36.850	297213	0.03365	0.765	0.349		
36.250	292374	0.03420	0.765	0.383		
35.650	287534	0.03478	0.775	0.424		
35.050	282695	0.03537	0.808	0.468		
34.450	277856	0.03599	0.854	0.491		
33.850	273016	0.03663	0.900	0.498		
33.250	268177	0.03729	0.942	0.487		
32.650	263338	0.03797	0.970	0.471		
32.050	258499	0.03868	0.992	0.451		
31.450	253659	0.03942	1.000	0.421		
30.850	248820	0.04019	0.991	0.401		
30.250	243981	0.04099	0.978	0.401		
29.650	239141	0.04182	0.973	0.405		

(continued)

TABLE I *(Continued)*

Yttrium Aluminum Garnet (YAG)

eV	cm^{-1}	μm	n	k	n	k
28.960	233576	0.04281	0.977	0.407		
28.302	228269	0.04381	0.982	0.408		
27.673	223196	0.04480	0.981	0.393		
27.072	218349	0.04580	0.964	0.381		
26.496	213703	0.04679	0.938	0.383		
25.944	209251	0.04779	0.913	0.394		
25.414	204976	0.04879	0.889	0.414		
24.906	200879	0.04978	0.872	0.447		
24.418	196943	0.05078	0.870	0.483		
23.948	193152	0.05177	0.877	0.501		
23.496	189507	0.05277	0.869	0.511		
23.061	185998	0.05376	0.852	0.534		
22.642	182619	0.05476	0.838	0.566		
22.238	179360	0.05575	0.826	0.604		
21.847	176207	0.05675	0.820	0.651		
21.471	173174	0.05775	0.825	0.712		
21.107	170238	0.05874	0.857	0.765		
20.755	167399	0.05974	0.894	0.795		
20.415	164657	0.06073	0.915	0.819		
20.085	161995	0.06173	0.940	0.854		
19.767	159430	0.06272	0.972	0.882		
19.611	158172	0.06322	0.988	0.895		
19.458	156938	0.06372	1.005	0.909		
19.307	155720	0.06422	1.025	0.922		
19.158	154518	0.06472	1.045	0.930		
19.012	153341	0.06521	1.064	0.937		
18.868	152179	0.06571	1.082	0.943		
18.726	151034	0.06621	1.099	0.948		
18.587	149913	0.06671	1.114	0.952		
18.449	148800	0.06720	1.126	0.960		
18.313	147703	0.06770	1.142	0.971		
18.180	146630	0.06820	1.161	0.980		
18.048	145566	0.06870	1.181	0.990		
17.918	144517	0.06920	1.205	0.997		
17.790	143485	0.06969	1.230	0.999		
17.664	142469	0.07019	1.254	1.000		
17.540	141469	0.07069	1.277	0.995		
17.417	140476	0.07119	1.295	0.992		
17.296	139501	0.07168	1.313	0.989		
17.177	138541	0.07218	1.331	0.987		
17.059	137589	0.07268	1.350	0.986		
16.943	136653	0.07318	1.372	0.986		
16.828	135726	0.07368	1.399	0.984		
16.715	134814	0.07418	1.427	0.974		
16.604	133919	0.07467	1.455	0.959		
16.494	133032	0.07517	1.481	0.938		
16.385	132153	0.07567	1.499	0.907		

TABLE I *(Continued)*

Yttrium Aluminum Garnet (YAG)

eV	cm^{-1}	μm	n	k	n	k
16.279	131298	0.07616	1.511	0.882		
16.173	130443	0.07666	1.518	0.851		
16.068	129596	0.07716	1.518	0.821		
15.965	128765	0.07766	1.510	0.793		
15.864	127951	0.07816	1.498	0.775		
15.763	127136	0.07866	1.487	0.759		
15.664	126338	0.07915	1.474	0.744		
15.566	125547	0.07965	1.461	0.734		
15.470	124773	0.08015	1.446	0.723		
15.374	123999	0.08065	1.429	0.716		
15.280	123241	0.08114	1.408	0.713		
15.187	122490	0.08164	1.384	0.715		
15.095	121748	0.08214	1.364	0.729		
15.004	121014	0.08263	1.351	0.745		
14.914	120289	0.08313	1.342	0.763		
14.825	119571	0.08363	1.337	0.783		
14.737	118861	0.08413	1.338	0.803		
14.651	118167	0.08463	1.344	0.821		
14.565	117474	0.08513	1.353	0.837		
14.480	116788	0.08563	1.364	0.847		
14.396	116111	0.08612	1.375	0.855		
14.314	115449	0.08662	1.386	0.861		
14.232	114788	0.08712	1.397	0.866		
14.151	114135	0.08762	1.407	0.867		
14.071	113489	0.08811	1.416	0.868		
13.992	112852	0.08861	1.426	0.867		
13.914	112223	0.08911	1.431	0.863		
13.837	111602	0.08960	1.435	0.861		
13.760	110981	0.09011	1.435	0.857		
13.685	110376	0.09060	1.433	0.857		
13.610	109771	0.09110	1.431	0.858		
13.536	109174	0.09160	1.428	0.862		
13.463	108586	0.09209	1.426	0.868		
13.390	107997	0.09260	1.424	0.876		
13.319	107424	0.09309	1.423	0.885		
13.248	106851	0.09359	1.423	0.894		
13.178	106287	0.09408	1.424	0.906		
13.109	105730	0.09458	1.428	0.918		
13.040	105174	0.09508	1.433	0.929		
12.972	104625	0.09558	1.438	0.941		
12.905	104085	0.09608	1.447	0.955		
12.838	103545	0.09658	1.459	0.965		
12.772	103012	0.09708	1.469	0.973		
12.707	102488	0.09757	1.480	0.982		
12.643	101972	0.09807	1.492	0.990		
12.579	101456	0.09857	1.505	0.997		
12.516	100948	0.09906	1.518	1.001		

(continued)

TABLE I *(Continued)*

Yttrium Aluminum Garnet (YAG)

eV	cm^{-1}	μm	n	k	n	k
12.453	100439	0.0996	1.531	1.005		
12.391	99939.4	0.1001	1.543	1.007		
12.330	99447.4	0.1006	1.554	1.010		
12.269	98955.4	0.1011	1.565	1.011		
12.209	98471.4	0.1016	1.576	1.013		
12.149	97987.5	0.1021	1.585	1.012		
12.090	97511.7	0.1026	1.592	1.013		
12.032	97043.9	0.1030	1.600	1.016		
11.974	96576.1	0.1035	1.611	1.019		
11.917	96116.3	0.1040	1.616	1.014		
11.860	95656.6	0.1045	1.621	1.021		
11.804	95204.9	0.1050	1.627	1.022		
11.748	94753.3	0.1055	1.632	1.028		
11.719	94519.4	0.1058	1.636	1.031		
11.609	93632.2	0.1068	1.648	1.038		
11.502	92769.2	0.1078	1.658	1.058		
11.462	92446.5	0.1082	1.668	1.070		
11.356	91591.6	0.1092	1.702	1.085		
11.252	90752.8	0.1102	1.733	1.093		
11.150	89930.1	0.1112	1.763	1.102		
11.050	89123.6	0.1122	1.800	1.109		
10.952	88333.1	0.1132	1.835	1.105		
10.856	87558.9	0.1142	1.871	1.103		
10.761	86792.6	0.1152	1.903	1.090		
10.668	86042.5	0.1162	1.929	1.080		
10.576	85300.5	0.1172	1.954	1.071		
10.486	84574.6	0.1182	1.983	1.061		
10.398	83864.9	0.1192	2.004	1.044		
10.311	83163.2	0.1202	2.023	1.035		
10.225	82469.5	0.1213	2.044	1.027		
10.141	81792.0	0.1223	2.073	1.019		
10.058	81122.6	0.1233	2.094	0.998		
9.977	80469.3	0.1243	2.113	0.984		
9.897	79824.1	0.1253	2.126	0.967		
9.818	79186.9	0.1263	2.145	0.959		
9.740	78557.8	0.1273	2.160	0.941		
9.664	77944.8	0.1283	2.169	0.929		
9.589	77339.9	0.1293	2.189	0.926		
9.515	76743.0	0.1303	2.204	0.910		
9.442	76154.3	0.1313	2.213	0.901		
9.370	75573.5	0.1323	2.240	0.901		
9.299	75000.9	0.1333	2.257	0.882		
9.229	74436.3	0.1343	2.277	0.873		
9.161	73887.9	0.1353	2.294	0.856		
9.093	73339.4	0.1364	2.307	0.845		
9.027	72807.1	0.1373	2.336	0.838		
8.961	72274.8	0.1384	2.352	0.815		

TABLE I *(Continued)*

Yttrium Aluminum Garnet (YAG)

eV	cm^{-1}	μm	n	k	n	k
8.896	71750.5	0.1394	2.371	0.803		
8.833	71242.4	0.1404	2.399	0.785		
8.770	70734.3	0.1414	2.411	0.754		
8.708	70234.2	0.1424	2.412	0.739		
8.647	69742.2	0.1434	2.440	0.734		
8.586	69250.2	0.1444	2.446	0.715		
8.527	68774.3	0.1454	2.486	0.717		
8.468	68298.5	0.1464	2.522	0.687		
8.410	67830.7	0.1474	2.578	0.640		
8.391	67677.4	0.1478	2.578	0.613		
8.334	67217.7	0.1488	2.583	0.567		
8.279	66774.1	0.1498	2.581	0.522		
8.224	66330.5	0.1508	2.574	0.487		
8.169	65886.9	0.1518	2.577	0.460		
8.116	65459.4	0.1528	2.585	0.428		
8.063	65032.0	0.1538	2.593	0.387		
8.010	64604.5	0.1548	2.598	0.331		
7.959	64193.2	0.1558	2.565	0.275		
7.908	63781.8	0.1568	2.533	0.242		
7.858	63378.5	0.1578	2.497	0.219		
7.808	62975.3	0.1588	2.467	0.209		
7.759	62580.1	0.1598	2.444	0.206		
7.710	62184.9	0.1608	2.433	0.202		
7.663	61805.8	0.1618	2.421	0.195		
7.615	61418.6	0.1628	2.415	0.190		
7.569	61047.6	0.1638	2.412	0.180		
7.523	60676.6	0.1648	2.409	0.165		
7.477	60305.6	0.1658	2.402	0.149		
7.432	59942.6	0.1668	2.396	0.133		
7.388	59587.8	0.1678	2.386	0.115		
7.344	59232.9	0.1688	2.373	0.0974		
7.301	58886.1	0.1698	2.356	0.0838		
7.258	58539.3	0.1708	2.342	0.0726		
7.215	58192.4	0.1718	2.326	0.0630		
7.173	57853.7	0.1728	2.313	0.0549		
7.132	57523.0	0.1738	2.298	0.0479		
7.091	57192.3	0.1748	2.285	0.0431		
7.051	56869.7	0.1758	2.275	0.0369		
7.011	56547.1	0.1768	2.261	0.0318		
6.971	56224.5	0.1779	2.252	0.0271		
6.932	55909.9	0.1789	2.241	0.0205		
6.893	55595.4	0.1799	2.228	0.0159		
6.855	55288.9	0.1809	2.217	0.0129		
6.817	54982.4	0.1819	2.208	0.00806		
6.780	54684.0	0.1829	2.195	0.00406		
6.743	54385.5	0.1839	2.183	0.00204		0.0020 [6]
6.600	53232.2	0.1879		1.44E-4 [5]		1.51E-4

(continued)

TABLE I *(Continued)*

Yttrium Aluminum Garnet (YAG)

eV	cm^{-1}	μm	n	k	n	k
6.550	52828.9	0.1893		5.71E-5		6.25E-5
6.500	52425.6	0.1907	2.120	2.26E-5		2.78E-5
6.450	52022.3	0.1922		8.96E-6		1.37E-5
6.400	51619.1	0.1937		3.55E-6		6.01E-6
6.250	50409.3	0.1984	2.088			3.03E-6
6.000	48392.9	0.2066	2.059			2.18E-6
5.750	46376.5	0.2156	2.033			1.84E-6
5.500	44360.1	0.2254	2.009			1.44E-6
5.250	42343.8	0.2362	1.987			9.06E-7
5.000	40327.4	0.2480	1.968			6.85E-7
4.750	38311.0	0.2610	1.950			5.67E-7
4.500	36294.7	0.2755	1.933			4.23E-7
4.250	34278.3	0.2917	1.918			
4.000	32261.9	0.3100	1.905			
3.750	30245.6	0.3306	1.892			
3.500	28229.2	0.3542	1.881			
3.250	26212.8	0.3815	1.871			
3.0996	25000	0.4000	1.8650 [7]			
3.0614	24691.4	0.4050			1.85977 [8]	
2.8568	23041.5	0.4340			1.85282	
2.8437	22935.8	0.4360			1.85246	
2.7552	22222.2	0.4500	1.8532			
2.5511	20576.1	0.4860			1.84367	
2.4797	20000	0.5000	1.8450			
2.11	17018.4	0.5876			1.83260	
2.105	16977.9	0.5890			1.83247	
2.0664	16666.7	0.6000	1.8347			
1.89	15243.9	0.6560			1.82785	
1.7712	14285.7	0.70	1.8285			
1.5498	12500	0.80	1.8245			
1.3776	11111.1	0.90	1.8222			
1.2399	10000	1.00	1.8197			
1.1271	9090.9	1.10	1.8170			
1.0332	8333.3	1.20	1.8152			
0.8856	7142.9	1.40	1.8121			
0.7749	6250.0	1.60	1.8093			
0.6888	5555.6	1.80	1.8065			
0.6199	5000.0	2.00	1.8035			
0.5636	4545.5	2.20	1.8004			
0.5166	4166.7	2.40	1.7970			
0.4769	3846.2	2.60	1.7935			
0.4428	3571.4	2.80	1.7896			
0.4133	3333.3	3.00	1.7855			
0.3875	3125.0	3.20	1.7810			
0.3647	2941.2	3.40	1.7764			
0.3444	2777.8	3.60	1.7713			
0.3263	2631.6	3.80	1.7659			

TABLE I *(Continued)*

Yttrium Aluminum Garnet (YAG)

eV	cm^{-1}	μm	n	k	n	k
0.3100	2500.0	4.00	1.7602			
0.2914	2350.0	4.2553	1.76 [20]	4.51E-6 [6]	1.77 [21]	
0.2901	2340.0	4.2735	1.75	4.97E-6	1.77	
0.2889	2330.0	4.2918	1.75	5.63E-6	1.77	
0.2876	2320.0	4.3103	1.75	6.30E-6	1.77	
0.2864	2310.0	4.3290	1.75	6.99E-6	1.77	
0.2852	2300.0	4.3478	1.75	7.76E-6	1.77	
0.2839	2290.0	4.3668	1.75	8.63E-6	1.77	
0.2827	2280.0	4.3860	1.75	9.55E-6	1.77	
0.2814	2270.0	4.4053	1.75	1.05E-5	1.77	
0.2802	2260.0	4.4248	1.75	1.13E-5	1.77	
0.2790	2250.0	4.4444	1.75	1.23E-5	1.77	
0.2777	2240.0	4.4643	1.75	1.33E-5	1.77	
0.2765	2230.0	4.4843	1.75	1.45E-5	1.76	
0.2752	2220.0	4.5045	1.75	1.58E-5	1.76	
0.2740	2210.0	4.5249	1.75	1.70E-5	1.76	
0.2728	2200.0	4.5455	1.75	1.83E-5	1.76	
0.2715	2190.0	4.5662	1.75	1.95E-5	1.76	
0.2703	2180.0	4.5872	1.75	2.09E-5	1.76	
0.2690	2170.0	4.6083	1.74	2.23E-5	1.76	
0.2678	2160.0	4.6296	1.74	2.35E-5	1.76	
0.2666	2150.0	4.6512	1.74	2.46E-5	1.76	
0.2653	2140.0	4.6729	1.74	2.56E-5	1.76	
0.2641	2130.0	4.6948	1.74	2.65E-5	1.76	
0.2628	2120.0	4.7170	1.74	2.64E-5	1.76	
0.2616	2110.0	4.7393	1.74	2.59E-5	1.76	
0.2604	2100.0	4.7619	1.74	2.50E-5	1.76	
0.2591	2090.0	4.7847	1.74	2.38E-5	1.75	
0.2579	2080.0	4.8077	1.74	2.28E-5	1.75	
0.2566	2070.0	4.8309	1.74	2.19E-5	1.75	
0.2554	2060.0	4.8544	1.74	2.10E-5	1.75	
0.2542	2050.0	4.8780	1.74	2.01E-5	1.75	
0.2529	2040.0	4.9020	1.73	1.89E-5	1.75	
0.2517	2030.0	4.9261	1.73	1.89E-5	1.75	
0.2505	2020.0	4.9505	1.73	2.02E-5	1.75	
0.2492	2010.0	4.9751	1.73	2.24E-5	1.75	
0.2480	2000.0	5.0000	1.73	2.45E-5	1.75	
0.2467	1990.0	5.0251	1.73	2.64E-5	1.75	
0.2455	1980.0	5.0505	1.73	2.84E-5	1.74	
0.2443	1970.0	5.0761	1.73	3.08E-5	1.74	
0.2430	1960.0	5.1020	1.73	3.30E-5	1.74	
0.2418	1950.0	5.1282	1.73	3.51E-5	1.74	
0.2405	1940.0	5.1546	1.72	3.71E-5	1.74	
0.2393	1930.0	5.1813	1.72	3.91E-5	1.74	
0.2381	1920.0	5.2083	1.72	4.11E-5	1.74	
0.2368	1910.0	5.2356	1.72	4.30E-5	1.74	
0.2356	1900.0	5.2632	1.72	4.49E-5	1.74	

(continued)

TABLE I *(Continued)*

Yttrium Aluminum Garnet (YAG)

eV	cm^{-1}	μm	n	k	n	k
0.2343	1890.0	5.2910	1.72	4.74E-5	1.74	
0.2331	1880.0	5.3191	1.72	5.02E-5	1.73	
0.2319	1870.0	5.3476	1.72	5.29E-5	1.73	
0.2306	1860.0	5.3763	1.72	5.62E-5	1.73	
0.2294	1850.0	5.4054	1.71	5.97E-5	1.73	
0.2281	1840.0	5.4348	1.71	6.30E-5	1.73	
0.2269	1830.0	5.4645	1.71	6.63E-5	1.73	
0.2257	1820.0	5.4945	1.71	6.99E-5	1.73	
0.2244	1810.0	5.5249	1.71	7.38E-5	1.72	
0.2232	1800.0	5.5556	1.71	7.77E-5	1.72	
0.2219	1790.0	5.5866	1.71	8.31E-5	1.72	
0.2207	1780.0	5.6180	1.71	8.85E-5	1.72	
0.2195	1770.0	5.6497	1.70	9.53E-5	1.72	
0.2182	1760.0	5.6818	1.70	1.02E-4	1.72	
0.2170	1750.0	5.7143	1.70	1.10E-4	1.72	
0.2157	1740.0	5.7471	1.70	1.19E-4	1.71	
0.2145	1730.0	5.7803	1.70	1.29E-4	1.71	
0.2133	1720.0	5.8140	1.70	1.40E-4	1.71	
0.2120	1710.0	5.8480	1.70	1.53E-4	1.71	
0.2108	1700.0	5.8824	1.69	1.70E-4	1.71	
0.2095	1690.0	5.9172	1.69	1.79E-4	1.71	
0.2083	1680.0	5.9524	1.69	1.88E-4	1.70	
0.2071	1670.0	5.9880	1.69	2.16E-4	1.70	
0.2058	1660.0	6.0241	1.69	2.55E-4	1.70	
0.2046	1650.0	6.0606	1.68	3.34E-4	1.70	
0.2033	1640.0	6.0976	1.68	4.65E-4	1.70	
0.2021	1630.0	6.1350	1.68	6.05E-4	1.70	
0.2009	1620.0	6.1728	1.68	7.27E-4	1.69	
0.1996	1610.0	6.2112	1.68	8.56E-4	1.69	
0.1984	1600.0	6.2500	1.68	9.51E-4	1.69	
0.1971	1590.0	6.2893	1.67	9.84E-4	1.69	
0.1959	1580.0	6.3291	1.67	1.01E-3	1.68	
0.1947	1570.0	6.3694	1.67	1.18E-3	1.68	
0.1934	1560.0	6.4103	1.67	1.64E-3	1.68	
0.1922	1550.0	6.4516	1.66	2.09E-3	1.68	
0.1909	1540.0	6.4935	1.66	2.54E-3	1.68	
0.1897	1530.0	6.5359	1.66	2.75E-3	1.67	
0.1885	1520.0	6.5789	1.66	2.82E-3	1.67	
0.1872	1510.0	6.6225	1.65	2.87E-3	1.67	
0.1860	1500.0	6.6667	1.65	3.15E-3	1.66	
0.1847	1490.0	6.7114	1.65	3.33E-3	1.66	
0.1835	1480.0	6.7568	1.65	3.49E-3	1.66	
0.1823	1470.0	6.8027	1.64	3.66E-3	1.66	
0.1810	1460.0	6.8493	1.64	3.88E-3	1.65	
0.1798	1450.0	6.8966	1.64	3.97E-3	1.65	
0.1785	1440.0	6.9444	1.64	3.94E-3	1.65	
0.1773	1430.0	6.9930	1.63	4.02E-3	1.64	

TABLE I *(Continued)*

Yttrium Aluminum Garnet (YAG)

eV	cm^{-1}	μm	n	k	n	k
0.1761	1420.0	7.0423	1.63	3.84E-3	1.64	
0.1748	1410.0	7.0922	1.63	3.83E-3	1.64	
0.1736	1400.0	7.1429	1.62	3.89E-3	1.63	
0.1723	1390.0	7.1942	1.62	3.94E-3	1.63	
0.1711	1380.0	7.2464	1.61	3.88E-3	1.63	
0.1699	1370.0	7.2993	1.61	3.50E-3	1.62	
0.1686	1360.0	7.3529	1.61	2.47E-3	1.62	
0.1674	1350.0	7.4074	1.60	2.18E-3	1.61	
0.1661	1340.0	7.4627	1.60	2.07E-3	1.61	
0.1649	1330.0	7.5188	1.60	2.10E-3	1.60	
0.1637	1320.0	7.5758	1.59	2.18E-3	1.60	
0.1624	1310.0	7.6336	1.59	2.28E-3	1.60	
0.1612	1300.0	7.6923	1.58	2.72E-3	1.59	
0.1599	1290.0	7.7519	1.58	2.96E-3	1.59	
0.1587	1280.0	7.8125	1.57	3.21E-3	1.58	
0.1575	1270.0	7.8740	1.57	3.58E-3	1.57	
0.1562	1260.0	7.9365	1.56	4.07E-3	1.57	
0.1550	1250.0	8.0000	1.56	4.43E-3	1.56	
0.1537	1240.0	8.0645	1.55	4.49E-3	1.56	
0.1525	1230.0	8.1301	1.54	4.41E-3	1.55	
0.1513	1220.0	8.1967	1.54	4.48E-3	1.54	
0.1500	1210.0	8.2645	1.53	4.74E-3	1.54	
0.1488	1200.0	8.3333	1.53	4.99E-3	1.53	
0.1475	1190.0	8.4034	1.52	5.25E-3	1.52	
0.1463	1180.0	8.4746	1.51	5.51E-3	1.52	
0.1451	1170.0	8.5470	1.50	5.80E-3	1.51	
0.1438	1160.0	8.6207	1.50	6.17E-3	1.50	
0.1426	1150.0	8.6957	1.49	6.51E-3	1.49	
0.1413	1140.0	8.7719	1.48	6.90E-3	1.48	
0.1401	1130.0	8.8496	1.47	7.31E-3	1.47	
0.1389	1120.0	8.9286	1.46	7.69E-3	1.46	
0.1376	1110.0	9.0090	1.45	8.04E-3	1.45	
0.1364	1100.0	9.0909	1.44	8.22E-3	1.44	
0.1351	1090.0	9.1743	1.43	8.02E-3	1.43	
0.1339	1080.0	9.2593	1.42	7.98E-3	1.41	
0.1327	1070.0	9.3458	1.41	8.18E-3	1.40	
0.1314	1060.0	9.4340	1.39	8.88E-3	1.39	
0.1302	1050.0	9.5238	1.38	9.72E-3	1.37	
0.1289	1040.0	9.6154	1.36	0.0105	1.36	
0.1277	1030.0	9.7087	1.35	0.0116	1.34	
0.1265	1020.0	9.8039	1.33	0.0120	1.32	
0.1252	1010.0	9.9010	1.31	0.0125	1.30	
0.1240	1000.0	10.000	1.30	0.0142	1.28	0.0122 [20]
0.1234	995.0	10.050	1.29	0.0148	1.27	0.0127
0.1227	990.0	10.101	1.28	0.0157	1.26	0.0133
0.1221	985.0	10.152	1.26	0.0161	1.24	0.0139
0.1215	980.0	10.204	1.25	0.0166	1.23	0.0146

(continued)

TABLE I *(Continued)*

Yttrium Aluminum Garnet (YAG)

eV	cm^{-1}	μm	n	k	n	k
0.1209	975.0	10.256	1.24	0.0171	1.22	0.0153
0.1203	970.0	10.309	1.23	0.0171	1.20	0.0160
0.1196	965.0	10.363	1.22	0.0172	1.19	0.0169
0.1190	960.0	10.417	1.20	0.0174	1.18	0.0178
0.1184	955.0	10.471	1.19	0.0182	1.16	0.0188
0.1178	950.0	10.526	1.17	0.0187	1.14	0.0198
0.1172	945.0	10.582	1.16	0.0196	1.12	0.0210
0.1165	940.0	10.638	1.14	0.0206	1.11	0.0223
0.1159	935.0	10.695	1.13	0.0216	1.09	0.0238
0.1153	930.0	10.753	1.11	0.0225	1.07	0.0254
0.1147	925.0	10.811	1.09	0.0242	1.04	0.0272
0.1141	920.0	10.870	1.07	0.0259	1.02	0.0293
0.1134	915.0	10.929	1.05	0.0285	0.99	0.0316
0.1128	910.0	10.989	1.03	0.0384	0.97	0.0343
0.1122	905.0	11.050	1.00	0.0427	0.94	0.0374
0.1116	900.0	11.111	0.97	0.0462	0.90	0.0410
0.1110	895.0	11.173	0.95	0.0492	0.87	0.0453
0.1103	890.0	11.236	0.92	0.0528	0.83	0.0505
0.1097	885.0	11.299	0.88	0.0571	0.79	0.0568
0.1091	880.0	11.364	0.85	0.0637	0.74	0.0648
0.1085	875.0	11.429	0.80	0.0938	0.68	0.0752
0.1079	870.0	11.494	0.76	0.116	0.62	0.0894
0.1072	865.0	11.561	0.71	0.158	0.55	0.110
0.1066	860.0	11.628	0.65	0.216	0.46	0.143
0.1060	855.0	11.696	0.58	0.250	0.35	0.204
0.1054	850.0	11.765	0.50	0.298	0.25	0.313
0.1048	845.0	11.834	0.41	0.353	0.20	0.446
0.1041	840.0	11.905	0.32	0.413	0.17	0.574
0.1035	835.0	11.976	0.27	0.419 [19]	0.16	0.694
0.1029	830.0	12.048	0.24	0.546	0.16	0.810
0.1023	825.0	12.121	0.23	0.668	0.16	0.926
0.1017	820.0	12.195	0.23	0.788	0.18	1.05
0.1010	815.0	12.270	0.25	0.909	0.20	1.17
0.1004	810.0	12.346	0.27	1.04	0.23	1.31
0.0998	805.0	12.422	0.32	1.17	0.28	1.47
0.0992	800.0	12.500	0.39	1.32	0.37	1.66
0.0986	795.0	12.579	0.51	1.49	0.56	1.87
0.0979	790.0	12.658	0.74	1.65	0.93	2.05
0.0973	785.0	12.739	1.14	1.67	1.50	1.85
0.0967	780.0	12.821	1.47	1.30	1.62	1.24
0.0961	775.0	12.903	1.34	0.864	1.31	0.879
0.0955	770.0	12.987	1.02	0.704	0.94	0.808
0.0948	765.0	13.072	0.72	0.775	0.64	0.945
0.0942	760.0	13.158	0.54	0.984	0.47	1.18
0.0936	755.0	13.245	0.48	1.22	0.41	1.43
0.0930	750.0	13.333	0.49	1.44	0.40	1.67
0.0924	745.0	13.423	0.55	1.66	0.44	1.92

TABLE I *(Continued)*

Yttrium Aluminum Garnet (YAG)

eV	cm^{-1}	μm	n	k	n	k
0.0917	740.0	13.514	0.67	1.88	0.53	2.19
0.0911	735.0	13.605	0.88	2.09	0.71	2.48
0.0905	730.0	13.699	1.24	2.24	1.03	2.78
0.0899	725.0	13.793	1.73	2.11	1.60	2.94
0.0893	720.0	13.889	1.91	1.57	2.22	2.58
0.0886	715.0	13.986	1.52	1.24	2.25	1.94
0.0880	710.0	14.085	1.10	1.49	1.77	1.71
0.0874	705.0	14.184	1.09	1.98	1.31	2.11
0.0868	700.0	14.286	1.44	2.39	1.35	3.03
0.0862	695.0	14.388	2.04	2.53	2.60	4.17
0.0855	690.0	14.493	2.63	2.26	4.93	2.70
0.0849	685.0	14.599	2.92	1.75	4.31	1.00
0.0843	680.0	14.706	2.92	1.29	3.65	0.520
0.0837	675.0	14.815	2.80	0.973	3.22	0.337
0.0831	670.0	14.925	2.65	0.762	2.92	0.247
0.0825	665.0	15.038	2.50	0.619	2.70	0.195
0.0818	660.0	15.152	2.37	0.519	2.52	0.162
0.0812	655.0	15.267	2.25	0.448	2.36	0.140
0.0806	650.0	15.385	2.13	0.396	2.23	0.125
0.0800	645.0	15.504	2.03	0.358	2.11	0.114
0.0794	640.0	15.625	1.93	0.329	2.01	0.106
0.0787	635.0	15.748	1.84	0.309	1.90	0.101
0.0781	630.0	15.873	1.75	0.295	1.80	0.0983
0.0775	625.0	16.000	1.66	0.286	1.71	0.0974
0.0769	620.0	16.129	1.57	0.284	1.61	0.0986
0.0763	615.0	16.260	1.48	0.287	1.51	0.102
0.0756	610.0	16.393	1.38	0.297	1.40	0.108
0.0750	605.0	16.529	1.27	0.316	1.28	0.119
0.0744	600.0	16.667	1.15	0.350	1.15	0.136
0.0738	595.0	16.807	1.02	0.409	1.00	0.165
0.0732	590.0	16.949	0.87	0.515	0.81	0.224
0.0725	585.0	17.094	0.72	0.712	0.56	0.374
0.0719	580.0	17.241	0.65	1.030	0.39	0.701
0.0713	575.0	17.391	0.79	1.485	0.39	1.09
0.0707	570.0	17.544	1.66	1.744	0.62	1.55
0.0701	565.0	17.699	1.87	0.739	1.53	1.59
0.0694	560.0	17.857	1.40	0.471	1.46	0.678
0.0688	555.0	18.018	1.06	0.486	0.93	0.501
0.0682	550.0	18.182	0.80	0.613	0.51	0.672
0.0676	545.0	18.349	0.62	0.816	0.32	0.984
0.0670	540.0	18.519	0.54	1.04	0.26	1.25
0.0663	535.0	18.692	0.51	1.26	0.24	1.49
0.0657	530.0	18.868	0.54	1.47	0.26	1.71
0.0651	525.0	19.048	0.63	1.68	0.30	1.94
0.0645	520.0	19.231	0.84	1.81	0.40	2.17
0.0639	515.0	19.417	1.03	1.69	0.62	2.38
0.0632	510.0	19.608	0.91	1.56	0.92	2.31

(continued)

TABLE I *(Continued)*

Yttrium Aluminum Garnet (YAG)

eV	cm^{-1}	μm	n	k	n	k
0.0626	505.0	19.802	0.74	1.66	0.81	2.07
0.0620	500.0	20.000	0.66	1.85	0.53	2.19
0.0614	495.0	20.202	0.65	2.05	0.39	2.49
0.0608	490.0	20.408	0.68	2.26	0.36	2.81
0.0601	485.0	20.619	0.75	2.47	0.38	3.16
0.0595	480.0	20.833	0.87	2.67	0.43	3.55
0.0589	475.0	21.053	1.07	2.81	0.55	4.02
0.0583	470.0	21.277	1.08	2.88	0.76	4.63
0.0577	465.0	21.505	1.15	3.23	1.20	5.45
0.0570	460.0	21.739	1.46	3.60	2.32	6.55
0.0564	455.0	21.978	2.01	3.89	5.27	6.72
0.0558	450.0	22.222	2.90	3.87	6.56	3.52
0.0552	445.0	22.472	3.59	2.93	5.22	1.93
0.0546	440.0	22.727	2.87	2.11	3.89	1.91
0.0539	435.0	22.989	2.36	2.77	3.81	3.36
0.0533	430.0	23.256	3.02	3.24	5.84	2.51
0.0527	425.0	23.529	3.79	2.83	5.19	1.00
0.0521	420.0	23.810	3.97	2.05	4.42	0.588
0.0515	415.0	24.096	3.68	1.40	3.81	0.454
0.0508	410.0	24.390	3.11	1.01	3.21	0.450
0.0502	405.0	24.691	2.22	0.988	2.43	0.670
0.0496	400.0	25.000	1.47	2.24	1.60	2.12
0.0490	395.0	25.316	2.84	3.34	4.41	3.55
0.0484	390.0	25.641	3.47	2.27	3.82	1.85
0.0477	385.0	25.974	3.90	1.61	4.12	0.841
0.0471	380.0	26.316	2.64	1.44	2.37	1.32
0.0465	375.0	26.667	2.51	3.34	6.40	3.40
0.0459	370.0	27.027	4.98	2.45	4.90	0.393
0.0453	365.0	27.397	4.43	1.14	4.14	0.198
0.0446	360.0	27.778	3.87	0.770	3.71	0.153
0.0440	355.0	28.169	3.42	0.626	3.36	0.147
0.0434	350.0	28.571	2.97	0.588	3.01	0.172
0.0428	345.0	28.986	2.39	0.698	2.55	0.260
0.0422	340.0	29.412	1.59	1.39	1.75	0.661
0.0419	338.0	29.586	1.43	2.04	1.33	1.24
0.0417	336.0	29.762	1.55	2.81	1.23	2.17
0.0414	334.0	29.940	2.05	3.64	1.56	3.26
0.0412	332.0	30.120	3.16	4.27	2.72	4.52
0.0409	330.0	30.303	4.69	3.96	5.44	4.39
0.0407	328.0	30.488	5.40	2.74	6.16	2.01
0.0404	326.0	30.675	5.27	1.80	5.49	0.932
0.0402	324.0	30.864	4.96	1.27	4.95	0.535
0.0399	322.0	31.056	4.66	0.974	4.57	0.355
0.0397	320.0	31.250	4.41	0.796	4.30	0.260
0.0394	318.0	31.447	4.19	0.681	4.09	0.204
0.0392	316.0	31.646	4.01	0.604	3.91	0.170
0.0389	314.0	31.847	3.84	0.551	3.76	0.148

TABLE I *(Continued)*

Yttrium Aluminum Garnet (YAG)

eV	cm^{-1}	μm	n	k	n	k
0.0387	312.0	32.051	3.68	0.516	3.62	0.134
0.0384	310.0	32.258	3.53	0.494	3.49	0.126
0.0382	308.0	32.468	3.38	0.485	3.36	0.125
0.0379	306.0	32.680	3.21	0.491	3.22	0.129
0.0377	304.0	32.895	3.03	0.516	3.06	0.141
0.0374	302.0	33.113	2.81	0.574	2.88	0.167
0.0372	300.0	33.333	2.54	0.692	2.64	0.219
0.0369	298.0	33.557	2.20	0.948	2.29	0.338
0.0367	296.0	33.784	1.85	1.52	1.72	0.697
0.0365	294.0	34.014	1.84	2.49	1.25	1.894
0.0362	292.0	34.247	2.59	3.68	1.90	3.754
0.0360	290.0	34.483	4.67	4.04	5.61	4.466
0.0357	288.0	34.722	5.80	2.28	5.95	1.202
0.0355	286.0	34.965	5.40	1.17	5.07	0.463
0.0352	284.0	35.211	4.96	0.738	4.59	0.252
0.0350	282.0	35.461	4.64	0.539	4.30	0.164
0.0347	280.0	35.714	4.41	0.433	4.10	0.120
0.0345	278.0	35.971	4.23	0.369	3.96	0.0941
0.0342	276.0	36.232	4.09	0.327	3.84	0.0776
0.0340	274.0	36.496	3.98	0.298	3.75	0.0665
0.0337	272.0	36.765	3.88	0.277	3.67	0.0587
0.0335	270.0	37.037	3.79	0.262	3.60	0.0529
0.0332	268.0	37.313	3.72	0.250	3.53	0.0485
0.0330	266.0	37.594	3.65	0.240	3.48	0.0452
0.0327	264.0	37.879	3.59	0.233	3.42	0.0426
0.0325	262.0	38.168	3.53	0.227	3.38	0.0407
0.0322	260.0	38.462	3.47	0.222	3.33	0.0392
0.0320	258.0	38.760	3.42	0.219	3.28	0.0382
0.0317	256.0	39.063	3.37	0.217	3.24	0.0375
0.0315	254.0	39.370	3.32	0.215	3.20	0.0372
0.0312	252.0	39.683	3.27	0.215	3.15	0.0372
0.0310	250.0	40.000	3.22	0.216	3.11	0.0377
0.0307	248.0	40.323	3.17	0.218	3.06	0.0386
0.0305	246.0	40.650	3.12	0.221	3.02	0.0401
0.0303	244.0	40.984	3.07	0.226	2.97	0.0423
0.0300	242.0	41.322	3.01	0.233	2.91	0.0454
0.0298	240.0	41.667	2.94	0.242	2.85	0.0499
0.0295	238.0	42.017	2.87	0.256	2.78	0.0563
0.0293	236.0	42.373	2.79	0.275	2.70	0.0657
0.0290	234.0	42.735	2.70	0.302	2.60	0.0801
0.0288	232.0	43.103	2.58	0.342	2.48	0.103
0.0285	230.0	43.478	2.44	0.409	2.31	0.145
0.0283	228.0	43.860	2.23	0.527	2.06	0.231
0.0280	226.0	44.248	1.95	0.774	1.64	0.464
0.0278	224.0	44.643	1.65	1.36	1.14	1.30
0.0275	222.0	45.045	1.74	2.48	1.46	2.80
0.0273	220.0	45.455	3.29	3.91	3.96	4.10

(continued)

TABLE I *(Continued)*

Yttrium Aluminum Garnet (YAG)

eV	cm^{-1}	μm	n	k	n	k
0.0270	218.0	45.872	5.65	1.92	5.29	1.35
0.0268	216.0	46.296	4.81	0.559	4.50	0.469
0.0265	214.0	46.729	4.24	0.267	4.05	0.239
0.0263	212.0	47.170	3.91	0.176	3.78	0.149
0.0260	210.0	47.619	3.69	0.142	3.60	0.106
0.0258	208.0	48.077	3.53	0.129	3.46	0.0817
0.0255	206.0	48.544	3.40	0.125	3.35	0.0672
0.0253	204.0	49.020	3.29	0.126	3.26	0.0581
0.0250	202.0	49.505	3.19	0.131	3.18	0.0523
0.0248	200.0	50.000	3.10	0.138	3.10	0.0489
0.0245	198.0	50.505	3.02	0.148	3.02	0.0472
0.0243	196.0	51.020	2.93	0.160	2.95	0.0470
0.0241	194.0	51.546	2.84	0.177	2.87	0.0483
0.0238	192.0	52.083	2.74	0.199	2.79	0.0513
0.0236	190.0	52.632	2.63	0.230	2.69	0.0568
0.0233	188.0	53.191	2.51	0.274	2.59	0.0660
0.0231	186.0	53.763	2.35	0.344	2.45	0.0822
0.0228	184.0	54.348	2.17	0.466	2.27	0.114
0.0226	182.0	54.945	1.95	0.713	2.01	0.198
0.0223	180.0	55.556	1.88	1.24	1.58	0.576
0.0221	178.0	56.180	2.61	1.68	2.33	1.49
0.0218	176.0	56.818	2.78	0.743	2.36	0.491
0.0216	174.0	57.471	1.95	0.588	1.62	0.444
0.0213	172.0	58.140	1.14	1.20	0.74	1.14
0.0211	170.0	58.824	0.92	2.33	0.57	2.38
0.0208	168.0	59.524	1.13	3.56	0.78	3.82
0.0206	166.0	60.241	1.97	5.20	1.87	6.22
0.0203	164.0	60.976	5.40	6.80	8.97	5.77
0.0201	162.0	61.728	7.93	2.64	7.04	0.998
0.0198	160.0	62.500	6.56	0.887	5.74	0.387
0.0196	158.0	63.291	5.71	0.423	5.11	0.211
0.0193	156.0	64.103	5.21	0.245	4.73	0.135
0.0191	154.0	64.935	4.87	0.159	4.47	0.0953
0.0188	152.0	65.789	4.64	0.111	4.29	0.0718
0.0186	150.0	66.667	4.46	0.0822	4.15	0.0567
0.0183	148.0	67.568	4.31	0.0636	4.04	0.0463
0.0181	146.0	68.493	4.20	0.0509	3.95	0.0389
0.0179	144.0	69.444	4.10	0.0421	3.87	0.0335
0.0176	142.0	70.423	4.02	0.0357	3.80	0.0294
0.0174	140.0	71.429	3.95	0.0310	3.75	0.0262
0.0171	138.0	72.464	3.89	0.0275	3.69	0.0239
0.0169	136.0	73.529	3.83	0.0249	3.65	0.0221
0.0166	134.0	74.627	3.78	0.0230	3.60	0.0210
0.0164	132.0	75.758	3.72	0.0220	3.56	0.0206
0.0161	130.0	76.923	3.67	0.0222	3.51	0.0214
0.0159	128.0	78.125	3.60	0.0250	3.46	0.0247
0.0156	126.0	79.365	3.50	0.0376	3.39	0.0358

TABLE I *(Continued)*

Yttrium Aluminum Garnet (YAG)

eV	cm^{-1}	μm	n	k	n	k
0.0154	124.0	80.645	3.27	0.129	3.24	0.0901
0.0151	122.0	81.967	4.23	1.01	3.18	0.994
0.0149	120.0	83.333	3.92	0.0933	3.82	0.123
0.0146	118.0	84.746	3.77	0.0412	3.64	0.0373
0.0144	116.0	86.207	3.70	0.0282	3.56	0.0214
0.0141	114.0	87.719	3.65	0.0227	3.52	0.0157
0.0139	112.0	89.286	3.62	0.0197	3.49	0.0129
0.0136	110.0	90.909	3.59	0.0178	3.46	0.0112
0.0134	108.0	92.593	3.57	0.0165	3.44	0.0100
0.0131	106.0	94.340	3.55	0.0155	3.42	0.00916
0.0129	104.0	96.154	3.53	0.0147	3.41	0.00849
0.0126	102.0	98.039	3.51	0.0141	3.39	0.00794
0.0124	100.0	100.00	3.50	0.0135	3.38	0.00748
			3.510 [22]	0.0167 [22]		
0.0118	95.0	105.26	3.443	0.0140		
0.0112	90.0	111.11	3.396	0.0121		
0.0105	85.0	117.65	3.362	0.0108		
0.0099	80.0	125.00	3.335	0.0099		
0.0093	75.0	133.33	3.314	0.00922		
0.0087	70.0	142.86	3.298	0.00838		
0.0081	65.0	153.85	3.284	0.00688		
0.0074	60.0	166.67	3.273	0.00542		
0.0068	55.0	181.82	3.263	0.00437		
0.0062	50.0	200.00	3.255	0.00375		
0.0056	45.0	222.22	3.249	0.00323		
0.0050	40.0	250.00	3.243	0.00252		
0.0043	35.0	285.71	3.239	0.00179		
0.0037	30.0	333.33	3.235	0.00125		
0.0031	25.0	400.0	3.232	0.00060		
0.0	0.0		3.26 [20]	0.0	3.18 [21]	0.0
			3.225 [22]		3.26 [23]	

TABLE II

Sellmeier Dispersion Equation Constants for Yttrium Aluminum Garnet

Term [(Eq. (2)]	Tomiki [2]	Tropf [11]	Wemple [12]	Zharikov [13]
λ_1	0.11227	0.1095	0.1117	0.1110
λ_2		17.825		
A_1	2.2831	2.293	2.2883	2.2736
A_2		3.705		
Range (μm)	0.4–1	0.4–4	0.4–0.9	0.4-0.6

TABLE III

Thermo-optical Coefficients of Yttrium Aluminum Garnet

Wavelength (μm)	dn/dT (10^{-6}/K)	Temperature (°C)	Reference
0.4579	11.9	30–45	[10]
0.4765	12.0	30–45	[10]
0.4880	11.6	30–45	[10]
0.4965	11.4	30–45	[10]
0.5017	11.4	30–45	[10]
0.508	10.2	20–120	[8]
0.5146	10.6	30–45	[10]
	12.2	27	[16]
0.546	11.5	23–372	[13]
0.6328	10.4	30–45	[10]
	9.86	75–110	[15]
	7.3[a]	27–58	[14]
0.644	9.4	20–120	[8]
1.06	10.0	23–372	[13]
1.0642	9.1	30–45	[10]

[a] Neodynium-doped YAG.

TABLE IV

Transverse (and Longitudinal) Optical Phonon Frequencies in Yttrium Aluminum Garnet

Mode	Gledhill [20]	Hoffmeister [21]	Hurrell [18]
F_{1u}	122.25(122.65)	121.7(122.2)	119(125)
F_{1u}	163.4(172.3)	164.2(173.0)	165(181)
F_{1u}	177.5(180.2)	177.9(179.8)	
F_{1u}	219.0(224)	219.6(224.7)	217.8(227)
F_{1u}	289.7(296.0)	288.8(295.8)	289(298)
F_{1u}	330.2(340)	328.5(338.0)	329(341)
F_{1u}	372.5(378)	374.3(380.4)	370(379)
F_{1u}	387.3(388)	388.3(391.2)	—
F_{1u}	394.5(402.5)	395.1(402.4)	392(403)
F_{1u}	427.8(438.3)	430.6(438.6)	429(437)
F_{1u}	445.5(471.5)	451(547.8?)	466(471)
F_{1u}	472.3(510.8)	—	482(505)
F_{1u}	516.5(549.0)	509.7(506.3?)	521(551)
F_{1u}	569.2(585.0)	565(582.6)	569.5(591.8)
F_{1u}	692.0(712.0)	690/3(708.4)	690(707)
F_{1u}	723(765)	720.8(766.5)	737(769)
F_{1u}	782(840.5)	784.9(857.7)	811(921)?

Zircon ($ZrSiO_4$)

EDWARD D. PALIK
Institute for Physical Science and Technology
and
R. KHANNA
Department of Chemistry and Biochemistry
University of Maryland
College Park, Maryland

The interest in zircon is primarily as a gemstone. Many varieties and colors are found all over the world. The colors are due to the impurities, which give line absorption in the visible. We will not discuss these extrinsic effects in any detail. Many of the properties of zircon are summarized by Deer *et al.* [1].

$ZrSiO_4$ is a tetragonal crystal with space group symmetry I4/amd (D_{4h}). The clear crystal is termed high zircon, but containing impurities, it may have various colors. A somewhat amorphous phase made up of some SiO_2 and ZrO_2 is called low zircon and bears a green color [2].

The crystal form should have four E_u ($\mathbf{E}\perp\mathbf{c}$) and three A_{2u} ($\mathbf{E}\parallel\mathbf{c}$) vibration modes in the infrared spectral region. The IR from 200 to 1100 cm^{-1} has been studied by Dawson *et al.* [3]. Gem-quality crystals from Ceylon were oriented, cut, and mechanically polished. An RIIC Michelson interferometer FS-720 was used at low frequencies, while single-beam and double-beam grating spectrometers (both built in the King's College physics department) were used at higher frequencies. The samples were either at 300 K or 100 K. Wire-grid polarizers were made of gold lines on AgCl or polyethylene sheets. The reflectivity spectrum was Kramers–Kronig (K-K) analyzed, but no mention was made of including the high-frequency reflectivity above the band gap. No Lorentz-oscillator analysis of reflectivity was made (which is often useful for comparison). The absorption spectrum was also measured for samples of thickness 0.3 to 3 mm with the *c*-axis in the plane of the samples. The data were presented in small graphs of ϵ' (real dielectric function) and ϵ'' (imaginary dielectric function) for polarization $\parallel$(e) and $\perp$(o) to the *c*-axis. These graphs were expanded by photocopying and read, and the 300 K data are listed in Table I. There is a significant

Copyright © 1998 by Academic Press.
All rights of reproduction in any form reserved
ISBN 0-12-544423-0/$25.00.

uncertainty in n and k, especially where these parameters are changing rapidly. Although we include n to three figures and k to two figures, the reading uncertainty is surely $\pm 20\%$. There is also an uncertainty in the wave number of probably ± 3 cm^{-1}. Four E_u modes are observed. Three A_{2u} modes are seen with a hint of a fourth one.

The A_{2u} modes ($\mathbf{E} \| \mathbf{c}$) have been measured by Gervais *et al.* [4]. The sample was a natural crystal, mechanically polished and then annealed at 1300 K. Both a K-K analysis and an oscillator model have been used to fit the reflectivity. The oscillator model gave the complex dielectric function as

$$\epsilon = \epsilon' - i\epsilon'' = \epsilon_\infty + \sum_j \frac{\Delta\epsilon_j \, \omega_j^2}{(\omega_j^2 - \omega^2 + i\Gamma_j\omega)}.$$

The parameters at 295 K for four oscillators are given in Table II. Note that group theory predicts only three A_{2u} modes, and a fourth mode has been added at high frequency for the model fit. The dc dielectric constant is calculated to be $\epsilon'_o(\mathrm{e}) = 10.71$.

We have calculated n(e) and k(e) to extend and fill in the gaps of the data of Dawson *et al.* [3] and also give them in Table I. The magnitudes of n and k are similar for the two sets of data, but do differ by $\pm 20\%$ in places if account is taken of the mode frequencies being slightly different. This gives slightly shifted spectra.

Dawson *et al.* [3] measured the transmittance of thin plates at 100 and 300 K with polarized radiation. They displayed absorption spectra with arbitrary but linear ordinate. They also gave the peak absorption coefficient $\alpha = 4\pi k/\lambda$ at three points in the spectrum. (We assume these are low-temperature data; if this is the wrong choice, there are up to 20% differences.) These are ($\perp$: 887 cm^{-1}, 85000 cm^{-1}; 1900 cm^{-1}, 70 cm^{-1}; 2750 cm^{-1}, ~0 cm^{-1}); ($\|$: 994 cm^{-1}, 93000 cm^{-1}; 1900 cm^{-1}, 100 cm^{-1}; 2750 cm^{-1}, 1.4 cm^{-1}). Assuming we can make the comparison of absorption coefficient with arbitrary absorption, we have calculated k in the two- and three-phonon absorption region near 1900 and 2800 cm^{-1}, respectively. We did not use a grid fine enough to show all the details of the observed spectral lines. The results are listed in Table I.

We could find no near-IR, visible data for n(o) and n(e) obtained by prism minimum-deviation methods.

Many books on gems give the indices of refraction at the Na D line (0.5890 μm) but usually do not quote the source. Clear high zircon has n(o) = 1.925 and n(e) = 1.984 in one gem book [5] and is given a range of values n(o) = 1.924–1.934 and n(e) = 1.970–1.977 in another book [1]. However, because of the ubiquitous presence of impurities, which change the color of the gem, these constants can vary drastically; therefore, we should focus on clear high zircon.

Vance [6] has measured the visible and near-IR transmittance of various

gem stones of low zircon at 15 and 290 K. The spectra contain many weak, sharp lines attributed to impurity atoms of U and Th. It is believed that high zircon containing U and Th degenerates into low zircon over the years because of the radioactive decay of the impurity atoms. Only the low-temperature spectra are given in graphs, and they are labeled as σ polarized. The atomic impurities often appear only in σ or π polarization. We assume this refers to and perpendicular and parallel to the c-axis of the crystal. The c-axis was presumably located in the plane of these gem samples. One σ spectrum shows the onset of band-edge absorption. Even though the spectrum was obtained at 15 K, we have smoothed out the impurity structure and show k(o) in Table II, since we can find no detailed study of the absorption edge at room temperature. This is not quite the correct thing to do, since low zircon is an "amorphous" mixture of SiO_2 and ZrO_2 (but showing a c-axis). But the band gap of crystalline SiO_2 is $\sim$ 9 eV, while that of crystalline ZrO_2 (zirconia) is $\sim$ 3 eV. We would expect a mixture to have a band gap somewhere in between these limits. Deer *et al.* [1] gives several references to optical absorption studies, but none of these were quantitative regarding k.

We could find no data above the band gap into the UV that could yield the optical constants and, therefore, cannot obtain an accurate value of the band gap.

The data listed in Table I are plotted in Fig. 1. The ordinary n(o) and k(o), primarily from Dawson *et al.* [3], are shown in Fig. 1a; the extraordinary n(e) and k(e), primarily from Dawson *et al.* [3] are shown in Fig. 1b; the extraordinary n(e) and k(e) from Gervais *et al.* [4] are shown in Fig. 1c for comparison.

ACKNOWLEDGMENT

We thank James E. Shigley, Director of Research, Gemological Institute of America, 1630 Stewart St., Santa Monica, CA 90404-4088 for kindly providing us with a copy of the zircon section of Deer *et al.* [1].

REFERENCES

1. W. A. Deer, R. A. Howie, and J. Zussman, "Rock-Forming Minerals," Vol. 1A, 2nd Ed., Orthosilicates, p. 431. Longmans, London, 1982.
2. R. Webster, "Gems," p. 131. Newnes-Butterworth, London, 1975.
3. P. Dawson, M. M. Hargreave, and G. R. Wilkinson, The vibrational spectrum of zircon ($ZrSiO_4$). *J. Phys. C: Solid State Phys.* **4**, 240 (1971).
4. F. Gervais, B. Piriou, and F. Cabannes, Anharmonicity in silicate crystals: temperature dependence of Au type vibrational modes in $ZrSiO_4$ and $LiAlSi_2O_6$. *J. Phys. Chem. Solids* **34**, 1785 (1973).
5. R. T. Liddicoat, Jr., "Handbook of Gem Identification," p. 272. Gemological Institute of America, Santa Monica, CA, 1969.
6. E. R. Vance, The anomolous optical absorption spectrum of low zircon. *Minerol. Mag.* **39**, 709 (1974).

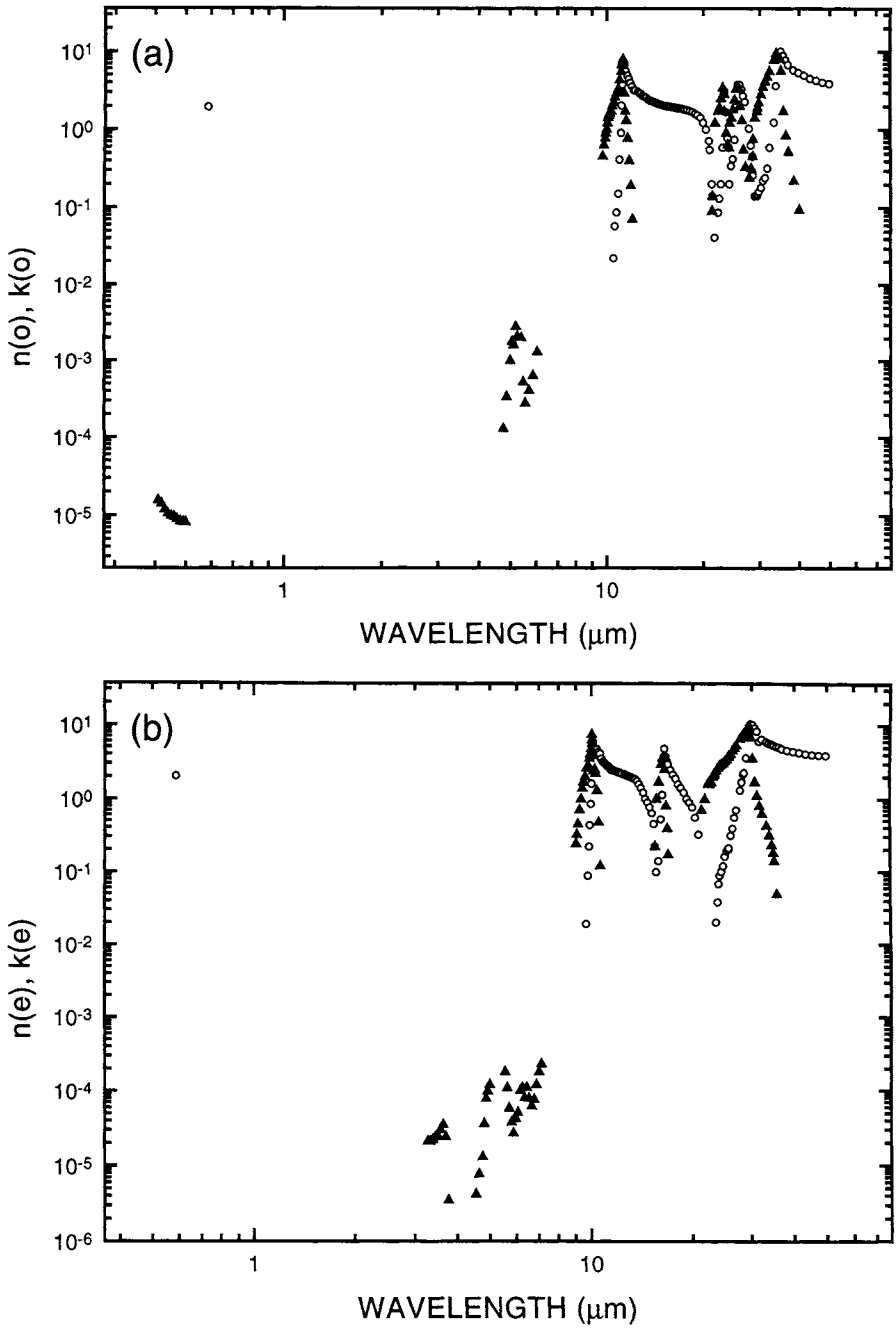

Fig. 1. (a) Log–log plot of n(o) (○○○) and k(o) (▲▲▲) versus wavelength in micrometers for zircon, primarily from Dawson et al. [3]. (b) Log–log plot of n(e) (○○○) and k(e) (▲▲▲) versus wavelength in micrometers for zircon, primarily from Dawson *et al.* [3].

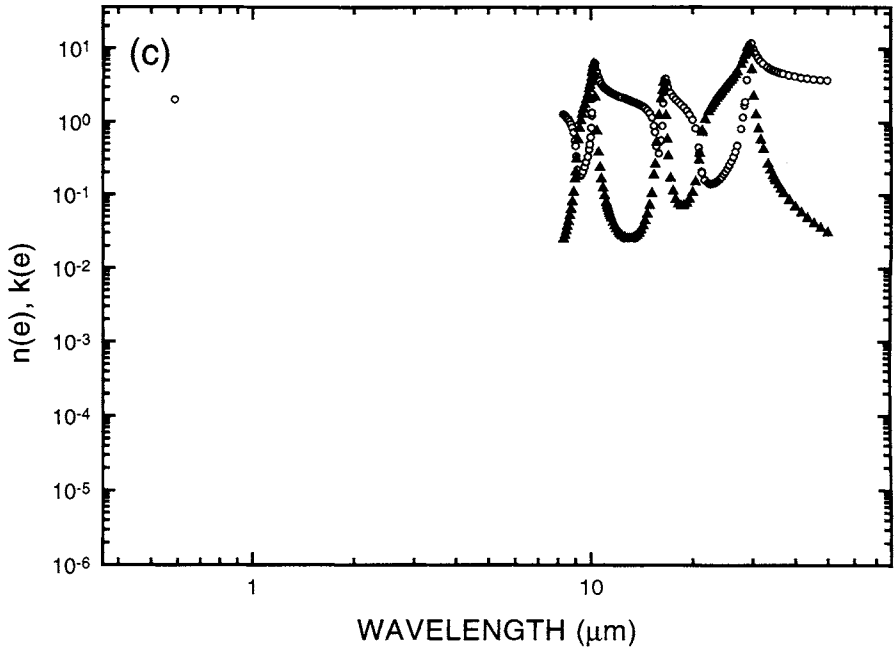

Fig. 1, cont'd. (c) Log–log plot of n(e) (○○○) and k(e) (▲▲▲) versus wavelength in micrometers for zircon, primarily from Gervais *et al.* [4].

TABLE I

Values of n and k for Zircon ($ZrSiO_4$) Obtained from Various References

eV	cm^{-1}	μm	n(o)	k(o)	n(e)	n(e)	k(e)	k(e)
3.024	24390	0.41		1.55E-5 [6]				
2.952	23810	0.42		1.40E-5				
2.883	23256	0.43		1.19E-5				
2.818	22727	0.44		1.05E-5				
2.755	22222	0.45		9.77E-6				
2.695	21739	0.46		9.51E-6				
2.638	21277	0.47		8.86E-6				
2.583	20833	0.48		8.40E-6				
2.530	20408	0.49		8.18E-6				
2.480	20000	0.50		8.15E-6				
2.105	16980	0.5890	1.925 [5]		1.984 [5]			
0.3782	3050	3.279					2.1E-5 [3]	
0.3720	3000	3.333					2.1E-5	
0.3658	2950	3.390					2.2E-5	
0.3596	2900	3.448					2.4E-5	
0.3534	2850	3.509					2.5E-5	
0.3472	2800	3.571					3.0E-5	
0.3410	2750	3.636					3.5E-5	
0.3348	2700	3.704					2.4E-5	
0.3286	2650	3.774					3.5E-6	
0.2728	2200	4.545					4.2E-6	
0.2666	2150	4.651					7.7E-6	
0.2604	2100	4.762		1.3E-4 [3]			1.3E-5	
0.2573	2075	4.819					3.6E-5	
0.2542	2050	4.878		3.4E-4			7.9E-5	
0.2511	2025	4.938					9.8E-5	
0.2480	2000	5.000		1.0E-3			1.2E-4	

0.2449	1975	5.063	1.8E-3				
0.2418	1950	5.128	1.6E-3				
0.2387	1925	5.195	2.8E-3				
0.2356	1900	5.263	2.1E-3				
0.2294	1850	5.405	2.0E-3				
0.2263	1825	5.479	5.3E-4				
0.2232	1800	5.556	2.8E-4			1.8E-4	
0.2201	1775	5.634				1.1E-4	
0.2170	1750	5.714	4.1E-4			5.8E-5	
0.2139	1725	5.797				3.8E-5	
0.2108	1700	5.882	6.4E-4			2.7E-5	
0.2077	1675	5.970				4.2E-5	
0.2046	1650	6.061	1.3E-3			5.1E-5	
0.2015	1625	6.154				1.0E-4	
0.1984	1600	6.250				1.1E-4	
0.1953	1575	6.349				8.0E-5	
0.1922	1550	6.452				1.1E-4	
0.1891	1525	6.557				7.9E-5	
0.1860	1500	6.667				6.2E-5	
0.1829	1475	6.780				7.6E-5	
0.1798	1450	6.897				1.2E-4	
0.1767	1425	7.018				1.8E-4	
0.1736	1400	7.143				2.3E-4	
0.1488	1200	8.333		1.26 [4]			2.48E-2 [4]
0.1475	1190	8.403		1.22			2.80E-2
0.1463	1180	8.475		1.18			3.19E-2
0.1451	1170	8.547		1.13			3.68E-2
0.1438	1160	8.621		1.08			4.30E-2
0.1426	1150	8.696		1.01			5.13E-2
0.1413	1140	8.772		0.932			6.27E-2
0.1401	1130	8.850		0.836			7.95E-2

(continued)

TABLE I *(Continued)*

$ZrSiO_4$

eV	cm^{-1}	μm	*n*(o)	*k*(o)	*n*(e)	*n*(e)	*k*(e)	*k*(e)
0.1389	1120	8.929				0.714		1.07E-1
0.1376	1110	9.009				0.549		1.62E-1
0.1371	1106	9.041				0.467	2.4E-1 [3]	2.02E-1
0.1364	1100	9.091				0.338	3.2E-1	3.09E-1
0.1351	1090	9.174				0.218	4.5E-1	5.72E-1
0.1339	1080	9.259				0.186	7.1E-1	8.17E-1
0.1327	1070	9.346				0.180	1.0E0	1.04E0
0.1314	1060	9.434				0.189	1.4E0	1.27E0
0.1302	1050	9.524				0.208	1.7E0	1.50E0
0.1289	1040	9.615				0.238	2.0E0	1.75E0
0.1277	1030	9.709		4.5E-1 [3]	0.019 [3]	0.279	2.6E0	2.04E0
0.1265	1020	9.804		6.3E-1	0.088	0.332	2.8E0	2.39E0
0.1252	1010	9.901		7.7E-1	0.22	0.418	3.5E0	2.86E0
0.1246	1005	9.950		8.9E-1	0.43	0.493	4.0E0	3.17E0
0.1240	1000	10.00		1.0E0	0.86	0.613	4.7E0	3.56E0
0.1234	995	10.05		1.2E0	1.61	0.820	6.2E0	4.06E0
0.1227	990	10.10		1.4E0	5.20	1.21	5.6E0	4.72E0
0.1226	989	10.11		1.4E0	5.48	1.33	5.5E0	4.88E0
0.1221	985	10.15		1.5E0	5.88	2.07	3.8E0	5.58E0
0.1215	980	10.20		1.6E0	4.69	4.07	2.4E0	6.18E0
0.1209	975	10.26		1.7E0	4.48	6.41	2.5E0	4.42E0
0.1203	970	10.31		1.7E0	4.58	6.23	2.2E0	2.18E0
0.1190	960	10.42		2.0E0	4.65	4.85	1.3E0	7.46E-1
0.1178	950	10.53	0.022 [3]	2.2E0	4.27	4.08	4.7E-1	3.82E-1
0.1165	940	10.64	0.057	2.6E0	4.00	3.62	1.2E-1	2.37E-1
0.1153	930	10.75	0.086	2.9E0	3.46	3.31		1.64E-1
0.1141	920	10.87	0.15	3.3E0	3.16	3.09		1.22E-1

0.1128	910	10.99	0.41	4.3E0	3.00	2.92		9.54E-2
0.1116	900	11.11	0.90	5.5E0	2.83	2.79		7.72E-2
0.1110	895	11.17	2.01	6.7E0	2.79	2.73		7.02E-2
0.1103	890	11.23	3.74	7.3E0	2.74	2.68		6.42E-2
0.1097	885	11.30	6.35	7.1E0	2.69	2.63		5.91E-2
0.1091	880	11.36	6.95	2.9E0	2.64	2.58		5.47E-2
0.1085	875	11.43	5.76	1.7E0	2.55	2.54		5.08E-2
0.1079	870	11.49	5.53	1.3E0	2.45	2.50		4.75E-2
0.1066	860	11.63	4.86	7.7E-1	2.41	2.43		4.19E-2
0.1054	850	11.76	4.38	4.0E-1	2.37	2.37		3.76E-2
0.1041	840	11.90	3.94	1.9E-1	2.32	2.31		3.42E-2
0.1029	830	12.05	3.54	7.1E-2	2.28	2.26		3.15E-2
0.1017	820	12.19	3.17		2.24	2.21		2.94E-2
0.1004	810	12.34	3.16		2.19	2.16		2.78E-2
0.09919	800	12.59	3.00		2.14	2.12		2.65E-2
0.09795	790	12.66	2.91		2.10	2.07		2.57E-2
0.09671	780	12.82	2.83		2.05	2.03		2.52E-2
0.09547	770	12.99	2.68		2.00	1.99		2.50E-2
0.09423	760	13.16	2.61		1.95	1.94		2.51E-2
0.09299	750	13.33	2.55		1.90	1.90		2.56E-2
0.09175	740	13.51	2.39		1.83	1.85		2.66E-2
0.09051	730	13.70	2.32		1.73	1.80		2.80E-2
0.08927	720	13.89	2.28		1.58	1.74		3.02E-2
0.08803	710	14.08	2.24		1.41	1.68		3.32E-2
0.08679	700	14.29	2.19		1.22	1.62		3.77E-2
0.08555	690	14.49	2.14		1.00	1.54		4.42E-2
0.08431	680	14.70	2.10		0.89	1.44		5.44E-2
0.08307	670	14.92	2.05		0.77	1.32		7.15E-2
0.08183	660	15.15	2.02		0.63	1.15		1.04E-1
0.08059	650	15.38	2.00		0.45	0.882		1.85E-1
0.08009	646	15.48	1.98		0.22	0.726	2.2E-1	2.62E-1
0.07935	640	15.62	1.97		0.099	0.466	1.0E0	5.35E-1

(continued)

TABLE I *(Continued)*

$ZrSiO_4$

eV	cm^{-1}	μm	n(o)	k(o)	n(e)	n(e)	k(e)	k(e)
0.07811	630	15.87	1.95		0.14	0.368	1.7E0	1.24E0
0.07687	620	16.13	1.92		0.52	0.560	2.9E0	2.10E0
0.07625	615	16.26	1.91		1.14	0.886	3.5E0	2.71E0
0.07563	610	16.39	1.90		3.32	1.82	3.6E0	3.48E0
0.07538	608	16.45	1.89		3.71	2.57	3.7E0	3.62E0
0.07501	605	16.53	1.88		4.73	3.81	2.5E0	2.96E0
0.07439	600	16.67	1.87		3.69	3.91	8.1E-1	1.22E0
0.07377	595	16.81	1.86		3.19	3.36	3.9E-1	5.77E-1
0.07315	590	16.95	1.84		2.92	2.97	1.7E-1	3.39E-1
0.07191	580	17.24	1.82		2.45	2.51		1.69E-1
0.07067	570	17.54	1.79		2.12	2.23		1.11E-1
0.06943	560	17.86	1.76		1.87	2.03		8.56E-2
0.06819	550	18.18	1.73		1.58	1.87		7.40E-2
0.06695	540	18.52	1.67		1.41	1.72		6.97E-2
0.06571	530	18.87	1.58		1.22	1.58		7.04E-2
0.06447	520	19.23	1.52		1.00	1.43		7.56E-2
0.06323	510	19.61	1.41		0.89	1.26		8.65E-2
0.06199	500	20.00	1.22		0.77	1.07		1.07E-1
0.06075	490	20.41	1.00		0.55	0.814		1.50E-1
0.05951	480	20.83	0.71		0.32	0.446		2.99E-1
0.05926	478	20.92	0.55			0.368		3.71E-1
0.05827	470	21.28	0.20	9.0E-2		0.207	7.0E-1	7.21E-1
0.05815	469	21.32	0.14	1.4E-1		0.198		7.61E-1
0.05703	460	21.74	0.041	1.2E0		0.158	1.0E0	1.08E0
0.05573	450	22.22	0.086	1.7E0		0.143	1.6E0	1.39E0
0.05517	445	22.47	0.13	1.9E0		0.140	1.6E0	1.54E0
0.05455	440	22.73	0.20	2.5E0		0.140	1.7E0	1.68E0

0.05393	435	22.99	0.59	3.4E0		0.142	2.0E0	1.83E0
0.05337	430	23.23	3.13	2.8E0		0.144	2.1E0	1.96E0
0.05331	430	23.25	2.97	1.7E0		0.145	2.2E0	1.98E0
0.05269	425	23.53	1.67	9.0E-1	0.020	0.150	2.4E0	2.13E0
0.05207	420	23.81	0.78	6.4E-1	0.038	0.156	2.6E0	2.29E0
0.05170	417	23.98	0.59	5.9E-1	0.068	0.161	2.7E0	2.39E0
0.05145	415	24.10	0.20	1.2E0	0.088	0.165	2.8E0	2.46E0
0.05083	410	24.39	0.34	1.4E0	0.10	0.175	2.9E0	2.64E0
0.05021	405	24.69	0.42	1.8E0	0.12	0.189	3.0E0	2.83E0
0.04959	400	25.00	0.74	2.4E0	0.16	0.205	3.2E0	3.03E0
0.04897	395	25.32	1.94	3.3E0	0.19	0.226	3.4E0	3.26E0
0.04835	390	25.64	3.54	3.4E0	0.20	0.252	3.7E0	3.51E0
0.04829	389	25.67	3.75	3.5E0	0.21	0.256	3.8E0	3.53E0
0.04773	385	25.97	3.74	2.0E0	0.31	0.286	4.0E0	3.79E0
0.04711	380	26.32	3.27	1.30E0	0.39	0.331	4.5E0	4.11E0
0.04649	375	26.67	2.70	5.5E-1	0.55	0.392	4.9E0	4.48E0
0.04587	370	27.03	2.26	3.3E-1	0.70	0.478	5.3E0	4.92E0
0.04463	360	27.78	1.03	2.4E-1	1.31	0.807	6.5E0	6.17E0
0.04401	355	28.17	0.63	3.2E-1	1.70	1.16	7.1E0	7.11E0
0.04352	351	28.49	0.45	4.5E-1	2.17	1.70	7.6E0	8.14E0
0.04339	350	28.57	0.26	7.5E-1	2.26	1.90	7.7E0	8.45E0
0.04277	345	28.98	0.14	1.4E0	3.58	3.79	7.0E0	10.4E0
0.04215	340	29.41	0.14	1.7E0	7.43	9.03	8.1E0	10.8E0
0.04191	338	29.58	0.15	1.9E0	9.67	11.2	9.7E0	8.82E0
0.04153	335	29.85	0.16	2.2E0	10.3	11.6	6.8E0	5.21E0
0.04091	330	30.30	0.18	2.8E0	10.1	9.84	3.5E0	2.28E0
0.04029	325	30.77	0.22	3.5E0	9.11	8.41	1.7E0	1.26E0
0.03968	320	31.25	0.24	4.1E0	8.26	7.46	1.1E0	8.11E-1
0.03905	315	31.75	0.32	4.7E0	5.97	6.79	8.0E-1	5.71E-1
0.03843	310	32.26	0.59	5.5E0	6.43	6.30	6.2E-1	4.26E-1
0.03720	300	33.33	1.23	7.7E0	5.93	5.60	4.2E-1	2.67E-1
0.03657	295	33.90	3.60	9.4E0	5.66	5.35	3.1E-1	2.21E-1

(continued)

TABLE I *(Continued)*

$ZrSiO_4$

eV	cm^{-1}	μm	n(o)	k(o)	n(e)	n(e)	k(e)	k(e)
0.03595	290	34.48	7.91	8.2E0	5.48	5.14	2.3E-1	1.85E-1
0.03558	287	34.84	9.70	8.1E0	5.36	5.03	1.8E-1	1.68E-1
0.03533	285	35.09	10.0	5.6E0	5.29	4.96	1.4E-1	1.58E-1
0.03472	280	35.71	8.82	1.7E0	5.10	4.81	4.9E-2	1.37E-1
0.03409	275	36.36	7.73	8.4E-1	5.00	4.68		1.20E-1
0.03347	270	37.04	6.73	5.2E-1	4.79	4.56		1.05E-1
0.03224	260	38.46	5.75	2.2E-1	4.53	4.36		8.41E-2
0.03100	250	40.00	5.29	9.4E-2	4.41	4.20		6.85E-2
0.02976	240	41.67	4.90		4.24	4.07		5.70E-2
0.02852	230	43.48	4.47		4.04	3.96		4.80E-2
0.02728	220	45.45	4.24		3.94	3.87		4.10E-2
0.02604	210	47.62	4.00		3.91	3.79		3.53E-2
0.02480	200	50.00	3.87		3.87	3.72		3.07E-2

TABLE II

Oscillator Parameters for A_{2u} Vibrational Modes at 295 K; $\epsilon_\infty = 3.8$

$\Delta\epsilon_j$	ω_j (cm^{-1})	Γ_j (cm^{-1})
5.75	339	9.5
0.36	605.7	9.5
0.78	977	12.2
0.022	1020	65

This page is intentionally left blank